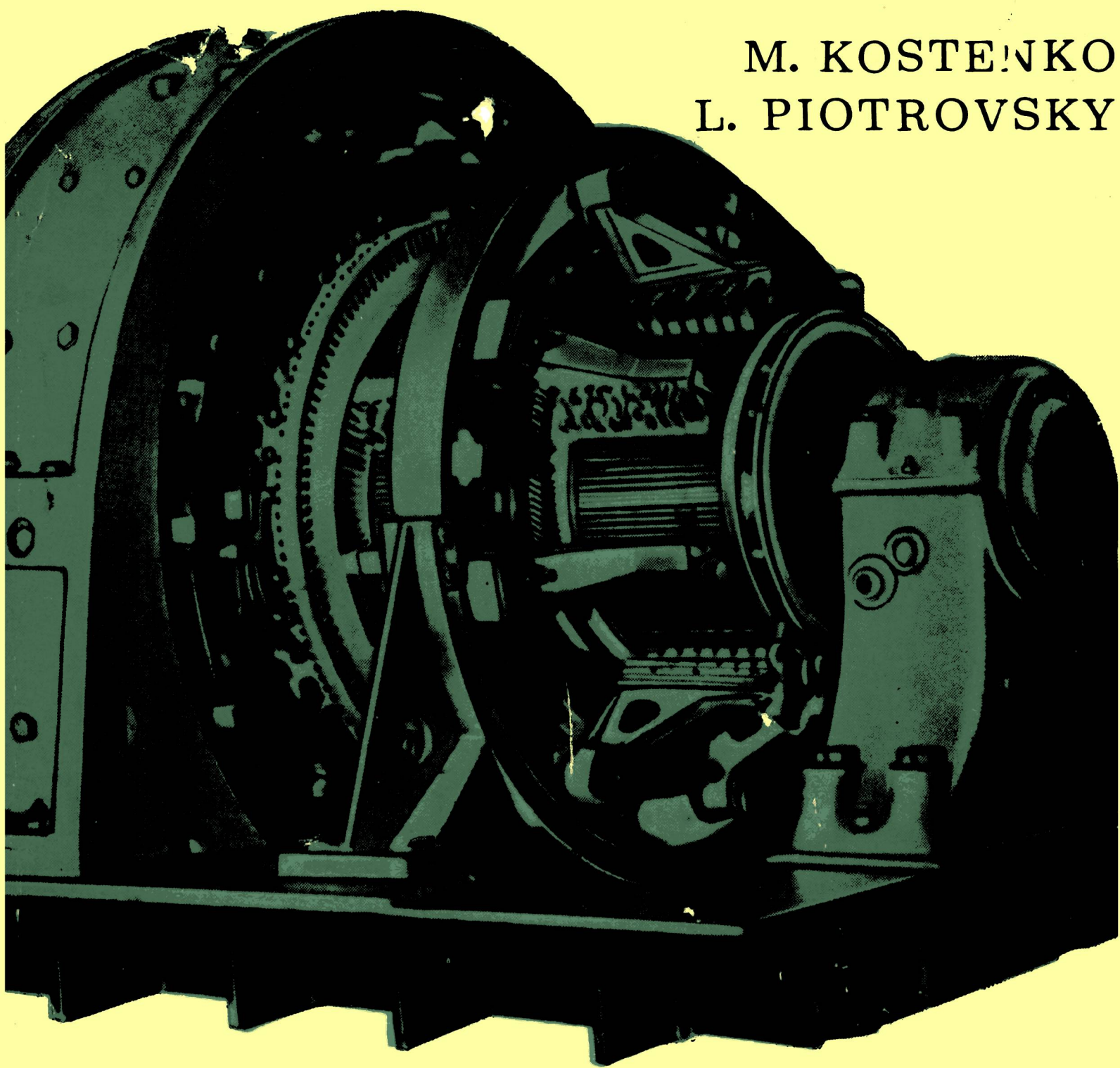


M. KOSTENKO
L. PIOTROVSKY



ELECTRICAL MACHINES

VOLUME II

MIR PUBLISHERS

M. KOSTENKO, L. PIOTROVSKY

ELECTRICAL MACHINES

IN TWO VOLUMES

VOL. 2

ALTERNATING CURRENT MACHINES

TRANSLATED FROM THE RUSSIAN BY A. CHERNUKHIN

MIR PUBLISHERS · MOSCOW

First published 1962
Second printing 1964
Second edition 1968
Third edition 1974

Revised from the 1972 Russian edition

This book has been recommended for republication by Indian specialists under the programme of the Joint Indo-Soviet Board to make the best Soviet textbooks available for Indian students.

На английском языке

© English translation, Mir Publishers, 1974

М. П. КОСТЕНКО, Л. М. ПИОТРОВСКИЙ

ЭЛЕКТРИЧЕСКИЕ МАШИНЫ

Том II

МАШИНЫ ПЕРЕМЕННОГО ТОКА

ИЗДАТЕЛЬСТВО «ЭНЕРГИЯ»

Москва

Ленинград

CONTENTS

Notation	12
--------------------	----

PART ONE

GENERAL INFORMATION ON A. C. MACHINES

Chapter 1. Basic Types of A. C. Machines and Their Design	19
1-1. Basic Types of A. C. Machines	19
1-2. Operating Principle of a Synchronous Machine	19
1-3. Fundamental Designs of Synchronous Machines	21
1-4. Design of Non-Salient-Pole Synchronous Machines	23
1-5. Turbogenerators for Atomic Power Stations	25
1-6. Design of Salient-Pole Synchronous Machines	29
1-7. High-Frequency and Special Synchronous Machines	37
1-8. Principal Elements of Non-Commutator Induction Machines	40
1-9. Operating Principle of the Induction Machine	42
1-10. Operating Conditions of the Induction Machine	43
1-11. Fundamental Relations. Electromagnetic Torque of the Induction Machine	45
1-12. Principle of A. C. Machine Winding Design	46
Chapter 2. Electromotive Forces in A. C. Machine Windings	51
2-1. Basic Characteristics of A. C. Machine E. M. F.	51
2-2. E. M. F. of a Conductor	51
2-3. E. M. F. of a Turn and of a Concentrated Winding with a Full (Diametrical) Pitch	55
2-4. E. M. F. of a Full-Pitch Distributed Winding	56
2-5. E. M. F. of a Concentrated Short-Pitch Winding	60
2-6. General Expression for E. M. F. of A. C. Machine Armature Winding	64
2-7. Combination of E. M. F. s	67
Chapter 3. Windings of Alternating Current Machines	68
3-1. Three-Phase Double-Layer Lap Windings with q an Integer	68
3-2. Three-Phase Double-Layer Wave Windings with q an Integer	75
3-3. Three-Phase Single-Layer Windings with Coils of Equal Width	77
3-4. Three-Phase Single-Layer Concentric Windings with a Whole Number of Slots per Pole per Phase	80
3-5. E. M. F.s Due to Tooth-Ripple Harmonics	85
3-6. Three-Phase Fractional-Slot Windings	87
3-7. Insulation of Windings	98

Chapter 4. Magnetizing Force of Alternating Current Windings	103
4-1. General	103
4-2. Equations of Pulsating and Travelling Waves	103
4-3. Magnetizing Force of a Winding Phase	108
4-4. Magnetizing Force of a Three-Phase Winding	114
4-5. Analysis of Magnetizing Force Curve of Integral-Slot q Windings	119
4-6. Magnetizing Force of Fractional-Pitch Windings	124
4-7. Magnetic Field of an A. C. Winding	125
Chapter 5. Inductive Reactances of A. C. Machine Windings	128
5-1. Inductive Reactances of Air-Gap Magnetic Fields	128
5-2. General Expressions for Inductive Leakage Reactances	130
5-3. Slot Permeance	134
5-4. Permeance of End Connections	138
5-5. Differential Leakage Inductive Reactance	139
5-6. Leakage Inductive Reactances of Stator and Rotor Windings of a Synchronous Machine	140
Chapter 6. Heating and Cooling of Rotating Electrical Machines	143
6-1. Insulating Materials Used in Electrical Machinery and Their Required Properties	143
6-2. Permissible Temperature Limits and Temperature-Rise Limits	145
6-3. Heat Transfer in Electrical Machines	148
6-4. Theory of Solid Body Heating	152
6-5. Main Rated Machine Duties	157
6-6. Machine Heating in Continuous Duty	158
6-7. Machine Heating in Short-Time Duty	159
6-8. Machine Heating in Short-Time Intermittent Duty	160
6-9. Ventilation of Electrical Machines	160
Chapter 7. Cooling Systems for Turbogenerators and Hydrogenerators	165
7-1. Ventilation of Turbogenerators with Ordinary Cooling	165
7-2. Systems of Direct Cooling of Turbogenerator Windings	167
7-3. The Main Trends in the Development of Turbogenerator Cooling	174
7-4. Cooling Systems for Hydrogenerators	176

PART TWO

SYNCHRONOUS MACHINES

Chapter 8. Armature Reaction of a Synchronous Machine at Balanced Load	183
8-1. Armature-Reaction Phenomenon in a Polyphase Synchronous Generator at Balanced Load	183
8-2. Armature Reaction of a Non-Salient-Pole Synchronous Machine	186
8-3. Armature Reaction of a Salient-Pole Synchronous Machine. Two-Reaction Theory.	189
Chapter 9. Voltage Diagrams of a Three-Phase Synchronous Generator at Balanced Load	203
9-1. General	203
9-2. E. M. F. and the Potier Diagrams of a Three-Phase Non-Salient-Pole Synchronous Generator	205
9-3. E. M. F. Diagram of a Salient-Pole Three-Phase Synchronous Generator at Balanced Load (Blondel Diagram)	208

9-4. Modified E. M. F. Diagram	211
9-5. E. M. F. Diagram for Short Circuit	213
9-6. Synchronous Machine Inductive Reactances in Steady-State Balanced Operation	215
9-7. Determination of Voltage Rise and Drop by Means of Voltage Diagrams	218
9-8. Determination of Voltage Change from the E. M. F. Diagram for a Salient-Pole Machine According to Design Data	219
9-9. Determination of Voltage Change by Means of the Potier Diagram	221
9-10. Simplified Practical Diagram (Swedish Diagram)	226
9-11. Determination of Voltage Change by the Simplified E. M. F. Diagram	230
9-12. Experimental Data of E. M. F. Diagram Comparison	232
Chapter 10. Single-Phase Synchronous Generator	233
10-1. Armature Reaction of a Single-Phase Generator	233
10-2. Voltage Diagram of a Single-Phase Generator	236
10-3. Comparison of Output of Single-Phase and Three-Phase Synchronous Generators of the Same Size	236
Chapter 11. Characteristics of a Synchronous Generator	238
11-1. System of Relative Units (per Unit Values)	238
11-2. No-Load Characteristic	242
11-3. Short-Circuit Characteristic	243
11-4. Short-Circuit Ratio :	245
11-5. Load Characteristics	246
11-6. External Characteristics	247
11-7. Regulation Characteristics	248
11-8. Losses and Efficiency of a Synchronous Generator	248
Chapter 12. Parallel Operation of Synchronous Machines	251
12-1. General	251
12-2. Parallel Connection of Synchronous Generators	252
12-3. Angle Characteristics of a Synchronous Machine	257
12-4. Static Overload Capacity of a Synchronous Machine Operating in Parallel in an Electrical System	263
12-5. Generator and Motor Duties. Overexcitation and Underexcitation of a Synchronous Machine	267
12-6. Current Diagrams of Synchronous Machines	274
Chapter 13. Synchronous Motor and Synchronous Condenser	281
13-1. Physical Aspects of Synchronous Machine Motoring Duty	281
13-2. Powers and Torques of a Synchronous Motor	282
13-3. Voltage Diagrams of a Synchronous Motor	284
13-4. Synchronous Motor Operating from High-Capacity Power System	285
13-5. Performance Characteristics of a Synchronous Motor	287
13-6. Methods of Starting Synchronous Motors	288
13-7. Features of Asynchronous Starting of Synchronous Motors	292
13-8. Methods of Asynchronous Starting	300
13-9. Synchronous Condenser	306
Chapter 14. Asymmetrical Steady-State Duties of a Three-Phase Synchronous Generator	311
14-1. General	311
14-2. Reactances and Resistances of a Synchronous Machine for Currents of Various Sequences	313

14-3. Asymmetrical Short Circuits of a Three-Phase Synchronous Generator	319
14-4. Voltage Diagrams for Short Circuits	327
14-5. Voltage Diagrams for Unbalanced Load	328
14-6. Construction of Short-Circuit Triangles for Steady-State Short Circuits of a Generator, with Account of Magnetic Circuit Saturation	331
Chapter 15. Sudden Short Circuit of a Synchronous Machine	336
15-1. Physical Picture of a Sudden Short Circuit	336
15-2. Flux Linkages of Stator and Rotor Windings of a Synchronous Machine	345
15-3. Analytical Investigation of the Sudden Short-Circuit Process	349
15-4. Sudden Short Circuit of a Synchronous Non-Salient-Pole Machine with Damper Windings on the Direct and Quadrature Axes	356
15-5. Equivalent Circuits for Synchronous Machine Inductive Reactances with a Sudden Short Circuit	361
15-6. Time Constants of a Symmetrical Polyphase Short Circuit	364
15-7. Sudden Short Circuit of a Polyphase Salient-Pole Synchronous Machine.	366
15-8. Total, Maximum Asymmetric and Effective Currents of a Polyphase Symmetrical Short Circuit	367
15-9. Sudden Asymmetrical Short Circuit of a Synchronous Machine	372
Chapter 16. Oscillations of Synchronous Machines	377
16-1. General Physical Picture of Oscillations	377
16-2. Forced Oscillations of a Synchronous Machine	385
16-3. Natural and Forced Oscillations of a Synchronous Generator on Infinite-Power Bus-Bar	387
16-4. Forced Oscillations of a Synchronous Generator Operating Alone	398
Chapter 17. Rotary Converter	400
17-1. Operating Principle of a Rotary Converter and Its Basic Relations	400
17-2. Relations Between Converter E. M. F. s	400
17-3. Relations Between Converter Currents	402
17-4. Losses in Armature Winding of a Converter	403
17-5. Starting of a Converter	407
17-6. Voltage Regulation of a Converter	408
17-7. Oscillations of a Converter	409
17-8. Application of Converters	410

PART THREE

INDUCTION MACHINES

Chapter 18. Three-Phase Induction Machine with Locked Rotor	413
18-1. General	413
18-2. Induction Machine on No-Load, $n = 0$	413
18-3. Short Circuit of an Induction Machine	416
18-4. Squirrel-Cage Parameters	418
18-5. Locked-Rotor Induction Machine Under Load	423
18-6. The Induction Regulator	424
Chapter 19. Three-Phase Induction Machine with Rotor Running	430
19-1. Principal Phenomena	430
19-2. Rotor E. M. F. Equation and Current	432
19-3. Speed of Rotation of Rotor Magnetizing Force	433
19-4. Magnetizing Force Equation and Flux Vector Diagrams of an Induction Machine	433

19-5. Equivalent Circuits of an Induction Machine	437
19-6. Operating Conditions and Vector Diagrams of an Induction Machine	446
Chapter 20. Torques and Power of an Induction Machine	451
20-1. Energy Diagrams of an Induction Machine	451
20-2. Torques of an Induction Machine	453
20-3. Electromagnetic Torque of an Induction Machine	454
20-4. Relation Between Torque M_{em} and Slip	459
20-5. Maximum Electromagnetic Torque and Maximum Power	459
20-6. Starting Torque of an Induction Motor	461
20-7. Relation Between Torque and Resistance of Rotor Circuit	465
20-8. Relation Between Torque M_{em} and Frequency f_1 with $\frac{U_1}{f_1} = \text{const}$	466
20-9. Kloss's Formula for Relative Torque	466
20-10. Maximum Mechanical Power	468
20-11. Hysteresis Torque	469
20-12. Parasitic Torques of an Induction Motor	471
20-13. Asynchronous Parasitic Torques	472
20-14. Tooth-Ripple Harmonics	474
20-15. Synchronous Torques	474
20-16. Vibration Torques	475
20-17. Preventive Measures Against Parasitic Torques	476
20-18. Performance Characteristics of an Induction Motor	478
Chapter 21. Circle Diagrams for an Induction Machine	483
21-1. Main Concepts of Theory of Loci of A. C. Machines in Symbolic Form	483
21-2. Improved Circle Diagram	487
21-3. Precise Circle Diagram	504
21-4. Current Loci for Induction Machines with Variable Parameters	510
21-5. No-Load Test	513
21-6. Short-Circuit Test	513
21-7. Construction of Circle Diagrams According to Experimental Data	516
21-8. Application of Approximate Circle Diagram	517
Chapter 22. Starting of Three-Phase Induction Motors	521
22-1. General	521
22-2. Starting Currents of Induction Motors	521
22-3. Disconnection of an Induction Motor from the Line	523
22-4. Acceleration of an Induction Motor at Starting	523
22-5. Starting of Phase-Wound Motors	526
22-6. Starting of Squirrel-Cage Motors	529
Chapter 23. Induction Motors Using Skin Effect in the Rotor Winding	535
23-1. Double Squirrel-Cage Motor	535
23-2. Deep Bar Motor	549
23-3. Comparison of Double Squirrel-Cage and Deep Bar Motors	558
23-4. Calculation of Starting Characteristics of a Salient-Pole Synchronous Motor with a Damper System	560
Chapter 24. Speed Control of Three-Phase Induction Motors	565
24-1. Methods of Speed Control	565
24-2. Changing the Number of Poles	566
24-3. Changing the Primary Frequency	570
24-4. Changing the Resistance in the Rotor	571
24-5. Cascaded Induction Motors	573

Chapter 25. Single-Phase Induction Motors	579
25-1. Principle of Operation	579
25-2. Equivalent Circuit for a Single-Phase Motor	581
25-3. Circle Diagram of a Single-Phase Motor	583
Chapter 26. Special Operating Conditions and Types of Induction Machines . .	586
26-1. Electrical Braking of Induction Motors	586
26-2. Doubly Fed Induction Motor	587
26-3. Electromagnetic Slipping Clutches	589
26-4. Induction Machines for Automatic Devices	590

PART FOUR

ALTERNATING-CURRENT COMMUTATOR MACHINES

Chapter 27. General Theoretical Problems	595
27-1. Brief History of A. C. Commutator Machines	595
27-2. E. M. F.s Induced in Armature of an A. C. Commutator Machine . .	597
27-3. Armature Currents of an A. C. Commutator Machine	602
27-4. Armature Winding Magnetizing Force of a Polyphase Commutator Machine	603
27-5. Commutation in A. C. Commutator Machines	606
Chapter 28. Single-Phase Commutator Motors	612
28-1. Principle of Operation and Torque of a Single-Phase Series Motor . .	612
28-2. Vector Diagram of a Single-Phase Series Motor	613
28-3. Methods of Improving Commutation of Single-Phase Series Motors .	615
28-4. Characteristics of a Single-Phase Series Motor	618
28-5. Application of Single-Phase Commutator Motors	620
28-6. Repulsion Motor with Two Windings on the Stator	621
28-7. Repulsion Motor with One Winding on the Stator and with One Set of Brushes (Thomson Motor)	624
28-8. Characteristics of a Thomson Repulsion Motor	625
28-9. Repulsion Motor with One Winding on the Stator and Two Sets of Brushes (Deri Motor)	627
Chapter 29. Three-Phase Shunt and Series Commutator Motors	628
29-1. General	628
29-2. General Principles of Shunt Polyphase Commutator Machines	628
29-3. General Equations of Polyphase Shunt Commutator Machine Operation and Their Circle Diagrams	629
29-4. Introduction of an Additional E. M. F. into the Secondary Circuit of an Induction Machine	633
29-5. Power Supplied from the Source of an Additional E. M. F.	636
29-6. Frequency Conversion by Means of a Commutator	636
29-7. Three-Phase Shunt Motor with Double Set of Brushes (Schrage-Richter Motor)	639
29-8. Regulation of Speed and Power Factor of Schrage-Richter Motor . .	640
29-9. Vector Diagrams of Schrage-Richter Motor	642
29-10. Characteristics of Schrage-Richter Motor	644
29-11. Three-Phase Series Commutator Motor. Diagrams and Operating Prin- ciple	650
29-12. Fundamental Equations of Three-Phase Series Commutator Motors .	655
29-13. Circle Diagrams of Current and Voltage	659
29-14. Connection Diagrams of a Three-Phase Series Commutator Motor, Its Characteristics and Applications	660

Chapter 30. Cascade Connections of Induction and Commutator Machines . .	664
30-1. General	664
30-2. Mechanical Cascade of an Induction Motor with a Rotary Converter and a D. C. Motor as the Regulating Machine (Kramer Cascade)	665
30-3. Cascade with Electrical Connection (Scherbius Cascade)	667
30-4. Characteristics of Mechanical and Electrical Cascade Connections . .	668
Chapter 31. Polyphase Commutator Generators	671
31-1. Operating Principle and Fundamental Relations	671
31-2. Compensated Commutator Salient-Pole Generator with Field Winding on Stator (Scherbius Generator)	671
31-3. Compensated Commutator Non-Salient-Pole Generator	672
31-4. Applications of a Commutator Generator	675
31-5. Thyristors or Silicon Controlled Rectifiers	676
Bibliography	677
Index	691

NOTATION

A	= Area; constant; electric loading; live load; loss of energy
a	= Integer; number of pairs of parallel paths; space angular coordinate along air-gap
B	= Complex number; flux density
b	= Integer; length (of magnetic tube); width
C	= Capacitance; coefficient; constant; integration constant
c	= Integer; specific heat; value of pole-shoe or slot skew
D	= Diameter; stator bore
E	= Electromotive force (e. m. f.)
e	= Base of natural logarithms; instantaneous e. m. f.
F	= Magnetomotive force (m. m. f.)
f	= Elementary force; frequency
G	= Weight
g	= Acceleration of gravity
H	= Height; magnetic field intensity or magnetizing force
h	= Height
I	= Current
i	= Current
J	= Moment of inertia
K	= Coefficient; factor
k	= Coefficient; factor; integer; ratio
L	= Inductance; leakage inductance
l	= Length
M	= Centre vector; electromagnetic torque; torque (moment)
m	= Number of phases; scale of circle diagram; torque produced by one conductor
N	= Number; number of conductors
n	= Exponent; speed
P	= Capacity; input; output; power
p	= Losses; number of pole pairs
Q	= Amount of heat; number of slots per pole pitch
q	= Amount of heat per unit; cross-sectional area; number of slots per pole per phase
R	= Radius; resistance (total)
R_{μ}	= Reluctance

r	= Resistance
S	= Number of tooth divisions
SCR	= Short-circuit ratio
s	= Slip of induction machine
T	= Heating time constant; period of time
t	= Time
U	= Voltage
u	= Voltage
Δu	= Voltage drop or rise
V	= Air consumption rate (ventilation)
v	= Linear speed at rotor periphery; velocity
w	= Number of coil turns
X	= Inductive reactance (total)
x	= Inductive reactance
Y	= Star connection
y	= Pitch; winding pitch
Z	= Impedance; number of armature slots
z	= Impedance

Greek Letter Symbols

α (alpha)	= Angle; emissivity; factor; pole arc coefficient; 120° turn operator
β (beta)	= Angle; relative winding pitch
γ (gamma)	= Angle; ratio between lagging and leading currents; ratio between wound part of pole and full pole pitch
Δ (delta)	= Delta connection; increment; ratio
δ	= Air-gap between stator and rotor
ϵ (epsilon)	= Relative shortening of winding pitch
η (eta)	= Efficiency
Θ (theta)	= Angle; angle between E_m and U ; power angle; temperature (absolute)
θ	= Ratio of excitation currents; temperature
Λ (lambda)	= Permeance
λ	= Coefficient of thermal conductivity; convection coefficient; emissivity; surface heat-transfer coefficient; unit permeance
μ (mu)	= Permeability
ν (nu)	= Characteristic of short circuit; order of harmonic
ξ (ksi)	= Equivalent conductor height (dimensionless quantity)
π (pi)	= 3.14 ... = ratio of circumference of circle to its diameter
ρ (rho)	= Angle of brush shift; resistivity
Σ (sigma)	= Summation sign
σ	= Correction factor; leakage factor
τ (tau)	= Leakage factor; pole pitch; temperature drop or rise

Φ (phi)	= Magnetic flux
φ	= Phase angle
Ψ (psi)	= Full flux linkage
ψ	= Angle between e. m. f. and current vectors: flux linkage; phase angle
Ω (omega)	= Angular speed of rotation; mechanical rotational speed of rotor
ω	= Angular speed of rotation

Subscripts

<i>a</i>	= active; air; armature; asynchronous; autotransformer; stator
<i>ad</i>	= armature direct-axis
<i>add</i>	= additional
<i>adv</i>	= phase advancer
<i>amb</i>	= ambient
<i>ap</i>	= aperiodic
<i>aq</i>	= armature quadrature-axis
<i>asyn</i>	= asynchronous
<i>av</i>	= average
<i>bot</i>	= bottom
<i>br</i>	= brass; brush
<i>C</i>	= capacitive
<i>c</i>	= cage; cascade; coil
<i>cm</i>	= cooling medium
<i>com</i>	= commutation
<i>comp</i>	= compensating
<i>con</i>	= conductor
<i>conv</i>	= convection
<i>cop</i>	= copper
<i>cp</i>	= commutating pole
<i>cs</i>	= coil section of armature winding
<i>d</i>	= damper system; direct-axis; distribution; duct; decay
<i>db</i>	= damper bar
<i>dc</i>	= direct current
<i>dcm</i>	= direct current machine
<i>dif</i>	= differential
<i>dr</i>	= drive
<i>dω</i>	= damper winding
<i>e</i>	= effective; electric
<i>ec</i>	= external (power) circuit
<i>ed</i>	= eddy current
<i>em</i>	= electromagnetic
<i>end</i>	= end connection
<i>eq</i>	= equivalent
<i>ew</i>	= excitation (field) winding

<i>exc</i>	= excitation
<i>f</i>	= field; form
<i>fc</i>	= frequency converter
<i>fin</i>	= final
<i>h</i>	= heat; hysteresis
<i>hyp</i>	= hypersynchronous
<i>i</i>	= current; ideal; internal
<i>in</i>	= inertia
<i>ins</i>	= insulation
<i>int</i>	= intermediate
<i>L</i>	= Inductive
<i>l</i>	= line; load
<i>lim</i>	= limiting
<i>M</i>	= torque
<i>m</i>	= main; maximum
<i>ma</i>	= mean annual
<i>max</i>	= maximum
<i>md</i>	= mean daily
<i>mech</i>	= mechanical
<i>min</i>	= minimum
<i>mot</i>	= motor
<i>o</i>	= initial; open; original
<i>op</i>	= operating
<i>ov</i>	= overload
<i>p</i>	= pitch; pole; Potier; power; primary; pulsating; pulse
<i>pa</i>	= pole arc
<i>ph</i>	= phase
<i>pi</i>	= pull-in
<i>pr</i>	= primary; prime-mover
<i>ps</i>	= pole shoe
<i>q</i>	= quadrature-axis
<i>r</i>	= rated; reactive; resistance; rotor
<i>rad</i>	= radiation
<i>rc</i>	= radiation and convection; rotary converter
<i>res</i>	= residual; resistance
<i>rev</i>	= reverse; revolution
<i>s</i>	= slip; slot; stator; surface
<i>sc</i>	= shading coil
<i>se</i>	= self-excitation
<i>sec</i>	= second
<i>sh</i>	= short circuit; short-pitch
<i>sh_t</i>	= short-time
<i>sig</i>	= signal
<i>sk</i>	= skew
<i>sl</i>	= slot
<i>sm</i>	= surrounding medium

<i>sp</i>	= space; speed
<i>sq</i>	= squirrel-cage
<i>st</i>	= start; steel
<i>st. st</i>	= steady state
<i>stat</i>	= static (braking) torque
<i>str</i>	= straight
<i>sub</i>	= subsynchronous
<i>sus</i>	= sustained
<i>sym</i>	= symmetrical
<i>syn</i>	= synchronous
<i>t</i>	= tank (of transformer); test; tooth; torque
<i>tn</i>	= turn
<i>tot</i>	= total
<i>tr</i>	= transformer; transient
<i>u</i>	= unit
<i>w</i>	= winding
<i>x</i>	= inductive reactance
<i>z</i>	= impedance; zero
δ	= air-gap
λ	= flux
μ	= magnetizing; saturation
σ	= leakage; leakage tube
0	= no-load; zero; zero-sequence
1	= positive-sequence; primary system or winding
2	= negative-sequence; secondary system or winding

PART ONE

GENERAL INFORMATION ON A.C. MACHINES

Chapter

I

BASIC TYPES OF A.C. MACHINES AND THEIR DESIGN

1-1. Basic Types of A.C. Machines

There are two basic types of alternating current machines, synchronous and asynchronous. The latter, usually referred to as induction machines, are further subdivided into non-commutator and commutator machines.

A synchronous machine is a machine in which a strictly constant relation exists between the speed n and the supply frequency f , viz.

$$f = pn \text{ or } n = \frac{f}{p} \quad (1-1)$$

where p is the number of pole pairs.

The synchronous machine is excited by direct current which is fed to the field winding from a d.c. power source or from a special d.c. machine called an *exciter*. Low-power synchronous machines may be constructed with permanent magnets, or as the so-called reluctance synchronous machine which has no special d.c. excitation (field) winding (Chapter 12).

An induction machine is a machine in which the speed n for a given frequency f depends on the load, and in which, consequently, there exists the relationship

$$f \neq pn \quad (1-2)$$

In an induction machine, the magnetic field is produced by an alternating current supplied from some a. c. power source.

Both synchronous and induction machines possess reversibility and may operate either as generators or as motors.

Synchronous machines are mainly used as alternators for the production of a. c. power at electric power stations. They are also widely used as synchronous motors and as synchronous condensers, which are synchronous motors operating under no-load conditions (see Chapter 13).

In contrast to synchronous machines, their asynchronous counterparts are mostly used as motors.

1-2. Operating Principle of a Synchronous Machine

The operating principle of a synchronous machine is fundamentally the same as that of a d. c. machine, but, unlike the latter, in a synchronous machine there is no need to rectify the varying in time e. m. f.

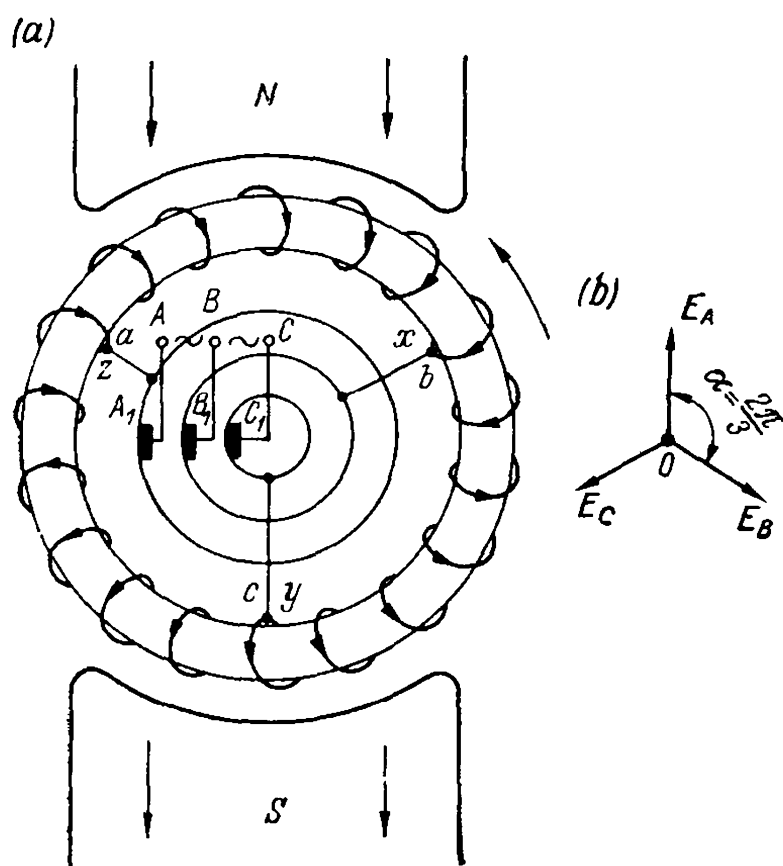


Fig. 1-1. Schematic diagram of a three-phase synchronous generator

which is induced in the armature winding. Consequently, a synchronous machine does not require a commutator. Fig. 1-1a shows schematically a two-pole generator with a ring armature. To obtain the simplest form of a three-phase synchronous generator from this arrangement, it is necessary to select three points a , b and c on the armature periphery spaced at an angle $\alpha = \frac{2\pi}{3}$, connect them to a. c. supply mains via three slip rings on the shaft, brushes A_1 , B_1 and C_1 in contact with the rings and terminals A , B and C . In this case we have an armature carrying three delta-connected phase windings $a-x$, $b-y$ and $c-z$.

When the armature rotates in a magnetic field, e.m.f.s E_A , E_B and E_C are induced in the $a-x$, $b-y$ and $c-z$ windings. These forces have a frequency $f = pn$ and are displaced by an angle $\alpha = \frac{2\pi}{3}$ (Fig. 1-1b).

If the load in the circuit is balanced, the machine generates a three-phase symmetrical current system I_A , I_B , I_C , the current in each phase winding being, in the general case, displaced with respect to the e.m.f. of this winding by an angle φ determined by the character of the load. It may be shown (for greater detail see Chapter 4) that such a current system produces a magnetic field whose fundamental wave rotates with a speed $n = \frac{f}{p}$ relative to the armature but oppositely directed. Consequently, this field is stationary with respect to the pole field and is in constant interaction with it. This is the fundamental principle of synchronous machine operation. The mechanical energy delivered to the machine from the shaft is converted into electric energy, i.e., the machine operates as a synchronous generator. However, according to the principle of reversibility, such a machine can operate as a synchronous motor if it is supplied with electric energy from a three-phase circuit through brushes A_1 , B_1 and C_1 .

In the general case, an m -phase system can be set up if in a two-

pole machine we take m points evenly spaced around the armature periphery ($\alpha = \frac{2\pi}{m}$) and bring them out to a.c. mains through a system of m slip rings fitted on the shaft and m brushes riding on the rings.

1-3. Fundamental Designs of Synchronous Machines

The arrangement of the main parts of the synchronous machine shown in Fig. 1-1a (fixed poles and a rotating armature) is good only for low-power synchronous machines. It is not good practice to use this design for medium- and high-power synchronous machines, which are built for voltages as high as 27 kilovolts and for currents up to several thousands of amperes, since in such conditions the slip rings will not function reliably.

Long experience in the design and operation of synchronous machines has shown that the most economical and convenient machine is one whose main parts have an arrangement opposite to that shown in Fig. 1-1a, namely, the poles, excited by direct current, are arranged on the rotating part of the machine, termed the *rotor*, while the a.c. armature winding is placed on the stationary part, the *stator*. Therefore, in further discussions it is this type of machine which we shall bear in mind first of all.

From the standpoint of design two basic types of synchronous machines are distinguished, namely, cylindrical-rotor or non-salient-pole machines, in which the field poles do not project (see Fig. 1-2), and salient-pole machines in which the field poles project (see Fig. 1-10, etc.).

The design of a synchronous machine followed depends on its speed of rotation n .

With a given frequency, the highest speed is developed by machines with $p=1$ and $p=2$ pairs of poles; for $f=50$ Hz we have, in the first case, $n=50$ rps or 3000 rpm, and, in the second case, $n=25$ rps or 1500 rpm. In such high-power machines the peripheral speed of the rotor is so great (see Table 1-1) that, for ensuring adequate mechanical strength, as well as better arrangement and securing of the excitation winding, the latter has to be distributed over the entire rotor surface, i.e., the machine must be of the non-salient-pole type. If $p \geq 3$, the rotor peripheral speed decreases and such synchronous machines are generally designed as salient-pole ones, since this simplifies their manufacture.

Synchronous generators or alternators are most frequently driven by steam or water turbines. In the first case the synchronous generator is referred to as a *turbogenerator* and in the second case as a *hydrogenerator*. Steam turbines are high-speed units and, accordingly, turbogenerators are built as non-salient-pole machines. On the other hand, hydrogenerators are salient-pole machines, since hydraulic turbines

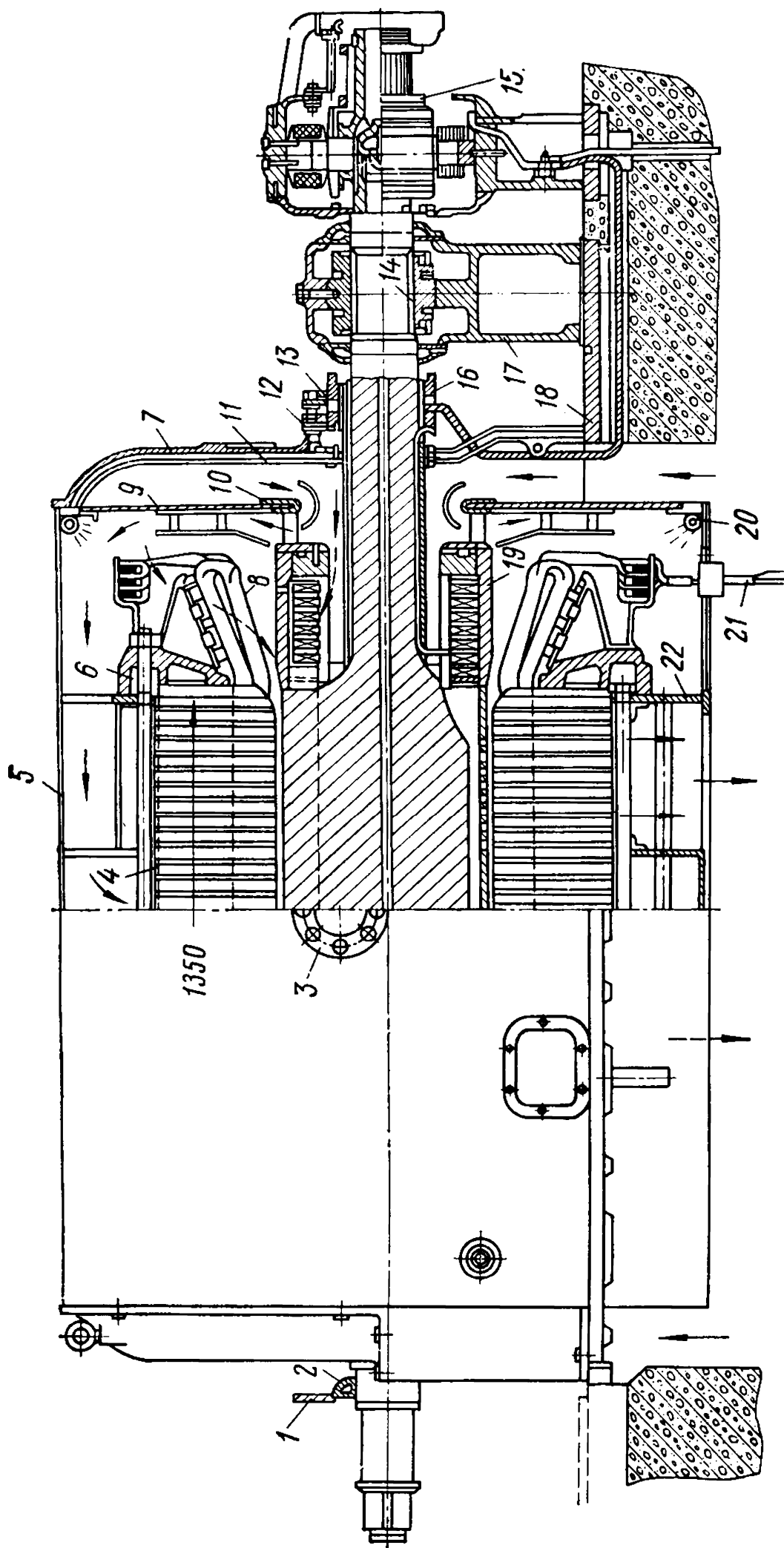


Fig. 1-2. Longitudinal section of air-cooled turbogenerator:

1 — oil seal holder at turbine side; 2 — oil seal; 3 — stator lifting device; 4 — stator core; 5 — frame housing; 6 — stator clamping ring; 7 — outer shield; 8 — stator winding; 9 — inner shield; 10 — ventilation shield; 11 — shield packing; 12 — brush holder; 13 — brush; 14 — bushing; 15 — exciter; 16 — contact ring; 17 — bearing; 18 — bed plate; 19 — rotor; 20 — fire-prevention pipe; 21 — terminals; 22 — frame

run at low speeds. Synchronous generators driven by internal-combustion engines, and synchronous motors and condensers are of a salient-pole design. However, in cases when synchronous motors are required for high-speed operation (for instance, for driving a turbocompressor), they are designed, similar to turbogenerators, as two-pole non-salient-pole machines.

1-4. Design of Non-Salient-Pole Synchronous Machines

Let us consider the features of such machines, taking a turbogenerator as an example.

At present practically all turbogenerators are designed with two poles, since with an increase of speed the efficiency of steam turbines appreciably improves and, due to a certain reduction in turbine and generator size, manufacturing costs are decreased.

Figure 1-2 gives a longitudinal section of a two-pole, 6000-kW, 3000-rpm turbogenerator produced by the "Elektrosila" Works, whose design is also typical of large-power machines. The most vital part of the turbogenerator, both from the mechanical and the thermal standpoint, is the rotor. At the rated speed of rotation, the linear speeds at the rotor periphery of a four-pole turbogenerator reach 125 to 145 metres per second. In two-pole high-power turbogenerators the speeds are as great as 170 to 185 metres per second. The centrifugal forces developed at these speeds produce very great mechanical stresses in some parts of the rotor. This is why the rotor of a modern turbogenerator is generally made from a massive solid steel forging (Fig. 1-3)

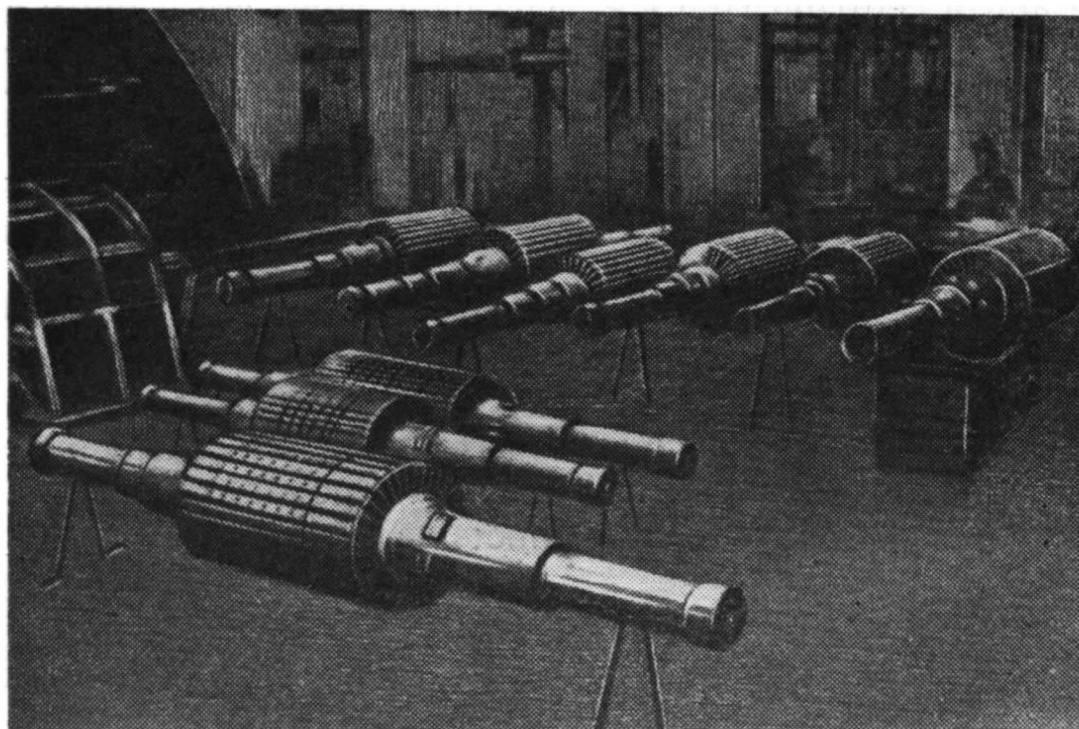


Fig. 1-3. Turbogenerator rotors

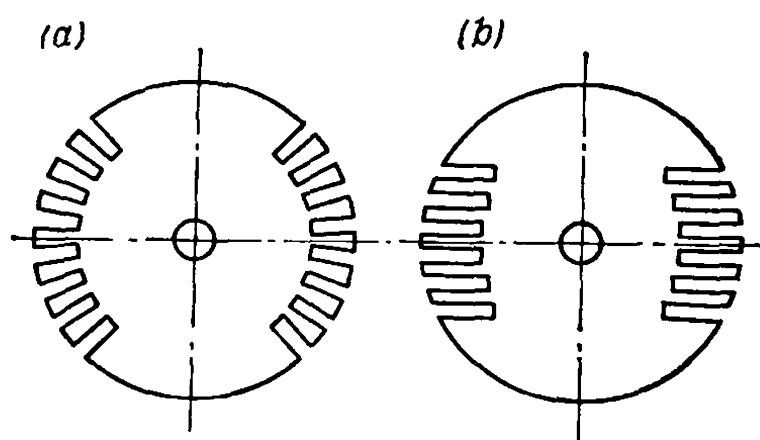


Fig. 1-4. Turbogenerator rotor slots

re axial length of the rotor a central hole is bored, serving, firstly, for testing the material of the forging in the central zone and, secondly, for relieving dangerous internal stresses in the forging.

Slots are milled in the rotor for inserting and securing the excitation winding. There are distinguished *radial-slot* and *parallel-slot* rotors (Fig. 1-4a and b). We shall consider the radial-slot design.

Approximately one-third of a pole pitch is left without slots and forms the so-called large tooth through which the main part of the generator magnetic flux passes.

Owing to the high speeds at the rotor periphery, the rotor winding is secured in the slots by means of metal wedges, the main shapes of which are shown in Fig. 1-5a and b. The wedges are made both of non-magnetic steel and non-magnetic alloys.

The end connections of the rotor winding are secured in place by means of retaining bands. A band consists of two parts, a band ring *B* (Fig. 1-6) and a centring ring *CR*. The band rings are usually made of non-magnetic steel with an ultimate tensile strength of 700 to 1000 N/mm² and a yield point of 450 to 900 N/mm². The band rings are highly stressed mechanically, since, in addition to the stress developed by their own weight, they must also sustain the pressure exerted by the winding as a result of the centrifugal forces developed by the revolving rotor.

The machine is usually excited by exciters coupled to or seated on the turbogenerator shaft (see Fig. 1-2).

The stator of a turbogenerator consists of an active part, i.e., the core, in which the stator winding is arranged, and a frame, which together with the end shields serves to secure the stator-core iron and to provide a system of ventilating ducts and chambers.

Alloyed electrical sheet steel 0.5- and 0.35-mm thick is used for turbogenerator stator cores. The steel laminations are insulated on both sides with a special varnish.

whose high strength is the result of a complicated process of heat treating and machining operations. In large machines use is made of a special chrome-nickel-molybdenum steel having an ultimate tensile strength of about 800 N/mm², a yield point of 550 to 600 N/mm², and an elongation of about 20 per cent. Along the entire

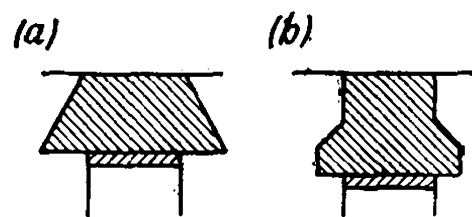


Fig. 1-5. Rotor-slot wedges

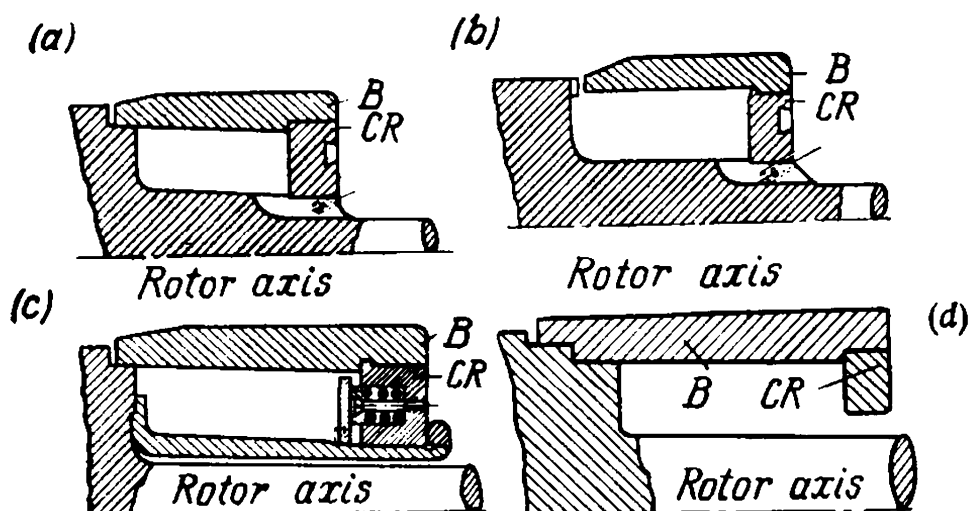


Fig. 1-6. Rotor band rings

In the axial direction the stator core consists of stacks 3 to 6 cm thick separated by ventilating ducts 5 to 10 mm wide (see Fig. 1-2). To make the core structure more rigid, it is compressed from both sides by means of special clamping plates of non-magnetic iron or steel.

Of immense importance is the problem of turbogenerator ventilation. The difficulties that arise in this connection are due to the large length of the machines and to the small diameter of the rotors. This has resulted in the development of special ventilating methods used only in turbogenerators and discussed in Chapter 7.

The characteristics of some turbogenerators produced by various manufacturers are given in Table 1-1, where

P = active power

U = line voltage

D = rotor diameter

L = length of active part of machine

q = number of stator slots per pole per phase

δ = air-gap between stator and rotor

A = line load

$C_A = D^2 L n / P_{kv.A} = \text{Arnold's constant}$

SCR = short-circuit ratio

η = efficiency

G_r = weight of rotor

G = total weight of machine

x_d, x'_d, x''_d = quadrature-axis synchronous, transient and subtransient reactance

GD^2 = flywheel moment.

1-5. Turbogenerators for Atomic Power Stations

In the last few years atomic power stations have been gaining in popularity in many countries. These stations use nuclear reactors instead of combustion chambers of steam boilers where organic fuel

P		U, kV	n, rpm	η, %	D, cm	L, cm	δ, cm	q	A·10 ⁻² A/m	C _A ·10 ⁻⁴	Short- cir- cuit ratio
MVA	MW										
Two-pole turbogene											
15	12	10.5	3000	97.1	68	190	2.5	14	483	20.3	0.646
37.5	30	10.5	3000	98.3	81.6	270	2.7	9	815	16.3	0.437
75	60	10.5	3000	98.5	93	280	5	12	917	11.9	0.675
117	100	10.5	3000	98.5	100	310	6.4	10	1095	10.1	0.605
176	150	18	3000	98.5	100	380	8.5	7	1299	8.86	0.615
235	200	15.75	3000	98.7	107.5	430	8	10	1335	8.38	0.57
235	200	15.75	3000	98.7	107.5	500	10	10	1293	10.4	0.58
220	200	18.5	3000	—	101.6	456	8	—	1290	8.6	—
260	208	18	3600	—	99	440	9.5	8	—	8.48	—
262	236	12	3600	98.8	—	—	—	—	—	—	0.58
295	250	20	3000	—	115	420	5.75	6	1750	6.84	0.536
312	250	24	3000	98.88	105	540	7.5	6	1435	7.48	0.57
353	300	20	3000	98.7	107.5	600	9.5	9	1380	8.15	0.624
353	300	20	3000	98.7	112	580	9.0	10	1500	8.34	0.524
400	300	21	3000	98.6	—	—	—	—	—	—	0.44
396	336	24	3600	—	—	—	—	—	—	—	0.61
412	350	19.5	3000	—	112	540	9.0	—	1745	6.65	0.53
442	375	22	3600	98.75	99.06	622	9.5	8	—	7.07	0.58
471	400	20	3600	—	106.8	560	10	—	1758	6.87	0.56
588	500	22	3000	98.7	114.3	571	8.1	9	2035	4.96	0.437
588	500	20	3000	98.8	112.5	635	9.5	8	1975	5.6	0.42
588	500	20	3000	98.8	112	620	10	8	1965	5.51	0.45
667	600	20	3000	98.96	115	650	—	7	—	—	0.4
706	600	23	3600	—	—	725	—	—	2000	—	0.5
776	660	23.5	3000	98.58	117	750	9.5	—	2010	5.36	0.51
889	800	24	3000	98.82	120	—	—	—	—	4.76	0.475
907	815	26	3600	—	—	—	—	—	—	—	—
1333 *	1200	24	3000	99.03	1250	—	—	—	—	—	0.437
Four-pole turtogene											
55.5	50	10.5	1500	97.89	133.5	376	4.25	9	730	16.1	0.76
117.5	100	15.75	1500	97.8	152	550	5.25	7	761	18.4	0.8
121	115	18	1800	97.65	139.5	720	5.0	7	689	18.1	—
400	340	17	1800	—	—	—	—	5	—	—	0.65
588 *	500	20	1500	98.6	180.0	—	—	—	—	5.29	0.5
775	660	21	1500	98.7	170	600	7.0	—	2210	3.94	0.45
1110 *	1000	27	1500	98.9	190	—	—	—	—	4.76	0.63
1126	1021	22	1800	—	171	720	—	—	—	—	0.5
1280	1152	22	1800	—	164	890	10	—	—	4.25	0.6
1350	1215	27	1800	—	—	—	—	—	—	—	—
1400 *	1260	22	1800	—	176	800	—	—	2650	—	0.6
1500 *	1200	27	1500	99	180	788	—	—	—	—	0.5

Note. Notations of cooling systems in table: A—air; HO—ordinary hydrogen; HD—hydrogen

* Data of generators in design stage.

TABLE 1-1

x_d f. u	x'_d f. u	x''_d f. u	G_r tons	G tons	GD^2 10^{-4} N·m ²	Cooling system for winding		Manufacturer or company	Country
						sta- tor	ro- tor		
rators, 2p=2									
2.07	0.2	0.13	9.5	39	2.6	A	A	Lisva Works	USSR
2.65	0.26	0.15	16.5	83	5.4	HO	HO	Lisva Works	USSR
1.66	0.22	0.15	24.2	125	8.85	HO	HD	Elektrosila Works	USSR
1.79	0.26	0.18	29.8	175	13	HO	HD	Elektrosila Works	USSR
1.71	0.3	0.21	33.5	200	17.8	W	HD	Elektrosila Works	USSR
1.84	0.27	0.19	42	256	21.2	W	HD	Elektrosila Works	USSR
1.84	0.27	0.19	48	313	25	HD	HD	Elektrot'yazhmash	USSR
1.42	0.25	0.18	42	—	—	HD	HD	AEI-EE	England
—	—	—	—	353	—	OD	HD	General Electric	USA
1.68	0.334	0.28	—	—	—	HD	HD	Hitachi	Japan
—	—	—	50	275	—	W	HD	SEM	France
—	—	—	49	278	25	HD	HD	Jeumont-Schneider	France
1.7	0.26	0.17	55	350	29.8	W	HD	Elektrosila Works	USSR
2.21	0.3	0.19	56.5	366	31	HD	HD	Elektrot'yazhmash	USSR
—	—	0.254	54	376	—	W	HD	Brown Boveri	Switzerland
—	0.307	0.208	50	255	—	HD	HD	Mitsubishi	Japan
2.14	0.24	0.169	56	—	—	W	HD	AEI-EE	England
1.66	0.292	0.236	45.5	325	—	W	HD	Tosiba	Japan
—	—	—	55	—	—	W	HD	AEI-EE	England
—	—	—	62.1	449	37	W	HD	AEI-EE	England
2.46	0.36	0.233	65	362	40	W	HD	Elektrosila Works	USSR
2.38	0.36	0.243	60	347	—	W	W	Elektrot'yazhmash	USSR
2.68	0.38	0.265	75	450	—	HD	HD	Jeumont-Schneider	France
2.2	0.304	0.216	67	—	—	W	HD	AEI-EE	England
2.36	0.263	0.192	84	—	—	W	HD	AEI-EE	England
—	0.314	—	80	515	—	W	HD	Elektrosila Works	USSR
—	—	—	74.5	405	—	W	HD	General Electric	USA
—	0.361	—	—	610	—	W	—	Elektrosila Works	USSR
rators, 2p=4									
1.41	0.235	0.134	58	146	46.7	A	A	Elektrosila Works	USSR
1.35	0.26	0.15	93	243	110	A	A	Kharkov-Electric Works	USSR
—	—	—	103.6	—	102.5	A	A	Allis-Chalmers	USA
—	—	—	93.5	383	—	HO	HO	Mitsubishi Works	Japan
—	0.4	—	—	444	—	W	HD	Elektrosila Works	USSR
—	0.44	—	140	450	—	W	HD	AEG	FGR
—	0.39	—	—	690	—	W	HD	Elektrosila Works	USSR
—	—	—	165	710	—	HD	HD	Westinghouse	USA
—	—	—	176	595	—	W	HD	General Electric	USA
—	—	—	207	700	—	W	HD	Brown-Boveri	Switzerland
—	0.51	0.34	176	626	—	W	HD	AEI-EE	England
—	0.47	0.25	198	668	—	W	W	Kraftwerkunion	FGR

direct; W — water; OD — oil direct; f. u — fraction unit.

or gas is burnt. The most generally employed type of reactor is the water-water reactor in which water is used as a moderator, and as a cooling medium. Such reactors generate steam with relatively low parameters: temperature 280 to 320 °C, pressure 600 to 800 N/cm². For this reason, the 1500- or 1800-rpm turbogenerators are more economical machines than the high-speed 3000- or 3600-rpm turbogenerators used for thermal power stations with higher steam parameters.

The efficiency of atomic power stations as a whole is considerably increased with an increase in reactor power, and also when each reactor utilizes a turbogenerator unit of appropriate power. This was the principal stimulus for rapid development and growth of power of four-pole turbogenerators. Practically all turbogenerators rated at 500 MW and more, at 1500 and 1800 rpm, shown in Table 1-1 have been made or are being designed for operation at power plants.

The operating conditions of turbogenerators at atomic power stations do not require any specific design features for the generators; however, the necessity of the manufacturing very powerful turbogenerators creates a series of complex problems.

The main feature of the high-power turbogenerator design is that the rotor diameters of such machines are considerably (about 1.414 times) larger than those of two-pole generator rotors of a similar power. The rotor diameters of modern turbogenerators reach 1800 mm. The peripheral speed of the rotor in this case, however, is lower than that of two-pole machines, since their speed is reduced by 50 per cent. This is why the mechanical stress in the rotors is reduced which increases their reliability. Besides, the level of vibrations of the stator core in four-pole turbogenerators is reduced and therefore there is no need to use elastic suspension for the core; the increase in rotor mass permits the flywheel moment to be increased, this being favourable for the stability of generator operation in the mains. The decrease in the magnetic flux per pole makes it possible to decrease the height of the core yoke and correspondingly to reduce the stator mass and diameter. An increase in the rotor diameter permits a decrease in the relative length of the rotor and an increase in its resistance to vibration.

The above advantages allow the four-pole turbogenerators to be constructed with much greater power than that of two-pole units.

The main difficulties in constructing high-power turbogenerators for atomic power stations are connected with the design of rotors of increased dimensions and mass. If the mass of the rotors of two-pole 800-1200-MW turbogenerators does not exceed 100 tons and the rotors may be made from a single forging, then the mass of rotors for four-pole generators of the same power may reach 200 tons.

At present the maximum possible mass of a single rotor forging is, in Europe, 140 tons and, in the USA, about 180 tons. Therefore, for 800- to 1000-MW machines new methods for manufacturing rotor

forgings should be found. Therefore several versions of composite rotor designs have been developed. Simultaneously, research is being carried out with a view to developing a combined welded and forged structural rotor member. The designers are confronted with the task of developing such rotors having masses up to 300-350 tons.

A comparison of the main parameters of four- and two-pole turbogenerators (Table 1-1) shows that their values are quite close with a few exceptions. For example, the electromagnetic loads for the four-pole machines are somewhat lower than for two-pole generators of comparable power and the value of the transient reactance is a little higher.

Most of the high-power turbogenerators already constructed for atomic power stations and in the design stage have water cooling of stator windings and direct hydrogen cooling of rotor windings. Some manufacturers (Westinghouse, Jeumont-Schneider, Mitsubishi) however also use hydrogen as cooling medium for stator windings of high-power generators. But Westinghouse has introduced water-cooling for stator windings of turbogenerators of 1000 MW and more.

The most widely used high-power turbogenerators have the excitation systems with static converters powered by alternating current generators joined to the rotor shaft. However, with increase in unit power the rotor current abruptly increases (up to 10-12 kA), which considerably complicates the design of the brush gear and reduces the reliability of turbogenerator operation.

Among various ways of solving the problem of supplying current to the rotor winding, the most promising is the brushless excitation circuit with rotary rectifiers. At present such a system, with rotary silicon diodes is used in practically all turbogenerators manufactured by Westinghouse. Similar systems are used by other foreign manufacturers and in the USSR.

Research is being conducted with the aim of improving the excitation circuit by replacing the rotary diodes with thyristors. The brushless excitation circuit is evidently the most progressive solution and will find ever-increasing application.

1-6. Design of Salient-Pole Synchronous Machines

Horizontal-shaft design is conventional for salient-pole machines and is employed for the overwhelming majority of synchronous motors, for all synchronous condensers and for generators designed for coupling to internal-combustion engines, and, in many cases, also for hydrogenerators with comparatively high speeds (200 rpm and above).

High-power, low-speed hydrogenerators installed in low-head hydropower plants are built with a vertical shaft coupled through a flange to the shaft of the hydroturbine arranged under the generator. Motors for large water pumps are also built with a vertical shaft.

Salient-pole synchronous machines differ greatly in design from non-salient-pole ones. For instance, in a turbogenerator of maximum capacity the length of the rotor L exceeds the bore D about 6 times (Table 1-1), while low-speed hydrogenerators may have bores of up to 15 m and an $\frac{L}{D}$ ratio of 0.15 to 0.20.

Among the many types of salient-pole synchronous machines, the vertical-shaft hydrogenerators installed in hydroelectric power plants are of the greatest importance.

There are two main types of such generators, the suspended-type in which the thrust bearing is arranged on the upper spider above the rotor (Fig. 1-7a and b), and the umbrella-type in which the thrust bearing is mounted on the lower spider (Fig. 1-7c and d) or on the turbine cover (Fig. 1-7e).

Nowadays high-power hydrogenerators are generally designed of the umbrella-type to reduce the weight and height of the generator which, in turn, makes it possible to reduce the height of the station building. This is explained by the fact that the upper spider is of a greater diameter than the lower one, and, when the total weight of the generator rotor, turbine rotor and the water reaction force are transmitted to the upper spider (the suspended design), its dimensions have to be considerably increased.

A longitudinal section of a suspended-type generator is shown in Fig. 1-8, while Fig. 1-9 gives a longitudinal section of the hydroelect-

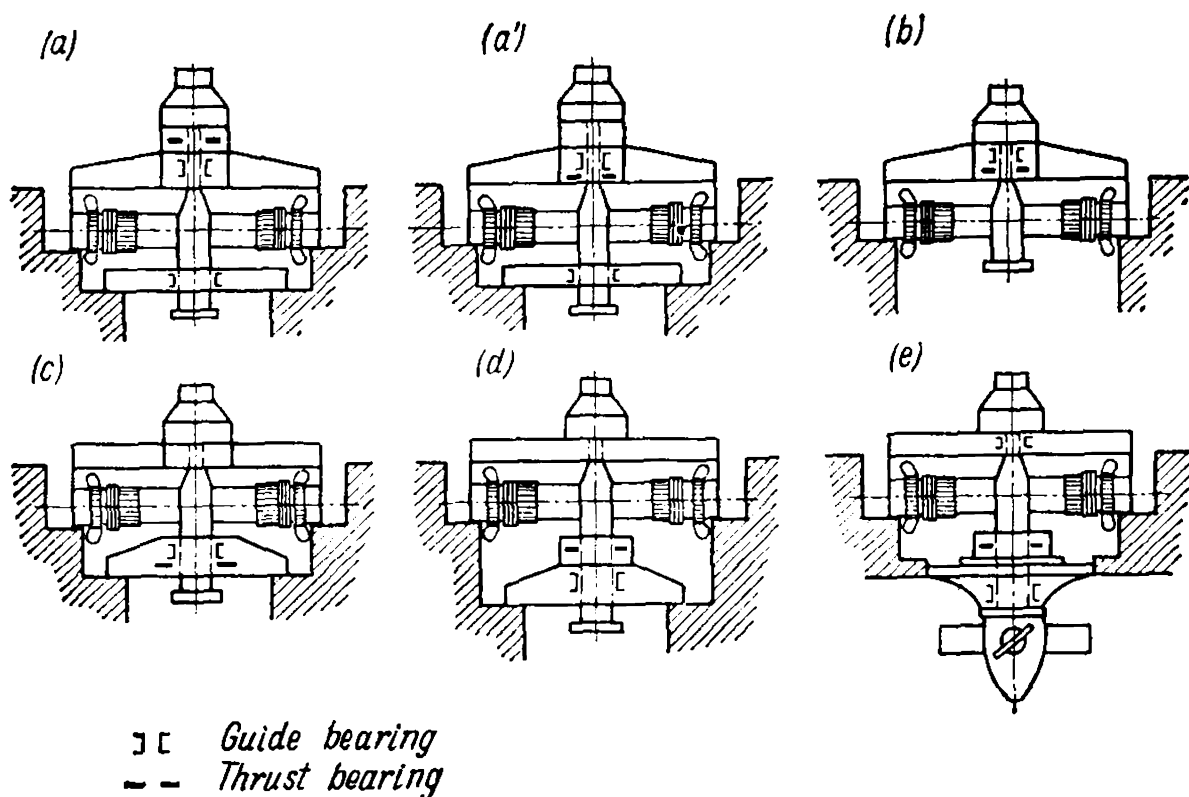


Fig. 1-7. Types of hydrogenerators:

a and a' — suspended with two guide bearings; b — suspended with one guide bearing, without lower spider; c and d — umbrella with one guide bearing; e — umbrella with thrust bearing on turbine cover and one guide bearing

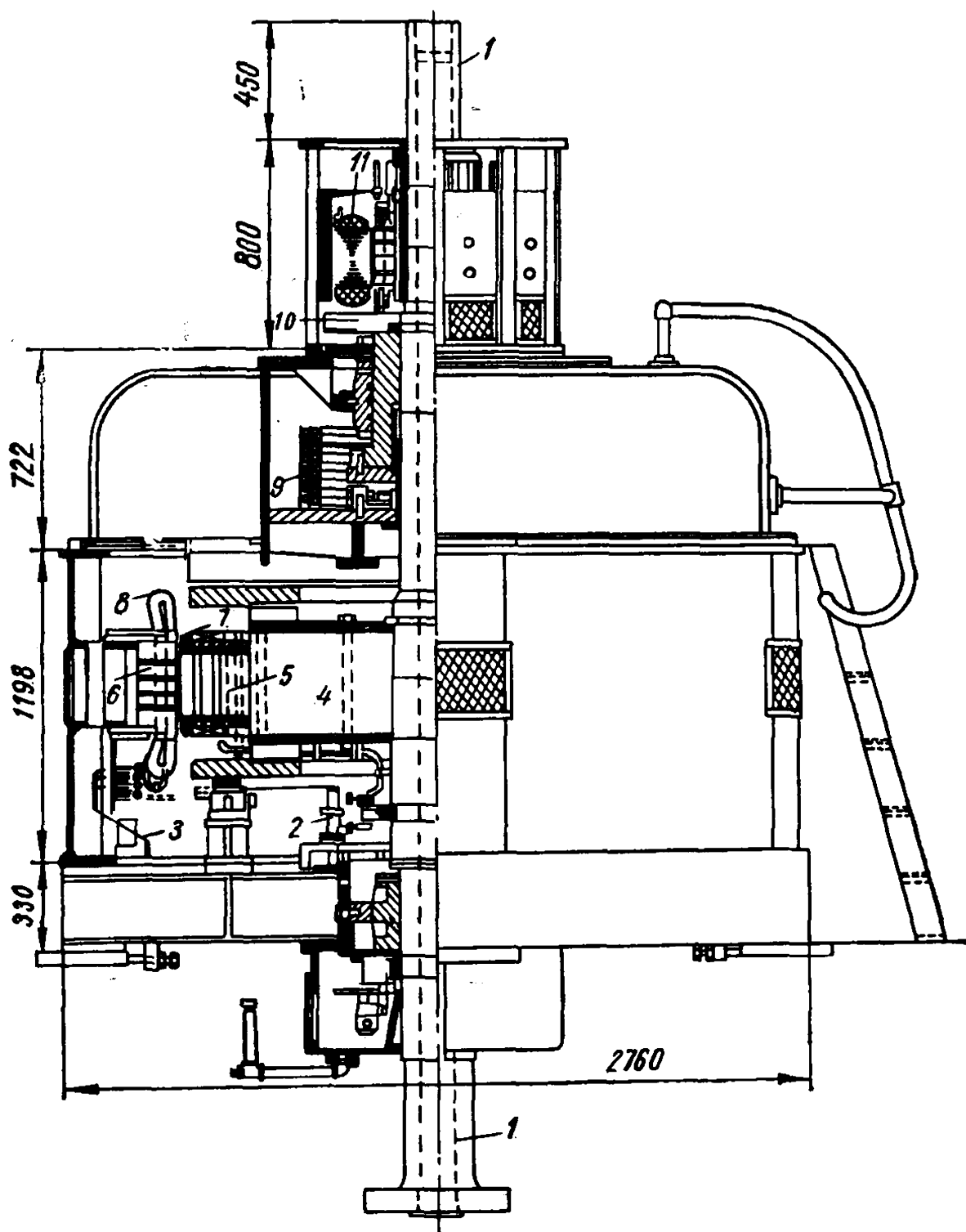


Fig. 1-8. Longitudinal section of suspended-type hydrogenerator:

- 1 — generator shaft; 2 — slip rings and rockers; 3 — generator terminals;
 4 — rotor spider; 5 — pole core; 6 — stator core; 7 — excitation field winding;
 8 — stator winding; 9 — thrust-bearing housing; 10 — exciter fan; 11 — exciter

ric unit designed for use at the Volga hydroelectric station. This unit consists of a low-speed umbrella-type hydrogenerator with the thrust bearing mounted on the cover of the turbine, with ratings of 123 000 kVA, 13 800 V, 68.2 rpm, and a power factor of 0.85. The generator split stator consists of six sections and is mounted on bed plates. One of the most difficult problems in high-power hydrogenerator design is the thrust bearing, which must withstand an extremely

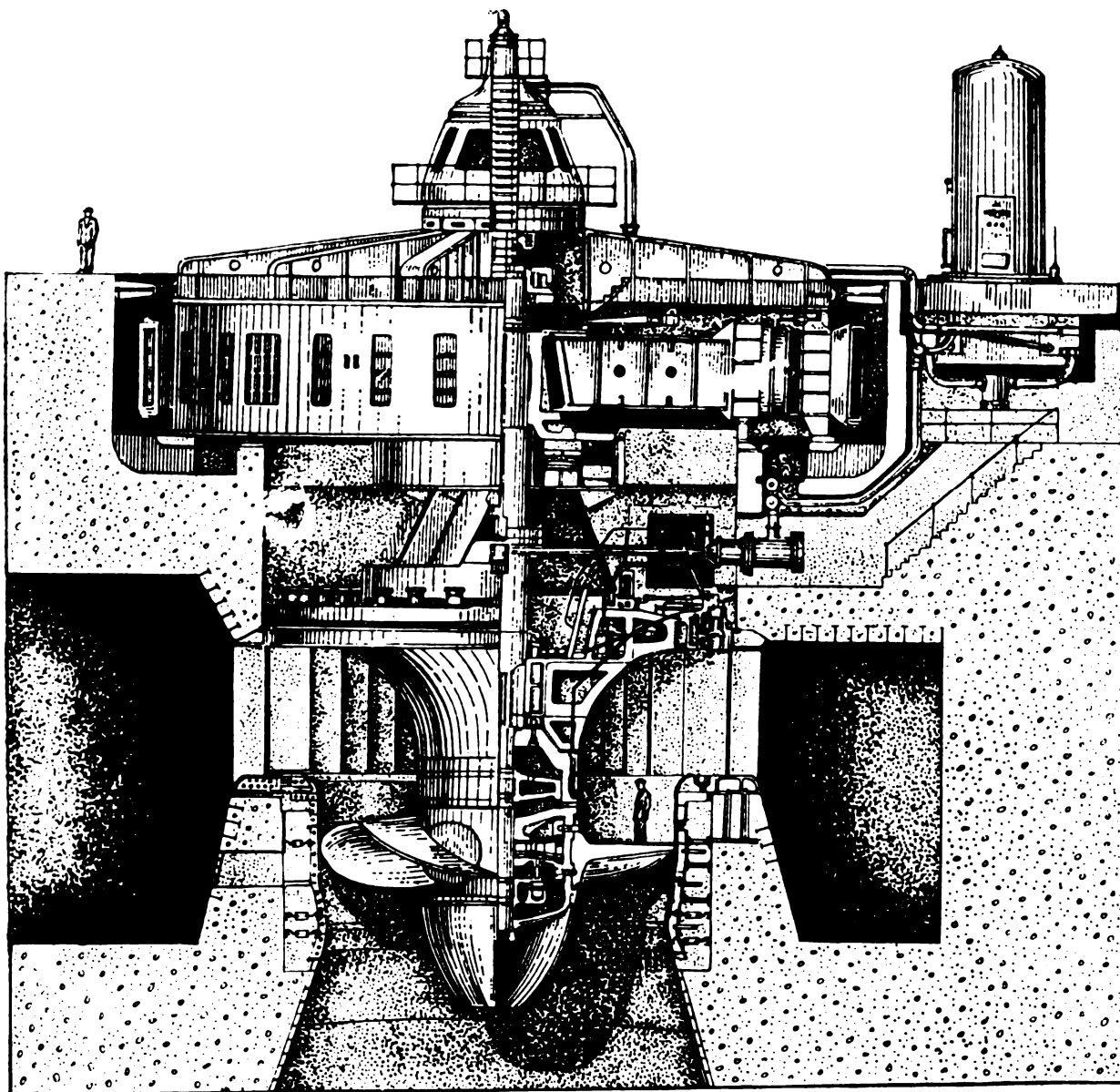


Fig. 1-9. Water-power unit of Volga hydroelectric station named after V. Lenin

heavy weight of the rotating parts and the reaction of water flowing into the turbine. In the hydrogenerator under consideration the total load on the bearing surfaces reaches 3400 tons and the thrust bearing is supported by a pedestal on the turbine cover.

This design eliminates the need for a lower spider and results in a considerable saving in structural steel (about 200 tons). The pole cores are assembled of thin steel sheets secured with studs. The rotor winding is made of copper strips with asbestos-paper insulation between the strips. The generator is provided with a damper winding laid in slots in the pole shoes. The machine is ventilated by means of a closed-circuit self-cooling system (Chapter 6).

Figure 1-10 shows the rotor of a horizontal high-speed 80 000-kVA, 428-rpm hydrogenerator built for the French Malgovert hydroelectric station. The generator is driven by two hydroturbines with bucket-

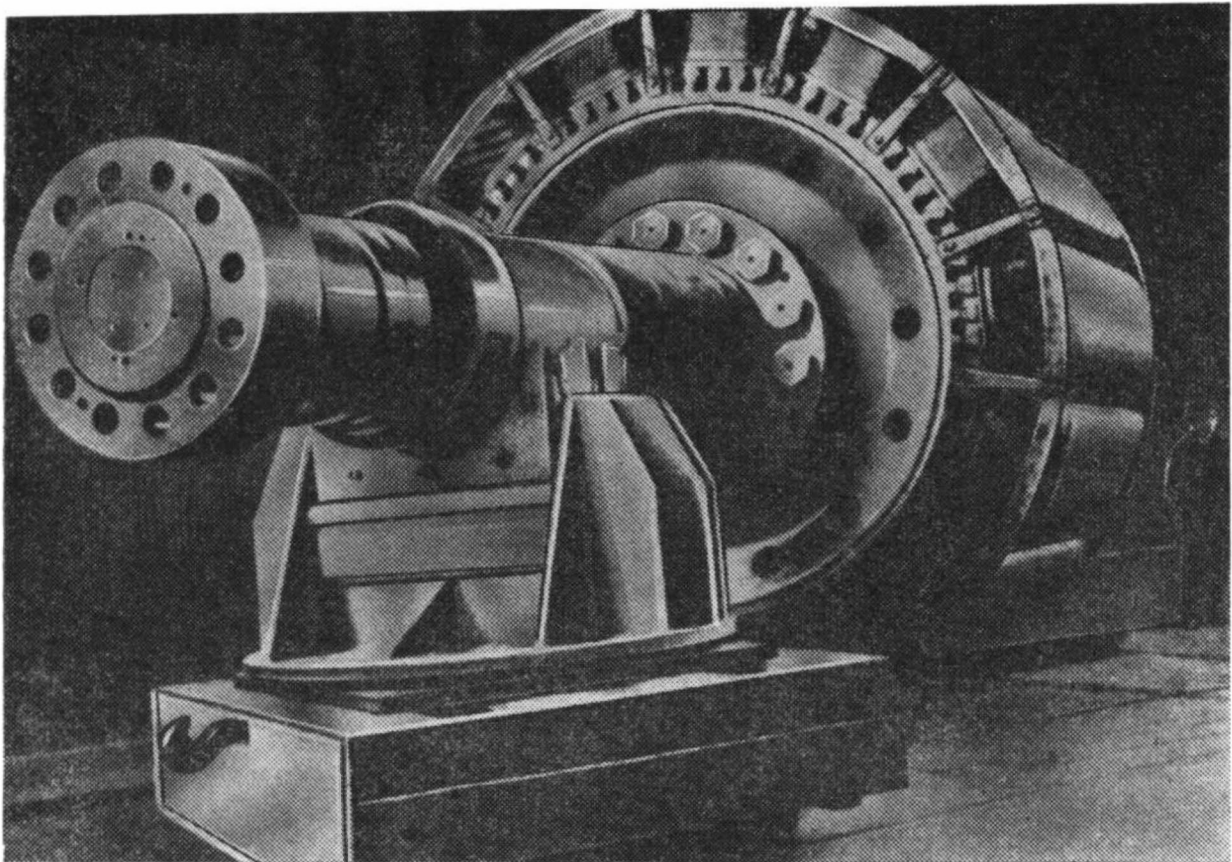


Fig. 1-10. Rotor of 80 000-kVA, 428-rpm horizontal-type hydrogenerator for Malgovert hydroelectric station (France)

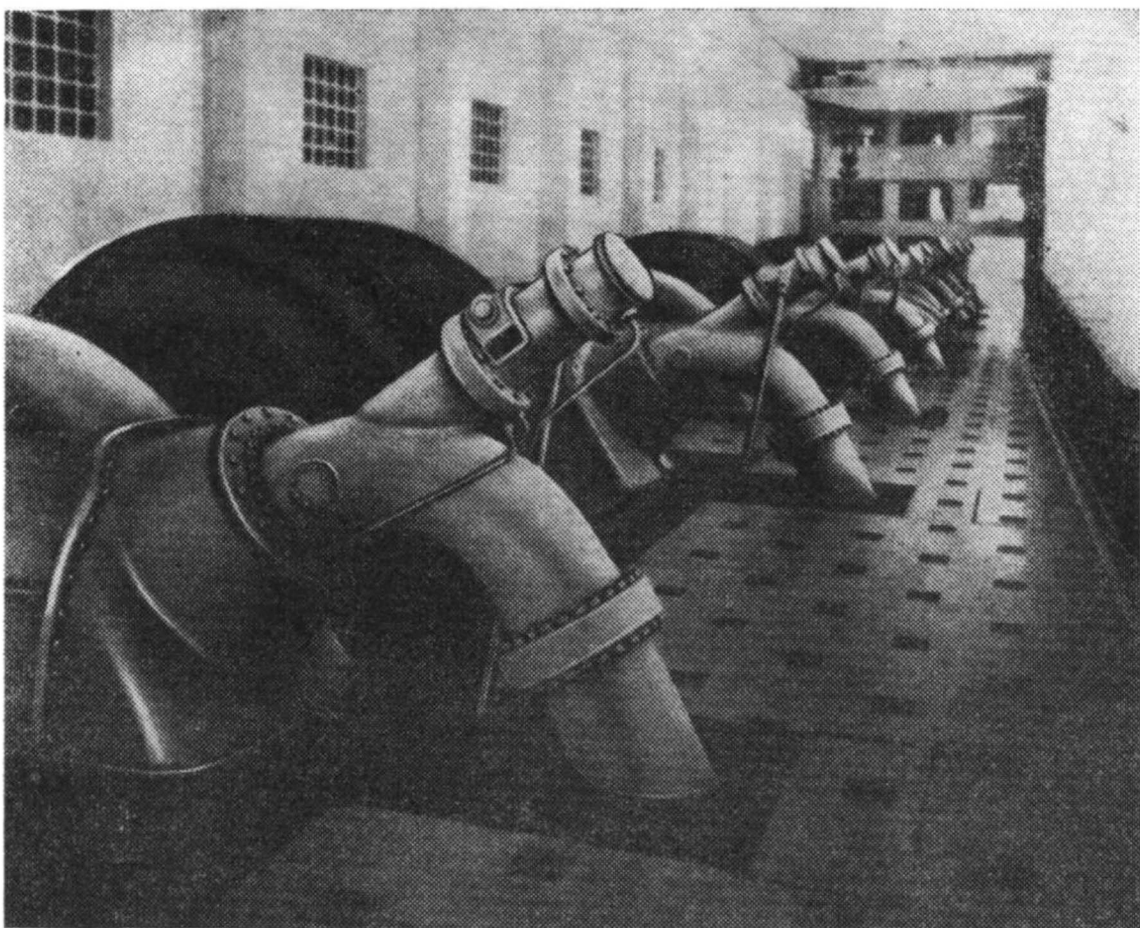


Fig. 1-11. Hydroelectric units of Malgovert station

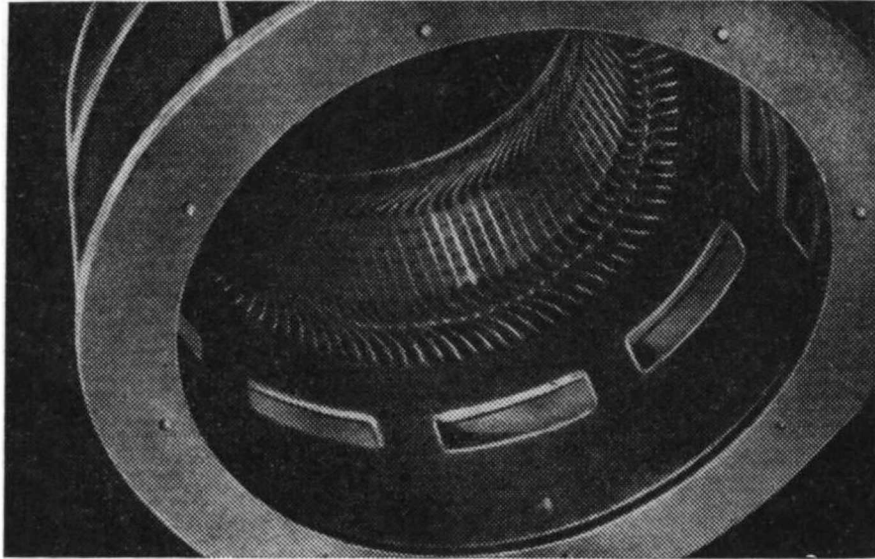


Fig. 1-12. Stator of 250-kVA, 600-rpm vertical hydrogenerator

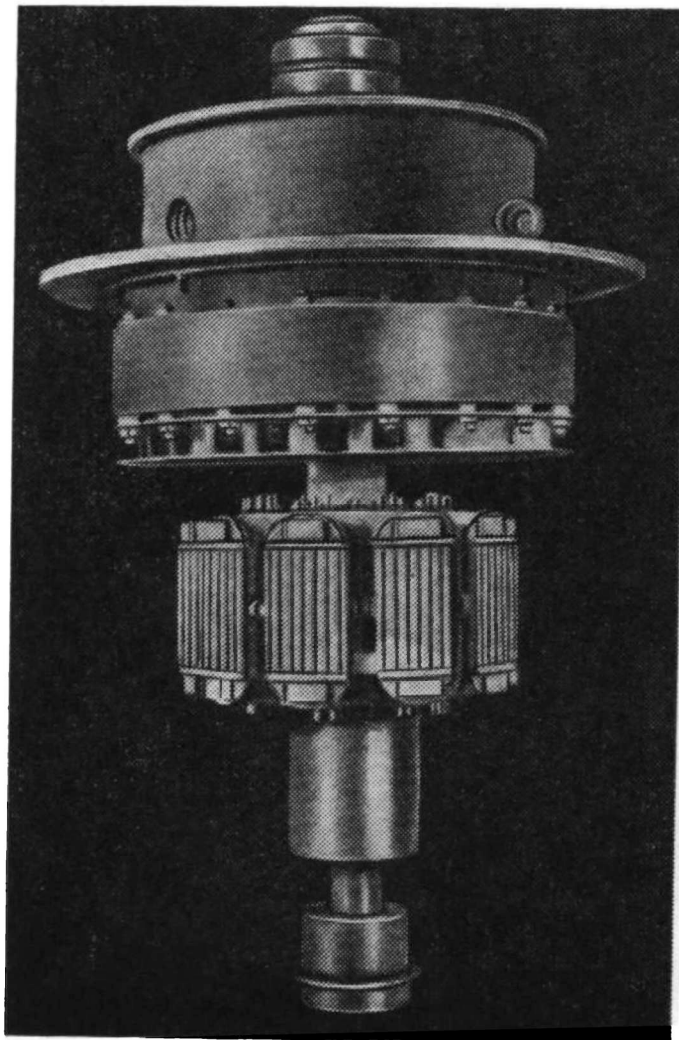


Fig. 1-13. Rotor and upper spider of 250-kVA, 600-rpm hydrogenerator

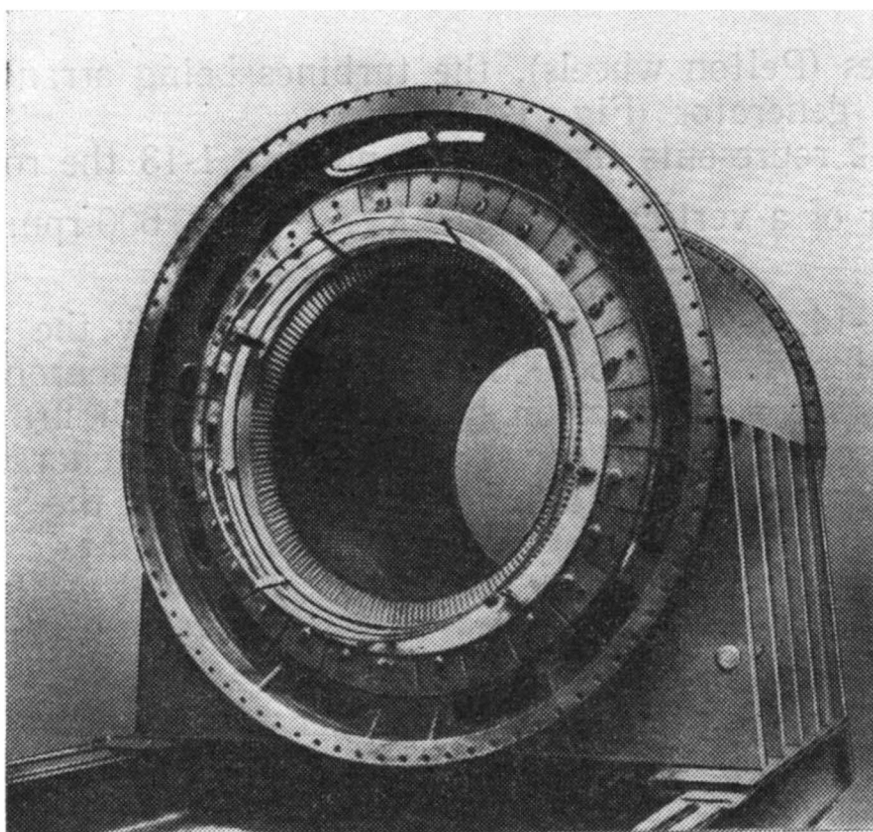


Fig. 1-14. Stator of the Alsthom 60 000-kVA, 1000-rpm synchronous condenser without winding (France)

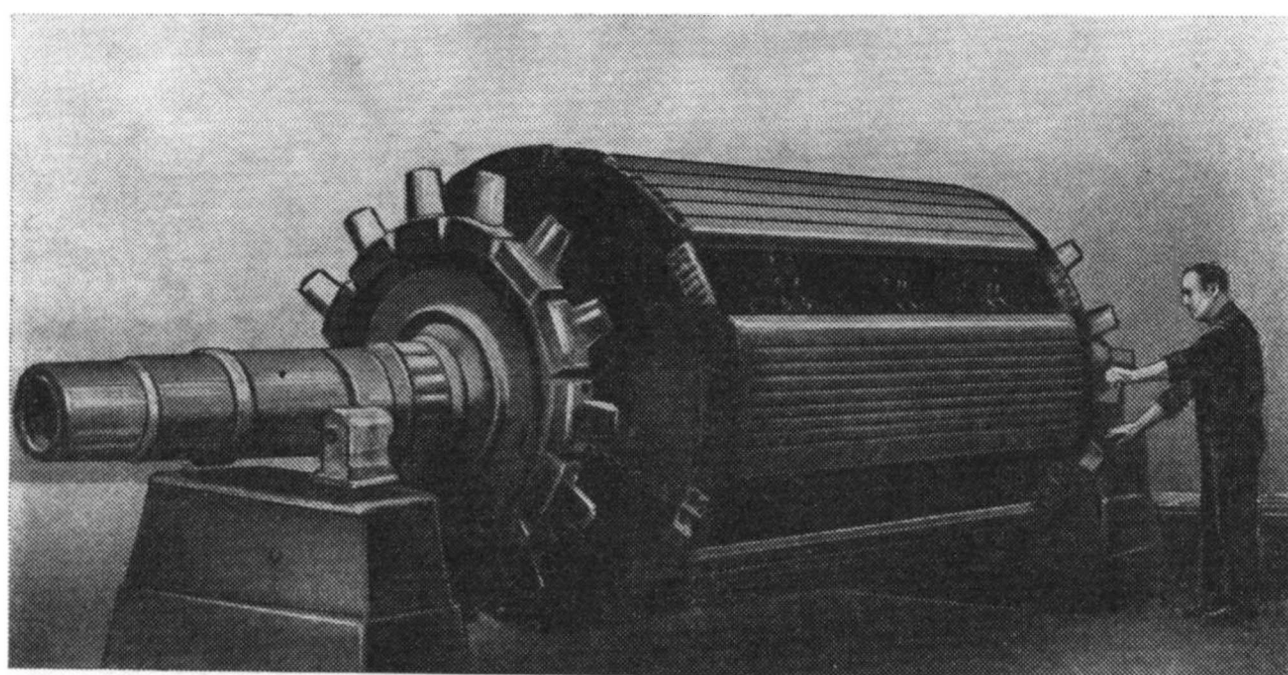


Fig. 1-15. Rotor of the Alsthom 60 000-kVA, 1000-rpm synchronous condenser

shaped blades (Pelton wheels), the turbines being arranged on both sides of the generator (Fig. 1-11).

Figure 1-12 represents the stator, and Fig. 1-13 the rotor and the upper spider of a vertical type 250-kVA, $\frac{400}{230}$ -V, 600-rpm hydrogenerator.

Figures 1-14, 1-15 and 1-16, respectively, show the stator, rotor and a generator view of a 60 000-kVA, 1000-rpm synchronous condenser for an outdoor installation built by the French firm Alsthom.

For purposes of illustration Table 1-2 presents characteristics of some hydrogenerators with different speeds made in the Soviet Union and abroad.

Salient-pole generators are frequently provided with a damper winding on the rotor to damp rotor oscillations under transient conditions (Chapter 16) and to facilitate operation under unbalanced load conditions (Chapter 14). The damper winding consists of copper bars laid in slots on the pole shoes and interconnected at the ends by means of short-circuiting segments. The segments of individual poles in modern generators are usually welded together to form common rings (see Fig. 1-10) resulting in a short-circuited squirrel-cage winding similar to that used in induction machines with squirrel-cage rotors (Sec. 1-7).

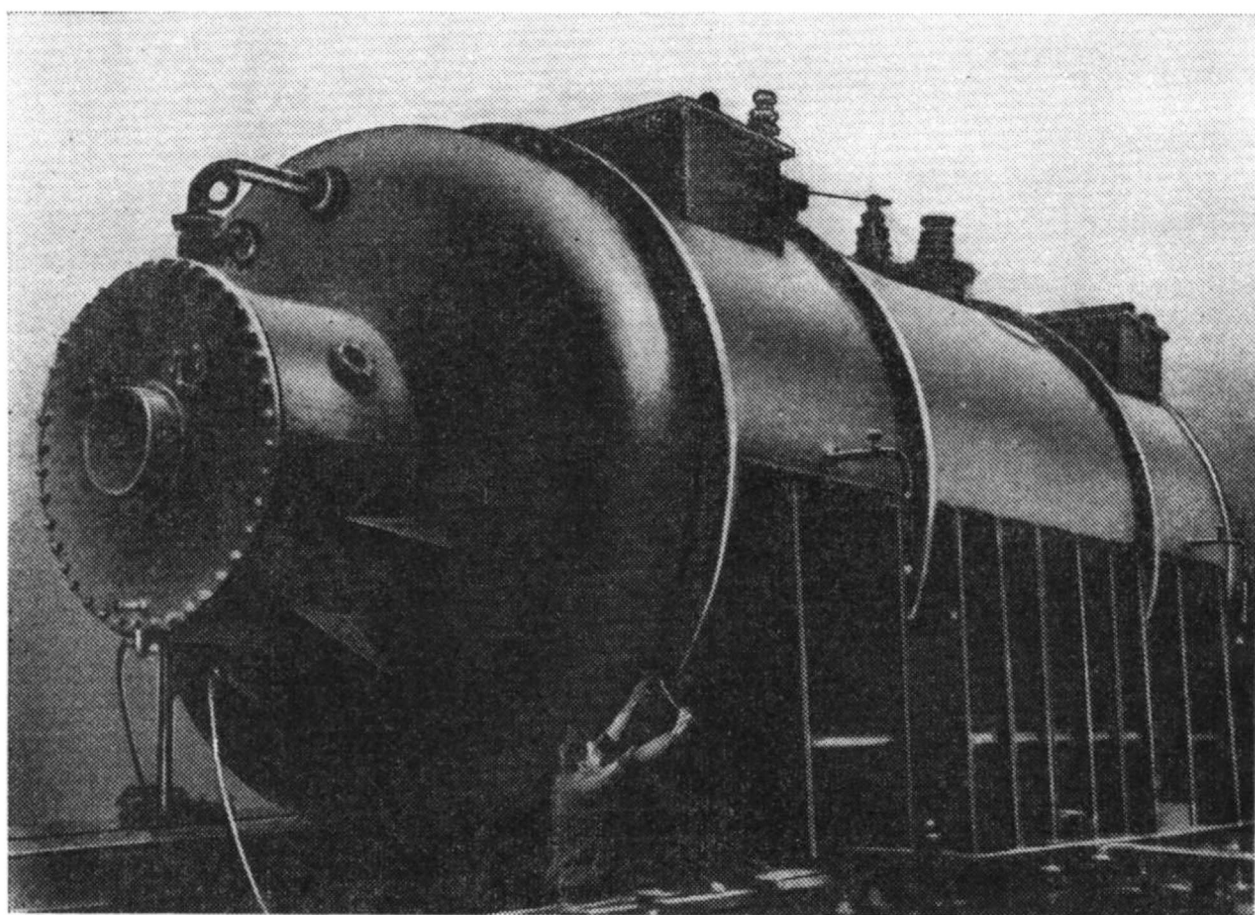


Fig. 1-16. General view of Alsthom 60 000-kVA, 1000-rpm synchronous condenser

Salient-pole synchronous motors and condensers are, in general, of the same design as salient-pole generators. Their rotors (Fig. 1-15), in addition to the excitation winding, carry a starting winding, differing from the damper winding of a generator only in that the bars are made of alloys with a higher resistivity.

1-7. High-Frequency and Special Synchronous Machines

Single-phase machines rated at 500 to 15 000 Hz and outputs up to several hundred kilowatts are used at present for feeding induction furnaces in metal-melting plants, for induction hardening of steel and for heating metals in forging and pressing shops.

In such machines the high-frequency e.m.f. is induced by means of magnetic flux pulsations caused by the relative movement of the stator and rotor teeth. Both the a.c. winding and the d.c. excitation winding are arranged on the stator, while the rotor carries no winding at all. To avoid the induction of a high-frequency e.m.f. in the exciting winding, measures are taken to keep the magnetic flux linkage with this winding constant during rotation of the rotor. Thin electrical sheet steel (0.2 to 0.3 mm thick) is used for the sections of the magnetic circuit in which the pulsating magnetic field acts.

Figure 1-17 depicts a high-frequency inductor generator with a ring field winding placed between two stator stacks assembled from sheet steel laminations. Each stack carries a.c. windings consisting of coils, each encircling one stator tooth. The rotor of the machine is of solid steel and has slots milled axially. The number of stator and rotor slots Z is the same. The direction of the magnetic lines of the

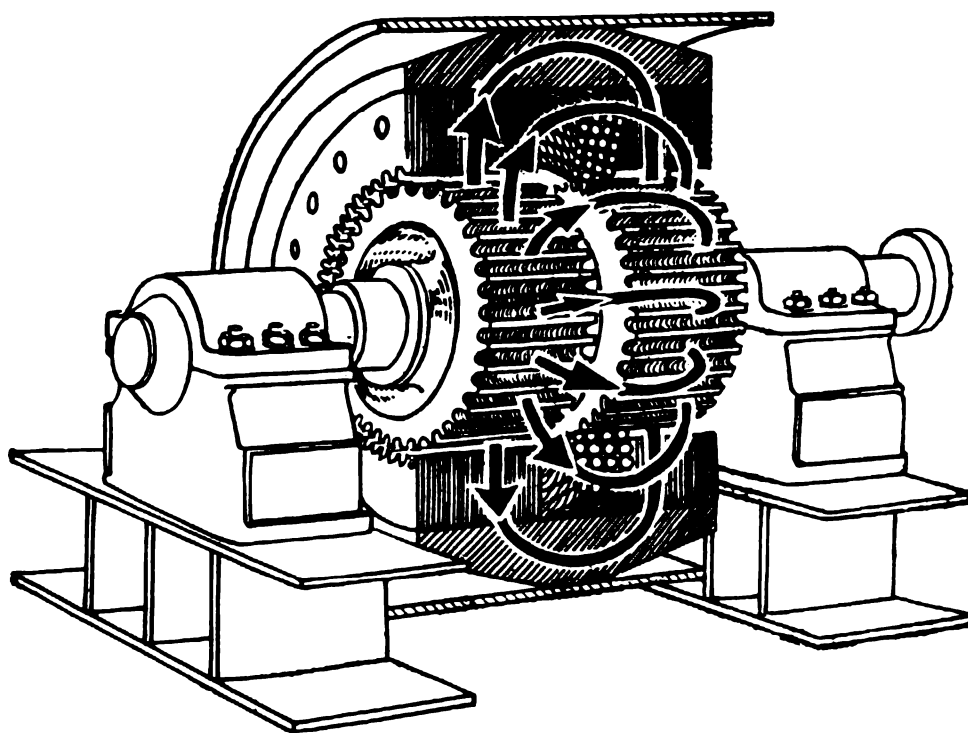


Fig. 1-17. High-frequency inductor generator (without a working winding on the stator)

Name of power plant	P		U kV	2p	η rpm	η %	D _i cm	L cm	δ cm	Z	A·10 ⁻² A/m	C·10 ⁻⁴
	MVA	MW										

Hydraulic turbogene

Fiynman	100	90	16.5	40	150	98	782	190	2.5	396	565	17.4
Bhakra	100	90	11	36	167	—	681	274	2.5	378	620	21.2
Trangslet	100	100	14.8	28	214	98.8	590	260	—	264	565	19.4
Ust-Kamenogorskaya	103.5	83	13.8	72	83.3	97.55	1100	180	1.8	486	610	17.6
Tagokura	105	94.5	13.2	36	167	98	—	—	—	—	—	—
Harspranget	105	94.5	16	36	167	98.1	840	245	3.05	432	413	27.5
Bovona	107.5	86	12	14	428	—	320	190	—	—	—	7.75
Kariba	111.1	100	18	36	166.7	97.57	785	196	—	—	—	18.1
Vianden	115	103.5	13.8	14	428	98.4	440	195	3.0	222	775	14.1
Votkinskaya	118	100	13.8	96	62.5	97.53	1430	170	2.3	756	553	21.7
Tokke I	120	96	16	16	375	—	450	260	—	—	—	16.6
Volga, Lenin	127.8	115	13.8	88	68.2	97.62	1430	200	2.3	756	451	21.8
Bhakra	134	120	11	32	187.5	98.31	720	230	2.4	408	635	16.7
Tokke III	140	—	—	20	300	—	490	284	—	—	—	14.6
Stornorfors	150	135	18	48	125	98.19	980	250	2.5	432	450	20
Volga, 22 Congress	160	128	13.8	88	68.2	96.3	1429	130	1.8	726	1085	11.3
Sanminsya	176	150	15.75	60	100	97.6	1190	200	2.4	594	663	16.1
Infernillo	188.6	179	13.8	44	136.5	98.3	1015	140	2.0	276	684	10.4
Tonsted	190	161.5	12	16	375	98.8	480	220	—	—	—	10
Aswan	206	175	15.75	60	100	98.1	1190	230	2.2	648	657	15.8
Zeitevare	225	214	17	30	200	98.5	740	200	—	—	830	9.75
Bratskaya	264.7	225	15.75	48	125	98.22	1100	250	2.5	504	708	14.3
Nourekская	353	300	15.75	30	200	97.87	830	174	3.2	270	1342	6.8
Krasnoyarskaya	590	500	15.75	64	93.8	98.25	1610	175	2.6	576	1128	7.21

Hydraulic turbogene

Robert Sounders	60	57	13.8	76	94.7	97.38	901	211	1.03	396	528	27.1
Bonneville	60	54	15	96	75	—	1025	114	—	—	—	15
Vollitch	75	60	13.8	20	360	96.6	397	238	1.68	240	605	18.1
Adam Beck	80.5	76.5	13.8	48	150	—	742.9	192	1.43	414	602	19.5
Hoover Dam	82.5	82.5	16.5	40	180	—	725	240	—	—	—	27.6
Priest	83	79	13.8	84	85.7	—	1067	147	2.1	450	934	17.3
Rapinds Sakuma	93	83.7	13.2	36	167	—	667	235	2.7	270	525	18.7
Brownlee	100.11	90.1	13.8	56	128.6	97.6	830	214	—	360	578	19
Kemano	106	85	13.8	22	327	97.3	498	246	2.53	—	—	18.8
Rocky Rich	107	—	—	80	90	—	1063	180	—	—	—	17.2
Grand Coulee	108	108	13.8	60	120	—	970	200	—	—	—	20.9
Lower Gen	115	100	13.8	20	360	97.98	424	234	—	—	—	13.2
Bersimis	138	131	13.8	26	277	—	512	287	—	—	609	15.1
Furnas	160	152	15	48	150	98.27	950	176	2.5	468	644	14.9
Shute des Passes	165	148.5	14.4	36	200	98.04	695	243	—	—	—	14.2
Robert Moses	167	150	13.8	60	120	—	1040	214	—	—	—	16.6

Note. Notations in table: D_i=diameter of stator bore; F=load on footstep bearing; H=sus

TABLE 1-2

Shortcircuit ratio	X_d f. u.	x_d' f. u.	x_d'' f. u.	F , tons	G_p , tons	G , tons	$GD^2 \cdot 10^{-7}$, N.m ²	Modification	Manufacturer or company	Country	Year
--------------------	----------------	-----------------	------------------	------------	--------------	------------	--	--------------	----------------------------	---------	------

rators, $f=50$ Hz

1.52	0.746	0.278	0.193	1100	452	845	16	H	Elektrosila	USSR	1957
—	0.95	0.3	0.19	850	—	548	10.55	H	AEI-EE	England	1960
—	—	—	—	470	—	—	4.36	H	ASEA	Sweden	1959
1.27	0.886	0.348	0.258	1030	491	986	39	H	Elektrosila	USSR	1951
1.2	0.912	0.27	0.18	900	460	820	15.5	U	Mitsubishi	Japan	1963
—	0.65	0.22	0.15	815	465	796.5	21.36	H	ASEA	Sweden	1961
—	1.67	0.5	0.3	—	—	—	1.67	Ho	BBC	Switzerland	—
1.715	0.678	0.234	0.146	680	—	—	—	U	AEI-EE	England	1962
0.8	1.35	0.3	0.2	—	197	375	1.9	—	—	—	—
1.75	0.649	0.292	0.22	2800	592	1170	80	U	Elektrosila	USSR	1961
—	1.0	0.23	0.15	455	—	—	—	—	BBC	Switzerland	1958
2.27	0.524	0.197	0.148	3400	767	1410	121	U	Elektrosila	USSR	1953
1.19	0.97	0.285	0.174	1200	435	810	14	H	Elektrosila	USSR	1964
—	1	0.25	—	455	—	—	3.97	H	BBC	Switzerland	—
—	0.65	0.22	0.15	950	445	915	30.4	U	ASEA	Sweden	1955
—	1.753	0.565	0.398	2600	572.6	1080	100	U	Elektrosila	USSR	1961
1.1	1.02	0.352	0.247	2000	566	1200	58	H	Uralelektrotiyazhmash	USSR	1960
—	1	0.32	0.2	—	600	—	22.5	H	Alsthom	France	1962
—	1	0.32	—	—	—	420	3	—	BBC	Switzerland	1966
—	0.998	0.328	0.216	2100	700	1350	73	U	Elektrosila	USSR	1966
—	0.75	0.28	0.2	—	300	550	—	—	ASEA	Sweden	1967
1.04	1.073	0.353	0.241	1400	654	1300	52	H	Elektrosila	USSR	1960
0.627	1.672	0.472	0.34	—	—	1075	21.5	U	Uralelektrotiyazhmash	USSR	—
0.67	1.57	0.41	0.3	2600	884	1650	187	U	Elektrosila	USSR	1965

rators, $f=60$ Hz

2.74	—	0.23	0.188	1500	267	476	12.9	U	General Electric	Canada	1955
—	0.56	—	—	1370	—	—	20	U	General Electric	USA	1938
1.04	1.178	0.282	0.179	—	—	—	1.5	H	—	USA	1952
—	0.92	0.3	0.26	635	315	541	10.2	—	—	USA	—
2.4	0.49	0.21	—	910	500	908	18.6	—	Westinghouse	USA	1955
1.24	1.04	0.51	—	1600	—	—	28.8	U	AEI-EE	England	1956
—	0.582	0.21	0.178	—	—	845	11.5	—	Hitachi	Japan	1956
1.1	—	—	—	—	307	600	13.2	—	Westinghouse	USA	—
1	1.132	0.286	0.202	430	290	516	2.77	U	AEI-EE	England	1954
—	1.13	0.31	—	1563	—	—	25	U	Westinghouse	USA	1961
1.66	0.64	0.3	—	910	—	—	29.4	H	Westinghouse	USA	1941
1.1	1.07	0.282	0.195	—	—	—	1.82	—	—	—	1960
1.3	0.98	0.37	—	496	—	—	—	—	General Electric	Canada	1956
1.9	0.82	0.29	0.205	1060	442	767	26.1	U	Siemens	FGR	1961
—	1.2	0.36	—	—	—	—	2.84	U	AEI-EE	England	1959
—	0.96	0.29	—	1107	—	—	47.5	U	General Electric	USA	1960

pension-type; U=umbrella-type; Ho=horizontal-type; f. u=fraction unit.

excitation field is shown in Fig. 1-17 by thick arrows. When the rotor teeth travel relative to the stator, the flux in the stator teeth will pulsate with a frequency $f=Zn$ and an e.m.f. of the same frequency will be induced in the stator coils. The teeth of one stator stack are displaced in relation to the teeth of the other one by half of a tooth pitch. For this reason the magnitude of the total flux does not change and no e.m.f. is induced in the field winding.

Lately synchronous machines with claw-like poles and a d.c. field winding on the stator have again come into use. A series of such machines has been designed by the Latvian Academy of Sciences [78].

1-8. Principal Elements of Non-Commutator Induction Machines

Here we shall bear in mind first of all the three-phase non-commutator induction machine because of its great importance (the term "non-commutator" has been omitted below, for purposes of brevity).

The stator of a three-phase induction machine is designed similar to that of a three-phase synchronous machine and also contains a similar three-phase winding for connection to an a.c. three-phase power line.

The rotor of an induction machine is a cylindrical body assembled of electrical sheet steel laminations with slots for accommodation of the winding. There are distinguished:

(a) induction machines with a *phase-wound rotor* (Fig. 1-18a) in which the rotor winding is of the same type as the three-phase winding on the stator. The rotor windings are generally star connected, and

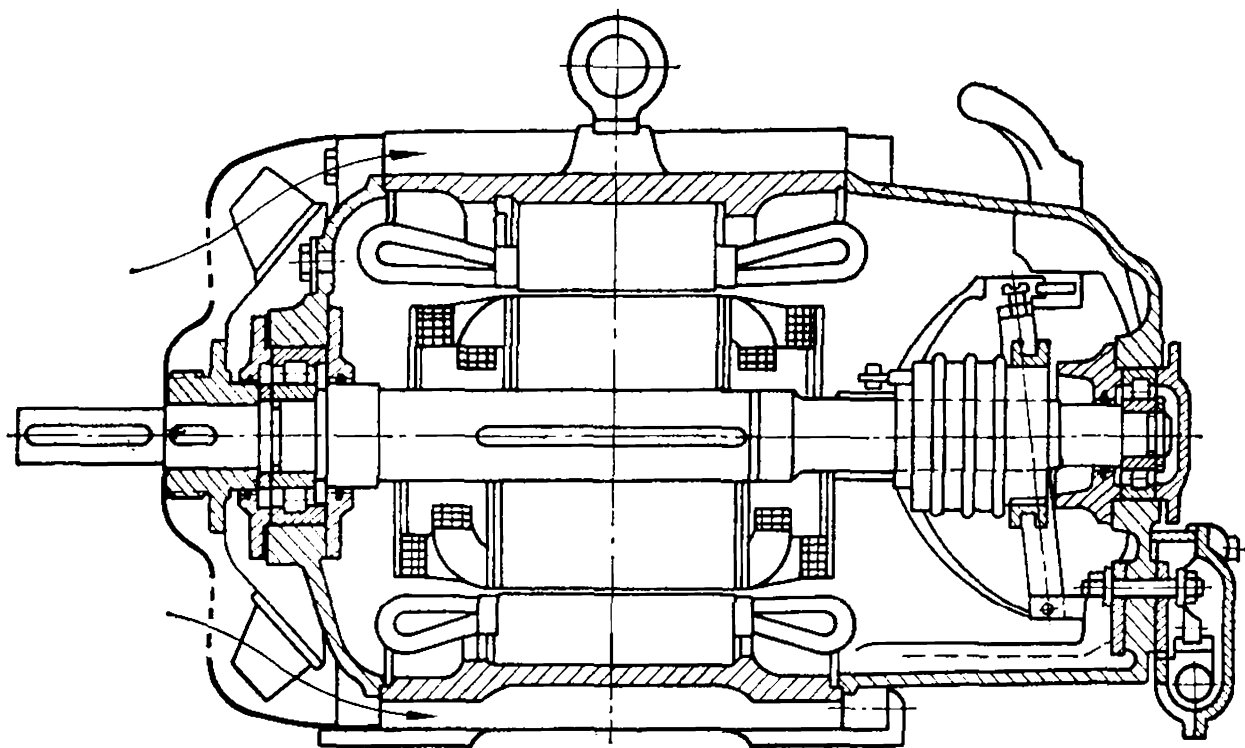


Fig. 1-18a. Longitudinal section of an induction motor with a phase-wound rotor

their ends are brought out via slip rings and brushes to a starting rheostat (Fig. 1-18b);

(b) induction machines with a *squirrel-cage rotor*, or simply *squirrel-cage machines*. They are built in three main modifications: with a single squirrel-cage rotor, a deep-bar rotor, and a double squirrel-cage rotor. These differ from each other in their starting characteristics (Ch. 23).

In the single squirrel-cage rotor machines the rotor slots stamped in the steel laminations generally have an oval shape with a varying depth-to-width ratio (Fig. 1-19). The slots, closed on top with a thin bridge 0.4 to 0.5 mm thick, are filled with aluminium. Simultaneously aluminium rings are cast at both ends of the rotor which connect the bars cast in the slots. The cast aluminium squirrel cage thus obtained is often provided at both sides with blades adjacent to the end rings to intensify cooling.

The form of the slot in a deep-bar rotor is shown in Fig. 1-20 on the left. The cage is made of rectangular copper bars, while the shorting rings R are generally made from strip copper and have slots milled in them to suit the dimensions of the bars. The cage bars are brazed to the shorting rings R with a high-heat solder.

In a double squirrel-cage rotor, the upper cage S (Fig. 1-21a), with a relatively high resistance and low inductive reactance, is made of brass or special bronze and serves as the starting winding when such a machine operates as a motor. The lower cage W , on the contrary, is made of copper with the lowest possible resistance and is the working winding of the motor.

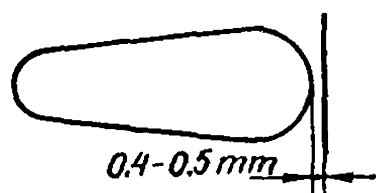


Fig. 1-19. Closed rotor slot

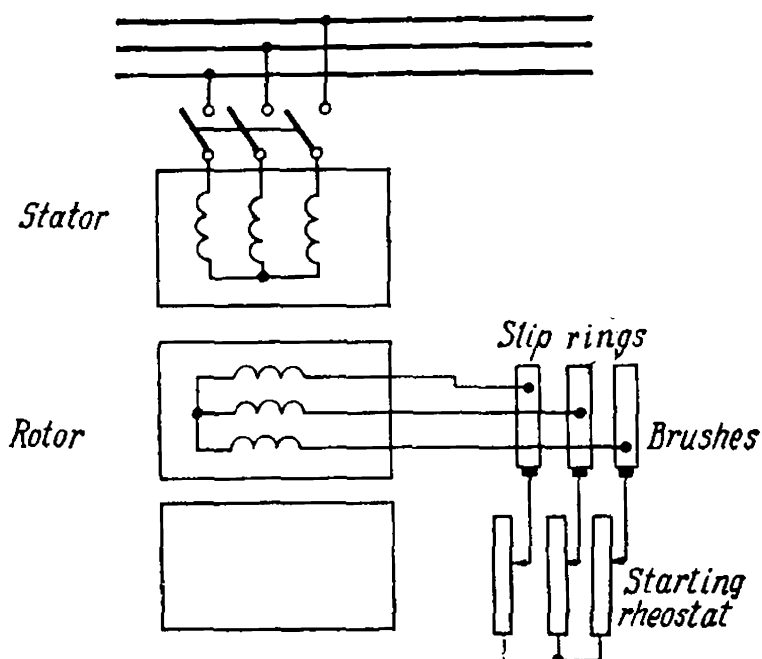


Fig. 1-18b. Connection diagram of an induction motor with a phase-wound rotor

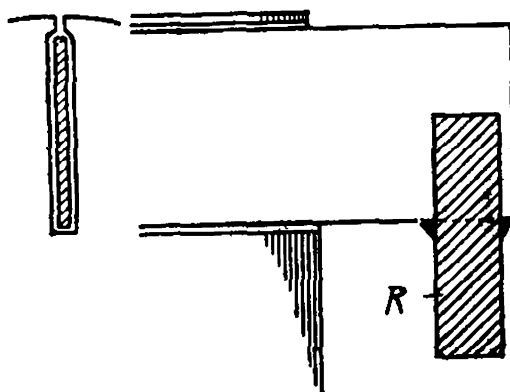


Fig. 1-20. Motor with deep-bar rotor

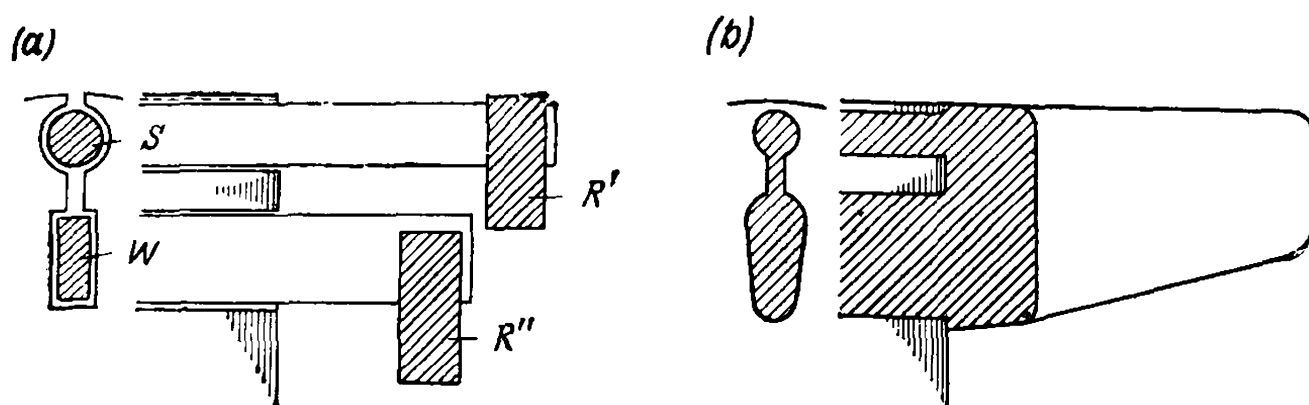


Fig. 1-21. Double squirrel-cage rotor:
a — with two windings; *b* — with aluminium casting

The upper and lower cages may both have round slots, or the upper cage may have round slots and the lower cage rectangular or oval ones.

The shorting rings R' and R'' for both cages are usually made of copper.

Figure 1-21*b* shows the form of the slots and rings when the rotor windings are made by pouring in aluminium. In this case the neck between the upper and lower cages is also filled with aluminium, and the motor as a whole is now of a deep-bar rotor type, but with a shaped slot. Consequently, such a motor can be considered as an intermediate form between a deep-bar rotor motor and one with a double squirrel-cage rotor.

There exist many other designs of squirrel-cage rotors. The “Elektrosila” Works, for example, successfully uses the bottle-shaped slot (Fig. 1-22) with copper bars of the corresponding shape. The properties of these motors are similar to those of the deep-bar and double squirrel-cage-rotor ones.

1-9. Operating Principle of the Induction Machine

Induction machine operation is based on the principle of electromagnetic interaction between the rotating magnetic field produced by the three-phase current supplied to the stator winding from a power source, and the currents induced in the rotor winding when its conductors are crossed by the rotating field. Thus, the operation of the induction machine is physically similar to that of a transformer. The stator may be considered as the primary and the rotor as the secondary winding, which, in the general case, is able to revolve with a speed n .

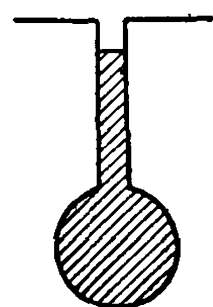


Fig. 1-22. Bottle-shaped slot

The speed of a sinusoidal rotating field is

$$n_1 = \frac{f}{p}$$

Electromagnetic interaction between the two parts of the induction machine (non-commutator) is possible only when the speeds of the rotating field (n_1) and the rotor (n) differ, i.e., on condition that $n \neq n_1$, since at $n = n_1$ the field would be stationary relative to the rotor, and no currents would be induced in the rotor winding.

The relation

$$s = \frac{n_1 - n}{n_1} \text{ or } s = \frac{n_1 - n}{n_1} 100\% \quad (1-3)$$

is termed the *slip* of the induction machine.

1-10. Operating Conditions of the Induction Machine

Depending on the relation between the speeds n_1 and n , the following operating conditions of the induction machine are distinguished: motoring, generating and electromagnetic braking. Let us consider briefly the features of each of them.

Motoring Operation. Let us assume that, in connecting the stator to three-phase mains, we have left the rotor circuit open. In this case $n = 0$ and the induction machine is similar to a transformer under no-load conditions. The magnetic field of the stator rotates in relation to the rotor with a speed n_1 and induces in the rotor winding an e.m.f. E_2 which has the frequency of the mains f and the direction determined by the right-hand rule (Fig. 1-23a).

If we now close the rotor circuit, a current I_2 will flow through the rotor winding whose active component coincides with the direction

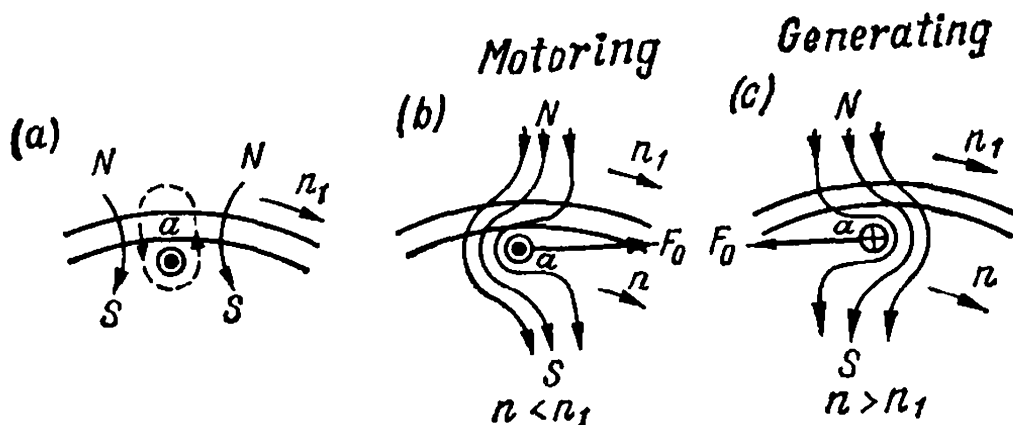


Fig. 1-23. Operating principles of an induction machine in motoring and generating conditions

of e.m.f. E_2 . The interaction of the flux (dotted lines in Fig. 1-23a) produced by this current with the stator flux will produce the resultant flux shown in Fig. 1-23b. We see that in these conditions the force F_0 applied to conductor a produces a torque at the machine shaft which tends to turn the rotor in the direction of flux rotation. The combined torques produced by the separate conductors form the resultant torque M of the machine. If this torque is sufficient to overcome the braking torque at the shaft, the rotor will start to run and develop a certain speed n . In this case the electric energy supplied to the stator from the power source is converted into mechanical energy at the shaft, i.e., the machine operates as a motor.

The speed n at which the motor runs depends on its load. At no-load the speed n becomes almost equal to n_1 , but cannot reach it, since at $n=n_1$ the machine could not operate as a motor.

Hence, an induction machine operates as a motor within the range from $n=0$ to $n=n_1$, i.e., at slips from $s=+1$ to $s=0$.

Generating Operation. Let us assume that with the help of a prime mover, we accelerate the rotor of an induction machine to a speed n greater than n_1 . In this case the slip becomes negative and the direction of flux rotation relative to the rotor is opposite to that when the machine operates as a motor. Accordingly the direction of the e.m.f. and the current in conductor a , as well as the sign of the shaft torque are also reversed (Fig. 1-23c). Consequently, the torque developed by the induction machine becomes a braking torque in relation to the driving torque of the prime mover. Under such conditions the induction machine operates as a generator and converts the mechanical energy supplied to it from the shaft of the prime mover into electric energy delivered to the power circuit.

Theoretically we may accelerate the rotor with respect to the rotating flux as much as desired. Therefore, *when an induction machine operates as a generator, the slip is within the range from $s=0$ to $s=-\infty$.*

In practice the transition from motoring to generating operation is possible, for instance, when a load is lowered by a crane, or when a train runs downhill.

Electromagnetic Braking. Suppose that under the influence of some external force the rotor of an induction machine begins to run in the direction *opposite to the magnetic flux rotation*. In this case energy is fed to the induction machine from two sources, electric energy from the power source and mechanical energy from the prime mover. Such performance is referred to as the *electromagnetic braking*. It starts at $n=0$ and may continue theoretically to $n=-\infty$. Therefore, *in an induction machine operating in braking conditions the slip is within the range of $s=+1$ to $s=\frac{n_1 - (-\infty)}{n_1} = +\infty$.*

In practice electromagnetic braking is used mainly when lowering loads with mechanical handling equipment.

1-11. Fundamental Relations.

Electromagnetic Torque of the Induction Machine

The rotor in an induction machine runs relative to the magnetic field with a speed $n_1 - n$. Hence the e.m.f.s induced in the rotor have a slip frequency

$$f_2 = p(n_1 - n) = pn_1 \frac{n_1 - n}{n_1} = fs \quad (1-4)$$

Let us assume the resultant magnetic flux in the air-gap of the machine to be constant ($\Phi = \text{const}$). Let E_2 be the e.m.f. induced in the rotor winding and $x_2 = 2\pi f L_2$ be its leakage inductive reactance at standstill, i.e., at a slip $s=1$. Then, for a running rotor, that is, at the slip s , we have

$$E_{2s} = E_2 \frac{f_2}{f} = E_2 s \quad (1-5)$$

and

$$x_{2s} = x_2 \frac{f_2}{f} = x_2 s \quad (1-6)$$

Hence,

$$I_2 = \frac{E_{2s}}{\sqrt{r_2^2 + (x_{2s})^2}} \quad (1-7a)$$

and

$$\cos \psi_2 = \frac{r_2}{z_2} = \frac{r_2}{\sqrt{r_2^2 + (x_{2s})^2}} \quad (1-7b)$$

where r_2 is the resistance of the rotor winding, and ψ_2 is the angle of displacement between the e.m.f. E_{2s} and the current I_2 .

The electromagnetic torque M at the shaft of an induction machine is produced as a result of interaction of the flux Φ , here assumed to be constant, and the active component of the current in the rotor winding $I_2 \cos \psi_2$.

Thus,

$$M = k \frac{E_{2s}}{\sqrt{r_2^2 + (x_{2s})^2}} \frac{r_2}{\sqrt{r_2^2 + (x_{2s})^2}} = k \frac{E_{2s} r_2}{r_2^2 + (x_{2s})^2} \quad (1-8)$$

where k is a proportionality factor.

From equation (1-8) it follows that the torque M of an induction machine is positive, i.e., a driving one, for $s > 0$ (motoring and electromagnetic braking conditions) and negative, i.e., braking for $s < 0$ (generating conditions). For $s=0$ and $s=\pm\infty$, the torque M vanishes. The slip $s=s_{max}$ corresponding to the maximum value of the torque

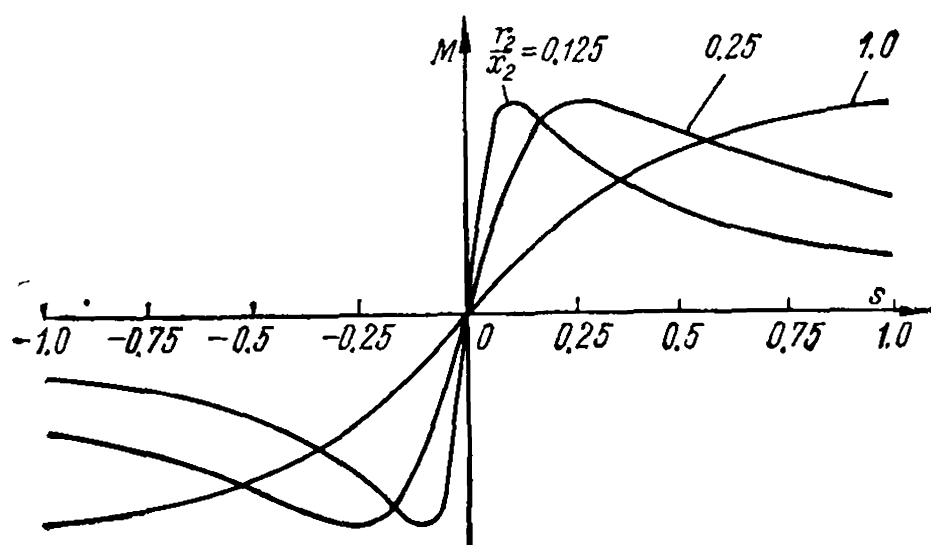


Fig. 1-24. Torque-slip curves of an induction machine for different active resistances of rotor circuit

$M = M_{max}$ is obtained by solving the equation

$$\frac{dM}{ds} = kE_2 \frac{r_2 [r_2^2 + (x_2 s)^2] - s r_2 2s x_2^2}{[r_2^2 + (x_2 s)^2]^2} = 0$$

whence

$$s_{max} = \pm \frac{r_2}{x_2} \quad (1-9)$$

Substituting this value for s_{max} in equation (1-8) we get

$$M_{max} = \pm k \frac{E_2}{2x_2} \quad (1-10)$$

It thus follows that the magnitude of the maximum torque does not depend on the rotor resistance r_2 ; only the slip s_{max} at which the torque M reaches its maximum value depends on it.

The relations $M = f(s)$ for $x_2 = \text{const}$ and various values of the rotor resistance r_2 are represented in Fig. 1-24. The theory of the induction machine is set forth in greater detail in Part Three.

1-12. Principle of A.C. Machine Winding Design

At present a.c. machines mainly have double-layer windings which have much in common with the double-layer armature windings of d.c. machines and which, therefore, may be produced on the basis of such armature windings.

In Volume I, Chapter 3 of this book, the potential polygons of d.c. machine armature windings have been considered. These polygons are obtained by consecutive vector summation of the *fundamental harmonic vectors* of the e.m.f.s in all the coil sections in the sequence of their arrangement around the winding circuit, which closes on itself. With a sufficiently large (theoretically with an infinitely large) number of

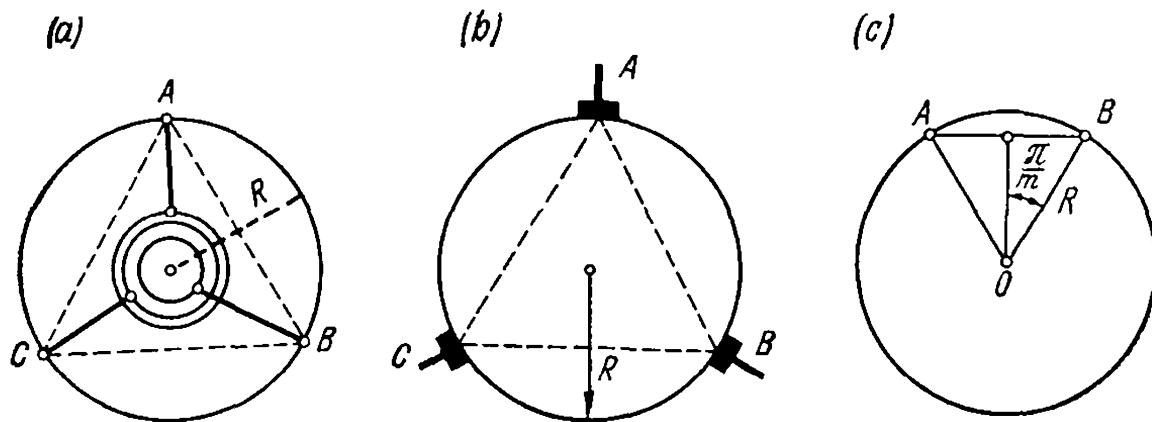


Fig. 1-25. Obtaining a three-phase winding from a closed d. c. machine armature winding

slots and coil sections, the potential polygon becomes a circle, or, with $2a$ parallel paths in the d.c. armature winding, it becomes a superimposed circles. In this case each part of the circle corresponds to a definite section of the closed winding.

Proceeding from such a concept, it may easily be seen that the simplest way to obtain an a.c. winding is from a conventional closed two-layer d.c. winding, if, in each section constituting a complete potential polygon, we make a number of taps corresponding to the number of phases in the machine. The equipotential points of these taps should be connected together, and then each phase will have a number of parallel paths a equal to the number of pairs of parallel paths of the initial d.c. winding.

Figure 1-25a shows the potential circle of a d.c. winding and the diagram of slip ring connections to one current path for a three-phase system. Such a winding is used in rotary converters, since in such machines the armature winding has to be made like a closed d.c. winding, joined at one side to the commutator, and at the other side to the slip rings (Chapter 17).

A similar winding is the armature winding of a three-phase a.c. commutator machine, the only difference being that the winding is divided into sections corresponding to the different phases, not by means of taps connected to slip rings, but by brushes contacting the commutator (Fig. 1-25b).

The sides of the triangles ABC in Fig. 1-25a and b represent simultaneously both the phase and line voltages of the winding, since the phase windings are delta-connected.

The length of the arc AB between adjacent points in Fig. 1-25a and b corresponds to the algebraic sum of the e.m.f.s of the given winding section or phase, while the corresponding chord AB will correspond to their vector sum giving the voltage between rings or brushes A and B .

The ratio between the vector sum of the e.m.f.s in the phase sections of the winding and the algebraic sum of these e.m.f.s is a measure of winding utilization and is referred to as the *winding distribution factor*.

In this case, for $m=3$ and a very large number of slots, we have

$$k_{d\infty} = \frac{\text{chord } AB}{\text{arc } AB} = \frac{R \sqrt{3}}{\frac{1}{3} 2\pi R} = \frac{3 \sqrt{3}}{2\pi} = 0.827$$

In the general case, if the machine has m phases (Fig. 1-25c), then for a very large number of slots we get

$$k_{d\infty} = \frac{2R \sin \frac{\pi}{m}}{\frac{1}{m} 2\pi R} = \frac{\sin \frac{\pi}{m}}{\frac{\pi}{m}} = \frac{m}{\pi} \sin \frac{\pi}{m} \quad (1-11)$$

In particular, with $m=6$ we have

$$k_{d\infty} = \frac{6 \times \sin 30^\circ}{\pi} = \frac{3}{\pi} = 0.955$$

Thus, for a three-phase winding, the phase e.m.f. decreases by 17.3 per cent in comparison with the algebraic sum of the e.m.f.s of the winding phase elements, whereas for a six-phase winding it decreases only by 4.5 per cent. Hence the armatures of polyphase commutator machines and rotary converters are sometimes built as six-phase machines.

The phase windings pictured in Fig. 1-25a can be star connected if we cut the d.c. armature winding into three parts (Fig. 1-26a), assuming that $2a=2$. In this case the line voltage increases $\sqrt{3}$ times (only the first harmonic is taken into account), but the utilization of the winding and its distribution factor will remain as above, namely $k_{d\infty}=0.827$ (Fig. 1-26b).

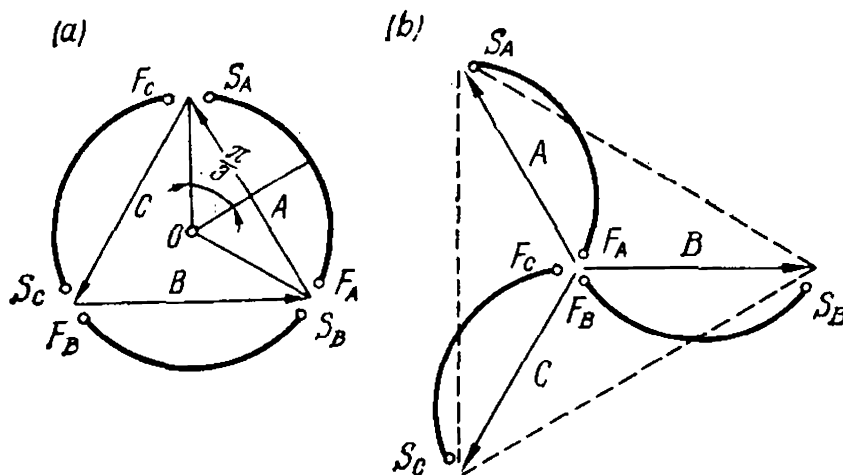


Fig. 1-26. Obtaining a 120° phase belt three-phase winding from a cut d. c. machine armature winding

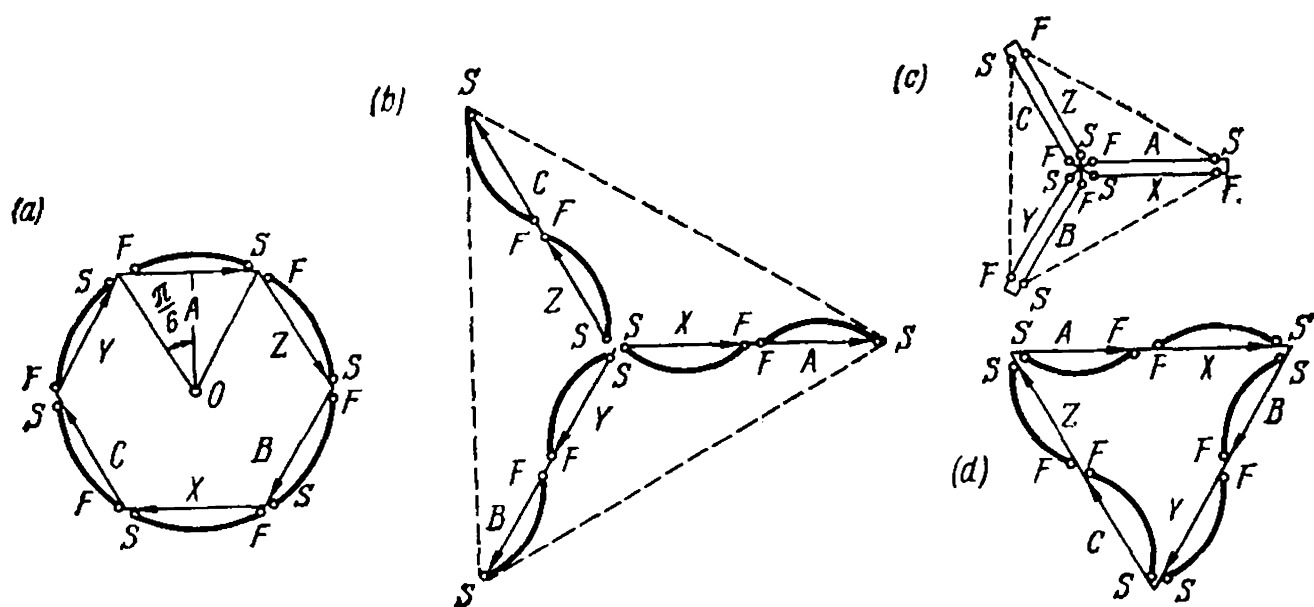


Fig. 1-27. Obtaining a 60° phase belt three-phase winding from a cut d.c. winding

Better results are obtained from three-phase windings if the e.m.f. polygon is divided into six belts (Fig. 1-27a). For the e.m.f.s of opposite half-phases (for instance *A* and *X*) to act concurrently in the circuit, the end of half-phase *A* should be connected with the end of half-phase *X* (Fig. 1-27b). In a uniformly distributed winding (number of slots $Z = \infty$) we obtain a distribution factor equal to

$$k_{d\infty} = \frac{6}{\pi} \cdot \sin \frac{\pi}{6} = \frac{3}{\pi} = 0.955$$

Thus it can be seen that in a winding with a phase belt of 60°, copper utilization is improved $\frac{0.955}{0.827} = 1.15$ times (i.e., by 15 per cent) over that in a winding with a 120° phase belt. In the same manner, a winding with a 60° belt allows each of the sections constituting the e.m.f. polygons to form two parallel groups by connecting in parallel the start and the finish of one half-phase with the finish and the start of the corresponding half-phase (Fig. 1-27c). The half-phases may also be delta connected (Fig. 1-27d).

A real winding is laid in a finite number of slots Z . For all the half-phases of a winding with a 60° belt to be identical, and to obtain a symmetrical winding in the simplest possible way, the number of slots in one belt, i.e., the number of slots per pole per phase

$$q = \frac{Z}{2pm} \quad (1-12)$$

should be a whole number. Such windings are referred to as windings with an integral number of slots per pole per phase and are universally adopted. In the following chapters we deal primarily with such windings. Windings with a fractional q are discussed separately (Sec. 3-6).

A winding consists of coils similar to those of the d.c. machine armature winding coil sections. In the general case a coil may consist of a number of series-connected turns having common insulation from the frame. Each 60° belt includes a group of several series-connected coil sections. One phase includes coil groups displaced from each other around the armature circumference by 180 electrical degrees. The number of coil groups in each phase of this type of winding, obtained from the two-layer d.c. armature windings, is equal to the number of poles $2p$. These groups may be both series- and parallel-connected in accordance with the principle discussed above.

Chapter

2

ELECTROMOTIVE FORCES IN A.C. MACHINE WINDINGS

2-1. Basic Characteristics of A.C. Machine E.M.F.

The e.m.f. of an alternating current is characterized by three main parameters: magnitude, frequency and wave-form.

An e.m.f. of the required magnitude and frequency is obtained in a comparatively simple way; it is more difficult to produce an e.m.f. of a specified wave-form. Generally it is required that the e.m.f. of a machine intended for industrial operation should have a practically sinusoidal wave-form. This especially concerns generators, since the higher harmonics in the e.m.f. harmfully influence not only the generator proper and most of the loads, by giving rise to increased losses, but also the transmission lines, by developing overvoltages at various sections and by creating inductive interference in nearby communication lines.

Let us consider the e.m.f. of an a.c. winding for a synchronous machine and begin with an analysis of the simplest case.

2-2. E.M.F. of a Conductor

Let us arrange a conductor a on the stator and pole shoes on the rotor parallel to the machine axis (Fig. 2-1). Let us next excite the machine and set it into rotation with a speed $n = \text{const.}$ The instantaneous value of the e.m.f. induced in the conductor a will then be

$$e_{con} = B_x lv \quad (2-1)$$

where B_x is the flux density at the point where the conductor is at the given moment of time.

Thus, the nature of the variation with time of the e.m.f. induced in the conductor, or, in other words, the wave-form of the conductor e.m.f. relative to time, exactly corresponds to the curve of magnetic flux density distribution in the air-gap along the armature periphery. To make the e.m.f. wave-form approach a sinusoid, it is necessary to produce a field having a wave-form containing the least number of higher harmonics. For this purpose, salient-pole synchronous machines are built

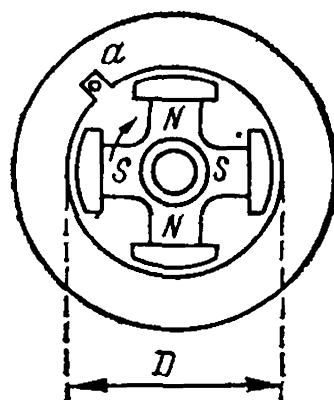


Fig. 2-1. E.m.f. of conductor

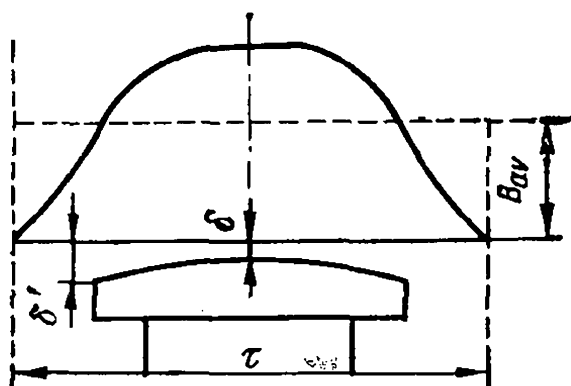


Fig. 2-2. Flux density distribution in gap over pole pitch

with a non-uniform gap along the pole periphery. Generally the outer end of the pole shoe is designed with a radius such that the gap δ' under the pole edges is 1.5 to 2 times the gap δ under the pole centre (Fig. 2-2). For the same purpose, in non-salient-pole machines the ratio of the wound part of the rotor to its pole pitch is made equal to about 0.75.

When the conductor moves through a double-pole pitch 2τ , this distance corresponds to the full time period T of the e.m.f.; therefore, the effective value of the conductor e.m.f. is

$$E_{con} = \sqrt{\frac{2}{T} \int_0^{\frac{T}{2}} e_{con}^2 dt} = lv \sqrt{\frac{2}{T} \int_0^{\frac{T}{2}} B_x^2 dt} = lvB \quad (2-2)$$

where the factor

$$B = \sqrt{\frac{2}{T} \int_0^{\frac{T}{2}} B_x^2 dt}$$

is the effective flux density.

The peripheral speed of the rotor is

$$v = \pi Dn = \frac{2\pi D}{2p} pn = 2\tau f$$

Let us call the ratio of the effective and mean values of the flux density B and B_{av} the *field form factor*

$$k_e = \frac{B}{B_{av}} \quad (2-3)$$

and substitute $2\tau f$ for v . Thus, taking into consideration that the total flux of one pole is

$$\Phi = \tau l B_{av}$$

we obtain

$$E_{con} = l 2\tau f k_e B_{av} = 2k_e \Phi f \quad (2-4)$$

For a sinusoidal field

$$k_e = \frac{\pi}{2\sqrt{2}} = 1.11$$

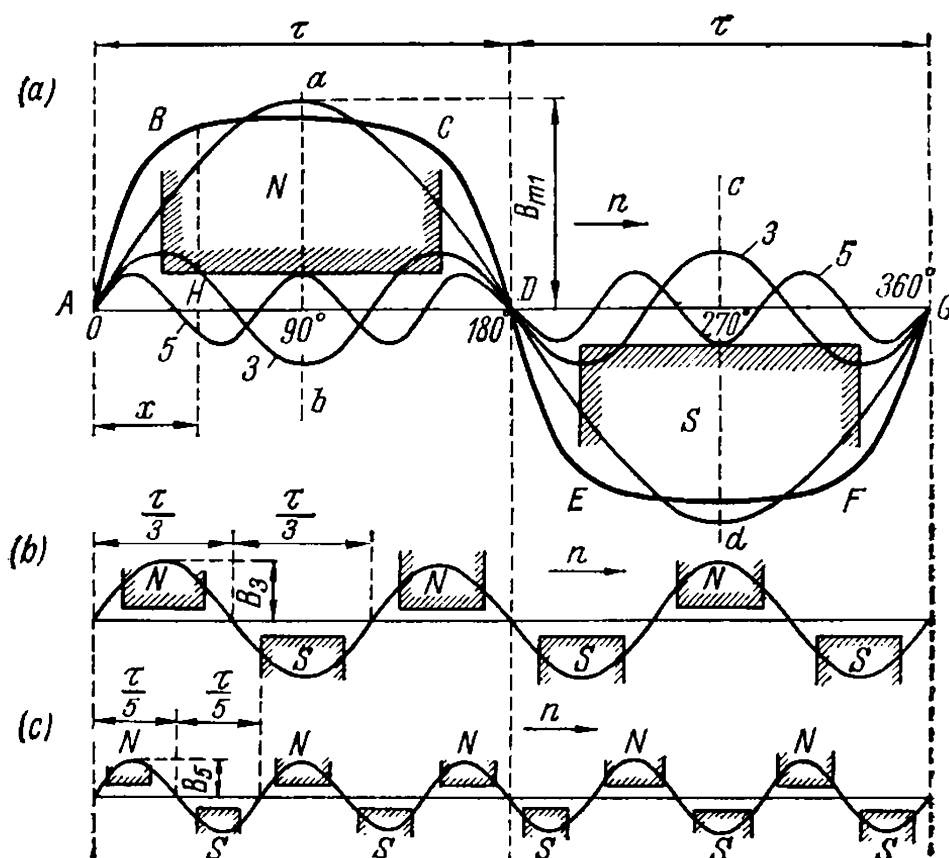


Fig. 2-3. Flux density distribution under poles:
 a—flux density wave-form resolved into harmonics;
 b and c—rotors producing third and fifth harmonics

hence, for the given case

$$E_{con} = \frac{\pi}{\sqrt{2}} \Phi f = 2.22 \Phi f \quad (2-5)$$

Let us determine the effective value of the conductor e.m.f. in the general case, for non-sinusoidal field distribution around the armature periphery.

We shall assume that the flux density curve is symmetrical with respect to the axis of abscissas, and also with respect to the pole axes ab and cd (Fig. 2-3a). Here the flux density curve, besides the first or the fundamental harmonic, contains higher harmonics of only odd orders: $v=3, 5, \dots$, i.e., $v=2k\pm 1$. All these harmonics intersect the axis of abscissas at common points A, D , etc.

Let us call the flux density harmonics *space* harmonics, since they are distributed over the armature periphery. The first harmonic of the flux density has an amplitude B_{m1} and a pole pitch τ which corresponds to the actual number of pole pairs p ; the higher harmonics have amplitudes $B_{m3}, B_{m5}, \dots, B_{mv}$ and pole pitches $\frac{\tau}{3}, \frac{\tau}{5}, \dots, \frac{\tau}{v}$ corresponding to the number of their pole pairs $3p, 5p, \dots, vp$ (Fig. 2-3b and c).

Each flux density harmonic determines a corresponding flux harmonic, namely

$$\Phi_1 = \tau l B_{av1} = \frac{2}{\pi} \tau l B_{m1} \quad (2-6a)$$

$$\Phi_3 = \frac{\tau}{3} l B_{av3} = \frac{2}{\pi} \frac{\tau}{3} l B_{m3} \quad (2-6b)$$

$$\dots \dots \dots \Phi_v = \frac{\tau}{v} l B_{avv} = \frac{2}{\pi} \frac{\tau}{v} l B_{mv} \quad (2-6c)$$

Since all the flux density harmonics of a pole field in a synchronous machine are stationary relative to the pole, they all rotate with the same speed n as the rotor. Therefore, the e.m.f. frequency induced in a conductor by each flux harmonic will be

$$f_1 = pn; \quad f_3 = 3pn; \dots; \quad f_v = vpn \quad (2-7)$$

According to equation (2-5), we have

$$E_{con1} = \frac{\pi}{\sqrt{2}} \Phi_1 f_1 = \sqrt{2} \tau l B_{m1} f_1 \quad (2-8a)$$

$$E_{con3} = \frac{\pi}{\sqrt{2}} \Phi_3 f_3 = \sqrt{2} \frac{\tau}{3} l B_{m3} 3f_1 = \sqrt{2} \tau l B_{m3} f_1 \quad (2-8b)$$

$$\dots \dots \dots E_{conv} = \frac{\pi}{\sqrt{2}} \Phi_v f_v = \sqrt{2} \frac{\tau}{v} l B_{mv} v f_1 = \sqrt{2} \tau l B_{mv} f_1 \quad (2-8c)$$

The effective value of the resultant e.m.f. of the conductor will be

$$\begin{aligned} E_{con} &= \sqrt{E_{con1}^2 + E_{con3}^2 + \dots + E_{conv}^2 + \dots} = \\ &= E_{con1} \sqrt{1 + \left(\frac{E_{con3}}{E_{con1}}\right)^2 + \dots + \left(\frac{E_{conv}}{E_{con1}}\right)^2 + \dots} = \\ &= E_{con1} \sqrt{1 + \left(\frac{B_{m3}}{B_{m1}}\right)^2 + \dots + \left(\frac{B_{mv}}{B_{m1}}\right)^2 + \dots} = \\ &= \frac{\pi}{\sqrt{2}} \Phi_1 f_1 \sqrt{1 + k_{B3}^2 + \dots + k_{Bv}^2 + \dots} \end{aligned} \quad (2-9)$$

where the factors

$$k_{B3} = \frac{B_{m3}}{B_{m1}}, \quad \dots, \quad k_{Bv} = \frac{B_{mv}}{B_{m1}}$$

represent the ratios between the amplitude values of the higher flux density harmonics B_{m3}, \dots, B_{mv} and the amplitude of the fundamental flux density wave B_{m1} .

Since the flux of one half-wave of a higher harmonic is either added to or subtracted from the flux of the half-wave flux density of the fun-

damental harmonic (Fig. 2-3a), the total flux per pole Φ is expressed by the following algebraic sum

$$\begin{aligned}\Phi &= \Phi_1 \pm \Phi_3 \pm \dots \pm \Phi_v \pm \dots = \Phi_1 \left(1 \pm \frac{\Phi_3}{\Phi_1} \pm \dots \pm \frac{\Phi_v}{\Phi_1} \pm \dots \right) = \\ &= \Phi_1 \left(1 \pm \frac{B_{m3}}{3B_{m1}} \pm \dots \pm \frac{B_{mv}}{vB_{m1}} \pm \dots \right) = \\ &= \Phi_1 \left(1 \pm \frac{1}{3} k_{B3} \pm \dots \pm \frac{1}{v} k_{Bv} \pm \dots \right) = \Phi_1 k_\Phi\end{aligned}\quad (2-10)$$

where k_Φ is the field form factor.

Hence, for the e.m.f. of a conductor we obtain

$$E_{con} = \frac{\pi}{\sqrt{2}} \Phi f_1 \frac{\sqrt{1 + k_{B3}^2 + \dots + k_{Bv}^2 + \dots}}{1 \pm \frac{1}{3} k_{B3} \pm \dots \pm \frac{1}{v} k_{Bv} \pm \dots} \quad (2-11)$$

By means of simple calculations it is not difficult to prove that, even if the higher flux density harmonics are significant, they have a comparatively small influence on the value of E_{con} , but, at the same time, they directly affect the wave-form of the conductor e.m.f. and, therefore, greatly distort it.

2-3. E.M.F. of a Turn and of a Concentrated Winding with a Full (Diametrical) Pitch

Figure 2-4 shows a turn with a full pitch $y = \tau$. As was already shown in Volume I, the e.m.f. of such a turn is obtained as the result of the vector subtraction of the e.m.f.s \dot{E}'_{con} and \dot{E}''_{con} induced in each of the conductors (1' and 1'' respectively) of the turn. Hence, the effective value of the e.m.f. of a full-pitch turn will be

$$E_{tn} = 2E_{con} \quad (2-12) \quad (a)$$

In the general case we may wind a coil by connecting w_c turns in series. If a machine has p pole pairs and identical coils are arranged under each pair of poles, then by connecting all the coils in series we form a so-called concentrated ($q=1$) winding consisting of $w = w_c p$ series-

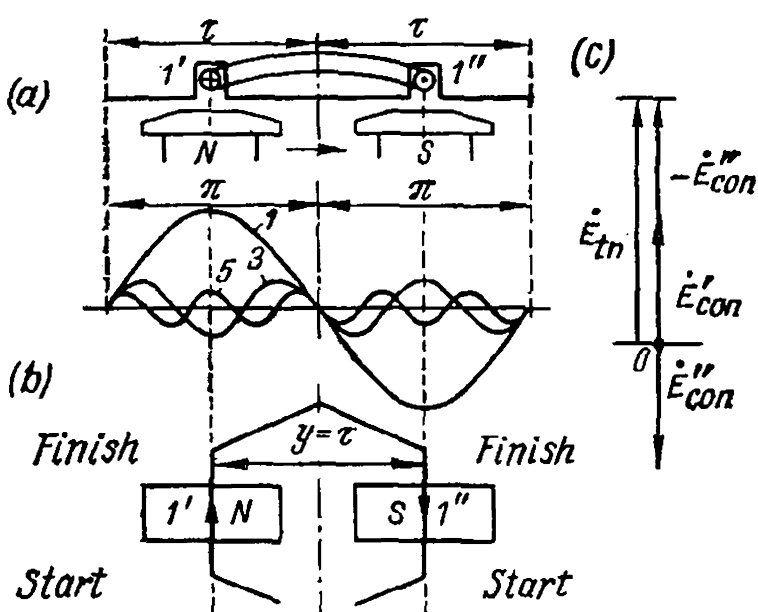


Fig. 2-4. E.m.f. of turn with pitch $y = \tau$

connected turns. Consequently, the e.m.f. of such a winding will be

$$\begin{aligned}
 E &= 2E_{con}\omega_c p = \frac{2\pi}{\sqrt{2}} \Phi_1 \omega f_1 \sqrt{1 + k_{B3}^2 + \dots + k_{Bv}^2 + \dots} = \\
 &= \frac{2\pi}{\sqrt{2}} \Phi \omega f_1 \frac{\sqrt{1 + k_{B3}^2 + \dots + k_{Bv}^2 + \dots}}{1 \pm \frac{1}{3} k_{B3} \pm \dots \pm \frac{1}{v} k_{Bv} \pm \dots} \quad (2-13)
 \end{aligned}$$

The e.m.f. of such a winding does not differ in form from the e.m.f. of a single conductor.

2-4. E.M.F. of a Full-Pitch Distributed Winding

The First E.M.F. Harmonic. The winding is generally designed not as a concentrated ($q=1$), but as a distributed one ($q>1$), i.e., the number of turns required per pole pair is not concentrated in one coil, but is distributed among several coils connected in series and arranged in q adjacent slots. Such an element of q coils is referred to as a *coil group*.

Let us suppose that the number of slots per pole pitch is $Q=6$ (Fig. 2-5). The coil group consists of four full-pitch coils ($y=\tau$); under each pole there are $q=4$ slots. All q coils are connected in series so that the start of one coil is connected to the finish of the next one.

For the first harmonic the angle of displacement between two adjacent slots and, consequently, between two adjacent coils will be

$$\gamma = \frac{\pi}{Q} = \frac{180^\circ}{6} = 30^\circ$$

Since at the moment under consideration coil 1 lies on the neutral, the instantaneous values of the e.m.f.s induced in coils 1, 2, 3, and 4 will be

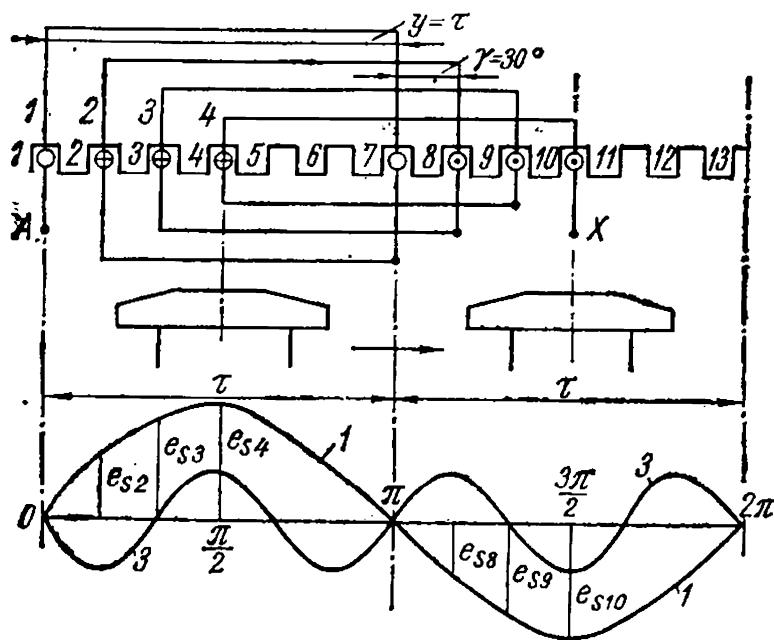


Fig. 2-5. E.m.f. distributed winding with pitch $y = \tau$

$$\begin{aligned}
 e_{c1} &= E_{cm} \sin 0^\circ = 0; \\
 e_{c2} &= E_{cm} \sin \gamma = E_{cm} \sin 30^\circ; \\
 e_{c3} &= E_{cm} \sin 2\gamma = E_{cm} \sin 60^\circ; \\
 e_{c4} &= E_{cm} \sin 3\gamma = E_{cm} \sin 90^\circ
 \end{aligned}$$

These e.m.f.s are shown in Fig. 2-6a by four vectors, each of which represents the maximum value of the coil e.m.f. or, by a suitable change in scale, its effective value E_c . Each vector is displaced relative to the adjacent one by an angle $\gamma=30^\circ$.

By geometrical summation of all four vectors, we obtain part of a regular polygon $OABCD$ (Fig. 2-6b), the resultant OD of which gives the effective value of the resultant e.m.f. E_q of four coils.

The projection of the resultant OD on the axis of ordinates gives the instantaneous value of the e.m.f. corresponding to the location

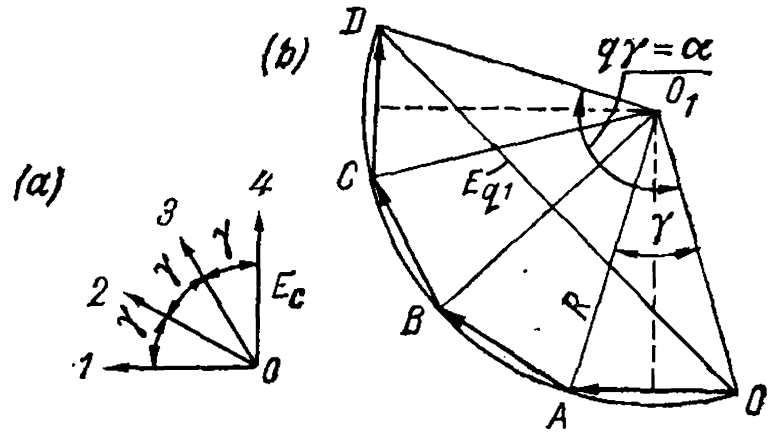


Fig. 2-6. E.m.f. star and polygon of coils shown in Fig. 2-5

of slots 1, 2, 3, and 4 relative to the pole in Fig. 2-5. At other moments the e.m.f. polygon will occupy other positions in its counterclockwise rotation about the centre O_1 with an angular frequency $\omega = 2\pi f$.

To determine $E_{q1} = OD$ we plot (Fig. 2-6b) the centre O_1 of a circle circumscribing the polygon. The radius of this circle, determined from the isosceles triangle OO_1A having the central angle γ , will be

$$R = \frac{E_c}{2 \sin \frac{\gamma}{2}}$$

Now $E_{q1} = OD$ can be determined from the isosceles triangle OO_1D with the angle $q\gamma$ at the vertex O_1 , namely

$$E_{q1} = 2R \sin \frac{q\gamma}{2} = E_c \frac{\sin \frac{q\gamma}{2}}{\sin \frac{\gamma}{2}}$$

If all the active sides of the coils were concentrated in one slot, the e.m.f. would be equal to qE_c . Hence, the ratio of the e.m.f. vector sum of a distributed winding to the e.m.f. of a concentrated winding with the same number of turns is

$$k_{d1} = \frac{E_{q1}}{qE_c} = \frac{E_c \sin \frac{q\gamma}{2}}{qE_c \sin \frac{\gamma}{2}} = \frac{\sin \frac{q\gamma}{2}}{q \sin \frac{\gamma}{2}} \quad (2-14)$$

The factor k_{d1} is referred to as the *winding differential* or *distribution factor*, the subscript "1" showing that it pertains to the first harmonic of the e.m.f.

For an m -phase winding with a phase belt $\frac{\pi}{m}$ (for $m=3$, with a 60° belt) the angle γ between two adjacent slots is

$$\gamma = \frac{\pi}{mq}$$

Substituting this value for γ in expression (2-14) for the distribution factors, relating to the fundamental harmonic of the e.m.f. of a polyphase winding we obtain

$$k_{d1} = \frac{\sin \frac{\pi}{2m}}{q \sin \frac{\pi}{2mq}} \quad (2-15)$$

Since the positions of the slots relative to the poles under all p pairs of poles are the same, the above conclusion may be applied to an entire winding consisting of qp series-connected coils, each of which comprises ω_c series-connected turns. Consequently, the effective value of the first e.m.f. harmonic of a full-pitch distributed winding will be

$$E_{q1} = \frac{2\pi}{\sqrt{2}} \Phi_1 f_1 qp \omega_c k_{d1} = \frac{2\pi}{\sqrt{2}} \Phi_1 f_1 \omega k_{d1} = 2\sqrt{2} \tau l B_{m1} f_1 \omega k_{d1} \quad (2-16)$$

Here $\omega = qp \omega_c$ is the number of series-connected turns in a winding phase.

Higher E.M.F. Harmonics of a Distributed Winding. The angle of displacement between two adjacent slots for a field harmonic of the v -th order is equal to $v\gamma$. The vectors of the e.m.f. induced by this harmonic in the armature winding are also displaced by the same angle. Reasoning as before for the first e.m.f. harmonic, we find the distribution factor of the winding for the v -th e.m.f. harmonic to be

$$k_{dv} = \frac{\sin \frac{vq\gamma}{2}}{q \sin \frac{v\gamma}{2}} = \frac{\sin \frac{v\pi}{2m}}{q \sin \frac{v\pi}{2mq}} \quad (2-17)$$

Thus, for example, the distribution factor of the winding shown in Fig. 2-5, for the third e.m.f. harmonic, will be

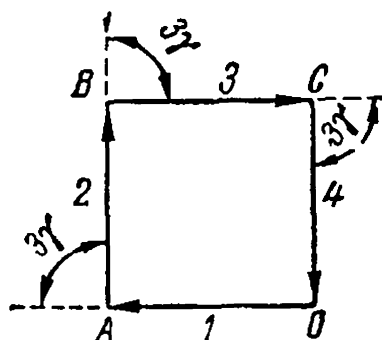


Fig. 2-7. Third e.m.f. harmonics of coil shown in Fig. 2-5

$$k_{d3} = \frac{\sin \frac{3 \times 4 \times 30^\circ}{2}}{4 \sin \frac{3 \times 30^\circ}{2}} = 0$$

Physically this is explained by the fact that the four e.m.f. vectors, shifted in phase by an angle $3\gamma = 3 \times 30^\circ = 90^\circ$, form a closed quadrangle (Fig. 2-7).

The harmonics of the order $v_{tc}=2Qk\pm1=2mqk\pm1$, where $k=1, 2, 3, \dots$, give values of the winding distribution factor equal to the factor k_{d1} for the fundamental harmonic.

Indeed

$$k_{d(2mqk\pm1)} = \frac{\sin \left[\frac{\pi}{2m} (2mqk \pm 1) \right]}{q \sin \left[\frac{\pi}{2mq} (2mqk \pm 1) \right]} = \pm \frac{\sin \frac{\pi}{2m}}{q \sin \frac{\pi}{2mq}} = \pm k_{d1}$$

The orders of these harmonics are strictly related to the number of slots per double pole pitch $2Q$. For instance, for $Q=6$ and $2Q=12$, with $k=1$, we obtain $v_{t1}=11$ and 13. These harmonics are referred to as *tooth-ripple harmonics*, or *tooth ripples*.

In a uniformly distributed winding, when the number of slots per pole per phase q may be assumed infinite, the winding distribution factor is equal to the ratio between the chord and the corresponding arc (Fig. 2-6b)

$$k_{d1} = \frac{\text{chord } OD}{\text{arc } OD} = \frac{2R \sin \frac{\alpha}{2}}{R\alpha} = \frac{\sin \frac{\alpha}{2}}{\frac{\alpha}{2}} \quad (2-18)$$

Accordingly, for a harmonic of the v -th order

$$k_{dv} = \frac{\sin \frac{v\alpha}{2}}{\frac{v\alpha}{2}} \quad (2-19)$$

For a three-phase winding $\alpha=60^\circ$, and with a uniformly distributed three-phase winding all the winding distribution factors for harmonics which are a multiple of three are equal to

$$k_{dv} = \pm \frac{2}{v} k_{d1} \quad (2-20)$$

and for all other harmonics

$$k_{dv} = \pm \frac{1}{v} k_{d1} \quad (2-21)$$

The signs “+” and “—” of the winding factors alternate every three harmonics.

Table 2-1 contains the distribution factors of single-phase windings for the fundamental and higher harmonics and for various ratios of the slot numbers Q and q , and Table 2-2 gives the corresponding values of the distribution factors for three-phase windings. The values of the factors for the fundamental and tooth-ripple harmonics are indicated by bold-face type.

TABLE 2-1

Dis- tribu- tion factor	Total number of slots per pole Q							
	3	4	4	5	5	6	6	6
	Number of slots per pole per phase q							
	2	2	3	2	3	2	3	4
k_{d1}	0.866	0.925	0.804	0.953	0.872	0.966	0.910	0.833
k_{d3}	0.000	0.385	-0.118	0.589	0.125	0.707	0.333	0.000
k_{d5}	-0.866	-0.385	-0.138	0.000	-0.333	0.259	-0.244	-0.224
k_{d7}	-0.866	-0.925	0.804	-0.589	0.127	-0.259	-0.244	0.224

Knowing these factors, we can determine the higher e.m.f. harmonics of a distributed winding

$$\begin{aligned} E_{qv} &= \frac{2\pi}{\sqrt{2}} \Phi_v f_v \omega k_{dv} = 2\sqrt{2} \frac{\tau}{v} l B_{mv} v f_1 \omega k_{dv} = \\ &= 2\sqrt{2} \tau l B_{mv} f_1 \omega k_{dv} \end{aligned} \tag{2-22}$$

Resultant E.M.F. of a Full-Pitch Distributed Winding. Similarly to formula (2-13) we obtain

$$E_q = \frac{2\pi}{\sqrt{2}} \Phi f_1 \omega k_{d1} \frac{\sqrt{1 + (k_{B3} k'_{d3})^2 + \dots + (k_{Bv} k'_{dv})^2 + \dots}}{1 \pm \frac{1}{3} k_{B3} \pm \dots \pm \frac{1}{v} k_{Bv} \pm \dots} \tag{2-23}$$

where

$$k'_{d3} = \frac{k_{d3}}{k_{d1}}, \dots, k'_{dv} = \frac{k_{dv}}{k_{d1}}$$

represent the relative values of the distribution factors for the higher harmonics.

The factor k_{d1} is less than unity, while the factors k_{d3}, \dots, k_{dv} are, as a rule, less than k_{d1} . Consequently, *the e.m.f. of a distributed winding is less than that of a concentrated winding with the same number of turns, but has a better wave-form.* In particular, we may have $k_{dv}=0$ (see Table 2-1). This means that the given harmonic is absent from the e.m.f. wave-form, although in the field wave-form it may be strongly manifested.

2-5. E.M.F. of a Concentrated Short-Pitch Winding

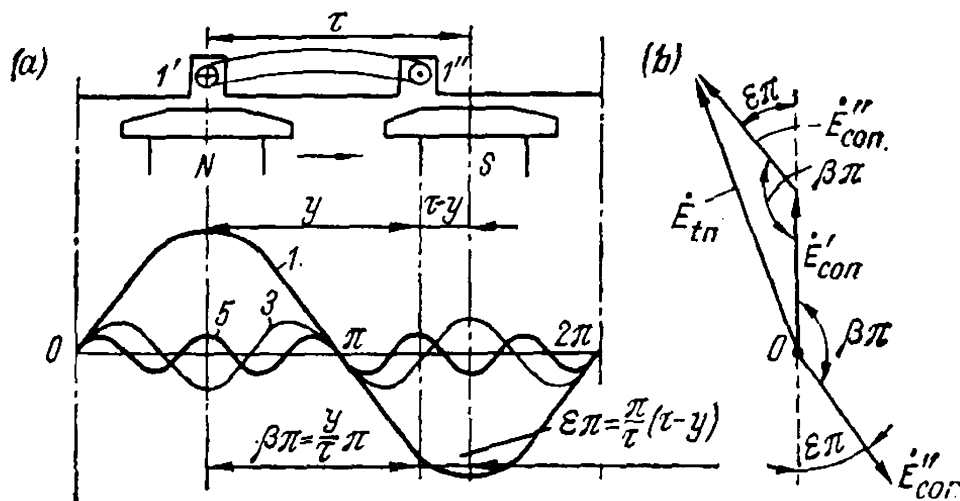
E.M.F. of a Short-Pitch Turn. Alternating-current windings are most frequently designed with a short pitch (Fig. 2-8a).

Let us denote the magnitude of the relative winding pitch by β , viz.

$$\beta = \frac{y}{\tau} \tag{2-24}$$

TABLE 2-2

Distribution factor	Total number of slots per pole Q										Uniformly distributed winding
	9	12	15	18	21	24	27	30			
	Number of slots per pole per phase q										
	3	4	5	6	7	8	9	10			
k_{d1}	0.960	0.958	0.957	0.957	0.957	0.956	0.955	0.955	0.955	0.955	
k_{d3}	0.667	0.654	0.646	0.644	0.642	0.641	0.640	0.639	0.636	0.636	
k_{d5}	0.217	0.205	0.200	0.197	0.195	0.194	0.194	0.193	0.191	0.191	
k_{d7}	-0.177	-0.158	-0.149	-0.145	-0.145	-0.141	-0.140	-0.140	-0.136	-0.136	
k_{d9}	-0.333	-0.270	-0.247	-0.236	-0.229	-0.225	-0.222	-0.220	-0.212	-0.212	
k_{d11}	-0.177	-0.126	-0.110	-0.102	-0.097	-0.095	-0.095	-0.092	-0.087	-0.087	
k_{d13}	0.217	0.126	0.102	0.092	0.086	0.085	0.081	0.079	0.075	0.075	
k_{d15}	0.667	0.270	0.200	0.172	0.158	0.150	0.145	0.141	0.127	0.127	
k_{d17}	0.960	0.158	0.102	0.084	0.075	0.070	0.066	0.064	0.056	0.056	
k_{d19}	0.980	-0.205	-0.110	-0.084	-0.072	-0.066	-0.062	-0.060	-0.050	-0.050	
k_{d21}	0.667	-0.654	-0.247	-0.172	-0.145	-0.127	-0.118	-0.112	-0.091	-0.091	
k_{d23}	0.217	-0.958	-0.149	-0.092	-0.072	-0.065	-0.057	-0.054	-0.041	-0.041	
k_{d25}	-0.177	-0.958	0.200	0.102	0.075	0.065	0.056	0.052	0.038	0.038	
k_{d27}	-0.333	-0.654	0.646	0.236	0.158	0.127	0.111	0.101	0.071	0.071	
k_{d29}	-0.177	-0.205	0.957	0.145	0.086	0.056	0.056	0.050	0.053	0.053	
k_{d31}	0.217	0.158	0.957	-0.197	-0.097	-0.070	-0.057	-0.050	-0.051	-0.051	
k_{d33}	0.667	0.270	0.646	-0.644	-0.229	-0.150	-0.118	-0.101	-0.058	-0.058	
k_{d35}	0.960	0.126	0.200	-0.957	-0.143	-0.085	-0.062	-0.052	-0.007	-0.007	
k_{d37}	0.960	-0.126	-0.149	-0.957	0.195	0.095	0.066	0.054	0.026	0.026	
k_{d39}	0.667	-0.270	-0.247	-0.644	0.642	0.225	0.145	0.112	0.049	0.049	
k_{d41}	0.217	-0.158	-0.110	-0.197	0.957	0.141	0.081	0.060	0.023	0.023	
k_{d43}	-0.177	0.205	0.102	0.145	0.957	-0.194	-0.095	-0.064	-0.022	-0.022	
k_{d45}	-0.333	0.654	0.200	0.256	0.642	-0.641	-0.022	-0.141	-0.042	-0.042	
k_{d47}	-0.177	0.958	0.102	0.102	0.195	-0.956	-0.140	-0.079	-0.020	-0.020	

Fig. 2-8. E.m.f. of turn with pitch $y < \tau$

The pitch of the winding will then correspond to an angle $\beta\pi$, the fundamental harmonics of the e.m.f.s in conductors $1'$ and $1''$ of the turn will be displaced by an angle $\beta\pi$ and the v -th harmonic by an angle $v\beta\pi$.

The vector diagram for the fundamental harmonic of a turn e.m.f. is plotted in Fig. 2-8b, according to which

$$\dot{E}_{tn1} = 2\dot{E}_{con1} \sin \frac{\beta\pi}{2} = 2\dot{E}_{con1} k_{p1} \quad (2-25)$$

where

$$k_{p1} = \sin \frac{\beta\pi}{2} \quad (2-26)$$

is the *pitch factor* of the winding for the first e.m.f. harmonic.

The factor k_{p1} may also be expressed through the relative value of pitch shortening

$$e = 1 - \beta$$

namely

$$k_{p1} = \cos \frac{e\pi}{2} \quad (2-27)$$

In the general case

$$E_{tnv} = 2E_{conv} k_{pv} \quad (2-28)$$

where

$$k_{pv} = \sin \frac{v\beta\pi}{2} \quad (2-29)$$

represents the pitch factor of the winding for the v -th harmonic.

It is not difficult to prove that the pitch factors for the tooth-ripple harmonics are also equal to the pitch factor for the fundamental harmonic. Indeed, the angle $\beta\pi$ corresponding to the pitch y may be expressed as $\beta\pi = \frac{y\pi}{\tau} = \frac{Q-S}{Q} \pi$, where S is the number of tooth in-

tervals by which the pitch is shortened. In this case

$$k_{p1} = \sin \frac{\beta\pi}{2} = \cos \frac{\pi}{2} \frac{S}{Q} \quad (2-30)$$

and for the tooth-ripple harmonics

$$\begin{aligned} k_{pvt} &= \sin \frac{v_t \beta \pi}{2} = \sin \left[(2Qk \pm 1) \frac{Q-S}{Q} \frac{\pi}{2} \right] = \\ &= \pm \cos \frac{\pi}{2} \frac{S}{Q} = \pm k_{p1} \end{aligned} \quad (2-31)$$

E.M.F. of a Short-Pitch Concentrated Winding. Let us make a winding of p short-pitch coils identically arranged with respect to the poles. If each coil consists of w_c turns connected in series and all the coils are also series-connected, we have a winding with a given short pitch consisting of $w = pw_c$ turns. The effective value of the resultant e.m.f. of such a winding is expressed by a formula similar to formula (2-23)

$$E = \frac{2\pi}{\sqrt{2}} \Phi f_1 w k_{p1} \frac{\sqrt{1 + (k_{B3} k'_{p3})^2 + \dots + (k_{Bv} k'_{pv})^2 + \dots}}{1 \pm \frac{1}{3} k_{B3} \pm \dots \pm \frac{1}{v} k_{Bv} \pm \dots} \quad (2-32)$$

Here

$$k'_{p3} = \frac{k_{p3}}{k_{p1}}, \quad k'_{pv} = \frac{k_{pv}}{k_{p1}}$$

are the relative pitch factor values for the higher harmonics.

The factor k_{p1} is less than unity, and the factors k_{p3}, \dots, k_{pv} are, as a rule, less than k_{p1} . Therefore, the e.m.f. of a short-pitch winding, other factors being equal, is less than that of a full-pitch winding, but has a better wave-form, since the higher e.m.f. harmonics are decreased k_{pv} times in comparison with the higher field harmonics. In a particular case k_{pv} may equal zero. For instance, let the winding pitch be $y = \frac{4}{5}\tau$, i.e., the relative pitch is $\beta = \frac{4}{5}$; then, for the fifth e.m.f. harmonic, according to equation (2-29), we have

$$k_{p5} = \sin \frac{5 \times 4\pi}{5 \times 2} = \sin 2\pi = 0$$

Thus, the fifth e.m.f. harmonic disappears. Physically this is explained by the fact that the fifth field harmonic induces in the coil sides e.m.f.s that are equal in value, but opposite in direction in the coil circuit (see Fig. 2-8). With a winding pitch shortened by $\frac{1}{v}\tau$ the v -th harmonic disappears from the wave-form winding e.m.f. Usually $\beta = 0.80$ to 0.85 , but in a number of cases a winding pitch value of $\left(\frac{1}{2} \text{ to } \frac{1}{3}\right)\tau$ is used.

Example 2-1. A three-phase induction motor with a phase-wound rotor having $2p=6$ poles has $Z_1=90$ stator slots, or $\frac{90}{6}=15$ slots per pole, and $Z_2=72$ rotor slots, or 12 slots per pole. The number of stator and rotor slots per pole per phase is, respectively, $q_1=5$, and $q_2=4$.

The stator winding pitch is from slot 1 to slot 13.

The relative pitch of the stator winding is

$$\beta_1 = \frac{12}{15} = 0.8$$

The distribution factor for $q_1=5$, from Table 2-2, is

$$k_{d1} = 0.957$$

The winding pitch factor, according to formula (2-26), is

$$k_{p1} = \sin 72^\circ = 0.951$$

The resultant stator winding factor

$$k_{w1} = 0.957 \times 0.951 = 0.91$$

The rotor winding pitch is from slot 1 to slot 13, hence the relative pitch is

$$\beta_2 = \frac{12}{12} = 1.0$$

The distribution factor for $q_2=4$, according to Table 2-2, is

$$k_{d2} = 0.958$$

The resultant rotor winding factor is

$$k_{w2} = 0.958 \times 1.0 = 0.958$$

2-6. General Expression for E.M.F. of A.C. Machine Armature Winding

At present the most widespread type of armature winding in a.c. machines is the short-pitch double-layer distributed winding (similar in type to a d.c. machine armature winding). Generalizing the conclusions drawn above in Secs. 2-4 and 2-5, we have:

for the first e.m.f. harmonic

$$E_1 = \pi \sqrt{2} \omega k_{d1} k_{p1} f_1 \Phi_1 = 2 \sqrt{2} \tau l \omega k_{w1} f_1 B_{m1} \quad (2-33)$$

for the v -th e.m.f. harmonic

$$E_v = \pi \sqrt{2} \omega k_{dv} k_{pv} f_v \Phi_v = 2 \sqrt{2} \tau_v l \omega k_{wv} f_v B_{mv} \quad (2-34)$$

Here

$$\tau_v = \frac{\tau}{v}$$

and

$$k_{w1} = k_{d1} k_{p1}, \dots, k_{wv} = k_{dv} k_{pv} \quad (2-35)$$

are winding factors for the first, ..., v -th harmonics.

Hence the resultant of the winding e.m.f. will be

$$E = \frac{2\pi}{\sqrt{2}} \omega k_{w1} f_1 \Phi \frac{\sqrt{1 + (k_{B3}k_3)^2 + \dots + (k_{Bv}k_v)^2 + \dots}}{1 \pm \frac{1}{3} k_{B3} \pm \dots \pm \frac{1}{v} k_{Bv} \pm \dots} \quad (2-36)$$

where

$$k_3 = \frac{k_{w3}}{k_{w1}} = \frac{k_{d3}k_{p3}}{k_{d1}k_{p1}}, \dots, k_v = \frac{k_{wv}}{k_{w1}} = \frac{k_{dv}k_{pv}}{k_{d1}k_{p1}}$$

are the relative winding factor values for the higher harmonics.

From the above it follows that the distribution of the winding and the shortening of its pitch, while somewhat decreasing the magnitude of the fundamental e.m.f., improve the form of the resultant e.m.f. wave, bringing it closer to a sinusoid.

Formulas (2-33) and (2-34) for the e.m.f. are often written in the following form

$$E_1 = \pi \sqrt{2} \omega k_{w1} f_1 \Phi_1 = 4.44 \omega k_{w1} f_1 \Phi_1 \quad (2-37)$$

$$E_v = \pi \sqrt{2} \omega k_{wv} f_v \Phi_v = 4.44 \omega k_{wv} f_v \Phi_v \quad (2-38)$$

Example 2-2. Compute the e. m. f. of the fundamental and the nearest higher harmonics, the 3rd, 5th and 7th, for a three-phase synchronous hydrogenerator with the following rated data: power $P = 16\,500$ kVA, line voltage $U_r = 11\,000$ V, current $I_r = 865$ A, power factor $\cos \varphi = 0.7$, frequency $f = 50$ Hz, number of pole pairs $2p = 12$, pole pitch $\tau = 0.693$ m, number of winding phase turns (star connection) $w_1 = 72$, number of slots per pole per phase $q_1 = 4$, relative winding pitch $\beta = \frac{5}{6}$ (the slot pitch $y = 1$ to 11), active length $l = 1.3$ m, amplitude of the harmonics $v = 1, 3, 5, 7$ of the excitation field in the air-gap

$$\begin{aligned} B_{m1} &= 0.75 \text{ T} & B_{m3} &= 0.039 \text{ T} \\ B_{m5} &= 0.035 \text{ T} & B_{m7} &= 0.02 \text{ T} \end{aligned}$$

We find the distribution factors for $q_1 = 4$ from Table 2-2

$$k_{d1} = 0.958; k_{d3} = 0.654; k_{d5} = 0.205; k_{d7} = -0.158$$

The winding pitch factors, by formula (2-29), are

$$\begin{aligned} k_{p1} &= \sin \frac{5}{6} \times \frac{\pi}{2} = \sin 75^\circ = 0.966 \\ k_{p3} &= \sin 3 \times \frac{5}{6} \times \frac{\pi}{2} = \sin 225^\circ = -0.707 \\ k_{p5} &= \sin 5 \times \frac{5}{6} \times \frac{\pi}{2} = \sin 375^\circ = 0.259 \\ k_{p7} &= \sin 7 \times \frac{5}{6} \times \frac{\pi}{2} = \sin 525^\circ = 0.259 \end{aligned}$$

The winding factors are

$$\begin{aligned}k_{w1} &= k_{d1}k_{p1} = 0.958 \times 0.966 = 0.925 \\k_{w3} &= k_{d3}k_{p3} = 0.654 \times (-0.707) = -0.462 \\k_{w5} &= k_{d5}k_{p5} = 0.205 \times 0.259 = 0.053 \\k_{w7} &= k_{d7}k_{p7} = -0.158 \times 0.259 = -0.041\end{aligned}$$

The flux of the fundamental harmonic, from formula (2-6a), is

$$\Phi_1 = \frac{2}{\pi} \times 0.693 \times 1.3 \times 0.75 = 0.43 \text{ Wb}$$

and the e. m. f. of the winding phase for the fundamental harmonic, according to formula (2-33), is

$$E_1 = \pi \sqrt{2} \times 72 \times 0.925 \times 50 \times 0.43 = 6350 \text{ V}$$

The relative amplitudes of the higher field harmonics are

$$\begin{aligned}k_{B3} &= \frac{0.039}{0.75} = 0.052 \\k_{B5} &= \frac{0.035}{0.75} = 0.047 \\k_{B7} &= \frac{0.02}{0.75} = 0.027\end{aligned}$$

The relative values of the e. m. f. higher harmonics, taking into account formulas (2-33) and (2-34), are

$$\begin{aligned}\frac{E_3}{E_1} &= -0.052 \times \frac{0.462}{0.925} = -0.026 \\ \frac{E_5}{E_1} &= 0.047 \times \frac{0.053}{0.925} = 0.00269 \\ \frac{E_7}{E_1} &= -0.027 \times \frac{0.041}{0.925} = -0.00120\end{aligned}$$

As can be seen, the relative value of the e. m. f. higher harmonics is much lower than the relative values of the flux density higher harmonics.

The absolute values of the phase e. m. f. higher harmonics are

$$\begin{aligned}E_3 &= -6350 \times 0.026 = -165 \text{ V} \\ E_5 &= 6350 \times 0.00269 = 17.1 \text{ V} \\ E_7 &= -6350 \times 0.00120 = -7.6 \text{ V}\end{aligned}$$

The effective value of the phase winding e. m. f., taking into account the higher harmonics up to and including $v=7$, is

$$E_{ph} = 6350 \sqrt{1 + 0.026^2 + 0.00269^2 + 0.00120^2} = 6352.16 \text{ V}$$

i.e., differs but slightly from the fundamental e. m. f. harmonic.

There will be no third harmonic in the line voltages, therefore the effective value of the line voltage, taking into account harmonics of up to $v=7$, will be

$$E_1 = 11\,000 \sqrt{1 + 0.00269^2 + 0.00120^2} = 11\,000.051 \text{ V}$$

i.e., a very negligible difference from the line e. m. f. fundamental harmonic value.

2-7. Combination of E.M.F.s

Alternating current machines are generally of a three-phase design. As in transformers, the phase windings may be star- or delta-connected. The methods of phase winding connection, the quantitative relations between phase and line voltages and currents, and the influence of the winding connection method on the wave-form of the line e.m.f. are dealt with in Volume I, Chapter 15. Each phase winding, however, is distributed along the armature periphery and, therefore, has a corresponding distribution factor. In three-phase machines the number of slots per pole per phase $q = \frac{1}{3}Q$, where Q is the number of slots per pole. Usually q is an integer, but in special cases windings are made with a fractional number of slots per pole per phase. Such windings are discussed separately (Sec. 3-6).

Chapter

3

WINDINGS OF ALTERNATING CURRENT MACHINES

3-1. Three-Phase Double-Layer Lap Windings with q an Integer

At the end of the first chapter we discussed the basic principles of obtaining three-phase double-layer windings by cutting into sections the closed double-layer windings employed in d.c. machines.

In this chapter the problems involved in designing three-phase windings are discussed in more detail.

Let us begin the examination of double-layer lap windings by considering the example of a full-pitch winding ($y=\tau$) having the following data (Fig. 3-1a): number of phases $m=3$, number of poles $2p=4$, number of slots $Z=36$, and number of slots per pole per phase

$$q = \frac{Z}{2pm} = \frac{36}{4 \times 3} = 3$$

The star of slot e.m.f.s of this winding is presented in Fig. 3-1b. When completing a path through the phase winding diagram (Fig. 3-1a), one part of the conductors is passed in the upward direction, the other part in the downward direction. For example, the conductors of the first coil of phase A in slot No. 1 are passed in the upward direction, the conductors in slot No. 10 downwards. In this case, to obtain the e.m.f. for a turn of this coil, it is necessary to subtract vector 10 from vector 1 (Fig. 3-1b). It is also possible to add to vector 1 vector $10'$, obtained from vector 10 by turning it through 180° . In accordance with this, Fig. 3-1b shows 36 slot e.m.f. vectors denoted by figures without primes, and also vectors which have been turned through 180° with respect to them and are denoted by figures with primes. To obtain the winding phase e.m.f., the vectors of the slots which are passed downwards and are denoted by figures without primes should be added.

If we agree to denote in a similar manner the sides of the coils, depending on the direction in which they are passed in completing a path around the winding diagram, the sequence of connection of the winding coils in Fig. 3-1a is as follows

$$\begin{aligned} A-1 & -10' -2 & -11' -3 & -12' - \\ & -21' -12 & -20' -11 & -19' -10 - \\ & -19 & -28' -20 & -29' -21 & -30' - \\ & -3' & -30 & -2' & -29 & -1' & -28 -X \end{aligned}$$

$$\begin{array}{l}
 B-7 \quad -16' -8 \quad -17' -9 \quad -18' - \\
 \quad -27' -18 \quad -26' -17 \quad -25' -16 \quad - \\
 \quad -25 \quad -34' -26 \quad -35' -27 \quad -36' - \\
 \quad -9' \quad -36 \quad -8' \quad -35 \quad -7' \quad -34 \quad -Y \\
 C-13 \quad -22' -14 \quad -23' -15 \quad -24' - \\
 \quad -33' -24 \quad -32' -23 \quad -31' -22 \quad - \\
 \quad -31 \quad -4' \quad -32 \quad -5' \quad -33 \quad -6' \quad - \\
 \quad -15' -6 \quad -14' -5 \quad -13' -4 \quad -Z
 \end{array}$$

If we take into consideration this winding coil connection sequence, the star of the slot e.m.f.s will have the form of three concentrated groups whose resultant vector geometrical sums have axes displaced 120° in relation to one another (Fig. 3-1c). This shows that as the result of such winding coil connection a regular three-phase system is produced.

In the winding diagram of Fig. 3-1a the phase belts forming the winding half-phases are clearly distinguished. Each of the six groups of connected coils, written in one line and forming a half-phase of the winding, has resultant e.m.f.s equal in magnitude and coinciding in phase. Such a winding makes it possible, therefore, to connect half-phases not only in series, as shown in the diagram in Fig. 3-1, but also in two and four parallel groups.

Figure 3-2a shows a diagram of a double-layer lap winding similar to that in Fig. 3-1a, but with a short pitch

$$2p = 4, \quad Z = 36, \quad q = 3, \quad y = \frac{7}{9} \tau$$

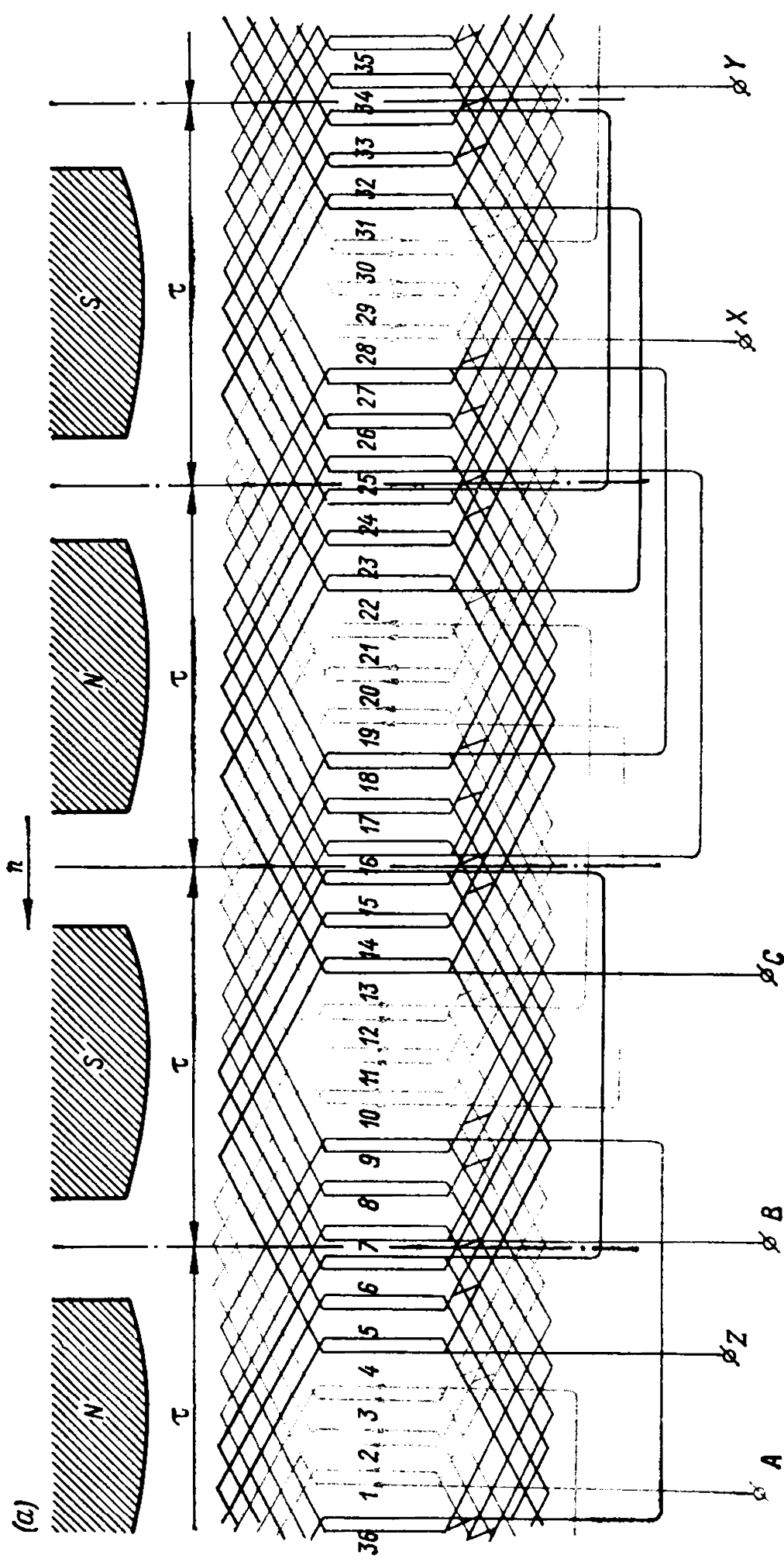
i.e., with a relative pitch $\beta = \frac{y}{\tau} = \frac{7}{9} = 0.778$.

The sequence of coil connection of this winding can be expressed as follows

$$\begin{array}{l}
 A_1-1' -8 \quad -2 \quad -9' -3 \quad -10' -X_1 \\
 X_2-19' -12 \quad -18' -11 \quad -17' -10 \quad -A_2 \\
 A_3-19 \quad -26' -20 \quad -27' -21 \quad -28' -X_3 \\
 X_4-1' \quad -30 \quad -36' -29 \quad -35' -28 \quad -A_4 \\
 B_1-7 \quad -14' -8 \quad -15' -9 \quad -16' -Y_1 \\
 Y_2-25' -18 \quad -24' -17 \quad -28' -16 \quad -B_2 \\
 B_3-25 \quad -32' -26 \quad -33' -27 \quad -34' -Y_3 \\
 Y_4-7' \quad -36 \quad -6' \quad -35 \quad -5' \quad -34 \quad -B_4 \\
 C_1-13 \quad -20' -14 \quad -21' -15 \quad -22' -Z_1 \\
 Z_2-31' -24 \quad -30' -23 \quad -29' -22 \quad -C_2 \\
 C_3-31 \quad -2' \quad -32 \quad -3' \quad -33 \quad -4' \quad -Z_3 \\
 Z_4-13' -6 \quad -12' -5 \quad -11' -4 \quad -C_4
 \end{array}$$

In Fig. 3-2a phase $A-X$ of the winding is connected in four parallel groups, but it can also be connected, as in a full-pitch winding, both in series and in two parallel groups, the latter being possible if we connect two series groups in parallel in each phase.

In general, a double-layer winding with q an integer and $2p$ similar coil groups in each phase can have such a number of parallel paths for



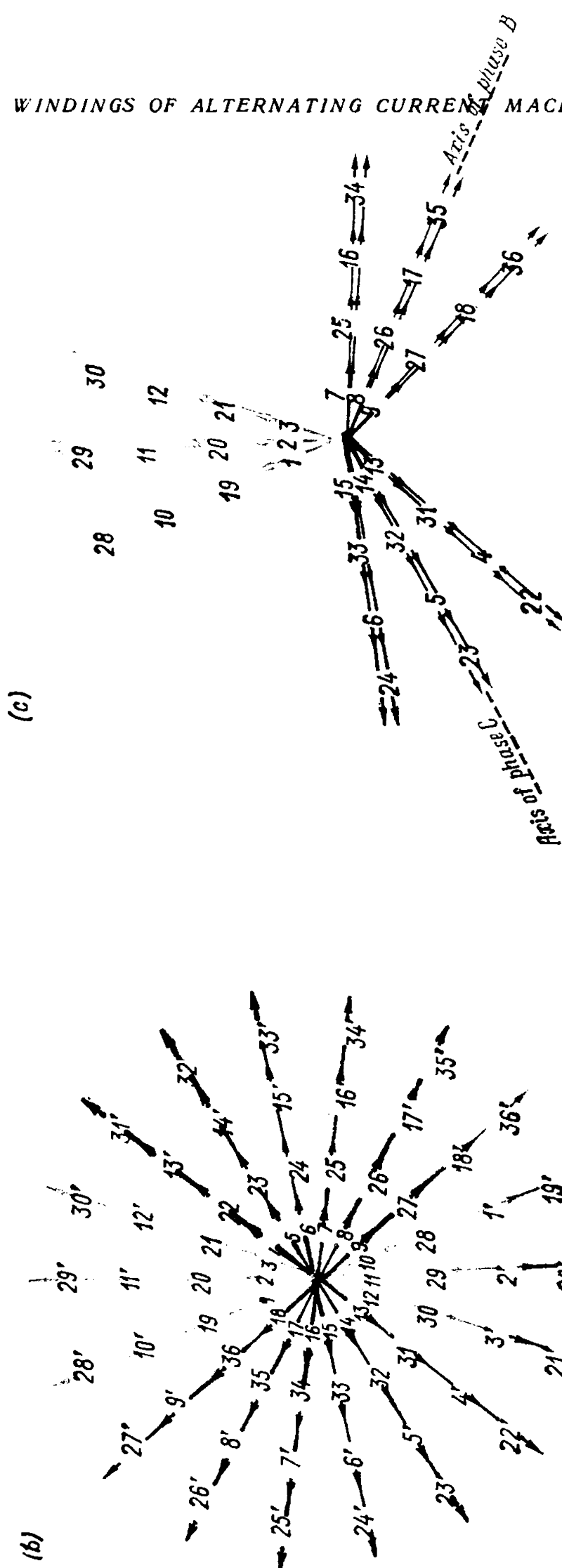
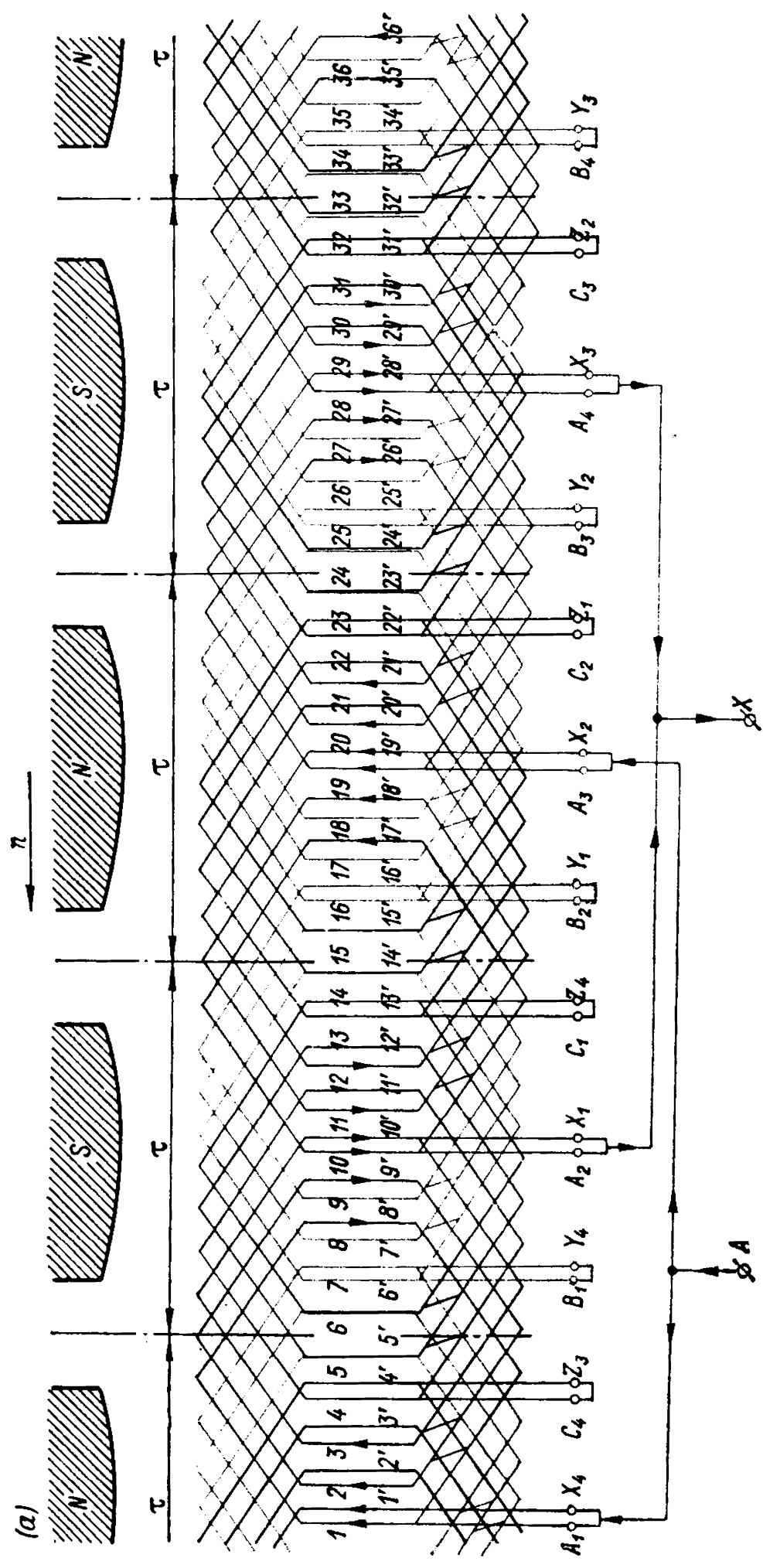


Fig. 3-1. Three-phase full-pitch double-layer lap winding with $Z = 36$, $2p = 4$ and $q = 3$:
a — winding diagram; b — star of slot e. m. f. s; c — star of winding e. m. f. s



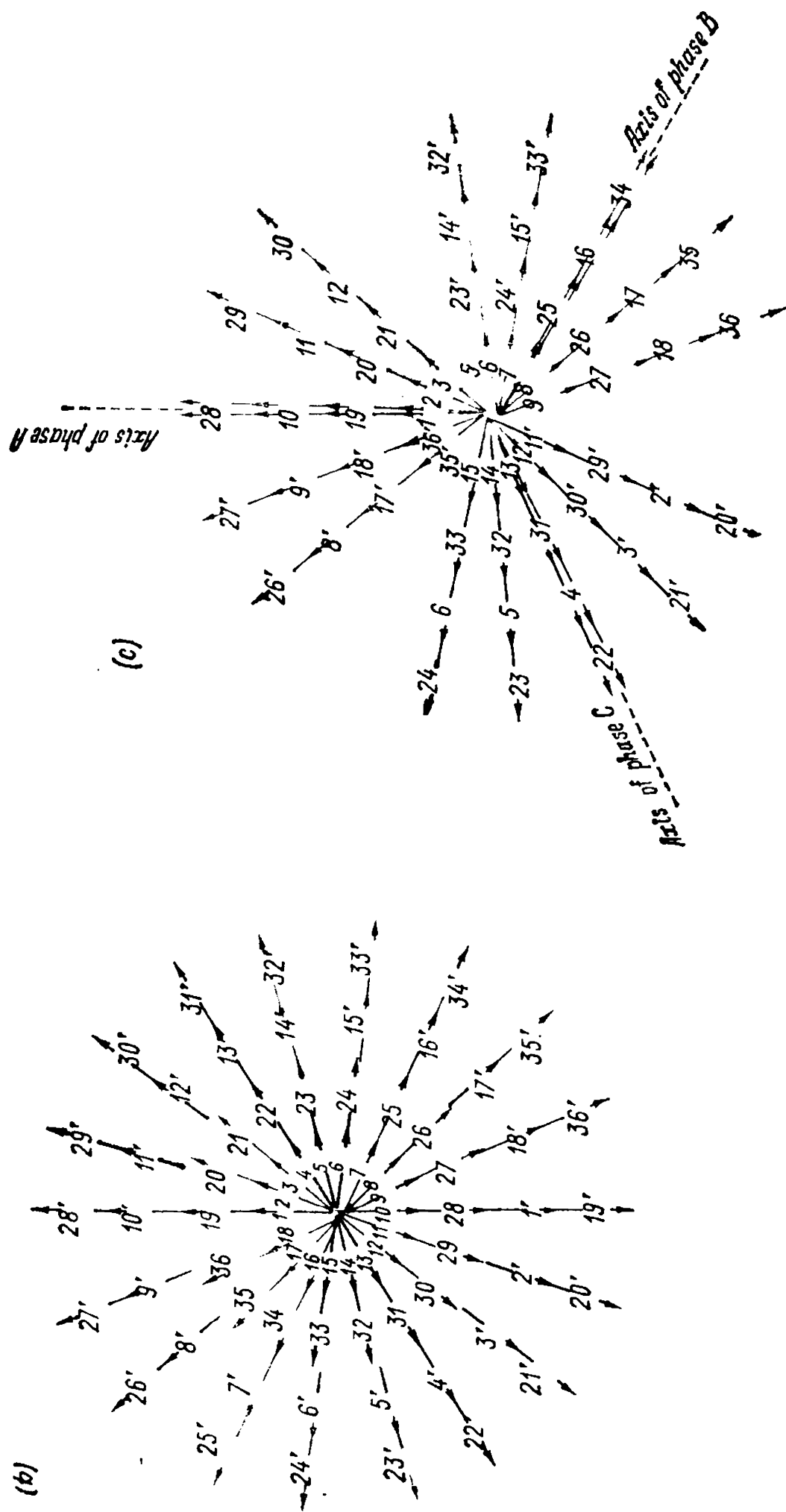


Fig. 3-2. Three-phase short-pitch double-layer lap winding with $Z = 36$, $2p = 4$, $q = 3$, $y = 7$, $\beta = \frac{7}{9}$:
a — winding diagram; b — star of slot e. m. f. s; c — star of winding e. m. f. s

which $2p:a$ equals an integer. In this case windings with $a=2$ and $a=2p$ are always possible. It is also essential that, along with equal e.m.f.s, all paths should have equal resistances and inductive reactances.

The star of slot e.m.f.s of the short-pitch winding also has 36 rays, or 18 rays per double-pole pitch, similar to that of the full-pitch winding in Fig. 3-1a. A comparison of the slot e.m.f. stars of windings with full and short pitches (Figs. 3-1b and 3-2b) shows that in the first case the ray zones of each phase are sharply set aside from the zones of the adjacent phases, and in the second case rays of adjacent phases mutually intersect, this increasing with shortening of the pitch.

Figure 3-2c shows the resultant star of slot e.m.f.s for a winding with coils connected as shown above. In this case the vector sums of the coil e.m.f.s in each phase are also displaced 120° relative to each other; therefore, again a regular three-phase winding is formed.

The end connections of both lap and wave double-layer stator windings (Sec. 3-2) are arranged on a conical surface, and are braced against radial forces when necessary by means of shrink rings made of non-magnetic materials.

At present double-layer windings of the above type find prevalent application owing to the following advantages:

1. The possibility of shortening the winding pitch by any number of tooth pitches and thus obtaining a better e.m.f. wave-form and also a better pattern of the magnetic field produced by the winding (see the following chapter).

2. Shorter end connections due to shortening of the pitch. This is accompanied by a saving in copper.

3. The possibility of forming a large number of absolutely equivalent parallel paths.

4. The simplicity of manufacturing the windings, since all the coils are of the same shape, and therefore can be form-wound.

The double-layer lap winding has the following disadvantages:

1. There are some difficulties in laying the last coils of the winding along a coil pitch due to the necessity of lifting and suspending the upper sides of the coils first laid in along the same pitch.

2. The necessity of lifting the coils of a whole pitch to get to a damaged lower coil side.

3. The impossibility of making a split stator without having to lift the coils out of the slots.

These disadvantages also apply to d.c. machine armatures. They are compensated in all types of machines, however, by the greater advantages of this winding over windings of other types.

In low-power induction motors, for greater convenience, the first coils are laid only in the lower part of the slots, while the last coils to be laid are arranged only in the upper parts of the slots. Though this leads to a slight asymmetry, it eliminates the necessity of holding the upper sides of the first-pitch coils when laying the last coils.

3-2. Three-Phase Double-Layer Wave Windings with q an Integer

In the lap windings discussed above the winding sections can be joined in series only by means of special connections between the coils. Since for each double-pole pitch two series-connected elements are obtained in each phase, the number of connections between coils in multiple-pole machines becomes very large; in bar-type windings (with single-turn coils) having turns of large cross-section this results in a great additional expenditure of copper. By applying the principle of the d.c. type wave winding, it is possible to obtain automatic connection of the conductors forming a phase without any intercoil connections. The usual type of d.c. wave winding, however, is impracticable, since to make a.c. windings it is necessary that the total number of coils, equal to the number of slots, should be divisible by three, while the formula for the resultant pitch of a d.c. wave winding

$$y_{res} = \frac{Z \pm 1}{p} = \frac{6pq \pm 1}{p}$$

does not satisfy this condition.

The winding used to obtain an a.c. wave winding has a resultant pitch equal to $y_{res} = \frac{Z}{p} = 6q$ which gives no displacement in a magnetic field when completing a path through the wave winding under different poles; but when the wave returns to the initial conductor, it artificially fails to close on itself by one bar, forward or backward, after which it begins a new path with the same pitch y_{res} , etc. A wave winding made according to this principle has two separate split sections and one intercoil connection per phase for any number of poles. This type of winding is used, for example, in the 15000-kW, 6000-V "Elektrosila" hydrogenerator with $Z=180$, $N_s=2$, $q=3$, $2p=20$ and pitches $y_{res} = \frac{180}{10} = 18$, $y_1=8$ and $y_2=10$. Here N_s is the number of effective conductors per slot.

It should be noted that wave windings with a short pitch, as well as lap windings, improve the electrical characteristics of a machine, but do not save copper in the end connections. Indeed, as in the above hydrogenerator, shortening of the front pitch in comparison with the diametral pitch to $y_1 = \frac{8}{9}\tau$ results in a corresponding increase of the back pitch to $y_2 = \frac{11}{9}\tau$, and the total length of the end connections does not change.

Wave windings with an integer number of slots per pole per phase are used most widely in the rotors of slip-ring induction motors, since fixed standard voltages are not required in this case, thus making possible extensive use of the bar-type winding. This simplifies winding manufacture and results in better utilization of the slot space

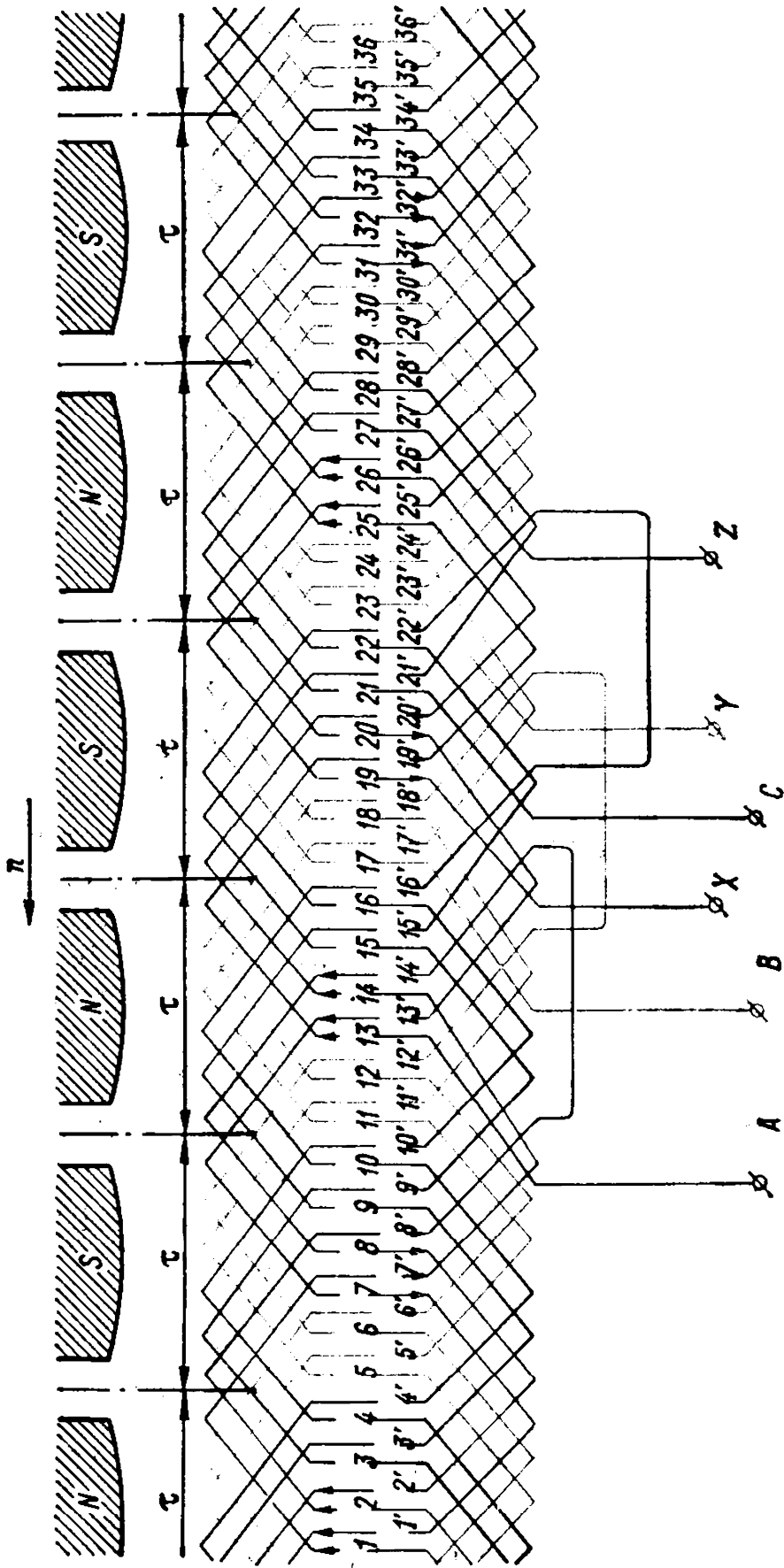


Fig. 3-3. Diagram of three-phase full-pitch double-layer wave winding with $Z = 36$, $2p = 6$, $q = 2$

owing to the decrease in the quantity of insulation. Rotor wave windings are usually wound with a diametral pitch.

Figure 3-3 shows a diagram of a full-pitch wave winding with $2p=6$, $Z=36$, $N_s=2$, $q=2$, $y_{res}=36:3=12$, $y_1=6$ and $y_2=6$.

3-3. Three-Phase Single-Layer Windings with Coils of Equal Width

Single-layer windings were extensively used in the past, but at present they have been almost completely replaced by double-layer windings and find application only in certain special cases. A great number of machines with single-layer windings are still in operation however.

Here the basic single-layer windings with equal-width coils are discussed. All the coils of these windings are similar in shape and may be wound on a common form. Such windings, for this reason, are also referred to as form-wound windings. These windings have the advantage that their pitch can be shortened, but, as in all single-layer windings, difficulties are encountered in arranging the end connections, since the winding is laid in the slots in one layer, while the end connections, owing to the intersection of their conductors, must be arranged in two (or more) planes.

Single-Layer Involute Windings. The simplest way to design a single-layer winding with equal-width coils is as follows.

If we double the number of slots or halve the number of coils in a double-layer lap winding and lay one active coil side in each slot so that the starts and finishes of the coils alternate, and the end connections alternatively go to the left and to the right, we obtain a single-layer lap winding.

Figure 3-4a shows a short-pitch single-layer lap winding with $y=\frac{9}{12}\tau$, $2p=4$, $Z=48$ and $q=4$. The star of slot e.m.f.s of this winding, with 24 rays per double-pole pitch, is pictured in Fig. 3-4b.

The pitch of a single-layer winding can be shortened only by an even number of tooth pitches. This winding is used mainly for bar windings where the bars and end connections are manufactured separately, and soldered together when the winding is laid in the slots.

The end connections of the winding considered above are arranged in two planes perpendicular to the machine axis, namely: the winding end-connection conductors inclined in Fig. 3-4a in one direction are in one plane, and those inclined in the other direction are in another plane. The conductors of the end connections are bent according to an involute curve, hence the name given to this winding. Such windings were widely used in former types of "Elektrosila" turbogenerators, and in a number of types of synchronous machines made in other countries.

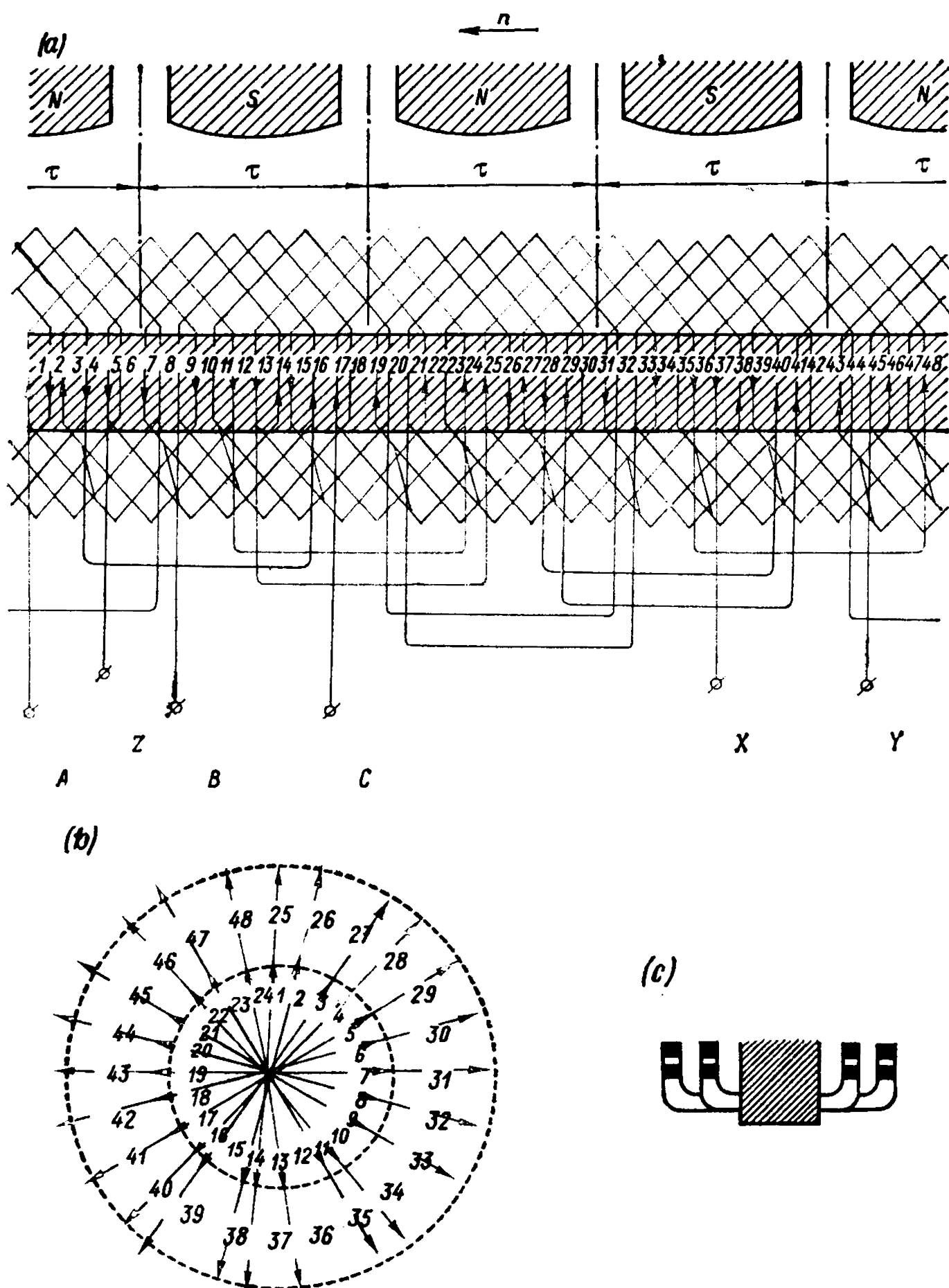


Fig. 3-4. Three-phase short-pitch single-layer involute lap winding with $Z = 48$,
 $2p = 4$, $q = 4$, $y = 9$, $\beta = \frac{9}{12}$:

a — winding diagram; *b* — e. m. f. star; *c* — arrangement of end connections

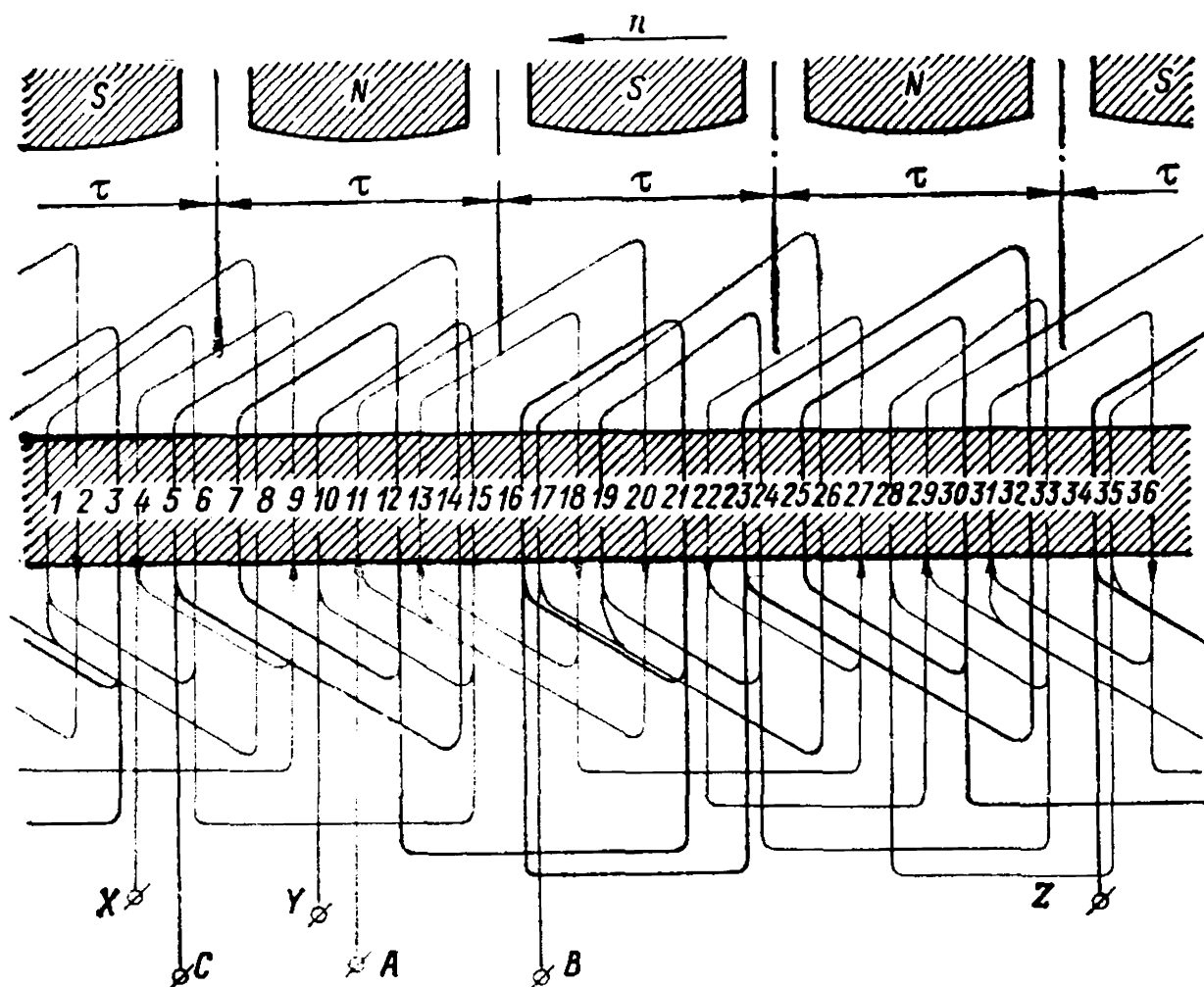


Fig. 3-5. Diagram of three-phase chain winding with $Z = 36$, $2p = 4$, $q = 3$, $y = 7$

When computing the distribution factors for windings of this type, it must not be forgotten that each coil group of such a winding contains $\frac{q}{2}$ coils, therefore, in formulas (2-15) and (2-17) $\frac{q}{2}$ is substituted for q .

Chain Winding. In low-power induction machines, where single-layer windings wound similar to those shown in Fig. 3-4 are sometimes used, the end connections are given another shape, since in this case the coils are multiturn, and when laid are easily deformed ("soft"). The diagram of such a winding with $m=3$, $Z=36$, $2p=4$, $q=3$ and $y=\frac{7}{9}\tau$ is shown in Fig. 3-5. The winding in Fig. 3-5 differs from that in Fig. 3-4 only in the shape of its end connections.

The winding in Fig. 3-5, owing to the appearance of the end connections, is referred to as a "chain" winding. Figure 3-6 shows an induction motor stator with a partly wound chain winding.

Single-Layer Mush Winding. Single-layer windings of the types discussed above can also be made, with even values of q , with the end connections of $\frac{q}{2}$ coils bent to one side and those of the adjacent $\frac{q}{2}$

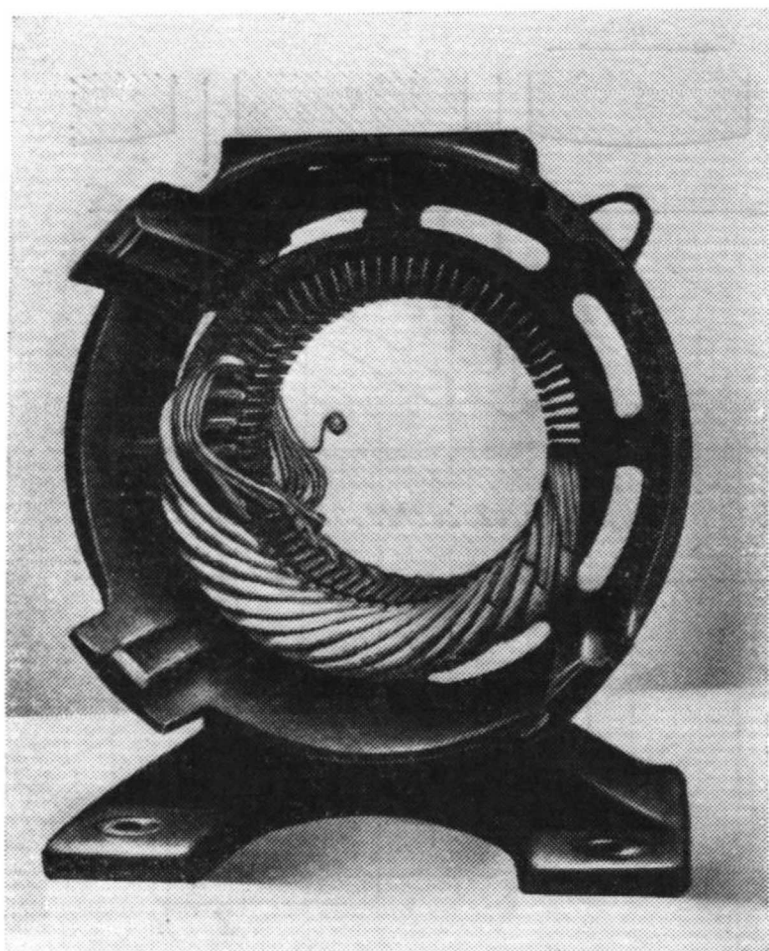


Fig. 3-6. Stator of an induction motor partly wound with a chain winding

coils bent to the other side, etc. Although their coil pitches are, in space, less than a pole pitch, these windings have, essentially, the electrical properties of full-pitch windings, since the belts of the different phases do not intersect, and all the conductors of a given phase could also be reconnected into turns and coils with a full pitch. Therefore, in computing the winding factors of these windings, their pitches should be considered full, and q taken equal to the actual number of slots per pole per phase. A diagram of a mush winding for $m=3$, $2p=4$, $Z=48$ and $q=4$ is presented in Fig. 3-7.

The end connections of these windings are arranged in the same way as those of the windings of Fig. 3-5. Since the coil pitch in this case is shortened in space, the end connections are shorter than in full-pitch coils, this being an advantage of mush windings over full-pitch windings.

The single-layer windings discussed above also allow the winding to be wound with p , and in part with $2p$, equal parallel branches.

3-4. Three-Phase Single-Layer Concentric Windings with a Whole Number of Slots per Pole per Phase

These windings were previously widely used in synchronous and induction machines, but today they are rarely used, and only in low-power machines.

Three-Phase Two-Tier Winding. Figure 3-8a shows a developed schematic diagram of this type of winding with $2p=6$ and $q=2$.

The star of the slot e.m.f.s of the winding, consisting of twelve rays per double-pole pitch, is shown in Fig. 3-8b.

As can be seen from Fig. 3-8a, the coil groups of the winding consist of concentric coils of different width which gave rise to their name. Since the end-connections of the winding are in two planes or tiers,

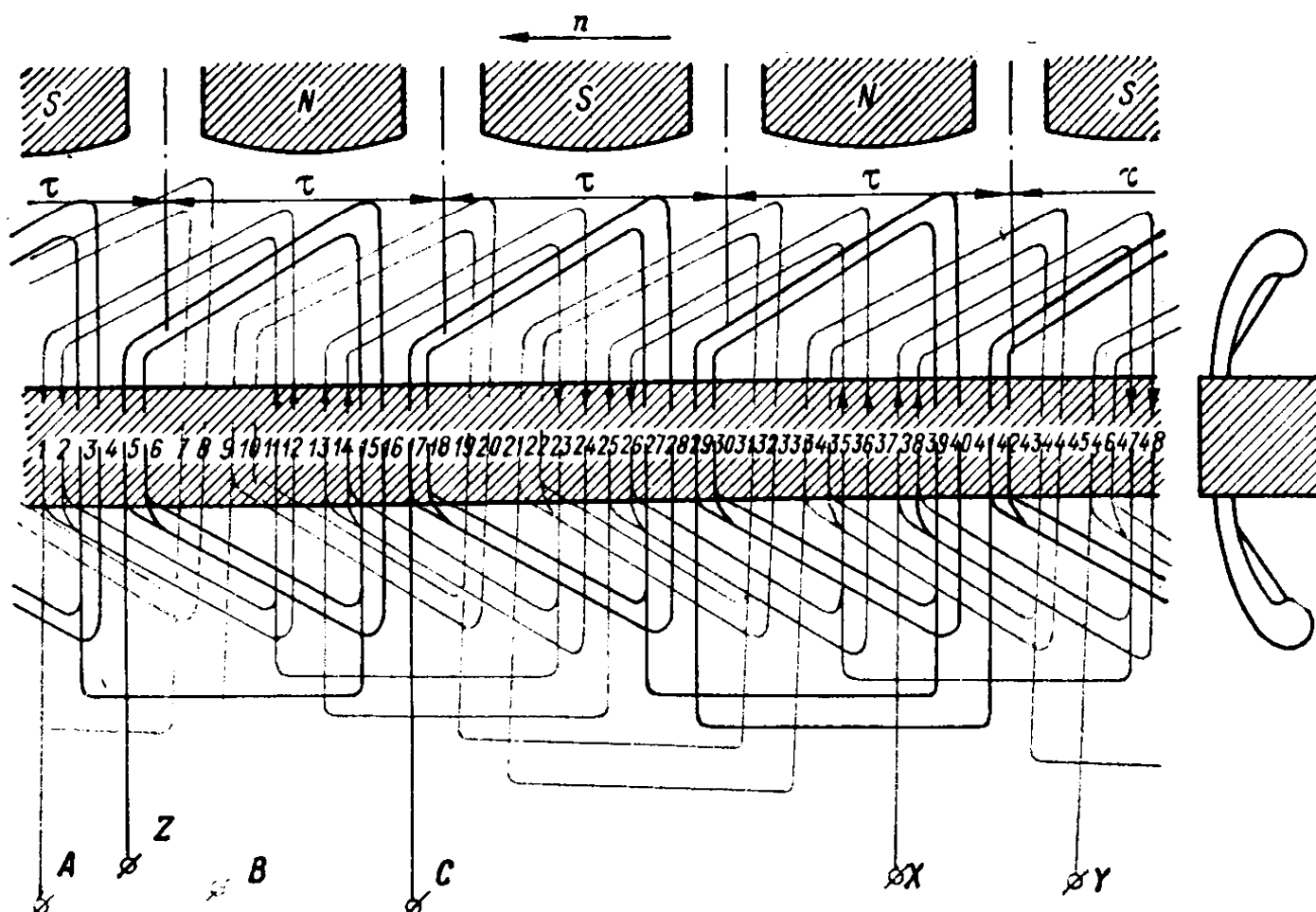


Fig. 3-7. Diagram of three-phase single-layer mush winding with $Z = 48$, $2p = 4$, $q = 4$

all q coil groups coming out of the slots go to one side. The end connections in the "short" and "long" tiers come out of the slots at different angles. In certain cases the coil sides in the "long" tier may be left unbent, as shown in Fig. 3-8c.

With an even number of pole pairs, the winding consists of an equal number of long and short coils. With an odd number of pole pairs (for example, $p=3, 5, 7$), one coil should be crank-shaped with the end connection bent in a special way (Fig. 3-8a), as in this case an odd number of coil groups is used in the machine ($mp=3p$). The presence of such a crank-shaped coil is undesirable because of certain difficulties in manufacture and in repairs, and also because of difficulties encountered when it is necessary to form parallel groups.

Straight winding coils (Fig. 3-8a) are quite easy to repair, since they may be unwound without disturbing the adjacent undamaged coils. If a curved coil must be repaired, it is first necessary to unwind two adjacent undamaged straight coils, and only then can the damaged curved coil be unwound and then rewound.

This type of winding requires a relatively large amount of copper, because its end connections are longer, their length being approximately $l_{end} = (2.4 \text{ to } 2.6)\tau$.

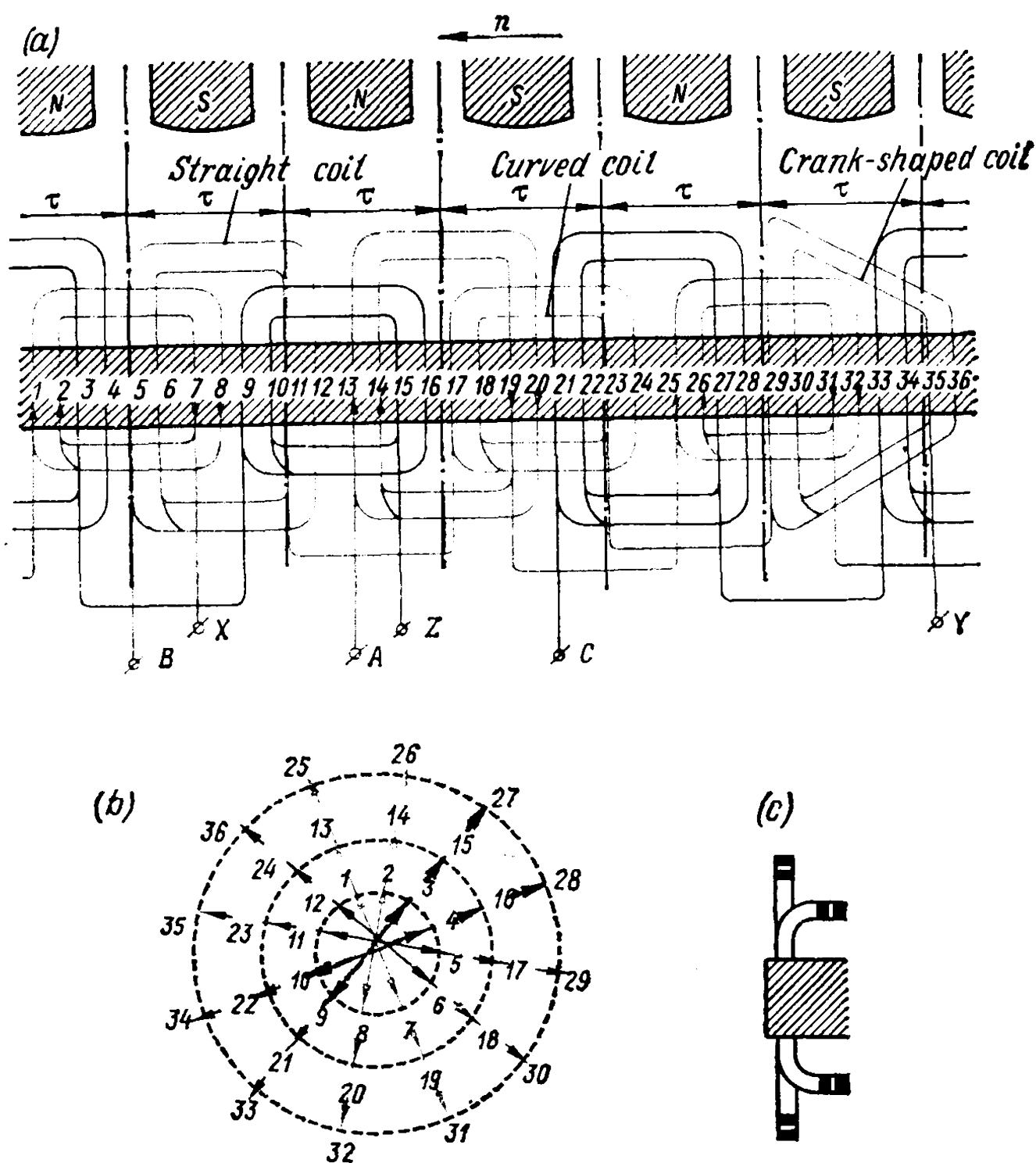


Fig. 3-8. Three-phase concentric two-tier winding with $Z = 36$, $2p = 6$, $q = 2$:
 a — winding diagram; b — e. m. f. star; c — end-connection arrangement

In concentric windings, difficulties arise when forming parallel branches, because coils of different shape have different resistances and inductive reactances, and the branches are therefore unequally loaded by the current.

Although the coils of concentric windings differ in pitch, these windings are essentially always full-pitch ones, because their phase belts do not intersect, and it is possible to reconnect all the phase conductors into full-pitch turns.

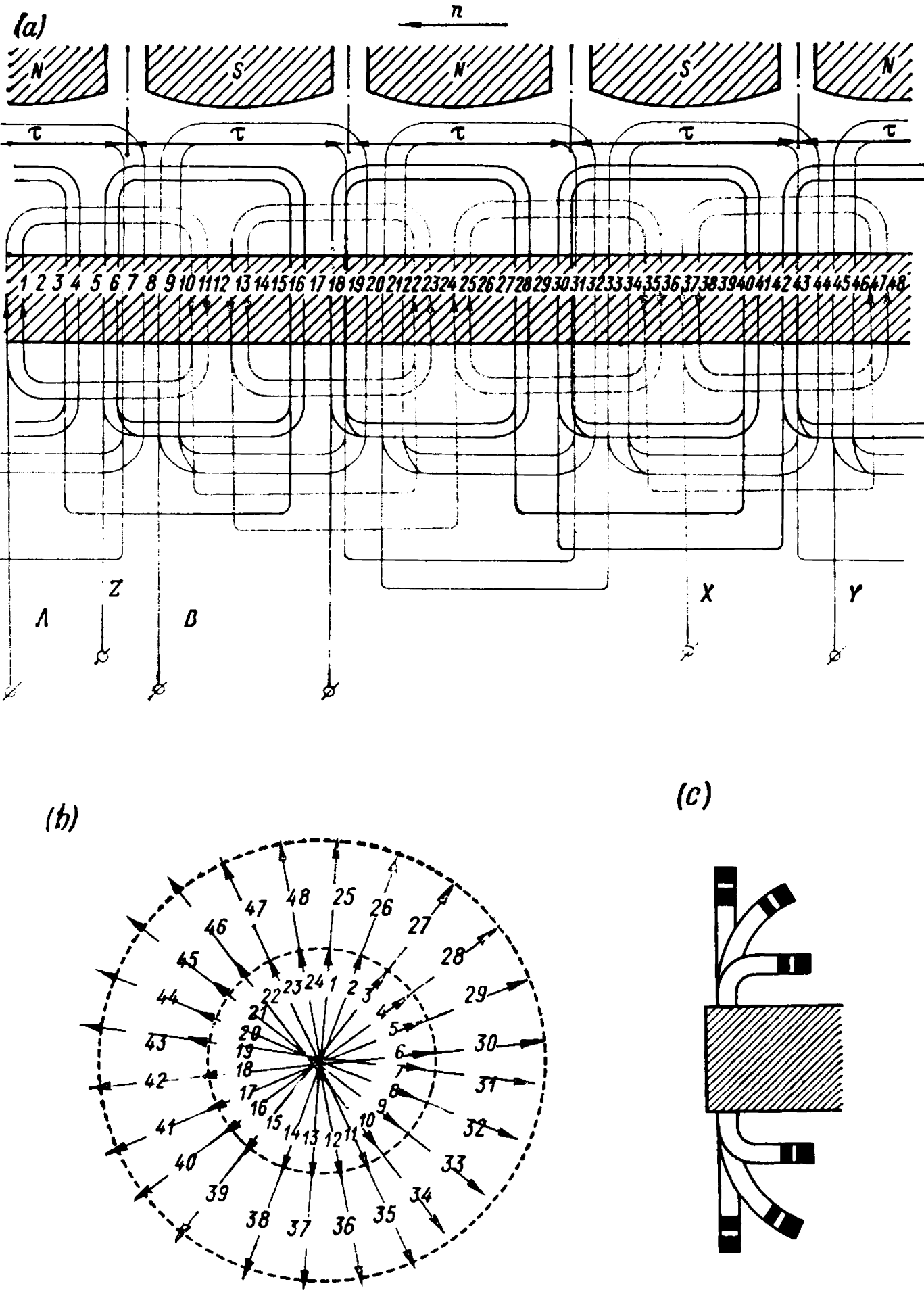


Fig. 3-9. Three-phase concentric three-tier winding with $Z = 48$, $2p = 4$, $q = 4$;
a — winding diagram; b — e. m. f. star; c — end-connection arrangement

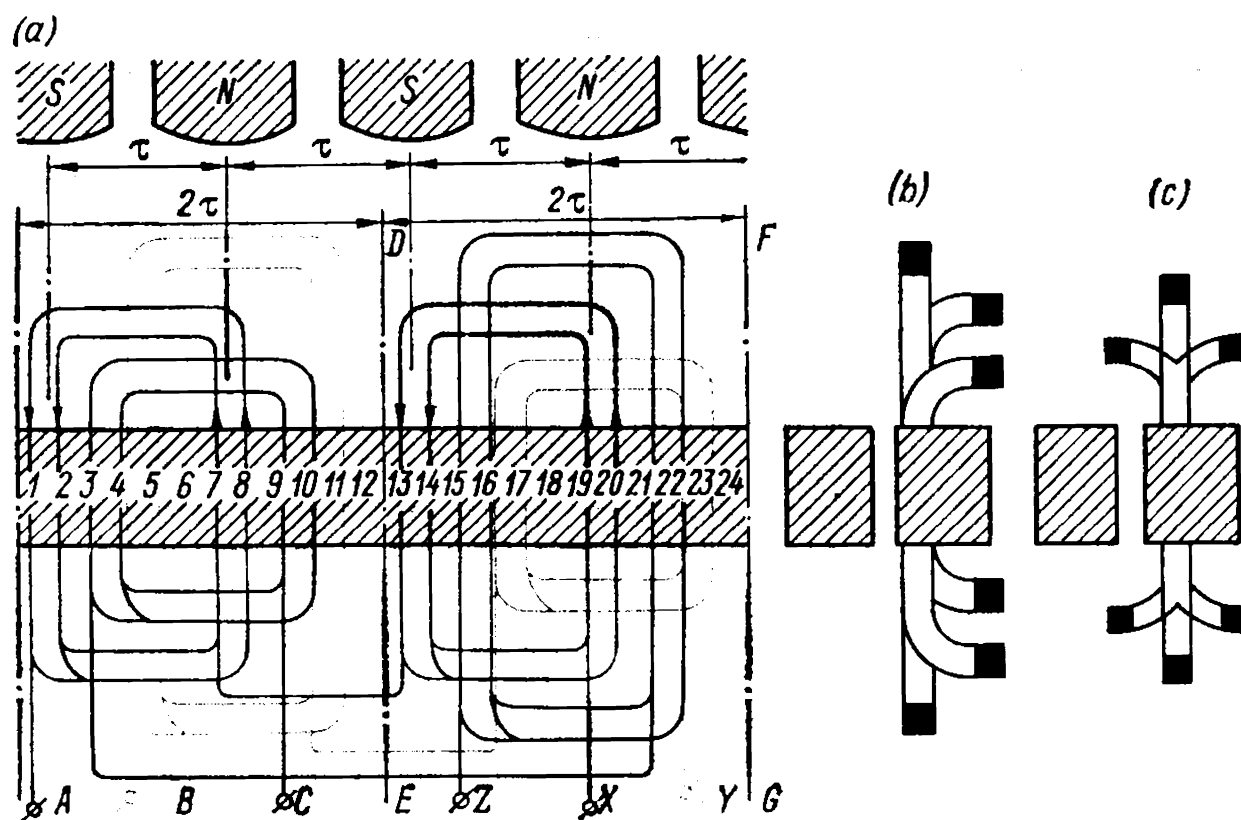


Fig. 3-10. Three-phase concentric three-tier winding for split stator with $Z = 24$, $2p = 4$, $q = 2$:

a — winding diagram; *b* and *c* — end-connection arrangement

Three-Phase Three-Tier Winding. A three-tier winding is generally used for an even number of slots per pole per phase q , which makes it possible to divide the group of coils belonging to one phase belt at the end connection into two halves with $\frac{q}{2}$ coils in each half, and to bend the group coils to go in opposite directions (Fig. 3-9a), and not in one direction, as with a two-tier winding (Fig. 3-8a). The end connections of the winding must be arranged in three tiers, as shown in Fig. 3-9c. The mean coil pitch of a three-tier winding is less than that of its two-tier counterpart, and therefore has somewhat shorter end connections.

The three-tier winding was often used in foreign-made motors and generators designed with $2p=2$ poles.

Three-Phase Three-Tier Winding for Split Stators. Figure 3-10a shows a winding diagram for $2p=4$ and $q=2$. In this winding, as in the two-tier type (Fig. 3-8a) all the coils of the slots belonging to the same phase belt are bent to the same side at the end connections, and not to both sides as in a conventional three-tier winding (Fig. 3-9a). This results in very uneven distribution of the conductors in the end connections, but provides the stator with a splitting line along which the coils remain intact and only the intercoil connections are cut. Lines *DE* and *FG* in Fig. 3-10a are convenient places for splitting the stator frame. Here it is necessary only to disconnect the intercoil

connections, without disturbing the main coils, which is impossible in other types of windings. In the winding considered above, however, the increased overhang of the end connections leads to a greater end-shield overhang with a consequent increase in machine length.

Figure 3-10*b* and *c* shows the arrangement of the coil end connections in the winding under consideration. Since with a split stator there is no necessity of removing the rotor in an axial direction, the coils of one phase may be bent towards the rotor; this makes it possible to shorten somewhat the length of the end connections, as can be seen from a comparison of the end connections in Fig. 3-10*b* and *c*.

3-5. E.M.F.s Due to Tooth-Ripple Harmonics

In Chapter 2 the fundamental and higher field harmonics produced by the excitation system of a synchronous machine were considered for the case when the stator surface is smooth, i.e., has no slots. Actually the slots distort the form of the excitation field by creating so-called tooth ripples, which also induce e.m.f.s in the stator winding.

Consider a rather ideal case where the excitation system of a synchronous machine produces, in the absence of stator slots, a rectangular field wave having a height B_{max} . With slots in the stator (Fig. 3-11*a*), the field has the form shown in Fig. 3-11*b* by the solid line. We may consider this curve to be the result of summation of a rectangular wave with a height B_{av} (Fig. 3-11*c*) and a tooth-ripple curve (Fig. 3-11*d*). Thus

$$B_{av} = \frac{B_{max}}{k_\delta}$$

where k_δ is the air-gap factor.

The rectangular wave with the height B_{av} contains, and in the same ratio, all the harmonics which are present when there are no slots on the stator. All these field harmonics rotate at the same speed as the rotor, and the e.m.f.s induced by them were discussed earlier. As to the magnitude of these e.m.f.

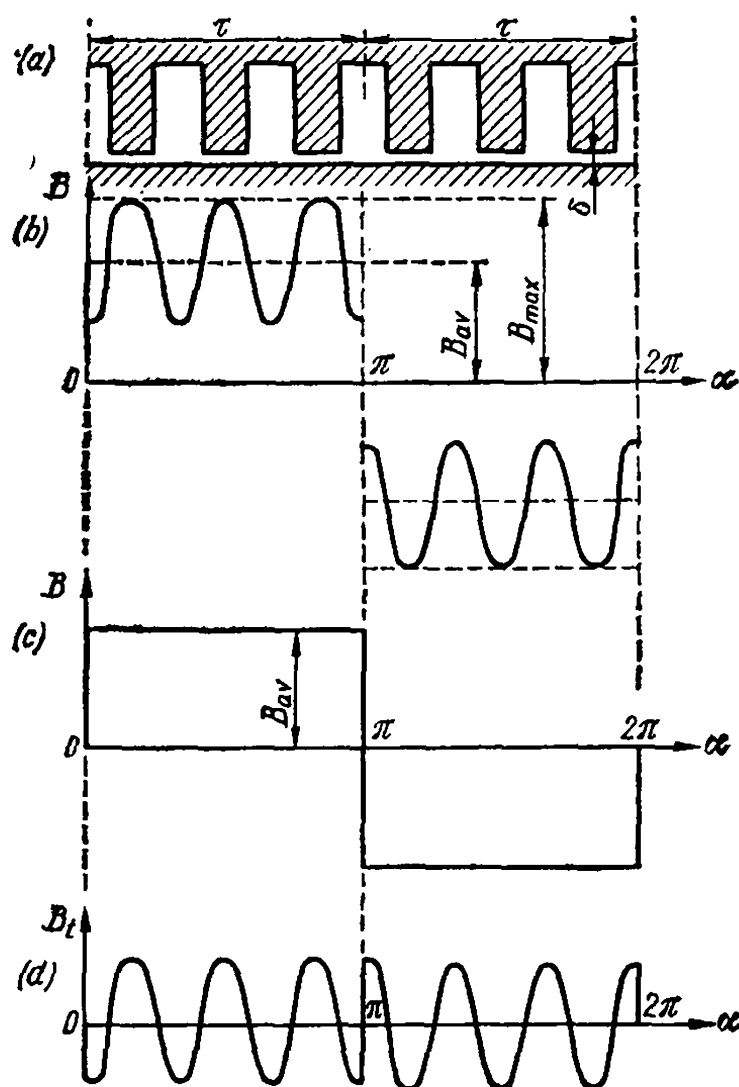


Fig. 3-11. Tooth ripples in air-gap

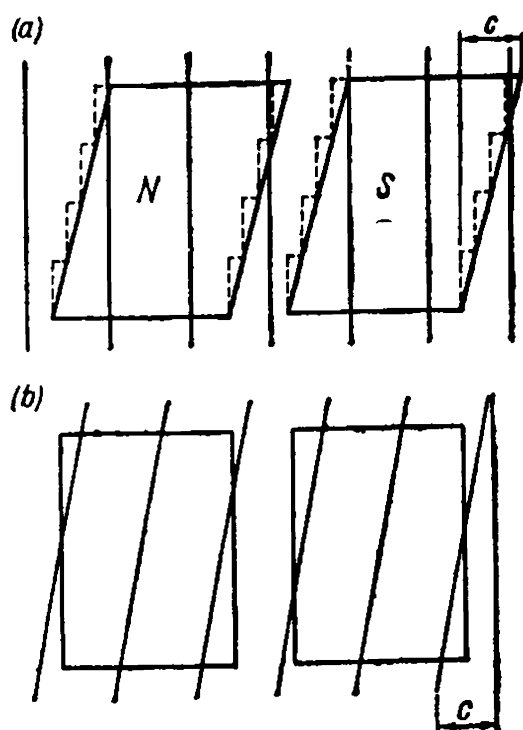


Fig. 3-12. Skewed poles (a) and slots (b) in a synchronous machine

the harmonics of this curve travel relative to the stator at different speeds, and induce e.m.f.s of different frequency in the stator winding.

The tooth ripples of the order $v_t = 2Qk \pm 1$, which induce e.m.f.s with the frequency $v_t f_1$ in the winding, are the most harmful, since these field harmonics have the greatest amplitudes, and with an integral q , as was shown previously, the winding factors for these harmonics are equal to the winding factor of the fundamental harmonic. Hence the winding does not suppress these e.m.f. harmonics when q is an integer. Tooth ripples can be effectively minimized by employing fractional q windings discussed below in Sec. 3-6. In addition, a considerable reduction of these e.m.f. harmonics can be obtained by skewing the pole shoes or stator slots by one stator-tooth interval.

Figure 3-12a gives a plan view of skewed pole shoes and Fig. 3-12b skewed stator slots. When the poles and pole shoes are assembled of stamped steel laminations, the shoes can easily be skewed in steps as illustrated by the dotted lines in Fig. 3-12a.

When the shoe or slot is skewed by some value c (Fig. 3-12b), the e.m.f.s induced in a series of consecutive points along a conductor are shifted in phase. The vector diagram of these e.m.f.s can be represented by an arc with a central angle $\frac{c}{\tau}\pi$ (Fig. 3-13). The vector sum of these e.m.f.s is represented by chord AB . It is necessary, therefore, to introduce into the formula of the e.m.f. an additional pole-shoe skew factor, equal to the ratio of the length of chord AB to the length of arc AB . Hence, for the first harmonic and for harmonics of any order

harmonics, the presence of teeth on the stator only decreases it. The decrease is determined by the air-gap factor.

The tooth ripples shown in Fig. 3-11d are more complex. This curve, having a period of 2π or two pole pitches, is symmetrical about the axis of abscissas, i.e., the section of the curve between $\alpha = \pi$ and $\alpha = 2\pi$, displaced one half-period to the left, is a mirror image of the section between $\alpha = 0$ and $\alpha = \pi$ with respect to the axis of abscissas. Therefore, the curve in Fig. 3-11d contains only odd harmonics ($v = 1, 3, 5, \dots$). Of greatest significance are, obviously, the harmonics of the order $v = 2Q \pm 1$. (Fig. 3-11a is for $2Q = 6$).

When the rotor poles travel relative to the stator, the shape of the curve in Fig. 3-11d changes. This means that

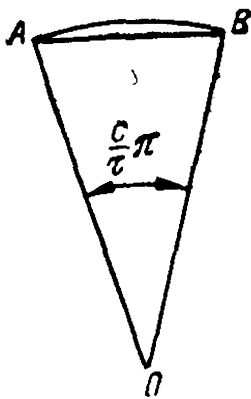


Fig. 3-13. To determination of pole-shoe skew factor

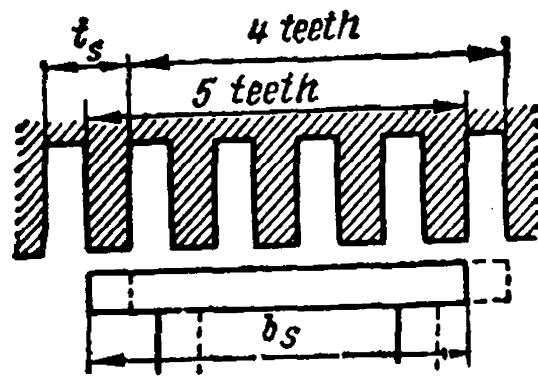


Fig. 3-14. Variation of air-gap permeance with $b_s = 4.5t_s$

v we have

$$k_{sk1} = \frac{\sin \frac{c}{\tau} \frac{\pi}{2}}{\frac{c}{\tau} \frac{\pi}{2}}, \quad k_{skv} = \frac{\sin \frac{vc}{\tau} \frac{\pi}{2}}{\frac{vc}{\tau} \frac{\pi}{2}} \quad (3-1)$$

Pole-shoe skewing obviously plays the same role as winding distribution or pitch shortening. With $c=t_{l1}$, the coefficient k_{sk1} is almost equal to unity, while k_{skv} for the tooth harmonics becomes very small, owing to which these harmonics are weakened in the e.m.f. curve.

Higher harmonics are also induced in an e.m.f. curve by longitudinal oscillations of the magnetic flux, a state which may develop under certain conditions.

To better understand this phenomenon, assume that $m=3$ and $q=2$; then $Q=mq=3 \times 2=6$ slots. If the pole arc is equal to 4.5 tooth intervals, then in the pole position shown in Fig. 3-14 by a solid line five teeth will be under the pole shoe, while in the position shown by dotted lines—only four teeth. This leads to a change in air-gap permeance and, consequently, to pulsations of the magnetic flux. When designing a machine, the possibility of such a phenomenon should be precluded, owing to the growth of additional losses in the steel caused by high-frequency oscillations of the flux.

3-6. Three-Phase Fractional-Slot Windings

General Principles of Arranging Fractional-Slot Windings. Synchronous generators with a small whole number of slots per pole per phase ($q=1, 2, 3$) may have appreciable tooth harmonic e.m.f.s induced in the stator windings, since in windings with q an integer the corresponding winding elements of each phase under different poles occupy similar positions with respect to the pole axis; the higher e.m.f. harmonics of all groups of the winding phase therefore add algebraically and their full magnitude participates in the resultant e.m.f.

of the entire machine. If a winding is wound with a fractional number of slots per pole per phase q , and has a sufficiently well selected fractional coefficient, the separate elements of the winding belonging to a given phase may be under different poles, in different positions relative to the magnetic field. The displacement of these elements relative to the pole axis may be chosen so that the winding factor for the fundamental wave will be reduced very insignificantly, but the winding factors for the higher harmonics are reduced to such a small value in comparison with these factors for a winding having q the nearest integer that the magnitude of the harmonics with respect to that of the fundamental e.m.f. wave may become quite negligible.

As is known, windings with a whole number of slots per pole per phase (integral-slot windings) are a.c. windings in which all the phase belts have the same number of slots. Windings having in different belts of the same phase a number of slots differing by unity are referred to as fractional-slot windings. The coil groups (belts) of each phase with a number of slots differing by unity must be symmetrically distributed around the machine periphery.

To arrange a multiphase winding with a fractional q , the resultant e.m.f.s of the separate phases should be equal in magnitude and shifted in phase relative to each other by $\frac{2\pi}{m}$.

It is best to investigate a winding with a fractional q proceeding from the star of the slot e.m.f.s.

The fractional number of slots per pole per phase is given by

$$q = a + \frac{b}{c} = \frac{ac + b}{c} \quad (3-2)$$

where a , b and c are integers, $\frac{b}{c}$ being a proper fraction with co-prime numbers. As will be seen from the following examples, the denominator c of the winding fraction is the divisor of the number of pole pairs. In a three-phase machine it must not be equal to or divisible by three, since only in this case will the coil groups differing in number of slot bars be uniformly arranged among the phases.

To make a winding with a fractional q , with completely filled stator slots, the number of slots in each phase of the winding arranged under poles of the same sign should be the same; this leads to the condition

$$\frac{Z}{2m} = \gamma = \text{integer}$$

If the number of slots Z and the number of pairs of poles p have a greatest common factor t , then, after arranging a winding section over $\frac{p}{t}$ pole pairs, we meet slot bars having respectively the same e.m.f. phase as in the initial group; therefore, the winding will have t

slot bars of equal phase and will make it possible to form t parallel groups.

With an even number of slots Z , and the greatest common factor of $t > 1$, after arranging a winding section over $p : 2t$ pole pairs, we meet slot bars with e.m.f.s displaced 180° with respect to the e.m.f. of the slot bars of the initial group. Such a winding makes it possible to form $2t$ parallel groups, the slot-bar groups with e.m.f.s displaced 180° with respect to the fundamental e.m.f. being joined to the common junctions not at their starts, but at their finishes.

To be able to form an m -phase winding, the number of slots not coinciding in phase which enter each simple winding of $\frac{Z}{t}$ slots must be divisible by m , therefore

$$\frac{Z}{tm} = \text{integer}$$

but since $\frac{Z}{2m} = \gamma$, we have the condition

$$\frac{2\gamma}{t} = \text{integer}$$

When plotting a star of slot e.m.f.s, account should be taken of the following conditions.

The electrical angle between the e.m.f.s of bars in two adjacent slots is

$$\alpha = \frac{p \times 360^\circ}{Z} = \frac{p \times 360^\circ}{2pmq} = \frac{180^\circ}{mq} \quad (3-3)$$

and with $m=3$

$$\alpha = \frac{60^\circ}{q} = \frac{c \times 60^\circ}{ac + b} \quad (3-4)$$

When Z and p are mutually prime numbers ($t=1$), the winding has no slots with e.m.f.s, coinciding in phase, therefore the least possible phase shift between the e.m.f.s of any two slots is equal to

$$\alpha' = \frac{360^\circ}{Z} \quad (3-5)$$

If we plot the star of slot e.m.f.s, then α' is the angle between adjacent e.m.f. vectors.

When the numbers Z and p have a greatest common factor t , the winding has t slots of the same phase. Here the winding may be divided into t simple windings, each with $\frac{Z}{t}$ slots. The angle α' between adjacent e.m.f. vectors in the star is therefore equal to

$$\alpha' = \frac{t \times 360^\circ}{Z} \quad (3-6)$$

Fractional-slot windings may be single-layer and double-layer. The latter, in turn, may be designed like lap and wave split d.c. armature windings. Double-layer windings have the advantage over single-layer ones in that they allow the use of form-wound coils placed in open stator slots. Some examples of double-layer fractional-slot windings will be examined below, since single-layer fractional-slot windings are practically not used in new machines at present.

Fractional-Slot Lap Windings. Let us examine the features of this type of winding, taking as an example a winding with $Z=30$, $2p=8$, $m=3$. The greatest common factor of Z and p is $t=2$. The number of slots per pole per phase is

$$q = \frac{Z}{2pm} = \frac{30}{8 \times 3} = 1 \frac{1}{4}$$

with $a=1$, $b=1$ and $c=4$. The electrical angle between adjacent slots is

$$\alpha = \frac{p \times 360^\circ}{Z} = \frac{4 \times 360^\circ}{30} = 48^\circ$$

The angle between adjacent vectors of the star of slot e.m.f.s is

$$\alpha' = \frac{t \times 360^\circ}{Z} = \frac{2 \times 360^\circ}{30} = 24^\circ$$

If we take into account that the e.m.f. of the lower conductors is displaced 180° with respect to the upper ones, then, for an odd number of e.m.f. vectors their number is doubled and the angle between adja-

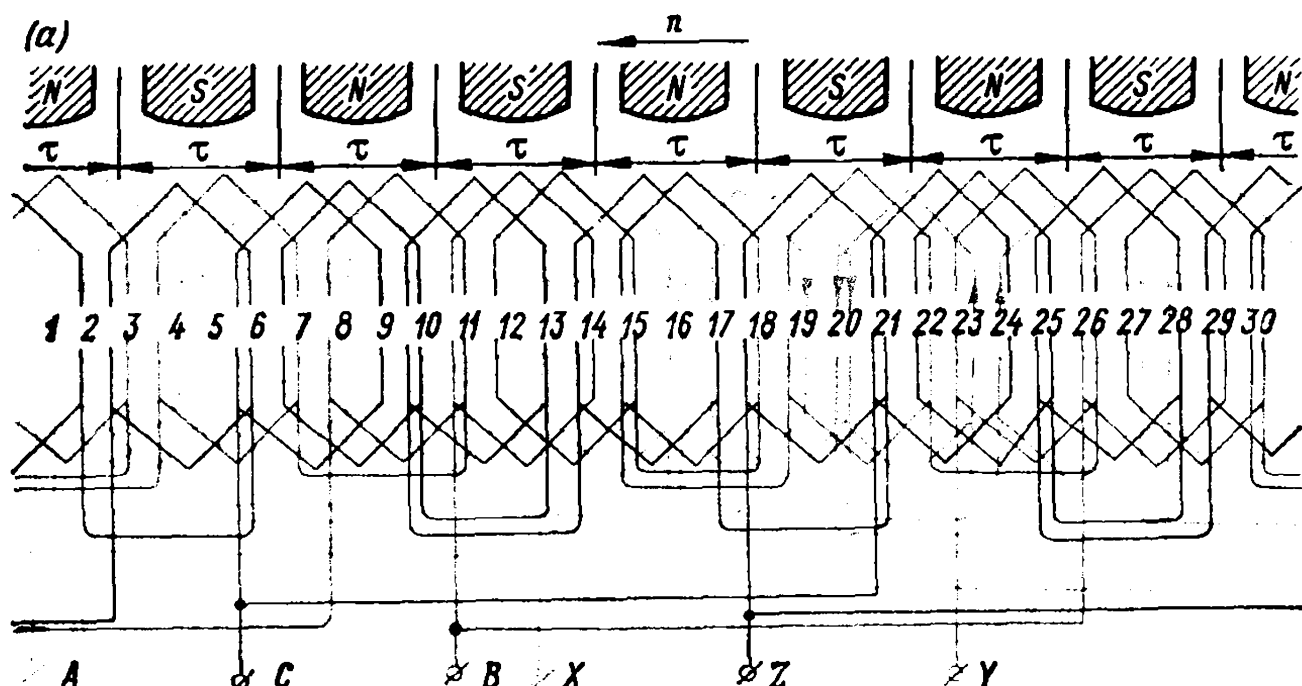


Fig. 3-15. Three-phase double-layer lap fractional-slot winding with $Z = 30$,

$$2p = 8, q = 1 \frac{1}{4}, y = 3, \beta = \frac{3}{3 \times 1 \frac{1}{4}} = 0.8:$$

a — winding diagram; b — star of slot e. m. f. s, c — star of winding e. m. f. s

cent vectors becomes (Fig. 3-15)

$$\alpha'' = \frac{t \times 360^\circ}{2Z} = 12^\circ$$

The number of slots per phase under poles of the same polarity is

$$\gamma = \frac{Z}{2m} = \frac{30}{6} = 5$$

and

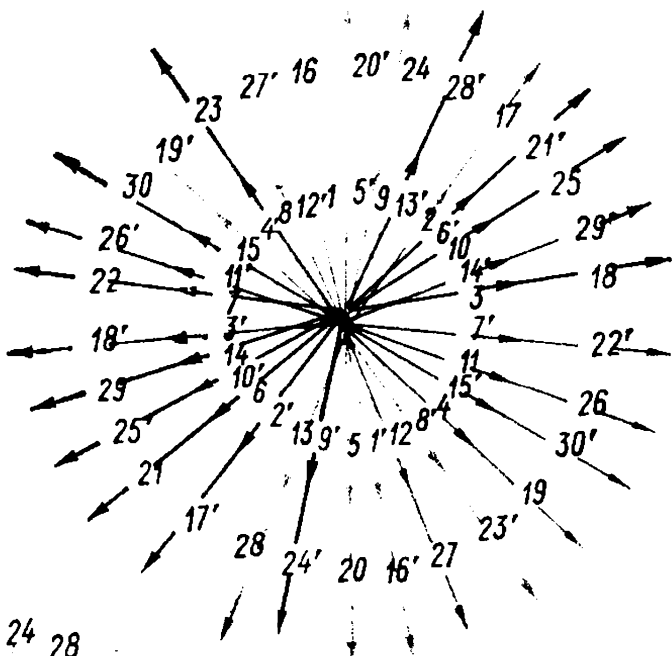
$$\frac{2\gamma}{t} = \frac{10}{2} = 5$$

Let the winding have a pitch from the first to the fourth slot so that

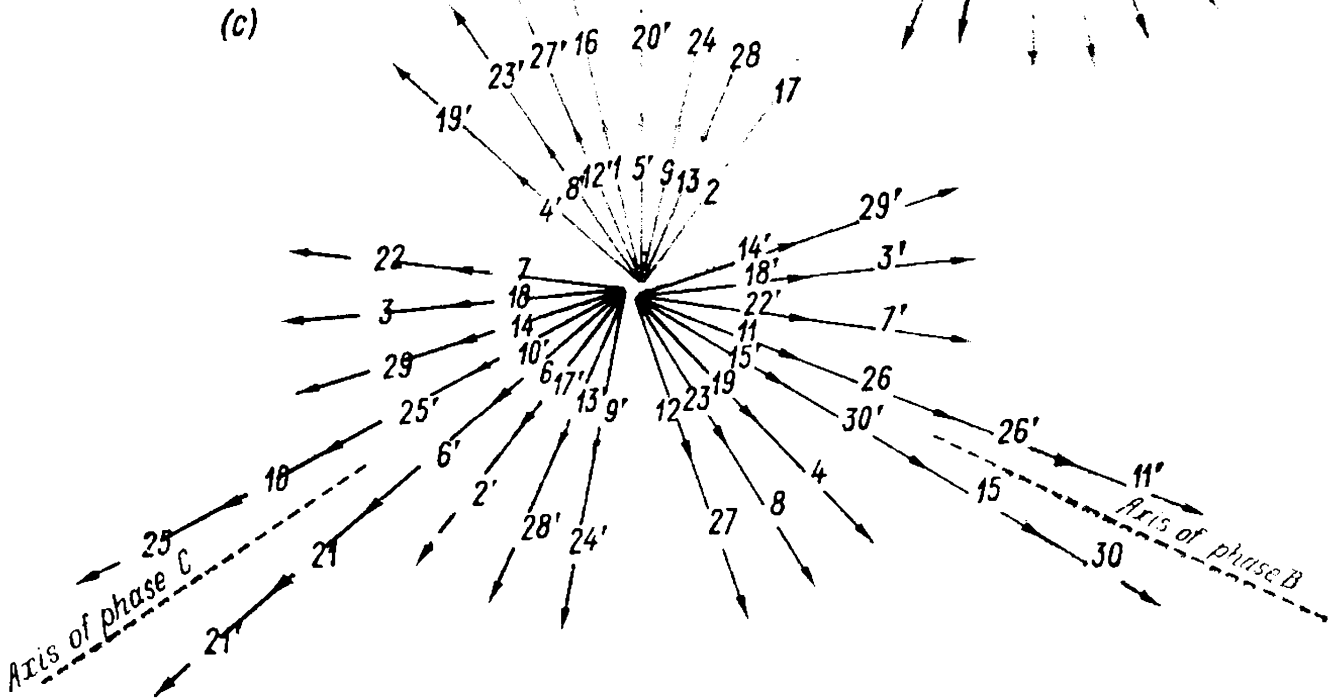
$$\beta = \frac{y}{\tau} = \frac{3}{3.75} = 0.8$$

Figure 3-15a shows a diagram of a winding with the data given above. The sequence of connection of the winding sections is as

(b)



(c)



follows

$A-1-4'-2-5'-8-5-9-12'-16'-13-16-19'-$
 $-17-20'-23'-20-24-27'-1'-28-X,$
 $B-11-14'-12-15'-18'-15-19-22'-26'-23-$
 $-26-29'-27-30'-3'-30-4-7'-11'-8-Y,$
 $C-6-9'-7-10'-13'-10-14-17'-21'-18-21-$
 $-24'-22-25'-28'-25-29-2'-6'-3-Z$

Every two groups of series-connected sections written in the same line and forming a winding half-phase have resultant e.m.f.s equal in magnitude and coinciding in phase. Therefore, they may be inter-connected either in series or in parallel.

The star of slot e.m.f.s of the winding is given in Fig. 3-15*b*. The star of the resultant groups of slot e.m.f.s, which corresponds to the above sequence of coil section connection, is pictured in Fig. 3-15*c*. The latter shows that the vector sums of the e.m.f.s of all the sections in each winding phase are displaced 120° relative to one another. This indicates that a regular three-phase winding with the required 120° displacement of the phase e.m.f.s has been obtained.

A double-layer winding makes it possible to obtain a number of parallel branches equal to *t*, i.e., to the greatest common factor for *Z* and *p*. In the above example with *Z*=30 and 2*p*=8 we have *t*=2, and the winding may have *a*=2 parallel groups as shown by the diagram in Fig. 3-15*a*.

The sequence of laying out this winding can be written as the following numerical series, where the numbers designate the quantity of slots (or the upper row of coil sides) belonging to each phase, the first figure in each table nest denoting the slots of the first phase, the second figure those of the second phase, and the third figure those of the third phase:

N	S	N	S	N	S	N	S
211	121	112	111	211	121	112	111

The principle of compiling the numerical series consists in the following. With $q=1\frac{1}{4}$, of each *c*=4 coil groups the *b*=1 group has *a*+1=2 coils, and the *c*—*b*=4—1=3 groups each have *a*=1 coil. By placing *b*=1 large groups (2 coils each) symmetrically between *c*—*b*=3 small groups (1 coil each) we obtain an element of the numerical series which, when repeated $\frac{Z}{ac+b} = \frac{30}{5} = 6$ times, will give a complete numerical series. In the case considered here, when the number of large groups in a numerical series element equals unity,

this group (the number 2) may be inserted anywhere in the numerical series element.

From the above numerical series it can be seen that after passing four poles, the figure sequence repeats itself in accordance with the phases which they belong to. This feature of the numerical series indicates that the slot conductors spaced four-pole pitches apart have e.m.f.s of the same phase, and the corresponding rays of the slot e.m.f. star therefore coincide in direction. This, in turn, indicates the possibility of obtaining in the given winding not only a series connection of all the conductors belonging to the same phase, but also a parallel connection of the two halves of the winding.

Example 3-1. Consider laying out of a fractional-slot lap winding for an “Elektrosila” hydrogenerator. The application of the above rules is simply illustrated by it.

The hydrogenerator had the following data:

$P=77\,500\text{ kVA},\ U_r=13\,800\text{ V},\ 2p=68,\ Z=600,$

$q=\frac{ac+b}{c}=\frac{2\times 17+16}{17}=\frac{50}{17}=2\frac{16}{17},$

$\alpha=\frac{60c}{ac+b}=\frac{60\times 17}{50}=20.4^\circ$

pitch 1-9, $3q=8.82$, the number of parallel branches $a=4$

$\beta=\frac{y}{\tau}=\frac{8}{8.82}=0.907$

The plotting of the star of slot e. m. f.s with a small value of α' would be very difficult, it is therefore more convenient to represent the arrangement of the winding with the help of a numerical table compiled according to the rules discussed above.

To obtain $q=2\frac{16}{17}$, every 50 slots in the winding must contain 16 coils with $q=3$ (triple coils) and one coil with $q=2$, (double coils) whence

$q=\frac{3\times 16+2}{17}=2\frac{16}{17}$

With $Z=600$ and $p=34$ we have $t=2$, and the winding is divided into two simple windings. The design of a winding with the distribution of the triple and double coils may be conveniently represented in the form of the following simple table of the numerical series:

N	S	N	S	N	S	N	S	N	S	N	S	N	S	N	S	N	S
333	333	333	333	333	323	333	333	333	333	333	233	333	333	333	333	332	
	333	333	333	333	333	323	333	333	333	333	333	233	333	333	333	333	332
333	333	333	333	333	323	333	333	333	333	333	233	333	333	333	333	332	
	333	333	333	333	333	323	333	333	333	333	333	233	333	333	333	333	332

It can be seen from the table that after passing 17 poles the winding assumes an identical position under a pole of opposite polarity and after 34 poles again comes under a pole of the same polarity.

Each phase winding has four coils with $q=2$, which are uniformly distributed around the machine periphery every 30° in space. Between adjacent double coils of different phases there are always 16 triple coils, and between the starts of double coils there is a phase shift equal in electrical degrees to

$$3 \times 360^\circ - 50\alpha = 3 \times 360^\circ - 50 \times 20.4^\circ = 1080^\circ - 1020^\circ = 60^\circ$$

The table shows that the winding makes it possible to form not two, but even four parallel branches, since besides the two main groups there are two additional groups with the same number of double and triple coils. The e.m.f.s of adjacent groups are not in phase, but displaced by 180° , since they start in the numerical tables from poles of different polarities. This, however, does not prevent them from being connected into parallel branches, for the start of one group may be connected with the finish of the other group at the common junctions of the parallel groups.

The star of slot e.m.f.s has $\frac{Z}{t} = \frac{600}{2} = 300$ vectors of different phase and 2 inphase vectors in each ray.

Fractional-Slot Wave Windings. The construction of the slot e.m.f. star and distribution of the slots between the phases in a fractional-slot wave winding are the same as for a fractional-slot lap winding.

Fractional-slot wave windings are a modification of the previously discussed integral-slot wave windings. The difference consists in that at certain predetermined places the regular coil group is altered by increasing or decreasing by one the number of coils in a group. In a lap winding such an alteration of the number of slots in a given phase group leads to violation of the natural development of the winding wave-form, and it is therefore necessary to add an insert to a wave by means of a by-passing jumper which decreases the number of slots in the given group by one.

These additions or removals of the number of coils in the natural wave group should be uniformly distributed around the stator of the machine periphery. Figure 3-16a shows such an additional by-pass,

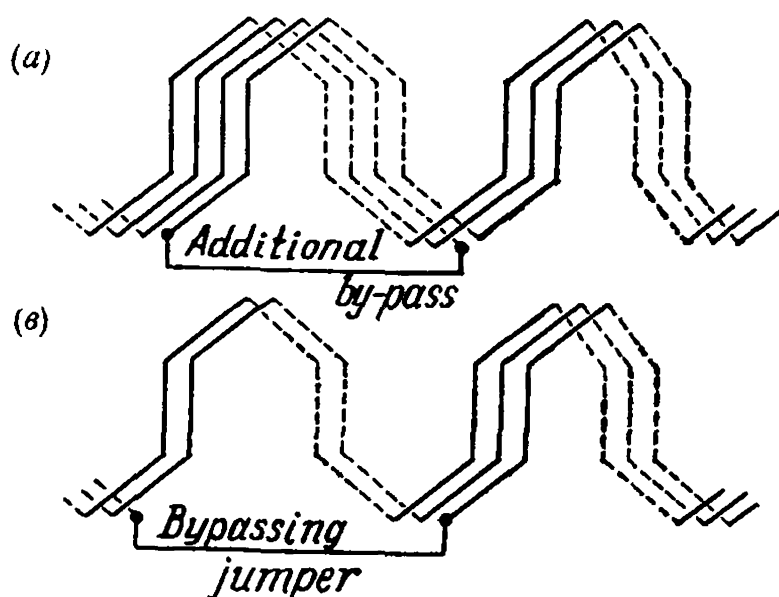


Fig. 3-16. Added wave and bypassing jumper of fractional-slot wave windings

which increases the number of coils in a given group from three to four, while Fig. 3-16b shows a by-passing jumper which reduces the number of coils from three to two. The least number of additional by-passes and jumpers is attained in windings where the number of slots per pole per phase for a given fractional denominator c has the least difference from integer, i.e., for such values of q as $2\frac{1}{5}$, $2\frac{4}{5}$, $2\frac{1}{8}$, and $2\frac{7}{8}$.

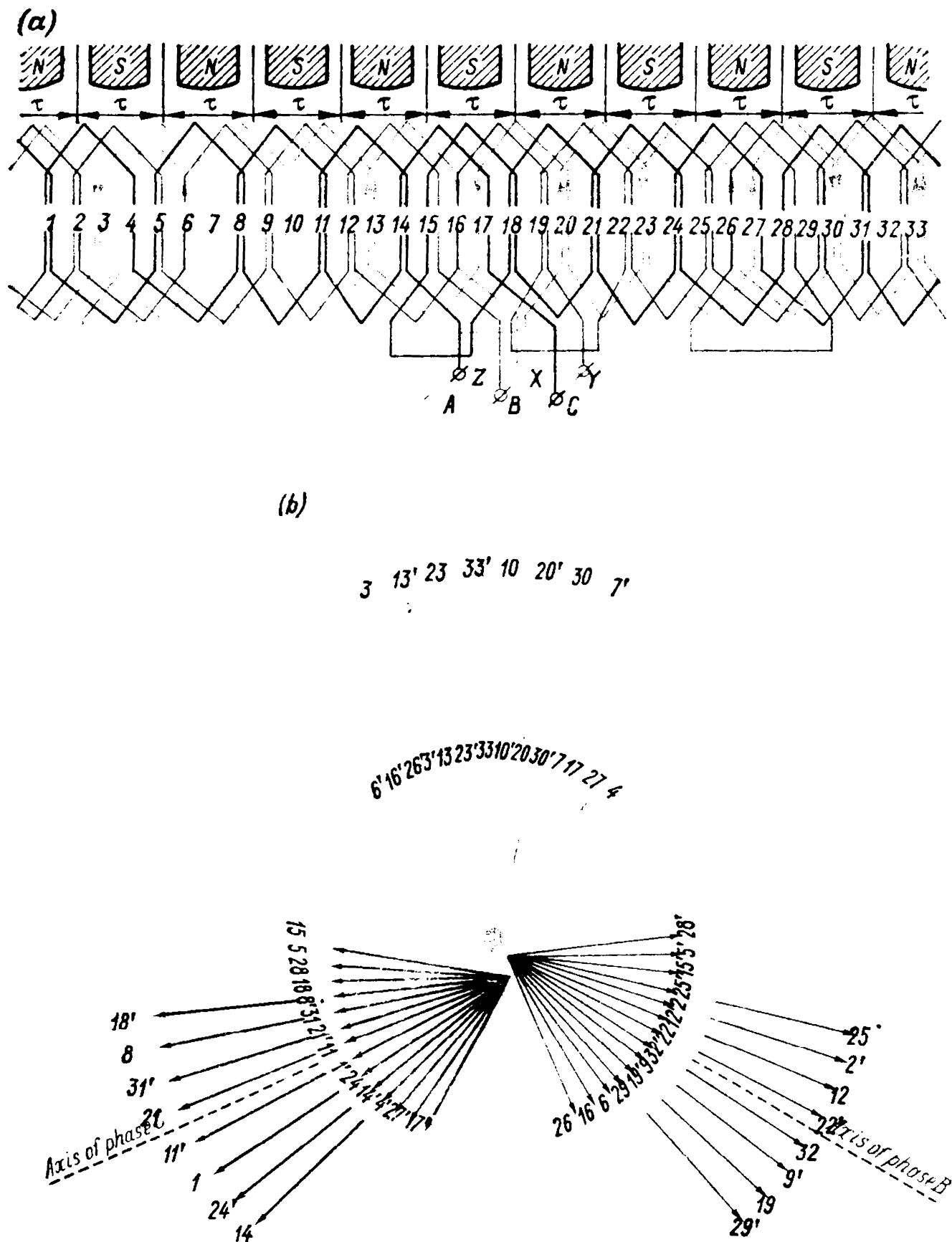


Fig. 3-17. Three-phase two-layer fractional-slot wave winding with $Z = 33$, $2p = 10$, $q = \frac{1}{10}$, $y = 3$, $\beta = \frac{3}{3,3} = 0.91$:
 a — winding diagram; b — e. m. f. star

Figure 3-17a shows a diagram for such a wave winding with $Z=33$, $p=5$, $q=1\frac{1}{10}$, $\beta=\frac{y}{\tau}=\frac{3}{3.3}=0.91$. This winding is a modification of a wave winding for the same number of poles $2p=10$ and a whole number of slots $q=1$ in which the increase in the number of slots per pole per phase makes it necessary to increase the total number of slots by $\frac{1}{10}\times 2p\times 3=\frac{1}{10}\times 10\times 3=3$ slots. These three additional slots are uniformly arranged along the stator periphery. This requires three additional by-passes—one per phase—designed as shown in Fig. 3-16a. Since one of these jumpers can be placed at the winding terminals, it can be omitted. As a result, the diagram in Fig. 3-17a, where $q=1\frac{1}{10}$, in comparison with the diagram in Fig. 3-3 where q is an integer, has only two additional jumpers instead of three, bringing the total number of jumpers to five. The slot e.m.f. vectors of the winding, combined into three sectors, are shown in Fig. 3-17b. The winding is represented by the following series:

N	S	N	S	N	S	N	S	N	S
111	112	111	111	111	211	111	111	121	111

Example 3-2. Consider a practical case of a fractional-slot wave winding. A hydrogenerator with a wave winding has the following data:

$P=32\,000\text{ kVA},\ U_r=10\,500\text{ V},\ n=375\text{ rpm},\ 2p=16,$
 $Z=189,\ q=3\frac{15}{16},\ \text{pitch } 1\text{-}11,\ \beta=\frac{y}{\tau}=0.8465$

The hydrogenerator winding corresponds to a winding with a whole number of slots $q=4$ and $Z=192$, the total number of slots of which has been decreased by $\left(4-3\frac{15}{16}\right)\times 2\times 8\times 3=\frac{1}{16}\times 48=3$ slots. It should therefore have three by-passing jumpers for decreasing the number of slots of the three groups from four to three. Since one jumper can be placed at the terminals the total number of jumpers equals five.

The star of the slot e. m. f. has 189 rays in the given case, which makes this winding equivalent to a winding with a number of slots per pole per phase of $q_{eq}=63$.

The numerical series of the winding is as follows:

N	S	N	S	N	S	N	S	N	S	N	S	N	S	N	S
444	444	441	443	444	444	444	444	444	344	444	444	441	444	434	444

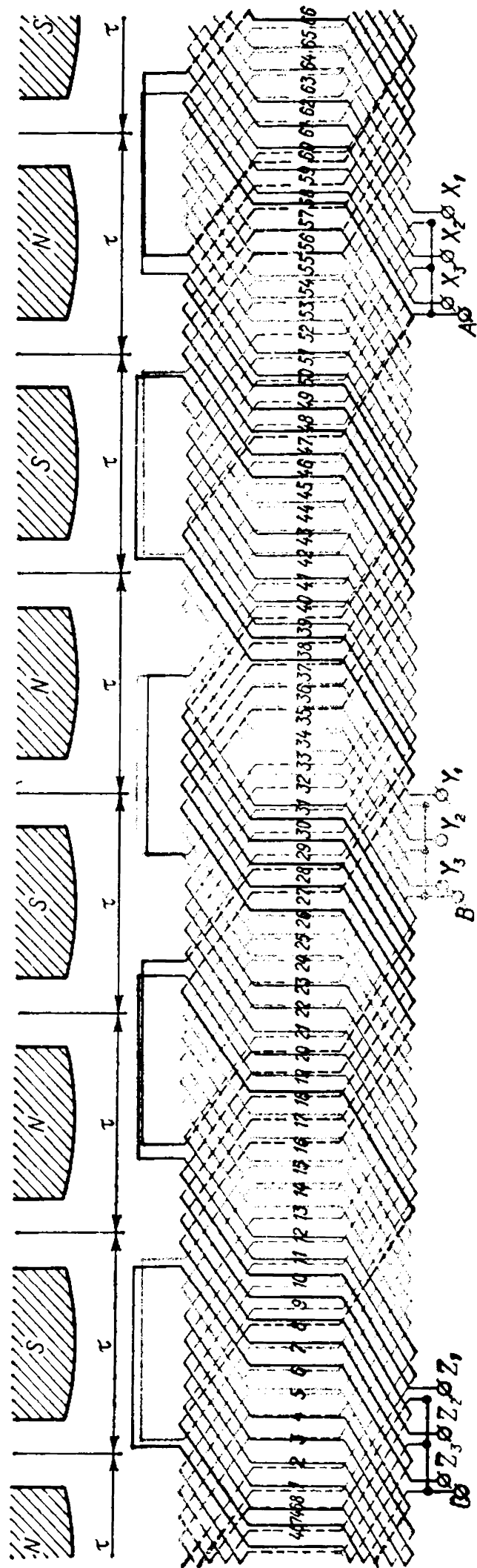


Fig. 3-18. Three-phase wave winding of hydrogenerator with $Z = 468$, $2p = 48$, $a = 3$, $q = 3\frac{1}{4}$ and pitches 1-10, 10-20

As can be seen from the above series, this winding can be obtained from a winding with a whole number $q=4$ by replacing fours with threes at three places equally spaced around the machine periphery one in each phase.

Hydrogenerators are sometimes built with more complicated winding designs. Figure 3-18 shows as an example a diagram of the wave winding used in the 160-MVA, 15-kV, 150-rpm, 60-Hz hydrogenerator installed by the firm Siemens-Schuckert at the Furnas Power Plant in Brazil.

Fractional-slot windings are also used in synchronous and induction motors, but for another purpose. For motors there is no such stringent requirement to the resultant e.m.f. wave-form with respect to its harmonic content as for generators. With synchronous and induction motors, the use of these windings is connected with the use of the same stamping dies having a definite number of slots for machines with different numbers of poles. Therefore, with the same number of slots, for one number of poles q may be obtained equal to an integer, and for another number of poles—equal to a fraction. For example, with $Z=36$, for $2p=4$ we have $q=3$, for $2p=6$ we have $q=2$, and for $2p=8$ we have $q=1\frac{1}{2}$.

3-7. Insulation of Windings

The coil of a winding is placed in slots punched in sheet steel laminations assembled into stator stacks. The slots may have the following shapes, depending on the rating and voltage of the machine: (1) open; (2) semi-open; (3) semi-closed; (4) closed.

The open and semi-open slots are generally of a rectangular shape (Fig. 3-19*a* and *b*), the semi-closed and closed slots are either rectangular or trapezoidal with rounded corners (Fig. 3-19*c*, *d* and *e*).

The method of winding layout and the type of insulation used depend to a considerable degree on the slot shape.

With closed slots there may be two methods of laying the windings and slot insulation. By the first method, the so-called *pull-through* or *draw-in winding* (Fig. 3-20), a casing made beforehand is inserted into the slot to fit its shape, or the slot is lined with some kind of sheet insulation. Then the slot is filled with wooden or metal pins correspon-

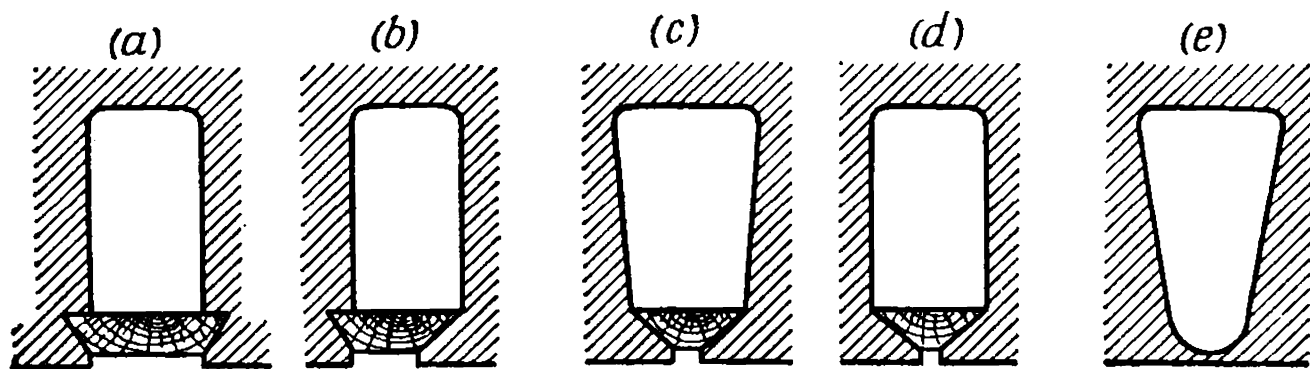


Fig. 3-19. Slot shapes

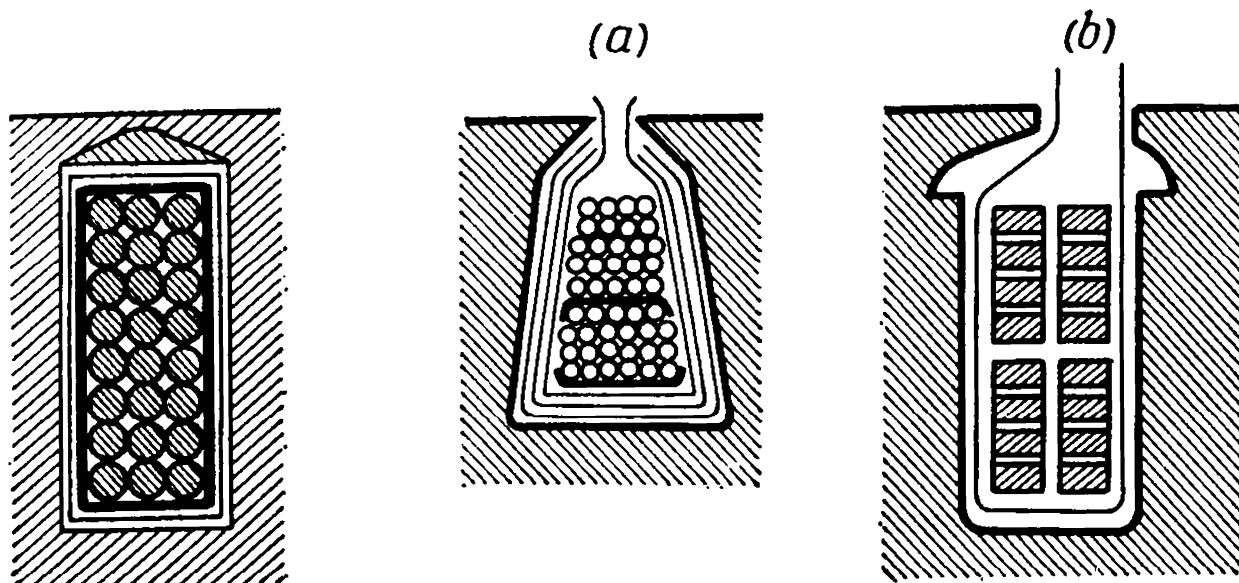


Fig. 3-20. Slot with pull-through winding

Fig. 3-21. Slots with winding in place:
a — semi-closed; b — semi-open

ding in size to the winding wire, and the pins are gradually, in a definite sequence, replaced by the winding wire. By the second method, the so-called *compound split winding*, the coils are form-wound, compound-impregnated under pressure and further insulated at the slot part. Next the end connection is split at one side, and the coil is laid in the slots, after which the split conductors of the end connections are soldered and the end part insulated.

At present closed slots are rarely used because of the time-consuming operations of inserting the winding by the above methods.

With semi-closed slots, either of the above methods can be used for laying out the windings, but semi-closed slots are employed today mainly for low-voltage machines having the so-called *mush windings* using round wire. The semi-closed slot sheet insulation is inserted so that its edges project beyond the slot opening (Fig. 3-21a) each coil is first wound on a former, and then the winding is placed by dropping each wire into its slot.

Semi-open slots are used for medium-power low-voltage machines (up to 500 V). The frame insulation is of sheet material and, as with a *mush winding*, is preliminarily inserted into the slot (Fig. 3-21b). The coils, each consisting of two parts divided along the slot width, are first wound on a form and shaped. The width of the slot opening is such that one-half of a section can be inserted through it. The winding is inserted through the slot opening one half-coil at a time. The winding, after being laid and secured in the slots and end connections, is impregnated with an insulating varnish.

When open slots are used, the coils are first wound on forms, fully insulated, and in a completely finished form are placed in the slot. To insulate the coil, the following methods are used: (1) continuous

insulation of the coil with mica tape, with subsequent vacuum drying and impregnating with compounds in special tanks; (2) continuous insulation with black or yellow varnished cloth with repeated drying and impregnation with insulating varnishes; (3) compound insulation employing varnished cloth for the inner layers and mica tape for the outer layers; (4) continuous insulation employing an impregnated glass tape, either alone or in combination with mica tape; (5) pressing of micafoil insulation into the slot portion of the coil section.

The end connections in the first four methods are insulated in the same way as the slot portion, but using a somewhat smaller number of tape layers. By the fifth method the end connections are insulated either with varnished cloth or with a mica tape, and where the coil comes out from the slot there will be a junction of the two types of insulation.

Closed slots for stators are practically not employed nowadays. Split and pulled-through windings have also become obsolete. Semi-closed slots are used for low-voltage low- and medium-power machines. Semi-open slots are used in low-voltage medium-power synchronous and induction machines. Open slots are used in all high-voltage machines, in medium- and high-power low-voltage synchronous machines, and also sometimes in induction machines when production conditions make them more advantageous than semi-open slots.

In the practice of USSR electrical machine-building works press moulded micafoil insulation and continuous mica tape insulation are used in high-voltage machines with a rating of 3000 to 3150 V with open slots. For voltages of 6000 to 6300 V and higher continuous insulation with mica tape is preferred. For voltages up to 3150 V the press moulding of the slot portion is accomplished with five layers of micafoil tape 0.25 mm thick. With continuous insulation for 3150 V (Fig. 3-22a), depending on the operating conditions of the machine, five to six half-

lapped layers of mica tape 0.13 mm thick are used for the slot portion and one layer less for the end connections. For a voltage of 6300 V (Fig. 3-22b), nine layers are used for the slot portion and eight for the end connections. Over the mica tape the coil section is wound end-to-end with one layer of twill or ferroasbestos tape.

In low-voltage low-power machines the insulation of the turns is limited to the usual insulation of the wire, which consists of a layer of ena-

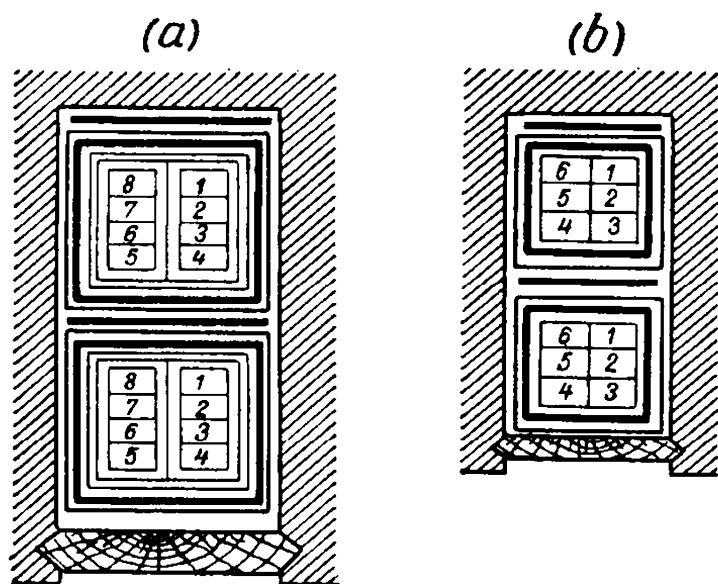


Fig. 3-22. Open slots with inserted winding

mel and a layer of cotton taping.

In high-power machines use is made of wire with double-cotton taping, or with taping and braiding as well as with asbestos insulation.

According to the allowable heating limits, the above types of insulation relate to Class A (Sec. 6-1) which permits a temperature of 100°C , since they all contain a quite considerable amount of Class A insulation (paper, cotton yarn).

In high-voltage machines, besides the wire insulation, additional interturn insulation is employed, usually of mica tape. Depending on the voltage per turn and the power rating of the machine, this insulation may consist of one or maximum of two or three layers of mica tape.

Compound-impregnated insulation, although it belongs to Class B, cannot withstand temperature rise above 105°C , since conventional impregnating compounds soften and begin to flow at higher temperatures. To obtain Class B insulation, which has an allowable maximum temperature of 120°C , it is necessary, according to the existing standards, to insulate the wire with asbestos, multilayer micafoil on a silk substrate or mica-and-fibreglass thermosetting binder.

Finished stator coil sections, when being laid in the stator, are subjected to high-voltage tests, the test voltage depending on the rated voltage of the machine. Figure 3-23 gives standards for testing the winding insulation relative to the frame at different stages of production, depending on the rated voltage of the machine. For coil sections of large and important machines, the dielectric loss angle $\tan \delta$ is determined at voltages within 0.5 to 1.5 times the rated voltage by means of Schering's bridge. In good-quality coil sections the value of $\tan \delta$ at the rated voltage should not exceed 0.08 to 0.1, and the variation of $\tan \delta$ within 1.0 to 1.5 U_r should not exceed 0.02.

The quality of the insulation in machines determines their reliability in operation. Therefore, the greatest importance should be attached to the choice of the insulation to be used and its manufacture. The part played by the insulation relates not only to dielectric strength. Since the losses incurred in the copper usually pass through the insulation into the surroundings, besides the dielectric strength and

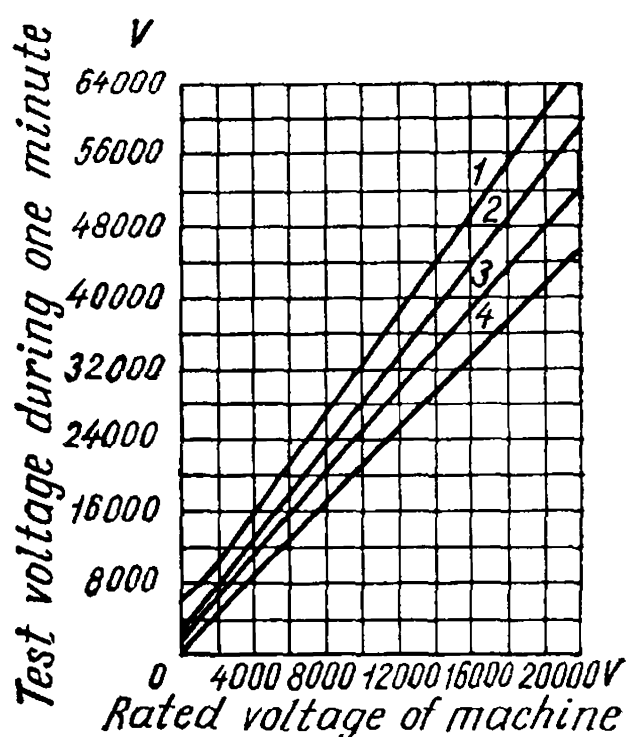


Fig. 3-23. Test voltages for windings: 1 — for uninserted coils; 2 — for coils inserted, but not interconnected; 3 — for coils connected into a winding; 4 — for finished machine

heat resistance of the insulation, its thermal conductivity must also be given attention. This, to a considerable degree, is achieved by proper impregnation and compounding. Also of paramount importance are the mechanical strength, moisture impermeability, oil resistance and other properties of the insulation.

At present new synthetic insulations based on thermosetting binders are widely used. The USA firm Westinghouse, for example, uses insulation of the thermoplastic type, the firm General Electric uses Micopal, and the French firm Alsthom—Isotenax.

Chapter

4

MAGNETIZING FORCE OF ALTERNATING CURRENT WINDINGS

4-1. General

The magnetic field of a machine winding depends on the arrangement of the conductors in the winding and the current flowing through them, and on the configuration of the magnetic circuit of the machine and the magnetic properties of its separate sections. The main object of winding field calculation is to determine the distribution of the flux density along the air-gap of the machine, since this distribution affects: (1) the magnitudes and shapes of the e.m.f.s induced in the windings, and (2) the magnitude and kind of electromagnetic forces induced which produce the torque of the machine.

The magnetic field of a winding is determined through its magnetizing force, which depends on the design of the winding and the currents flowing in it. The winding magnetizing force is determined and used for calculation of the winding field in this chapter for a machine with a uniform air-gap. The features due to a non-uniform gap and those of the magnetic field of fractional-slot windings will be discussed separately in Sec. 4-6.

4-2. Equations of Pulsating and Travelling Waves

Both rotating magnetic field and fields stationary in space, but pulsating in time, may be produced in electrical machines. We shall first consider, therefore, the general problems connected with such fields.

The mathematical expression of a wave pulsating with time according to a sinusoidal law and distributed in space also according to a sinusoidal law can be written in the following form

$$F_{[t, a]} = F_m \sin \omega t \cos \frac{2\pi}{T_{sp}} x = F_m \sin t' \cos a \quad (4-1)$$

Here

$$t' = \omega t \frac{2\pi}{T} t; \quad a = \frac{2\pi}{T_{sp}} x$$

where T = wave time period

T_{sp} = wave space period

F_m = wave amplitude.

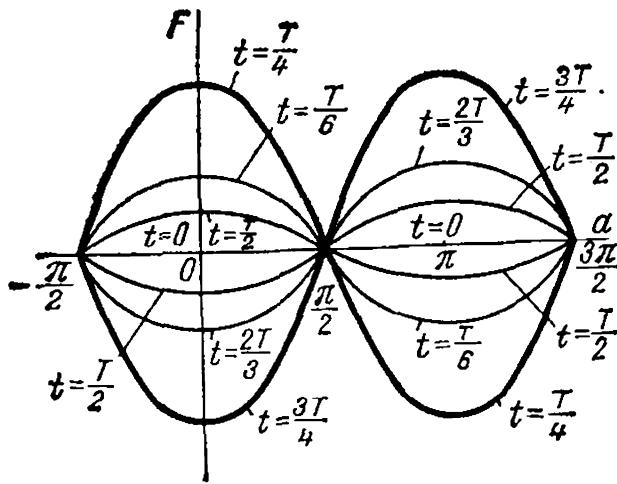


Fig. 4-1. Pulsating wave at different moments of time

$a=0, \pi, 2\pi, \dots$, at which the function (4-1), changing with time according to a sinusoidal law, reaches maximum positive and negative values. The former points are referred to as *nodes* of the wave, and the latter as *antinodes*.

The mathematical expression of a travelling wave is

$$F_{[t, a]} = F_m \sin(t' \pm a) \quad (4-2)$$

The quantities t' and a here are the same as above.

In contrast to a pulsating wave, the maximum value of a travelling wave does not drop to zero during the entire space period for any time value. The maximum of the wave travels to the right or to the left with an increase in time t in the generally used system of coordinates, whence the concept of right- and left-travelling waves.

Figure 4-2 shows the position of the wave

$$F_{[t, a]} = F_m \sin(t' + a) \quad (4-3)$$

for the time values $t'=0$ and $t'=\frac{\pi}{2}$. Since with an increase in time the wave maximum shifts to the left, it is evident that the plus sign before a corresponds to a left-travelling wave. Figure 4-3 shows the po-

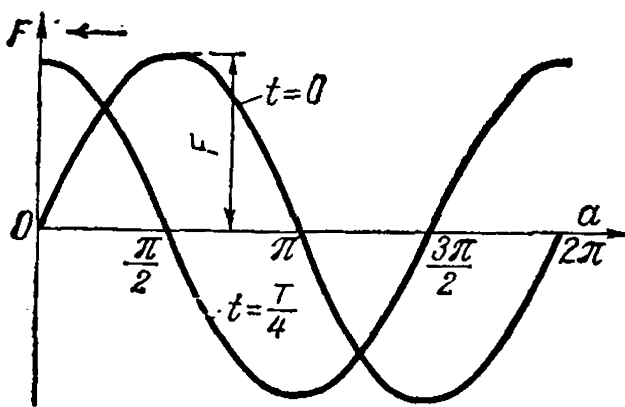


Fig. 4-2. Position of backward (left) travelling wave for two moments

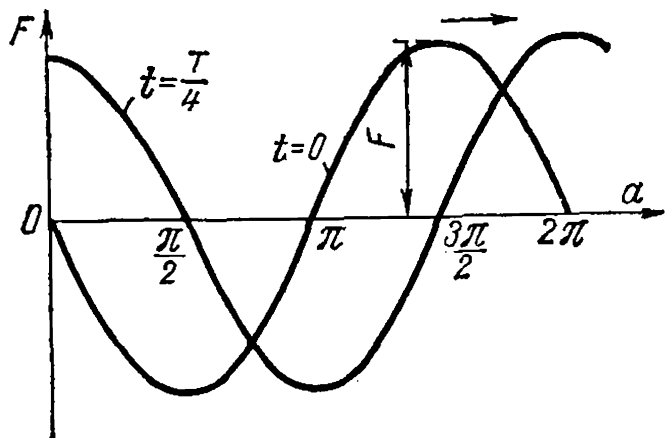


Fig. 4-3. Position of forward (right) travelling wave at two moments

sitions of the wave

$$F_{[t, a]} = F_m \sin(t' - a) \quad (4-4)$$

for the time values $t' = 0$ and $t' = \frac{\pi}{2}$. Here the wave maximum shifts to the right, so that the minus sign before a corresponds to a right-travelling wave.

The concept of right- and left-travelling waves is connected with the system of coordinates. If we change the positive direction of the axis of abscissas in the coordinate system there will be a corresponding change in the direction of travel of these waves in the plane of the drawing.

In a.c. electrical machines, the magnetic field travelling along the air-gap circumference becomes a rotating field, therefore, in further discussions, we shall consider rotating waves of magnetizing force and magnetic fields.

The rotating field of a machine can be resolved into two pulsating fields displaced in space and in time. Indeed, from equation (4-2) it follows that the value of the magnetizing force at a given instant t and point x on the stator periphery is expressed as

$$\begin{aligned} F_{[t, a]} &= F_m \sin(t' \pm a) = F_m \sin t' \cos a \pm F_m \cos t' \sin a = \\ &= F_m \sin t' \cos a \pm F_m \sin\left(t' - \frac{\pi}{2}\right) \cos\left(a - \frac{\pi}{2}\right) = F_{a1} + F_{a2} \end{aligned} \quad (4-5)$$

where

$$F_{a1} = F_m \sin t' \cos a$$

is a pulsating field for which the origin of coordinates is opposite to the wave antinode, and

$$F_{a2} = \pm F_m \sin\left(t' - \frac{\pi}{2}\right) \cos\left(a - \frac{\pi}{2}\right)$$

is a pulsating field shifted from field F_{a1} in space and in time by an angle of $\pm \frac{\pi}{2}$.

The pulsating field can be resolved into two oppositely rotating fields with amplitudes equal to one-half of the maximum amplitude of the pulsating field. This condition follows from the trigonometric transformation of equation (4-1) for a pulsating field wave

$$F_{[t, a]} = F_m \sin t' \cos a = \frac{1}{2} F_m \sin(t' - a) + \frac{1}{2} F_m \sin(t' + a) \quad (4-6)$$

This resolution is depicted graphically in Fig. 4-4.

A sinusoidal rotating field can be obtained from three sinusoidal pulsating fields displaced in space and in time with respect to each other by $\frac{2\pi}{3}$,

the invariable amplitude of this rotating field being equal to $\frac{3}{2}$ of the

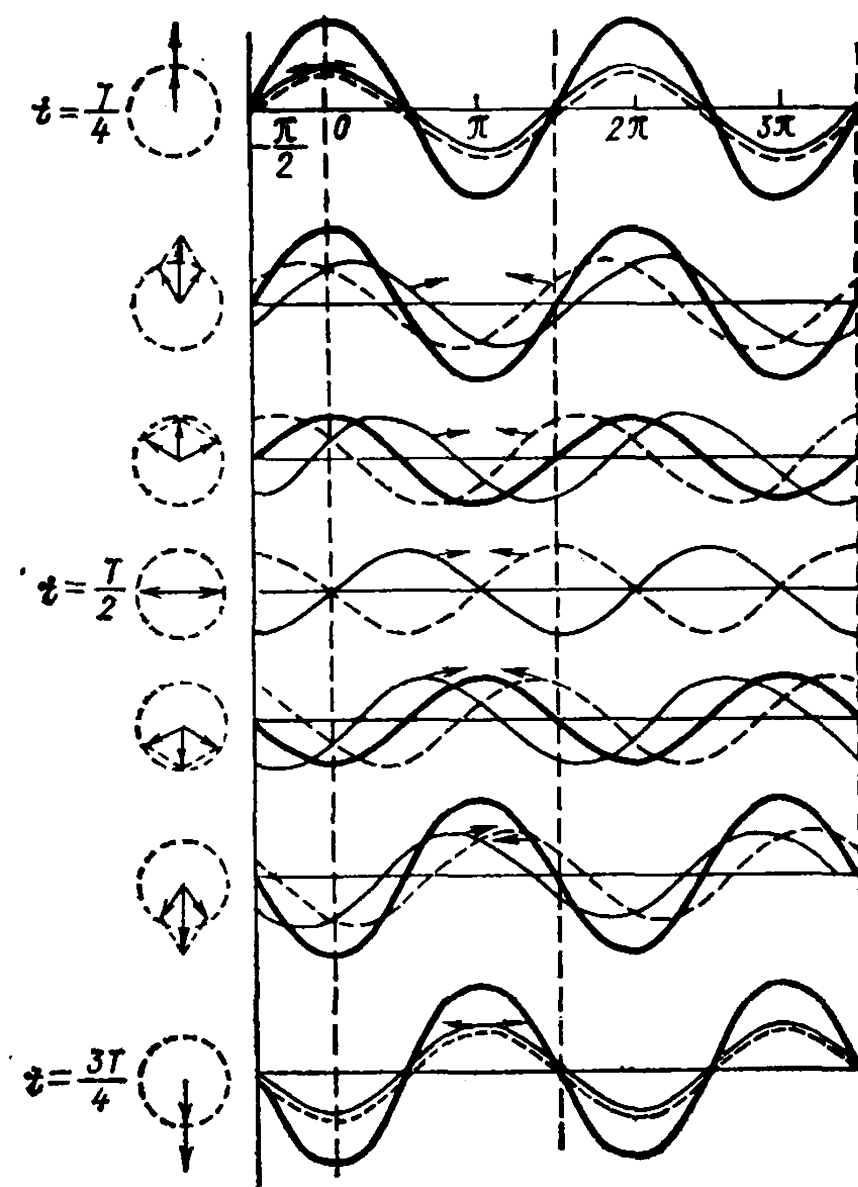


Fig. 4-4. Resolution of pulsating field into two rotating fields

amplitude of each of the pulsating fields. This can be proved trigonometrically, if we summate the expressions for the three pulsating fields after resolving them preliminarily into fields travelling in opposite directions

$$F_{A[t, a]} = F_m \sin t' \cos a = \frac{1}{2} F_m \sin (t' - a) + \frac{1}{2} F_m \sin (t' + a) \quad (4-7)$$

$$\begin{aligned} F_{B[t, a]} &= F_m \sin \left(t' - \frac{2\pi}{3} \right) \cos \left(a - \frac{2\pi}{3} \right) = \\ &= \frac{1}{2} F_m \sin (t' - a) + \frac{1}{2} F_m \sin \left(t' + a - \frac{4\pi}{3} \right) \end{aligned} \quad (4-8)$$

$$\begin{aligned} F_{C[t, a]} &= F_m \sin \left(t' - \frac{4\pi}{3} \right) \cos \left(a - \frac{4\pi}{3} \right) = \\ &= \frac{1}{2} F_m \sin (t' - a) + \frac{1}{2} F_m \sin \left(t' + a - \frac{2\pi}{3} \right) \end{aligned} \quad (4-9)$$

The sum of the left-travelling fields is

$$\frac{1}{2} F_m \left[\sin(t' + a) + \sin\left(t' + a - \frac{4\pi}{3}\right) + \sin\left(t' + a - \frac{2\pi}{3}\right) \right] = 0$$

i.e., in the given case, when the pulsating fields with a phase lag angle of $\frac{2\pi}{3}$ are arranged in the positive direction of the axis of abscissas, the left-travelling fields are mutually balanced, and the sum of the right-travelling fields is

$$F_{[t, a]} = F_{A[t, a]} + F_{B[t, a]} + F_{C[t, a]} = \frac{3}{2} F_m \sin(t' - a) \quad (4-10)$$

The statement proved above also follows from the graphical summation of three pulsating fields with the indicated shifts from one another given in Fig. 4-5.

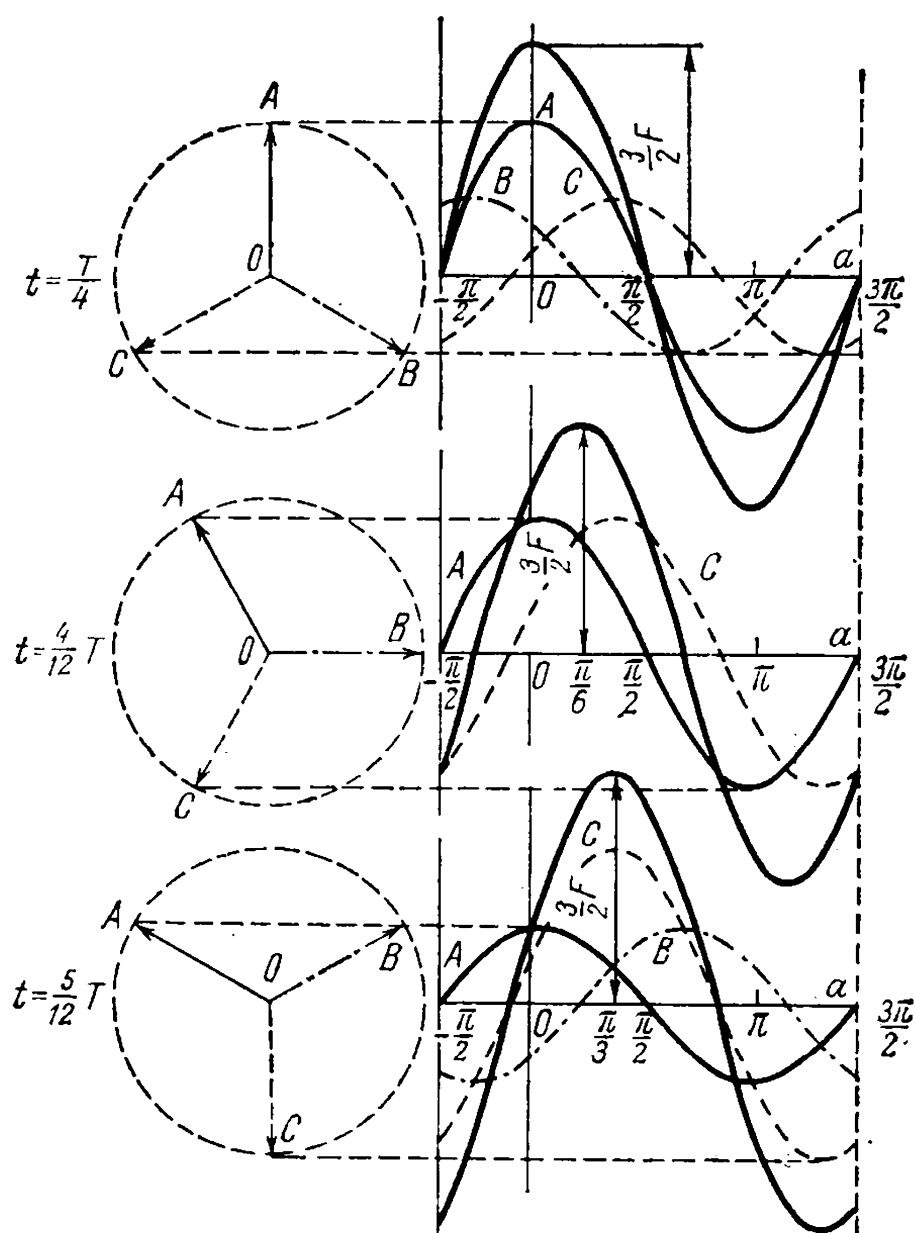


Fig. 4-5. Summation of three pulsating waves shifted 120° in space and time

A rotating field can be similarly obtained from m pulsating fields, displaced by an angle of $\frac{2\pi}{m}$ from one another. The resultant right-travelling field, in this case, will equal

$$F_{[t, a]} = F_{A[t, a]} + F_{B[t, a]} + \dots + F_{m[t, a]} = \frac{m}{2} F_m \sin(t' - a) \quad (4-11)$$

For example, in a two-phase system ($m=2$)

$$F_{A[t, a]} = F_m \sin t' \cos a = \frac{1}{2} F_m \sin(t' - a) + \frac{1}{2} F_m \sin(t' + a)$$

$$\begin{aligned} F_{B[t, a]} &= F_m \sin\left(t' - \frac{\pi}{2}\right) \cos\left(a - \frac{\pi}{2}\right) = \\ &= \frac{1}{2} F_m \sin(t' - a) + \frac{1}{2} F_m \sin(t' + a - \pi) \end{aligned}$$

and the resultant field is

$$F_{[t, a]} = F_{A[t, a]} + F_{B[t, a]} = F_m \sin(t' - a)$$

4-3. Magnetizing Force of a Winding Phase

Coil Magnetizing Force. Consider the field of a double-pole machine produced by a full-pitch coil laid along a uniform air-gap (Fig. 4-6a). The nature of the magnetic field is depicted in Fig. 4-6a by the lines

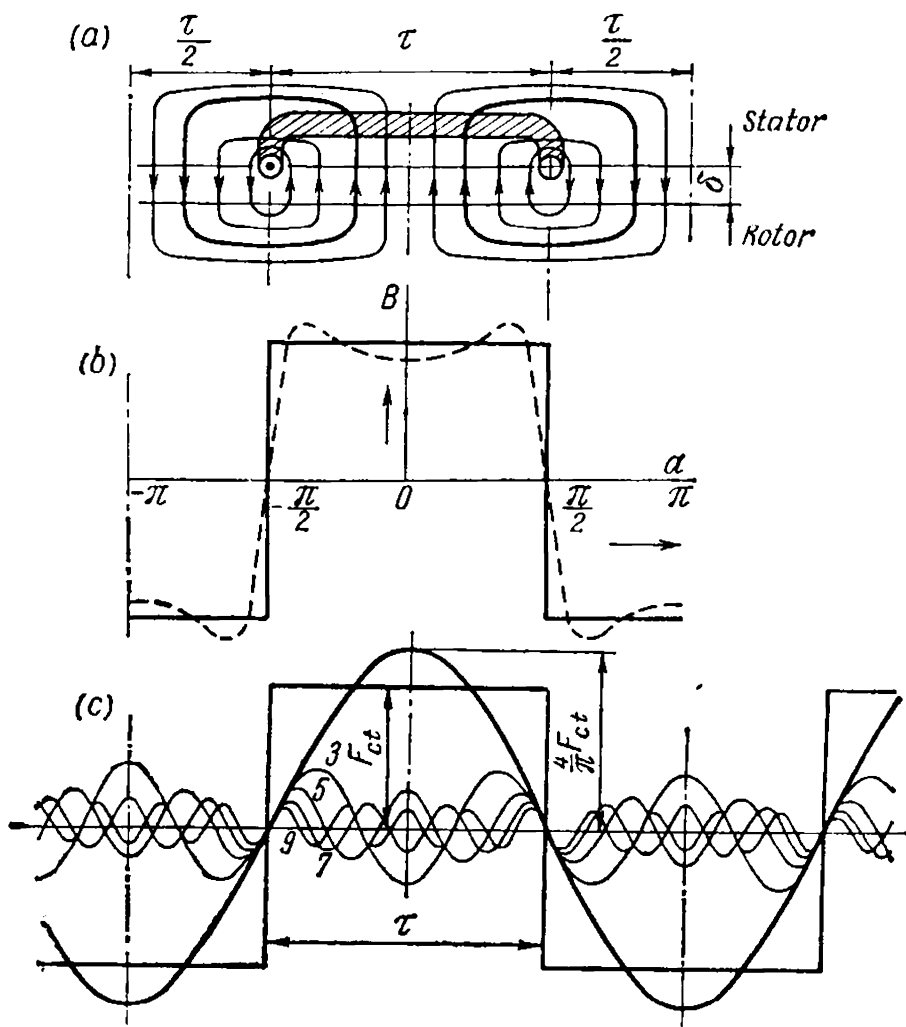


Fig. 4-6. Magnetic field in a gap produced by a full-pitch coil

of magnetic flux in the air-gap, and the flux density B_δ distribution by the dotted curve in Fig. 4-6b. The concavity of this curve is due to the influence of the finite permeability of the steel. If we assume $\mu = \infty$ for steel and neglect field distortion near the coil conductors, then the distribution of B_δ along the gap will be represented by the rectangular-shaped wave shown in Fig. 4-6b by the solid line. The relation between the total current of the coil $\omega_c i_c$ (ω_c is the number of turns in the coil, and i_c , the current in it) and the field strength H is determined by the total current law

$$\boxed{\omega_c i_c = \oint \mathbf{H} d\mathbf{l}} \quad (4-12)$$

the integration being carried out around any closed path enveloping the coil, for instance, along the path shown in Fig. 4-6a by a heavy line.

If we assume that for steel $\mu = \infty$, then the magnetic flux intensity in the steel $H = 0$. Furthermore, since the gap length δ is small in comparison with the pole pitch τ , we can assume that the magnetic lines cross the air-gap radially and the field strength along the gap is constant, varying only in direction according to Fig. 4-6a, b.

For these conditions

$$\oint \mathbf{H} d\mathbf{l} = 2\delta H \quad (4-12a)$$

and, therefore

$$\omega_c i_c = 2\delta H$$

whence

$$H = \frac{1}{\delta} \frac{\omega_c i_c}{2}$$

Consequently, the instantaneous value of the field flux density in the gap at a given point will be

$$B_{(t, a)} = \mu_0 H = \frac{\mu_0}{\delta} \frac{\omega_c i_c}{2} = \lambda_\delta F_{ct} \quad (4-13)$$

In the SI system

$$\boxed{\mu_0 = 4\pi \times 10^{-7} \text{ H/m} = 1.26 \times 10^{-8} \text{ H/cm}}$$

The quantity

$$\lambda_\delta = \frac{\mu_0}{\delta} \quad (4-14)$$

will be referred to as the *specific air-gap permeance*, i.e., the permeance per unit of surface perpendicular to the magnetic density lines in the gap.

The quantity

$$F_{ct} = \frac{1}{2} \omega_c i_c \quad (4-15)$$

is the magnetizing force necessary for conducting the magnetic flux through one air-gap.

The coil magnetizing force varies along the gap in the form of a rectangular wave (Fig. 4-6c) with a height F_{ct} .

With a uniform gap and unsaturated steel, the flux density curve along the gap coincides in shape with the magnetizing force curve, since $\lambda_\delta = \text{const}$. With a non-uniform gap, and with account of steel saturation, expression (4-13) can also be used for calculating the gap field, but here it is necessary to consider the permeance λ_δ as a function of the gap coordinate and of the magnetic conditions of the steel. These considerations will be given below.

The magnetizing force of a winding coil determined as indicated above can be taken as the basis for analysis of the air-gap magnetic field.

For convenience of analysis of the processes taking place in a machine, the field curve in the gap and, correspondingly, the magnetizing force curve can be resolved into harmonics.

The magnetizing force curve for a full-pitch coil (Fig. 4-6c), owing to its symmetry relative to the axis of abscissas, contains only odd harmonics ($\nu = 1, 3, 5, \dots$), and if the axis of ordinates is directed along the coil axis, it can be written as

$$F_{[t, a]} = F_{ct1} \cos a + F_{ct3} \cos 3a + \dots + F_{ct\nu} \cos \nu a + \dots \quad (4-16)$$

The instantaneous amplitude value for a harmonic of the ν -th order is, according to Fig. 4-6c,

$$F_{ct\nu} = \frac{2}{\pi} \int_{-\frac{\pi}{2}}^{\frac{\pi}{2}} F_{ct} \cos \nu a \, da = \frac{4}{\pi} \frac{1}{\nu} F_{ct} \sin \frac{\nu\pi}{2} \quad (4-17)$$

For the odd harmonics

$$\sin \frac{\nu\pi}{2} = \pm 1$$

Equation (4-16), when an alternating current equal to

$$i_c = \sqrt{2} I_c \sin t' \quad (4-18)$$

flows through the coil, represents the sum of the pulsating waves of magnetizing force, since their amplitudes $F_{ct\nu}$ change with time according to a sinusoidal law.

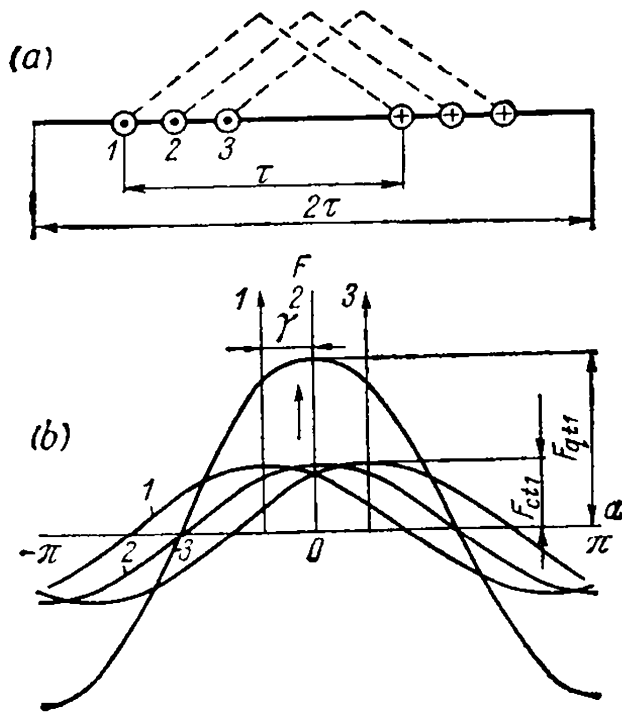


Fig. 4-7. Magnetizing force of a full-pitch coil group

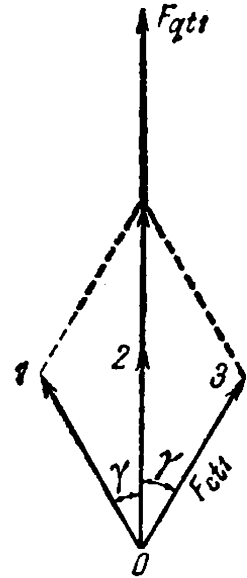


Fig. 4-8. Summation of coil group magnetizing forces

Magnetizing Force of a Full-Pitch Coil Group. Consider q full-pitch coils arranged along a double-pole pitch and belonging to one phase (Fig. 4-7a, $q=3$).

Figure 4-7b shows the fundamental ($v=1$) magnetizing force harmonics of q coils each displaced by an angle $\gamma = \frac{\pi}{mq}$ equal to the displacement angle of two adjacent slots for a fundamental wave.

The summated fundamental magnetizing force harmonics of the separate coils of a group with an amplitude F_{ct1} produce the fundamental magnetizing force harmonic of a group with an amplitude F_{qt1} . The axis of the group magnetizing force will be arranged along the axis of the coil group (Fig. 4-7b).

Thus, the q magnetizing forces, varying in space, and displaced from one another by an angle γ , can be represented in the same way as when adding q sinusoidally time-varying e.m.f.s represented as q vectors displaced by an angle γ from one another (Fig. 4-8). Therefore, the instantaneous amplitude value of the first harmonic will be

$$F_{qt1} = F_{ct1} q k_{d1} \quad (4-19)$$

where k_{d1} is the same winding distribution factor for the fundamental harmonic which was obtained when calculating the e.m.f. Accordingly, for a magnetizing force harmonic of the v -th order we have

$$F_{qtv} = q F_{ctv} k_{dv} \quad (4-20)$$

where k_{dv} is the winding distribution factor for the harmonic calculated according to formula (2-17).

The magnetising force of a full-pitch coil group should, consequently, be written as

$$F_{q[l, a]} = F_{qt1} \cos a + F_{qt3} \cos 3a + \dots + F_{qtv} \cos va + \dots \quad (4-21)$$

the origin of coordinates being at the group axis (Fig. 4-7).

Magnetizing Force of Winding Phase. To obtain an expression for the magnetizing force of a fractional-pitch winding, let us consider one phase of the double-layer winding with $2p=2$ shown in Fig. 4-9a, where the direction of the current in the coils is also indicated.

Generally, in such a winding the conductors of the top layer are connected to those of the bottom layer with a pitch $y = \beta\tau < \tau$. To produce a magnetizing force however, it is the arrangement of the conductors and the direction of currents in them that are of importance, and not the sequence of their connection. Therefore, it may be considered that the top layer of conductors in Fig. 4-9a comprises q full-pitch coils, and the bottom layer also comprises full-pitch coils (in Fig. 4-9a, $q=4$). Hence the magnetizing force fundamental harmonics of the top and bottom layers F_{top1} and F_{bot1} are the previously discussed sine waves which have an amplitude F_{qt1} and are displaced by the angle $\left(1 - \frac{y}{\tau}\right)\pi = (1 - \beta)\pi$, corresponding to the displacement of the winding layers (Fig. 4-9b).

The magnetizing forces F_{top1} and F_{bot1} are therefore summated in the same way as the e.m.f.s in fractional-pitch winding coils.

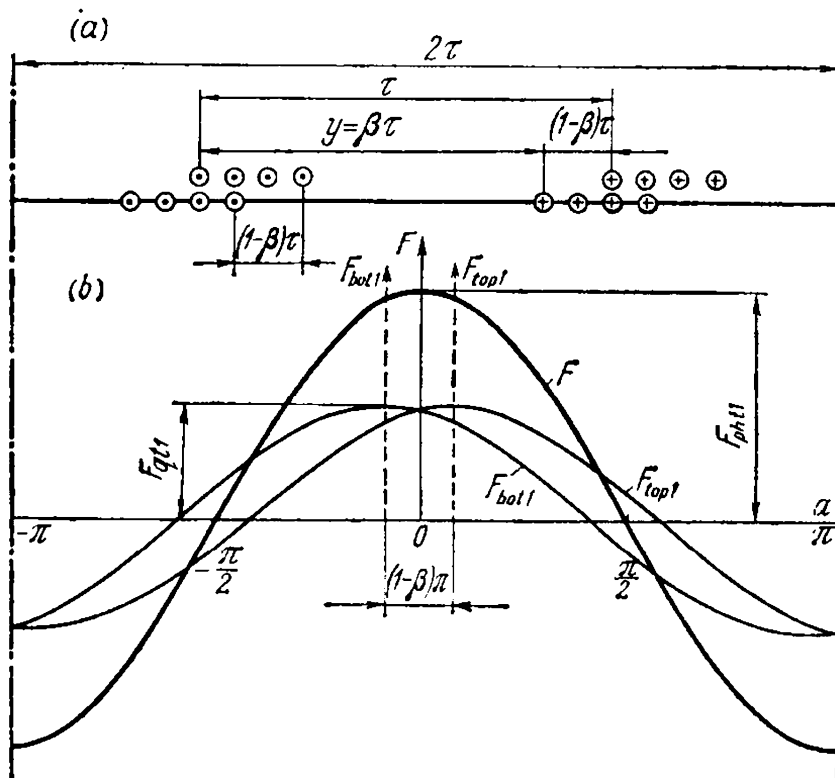


Fig. 4-9. Magnetizing forces of two fractional-pitch coil groups

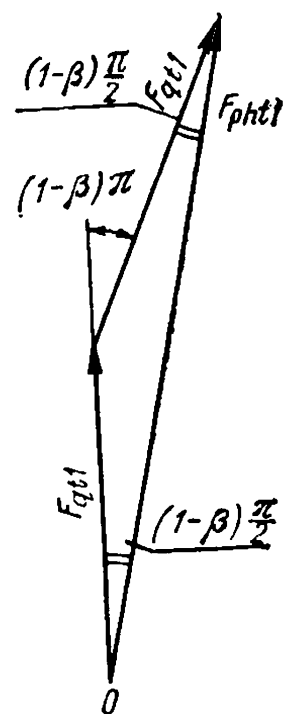


Fig. 4-10. Summation of magnetizing forces of two fractional-pitch coil groups

Hence (Fig. 4-10)

$$F_{ph1} = 2F_{qt1}k_{p1} \quad (4-22)$$

where k_{p1} is the pitch factor for the fundamental harmonic determined by formula (2-26).

To express the magnetizing force F_{ph1} in its final form, formulas (4-15), (4-17) and (4-19) can be used

$$F_{ph1} = 2qF_{ct1}k_{d1}k_{p1} = 2q \frac{4}{\pi} F_{ct}k_{w1} = \frac{4}{\pi} q\omega_c k_{w1}i_c \quad (4-23)$$

where $k_{w1} = k_{d1}k_{p1}$ is the resultant winding factor for the fundamental harmonic.

Similarly, for the v -th harmonic we have

$$F_{phv} = \frac{4}{\pi} \frac{1}{v} q\omega_c k_{wv}i_c \quad (4-24)$$

where

$$k_{wv} = k_{dv}k_{pv}$$

A machine having $p=1$ pole pairs was considered above. With $p>1$ and an integer number of slots per pole per phase, the magnetizing force owing to winding symmetry, will be similar to that in the above machine over each pole pair arc. When all the coil groups of the winding are connected in series, the number of turns per phase will be

$$\omega = 2pq\omega_c \quad (4-25)$$

and the coil current

$$i_c = \sqrt{2} I \sin \omega t$$

where I is the effective phase current.

Upon introducing these relations into equations (4-23) and (4-24), we obtain

$$F_{ph1} = F_{ph1} \sin \omega t \quad (4-26)$$

$$F_{phv} = F_{phv} \sin \omega t \quad (4-27)$$

where

$$F_{ph1} = \frac{2}{\pi} \sqrt{2} \frac{\omega k_{w1}}{p} I = 0.9 \frac{\omega k_{w1}}{p} I \quad (4-28)$$

$$F_{phv} = \frac{2}{\pi} \sqrt{2} \frac{\omega k_{wv}}{vp} I = 0.9 \frac{\omega k_{wv}}{vp} I \quad (4-29)$$

It is not difficult to see that expressions (4-28) and (4-29) are valid also for a winding with parallel branches if we take ω as the number of series-connected turns in a phase or the number of turns in one branch, and I as the total phase current.

These expressions are also valid for single-layer windings.

The expression for the total magnetizing force of a phase can now be written as

$$F_A = F_{ph1} \sin t' \cos a + F_{ph3} \sin t' \cos 3a + \dots + F_{phv} \sin t' \cos va \quad (4-30)$$

where, in the given case, the angle a is counted from the winding phase axis (Fig. 4-9).

The following conclusions can be drawn from the above:

1. The magnetizing force of a winding phase is the sum of the fundamental and higher space magnetizing force harmonics, invariably located in space.

2. The amplitude of the fundamental magnetizing force harmonic of a separate coil is arranged in space along the axis of the corresponding coil, and the amplitude of the fundamental magnetizing force harmonic of a winding phase is arranged along the phase axis.

3. The amplitudes of the fundamental and higher harmonics pulsate with time according to the same law as that followed by the current feeding the winding.

4. The amplitude of the harmonic is inversely proportional to its order and proportional to the winding factor for the given harmonic.

5. The distribution and pitch shortening of the winding influence the magnetizing force wave-form in the same manner as they influence the e.m.f. wave-form, i.e., bring it closer to a sine wave.

4-4. Magnetizing Force of a Three-Phase Winding

With three-phase current we have on the machine armature three systems of windings 120 and 240 electrical degrees apart in space, fed with sine-wave currents shifted in phase also by 120° and 240°. For such windings the following magnetizing force equations can be written if the origin of coordinates is selected along the axis of phase A

$$\begin{aligned} F_{A(t, a)} &= \\ &= [F_{ph1} \cos a + F_{ph3} \cos 3a + F_{ph5} \cos 5a + \dots + F_{phv} \cos va + \dots] \sin t' \end{aligned} \quad (4-31)$$

$$\begin{aligned} F_{B(t, a)} &= \left[F_{ph1} \cos \left(a - \frac{2\pi}{3} \right) + F_{ph3} \cos 3 \left(a - \frac{2\pi}{3} \right) + \right. \\ &\quad \left. + F_{ph5} \cos 5 \left(a - \frac{2\pi}{3} \right) + \dots + F_{phv} \cos v \left(a - \frac{2\pi}{3} \right) \right] \sin \left(t' - \frac{2\pi}{3} \right) \end{aligned} \quad (4-32)$$

$$\begin{aligned} F_{C(t, a)} &= \left[F_{ph1} \cos \left(a - \frac{4\pi}{3} \right) + F_{ph3} \cos 3 \left(a - \frac{4\pi}{3} \right) + \right. \\ &\quad \left. + F_{ph5} \cos 5 \left(a - \frac{4\pi}{3} \right) + \dots + F_{phv} \cos v \left(a - \frac{4\pi}{3} \right) \right] \sin \left(t' - \frac{4\pi}{3} \right) \end{aligned} \quad (4-33)$$

The resultant magnetizing force for each single harmonic can be found by summing the given harmonics of all three phases.

For the fundamental magnetizing force harmonic of a three-phase winding we obtain, according to Sec. 4-2 formulas (4-7) to (4-10), the following expression

$$F_{1(t, a)} = \frac{3}{2} F_{ph1} \sin(\omega t - a) = F_1 \sin(\omega t - a) \quad (4-34)$$

Hence it follows that the fundamental harmonic of the resultant magnetizing force in a three-phase winding is no longer a wave pulsating in space as with a single phase in a winding, but a wave travelling to the right around the stator periphery. The amplitude of this wave is equal to the resultant magnetizing force of the fundamental harmonic per pole

$$F_1 = \frac{3}{2} F_{ph1} = \frac{3 \sqrt{2}}{\pi} \frac{\omega k_{w1}}{p} I = 1.35 \frac{\omega k_{w1}}{p} I \quad (4-35)$$

It is easy to show similarly that, for any other number of phases m , with the windings displaced by an angle $\frac{2\pi}{m}$ and the current in them displaced in time by the same angle, the amplitude of the fundamental magnetizing force wave will be equal to

$$F_1 = \frac{m}{2} F_{ph1} = \frac{m \sqrt{2}}{\pi} \frac{\omega k_{w1}}{p} I = 0.45 \frac{m \omega k_{w1}}{p} I \quad (4-36)$$

To find the speed with which the sinusoidal wave of the fundamental magnetizing force harmonic, determined by equation (4-34), travels along the air-gap, let us take a point rigidly fixed on this wave and travelling together with it. For such a point

$$\sin(\omega t - a) = \text{const}$$

or

$$\omega t - a = \text{const}$$

By differentiating this expression with respect to the time t , we obtain

$$\omega - \frac{da}{dt} = 0$$

whence the angular speed of the wave is

$$\frac{da}{dt} = \omega \quad (4-37)$$

i.e., any point rigidly fixed on a rotating magnetizing force wave travels around the stator periphery with an angular speed ω . In a synchronous machine the rotor runs at the same angular speed (in electrical angular units) and in the same direction, i.e., the fundamental

magnetizing force wave of the stator winding travels around the stator synchronously with the rotor.

The content of the above mathematical analysis of the stator winding magnetizing force with respect to its fundamental harmonic can be formulated as follows.

When there are three sinusoidal magnetizing forces on a stator, 120 electrical degrees apart and pulsating with a shift in time of 120°, we substitute for each of them two oppositely directed sinusoidal magnetizing forces having amplitudes equal to one-half of that of the pulsating magnetizing force and travelling. The magnetizing forces travelling in the direction opposite to rotor rotation are eliminated, since they are shifted 120° from one another, while the magnetizing forces travelling in the rotor direction coincide and give a resultant sinusoidal magnetizing force in space with an amplitude equal to $\frac{3}{2}$ times the maximum amplitude of the pulsating magnetizing force travelling synchronously with the rotor.

In a similar manner the magnetizing forces of any higher harmonic of all three phases can be summated. For $v=3$ we obtain

$$F_{a3} = F_{ph3} \left[\sin \omega t \cos 3a + \sin \left(\omega t - \frac{2\pi}{3} \right) \cos 3 \left(a - \frac{2\pi}{3} \right) + \sin \left(\omega t - \frac{4\pi}{3} \right) \cos 3 \left(a - \frac{4\pi}{3} \right) \right] = 0$$

and for $v=5$

$$\begin{aligned} F_{a5} &= F_{ph5} \left[\sin \omega t \cos 5a + \sin \left(\omega t - \frac{2\pi}{3} \right) \cos 5 \left(a - \frac{2\pi}{3} \right) + \sin \left(\omega t - \frac{4\pi}{3} \right) \cos 5 \left(a - \frac{4\pi}{3} \right) \right] = \\ &= \frac{3}{2} F_{ph5} \sin (\omega t + 5a) = F_5 \sin (\omega t + 5a) \end{aligned}$$

correspondingly

$$\begin{aligned} F_{a7} &= \frac{3}{2} F_{ph7} \sin (\omega t - 7a) = F_7 \sin (\omega t - 7a) \\ F_{a11} &= \frac{3}{2} F_{ph11} \sin (\omega t + 11a) = F_{11} \sin (\omega t + 11a) \\ F_{a13} &= \frac{3}{2} F_{ph13} \sin (\omega t - 13a) = F_{13} \sin (\omega t - 13a) \end{aligned}$$

and for the harmonics of the v -th order

$$F_{av} = \frac{3}{2} F_{phv} \sin (\omega t \pm va) = F_v \sin (\omega t \pm va) \quad (4-38)$$

where

$$F_v = \frac{3}{2} F_{phv} = \frac{3 \sqrt{2}}{\pi} \frac{\omega k_{wv}}{vp} I = 1.35 \frac{\omega k_{wv}}{vp} I \quad (4-39)$$

The resultant magnetizing force of three phases including all harmonics is

$$F_{[t, a]} = F_1 \sin(t' - a) + F_5 \sin(t' + 5a) + F_7 \sin(t' - 7a) + \\ + F_{11} \sin(t' + 11a) + F_{13} \sin(t' - 13a) + \dots + F_v \sin(t' \pm va) \quad (4-40)$$

In the expression for the resultant magnetizing force, all harmonics of the order $v=3k$ (a multiple of three) vanish. All harmonics of the order $v=6k-1$, i.e., $v=5, 11, 17$, have the multiplier $\sin(\omega t + va)$ and, therefore, run to the left, opposite to the direction of travel of the fundamental wave.

All harmonics of the order $v=6k+1$, i.e., $v=1, 7, 13, \dots$, have the multiplier $\sin(\omega t - va)$ and run, therefore, to the right, i.e., in the direction of the fundamental wave and the rotor.

The above can be formulated as follows: if, for obtaining the order of a harmonic in the formula

$$v=6k \pm 1$$

where k is an integer, it is necessary to use the plus sign, the rotation of the harmonic will coincide with that of the fundamental harmonic. If the minus sign must be used, the direction is opposite to the direction of rotation of the fundamental harmonic.

Since all the magnetizing force harmonics are produced by sine-wave currents of the fundamental frequency f , they have the same fundamental frequency f . On the other hand, a space harmonic of the v -th order has, when compared with the fundamental space harmonic, a space period v times smaller and, therefore, a number of pole pairs v times greater.

Consequently, $f = v p n_v$, whence the speed of rotation of the harmonic relative to the winding is

$$n_v = \frac{f}{vp} = \frac{n_1}{v} \quad (4-41)$$

The speed of the v -th space magnetizing force harmonic relative to the rotor of a synchronous machine is

$$n_{vr} = \frac{f}{vp} \pm n_r \quad (4-42)$$

where the minus sign pertains to a harmonic travelling in the direction of the fundamental magnetizing force wave, and the plus sign, accordingly, to a harmonic travelling in the opposite direction.

Let us determine the speed of rotation of the magnetizing force harmonics relative to the stator and rotor systems of a synchronous machine. For the fifth and eleventh magnetizing force harmonics, the

speeds relative to the stator and the stationary rotor are equal to (in rps)

$$n_5 = \frac{1}{5} n_1 \quad \text{and} \quad n_{11} = \frac{1}{11} n_1$$

whence

$$n_1 = 5n_5 = 11n_{11}$$

With a uniform air-gap and an unsaturated magnetic circuit, the flux density in the air-gap is proportional to the magnetizing force. Therefore, each magnetizing force harmonic of the v -th order produces a field harmonic of the same order.

With a stationary rotor and the fifth magnetizing force harmonic rotating relative to it at a speed of n_5 rps and the eleventh harmonic rotating at a speed of n_{11} rps, e.m.f.s will be induced in the rotor having a frequency

$$f_2 = 5pn_5 = 11pn_{11} = f_1$$

When the rotor revolves with a speed of $n_1 = 5n_5 = 11n_{11}$ in the direction opposite to that of these harmonics, e.m.f.s of higher frequency will be induced in the rotor, namely

$$f_{2(5)} = 5p(n_1 + n_5) = 5p \times 6n_5 = 6f_1$$

and

$$f_{2(11)} = 11p(n_1 + n_{11}) = 11p \times 12n_{11} = 12f_1$$

For the seventh and thirteenth magnetizing force harmonics rotating in the direction of the rotor, correspondingly

$$f_{2(7)} = 7p(n_1 - n_7) = 7p \times 6n_7 = 6f_1$$

$$f_{2(13)} = 13p(n_1 - n_{13}) = 13p \times 12n_{13} = 12f_1$$

Thus, the fifth and seventh harmonics produce in the rotor a frequency of $6f_1$, the 11th and the 13th, a frequency of $12f_1$, the 17th and 19th, a frequency of $18f_1$, and so on.

Thus it is apparent that the presence of higher space harmonics in a magnetizing force curve with a uniform air-gap does not induce higher time harmonics in the stator winding e.m.f. The fluxes due to these magnetizing force harmonics move relative to the rotor, however giving rise to eddy current losses in it and thus reducing the efficiency of the machine. For this reason everything possible should be done to reduce the higher harmonics in the magnetizing force curve of a machine.

In the general case, when the current is non-sinusoidal, each current time harmonic gives rise to its own series of magnetizing force harmonics. The speed of a magnetizing force of the v -th order induced by the μ -th current harmonic is determined from the equation

$$n_v = \frac{f_\mu}{vp} = \frac{n_1 \mu}{v} \quad (4-43)$$

The angular speed of a v -th order magnetizing force induced by a μ -th current harmonic, in relation to the rotor, is

$$n_{\mu r} = \frac{f\mu}{\mu p} \pm n_r = \frac{f}{p} \pm n_r \quad (4-44)$$

where the minus sign corresponds to a magnetizing force rotating in the direction of the rotor.

4-5. Analysis of Magnetizing Force Curve of Integral-Slot q Windings

A glance at Fig. 4-6c shows that the curve of a coil magnetizing force is a broken line, which abruptly changes its direction at points where current-carrying conductors are arranged. The magnitude of this change at a point where there is a coil side with w_c coil turns and a current i_c is $w_c i_c$. At sections with no current-carrying conductors, the curve ordinates do not change, and the magnetizing force curve is horizontal.

The magnetizing force curve of a whole winding can be obtained by superposing the magnetizing force curves of the constituent winding or coil elements.

From the above follows the so-called integral method of magnetizing force curve construction.

First the distribution of the winding coil sides along the air-gap is shown, the sides being marked to show the phase which they belong to. Next the magnitude and direction of the currents in separate coil conductors are determined for the moment under consideration. Then, moving forward from left to right, or winding magnetizing force broken curve is drawn, making an abrupt vertical change at points where each coil side is arranged either upward or downward, depending on the direction of current, equal to the total current in the given section. The resulting broken line is then divided by the axis of abscissas into two parts, upper and lower, so that the sum of the areas of the upper curve sections is equal to that of the lower sections. This follows from the principle of equality of the sums of the magnetic fluxes induced by the north poles to those induced by the south poles.

For a whole number of slots q per pole per phase it is sufficient to plot the magnetizing force curve over a double-pole pitch, since the curve repeats itself thereafter. The curves of the magnetizing force of stepped positive half-waves will be symmetrical to the negative ones.

In double layer winding, the magnitude of the jump in the magnetizing force curve at each point is determined by the value of the current and its direction in both the upper and lower coil section sides:

$$w_c(i_{top} + i_{bot})$$

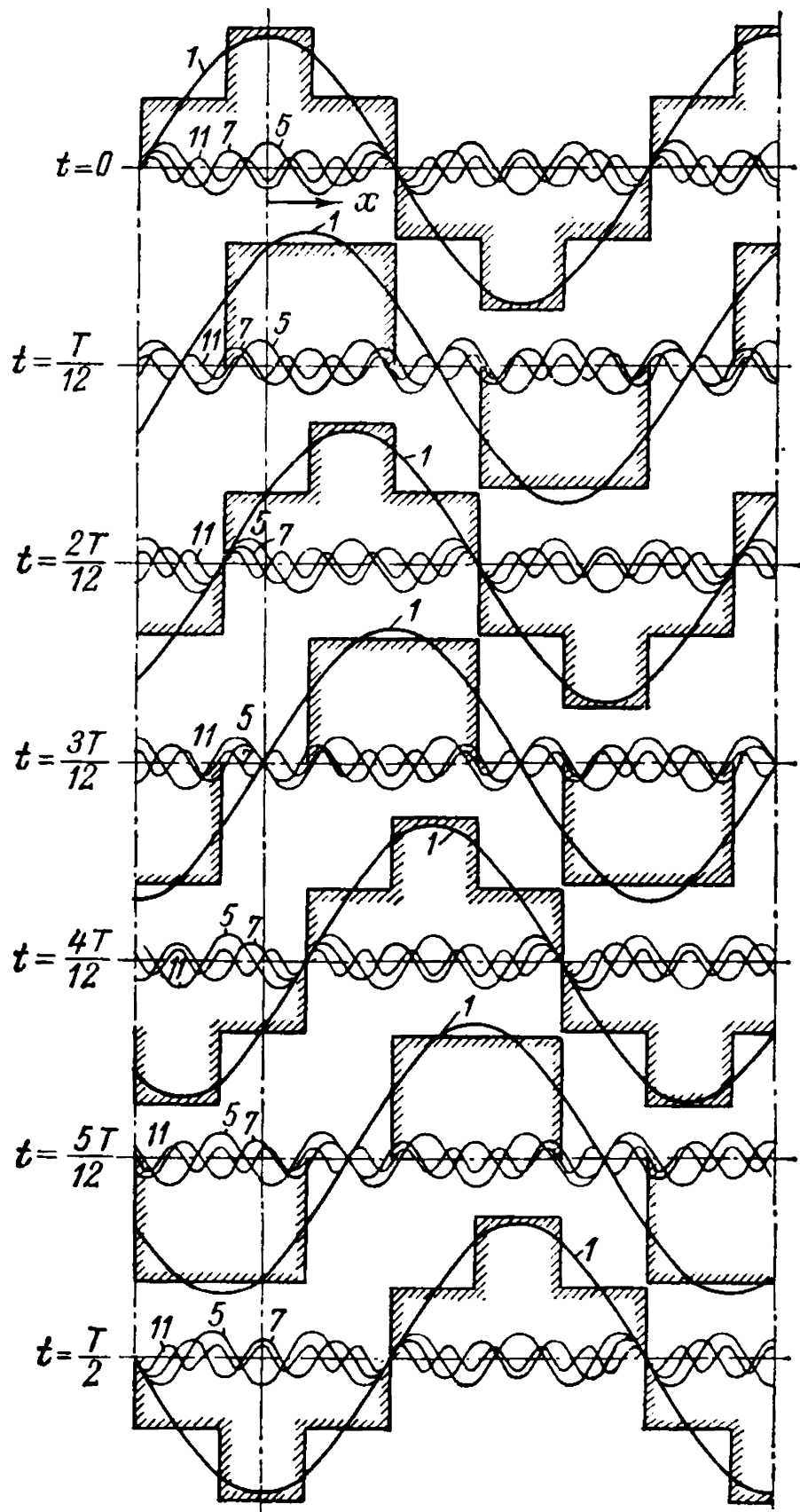


Fig. 4-11. Magnetizing force curves of three-phase single-layer full-pitch winding with $q = 1$ for different moments

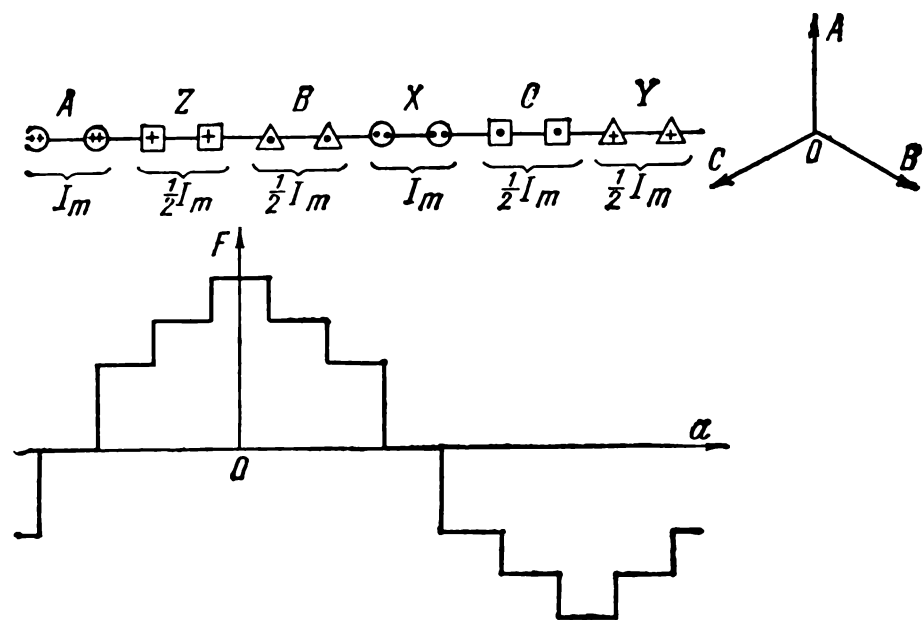


Fig. 4-12. Magnetizing force curve of three-phase single-layer full-pitch winding with $q = 2$

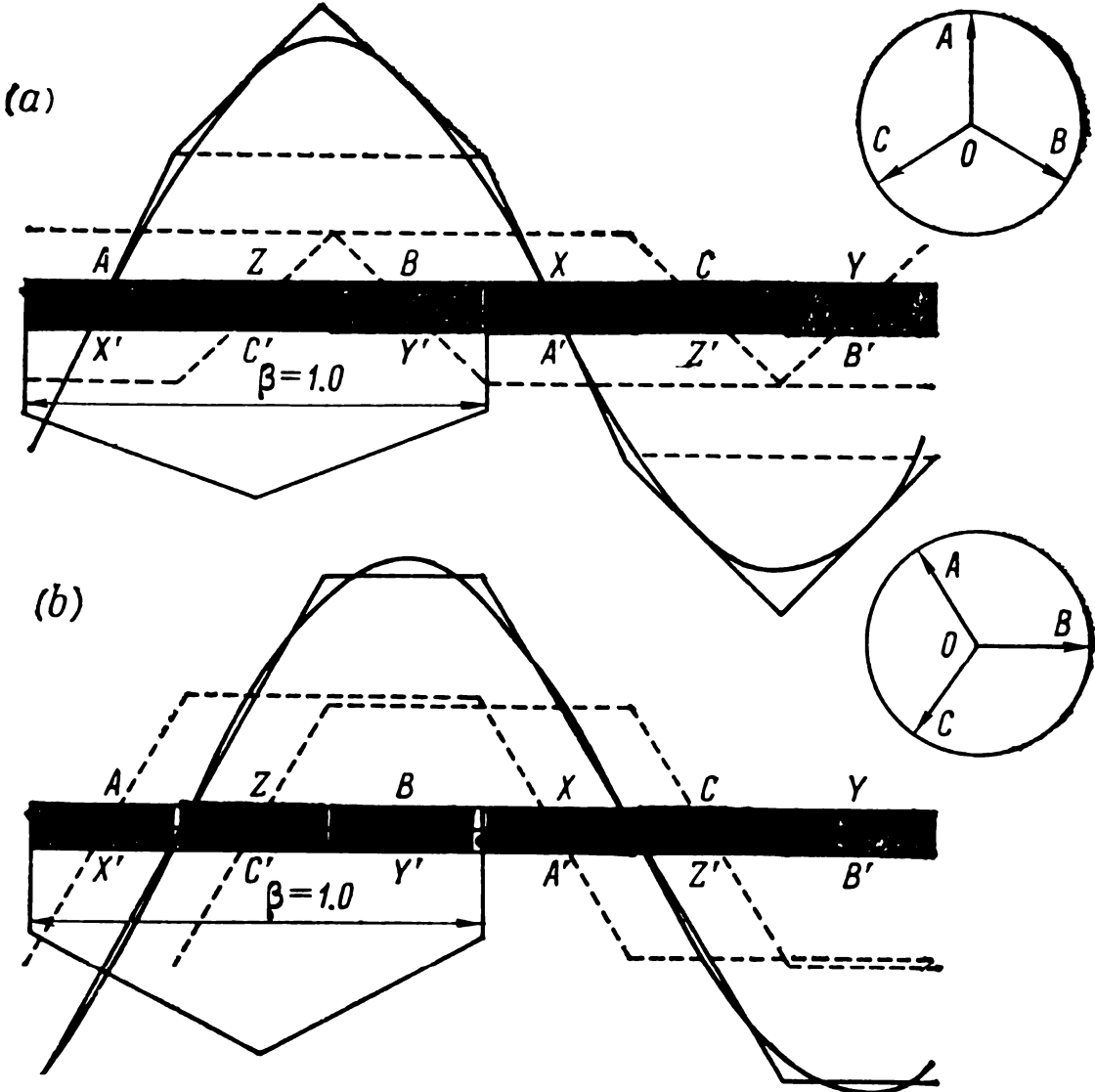


Fig. 4-13. Magnetizing force curves of uniformly distributed full-pitch winding for two moments

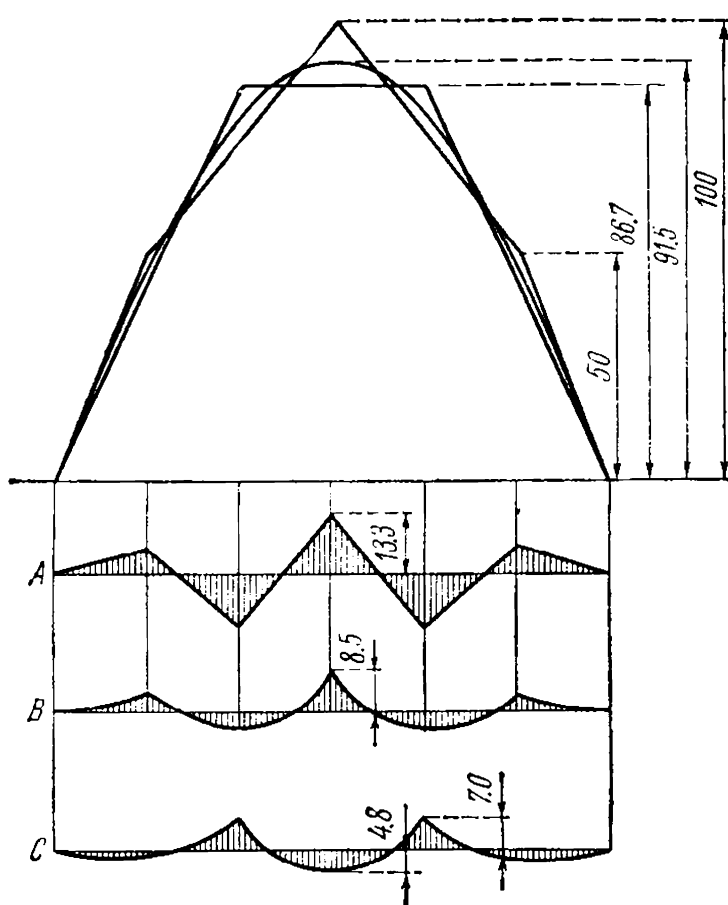


Fig. 4-14. Superposed curves of Fig. 4-13

phase diametrical full-pitch winding with $q=1$ for different moments of time and the resolution of the basic magnetizing force curve into harmonics.

As an illustration of the above, Fig. 4-12 depicts over a double-pole pitch the magnetizing force curve of a full-pitch three-phase single-layer winding with $q=2$ for the moment when $i_A = I_m$ and $i_B = i_C = -\frac{1}{2} I_m$.

Figure 4-13 pictures magnetizing force curves of a two-layer uniformly distributed full-pitch winding ($\beta=1.0$) for two moments differing by 30° , and also the sine curve of the fundamental magnetizing force harmonic. All these curves are superposed in Fig. 4-14 to take an account of the changes which the magnetizing forces undergo in travelling along the air-gap. Curve A in the lower part of Fig. 4-14 depicts the differences between the magnetizing forces for the moments of time indicated above at which the extreme magnetizing force curve shapes are obtained. Curves B and C show the differences between the extreme shapes of the magnetizing force curves and the sine curve of the fundamental magnetizing force harmonic.

Figure 4-15 illustrates magnetizing force curves of a double-layer uniformly distributed winding with a short pitch $y = \frac{5}{6}\tau$ for the same moments of time as in Fig. 4-13.

In a uniformly distributed winding ($q=\infty$), the magnetizing force wave ordinates change not abruptly, but continuously. As a result, sloping lines appear instead of vertical magnetizing force curve sections.

Two shapes are characteristic of magnetizing force curves plotted for a given winding for different moments of time. One corresponds to the moment when the current in one of the phases (for example, in phase A) is maximum in value, the other to the moment when the current in one phase (for example, in phase B) equals zero. Let us refer to these shapes as extreme ones.

Figure 4-11 shows magnetizing force curves of a three-

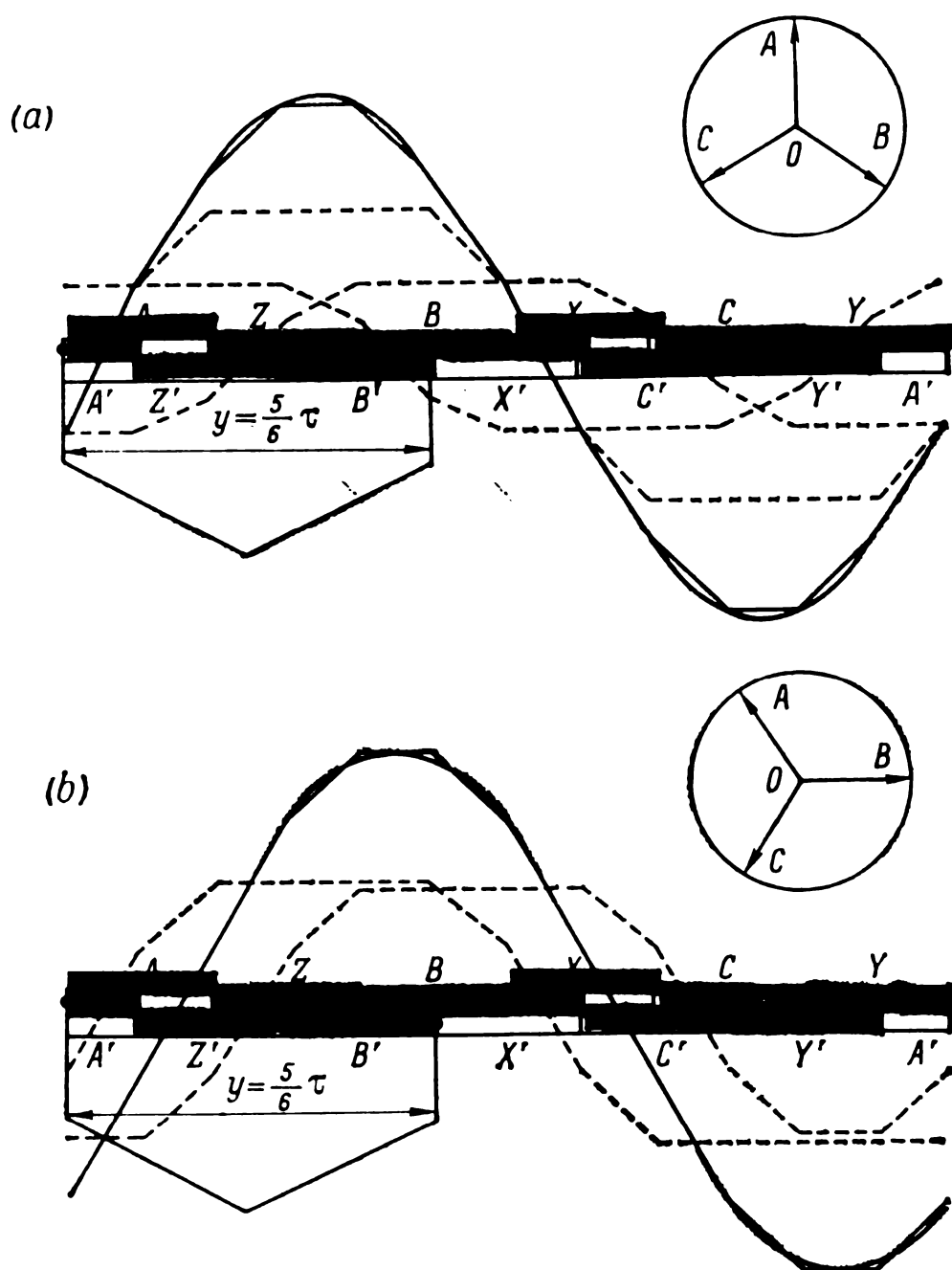


Fig. 4-15. Magnetizing force curves of double-layer uniformly distributed winding with relative pitch $\beta = \frac{5}{6}$ for two moments

Comparison of magnetizing force curves for a full pitch and a short pitch with $\beta = \frac{5}{6} = 0.833$ shows that, in the latter case, the magnetizing force curve is much closer to a magnetizing force sine curve than the full-pitch curve. This also follows from the analysis of the expressions obtained for the magnetizing force. For a pitch of $\beta = \frac{5}{6}$ according to equation (2-29) we have

$$\frac{k_{p5}}{k_{p1}} = \frac{\sin \left(5 \times \frac{5}{6} \times \frac{\pi}{2} \right)}{\sin \left(\frac{5}{6} \times \frac{\pi}{2} \right)} = \frac{0.259}{0.966} = 0.268$$

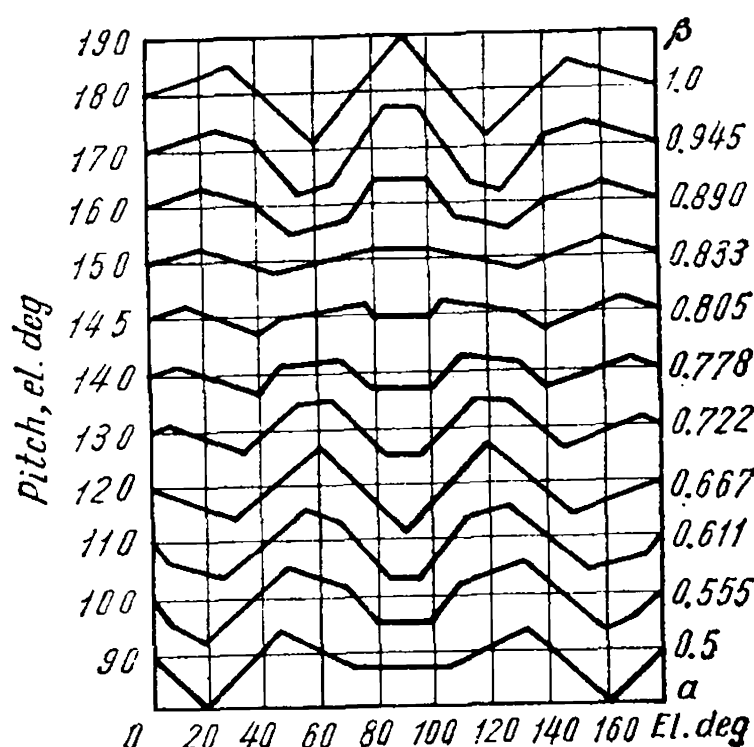


Fig. 4-16. Differences in magnetizing force curves for two moments differing by 30° , for different short pitches

netizing forces for two basic moments of time displaced by 30° for different short pitches ranging from $\beta=1.0$ to $\beta=0.5$. These curves show that the best results are obtained at relative pitch values within $\beta=0.833$ to $\beta=0.805$. For a pitch with $\beta=0.667$ the same harmonic content is obtained as with a pitch with $\beta=1.0$.

Example 4-1. Determine the amplitudes of the fundamental and higher magnetizing force harmonics $v=1, 5$ and 7 for the synchronous generator with $q=4$ considered in Example 2-2. Using the initial and computed data of the above example, by means of formulas (4-35) and (4-39) we get:

$$F_1 = 1.35 \times \frac{72 \times 0.925}{6} \times 865 = 13,000 \text{ A}$$

$$F_5 = 1.35 \times \frac{72 \times 0.053}{5 \times 6} \times 865 = 148 \text{ A}$$

$$F_7 = 1.35 \times \frac{72 \times 0.041}{7 \times 6} \times 865 = 82 \text{ A}$$

This example shows that the magnetizing force higher harmonics obtained are very small compared with the magnetizing force of the fundamental harmonic.

4-6. Magnetizing Force of Fractional-Pitch Windings

The magnetizing force curve of a fractional-pitch winding can be plotted by the graphical method described in the previous section, but, since the symmetrical part of the winding occupies not two, but $2p : t$ pole pitches, where t is the greatest common factor of the number

and

$$\begin{aligned} \frac{k_{p7}}{k_{p1}} &= \frac{\sin \left(7 \times \frac{5}{6} \times \frac{\pi}{2} \right)}{\sin \left(\frac{5}{6} \times \frac{\pi}{2} \right)} = \\ &= \frac{0.259}{0.966} = 0.268 \end{aligned}$$

Therefore, with a short pitch of $\beta=\frac{5}{6}$, the fifth and seventh harmonics decrease to 0.268 of their diametral pitch value, which results in an appreciable decrease in the relative harmonic content.

To compare the influence of pitch shortening on the relative value of high-order harmonics, Fig. 4-16 gives the differences between mag-

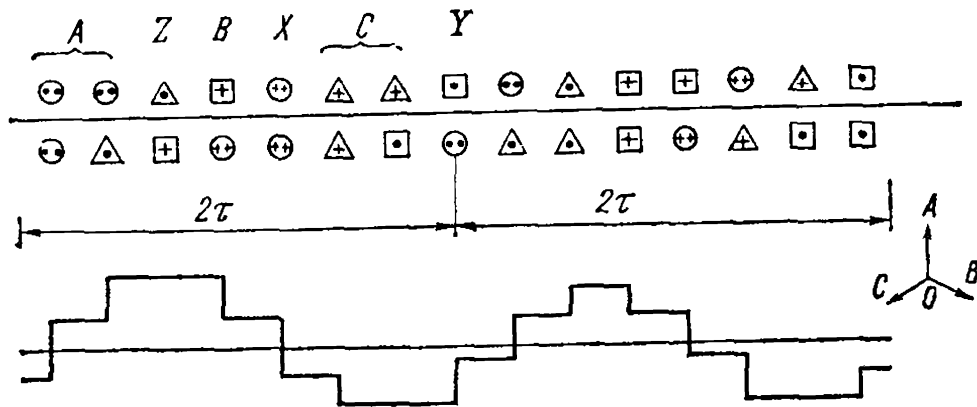


Fig. 4-17. Magnetizing force curve of three-phase double-layer winding with $q = 1\frac{1}{4}$ and $\beta = 0.8$

of slots Z and p (see Sec. 3-6), the magnetizing force curve should be constructed for at least $2p : t$ pole pitches.

Figure 4-17 shows the magnetizing force curve over a distance of 4τ discussed in Chapter 3 (Fig. 3-15) for a three-phase double-layer winding with $Z=30$, $2p=8$, $t=2$ and $q=1\frac{1}{4}$ for the moment when the current in phase A is maximum.

A glance at Fig. 4-17 shows that the magnetizing force forms four stepped poles, but the period of the curve is not 2τ , but 4τ . The curve therefore also contains a harmonic with a period two times that of the fundamental wave. Thus, a fractional-pitch winding also produces lower-order magnetizing force harmonics rotating with a speed as many times greater than the fundamental harmonic speed, as the space harmonic periods are.

Furthermore, since the curve in Fig. 4-17 is not symmetrical with respect to the axis of abscissas, it can be concluded that a fractional pitch winding, besides odd harmonics, also induces even harmonics.

The magnetizing force harmonic amplitudes of a fractional-pitch winding can be calculated with the help of the same equations as for integral-pitch windings if the winding factors are properly determined. It can be shown that the winding factors for the harmonics which also exist in a magnetizing force curve with a fractional q ($v=1, 3, 5, 7, \dots$) are calculated by the same formulas as for an integral q by substituting for q the equivalent number of slots per pole per phase of the fractional-pitch winding $q_{eq}=ac+b$.

4-7. Magnetic Field of an A.C. Winding

With a uniform air-gap and in the absence of saturation, the flux density B in the gap is proportional to the magnetizing force F_a

$$B = \lambda_\delta F_a$$

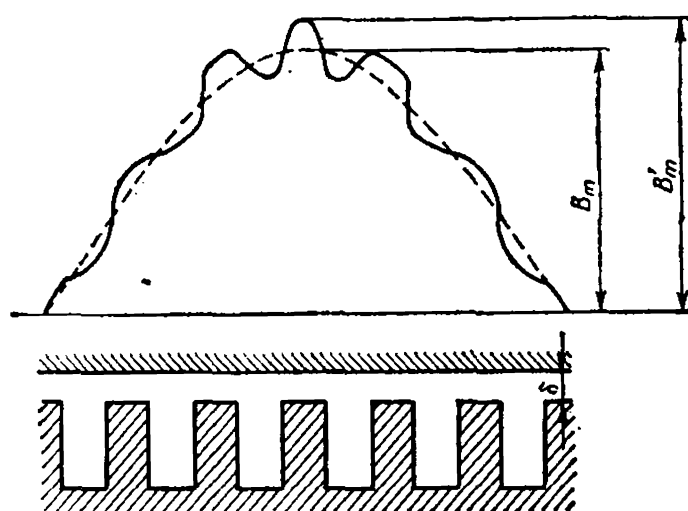


Fig. 4-18. Changes in field curve due to presence of teeth

where

$$\lambda_{\delta} = \frac{\mu_0}{\delta} \quad (4-45)$$

is the air-gap permeance [formula (4-14)].

Where a tooth and slot construction is involved, the magnetic field becomes distorted.

The solid line in Fig. 4-18 shows the curve of the field produced by the fundamental magnetizing force harmonic when one of the gap surfaces is toothed. If the fundamental harmonic is separated from this

curve, its amplitude B_m will be smaller than the amplitude B'_m with a uniform gap.

It can be assumed with sufficient accuracy that

$$\frac{B'_m}{B_m} = k_{\delta}$$

where k_{δ} is the air-gap factor.

Thus, with non-uniformity of the air-gap due to the presence of teeth and slots, for calculation of the fundamental field harmonic produced by the fundamental magnetizing force harmonic, the gap permeance must be considered equal to

$$\lambda_{\delta} = \frac{\mu_0}{k_{\delta} \delta} \quad (4-46)$$

If the steel is saturated, the flux density in the gap also decreases and, in addition, is distorted. For example, the fundamental magnetizing force harmonic with the steel saturated produces not a sinusoidal field curve, but a flattened one. This distortion is comparatively small, however, since, owing to the presence of the air-gap and moderate flux densities in the steel under normal operating conditions, the reluctance of the steel portions of the magnetic circuit is comparatively small. It can be considered that the amplitude of the fundamental field harmonic induced by the fundamental magnetizing force harmonic decreases in proportion to the saturation factor k_{μ} , which, for the given magnetic state of the steel, is equal to the ratio of the total magnetic circuit magnetizing force to the air-gap magnetizing force. The factor k_{μ} is determined from the calculated data of the magnetic circuit from the no-load curve of the machine.

Consequently, taking into account the serrated surface of the air-gap and the saturation, the air-gap permeance, when computing the

fundamental field harmonic, should be assumed equal to

$$\lambda_\delta = \frac{\mu_0}{k_\delta k_\mu \delta} \quad (4-47)$$

Greater complications are encountered with the higher magnetizing force harmonics, whose fields are more affected by non-uniformity of the gap. Non-uniformity of the gap leads, furthermore, to the appearance of additional field harmonics, as can be seen from Fig. 4-18. For approximate computations it can be assumed that gap non-uniformity and saturation affect the higher-order harmonic field in the same way as the fundamental harmonic field, i.e., relation (4-47) can be used.

The influence of salient-pole rotor design of a synchronous machine on the fundamental harmonic of an a.c. winding field is discussed in Chapter 8.

Chapter

5

INDUCTIVE REACTANCES OF A.C. MACHINE WINDINGS

5-1. Inductive Reactances of Air-Gap Magnetic Fields

When analysing a.c. winding magnetizing force (Sec. 4-4), it was indicated that with a uniform gap each winding magnetizing force harmonic produces a sinusoidally distributed magnetic field wave, all field harmonics inducing e.m.f.s of fundamental frequency in the winding which produced them.

The e.m.f. induced in a winding phase by a ν -th field harmonic, produced by the given phase, is the e.m.f. of self-inductance of the winding phase due to the ν -th field harmonic. If we consider the e.m.f. in a phase produced by the ν -th field harmonic of this and the other phases of the same winding with balanced loading then this e.m.f. may be termed the phase self-inductance e.m.f. due to the ν -th harmonic, allowing for mutual inductance of the other phases.

If the machine active steel is not saturated, the harmonics of the magnetic field in the gap and also the e.m.f.s induced by them are proportional to the winding current I , and these e.m.f.s in the winding can be taken into account as voltage drops in the given winding due to the current I in the appropriately calculated inductive reactances.

Let us calculate the inductive reactances corresponding to the harmonics of the magnetic field in the air-gap.

The amplitude of the ν -th order magnetizing force harmonic F_ν is determined by equation (4-39). With a uniform gap having a width δ all around the periphery, the magnetizing force harmonic produces a sinusoidally distributed field harmonic with an amplitude $B_{\nu m} = \frac{\mu_0}{\delta} F_\nu$.

Actually the gap, owing to the presence of slots and teeth, is not uniform. In a non-salient-pole machine this can be taken into account, as a first approximation, by dividing the obtained value of $B_{\nu m}$ by the air-gap factor k_δ (see Vol. I, Chapter 2), this giving sufficiently accurate results for the fundamental field harmonic and somewhat less accurate results for higher-order harmonics. Similarly, by introducing the factor k_μ , steel saturation can be taken into account (see Sec. 4-7).

Hence for $B_{\nu m}$ we obtain

$$B_{\nu m} = \frac{\mu_0}{k_\delta k_\mu \delta} F_\nu \quad (5-1)$$

Since the pole pitch of a higher harmonic is

$$\tau_v = \frac{\tau}{v} = \frac{\pi D}{2vp}$$

the magnetic flux of the v -th order harmonic will be

$$\Phi_v = \frac{2}{\pi} B_{vm} \tau_v l = \frac{\mu_0 D l}{k_\delta k_\mu \delta} \frac{1}{vp} F_v \quad (5-2)$$

Here and below D is the diameter of the stator bore. A specialist of the Brown-Boveri firm [123, 124] proposes to use an average diameter over the machine gap as the design diameter, i.e. $D_{des} = \frac{(D+D_2)}{2}$, where D_2 is the rotor diameter.

In machines with a relatively great air-gap (turbogenerators) the design diameter is appreciably smaller than that of the stator bore. This results in a certain increase in the values of the line load magnetic density and in a change in the design values of the parameters.

Substituting the above expression for Φ_v in formula (2-38), we obtain the e.m.f. induced in the winding by the v -th harmonic.

With an account taken of the mutual inductance of the other phases, we find the inductive reactance of the winding self-inductance for the v -th-order harmonic $x_v = \frac{E_v}{I}$, taking into consideration the value of F_v from formula (4-39) and substituting f for f_v

$$x_v = 2mf \frac{\mu_0 D l}{k_\delta k_\mu \delta} \frac{\omega^2 k_{wv}^2}{v^2 p^2} \quad (5-3)$$

As any inductive reactance, x_v is proportional to the frequency f and to the square of the number of turns ω .

The amplitude of the magnetizing force of an entire m -phase winding is $\frac{m}{2}$ times greater than the magnetizing force amplitude of one phase. The self-inductance reactance of a phase in a winding due to the v -th-order field harmonic in the proper sense of the word, i.e., due to the field proper of the given phase, will therefore be equal to

$$x'_v = 4f \frac{\mu_0 D l}{k_\delta k_\mu \delta} \frac{\omega^2 k_{wv}^2}{v^2 p^2} \quad (5-4)$$

As can be seen from expressions (5-3) and (5-4), the reactances x_v and x'_v rapidly decrease with an increase in the harmonic order v . The main physical processes taking place in a machine are connected with the fundamental field harmonic ($v=1$). Therefore the leading part is played by the self-inductance reactance of the phase, with the mutual inductance due to other phases for the fundamental wave ta-

ken into account

$$x_1 = 2mf \frac{\mu_0 D l}{k_\delta k_\mu \delta} \frac{\omega^2 k_{w1}^2}{\rho^2} \quad (5-5)$$

and by the own self-inductance reactance of the phase for the fundamental harmonic

$$x'_1 = 4f \frac{\mu_0 D l}{k_\delta k_\mu \delta} \frac{\omega^2 k_{w1}^2}{\rho^2} \quad (5-6)$$

The field harmonics of a given winding, for instance a stator winding, also induce mutual inductance e.m.f.s in the other windings of the machine, for example, in the rotor winding. We shall obtain the corresponding mutual inductance reactances, if in formulas (5-3), (5-4), (5-5) and (5-6) we substitute $\omega_1 \omega_2 k_{w1} k_{w2}$ for $\omega^2 k_{w1}^2$, where the subscripts 1 and 2 indicate the corresponding windings. Here instead of f it is necessary to use the actual frequency of the self-inductance e.m.f., and, instead of m , the number of phases in the winding whose current induces the e.m.f. under consideration. Since often $m_1 \neq m_2$, it also follows, generally speaking, that $x_{12} \neq x_{21}$.

The corresponding self- and mutual inductances of a winding can be obtained by dividing the reactances x by $\omega = 2\pi f$.

5-2. General Expressions for Inductive Leakage Reactances

The basic physical processes occurring in a machine, including the processes of mutual inductance between the windings of the machine, take place together with the fundamental field harmonic in the air-gap. All the other magnetic fields of the winding (the field in the slots, in the end connections, and the higher harmonics of the field) either do not link with any other winding and do not induce an e.m.f. of mutual inductance in them (the field in the slots, when only one winding is in them), or link very weakly with other windings (the end-connections and higher harmonic fields) and their mutual inductance and linkages are of secondary importance. These linkages, consequently, may be neglected when considering most of the problems.

All these fields belong to the leakage field of the winding, their principal action is to induce in the winding an e.m.f. of self-inductance, or the so-called leakage e.m.f., accounted for by the inductive leakage reactance.

Leakage fields encounter mainly air-gap reluctances. The reluctance of the steel parts may therefore be disregarded for practical purposes and it is considered that the leakage inductance $L_\sigma = \text{const.}$

The leakage electromotive force is

$$e_\sigma = - \frac{d(L_\sigma i)}{dt} = - L_\sigma \frac{di}{dt}$$

But $i = I_m \sin \omega t$ and therefore

$$e_\sigma = -\omega L_\sigma I_m \cos \omega t = -x_\sigma I_m \cos \omega t$$

Here x_σ is the inductive leakage reactance, equal to

$$x_\sigma = \omega L_\sigma \quad (5-7)$$

The leakage inductance of a winding, in the general case, is equal to

$$L_\sigma = \frac{\sum \omega_x \Phi_x}{i} \quad (5-8)$$

where Φ_x is a magnetic inductance tube flux linking ω_x turns, and the summation covers all the flux tubes.

For one coil side, with s_s conductors per slot, and laid in one slot we have

$$L_{\sigma 1} = \frac{\sum s_x \Phi_x}{i}$$

Here the flux is

$$\Phi_x = \frac{s_x i}{R_x}$$

and the reluctance of a tube is

$$R_x = \frac{b_x}{\mu_x A_x}$$

where b_x is the length of the leakage flux tube, and A_x is its cross-sectional area, which may be considered constant. Since the leakage fields close through air, it may be assumed that $\mu_x = \mu_0$.

If instead of the reluctance R_x we use its reciprocal, i.e., the permeance Λ_x , then

$$\Lambda_x = \frac{1}{R_x} = \lambda'_x l_x \mu_0$$

where λ'_x is the permeance of the leakage flux per unit of turn length. Hence

$$\Phi_x = s_x \Lambda_x i = \mu_0 s_x \lambda'_x l_x i$$

and

$$L_{\sigma 1} = \mu_0 \sum s_x^2 \lambda'_x l_x \quad (5-9)$$

In the general case the fluxes Φ_x link with various numbers of conductors s_x (Fig. 5-1a).

Let us transform the expression for flux linkage $\sum \Phi_x s_x$ so that the leakage flux Φ_x , linking with the full number of conductors s_s in the slot, will give equal flux linkage. For this purpose let us substitute in expression (5-9) $s_s^2 \lambda_x$ for the product $s_x^2 \lambda'_x$, where

$$\lambda_x = \left(\frac{s_x}{s_s} \right)^2 \lambda'_x$$

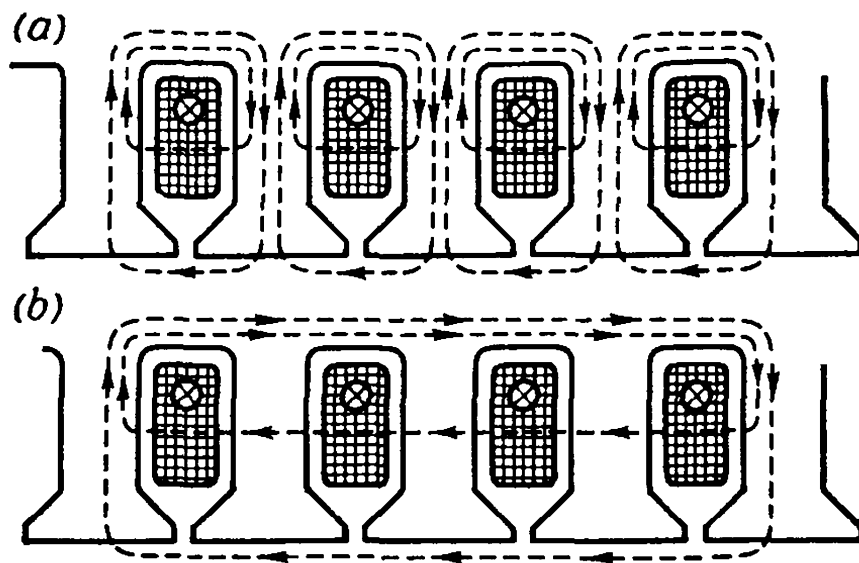


Fig. 5-1. Slot-leakage magnetic field

is the equivalent permeance for the case when the leakage flux links with the total number of conductors s_s laid in the slot. Hence

$$L_{\sigma 1} = \mu_0 s_s^2 \sum \left(\frac{s_x}{s_s} \right)^2 \lambda'_x l_x = \mu_0 s_s^2 \sum \lambda_x l_x \quad (5-10)$$

If the winding of a given phase is laid not in one, but in q slots, the leakage e.m.f. of the slots increases q times. Indeed, the leakage flux diagram (Fig. 5-1a), in which a separate leakage field is produced around each slot, can be replaced by a diagram (Fig. 5-1b) in which all q slots are linked by one common leakage flux. Since the magnetizing force of q slots increases q times as compared with the magnetizing force of one slot, and since the reluctance likewise increases the same number of times, the magnitude of the magnetic leakage flux remains the same, while the flux linkage and the leakage e.m.f. increase q times.

If, for example, we have a single-layer winding with p pairs of poles and all the p groups of a coil section are series-connected, the e.m.f. and the inductive leakage reactance will increase p times. The total number of series-connected turns will be $w = s_s q p$. Therefore, the leakage inductance of a winding phase due to the leakage field of the slots is equal to

$$L_{\sigma s} = q p L_{\sigma 1} = s_s^2 q p \mu_0 \sum \lambda_x l_x = \frac{\mu_0 w^2}{p q} \sum \lambda_x l_x \quad (5-11)$$

The inductive leakage reactance of the slots of the entire phase of a winding is equal to

$$x_{\sigma s} = \omega L_{\sigma s} = 2\pi f \mu_0 \frac{w^2}{p q} \sum \lambda_x l_x \quad (5-12)$$

The expression obtained above will be valid for all types of windings if we properly calculate the sum $\sum \lambda_x l_x$.

The inductive reactance of the end connections of a single-layer winding depends on the number of conductors running together in close contact. In a two-tier single-layer winding, the whole group of conductors coming out of q slots forms one common bunch of conductors encompassed by a common leakage flux (Fig. 5-2). The leakage e.m.f. and the inductive reactance of the end connections therefore increase q^2 times and in the given case

$$x_{\sigma \cdot end} = 2\pi f s_s^2 q^2 p \mu_0 \sum \lambda_x l_x = 2\pi f \mu_0 \frac{\omega^2}{pq} q \sum \lambda_x l_x \quad (5-13)$$

In a three-tier single-layer winding, at the end connections, where the parts of the overhang are straight, the inductive reactance increases q^2 times, but in the regions where the wires go in opposite directions the reactance increases only $\left(\frac{q}{2}\right)^2$ times. It may be assumed that the permeance per unit of length in a three-tier winding is 1.5 times less than that in a two-tier winding.

In double-layer d.c. type windings the length of the end connections is relatively small. According to information given by the "Elektrosila" Works, the inductive reactance of the end connections in comparison with that of a two-tier winding is roughly halved.

Since for the slot portion and tooth heads it should be assumed that $l_x = 2l$, where l is the length of the active steel, and for the end connection, $l_x = 2l_{end}$, where l_{end} is the length of the end connection, the value $\sum \lambda_x l_x$ for the slot and end-connection leakage in the general case may be represented as

$$\sum \lambda_x l_x = 2l\lambda_s + 2l_{end}\lambda_{end}q = 2l\left(\lambda_s + q\lambda_{end}\frac{l_{end}}{l}\right) \quad (5-13a)$$

where λ_s = equivalent permeance for the slot leakage fields

λ_{end} = equivalent permeance of the end connections.

Thus the equation for the inductive reactance of the slots and the end connections becomes

$$x_{\sigma s \text{ end}} = 4\pi f \mu_0 \frac{l\omega^2}{pq} \left(\lambda_s + q\lambda_{end} \frac{l_{end}}{l} \right) \quad (5-14)$$

Here $\mu_0 = 4\pi \times 10^{-7} \text{ H/m} = 1.26 \times 10^{-8} \text{ H/cm}$.

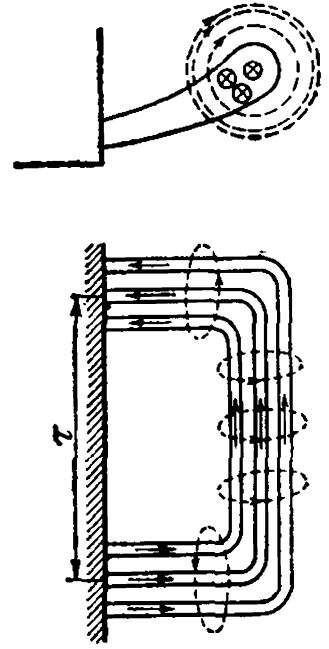


Fig. 5-2. Magnetic field of end-connection leakage

The higher field harmonics of the winding in the gap form the so-called differential leakage field of the winding. Differential leakage inductive reactance can be obtained, with some approximation, by summation of all the x_v according to formula (5-3) for values of $v > 1$.

In machines with a relatively small air-gap the magnitude of the differential leakage inductive reactance may be of the same order as the slot leakage or end-connection leakage reactance.

5-3. Slot Permeance

The distribution of the leakage flux Φ_{os} along the slot height is shown in Fig. 5-3. The reluctance of the steel is neglected. Therefore,

assuming that the magnetic lines cross the gap everywhere as straight and parallel lines, we can consider the length of each elementary tube, which determines its reluctance, to be equal to the width of the slot at the given point.

For the leakage fluxes encompassing a whole number of slot conductors s_s , the tube permeance per unit of slot length λ_x is determined as the ratio of the tube width along the slot height to the tube length across the slot width. Thus, for the slot in Fig 5-3a the permeance is:

for the portion with the height h_2

$$\lambda_{s2} = \frac{h_2 \times 1}{b_1} = \frac{h_2}{b_1}$$

for the portion with the height h_3

$$\lambda_{s3} = \frac{h_3}{\frac{1}{2}(b_1 + b_2)} = \frac{2h_3}{b_1 + b_2}$$

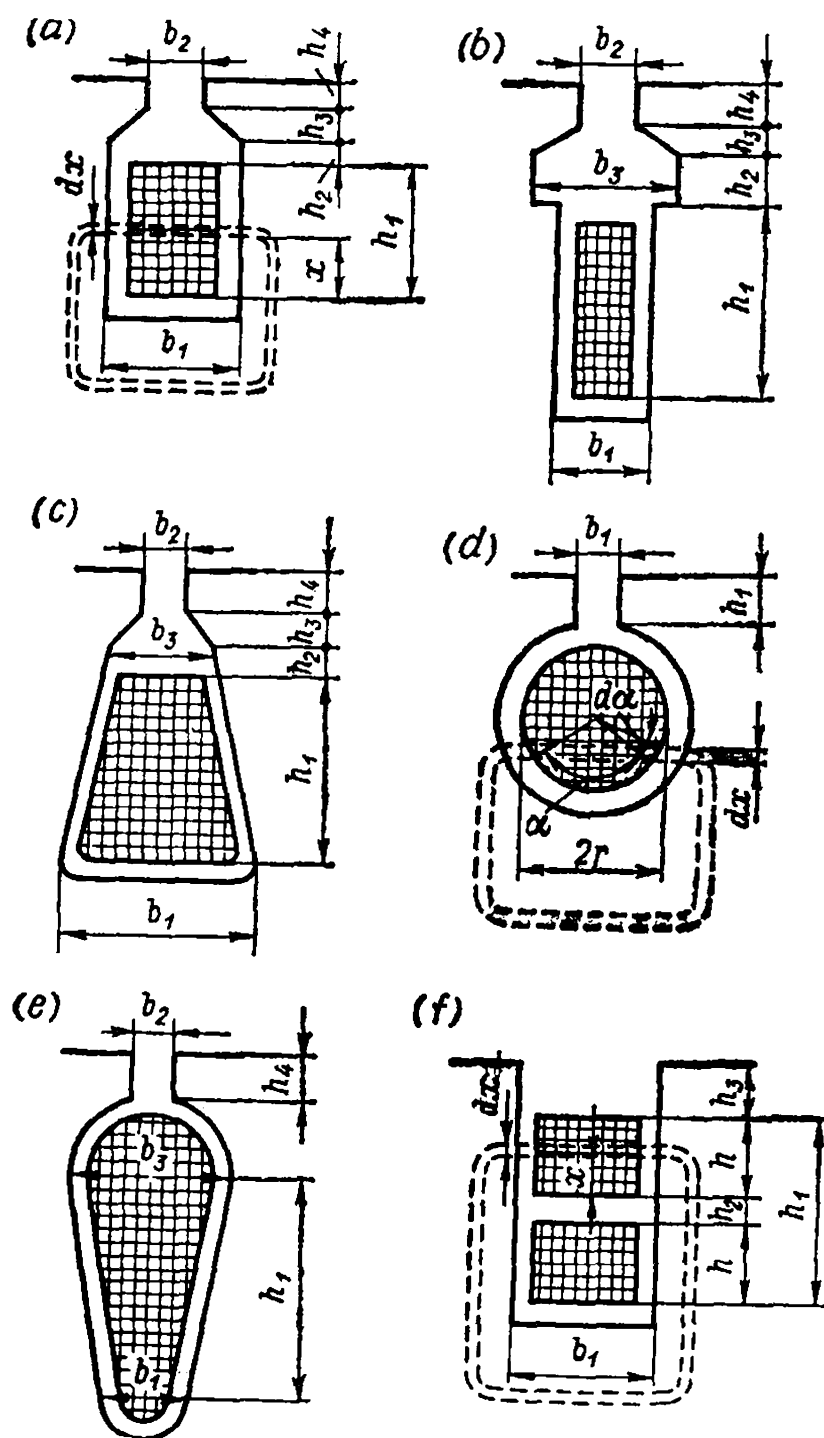


Fig. 5-3. To calculation of slot permeance

for the portion with the height h_4

$$\lambda_{s4} = \frac{h_4 \times 1}{b_2} = \frac{h_4}{b_2}$$

For the leakage fluxes acting only on part of the conductors along the height h_1 (Fig. 5-3a), it is necessary to determine the equivalent permeance corresponding to the leakage flux which would act on all s_s slot conductors.

An elementary tube with a width dx located at a height x from the slot bottom (Fig. 5-3a) has an elementary permeance

$$\lambda'_x = \frac{dx \times 1}{b_1} = \frac{dx}{b_1}$$

This tube links with the number of slot conductors

$$s_x = s_s \frac{x}{h_1}$$

The flux-linkage of this tube per unit of armature length is proportional to

$$s_x^2 \lambda'_x = \frac{s_s^2}{h_1^2 b_1} x^2 dx$$

The total flux-linkage for all the conductors along a height h_1 is proportional to

$$\sum_0^{h_1} s_x^2 \lambda_x = \int_0^{h_1} \frac{s_s^2}{h_1^2 b_1} dx = s_s^2 \frac{h_1}{3b_1} = s_s^2 \lambda_{s1}$$

The total equivalent permeance of the entire slot is

$$\lambda_s = \lambda_{s1} + \lambda_{s2} + \lambda_{s3} + \lambda_{s4} = \frac{h_1}{3b_1} + \frac{h_2}{b_1} + \frac{2h_3}{b_1 + b_2} + \frac{h_4}{b_2} \quad (5-15a)$$

For the form of slot shown in Fig. 5-3b we obtain in a similar way the permeance

$$\lambda_s = \frac{h_1}{3b_1} + \frac{h_2}{b_3} + \frac{2h_3}{b_2 + b_3} + \frac{h_4}{b_2} \quad (5-15b)$$

For the form of slot in Fig. 5-3c

$$\lambda_s = \frac{2h_1}{3(b_1 + b_3)} + \frac{h_2}{b_3} + \frac{2h_3}{b_2 + b_3} + \frac{h_4}{b_2} \quad (5-15c)$$

For a round slot uniformly filled with conductors, an elementary tube with a width dx and a specific permeance

$$\frac{dx}{2r \sin \frac{\alpha}{2}} = \frac{d \left(-r \cos \frac{\alpha}{2} \right)}{2r \sin \frac{\alpha}{2}} = \frac{d\alpha}{4}$$

is linked with a number of conductors

$$s_x = \frac{s_s}{\pi r^2} \left(\frac{\alpha r^2}{2} - \frac{r^2 \sin \alpha}{2} \right) = \frac{s_s}{2\pi} (\alpha - \sin \alpha)$$

Therefore, the flux-linkage of a round slot is proportional to

$$\int_0^{2\pi} \left(\frac{s_x}{s_s} \right)^2 \frac{d\alpha}{4} = \int_0^{2\pi} \frac{(\alpha - \sin \alpha)^2 d\alpha}{16\pi^2} = \frac{1}{16\pi^2} \left(\frac{8\pi^3}{3} + 4\pi + \pi \right) = 0.623$$

The total equivalent permeance of the entire round slot according to Fig. 5-3d is

$$\lambda_s = 0.623 k_{rd} + \frac{h_1}{b_1} \quad (5-15d)$$

With a solid round conductor account should be taken of screening of the leakage fields, by means of a factor $k_{rd} > 1$.

For the slot form shown in Fig. 5-3e

$$\lambda_s = \frac{2h_1}{3(b_1 + b_3)} + 0.623 + \frac{h_4}{b_2} \quad (5-15e)$$

For a double-layer winding with the conductors distributed in the slot according to Fig. 5-3f and having $\frac{s_s}{2}$ conductors in the top and the bottom layers, the self-inductance of the conductors in the two layers and their mutual inductance should be taken into consideration.

For the leakage flux-linkage of self-inductance of the conductors in the bottom layer, we have

$$\sum \lambda_{x1} s_{x1}^2 = \frac{s_s^2}{4} \left(\frac{h}{3b_1} + \frac{h_2 + h + h_3}{b_1} \right) = \frac{s_s^2}{4} \left(\frac{4h}{3b_1} + \frac{h_2 + h_3}{b_1} \right)$$

and for the top layer

$$\sum \lambda_{x2} s_{x2}^2 = \frac{s_s^2}{4} \left(\frac{h}{3b_1} + \frac{h_3}{b_1} \right)$$

whence the corresponding permeances are

$$\lambda_{s1} = \frac{1}{4} \left(\frac{4h}{3b_1} + \frac{h_2 + h_3}{b_1} \right)$$

$$\lambda_{s2} = \frac{1}{4} \left(\frac{h}{3b_1} + \frac{h_3}{b_1} \right)$$

In a full-pitch winding, the currents in the top and bottom layers are of equal magnitude, but in a short-pitch winding some of the slots contain layers of conductors which may carry currents belonging to different phases.

The flux-linkage of an elementary tube of conductors of the bottom layer with conductors of the top layer, in case of diameter pitch (Fig. 5-3f), is proportional to

$$\frac{s_s}{2} \left(\frac{s_s}{2} \frac{x}{h} \right) \frac{dx}{b_1} = \frac{s_s^2}{4} \frac{x dx}{hb_1}$$

The linkage of the top-layer flux with all the conductors of the bottom layer at a height h is proportional to the integral of the previous expression

$$\int_0^h \frac{s_s^2}{4} \frac{x dx}{hb_1} = \frac{s_s^2}{4} \frac{h}{2b_1}$$

Besides, the top-layer flux passing along the upper part of the slot free from conductors gives a flux-linkage with the conductors of the bottom layer proportional to

$$\frac{s_s^2}{4} \frac{h_3}{b_1}$$

Therefore, the following permeance corresponds to the flux-linkage of the bottom layer due to the top-layer flux

$$\lambda_{s12} = \frac{1}{4} \left(\frac{h}{2b_1} + \frac{h_3}{b_1} \right)$$

Similarly, the same permeance corresponds to the top-layer flux-linkage due to the bottom-layer flux

$$\lambda_{s21} = \lambda_{s12} = \frac{1}{4} \left(\frac{h}{2b_1} + \frac{h_3}{b_1} \right)$$

The resultant equivalent permeance of a full-pitch double-layer winding with a slot of the form shown in Fig. 5-3f will be

$$\lambda_s = \lambda_{s1} + \lambda_{s2} + \lambda_{s12} + \lambda_{s21} = \frac{1}{4} \left(\frac{8h}{3b_1} + \frac{h_2}{b_1} + \frac{4h_3}{b_1} \right) \quad (5-16)$$

Substituting $\frac{h_1 - h_2}{2}$ for h (Fig. 5-3f) we have

$$\lambda_s = \frac{h_1}{3b_1} - \frac{h_2}{12b_1} + \frac{h_3}{b_1} \quad (5-17)$$

whence, neglecting the term $\frac{h_2}{12b_1}$, we have

$$\lambda_s \cong \frac{h_1}{3b_1} + \frac{h_3}{b_1} \quad (5-18)$$

With a short-pitch winding, the lower layer will be displaced with respect to the upper layer by an angle $(1-\beta)\pi$.

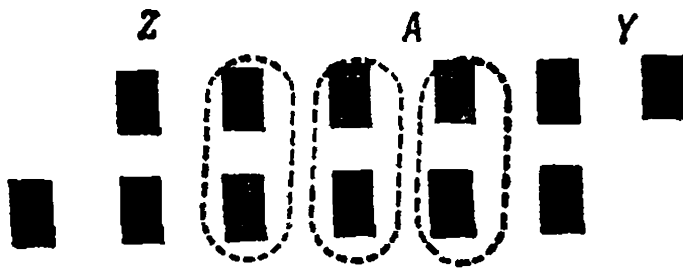


Fig. 5-4. Effect of fractional-pitch on slot-leakage field

Figure 5-4 shows the distribution of the layers of a winding with $q=2$ and $\beta=\frac{5}{6}=0.833$. In the middle slot of those encircled with a dotted line, both layers belong to phase A; in the right-hand encircled slot,

only the top layer belongs to phase A, the bottom layer belonging to phase B; in the left-hand encircled slot, the bottom layer belongs to phase A, while the top layer belongs to phase C. In a three-phase system, the currents of the adjacent phases located on one side of a given phase lead its current by 60° , those on the other side lag behind its current by 60° . The resultant magnetizing force and the leakage permeance therefore decrease. This decrease of permeance for a short-pitch winding within the range of $\frac{2}{3}<\beta<1.0$, as the analysis of this problem shows, occurs according to the ratio

$$k_{sh} = \frac{3\beta + 1}{4}$$

Thus, for a double-layer winding with a pitch within the range of $\frac{2}{3}<\beta<1.0$, the formula for the equivalent permeance of a slot according to Fig. 5-3f can be written in the following form:

$$\lambda_s = \left(\frac{h_1}{3b_1} + \frac{h_3}{b_1} \right) k_{sh} = \left(\frac{h_1}{3b_1} + \frac{h_3}{b_1} \right) \frac{3\beta + 1}{4} \quad (5-19)$$

5-4. Permeance of End Connections

The end-connection leakage is determined mathematically with greater difficulty than the slot leakage. A number of formulas for different cases of end-connection arrangement have been found by empirical methods. Because the available deductions of end-connection leakage equations are rather complicated and, notwithstanding this, still remain only approximate, we shall give here some of the more commonly used formulas without presenting their deductions.

For single-layer two-tier windings (see Fig. 3-8), the following formula is used

$$\Lambda_{end} = l_{end} \lambda_{end} = 0.67 l_{end} - 0.43 \tau \quad (5-20)$$

If separate coils are not grouped into one head, but are divided into two heads, as in single-layer three-tier windings (see Figs. 3-7 and 3-9) and in single-phase windings, the leakage values become approxi-

mately $\sqrt{2}$ times less and, therefore

$$\Lambda_{end} = l_{end} \lambda_{end} = 0.47 l_{end} - 0.3 \tau \quad (5-21)$$

A formula is obtained for a double-layer winding with cone-shaped end connections, which takes account of the axial and tangential end-connection fields, and gives good results for two-layer basket stator windings of turbo- and hydrogenerators

$$\Lambda_{end} = l_{end} \lambda_{end} = 0.57 \tau k_{sh} = 0.57 \frac{3\beta - 1}{2} \tau \quad (5-22)$$

where the factor

$$k_{sh} = \frac{3\beta - 1}{2}$$

takes into account the influence of pitch shortening.

5-5. Differential Leakage Inductive Reactance

Using equation (5-3), the expression for the inductive differential leakage reactance of a winding phase, taking into account the mutual inductance due to higher field harmonics of the other phases of the given winding, can be rewritten as

$$x_{dif} = \sum_{v>1} x_v = 2mf \frac{\mu_0 D l}{k_\delta k_{\mu\delta}} \frac{w^2}{p^2} \sum_{v>1} \frac{k_{wv}^2}{v^2} \quad (5-23)$$

where the summation extends to all harmonics except the fundamental one ($v=1$).

The ratio of x_{dif} to the inductive reactance x_1 due to the fundamental field harmonic in the air-gap x_1 [see formula (5-5)] is referred to as the differential leakage factor

$$k_{dif} = \frac{x_{dif}}{x_1} = \frac{1}{k_{w1}^2} \sum_{v>1} \frac{k_{wv}^2}{v^2} \quad (5-24)$$

Figure 5-5 gives the values of k_{dif} as a function of the relative pitch β for several values of q .

The value of the differential leakage reactance can be computed using known values of k_{dif} by means of the formula

$$x_{dif} = k_{dif} x_1 \quad (5-25)$$

or, if we rewrite the expression for x_{dif} in the form of formula (5-14)

$$x_{dif} = \frac{4\pi f \mu_0 l w^2}{pq} \lambda_{dif} \quad (5-26)$$

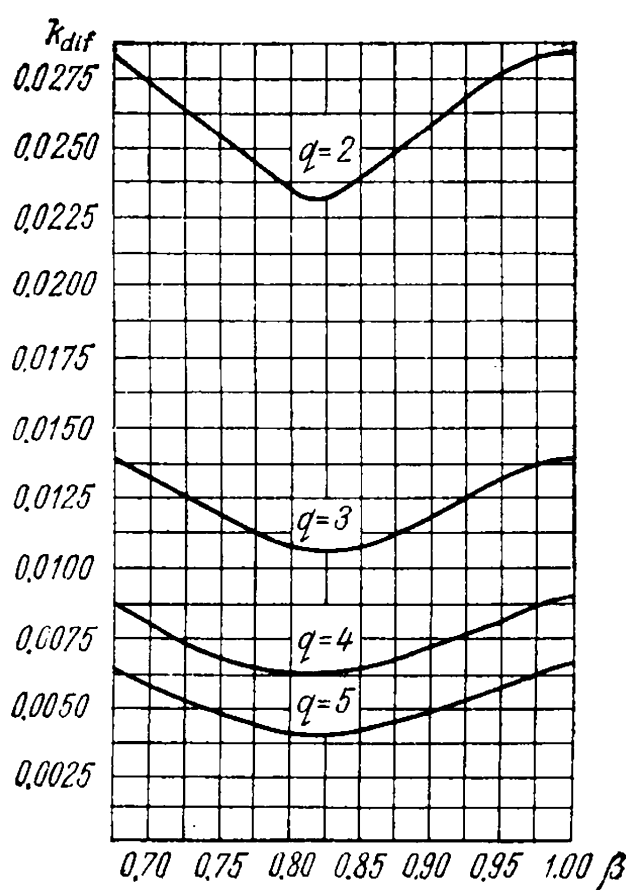


Fig. 5-5. Curves of differential leakage factor

where λ_{dif} is the permeance of the differential leakage flux, which, according to the above relationships, is equal to

$$\lambda_{dif} = \frac{mqk_{w1}^2\tau}{\pi^2k_{\delta}k_{\mu}\delta} k_{dif} = \frac{Zk_{w1}^2\tau}{2p\pi^2k_{\delta}k_{\mu}\delta} k_{dif} \quad (5-27)$$

The influence of nonuniformity of the air-gap when deriving formula (5-3) used above was accounted for by dividing the amplitudes of the field harmonics by k_{δ} . Actually, the differential leakage due to the action of the slot openings decreases to a greater degree. When the rotor has windings of the squirrel-cage type, or when a massive rotor is used, the differential leakage of the stator winding also reduces owing to damping of the higher harmonic fields by the rotor. In salient-pole synchronous machines x_{dif} also decreases because of weakening of the field in the space between the poles. All this is taken into account in computation practice by means of various approximate factors.

5-6. Leakage Inductive Reactances of Stator and Rotor Windings of a Synchronous Machine

The leakage inductive reactance of a synchronous machine stator winding is determined by the general formulas given in the present chapter for the permeances and inductive reactances of a.c. electrical machines.

The inductive reactance of the secondary rotor system of a salient-pole synchronous machine for the transient dynamic duties is determined from the general concepts and geometrical relations pictured in Fig. 5-6.

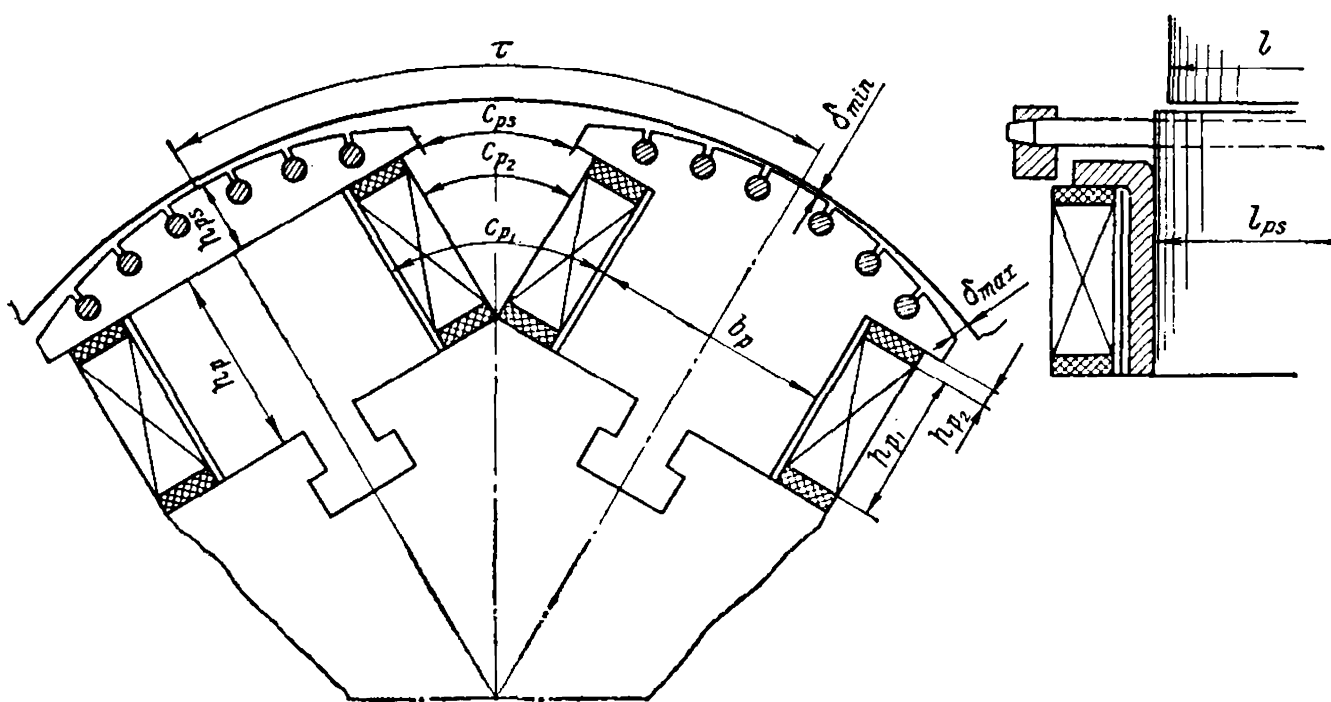


Fig. 5-6. Arrangement of poles of a salient-pole synchronous machine

The leakage permeance of the field winding is determined by the general method as for the leakage permeance of a slot, which the space between the poles is conditionally considered to be

$$\lambda_{exc.s} = 2 \left[\frac{h_{p1}}{3c_{p1}} + \frac{h_{p2}}{c_{p2}} + \frac{h_{ps}}{c_{ps}} + \frac{(l_{ps} - l) + 0.5h_p + 0.125b_p}{2l_{ps}} \right] \quad (5-28)$$

The first three terms take into account the permeance over the length of the machine, and the fourth term takes into account the permeance over the end part of the poles.

The leakage permeance of the damper system is the sum of the leakage permeances for the slot portion λ_{ds} and for the end connections $\lambda_{d.end}$. The former is determined by formula (5-15d) for a round slot (Fig. 5-3d), and the latter can be found by the formula

$$\lambda_{d.end} \cong 0.06 \frac{\tau}{l} N_{rod} \quad (5-29)$$

where N_{rod} is the number of damping rods per pole.

Example 5-1. Calculate the stator and rotor winding inductive reactances of a three-phase induction motor with a phase-wound rotor. The motor data are: $P_r = 250$ kW, $U_1 = 3000$ V, $\eta = 90\%$, $\cos \varphi_r = 0.89$, $2p = 6$, outer diameter of stator steel $D_a = 730$ mm, stator bore $E = 523.3$ mm, pole pitch $\tau = 275$ mm, length of active steel with ducts 364 mm, radial ventilation ducts 6×10 mm = 60 mm, effective length of steel $l = 364 - \frac{1}{2} \times 60 = 334$ mm, number of stator slots $Z_1 = 90$, number of series-connected stator turns $w_1 = 210$, number of slots per pole per phase $q_1 = 5$, winding stator slot pitch 1 to 13, relative stator winding pitch $\beta_1 = \frac{12}{15} = 0.8$. The stator slots (the slot shape is shown in Fig. 5-3f) have the dimensions: $h = 18.5$ mm, $h_1 = 42$ mm, $h_2 = 5$ mm, $h_3 = 8$ mm, and $b_1 = 9.8$ mm, winding factors of stator windings (see example in Ch. 2), $k_{d1} = 0.957$, $k_{p1} = 0.951$, $k_{w1} = 0.91$. The leakage permeance of the slot portion of the stator winding $\lambda_s = 1.87$ [formula (5-17)] taking into account the shortening factor of the slot portion of the winding $k_{sh.s} = 0.85$ [formula (5-19)]. The leakage permeance of the end connections of the stator winding $\lambda_{end} = 1.64$ [formulas (5-14) and (5-22)] taking into account the shortening factor of the end connections of the winding $k_{sh.end} = 0.7$ [formula (5-22)]. The air-gap $\delta = 1$ mm, air-gap factor $k_\delta = 1.6$, saturation factor of the magnetic circuit $k_\mu = 1.1$.

The differential leakage permeance, according to formula (5-27), is

$$\lambda_{dif} = \frac{3 \times 5 \times 0.91^2 \times 27.5}{\pi^2 \times 0.1 \times 1.6 \times 1.1} \times 0.004 = 0.08$$

where the differential leakage factor according to the curves of Fig. 5-5 for $q = 5$ and $\beta = 0.8$ is equal to $k_{dif} = 0.004$.

The sum of the leakage permeances is $\sum \lambda_1 = 3.59$. The inductive reactance of the stator winding, from formula (5-14), is

$$x_1 = 4\pi \times 50 \times 1.26 \times 10^{-8} \times \frac{33.4 \times 210^2}{3 \times 5} \times 3.59 = 2.78 \Omega$$

The rotor data are: $Z_2 = 72$, $q_2 = 4$, number of turns per phase $w_2 = 24$, the winding pitch is diametric, therefore $\beta_2 = 1$. The resulting secondary winding

factor, according to Table 2-2

$$k_{w2} = k_{d2} = 0.958$$

The rotor slot leakage permeance (the slot shape is shown in Fig. 5-3a), with slot dimensions of $h_1 = 38$ mm, $h_2 = 0.5$ mm, $h_3 = 1.5$ mm, $b_1 = 8.2$ mm and $b_2 = 1.5$ mm, is $\lambda_{s2} = 2.24$ [formula (5-15a)], and $\lambda_{end2} = 1.88$ [formula (5-22)].

The differential leakage permeance [formula (5-27)] is

$$\lambda_{dif2} = \frac{3 \times 4 \times 0.958^2 \times 27.5}{\pi^2 \times 0.1 \times 1.6 \times 1.1} \times 0.008 = 1.4$$

where the differential leakage factor according to the curves of Fig. 5-5 for $q_2 = 4$ and $\beta_2 = 1.0$ is equal to $k_{dif} = 0.008$.

The sum of the leakage reactances is $\sum \lambda_2 = 5.52$.

The rotor winding inductive reactance, from formula (5-14),

$$x_2 = 4\pi \times 50 \times 1.26 \times 10^{-8} \times \frac{33.4 \times 24^2}{3 \times 4} \times 5.52 = 0.07 \Omega$$

The secondary circuit inductive reactance, reduced to the primary circuit, is

$$x_2' = 0.07 \left(\frac{210 \times 0.91}{24 \times 0.958} \right)^2 = 4.7 \Omega$$

Chapter

6

HEATING AND COOLING OF ROTATING ELECTRICAL MACHINES

6-1. Insulating Materials Used in Electrical Machinery and Their Required Properties

The losses of electric and mechanical energy in electrical machines take place as a result of conversion of these kinds of energy into heat energy which leads to heating of various parts of the machine. To ensure reliable operation of electrical machines, the heating of any part of a machine must be kept within certain limits.

The most important and difficult task is to ensure reliable operation of the winding insulation in a machine, since insulating materials begin to fail at relatively low temperatures. Therefore, the allowable load on a machine is determined, first of all, by the permissible maximum temperature of the insulating materials used in it.

The insulating materials used in electrical machinery are divided on the basis of their thermal stability into classes: Y, A, E, B, F, H and C. Class Y insulation includes non-impregnated fibrous materials of cellulose and silk, not immersed into a liquid electrical insulation material, and also other materials or combinations of materials corresponding to this class. The temperature characterizing the thermal stability of Class Y materials is 90 °C. Class A includes impregnated fibrous materials of cellulose or silk immersed into a liquid electrical insulation material, and also other materials and combinations of materials corresponding to this class. The thermal stability of materials of Class A is 105 °C. Class E includes certain synthetic organic films, and other materials corresponding to this class with thermal stability of 120 °C. Class B includes materials on a mica base (including those on organic substrates), asbestos and fibreglass used together with organic binders and impregnating compounds, and also similar materials with thermal stability of 130 °C. Class F with thermal stability of 155 °C includes materials on a mica base, asbestos and fibreglass used in combination with synthetic binders and impregnating compounds. Class H with a heat resistance of 180 °C includes materials on a mica base, asbestos and fibreglass used in combination with silicon organic binders and impregnating compounds. Class C with thermal stability above 180 °C includes mica, ceramics, glass and quartz used without organic binders.

Each insulation class has a certain allowable limiting heating temperature limits ϑ_{lim} , at which the insulation can function reliably

for a sufficiently long period compatible with operation of the electrical machine. The experience available and the research carried out in this field have shown that the service life of Class A insulation, for instance, can be expressed by the formula

$$t_{ins} = Ce^{-\alpha\vartheta} = 7.15 \cdot 10^4 e^{-0.088\vartheta} \quad (6-1)$$

In this formula the time t_{ins} is measured in years; $C=7.15 \times 10^4$ and $\alpha=0.088$ are experimentally determined factors, e is the base of natural logarithms and ϑ is the temperature of the insulation in degrees Centigrade.

From this formula it follows that: (a) Class A insulation can function reliably for 16 to 20 years at a temperature limit $\vartheta_{lim}=95$ to 90°C ; (b) Class A insulation for every increase of temperature by 8°C loses half its service life. Thus, if the service life of this insulation at $\vartheta=95^\circ\text{C}$ is 16 years, at 110°C it drops to 4 years, and at 150°C , to several days.

Matters are more complicated with mica, asbestos and fine-fibre glass (glass-fibre silk), which are the substrate of Class B insulation. These materials, when used alone, are capable of withstanding high temperatures. In electrical machinery, however, they are employed not in the pure state, but as products containing binders—varnishes, compounds, resins, etc. These substances are affected to a greater degree by the temperature than the basic insulating material and, correspondingly, they reduce the service life of the insulation. This is why work is continuously being carried out to develop more thermal stability binders.

In addition to the required thermal stability properties, insulating materials must meet a number of other requirements, among which the most important are: (a) high dielectric strength of the materials, both at the normal ambient temperature and at the working temperature of the machine; (b) ability of the insulating material to withstand mechanical stresses and to maintain the necessary degree of elasticity, a property which should be retained even under the prolonged heating in service (see Table 6-1 below); (c) the lowest possible dielectric losses both in cold and warm conditions of the insulation; (d) high resistivity of the material when heated; (e) ease of working and application; (f) low cost of the material.

These requirements are the more important, the greater the machine output and the higher its rated voltage.

An excessive temperature rise may also adversely influence the mechanical operating conditions of a given machine part. Thus, for instance, the commutator may lose its regular geometrical shape, soldered joints between the armature winding and the commutator may break, bearings may fail, etc. These difficulties can be avoided, however, by proper design of the machine and observance of proper operating conditions.

It does not follow from the above that it is necessary to design machines with a low temperature rise. Such a machine could easily be built if low electromagnetic loadings for the active materials were incorporated, i.e., if we were to allow poor utilization of the materials, but the machine would be too heavy and costly and would have a very high moment of gyration. Therefore, the correct solution to the problem is to build a machine with good utilization of its materials, with the required efficiency and a sufficiently long service life. It should also be borne in mind that, other conditions being equal, the temperature of the machine will rise the higher, the poorer the cooling, and vice versa. Consequently, the problem of temperature rise in a machine is inseparable from the problem of its cooling and, in particular, the problem of its ventilation. In recent years these problems have acquired great importance in connection with the tendency to intensify machine utilization without deterioration of performance.

The following sections of this chapter are devoted to problems of a general nature, i.e., those necessary for the understanding of heating and cooling phenomena in all types of electrical machines. The features of heating and cooling of turbo-, and hydrogenerators are considered in Chapter 7.

6-2. Permissible Temperature Limits and Temperature-Rise Limits

The temperature ϑ of a given machine part depends not only on the losses occurring in it, but also on the temperature ϑ_{cm} of the cooling medium — air, hydrogen, water, etc.— used for cooling the machine. The difference

$$\vartheta - \vartheta_{cm} = \tau \quad (6-2)$$

is the *temperature rise* of the given part of the machine with respect to the temperature of the cooling medium.

To ensure the required service life of a machine, GOST* 183-66, for electrical machines establishes a standard temperature of the cooling medium ϑ_{cm} and the allowable temperature-rise limits τ_{lim} .

According to GOST 183-66, air is taken as the basic cooling medium. Since under actual conditions of machine operation the ambient air temperature may vary within a very wide range, the standard defines the permissible temperature limit for air as $\vartheta_{cm} = +40^\circ\text{C}$.

The permissible temperature-rise limits τ_{lim} are established by GOST 183-66 for windings, and for other generally not insulated machine parts, depending on the method of temperature measurement (Table 6-1). The following methods are generally used: (a) thermometer method, (b) resistance method and (c) embedded temperature indicator method.

* GOST—USSR State Standard.

The thermometer method is simple and gives sufficiently reliable results, but it cannot be used to measure the temperatures of the inner most heated machine parts.

The resistance method is used to measure the winding temperature, but it gives only the mean temperature value.

Thermocouples or resistance thermometers are customarily used as temperature indicators. They are embedded in the winding or in other machine parts during its manufacture, or are inserted for testing in spots where the maximum temperature is expected. This method gives the most accurate results, but it is more complicated than the other methods.

The allowable temperature limit ϑ_{lim} for insulating materials of different classes is obtained as the sum $\tau_{lim} + \vartheta_{cm} = \tau_{lim} + 40^\circ$. The temperature-rise limits for Class C insulation are not standardized.

Electrical machines must be designed and built so that their temperature rises at the rated load are within the given limits. If under actual operating conditions the ambient temperature is higher than the standard one (40°C), the load carried by the machine must be correspondingly reduced. If during certain periods of operation (for instance, in winter), the ambient temperature is below 40°C , this does not mean that the machine may be loaded above its power rating, except in emergencies, since the established limits of τ_{lim} are based on the necessity of ensuring normal service life, taking into account the natural variations of the ambient temperature.

6-3. Heat Transfer in Electrical Machines

Heat is transferred from one machine part to another and to the surrounding medium by conduction, radiation and convection.

Heat Transfer by Conduction is of significance in electrical machinery mainly in solid bodies (copper, steel, insulation), whereas in gases (air, hydrogen) and liquids (oil, water) convection is of the main importance.

If we have two parallel surfaces (for instance, the winding copper and the machine slot walls), each with an area A and with constant temperatures ϑ_1 and ϑ_2 , then the following amount of heat is conducted per unit of time through the medium between these surfaces (the insulation)

$$Q = \frac{\lambda_{int} A}{\delta} (\vartheta_1 - \vartheta_2) \quad (6-3)$$

where δ is the distance between the surfaces (in our case the insulation thickness), and λ_{int} is the coefficient of thermal conductivity of the intermediate medium, numerically equal to the quantity of heat transferred through a unit of area in a unit of time with a temperature difference of 1°C and over a distance between the surfaces equal to a unit of length.

TABLE 6-2

Material	Specific gravity, g/cm ³	Specific heat, W/sec deg·kg	Coefficient of thermal conductivity, W deg/cm
Copper, red	8.9	388	3.85
Aluminium	2.55	880	2.05
Electrical sheet steel:			
grade 31	7.8	460	0.46
" 32	7.75	—	0.32
" 33	7.65	—	0.25
" 34	7.6	480	0.20
Brass	8.6	386	1.0
Asbestos	2.5	818	0.0019
Mica	3.0	813	0.0036
Micafolium	2.3	880	0.0012-0.0017
Mica tape	2.4	1050	0.0015-0.006
Varnished cloth	—	—	0.002
Cotton	1.48	1520	0.0007
Pressboard	1.15	1760	0.0017
Paper	0.9	1680	0.0012
Transformer oil	0.95	1800	0.0016
Water	1.00	4184	0.0063
Air, 20 °C	0.0012	1000	0.00025
Hydrogen	0.000084	980	0.00175
Class A insulation	1.3	1470	0.0012
Class B insulation (continuous)	2.3	1170	0.0015-0.002
Sheet steel (across laminations)	—	—	0.01

The coefficients of thermal conductivity, specific gravities and specific heats for some materials are given in Table 6-2.

If, for example, the losses in a winding are such that 0.25 W is transferred through 1 cm² of the insulation and the latter (Class A) is 0.5 mm or 0.05 cm thick, the temperature drop in the insulation will be

$$\tau_{ins} = \vartheta_1 - \vartheta_2 = \frac{Q\delta}{\lambda_{int}S} = \frac{0.25 \times 0.05}{0.0012 \times 1} = 10.4^\circ\text{C}$$

Heat Transfer by Radiation. For an ideal black body the Stefan-Boltzmann law can be applied

$$q_{rad} = \alpha_{rad} (\theta_1^4 - \theta_{s.m}^4) \quad (6-4)$$

where q_{rad} = amount of heat radiated by a unit of area of the given body in a unit of time

α_{rad} = emissivity

θ_1 and $\theta_{s.m}$ = absolute temperatures of the emitting surface and the surrounding medium.

Experiments show that α_{rad} can be taken equal to 5.65×10^{-8} W/deg·m². For a non-ideal black body this value decreases, the rate of decrease depending on the nature of the radiating surface. Thus, for example, for cast-iron or steel surfaces, and for varnished insulation, the rate of decrease is 3-10%. Assuming 15% to provide a margin of safety, we get

$$q_{rad} = 4.8 \times \left[\left(\frac{\theta_1}{100} \right)^4 - \left(\frac{\theta_{cm}}{100} \right)^4 \right] \tag{6-5}$$

Here q_{rad} is determined in W/m². But

$$\begin{aligned} \left(\frac{\theta_1}{100} \right)^4 - \left(\frac{\theta_{cm}}{100} \right)^4 &= \frac{\theta_1 - \theta_{cm}}{100} \left[\left(\frac{\theta_1}{100} \right)^3 + \right. \\ &\quad \left. + \left(\frac{\theta_1}{100} \right)^2 \left(\frac{\theta_{cm}}{100} \right) + \left(\frac{\theta_1}{100} \right) \left(\frac{\theta_{cm}}{100} \right)^2 + \left(\frac{\theta_{cm}}{100} \right)^3 \right] \end{aligned}$$

The difference $\theta_1 - \theta_{cm} = (273 + \vartheta_1) - (273 + \vartheta_{cm}) = \vartheta_1 - \vartheta_{cm} = \tau$ is the temperature rise of a body; as to the sum in brackets, it varies relatively little within the conventional temperature limits for electrical machines. Formula (6-5) can therefore be rewritten as

$$q_{rad} = \lambda_{rad} \tau \tag{6-6}$$

where λ_{rad} is the transformed emissivity measured in W per m² with a temperature rise of $\tau = 1^\circ\text{C}$.

In contrast to α_{rad} , the value of λ_{rad} depends on the temperatures θ_1 and θ_{cm} and, hence, is not a constant. Values of λ_{rad} are given in Table 6-3 for various temperature rises of the body and ambient temperatures ϑ_{cm} . It can be assumed that, on the average, for air-cooled electrical machines $\tau = 40^\circ\text{C}$ and $\vartheta_{cm} = 20^\circ\text{C}$. Hence

$$\lambda_{rad} = 6 \text{ W/deg} \cdot \text{m}^2$$

The total heat radiated by a surface is

$$Q_{rad} = \lambda_{rad} A \tau \tag{6-7}$$

Heat Transfer by Convection. Liquid or gas particles in contact with a heated body become less dense and are compelled to rise, giving

TABLE 6-3

$\tau, ^\circ\text{C}$	$\theta_{cm}, ^\circ\text{C}$			$\tau, ^\circ\text{C}$	$\theta_{cm}, ^\circ\text{C}$		
	10	20	30		10	20	30
5	4.63	5.03	5.55	40	5.44	6.05	6.59
20	4.91	5.42	5.98	80	6.67	7.30	7.98

place to colder particles which also become warmer and rise. This phenomenon will be referred to as *natural convection*, as distinct from *artificial convection* which is caused by artificial circulation of the cooling medium, for instance, by blowing air at the surface being cooled with the aid of a fan.

Let us first consider natural convection.

Similar to formula (6-6), the heat dissipated by convection from a unit of surface area can be expressed as

$$q_{conv} = \lambda_{conv} \tau \quad (6-8)$$

where λ_{conv} is the convection coefficient equal to the amount of heat rejected from a unit of surface with a temperature rise of 1 °C, and τ is the temperature rise of the surface being cooled above the temperature of the cooling medium.

According to experimental data we have

$$\lambda_{conv} = C_{conv} \sqrt[4]{\frac{\tau}{H}} \quad (6-9)$$

where C_{conv} is a constant varying within rather wide limits depending on the conditions of the experiment, and H is the height of the surface in metres.

With the average values of C_{conv} , τ and H for electrical machines and transformers, it can be assumed that with air convection

$$\lambda_{conv} = 8 \text{ W/deg} \cdot \text{m}^2$$

The total heat rejected by convection from a surface with the area A will be

$$Q_{conv} = \lambda_{conv} A \tau \quad (6-10)$$

According to equations (6-7) and (6-10), the heat rejected from a surface by radiation and convection is equal to

$$Q = \lambda_{rc} A \tau \quad (6-11)$$

where

$$\lambda_{rc} = \lambda_{rad} + \lambda_{conv}$$

is the coefficient of thermal conductivity by radiation and convection, equal, in ordinary conditions, to $\lambda_{rc} = 14 \text{ W/deg} \cdot \text{m}^2$.

The relations (6-7) and (6-10) or (6-11) are used for temperature-rise calculations in conditions where there is no artificial convection.

In electrical machines, the conditions for heat dissipation by radiation and convection differ for various surfaces. In modern ventilated machines the heat removed by artificial convection prevails over that removed by radiation to such a degree that the latter is usually neglected.

Heat Rejection from Ventilated Surfaces. Here it is necessary to distinguish two cases: (a) heat rejection from an open ventilated surface, and (b) heat rejection from a closed ventilated surface. An example of the first case is the cooling of the outer surface of a commutator in an open-type machine and the cooling of a transformer tank; an example of the second case is the cooling of the duct surfaces in machines with internal ventilation. The increase in heat rejection in these conditions is due practically only to the increase in convection. The study of this problem is made difficult by the great variety of electrical machine designs and by the complexity of the aerodynamic phenomena in the internal ducts and spaces of a machine. Therefore, the increase in heat rejection when ventilating open surfaces is taken into account by means of empirical formulas. One of the most widely used formulas is

$$\lambda'_{conv} = \lambda_{conv} (1 + C_a \sqrt{v}) \quad (6-12)$$

Here λ'_{conv} = coefficient of heat transfer from a ventilated surface
 λ_{conv} = coefficient of heat transfer for natural convection
 v = air velocity relative to the cooled surface in m/sec
 C_a = empirical coefficient.

If the stream of air is uniform over the entire surface, then according to experimental data, $C_a \cong 1.3$; when the stream is not uniform, the coefficient C_a drops, for instance, to $C_a \cong 0.5$ for the frames of locomotive traction motors.

6-4. Theory of Solid Body Heating

Although an electrical machine consists of a number of parts differing in physical properties, machine heating can be analysed on the basis of the theory of heating of an ideal solid body, i.e., a homogeneous body possessing the property of uniform dissipation of heat from its entire surface and of infinitely great thermal conductivity.

Consider a body in which Q heat units are liberated in a unit of time. The heat energy liberated in the body during an infinitely small time dt will then be equal to $Q dt$.

If during this period the temperature of the body rises by $d\tau$ degrees, the heat energy absorbed by the body will then equal $Gc d\tau$, where G is the mass of the body and c its specific heat.

If in the process of heating of the body the temperature of its surface rises by τ degrees with respect to the surrounding medium, the heat energy dissipated by the body into the surroundings by radiation, convection and conduction during the time dt will equal $A\lambda\tau dt$, where A is the surface area of the body and λ is the surface heat-transfer coefficient.

The difference between the heat energy liberated in the body ($Q dt$) and the heat energy dissipated by the body into the surrounding me-

dium ($A\lambda\tau dt$) will be spent for raising the temperature of the body. The fundamental differential equation of heating can therefore be written as

$$Q dt - A\lambda\tau dt = Gc d\tau \quad (6-13)$$

Heat energy dissipation from the surface of a body will increase with the temperature rise τ , and, therefore, the part of the heat energy spent on the body temperature-rise decreases. Consequently, the heating process gradually begins to slow down. When, finally, the temperature difference attains its final temperature-rise value τ_{fin} , at which the entire heat energy liberated in the body is dissipated from the surface, the body temperature will cease to rise ($d\tau=0$) and a steady thermal state of the body sets in. Here equation (6-13) becomes

$$Q dt - A\lambda\tau_{fin} dt = 0$$

whence

$$\tau_{fin} = \frac{Q}{A\lambda} \quad (6-14)$$

Thus, the steady-state final temperature rise τ_{fin} is directly proportional to the heat flow Q and inversely proportional to the body surface area A and the heat transfer coefficient λ , but does not depend on the specific heat c and mass G of the body.

Divide (6-13) by $A\lambda$ and let

$$T = \frac{Gc}{A\lambda} \quad (6-15)$$

Thus

$$(\tau_{fin} - \tau) dt = T d\tau$$

or

$$\frac{dt}{T} = \frac{d\tau}{\tau_{fin} - \tau} \quad (6-16)$$

Using formulas (6-14) and (6-15), the expression for T can be rewritten as

$$T = \frac{Gc\tau_{fin}}{Q} \quad (6-17)$$

A glance at formula (6-17) shows that T can be interpreted as the time during which a body with a mass G and specific heat c is heated to τ_{fin} if the heat flow developed in the body equals Q and if there is no heat dissipation from the surface of the body. The quantity T is, therefore, referred to as the *heating time constant*. According to formula (6-15), the heating time constant T is directly proportional to the total heat capacity Gc of the body and inversely proportional to the total heat dissipation $A\lambda$ from its surface, being independent of the heat flow value Q .

Since the volume of a body increases in proportion to the third power, and the surface area in proportion to the second power of its linear

dimensions, the time constant of the body increases, other conditions being equal, in proportion to the first power of the linear dimensions. Because of this, larger machines also have a greater heating time constant. With greater ventilation the heating time constant decreases, since λ increases. The heating time constant for conventional electrical machines ranges from 0.5 to 3-4 hours.

Integration of formula (6-16) gives for the common integral the expression

$$\frac{t}{T} = -\log_e (\tau_{fin} - \tau) + C \quad (6-18)$$

where C is the integration constant, which can be determined from the initial conditions.

If at the initial moment $t=0$ the body has an initial temperature rise $\tau_{s.m}$ above the surrounding medium, we have, according to formula (6-18)

$$C = \log_e (\tau_{fin} - \tau_{s.m})$$

Substituting for C in (6-18), we get

$$\frac{t}{T} = \log_e \frac{\tau_{fin} - \tau_{s.m}}{\tau_{fin} - \tau}$$

whence, for the temperature rise τ as a function of time, we find

$$\tau = \tau_{fin} \left(1 - e^{-\frac{t}{T}} \right) + \tau_{s.m} e^{-\frac{t}{T}} \quad (6-19)$$

If, at the initial moment $t=0$, the initial temperature rise is $\tau_{s.m}=0$, equation (6-19) acquires a more simple form

$$\tau = \tau_{fin} \left(1 - e^{-\frac{t}{T}} \right) \quad (6-20)$$

At $t=0$ equation (6-20) gives $\tau=0$, and at $t=\infty$ we have $\tau=\tau_{fin}$.

From formula (6-19) we can also obtain the law of cooling of a body heated to a temperature rise of $\tau_{s.m}$. Indeed, if no heat is liberated in the body ($Q=0$), then, according to formula (6-14), we have $\tau_{fin}=0$, and from formula (6-19)

$$\tau = \tau_{s.m} e^{-\frac{t}{T}} \quad (6-21)$$

In accordance with formulas (6-19) and (6-21), the heating and cooling of a body take place according to an exponential law. In Fig. 6-1a curves 1 and 2 are the curves of a body heating $\tau=f(t)$ with $\tau_{s.m} \neq 0$ and $\tau_{s.m}=0$, and curve 3 is a cooling curve $\tau=f(t)$. For time periods

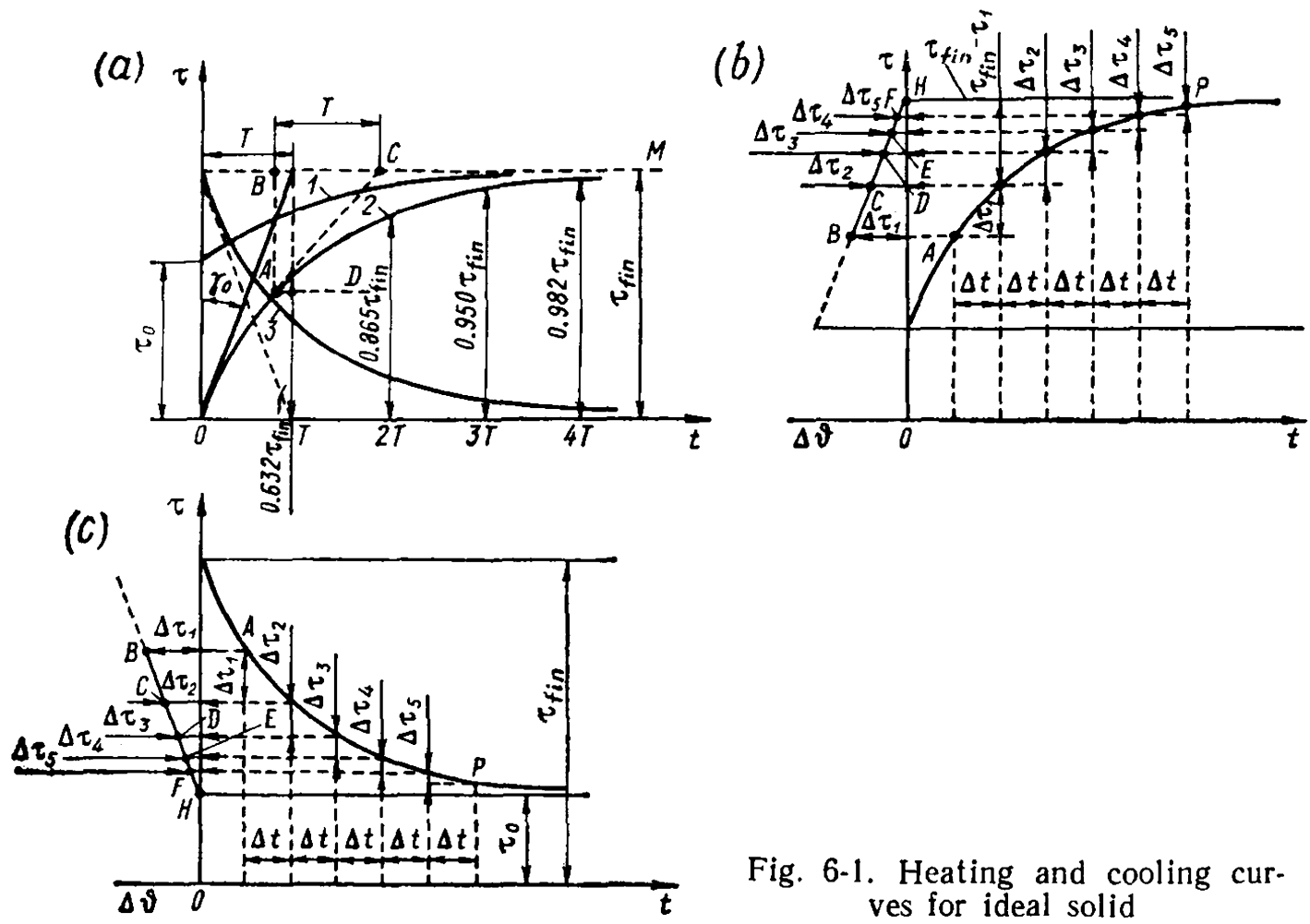


Fig. 6-1. Heating and cooling curves for ideal solid

$t=T, 2T, 3T, \dots$ the quantity $\frac{\tau}{\tau_{fin}}$ will have the following values:

t	$\dots\dots\dots$	T	$2T$	$3T$	$4T$
$\frac{\tau}{\tau_{fin}}$	$\dots\dots\dots$	0.632	0.865	0.95	0.982

The given data show that a body attains a steady-state temperature rise τ_{fin} during a time interval which is practically equal to four heating time constants.

By using heating curves it is possible to determine the heating constant T graphically. To prove this, let us differentiate equation (6-19) with respect to t . We obtain

$$\frac{d\tau}{dt} = \frac{(\tau_{fin} - \tau_{s. m})}{T} e^{-\frac{t}{T}}$$

But, according to the same equation (6-19)

$$(\tau_{fin} - \tau_{s. m}) e^{-\frac{t}{T}} = \tau_{fin} - \tau$$

Therefore

$$\frac{d\tau}{dt} = \frac{\tau_{fin} - \tau}{T}$$

or

$$T = (\tau_{fin} - \tau) : \frac{d\tau}{dt}$$

This relationship is the basic one for the graphical determination of T .

Consider now triangle ABC in Fig. 6-1a, where AC is a part of the tangent to the heating curve at some point A corresponding to the values t and τ .

For this triangle we have

$$BC = AB : \tan \angle BCA$$

But

$$AB = \tau_{fin} - \tau$$

and

$$\angle BCA = \angle CAD$$

is the angle of inclination of the tangent to the curve, the tangent of this angle being equal to the derivative of the function at the given point, i.e.

$$\tan \angle BCA = \frac{d\tau}{dt}$$

From a comparison of the relationships obtained it follows that in Fig. 6-1a we have $BC = T$, i.e., the heating time constant T can be determined as the subtangent BC (Fig. 6-1a) subtended by a tangent to the heating curve at any point on straight line BCM of the final temperature rise. In particular, T can also be determined by drawing a tangent to the heating or cooling curve at the initial point $t=0$ (Fig. 6-1a).

By utilizing the properties of an exponential function, it is also possible to determine graphically the final temperature rise τ_{fin} from some section of the heating or cooling curve. This can be shown by using the expression obtained for the derivative $\frac{d}{dt}$.

From this expression we have

$$\tau_{fin} - \tau = T \frac{d\tau}{dt}$$

Substitute for the derivative $\frac{d\tau}{dt}$ the ratio of small finite increments $\frac{\Delta\tau}{\Delta t}$, assuming $\Delta t = \text{const.}$

Hence

$$\tau_{fin} - \tau = \frac{T}{\Delta t} \Delta\tau = k \Delta\tau$$

i.e., the difference $\tau_{fin} - \tau$ with $\Delta t = \text{const}$ is a linear function of the increment $\Delta\tau$.

This leads to the following method of construction for the determination of τ_{fin} (Fig. 6-1b). On section AP of the heating curve, after dividing the corresponding time section into equal intervals

$$\Delta t_1 = \Delta t_2 = \Delta t_3 = \dots = \Delta t$$

find the corresponding temperature increments $\Delta\tau_1, \Delta\tau_2, \Delta\tau_3, \dots$ etc. By laying off along the axis of abscissas to the left of the origin of coordinates the increments of $\Delta\tau$ obtained for the corresponding temperature difference values $\tau_{fin} - \tau_1, \tau_{fin} - \tau_2, \tau_{fin} - \tau_3, \dots$ etc., and then drawing a straight line through ends B, C, D, E, F of the plotted increments $\Delta\tau_1, \Delta\tau_2, \Delta\tau_3, \dots$ to the intersection with the axis of ordinates at point H , we find the final value of the temperature rise

$$\tau_{fin} = OH$$

This plotting procedure can also be used for determining the final temperature for the cooling curve (Fig. 6-1c).

In view of the errors inherent in graphical methods and the deviations of the heating curves from an ideal exponential relationship, the above graphical methods are used in practice only when extrapolation is not extended too far.

Theoretically, the heating time constant T for a given machine part remains a constant. Actually, it varies somewhat. This can be explained mainly by the inconstancy of the coefficients λ_{rad} and λ_{conv} . Indeed, with an increase in temperature the losses in the windings increase, whereas in the bearings they decrease. Furthermore, the air gets heated when it flows through the ventilating ducts, and the temperature of the cooling medium therefore attains different values at various sections of the surface being cooled.

Experiment shows, however, that the process of temperature rise in real bodies will follow quite closely the law of temperature rise in an ideal body if their thermal conductivity is sufficiently high (in the case of metals) and if the rate of heat liberation is sufficiently moderate, i.e., with normal loads of electrical machines.

6-5. Main Rated Machine Duties

According to GOST 183-66, three rated duties are established for electrical machines, depending on the character of the load and its duration: (a) continuous, (b) short-time, and (c) short-time intermittent.

A machine is rated for *continuous* duty if its operating period is indefinitely long so that the temperatures of all parts of the machine attain practically steady values at a constant ambient air temperature. The machine can be operated in this duty for an infinitely long period, the temperature rise of its parts not exceeding the limits specified by the standards and those given for certain cases in Sec. 6-1.

Short-time duty is such which requires a machine operation of a certain specified short period indicated on the nameplate without exceeding the specified limits of temperature rise for any separate parts. The period of operation of the machine is so short that the temperature rise in the machine with the ambient temperature being invariable, does not reach a steady value, and the period of rest or no-load operation is so long that the machine practically returns to its cold state.

Short-time intermittent duty is a duty in which short-time operating intervals alternate with so-called pauses, i.e., with short-time rest or no-load intervals.

The intermittent duty cycle is characterized by the relative duration of the operating interval which, being given on the nameplate, is the ratio of time of the operating interval to full-cycle duration (operating interval plus pause interval).

A machine in short-time intermittent duty can operate with the duty factor indicated on the nameplate for an infinitely long time without exceeding the limits of the temperature rise specified by the relevant standard.

This duty is characterised by a relative (in per cent) duration of the on-load interval (duty factor) found by the following formula

$$\text{duty factor} = \frac{t_a}{t_a + t_b}$$

where t_a is on-load interval; t_b is a pause interval.

6-6. Machine Heating in Continuous Duty

The majority of electrical machines, with the exception of traction machines, are designed for continuous operation. In addition, the calculation of the temperature rise for continuous duty serves as the basis for calculations of the temperature rise in short-time and short-time intermittent duties. Hence it follows that the thermal calculation for continuous duty is the fundamental one.

The thermal calculations of electrical machines are quite complicated and are discussed in greater detail in the course on electrical machine design. Here we shall deal only with the procedure of calculation for continuous duty, when the temperature rise attains steady values.

The losses in the machine parts are known from the electrical calculations. The direction of the heat flows and the quantities of heat rejected from the surfaces being cooled can be established from the design of the machine. Also determined are the velocities of the air, the coefficient of heat transfer and the areas of the cooled surfaces being cooled. Next are determined: (a) the temperature drop τ_{ins} in the insulation of the winding by formula (6-3), and (b) the tempera-

ture rise $\tau_{s\ cm}$ of the surface being cooled above the temperature of the cooling medium by formula (6-11).

In addition, when gases and liquids move in the ducts, it is necessary to take into account the average temperature rise of the cooling medium itself $\Delta\tau_{cm\cdot av}$.

The temperature rise of a winding above the temperature of the cooling medium entering the machine $\tau_{w\ cm}$ is expressed by the sum

$$\tau_{w.\ cm} = \tau_{ins} + \tau_{s.\ cm} + \Delta\tau_{cm.\ av} \quad (6-22)$$

The temperature rise values obtained should not exceed the values permitted by GOST 183-66.

In view of the complexity of the aerodynamic phenomena in a machine, the velocities of the cooling medium for any surfaces and the corresponding heat transfer coefficients can be determined only approximately. It is also difficult to determine with sufficient accuracy the directions and magnitudes of the separate thermal flows in a machine. Therefore, the thermal calculations give satisfactory results only when sufficient experimental data are obtained.

6-7. Machine Heating in Short-Time Duty

To determine the temperature rise in separate machine parts in short-time duty $\tau_{sh.\ t}$ we first find, using the method described in Sec. 6-6, the temperature rise τ_{fin} when the machine operates under the given load in continuous duty, and also set the heating time constants T . Knowing the duration $t_{sh.\ t}$ of the short-time duty, it is possible to find the temperature rise in this duty by means of formula (6-20)

$$\tau_{sh.\ t} = \tau_{fin} \left(1 - e^{-\frac{t_{sh.\ t}}{T}} \right) \quad (6-23)$$

The values of $\tau_{sh.\ t}$ should fall within the limits specified by GOST 183-66.

Obviously, $\tau_{fin} > \tau_{sh.\ t}$ and, compared with continuous duty, the permissible value of $\tau_{sh.\ t}$ can be

$$\frac{\tau_{fin}}{\tau_{sh.\ t}} = \frac{1}{1 - e^{-\frac{t_{sh.\ t}}{T}}}$$

times greater. The permissible losses in the machine can also be the same number of times greater. Therefore, with given dimensions, the output of machines with a short-time duty is greater than that of machines with a continuous duty.

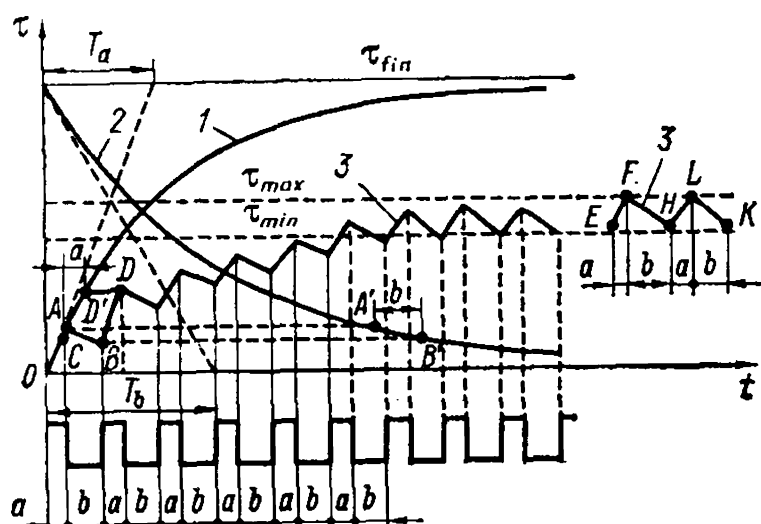


Fig. 6-2. Temperature rise curve for intermittent load

6-8. Machine Heating in Short-Time Intermittent Duty

Suppose a machine starts short-time intermittent operation from a cold state. Let the operating time be t_a , and the pause t_b .

The heating of the machine during the first period of operation will correspond to section Oa on heating curve 1 in Fig. 6-2; this curve can be plotted if the heating time constant T_a and the steady-state temperature rise τ_{fin} for continuous duty at the given power output are known.

Next a pause sets in, and the machine begins to cool. Cooling takes place along a curve parallel to section $A'B'$ of curve 2 in Fig. 6-2. This curve can also be plotted if τ_{fin} and the time constant T_b for cooling are known. If the ventilating conditions during the pause are the same as in operation, the time constants of curves 1 and 2 in Fig. 6-2 are identical. If the machine during the pause is at standstill and is not ventilated, the time constant of curve 2 will be greater than that of curve 1.

During the second and subsequent cycles of operation, the temperature rises parallel to the corresponding sections of curve 1, while cooling takes place parallel to the corresponding parts of curve 2. As a result, we obtain a zigzag curve 3 shown in Fig. 6-2 by a solid line. After some time the above duty becomes practically uniform, and the temperature rise of the machine varies within the range from τ_{max} to τ_{min} .

It can be seen that τ_{max} is smaller than τ_{fin} for continuous duty. Accordingly, a machine used for short-time intermittent duty, with the same dimensions and the same cooling conditions, can have $\tau_{fin} : \tau_{max}$ times higher losses and a correspondingly greater output. When it is desirable to use a machine designed for continuous duty for short-time intermittent operation, its output may be increased if this is permitted by other operating conditions of the machine, for instance, commutating conditions or overload torque capacity.

It can be seen that τ_{max} is smaller than τ_{fin} for continuous duty. Accordingly, a machine used for short-time intermittent duty, with the same dimensions and the same cooling conditions, can have $\tau_{fin} : \tau_{max}$ times higher losses and a correspondingly greater output. When it is desirable to use a machine designed for continuous duty for short-time intermittent operation, its output may be increased if this is permitted by other operating conditions of the machine, for instance, commutating conditions or overload torque capacity.

6-9. Ventilation of Electrical Machines

The following types of machines are distinguished according to the method of cooling:

(a) machines with natural cooling, which have no special ventilating devices;

(b) machines with internal self-ventilation, which are cooled by means of fans or other special devices integral with the rotating part of the machine;

(c) machines with external self-ventilation, i.e., machines whose outer surface is cooled by self-ventilation, while the active parts of the machine are inaccessible for the external air;

(d) machines with external ventilation, in which the cooling gaseous or liquid medium is supplied by a special device placed outside the machine, for instance, a fan or a pump.

The majority of machines are air-cooled. The specific gravity of air is $\gamma = 1.1 \text{ kg/m}^3$ and its specific heat is $c = 1000 \text{ W}\cdot\text{s/deg}\cdot\text{kg}$. In conventional machines the temperature of the air coming out of the machine rises above the temperature of the entering air by $\tau_{air} = 18$ to 27°C . According to these data, the air consumed per kW of losses in the machine amounts to

$$V = \frac{1000}{\gamma \tau_{air} c} = \frac{1000}{1.1 (18 \text{ to } 27) \times 1000} = 0.033 \text{ to } 0.05 \text{ m}^3/\text{s}$$

or 2 to 3 m^3/min . The aim of a ventilating system is to feed the required quantity of air through a machine with the minimum windage losses and with effective cooling of the most heated machine parts.

Let us consider, in brief, the characteristic features of various cooling methods.

Machines with Natural Cooling. At present this method of cooling is used only in small fractional-horsepower machines with outputs of several tens or hundreds of watts, since the conditions of cooling are comparatively favourable.

Machines with Internal Self-Cooling. Depending on the direction of the air flowing in a ventilated machine, there are distinguished suction or exhaust ventilation (Fig. 6-3a), and forced ventilation (Fig. 6-3b). Exhaust ventilation is used more frequently, the fan being mounted on the drive side. A valuable advantage of this method of ventilation is that cold air enters the machine, while in machines with forced ventilation the air is heated owing to losses in the fan. Experimental data show that the air temperature rise due to this heating reaches $3\text{--}7^\circ\text{C}$; the result is that the volume of air delivered into the

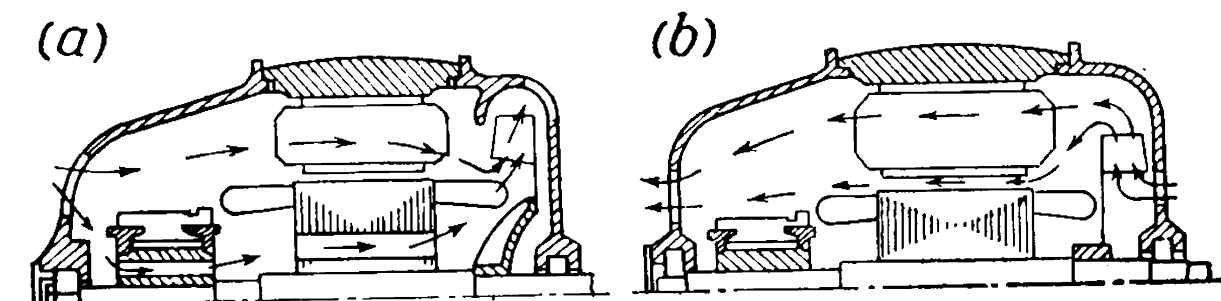


Fig. 6-3. Exhaust and forced ventilation

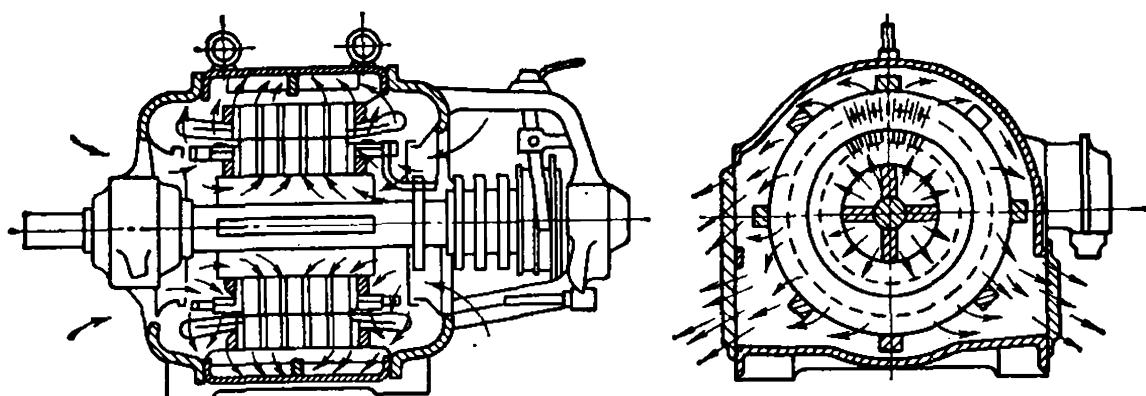


Fig. 6-4. Simple radial ventilation of an induction motor

machine must be increased by 15-20%, the windage losses thus growing by 50-70%.

Depending on how the air flows over the heated machine parts, two fundamental ventilation systems are distinguished: radial and axial-flow.

A simple radial ventilation system used in an induction machine with radial cooling ducts is shown schematically in Fig. 6-4. The core consists of separate stacks each 4-8 cm thick, the width of the cooling duct being 10 mm.

A synchronous machine radial ventilation system is shown in Fig. 6-5. A system of multi-jet radial ventilation used in turbogenerators is discussed in Chapter 7.

Some of the advantages of the radial ventilation system are: minimum energy losses in ventilation and sufficiently uniform heating of the machine in an axial direction. Among the disadvantages of this ventilation system are that it makes the machine less compact, since the cooling ducts occupy up to 20% of the armature length; the heat rejection is less than that in other systems, and the system is sometimes unstable with respect to the quantity of cooling air flowing through the machine. Thus, for instance, an armature axial displacement by 2-3 mm to either side from the position shown in Fig. 6-4 involves a 20 to 30 per cent change in the quantity of cooling air.

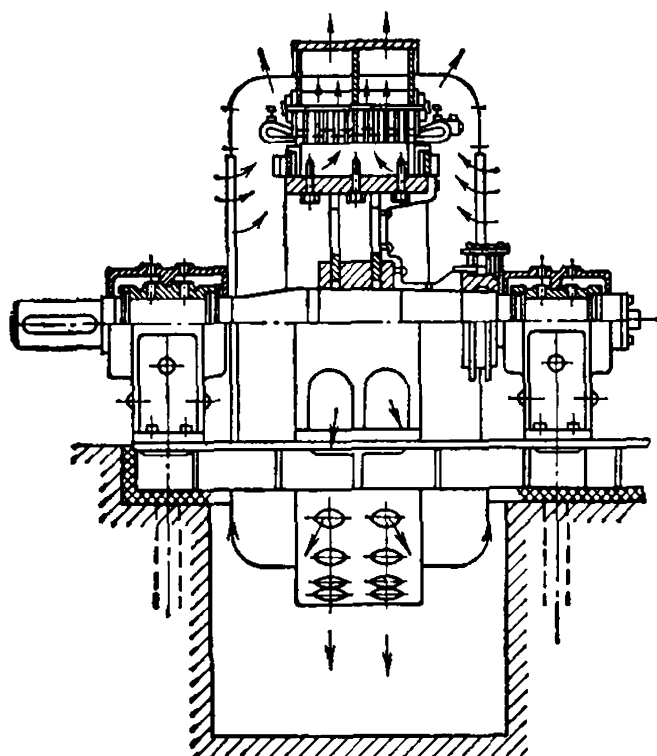


Fig. 6-5. Simple radial ventilation of a synchronous machine

The axial-flow ventilation system as employed in induction machines is illustrated in Fig. 6-6. If the axial ducts are arranged only on the rotating part, the

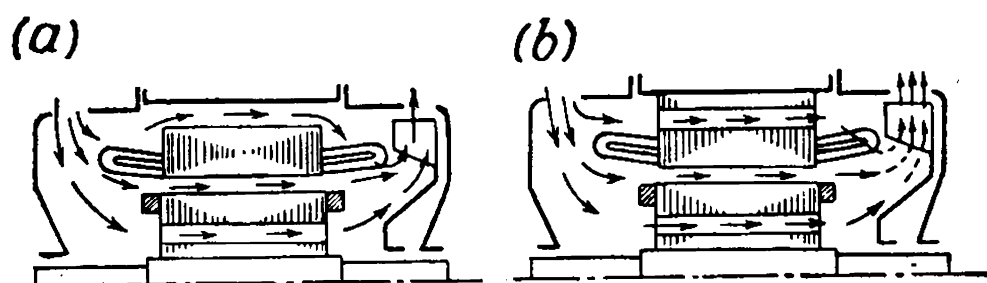


Fig. 6-6. Simple and double axial-flow ventilation

system is termed a simple axial-flow one (Fig. 6-6a), if arranged on both parts of the machine, it is referred to as a double axial-flow system (Fig. 6-6b).

A disadvantage of axial-flow ventilation is non-uniform heat transfer. Indeed, the right-hand part of the machine in Fig. 6-6a is cooled less because the air, in passing through the axial ducts, becomes heated. Mixed-flow ventilation systems are also used.

Detailed calculations and investigations show that in machines of low and, partly, of medium output the best results are obtained with an axial-flow ventilation system; in machines of medium and high output the radial system gives better results.

Machines with external self-ventilation are used when the air contains explosive gases or acid vapours which may destroy the insulation, and the machines must be totally enclosed, i.e., arranged so that the air cannot enter them. All the heat developed in such a machine can be dissipated into the surrounding medium only from the external surface of the frame. Under conditions of natural cooling a heavy and expensive machine is obtained, whereas by forced cooling of the external surface of the frame the output of the machine is increased 2 or 3 times.

The frame is cooled by a fan installed behind the end shields (Fig. 6-7). To increase heat transfer from the inner part of the machine to the outer surface, the air inside the machine is made to circulate with the help of special internal fans.

Machines with Separate Cooling. In these machines cooling air is supplied to the machine with the aid of a separate fan, i.e., one provi-

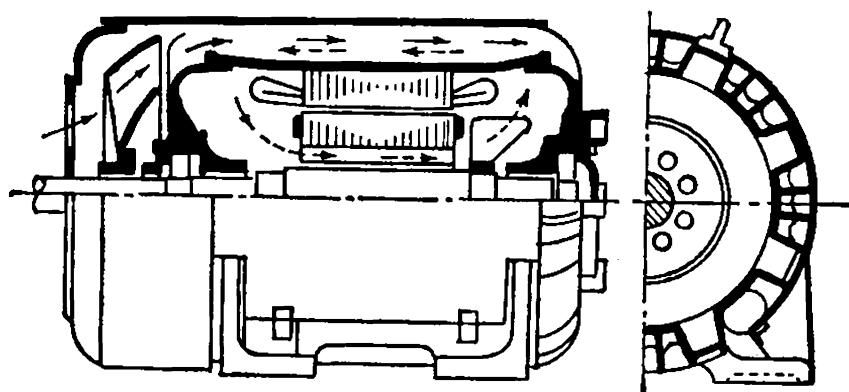


Fig. 6-7. Machine with forced external cooling

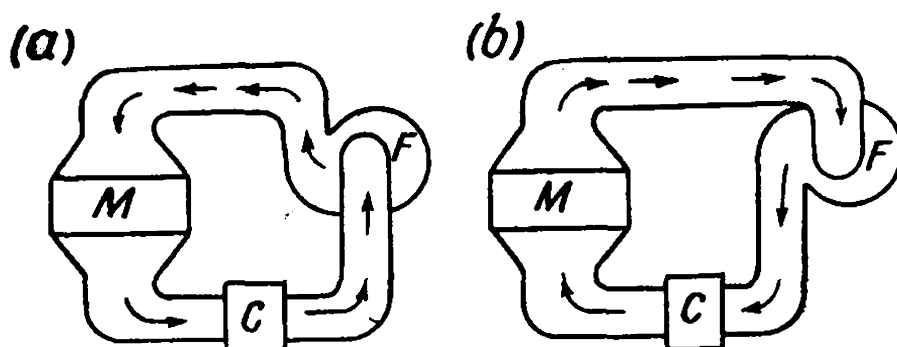


Fig. 6-8. Closed-circuit cooling system

ded with its own drive. By regulating the fan speed, depending upon the load, we can either force or attenuate cooling. For instance, at partial load it is good to decrease the fan speed. The windage losses are thus considerably reduced (approximately in proportion to the cube of the speed), improving the total machine efficiency.

Open-Circuit and Closed-Circuit Ventilation. Both self-ventilation and separate ventilation may be of two kinds: open-circuit, and closed-circuit.

In an open-circuit ventilation system a machine is cooled by the intake of cold air, which passes through the machine and is expelled into the atmosphere. To prevent clogging of the machine with dust which the air always contains, a filter may be mounted at the air intake, but it must be frequently cleaned. In addition, the filter increases the resistance to air flow, requiring an increase in fan power.

The closed-circuit ventilation system is one in which the same air volume passes through a closed circuit: it passes through the machine, becomes heated, then it passes through air coolers, is cooled, and returns to the machine. The air thus circulates in a closed system either in the direction fan *F*—machine *M*—air cooler *C* (Fig. 6-8*a*) or in the direction fan *F*—air cooler *C*—machine *M* (Fig. 6-8*b*). In the latter case the cold air enters directly from the air cooler into the machine; in the first case it is slightly heated in its passage through the fan.

The closed-circuit ventilation system is widely used with large synchronous generators.

Chapter 7

COOLING SYSTEMS FOR TURBOGENERATORS AND HYDROGENERATORS

7-1. Ventilation of Turbogenerators with Ordinary Cooling

Air-Cooling System. The problem of selection of a cooling system for turbogenerators has always received considerable attention because the high speeds enable reducing their overall dimensions compared with those of other types of machines.

In the early stage of their development turbogenerators were designed exclusively with air cooling, and this system attained a high degree of perfection. The maximum power of turbogenerator units with air cooling reached 100 MW.

Further development of the turbogenerators' cooling systems was achieved by utilizing hydrogen gas as a cooling medium. Therefore at the present time, air cooling is used only for comparatively small-power units (up to 30 to 40 MW). Such machines usually use the multi-jet radial closed-circuit ventilation system.

Fig. 7-1 shows a simplified diagram of turbogenerator with the air ventilating equipment being installed in the basement. The air is

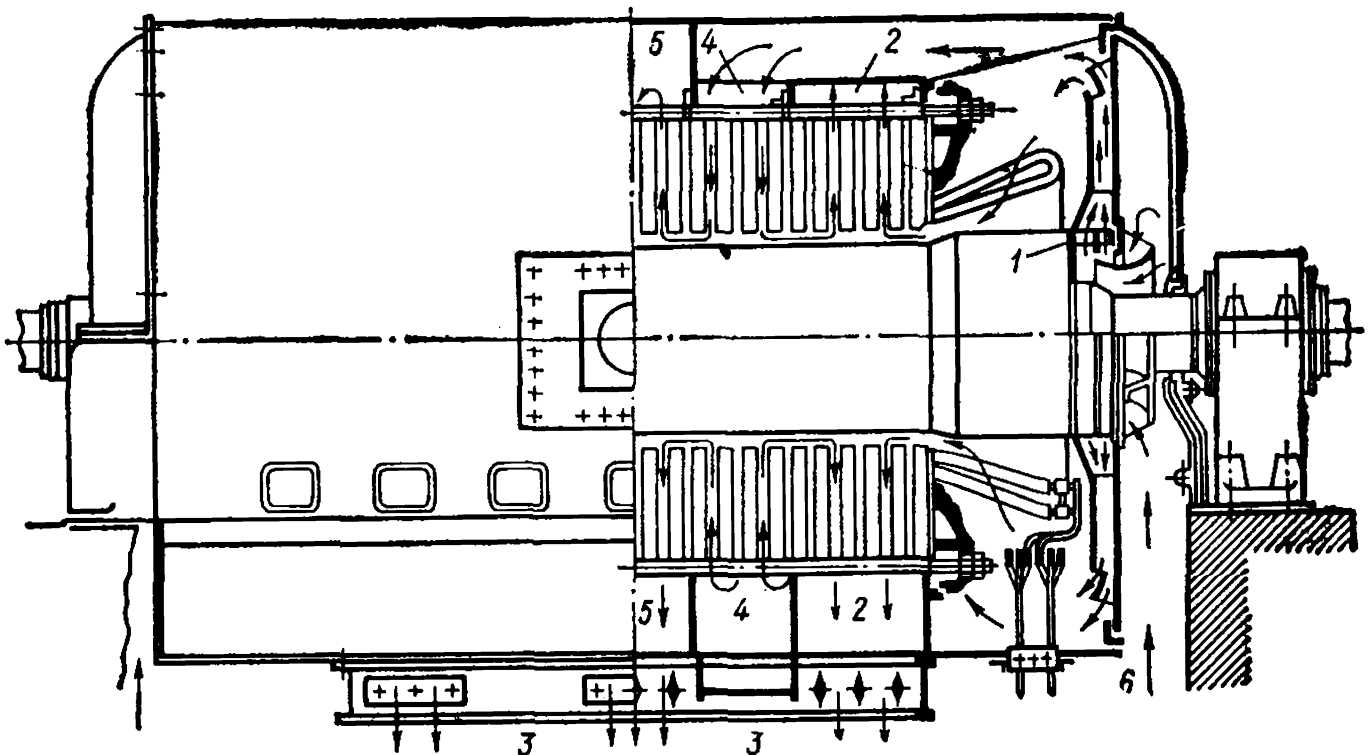


Fig. 7-1. Radial closed-circuit air ventilation system of turbogenerator

circulated by two fans 1 built in at each end of the rotor. Part of the air injected by the fan flows round the stator winding end connections, passes into the air gap between stator and rotor and is discharged through radial channels at the end-faces of the stator core, into the annular hot-air channels 2 and then, through the basement duct, via common outlet chamber 3, into air-coolers. The other part of the cooling air passes between chamber 2 and the generator casing into annular chamber 4, then through radial channels is directed into the machine air gap and from there, into hot-air chambers 5 and 2, and further through the common outlet chamber 3 into the air-coolers. From the air-coolers the air is again directed to fans through chambers 6 and then to the machine.

The ventilation system shown in Fig. 7-1 is termed the three-jet system, according to the number of hot-air flows coming out of the generator. In turbogenerators with a large core length multi-jet systems are used; in small-power generators the two-jet and single-jet systems are used.

Hydrogen Cooling System. In the period of 1940-1948 turbogenerators with hydrogen cooling became widely used. With hydrogen the cooling efficiency considerably increases, and the friction losses of the rotor rotating in gas are reduced; with air cooling these losses constitute a considerable portion of the total losses. The advantages of hydrogen cooling are due to the fact that thermal conductivity of this gas is 6, 7 times greater than that of air. In a hydrogen medium the heat resistance of the frame winding insulation is also reduced. As a result the hydrogen system of cooling permits construction of more powerful machines without increasing their size. Besides, technical hydrogen is about 10 times lighter than air and therefore there is a corresponding reduction in windage losses and in rotor friction losses in gas.

Calculations show that the efficiency of 50-100 MW turbogenerators at 3000 rpm and full loads increases by 0.8% compared with the efficiency of machines with air cooling, and attains 98.6 to 98.8%.

The use of hydrogen cooling prolongs the service life of the insulation, since the corona phenomenon does not cause formation of ozone (which intensifies oxidation) and of harmful nitrogen compounds. Hydrogen does not sustain combustion, therefore there is no need for fire-extinguishing facilities.

The disadvantage of hydrogen cooling is the explosion hazard of the hydrogen-air mixture, which calls for sealing the entire machine casing filled with hydrogen, and increasing the mechanical strength of the turbogenerator frame in order to preclude internal damage to the machine by hydrogen explosion. Besides, the plants must have a hydrogen installation to produce gas, control its purity, feed and clean the facilities.

The turbogenerator gas circulation diagram with hydrogen cooling has not changed much. Its main specific feature is that for proper sealing the gas-coolers of such turbogenerators must be mounted directly inside the stator frame. The gas-coolers are installed horizontally along the circumference, or vertically in the end parts of the stator frame; all this somewhat complicates the frame design. The end shields are made mechanically strong and are hermetically joined with the frame. The places where the ends of the rotor shaft come out are fitted with special oil seals to avoid leakage of hydrogen. The generator leads are also hermetically sealed. In Fig. 7-2 is shown the longitudinal section of a 150-MW turbogenerator with an ordinary system of hydrogen cooling.

One of the turbogenerator units most affected by heat is the rotor, the cooling of which in an ordinary version is achieved by circulation of gas which cools the external surface of the rotor. For better cooling the surface of the rotor drum has special helical grooves. Turbogenerators with an ordinary system of hydrogen cooling are made for powers up to 150-200 MW.

Hydrogen cooling is used also in large synchronous condensers.

7-2. Systems of Direct Cooling of Turbogenerator Windings

Main Advantages of Direct Cooling. With ordinary cooling the entire heat liberated from the copper of the windings is removed, mainly, from the surface of the steel cores in which the windings are enclosed. In this case the heat flow on its way overcomes a series of heat resistances, the sum of the temperature gradients in which makes up the temperature rise of the winding copper. The temperature rise in the copper represents the sum of the following components: (a) temperature gradient in the winding insulation; (b) gradient in the teeth; (c) gradient on the surface of heat removal; (d) temperature rise of the cooling gas.

One of the ways of improving the cooling is to increase the hydrogen pressure in the stator frame. For more intensive cooling of the field winding some manufacturers provide additional ventilating channels in the winding slot bottoms and in the rotor teeth.

In Fig. 7-3a are shown the relative values of the above components of the temperature rise and their variations versus hydrogen pressure. As seen in the figure, the main components of the temperature rise for ordinary cooling are the temperature gradients in the insulation and in the rotor teeth. With an increase in hydrogen pressure the temperature gradients across the rotor surface as well as the temperature rise of hydrogen decrease; the temperature gradients in the insulation and in the steel (in the rotor teeth) remain constant. With additional ventilating channels in the core steel, only the temperature gradient in the teeth is reduced. Therefore the possibility of increasing the

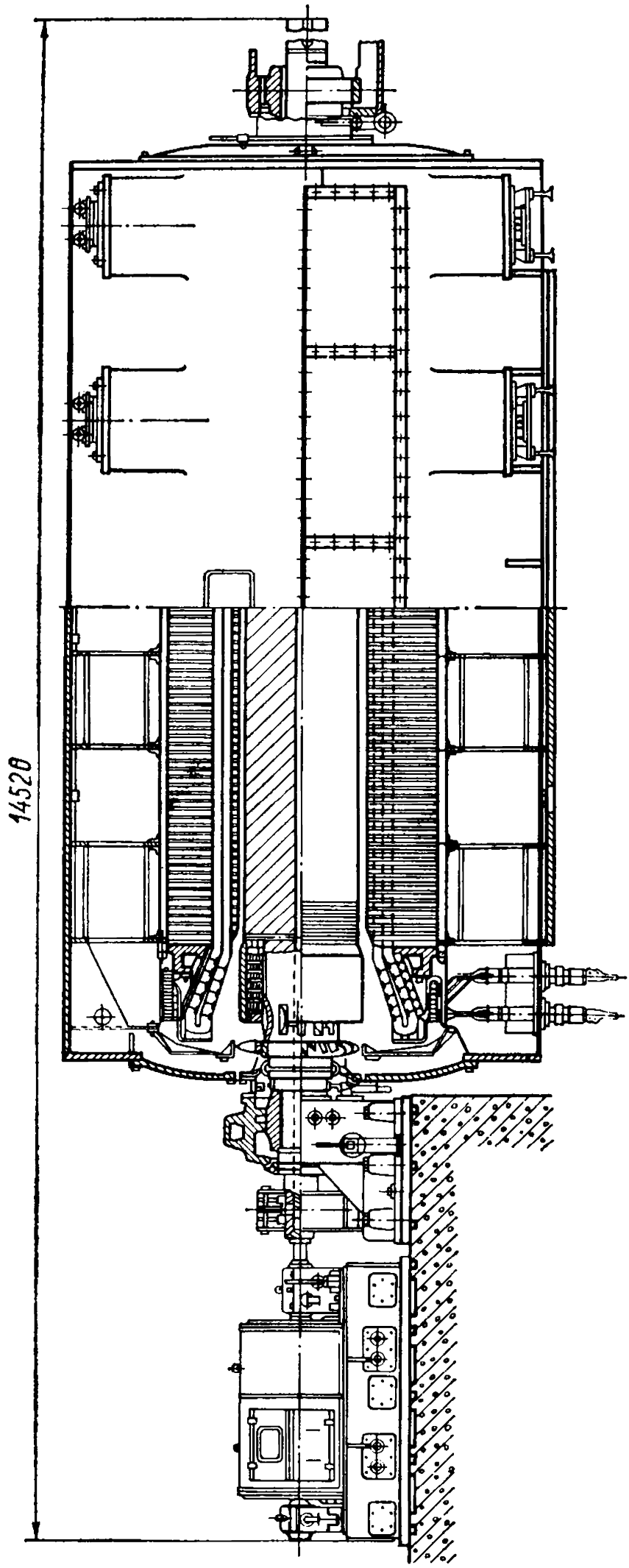


Fig. 7-2. Longitudinal section of 150-MW turbogenerator with hydrogen cooling

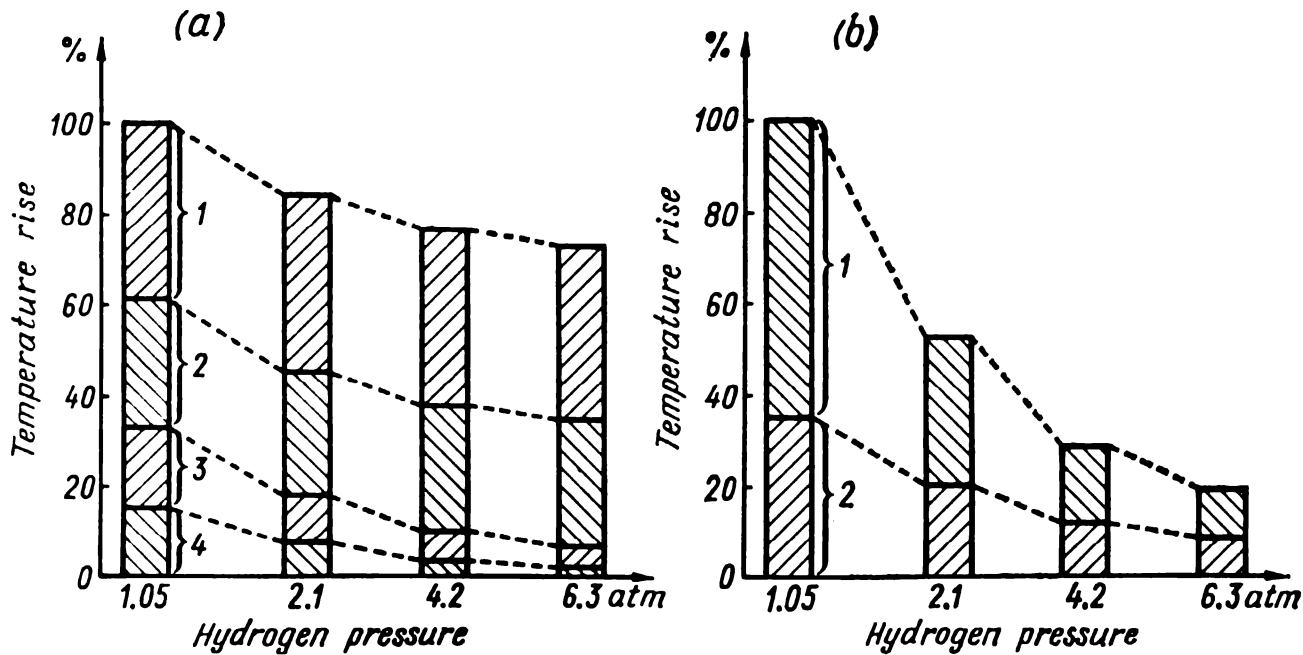


Fig. 7-3. Rotor winding temperature rise and its components versus hydrogen pressure:

a — for ordinary cooling

1 — in insulation; 2 — in rotor tooth; 3 — on rotor surface;
4 — temperature rise of gas in the air-gap

b — for direct cooling

1 — temperature rise of gas; 2 — temperature drop at the channel surface

effectiveness of turbogenerator systems with ordinary cooling is very limited.

The effectiveness of winding cooling was greatly increased as a result of using systems with direct cooling. To ensure direct cooling in winding conductors internal channels are provided through which the cooling medium circulates (Fig. 7-4). In this case the main heat

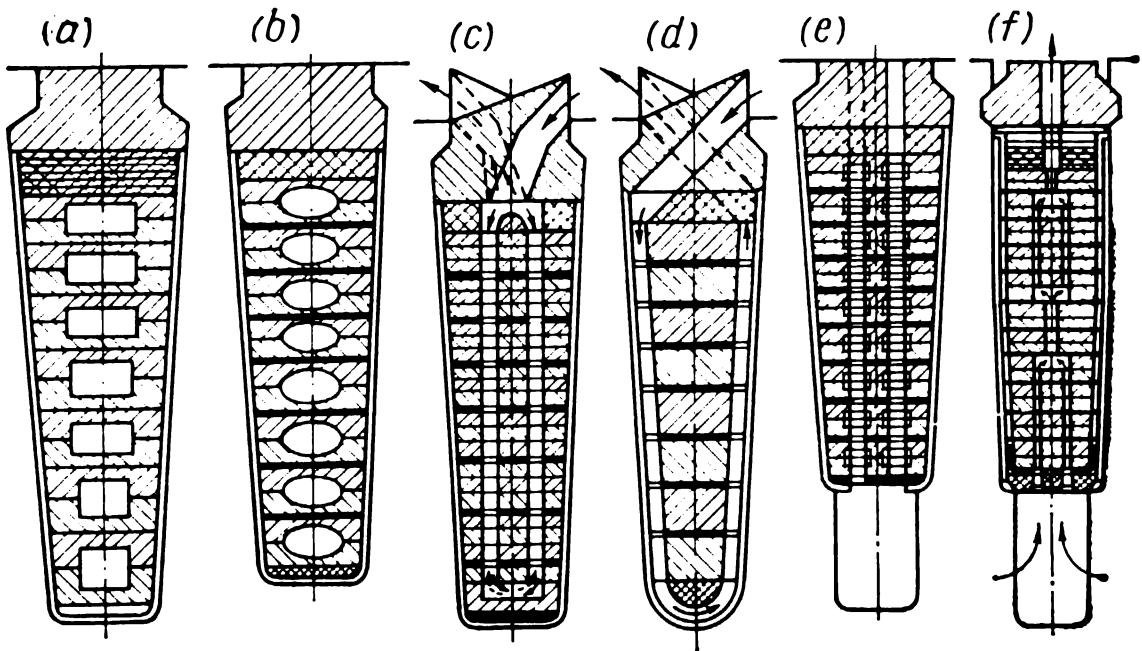


Fig. 7-4. Design variants of internal channels in the rotor winding

barriers that hinder the dissipation of losses are eliminated and the total temperature rise in the copper has only two components: temperature rise of gas in duct τ_1 and temperature gradient across the duct surface τ_2 , i.e. at the outlet of the cooling gas from the internal duct

$$\tau = \tau_1 + \tau_2 = \frac{q_1 l}{cV} + \frac{q_1}{\alpha P} = q_1 \left(\frac{l}{cV} + \frac{1}{\alpha P} \right)$$

where q_1 = losses in the copper of the winding per unit length of internal channel;

l = length of channel;

c = specific heat of the cooling medium;

V = expenditure of cooling medium through channel;

α = heat-transfer coefficient from the channel surface;

P = perimeter of the cooling channel.

As a result of direct contact of the cooling medium with the conductors the intensity of heat dissipation increases considerably and this permits one to considerably increase the permissible current density in the winding.

With hydrogen cooling the effectiveness of direct cooling systems increases with an increase in gas pressure to a much greater degree than in the case of ordinary cooling (Fig. 7-3b).

Direct Cooling of Rotor Winding. Rotor windings are cooled mainly by hydrogen under high pressure.

Since practically all leading turbogenerator plants have been elaborating new methods for direct cooling, modern practice utilizes many different variants of cooling system designs, especially as regards the inner channels in the winding conductors.

Several versions of internal channels are shown in Fig. 7-4. Though very diverse the internal channels of the rotor winding are usually divided into three groups:

(1) axial cooling systems with internal channels in the conductors (Fig. 7-4a, b);

(2) diagonal systems with side or internal channels in the coils, with separate delivery of cooling gas into the inner channels with the help of gas intakes on the rotor surface (Fig. 7-4c, d);

(3) radial-axial or radial systems with delivery of cooling gas through channels under the slots (Fig. 7-4e, f).

In the axial systems the cooling gas enters the internal channels from the butt ends of the rotor, passes through the channels in the winding up to the middle of the rotor and comes out in the air-gap of the machine through radial ducts in the coil and in the rotor wedges.

The channels in such systems are of considerable length, and in order to ensure intensive gas flow in them an increased pressure is required at the channel inlet which is produced by a special high-pressure fan. Built-in centrifugal fans with an increased external dia-

meter, or multistage axial fans are usually used for this purpose. Even at high gas flow rates in the channels (40-60 m/sec), the axial systems are characterized by a considerable non-uniformity of heating of the windings along the rotor length.

Diagonal multi-jet cooling systems are self-pressurized systems, in which the pressure, necessary for gas-circulation in the channels, is created by the gas intakes and deflectors arranged on the surface of the rotor. The surface of the rotor drum is in this case divided into a series of annular sections with a system of inlet and outlet ducts, which are joined in pairs by internal diagonal channels, made in the form of helical holes running along the perimeter of the coil. In this system the circulation of the gas in the channels is caused by the pressure set up at the channel inlet (gripping baffle plates) and by the vacuum at the deflector outlet.

The advantage of the multi-jet diagonal system is that more uniform cooling along the rotor length is at this attained, thus eliminating the need for a high-pressure fan, and the overall circulation of the gas is carried out by ordinary fans.

The radial-axial system provides for axial ducts in the conductors and the cooling air is delivered to them from the channel under the slot through radial ducts in the coil located at definite intervals along the rotor length. The cooling gas from the supply radial channel is distributed to both sides through axial ducts, passes a definite section and enters the machine air gap through radial ducts in the coil and in the rotor wedge. With this circuit it is possible to have a double counterflow cooling system for each coil (Fig. 7-4e) which ensures more uniform heating of the rotor.

In the radial systems, with the cooling gas delivered from the channel under the slot in the coils of the field winding radial through slots are made along the entire length of the rotor drum via which the gas passes from the channel under the slot into the machine air-gap.

In the last few years much research work has been accomplished evolving the design of turbogenerator rotors with water cooling. At present a variety of experimental water-cooled rotors have been devised for different types of turbogenerators rated at 30 to 1000 kW and more. Some of these generators are successfully operating at electric power stations.

The rotor winding with water cooling is made of rolled hollow conductors (Fig. 7-5). All winding conductors are grouped in several parallel hydraulic circuits, to each of which a sealed inlet is provided as well as an outlet for the cooling water. For these purposes highly purified distilled water is used.

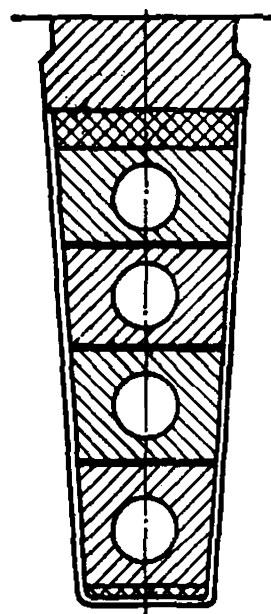


Fig. 7-5. Cross-section of rotor slot with water-cooled winding

Internal Cooling of Stator Winding. With direct cooling of the rotor winding the most heated area is the stator winding of the generator, therefore in modern large turbogenerators provision is made for internal cooling of stator winding bars.

Because of the high voltage, for stator winding axial cooling systems are solely used which make it possible to ensure continuous insulation along the entire bar length. The cooling is performed by gas or liquid.

With gas cooling, which is generally used when for rotor winding cooling an axial gas system and a high-pressure fan are provided, the stator winding is cooled by a gas flow passing along the entire length of the internal channels. The internal channels in the bars are made by laying thin-walled tubes of non-magnetic metal with high resistivity inside the plaited bar (Fig. 7-6a). To prevent short-circuiting the tubes have a thin insulation along the entire length and the ends of the tubes coming out of the bar are protected by special rings made of insulating material. The high-pressure fan directs the cooling gas into the tubes from the high-pressure chamber, passes along the entire winding length and comes out into the low-pressure zone at the other side of the generator.

In turbogenerators with a multi-jet diagonal cooling system liquid-cooled stator windings are utilized. At first transformer oil was used as coolant since it has high dielectric properties. The bars of the stator winding with such cooling are usually made of copper tubes (Fig. 7-6b). The liquid is charged into the bar channels through sealed hoses made of insulating material, from the distribution header. This is a closed-circuit system in which the liquid is discharged from the winding into an external hydraulic unit, containing the pump, heat-exchangers and purifying facilities.

The most widely used cooling medium at present is distilled water, which has adequate dielectric properties, a considerably larger heat

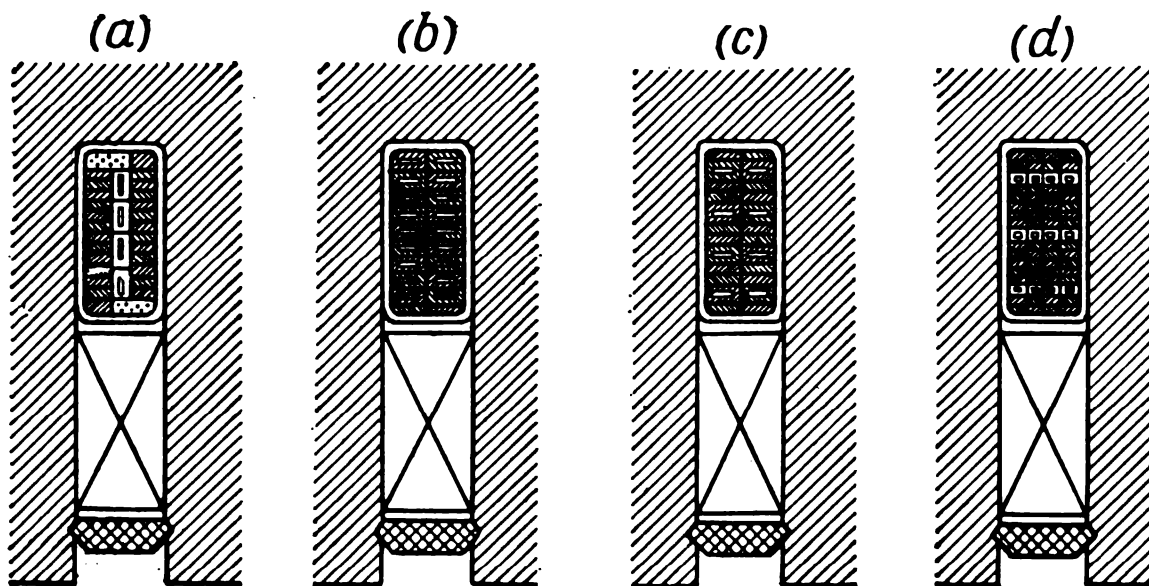


Fig. 7-6. Cross-sections of stator winding bars with internal cooling

capacity and 7 to 9 times lower viscosity. Therefore with water cooling the intensity of heat dissipation is greatly increased and the pressure required for providing circulation of the water in the channels may be reduced. The stator winding bars, with water cooling, are usually made of hollow and solid conductors (Fig. 7-6c). In such bars by reducing the thickness of the solid conductors the additional losses in the winding copper are reduced. To further reduce the additional losses in the winding of the large-power machines it is advisable to replace the hollow conductors in the bar by thin-walled metal tubes. The tubes are arranged in a vertical row across the bar as in bars with gas cooling (Fig. 7-6a) or in horizontal rows as in Fig. 7-6d.

Cooling Medium Circulation Circuits of Machines with Direct Cooling of Windings. Turbogenerators with direct cooling of windings are usually filled with hydrogen at high pressure. The gas circulation circuit in the machine depends on the rotor winding cooling system.

In turbogenerators with axial gas cooling of windings, the stator core is made either with an axial or with a radial system of cooling.

With axial cooling the core is made of steel segments with ducts in the teeth and in the yoke. When the core is assembled the through axial channels are formed through which the cooling gas moves together with the gas flowing along the channels of the stator windings.

In turbogenerators with a radial system of cooling the stator core has the usual arrangement, i.e. it consists of packs among which the ventilating channels are arranged. To reduce the flow of the cooling gas through the core channels, which have a sufficiently large cross-section, the inlet ducts in the distribution chamber of the stator are made narrow.

The pressure head is provided by multistage fans both in axial and in radial cooling systems. One of the variants of the gas circulation diagram in a turbogenerator with a two-way axial system for cooling the rotor winding and with a gas system for cooling the stator winding is shown in Fig. 7-7.

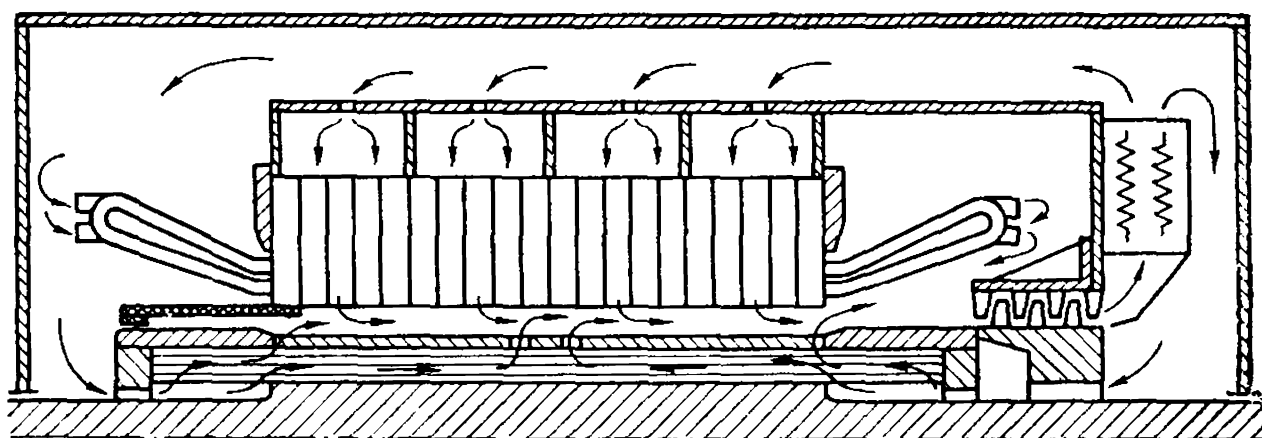


Fig. 7-7. Two-way axial gas cooling system of rotor winding

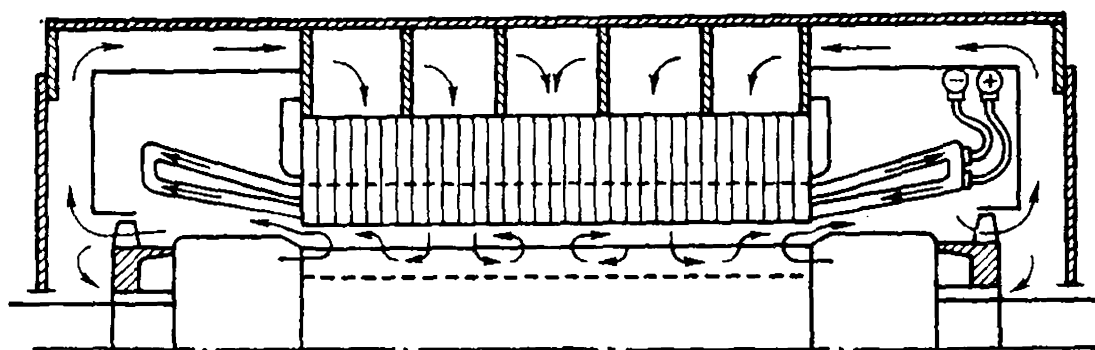


Fig. 7-8. Circulation of gas in turbogenerator with diagonal system of rotor winding cooling

Fig. 7-8 shows the circulation of the cooling gas in a turbogenerator with a multi-jet diagonal system of rotor winding cooling and with water cooling of the stator winding.

The use of methods for direct cooling of the windings has opened up wide perspectives for further development of turbogenerator construction. With the same dimensions it has become possible to build generators of power two to three times greater than with ordinary cooling.

In modern practice batch-produced 500- to 600-MW turbogenerators are put out, 800- to 1000-MW machines have been constructed and even more powerful generators are being designed.

7-3. The Main Trends in the Development of Turbogenerator Cooling

The analysis of the development of power engineering and turbogenerator construction shows that in the future the power of turbogenerator units is to increase to 1600-2500 MW. The construction of such machines will require further improvement of the cooling systems as well as the solution of many other problems, and at present major work is being carried out to solve these problems.

All-Water Cooling Systems. Experimental turbogenerators have been manufactured with all-water cooling. The water-cooling is used not only for stator and rotor windings but also for the stator core and for various separate subassemblies and elements. The stator core is cooled by special cooling elements made in the form of cast segments with a cooling tube inside and installed in the core between the packs. The length of the active steel in the core is not reduced, compared with the turbogenerators using radial gas systems, since the thickness of the cooling segments, which are arranged along the entire periphery of the core instead of inter-pack spacers does not usually exceed the width of the radial channels.

Along with cores having a radial system of cooling new core types with an axial system of water cooling are under development in which the cooling water flows inside the insulated metal tubes, mounted in axial channels of the stator core.

In turbogenerators with all-water cooling it is possible to provide more effective cooling and thus to increase the unit power of machines. This, however, requires that a multi-parallel cooling system for the rotor winding be provided as well as water cooling of the pressing plates, damping screens in the stator, and other elements.

Liquid Systems With an Oil-Filled Stator. In turbogenerators with such a cooling system the stator is sealed, this being attained by mounting inside the stator bore an insulating cylinder the ends of which are hermetically joined to the stator end shields. The stator is filled with insulating oil. In the winding bars and in the stator core are provided axial channels through which the oil circulates by means of a pump mounted in the external hydraulic unit. An oil-cooled system ensures a uniform and adequate cooling of the windings and core of the stator.

In such a machine the bars of the stator winding are usually made with paper and oil insulation, this permitting an increase in generator voltage up to 36 kV. The winding of the rotor is water-cooled. Experimental 60- to 300-MW turbogenerators with oil-filled stators have been manufactured.

Evaporative Systems. In the USSR and abroad evaporative cooling systems are being developed in which the heat dissipation is due to the boiling of a liquid, and the vapour formed is removed into the coolers. With evaporative cooling the expenditure of the liquid is approximately 13 to 14 times compared with water cooling. The use of such a system, however, depends on the solution of many other problems stemming from the presence of a vapour-liquid mixture in the machine. To overcome these difficulties sealed systems of evaporative water cooling of rotor winding have been designed similar to water-cooled systems.

Investigations are in progress for using freon gas for evaporative cooling of the rotor and the stator core.

Cooling Systems with Artificial Refrigeration. The first step in the investigation of this trend was the study of water-type systems with the use of freon gas which is cooled in a refrigerating plant to minus 30 to 40 °C. This enables reducing the temperature in the winding and the corresponding losses in it. Such a system will, however, be economical only when the loss reduction exceeds the power expended in the refrigerating plant. Therefore the most promising version is cryogenic cooling of turbogenerators which allows the use of superconductors and pure metals. Turbogenerators with cryogenic cooling should have a modified design, because the windings being cooled by a liquid gas must be placed in special cryostats; the cryostat for the stator winding must be made of insulating material.

The results of investigations show that the best design is when the rotor winding is made of a superconductor and is inserted in a metal cryostat and when the stator winding is made of highly purified alu-

minium. The electric resistance of pure aluminium at cryogenic temperatures is reduced tens of times and also, as distinct from superconductors, it does not lose its high electric conductivity in the presence of strong alternating magnetic fields.

Other designs of turbogenerators are also being investigated in which the rotor winding is made of superconductors with cryogenic cooling, and a stator is of conventional design.

7-4. Cooling Systems for Hydrogenerators

The closed-circuit cooling system typical for a large hydrogenerator is shown in Fig 7-9. The cooling air in the machine is circulated with

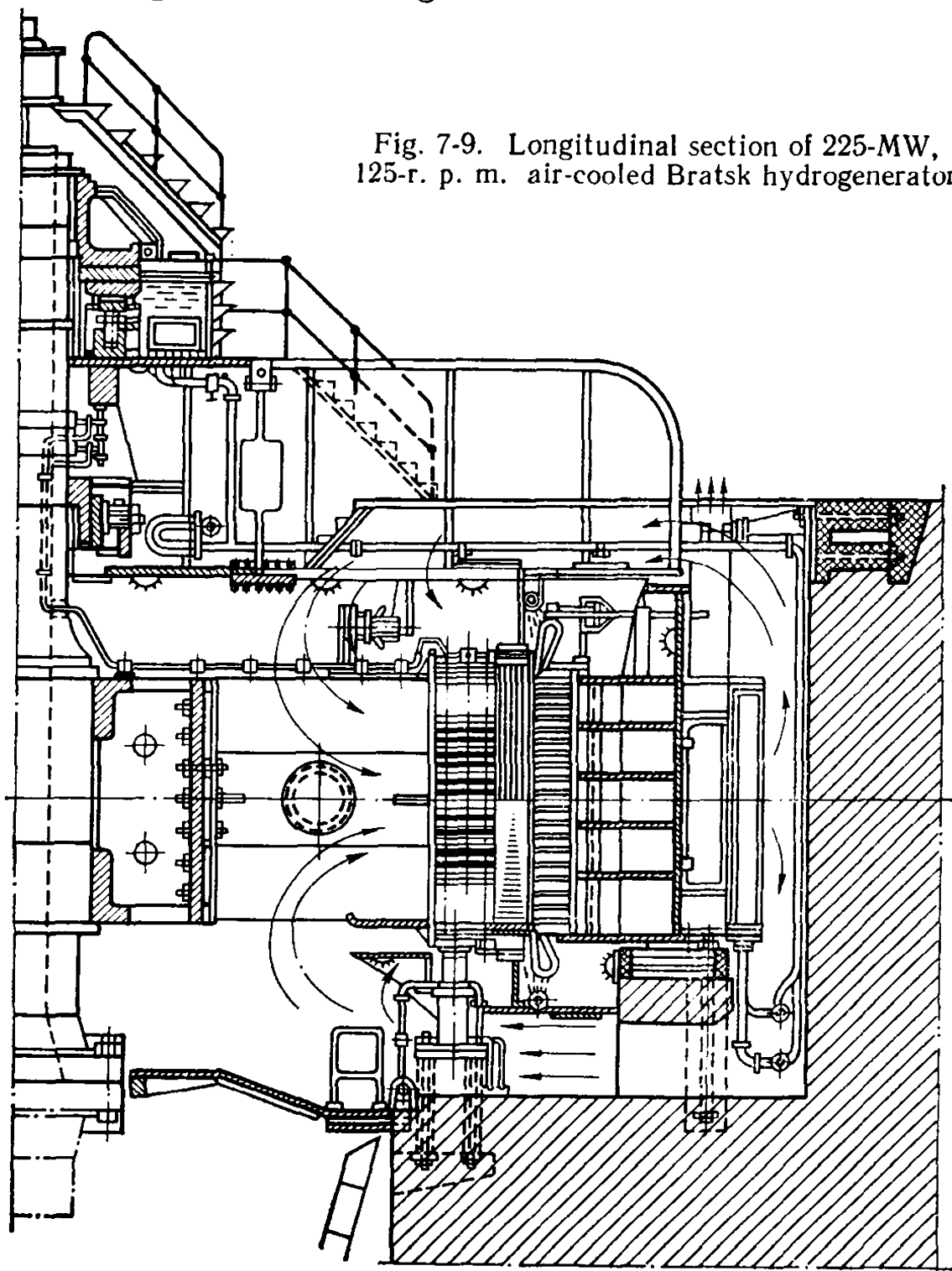


Fig. 7-9. Longitudinal section of 225-MW, 125-r. p. m. air-cooled Bratsk hydrogenerator

the aid of pressure elements, i.e. the rotor with fans fixed at its ends. The air leaving the rotor and fans, moves into the generator air-gap and winding end connection chambers and further through the stator ventilating channels into the air coolers located on the stator frame. Coming out of the coolers the air enters the cold-air chamber behind the stator frame and passes in two parallel flows through the top and bottom spiders to the rotor spider and fans.

The rotor poles are cooled by the air delivered from the ventilating channels of the rotor rim. The stator winding is cooled from the insulating surface by air passing through the end-connection chambers and ventilating channels of the stator core. The other part of the heat is removed from the winding into the stator steel packs and then dissipated by air from the surface of the packs.

To increase cooling efficiency internal water cooling of stator windings and forced air cooling of the pole coils are used. The system of water cooling of the stator windings is made similar to the system used in turbogenerators.

Intensified air-cooling of the field windings is achieved mainly by expanding the cooling surfaces, and by increasing the speed of the air at the cooling surface.

The simplest method of expanding the surface of heat dissipation with ordinary cooling of the rotor poles is by tapering the external edges. As a result, the sides of the coils facing the interpole port have a saw-tooth cross-section, which considerably increases the total heat dissipation surface of the poles.

To increase the speed of the cooling gas at the coil surfaces in the interpole port a V-shape insert is installed along the entire length of the poles. As a result effective cross-section of the interpole port is considerably reduced and the cooling air coming out of the channels of the rotor rim is divided into two streams moving at a high speed at the surfaces of the pole coils.

The intensive cooling of the pole winding is attained by using an air-forced cooling system with transverse internal channels. A simplified diagram of such a system is shown in Fig. 7-10.

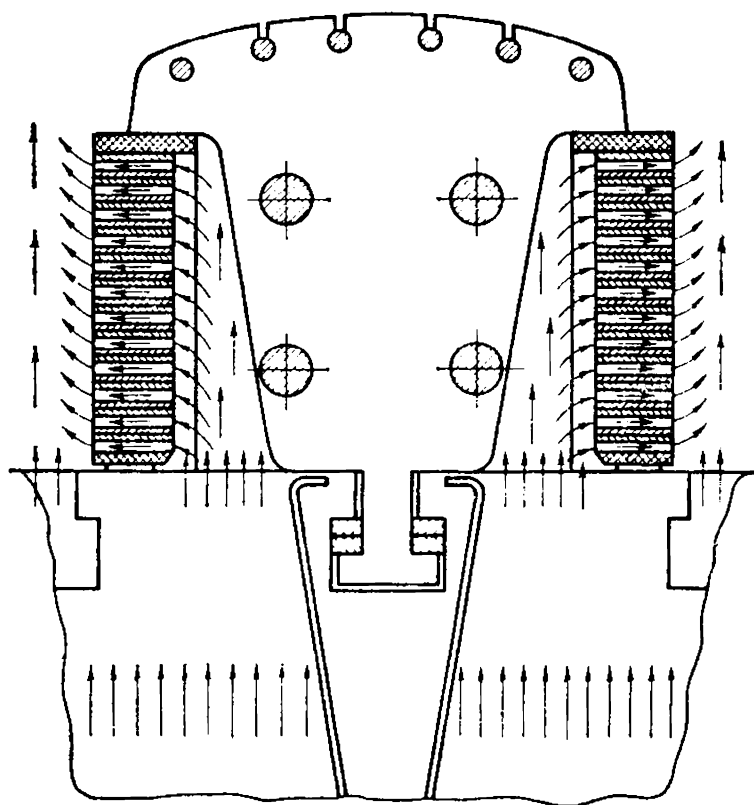


Fig. 7-10. Air-forced cooling system of hydro-generator rotor winding

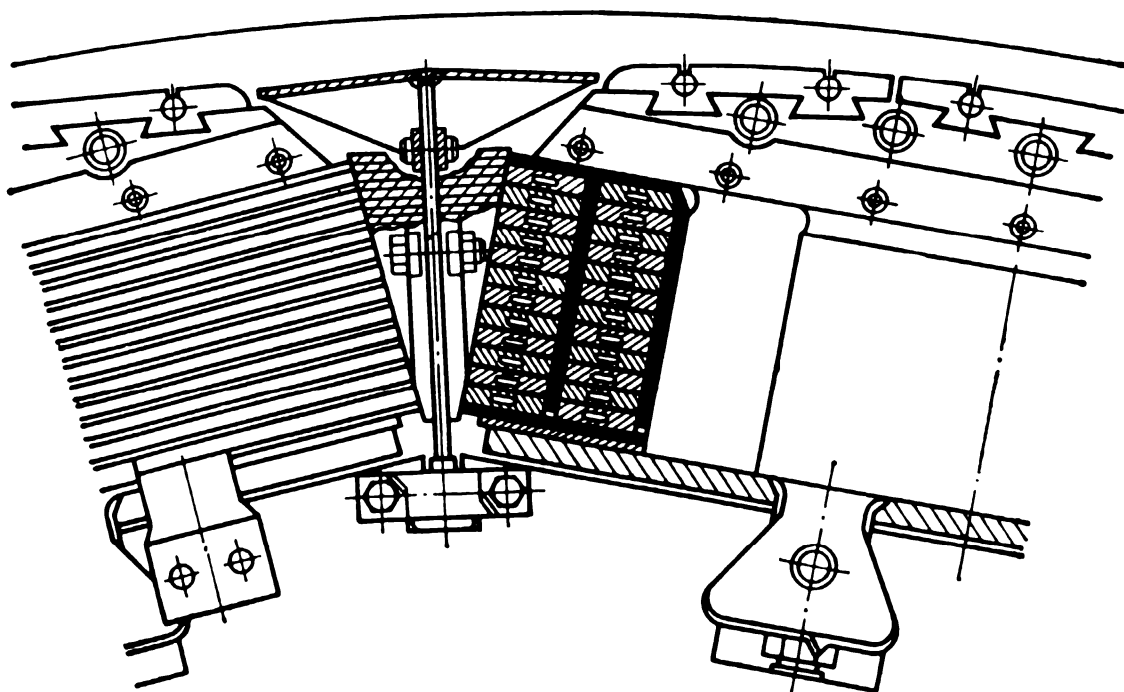


Fig. 7-11. Hydrogenerator rotor with internal water-cooled winding

The poles are made with gaps between the coils and the core. Into these gaps are placed several insulation struts which fix the position of the coils. Between the turns of the coils internal transverse ventilating channels are arranged which are formed by mounting insulating struts or by providing transverse grooves in the winding conductors.

The cooling air from the radial channels of the rotor rim enters the distribution chambers between the core and the coil and from the chambers through the system of transverse channels in the coil passes into the interpole port and then moves along the ventilating tracts of the stator.

There are also hydrogenerator designs with water-cooled rotor winding. Fig. 7-11 shows a transverse section of a 86-MVA, 428.5-rpm, 50-Hz hydrogenerator with direct water-cooling of pole windings, manufactured by Brown-Boveri (Switzerland) [62]. The 190-MVA, 375-rpm hydrogenerators manufactured by this firm for Norway have a similar cooling system. The stator and rotor of this machine are shown in Figs 7-12 and 7-13. A water-cooling system of this type has also been developed and used in the USSR.

There have also been designed and constructed experimental hydrogenerators with complete water-cooling in which the water cools not only the stator windings and the field windings but also the stator core, damping winding of the rotor and the pole cores. For example, the ASEA company (Sweden) has made a 225-MVA, 200-rpm hydrogenerator in which utilizes all-water cooling. In such generators a considerable reduction in windage losses is made possible by decreasing the volume of the circulating air, thus increasing the efficiency of the machine, because the windage losses with ordinary cooling are 15 to 30% of the total losses in the hydrogenerators.

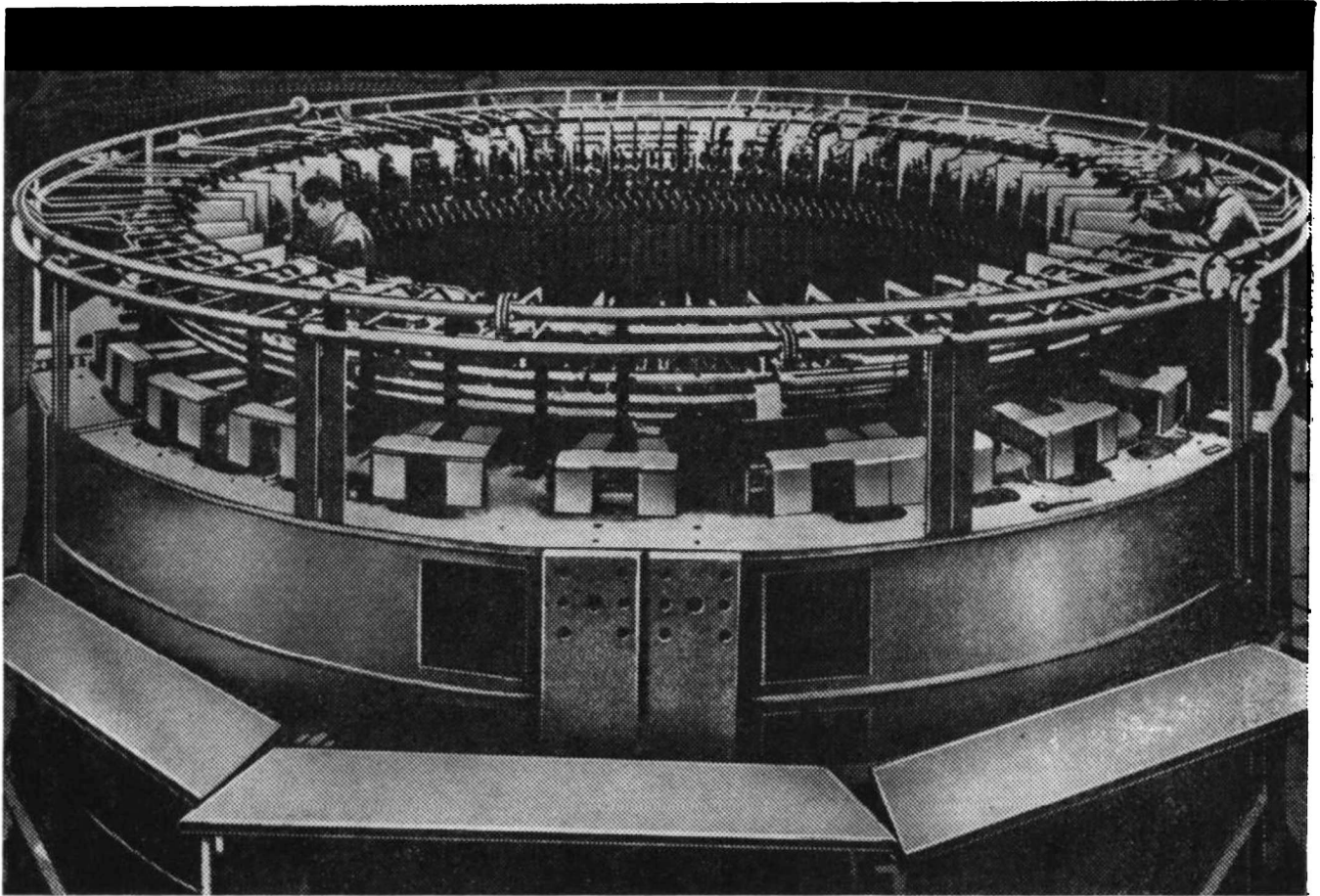


Fig. 7-12. Stator of 190-MVA, 375-r. p. m. hydrogenerator with all water-cooling

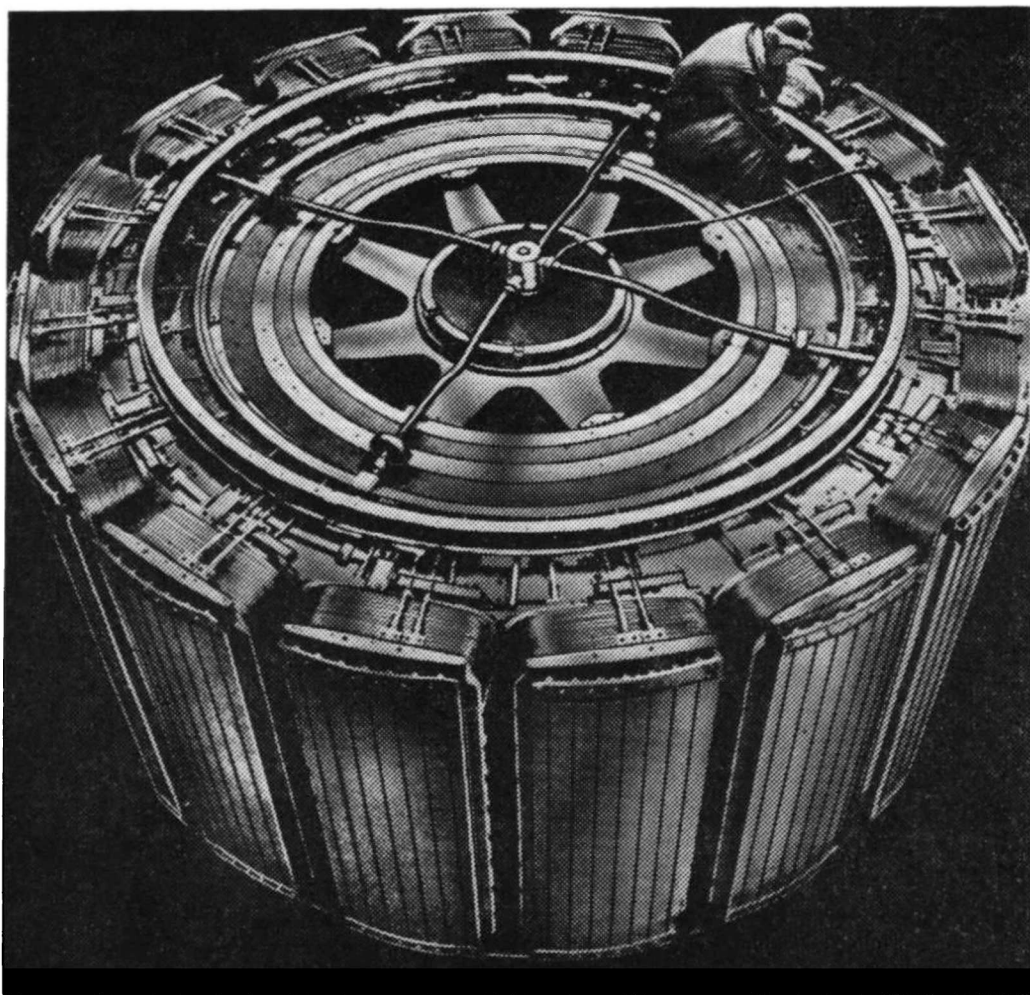


Fig. 7-13. Rotor of 190-MVA, 375-r. p. m. hydrogenerator with all-water cooling

PART TWO

SYNCHRONOUS MACHINES

Chapter

8

ARMATURE REACTION OF A SYNCHRONOUS MACHINE AT BALANCED LOAD

8-1. Armature-Reaction Phenomenon in a Polyphase Synchronous Generator at Balanced Load

Let us first consider the physical aspects of armature reaction and its effect on the field of a synchronous generator.

The current in the stator winding of a synchronous generator produces a magnetizing force whose fundamental wave, termed the armature-reaction magnetizing force, rotates in step with the rotor. The armature-reaction magnetizing force acts on the magnetizing force produced by the field winding and may either augment or weaken the excitation field of a machine and also distort the excitation magnetic field.

In a synchronous generator the displacement of the stator current I relative to the e.m.f. E_m induced in the stator winding by the field winding flux can be within the limits of $-\frac{\pi}{2} \leq \psi \leq \frac{\pi}{2}$, where ψ is the angle of displacement between the stator current I and the e.m.f. E_m . Let us first consider the limiting cases, when $\psi=0$, $\psi=\frac{\pi}{2}$ and $\psi=-\frac{\pi}{2}$.

Figure 8-1a shows the distribution of the stator currents and the fluxes of a synchronous generator with $\psi=0$. Clockwise rotation of the poles is assumed. The maximum of the fundamental wave of the field will be opposite the pole centres, and at the same points the conductors will have their maximum induced e.m.f.; with $\psi=0$ the conductors carrying the maximum current will also be at the same points, as shown in Fig. 8-1a. The mutual arrangement of the fundamental field wave (curve 2) and fundamental armature-reaction wave (curve 1) is shown in Fig. 8-1b. The armature-reaction magnetizing force is directed perpendicular to the magnetizing force of the poles, as in a d.c. machine when the brushes are on the neutral line. This results in distortion of the field wave-shape and in asymmetrical distribution of the flux density under the pole shoe. The flux density under the trailing edge increases somewhat, while under the leading edge it decreases. The axis of the resultant field (curve 3) is displaced under the action of the alternator armature-reaction magnetizing force opposite to the rotor rotation, this corresponding to a displacement of armature-field rotation in a d.c. machine.

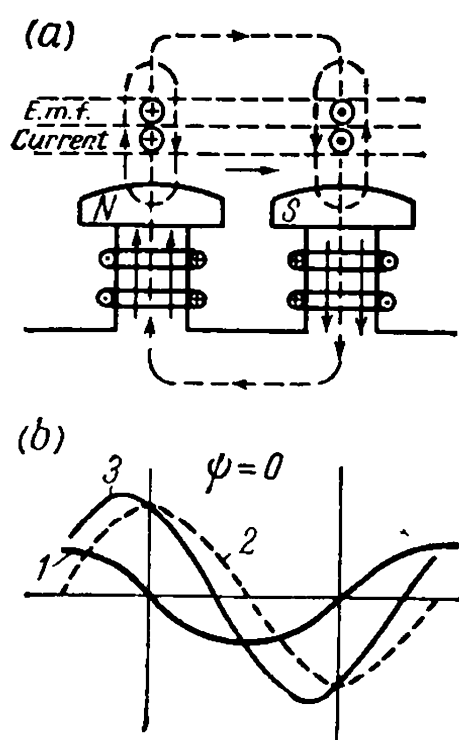


Fig. 8-1. Armature-reaction field with $\psi = 0$

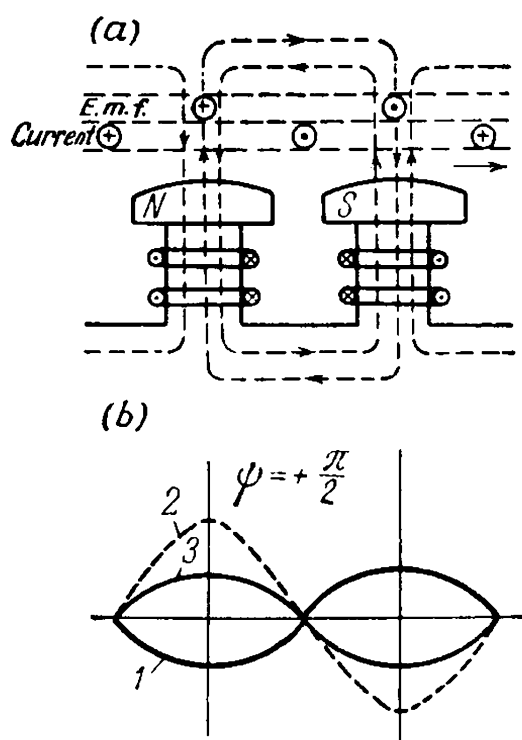


Fig. 8-2. Armature-reaction field with $\psi = \frac{\pi}{2}$

Figure 8-2a shows the distribution of currents and fluxes with $\psi = +\frac{\pi}{2}$, i.e., for a purely inductive load current relative to the e.m.f. E_m . The current maximum will be shifted in space by an angle $\frac{\pi}{2}$ from the e.m.f. maximum, which coincides with the centres of the poles. This shift will be opposite to the direction of rotor rotation, since the fundamental armature-reaction wave rotates in step with the field poles, while when $\psi = +\frac{\pi}{2}$, the current wave lags in phase behind the e.m.f. wave by an angle $\psi = -\frac{\pi}{2}$. The field produced by the armature-reaction magnetizing force will oppose the pole field flux and will therefore have a demagnetizing effect.

Figure 8-3a shows the distribution of the currents and fluxes with $\psi = -\frac{\pi}{2}$, i.e., for a purely capacitive load current I relative to the e.m.f. E_m . The current maximum will be shifted to the right from the e.m.f. maximum, which remains as before under the pole centres, and the armature reaction will therefore have a magnetizing effect on the field.

With intermediate values of ψ , for instance $0 < \psi < \frac{\pi}{2}$, i.e., with a mixed load of an inductive nature (Fig. 8-4), the sine wave of the fundamental harmonic magnetizing force of armature reaction can be resolved into two components with the amplitudes $F_a \cos \psi$ and

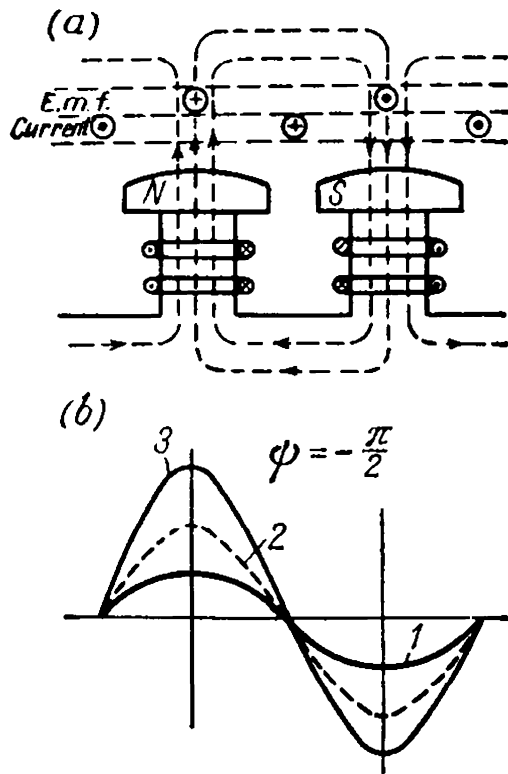


Fig. 8-3. Armature-reaction field with $\psi = -\frac{\pi}{2}$

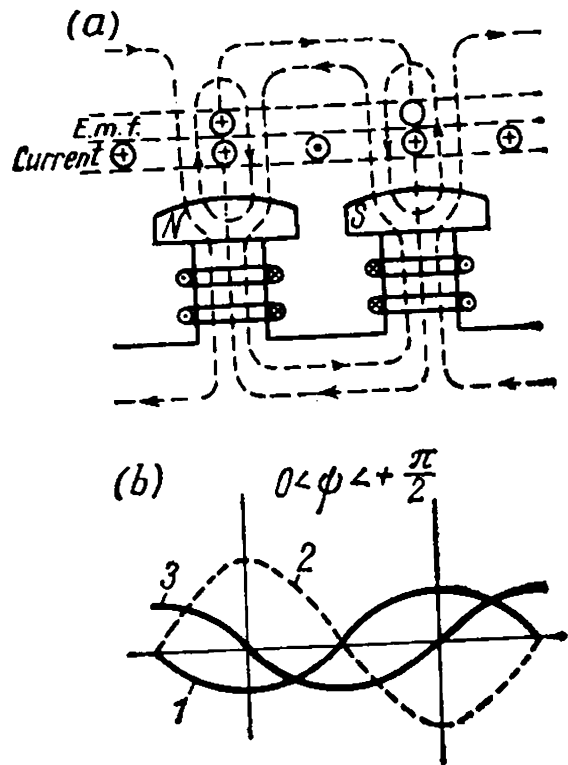


Fig. 8-4. Armature-reaction field with $0 < \psi < \frac{\pi}{2}$

$F_a \sin \psi$, whose vector sum is equal to the amplitude of the armature-reaction magnetizing force F_a . The value of $F_a = F_1$ is determined by equation (4-36)

$$F_a = \frac{m \sqrt{2}}{\pi} \frac{\omega k_{w1}}{p} I$$

The component

$$F_{aq} = F_a \cos \psi \tag{8-1}$$

will produce a quadrature-axis (cross-axis) armature reaction similar to that in Fig. 8-1, and the component

$$F_{ad} = F_a \sin \psi \tag{8-2}$$

will produce, accordingly, a direct-axis demagnetizing component of armature reaction similar to that in Fig. 8-2. With $0 > \psi > -\frac{\pi}{2}$ the armature-reaction magnetizing force F_a can also be resolved into the components

$$F_{aq} = F_a \cos \psi \text{ and } F_{ad} = F_a \sin \psi$$

of which the first is the quadrature-axis, and the second—the direct-axis component of the armature reaction, the latter increasing the excitation of the field as shown in Fig. 8-3. The quadrature-axis component of the magnetizing force with the amplitude F_{aq} is depicted in Fig. 8-4b by curve 3, and the direct-axis magnetizing force component, with the amplitude F_{ad} , is depicted by curve 1

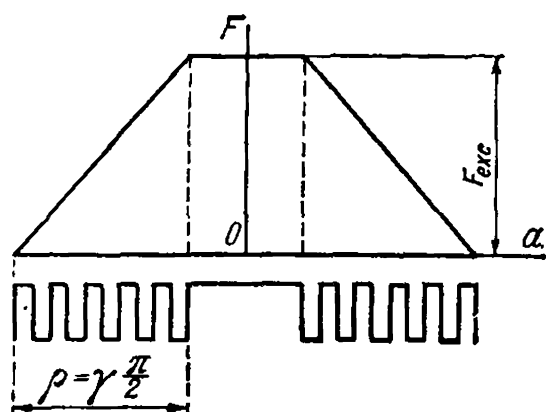


Fig. 8-5. Field winding magnetizing force of a non-salient-pole synchronous machine

The vector sum of the fundamental armature winding and field winding magnetizing force waves constitutes, in a synchronous machine, the magnetizing force producing the resultant magnetic flux.

When plotting vector diagrams of the magnetizing forces and e.m.f.s, it is necessary to know what value of the armature-reaction magnetizing force is equivalent to a certain value of the field magnetizing force, which makes it possible to determine the influence

of the reaction magnetizing force by using the no-load characteristic, along whose axis of abscissas, as is known, the magnetizing force or the field winding current proportional to it is plotted. When reducing the armature-reaction magnetizing force to the scale of the field magnetizing force, it is necessary to distinguish between non-salient- and salient-pole machines.

8-2. Armature Reaction of a Non-Salient-Pole Synchronous Machine

The field winding of a non-salient-pole machine is arranged over the greater part of the rotor periphery occupied by the small-tooth belt, while the other, the unwound part of the rotor, constitutes the belt of the large tooth (Fig. 8-5). Neglecting the influence of the slots, which make the magnetizing force curve of a stepped shape, the field magnetizing force can be assumed to be distributed around the periphery of a cylindrical rotor with non-salient poles according to a trapezoidal law (Fig. 8-5).

The ratio γ of the wound part of the pole to the full-pole pitch is generally within the limits of $\gamma=0.67$ to 0.80 .

Let us designate the space angular coordinate along the air-gap as a .

By resolving the trapezoidal curve of the field magnetizing force according to Fig. 8-5 into a Fourier series, with the origin of coordinates opposite the centre of the large tooth, we get

$$F = F_{exc1} \cos a + F_{exc3} \cos 3a + F_{exc5} \cos 5a + \dots$$

the amplitude of the v -th-order harmonic being:

$$F_{exc v} = \frac{2}{\pi} \int_{-\frac{\pi}{2}}^{\frac{\pi}{2}} F_{exc} \cos v a da = \frac{4}{\pi} \int_0^{(1-\gamma)\frac{\pi}{2}} F_{exc} \cos v a da + \frac{4}{\pi} \int_{(1-\gamma)\frac{\pi}{2}}^{\frac{\pi}{2}} \frac{\frac{\pi}{2} - a}{\gamma \frac{\pi}{2}} F_{exc} \cos v a da \quad (8-3)$$

Upon integration, and with a view to v being an odd number, we obtain

$$F_{exc v} = \frac{8}{\pi^2} \frac{F_{exc}}{\gamma} \frac{1}{v^2} \sin \frac{v\pi}{2} \sin v\gamma \frac{\pi}{2} \quad (8-4)$$

Here F_{exc} is the field winding magnetizing force per pole:

$$F_{exc} = w_{tn} i_{exc} \quad (8-5)$$

where i_{exc} = field (excitation) current
 w_{tn} = number of turns per pole.

For the fundamental harmonic ($v=1$), we obtain from expression (8-4)

$$F_{exc1} = \frac{8 \sin \frac{\gamma\pi}{2}}{\pi^2 \gamma} F_{exc} = k_{f. exc} F_{exc} \quad (8-6)$$

where the factor

$$k_{f. exc} = \frac{8 \sin \frac{\gamma\pi}{2}}{\pi^2 \gamma} \quad (8-7)$$

is termed the *form factor of the excitation field*, which determines the ratio of the flux density amplitude of the fundamental field wave to the actual maximum value of the field flux density.

The field magnetizing force with $i_{exc} = \text{const}$ is invariable in time, because the field winding is fed with direct current. The least relative harmonic content is obtained with $\gamma = 0.75$. The value of γ in turbo-generators is therefore generally taken close to this figure. For instance, with the twenty-four wound slots and the total of thirty-two slots used in some "Elektrosila" turbogenerators, we have $\gamma = \frac{24}{32} = 0.75$.

Let us find the field magnetizing force which produces the same fundamental wave flux as the armature-reaction magnetizing force of a given magnitude. Since with an unsaturated magnetic system the fluxes are proportional to the magnetizing forces which create them, we can, by taking the fundamental wave amplitude of the field winding magnetizing force and equating it to the fundamental wave amplitude of the armature-reaction magnetizing force find the expression for the armature-reaction magnetizing force to the scale of the field magnetizing force. The amplitude of the fundamental wave of the field winding magnetizing force per pole is found by equation (8-6). Accordingly, the amplitude of the fundamental wave of the armature reaction in a three-phase machine at a balanced load with a phase current I is equal to

$$F_a = \frac{m \sqrt{2}}{\pi} \frac{w k_w}{p} I \quad (8-8)$$

The value of the field magnetizing force $F_{exc \cdot eq}$ equivalent to the given value of the armature-reaction magnetizing force F_a is found if

the equivalent field magnetizing force $F_{exc. eq}$ is substituted for F_{exc} in equation (8-5) and is determined from the equality of the fundamental magnetizing force harmonics by equations (8-6) and (8-8). Thus

$$F_a = \frac{8 \sin \frac{\gamma \pi}{2}}{\pi^2 \gamma} F_{exc. eq} = k_{f. exc} F_{exc. eq}$$

whence for the factor reducing the armature-reaction magnetizing force to the field winding magnetizing force

$$k_a = \frac{F_{exc. eq}}{F_a} \tag{8-9}$$

we have

$$k_a = \frac{\pi^2 \gamma}{8 \sin \frac{\gamma \pi}{2}} = \frac{1}{k_{f. exc}} \tag{8-10}$$

For every machine the factor k_a has a certain definite value, and

$$F_{exc. eq} = k_a F_a = \frac{m \sqrt{2}}{\pi} \frac{\omega k_w}{p} k_a I \tag{8-11}$$

Assuming in equation (8-11)

$$F_{exc. eq} = \omega_{tn} i_{exc. eq}$$

it is also possible to find the field current $i_{exc. eq}$ equivalent to the armature current I .

Thus, the factor k_a makes it possible to express the armature magnetizing force in the scale of the field magnetizing force and, consequently, the no-load characteristic makes it possible to find the relation between the armature-reaction flux and the fundamental harmonic amplitude of the armature magnetizing force.

The relation between k_a and γ is given in Table 8-1. For the most frequently used ratio $\gamma=0.75$ we have $k_a=1$, and, consequently, the fundamental wave amplitude of the armature reaction is equal to the maximum of the equivalent field magnetizing force (to the height of the trapezoidal curve).

TABLE 8-1

γ	$\gamma \times 90^\circ$	k_a	γ	$\gamma \times 90^\circ$	k_a
0.60	54.0°	0.918	0.75	67.5°	1.000
0.66	59.4°	0.943	0.80	72.0°	1.035
0.70	63.0°	0.970			

The armature-reaction flux induces in the armature winding an armature-reaction e.m.f. E_a which, with $\mu = \text{const}$, is proportional to the armature current I

$$E_a = x_a I \quad (8-12)$$

The quantity x_a is termed the inductive reactance of the armature of a non-salient-pole machine, which according to relation (5-5) is

$$x_a = 2mf \frac{\mu_0 D l}{k_\delta k_\mu \delta} \frac{\omega^2 k_w^2}{p^2} \quad (8-13)$$

8-3. Armature Reaction of a Salient-Pole Synchronous Machine. Two-Reaction Theory [95, 98a]

The air-gap in a salient-pole machine, even when there are no slots on the stator, is not constant because of the presence of a large inter-polar air space.

The sine wave of the fundamental harmonic of the armature-reaction magnetizing force, when interacting with the fundamental harmonic of the field winding magnetizing force, produces a resultant magnetizing force whose axis is displaced from the rotor pole axis in a generator opposite to the direction of rotation.

Since the air-gap, being symmetrical with respect to the pole axis, becomes asymmetrical relative to the axis of the resultant magnetizing force, displaced from the pole axis, the resultant field wave obtained owing to the resultant magnetizing force will be asymmetrical and will contain higher harmonics of an appreciable magnitude. The form of the resultant field and the amplitude of the fundamental field wave for the same resultant magnetizing force amplitude will change depending on the angle ψ .

To appraise quantitatively the action of the armature reaction in a salient-pole machine, the phenomenon is considered as if the field magnetizing force and the reaction magnetizing force produce in the machine separate fluxes, which induce separate e.m.f.s in the stator winding. This greatly facilitates quantitative estimation. In the absence of saturation of the steel, it does not matter whether we first find from the magnetizing force components their resultant and the resultant flux in the machine and from this flux determine the e.m.f., or whether we find the fluxes of the magnetizing force components, and determine from them the e.m.f. components, and then, by vector addition of the e.m.f. components, find the resultant. There would be a difference if we took account of magnetic circuit saturation phenomena, but since with the relatively large air-gaps in synchronous machines saturation has a small influence, while its consideration involves great mathematical difficulties, these phenomena are neglected.

ted when analysing armature reaction and are allowed for only indirectly when plotting voltage diagrams.

With the above assumptions, the fundamental field wave induced by the field magnetizing force will vary in proportion to the amplitude of the fundamental magnetizing force wave. All the field wave harmonics will also vary in proportion to the amplitude of the fundamental magnetizing force wave. The amplitude of the fundamental wave of the reaction field, however, will depend not only on the fundamental wave of the armature-reaction magnetizing force, but also on the angle ψ . The harmonics in the armature-reaction field curve due to air-gap asymmetry will also depend on the angle ψ . If we would desire, as with a non-salient-pole machine, to find for the entire armature-reaction field the factor k_a , which allows us to express the armature-reaction magnetizing force in the scale of the field magnetizing force, then, obviously, the value of this factor would depend on the angle ψ , which would complicate analysis.

In analysing this problem use is made of the two-reaction theory introduced by Blondel, which consists in the following.

After separating the fundamental wave of the armature-reaction magnetizing force by the methods described above, we resolve it into two components along the main axes of the machine magnetic system: one, the direct-axis component producing magnetization whose axis coincides with the centre lines of the poles; and the other, the quadrature-axis component producing magnetization whose axis is midway between the field poles. The amplitude of the armature-reaction fundamental wave component along the direct axis will be

$$F_{ad} = F_a \sin \psi$$

and the amplitude of the quadrature-axis component is

$$F_{aq} = F_a \cos \psi$$

Since each of these components does not change its position relative to the pole axis, it is possible to find for each of them an appropriate factor, viz., k_{ad} for the direct-axis and k_{aq} for the quadrature-axis component. These factors make it possible to express for each of these components the armature-reaction magnetizing force in the scale of the field magnetizing force in a way similar to that used in finding the factor k_a for a non-salient-pole machine, which does not vary with the angle ψ . The only difference here is that in the stator winding of a non-salient-pole machine we consider one common fundamental wave e.m.f. E_a induced by the armature reaction, whereas in a salient-pole machine two e.m.f.s are considered: E_{ad} and E_{aq} , induced by the direct-axis and quadrature-axis armature reactions, and shifted in phase by 90° . Since the field forms produced by the same fundamental wave of the armature reaction when $\psi=0$ and $\psi=\pm\frac{\pi}{2}$ will be diffe-

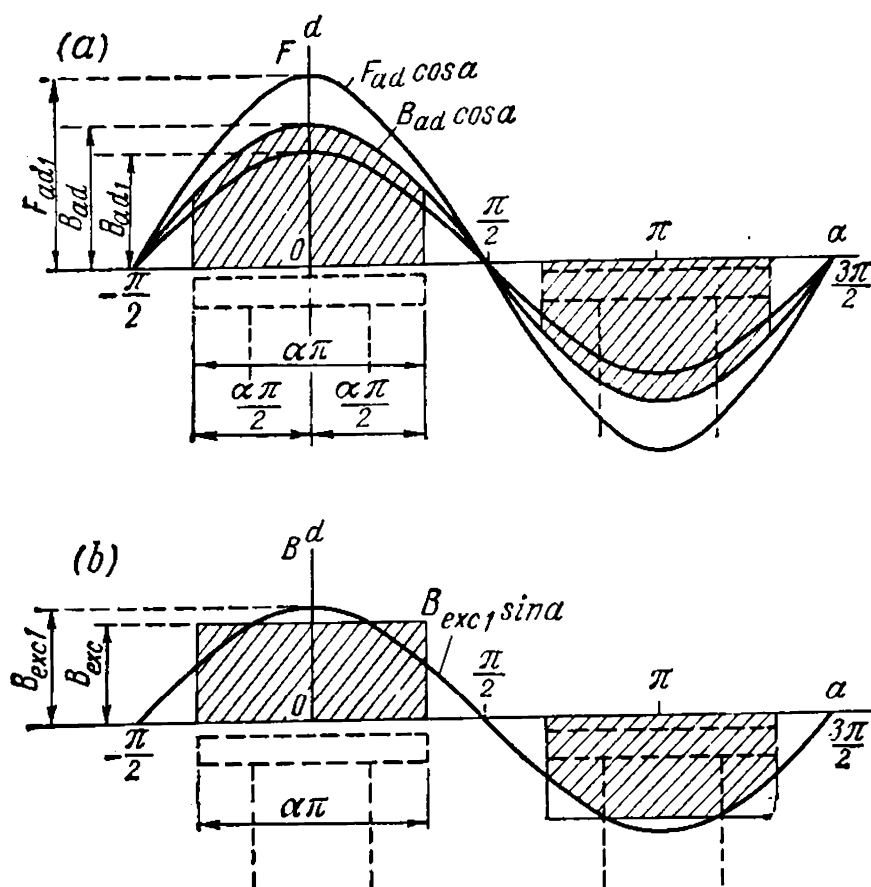


Fig. 8-6. Magnetizing force and magnetic field of direct-axis armature reaction and of field winding in a salient-pole synchronous machine

rent, it is obvious that the armature-reaction factors k_{ad} and k_{aq} for the direct and quadrature axes are also unequal. Let us analyse the armature reaction along the two axes.

Direct-Axis Armature Reaction. Figure 8-6a shows the position of the armature-reaction fundamental wave curve $F_{ad} \cos \alpha = F_a \cdot \sin \psi \cos \alpha$ relative to the pole system when $\psi = \pm \frac{\pi}{2}$. The ratio of the pole-shoe width to the pole pitch—the pole-arc coefficient—is designated by α . The shaded areas correspond to the flux density which is produced by the direct-axis sine-wave armature reaction on the assumption that the air-gap is uniform over the pole-shoe arc, but very small ($\delta \cong 0$), this allowing the edge effects to be neglected, and that the permeability of the magnetic circuit material is infinitely great. By neglecting the reluctance of the steel in the magnetic circuit and also the permeance of the space between the poles and the shoes (this being true for relatively small gaps), we can assume that the curve of the flux density in the air-gap has the same shape over the pole shoe as the magnetizing force curve. Since the field loses its sinusoidal form, it will induce in the stator winding e.m.f.s not only of the fundamental, but also of the higher harmonics. Let us find the factor k_{fd} which determines the decrease in the amplitude of the fundamental field wave

in comparison with a uniform air-gap, finding for this purpose the fundamental field harmonic shown in Fig. 8-6a by the shaded area.

If we place the origin of coordinates under the pole centre as in Fig. 8-6a, then all the sine terms in the expansion vanish, and only the cosine terms remain. The amplitude of the fundamental field harmonic B_{ad1} will be

$$B_{ad1} = \frac{2}{\pi} \int_{-\frac{\pi}{2}}^{\frac{\pi}{2}} B \cos a \, da = \frac{2}{\pi} \int_{-\frac{\alpha\pi}{2}}^{\frac{\alpha\pi}{2}} B_{ad} \cos^2 a \, da$$

since in the given case the flux density B differs from zero only within the region $-\frac{\alpha\pi}{2} \leq a \leq \frac{\alpha\pi}{2}$, where it is equal to $B_{ad} \cos a$. Here B_{ad} is the maximum value of the direct-axis armature-reaction flux density, i.e., the value of B under the pole-shoe centre.

By integration we obtain

$$B_{ad1} = \frac{B_{ad}}{\pi} \int_{-\frac{\alpha\pi}{2}}^{\frac{\alpha\pi}{2}} (1 + \cos 2a) \, da = \frac{B_{ad}}{\pi} \left[a + \frac{\sin 2a}{2} \right]_{-\frac{\alpha\pi}{2}}^{\frac{\alpha\pi}{2}} = \frac{\alpha\pi + \sin \alpha\pi}{\pi} B_{ad} \quad (8-14)$$

The factor

$$k_{fd} = \frac{B_{ad1}}{B_{ad}} \quad (8-15)$$

which determines the degree of reduction in the amplitude of the fundamental harmonic of the direct-axis armature reaction field due to air-gap non-uniformity which is caused by the presence of an air space between the poles and pole shoes is called *the form factor of the direct-axis armature reaction*. From expressions (8-14) and (8-15), with $\delta = \text{const} \cong 0$

$$k_{fd} = \frac{\alpha\pi + \sin \alpha\pi}{\pi} \quad (8-16)$$

The maximum flux density of the armature-reaction direct-axis field in the general case, with stator toothings taken into account, is equal to

$$B_{ad} = \frac{\mu_0}{k_\delta \delta} F_{ad} \quad (8-17)$$

where δ is the size of the gap under the pole-shoe centre.

Let us now find the fundamental harmonic of the field produced by the pole magnetizing forces. If the gap under the pole shoe is uniform and very small, the excitation field has the form of a rectangular wave,

whose base is equal to $\alpha\pi$ (Fig. 8-6b). This curve has a fundamental harmonic whose amplitude is equal to

$$B_{exc1} = \frac{2}{\pi} \int_{-\frac{\alpha\pi}{2}}^{\frac{\alpha\pi}{2}} B_{exc} \cos a \, da = \frac{4}{\pi} \sin \frac{\alpha\pi}{2} B_{exc} \quad (8-18)$$

In the general case B_{exc} is the maximum value of the excitation field flux density under the pole-shoe centre and is equal to

$$B_{exc} = \frac{\mu_0}{k_\delta \delta} F_{exc} \quad (8-19)$$

The ratio of the amplitude of the fundamental wave flux density of the excitation field B_{exc1} to the maximum flux density of this field

$$k_{f.exc} = \frac{B_{exc1}}{B_{exc}} \quad (8-20)$$

is called the *form factor of the excitation field*.

With a very small and uniform gap under the pole shoe this factor is, according to (8-18), equal to

$$k_{f.exc} = \frac{4}{\pi} \sin \frac{\alpha\pi}{2} \quad (8-21)$$

We find the field winding magnetizing force $F_{exc.d}$ equivalent to the armature-reaction direct-axis magnetizing force F_{ad} from the condition of equality of the fundamental harmonics of the magnetic field produced by these magnetizing forces:

$$\frac{\mu_0}{\delta k_\delta} F_{exc.d} k_{f.exc} = \frac{\mu_0}{\delta k_\delta} F_{ad} k_d$$

whence

$$F_{exc.d} = \frac{k_{fd}}{k_{f.exc}} F_{ad} = k_{ad} F_{ad}$$

The factor

$$k_{ad} = \frac{k_{fd}}{k_{f.exc}} \quad (8-22)$$

is called the factor for reducing the direct-axis armature-reaction magnetizing force to the field winding magnetizing force, or, in short, the direct-axis reaction factor.

When $\delta = \text{const} \cong 0$, according to (8-16) and (8-21), the factor is equal to

$$k_{ad} = \frac{\alpha\pi + \sin \alpha\pi}{4 \sin \frac{\alpha\pi}{2}} \quad (8-23)$$

Practical data pertaining to these factors are given below.

With a known value of k_{ad} the equivalent field magnetizing force $F_{exc.d}$ is determined from the relation

$$F_{exc.d} = k_{ad} F_{ad} = \frac{m \sqrt{2}}{\pi} \frac{\omega k_w}{p} k_{ad} I \sin \psi \quad (8-24)$$

Substituting here

$$F_{exc.d} = \omega_{exc} i_{exc.d} \quad (8-25)$$

we can also find the excitation current $i_{exc.d}$ which is equivalent to the direct-axis component of the stator current $I_d = I \sin \psi$. By the given method we find

$$i_{exc.d} = \frac{m \sqrt{2}}{\pi} \frac{\omega k_w}{p \omega_{exc}} k_{ad} I_d \quad (8-26)$$

The e.m.f. E_{ad} induced in the stator winding by the direct-axis armature reaction magnetizing force F_{ad} is the self-inductance e.m.f. of a stator phase winding due to this field, with the mutual inductance of the other stator phases taken into account. With $\mu = \text{const}$, the e.m.f. E_{ad} is proportional to F_{ad} and, consequently, to the direct-axis stator current component I_d :

$$E_{ad} = x_{ad} I_d \quad (8-27)$$

The proportionality factor x_{ad} is the inductive reactance of the direct-axis armature reaction.

As a result of the non-uniformity of the air-gap in a salient-pole machine, which is due to the configuration of the pole shoe, the fundamental harmonic of the armature-reaction direct-axis field decreases in proportion to k_{fd} , and the value of x_{ad} will be found by multiplying x_a from (8-13) by k_{fd} :

$$x_{ad} = 2mf \frac{\mu_0 D l}{k_\delta k_\mu \delta} \frac{\omega^2 k_w^2}{p^2} k_{fd} \quad (8-28)$$

Relation (8-28) distinctly reveals the dependence of x_{ad} on the design features of the machine.

Quadrature-Axis Armature Reaction. The armature reaction along the quadrature axis can be investigated in a similar manner. Figure 8-7 shows the position of the fundamental wave of the quadrature-axis armature reaction which has an amplitude $F_{aq1} = F_a \cos \psi$, and which produces the cross magnetization of the machine and does not directly interact with the field magnetizing force. The shaded areas depict the field produced by the quadrature reaction when assuming that the air-gap is uniform and negligibly small over the entire pole-shoe arc ($\delta \cong 0$), and that the permeability of the magnetic circuit material is infinitely large.

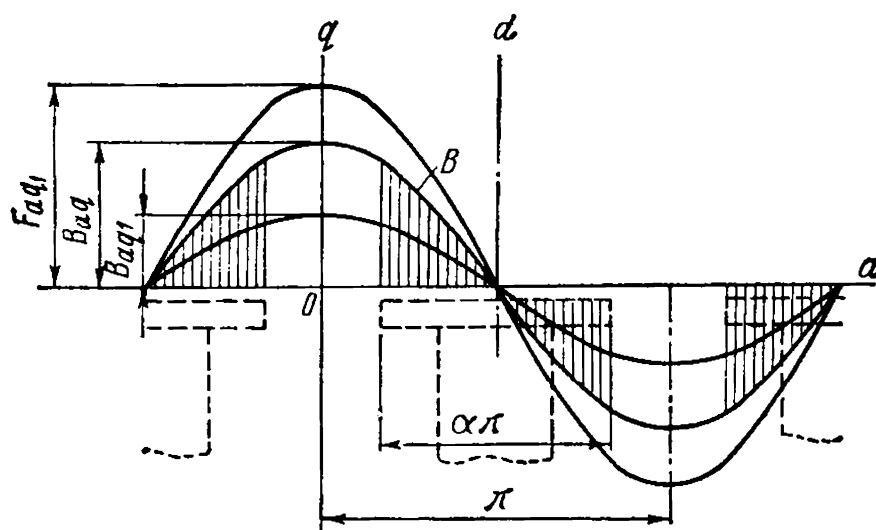


Fig. 8-7. Magnetizing force and magnetic field of a quadrature-axis armature reaction in a salient-pole synchronous machine

Under these conditions the curve of the flux density B over the pole-shoe arc changes relative to the quadrature axis q according to the law $B = B_{aq} \cos a$, and relative to the direct axis d according to the law $B = B_{aq} \sin a$. Here B_{aq} is the maximum value of the flux density of the quadrature-reaction field for the condition that the gap δ is uniform along the entire periphery:

$$B_{aq} = \frac{\mu_0}{k_\delta \delta} F_{aq}$$

Let us designate by k_{fq} the *form factor of the quadrature-reaction field*:

$$k_{fq} = \frac{B_{aq1}}{B_{aq}} \quad (8-29)$$

where B_{aq1} is the amplitude of the fundamental harmonic of the quadrature-reaction magnetic field. The factor k_{fq} determines the rate of decrease of B_{aq1} relative to B_{aq} due to gap non-uniformity resulting from the presence of an air space between the poles.

The value of B_{aq1} , when $\delta = \text{const} \cong 0$ over the pole-shoe arc, is determined, according to Fig. 8-7, if the coordinate a is measured from axis d , by the expression:

$$\begin{aligned} B_{aq1} &= \frac{2}{\pi} \int_{-\frac{\pi}{2}}^{+\frac{\pi}{2}} B \sin a \, da = \frac{2}{\pi} \int_{-\frac{\alpha\pi}{2}}^{+\frac{\alpha\pi}{2}} B_{aq} \sin^2 a \, da = \\ &= \frac{B_{aq}}{\pi} \int_{-\frac{\alpha\pi}{2}}^{+\frac{\alpha\pi}{2}} (1 - \cos 2a) \, da = \frac{B_{aq}}{\pi} \left[a - \frac{\sin 2a}{2} \right]_{-\frac{\alpha\pi}{2}}^{+\frac{\alpha\pi}{2}} = \frac{\alpha\pi - \sin \alpha\pi}{\pi} B_{aq} \end{aligned} \quad (8-30)$$

which gives the following value of k_{fq} for $\delta = \text{const} \cong 0$:

$$k_{fq} = \frac{\alpha\pi - \sin \alpha\pi}{\pi} \quad (8-31)$$

Let us determine the equivalent value of the field magnetizing force $F_{exc. q}$ which, when acting along the quadrature axis, will produce the same fundamental field harmonic as the given value of the quadrature-reaction magnetizing force F_{aq} . According to the previous considerations, between $F_{exc. q}$ and F_{aq} there should be maintained the relation

$$\frac{\mu_0}{k_\delta \delta} F_{exc. q} k_{f. exc} = \frac{\mu_0}{k_\delta \delta} F_{aq} k_{fq} \quad (8-32)$$

where $k_{f. exc}$ has the same value as in expression (8-21), used when considering the direct-axis reaction of the armature.

From (8-32) we find

$$F_{exc. q} = k_{aq} F_{aq} \quad (8-33)$$

where

$$k_{aq} = \frac{k_{fq}}{k_{f. exc}} \quad (8-34)$$

is the factor reducing the quadrature-axis armature reaction magnetizing force to the field winding magnetizing force or, in short, the quadrature-axis reaction factor.

With $\delta = \text{const} \cong 0$, the factor k_{aq} , from equations (8-21) and (8-31), is equal to

$$k_{aq} = \frac{\alpha\pi - \sin \alpha\pi}{4 \sin \frac{\alpha\pi}{2}} \quad (8-35)$$

With a known value of k_{aq} the equivalent field magnetizing force is found from the relation

$$F_{exc. q} = k_{aq} F_{aq} = \frac{m \sqrt{2}}{\pi} \frac{\omega k_w}{p} k_{aq} I \cos \psi \quad (8-36)$$

If we substitute in (8-36)

$$F_{exc. q} = \omega_{tn} i_{exc. q} \quad (8-37)$$

we can find the excitation current i_{aq} equivalent to the quadrature-axis armature current component

$$I_q = I \cos \psi \quad (8-38)$$

The fundamental harmonic of the armature quadrature-axis reaction field induces in the armature winding an e.m.f.

$$E_{aq} = x_{aq} I_q \quad (8-39)$$

where x_{aq} is the inductive reactance of the quadrature-axis armature reaction.

The expression for x_{aq} may be obtained from formula (8-28) if we substitute k_{fq} for k_{fd} and omit the saturation factor k_{μ} , since the quadrature-axis armature reaction fluxes, closing through the large air spaces between the poles, depend only slightly on the saturation. Thus,

$$x_{aq} = 2mf \frac{\mu_0 D l}{k_{\delta} \delta} \frac{\omega^2 k_w^2}{p^2} k_{fq}$$

(8-40)

Armature-Reaction Factors. The values of the factors k_{fd} , k_{fq} , k_{ad} , k_{aq} and $k_{f. exc}$ for a uniform and very small gap under the pole shoe, obtained from equations (8-16), (8-21), (8-23), (8-31) and (8-35), are given in Table 8-2. A glance at the table shows that k_{fq} and k_{aq} are respectively less than k_{fd} and k_{ad} and become equal to them only when $\alpha=1$, i.e., when the pole shoes of adjacent poles come into contact.

TABLE 8-2

Factor	$\alpha=b/\tau$						
	0.4	0.5	0.6	0.667	0.7	0.8	1.0
k_{fd}	0.703	0.818	0.913	0.943	0.958	0.987	1.000
k_{fq}	0.097	0.182	0.287	0.391	0.442	0.613	1.000
$k_{f. exc}$	0.749	0.900	1.032	1.104	1.135	1.212	1.275
k_{ad}	0.938	0.910	0.883	0.853	0.843	0.813	0.785
k_{aq}	0.129	0.202	0.288	0.354	0.389	0.505	0.785

In real machines the air-gap under the pole shoe has a finite value and, to decrease the influence of the armature reaction, it is even made much larger than, for instance, in induction machines. In addition, to obtain an excitation field form as close as possible to a sine wave, the air-gap under the pole shoe is made to increase towards the edges of the pole shoe instead of being a uniform one.

In practice the shape of the pole shoe is circumscribed by a radius somewhat smaller than that of the stator bore. The ratio of the maximum gap δ_{max} under the edge of the pole shoe to its value δ under the centre of the shoe is generally chosen within the limits of $\frac{\delta_{max}}{\delta} = 1.5$ to 2.0.

As a result, an armature-reaction flux of an appreciable magnitude also appears in the interpolar space, and the field wave forms will noticeably differ from those shown in Figs. 8-6 and 8-7. The forms of the field waves and the values of the corresponding factors are established in this case by a graphical plotting of the fields in the air-gap of a machine.

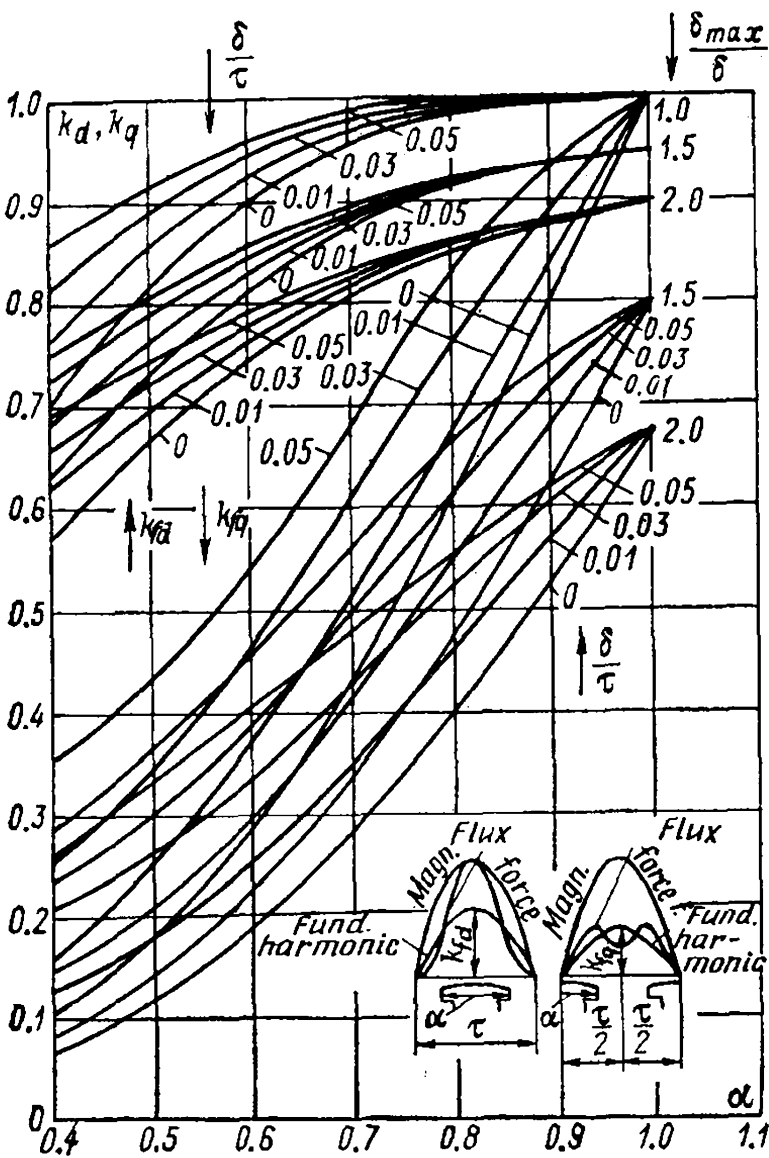


Fig. 8-8. Curves for determining factors k_{fd} and k_{fq}

Shown in Figs. 8-8, 8-9, 8-10, 8-11 and 8-12 are the curves of the factors $k_{fd}, k_{fq}, k_{f.exc}, k_{ad}$ and k_{aq} as functions of α , based on research carried out by M. Kostenko and B. Konik [116]. Figures 8-13 and 8-14 contain curves for determining the field form factor (k_f) and the pole-arc flux factor (k_{pa}). The curves are given for various ratios of the gap width under the pole-shoe centre δ to the pole pitch τ and for various ratios of δ to the maximum gap δ_{max} (at the pole-shoe edge), including a uniform gap over the pole-shoe arc ($\frac{\delta_{max}}{\delta}=1$).

Reduction of Field Winding Parameters to Stator. In analysing the processes occurring in transformers we reduce the secondary winding to the primary one (see Vol. I, Ch. 13) and obtain the parameters of the reduced

secondary winding by multiplying the real secondary winding parameters by the reduction factor k^2 . In studying various transient phenomena in synchronous machines, when the mutual inductance of the stator and rotor windings is manifested similarly to that of transformer windings, the rotor windings of a synchronous machine are also reduced to the stator winding.

Let us determine the factor $k_{exc.s}$ for reducing the field winding parameters to stator parameters, proceeding from the equality of the losses in the reduced and real windings. As the study of the transformer has shown, this condition must be observed when reducing the windings.

The losses in a real field winding are equal to

$$p_{exc} = i_{exc}^2 r_{exc}$$

When reducing a real field winding, we replace it with a winding identical with an m -phase stator winding, in which the reduced ex-

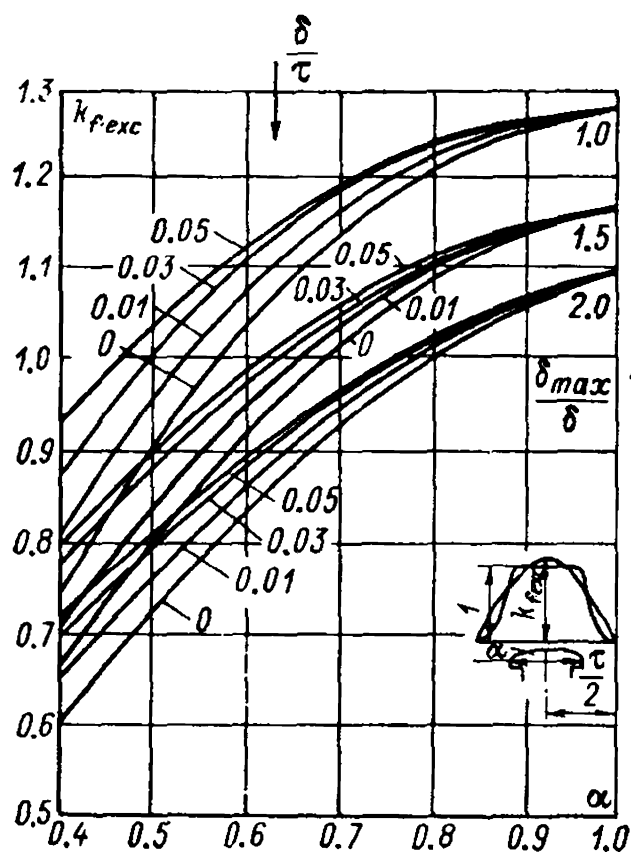


Fig. 8-9. Curves for determining factor $k_{f,exc}$

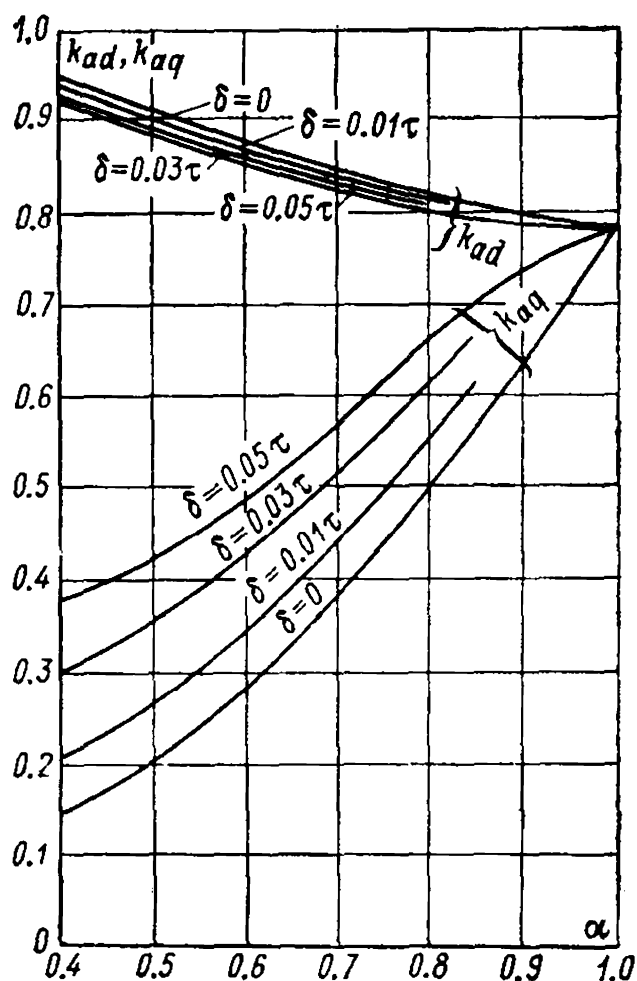


Fig. 8-10. Curves for determining factors k_{ad} and k_{aq} with $\frac{\delta_{max}}{\delta} = 1.0$

citation current has an effective value $I_{d,eq}$ equivalent to the excitation current i_{exc} .

The losses in the reduced winding will be

$$p'_{exc} = m I_{d,eq}^2 r'_{exc}$$

where r'_{exc} is the reduced resistance of the field winding.

By equating $p_{exc} = p'_{exc}$, we get

$$r'_{exc} = \frac{i_{exc}^2}{m I_{d,eq}^2} r_{exc} = k_{exc.s} r_{exc} \quad (8-41)$$

where the multiplier of r_{exc}

$$k_{exc.s} = \frac{i_{exc}^2}{m I_{d,eq}^2}$$

is the sought reduction factor.

The relation between i_{exc} and $I_{d,eq}$ is determined by equation (8-26), in which it is necessary to assume that $I_d = I_{d,eq}$. For $k_{exc.s}$ we obtain

$$k_{exc.s} = \frac{2m}{\pi^2} \frac{\omega^2 k_{\omega 1}^2}{\rho^2 \omega_{exc}^2} k_{ad}^2 \quad (8-42)$$

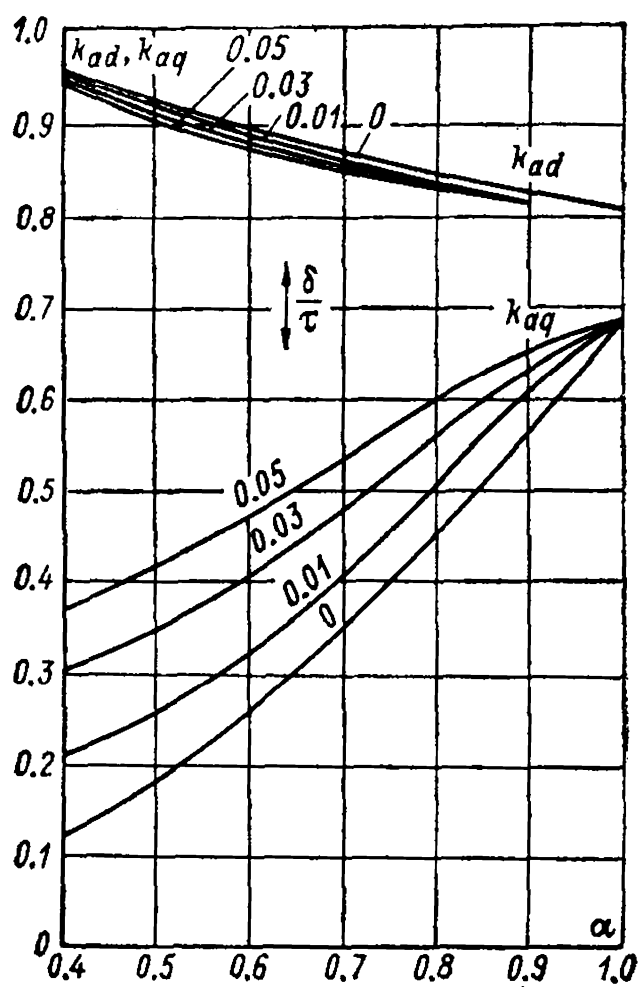


Fig. 8-11. Curves for determining factors k_{ad} and k_{aq} with $\frac{\delta_{max}}{\delta} = 1.5$

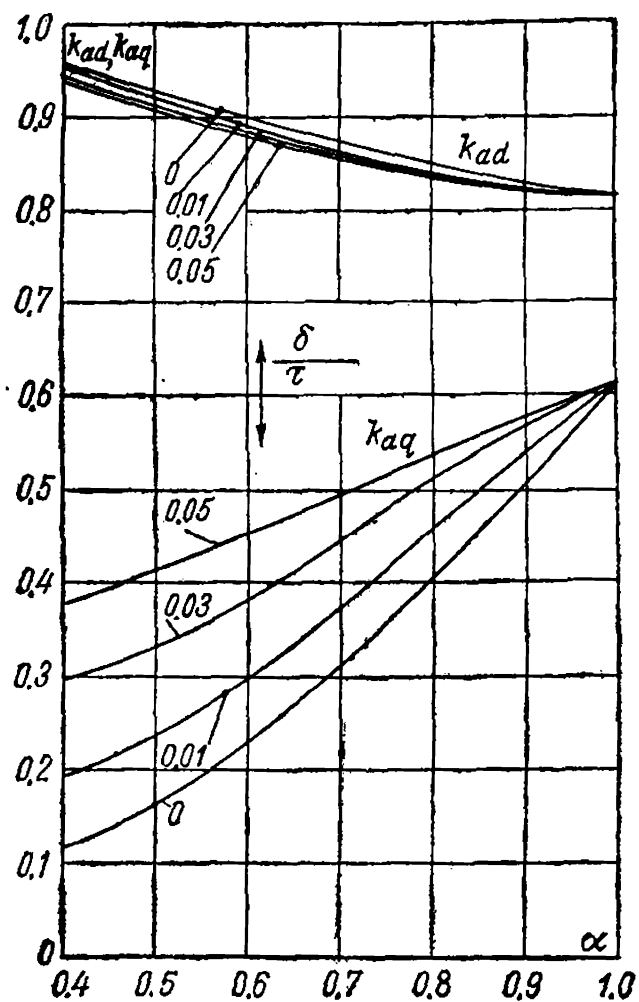


Fig. 8-12. Curves for determining factors k_{ad} and k_{aq} with $\frac{\delta_{max}}{\delta} = 2.0$

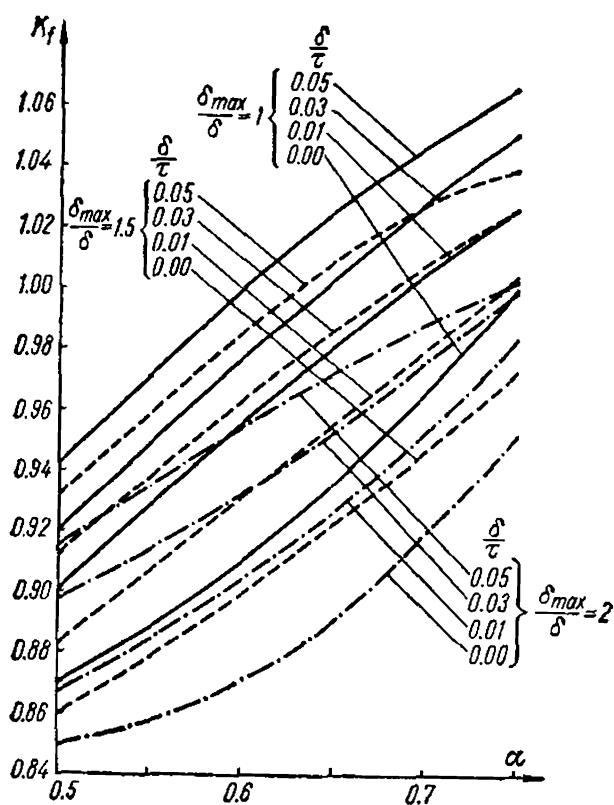


Fig. 8-13. Curves for determining the field form factor k_f

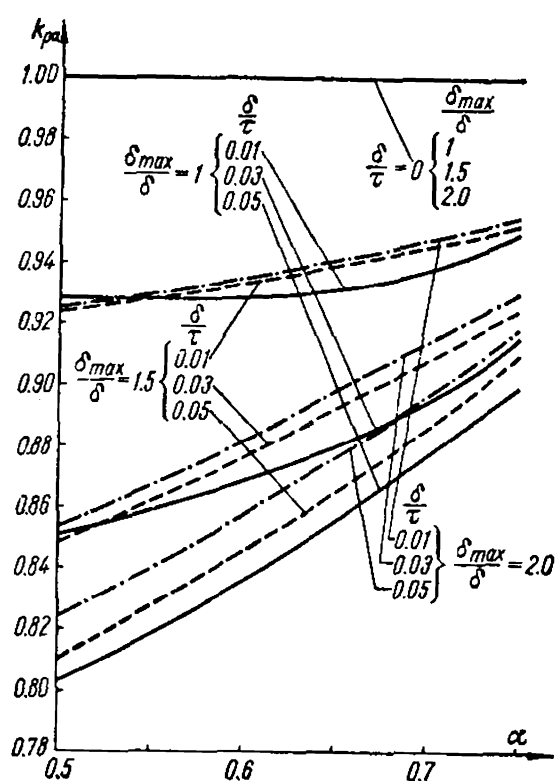


Fig. 8-14. Curves for determining the pole-arc flux factor $k_{pa} = \frac{\Phi_{pa}}{\Phi}$ (ratio of the magnetic flux entering the pole shoe to the total magnetic flux)

In dealing with transient phenomena, account should also be taken of the inductance $L_{\sigma exc}$, or the field winding leakage reactance x_{exc} due to: (a) the leakage fluxes of the field winding existing in the interpolar space, similar to the stator slot, (b) the end connections of the field winding, and (c) to the higher harmonics of the excitation field in the air-gap. Formulas for the calculation of $L_{\sigma exc}$ and x_{exc} are given in special manuals.

The parameters $L_{\sigma exc}$ and x_{exc} are reduced to the stator by means of the same factor as is used for r_{exc} .

Thus, the reduced values of the field winding parameters will be

$$\begin{aligned} r'_{exc} &= k_{exc. s} r_{exc. s}; & L'_{\sigma exc} &= k_{exc. s} L_{\sigma exc}; \\ x'_{exc} &= k_{exc. s} x_{exc} \end{aligned} \quad (8-43)$$

Example 8-1. A vertical salient-pole three-phase hydrogenerator has the following data: output $P=71\,500$ kVA, $U_r=13\,800$ V, $I_r=2990$ A, $f=50$ Hz, $\cos \varphi=0.8$, $2p=96$, $n=62.5$ rpm, $Z_1=684$, $q_1=2\frac{3}{8}$.

Design data: $D=12.92$ m, effective length of active steel of stator $l=1.5$ m, pole pitch $\tau=42.3$ cm, minimum air-gap $\delta_{min}=18.5$ mm, ratio $\frac{\delta_{max}}{\delta_{min}}=1.54$, $\frac{\delta_{min}}{\tau}=0.044$. The total air-gap factor $k_\delta=1.16$, $\alpha=0.733$. The saturation factor in operation at the rated load is $k_\mu=1.11$.

Winding data: series-connected number of turns in a stator phase winding $w_1=114$, the resultant winding factor for the fundamental harmonic is

$$k_{w1}=k_{d1}k_{p1}=0.955 \times 0.982=0.937$$

The number of field winding turns per pole $w_{exc}=17.5$. Using the curves of Figs. 8-8, 8-9 and 8-11 for the above values of α , $\frac{\delta_{max}}{\delta_{min}}$ and $\frac{\delta_{min}}{\tau}$, we find the factors of the armature reaction:

$$k_{fd}=0.9, \quad k_{fq}=0.6 \quad \text{and} \quad k_{f. exc}=1.08$$

whence

$$\begin{aligned} k_{ad} &= \frac{k_{fd}}{k_{f. exc}} = \frac{0.9}{1.08} = 0.833 \\ k_{aq} &= \frac{k_{fq}}{k_{f. exc}} = \frac{0.6}{1.08} = 0.555 \end{aligned}$$

When the magnetic circuit is not saturated ($k_\mu=1.0$) the inductive reactance of the direct-axis armature reaction is calculated by means of formula (8-28):

$$x_{ad}=2 \times 3 \times 50 \times \frac{4\pi \times 10^{-7} \times 12.92 \times 1.5}{1.16 \times 0.0185} \times \frac{114^2 \times 0.937^2}{48^2} \times 0.9 = 1.52 \, \Omega$$

The saturated value of this reactance at rated operating conditions with a saturation factor of $k_\mu=1.11$ is

$$x_{ad. r} = \frac{x_{ad}}{k_\mu} = \frac{1.52}{1.11} = 1.37 \, \Omega$$

The inductive reactance of the quadrature-axis armature reaction, according to formula (8-40), is

$$x_{aq} = 2 \times 3 \times 50 \times \frac{4\pi \times 10^{-7} \times 12.92 \times 1.5}{1.16 \times 0.0185} \times \frac{114^2 \times 0.937^2}{48^2} \times 0.6 = 1.01 \Omega$$

The rated impedance, taken as the unit,

$$Z_r = \frac{U_r}{\sqrt{3} I_r} = \frac{13\,800}{\sqrt{3} \times 2990} = 2.67 \Omega$$

The reactances in relative units are:

1. Unsaturated

$$\underline{x}_{ad} = \frac{1.52}{2.67} = 0.57$$

2. Saturated

$$\underline{x}_{ad, r} = \frac{1.37}{2.67} = 0.513$$

3. Quadrature-axis

$$\underline{x}_{aq} = \frac{1.01}{2.67} = 0.382$$

The stator winding leakage reactance in relative units, using the machine data, is:

$$\underline{x}_{\sigma a} = 0.125$$

The parameters of the 71 500-kVA hydrogenerator in steady-state conditions are:

direct-axis

$$\begin{aligned} \underline{x}_{ad} &= 0.57; \quad \underline{x}_{\sigma a} = 0.125; \\ \underline{x}_d &= 0.57 + 0.125 = 0.695 \end{aligned}$$

quadrature-axis

$$\underline{x}_{aq} = 0.382; \quad \underline{x}_q = 0.382 + 0.125 = 0.507$$

The resistances of the stator and rotor windings at 75°C, according to the machine data, are

$$\begin{aligned} r_a &= 0.0125 \Omega \\ r_{exc} &= 0.228 \Omega \end{aligned}$$

The stator winding resistance in relative units is

$$\underline{r}_a = \frac{r_a}{Z_r} = \frac{0.0125}{2.67} = 0.00468$$

The resistance of the field winding reduced to the stator winding from formula (8-43), is

$$\begin{aligned} \underline{r}'_{exc} &= k_{exc, s} \cdot r_{exc} = \frac{2 \times 3}{\pi^2} \times \frac{114^2 \times 0.937^2}{48^2 \times 17.5^2} \times 0.833^2 \times 0.228 = \\ &= 0.0068 \times 0.228 = 0.00155 \Omega \end{aligned}$$

and in

and in relative units

$$\underline{r}_{exc} = \frac{\underline{r}'_{exc}}{Z_r} = \frac{0.00155}{2.67} = 0.00058$$

Chapter

9

VOLTAGE DIAGRAMS OF A THREE-PHASE SYNCHRONOUS GENERATOR AT BALANCED LOAD

9-1. General

The voltage diagram is of very great importance for analysing the operating conditions of a synchronous machine. It can be used to obtain the relative variation of the synchronous generator voltage, the voltage increase with a drop in load and the voltage decrease in transition from no-load operation to operation under load. The solution of these problems is of great importance for: (a) initial machine design when the required excitation current values are determined for various operating conditions, and (b) when testing a finished machine to decide whether the machine conforms to given specifications. The voltage diagram makes it possible to determine the operating conditions of a machine without actually applying the load, which is quite a difficult problem when a high-power machine is involved.

Voltage diagrams make it possible to obtain the basic characteristics of a machine by calculation. Finally, the voltage diagram makes it possible to determine the power angle θ , i.e., the angle between the e.m.f. induced by the excitation field and the voltage across the terminals. The angle θ plays a very important role in the analysis of the torques and outputs developed by a machine both in steady-state and transient conditions.

The vector difference between the e.m.f. \dot{E}_m induced by the excitation flux and voltage \dot{U} across the terminals of a synchronous machine depends on the influence of the armature reaction and on the voltage drops in the resistance and leakage inductive reactance of the armature winding.

Since the armature reaction depends to a very great extent on the type of the machine (salient-pole or non-salient-pole), the kind of load (inductive, active or capacitive), and on the degree of load symmetry (balanced or unbalanced), all these factors must be duly considered when plotting a voltage diagram.

It must not be forgotten that all the e.m.f.s and voltages participating as components in the voltage diagram should correspond to the fundamental harmonic; therefore, all the e.m.f.s and voltages should be preliminarily resolved into harmonics and the fundamental wave separated from each of them. In Chapter 8 an analysis was carried

out which allowed us to obtain the fundamental voltage wave induced by the armature-field components revolving in step with the machine rotor.

When a new machine is being placed into service, a vector diagram is plotted from the test data based on the experimental no-load and short-circuit characteristics.

The voltage across the terminals is the result of the action of the following factors: (a) the main pole magnetizing force producing the flux Φ_m which induces the main e.m.f. E_m ; (b) the direct-axis armature reaction magnetizing force F_{ad} proportional to the load-current component I_d , reactive relative to the e.m.f. E_m ; (c) the quadrature-axis armature reaction magnetizing force F_{aq} proportional to the current component I_q , active relative to the e.m.f.; (d) the leakage e.m.f. $E_{\sigma a} = x_{\sigma a} I$ proportional to the load current I ; (e) the voltage drop in the stator winding resistance $I r_a$. Since when $I = I_r$ the voltage drop $I r_a$ is less than one per cent of the rated voltage, in most cases it may be neglected.

The diagram can be plotted in two different ways. In the first one it is assumed that each magnetizing force exists separately and induces its own magnetic flux, the latter producing its own e.m.f. Thus, four separate fluxes and, accordingly, four e.m.f.s produced by them appear in the machine: (1) the excitation flux Φ_m and the main e.m.f. \dot{E}_m ; (2) the flux Φ_{ad} and the e.m.f. \dot{E}_{ad} of the direct-axis armature reaction; (3) the flux Φ_{aq} and e.m.f. \dot{E}_{aq} of the quadrature-axis armature reaction; and (4) the flux $\Phi_{\sigma a}$ and the e.m.f. $\dot{E}_{\sigma a}$ of armature-winding leakage.

If we also take into account the active voltage drop, which, when taken with the opposite sign, can be formally considered as an e.m.f. $\dot{E}_r = -I r_a$, the vector sum of the e.m.f.s listed above gives as a result the magnitude and phase of the terminal voltage vector \dot{U} .

Since the vector summation of fluxes and the corresponding e.m.f.s induced by them by the superposition method is permissible only when the reluctances are constant in all sections of the magnetic circuit of the machine, this method is directly applicable in conditions of an unsaturated magnetic circuit of a synchronous machine. When using this method for machines with a saturated circuit, account should be taken of the actual reluctances of the parts of the magnetic circuit in the given duty and the reluctances assumed to be constant so far as the given duty is concerned. The results obtained will be correct, although it is difficult to determine the real magnetic conditions of the machine.

Since in this method the vectors of the synchronous machine e.m.f.s are summated, the voltage vector diagram obtained can be called an e.m.f. diagram.

From the theoretical viewpoint, this diagram is of very great methodological importance, since it allows us to assess, with the necessary completeness, all the factors determining, in the final run, the voltage across the terminals of a synchronous generator, although for purposes of calculation and test it is somewhat complicated. Therefore, for a number of practical purposes, the e.m.f. diagram is modified to make it simpler and more convenient.

Of greatest interest is the Blondel two-reaction theory, according to which all fluxes induced by the load current I , including the leakage $\Phi_{\sigma a}$, are resolved along the direct and quadrature axes. In this connection there is introduced for synchronous machines the concept of direct- and quadrature-axis inductive reactances x_d and x_q , which are basic parameters of a synchronous machine and serve for appraising its properties.

By the second method we can first determine the resultant magnetizing force of the generator, obtained as the result of interaction of the field magnetizing force with the armature-reaction magnetizing force, and, having found from it the resultant flux in the air-gap Φ_δ , determine the e.m.f. E_δ actually induced in the machine. By geometrically subtracting from the e.m.f. E_δ the voltage drop in the leakage reactance $jI x_{\sigma a}$ and in the resistance $I r_a$, we can find the resultant voltage across the generator terminals.

The diagram of magnetizing forces and e.m.f.s obtained is called the Potier, or e.m.m.f., diagram.

For balanced load conditions, assuming that the parameters of all phases are equal, the diagram may be plotted only for one phase.

It should be noted that vector diagrams plotted for a synchronous generator operating in generating duty may be readily extended to its operation as a synchronous motor and a synchronous condenser.

The simplest voltage diagram is obtained for balanced load of a synchronous non-salient-pole generator with an unsaturated magnetic system. We shall therefore begin our discussion with such a generator.

9-2. E.M.F. and the Potier Diagrams of a Three-Phase Non-Salient-Pole Synchronous Generator

Let us first construct an e.m.f. diagram of a synchronous non-salient-pole generator for an inductive load, when $0 < \psi < 90^\circ$. Align the vector of the voltage across the generator terminals with the positive direction of the axis of ordinates (Fig. 9-1a) and draw the current vector I lagging behind the voltage vector \dot{U} by the angle φ . Then draw the vector of the e.m.f. \dot{E}_m produced by the magnetic excitation flux Φ_m , leading the current vector I by the angle ψ . According to the general rule, the flux Φ_m leads the e.m.f. vector \dot{E}_m by 90° .

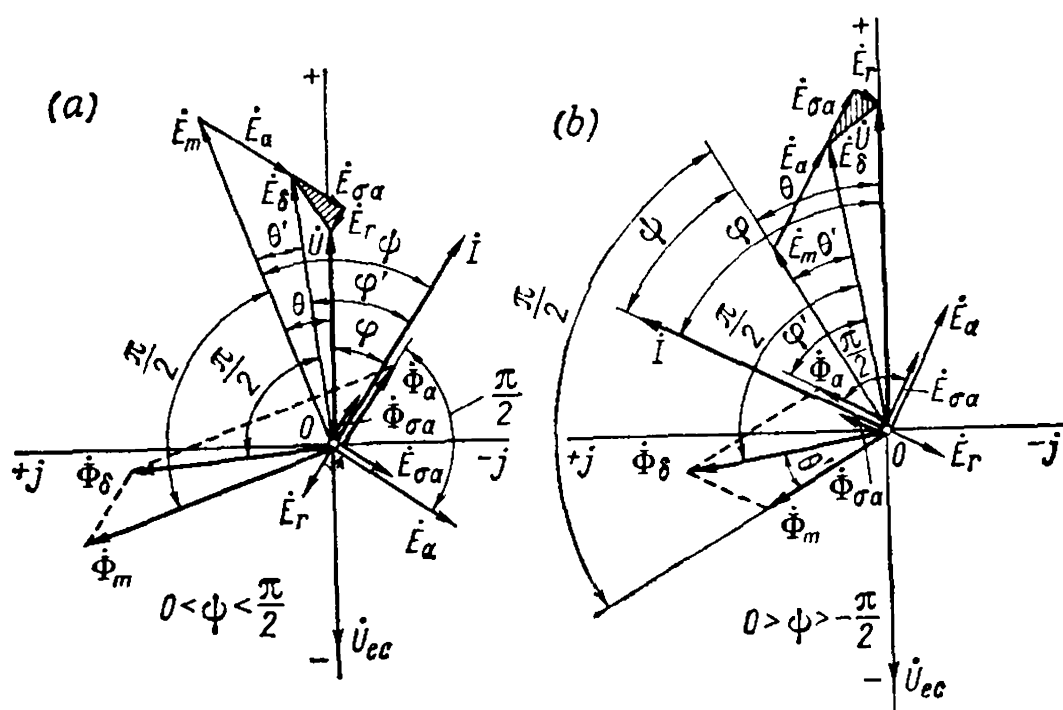


Fig. 9-1. E. m. f. diagrams of a non-salient-pole generator

The fundamental wave of the armature-reaction magnetizing force F_a of a synchronous generator rotates in step with its rotor. In a non-salient-pole machine the difference between the permeances along the direct and quadrature axes may be neglected, and it may be assumed that the magnetizing force F_a produces only a sine wave of the reaction flux Φ_a . This flux coincides in phase with the current I and induces in the stator winding an e.m.f. \dot{E}_a lagging in phase behind I by 90° . If x_a is the inductive reactance of the armature reaction in a non-salient-pole machine, then $\dot{E}_a = -jI x_a$.

By vector summation of the flux vectors Φ_m and Φ_a and, respectively, the e.m.f. vectors \dot{E}_m and \dot{E}_a , we obtain the vector of the resultant flux Φ_δ which actually exists in the generator air-gap and determines the saturation of its magnetic circuit, and the vector of the resultant e.m.f. \dot{E}_δ in the stator winding, proportional to the flux Φ_δ and lagging behind it by 90° .

Together with the armature-reaction flux there exists a stator winding leakage flux $\Phi_{\sigma a}$, whose vector, like that of the flux Φ_a , coincides in phase with the current I and produces in the stator winding a leakage e.m.f. of the fundamental frequency $\dot{E}_{\sigma a} = -jI x_{\sigma a}$, lagging in phase behind the current I by 90° . Here $x_{\sigma a}$ is the leakage reactance of the stator winding. Besides, it is necessary to take account of the e.m.f. $\dot{E}_r = -I r_a$, which is opposite in phase to the current I ; here r_a is the resistance of the stator winding.

By vector summation of the e.m.f. vectors \dot{E}_m , \dot{E}_a , $\dot{E}_{\sigma a}$ and \dot{E}_r or, what is the same, the e.m.f.s \dot{E}_δ , $\dot{E}_{\sigma a}$ and \dot{E}_r , we obtain the vector \dot{U}

of the voltage across the generator terminals. The angle φ by which the current I lags behind the voltage \dot{U} is determined by the parameters of the external power circuit which the generator is connected to. The vector \dot{U}_{ec} of the external circuit voltage opposes the generator voltage vector \dot{U} .

Figure 9-1b shows a similarly plotted e.m.f. diagram for a capacitive load, where the current I leads the e.m.f. \dot{E}_m by an angle $\psi < 0$, and $0 > \psi > -\frac{\pi}{2}$.

Comparing the diagrams in Fig. 9-1a and 9-1b, we see that with an inductive load the armature reaction produces a demagnetizing effect on the excitation system, while with a capacitive load, on the contrary, it produces a magnetizing effect. Therefore, in the first case we have $\Phi_\delta < \Phi_m$ and in the second $\Phi_\delta > \Phi_m$. Since generally $E_r < E_{\sigma a}$, with a capacitive load we usually have not only $U > E_m$, but also $U > E_\delta$.

When plotted the vector diagrams for a synchronous machine, the e.m.f.s \dot{E}_a , $\dot{E}_{\sigma a}$ and \dot{E}_r are generally replaced by their inverse values, which are the inductive and active voltage drops in the given sections of the circuit, i.e.,

$$-\dot{E}_a = jI x_a, \quad -\dot{E}_{\sigma a} = jI x_{\sigma a}, \quad -\dot{E}_r = I r_a$$

Here the voltage diagram gives, obviously, the resolution of the e.m.f. \dot{E}_m induced by the excitation flux into components represen-

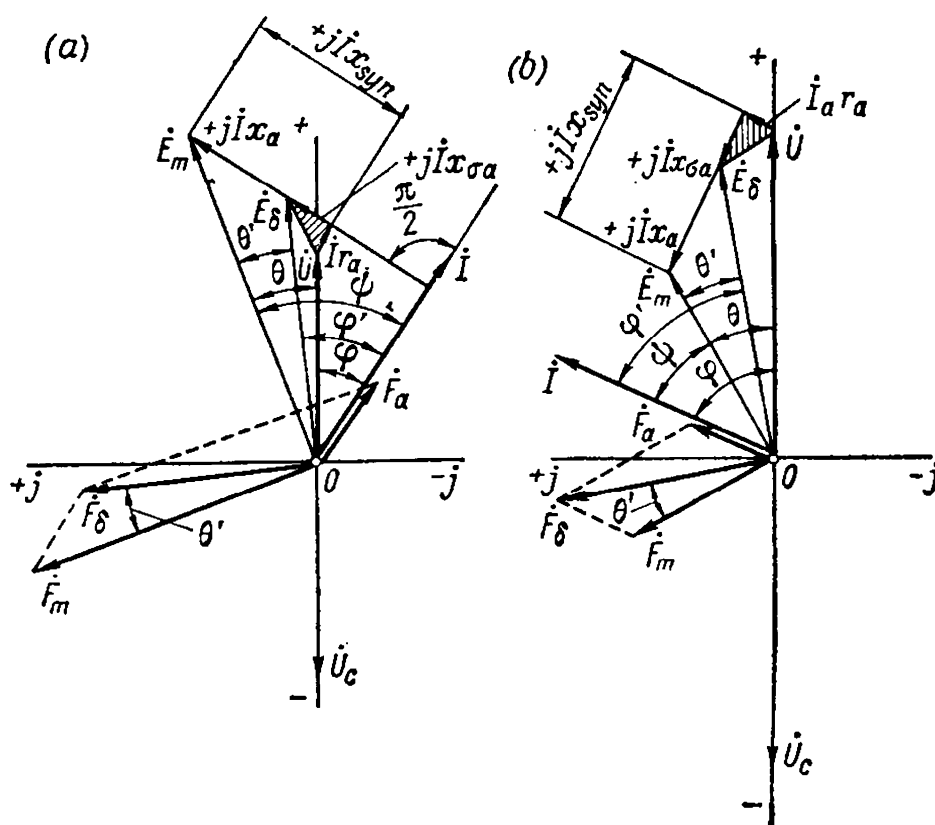


Fig. 9-2. The Potier diagrams for a non-salient-pole generator

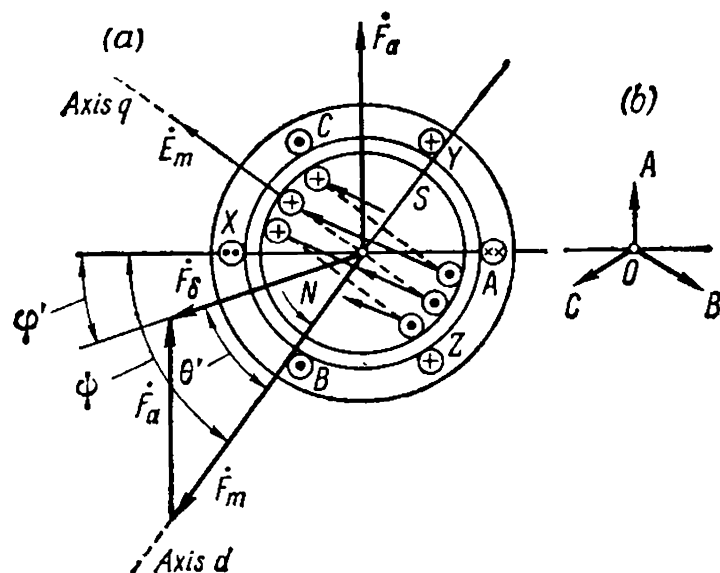


Fig. 9-3. Space diagram for non-salient-pole generator magnetizing force

ting the voltage drops $jI x_a$, $jI x_{\sigma a}$ and $I r_a$ and the generator terminal voltage \dot{U} . On the other hand, the voltage diagram instead of the fluxes $\dot{\Phi}_m$, $\dot{\Phi}_a$ and $\dot{\Phi}_\delta$ shows the magnetizing forces \dot{F}_m , \dot{F}_a and \dot{F}_δ . This makes it possible to call it the Potier diagram. Thus, the general-form e.m.f. diagrams for leading and lagging currents in Fig. 9-1a and b become the Potier diagrams in Fig. 9-2a and b.

The voltage drop vectors $jI x_a$ and $jI x_{\sigma a}$ in Fig. 9-2a and b can be replaced with a common voltage drop vector

$$jI x_a + jI x_{\sigma a} = jI x_{syn}$$

where the reactance

$$x_{syn} = x_a + x_{\sigma a}$$

is termed the synchronous inductive reactance of a non-salient-pole machine.

It is interesting to show the relative arrangement in space of the main parts of a machine—the stator and rotor and the windings on them—together with the magnetizing forces produced by them. Figure 9-3a presents the position of the rotor for the moment corresponding to the instantaneous current values of Fig. 9-3b. The angle ψ shows the displacement in space of the conductors carrying the maximum current I from the conductors which have the maximum e.m.f. \dot{E}_m and lie opposite to the pole axis. The current I lags behind the e.m.f. \dot{E}_m in time by the same angle ψ . If we add the magnetizing force vector \dot{F}_a to the excitation winding magnetizing force vector \dot{F}_m , we obtain the resultant magnetizing force vector \dot{F}_δ which lags in space behind \dot{F}_m by the same angle θ' by which the e.m.f. \dot{E}_δ lags behind the e.m.f. \dot{E}_m in time.

9-3. E.M.F. Diagram of a Salient-Pole Three-Phase Synchronous Generator at Balanced Load (Blondel Diagram) [95, 98a]

In a salient-pole machine the fundamental wave of the armature-reaction magnetizing force F_a rotates in step with the rotor and, owing to the non-uniformity of the air-gap between the rotor and the stator, induces a non-sinusoidal armature-reaction magnetic flux which indu-

ces, in turn, a non-sinusoidal armature-reaction e.m.f. To include the armature-reaction e.m.f. in the voltage diagram, the fundamental wave should be separated from it. This is achieved, as was shown in Sec. 8-3, with the aid of a method based on the Blondel two-reaction theory. According to this method the fundamental wave of the armature reaction is resolved into two components: the direct and quadrature components \dot{F}_{ad} and \dot{F}_{aq} . By separating the fundamental wave from the fluxes produced by the direct- and quadrature-axes reactions, we find (see Sec. 8-3) with the aid of the factors k_{ad} and k_{aq} of the armature reaction field (which are definite functions of the geometrical relations of the pole system) the direct- and quadrature-axis armature-reaction magnetizing forces (equivalent or reduced to the excitation winding):

$$\dot{F}'_{ad} = k_{ad} \dot{F}_a \sin \psi \quad \text{and} \quad \dot{F}'_{aq} = k_{aq} \dot{F}_a \cos \psi$$

These armature-reaction components \dot{F}'_{ad} and \dot{F}'_{aq} will produce the fundamental wave fluxes $\dot{\Phi}'_{ad}$ and $\dot{\Phi}'_{aq}$, which will induce the armature-reaction direct-axis e.m.f.s \dot{E}_{ad} and quadrature-axis e.m.f.s \dot{E}_{aq} having the fundamental wave frequency.

The resolution shown above makes it possible to construct a voltage diagram for a salient-pole machine practically by the method used for a non-salient-pole machine, only substituting for the total armature-reaction e.m.f. \dot{E}_a its components \dot{E}_{ad} and \dot{E}_{aq} .

Figure 9-4a shows a voltage diagram for a lagging current ($0 < \psi < \frac{\pi}{2}$), constructed by this method as follows. The current \dot{I} is resolved

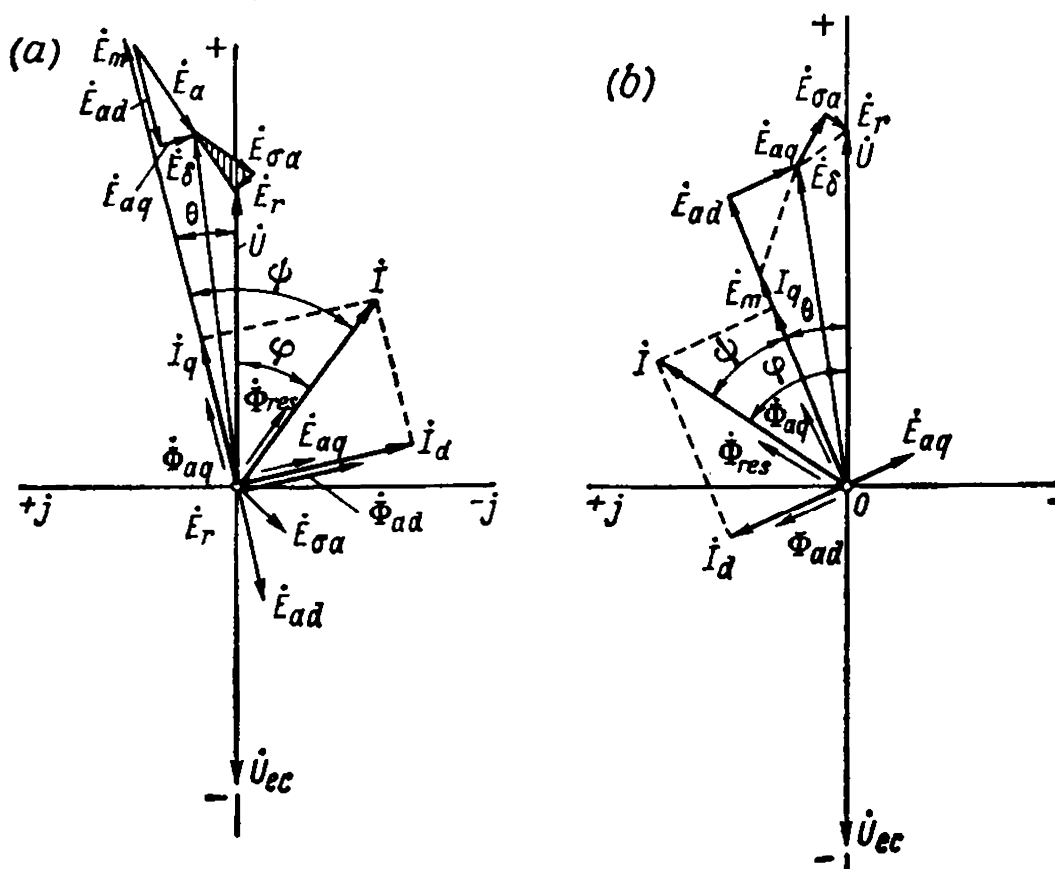


Fig. 9-4. E. m. f. diagrams of a salient-pole generator

into the quadrature-axis component $\dot{I}_q = \dot{I} \cos \psi$ coincident with the e.m.f. vector \dot{E}_m and active relative to it, and the direct-axis component $\dot{I}_d = \dot{I} \sin \psi$, which lags on \dot{E}_m in phase by 90° and is reactive relative to it. The current \dot{I}_q induces the magnetizing force \dot{F}_{aq} and flux $\dot{\Phi}_{aq}$ of the quadrature-axis armature reaction in phase with the current \dot{I}_q , while the current \dot{I}_d induces the magnetizing force \dot{F}_{ad} and flux $\dot{\Phi}_{ad}$ of the direct-axis armature reaction in phase with the current \dot{I}_d . The fluxes $\dot{\Phi}_{aq}$ and $\dot{\Phi}_{ad}$ induce in the stator winding the e.m.f.s \dot{E}_{aq} and \dot{E}_{ad} , which are of fundamental frequency and lag behind the corresponding fluxes $\dot{\Phi}_{aq}$ and $\dot{\Phi}_{ad}$ by 90° .

If the magnetic circuit is not saturated, it may be assumed that $E_{aq} \equiv \Phi_{aq} \equiv F_{aq} \equiv I_q$ and $E_{ad} \equiv \Phi_{ad} \equiv F_{ad} \equiv I_d$, and the e.m.f.s E_{aq} and E_{ad} may be expressed as follows:

$$\left. \begin{aligned} \dot{E}_{aq} &= -j\dot{I}_q x_{aq} = -j\dot{I} \cos \psi x_{aq} \\ \dot{E}_{ad} &= -j\dot{I}_d x_{ad} = -j\dot{I} \sin \psi x_{ad} \end{aligned} \right\} \quad (9-1)$$

Here x_{aq} and x_{ad} are the *inductive reactances of the armature reaction along the quadrature and direct axes*.

Since in a salient-pole machine the armature-reaction factors k_{aq} and k_{ad} are not equal (Figs. 8-10, 8-11 and 8-12), we have

$$\frac{E_{ad}}{E_{aq}} = \frac{k_{ad} \sin \psi}{k_{aq} \cos \psi} = \frac{k_{ad}}{k_{aq}} \tan \psi$$

For this reason the armature-reaction e.m.f. $E_a = \sqrt{E_{ad}^2 + E_{aq}^2}$

and its vector lag behind the current \dot{I} in phase by an angle other than 90° , whereas in a non-salient-pole machine, where $k_{aq} = k_{ad}$, the e.m.f. \dot{E}_a lags behind the current \dot{I} by exactly 90° (see diagram in Fig. 9-2a and b).

By plotting the e.m.f. vectors $\dot{E}_{\sigma a} = -j\dot{I}x_{\sigma a}$ and $\dot{E}_r = -\dot{I}r_a$ and by vector addition of the e.m.f.s \dot{E}_m , \dot{E}_{ad} , \dot{E}_{aq} , $\dot{E}_{\sigma a}$, and \dot{E}_r , we obtain the generator terminal voltage vector \dot{U} which leads the current vector \dot{I} by an angle φ (Fig. 9-4a).

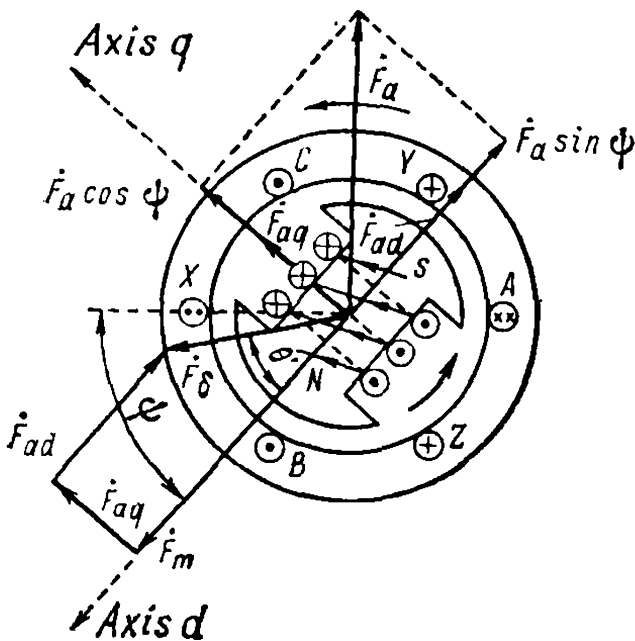


Fig. 9-5. Space diagram of salient-pole generator magnetizing force

A similar e.m.f. diagram for a leading current ($0 > \varphi > -\frac{\pi}{2}$) is constructed in Fig. 9-4b.

The space arrangement of the pole system and the stator current system with inductive load has the form indicated in Fig. 9-5.

9-4. Modified E.M.F. Diagram

The e.m.f. diagrams in Fig. 9-4a and b are usually modified so that instead of the e.m.f. vectors \dot{E}_{ad} , \dot{E}_{aq} , $\dot{E}_{\sigma a}$ and \dot{E}_r there are introduced (Fig. 9-6) the voltage drops

$$-\dot{E}_{ad} = j\dot{I}_d x_{ad}; \quad -\dot{E}_{aq} = j\dot{I}_q x_{aq}; \quad -\dot{E}_{\sigma a} = j\dot{I} x_{\sigma a}; \quad -\dot{E}_r = \dot{I} r_a$$

When constructing this diagram, we lay out the generator terminal voltage vector \dot{U} in the positive direction of the axis of ordinates and draw the current vector \dot{I} at an angle φ to it. To the voltage vector

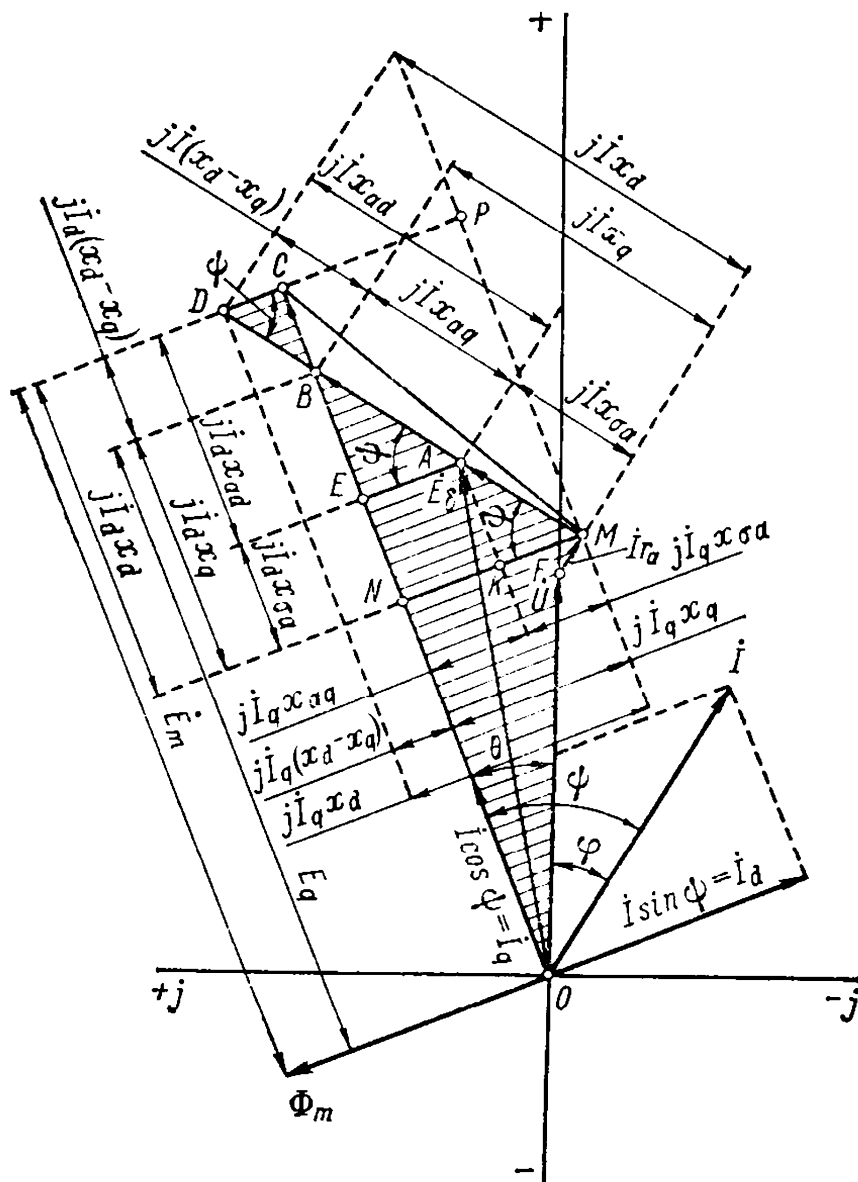


Fig. 9-6. Modified e. m. f. diagram of a salient-pole generator

$\overline{OF} = \dot{U}$ we add the active voltage drop vector $\overline{FM} = \dot{I}r_a$ and the inductive leakage voltage drop vector $\overline{MA} = j\dot{I}x_{\sigma a}$. The closing line \overline{OA} of the vectors is the resultant e.m.f. vector \dot{E}_σ induced by the air-gap flux Φ_δ .

Suppose the direction of the e.m.f. vector \dot{E}_m is known, then the angle ψ between the vectors \dot{E}_m and \dot{I} will also be known. By dropping perpendiculars from the end of the current vector \dot{I} to the direction of vector \dot{E}_m and to the direction normal to it, we obtain the quadrature-axis current component $\dot{I}_q = \dot{I} \cos \psi$ and the direct-axis component $\dot{I}_d = \dot{I} \sin \psi$. A perpendicular from end A of the e.m.f. vector \dot{E}_δ onto the direction of vector \dot{E}_m will denote the voltage drop due to the quadrature-axis armature reaction $\overline{EA} = j\dot{I}_q x_{aq}$. By laying off from point \dot{E} the voltage drop due to the direct-axis armature reaction $\overline{CE} = j\dot{I}_d x_{ad}$, we obtain both the magnitude and the direction of the full e.m.f. vector $\overline{OC} = \dot{E}_m$ induced by the excitation flux.

If we resolve the inductive reactance voltage drop vector $\overline{AM} = j\dot{I}x_{\sigma a}$ into components similar in direction to the e.m.f. \dot{E}_m and directed perpendicularly to it,

$$\begin{aligned}\overline{AK} &= j\dot{I}x_{\sigma a} \sin \psi = j\dot{I}_d x_{\sigma a} \\ \overline{KM} &= j\dot{I}x_{\sigma a} \cos \psi = j\dot{I}_q x_{\sigma a}\end{aligned}$$

then

$$\overline{CN} = \overline{CE} + \overline{EN} = \overline{CE} + \overline{AK} = j\dot{I}_d x_{ad} + j\dot{I}_d x_{\sigma a} = j\dot{I}_d (x_{ad} + x_{\sigma a}) = j\dot{I}_d x_d$$

Accordingly

$$\begin{aligned}\overline{NM} &= \overline{NK} + \overline{KM} = \overline{EA} + \overline{KM} = j\dot{I}_q x_{aq} + j\dot{I}_q x_{\sigma a} = \\ &= j\dot{I}_q (x_{aq} + x_{\sigma a}) = j\dot{I}_q x_q\end{aligned}$$

The inductive reactances

$$x_d = x_{ad} + x_{\sigma a} \quad \text{and} \quad x_q = x_{aq} + x_{\sigma a}$$

are called the synchronous inductive reactances of a synchronous salient-pole machine for the direct and quadrature axes, respectively.

The parameters x_d and x_q are of very great importance for the analysis of synchronous machine performance. From the diagram in Fig. 9-6 we have, further

$$\overline{AB} = \frac{\overline{EA}}{\cos \psi} = \frac{j\dot{I}_q x_{aq}}{\cos \psi} = j\dot{I} x_{aq}$$

and

$$\overline{BE} = \overline{AB} \sin \psi = j\dot{I}x_{aq} \sin \psi = j\dot{I}_d x_{aq}$$

Hence

$$\overline{CB} = \overline{CE} - \overline{BE} = j\dot{I}_d x_{ad} - j\dot{I}_d x_{aq} = j\dot{I}_d (x_{ad} - x_{aq}) = j\dot{I}_d (x_d - x_q)$$

Accordingly

$$\overline{BD} = \frac{\overline{CB}}{\sin \psi} = \frac{j\dot{I}_d (x_d - x_q)}{\sin \psi} = \frac{j\dot{I} \sin \psi (x_d - x_q)}{\sin \psi} = j\dot{I} (x_d - x_q)$$

$$\overline{CD} = \overline{BD} \cos \psi = j\dot{I} (x_d - x_q) \cos \psi = j\dot{I}_q (x_d - x_q)$$

In a non-salient-pole synchronous machine $x_d - x_q = 0$, and the vector lengths

$$\overline{CB} = j\dot{I}_d (x_d - x_q) = 0; \quad \overline{CD} = j\dot{I}_q (x_d - x_q) = 0$$

and, consequently, the vector diagram in Fig. 9-6 takes the form previously discussed in Fig. 9-2a.

9-5. E.M.F. Diagram for Short Circuit

The e.m.f. diagram for a balanced, i.e., three-phase steady-state short circuit (Fig. 9-7a) is obtained from the diagram in Fig. 9-6 if we assume therein that the voltage $U = 0$. The resistance r_a is considerably less than the inductive reactances $x_{\sigma a}$, x_{ad} and x_{aq} and may therefore be neglected. Correspondingly, the quadrature-axis current component \dot{I}_q practically vanishes, and the entire short-circuit current is essentially direct-axis, i.e., $\psi_{sh} \cong 90^\circ$ and $\dot{I}_d = \dot{I}_{sh}$. For this reason in Fig. 9-7a we practically have $\dot{I}r_a \cong 0$ and $j\dot{I}_q x_{aq} \cong 0$. Therefore,

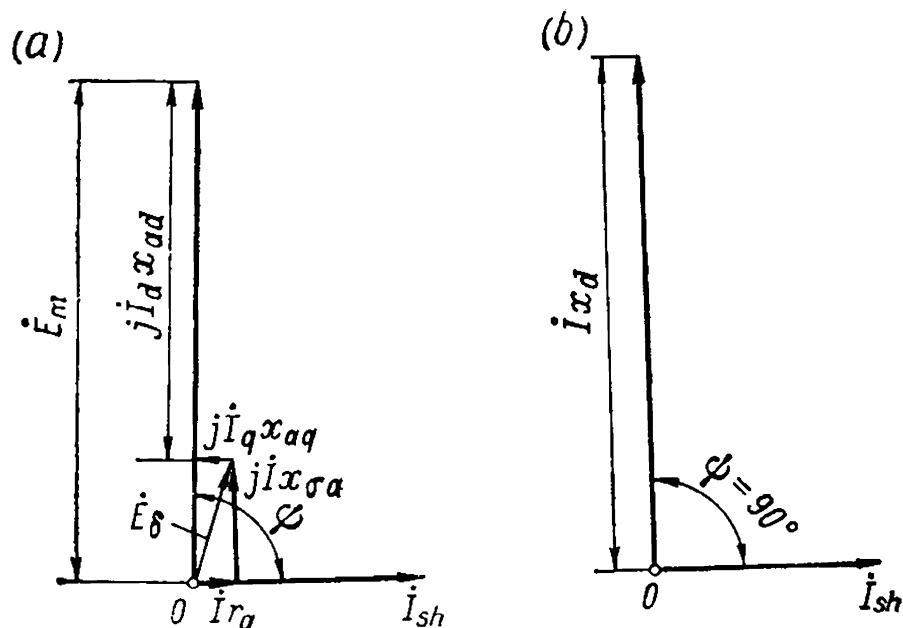


Fig. 9-7. E. m. f. diagram for short circuit

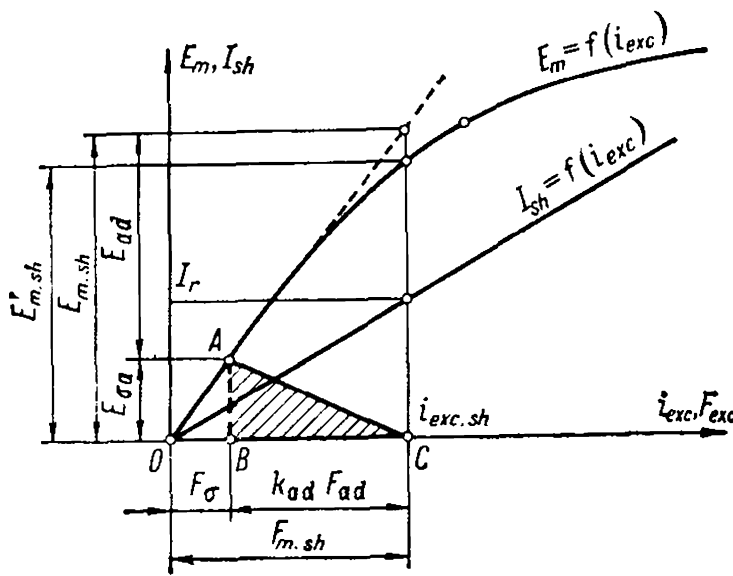


Fig. 9-8. No-load and short-circuit characteristics

the diagram in Fig. 9-7a can be replaced, without any significant error, with the diagram in Fig. 9-7b, from which it can be seen that the short-circuit current I_{sh} is determined by the magnitude of the e.m.f. E_m , i.e., by the excitation current and the synchronous direct-axis inductive reactance x_d , and

$$I_{sh} \cong \frac{E_m}{x_{\sigma a} + x_{ad}} = \frac{E_m}{x_d} \quad (9-2)$$

Thus, the armature-reaction flux in short circuit is completely demagnetizing.

Since the leakage inductive reactance $x_{\sigma a}$ is much smaller than the synchronous reactance x_d , the resultant e.m.f. \dot{E}_δ which, according to Fig. 9-7a, with $r_a = 0$ becomes $\dot{E}_\delta = -j\dot{I}x_{\sigma a}$, is small in comparison with the e.m.f. E_m . Consequently, the resultant magnetic flux Φ_δ in short circuit is very small, and the machine does not become saturated. Therefore in equation (9-2) we have to do with the saturated value of x_d .

Figure 9-8 gives the no-load characteristic $E_m = f(i_{exc})$ and the three-phase short-circuit characteristic $I_{sh} = f(i_{exc})$.

If on the short-circuit characteristic curve we take the excitation current $i_{exc.sh}$ corresponding, for example, to the rated current $I_{sh} = I_r$, then on the no-load characteristic curve we can find the e.m.f. $E_{m.sh}$ induced by this excitation current at no-load when the machine is saturated to a certain degree. The e.m.f. $E_{m.sh}$ corresponding to this excitation current in short circuit can be found on the extension of the straight part of the no-load characteristic. The excitation current $i_{exc.sh}$ corresponds to a full excitation magnetizing force $F_{m.sh}$. If from $F_{m.sh}$ we subtract the direct-axis armature-reaction magnetizing force F_{ad} , reduced to the field winding (see Sec. 8-3), i.e., $k_{ad}F_{ad}$, the remaining magnetizing force F_σ determines, from the no-load characteristic, the stator winding leakage e.m.f. $E_{\sigma a}$. The direct-axis armature-reaction e.m.f. E_{ad} will be determined as the difference between the e.m.f.s $E_{m.sh}$ and $E_{\sigma a}$:

$$E_{ad} = E_{m.sh} - E_{\sigma a}$$

The triangle ABC obtained from the no-load and short-circuit characteristics and having legs $AB = E_{\sigma a} = Ix_{\sigma a}$ and $BC \equiv F_{ad}$ is referred to as the *short-circuit triangle* or the *reactive triangle*. The

triangle is of major significance in the construction of synchronous machine characteristics.

9-6. Synchronous Machine Inductive Reactances in Steady-State Balanced Operation

To characterize these reactances, let us investigate the physical aspects of magnetic flux distribution corresponding to no-load operation (Fig. 9-9) and a steady-state three-phase short circuit of a machine (Fig. 9-10).

In these figures only one phase is shown, because we consider here a three-phase steady-state short circuit at a moment when the current in the depicted phase attains its maximum, i.e., when the resultant armature-reaction flux is along the axis of the given phase. The magnetic lines of the pole field are shown by solid lines, and the magnetic lines induced by the stator current, by dotted lines.

For simplicity, the stator winding phase, the same as the magnetic flux lines, is shown as a circuit encircling the stator iron stack, and only from one side.

In a steady-state short circuit the excitation winding flux Φ_m (Fig. 9-10a) induces in the stator winding the same e.m.f. E_m as under no-load at the same excitation and without saturation. Since in short circuit the voltage across the machine terminals is zero, the e.m.f. E_m should be balanced, if we neglect the resistance of the armature winding, by the armature-reaction e.m.f. $-jI_d x_{ad}$ and the leakage e.m.f. $-jI_d x_{\sigma a}$ induced by the armature-reaction flux Φ_{ad} and

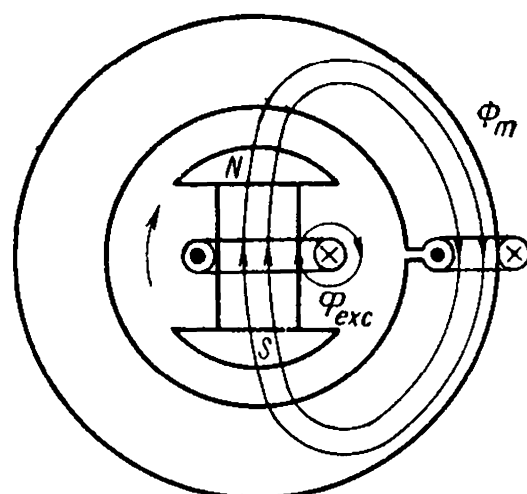


Fig. 9-9. Magnetic field of a synchronous generator at no-load

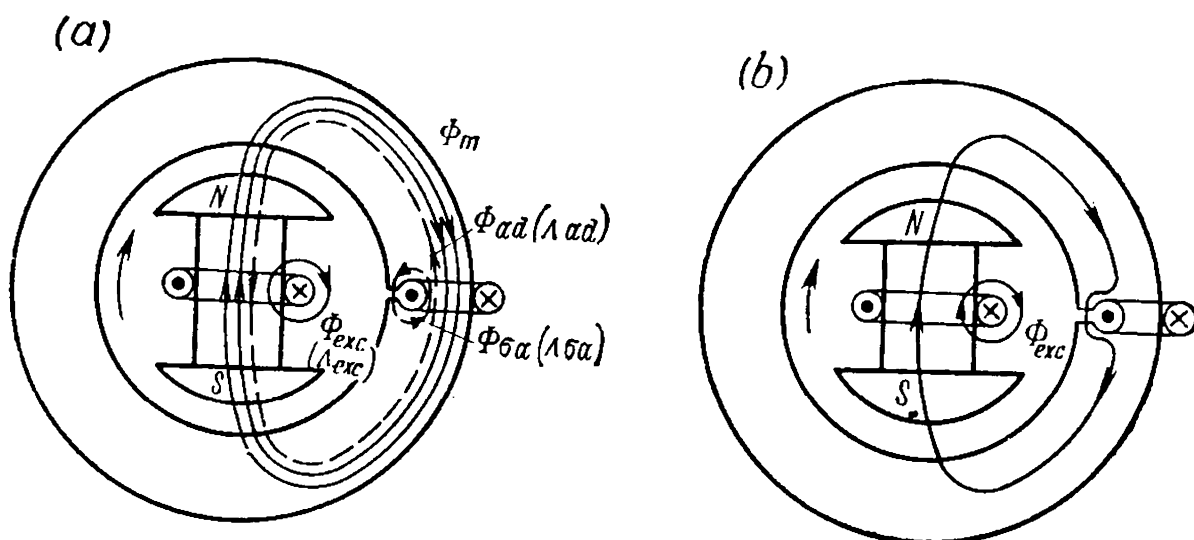


Fig. 9-10. Magnetic field of a synchronous generator in steady-state short-circuit conditions

the stator winding leakage flux $\Phi_{\sigma a}$ which together equal the flux Φ_m , but are opposite in direction.

Consequently, $\dot{E}_m - j\dot{I}_d x_{ad} - j\dot{I}_d x_{\sigma a} = 0$.

In other words, the e.m.f. E_m is equal to the sum of the voltage drops in the direct-axis inductive reactance x_{ad} of the armature reaction and in the leakage inductive reactance $x_{\sigma a}$, i.e.,

$$\dot{E}_m = j\dot{I}_d x_{ad} + j\dot{I}_d x_{\sigma a} = j\dot{I}_d (x_{ad} + x_{\sigma a}) = j\dot{I}_d x_d \quad (9-3)$$

where x_d is the direct-axis synchronous inductive reactance. Relation (9-3) corresponds to the diagram in Fig. 9-7b and to expression (9-2) obtained from it.

According to Fig. 9-10a, the armature-reaction flux Φ_{ad} , which the permeance Λ_{ad} corresponds to, and the stator leakage flux $\Phi_{\sigma a}$ with the permeance $\Lambda_{\sigma a}$ exist as if they pass separately through parallel paths, and, consequently, the permeance Λ_d for the entire flux produced by the stator current will be equal to the sum of the permeances of the component fluxes, i.e.,

$$\Lambda_d = \Lambda_{ad} + \Lambda_{\sigma a}$$

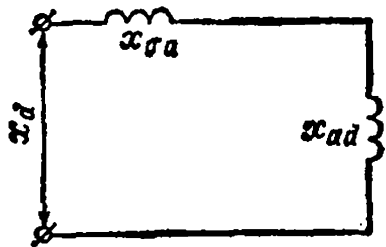
The same relation exists between the inductive reactances, which are proportional to the permeances of the corresponding fluxes:

$$x_d = x_{ad} + x_{\sigma a}$$

The direct-axis equivalent circuit of a synchronous machine corresponding to this equation for steady-state balanced conditions is presented in Fig. 9-11.

Finally, Fig. 9-10b shows the resultant fluxes for a steady-state short circuit.

To establish the concept of synchronous inductive reactance, let us consider the following experiment. A non-excited rotor of a synchronous machine is made to rotate at a synchronous speed. If we apply to the stator winding a three-phase balanced voltage of rated frequency and positive-phase sequence, through the winding will flow a current I which produces magnetic fields closing round the circuits of permeances Λ_{ad} and $\Lambda_{\sigma a}$ (Fig. 9-12), if the pole axis coincides with the axis of the armature-reaction field. These magnetic fields will induce in the stator winding the e.m.f.s $-jI x_{ad}$ and $-jI x_{\sigma a}$ balancing the applied voltage, and therefore



$$\dot{U} - j\dot{I} x_{ad} - j\dot{I} x_{\sigma a} = 0$$

Fig. 9-11. Direct-axis equivalent circuit of a synchronous machine for steady-state balanced conditions.

i.e., the applied voltage \dot{U} is equal to the sum of the voltage drops in the armature-reaction inductive reactance $j\dot{I} x_{ad}$ and the

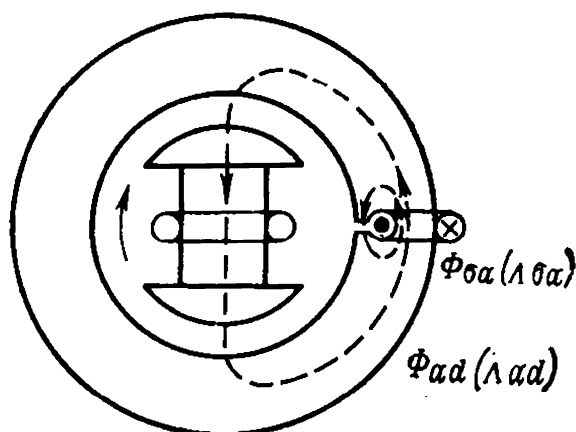


Fig. 9-12. Magnetic field of a synchronous generator for experimental determination of direct-axis synchronous reactance

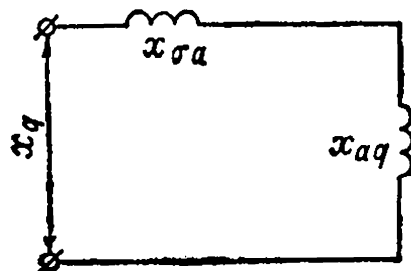


Fig. 9-13. Quadrature-axis equivalent circuit of a synchronous machine for balanced steady-state condition

leakage reactance $j\dot{I}x_{\sigma a}$. Therefore

$$\dot{U} = j\dot{I}(x_{ad} + x_{\sigma a}) = j\dot{I}x_d$$

i.e.,

$$\dot{I} = \frac{\dot{U}}{jx_d} = \frac{\dot{E}_m}{jx_d}$$

Hence, when connected to a circuit with a voltage \dot{U} , the stator winding will have a current equal to the steady-state short-circuit current at an excitation corresponding to the no-load e.m.f. $\dot{E}_m = \dot{U}$.

If in the experiment considered above the pole axis is perpendicular to the armature-reaction field axis, the machine will be, with respect to the applied voltage, a quadrature-axis synchronous inductive reactance $x_{aq} + x_{\sigma a} = x_q$. This reactance is represented, similar to the direct-axis synchronous inductive reactance, by the equivalent circuit shown in Fig. 9-13.

Thus, we can make the following definition: the synchronous inductive reactance is the reactance offered by a synchronous machine to a balanced three-phase voltage of rated frequency applied to its stator winding when the rotor is unexcited and rotates at synchronous speed; if the axis of the resultant armature-reaction field coincides with the pole axis, it will be the direct-axis synchronous inductive reactance, and if the axis of the resultant armature-reaction field is perpendicular to the pole axis, it will be the quadrature-axis synchronous inductive reactance.

The leakage reactance $x_{\sigma a}$ is relatively small and the synchronous inductive reactances depend mainly on the permeances met by the armature-reaction flux along the corresponding axes.

In salient-pole machines the reluctance of the direct-axis armature-reaction magnetizing force is less than that of the quadrature-axis

armature-reaction magnetizing force and, therefore, we have $x_{ad} > x_{aq}$ and, consequently, $x_d > x_q$.

In non-salient-pole machines, from theoretical and experimental data, the reluctance does not practically depend on the position of the armature-reaction magnetizing force axis relative to the main field of the poles, and, therefore, $x_{ad} = x_{aq}$ and $x_d = x_q$.

9-7. Determination of Voltage Rise and Drop by Means of Voltage Diagrams

When solving practical problems, it is frequently necessary to pre-determine the relative change in voltage for a drop in load from the rated value to zero, i.e., for a transition to no-load conditions with the excitation current and the speed maintained constant:

$$\Delta U = \frac{E_m - U_r}{U_r} \times 100\%$$

Generators are usually intended for operation with an inductive load, therefore a drop in load will result in a voltage rise and Δu will become positive. If the rated conditions were for a capacitive load, a drop in load would cause a drop in voltage and Δu would become negative. In other cases it is necessary to determine the voltage change when a generator operating at no-load and the rated voltage U_r is loaded to the rated values of the current and the power factor $\cos \varphi$ at the rated speed. Here

$$\Delta U = \frac{U - U_r}{U_r} \times 100\%$$

Under an inductive load the voltage across the terminals will fall, and Δu will be negative; under a capacitive load the voltage will rise and Δu will be positive.

The terms "rise" and "drop" of the voltage are thus arbitrary and are true only in the sense they are used in relation to the active and inductive loads of d.c. machines. With a capacitive load the armature-reaction effect causes an increase in the resultant magnetic flux in the machine and leads to a rise in voltage with an increase in load. In synchronous machines in the majority of cases we have to deal with active and inductive loads.

Note that the standards previously limited the voltage drop of generators (35-40%). This is explained by the fact that the automatic voltage regulators of those days were imperfect and the voltage was usually regulated manually. Today this does not present a problem, owing to the use of highly efficient quick-action regulators. Nevertheless, the voltage rise when the load is thrown off should not exceed a certain value in order to avoid damage to the insulation. For this reason the voltage rise is usually limited to 50% at rated speed and

with the exciting current corresponding to the rated values of the voltage, current and power factor.

In practice use is generally made of voltage rise diagrams, while voltage drop diagrams are mainly of theoretical interest.

In conclusion, Table 9-1 presents data on the voltage rise for various types of synchronous machines.

TABLE 9-1

Type of generator	Voltage rise, %		Steady-state short-circuit current-ratio at no-load excitation
	$\cos \varphi = 1$	$\cos \varphi = 0.8$	
Three-phase: high-speed	8-15	18-31	2.0-1.4
low-speed	9-13	18-25	2.5-2.0
turbogenerators	16-25	30-48	1.2-0.7
Single-phase generators, for railway substations	17-20	35-40	1.2-0.8

9-8. Determination of Voltage Change from the E.M.F. Diagram for a Salient-Pole Machine According to Design Data

Voltage Rise. Let us draw (Fig. 9-14*a*) the current vector $OH = I$ and, by laying out the voltage vector at an angle φ to it, and adding to it vectors $I r_a$ and $j I x_{sa}$, we obtain the e.m.f. vector E_δ produced

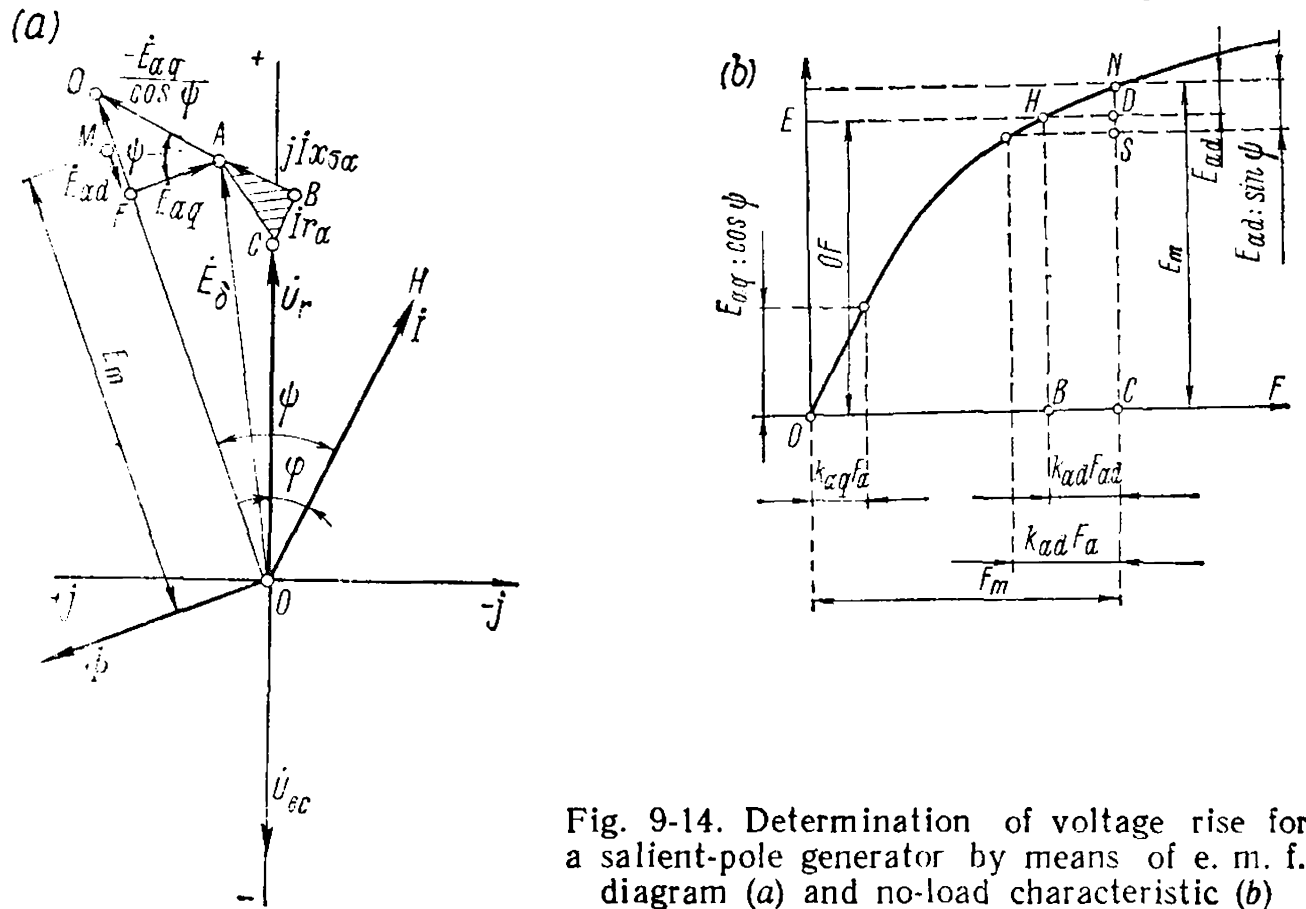


Fig. 9-14. Determination of voltage rise for a salient-pole generator by means of e. m. f. diagram (a) and no-load characteristic (b)

by the resultant flux in the air-gap Φ_δ . Knowing from the data of calculations the value of the armature-reaction magnetizing force

$$F_a = \frac{m}{\pi} \sqrt{2} \frac{\omega k_w}{\rho} I$$

and the quadrature-axis reaction factor k_{aq} , we get

$$\frac{k_{aq} F_{aq}}{\cos \psi} = k_{aq} F_a$$

where $k_{aq} F_{aq}$ is the magnetizing force of the quadrature-axis armature reaction reduced to the excitation winding.

It was shown in Sec. 9-4 that the vector $\frac{I}{I_q} \dot{E}_{aq} = \frac{\dot{E}_{aq}}{\cos \psi} = -j \dot{I} x_{aq}$ is proportional to the quadrature-axis armature-reaction e.m.f. \dot{E}_{aq} and coincides with the direction of this e.m.f., which is perpendicular to the vector of the e.m.f. \dot{E}_m induced by the excitation current.

Since the quadrature-axis reaction flux Φ_{aq} closes in the air-gaps between the poles, it may be assumed that for this flux the magnetic circuit is not saturated, and, therefore, it is possible to determine the value of the e.m.f. $E_{aq} : \cos \psi$ corresponding to the magnetizing force $k_{aq} F_a$ by using the initial straight part of the no-load characteristic (Fig. 9-14b). Let us lay off, next, the value found in Fig. 9-14b as segment $AD = -E_{aq} : \cos \psi$ on the continuation of line BA in Fig. 9-14a and connect point D with the origin of coordinates O . The line OD will be the direction of excitation e.m.f. vector E_m , the angle between the latter and the vector I being angle ψ . The perpendicular AF , dropped from point A to OD , is the quadrature-axis armature-reaction e.m.f. $\overline{FA} = \dot{E}_{aq} = -j \dot{I} x_{aq}$. The direct-axis armature-reaction magnetizing force may be determined from the calculation data, in accordance with the value of angle ψ found above, from the expression

$$k_{ad} F_{ad} = k_{ad} F_a \sin \psi$$

Having determined from the no-load characteristic of Fig. 9-14b the value OB of the excitation magnetizing force corresponding to the value of the voltage \overline{OF} from the diagram in Fig. 9-14a, and by adding to OB the direct-axis armature-reaction magnetizing force reduced to the rotor $k_{ad} F_{ad} = BC$, we find the voltage rise $ND = E_{ad}$ corresponding to this armature reaction, which can be laid off from point F in the diagram of Fig. 9-14a. The total e.m.f. produced by the excitation system at no-load will evidently be equal to

$$E_m = CN$$

The voltage rise is determined from the relation

$$\Delta U = \frac{E_m - U_r}{U_r} \times 100\%$$

Voltage Drop. When determining the approximate voltage drop, we assume that after the bend of the no-load curve the voltage increment is proportional to the excitation magnetizing force increment (Fig. 9-14b). Since the length of leg CD is small compared with that of leg OC , the distance OD (Fig. 9-6) to the end of the vector $E_{ad} : \sin \psi = AD$ is equal to $OC = E_m$ (Fig. 9-6). From the no-load characteristic (Fig. 9-14b) we find the excitation magnetizing force F_m and, subtracting from it the magnetizing force $k_{ad}F_{ad} : \sin \psi = k_{ad}F_a$, we obtain the difference $NS = E_{ad} : \sin \psi$.

After plotting the voltage drop triangle CBA with legs $\overline{CB} = \dot{I}r_a$ and $\overline{BA} = j\dot{I}x_{\sigma a}$ (Fig. 9-15), we draw the straight line PQ giving the direction of the vector \dot{U}_r at an angle φ to CB . We continue the line BA and lay off from point A the section $AR = -E_{ad} : \sin \psi$, and from point R with a radius E_m we intersect the line PQ at point O . Then \overline{OC} gives the required voltage \dot{U} , and the voltage drop is

$$\Delta U = \frac{U - E_m}{E_m} \times 100 = \frac{U - U_r}{U_r} \times 100\%$$

If it is desirable to use the above data to complete the rest of the diagram (Fig. 9-15), this can be done by the method used for determining the voltage rise (Fig. 9-14a), since we now know not only the direction of the voltage vector \dot{U} , but also its value $\dot{U} = \overline{OC}$.

9-9. Determination of Voltage Change by Means of the Potier Diagram

The e.m.f. diagram for a non-salient-pole synchronous machine with an unsaturated magnetic circuit discussed in Sec. 9-2 is based on the separate existence of the magnetic flux Φ_m due to the excitation poles, the armature-reaction flux Φ_a and the leakage flux $\Phi_{\sigma a}$, this making it possible to determine separately and summate geometrically the e.m.f.s E_m , E_a and $E_{\sigma a}$ induced by these fluxes.

When the magnetic circuit of a synchronous machine is saturated, the e.m.f.s E_m and E_a are no longer proportional to the magnetizing forces F_m and F_a , and for this reason their simple vector addition is no longer possible. In this case it is more appropriate to use the Po-

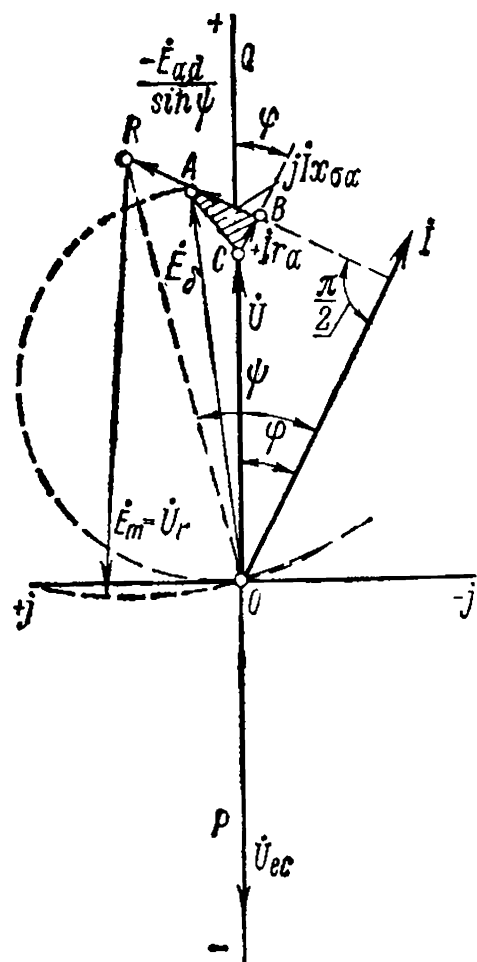


Fig. 9-15. Determination of voltage drop in a salient-pole generator

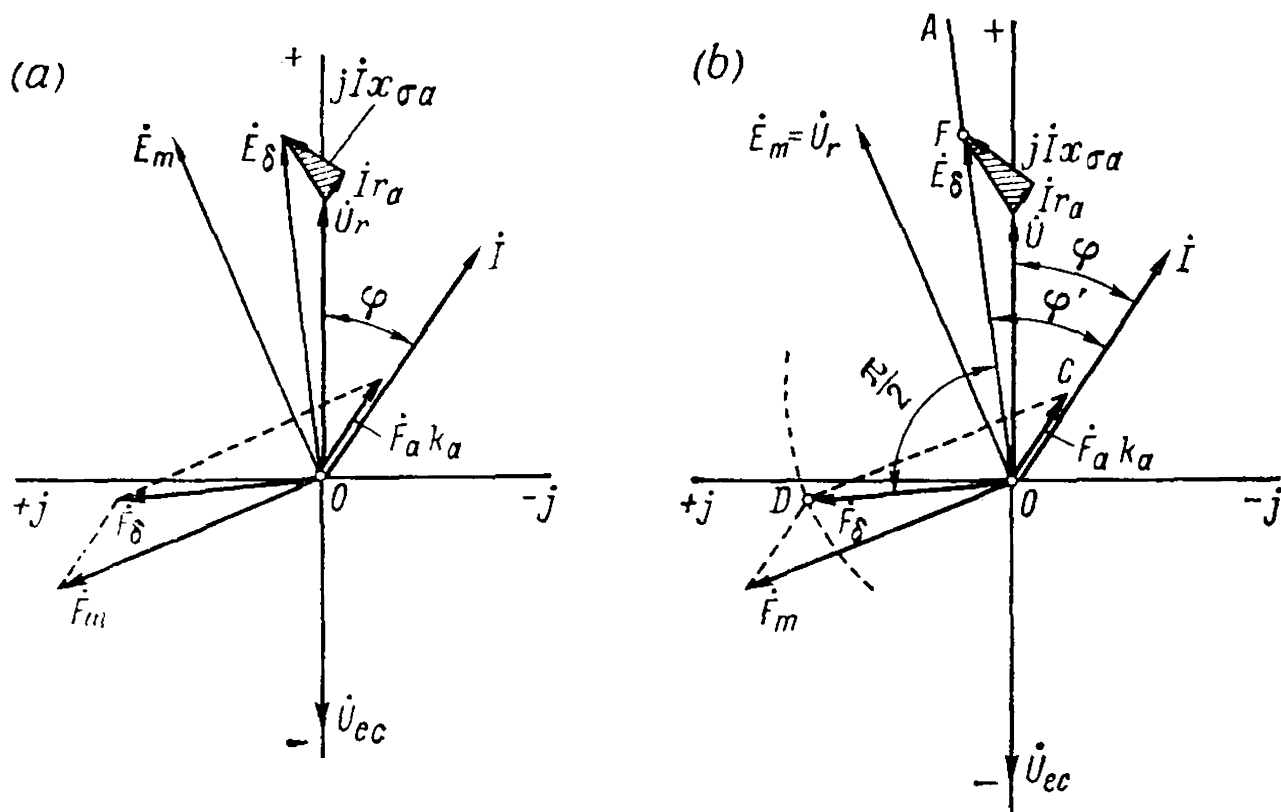


Fig. 9-16. Determination of voltage rise and drop for non-salient-pole generator by means of the Potier diagram

tier diagram method, where not the e.m.f.s but the magnetizing forces of the poles and the armature are geometrically summated and their resultant magnetizing force F_δ is determined, from which, with the aid of the no-load characteristic, the resultant e.m.f. E_δ is found. After this, by vector subtraction of the voltage drops $jI x_{\sigma a}$ and $I r_a$, the voltage across the terminals can be found.

The Potier diagram makes it possible to solve the problem of determining the rise and drop in voltage by means of both design and experimental data.

Voltage Rise. The quantities U , I , $\cos \varphi$, r_a and $x_{\sigma a}$ are known; find E_m and Δu .

We plot the voltage vector U_r at an angle φ to the current vector I (Fig. 9-16a) and, by vector addition of the voltage drops $jI x_{\sigma a}$ and $I r_a$, obtain the e.m.f. vector E_δ due to the resultant flux in the air-gap Φ_δ . From the no-load characteristic we find the magnetizing force F_δ and, by geometrically subtracting from it the armature-reaction magnetizing force $F_a k_a$, reduced to the field winding, we obtain the excitation magnetizing force F_m . From the no-load characteristic we find the e.m.f. E_m corresponding to the magnetizing force F_m , and then the voltage rise

$$\Delta U = \frac{E_m - U_r}{U_r} \times 100\%$$

Voltage Drop. The quantities $E_m = U_r$, I , $\cos \varphi$, r_a , $x_{\sigma a}$ and F_a are known; find U and ΔU .

When determining the voltage drop we assume an approximate angle ratio $\frac{\varphi'}{\varphi} = 1.05$ (Fig. 9-16b).

First we draw line OA at an angle $\varphi' = 1.05 \varphi$ to the current vector I . The direction of the magnetizing force vector \dot{F}_δ leads vector \dot{E}_δ by the angle $\frac{\pi}{2}$. After laying off the armature-reaction magnetizing force vector $\dot{F}_a k_a$ in the direction of vector I , we draw an arc from point C with a radius equal to the excitation magnetizing force \dot{F}_m , determined from the no-load characteristic for the value of the no-load voltage E_m . The point of intersection D of the arc with line OD determines both the value and direction of the vector of the resultant magnetizing force \dot{F}_δ ; this allows the vector $\dot{E}_\delta = \overline{OF}$ to be determined from the no-load characteristic. By subtracting geometrically the voltage drops $jI x_{\sigma a}$ and $I r_a$ from \dot{E}_δ , we find the voltage vector U , after which the voltage drop is found as

$$\Delta U = \frac{U - E_m}{E_m} \times 100 = \frac{U - U_r}{U_r} \times 100\%$$

If, as the result of the first construction, the ratio $\frac{\varphi'}{\varphi}$ will differ from 1.05, the procedure may be repeated, using the value of the ratio obtained as the first approximation.

Practical Construction of the Potier Diagram [81]. When plotting the Potier diagram, the quantities $x_{\sigma a}$ and $F_a k_a$ should be known. With known machine data, for instance, when designing a machine, these values are determined by calculation, but, when testing a finished machine, they are obtained experimentally from the no-load and load characteristics with $I = \text{const}$ and $\cos \varphi \cong 0$ (i.e., a purely inductive load), as follows.

Since when $\cos \varphi = 0$ ($\varphi > 0$) the entire armature reaction causes demagnetization of the excitation system, with $I = \text{const}$ the same value of the demagnetizing magnetizing force is obtained for all voltages beginning with $U = 0$, i.e., from the point corresponding to the excitation winding magnetizing force under a short circuit having the same current value (Fig. 9-17, point A). If the excitation is changed when determining the load characteristic for $\cos \varphi \cong 0$, apex B of the reactive triangle BAC in Fig. 9-17 slides along the no-load characteristic, while apex A draws the load curve. If for the rated voltage $U_r = KD$ we lay off from point D the length $DH = OA = F_{sh}$ determined from the short-circuit characteristic for the given value of the current I , and draw the line HQ parallel to the straight initial part of the no-load characteristic, it will be seen from the construction that $QF =$

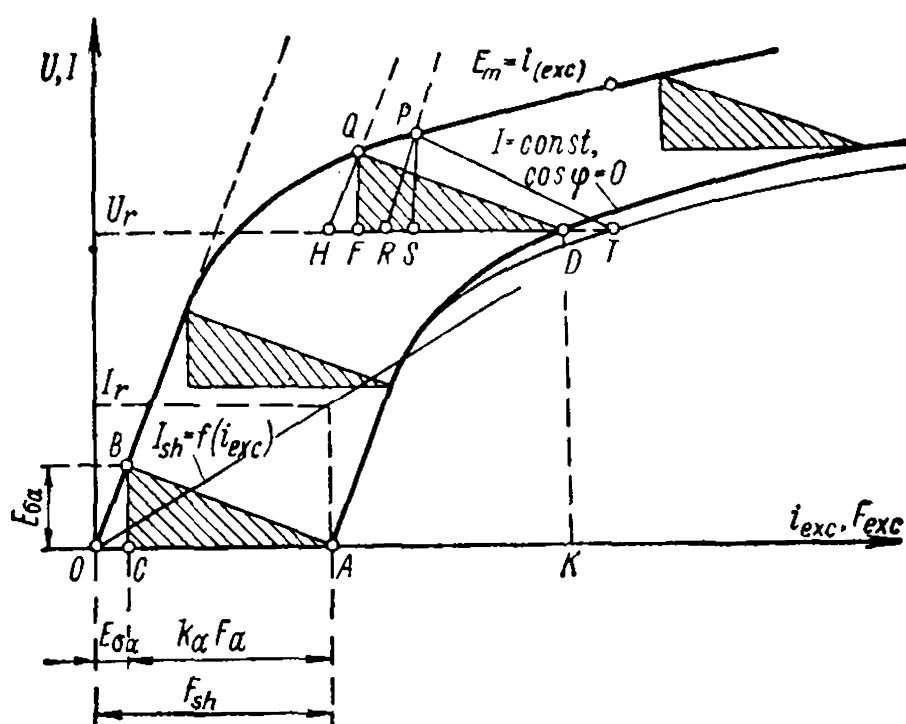


Fig. 9-17. Inductive load characteristic of a synchronous generator

$= BC = E_{\sigma a} = Ix_{\sigma a}$, whence

$$x_{\sigma a} = \frac{QF}{I}$$

and

$$FD = CA = k_a F_a$$

where k_a is the factor for reduction of the reaction magnetizing force of a non-salient-pole machine to the field winding (see Sec. 8-2).

The practical construction of a Potier diagram for determination of the voltage rise is performed in combination with the no-load characteristic, as follows (Fig. 9-18). After laying off on the axis of ordinates the value of the rated voltage U_r , we draw the current vector I at the angle φ to it. By geometrically adding to vector \dot{U}_r the voltage-drop vectors $I r_a$ and $j I x_{\sigma a}$, we obtain the e.m.f. E_δ due to the resultant flux Φ_δ .

By projecting the value $E_\delta = AB$ onto the axis of ordinates, we find from the no-load characteristic the resultant magnetizing force $F_\delta = OA$. Drawing the line $AC = k_a F_a$ at an angle $\varphi + \gamma = \varphi'$ to line AB , we find the resultant magnetizing force $F_{exc} = OC$. By turning OC onto the axis of abscissas into position OD , we find from the no-load characteristic corresponding to point D the e.m.f. E_m obtained when the load is thrown off. The difference $HG = HD - GD = E_m - U_r = \Delta u$ gives the voltage increment with the load thrown off, and the relative voltage

$$\Delta u = \frac{E_m - U_r}{U_r} \times 100 = \frac{GH}{DH} \times 100\%$$

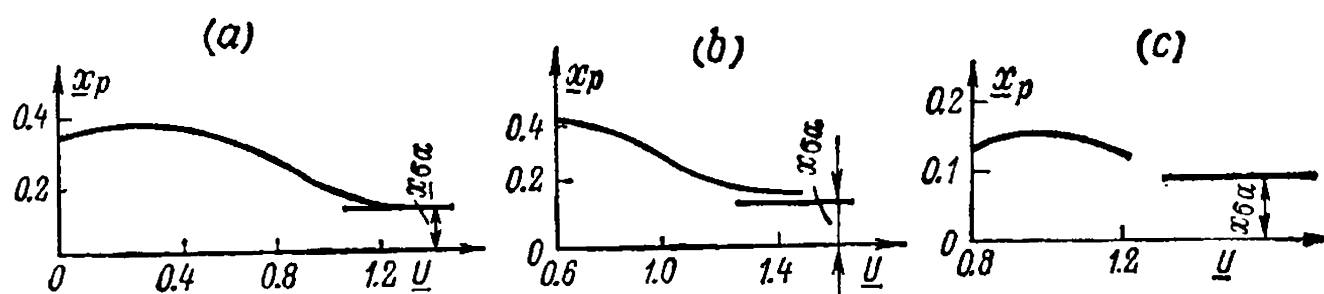


Fig. 9-20. The Potier inductive reactance versus saturation

$E_{\sigma a}$ and F_a determined from the no-load and the load characteristics with $\varphi \cong 0$ (Fig. 9-17), it must not be forgotten that the load characteristic of a salient-pole machine plotted from test data gives, with the given voltages, somewhat greater values of the excitation magnetizing force than those obtained when moving the reactive triangle apexes along the no-load characteristic. This deviation is explained by the increase in the reluctance of the poles resulting from the growth in the field winding leakage flux when the excitation current increases. The leakage e.m.f. $E_{\sigma a} = PS$ (Fig. 9-17), determined by the above method from the no-load and short-circuit characteristics and from the load characteristic for $\varphi = 0$, obtained experimentally and shown in Fig. 9-17 by a thin line, is greater than its actual value $BC = E_{\sigma a} = jI x_{\sigma a}$. Accordingly, the inductive reactance for plotting the Potier diagram will be

$$x_p = \frac{PS}{I} > \frac{BC}{I} = x_{\sigma a}$$

In machines with a relatively high saturation of the poles and a small excitation current, the inductive reactance x_p with an increase in i_{exc} will first grow and then drop (Fig. 9-20a). In the figure not the currents i_{exc} are laid off along the axis of abscissas, but the voltage values corresponding to them in relative units. In machines with a low saturation of the poles, the reactance x_p with an increase in i_{exc} immediately drops (Fig. 9-20b). In turbogenerators x_p may practically be assumed constant (Fig. 9-20c), which is explained by the small field winding leakage. With a view to the above, $x_{\sigma a}$ for a salient-pole machine should be determined for values of i_{exc} corresponding to (1.2 to 1.3) U_r from the load characteristic for $I = I_r$ and $\cos \varphi \cong 0$ (i.e., a purely inductive load), and for turbogenerators for the point $U = U_r$ from the same load characteristic.

9-10. Simplified Practical Diagram (Swedish Diagram)

The method of constructing a simplified diagram follows from the method of practical construction of the Potier diagram (Fig. 9-18). From the construction of the latter for different values of $\cos \varphi$ (Fig. 9-19), it can be seen that the end of the

armature-reaction magnetizing force vector $\vec{F}_a k_a$ follows curve MCN close to a circular one. The centre of this circle can be found by means of the following construction. From the no-load characteristic we find the excitation current $i_{exc0} = OA$ corresponding to the voltage U_r , and from the short-circuit characteristic we find the excitation current $i_{exc.sh} = OH$ corresponding to the current I_r (Fig. 9-21). We find further the excitation current $i_{exc} = OB$ from the load characteristic with $\cos \varphi \cong 0$ for the voltage U_r .

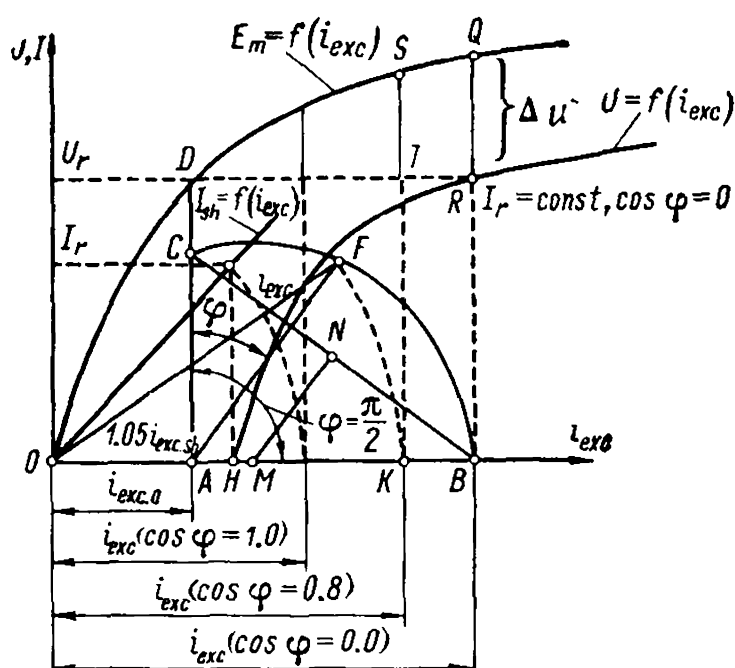


Fig. 9-21. The Potier simplified practical diagram

Having laid off $AC = 1.05 i_{exc.sh} = 1.05 OH$ on line AD , we connect points C and B with a straight line, and from the middle N of CB we draw a perpendicular to intersection with the axis of abscissas at point M . We now draw from centre M with the radius MB an arc CFB which is the locus of the excitation current of the poles for different values of $\cos \varphi$. By drawing a line from A at an angle φ to line AD , we obtain the point of intersection F with arc CFB ; the line OF then gives the value of the excitation current for a machine on load carrying a current I_r with the given power factor $\cos \varphi$. By turning radius OF to intersect the axis of abscissas, we find the excitation current $i_{exc} = OK$, and then from the no-load characteristic determine the e.m.f. $E_m = KS$.

The voltage rise is

$$\Delta u = \frac{KS - BR}{BR} \times 100 = \frac{E_m - U_r}{U_r} \times 100\%$$

When constructing the Swedish diagram for non-salient-pole machines of the turbogenerator type, it is recommended to lay off the length $AC = i_{exc.sh}$, since the increase in the excitation current value to $1.05 i_{exc.sh}$ is due to account being taken of the increase of the reluctance in the poles of a salient-pole machine under the influence of their leakage, which in non-salient-pole turbogenerators is very small.

Example 9-1. Plot a Potier diagram for a 71 500-kVA salient-pole hydrogenerator whose data are given in Example 8-1, when operating under the rated load at the rated power factor $\cos \varphi = 0.8$ and the rated output $P_r = 57\,200$ kW.

The diagram is constructed in relative units (the unit of voltage $E_{r.ph} = \frac{13\,800}{\sqrt{3}} = 7980$ V and the unit of current $I_r = 2990$ A).

Cos φ	Data		Experi- mental data
	according to Potier diagram	according to Swedish diagram	
1.0	1.2	1.185	1.195
0.9	1.47	1.465	1.45
0.8	1.58	1.57	1.57
0.7	1.64	1.64	1.67
0.6	1.7	1.69	1.74
0.0	1.83	1.83	1.83

current $I_r = 1.0$ is

$$x_p = E_p = 0.15$$

The given and experimental data have been used to plot the Potier diagram in Fig. 9-22 according to the method described above. The excitation current at the rated load current $I_r = 2990$ A and $\cos \varphi = 0.8$ was obtained equal to $i_{exc. r} = 1.58$ in relative units, or $i_{exc. r} = 1.58 \times 868 = 1370$ A, while with $\cos \varphi = 1.0$ the relative excitation current becomes equal to $i_{exc. r} = 1.2$ or $i_{exc. r} = 1.2 \times 868 = 1040$ A. According to the no-load

characteristic, with $\cos \varphi = 1.0$ the voltage rise is equal to $\Delta u = 10\%$, with $\cos \varphi = 0.8$ we have $\Delta u = 21\%$, and with $\cos \varphi \approx 0$ we have $\Delta u = 26.5\%$.

A simplified Swedish diagram in accordance with Fig. 9-21 has been constructed for the same 71 500-kVA generator in Fig. 9-23 by means of the method described in Sec. 9-10. A comparison of the results of determining the excitation current for various $\cos \varphi$ and the same rated current $I_r = 2990$ A by means of the Potier and Swedish diagrams and of experimental data for the same generator is given in the following table with the excitation current given in relative units.

It is necessary to note the good coincidence of the data obtained from the Potier and Swedish diagrams with experimental data. Since the construction of the Swedish diagram is simpler than that of the Potier diagram, its great practical value should be recognized not only for non-salient-pole, but also for salient-pole machines.

9-11. Determination of Voltage Change by the Simplified E.M.F. Diagram

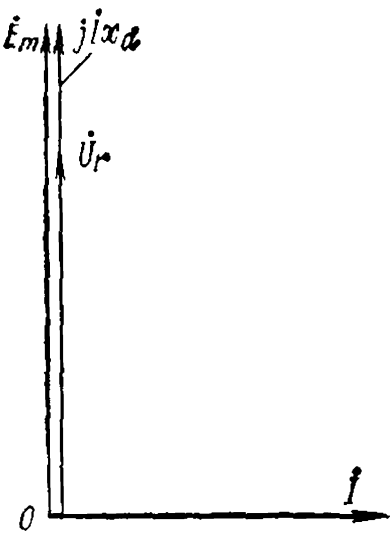
Voltage Rise. The values $U = U_r$, I , $\cos \varphi$ and the synchronous reactance x_{syn} are known. It is necessary to find E_m and Δu .

Lay off (Fig. 9-24) the current vector \vec{I} and draw the vector $\vec{U} = \vec{U}_r$ at an angle $\varphi > 0$ to it. From the end of vector \vec{U} lay off vector $\vec{I}r_a$ coinciding in direction with the current vector, and from the end of vector $\vec{I}r_a$ the vector $j\vec{I}x_{syn}$ leading the current vector \vec{I} by 90° . The closing vector will be the e.m.f. E_m both in value and in phase. The voltage rise is

$$\Delta u = \frac{OC - OA}{OA} \times 100 = \frac{E_m - U_r}{U_r} \times 100\%$$

Voltage Drop. The values $E_m = U_r$, I , $\cos \varphi$, r_a and x_{syn} are known. Find U and Δu .

Lay off the current vector \vec{I} (Fig. 9-24) and at an angle φ to it draw the straight line OK . At the origin of coordinates below the axis of abscissas add the triangle $OA'B'$ with legs $\vec{OB'} = j\vec{I}x_{syn}$ and $\vec{A'B'} = \vec{I}r_a$. From point A' draw an arc with the radius U_r to intersect the line OK at point A . Vector \vec{OA} is the voltage U being sought, and the voltage



portion of the no-load characteristic, but as the voltage difference $QB - BR = QR = Ix_{syn}$ (Fig. 9-21) obtained for the excitation current corresponding to the voltage U_r on the load characteristic with $\cos \varphi = 0$ for the current I_r . The basis for this method is that with $\cos \varphi \cong 0$ the voltage drop due to the effect of the armature reaction and the stator winding leakage is added algebraically to the voltage (Fig. 9-25).

9-12. Experimental Data of E.M.F. Diagram Comparison

Fig. 9-25. Diagram of e. m. f. with inductive load

As an example of comparison of the above voltage diagram with experimental data obtained for salient-pole machines, the results of tests of the main generators of the Volkhov hydroelectric station are given. The tests were carried out under the supervision of Prof. V. Tolvinsky. The main characteristics of the "Elektrosila" Kirov generator are $P_r = 8750$ kVA, $U_r = 11\,000$ V, $I_r = 460$ A, $\cos \varphi = 0.8$, $n = 75$ rpm.

The voltage rises obtained from e.m.f. diagrams and from tests are given in Table 9-2.

From the data of Table 9-2 we can conclude that these diagrams give practically very closely coinciding results well agreeing with experimental data, and they should hence be recognized as practically equivalent.

TABLE 9-2

Operating conditions				Voltage rise %			
Load, kW	Voltage, V	Current, A	cos φ	from diagrams			from tests
				Potier	simplified with correction	simplified Swedish	
7000	11 000	460	0.8	26.7	26.7	27.7	27.7
8750	11 000	460	1.0	13.5	14.1	14.5	14.1
7700	11 000	506	0.8	28.8	28.8	28.9	29.8
9620	11 000	506	1.0	14.42	15.5	16.4	—

Chapter 10

SINGLE-PHASE SYNCHRONOUS GENERATOR

10-1. Armature Reaction of a Single-Phase Generator

A single-phase generator has only one stator winding carrying a single-phase alternating-current, and, therefore, a pulsating armature-reaction magnetizing force wave is induced in it. The wave, in accordance with the general rule (Sec. 4-2), can be resolved into two components of one-half amplitude rotating in opposite directions. The direct rotating e.m.f. wave moves in step with the rotor and interacts with the field winding magnetizing force exactly in the same manner as in a polyphase synchronous generator, while the opposite wave rotates in a direction opposite to that of the rotor with a double-speed relative to it. The rotor windings, with respect to the counter-synchronous magnetizing force are transformer secondaries, therefore, currents of double frequency are produced in them that screen the field which induces these currents.

If the rotor has a full damper winding, i.e., along both the direct and quadrature axes, the counter-synchronous field will be practically suppressed in the same way as the mutual inductance field is damped in a transformer on short circuit. But, if the rotor has no damper winding along the quadrature axis, and has a field winding along the direct axis, and, in addition, a damper winding along the same axis, the flux Φ_{2d} along the direct axis will be damped, and only the quadrature-axis flux Φ_{2q} will remain. If all the windings on the rotor are open, then, also, in a non-salient-pole rotor having a uniform air-gap, the counter-synchronous field will not be completely suppressed and will induce an e.m.f. of fundamental frequency in the stator winding.

With open windings on a non-salient-pole rotor, with different permeances along the direct and quadrature axes proportional to the inductive reactances, the permeance for the counter-synchronous field will change in accordance with the law

$$\Lambda_2 = \frac{1}{2} k (x_d + x_q) - \frac{1}{2} k (x_d - x_q) \cos 2\omega t \quad (10-1)$$

if with $t = 0$ the axis of the single-phase stator winding coincides with the quadrature axis of the machine.

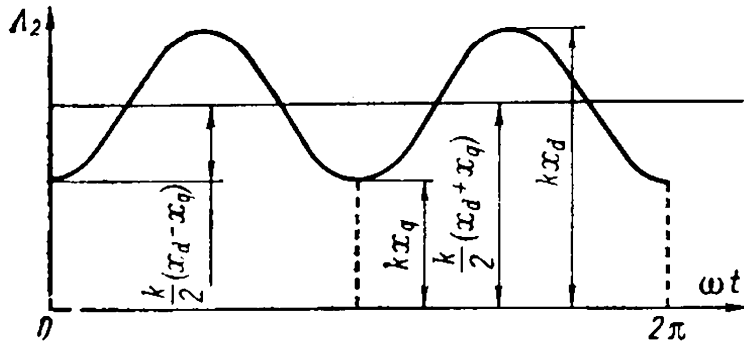


Fig. 10-1. Variation in permeance for the stator flux of single-phase synchronous generator

From equation (10-1) it can be seen that the permeance for a counter-synchronous field consists of two parts, the first of which, $\frac{1}{2}k(x_d + x_q)$, is constant and is the value of the mean permeance, and the second, $-\frac{1}{2}k(x_d - x_q)\cos 2\omega t$, varies according to the double-frequency law and has an amplitude equal to the half-difference of the permeances along the direct and quadrature axes (Fig. 10-1).

The change in the flux induced by the counter-synchronous magnetizing force in the stator winding circuit follows the equation

$$\begin{aligned}
 \Phi_2 &= \frac{1}{2} \Lambda_2 F_a \sin \omega t = \frac{1}{4} F_a k (x_d + x_q) \sin \omega t - \\
 &\quad - \frac{1}{4} F_a k (x_d - x_q) \sin \omega t \cos 2\omega t = \\
 &= \Phi'_{2m} \sin \omega t - \Phi''_{2m} \sin \omega t \cos 2\omega t = \\
 &= \Phi'_{2m} \sin \omega t - \frac{1}{2} \Phi''_{2m} (\sin 3\omega t - \sin \omega t) = \\
 &= \left(\Phi'_{2m} + \frac{1}{2} \Phi''_{2m} \right) \sin \omega t - \frac{1}{2} \Phi''_{2m} \sin 3\omega t = \\
 &= \Phi'_{2m} \sin \omega t - \frac{1}{2} \Phi''_{2m} \sin 3\omega t
 \end{aligned} \tag{10-2}$$

where

$$\Phi'_{2m} = \frac{1}{4} F_a k (x_d + x_q) \tag{10-3}$$

and

$$\Phi''_{2m} = \frac{1}{4} F_a k (x_d - x_q) \tag{10-4}$$

Equation (10-2) shows that in a salient-pole machine the counter-synchronous field induces e.m.f.s of both a fundamental and a triple frequency in the stator winding. In a non-salient-pole machine with open rotor windings $x_d = x_q$ and the flux Φ'_{2m} and, consequently, the third harmonic of the e.m.f. vanish.

With a field winding closed and no damper winding on the rotor

$$\Phi'_{2m} = \frac{1}{4} F_a k (x'_d + x_q) \tag{10-5}$$

$$\Phi'_{2m} = \frac{1}{4} F_a k (x'_d - x_q) \tag{10-6}$$

With a field winding closed and with a damper winding on the rotor

$$\Phi'_{2m} = \frac{1}{4} F_a k (x'_d + x''_q) \quad (10-7)$$

$$\Phi''_{2m} = \frac{1}{4} F_a k (x''_d - x''_q) \quad (10-8)$$

Here x'_d and x''_d are the equivalent direct-axis inductive reactances, and x'_q and x''_q are the quadrature-axis reactances with a view to the transformer coupling of the stator winding with the short-circuited rotor windings relative to the counter-synchronous field. From equation (10-8) it follows that with a complete damper winding on the rotor, when $x''_q \cong x''_d$, the third e.m.f. harmonic disappears, but if there is no quadrature-axis damper winding, then $x_q \neq x'_d$ (no direct-axis damper winding) or $x_q \neq x''_d$ (there is a direct-axis damper winding), and a third e.m.f. harmonic therefore appears.

The flux Φ_{2d} produced by the counter-synchronous magnetizing force may induce in the field winding a very high voltage U_2 of double frequency, which may be detrimental to the insulation of the winding if it is accidentally opened or broken. Adding up with the d.c. excitation current (Fig. 10-2), the double-frequency current i_2 increases the effective value of the resultant current in the field winding to the value

$$i = \sqrt{i_{exc}^2 + I_2^2}$$

where I_2 is the effective value of the alternating current i_2 .

To eliminate the above undesirable phenomena, a damper winding is arranged on the pole shoes in the form of short-circuited low-resistance circuits embracing the poles, designed as shorted copper turns of sufficiently large cross section (Fig. 10-3a) or as copper rods placed in special slots in the pole shoes and connected at the ends by copper strips

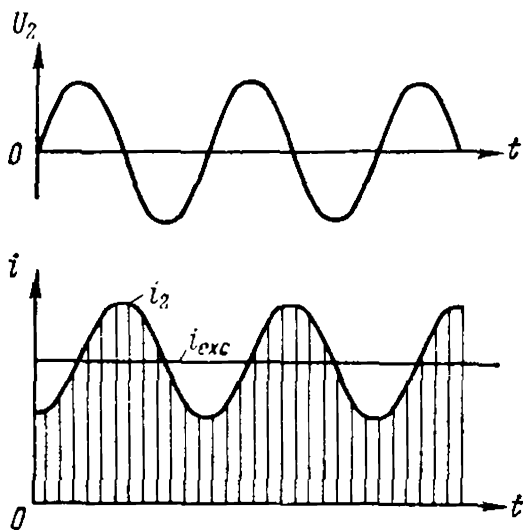


Fig. 10-2. Voltage and current induced in the field winding of a single-phase synchronous generator

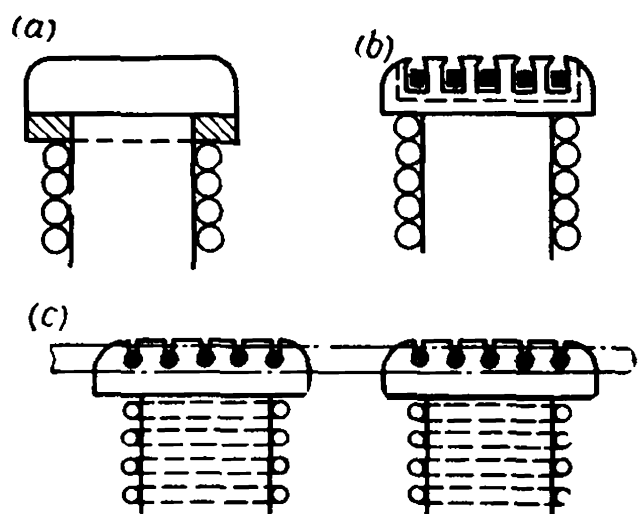


Fig. 10-3. Forms of damper windings of single-phase synchronous generator

of large cross section (Fig. 10-3*b*) in the form of a squirrel cage. The action of these damper windings is so intensive that the field winding is practically relieved of the double-frequency currents, and, in addition, no overvoltages appear when the excitation circuit is broken.

The damper windings shown in Fig. 10-3*a* and *b* do not noticeably influence the quadrature pulsating flux Φ_{2q} and do not eliminate the third e. m. f. harmonic in the stator winding. To eliminate this e.m.f., it is necessary to achieve at least approximate equality of both the direct and quadrature-axis equivalent inductive reactances; for this purpose the squirrel-cage rods placed in the pole shoes must be connected by common short-circuiting rings (Fig. 10-3*c*) to form together with the rods a complete squirrel cage. The direct-axis pulsating field Φ_{2d} is damped by the flux formed by the circuits on the surface of the pole shoe, while the quadrature-axis pulsating field Φ_{2q} is damped by the flux formed by the circuits between the adjacent poles.

In non-salient-pole machines of the turbogenerator type the rotor is usually a solid body, and the eddy currents produced in it have a damping action both on the direct- and the quadrature-axis pulsating field.

10-2. Voltage Diagram of a Single-Phase Generator

The voltage diagram for a single-phase generator is constructed similar to that for a three-phase generator, the value of the armature-reaction magnetizing force, namely its synchronously rotating component due to the single-phase winding on the stator, is small compared with the value for a three-phase generator. This value per pole is equal to

$$F_a = \frac{\sqrt{2}}{\pi} \frac{\omega k_w}{p} I = 0.45 \frac{\omega k_w}{p} I$$

The inductive voltage drop in the stator winding of a single-phase generator corresponding to the voltage drop in the leakage reactance of a three-phase generator is considerably higher, since, in addition to the inductive drop $Ix_{\sigma a}$ in the leakage reactance, it is necessary to include the e.m.f. due to the counter-synchronous field. When a complete squirrel cage is used, the counter-synchronous field will be practically damped, and the inductive voltage drop will therefore be smaller.

10-3. Comparison of Output of Single-Phase and Three-Phase Synchronous Generators of the Same Size

If in a three-phase generator with star-connected windings one phase is disconnected and the generator is fed through the remaining two phases, a single-phase synchronous generator is obtained, whose working winding will occupy only two-thirds of the slots.

The total output of a three-phase machine is

$$P_3 = 3U_{ph}I = \sqrt{3}U_l I$$

When operating with two phases in single-phase connection

$$P_1 = \sqrt{3}U_{ph}I = U_l I$$

The output ratio is

$$\frac{P_1}{P_3} = \frac{1}{\sqrt{3}} = 0.578$$

The electrical losses in the stator windings, with $I_1 = I_3 = I$, will be in the proportion

$$\frac{2I^2 r_a}{3I^2 r_a} = \frac{2}{3} = 0.667$$

If we suppose that the given dimensions allow equal losses in the stator windings in both cases, the following current ratio is permissible

$$\frac{I_1}{I_3} = \sqrt{\frac{3}{2}} = 1.225$$

and, therefore, the power ratio will be

$$\frac{P_1}{P_3} = \frac{U_l I_1}{\sqrt{3}U_l I_3} = \frac{1}{\sqrt{3}} \sqrt{\frac{3}{2}} = \frac{1}{\sqrt{2}} = 0.707$$

It must also be taken into account that in a single-phase machine the stator winding has relatively short end connections, which reduces the value of the stator winding resistance and cuts somewhat the losses in the winding. Since in the heating of a machine the main contribution is due to the losses in the slot part of the winding, the reduction in the length of the end connections will have no practical influence on the admissible power rating of a single-phase machine.

The value of the excitation current under load at a phase angle $\varphi \neq 0$ will, in a single-phase machine, be somewhat smaller owing to the reduction in the magnitude of the armature reaction, but the inductive voltage drop will be somewhat greater.

Chapter II

CHARACTERISTICS OF A SYNCHRONOUS GENERATOR

11-1. System of Relative Units (per Unit Values)

Synchronous machines of various design, voltage and output are best compared by expressing their basic quantities and parameters not in physical units, but in relative units, which can be calculated as a percentage or fraction of the quantities taken as the unit. The following quantities serve as units in this system:

1. The full power rating of a machine $P_r = mU_r I_r$.
2. The rated phase voltage at no-load $U_r = E_m$.
3. The rated phase current I_r .
4. The rated impedance

$$z_r = \frac{U_r}{I_r} = \frac{E_m}{I_r} \quad (11-1)$$

5. The rated angular rotor speed Ω_r , i.e., the angular speed at rated frequency.

6. An angle equal to one radian.

7. The time during which the phase of the current and voltage at rated frequency changes by one radian, or, which is the same, the time during which the rotating field at rated frequency revolves through one radian (electrical).

The above values of voltage, current and impedance are the units for the corresponding stator circuit quantities. For the excitation circuit, the units are defined as follows.

The unit of current in the excitation circuit is assumed to be the excitation current $i_{exc.r}$ which induces in the air-gap a fundamental harmonic of magnetic flux of the same magnitude as that induced by the rated stator current on balanced load when the armature reaction is completely a direct-axis one. According to relation (8-26), the unit of the excitation current is

$$i_{exc.r} = \frac{m \sqrt{2}}{\pi} \frac{w k_w}{p w_{exc}} k_{ad} I_r \quad (11-2)$$

The unit of voltage in the excitation circuit is the voltage $u_{exc.r}$ determined from the full rated output P_r and the unit excitation current

$$u_{exc.r} = \frac{P_r}{i_{exc.r}} = \frac{m U_r I_r}{i_{exc.r}} \quad (11.3)$$

From equations (11-2) and (11-3) we also have

$$u_{exc.r} = \frac{\pi}{\sqrt{2}} \frac{p\omega_{exc}}{\omega k_w k_{ad}} U_r \quad (11-4)$$

The unit of impedance of the excitation circuit is equal to the ratio of the corresponding voltage and current units

$$z_{exc.r} = \frac{u_{exc.r}}{i_{exc.r}} \quad (11-5)$$

or, from equations (11-1), (11-2) and (11-4)

$$z_{exc.r} = \frac{\pi^2}{2m} \frac{p^2 \omega_{exc}^2}{\omega^2 k_w^2 k_{ad}^2} z_r \quad (11-6)$$

From a comparison of equations (8-42) and (11-6) it also follows that

$$z_{exc.r} = \frac{z_r}{k_{exc.s}} \quad (11-7)$$

i.e., the rated or unit values of the stator and rotor circuit impedances are related by the reduction factor for the rotor quantities.

The symbols denoting the various quantities expressed in relative units will be underlined.

The e.m.f., magnetizing force, and other diagrams can also be constructed in relative units. If, for instance, the e.m.f. diagram of a salient-pole generator (Fig. 9-4) is constructed in relative units, then

$$\underline{U}_r = 1; \quad \underline{E} = \frac{E}{U_r}; \quad \underline{E}_\delta = \frac{E_\delta}{U_r}; \quad \underline{E}_{aq} = \frac{E_{aq}}{U_r}; \quad \underline{E}_{ad} = \frac{E_{ad}}{U_r}$$

Similarly

$$\underline{I}_r = 1; \quad \underline{I}_q = \frac{I_q}{I_r}; \quad \underline{I}_d = \frac{I_d}{I_r}$$

For all the inductive reactances

$$\underline{x} = \frac{x I_r}{U_r} = \frac{x}{z_r}$$

For example

$$\underline{x}_d = \frac{x_d}{z_r}; \quad \underline{x}_q = \frac{x_q}{z_r}$$

The corresponding resistance is

$$\underline{r}_a = \frac{r_a I_r}{U_r} = \frac{r_a}{z_r}$$

The inductive reactance x_{ad} of the direct-axis armature reaction in relative units is

$$\underline{x}_{ad} = \frac{x_{ad}}{z_r} = x_{ad} \frac{I_r}{E_m}$$

By substituting for x_{ad} , I_r and E_m their values from expressions (8-28), (8-8) and (2-37), respectively, we get the following expression for the relative inductive reactance of the direct-axis armature reaction

$$\underline{x}_{ad} = \mu_0 \left(\frac{D}{\rho \delta'} \right) \left(\frac{F_{al}}{\Phi_1} \right) k_{fd} \quad (11-8a)$$

Taking into account that the line load per centimetre of armature periphery is

$$A = \frac{2m\omega l}{\pi D}$$

and the magnetic flux of the fundamental harmonic

$$\Phi_1 = B_{\delta 1} \frac{Dl}{\rho}$$

we can obtain the following expression for the relative inductive reactance

$$\underline{x}_{ad} = \mu_0 \left(\frac{D}{\rho \delta'} \right) \left(\frac{A k_{w1}}{\sqrt{2} B_{\delta 1}} \right) k_{fd} \quad (11-8b)$$

Thus, from formulas (11-8a) and (11-8b) it follows that

$$\frac{F_{al}}{\Phi_1} = \frac{A k_{w1}}{\sqrt{2} B_{\delta 1}}$$

Since $\frac{D}{\rho} = \frac{2}{\pi} \tau$ and $\delta' = k_{\delta} \delta$, it is possible to write expression (11-8b) for the relative inductive reactance in another way

$$\underline{x}_{ad} = \frac{\mu_0 \sqrt{2} k_{fd} k_{w1}}{\pi k_{\delta}} \left(\frac{\tau}{\delta} \frac{A}{B_{\delta 1}} \right) \quad (11-8c)$$

or, assuming the average values for $k_{fd} \cong 0.87$, $k_{w1} \cong 0.91$ and $k_{\delta} \cong 1.1$, we obtain the following approximate generalized expression for the relative inductive reactance of the direct-axis armature reaction

$$\underline{x}_{ad} \cong 0.4 \left(\frac{\tau}{\delta} \frac{A}{B_{\delta 1}} \right) \quad (11-8d)$$

Similarly, for the inductive reactance of the quadrature-axis armature reaction we have

$$\underline{x}_{aq} = x_{aq} \frac{I_r}{E_m} = \mu_0 \left(\frac{D'}{\rho \delta'} \right) \left(\frac{F_{al}}{\Phi_1} \right) k_{fq} = \mu_0 \left(\frac{D}{\rho \delta'} \right) \left(\frac{A k_{w1}}{\sqrt{2} B_{\delta 1}} \right) k_{fq} \quad (11-9a)$$

If it is assumed that on an average $\frac{k_{fq}}{k_{fd}} \cong 0.6$, an approximate general expression is obtained for the quadrature-axis armature reaction

$$\underline{x}_{aq} \cong 0.24 \left(\frac{\tau}{\delta} \frac{A}{B_{\delta 1}} \right) \quad (11-9b)$$

For the stator winding the relative inductive reactance is

$$\underline{x}_{\sigma a} = x_{\sigma a} \frac{l_r}{E_m}$$

By substituting for $x_{\sigma a}$ and E_m their values from formulas (5-14) and (2-37), respectively, and since from formula (8-8)

$$l_r = \frac{\pi p}{m \sqrt{2} \omega k_{w1}} F_a$$

we get for the relative inductive reactance

$$\underline{x}_{\sigma a} = \frac{2\pi\mu_0}{k_{w1}^2} \left(\frac{F_a l}{\Phi_1} \right) \frac{\lambda_s}{mq} = \frac{2\pi\mu_0}{k_{w1}} \left(\frac{A}{B_{\delta 1}} \frac{1}{\sqrt{2}} \right) \frac{\lambda_s}{mq} \quad (11-10)$$

where

$$\lambda_s = \lambda_{sl} + q\lambda_{end} \frac{l_{end}}{l} + \lambda_{dif}$$

For the relative inductive reactance of the field winding after reducing it to the stator system, the following expression is obtained in stator relative units

$$\underline{x}_{exc. s} = \left(\frac{4}{\pi} \right)^2 \left(\frac{F_a l}{\Phi_1} \right) k_{ad}^2 2\lambda_{exc. s} + \underline{x}_{dif} \quad (11-11a)$$

or

$$\underline{x}_{exc. s} = \left(\frac{4}{\pi} \right)^2 \left(\frac{Ak_{w1}}{\sqrt{2}B_{\delta 1}} \right) k_{ad}^2 2\lambda_{exc. s} + \underline{x}_{dif} \quad (11-11b)$$

where

$$\underline{x}_{dif} = \left(\frac{4}{\pi} k_{ad} k_{\Phi} - 1 \right) \underline{x}_{ad}$$

The leakage permeance per centimetre of machine length is determined as follows [formula (5-28)]

$$\lambda_{exc. s} = 2 \left(\frac{h_{m1}}{3c_{m1}} + \frac{h_{m2}}{c_{m2}} + \frac{h_p}{c_p} + \frac{(l_p - l) + 0.5h_m + 0.125b_m}{2l_p} \right)$$

For the short-circuited secondary system of the squirrel-cage type on the rotor of a synchronous machine

$$\underline{x}_{ds} = 8\mu_0 \left(\frac{F_a l}{\Phi_1} \right) \frac{\lambda_d}{n_{db}} = 8\mu_0 \left(\frac{Ak_{w1}}{B_{\delta 1} \sqrt{2}} \right) \frac{\lambda_d}{n_{db}} = 4\sqrt{2}\mu_0 \left(\frac{A}{B_{\delta 1}} \right) k_{w1} \frac{\lambda_d}{n_{db}} \quad (11-12)$$

where λ_d is the leakage permeance, which is determined in the same way as for a squirrel-cage induction motor, and n_{db} is the number of damping bars per pole.

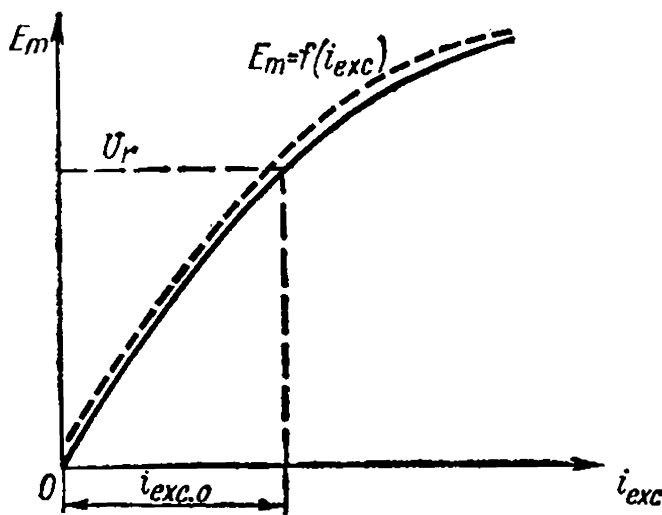


Fig. 11-1. No-load characteristic of a synchronous generator

11-2. No-Load Characteristic

The no-load characteristic, giving the relation $E_m = f(i_{exc})$, is obtained for both the voltage rise and voltage drop branches. The area confined within these curves is determined by the hysteresis of the rotor magnetic circuit. When using the no-load characteristic for the construction of voltage diagrams and other characteristics, the descending branch should be taken with zero placed at the point of intersection

of the curve and the axis of abscissas (Fig. 11-1, solid line).

The no-load characteristic, as well as the other characteristics of a synchronous generator, can be constructed in relative units, which makes it possible to better appraise machine performance.

In constructing the no-load characteristic, however, the unit used is not the excitation current $i_{exc,r}$, as in the previous section, but the excitation current $i_{exc,0}$ corresponding to the rated voltage on the no-load characteristic (Fig. 11-1). The ratio of the excitation current to the current $i_{exc,0}$ will be designated by the underlined symbol $\underline{i}_{exc,0}$

$$\underline{i}_{exc,0} = \frac{i_{exc}}{i_{exc,0}}$$

The advantage of selecting this excitation current unit for the no-load characteristics is that the no-load characteristics of different generators constructed in similar relative units intersect at a common point

$$\underline{E}_m = \frac{E_m}{U_r} = 1; \quad \underline{i}_{exc,0} = 1$$

This makes it possible to easily compare the degree of saturation of individual machines.

When calculating electrical systems incorporating a considerable number of synchronous generators, use is made of a normal no-load characteristic obtained as the average for a great number of tested machines. This normal no-load characteristic is given in the following form

$\underline{i}_{exc,0}$	0.5	1.0	1.5	2.0	2.5	3.0	3.5
$\underline{U} = \underline{E}_m$	0.58	1.0	1.21	1.33	1.40	1.46	1.51

and is depicted in Fig. 11-2 by dotted line 3.

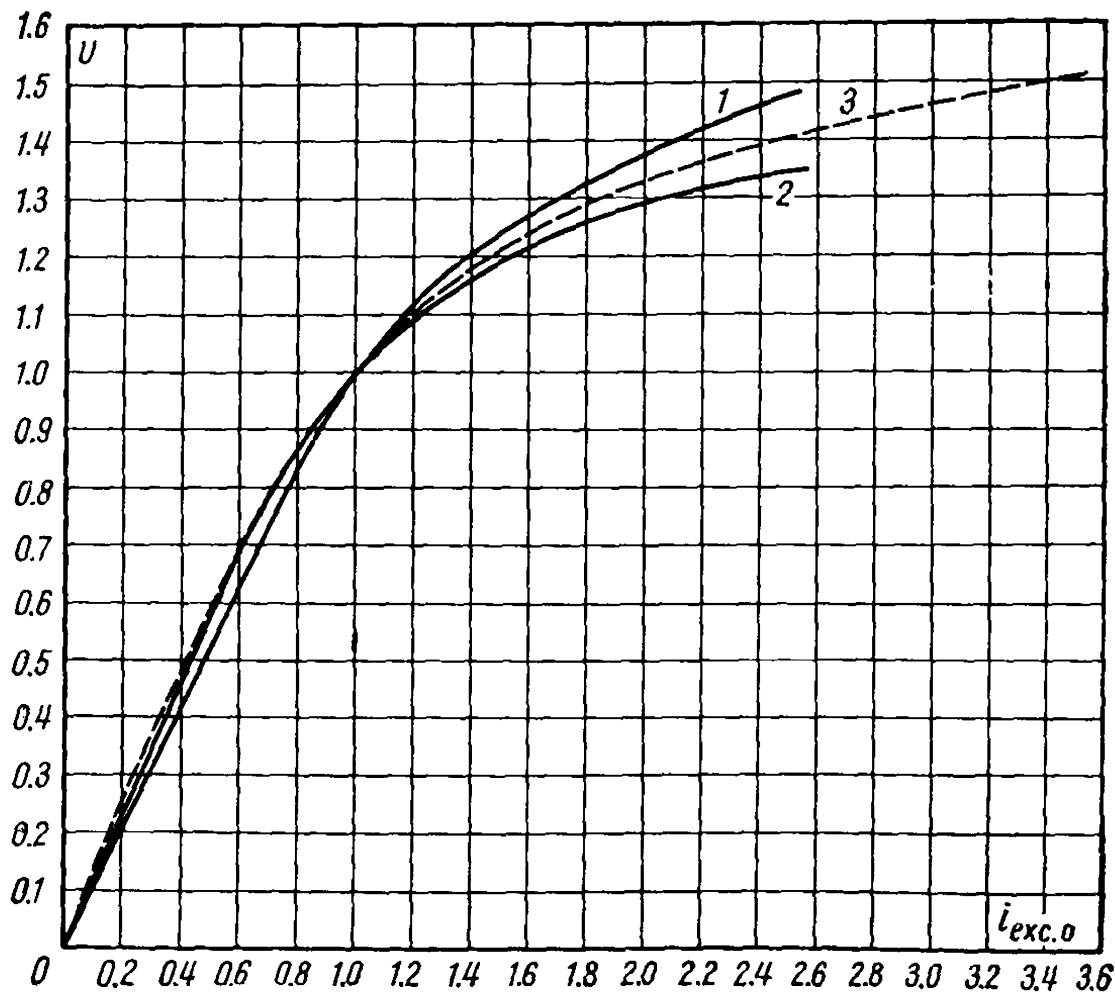


Fig. 11-2. No-load characteristics in relative units:
 1 — 50 000-kW turbogenerator, $2p = 4$; 2 — 57 200-kW hydrogenerator,
 $2p = 96$; 3 — normal characteristic

When finding the no-load characteristic of a definite synchronous machine, it is compared with the normal characteristic. For example, shown in Fig. 11-2 are the no-load characteristics of a 50 000-kW turbogenerator and a 57 200-kW hydrogenerator, compared with the normal characteristic.

A glance at this figure shows that the characteristics of real generators coincide quite closely with the normal characteristic. This is true for the absolute majority of cases.

11-3. Short-Circuit Characteristic

A three-phase short-circuit characteristic (Fig. 11-3) gives the relation

$$I_{sh3} = f(i_{exc}) \text{ with } f = \text{const and } U = 0$$

The short-circuit characteristic, together with the no-load characteristic, makes it possible to determine the reactive triangle (see Fig. 9-17). Since the resultant flux Φ_δ of a machine induces at short

circuit only a small e.m.f. E_δ making up for the voltage drop $r_a \dot{I} + jx_{sa} \dot{I}$ (see Fig. 9-7), the magnetic system of the machine is unsaturated, and therefore the short-circuit characteristic is straight, having a bend only when the currents considerably exceed the rated current I_r .

The relations

$$I_{sh2} = f(i_{exc}); \quad I_{sh1} = f(i_{exc})$$

obtained for two-phase and single-phase short circuits are also linear, but, because of a smaller armature reaction, the characteristic $I_{sh2} = f(i_{exc})$ passes above the characteristic $I_{sh3} = f(i_{exc})$, and the characteristic $I_{sh1} = f(i_{exc})$ is still higher than the characteristic $I_{sh2} = f(i_{exc})$ (Fig. 11-3).

If we find the short-circuit characteristic at a varying speed, the short-circuit current will be practically independent of the speed, because the inductive reactances and the e.m.f. induced by the field winding vary with the frequency and, consequently, are proportional to the speed; therefore

$$I_{sh} = \frac{E_m}{\sqrt{r_a^2 + x_d^2}} \cong \frac{E_m}{x_d} = \text{const}$$

Only at very low frequencies, when the influence of the resistance r_a on the value of z_d becomes appreciable, does the characteristic $I_{sh} = f(n)$ have a bend when $i_{exc} = \text{const}$ and drop to a value of $I_{sh} = 0$ at $n = 0$ (Fig. 11-4).

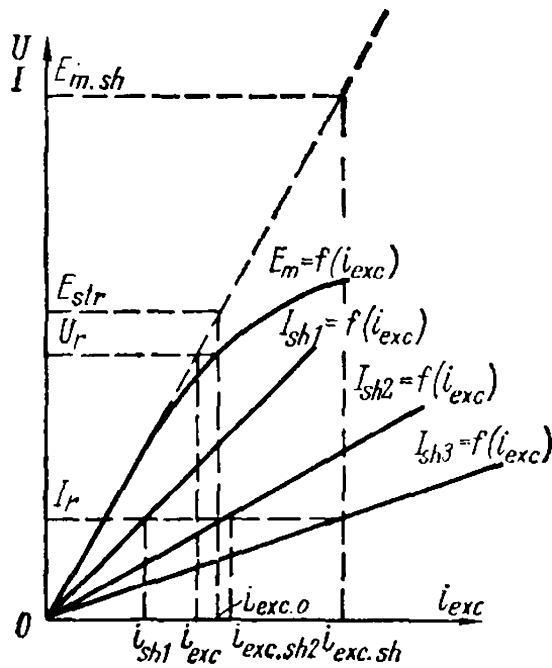


Fig. 11-3. Short-circuit characteristic of a synchronous generator

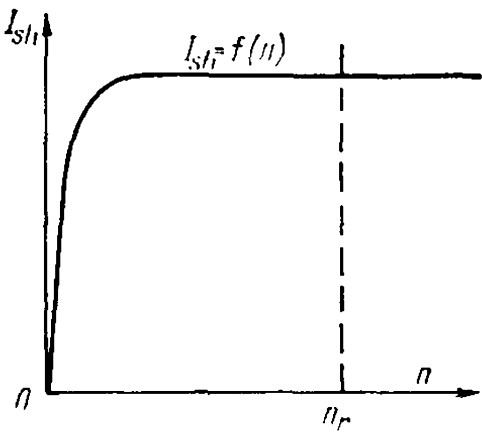


Fig. 11-4. Short-circuit current of a synchronous generator versus speed

11-4. Short-Circuit Ratio

Of great importance for appraising the properties of a synchronous machine is the ratio of the excitation current $i_{exc} = i_{exc.0}$, corresponding to the rated voltage $E_m = U_r$ on the no-load characteristic, to the excitation current $i_{exc.sh}$, corresponding to the rated current $I_{sh3} = I_r$ on the three-phase short-circuit characteristic (Fig. 11-3). This ratio $\frac{i_{exc.0}}{i_{exc.sh}}$ is called the *short-circuit ratio* (SCR) and mainly characterizes the influence of the armature reaction on the field winding of a synchronous machine.

Designate the e.m.f. obtained with an excitation current $i_{exc} = i_{exc.0}$ on the extension of the straight part of the no-load characteristic as E_{str} . Then (Fig. 11-3)

$$\text{SCR} = \frac{i_{exc.0}}{i_{exc.sh}} = \frac{E_{str}}{E_{m.sh}}$$

But $E_{m.sh} = I_r x_d = I_r (x_{\sigma a} + x_{ad})$, therefore

$$\frac{E_{m.sh}}{U_r} = \frac{x_d I_r}{U_r} = \frac{x_d}{z_r} = \underline{x_d}$$

Hence,

$$\text{SCR} = \frac{i_{exc.0}}{i_{exc.sh}} = \frac{E_{str}}{E_{m.sh}} \frac{U_r}{U_r} = \frac{E_{str}}{U_r} \frac{1}{\underline{x_d}} = \frac{i_{exc.0}}{i_{exc.r}} \frac{1}{\underline{x_d}} \quad (11-13)$$

With an unsaturated magnetic system in a synchronous machine

$$\frac{i_{exc.r}}{i_{exc.0}} = 1$$

and

$$\text{SCR} = \frac{1}{\underline{x_d}}$$

Thus, in an unsaturated machine the SCR is equal to the reciprocal of the relative value of the direct-axis synchronous reactance x_d . With a saturated magnetic circuit, when determining the SCR this value should be multiplied by the ratio $i_{exc.0} : i_{exc.r}$ of the values of the magnetizing current obtained from the no-load characteristic for the rated voltage on the saturated and straight parts.

For synchronous non-salient-pole turbogenerator-type machines, the SCR ranges from 0.4 to 0.7. For synchronous salient-pole hydrogenerators the SCR varies from 1.0 to 1.4.

Synchronous machines with a low SCR have greater changes in voltage with fluctuations in load, are less stable when operated in parallel, and have a lower value of the charging current when the ge-

erator works into the capacitance of a disconnected transmission line. Such a generator, however, is relatively cheaper.

The utilization of the active materials in a machine with a low SCR is better than in a machine with a high one. An increase in the air-gap results in an increase of the SCR and a reduction of the synchronous reactance. This improves parallel operation of a generator with other stations (especially if a long transmission line is used) and makes generator operation more stable under load fluctuations.

An increase in the air-gap of a generator, however, simultaneously leads to its greater weight and poorer performance. This is explained by the fact that a change in the air-gap alters the reluctance of the machine, which leads to a nearly proportional change in the excitation current. The short-circuit excitation current, however, varies only slightly, since the excitation magnetizing force which overcomes the reluctance of the air-gap is only a relatively small part of the total magnetizing force of the field winding in short-circuit conditions, the most significant part of which compensates the armature-reaction magnetizing force.

Example 11-1. Determine the short-circuit ratio (SCR) for the salient-pole 71 500-kVA hydrogenerator whose data are given in Example 9-1 (page 227). The no-load characteristic $E_m = f(i_{exc})$ and short-circuit characteristic make it possible to find the SCR for the given hydrogenerator according to Sec. 11-4.

By continuing the linear portion of the no-load characteristic (Fig. 11-2) we find the excitation current in relative units $\underline{i}_{exc.0} = 0.83$, corresponding to the rated voltage with an unsaturated machine. From the short-circuit characteristic, in relative units,

$$\underline{i}_{exc.sh} = 0.61$$

Hence

$$SCR = \frac{0.83}{0.61} = 1.36$$

Approximately

$$SCR \cong \frac{1}{\underline{x}_d} = \frac{1}{0.695} = 1.44$$

11-5. Load Characteristics

The load characteristics give the relation:

$$U = f(i_{exc}) \text{ for } I = \text{const}, f = \text{const and } \cos \varphi = \text{const}$$

Of the greatest practical importance is the load characteristic for $\cos \varphi \cong 0$ and $\varphi \cong \frac{\pi}{2} > 0$ (Fig. 11-5), since it allows the inductive reactance x_p to be determined for construction of the Potier diagram.

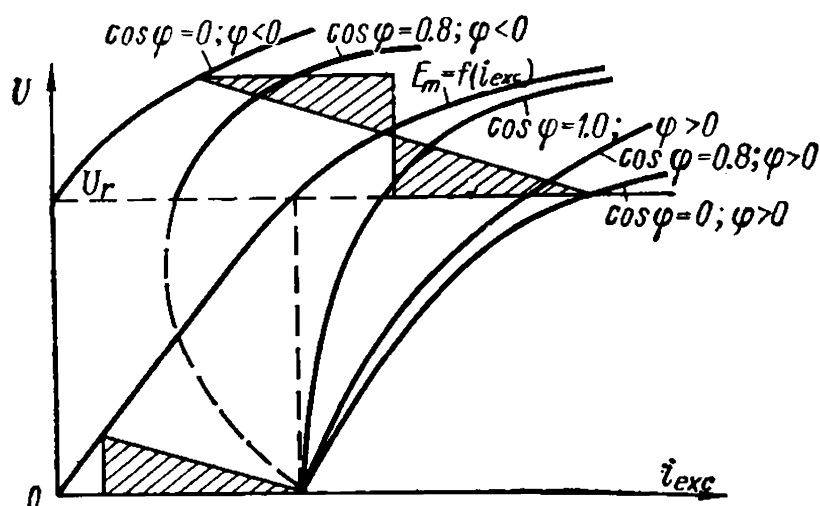


Fig. 11-5. Load characteristics of a synchronous generator

The load characteristics for $\cos \varphi = 0.8$ ($\varphi > 0$) and $\cos \varphi = 1$ lie above the curve for $\cos \varphi = 0$ and are not parallel to the no-load characteristic $E_m = f(i_{exc})$. The curves for $\cos \varphi = 0.8$ and $\cos \varphi = 0$, but with a leading current ($\varphi < 0$), lie above the no-load characteristic. Here the curve for $\cos \varphi = 0$ can also be obtained by moving the reactive triangle along the no-load characteristic, but this is done with the triangle inverted, since in this instance the inductive voltage drop $+jI x_p$ causes an increase in voltage, while the armature reaction produces a magnetizing effect (Fig. 11-5).

11-6. External Characteristics

The external characteristics give the relation

$$U = f(I) \text{ for } i_{exc} = \text{const}, f = \text{const and } \cos \varphi = \text{const}$$

Under inductive load with $0 < \varphi < \frac{\pi}{2}$, the armature reaction and the voltage drop $r_a I + j x_{sa} I$ cause the voltage to fall. This is why the external characteristic has a steeply drooping nature (Fig. 11-6), the voltage drop growing with a reduction in the value of $\cos \varphi$. For a leading $\cos \varphi$, which corresponds to $0 > \varphi > -\frac{\pi}{2}$, these factors act to increase the voltage and, therefore, with a reduction of $\cos \varphi$ the voltage rise increases. With $U = 0$ (short circuit) all the characteristics intersect at one point corresponding to the value of the three-phase short-circuit current.

In non-salient-pole synchronous machines of the turbogenerator type the relative magnitude of the armature reaction is generally

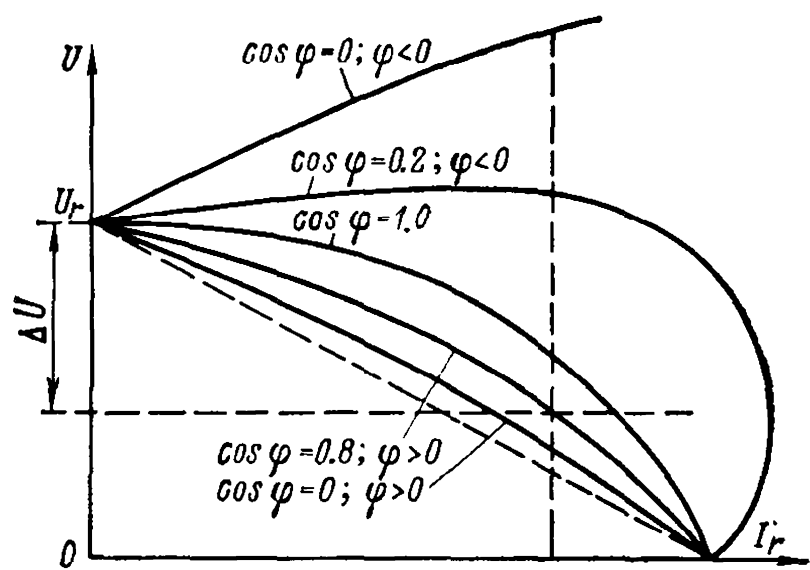


Fig. 11-6. External characteristics of a synchronous generator

greater than in salient-pole machines (for instance, hydrogenerators); for this reason the relative voltage drop under an inductive load and the voltage rise under a capacitive load are greater in the first case.

11-7. Regulation Characteristics

The regulation characteristics give the relation

$$i_{exc} = f(I) \text{ for } U = \text{const}, f = \text{const and } \cos \varphi = \text{const}$$

To maintain the voltage $U=\text{const}$ with an increasing inductive load, it will be necessary to increase the excitation current, while under a capacitive load the excitation must be decreased, as can be seen from the external characteristics. With a reduction of $\cos \varphi$, a

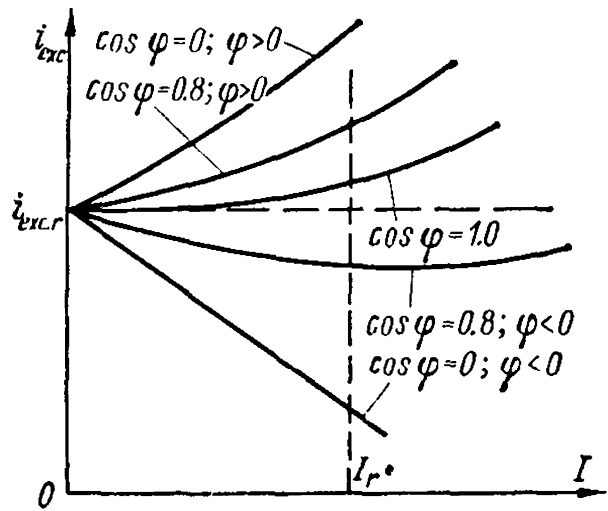


Fig. 11-7. Regulation characteristics of a synchronous generator

corresponding greater change of the excitation current is required, the regulation curves for various values of $\cos \varphi = \text{const}$ are therefore of the nature shown in Fig. 11-7.

11-8. Losses and Efficiency of a Synchronous Generator

All losses occurring in a synchronous machine can be divided into two groups: basic and additional. The basic losses are those which appear as a result of the basic electromagnetic and mechanical pro-

cesses taking place in the machine. They include the main copper losses in the stator and field windings, the losses in the stator active steel, the friction losses in the stator active steel, the friction losses in the bearing and slip-ring brushes, and the windage losses.

The additional losses include those resulting from the secondary processes of an electromagnetic nature. Some of them occur during no-load operation of a machine, others under load. Accordingly we distinguish additional no-load losses and additional short-circuit losses. The causes of the additional losses are the stator leakage fluxes, the higher magnetizing force harmonics of the stator and rotor, and losses due to the toothed nature of the stator and rotor.

The main cause of the additional losses are the stator leakage fluxes. They produce additional losses in the slot and end-connection parts of the stator winding, and in all metal parts where the leakage flux penetrates, i.e., in the shields, clamping end-plates, bandages, etc.

The higher magnetizing force harmonics cause additional losses in the stator and rotor surfaces, moving relative to them at different speeds. Since these losses do not penetrate deeply into the metal parts because of the shielding effect of the eddy currents, they are called surface losses.

The tooth-ripple harmonics of the magnetic field partly cause the surface losses on the stator and rotor surfaces due to quadrature-flux oscillations, and partly the pulsating losses due to the direct-flux oscillations in the teeth. The pulsating losses are usually small in comparison with the surface losses.

The additional losses can be reduced by: (a) dividing the stator winding conductors along the height of the slot into a number of elementary conductors and transposing them in the active and, sometimes, in the end connections of the winding; (b) designing the winding with a corresponding short pitch and with a conical arrangement of the end connections; (c) the use of clamping plates, bandages, etc., of non-magnetic steel; (d) grooving of the rotor in turbogenerators.

The efficiency of a synchronous generator is calculated by the formula

$$\eta = 1 - \frac{\sum p}{P + \sum p}$$

where P is the useful power and $\sum p$ is the sum of all losses.

According to data of the "Elektrosila" Works, the efficiency of air-cooled turbogenerators operating at full load and a power factor $\cos \varphi = 0.8$ ranges from 92 to 95% for 500- to 3000-kW turbogenerators, and from 95 to 98.8% for 3500- to 300 000-kW turbogenerators. With hydrogen cooling, the efficiency of a turbogenerator is increased at full load by about 0.8%. Hydrogenerators have practically the same efficiency as turbogenerators.

Given below are the values of various losses and the efficiencies for a 20-MVA hydrogenerator with $n=187$ rpm and $\cos \varphi=0.8$ (Table 11-1) and a 25-MVA turbogenerator with $n=3000$ rpm (Table 11-2) at rated load.

TABLE 11-1

Kind of losses	Losses, kW
Mechanical losses	125.7
Steel losses (including additional losses)	141.2
Copper losses:	
(a) stator	102
(b) rotor	101
Additional short-circuit losses	58.1
Total losses	528.0
Efficiency (per cent) at full load and $\cos \varphi=0.8$	96.8

TABLE 11-2

Kind of losses	Losses in turbogenerators of old modification, kW	Losses in turbogenerators of new modification, kW
Losses due to rotor air friction	150	102
Windage losses	200	100
Bearing losses	90	70
Steel losses	123	85
Copper losses in stator	47	60
Copper losses in rotor	72	90
Additional short-circuit losses	74	74
Additional no-load losses	36	34
Total losses	792	615
Efficiency (per cent) at full load	96.9	97.6

Chapter

12

PARALLEL OPERATION OF SYNCHRONOUS MACHINES

12-1. General

Modern power stations employ several generators which are operated in parallel. This is due to the fact that the power station load varies considerably both during the day and during the different seasons of the year, hence, one generator having the maximum installed capacity of the station would have to operate for long periods under small load, i.e., at reduced efficiency, both of the generator and of the prime mover. Also, modern power stations have so high an output that it is as yet difficult to build a single generator with such a rating.

To increase the reliability of supply to large industrial centres, the latter are fed from several power plants joined into a common supply mains. This has a number of advantages, viz.: (1) the installed spare capacity for emergency and repair can be reduced; (2) the load can be distributed among the plants more efficiently to make the entire power system more economical; (3) the maximum utilization of water power is achieved when hydroelectric and steam-power stations operate in parallel, etc. Thus, the number of generators operated in parallel is further increased. The reliable parallel operation of generators, however, requires the observance of a number of conditions.

For successful parallel operation of synchronous generators in a common supply mains, all the generators must have exactly the same frequency, i. e., they must all run synchronously. Since the prime movers driving the synchronous generators cannot maintain precisely the same speed of rotation, the synchronous operation of a number of generators would be impossible if they were not maintained in this condition automatically by the so-called *synchronizing torque* appearing during parallel operation. When synchronous generators are operating in parallel they may be subject to oscillations or swinging, depending on the angular displacement of the rotor over a certain part of the pole pitch. An important problem of parallel operation is the connection of a new generator to the buses of a station which generators feeding the system have already been connected to.

12-2. Parallel Connection of Synchronous Generators

When switching in a generator for parallel operation, the same general rules are to be observed as when connecting a new d.c. generator to a system already in operation, i.e., at the moment of connection:

1. *The electromotive force of the generator being connected should be equal to the line voltage, and*

2. *The polarity of the generator being connected should correspond to that of the line.*

Since with an alternating current the polarity changes with the line frequency, the appropriate polarity must be selected at the instant the generator connection is made.

With alternating current there arises a third requirement, viz.:

3. *The frequencies of the systems to be connected should be practically equal.*

To comply with all these requirements, it is necessary to use special synchronizing devices, the simplest of which are phasing lamps. With single-phase generators the lamps can be connected in two ways (Fig. 12-1): for extinction (generator *II*) and for burning (generator *III*). Figure 12-1 shows a moment when the rotors of all three generators are in identical conditions relative to the stator winding, and therefore this moment is appropriate for connecting both generators (*II* and *III*) to the buses of the power system to which unloaded generator *I* is already connected, since the instantaneous polarities of the machines being connected will be the same. For generator *II*, in the circuit consisting of the winding of generator *I*, the phasing lamps and the winding of generator *II*, the voltage of generator *I* and the e.m.f. of generator *II* are in opposition and the voltage across the phasing lamps will be zero, therefore they will go out. For generator *III*, on the contrary, owing to their cross connection, the lamps will be under a voltage which is the sum of the voltage of generator

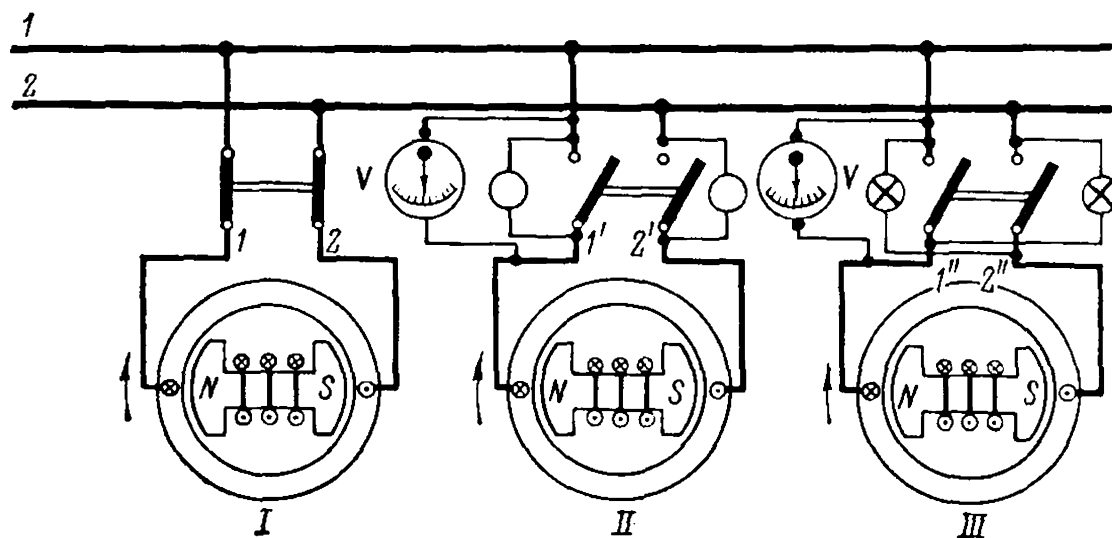


Fig. 12-1. Parallel connection of single-phase synchronous generators

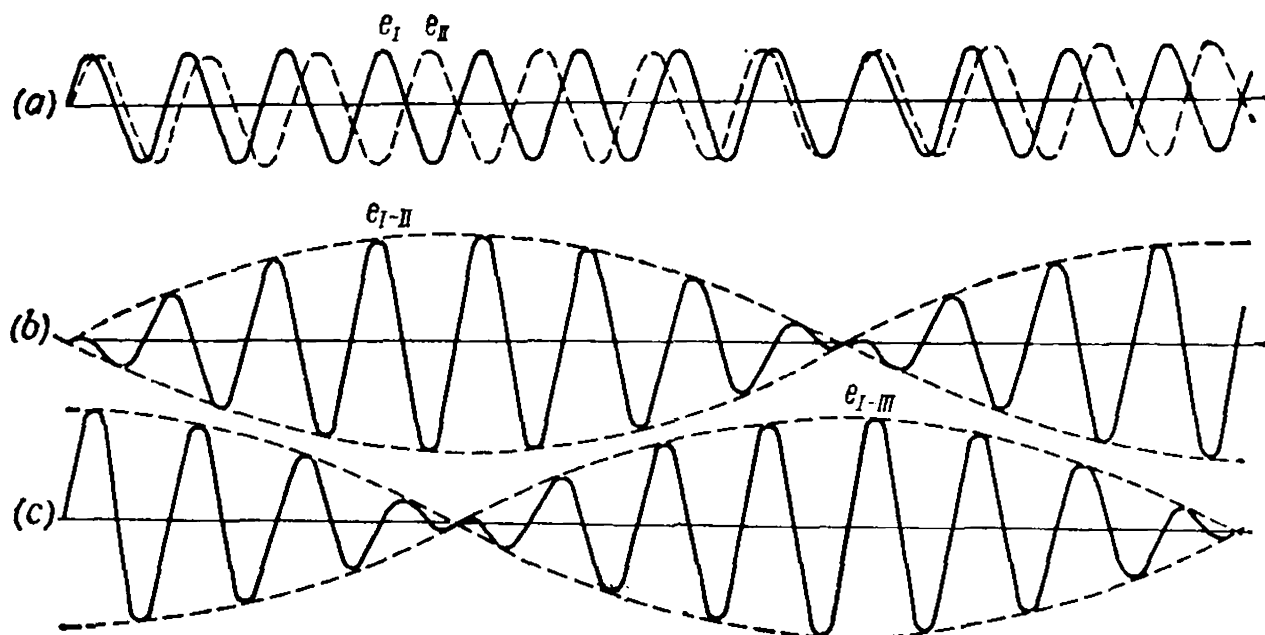


Fig. 12-2. Change in voltage across lamp terminals in synchronization

I and the e.m.f. of generator III , and will therefore burn very brightly.

The appropriate moment for parallel connection shown in Fig. 12-1 is chosen as follows. The generators to be connected are operated at a frequency $f_2 = f_1 \pm \Delta f_1$. The line voltage will be shown by a sine-wave curve e_I with the frequency f_1 , the voltage of the generator to be connected by curve e_{II} with the frequency f_2 (Fig. 12-2a) and the voltage across the phasing lamps of generator II by curve e_{I-II} having the form of a beat wave (Fig. 12-2b). At the moment when the lamps of generator II burn brightly, the phase difference between the e.m.f.s e_I and e_{II} will be maximum, while at the moment when the lamps go out, the e.m.f.s will be in phase. With the lamps connected for burning (for generator III) the moment of coincidence in phase of e.m.f.s e_I and e_{III} will correspond to the maximum of the beating voltage e_{I-III} and this will indicate the moment favourable for connection of generator III to the buses of the circuit (Fig. 12-2c).

The phasing lamps cannot give an absolutely accurate indication of the moment appropriate for connection, since the lamps begin to burn only at one-third of the normal voltage. Therefore, when the lamps are connected for extinction, the machine has to be switched-in during the beginning of the dark period, approximately at its middle. When the lamps are connected for burning, the moment of connection also cannot be determined with sufficient accuracy, since on the portion of the curve near a favourable moment of burning the beating e.m.f. e_{I-III} changes over a very flat portion of the wave. Better results are obtained in parallel connection to adjacent points in addition to the phasing lamps, of a null voltmeter with a mid-scale zero (Fig. 12-1), since passage of the voltmeter pointer through zero de-

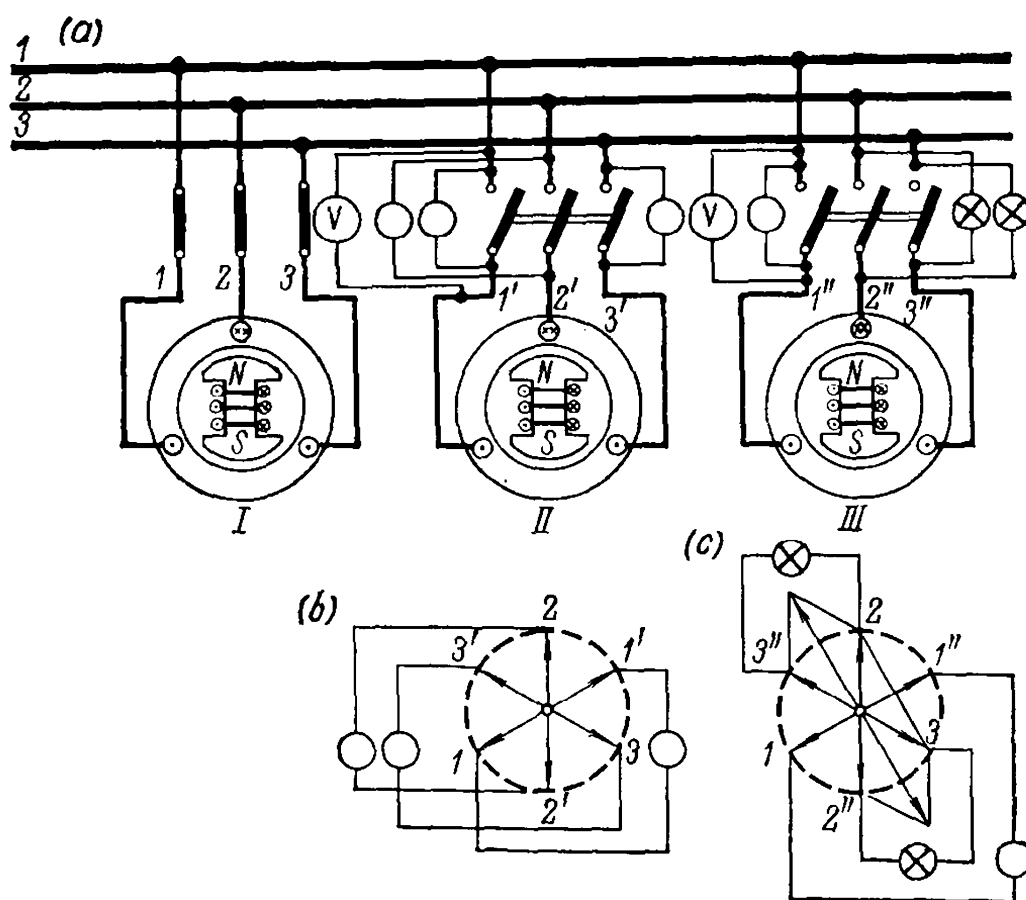


Fig. 12-3. Parallel connection of three-phase synchronous generators

termines the favourable moment more precisely than do the phasing lamps.

The synchronization of three-phase machines is essentially the same as for single-phase machines, the only difference being that three lamps are required.

To the three requirements for correct synchronization given above, one more requirement must be added for three-phase machines, which is as follows:

4. *The phase sequence at the points being connected should be the same.*

Figure 12-3a shows the moment favourable for connecting three-phase generators II and III to the buses of the circuit which three-phase generator I is already connected to. The phasing lamps of generator II are connected for extinction. In addition, a null voltmeter is included across the points 1-1' of the first phase being connected. Figure 12-3b depicts voltage diagrams of generators I and II with respect to the circuit made up of the windings of these generators and their phasing lamps. The sum of the vectors across whose ends the lamps are conventionally connected gives the voltage across the terminals of the corresponding lamp. From Fig. 12-3b it can be seen that the resultant voltage across each lamp will be zero, and they should hence go out and thus indicate the moment favourable for switching-in of generator II.

The lamp across the first phase of generator *III* between points 1-1" is connected for extinction, while the lamps of the second and third phases are cross-connected between points 2-3" and 3-2". Therefore, as can be seen from the diagram in Fig. 12-3c, the line voltage will be applied across these lamps for generator *III*, and they will burn quite brightly. This indicates a moment favourable for connecting generator *III*.

When the lamps are connected for extinction, they will all light and go out simultaneously, and there will be practically the same results when single-phase generator *II* (Fig. 12-1) will be connected.

In the synchronizing circuit of generator *III* (Fig. 12-3a) one lamp is connected across the first phase and the other two are cross-connected. This connection with a certain difference in frequencies results, as follows from Fig. 12-3c, in successive lighting and extinction of the lamps, and produces the impression of light rotation when the lamps are arranged in a circle. The lamp lighting frequency and, consequently, the apparent speed of light rotation will correspond to the difference between the line frequency and that of the generator being connected. When the generator being connected runs at a speed below the synchronous one the light will rotate in one direction, and at a speed above synchronous the rotation of the light will be reversed. Thus, the direction of light rotation indicates whether the speed of the incoming generator is to be increased or decreased to bring it into synchronism. This cannot be attained when the lamps are connected for extinction.

The proper moment for connection is indicated more precisely by the phasing lamp connected for extinction in the first phase, and by the null voltmeter connected across this lamp.

If in an extinction connection scheme (Fig. 12-3a, *II*) light rotation takes place, it is obvious that the connections in Fig. 12-3a, *III* were actually obtained, this being due to a wrong connection to the same knife-switch of the non-corresponding circuit and machine phases. In this case it is necessary to interchange any two of the conductors running from the line or the generator to the knife-switch, or to reverse the direction of machine rotation. Synchronization should be carried out only after making sure that the phase sequence of the power circuit and the machine is the same.

The lamps used for synchronizing must be connected through potential transformers when the synchronous generators have a voltage higher than that permissible for the lamps. If the machines to be connected are three-phase generators, it is first necessary to make sure that the potential transformers belong to the same group, since if by chance the transformer of one generator corresponds to the Y/Y-12 group, and that of the other generator to the Y/Y-6 group, the extinction of the lamps connected to the adjacent points will correspond not to phase coincidence of the voltages, but to a phase difference of

180°. In this case, with the lamps connected for extinction, a current surge corresponding to a sudden short circuit will occur. If we were to connect in this manner a generator to buses to which several other generators were already connected, a very serious failure of the system may occur due to the following reasons.

Suppose four identical generators were connected to the buses and a fifth, similar generator with wrongly connected phasing lamps is suddenly switched-in. The equivalent inductive reactance of the four generators operating in parallel will be $0.25x$, and that of the newly connected generator will be x , where x is the inductive reactance of a generator *. The current of a single generator with a sudden short circuit is

$$I_{sh} = \frac{E_m}{x}$$

but if the above wrong connection is made

$$I'_{sh} = \frac{E_m + E_m}{x + 0.25x} = 1.6 \frac{E_m}{x} = 1.6 I_{sh}$$

The stresses in the end connections, being designed for a current I_{sh} , will now increase by $1.6^2 \cong 2.5$ times and may cause damage to the machine. If only one generator were connected to the buses, however, then

$$I''_{sh} = \frac{2E_m}{2x} = \frac{E_m}{x} = I_{sh}$$

i.e., a current surge equal to a sudden short circuit of the generator would occur and, since the end connections should be designed for such stresses, there should be no damage to the windings.

In modern power stations improved synchronizing devices are used. Where non-automatic synchronization is practised, lamp-light rotation is replaced by rotation of the pointer of a special synchronoscope operating on the frequency difference between the power circuit and the generator to be connected. The rotating pointer allows the moment of synchronism to be found more precisely. In conjunction with a null voltmeter and a double frequency meter giving indications of the line frequency and the frequency of the generator to be connected on two parallel scales, the instrument assures complete reliability of synchronization.

There also exist automatic synchronization devices which perform the entire process of synchronization and connection of a generator automatically, without the participation of an operator.

Automatic synchronization devices, which connect a generator with great precision of phase coincidence of the system voltage and

* With no damper winding on the rotor the inductive reactance x is the transient reactance x'_d , while with a damper winding it is the subtransient reactance x''_d .

the voltage of the generator, often greatly extend the synchronization process, since operating conditions in the system change, particularly during emergency conditions, when rapid connection of standby generators is of the utmost importance.

To avoid using complicated automatic synchronization schemes and to increase the speed and reliability of synchronization, the recent trend in the USSR is to use the so-called self-synchronization of generators, in which the unexcited generator is brought up to a speed approximately equal to that of synchronism, is connected to the power circuit with an additional resistance in its field winding circuit, and is then excited. The excited generator then pulls itself into synchronism in a manner similar to a synchronous motor after an asynchronous start. The field winding is preliminarily closed through the additional resistance to weaken the stator current surge, since the armature-reaction flux, in increasing from zero to a certain value upon connection to the circuit, induces a current in the closed excitation circuit, owing to which the process is similar to connecting a transformer with a closed secondary. The function of this additional resistance in the excitation circuit is performed by the field damping resistor, which serves the following purpose.

When turn-to-turn and interphase short circuits occur and the generator is switched out of the circuit, it is simultaneously necessary to quickly eliminate the magnetic excitation field in order to limit the duration of the harmful effect of the short-circuit current in the stator winding. Breaking of the excitation current by means of some high speed device is inadmissible. However, since the rapid disappearance of the excitation flux would induce large e.m.f.s dangerous to the insulation in the generator field winding. For this reason the field winding is first shunted by a resistance 5 to 10 times that of the field winding and the exciter is then disconnected. The current in the winding drops to zero with a definite time constant, and the excitation field disappears.

In self-synchronization the stator of a generator must never be connected to a power system with the excitation circuit left open, because the large e.m.f. induced in the field winding may damage the insulation.

12-3. Angle Characteristics of a Synchronous Machine

The power of a synchronous machine is expressed by means of electrical quantities measured at the stator terminals by using the well-known relation

$$P = mUI \cos \varphi$$

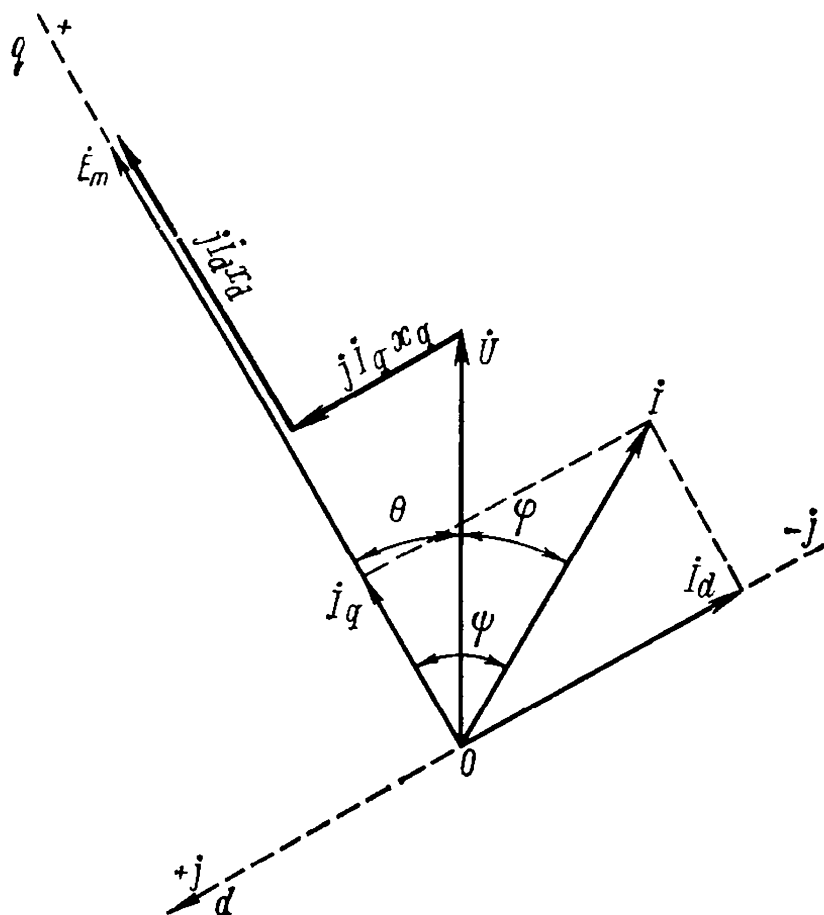


Fig. 12-4. Voltage diagram of a salient-pole synchronous generator

When investigating problems relating to parallel operation of machines with a power circuit, i. e., with other synchronous machines, it is more convenient to express the power in terms of quantities which characterize the effect on the operating conditions of the latter of factors which are external relative to the stator winding. These quantities are: (1) the line voltage U , (2) the e.m.f. E_m induced in the stator winding by the excitation current, and (3) the angle θ between the vectors \dot{U} and \dot{E}_m determined by the angular position of the rotor relative to the resultant

rotating magnetic flux of the stator. These external causes completely determine the operating conditions of the stator winding. Hence, the power P can also be definitely determined through the machine parameters E_m , U and θ :

$$P = f(E_m, U, \theta) \quad (12-1)$$

When $U = \text{const}$, $f = \text{const}$ (infinitely powerfull mains) and $E_m = \text{const}$ (constant excitation), the power of the machine P depends only on the angle θ , and the relation $P = f(\theta)$ is referred to as the *angle characteristic* of a synchronous machine.

In modern power systems the resistances of the stator windings in synchronous machines and in transmission lines are usually much less than their inductive reactances, and their influence on generator and line performance is small. Let us therefore first find relation (12-1), neglecting the resistances.

The voltage vector diagram of a salient-pole generator for a stator with a resistance $r_a = 0$ is shown in Fig. 12-4. By projecting the voltages and the e.m.f. s onto the directions of the d and q axes, we obtain

$$\dot{E}_m = \dot{U} \cos \theta + \dot{I}_d x_d \quad (12-2)$$

$$0 = \dot{U} \sin \theta - \dot{I}_q x_q \quad (12-3)$$

whence

$$\dot{I}_d = \frac{\dot{E}_m - \dot{U} \cos \theta}{x_d} \quad (12-4)$$

$$\dot{I}_q = \frac{\dot{U} \sin \theta}{x_q} \quad (12-5)$$

Assuming that the plane of the diagram in Fig. 12-4 is a complex coordinate plane, we can write

$$\dot{U} = \dot{U} \cos \theta - j \dot{U} \sin \theta \quad (12-6)$$

$$\dot{I} = \dot{I}_q - j \dot{I}_d \quad (12-7)$$

The complex of the generator power is

$$\dot{P}_\varphi = m \dot{U} \dot{I}^* \quad (12-8)$$

where \dot{U}^* is the conjugated complex of the voltage \dot{U} .

By substituting in equation (12-8) for \dot{U} and \dot{I} their values from equations (12-6) and (12-7), we obtain

$$\begin{aligned} \dot{P}_\varphi &= m (\dot{U} \cos \theta + j \dot{U} \sin \theta) (\dot{I}_q - j \dot{I}_d) = \\ &= m (\dot{U} \dot{I}_q \cos \theta + \dot{U} \dot{I}_d \sin \theta) - jm (\dot{U} \dot{I}_d \cos \theta - \dot{U} \dot{I}_q \sin \theta) \end{aligned} \quad (12-9)$$

The real component of \dot{P}_φ determines the active power of a machine:

$$P = m (U I_q \cos \theta + U I_d \sin \theta) \quad (12-10)$$

By substituting their values for I_d and I_q in equation (12-10), we obtain the required relation:

$$P = \frac{m E_m U}{x_d} \sin \theta + \frac{m U^2}{x_q} \sin \theta \cos \theta - \frac{m U^2}{x_d} \sin \theta \cos \theta$$

or, finally,

$$P = \frac{m E_m U}{x_d} \sin \theta + \frac{m U^2}{2} \left(\frac{1}{x_q} - \frac{1}{x_d} \right) \sin 2\theta$$

(12-11)

The first term of expression (12-11)

$$P_E = \frac{m E_m U}{x_d} \sin \theta \quad (12-12)$$

gives the fundamental component of the generator power depending both on the line voltage U and on the excitation or the e.m.f. E_m , while the second term

$$P_U = \frac{m U^2}{2} \left(\frac{1}{x_q} - \frac{1}{x_d} \right) \sin 2\theta \quad (12-13)$$

gives the additional component of the power which does not depend on machine excitation.

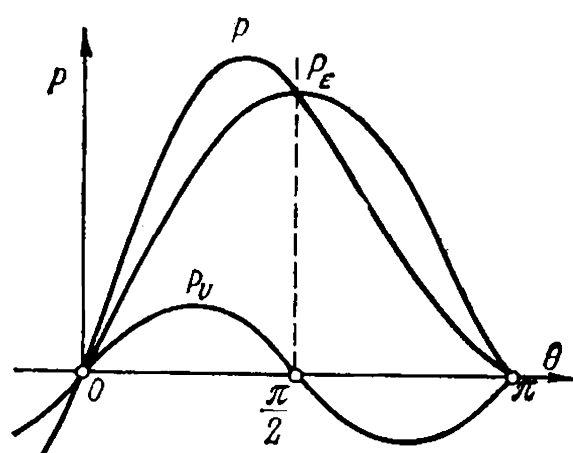


Fig. 12-5. Power-angle characteristic of a salient-pole generator with $r_a = 0$

In the absence of excitation ($E_m = 0$) a salient-pole generator ($x_d \neq x_q$) can develop the power P_U , since it is able under these conditions to rotate synchronously and to develop a torque because the armature-reaction flux tends to pass through the rotor along the path of least reluctance, i.e., along the direct axis. For more detailed consideration of these operating conditions see Sec. 12-6. In a non-salient-pole machine $x_d = x_q$, consequently, $P_U = 0$, and

$$P = \frac{mE_m U}{x_d} \sin \theta \quad (12-14)$$

Figure 12-5 shows the curves of both components (P_E , P_U) and the resultant power (P) of a salient-pole generator as a function of the angle θ with $E_m = \text{const}$ and $U = \text{const}$. It is assumed that the parameters x_d and x_q are constant. With respect to x_d this is not entirely true, since the saturation of the magnetic circuit will also vary with a change in operating conditions; we shall not take this change into account, however.

The maximum power of a non-salient-pole generator is obtained at the angle $\theta = \frac{\pi}{2}$. Under the influence of the component P_U the maximum power of a salient-pole generator is slightly shifted towards angles of $\theta < \frac{\pi}{2}$, and the value of the maximum power also slightly changes.

When negative values of the angle θ and values of $\theta > \pi$ are taken into consideration, the curve of the power P is a periodic one having positive and negative parts. The parts with a positive P ($0 < \theta < \pi$, $2\pi < \theta < 3\pi$, etc.) correspond to generator duties, and the parts with a negative P ($-\pi < \theta < 0$, $\pi < \theta < 2\pi$, etc.) correspond to motor duties. The duties corresponding to angles of θ differing by 2π and its multiples are equivalent. When a rotor runs at a non-synchronous speed, the angle θ continuously changes (for example, when it runs at above-synchronous speed, the angle θ continuously increases) and the machine alternately passes from generating to motoring and vice versa.

The power transferred electromagnetically via the magnetic field of the air-gap from the rotor of a synchronous generator to its stator is called the *electromagnetic* power. A part of it, generally a small one, is spent on losses in the generator steel, the remainder is converted into the electric power of the stator winding. In all further discussion we assume that the electromagnetic power is that part which is converted into the electric power of the stator winding, and will denote

it by P_{em} . If we assume, as in deriving formula (12-11), that the resistance of the stator winding is zero and, consequently, that there are no losses in the winding, the electromagnetic power P_{em} will be equal to the power P delivered by the generator to the power circuit:

$$P_{em} = \frac{mE_m U}{x_d} \sin \theta + \frac{mU^2}{2} \left(\frac{1}{x_q} - \frac{1}{x_d} \right) \sin 2\theta \quad (12-15)$$

When a generator is on load, its rotor is subjected to the braking action of the electromagnetic torque M_{em} , whose value is determined by the electromagnetic power P_{em} and by the mechanical angular speed of the rotor Ω :

$$M_{em} = \frac{P_{em}}{\Omega} = \frac{mE_m U}{\Omega x_d} \sin \theta + \frac{mU^2}{2\Omega} \left(\frac{1}{x_q} - \frac{1}{x_d} \right) \sin 2\theta \quad (12-16)$$

In motor duty the torque M_{em} changes its sign and acts on the rotor in the direction of its rotation, since it is a motor torque.

In a salient-pole synchronous machine the electromagnetic torque M_{em} also has two components:

$$M_{em} = M_{em \cdot E} + M_{em \cdot U} \quad (12-17)$$

where the fundamental torque

$$M_{em \cdot E} = \frac{mE_m U}{\Omega x_d} \sin \theta \quad (12-18)$$

is a function of both the excitation e.m. f. E_m and the voltage U , while the additional, parametric torque

$$M_{em \cdot U} = \frac{mU^2}{2\Omega} \left(\frac{1}{x_q} - \frac{1}{x_d} \right) \sin 2\theta \quad (12-19)$$

depends only on the voltage and also exists in an unexcited machine ($E_m=0$).

Let us note, finally, that in the formulas given above the voltage U is not only the voltage across the machine terminals, but also the voltage at any point of the line connecting the machine to the power system. Here, instead of x_d and x_q , the inductive reactances $x_d + x_l$ and $x_q + x_l$ are used, x_l being the reactance of the line up to the given point having the voltage U .

For practical calculations it is convenient to choose a point of the power system or line where the voltage U may be considered constant: $U = \text{const}$; this is always possible, if the capacity of the generator under consideration is small in comparison with the power of all the generators feeding the given circuit.

It is sometimes (as, for example, in studying the damping moments of synchronous machines during power swings) also of interest to determine the influence of the resistances of the stator circuit on the

power-angle characteristics. Let us consider this problem for a non-salient-pole machine ($x_d = x_q$).

Figure 12-6 depicts the voltage diagram of a non-salient-pole generator. By projecting the e.m.f.s and the voltages onto the axes d and q , we obtain

$$E_m = U \cos \theta + I_q r_a + I_d x_d$$

$$0 = U \sin \theta + I_d r_a - I_q x_q$$

whence

$$I_d = \frac{(E_m - U \cos \theta) x_d - U r_a \sin \theta}{z_d^2} \quad (12-20)$$

$$I_q = \frac{(E_m - U \cos \theta) r_a + U x_d \sin \theta}{z_d^2} \quad (12-21)$$

where

$$z_d^2 = r_a^2 + x_d^2 \quad (12-22)$$

By substituting for I_d and I_q in equation (12-10) their values from equations (12-20) and (12-21), we get

$$P = \frac{mU}{z_d} \frac{E_m (r_a \cos \theta + x_d \sin \theta) - U r_a}{z_d}$$

If we designate

$$\frac{r_a}{z_d} = \sin \alpha; \quad \frac{x_d}{z_d} = \cos \alpha \quad (12-23)$$

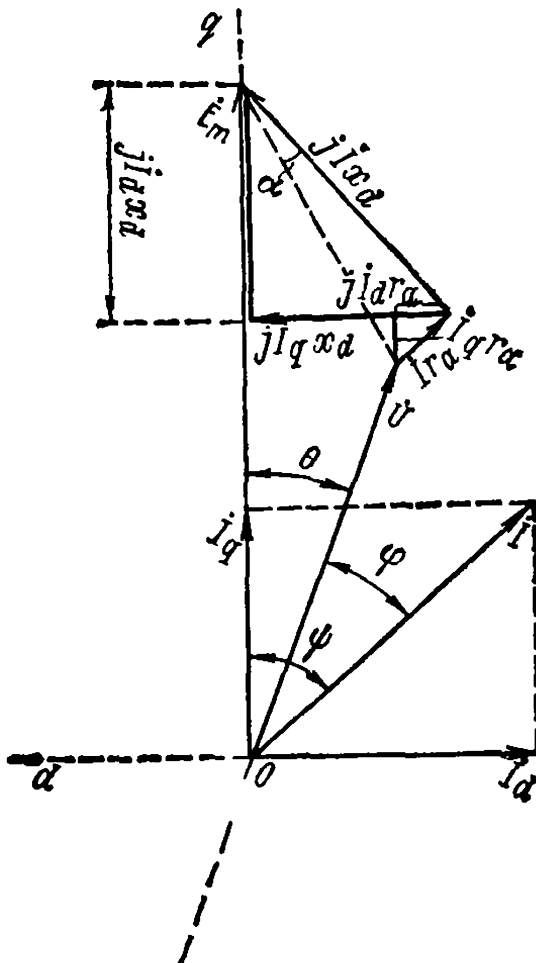


Fig. 12-6. Voltage diagram of a non-salient-pole synchronous generator

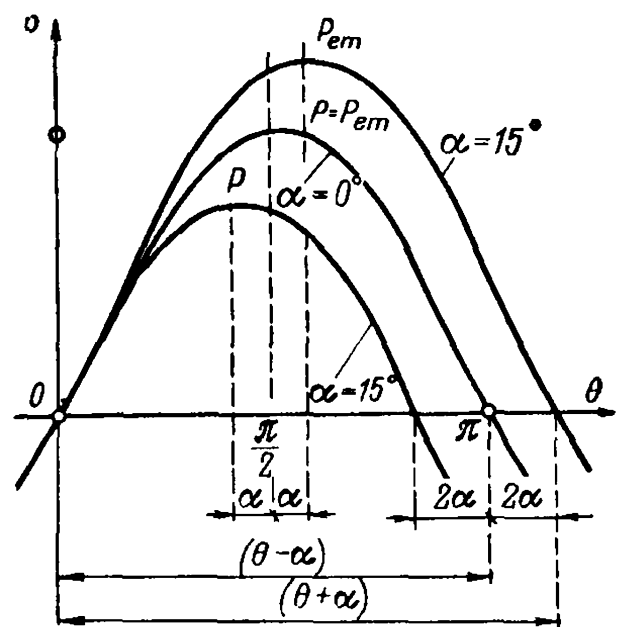


Fig. 12-7. Power-angle characteristics of a non-salient-pole synchronous generator with $r_a \neq 0$

we finally obtain for the useful power delivered to a circuit

$$P = \frac{mU}{z_d} [E_m \sin(\theta + \alpha) - U \sin \alpha] \quad (12-24)$$

The value of the electromagnetic power can be obtained in accordance with Fig. 12-6 in terms of the e.m.f. E_m and current I_q :

$$P_{em} = mE_m I_q$$

or, by substituting for I_q its value from equation (12-21) and taking into account relations (12-23):

$$P_{em} = \frac{mE_m}{z_d} [E_m \sin \alpha + U \sin(\theta - \alpha)] \quad (12-25)$$

Figure 12-7 gives the power-angle characteristics of a non-salient-pole generator with $E_m = U = \text{const}$ for $\alpha = 15^\circ$ and $\alpha = 0$.

12-4. Static Overload Capacity of a Synchronous Machine Operating in Parallel in an Electrical System

Static Overload Capacity. In the actual operation of a synchronous generator connected to the buses of a system its load never remains strictly constant, but is subjected to continuous changes because of switching-on and -off of loads, variations in load, and other causes. During changes in the operating conditions of a synchronous machine, various transient phenomena occur in it. For instance, when the direct-axis component of the stator current changes, the direct-axis armature-reaction flux changes, owing to which an additional current is induced in the field winding and also in the damper winding, if present. These additional currents will cause a change in the magnetic fluxes, electromagnetic torques and electric power of the machine in comparison with their values under steady-state operating conditions at the same voltage U , angle θ and excitation voltage.

Here we shall deal only with those variations of generator operating conditions which occur very slowly; hence the transient phenomena may be disregarded. It may then be assumed that any change in the generator power will take place in accordance with the relations obtained in the previous section. Such operating conditions are static, and the power-angle characteristics corresponding to them will be termed *static* characteristics.

Let us consider the conditions of parallel operation of a generator with invariable excitation ($E_m = \text{const}$) feeding into an infinitely powerful mains ($U = \text{const}$, $f = \text{const}$). For simplicity we shall consider a non-salient-pole machine ($x_q = x_d$); the features relating to a salient-pole machine will be discussed separately.

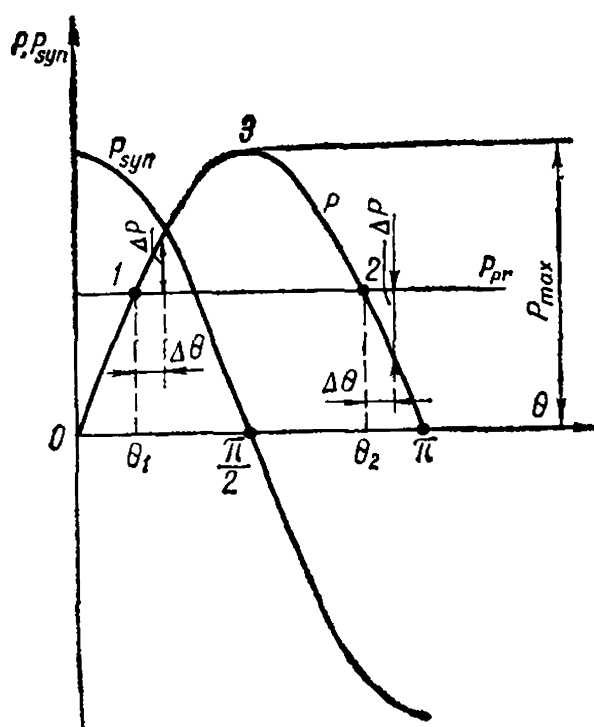


Fig. 12-8. To determination of static over-load capacity of synchronous generator

The power-angle characteristic of a non-salient-pole generator with $E_m = \text{const}$, $U = \text{const}$ and $f = \text{const}$ is given in Fig. 12-8.

Designate the output at the shaft of the prime mover (a steam or hydraulic turbine), less the mechanical losses and the losses in the steel, as P_{pr} . Since we neglect the losses in the stator circuit, the output P delivered to the power circuit by the generator under steady-state operating conditions will also be equal to P_{pr} . The output P_{pr} of the prime mover does not depend on the angle θ and is therefore shown in Fig. 12-8 by a horizontal line. The intersections of the straight line P_{pr} with the curve P in Fig. 12-8 indicate two possible steady-state conditions of operation, corresponding to points 1 and 2.

Only the condition corresponding to point 1, however, is stable.

In fact, if, as a result of the above inevitable variations in operating conditions, the rotor of the generator is somewhat accelerated, and the angle θ increases by a small value $\Delta\theta$, a positive increment in generator output ΔP will correspond to this change of angle at point 1, but the turbine will retain its output. The generator will deliver to the buses an output greater than that obtained from the turbine, therefore the rotor will be retarded, the angle θ will decrease and the generator return to the operating condition corresponding to point 1. At point 2, on the contrary, a negative output increment $-\Delta P$ corresponds to a positive increment $\Delta\theta$, the angle θ increases still more and the generator pulls out of synchronism.

Thus, the criterion for stable operation under the above conditions is to meet the requirement

$$\frac{\Delta P}{\Delta \theta} > 0$$

or, at the limit,

$$\frac{dP}{d\theta} > 0 \quad (12-26)$$

If negative increments of angle θ are considered, it is easy to see that we arrive at the same results.

The ascending branch of the curve in Fig. 12-8 ($0 < \theta < \frac{\pi}{2}$) corres-

ponds to steady-state operating conditions, and the descending branch ($\frac{\pi}{2} < \theta < \pi$) to unstable operating conditions of a non-salient-pole generator when $U = \text{const}$ and $E_m = \text{const}$. Here the angle $\theta = \frac{\pi}{2}$ and the output

$$\boxed{P_{max} = \frac{mE_m U}{x_d}} \quad (12-27)$$

corresponds to the limit of static overload capacity (stability) of a non-salient-pole machine (point 3 in Fig. 12-8).

In a salient-pole machine the maximum output P_{max} and, respectively, the limit of static stability are reached at an angle $\theta < \frac{\pi}{2}$ (see Fig. 12-5).

The ratio

$$k_{ov} = \frac{P_{max}}{P_r} \quad (12-28)$$

is called the *overload capacity* of a synchronous machine or the *static overload capacity factor*.

For non-salient-pole machines

$$k_{ov} \cong \frac{1}{\sin \theta_r} \quad (12-29)$$

where θ_r is the value of the angle θ at rated load; this angle, for turbogenerators, usually ranges from 25 to 30° , for which values $k_{ov} \cong 2.0$.

According to equation (12-27) the maximum output of a generator depends on E_m , U and x_d . The voltage U depends on the operating conditions of the power circuit and must be kept constant as far as possible. The e.m.f. (see Figs. 12-4 and 12-6) is determined at the given operating conditions by the voltage U and the parameters of the machine. However, a comparatively large change in the parameters does not change the e.m.f. E_m to the same extent. Therefore, the maximum output or the overload capacity of a given machine is the greater, the less its direct-axis inductive reactance x_d or the greater its short-circuit ratio. With respect to equation (12-29) this follows from the fact that with a reduction of x_d , the angle θ_r corresponding to the rated load decreases. However, the reduction of x_d and the corresponding increase in overload capacity are linked with the necessity of increasing the dimensions of the machine (see Sec. 11-4) and its cost.

Synchronizing Power and Synchronizing Torque. With a given small departure $\Delta\theta$ from steady-state conditions, the power output unbalance ΔP which causes the machine to return to its initial conditions will be the larger, the steeper the rise of the curve P with a change in

the angle θ , i.e., the greater the derivative

$$P_{syn} = \frac{dP}{d\theta} \quad (12-30)$$

The quantity P_{syn} will be called the *synchronizing power coefficient*, and the quantity

$$\Delta P = \frac{dP}{d\theta} \Delta\theta = P_{syn} \Delta\theta \quad (12-31)$$

the *synchronizing power*.

For a non-salient-pole machine, according to equation (12-14), the synchronizing power coefficient is

$$P_{syn} = \frac{mE_m U}{x_d} \cos \theta \quad (12-32)$$

and for a salient-pole machine, according to relation (12-11)

$$P_{syn} = \frac{mE_m U}{x_d} \cos \theta + mU^2 \left(\frac{1}{x_q} - \frac{1}{x_d} \right) \cos 2\theta \quad (12-33)$$

The curve of the synchronizing power coefficient $P_{syn} = f(\theta)$ for a non-salient-pole generator is shown in Fig. 12-8.

The synchronizing power ΔP , equal to the unbalance between the generator and turbine power output, corresponds to a synchronizing torque on the generator rotor

$$\Delta M = \frac{\Delta P}{\Omega} = \frac{P_{syn}}{\Omega} \Delta\theta \quad (12-34)$$

caused by the difference between the electromagnetic torque of the generator and the torque of the turbine.

The quantity

$$M_{syn} = \frac{P_{syn}}{\Omega} \quad (12-35)$$

will be referred to as the *synchronizing torque coefficient*.

For a non-salient-pole machine

$$M_{syn} = \frac{mE_m U}{\Omega x_d} \cos \theta \quad (12-36)$$

and for a salient-pole machine

$$M_{syn} = \frac{mE_m U}{\Omega x_d} \cos \theta + \frac{mU^2}{\Omega} \left(\frac{1}{x_q} - \frac{1}{x_d} \right) \cos 2\theta \quad (12-37)$$

The synchronizing power coefficient P_{syn} and the synchronizing torque coefficient M_{syn} are positive within stable operation ranges and negative within unstable ones. Therefore, the criterion of static stability, instead of non-equality (12-26), can also be written in the

form of

$$P_{syn} > 0 \text{ or } M_{syn} > 0$$

The coefficients P_{syn} and M_{syn} can also be considered as quantities characterizing the degree of static stability of a machine: the greater P_{syn} and M_{syn} , the greater the forces tending to return the generator rotor to its initial steady-state operating conditions. At the limit of static stability the factors become $P_{syn} = M_{syn} = 0$.

Example 12-1. The hydrogenerator considered in Examples 8-1 and 9-1 (pp. 201 and 227), with $P_r = 57\,200$ kW, $x_d = 0.695$ and $x_q = 0.507$, has an e.m.f. in relative units at rated load, obtained from the Potier diagram for $\cos \varphi = 0.8$, equal to $E_m = i_{exc. r} = 1.58$ (unsaturated conditions) and $\theta = 16^\circ 40'$. With these data and the rated voltage across the terminals $\underline{U}_r = 1.0$, the electromagnetic power in relative units, by formula (12-15), is

$$\begin{aligned} \underline{P}_{em} &= \frac{3 \times 1.58 \times 1.0}{0.695} \sin 16^\circ 40' + \frac{3 \times 1.0^2}{2} \left(\frac{1}{0.507} - \frac{1}{0.695} \right) \sin 2 \times 16^\circ 40' = \\ &= 6.82 \times 0.287 + 0.795 \times 0.55 = 2.4 \end{aligned}$$

The rated power of the generator in relative units is

$$\underline{P}_r = 3 \times 1.0 \times 1.0 \times 0.8 = 2.4$$

The synchronizing power coefficient at $\theta = 16^\circ 40'$ is, by formula (12-33),

$$\begin{aligned} \underline{P}_{syn} &= \frac{3 \times 1.58 \times 1.0}{0.695} \cos 16^\circ 40' + 3 \times 1.0^2 \left(\frac{1}{0.507} - \frac{1}{0.695} \right) \cos 2 \times 16^\circ 40' = \\ &= 6.82 \times 0.96 + 1.59 \times 0.835 = 7.86 \end{aligned}$$

whence

$$\frac{P_{syn}}{P_r} = \frac{7.86}{2.4} = 3.28$$

12-5. Generator and Motor Duties.

Overexcitation and Underexcitation of a Synchronous Machine

A synchronous machine, like rotating electrical machines, is reversible and, when operating in parallel with a power circuit, makes it possible to change from generating to motoring and vice versa. This change is connected with a change in the angle θ and, correspondingly, in the angle ψ .

Figures 12-9, 12-10 and 12-11 show simplified voltage diagrams for a non-salient-pole machine without losses in the stator winding.

When the angle ψ changes within the limits $-\frac{\pi}{2} < \psi < \frac{\pi}{2}$ (Fig. 12-9a and b), the synchronous machine operates as a generator. When the angle ψ changes within the limits $\frac{\pi}{2} < \psi < \pi$ and $-\frac{\pi}{2} > \psi > -\pi$ (Fig. 12-10a and b), the electromagnetic power P_{em} changes its sign, and the machine operates as a motor. Finally, when $\psi = \frac{\pi}{2}$ and $\psi = -\frac{\pi}{2}$, i. e.,

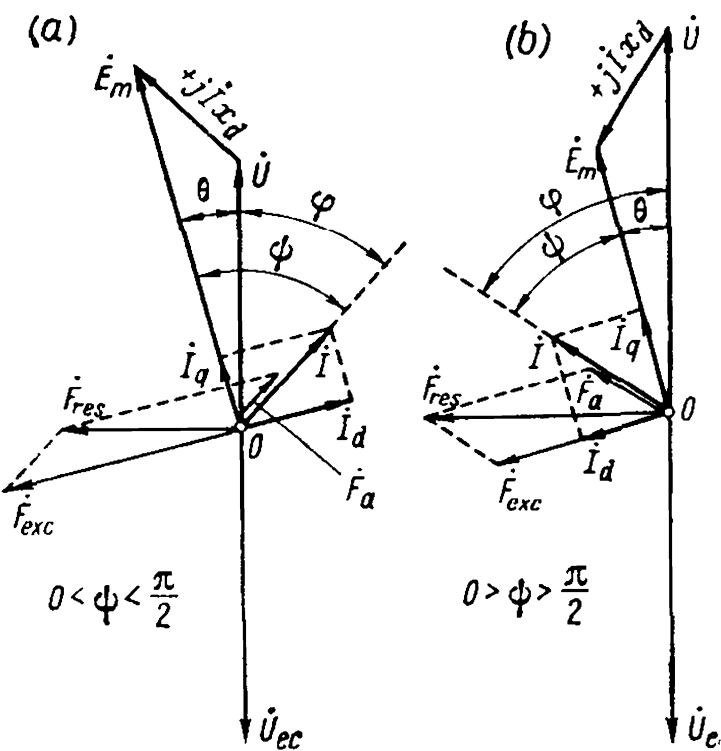


Fig. 12-9. Simplified voltage diagrams of a synchronous generator:
a — overexcited; b — underexcited

for boundary values of the angle ψ with $\cos \varphi=0$, the electromagnetic power $P_{em}=0$ and the machine operates with respect to the power circuit as if it were an equivalent inductance or capacitance, which corresponds to the operating conditions of a synchronous condenser (Fig. 12-11a and b).

The operating conditions of electrical machines, both d.c. and a.c., when considering them as generators, are best investigated on the basis of the e.m.f. E_m , the latter being resolved into components that balance the voltage drop, on one hand, and the external power circuit voltage U_{ec} , on the other hand. When analysing

motoring duty, it is better to take the circuit voltage U_{ec} applied to the motor as the basis and resolve it into components balancing the voltage drop and the counter e.m.f. E_m .

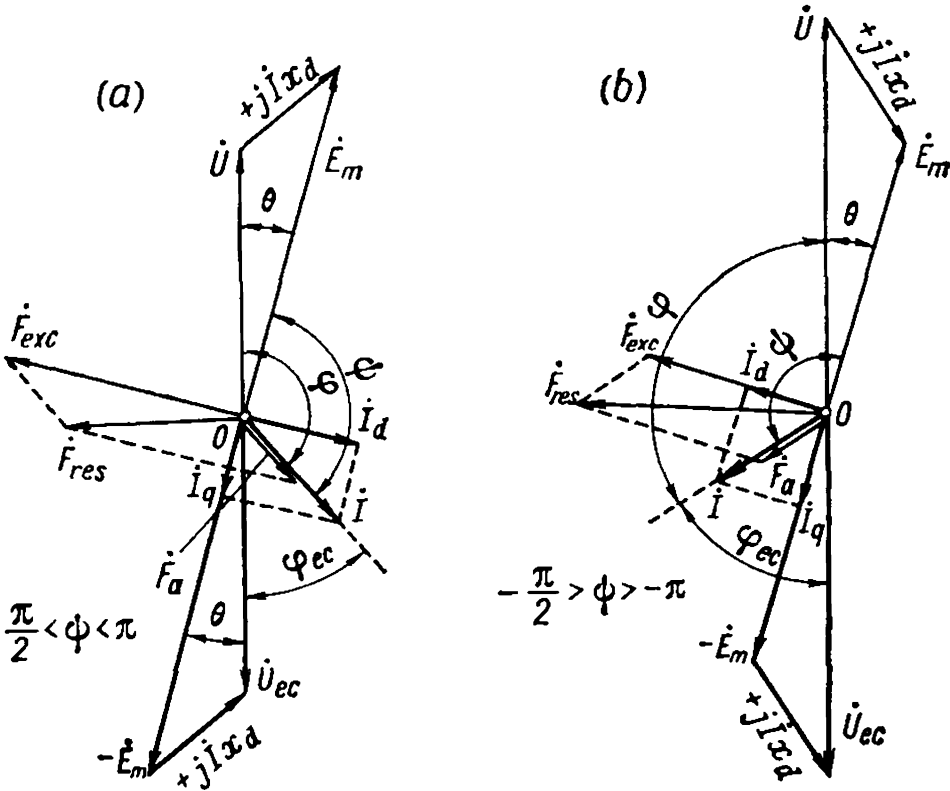


Fig. 12-10. Simplified voltage diagrams of a synchronous motor:
a — overexcited; b — underexcited

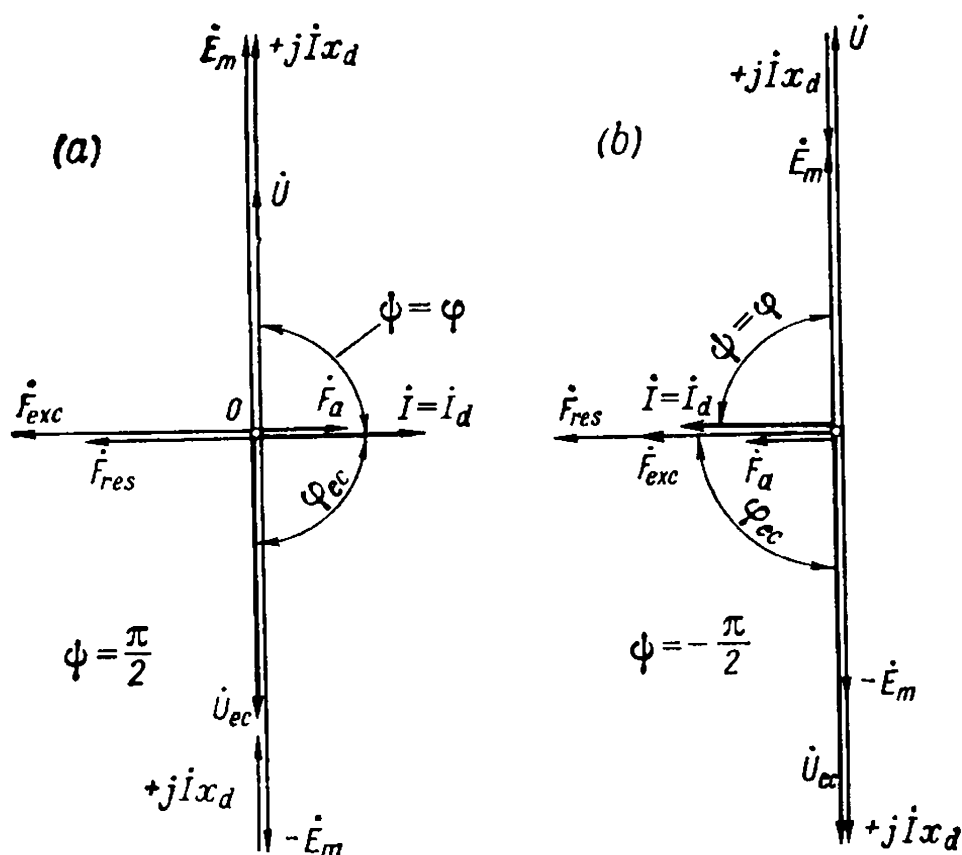


Fig. 12-11. Simplified vector diagrams of a synchronous condenser:

a — overexcited; *b* — underexcited

With such an approach, for instance, with a d.c. shunt-wound machine operating in parallel with the external circuit, we can express generator conditions by the equations

$$E_m = U_{ec} + r_a I_a \quad \text{and} \quad I_a = \frac{E_m - U_{ec}}{r_a}$$

Generating duty in a d.c. machine is obtained when $E_m > U_{ec}$. When $E_m < U_{ec}$, the machine transfers to motoring duty, for which

$$-U_{ec} = -E_m + r_a I_a \quad \text{and} \quad I_a = \frac{-U_{ec} - (-E_m)}{r_a} = \frac{-U_{ec} + E_m}{r_a}$$

Similarly, when considering a synchronous non-salient-pole machine operating in parallel with the external circuit, neglecting the active voltage drop, we consider generating duty on the basis of the e.m.f. E_m , resolving it into components $jI_d x_d$ and \dot{U} (Fig. 12-9*a* and *b*), and motoring duty on the basis of the circuit voltage \dot{U}_{ec} , resolving it into the components $jI_d x_d$ and $(-\dot{E}_m)$, as shown in Fig. 12-10*a* and *b*. A machine operated as a synchronous condenser is an unloaded synchronous motor, and here we also proceed from the circuit voltage \dot{U}_{ec} , resolving it into the components $jI_d x_d$ and $(-\dot{E}_m)$ (Fig. 12-11*a* and *b*).

Depending on what quantity is taken as the basis—the e.m.f. \dot{E}_m or the circuit voltage \dot{U}_{ec} —we determine the power factor $\cos \varphi$ for generating duty from the angle of displacement φ of the current \dot{I} (Fig. 12-9a and b) relative to the generator voltage \dot{U} , and, for motor and synchronous condenser duty, from the angle of displacement φ_{ec} of the current \dot{I} relative to the voltage \dot{U}_{ec} (Figs. 12-10a and b and 12-11a and b).

A glance at the voltage diagrams shows that a synchronous machine operates as a generator when \dot{I}_q coincides in direction with \dot{E}_m , as a motor when \dot{I}_q is in opposition to \dot{E}_m , and as a synchronous condenser when \dot{I} is practically perpendicular to \dot{E}_m .

Depending on the value of the excitation current, a synchronous machine acts in the circuit either as an inductive or a capacitive load, i.e., in addition to consuming or delivering active power from or to the circuit, the machine also behaves with respect to the circuit as an inductance or a capacitance.

If the current vector \dot{I} is in opposition to the circuit voltage vector \dot{U}_{ec} (Fig. 12-12a—generating duty), or is in phase with the circuit voltage (Fig. 12-12b—motoring duty), the synchronous machine has no inductive or capacitive effect on the line. If the current vector \dot{I} contains a component leading the circuit voltage \dot{U}_{ec} (Figs. 12-9a, 12-10a, and 12-11a), the synchronous machine has a capacitive effect on the circuit and delivers reactive power to the line, this power being consumed by induction motors, transformers, etc. Here the synchronous machine has an overexcited magnetic system, irrespective of whether it operates as a generator or a motor.

Conversely, if a synchronous machine has a component of the current vector \dot{I} lagging behind the circuit voltage vector \dot{U}_{ec} , it exerts an inductive influence, irrespective of whether it operates as a generator or a motor (Figs. 12-9b, 12-10b and 12-11b). Now the synchronous machine is underexcited and takes reactive power from the line, as well as current producing an armature reaction which additionally magnetizes its magnetic system.

When two synchronous generators connected in parallel operate under no-load, no equalizing current will flow between them only when their e.m.f.s produced by the excitation flux are $\dot{E}_{m1} = \dot{E}_{m2} = \dot{U}$. If now we increase the excitation of one of the machines and decrease the excitation of the other, for example, $\dot{E}_{m1} > \dot{E}_{m2}$, the voltage across the common terminals of these machines (if they are of the same type) will equal the half-sum of the e.m.f.s \dot{E}_{m1} and \dot{E}_{m2} , i.e.,

$$\dot{U} = \frac{\dot{E}_{m1} + \dot{E}_{m2}}{2}$$

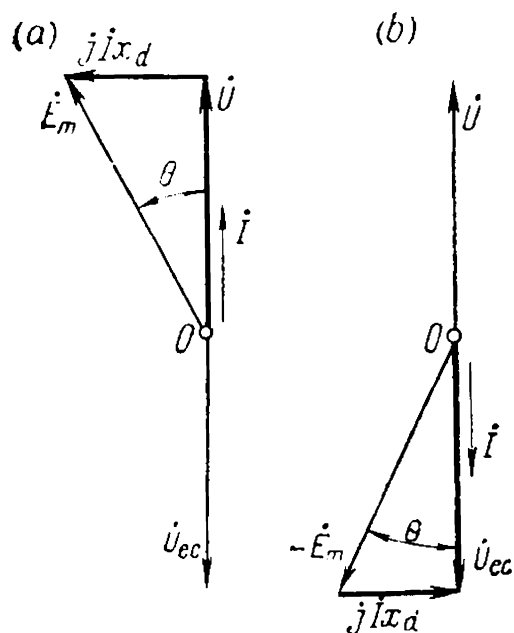


Fig. 12-12. Simplified vector diagrams of a synchronous machine with $\varphi = 0$:
 a — generator; b — motor

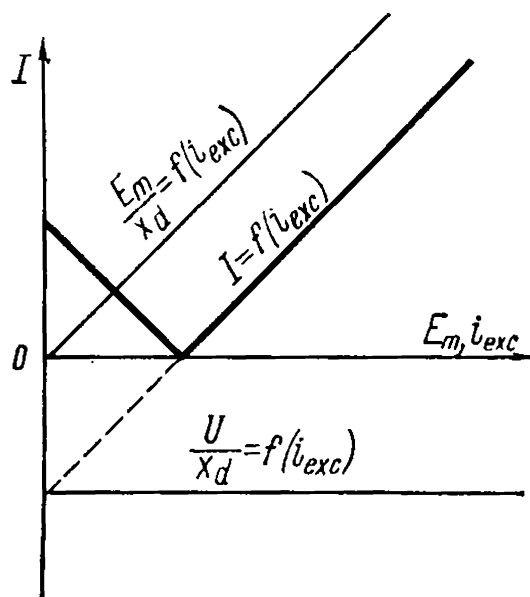


Fig. 12-13. Relation between stator current I and excitation current i_{exc} for a synchronous generator at no-load

and a reactive current will flow between them which will produce an armature reaction magnetizing the magnetic system of the underexcited machine with $E_m < U$ and demagnetizing the overexcited machine with $E_m > U$. The voltage diagram for an overexcited machine is given in Fig. 12-11a, and for an underexcited machine in Fig. 12-11b.

The value of this reactive current is

$$I = \frac{E_m - U}{x_d}$$

the positive sign of the current I indicating that it lags 90° behind the generator voltage U ; the negative sign indicates a phase lead of 90° . The current will be opposite in phase with respect to the circuit voltage U_{ec} . If we lay off the e.m.f. E_m or the excitation current i_{exc} for an unsaturated magnetic system along the axis of abscissas (Fig. 12-13), and the effective value of the current I along the axis of ordinates, the relation $I = f(E_m)$ or $I = f(i_{exc})$ will be represented by two intersecting straight lines.

Thus, when synchronous machines are operating in parallel, a change in the excitation of any of them causes only the appearance of an equalizing reactive current, and does not change the active power, as in parallel operation of d.c. machines. To change the load, or to transfer a synchronous machine from motoring to generating duty, the angle θ should be changed as follows from equations (12-11) and (12-14); this is achieved only by acting on the prime mover. For example, to raise the output of a generator, it is necessary to raise the output of the prime mover which drives it, i.e., increase the torque on the prime

θ is $\frac{\pi}{2}$, after which the machine falls out of step. Therefore, point K is at the limit of stable operation, while point M is already in the zone of unstable operation of a synchronous machine.

With a larger constant load a new diagram will be obtained with line $A'B'$ passing above line AB (Fig. 12-14).

The diagram of Fig. 12-14 makes it possible to plot a U-shaped curve for the relation $I=f(i_{exc})$ and a curve for $\cos \varphi=f(i_{exc})$ with $P=\text{const}$ and $U=\text{const}$. Since for each load in Fig. 12-14 there is a separate line AB , we obtain a separate U-shaped curve for each load. Figure 12-15 presents the U-shaped curves $I=f(i_{exc})$ for no-load conditions (curve A), for half-load (curve B) and for full load (curve C), as well as the corresponding curves a , b and c for $\cos \varphi=f(i_{exc})$. Curve A for no-load operation has the form of two intersecting straight lines, as follows from the construction of Fig. 12-13. The dotted curve corresponds to the limits of steady-state operation.

When a synchronous machine operates as a motor with $P=\text{const}$ and $U_{ec}=\text{const}$, we must plot the diagram on the basis of the voltage U_{ec} across the terminals. Figure 12-16 shows a diagram corresponding to the voltage diagram of Fig. 12-10a. Here the resultant flux vector $\dot{\Phi}_{res}$ and the resultant magnetizing force vector \dot{F}_{res} in the simplified diagram lag behind the voltage vector \dot{U}_{ec} by 90° . The U-shaped curves for a motor are of the same nature as for a generator, the only difference being that an overexcited motor has leading currents and an underexcited motor lagging currents, while in generators we obtain lagging currents with overexcitation and leading currents with underexcitation. This is explained by the fact that the current displacement in a generator is counted from the generator voltage \dot{U} , and in a motor, from the circuit voltage $\dot{U}_{ec}=-\dot{U}$.

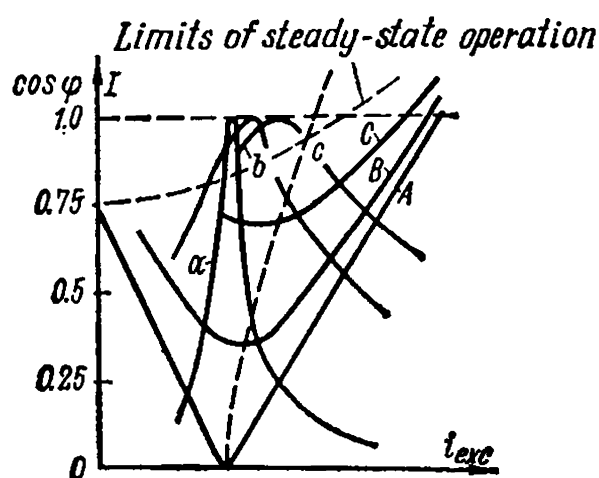


Fig. 12-15. U-shaped curves of a synchronous generator

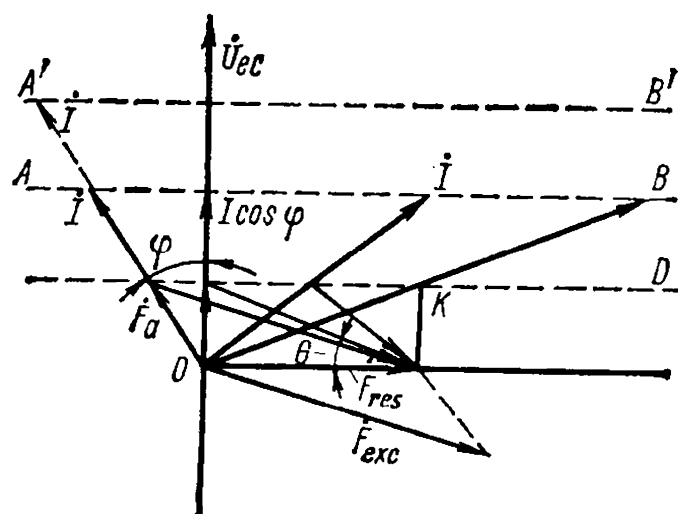


Fig. 12-16. Relation between stator current I and excitation current i_{exc} for a synchronous motor

12-6. Current Diagrams of Synchronous Machines

Equation of Current Diagram. When the operating conditions of a synchronous machine change, the current I in the stator winding changes in magnitude and phase relative to the terminal voltage U . If the parameters of the machine (x_d , x_q , r_a) are constant, then with a change in load or in the angle θ the end of the vector I , when $U = \text{const}$ and $E_m = \text{const}$, moves along a certain curve termed the *current diagram*. In the simplest case the current diagram is a circle, and is called the *current circle diagram*. For example, from the voltage diagram of a non-salient-pole machine (Fig. 12-9) it can be seen that, with a fixed position of vector \dot{U} and rotation of the vector \dot{E}_m , whose magnitude is constant, through an angle 2π , the end of the vector $jI x_d$ describes a circle; consequently, when $x_d = \text{const}$, the end of the current vector I also describes a circle.

The current diagram illustrates the relations between the quantities characterizing synchronous machine operation.

Let us consider the construction of a current diagram for a synchronous machine in motoring duty and, for simplicity, assume that the resistance of the stator winding is zero.

Figure 12-17 shows a voltage diagram of an overexcited salient-pole motor with $r_a = 0$. The following expressions for the direct-axis and quadrature-axis components of the stator current are found from the diagram

$$I_d = \frac{U_{ec} \cos \theta - E_m}{x_d} \quad (12-38)$$

$$I_q = \frac{U_{ec} \sin \theta}{x_q} \quad (12-39)$$

Expressions (12-38) and (12-39) coincide with expressions (12-4) and (12-5) obtained for generating duty.

Superpose the plane of the diagram in Fig. 12-17 on the complex coordinate plane, the axis of real numbers coinciding with the direction of the circuit voltage vector \dot{U}_{ec} . Then, according to Fig. 12-17, the stator current can be expressed as

$$I = I_q e^{-j\theta} + I_d e^{j\left(\frac{\pi}{2} - \theta\right)} \quad (12-40)$$

By substituting for I_d and I_q their values from equations (12-38) and (12-39), and taking into ac-

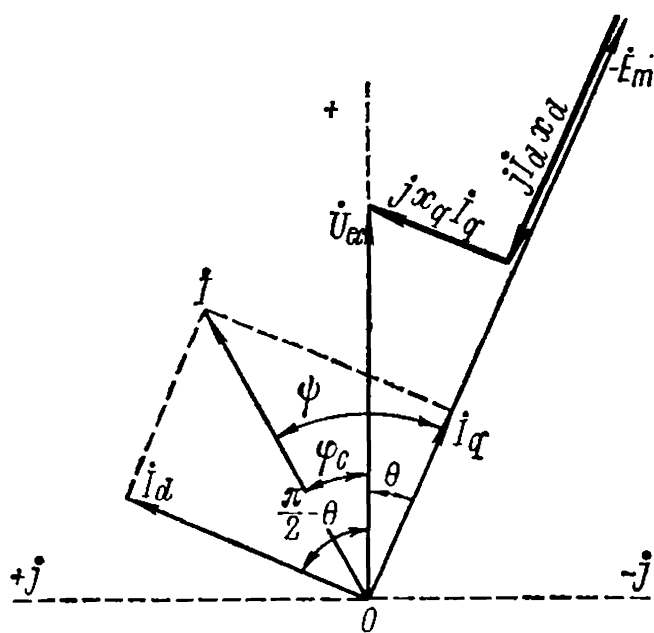


Fig. 12-17. Voltage diagram of a salient-pole synchronous motor

count the relations

$$\begin{aligned}\sin \theta &= \frac{e^{j\theta} - e^{-j\theta}}{2j} = \frac{1}{2} e^{-j\frac{\pi}{2}} (e^{j\theta} - e^{-j\theta}) \\ -\cos \theta &= -\frac{e^{j\theta} + e^{-j\theta}}{2} = \frac{1}{2} e^{-j\pi} (e^{j\theta} + e^{-j\theta})\end{aligned}$$

we get

$$\begin{aligned}\dot{I} &= \frac{U_{ec}}{2x_q} e^{-j\left(\frac{\pi}{2} + \theta\right)} \times (e^{j\theta} - e^{-j\theta}) + \\ &+ \frac{U_{ec}}{2x_d} e^{-j\left(\frac{\pi}{2} + \theta\right)} (e^{j\theta} + e^{-j\theta}) + \frac{E_m}{x_d} e^{j\left(\frac{\pi}{2} - \theta\right)} = \\ &= \frac{U_{ec}}{2} \left(\frac{1}{x_q} + \frac{1}{x_d}\right) e^{-j\frac{\pi}{2}} + \frac{U_{ec}}{2} \left(-\frac{1}{x_q} + \frac{1}{x_d}\right) e^{-j\left(\frac{\pi}{2} + 2\theta\right)} + \\ &+ \frac{E_m}{x_d} e^{j\left(\frac{\pi}{2} - \theta\right)}\end{aligned}\quad (12-41)$$

or

$$\dot{I} = \dot{M} + \dot{R}_U e^{-j2\theta} + \dot{R}_E e^{-j\theta} \quad (12-42)$$

where

$$\dot{M} = \frac{U_{ec}}{2} \left(\frac{1}{x_q} + \frac{1}{x_d}\right) e^{-j\frac{\pi}{2}} \quad (12-43)$$

$$\dot{R}_U = \frac{U_{ec}}{2} \left(\frac{1}{x_q} - \frac{1}{x_d}\right) e^{j\frac{\pi}{2}} \quad (12-44)$$

$$\dot{R}_E = \frac{E_m}{x_d} e^{j\frac{\pi}{2}} \quad (12-45)$$

Expression (12-42) is the required current diagram equation, according to which, when $\dot{U}_{ec} = \text{const}$ and $E_m = \text{const}$, the magnitude and the direction of the current vector are defined by the value of the angle θ .

Non-Salient-Pole Machine. In a non-salient-pole machine $x_q = x_d$ and, therefore, $R_U = 0$ and

$$\dot{I} = \dot{M} + \dot{R}_E e^{-j\theta} \quad (12-46)$$

where

$$\dot{M} = \frac{U_{ec}}{x_d} e^{-j\frac{\pi}{2}} \quad \text{and} \quad \dot{R}_E = \frac{E_m}{x_d} e^{j\frac{\pi}{2}} \quad (12-47)$$

From equation (12-46) it follows that as θ changes within the limits of 0 to 2π , the end of the current vector describes a circle whose centre is determined by vector M , while $R_E = E_m : x_d$ determines the magnitude of the radius vector. The diameter of the circle is, therefore, proportional to the e.m.f. produced by the excitation current.

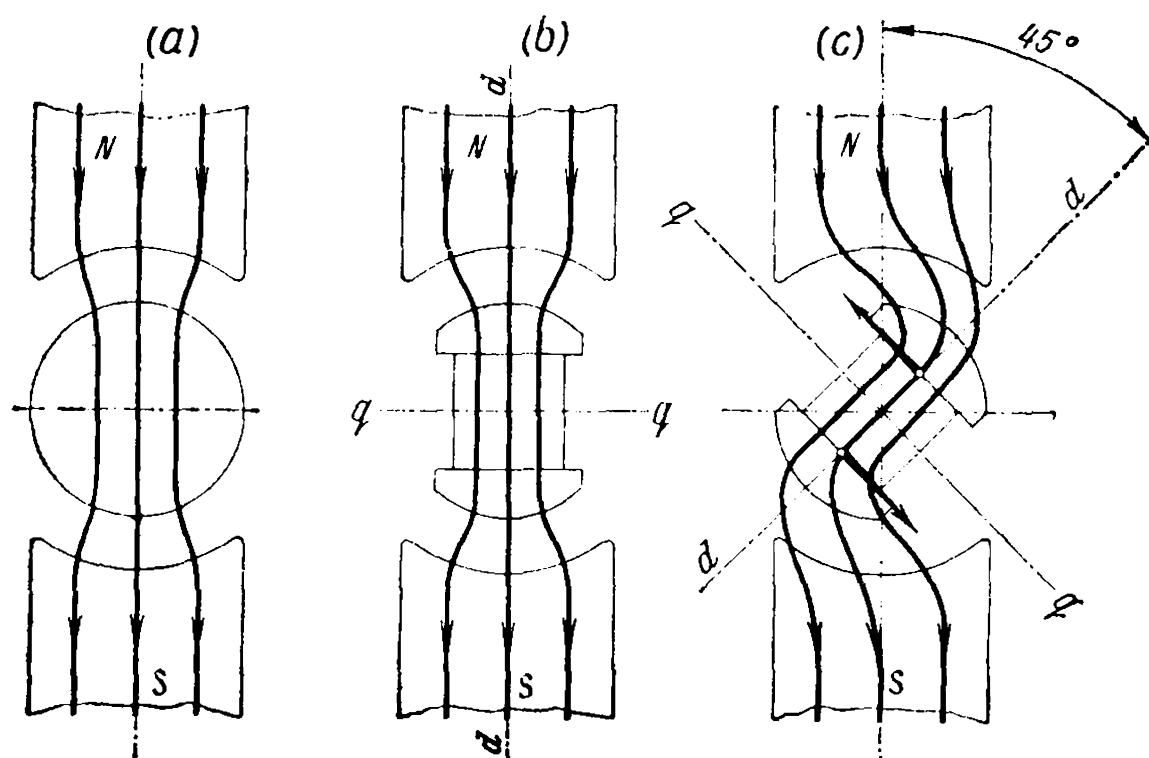


Fig. 12-19. Model of operation of a reaction synchronous machine

rotor (Fig. 12-19a) no reactive torque is developed because of the indifferent position of the rotor relative to the stator field.

The magnetic field of a reaction machine is produced only by the armature-reaction magnetic flux, whence the name given to this machine. Such a machine draws the reactive (lagging) current required for producing its magnetic field from the external circuit and operates with a low power factor ($\cos \varphi$). Figure 12-20 shows a vector diagram of a reaction motor. In a reaction machine $E_m = 0$ and, according to equation (12-45), $R_E = 0$. Equation (12-42) of the current diagram, therefore, becomes

$$\dot{I} = \dot{M} + \dot{R}_L e^{-j\theta} \quad (12-48)$$

The current diagram of a reaction machine according to equation (12-48) is a circle, the complete circle corresponding to a change in θ from 0 to π , and the change in θ from $\theta = \pi$ to $\theta = 2\pi$ corresponding to an identical circle superposed on the first one. Physically this is explained by the fact that the poles of a reaction machine obtain a certain polarity only under the influence of the stator field, and a displacement of 180 electrical degrees of the rotor relative to this field does not, therefore, change the operating conditions of the machine.

Figure 12-21 shows a circle diagram of a reaction machine when $x_d : x_q = 2$. Power va-

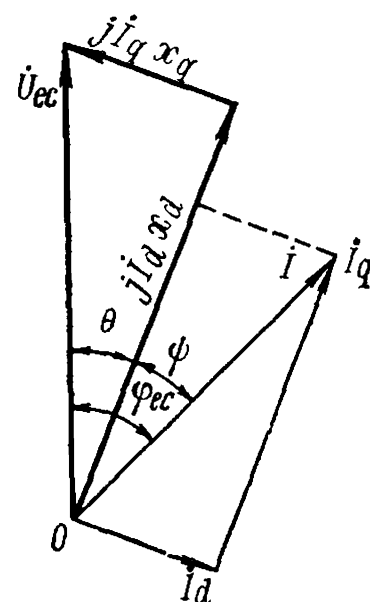


Fig. 12-20. Voltage diagram of a reaction synchronous motor

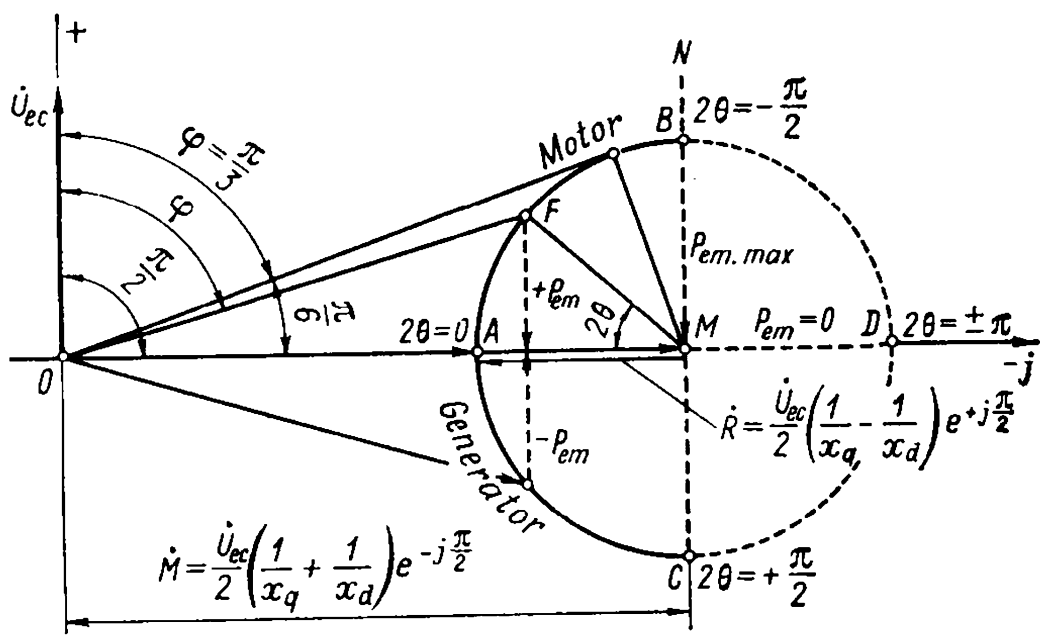


Fig. 12-21. Current circle diagram of a reaction synchronous machine

lues on this diagram are determined in the same way as on the diagram in Fig. 12-18.

The maximum power of a reaction machine is proportional to the circle radius R_U , and, according to equation (12-44), is the larger, the greater the ratio $x_d : x_q$. In reaction motors measures are taken to attain values as great as $x_d : x_q \cong 5$. For this purpose the rotor is assembled of steel laminations with non-magnetic strips, for example, aluminium, inserted between them (Fig. 12-22). At a given load, $\cos \varphi$ of a reaction motor is the higher, the greater the ratio $x_d : x_q$.

The no-load current of a reaction motor is

$$I_0 \cong \frac{U_{ec}}{x_d}$$

For ordinary salient-pole machines reactive operating conditions are, generally speaking, abnormal. If $x_d > 1$, however, such a machine may then, when $U_{ec} = U_r$, operate under reactive conditions and even carry a definite active load with $I = I_r$. Such conditions may

occur in a salient-pole machine carrying a small load when excitation disappears.

Single-phase reaction motors also find application. They are started by the induction method similar to capacitive induction motors (see Sec. 25-4).

Salient-Pole Machine. For an excited salient-pole machine, all the terms of equation

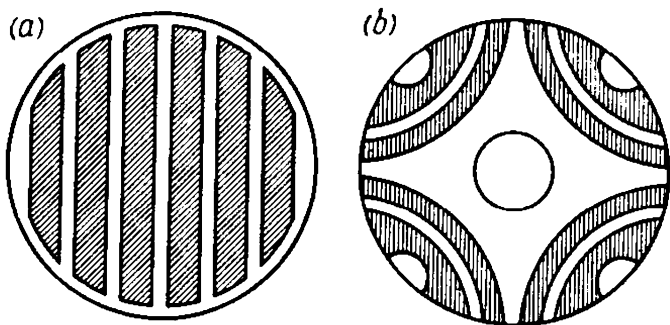


Fig. 12-22. Designs of a reaction synchronous machine rotor with:
a — number of poles $2p = 2$; b — $2p = 4$

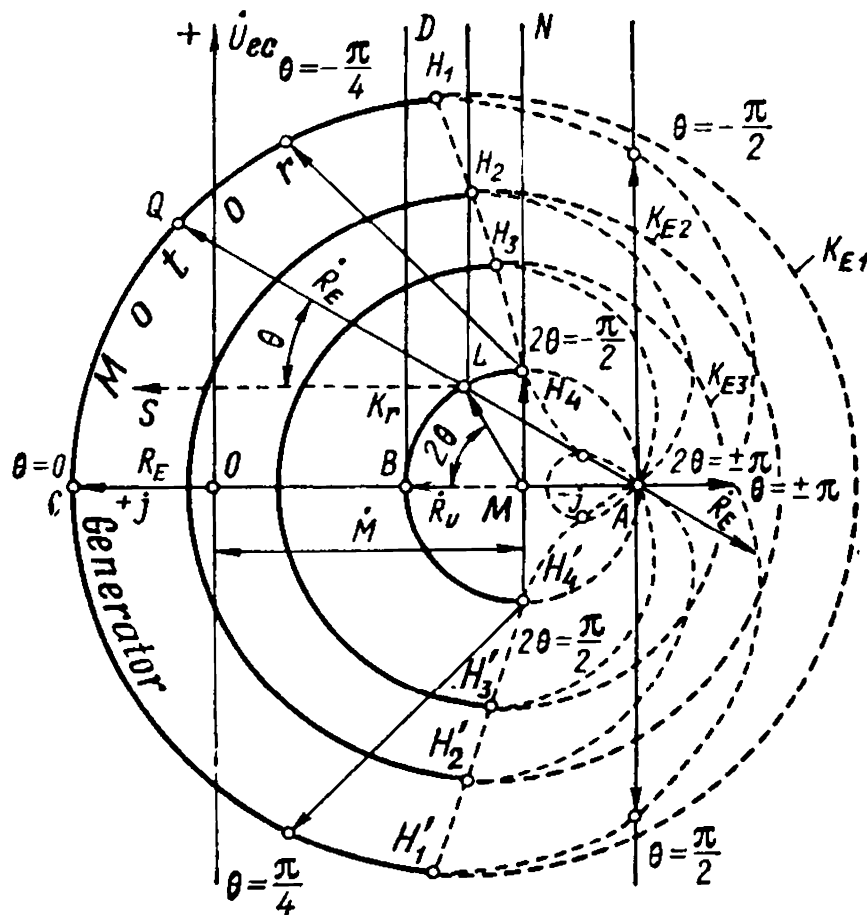


Fig. 12-23. Current diagram of a salient-pole synchronous machine

(12-42) are retained, and the current diagram acquires the form of a complicated curve called Pascal's limaçon. This diagram can be constructed as follows (Fig. 12-23).

First draw the voltage vector \dot{U}_{ec} along the vertical axis and lay off centre vector \dot{M} to the right of it at an angle $\frac{\pi}{2}$.

In the absence of excitation ($E_m = 0$), a salient-pole machine becomes a reaction machine, and equation (12-42) is converted to equation (12-48).

Now lay off vector \dot{R}_U to the left of vertical line MN at an angle $\frac{\pi}{2}$ to obtain point B , the position of the end of the current vector when $2\theta = 0$. By drawing the circle K_r with the radius R_U , we obtain a circle diagram of a salient-pole machine operating under reaction machine conditions.

Now, if we lay off vector \dot{R}_E to the right of the vertical line at an angle $\frac{\pi}{2}$, we obtain point C , the position of the current vector for an excited salient-pole machine when $\theta = 0$.

When the machine transfers to motoring at a definite value of the angle θ the radius-vector $\dot{R}_U e^{-j2\theta}$ turns counterclockwise from its

horizontal position MB through the angle 2θ to the position ML ; the radius-vector $\dot{R}_E e^{-j\theta}$ also turns counterclockwise from its horizontal position LS through the angle θ to the position LQ . Point Q defines the position of the end of the current vector for a given value of θ . From the above the following method of constructing the diagram is derived: the points L on circle K_r of a reaction machine which correspond to various values of θ are connected by a straight line, with point A on this circle corresponding to the angle $2\theta = \pm\pi$, and the values of radius-vector $R_E = LQ$ are then laid off on the extension of the straight lines.

The part of the current diagram above the axis of abscissas corresponds to motoring, and the part below the axis corresponds to generating duty.

Figure 12-23 shows three current diagrams corresponding to different values of the e.m.f. E_m .

When the excitation is decreased, the current diagram becomes smaller and, at $R_E < 2R_U$, a second inside loop of Pascal's limaçon appears inside the circle K_r .

The power P at the machine terminals and the electromagnetic power $P_{em} = P$ are determined from the diagram in Fig. 12-23 in the same way as from the diagrams in Figs. 12-18 and 12-21, i.e., from the scale value of the perpendicular dropped from the given point of the diagram onto the axis of abscissas. The scale m_p of the power here also equals $m_p = 3 U_{ec} m_i$.

If points $H_1, H_2, H_3, H_4, H'_1, H'_2, H'_3, H'_4$ on the current diagrams for different values of E_m and corresponding to the maximum values of the active current and power components are connected by a continuous curve, the latter will be the stability line, to the right of which conditions of unstable operation will exist. In the steady-state operation area the parts of the current diagram differ very little from the circles K_{E1}, K_{E2} and K_{E3} .

Chapter

13

SYNCHRONOUS MOTOR AND SYNCHRONOUS CONDENSER

13-1. Physical Aspects of Synchronous Machine Motoring Duty

When considering in Chapter 12 the operation of a synchronous machine connected in parallel with an external circuit, it was found that a machine can transfer from generating to motoring when the sign of the angle θ between the e.m.f. vector \dot{E}_m and the voltage vector \dot{U} changes. When a synchronous machine operates as a generator, the driving element is the rotor and the driven element is the resultant air-gap flux on the surface of the stator, which rotates in step with the rotor and in accordance with this the rotor flux axis leads the axis of the resultant flux $\dot{\Phi}_\delta$ by an angle θ' equal to the angle by which the internal e.m.f. \dot{E}_δ induced by the resultant flux $\dot{\Phi}_\delta$ lags behind the e.m.f. \dot{E}_m induced by the excitation flux (see Fig. 9-1). Under load the angle θ' differs from the angle θ between the excitation e.m.f. \dot{E}_m and the voltage \dot{U} by a small value due to the voltage drop in the resistance and the stator leakage reactance. For this reason, the magnetic lines in the air-gap, when load is carried, are not radially directed and the imaginary magnetic poles of the stator are shifted relative to the rotor poles as shown in Fig. 13-1a for generating duty.

If we gradually reduce the mechanical power applied to a generator shaft by the prime mover, the angles θ and θ' will begin to decrease. This will result in a reduction in the power delivered by the generator to the circuit which it is connected to.

When the angle θ and, together with it, the angle θ' become equal to zero (Fig. 13-1b), the generator will become completely unloaded, and the prime-mover will deliver the power required for covering the no-load losses to the generator. If we now disconnect the prime mover

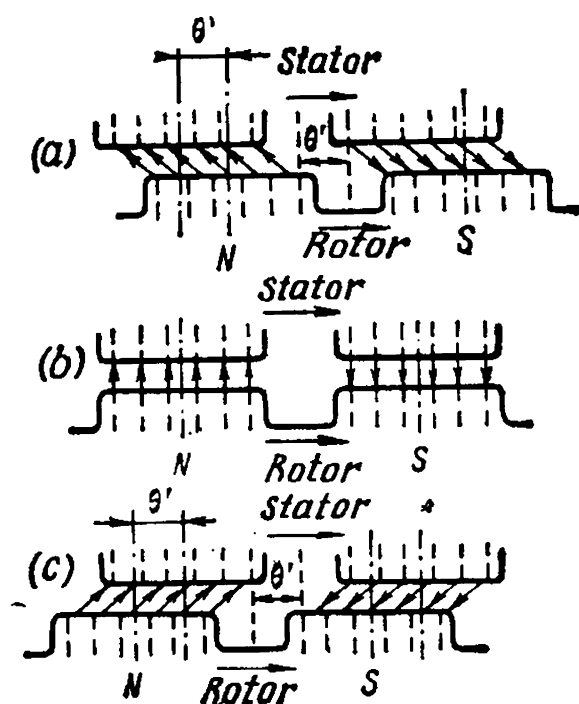


Fig. 13-1. Synchronous machine in various duties:

a — generating; b — at no-load; c — motoring

from the generator shaft, the angle θ' becomes negative, since the rotor begins to lag somewhat behind the stator flux, but the machine will continue to run in step with the resultant flux Φ_δ . The no-load losses of a synchronous machine will be balanced by the power taken from the external circuit, and the machine will operate as a synchronous motor at no-load. The driving element is now the stator flux, and the driven element, the rotor. If we load the shaft of a synchronous machine with an increasing breaking torque, the angle θ' , which has become negative, will grow with a corresponding increase in the mechanical power developed by the motor and in the electric power consumed by the motor from the power circuit via the stator (Fig. 13-1c).

Thus, if in generating duty a synchronous machine converts mechanical power obtained from the prime mover into electric power delivered to the external circuit connected to the stator winding, then in motoring duty, on the contrary, the synchronous machine converts electric energy received from the external circuit into mechanical power used by the working machine connected to the shaft of the synchronous machine. In both cases the synchronous speed determined by the power circuit frequency is retained. The maximum power which a synchronous motor can operate at without pulling out of step is a function, as in a generator, of the maximum overload capacity.

A very serious and difficult problem in the use of synchronous motors is the problem of starting and synchronizing them with the power supply circuit.

13-2. Powers and Torques of a Synchronous Motor

Let P_1 be the electric power delivered to a motor from the circuit. Part of this power is spent on covering the stator copper losses $p_{cop.s}$ and steel losses $p_{st.s}$, the remainder is the electromagnetic power P_{em} transferred from the stator to the rotor. Therefore,

$$P_{em} = P_1 - p_{cop.s} - p_{st.s} \quad (13-1)$$

The power P_{em} , less the mechanical friction and windage losses p_{mech} and the additional losses at the surface of the pole shoes p_{add} , is converted into useful power on the motor shaft, P_2 :

$$P_2 = P_{em} - p_{mech} - p_{add} = P_1 - p_{cop.s} - p_{st.s} - p_{mech} - p_{add} \quad (13-2)$$

If the exciter is on the same shaft as the motor, the useful power at the shaft of the motor-exciter unit is further decreased by the amount of power consumed by the exciter.

The electromagnetic torque of the motor is

$$M_{em} = \frac{P_{em}}{\Omega_{syn}} \quad (13-3)$$

where $\Omega_{syn} = 2\pi n$ is the synchronous angular speed of the rotor.

Since the transition from generating to motoring duty is called forth, as noted above, by a change in the sign of the angle θ between the e.m.f. vector \dot{E}_m and the voltage vector \dot{U}_{ec} , the expressions for the powers and torques of a synchronous machine in motoring duty can be obtained from the corresponding expressions for a generator by using the corresponding negative values of the angle θ . Here the power and torque for motoring duty, however, become negative, because the generator power was assumed to be positive when the formulas were deduced.

This change in the sign of the power indicates the change in the direction of power flow and the corresponding change in the duty. Manipulation with negative powers and torque is inconvenient, however, and this is why the power and the torque in motoring duty will be assumed positive in the discussions of synchronous motors. To obtain the required expression for the motor power or torque, substitute $-\theta$ for θ in the corresponding expression for generating duty and change the sign of the entire right-hand side of the expression, assuming that the angle θ for motoring duty is already positive.

Thus, from relations (12-24) and (12-25) for a non-salient-pole generator, we obtain for the electric power P_1 at the stator terminals of a non-salient-pole motor

$$P_1 = \frac{mU_{ec}}{z_d} [E_m \sin(\theta - \alpha) + U_{ec} \sin \alpha] \quad (13-4)$$

and for its electromagnetic power P_{em}

$$P_{em} = \frac{mE_m}{z_d} [U_{ec} \sin(\theta + \alpha) - E_m \sin \alpha] \quad (13-5)$$

When constructing the e.m.f. diagrams of synchronous machines, the losses in the steel and the additional losses are neglected, and they are consequently neglected in the expressions for electric and electromagnetic power. Keep this in mind when using these expressions.

For a salient-pole synchronous motor, neglecting the copper losses in the stator windings, from formula (12-11) we get

$$P_1 = P_{em} = \frac{mE_m U_{ec}}{x_d} \sin \theta + \frac{mU_{ec}^2}{2} \left(\frac{1}{x_q} - \frac{1}{x_d} \right) \sin 2\theta \quad (13-6)$$

When taking account of the stator copper losses and using formulas (13-4) and (13-5) for a salient-pole synchronous generator, we obtain

$$P_1 = \frac{mU_{ec}}{z_q} [E_q \sin(\theta - \alpha) + U_{ec} \sin \alpha] \quad (13-7)$$

$$P_{em} = \frac{mE_q}{z_q} [U_{ec} \sin(\theta + \alpha) - E_q \sin \alpha] \quad (13-8)$$

where

$$E_q = E_m - I_d(x_d - x_q) \quad (13-9)$$

is the equivalent e.m.f. of a salient-pole synchronous machine, if it is considered to be a non-salient-pole machine with a synchronous reactance x_{syn} equal to x_q of the salient-pole machine under consideration (see Fig. 9-6, where $E_q = OB$, and Fig. 13-2a and b).

Correspondingly, for the synchronizing power coefficient of a non-salient-pole synchronous motor, with account taken of the stator copper losses and using formula (12-25) for a generator, we have

$$P_{syn} = \frac{dP_{em}}{d\theta} = \frac{mE_m U_{ec}}{z_d} \cos(\theta + \alpha) \quad (13-10)$$

and for a salient-pole motor

$$P_{syn} = \frac{mE_q U_{ec}}{z_q} \cos(\theta + \alpha) \quad (13-11)$$

For a salient-pole motor without account of the stator copper losses we get

$$P_{syn} = \frac{mE_q U_{ec}}{x_q} \cos \theta + mU_{ec}^2 \left(\frac{1}{x_q} - \frac{1}{x_d} \right) \cos 2\theta \quad (13-12)$$

13-3. Voltage Diagrams of a Synchronous Motor

By using the e.m.f. diagrams of a salient-pole synchronous machine (Fig. 9-6) it is not difficult to construct the e.m.f. diagrams for salient-pole synchronous motors. The only difference is that when an e.m.f. diagram for a synchronous motor is being constructed, we do not plot on the diagram the voltage vector \dot{U} which the synchronous machine acts with on the power circuit and which is a component of the e.m.f. \dot{E}_m , but we plot the vector of the circuit voltage \dot{U}_{ec} opposite to it in direction, which the circuit acts with on the machine. The circuit voltage vector \dot{U}_{ec} is resolved into components of the voltage drops, as a result of which we obtain on the diagram the vector $-\dot{E}_m$ opposite to the e.m.f. vector \dot{E}_m due to the excitation flux, and which is the component of the circuit voltage balancing the e.m.f. \dot{E}_m . The vectors \dot{E}_m and \dot{U} are usually not shown on the diagram.

Figure 13-2a contains a vector diagram for a loaded synchronous motor with the load current \dot{I} lagging behind the vector \dot{U}_{ec} of the applied voltage by the angle φ , at which the motor is underexcited and induces with respect to the circuit voltage \dot{U}_{ec} an inductive current component $\dot{I} \sin \varphi$. An underexcited motor thus draws an inductive current and the corresponding reactive power from the line.

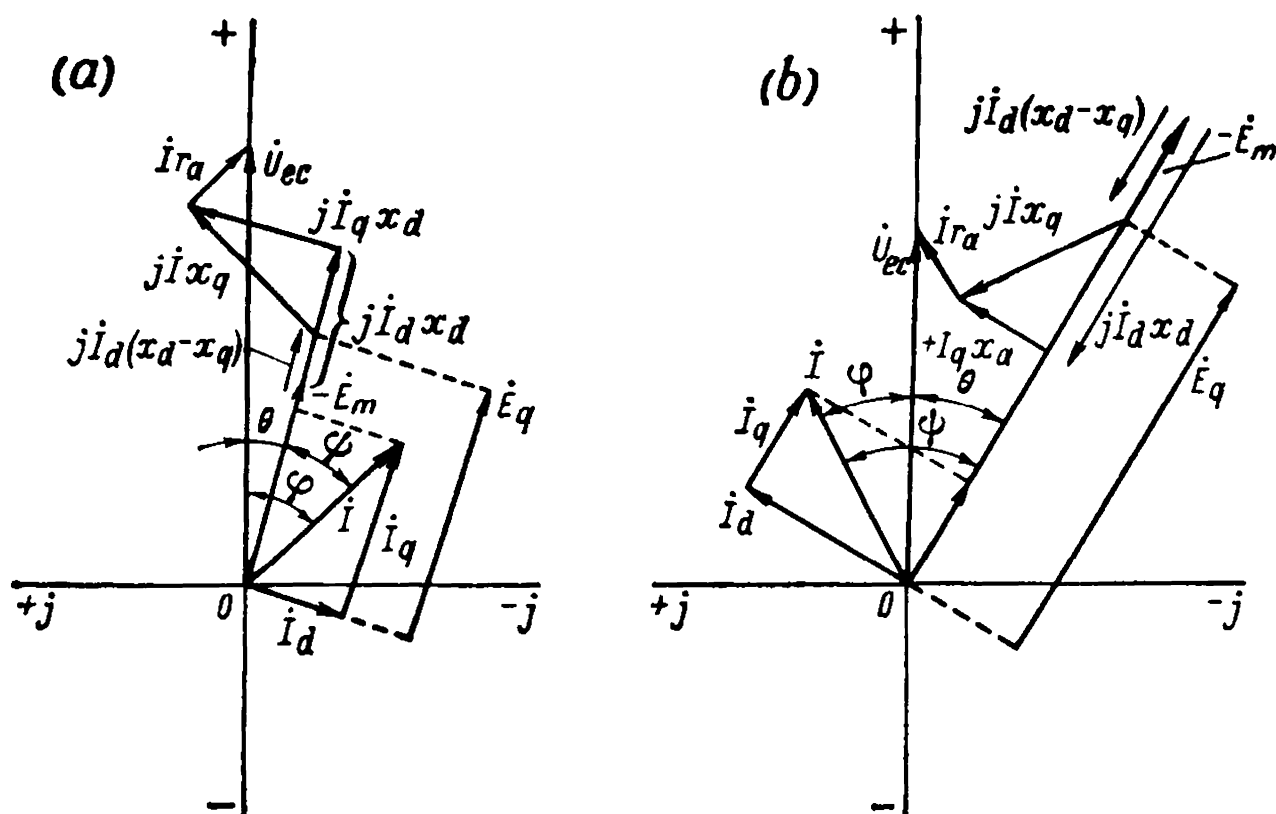


Fig. 13-2. Voltage diagrams of a synchronous motor:
 a — underexcited; b — overexcited

Figure 13-2b presents the corresponding diagram for a load current I leading the vector \dot{U}_{ec} of the applied voltage by the angle φ at which the motor is, conversely, overexcited and induces with respect to the line voltage \dot{U}_{ec} a capacitive current component $I \sin \varphi$. An overexcited motor, consequently, draws a leading current from the circuit and delivers reactive power to it.

13-4. Synchronous Motor Operating from High-Capacity Power System

Consider the operation of a synchronous motor when connected to a high-capacity system ($U_{ec} = \text{const}$, $f = \text{const}$) provided that the load on the motor shaft remains invariable ($M = \text{const}$) and the excitation current of the motor is varied ($i_{exc} = \text{var}$).

The operation of a synchronous motor under such conditions can be investigated, in a manner similar to the corresponding operation of a synchronous generator, on the basis of the simplified vector diagram, with which, neglecting the resistance of the stator winding, it may be assumed that the applied voltage vector \dot{U}_{ec} is equal in magnitude and opposite in phase to the e.m.f. vector \dot{E}_{res} due to the resultant flux Φ_{res} produced by the combined action of the stator and rotor magnetizing forces.

It should be noted, further, that since the electromagnetic power of a synchronous motor is

$$P_{em} \cong \frac{mE_m U_{ec}}{x_d} \sin \theta$$

the motor, when overexcited due to an increase in E_m , will have an increased P_{max} and, consequently, an increased overload capacity. It is necessary, however, to note that the motor will take a greater stator current, therefore motors intended for operation with overexcitation are somewhat heavier and more costly and have somewhat lower efficiencies than motors intended for operation with $\cos \varphi = 1$. Since motors of a given size, in conformance with temperature-rise conditions, practically retain their full power $P = mU_{ec}I$ even at overexcitation, their useful power $P_2 = \eta mU_{ec}I \cos \varphi$ correspondingly decreases.

Modern standard synchronous motors are rated for normal operation at $\cos \varphi = 1$ and $\cos \varphi = 0.8$ (leading).

13-5. Performance Characteristics of a Synchronous Motor

When a synchronous motor is supplied from an external circuit with $U_{ec} = \text{const}$ and $f = \text{const}$, and with constant excitation, its performance characteristics, which are the relation of the primary power P_1 , stator current I , efficiency η and power factor $\cos \varphi$ to the useful shaft power P_2 , have the form shown in Fig. 13-4, which is a case when $\cos \varphi = 1$ at no-load. When the load grows, the power factor $\cos \varphi$ of the motor, with $i_{exc} = \text{const}$, decreases somewhat. The efficiency of the motor rises to a certain maximum value and then begins to fall. The current at no-load and $\cos \varphi = 1$ is very low and corresponds to the no-load losses; with an increase in load the current grows almost linearly.

Figure 13-5 shows the characteristics $\cos \varphi = f\left(\frac{P_2}{P_r}\right)$ for different values of $\cos \varphi$ and at no-load. Synchronous motor operating conditions can be adjusted by changing the excitation current so that it gives the power factor $\cos \varphi = 1$ at the desired load. Curve 1 in Fig. 13-5 corresponds to $\cos \varphi = 1$ at no-load, curve 2 to $\cos \varphi = 1$ with $\frac{P_2}{P_r} = 0.5$, and curve 3 to $\cos \varphi = 1$ with $\frac{P_2}{P_r} = 1.0$. The greater the excitation of a synchronous motor, the higher the value of the leading no-load current and the greater the load at which $\cos \varphi = 1$ is reached.

The overload capacity of a synchronous motor, as well as of a synchronous generator, if we neglect the torque component due to

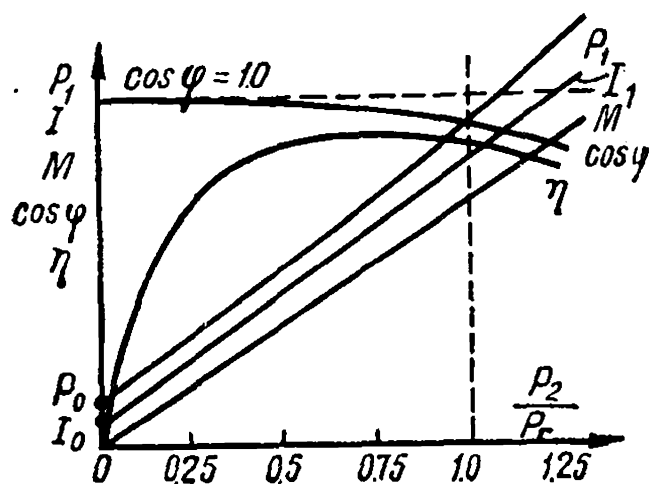


Fig. 13-4. Performance characteristics of a synchronous motor

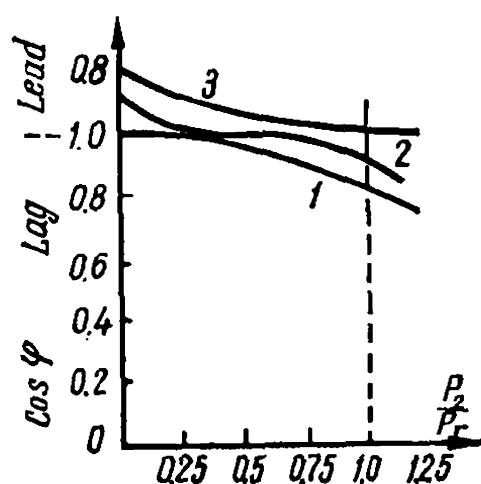


Fig. 13-5. Characteristics of $\cos \varphi = f\left(\frac{P_2}{P_c}\right)$ for different values of the excitation current

salient-pole design, is equal to:

$$k_{ov} = \frac{1}{\sin \theta_r}$$

In modern motors at the rated load the angle $\theta_r = 20$ to 30° and, consequently, $k_{ov} = 2$ to 3 .

13-6. Methods of Starting Synchronous Motors

Starting by Means of Auxiliary Motor. The synchronous motor and the synchronous condenser, the latter being in principle a synchronous motor operating at no-load under conditions of overexcitation, can be connected to a power circuit with the aid of a synchronizing device in the same way as a synchronous generator. For this purpose the machine must have a special starting motor on its shaft, capable of bringing it up to the synchronous speed at which synchronizing with the power circuit is possible. A comparatively low-power induction motor is generally used as the auxiliary motor. It has the same number of poles as the synchronous machine. With the help of this motor, the synchronous machine is accelerated to almost synchronous speed, after which the machine is switched in for parallel operation by the self-synchronization method.

Formerly, an induction motor was also used for this purpose with one pair of poles less than the synchronous machine, and it could thus accelerate the machine to a speed even somewhat higher than the synchronous speed. When the auxiliary motor was disconnected from the line, the machine began to slow down, smoothly passing through synchronous speed, thus permitting the synchronous machine to be connected to the circuit at the appropriate instant.

The disadvantage of this method is the impossibility of starting the motor under load, since it is unpractical to have a large starting

motor complicating and increasing the cost of the installation. This method is, therefore, used mainly for motor-generators which convert alternating current into direct current and can be started by a d.c. machine by using the generator at starting under motoring conditions; this method can also be used in high-power synchronous condensers.

Frequency-Change Starting. A synchronous motor may be started by this method when the frequency of the voltage applied to the motor is smoothly changed from zero to the rated value. The motor runs synchronously during the entire starting period.

When started by this method, the motor is fed from a separate synchronous generator whose speed is changed with the aid of a prime mover from zero to the rated value. The excitation of the generator and the motor for this method of starting cannot be ensured by means of exciters mounted on the same shaft, since they are not self-excited at low speeds.

For the motor to start running synchronously from the zero speed, the excitation currents of the generator and motor should be properly adjusted, and the rate of rise in the frequency should not be too high. Investigation of this problem indicates that the generator should have as large an excitation current as possible during the initial period of starting, and the motor excitation current at synchronous speeds should be of such a magnitude that the motor e.m.f. induced by it be approximately half the generator e.m.f. As the speed grows, the excitation current of the motor should be increased.

Frequency-change starting of synchronous motors is used in special installations.

Asynchronous Starting. General. A synchronous motor which has a starting cage on its rotor (see Sec. 1-5) can be started as a squirrel-cage induction motor. Asynchronous starting is today the main method of starting synchronous motors.

The field winding of a synchronous motor, with asynchronous starting, should be short-circuited or closed via a resistance whose value is about ten times that of the resistance of the field winding itself. If the latter were left open when the motor is started, such a high voltage would be induced across its terminals, owing to the great number of turns in the winding, that it could lead to a breakdown of the insulation.

With asynchronous starting, the stator winding of the synchronous motor is connected to an a.c. supply mains, a torque is developed in the motor (see Sec. 1-8), and it accelerates the motor to a speed close to a synchronous one. It runs similarly to an induction motor with some degree of slip or lagging behind the speed of the rotating magnetic field. If we now switch in direct current to the field winding, the presence of the constant-polarity poles results in periodic variations of the rotor speed phase swinging in relation to its average speed, and

it becomes possible at some moments not only to attain the synchronous speed, but also to exceed it for short intervals.

If the motor has attained such a speed, then after several decaying phase swingings it is pulled into step near the synchronous speed. The less the motor is loaded, the smaller is its slip relative to the synchronous speed and the easier is it pulled into synchronism under such swingings. Salient-pole motors at no-load and under a small load are frequently pulled into step without even applying the excitation, by virtue of the reactive torque. Conversely, with a load, the slip increases and the motor is pulled into step with greater difficulty. Thus, there exists a certain limiting braking torque depending on the so-called pull-in torque of the motor at which the motor is capable of pulling into step.

Thus, synchronous motors started as induction motors have the following three characteristic torques:

1. The *starting torque* M_{st} developed by the motor at standstill (slip $s = 1$).

2. The *pull-in torque* M_{pi} by which is meant the induction motor torque developed by the motor at 95% synchronous speed (slip $s = 0.05$).

3. The *maximum* or *pull-out torque* M_{max} corresponding to the maximum output of the motor at the synchronous speed and at rated voltage and excitation, and above which the motor falls out of step.

As indicated in Sec. 1-10, the torque of an asynchronous motor can be expressed in the following simplified form:

$$M = \frac{kE_2sr_2}{r_2^2 + (sx_2)^2}$$

It should be recalled that in this formula k is a proportionality factor; E_2 is the rotor e.m.f. at $s = 1$; s is the slip; r_2 and x_2 are the resistance and leakage reactance, respectively, of the rotor at standstill.

When the slip $s = 1$, the starting torque

$$M_{st} = \frac{kE_2r_2}{r_2^2 + x_2^2}$$

The maximum (pull-out) torque is obtained at a slip $s = \frac{r_2}{x_2}$ and is equal to

$$M_{max} = \frac{kE_2}{2x_2}$$

A more precise expression for the torque M_{max} of an induction machine is given in Sec. 20-3.

Thus, the maximum torque does not depend on the resistance r_2 of the starting winding; the resistance only influences the value of the slip $s = s_{max}$ at which the torque reaches its maximum.

Figure 13-6 shows the relation $M = f(s)$ with $x_2 = \text{const}$ and various values of the rotor resistance:

$$r_2' < r_2'' < r_2'''$$

When $r_2 = x_2$ (curve 3 in Fig. 13-6), the starting torque ($s = 1$) becomes equal to the maximum torque.

Depending on the operating conditions and the designation of the drive, various values of the starting and pull-in torques will be required.

For a drive with the braking torque increasing with speed, a low initial torque is required, but the pull-in torque must be considerably higher. Fans, for example, require the following torques

$$M_{st} = (0.2 \text{ to } 0.25) M_r \quad \text{and} \quad M_{pi} = M_r$$

For a drive with great friction at low speed, owing to its heavy masses, a greater starting torque is required, but since the motor may be pulled into step with the drive running light, the pull-in torque can be low. For instance, for a continuous non-regulated rolling-mill

$$M_{st} = (0.5 \text{ to } 1.0) M_r \quad \text{and} \quad M_{pi} \cong 0.4 M_r$$

Usually with a high pull-in torque M_{pi} a low starting torque M_{st} is required, and, conversely, with a high starting torque M_{st} a low pull-in torque M_{pi} is required. Consequently, a change in these relations can be attained by selecting the proper material for the starting cage.

To obtain high starting torques, a high resistance and adequate heat capacity of the cage are required. The cage is therefore made of brass, aluminium bronze or similar alloys. Since in this case, owing to the increased resistance of the starting cage, the slip s_{max} is greater, the pull-in torque is reduced and the motor is pulled into step with greater difficulty. If, on the contrary, the starting cage is made of low-resistance red copper, the motor will have a low starting torque and slip during the asynchronous steady-state running period, owing to which the pull-in torque is increased. The nature of the relation of the asynchronous starting-cage torque to the slip s is presented in Fig. 13-6 by curve 2 for the first case and by curve 1 for the second case.

Table 13-1 gives data for the "Elektrosila" Works synchronous motors of the 14th frame size for various numbers of poles, 3000 V and $\cos \varphi = 0.8$ (leading current) when the motor is started across the line.

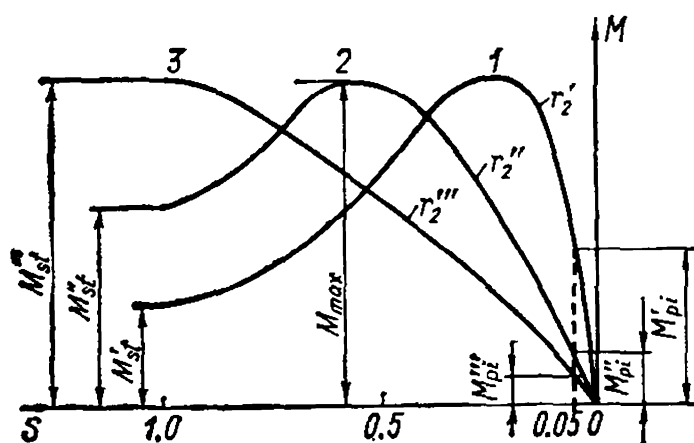


Fig. 13-6. Torque curves of synchronous motor starting winding

TABLE 13-1

Values	Pole pairs 2 <i>p</i>						
	4	6	8	10	12	14	16
<i>P</i> (kW)	360	285	220	182	148	115	93
<i>I</i> _{st} / <i>I</i> _r	5	5.2	5.1	4.6	4 0	3.9	3.8
<i>M</i> _{st} / <i>M</i> _r	2	2.3	2.4	2.6	1.8	1.4	1.3
<i>M</i> _{pi} / <i>M</i> _r	0.72	0.9	0.85	0.8	0 75	0.78	0.8
<i>M</i> _{max} / <i>M</i> _r	2.05	2.2	2.25	2.25	2 3	2.5	2 5

If it is desirable to reduce the starting current, this can be done by lowering the voltage across the terminals when starting. The current decreases in proportion to the voltage applied to the motor terminals, while the starting torque decreases as the square of the voltage (see Sec. 20-6).

13-7. Features of Asynchronous Starting of Synchronous Motors

Let us consider in greater detail the physical aspects of the motor starting process and its pulling into synchronism, assuming the motor field winding circuit to be closed and the starting winding unsymmetrical owing to the salient-pole design of the rotor.

Uniaxial Torque in Asynchronous Starting. A three-phase synchronous motor with a closed field winding, in the absence of a starting winding, is, with respect to starting, a motor with a three-phase primary winding and a single-phase secondary one. The latter produces a single-phase pulsating field which, in accordance with the general rule, can be resolved into direct and reverse travelling fields relative to the rotor system.

The pulsating rotor field, with a frequency $f_2 = sf_1$, produces one field which rotates in the direction of rotor rotation, and another field which rotates in the opposite direction. The speed of each field relative to the rotor is $n_1 - n$, where n_1 is the speed of the stator field, and n is the rotor speed.

The first (direct travelling) field has the speed

$$n_d = n + (n_1 - n) = n_1$$

with respect to the stationary stator winding, i.e., this field rotates in synchronism with the field produced by the stator winding at all speeds of the rotor.

The second field has the speed

$$n_{rev} = n - (n_1 - n) = 2n - n_1 = 2n_1 (1 - s) - n_1 = n_1 (1 - 2s)$$

with respect to the stationary stator winding. This field produces in the stator winding a current with the frequency

$$f' = pn_{rev} = pn_1(1 - 2s) = f_1(1 - 2s)$$

the frequency, at a slip of $s = 0.5$, becoming $f' = 0$.

Thus, at a rotor speed equal to one-half of the field speed, a counter-synchronous field is produced, stationary with respect to the stator winding, i.e., it has a frequency $f' = 0$. But, if the rotor has a speed somewhat less than $\frac{n_1}{2}$, a current is induced in the rotor winding with a frequency $f_2 > \frac{f_1}{2}$ and the counter-synchronous rotating field produced by this current will therefore rotate relative to the stator winding in a direction opposite to that of rotor rotation and of the main rotating field. Conversely, if the rotor speed is somewhat greater than $\frac{n_1}{2}$, the frequency $f_2 < \frac{f_1}{2}$ and the counter-synchronous field will rotate in the direction of rotor rotation and of the main rotating field. If in both cases the rotor speed n is close to half the synchronous speed $\frac{n_1}{2}$, low-frequency currents will be induced in the stator winding. These currents interacting with the counter-synchronous rotor field will produce appreciable additional asynchronous torques.

In the first case, when $n < \frac{n_1}{2}$, this additional torque will pull the motor in the direction of rotor rotation, and therefore have the nature of a motor torque. In the second case, when $n > \frac{n_1}{2}$, this torque will be directed against rotor rotation and have the nature of a braking torque. When $n = \frac{n_1}{2}$, the counter-synchronous field becomes stationary with respect to the stator winding, no additional currents are induced in it and the additional torques disappear.

The torque produced by the direct travelling field of the field winding is a motoring torque at all slips from $s = 1$ to $s = 0$. The value of this torque in the region of $s = 0.5$ also greatly decreases, however, since the reverse travelling field of the field winding is not damped by the additional stator currents. Therefore the resultant reactance of the field winding at $s = 0.5$ is high and the currents in it decrease.

The result is that the curve showing the relation between the torque M_{add} of the field winding and the slip has the form depicted in Fig.13-7a. The rotor of a motor not provided with a starting winding, even when it is started without load would not be able to develop a speed above half the synchronous one due to such a nature of the field winding torque. This phenomenon is called *uniaxial starting*.

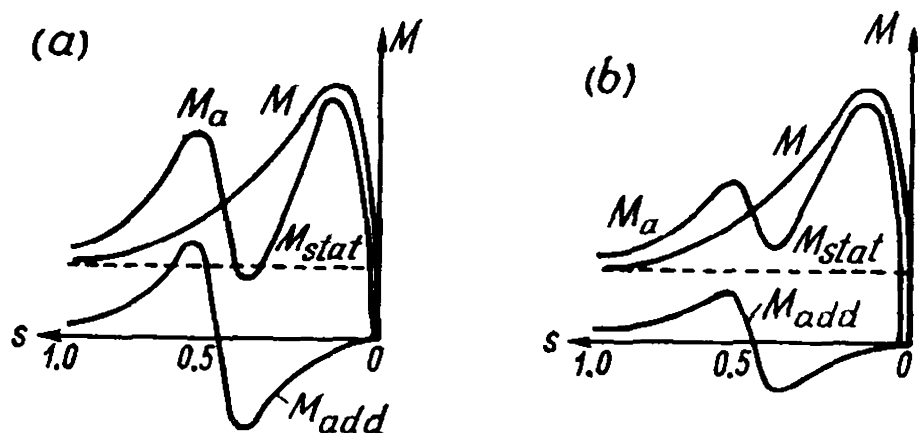


Fig. 13-7. Synchronous motor torque curves for asynchronous starting:

a — short-circuited field winding;
b — field winding closed through a resistance

With a starting winding present and the field winding short circuited, the uniaxial starting reveals itself in the form of a considerable distortion of the resultant torque curve M_a (Fig. 13-7*a*). With a large static braking torque M_{stat} on the shaft of the motor, the latter also cannot develop a speed exceeding half the synchronous speed. On the other hand, starting of a motor with the field winding open is impermissible because of the large e.m.f.s induced in the winding, which may damage its insulation, the slip rings, etc., and are also a hazard for the attending personnel. Therefore, when starting a motor under considerable load (approximately when $M_{stat} > 0.35 M_r$), it is necessary to short-circuit the field winding via an additional resistor during the starting period. A field discharge resistor, if available, can be used for this purpose (see Sec. 12-2).

When an additional resistor is inserted into the field winding circuit, the current induced in it decreases and brings about a decrease in the influence of the field winding torque. Practice shows that an additional resistance 5 to 10 times greater than the resistance of the field winding reduces the uniaxial starting phenomenon so that it does not present any special danger to the motor stopping its acceleration at speeds of $n \cong \frac{n_1}{2}$. Figure 13-7*b* pictures torque curves for the case when

an additional resistor is inserted into the excitation circuit. Here the field winding torque M_{add} decreases and the resultant torque M_a at the dangerous part is above the braking shaft torque M_{stat} , owing to which the motor can safely reach a speed close to synchronism.

The dip in the torque curve shown in Fig. 13-7 is also due to asymmetry of the starting winding of a salient-pole motor, since the currents of the starting winding because of this asymmetry also produce a magnetic field with an oppositely rotating component. If the bars of the starting winding are short-circuited by means of solid rings, however, this field and its effect are relatively small.

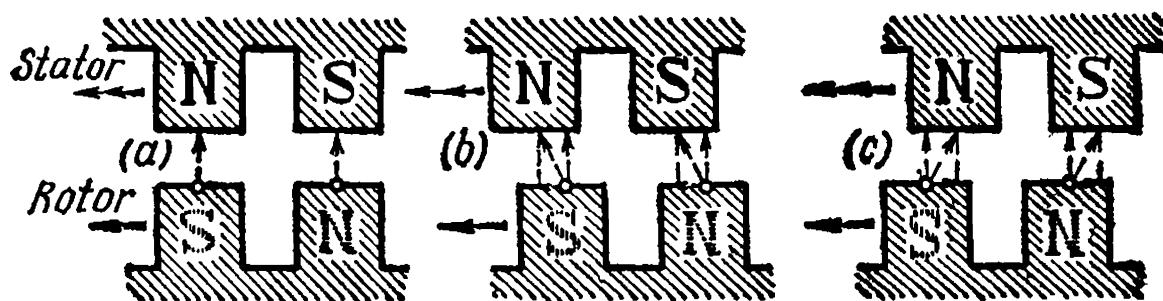


Fig. 13-8. Process of pulling an unexcited synchronous motor into synchronism

Pulling into Synchronism in Asynchronous Starting. Let us now consider the process taking place when a motor comes into synchronism. Under the influence of the asynchronous torque, the motor, when started under load, reaches approximately 95% of the synchronous speed and continues to run with a slip of $s \cong 0.05$ lagging behind the speed of the rotating field.

Suppose, at first, that the motor has no d.c. excitation. We can conceive the magnetic field as a permanent magnet pole system running at synchronous speed. At the moment when the axes of the salient rotor poles coincide with the axes of the rotating field poles, only radial attraction takes place. Since a machine always has an even number of poles, all the radial forces are balanced, and, therefore, no resultant effect is obtained (Fig. 13-8a).

Suppose now that the rotor poles lag somewhat behind the rotating field poles. As a result, a non-radial attraction force appears between the poles. This force can be resolved into its radial and tangential components (Fig. 13-8b). The radial component will be counter-balanced and give no effect, while the tangential component acting in the direction of rotor rotation produces an additional positive acceleration which increases its speed. If, owing to the difference in speed between the rotating field and the rotor, the rotor poles will somewhat lead the rotating field poles (Fig. 13-8c), then by resolving the force of attraction between the poles into its radial and tangential components, we shall find that the latter acts in the direction opposing rotor rotation and causes the appearance of a negative acceleration which lowers the rotor speed.

Hence, positive and negative variations in the rotor speed will be superposed on the average speed, causing fluctuations in the rotor speed under the influence of a reactive torque which is due to the salient-pole system on the rotor (Fig. 13-9, curve 1).

If we now allow a current to flow through the field winding (Fig. 13-10), the rotor poles will acquire a definite polarity, and the oscillatory process will proceed in a somewhat different manner. Here the rise in speed will occur only when the lagging rotor poles have a polarity opposite to that of the leading poles of the rotating field (Fig. 13-

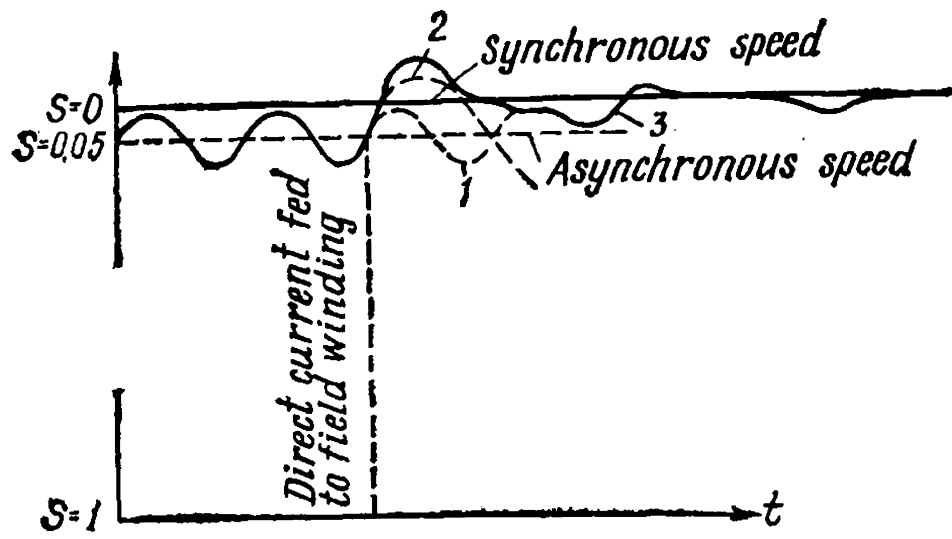


Fig. 13-9. Dependence of slip on the duration of starting a synchronous motor when pulling into synchronism fails to take place

10a), but when the polarity of these poles is identical, repulsion will take place with consequent slowing-down of the speed (Fig. 13-10c). Correspondingly, if the rotor poles lead the poles of the rotating field and have opposite polarity, mutual attraction and reduction of the speed will take place (Fig. 13-10b), but when they have the same polarity, repulsion and a rise in speed will take place (Fig. 13-10d).

The frequency of the accelerating and retarding pulses in the presence of excitation will be half that without excitation, owing to which the period of oscillations T will be two times greater (Fig. 13-9, curve 3) than in the first case (Fig. 13-9, curve 1). Owing to the greater period and greater pulse, the increase and decrease of the speed will be greater than in the first case. For this reason, the machine, fluctuating about the average asynchronous speed, will have a better chance of attaining the synchronous speed and even of exceeding it at certain

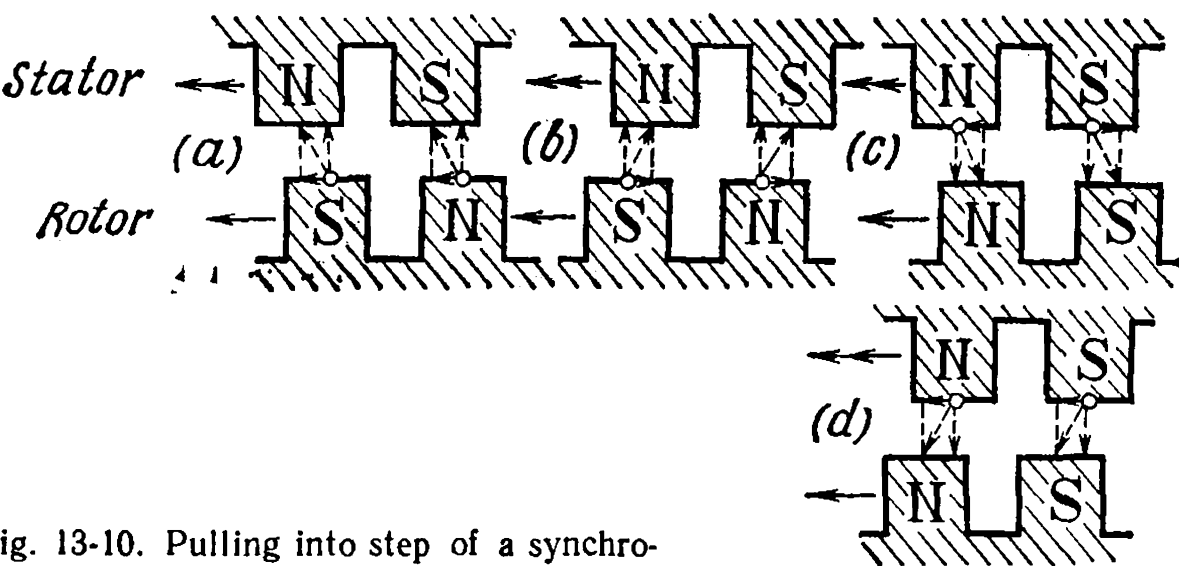


Fig. 13-10. Pulling into step of a synchronous motor

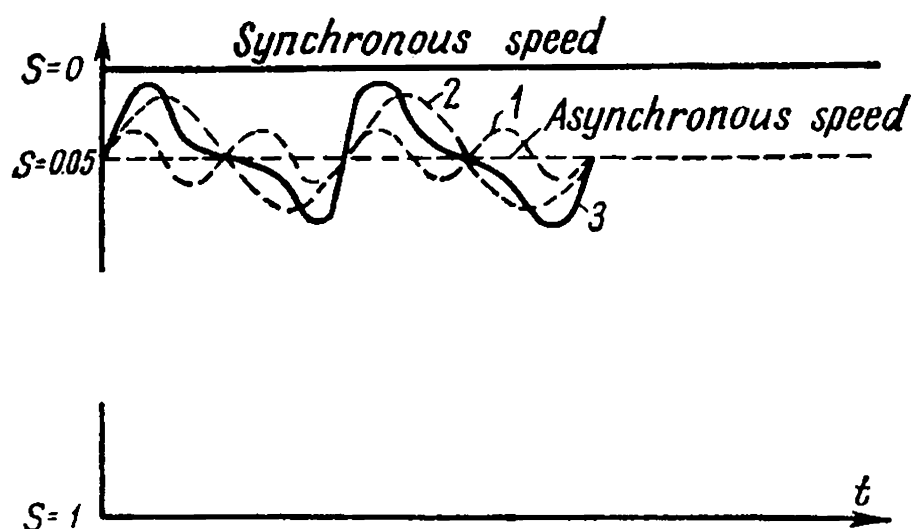


Fig. 13-11. Relation between slip and duration of asynchronous starting with pull into synchronism

moments. The resultant speed curve in the presence of salient poles (Fig. 13-9, curve 2) gives rise to a greater swing than with a non-salient-pole system, therefore, an excited machine is more easily pulled into step in the first case than in the second.

If during these fluctuations the speed of the rotor exceeds the synchronous one, then, when it slows down and passes through the synchronous speed, the synchronizing torque which holds the motor in synchronism will come into action, and rapidly damping oscillations follow (Fig. 13-11). After the oscillations are damped, the motor operates in synchronism with greater stability, since the maximum torque M_{max} , as seen from Table 13-1 containing data on several synchronous motors, is much greater than the pull-in torque M_{pi} .

Dynamics of the Motor Synchronizing Process. Let us consider in more detail the dynamics of the pull-in process of a rotor. Consider first the torques acting on the rotor.

From the moment the excitation current starts flowing at the end of the starting period, the electromagnetic torque M_{em} appears owing to the interaction between the excitation current and the stator current. This torque is determined by an expression of the type (12-16). It should be kept in mind that the rotor does not run in synchronism and the angle θ between the e.m.f. vector \vec{E}_m and the voltage vector \vec{U} therefore continuously changes. For simplicity, assume that we are dealing with a non-salient-pole synchronous motor. The expression for the torque M_{em} can then be written in the form

$$M_{em} = M_{max} \sin \theta$$

Besides, during the starting period, since the rotor does not run in synchronism with the stator magnetic field, it is already acted upon by the asynchronous torque M_a considered above (Fig. 13-7), depending on the slip s . When $s=0$, the angle $\theta = \text{const}$, and, conversely,

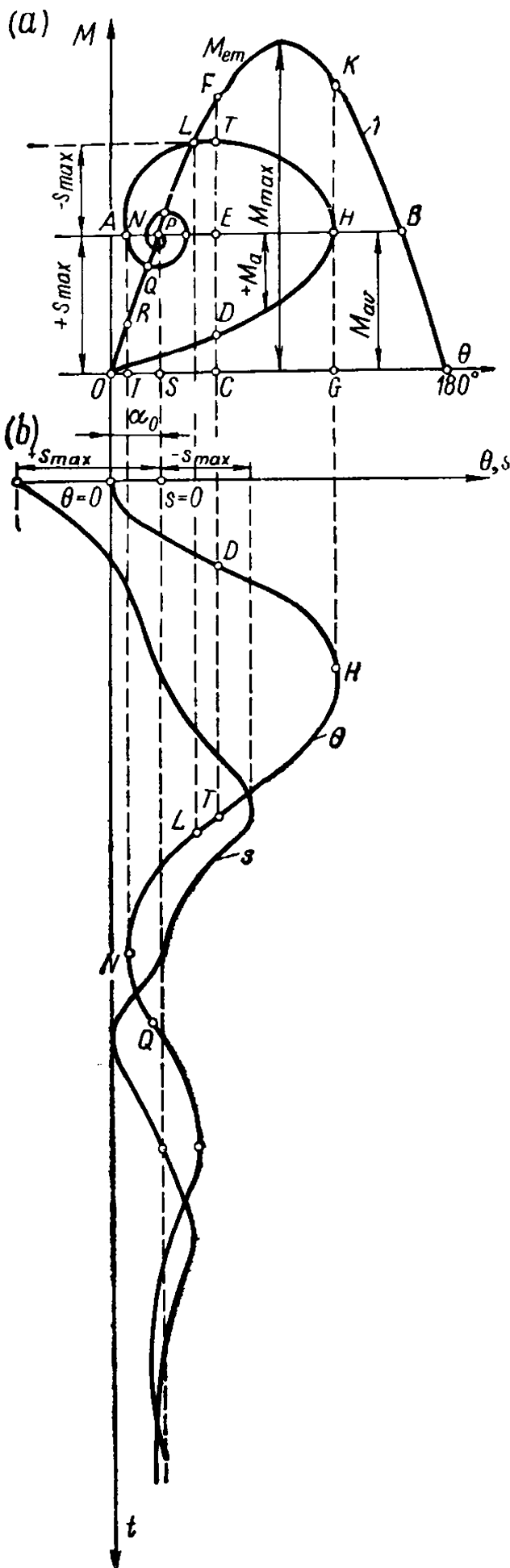


Fig. 13-12. Pulling into step of a synchronous motor with a moderate load on its shaft

the greater the slip s , the faster the change in θ . Therefore, s is proportional to $\frac{d\theta}{dt}$ and, since at low values of the slip s the torque M_a changes practically in proportion to s (Fig. 13-7), the expression for this torque can be written as

$$M_a = K_a \frac{d\theta}{dt}$$

Also acting on the rotor is the braking static torque of the drive M_{dr} which, generally speaking, depends on the speed, but here it may be assumed constant, since, from the moment of application of the excitation current ($s \approx 0.05$), the motor speed changes very slightly.

The quantity

$$M_j = M_{em} + M_a - M_{dr}$$

is the *excess* or *dynamic* torque inducing the change in the rotor speed and is proportional to the acceleration of the rotor or $\frac{d^2\theta}{dt^2}$.

Consider now, with the help of Fig. 13-12, the process of pulling a motor into synchronism.

In Fig. 13-12a the curve of the torque $M_{em} = M_{max} \sin \theta$ is shown by sine wave 1 . If the static torque $M_{stat} = \text{const} = OA$, it can be depicted by straight line AB parallel to the axis of abscissas. Assuming this straight line as the axis, we shall lay off downward from it the positive asynchronous torques M_a , and upward, the negative torques.

Suppose that before direct current is supplied to the field winding, the motor has a certain constant slip s and develops a constant

asynchronous torque M_a which counterbalances the static braking torque on the shaft $M_{stat}=OA$. The direct current may be switched on at the moment $t=0$ corresponding to any instantaneous position of the rotor with respect to the axis of the resultant flux. To simplify the reasoning, let us consider the most appropriate moment for switching on the current when the above axes coincide, i.e., when $\theta=0$. Under these conditions, when $t=0$, the electromagnetic torque $M_{em}=M_{max}=\sin \theta=0$, and the rotor of the motor does not accelerate at the initial moment. But since the motor is not running in synchronism, but with a slip $s \neq 0$, during the next moments the rotor begins to gradually lag behind the resultant flux Φ_δ , and the angle θ correspondingly increases. This results in the appearance of an electromagnetic torque $M_{em} > 0$. For example, when the angle $\theta=OC$, the torque $M_{em}=CF$. The greater torque causes an increase in motor speed which leads to a reduction in the slip and to a corresponding decrease in the asynchronous torque. Therefore, the torque M_a , which had the value AO at $\theta=0$ now, when $\theta=OC$, becomes equal to $ED < AO$. The resultant excess torque $M_j=FD=M_{em}+M_a-M_{stat}=CF+ED-CE$ accelerates the rotor and the slip s further decreases.

This process will continue until the motor attains its synchronous speed at point H when $\theta=OG$ and where the electromagnetic moment $M_{em}=GK$, the asynchronous torque $M_a=0$ and $M_j=HK$. Since the excess torque HK at this point also remains positive, it continues to accelerate the rotor so that its speed will further exceed the synchronous speed and the rotor will begin to run faster than the resultant flux Φ_δ . Owing to this, the angle θ now begins to decrease, and the slip s and the corresponding asynchronous torque will become negative. Therefore, the asynchronous generator torque will begin to retard the rotor.

When the rotor returns to the position where the angle θ again becomes equal to OC , the electromagnetic torque $M_{em}=CF$, the asynchronous torque $M_a=ET$ and the excess torque $M_j=FT=CF-ET-CE$, the latter still accelerating the motor until at point L on the curve of electromagnetic torque, with the angle $\theta=OS$, equilibrium of the torques is reached and the excess torque becomes zero. Since at this point the rotor has a certain negative slip, however, the angle will continue to decrease until at point N it again attains synchronous speed. Evidently at this point the asynchronous torque will again become equal to zero, but since the electromagnetic torque becomes equal to IR , i.e., less than the static torque M_{stat} , the braking torque increment NR again begins to increase the angle θ until equilibrium of the torques is reached at point Q .

Repeating this reasoning, we get the helical curve $ODHTLNQ$ (Fig. 13-12) ending at point P where equilibrium between the electromagnetic torque and the static torque is attained, but for the synchronous speed and asynchronous torque $M_a=0$. Here the process of start-

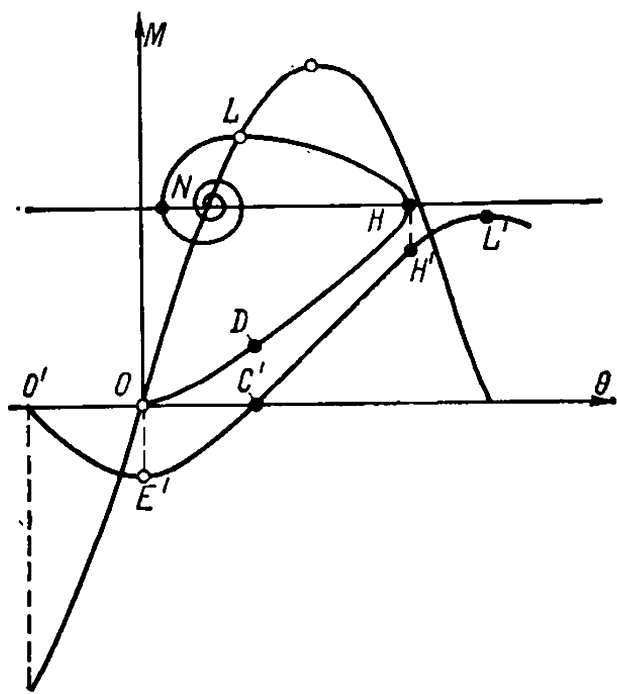


Fig. 13-13. Motor pulling into step with heavy load on the shaft

ing and pulling into synchronism ends and the motor runs in synchronism with the resultant flux Φ_{δ} . Figure 13-12b gives curves of the angle θ and slip s versus time t , the points D, H, T, \dots , on the curve corresponding to the points of the helix in Fig. 13-12a.

With an increase in the static torque, the slip which an unexcited motor operates with, is greater. Therefore the motor, when the excitation is on at the most favourable instant $\theta=0$, will now attain a smaller negative slip in accelerating along a curve of the form $ODHLN$ in Fig. 13-13. If the excitation is on with leading, for instance, at an angle $\theta=-60^\circ$, the torque M_{em} at the initial moment will have the

opposite sign, owing to which the slip will first increase, and the motor, gaining speed along curve $O'E'C'H'L'$ in Fig. 13-13, may not attain the synchronous speed and will oscillate in asynchronous duty along a curve similar to that shown in Fig. 13-9 (curve 3).

13-8. Methods of Asynchronous Starting

The main method of starting synchronous motors at present is the asynchronous method. Salient-pole motors of mass production are provided with a starting winding on the rotor and are designed for across-the-line starting. Across-the-line starting is always used where permissible from the standpoint of the effect of the starting current on the external circuit and voltage drops in it, and also of the motor temperature rise in starting. In most cases motors with ratings up to several hundreds of kilowatts, and quite often with ratings of a thousand kilowatts and higher have across-the-line starting.

In accordance with the general tendency in the USSR of further simplification of synchronous motor starting, the method of self-synchronization has been gaining ground, in which starting is accomplished with a permanently connected exciter, either mounted on the motor shaft or started simultaneously when separately mounted. Experience shows that, with a static braking torque at the shaft up to $M_{stat}=(0.25 \text{ to } 0.35) M_r$, uniaxial starting does not hinder the normal procedure. The field winding is connected directly to the exciter armature, the exciter in starting becoming self-excited and ensuring pull into synchronism at the end of starting. When starting under

heavy load, the field winding of the synchronous motor is shorted via a resistor (the field discharge resistor being used for this purpose, if available, see Sec. 12-2). When the speed near the synchronous one is reached, the field winding is connected to the exciter armature.

When it is necessary to reduce the voltage supplied to the motor in starting, a reactor of an autotransformer is inserted between the power line and the motor. Non-salient-pole synchronous motors with a massive rotor are used only for high speeds of rotation—3000 rpm—, and these motors do not require a special damper winding, since its function is performed by the rotor.

The asynchronous starting of non-salient-pole motors with massive rotors takes place in more severe conditions, since the currents induced in the massive rotor flow in its thin surface layer, causing a considerable local temperature rise. Therefore, in starting non-salient-pole motors, the starting voltage is often decreased with a corresponding increase in the starting time, since this makes the rotor temperature field more uniform.

Table 13-1 shows that the starting current ratio $\frac{I_{st}}{I_r}$ for across-the-line starting of such motors, as with induction motors, is about 4 to 5. When a large starting torque is not necessary, the starting current ratio can be reduced by using starting devices which lower the voltage across the motor terminals in starting; namely, an autotransformer, reactor or both devices together.

Autotransformer starting is accomplished as shown in Fig. 13-14. First breakers 1 and 3 are connected and then switch 2 is set to position *a*. When a speed near synchronism is attained, switch 2 is set in position *b*, the excitation switched on, and breaker 3 disconnected.

The resistor *R* in the circuit shown in Fig. 13-14 is inserted into the excitation circuit in asynchronous starting with the exciter disconnected and limits the development of the uniaxial effect.

Denote by I_{st} the starting current of the motor when it is directly connected to the power line, and by $I_{st.mot}$ its current when starting by means of an autotransformer. Let $I_{st.p}$ be the starting current of the autotransformer primary winding.

With across-the-line starting, the motor and line currents will be equal, since the motor voltage U_{mot} is equal to the circuit voltage U_{ec}

$$I_{st} = \frac{U_{ec}}{z_{mot}}$$

where z_{mot} is the motor impedance in starting.

When an autotransformer is used whose secondary voltage is U_{mot} , we have

$$I_{st.mot} = \frac{U_{mot}}{z_{mot}} = I_{st} \frac{U_{mot}}{U_{ec}}$$

To determine the starting current taken from the external circuit, we may assume that the outputs of the primary and secondary circuits of the autotransformer are equal, neglecting the voltage drop and losses in it

$$I_{st. p} U_{ec} \cong I_{st. mot} U_{mot}$$

whence

$$I_{st. p} \cong I_{st. mot} \frac{U_{mot}}{U_{ec}} = I_{st} \left(\frac{U_{mot}}{U_{ec}} \right)^2$$

The starting torque $M_{st. mot}$ when starting by means of an autotransformer decreases in proportion to the square of the applied voltage.

Both the current of the motor and its magnetic flux decrease proportionally, and, therefore

$$M_{st. mot} = M_{st} \left(\frac{U_{mot}}{U_{ec}} \right)^2$$

Thus, when an autotransformer is used, the starting torque of the motor and the starting current of the circuit decrease in proportion to the square of the voltage $\left(\frac{U_{mot}}{U_{ec}} \right)^2$, while the starting current in the motor itself decreases in proportion to the first power of the voltage.

In *reactance starting* (Fig. 13-15), the voltage across the motor terminals U_{mot} is lowered because of the voltage drop in the reactance,

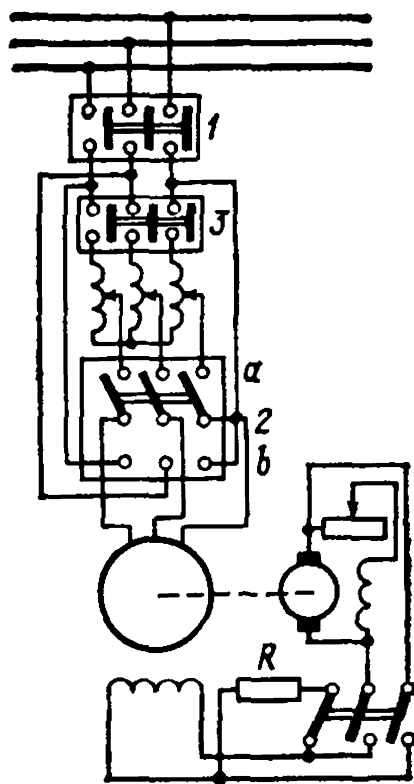


Fig. 13-14. Autotransformer starting of a synchronous motor

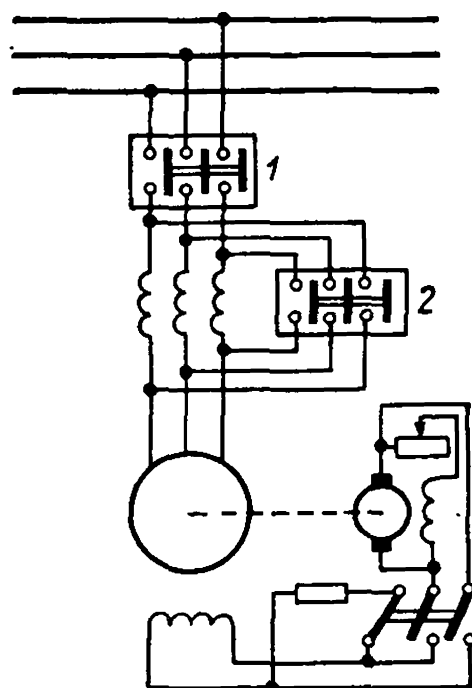


Fig. 13-15. Reactance starting of a synchronous motor

and the starting current of the motor is

$$I_{st. mot} = I_{st} \frac{U_{mot}}{U_{ec}}$$

Since equal currents pass through the motor and the reactor, then

$$I_{st. p} = I_{st. mot} = I_{st} \frac{U_{mot}}{U_{ec}}$$

The starting torque of the motor decreases in proportion to U_{mot}^2 and, therefore,

$$M_{st. mot} = M_{st} \left(\frac{U_{mot}}{U_{ec}} \right)^2$$

Thus, in reactance starting the starting torque decreases in proportion to the square of the voltage $\left(\frac{U_{mot}}{U_{ec}} \right)^2$, the starting current of the motor also decreases in proportion to $\frac{U_{mot}}{U_{ec}}$, but not to $\left(\frac{U_{mot}}{U_{ec}} \right)^2$ as in autotransformer starting.

The reactance starting of a synchronous motor is simpler and less expensive, but gives greater starting current ratios in the power circuit.

Starting of a Synchronous Motor by a Combined Scheme (Fig. 13-16) is used with large motors and under severe starting conditions. Figure 13-16 gives the circuit for a reversible motor. Here starting is in two stages, an autotransformer being used during the first stage, and a reactance during the second one. The following sequence of operations is observed. First breaker 4 is closed to complete the neutral of the autotransformer. Next breaker 1 is closed, and one of the breakers 2 or 3, depending on the desired direction of motor rotation (breaker 2 changes the positions of the two outer phases with respect to those connected by breaker 3). The motor now obtains, via the autotransformer, about 30% of the rated voltage. During this stage of starting, all the contactors C_1, C_2, C_3 and C_4 in the excitation circuit are open, and the field winding is therefore shorted through both resistors R_1

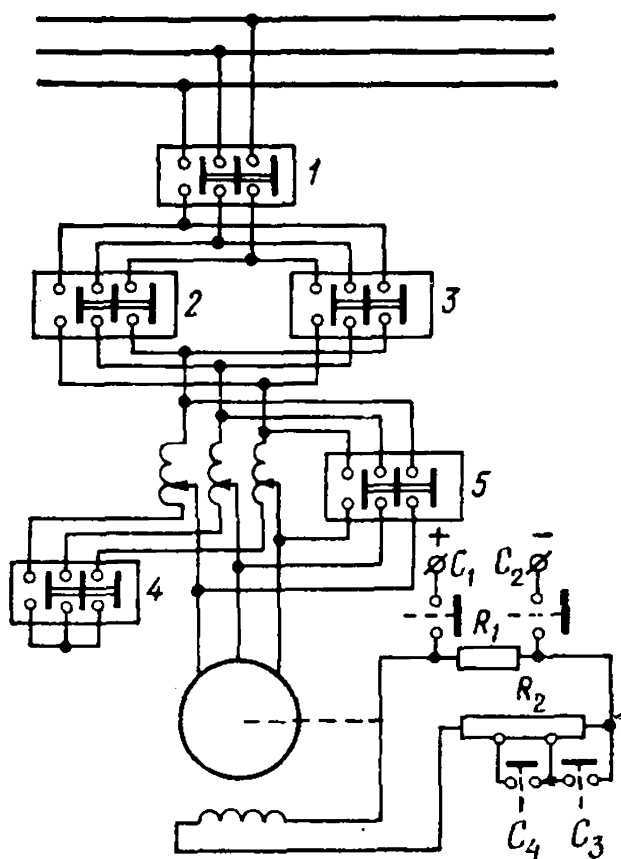


Fig. 13-16. Multistage autotransformer-starting circuit for a powerful synchronous motor

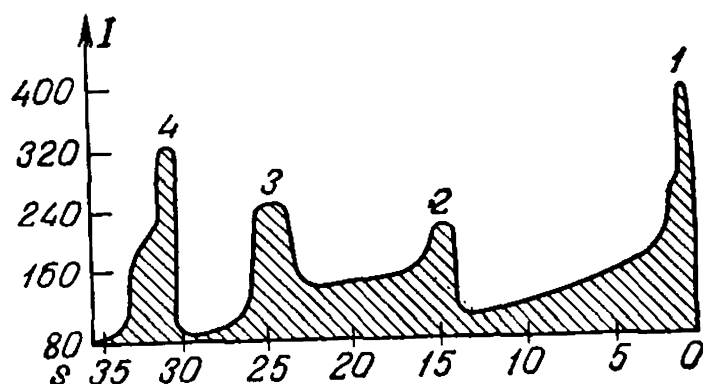


Fig. 13-17. Curve showing change in stator current of a 3000-kW, 83.7-rpm synchronous motor when starting according to the circuit in Fig. 13-16.

and R_2 , which here serve as current-limiting resistors. After the motor reaches 50 to 75% of its synchronous speed, a special frequency relay opens the neutral of the autotransformer with the aid of breaker 4 and the autotransformer begins to operate as a reactance, thus allowing the second-stage voltage to be applied to the motor, i.e., 70% of the rated voltage. By means of this starting scheme the motor attains 95% of its synchronous speed, and then a special low-frequency relay inserted in the excitation circuit of the motor closes contactors C_3 and C_4 to shunt part of resistor R_2 , and contactors C_1 and C_2 to connect the excitation circuit to a source of direct current. This results in application to the motor of an excitation higher than in normal duty and the motor is pulled into synchronism. After this breaker 5 is closed, which supplies full line voltage to the motor, and contactor C_4 is opened to increase the resistance of the excitation circuit and establish an excitation current conforming to normal duty.

Figure 13-17 gives a curve showing the change in current in a 3000-kW, 83.7-rpm synchronous motor traced by a pen-recorder when starting by the combined method considered above. The first current surge 1 corresponds to connection via the autotransformer at $0.32 U_{ec}$, the second surge 2 to connection at $0.7 U_{ec}$, the third surge 3 corresponds to delivery of excitation current by contactors C_1 and C_2 , and the fourth surge 4 corresponds to across-the-line switchover. In the scheme (Fig. 13-16) only one breaker 1 must be selected for the entire interrupting rating. Breaker 1 may be omitted, but then breakers 2 and 3 must have the entire interrupting rating. For non-reversible motors breakers 2 and 3 are not required. The advantages of starting by the combined scheme over starting by the scheme described earlier and illustrated in Fig. 13-14 consist in that the transfer from one voltage stage to another is accomplished without interruption of the current, a feature which is important for large motors.

Example 13-1. Determine the inductive reactances and resistances of the windings for a three-phase synchronous motor with $2p=6$, $P_r=225$ kW, $P=310$ kVA, $I_r=59.5$ A, $\cos \varphi$ (leading)=0.8; $U=3000$ V, $\eta=0.91$, and $\alpha=0.722$.

The motor has a stator with the following data, similar to those of the induction three-phase motor in Example 2-1: $D_a=730$ mm, $D=525$ mm, $l_0=364$ mm, $n_{sh} \times b_{sh}=6 \times 10=60$ mm, $l=364 - \frac{1}{2} \times 60=334$ mm, $q_1=5$, $Z_1=90$, $k_{w1}=0.957 \times 0.951=0.91$, $\delta=2.6$ mm, $\sum \lambda_1=3.59$

The number of wires per slot $7 \times 2 = 14$, the number of turns per phase

$$w_1 = \frac{90 \times 14}{2 \times 3} = 210$$

The inductive reactance of the stator winding

$$x_1 = 4\pi \times 50 \times 1.26 \times 10^{-8} \times \frac{33.4 \times 210^2}{3 \times 5} \times 3.59 = 2.78 \Omega$$

$$\tau = 276 \text{ mm}$$

$$A = \frac{I_r w_1 2m}{\pi D} = \frac{59.5 \times 210 \times 6}{\pi \times 52.5} = 433 \text{ A/cm}$$

$$B_{\delta 1} = \frac{U_{ph} p}{4.44 f D \cdot l w_1 k_{w1}} = \frac{1730 \times 3}{4.44 \times 50 \times 0.525 \times 0.334 \times 210 \times 0.91} = 0.7 \text{ T} = 7000 \text{ Gs}$$

$$z_r = \frac{U_{ph}}{I_r} = \frac{1730}{59.5} = 29.1 \Omega$$

From formula (8-28) we have

$$\begin{aligned} x_{ad} &= 2mf \frac{\mu_0 D \cdot l w_1^2 k_{w1}^2}{k_\delta \cdot k_\mu \cdot \delta \cdot \rho^2} k_d = 2 \times 3 \times 50 \times \\ &\times \frac{1.26 \times 10^{-8} \times 52.5 \times 33.4 \times 210^2 \times 0.91^2}{1.25 \times 1.11 \times 0.26 \times 3^2} \times 0.9 = 66 \Omega \\ k_\delta &= 1.25; \quad k_\mu = 1.11 \\ \frac{\delta}{\tau} &= \frac{2.6}{276} = 0.0098 \cong 0.01; \quad \frac{\delta_{max}}{\delta} = 1.5 \end{aligned}$$

According to the curves of Fig. 8-8 and Fig. 8-11 for $\alpha = 0.722$

$$k_d = 0.9; \quad k_q = 0.44; \quad k_{ad} = 0.83; \quad k_{aq} = 0.45$$

$$x_{aq} = x_{ad} \frac{k_q}{k_d} = 66 \times \frac{0.44}{0.9} = 32.2 \Omega$$

$$\underline{x}_{ad} = \frac{x_{ad}}{z_r} = \frac{66}{29.1} = 2.28$$

$$\underline{x}_{aq} = \frac{x_{aq}}{z_r} = \frac{32.2}{29.1} = 1.1$$

From formula (5-28)

$$\lambda_{exc.s} = 2 \left[\frac{h_{p1}}{3c_{p1}} + \frac{h_{p2}}{c_{p2}} + \frac{h_{ps}}{c_{ps}} + \frac{(l_{ps} - l_{tot}) + 0.5h_p + 0.125b_p}{2l_{ps}} \right]$$

$$h_{p1} = 70 \text{ mm}; \quad h_{p2} = 8 \text{ mm}; \quad h_{ps} = 12 \text{ mm};$$

$$c_{p1} = 90 \text{ mm}; \quad c_{p2} = 140 \text{ mm}; \quad c_{ps} = 70 \text{ mm};$$

$$(l_{ps} - l_{tot}) = 374 - 364 = 10 \text{ mm}; \quad b_p = 114 \text{ mm}$$

Hence

$$\lambda_{exc.s} = 1.13$$

According to formula (11-11b)

$$\begin{aligned} x_{exc.s} &= \left(\frac{4}{\pi}\right)^2 \times \left(\frac{433}{\sqrt{2}} \times \frac{0.91}{7000}\right) \times 0.83^2 \times 2 \times 1.13 + \\ &\quad + \left(\frac{4}{\pi} \times 0.83 \times 1.0 - 1\right) \times 2.28 = 0.101 + 0.129 = 0.23 \\ x_{exc.s} &= 0.23 \times 29.1 = 6.7 \Omega \end{aligned}$$

By formula (11-12)

$$x_{ds} = 8 \times 1.26 \times 10^{-6} \left(\frac{433 \times 10^2 \times 0.91}{\sqrt{2} \times 0.7} \right) \times \frac{1}{6} \times 1.91 = 0.128$$

where $\lambda_d = 1.91$.

Hence

$$\begin{aligned} x_{ds} &= 0.128 \times 29.1 = 3.73 \Omega \\ x_{qs} &= 0.75 \times x_{ds} = 0.75 \times 0.128 = 0.096 \\ x_{qs} &= 0.096 \times 29.1 = 2.79 \Omega \end{aligned}$$

The resistance of one phase of the stator winding at 75 °C is

$$r_1 = 0.61 \times 1.24 = 0.755 \Omega$$

The resistance of the field winding at 75 °C, with $w_{exc} = 42.5$ turns per pole, with a cross section $q_{exc} = 36.2 \text{ mm}^2$ and the length of one turn $l_{exc} = 1103 \text{ mm}$, is, for $2p = 6$,

$$r_{exc.75^\circ\text{C}} = 0.0217 \times \frac{42.5 \times 6 \times 1.103}{36.2} = 0.166 \Omega$$

The discharge resistance is chosen equal to the 10-fold value of the field winding resistance, therefore,

$$r_{exc.mot} = 0.166 \times (1 + 10) = 1.82 \Omega$$

The resistance of the field winding reduced to the stator system according to formula (8-42) is

$$\begin{aligned} r'_{exc} &= r_{exc.mot} k_{exc.st} = r_{exc.mot} \times \frac{2m}{\pi^2} \times \frac{w_1^2 k_{w1}^2}{p^2 w_{exc}^2} \times \\ &\quad \times k_{ad}^2 = 1.82 \times 2 \times 3 \left(\frac{210 \times 0.91 \times 0.83}{\pi \times 3 \times 42.5} \right)^2 = 1.56 \Omega \end{aligned}$$

13-9. Synchronous Condenser

A synchronous motor operating under no-load and consuming with respect to the line voltage a reactive leading or lagging current is called a *synchronous condenser*. This machine is used for improvement of the power factor $\cos \varphi$ and for regulation of the voltage in transmission lines and distribution networks.

To improve the power factor, the synchronous condenser operates in overexcited duty and therefore consumes from the line a capacitive current which compensates the lagging current of induction motors and transformers. This makes it possible to unload power circuits of inductive, lagging currents, which reduces losses in the line and im-

proves the utilization of the synchronous generators at the power stations.

When transmitting power over long lines, difficulties arise in keeping the voltages constant at the power receiving ends. With heavy inductive loads, the voltage at the load terminals is considerably lower than the generator voltage; conversely, at small loads, under the influence of capacitive reactances, the voltage at the load terminals may become even higher than the generator voltage. A synchronous condenser

carrying heavy loads in overexcited duty and, light loads in underexcited duty, permits a constant voltage to be maintained at the receiving ends of the power lines. A constant voltage is maintained by means of high-speed voltage regulators, which control the excitation current of the synchronous condenser. The maximum possible leading and lagging currents can be determined from the no-load characteristic of the condenser and of the short-circuit triangle (Fig. 13-18). The maximum possible lagging current $I_{L. max}$ consumed by a synchronous condenser from the power line is obtained when its excitation current is zero. Here the triangle occupies the position $a_1b_1c_1$, i.e., above the no-load characteristic. In overexcited duty the triangle occupies the position $a_2b_2c_2$, i.e., below the no-load characteristic. Here the maximum value of the reactive current $I_{C. max}$ may become greater than in underexcited duty, since its value will be limited only by the temperature rise of the active parts of the machine. Since the excitation current, when a leading current is consumed from the power line, is greater than in the case of a lagging current, the heating conditions of the synchronous condenser are more severe with a leading current. For this reason the rated capacity of the synchronous condenser will be that for overexcited duty.

From Fig. 13-18 it follows that

$$\frac{I_{C. max}}{I_{L. max}} = \frac{a_2c_2}{a_1c_1} = \frac{b_2c_2}{b_1c_1} \approx \frac{c_2H}{Hc_1} = \frac{i_{exc. max} - i_{exc. 0}}{i_{exc. 0}}$$

Since at $i_{exc} = 0$ we also have $E_m = 0$, then

$$U_{max} = x_d I_{L. max}$$

where x_d is the direct-axis synchronous reactance.

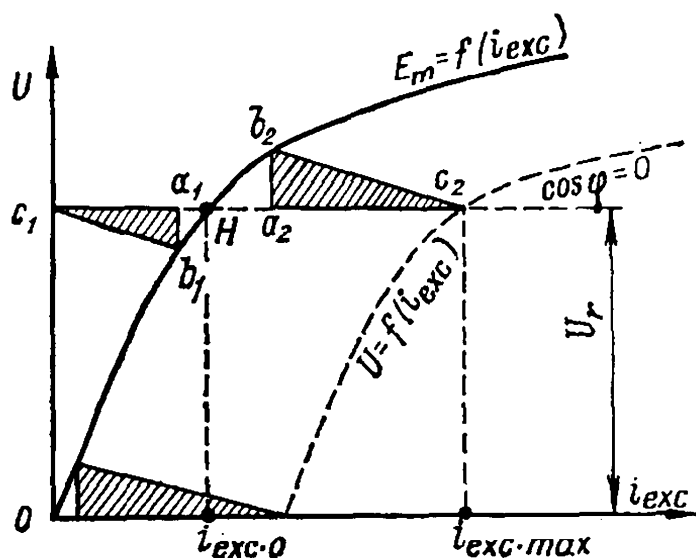


Fig. 13-18. Determination of maximum leading and lagging currents of a synchronous condenser

From the relations given above we find that

$$I_{L.max} = \frac{U_{max}}{x_d}$$

$$I_{C.max} = \frac{U_{max}}{x_d} \left(\frac{i_{exc.max}}{i_{exc.0}} - 1 \right) = \frac{U_{max}}{x_d} (\vartheta_{max} - 1)$$

where $\vartheta_{max} = \frac{i_{exc.max}}{i_{exc.0}}$ is the ratio of the maximum excitation current to the excitation current at which the stator current is minimum.

Consequently

$$I_{C.max} + I_{L.max} = U_{max} \frac{\vartheta_{max}}{x_d}$$

Usually in a synchronous condenser

$$\frac{I_{L.max}}{I_{C.max}} = \gamma_{max} = 0.5$$

and, consequently,

$$I_{C.max} + I_{L.max} = U_{max} \frac{\vartheta_{max}}{x_d} = 1.5 I_{C.max}$$

If the operating conditions of a power transmission line require that γ_{max} be higher than 0.5, it is necessary to decrease x_d . This may be done by increasing the air-gap, which, however, affects ϑ_{max} almost to the same degree as x_d , and the ratio $\frac{\vartheta_{max}}{x_d}$ remains nearly constant with an increase in the air-gap, i.e.

$$I_{C.max} + I_{L.max} = U_{max} \frac{\vartheta_{max}}{x_d} \cong \text{const}$$

Therefore, an increase in γ_{max} by changing the air-gap (with the same maximum possible magnetizing force of the field winding) results in a decrease of $I_{C.max}$, i.e., in a reduction in the utilization of the synchronous condenser. On the other hand, a decrease in γ_{max} below 0.5 leads to an increase in the surface losses in the synchronous condenser pole shoes. Practice shows that the value $\gamma_{max} = 0.5$ is the most favourable, both from the standpoint of losses and of synchronous condenser cost. Such machines are now termed standard synchronous condensers.

Since the curve optimum of the conditions dependent on γ_{max} has a gentle slope, it becomes possible, with a view to the needs of the electrical networks, to build synchronous condensers with $\gamma_{max} = 0.6$ without almost any increase in cost. For the series of synchronous condensers built in the USSR, the value of γ_{max} ranges from 0.5 to 0.66.

If, when using standard synchronous condensers ($\gamma_{max} = \frac{I_{L.max}}{I_{C.max}} = 0.5$) it is desirable, for a given value of the leading current $I_{C.max}$,

to obtain lagging currents with values of

$$I_{max} > I_{L.max} = \gamma_{max} I_{C.max} = 0.5 I_{C.max}$$

we must obviously use the machine *k* times more than its capacity and its utilization factor will become equal to

$$k = \frac{I_{L.max}}{I_L} = \frac{I_{L.max}}{I_{C.max}} \frac{I_{C.max}}{I_L} = \frac{\gamma}{\gamma_{max}}$$

where $\gamma = \frac{I_L}{I_{C.max}}$ is the desired ratio between the lagging and leading currents.

The utilization factors *k* of standard condensers for various values of γ are as follows:

γ	0.5	0.6	0.7	0.8	0.9	1.0
<i>k</i>	1.0	0.833	0.715	0.625	0.555	0.500

It is obvious that with low values of *k* the use of standard condensers for $\gamma > 0.5$ is unpractical.

At present the installation of synchronous condensers for circuit voltage regulation is being discontinued, since when the line voltage is increased it is necessary to underexcite the condenser, which, in turn, results in poor circuit power factors. Transformers provided with on-load voltage regulation are used instead.

For industrial enterprises which consume heavy inductive current, it is good to use synchronous motors operating with overexcitation.

The specifications of modern synchronous condensers produced in the USSR are given in Table 13-2:

TABLE 13-2

Type	Rated capacity with leading current, MVA	Voltage, kV	Speed, rpm	Losses at rated capacity, kW	Weight, tons		Exciting data		Starting current I_{st}/I_r with $U_{st} = U_r$
					rotor	total	current, A	voltage, V	
With air cooling									
KC 10000-6	10	6.3	1000	250	12.6	38.5	590	70	4.5
KC 15000-6	15	6.6	1000	330	17.5	49	560	105	6.0
KC 30000-11	30	10.5	750	613	44.5	100	600	170	5.4
With hydrogen cooling									
KCB-50000-11	50	11	750	750	46	145	1150	150	4.0
KCB-100000-11	100	11	750	1300	77	220	1350	230	5.2
KCB-160000-15	160	15.75	750	—	108	310	—	—	—

Synchronous condensers are started by the same methods as used for synchronous motors. Their starting, as compared with that of synchronous motors, takes place under more favourable conditions because of the absence of a mechanical load. To lighten the starting conditions and decrease the starting currents, powerful synchronous condensers are usually equipped with oil pumps which pump lubricating oil into the bearings of the machine before starting. The starting currents, depending on line requirements, usually amount to 30 to 100% of the rated current and can be reduced to 20% when oil is pumped into the bearings. The starting periods usually range from 20 to 60 seconds. Owing to its small air-gap, the synchronous condenser is a relatively light and inexpensive synchronous machine having relatively low losses.

Today very large synchronous condensers (50 to 200 MVA) are hydrogen-cooled and installed out of doors.

For more powerful synchronous condensers water-cooling is used. At present the firm ASEA has designed a 345-MVA, 18-kV, 900-rpm, 60-Hz synchronous condenser with entire water cooling. A synchronous condenser of a similar type, rated at 350 MVA and 750 rpm with water cooling is being designed at the "Ural Heavy Engineering" Works.

Chapter

14

ASYMMETRICAL STEADY-STATE DUTIES OF A THREE-PHASE SYNCHRONOUS GENERATOR

14-1. General

Unbalanced loading of a three-phase synchronous generator occurs when single-phase loads are non-uniformly distributed in the supply line, this leading to asymmetrical distribution of the current between the separate stator phase windings in the generator. As with asymmetrical load on a three-phase transformer, in the general case, if the generator has a grounded neutral, the asymmetrical currents in the stator winding phases may consist of all three symmetrical components: of the positive- I_1 , negative- I_2 and zero- I_0 phase sequences.

When electric energy is transmitted through a transformer and a transmission line, the neutral is practically grounded only on the high-voltage line side of the transformer, while the neutral of the generator itself is earthed only through a relatively large resistance determined by the conditions of generator protection. The zero-phase sequence current components appearing in the line in the event of single-phase and two-phase-to-earth short circuits circulate only in the line and transformers, and cannot flow into the generator circuit, in which practically only the positive- and negative-phase-sequence currents may flow.

Unbalanced loading may be caused by relatively high-power single-phase loads of a specific nature, such as, for instance, single-phase electrical furnaces and single-phase electrical railways, but even here appropriate distribution of the single-phase loads between the phases makes it possible to attain conditions at which the resultant load unbalance on the generators becomes relatively small.

According to GOST 183-66 for electrical machines, a three-phase current system is considered to be practically symmetrical if, when resolved into positive- and negative-phase sequence currents, it has a negative-phase sequence current not exceeding 5% of the positive one. According to the same standard, a continuous unbalanced loading of a turbogenerator is permissible up to a difference of 10% between the currents in the separate phases; the current difference for all other types of generators and synchronous condensers may reach 20%, the phase currents not exceeding their rated values. The difference of 10 to 20% between phase currents corresponds to a maximum value of the negative-sequence current of about 6 to 12%.

Compared with former USSR industrial standards, GOST 183-66 allows salient-pole synchronous generators to carry 2 to $2\frac{1}{2}$ times greater unbalanced loads. This to some extent serves to meet the requirements of operating personnel concerning the increase of the permissible unbalanced loading to increase the reliability of power system operation, and feeding of loads by operation under hypo-phase conditions (transmission-line operation with two phases or with two phases and earth) when it is necessary to repair one phase of the line. When the neutral of the transformer is grounded, the switching-out of one phase from the line immediately results in about a 17% flow of negative-sequence current, but when the neutral is insulated, the unbalance becomes still greater.

The presence of asymmetry with negative-sequence currents of about 10 to 15% and greater leads to an appreciable asymmetry of the voltages, this being unfavourable for the operation of three-phase induction motors in which an oppositely rotating field appears retarding rotor movement. On the other hand, the presence of noticeable negative-sequence currents in the stator winding of a synchronous generator gives rise to appreciable losses in the field winding, in the pole shoes of salient-pole generators and in the bodies of turbogenerator rotors, which reduces generator efficiency.

In modern turbogenerators with massive rotors in which the field windings, even under symmetrical duties, are heated to temperatures permissible only for the highest classes of rotor winding insulation, the presence of negative-sequence currents makes it necessary, first of all, to lower their output somewhat. The presence of noticeable negative-sequence currents in hydrogenerators without damper windings leads to the appearance of noise and vibrations which may unfavourably affect the safety of the numerous welds used in the structural parts of these machines. This requires the use of damper windings of sufficient capacity.

When analysing the phenomena taking place in asymmetrical loading and when short circuits of a synchronous machine occur, it is more convenient to use the method of symmetrical components and resolve the e.m.f.s, voltages and currents into their three symmetrical phase-sequence components: the positive-, negative-, and zero-phase sequences. Each of these systems is characterized by its own parameters, i.e., by the reactances (x_1 , x_2 , x_0), resistances (r_1 , r_2 , r_0) and impedances (z_1 , z_2 , z_0) of the corresponding sequence. In modern synchronous generators of sufficiently large rating the values of the resistances are very small in comparison with the inductive reactances. Therefore, the impedances z_1 , z_2 , z_0 may in most cases be replaced by the reactances x_1 , x_2 , x_0 , and the resistances r_1 , r_2 , r_0 taken into account only when determining the corresponding time constants (see Vol. I, Chap. 19).

The main task of this book is to explain the physical aspects of the above parameters and the empirical methods used in their determination. The calculation of the above components is the subject of special courses. Fundamental contributions to the theoretical investigation and physical interpretation of a.c. machine parameters by the method of symmetrical components are the works of L. Lomonosova, E. Pal, D. Gorodskoy and M. Kostenko.

14-2. Reactances and Resistances of a Synchronous Machine for Currents of Various Sequences

Positive-Sequence Inductive Reactance and Resistance. The system of positive-phase-sequence currents produces in a three-phase synchronous machine an armature magnetizing force whose fundamental harmonic runs in step with the rotor and, therefore, does not induce e.m.f.s in its windings. This corresponds to the generator operating under three-phase balanced load or under a steady-state three-phase short circuit. Hence it follows that the positive-phase-sequence reactance x_1 is equal to the value of the direct-axis synchronous reactance x_d or the quadrature-axis synchronous reactance x_q , depending on the kind of load and the angular position of the reaction magnetizing force relative to the rotor. In particular, with a sustained symmetrical short circuit, when the armature reaction acts along the direct axis ($r_a \cong 0$), the positive-sequence inductive reactance equals the unsaturated value of the direct-axis synchronous reactance x_d .

The positive-sequence resistance is equal to the resistance of the stator winding.

Negative-Sequence Inductive Reactance and Resistance. To define the concept of inductive negative-sequence reactance x_2 , consider those operating conditions of a synchronous machine when its rotor is brought up to synchronous speed with the field winding short-circuited, the exciter out of circuit and a symmetrical voltage of rated frequency, but of negative-phase sequence (Fig. 14-1), applied to the stator winding. Here the current I_2 (negative-sequence current) will flow through the stator winding.

The stator magnetizing force due to the negative-sequence currents I_2 produces a field rotating at double speed relative to the rotor and opposite to rotor rotation. In this case the stator winding of a synchronous generator may be considered as a transformer primary, and the rotor, including its field winding, damper windings, pole shoes and pole cores as short-circuited transformer secondary windings. The

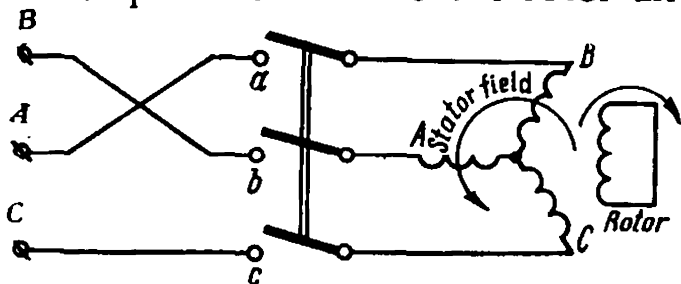


Fig. 14-1. Circuit for negative-phase-sequence current tests in stator winding of a synchronous machine

fact that in a conventional static transformer the field produced by the primary and secondary magnetizing forces is stationary in space, while in a synchronous generator it rotates at synchronous speed relative to the stator and at twice the synchronous speed relative to the rotor, does not violate the principle of transformer interaction of the stator and rotor circuits. This duty is equivalent to the braking duty of a three-phase induction motor whose rotor runs at synchronous speed against the field, with a slip $s=2$.

The action of the counter-synchronous field on the rotor winding system will differ from the action of the synchronous armature-reaction field. While the latter is stationary relative to the excitation field of the poles and with it forms the resultant flux, which also runs in synchronism with the rotor and determines the resultant positive-sequence e.m.f. of the synchronous machine, the counter-synchronous field induces in the rotor windings currents of double frequency which prevent this field from entering the rotor circuit system. As a result, the counter-synchronous field in the air-gap becomes, essentially, the leakage flux of the windings of a short-circuited transformer. Let us denote by $x'_{\sigma exc}$ the leakage inductive reactance of the rotor due to the counter-synchronous field, reduced to the stator system, by $x_{\sigma a}$ the leakage inductive reactance of the stator windings, and, by x_a the mutual inductive reactance through the air-gap equal, when reducing the rotor to the stator, to the armature-reaction stator reactance.

The inductive reactance x_2 of a synchronous salient-pole machine is not constant and depends on the instantaneous position of the pole axis relative to the stationary system of stator windings, since the leakage inductive reactances of the rotor and the reactances of mutual inductance along the direct axis (x_{ad}) and quadrature axis (x_{aq}) of a synchronous salient-pole machine are in the general case not equal.

Neglecting the influence of the relatively small resistances of the stator and the rotor, we obtain, for a synchronous machine without a damper winding on its rotor, as for a static transformer, the resultant short-circuit inductive reactance for the moment when the axis of the counter-synchronous armature field and the pole axis coincide:

$$\begin{aligned} x_{2d} &= x_{\sigma a} + \frac{1}{\frac{1}{x_{ad}} + \frac{1}{x'_{\sigma exc}}} = x_{\sigma a} + \frac{x_{ad}x'_{\sigma exc}}{x_{ad} + x'_{\sigma exc}} = \\ &= x_{\sigma a} + \frac{x'_{\sigma exc}}{\sigma_{2exc}} \cong x_{\sigma a} + x'_{\sigma exc} \end{aligned} \quad (14-1)$$

where the leakage factor of the secondary circuit is

$$\sigma_{2exc} = 1 + \frac{x'_{\sigma exc}}{x_{ad}} \cong 1$$

and at the moment when the axis of the counter-synchronous field is perpendicular to the pole axis and coincides with the quadrature axis:

$$x_{2q} = x_{\sigma a} + x_{aq} \quad (14-2)$$

The mean value of the inductive reactances x_{2d} and x_{2q} is assumed to be equal to the mean value of the negative-sequence reactance:

$$x_2 = \frac{1}{2} (x_{2d} + x_{2q}) = x_{\sigma a} + \frac{x'_{\sigma exc}}{2\sigma_{exc}} + \frac{1}{2} x_{aq} \quad (14-3)$$

For a synchronous machine with damper windings along the direct and quadrature axes, for the moment when the axis of the counter-synchronous armature field coincides with the pole axis, we have

$$x_{2d} = x_{\sigma a} + \frac{1}{\frac{1}{x_{ad}} + \frac{1}{x'_{\sigma exc}} + \frac{1}{x'_{\sigma dw.d}}} = x''_d \quad (14-4)$$

and for the moment when the axis of the counter-synchronous field coincides with the quadrature axis, we have

$$x_{2q} = x_{\sigma a} + \frac{1}{\frac{1}{x_{aq}} + \frac{1}{x'_{\sigma dw.q}}} = x''_q \quad (14-5)$$

The leakage inductive reactances $x'_{\sigma dw.d}$ and $x'_{\sigma dw.q}$ of the damper windings are usually small in comparison with $x_{\sigma a}$, $x_{\sigma exc}$, x_{ad} and x_{aq} . Therefore, when damper windings are used, we have, as the first approximation

$$\begin{aligned} x_{2d} &\cong x_{\sigma a} + x'_{\sigma dw.d} \cong x_{\sigma a} \\ x_{2q} &\cong x_{\sigma a} + x'_{\sigma dw.q} \cong x_{\sigma a} \end{aligned}$$

and, approximately,

$$x_2 = \frac{1}{2} (x_{2d} + x_{2q}) \cong x_{\sigma a}$$

If there is no suppression of the counter-synchronous field (the rotor is made of steel laminations, the field winding is open or connected across a very large resistance, damper windings are absent) and the reluctance of the air-gap is constant (a non-salient-pole machine, $x_{ad} \cong x_{aq}$), the counter-synchronous armature field will be of the same magnitude as the synchronous armature-reaction field when the machine operates as a three-phase generator, and, therefore, $x_2 = x_d$.

Thus, in the general case, x_2 may be within the range $x_{\sigma a} < x_2 < x_d$.

The negative-sequence resistance r_2 corresponding to the transformer coupling of the stator and rotor circuits due to the counter-synchronous field, as with a transformer, is practically equal to the sum of the resistances of the stator and rotor circuits, taking into consideration

for the rotor circuit resistances—as in an induction machine—the slip of the rotor relative to the counter-synchronous field equal to $2 - s$. It should be noted here that the resistance of the field (excitation) winding r_{exc} when damper windings are used may be neglected, since the resistance of the field winding is considerably lower than that of the damper windings, and the inductive reactance of the field winding is, conversely, much higher.

Thus, when a damper winding is used, its resistances along the direct and quadrature axes are assumed to be equal ($r_{dw.d} = r_{dw.q} = r_{dw}$) and we have:

$$r_2 \cong r_a + \frac{r'_{dw}}{2-s} \quad (14-6)$$

And, at synchronous speed of the rotor ($s=0$),

$$r_2 = r_a + \frac{r'_{dw}}{2} \quad (14-7)$$

with the rotor at standstill ($s=1$)

$$r_2 \cong r_a + r'_{dw} \quad (14-8)$$

In the absence of damper windings, with $s=0$

$$\begin{aligned} r_{2d} &\cong r_a + \frac{r'_{exc}}{2} \\ r_{2q} &\cong r_a \end{aligned}$$

and the mean value of the negative-sequence resistance will be

$$r_2 = \frac{1}{2} (r_{2d} + r_{2q}) \cong r_a + \frac{r'_{exc}}{4}$$

But, since $\frac{r'_{exc}}{4}$ is appreciably less than r_a , we may approximately assume for this case that $r_2 \cong r_a$.

It should be noted that r'_{exc} and r'_{dw} are the values of the resistances of the field and damper windings reduced to the stator winding.

The simplest way to determine the values of the negative-sequence resistances, reactances and impedances experimentally is by preliminary determination of the so-called subtransient impedances z''_d , z''_q and resistances r''_d and r''_q , by feeding two phases of the stator winding from a single-phase circuit with the machine at standstill and the field winding short-circuited (Fig. 14-2). During this experiment, a normal-frequency current of the order of $I \cong 0.25 I_r$ is passed through the stator winding and a constant voltage maintained across the terminals at different angular positions of the rotor. In this case the synchronous machine operates as a static transformer with a short-circuited secondary circuit, the transformer coupling between the primary and secondary circuits changing as the rotor turns.

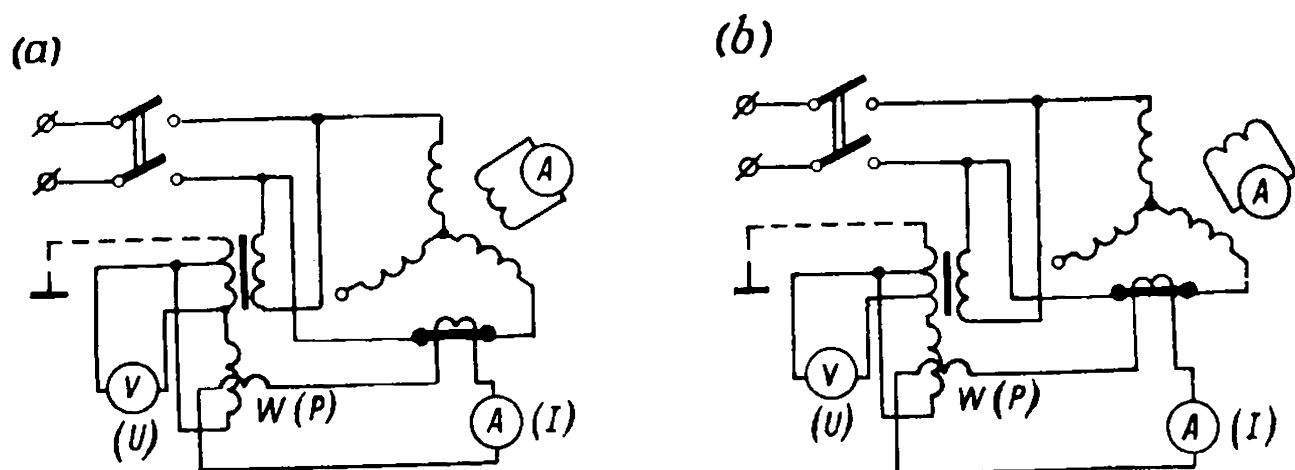


Fig. 14-2. Two-phase supply tests for determining direct-axis (a) and quadrature-axis (b) subtransient impedances with rotor at standstill

With a constant voltage applied across the terminals, the stator current does not remain constant, but attains a maximum value when the axis of the field winding coincides with the axis of the resultant stator winding flux, i.e., when the angle between these axes $\gamma=0$ (Fig. 14-2a), and attains a minimum value when these axes become perpendicular, i.e., when $\gamma=90^\circ$ (Fig. 14-2b). Although the screening effect of the rotor circuits also tells at $\gamma=90^\circ$, but since at $\gamma=0$ this effect is greater, the current increases above its value at $\gamma=90^\circ$. The current in the field winding will correspondingly be maximum at $\gamma=0$ and minimum at $\gamma=90^\circ$. The parameters for the given tests, as in a transformer short-circuit test, are obtained on the basis of the phase voltage, current, and power:

$$\begin{aligned} z_d'' &= \frac{U}{2I_{\max}}; & z_q'' &= \frac{U}{2I_{\min}} \\ r_d'' &= \frac{P_d}{2I_{\max}^2}; & r_q'' &= \frac{P_q}{2I_{\min}^2} \\ x_d'' &= \sqrt{z_d''^2 - r_d''^2}; & x_q'' &= \sqrt{z_q''^2 - r_q''^2} \\ x_2 &= \frac{1}{2}(x_d'' + x_q''); & r_2 &= \frac{1}{2}(r_d'' + r_q'') \end{aligned}$$

Zero-Sequence Inductive Reactance and Resistance. If we run the rotor of a synchronous machine at synchronous speed with the field winding short-circuited and apply a single-phase voltage of rated frequency to the stator winding, all three phases of which are connected in series (Fig. 14-3), through all three phases a current will flow of the same value and phase which, in accordance with the definition, will be the zero-sequence current I_0 . The voltage U_0 applied to the windings, if we neglect the resistance $3r_0=3r_a$ of the stator windings because of its relatively low value, will be balanced by the sum of

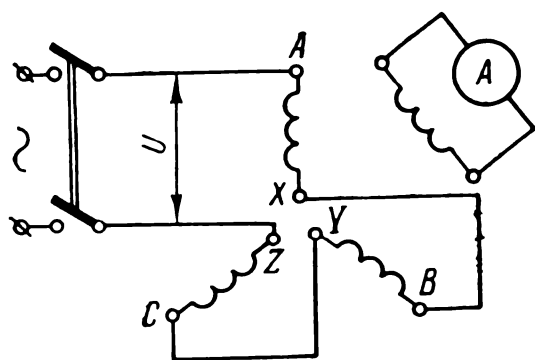


Fig. 14-3. Zero-sequence current tests in stator winding of a synchronous machine

the zero-sequence e.m.f.s of all three phases and, consequently,

$$U_0 \cong 3I_0 x_0$$

whence

$$x_0 \cong \frac{U_0}{3I_0}$$

The zero-sequence system currents in all the stator winding phases of a machine are equal in magnitude and coincide in phase, therefore, the fundamental magnetizing force harmonics of all phases, displaced in space by 120 electrical degrees, do not form a rotating magnetic field, but completely compensate each other so that their resultant fundamental harmonic field in the air-gap becomes zero. Consequently, the fundamental magnetizing force harmonics of the zero-sequence currents cannot produce armature-reaction fields, but produce only stator winding leakage fields. Similarly, the magnetizing forces of the 5th, 7th, 11th, 13th, etc., harmonics of the three phases also mutually balance one another. The third harmonic magnetizing forces of the zero-sequence currents in the three phases add together and produce in certain rotor positions (Fig. 14-4a) minor fluxes which link with its field winding and which, at synchronous rotor speeds, induce e.m.f.s of double and quadruple frequencies in the field winding. The same is true for the magnetizing force harmonics which are multiples of three. Since the air-gap in a synchronous machine is sufficiently large, the fluxes of harmonics which are a multiple of three are relatively small, and their mutual inductive linkage with the rotor circuits is of no appreciable importance.

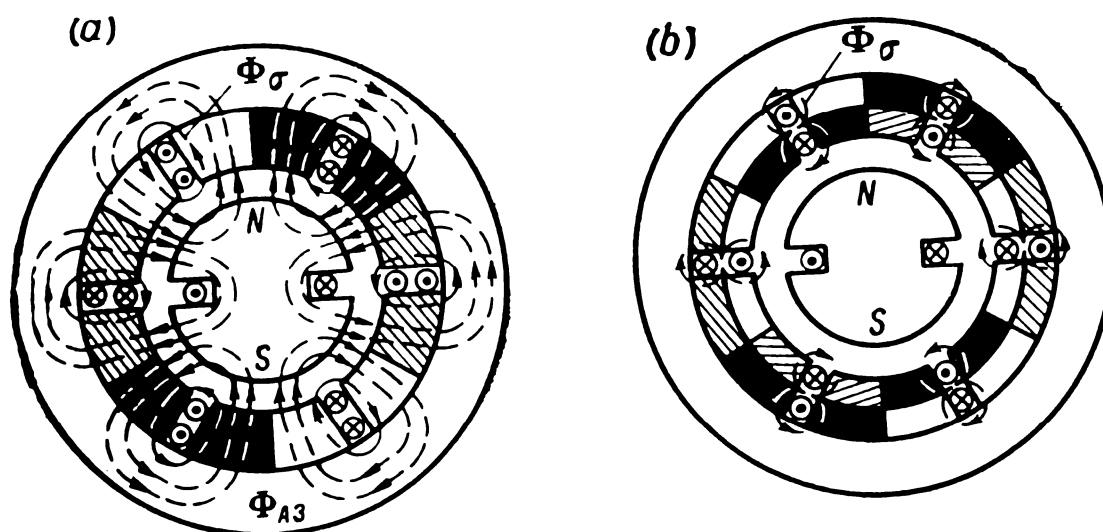


Fig. 14-4. Paths of zero-sequence fluxes and currents in a synchronous machine with full- (a) and short-pitch (b) winding

The distribution of the zero-sequence currents and of the fluxes produced by them for a full-pitch stator winding is presented in Fig. 14-4a. Here the distribution of the leakage fields in the slot parts of the winding is practically the same as for the positive-sequence currents, and the zero-sequence inductive reactance component corresponding to the leakage in the slots is therefore equal to the same reactive leakage component of the stator winding. In double-layer windings with a pitch shortened to $\frac{2}{3}\tau$ the zero-sequence currents in the conductors of the upper and lower layers flow in opposite directions (Fig. 14-4b), therefore the leakage fields in the slot parts of the winding and also in the air-gap become very small and x_0 drops to a very small value practically corresponding to the leakage fields of the end connections.

In the general case x_0 is within the range

$$0 < x_0 < x_{\sigma a}$$

where $x_{\sigma a}$ is the leakage reactance of the stator windings.

In conclusion, it should be noted that x_0 is practically independent of both the saturation of the main magnetic circuit of a machine and its duty.

As pointed out above, the zero-sequence currents do not produce fluxes which produce transformer coupling with the rotor windings. Therefore, the zero-sequence resistance r_0 may be assumed equal to the stator winding resistance r_a and, consequently, also equal to the positive-sequence resistance:

$$r_0 = r_1 = r_a$$

14-3. Asymmetrical Short Circuits of a Three-Phase Synchronous Generator

Asymmetrical short circuits occur quite often in networks connected to synchronous machines, in view of which it is of great practical importance to study these conditions. Below will be considered the simplest cases when a short circuit takes place across the terminals of a synchronous generator feeding a separate circuit and operating under no-load. If a short circuit occurs in the network, it is sufficient to add to the reactances x_{ad} and $x_{\sigma a}$ of the generator the reactances of the transmission line up to the point of short circuit for the corresponding phase sequences. The method of symmetrical components as applied to the analysis of asymmetrical operating conditions of a three-phase synchronous machine, similar to transformers (Vol. I, Chap. 19), makes it possible to determine the analytical relations between the phase voltages and currents $\dot{U}_a, \dot{U}_b, \dot{U}_c, \dot{I}_a, \dot{I}_b, \dot{I}_c$ and their symmetrical components $\dot{U}_1, \dot{U}_2, \dot{U}_0, \dot{I}_1, \dot{I}_2, \dot{I}_0$ and the e.m.f. of a synchronous ma-

chine, which is assumed to be symmetrically built, both with respect to geometrical distribution of the phase windings and to the number of turns in each winding. Owing to the fact that the phase e.m.f.s in this case form a positive-sequence symmetrical vector system, only the positive-sequence e.m.f. system remains, when the system is resolved into symmetrical components, and thus:

$$\dot{E}_1 = \dot{E}_a; \quad \dot{E}_2 = \dot{E}_0 = 0$$

The relation between the e.m.f.s and currents when using the symmetrical component method can be expressed, in the general case, in the form of the following system of nine equations:

$$\left. \begin{aligned} \dot{I}_a &= \dot{I}_0 + \dot{I}_1 + \dot{I}_2 \\ \dot{I}_b &= \dot{I}_0 + \alpha^2 \dot{I}_1 + \alpha \dot{I}_2 \\ \dot{I}_c &= \dot{I}_0 + \alpha \dot{I}_1 + \alpha^2 \dot{I}_2 \end{aligned} \right\} \quad (14-9)$$

$$\left. \begin{aligned} \dot{U}_a &= \dot{U}_0 + \dot{U}_1 + \dot{U}_2 \\ \dot{U}_b &= \dot{U}_0 + \alpha^2 \dot{U}_1 + \alpha \dot{U}_2 \\ \dot{U}_c &= \dot{U}_0 + \alpha \dot{U}_1 + \alpha^2 \dot{U}_2 \end{aligned} \right\} \quad (14-10)$$

$$\left. \begin{aligned} \dot{E}_0 &= Z_0 \dot{I}_0 + \dot{U}_0 = 0 \\ \dot{E}_1 &= Z_1 \dot{I}_1 + \dot{U}_1 = \dot{E}_a \\ \dot{E}_2 &= Z_2 \dot{I}_2 + \dot{U}_2 = 0 \end{aligned} \right\} \quad (14-11)$$

where α is the operator for a 120° -turn of the vector:

$$\alpha = e^{+j\frac{2\pi}{3}} = e^{-j\frac{4\pi}{3}} = -0.5 + j\frac{\sqrt{3}}{2}$$

Correspondingly,

$$\alpha^2 = -0.5 - j\frac{\sqrt{3}}{2}; \quad 1 + \alpha + \alpha^2 = 0; \quad \alpha - \alpha^2 = j\sqrt{3}; \quad \alpha^{3n} = 1; \\ \alpha^{3n+1} = \alpha; \quad \alpha^{3n+2} = \alpha^2$$

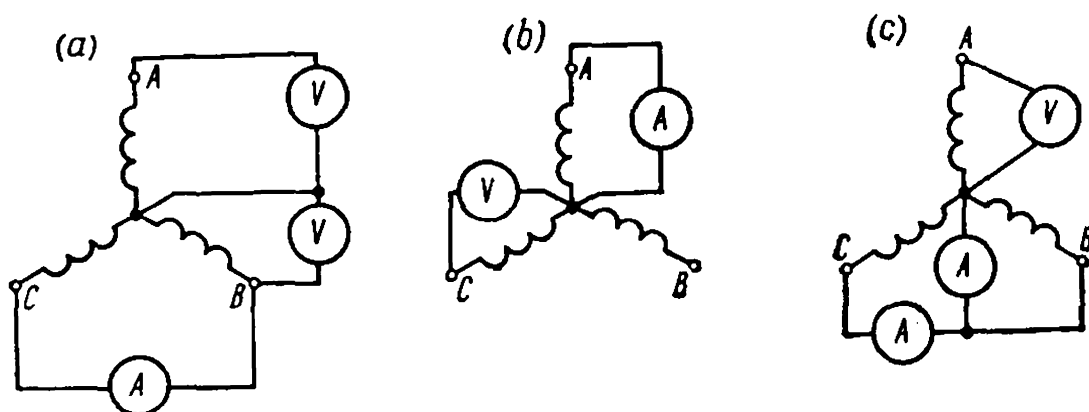


Fig. 14-5. Asymmetrical short circuit networks of a three-phase synchronous generator:

a — line-to-line; *b* — line-to-earth; *c* — double line-to-earth

To the nine equations (14-9), (14-10) and (14-11) are added three more equations resulting from the specific conditions of the problem which makes it possible to solve twelve equations with twelve variables, where E_a , Z_0 , Z_1 and Z_2 are the known quantities.

Line-to-Line Short Circuit. This case, as was noted above, is of the greatest interest when a synchronous generator feeds a transmission line through a transformer. All forms of asymmetrical short circuits in a transmission line are two-phase short circuits for synchronous generators. When a line-to-line fault occurs in *B* and *C* (Fig. 14-5*a*), we have

$$U_b = U_c; \quad I_a = 0; \quad I_b + I_c = 0$$

Summation of the system of equations (14-9) gives $I_0 = 0$. From the first equation of system (14-9) we then find that $I_1 + I_2 = 0$, and from the first equation of system (14-11), that $\dot{U}_0 = 0$.

By taking the difference between the second and third equations of system (14-10), we obtain $\dot{U}_1 = \dot{U}_2$. By taking the difference between the second and third equation of system (14-11) we find $(Z_1 + Z_2) I_1 = -\dot{E}_a$, whence for the currents of the positive and negative sequences we find

$$I_1 = -I_2 = \frac{\dot{E}_a}{Z_1 + Z_2} \quad (14-12)$$

Substituting for I_1 its value from equation (14-12) into the second equation of system (14-11), we get

$$\frac{Z_1 \dot{E}_a}{Z_1 + Z_2} + \dot{U}_1 = \dot{E}_a$$

whence we find the positive- and negative-sequence voltages:

$$\dot{U}_1 = \dot{U}_2 = \frac{Z_2 \dot{E}_a}{Z_1 + Z_2}$$

By substituting the values obtained for the symmetrical current and voltage components in equations (14-9) and (14-10), we get

$$\begin{aligned} \dot{I}_b = -\dot{I}_c &= (\alpha^2 - \alpha) \frac{\dot{E}_a}{Z_1 + Z_2} = -j\sqrt{3} \frac{\dot{E}_a}{Z_1 + Z_2} \quad (14-13) \\ \dot{U}_a &= 2 \frac{Z_2 \dot{E}_a}{Z_1 + Z_2}; \quad \dot{U}_b = \dot{U}_c = (\alpha^2 + \alpha) \frac{Z_2 \dot{E}_a}{Z_1 + Z_2} = -\frac{Z_2 \dot{E}_a}{Z_1 + Z_2} \end{aligned}$$

Expressing \dot{U}_a , \dot{U}_b and \dot{U}_c through the differences of the corresponding e.m.f.s and voltage drops induced by the symmetrical current components, we find that

$$\dot{U}_a = \dot{E}_a - \dot{E}_a + 2 \frac{Z_2 \dot{E}_a}{Z_1 + Z_2} = \dot{E}_a - \frac{(Z_1 - Z_2) \dot{E}_a}{Z_1 + Z_2}$$

whence, for phase *A* and similarly for phases *B* and *C*, we find

$$\left. \begin{aligned} \dot{U}_a &= \dot{E}_a - Z_1 \dot{I}_{a1} - Z_2 \dot{I}_{a2} \\ \dot{U}_b &= \dot{E}_b - Z_1 \dot{I}_{b1} - Z_2 \dot{I}_{b2} \\ \dot{U}_c &= \dot{E}_c - Z_1 \dot{I}_{c1} - Z_2 \dot{I}_{c2} \end{aligned} \right\} \quad (14-14)$$

where

$$\begin{aligned} \dot{I}_{a1} &= \dot{I}_1; \quad \dot{I}_{a2} = \dot{I}_2; \quad \dot{I}_{b1} = \alpha^2 \dot{I}_1; \\ \dot{I}_{b2} &= \alpha \dot{I}_2; \quad \dot{I}_{c1} = \alpha \dot{I}_1; \quad \dot{I}_{c2} = \alpha^2 \dot{I}_2 \end{aligned}$$

The absolute value of the short-circuit current according to equation (14-13) is

$$I_{sh} = \frac{\sqrt{3} E_a}{|Z_1 + Z_2|} \quad (14-15)$$

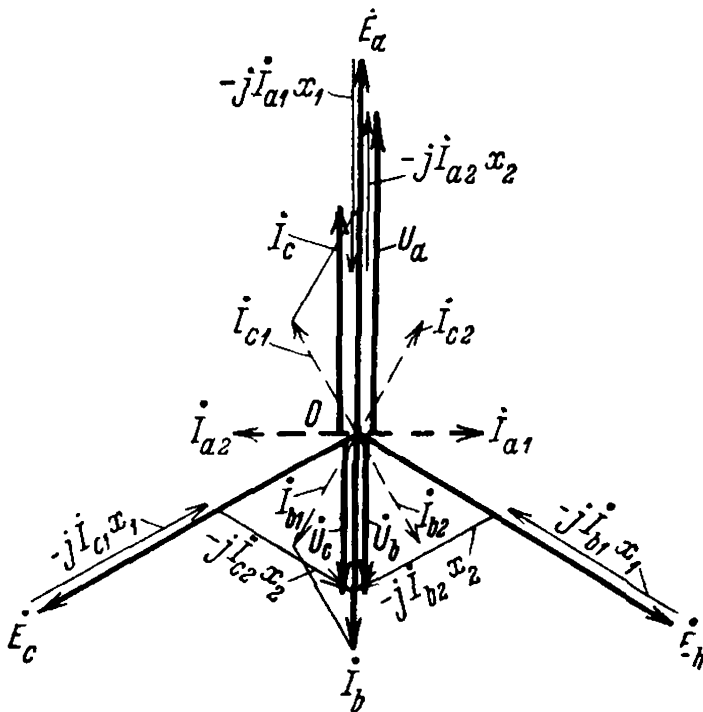


Fig. 14-6. Voltage diagram for double line-to-earth short circuit of a synchronous generator

An approximate vector diagram neglecting resistances for a double line-to-earth short circuit is shown in Fig. 14-6.

Line-to-Earth Short Circuit. When a short circuit of phase *A* takes place (Fig. 14-5*b*), we obtain the following additional equations:

$$\dot{I}_b = \dot{I}_c = 0 \quad \text{and} \quad \dot{U}_a = 0$$

By summing the system (14-9), we get $\dot{I}_a = 3\dot{I}_0$. If after this we take the difference between the second and third equations of system (14-9), we find

that $I_1 = I_2$. Then from the first equation of system (14-9) we obtain

$$I_0 = I_1 = I_2 = \frac{1}{3} I_a$$

By summing the system (14-11), we now obtain

$$I_0 (Z_0 + Z_1 + Z_2) = \dot{E}_a$$

whence

$$I_0 = I_1 = I_2 = \frac{\dot{E}_a}{Z_0 + Z_1 + Z_2} \quad (14-16)$$

From system (14-11) it can be found that

$$\left. \begin{aligned} \dot{U}_0 &= -Z_0 I_0 = -\frac{Z_0 \dot{E}_a}{Z_0 + Z_1 + Z_2} \\ \dot{U}_1 &= \dot{E}_a - Z_1 I_1 = \frac{(Z_0 + Z_2) \dot{E}_a}{Z_0 + Z_1 + Z_2} \\ \dot{U}_2 &= -Z_2 I_2 = -\frac{Z_2 \dot{E}_a}{Z_0 + Z_1 + Z_2} \end{aligned} \right\} \quad (14-17)$$

By substituting the values obtained for the symmetrical components of the voltages and currents in equations (14-9) and (14-10) we get

$$I_a = \frac{3\dot{E}_a}{Z_0 + Z_1 + Z_2}; \quad I_b = I_c = 0 \quad (14-18)$$

$$\begin{aligned} \dot{U}_b &= [(\alpha^2 - 1)Z_0 + (\alpha^2 - \alpha)Z_2] \frac{\dot{E}_a}{Z_0 + Z_1 + Z_2} \\ \dot{U}_c &= [(\alpha - 1)Z_0 - (\alpha^2 - \alpha)Z_2] \frac{\dot{E}_a}{Z_0 + Z_1 + Z_2} = 0 \end{aligned}$$

Expressing \dot{U}_a , \dot{U}_b and \dot{U}_c by the differences of the corresponding e.m.f.s and voltage drops due to the symmetrical components, we obtain for phase A

$$\dot{U}_a = \dot{E}_a - (Z_0 + Z_1 + Z_2) \frac{\dot{E}_a}{Z_0 + Z_1 + Z_2} = 0$$

whence for the A-phase voltage and similarly for the voltages of the other phases we obtain

$$\left. \begin{aligned} \dot{U}_a &= \dot{E}_a - Z_1 I_{a1} - Z_2 I_{a2} - Z_0 I_{a0} \\ \dot{U}_b &= \dot{E}_b - Z_1 I_{b1} - Z_2 I_{b2} - Z_0 I_{b0} \\ \dot{U}_c &= \dot{E}_c - Z_1 I_{c1} - Z_2 I_{c2} - Z_0 I_{c0} \end{aligned} \right\} \quad (14-19)$$

The absolute value of the short-circuit current according to equation (14-18) will equal

$$I_{sh} = \frac{3\dot{E}_a}{|Z_0 + Z_1 + Z_2|} \quad (14-20)$$

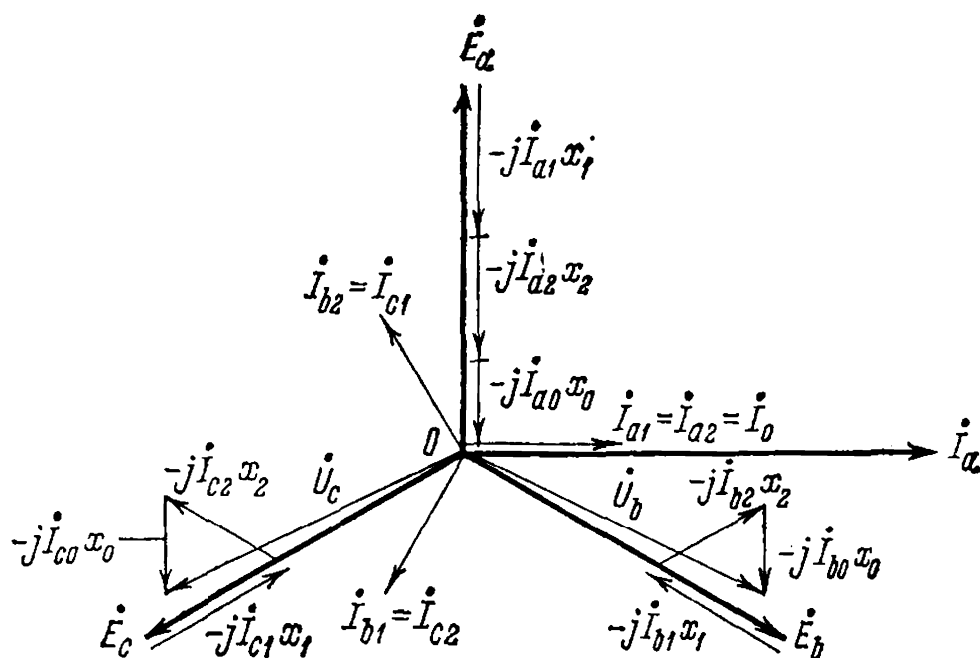


Fig. 14-7. Voltage diagram for line-to-earth short circuit of a synchronous generator

The approximate vector diagram for a line-to-earth short circuit is given in Fig. 14-7, neglecting the resistances.

Double Line-to-Earth Short Circuit. With a short circuit between phases *B* and *C* and the neutral (Fig. 14-5c) we have the additional equations

$$I_a = 0; \quad U_b = U_c = 0$$

Solving the problem the same way as in the above two cases of short circuit, on the basis of systems of equations (14-9), (14-10) and (14-11), we get the following values of the symmetrical current and voltage components

$$U_0 = U_1 = U_2 = \frac{Z_0 Z_2 \dot{E}_a}{Z_1 Z_2 + Z_1 Z_0 + Z_2 Z_0} \quad (14-21)$$

$$\left. \begin{aligned} I_0 &= -\frac{U_0}{Z_0} = -\frac{Z_2 \dot{E}_a}{Z_1 Z_2 + Z_1 Z_0 + Z_2 Z_0} \\ I_1 &= \frac{\dot{E}_a - U_1}{Z_1} = \frac{(Z_2 + Z_0) \dot{E}_a}{Z_1 Z_2 + Z_1 Z_0 + Z_2 Z_0} \\ I_2 &= -\frac{U_2}{Z_2} = -\frac{Z_0 \dot{E}_a}{Z_1 Z_2 + Z_1 Z_0 + Z_2 Z_0} \end{aligned} \right\} \quad (14-22)$$

Substituting their values for the symmetrical current and voltage components in equations (14-9) and (14-10), we obtain for the phase

currents and voltages

$$\left. \begin{aligned} \dot{I}_b &= [(\alpha^2 - 1)Z_2 + (\alpha^2 - \alpha)Z_0] \frac{\dot{E}_a}{Z_1Z_2 + Z_1Z_0 + Z_2Z_0} \\ \dot{I}_c &= [(\alpha - 1)Z_2 - (\alpha^2 - \alpha)Z_0] \frac{\dot{E}_a}{Z_1Z_2 + Z_1Z_0 + Z_2Z_0} \end{aligned} \right\} \quad (14-23)$$

$$\dot{U}_a = \frac{3Z_0Z_2\dot{E}_a}{Z_1Z_2 + Z_1Z_0 + Z_2Z_0} \quad (14-24)$$

By expressing \dot{U}_a , \dot{U}_b and \dot{U}_c through the differences of the corresponding e.m.f.s and voltage drops due to the symmetrical current components, we have

$$\dot{U}_a = \dot{E}_a - \frac{\dot{E}_a}{Z_1Z_2 + Z_1Z_0 + Z_2Z_0} (Z_1Z_2 + Z_1Z_0 - 2Z_2Z_0)$$

whence, for phase A and, similarly, for the other phases

$$\left. \begin{aligned} \dot{U}_a &= \dot{E}_a - Z_1\dot{I}_{a1} - Z_2\dot{I}_{a2} - Z_0\dot{I}_{a0} \\ \dot{U}_b &= \dot{E}_b - Z_1\dot{I}_{b1} - Z_2\dot{I}_{b2} - Z_0\dot{I}_{b0} \\ \dot{U}_c &= \dot{E}_c - Z_1\dot{I}_{c1} - Z_2\dot{I}_{c2} - Z_0\dot{I}_{c0} \end{aligned} \right\} \quad (14-25)$$

The absolute value of the short-circuit current in a phase, when the arguments Z_2 and Z_0 are equal, is

$$I_{sh} = \frac{\sqrt{3} \times V \sqrt{|Z_2^2 + Z_0Z_2 + Z_0^2|} E_a}{|Z_1Z_2 + Z_1Z_0 + Z_2Z_0|} \quad (14-26)$$

An approximate vector diagram of the currents and voltages for a double line-to-earth short circuit is given in Fig. 14-8, the resistances being neglected.

The values of the currents for different types of short circuits are summarized in Table 14-1, the current in the neutral conductor being designated as I_{shz} .

Since the resistances of the circuits, in comparison with

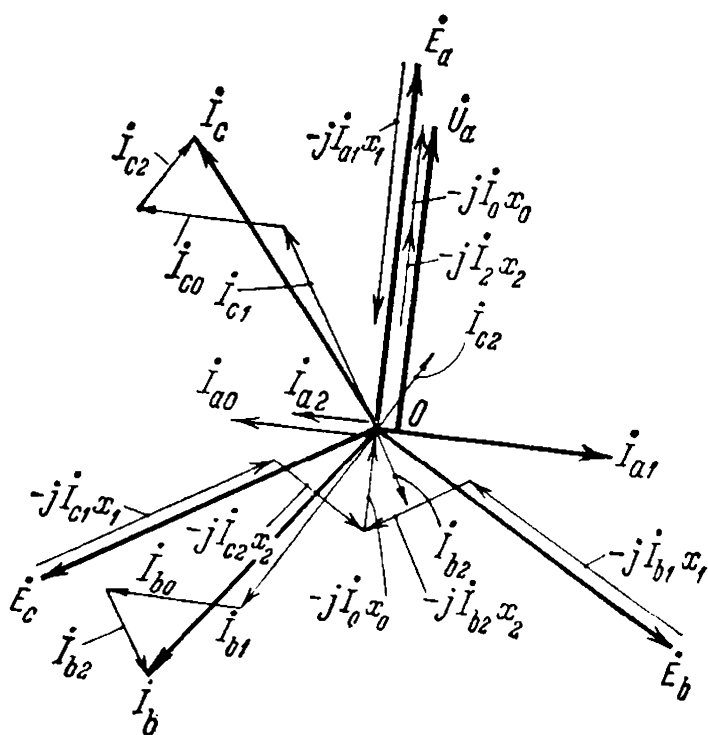


Fig. 14-8. Voltage diagram of a synchronous generator for double line-to-earth short circuit

TABLE 14-1

Current	Short circuit			
	on three lines	on two lines	on one line	on double line-to-earth
i_1	$\frac{\dot{E}_a}{Z_1}$	$\frac{\dot{E}_a}{Z_1 + Z_2}$	$\frac{\dot{E}_a}{Z_0 + Z_1 + Z_2}$	$\frac{(Z_0 + Z_2)\dot{E}_a}{Z_1Z_2 + Z_1Z_0 + Z_2Z_0}$
i_2	0	$-\frac{\dot{E}_a}{Z_1 + Z_2}$	$\frac{\dot{E}_a}{Z_0 + Z_1 + Z_2}$	$-\frac{Z_0\dot{E}_a}{Z_1Z_2 + Z_1Z_0 + Z_2Z_0}$
i_0	0	0	$\frac{\dot{E}_a}{Z_0 + Z_1 + Z_2}$	$-\frac{Z_2\dot{E}_a}{Z_1Z_2 + Z_1Z_0 + Z_2Z_0}$
i_{shz}	0	0	$\frac{3\dot{E}_a}{Z_0 + Z_1 + Z_2}$	$-\frac{3Z_2\dot{E}_a}{Z_1Z_2 + Z_1Z_0 + Z_2Z_0}$
i_{sh}	$\frac{\dot{E}_a}{ Z_1 }$	$\frac{\sqrt{3}\dot{E}_a}{ Z_1 + Z_2 }$	$\frac{3\dot{E}_a}{ Z_0 + Z_1 + Z_2 }$	$\frac{\sqrt{3}\sqrt{ Z_2^2 + Z_2Z_0 + Z_0^2 }\dot{E}_a}{ Z_1Z_2 + Z_1Z_0 + Z_2Z_0 }$

the reactances, are very small, the impedances Z may be without appreciable error replaced by the inductive reactances jx .

Example 14-1. Determine the magnitudes of the symmetrical and asymmetrical short-circuit currents for the hydrogenerator with $P_r=57\,200$ kW considered in Chapter 8, at the rated voltage ($U_r=1$), disregarding the resistances r_1 , r_2 and r_0 . The relative inductive reactances of the generator are: $\underline{x}_1=\underline{x}_d=0.695$; $\underline{x}_2=0.215$ and $\underline{x}_0=0.054$. According to Table 14-1 the current values for short circuits:

1. On three lines

$$\underline{I}_{sh3}=\frac{1}{\underline{x}_1}=\frac{1}{0.695}=1.44$$

2. On two lines

$$\underline{I}_{sh2}=\frac{\sqrt{3}}{\underline{x}_1+\underline{x}_2}=\frac{\sqrt{3}}{0.695+0.215}=1.91$$

3. On one line

$$\underline{I}_{sh1}=\frac{3}{\underline{x}_1+\underline{x}_2+\underline{x}_0}=\frac{3}{0.695+0.215+0.054}=3.12$$

4. On double line-to-earth

$$\begin{aligned} \underline{I}_{sh} &= \frac{\sqrt{3} \sqrt{\underline{x}_2^2 + \underline{x}_2 \underline{x}_0 + \underline{x}_0^2}}{(\underline{x}_1 \underline{x}_2 + \underline{x}_1 \underline{x}_0 + \underline{x}_2 \underline{x}_0)} = \\ &= \frac{\sqrt{3} \sqrt{0.215^2 + 0.215 \times 0.054 + 0.054^2}}{0.695 \times 0.215 + 0.965 \times 0.054 + 0.215 \times 0.054} = \sqrt{3} \frac{0.243}{0.2036} = 2.08 \end{aligned}$$

14-4. Voltage Diagrams for Short Circuits

Voltage Diagram for Line-to-Line Short Circuit (Fig. 14-6). When phases *B* and *C* are affected, assuming $r_a = 0$, from equations (14-12) and (14-14), we obtain

$$\dot{I}_0 = 0, \quad \dot{I}_{a1} = -\dot{I}_{a2} = -j \frac{\dot{E}_a}{x_1 + x_2} \quad (14-27)$$

$$\left. \begin{aligned} \dot{U}_a &= \dot{E}_a - jx_1 \dot{I}_{a1} - jx_2 \dot{I}_{a2} \\ \dot{U}_b &= \dot{E}_b - jx_1 \dot{I}_{b1} - jx_2 \dot{I}_{b2} \\ \dot{U}_c &= \dot{E}_c - jx_1 \dot{I}_{c1} - jx_2 \dot{I}_{c2} \end{aligned} \right\} \quad (14-28)$$

Having constructed the symmetrical system of e.m.f.s \dot{E}_a , \dot{E}_b and \dot{E}_c (Fig. 14-6), we lay off vectors $\dot{I}_1 = \dot{I}_{a1}$ lagging and $\dot{I}_2 = \dot{I}_{a2}$ leading by 90° with respect to the e.m.f. \dot{E}_a . Next we plot the system of vectors of the positive-sequence currents \dot{I}_{a1} , \dot{I}_{b1} , \dot{I}_{c1} and the negative-sequence currents \dot{I}_{a2} , \dot{I}_{b2} , \dot{I}_{c2} for the three phases. The vectors \dot{U}_a , \dot{U}_b and \dot{U}_c are plotted according to equation (14-28). The phase current vectors are plotted in accordance with equations:

$$\dot{I}_a = \dot{I}_{a1} + \dot{I}_{a2}, \quad \dot{I}_b = \dot{I}_{b1} + \dot{I}_{b2}$$

Voltage Diagram for Line-to-Earth Short Circuit (Fig. 14-7). For a short circuit of phase *A*, assuming $r_a \cong 0$, from equations (14-16) and (14-19), we have

$$\dot{I}_{a1} = \dot{I}_{a2} = \dot{I}_{a0} = -j \frac{\dot{E}_a}{x_0 + x_1 + x_2} \quad (14-29)$$

$$\left. \begin{aligned} \dot{U}_a &= \dot{E}_a - j\dot{I}_{a1}x_1 - j\dot{I}_{a2}x_2 - j\dot{I}_{a0}x_0 \\ \dot{U}_b &= \dot{E}_b - j\dot{I}_{b1}x_1 - j\dot{I}_{b2}x_2 - j\dot{I}_{b0}x_0 \\ \dot{U}_c &= \dot{E}_c - j\dot{I}_{c1}x_1 - j\dot{I}_{c2}x_2 - j\dot{I}_{c0}x_0 \end{aligned} \right\} \quad (14-30)$$

Having constructed the symmetrical system of e.m.f.s \dot{E}_a , \dot{E}_b and \dot{E}_c (Fig. 14-7), we lay off vectors $\dot{I}_{a1} = \dot{I}_{a2} = \dot{I}_{a0}$ lagging on \dot{E}_a by 90° . Then we plot the system of vectors of the positive-sequence currents \dot{I}_{a1} , \dot{I}_{b1} , \dot{I}_{c1} , negative-sequence currents \dot{I}_{a2} , \dot{I}_{b2} , \dot{I}_{c2} and zero-

sequence currents $\dot{I}_{a0} = \dot{I}_{b0} = \dot{I}_{c0}$, and also vectors \dot{U}_a , \dot{U}_b , \dot{U}_c according to equation (14-30). The vector of the phase current \dot{I}_a is plotted in accordance with the equation

$$\dot{I}_a = \dot{I}_{a0} + \dot{I}_{a1} + \dot{I}_{a2}$$

Voltage Diagram for Double Line-to-Earth Short Circuit. (Fig. 14-8). When the phases B and C and the neutral are affected, assuming $r_a = 0$ and according to (14-22), we obtain

$$\left. \begin{aligned} \dot{I}_{a1} &= -j \frac{(x_2 + x_0) \dot{E}_a}{x_1 x_2 + x_1 x_0 + x_2 x_0} \\ \dot{I}_{a2} &= j \frac{x_0 \dot{E}_a}{x_1 x_2 + x_1 x_0 + x_2 x_0} \\ \dot{I}_{a0} &= j \frac{x_2 \dot{E}_a}{x_1 x_2 + x_1 x_0 + x_2 x_0} \end{aligned} \right\} \quad (14-31)$$

The voltages \dot{U}_a , \dot{U}_b and \dot{U}_c are determined from equation (14-25) by substituting jx for Z .

Having constructed the symmetrical system of the vectors \dot{E}_a , \dot{E}_b and \dot{E}_c (Fig. 14-8), we lay off the vectors \dot{I}_{a1} lagging, and \dot{I}_{a2} and \dot{I}_{a0} leading \dot{E}_a by 90° . Then we construct the system of vectors of positive-sequence currents \dot{I}_{a1} , \dot{I}_{b1} , \dot{I}_{c1} , and of the negative-sequence currents \dot{I}_{a2} , \dot{I}_{b2} , \dot{I}_{c2} . The vectors \dot{U}_a , \dot{U}_b and \dot{U}_c are constructed according to equation (14-25). The vectors of the phase currents are plotted in accordance with the equations $\dot{I}_b = \dot{I}_{b0} + \dot{I}_{b1} + \dot{I}_{b2}$ and $\dot{I}_c = \dot{I}_{c0} + \dot{I}_{c1} + \dot{I}_{c2}$.

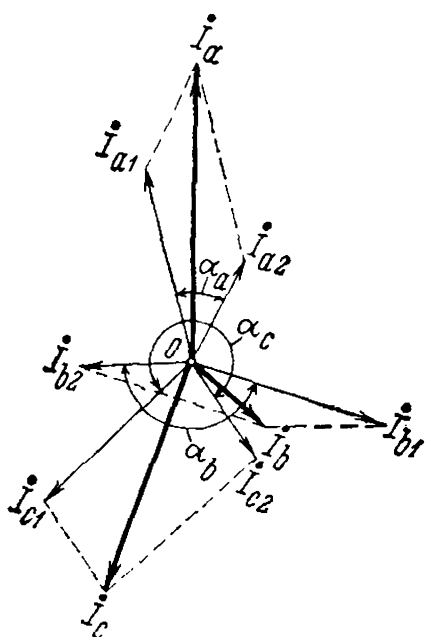


Fig. 14-9. Resolution of asymmetrical currents of a synchronous generator with unearthed neutral into positive- and negative-sequence current components

14-5. Voltage Diagrams for Unbalanced Load

Consider the most probable operating conditions of a non-salient-pole generator ($x_d = x_q = x_1$) in the absence of neutral earthing. Here the system of asymmetrical current vectors is resolved into two symmetrical systems of positive- and negative-sequence current vectors, the zero-sequence system being absent, since no current flows through the grounded wire. The system of positive-sequence currents will induce in the stator winding the e.m.f. $-j\dot{I}_1 x_1$ lagging 90° on the current vector \dot{I}_1 of this phase. The system

of negative-sequence currents induces an e.m.f. $-j\dot{I}_2x_2$ lagging on current vector \dot{I}_2 of the same phase by 90° .

Since the phase sequence of current vectors \dot{I}_1 and \dot{I}_2 is opposite, the angles of displacement α_a , α_b and α_c between the symmetrical component vectors of the phase currents are therefore different in all the phases (Fig. 14-9). As a result, although the amplitudes of the e.m.f.s $j\dot{I}_1x_1$ and $j\dot{I}_2x_2$ are the same in all phases, their vector sums are different for each phase, and, therefore, the resultant displacement angles θ_a , θ_b and θ_c between the voltage vectors $\dot{U}_a, \dot{U}_b, \dot{U}_c$ and the e.m.f. vectors $\dot{E}_a, \dot{E}_b, \dot{E}_c$ are also different for each phase. Thus, it is necessary to construct a voltage diagram separately for each phase. Such a construction is shown in Fig. 14-10.

The current vectors \dot{I}_{a1} , \dot{I}_{b1} and \dot{I}_{c1} are taken as the initial vectors for these constructions for each of the phases. The e.m.f.s \dot{E}_a, \dot{E}_b and \dot{E}_c are equal in magnitude and displaced with respect to the positive-sequence current vectors by the same angles $\psi_{a1} = \psi_{b1} = \psi_{c1}$. The e.m.f.s $-j\dot{I}_{a1}x_1$, $-j\dot{I}_{b1}x_1$ and $-j\dot{I}_{c1}x_1$ are therefore equal in magnitude and equally phase-shifted from the e.m.f.s \dot{E}_a, \dot{E}_b and \dot{E}_c . A glance at

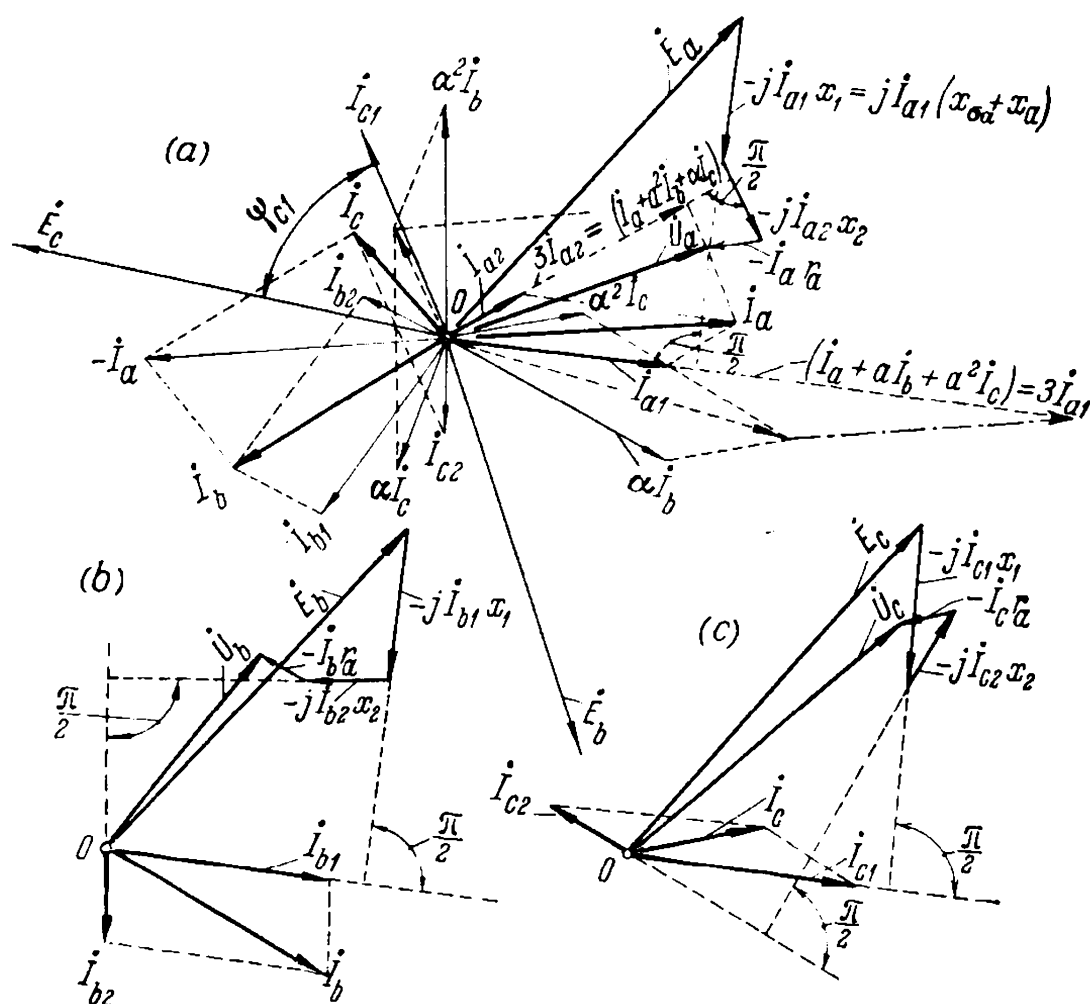


Fig. 14-10. Vector diagrams for three lines with unbalanced loading of a synchronous generator having unearthed neutral

Fig. 14-10 shows that these e.m.f.s occupy the same position with respect to the initial current vectors \dot{I}_{a1} , \dot{I}_{b1} and \dot{I}_{c1} on all the diagrams.

By then orientating on each diagram the vectors \dot{I}_{a2} , \dot{I}_{b2} , \dot{I}_{c2} and \dot{I}_a , \dot{I}_b , \dot{I}_c as in Fig. 14-9, we see that these systems of vectors are arranged on each of the diagrams differently with respect to the positive-sequence vectors. The negative-sequence currents will produce in each phase the e.m.f.s $-j\dot{I}_{a2}x_2$, $-j\dot{I}_{b2}x_2$ and $-j\dot{I}_{c2}x_2$ which lag on these currents by 90° in time. The e.m.f. vectors $-\dot{I}_a r_a$, $-\dot{I}_b r_a$ and $-\dot{I}_c r_a$ are directed opposite to the current vectors \dot{I}_a , \dot{I}_b and \dot{I}_c . By summation of the e.m.f.s induced in each of the phases, we find the terminal voltages \dot{U}_a , \dot{U}_b and \dot{U}_c .

It is possible to superpose all three diagrams in Fig. 14-10 onto a common diagram using the method of V. Tolvinsky [103]. Here it is not necessary to plot the voltage diagrams separately for each phase, the diagram in Fig. 14-11 being constructed directly. For this purpose, having constructed the voltage diagram for one phase, for instance, the diagram in Fig. 14-10a for phase A, we add at the origin O the currents \dot{I}_{b2} and \dot{I}_{c2} . As can be seen from the diagram in Fig. 14-11, with such a construction the sequence of the currents \dot{I}_{a2} , \dot{I}_{b2} and \dot{I}_{c2} will be not negative, but positive. The e.m.f.s $-j\dot{I}_{a2}x_2$, $-j\dot{I}_{b2}x_2$ and $-j\dot{I}_{c2}x_2$ will be shifted by 120° from each other on the diagram, also in a positive-sequence order. To construct the direction of the resultant currents \dot{I}_a , \dot{I}_b and \dot{I}_c on the superposed diagram of Fig. 14-11, it is necessary to add the current vectors \dot{I}_{a2} , \dot{I}_{b2} and \dot{I}_{c2} to the superposed initial current vector \dot{I}_1 . By joining the ends of vectors $-\dot{I}_a r_a$, $-\dot{I}_b r_a$

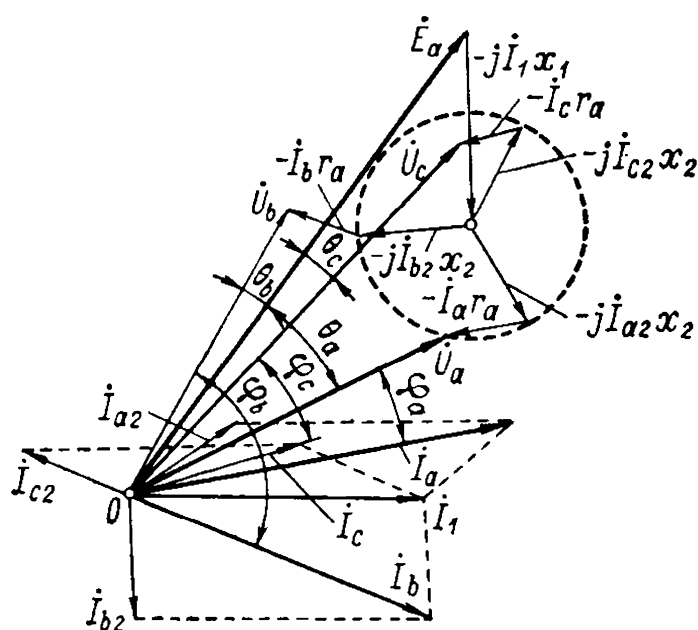


Fig. 14-11. Superposed vector diagram for unbalanced loading of a synchronous generator with unearthed neutral

and $-\dot{I}_c r_a$ with the origin of coordinates O , we obtain the voltages \dot{U}_a , \dot{U}_b , \dot{U}_c and their angles of displacement θ_a , θ_b , θ_c from the corresponding e.m.f.s \dot{E}_a , \dot{E}_b and \dot{E}_c .

The diagram in Fig. 14-11 makes it possible to construct the actual resultant vector diagram of the currents and e.m.f.s (Fig. 14-12). For this purpose we construct a diagram with the e.m.f.s \dot{E}_a , \dot{E}_b and \dot{E}_c equal in magnitude and displaced from each other by 120° . Then, according to Fig. 14-11, we construct a system of cur-

rents \dot{I}_a , \dot{I}_b and \dot{I}_c displaced from the corresponding e.m.f.s \dot{E}_a , \dot{E}_b and \dot{E}_c by the angles φ_a , φ_b and φ_c , and a system of voltages \dot{U}_a , \dot{U}_b and \dot{U}_c displaced from the corresponding e.m.f.s \dot{E}_a , \dot{E}_b and \dot{E}_c by the angles θ_a , θ_b and θ_c . It is easy to notice that the symmetrical star of the excitation e.m.f.s \dot{E}_a , \dot{E}_b and \dot{E}_c corresponding to no-load conditions is changed under the effect of an unbalanced load into an asymmetrical star of voltages \dot{U}_a , \dot{U}_b and \dot{U}_c . The corresponding lag angles φ_a , φ_b and φ_c of the resultant currents relative to the voltage vectors are different for all the phases.

In the most general case of unbalanced load, when, besides an oppositely rotating field, the windings carry currents coinciding in phase due to earthing of one of the phases when the generator neutral is earthed, the voltage diagrams can be constructed by fundamentally the same method. The asymmetrical system of currents \dot{I}_a , \dot{I}_b and \dot{I}_c is resolved into three symmetrical current systems — positive-, negative- and zero-sequences. Then the e.m.f.s must be constructed separately for the currents of each sequence. Obviously, the diagram of Fig. 14-10 will become more complicated only by the addition of the e.m.f.s $-j\dot{I}_{a0}x_0$, $-j\dot{I}_{b0}x_0$ and $-j\dot{I}_{c0}x_0$ lagging 90° in time behind the corresponding current vectors \dot{I}_{a0} , \dot{I}_{b0} and \dot{I}_{c0} .

On the superposed diagram constructed by the Tolvinsky method, the zero-sequence vectors will be arranged in negative-sequence order.

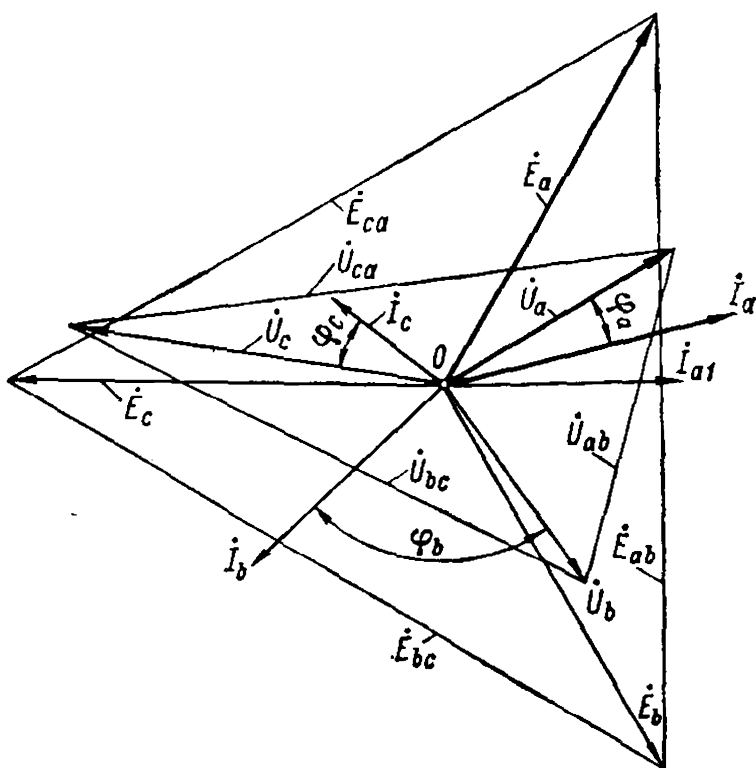


Fig. 14-12. Actual vector diagram for unbalanced loading of a synchronous generator corresponding to superposed diagram in Fig. 14-11.

14-6. Construction of Short-Circuit Triangles for Steady-State Short Circuits of a Generator, with Account of Magnetic Circuit Saturation

In a three-phase short circuit, the magnetic circuit of a machine, as shown above, remains practically unsaturated. With one- and two-phase short circuits, the relative value of the positive-sequence current producing the demagnetizing armature reaction is less, and therefore the magnetic circuit of a machine may be saturated to a

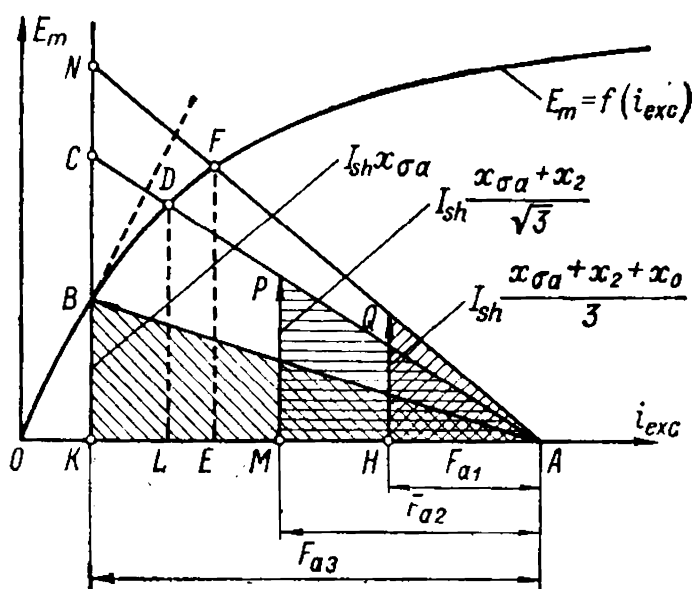


Fig. 14-13. Triangles for three-, two- and one-phase short circuits

the expressions obtained above for the currents of asymmetrical short circuits, the value of the reactance x_1 therefore becomes somewhat indefinite, and makes it more difficult to obtain sufficiently precise values of the short-circuit currents from these expressions. When it is necessary to find the values of the asymmetrical short-circuit currents more precisely, this difficulty can be overcome by the method considered below based on the no-load characteristic, which reflects magnetic-circuit saturation.

The quantitative relations given below in the text and figures for a one-phase short circuit proceed from the assumption that the generator neutral is dead-earthed. In actual practice the neutral is usually earthed through a large resistance and the generator current for a one-phase short circuit is considerably reduced.

With the generator positive-, negative- and zero-sequence inductive reactances known, it is possible to construct short-circuit triangles for two- and one-phase short circuits by the same method as for a three-phase short circuit (Fig. 14-13). With equal phase short-circuit currents I_{sh} in all three cases, the ratios of the armature-reaction magnetizing forces produced by the symmetrical positive-sequence current component will be

$$F_{a3} : F_{a2} : F_{a1} = \frac{3}{2} \times \frac{2\sqrt{2}}{\pi} \times \frac{\omega k_w}{p} I_{sh} : \frac{2}{2} \times \frac{\sqrt{3}}{2} \times \frac{2\sqrt{2}}{\pi} \times \frac{\omega k_w}{p} I_{sh} : \frac{1}{2} \times \frac{2\sqrt{2}}{\pi} \times \frac{\omega k_w}{p} I_{sh} = 3 : \sqrt{3} : 1 \quad (14-32)$$

Let us neglect the winding resistances. Then, the internal e.m.f. E_o induced in the stator winding by the resultant flux of the excitation current and the armature-reaction current due to the positive-sequence

certain extent, particularly when the short circuit occurs in the power line, and the value of the short-circuit current is thereby decreased.

As mentioned above, the saturation of the main magnetic circuit negligibly affects the values of the inductive leakage reactances $x_{\sigma a}$, the zero-sequence reactance x_0 and the negative-sequence reactance x_2 , but it appreciably affects the value of the armature-reaction reactance x_{ad} and, hence, the value of the positive-sequence reactance $x_1 = x_d = x_{\sigma a} + x_{ad}$. In

current, equal to

$$E_{\delta} = E_m - x_{ad}I_1 = E_a - x_{ad}I_1$$

will be, for a three-phase short circuit, equal to $x_{\sigma a}I_{sh}$, and, for a two-phase short-circuit, according to equations (14-12) and (14-15) to

$$E_{\sigma} = \frac{x_{\sigma a} + x_2}{\sqrt{3}} I_{sh}$$

and, finally, for a one-phase short circuit, according to equations (14-16) and (14-20) to

$$E_{\sigma} = \frac{x_{\sigma a} + x_2 + x_0}{3} I_{sh}$$

Thus, for the same current I_{sh} the short-circuit triangles BKA , PMA and QHA for all three cases will have the form shown in Fig. 14-13.

If in a two- and a one-phase short circuit we were to apply the same excitation to a generator as in a three-phase short circuit, the reaction magnetizing force and the leakage e.m.f. would so increase that apex P of the short-circuit triangle for a two-phase short circuit would shift to point D at the intersection of the no-load characteristic and the extension of the line AP , while apex Q of the short-circuit triangle for a one-phase short circuit would shift to point F at the intersection of the no-load characteristic and the extension of line AQ .

If, for a two-phase short circuit, the short-circuit triangle PMA becomes equal to ΔCKA , the short-circuit current should increase, as compared with a three-phase short circuit, in the ratio $\sqrt{3} : 1$, but if the same triangle PMA for a two-phase short circuit is equal to ΔDLA , the corresponding current will increase only in the ratio $\sqrt{3} \times \frac{LA}{KA}$. Similarly, if for a one-phase short circuit the short-circuit triangle becomes NKA instead of QHA , the current would increase in comparison with the three-phase short circuit in the ratio $3 : 1$. If the short-circuit triangle is equal to FEA , the current will increase only in the ratio $3 \times \frac{EA}{KA}$.

Thus, with equal excitation currents, in all three cases the short-circuit currents will be in the ratio of

$$1 : \sqrt{3} \times \frac{AL}{KA} : 3 \times \frac{EA}{KA}$$

For turbogenerators with a total leakage of 10%, this ratio will be $1 : 1.57 : 2.73$. For low-speed generators with a leakage of 30%, this relationship will be $1 : 1.33 : 2.3$. As an average for preliminary calculations, the ratio for sustained short circuits may be assumed to be $1 : 1.5 : 2.5$. The precise ratio can be determined by the method

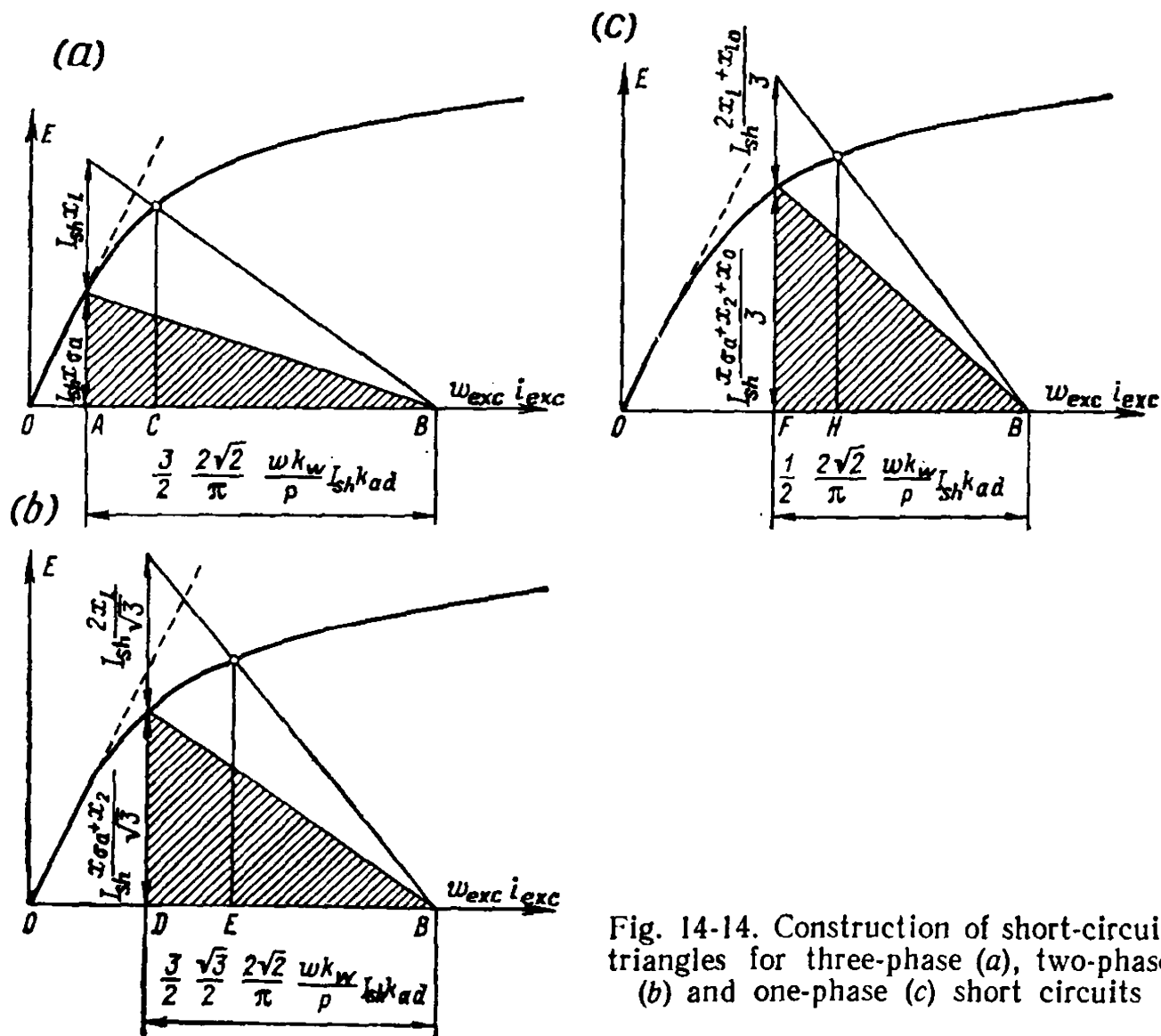


Fig. 14-14. Construction of short-circuit triangles for three-phase (a), two-phase (b) and one-phase (c) short circuits

described above from the no-load characteristic and the short-circuit triangles.

If the short circuit occurs not at the terminals of the generator itself, but in the line, then in constructing the short-circuit triangle its vertical side must be lengthened by the value of the reactive voltage drop in the line. It should then be taken into account here that, in accordance with the analysis of asymmetrical short circuits made above, when short circuits occur in the line it is necessary to add to each of the reactances x_0 , x_1 and x_2 of the machine itself the corresponding sequence reactances of the transmission line.

For transmission lines the positive- and negative-sequence reactances are equal to $x_{11} = x_{12} = x_1$, and the zero-sequence reactance x_{10} is less than the former two. Thus if, for example, with a two-phase short circuit at the generator terminals the internal e.m.f. E_δ is equal to

$$E_\delta = \frac{x_{0a} + x_2}{\sqrt{3}} I$$

then with a two-phase short circuit in the line, it will be

$$E_{\delta} = \left(\frac{x_{\sigma a} + x_2}{\sqrt{3}} + \frac{2x_l}{\sqrt{3}} \right) I$$

Figure 14-14 shows the corresponding constructions for a short circuit in the line. Obviously, the current with a three-phase short circuit in the line will decrease in the ratio $CB:AB$ (Fig. 14-14a), with a two-phase short circuit in the ratio $EB:DB$ (Fig. 14-14b), and with a one-phase short circuit in the ratio $HB:FB$ (Fig. 14-14c).

If in a synchronous generator one turn or a part of a winding is short-circuited, then, owing to the very small demagnetizing effect due to the armature-reaction magnetizing force of this part of the winding, the excitation e.m.f. will be counteracted mainly by the e.m.f. induced by the leakage fields. Since the value of this e.m.f. at the rated current is a relatively small part of the total e.m.f. due to the excitation flux (12-20%), the current will continue to increase at a high rate until these e.m.f.s are balanced. The thermal effect of the current in the short-circuited turn becomes extremely great. As a result, the insulation is usually easily damaged, and short-circuiting of the winding to the machine frame takes place.

Chapter

15

SUDDEN SHORT CIRCUIT OF A SYNCHRONOUS MACHINE

15-1. Physical Picture of a Sudden Short Circuit

A sudden short circuit in the stator windings of a synchronous machine, though of relatively short duration, is a very difficult process both for the machine itself and for all the apparatus, transmission lines and networks connected to it, since the current surges occurring at a sudden short circuit may exceed the rated current values 10 to 15 times.

The process of a sudden short circuit differs greatly from that of a steady-state short circuit. In a symmetrical steady-state short circuit, the armature-reaction magnetizing force has an amplitude constant in relation to time and, since it runs in synchronism with the rotor, does not induce currents in the rotor windings. With a sudden short circuit, however, the stator current varies in magnitude and results in the armature-reaction flux also varying and inducing currents in the rotor windings which, in turn, influence the stator currents. The presence of such transformer linkages between the stator and the rotor makes the sudden short-circuit process very complicated.

Here we shall first limit ourselves to analysis of the so-called symmetrical sudden short circuit at no-load operation, when an excited synchronous generator under no-load has all phases of the stator winding at the output terminals short-circuited simultaneously. The moment of the short circuit will be taken as the time origin ($t=0$).

Since the number of phases in a polyphase machine does not change in principle the picture of the sudden short-circuit process, let us consider the simplest non-salient-pole two-phase synchronous machine carrying on its rotor, besides the direct-axis field winding closed through the exciter, an additional short-circuited damper winding along the quadrature axis, whose parameters r_{dw} and L_{dw} are equal to those of the field winding. For greater clarity we shall, as in d.c. machines, place a two-phase ring winding on the stator instead of a drum winding. Suppose that at the initial moment of the short circuit, i.e., $t=0$ (Fig. 15-1) the phase axis $A-A'$ is on the direct axis of the rotor, and the phase axis $B-B'$ is on the quadrature axis, owing to which the e.m.f. in phase $B-B'$, at $t=0$, has a maximum value, and the e.m.f. in phase $A-A'$ is zero. The field winding produces a useful magnetic flux $\Phi_{m.exc}$ completely linked at the moment $t=0$ with

phase $A-A'$, the magnetic flux in the winding circuit of phase $B-B'$ being zero*. Furthermore, the field winding has a linkage flux $\Phi_{\sigma exc}$ that links only with this winding.

When the rotor turns through 90 electrical degrees from the initial short-circuit position, the stator and rotor windings will be arranged as shown in Fig. 15-2a. The useful excitation flux $\Phi_{m.exc}$ will now be excluded from the stator winding of phase $A-A'$ and directed into the winding of phase $B-B'$.

Let us first suppose that the resistances of the stator windings and field winding equal zero, i.e., the windings are superconductive electric circuits. Since the flux linkages of superconductive circuits must remain constant under any conditions, then when the rotor turns such currents should be induced in the stator and rotor windings that the resultant flux linkages of all the windings remain the same as at the initial moment of the short circuit (Fig. 15-1).

For this reason, when the rotor turns from the initial position at $t = 0$ through $\gamma = 90^\circ$ (Fig. 15-2a), phase $A-A'$ will have a current induced in it of such a direction that the flux $\Phi_{mA} + \Phi_{\delta A}$ produced by it and depicted by dotted lines in Fig. 15-2a crosses the circuit of phase $A-A'$ in the same direction as the pole flux in Fig. 15-1. Since, however, the flux Φ_{mA} also links with the damper winding, a current will be induced in the latter of a direction such that the flux $\Phi_{m.dw} + \Phi_{\sigma dw}$ produced by it and shown by solid lines in Fig. 15-2a opposes the flux of phase $A-A'$. As a result, currents appear in phase $A-A'$ and in the damper winding such that the flux linkages of these windings must remain the same as at $t = 0$ (Fig. 15-1) when the rotor rotates (Fig. 15-2a).

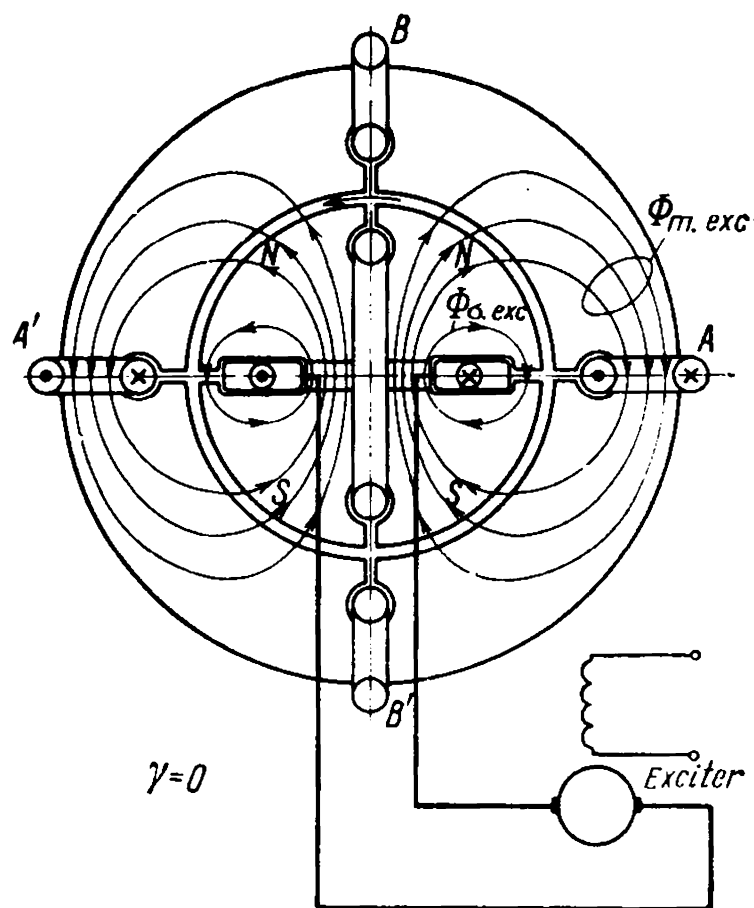


Fig. 15-1. Flux paths of a synchronous machine at the initial moment of sudden short circuit

* In the general case it would be more correct to apply the term flux linkages, but in the selected examples with single-turn windings on the stator and rotor, the flux linkages in Fig. 15-1 and others are equal to the fluxes, and, therefore, in these conditions we may apply the term fluxes.

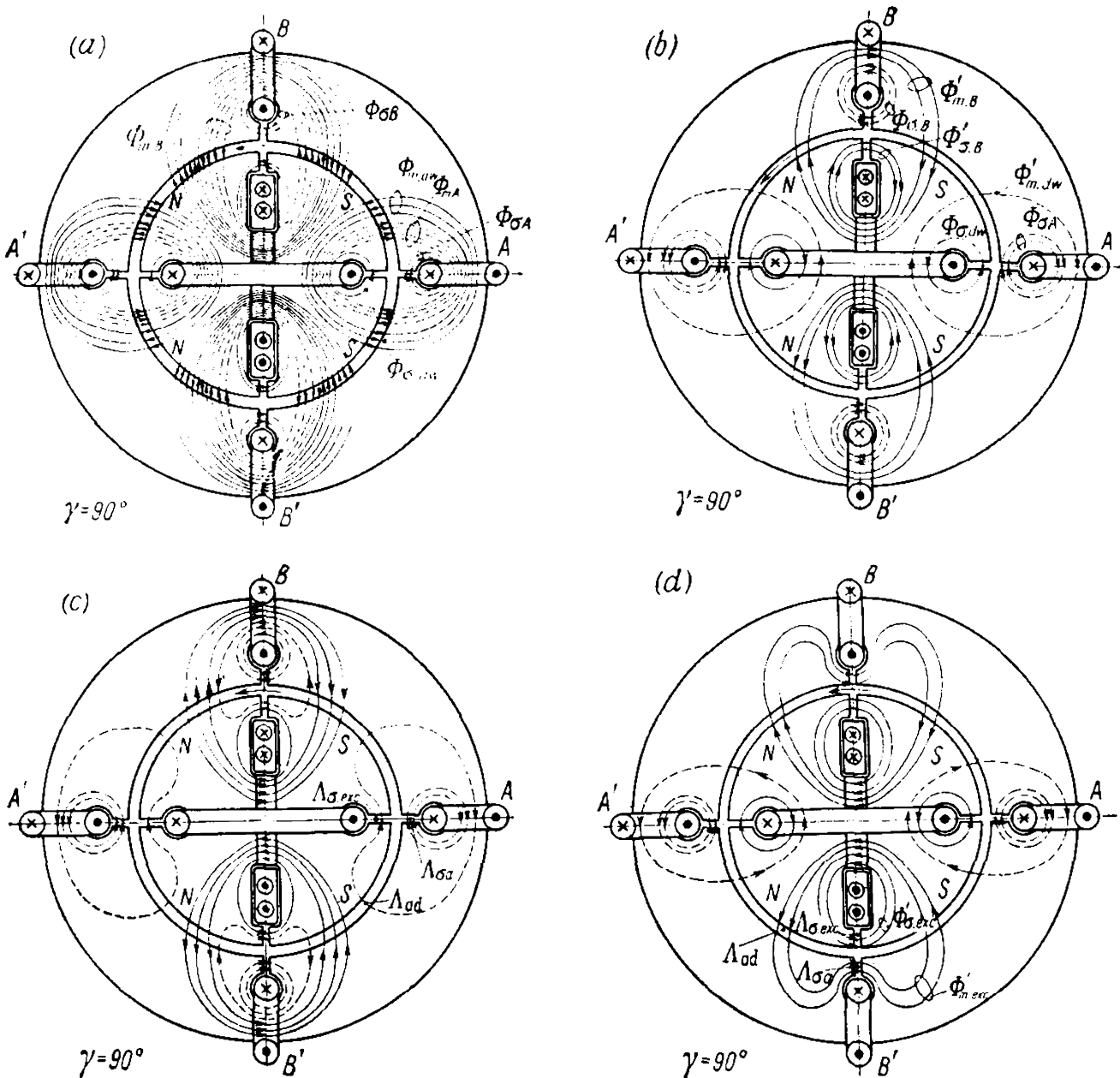


Fig. 15-2. Flux paths of a synchronous machine in a quarter of a period from the beginning of the sudden short circuit

In a similar manner, the penetration of the excitation flux into the circuit of phase $B-B'$ produces a current creating the flux $\Phi_{mB} + \Phi_{\sigma B}$ which is directed against the pole flux. Since the flux Φ_{mB} in passing through the rotor links with the field winding, an additional current is induced in the latter preventing the decrease of the flux linkage with this winding. As a result, currents will flow in phase $B-B'$ and in the field winding such that their flux linkages, when the rotor rotates (Fig. 15-2a), will be the same as at $t = 0$ (Fig. 15-1).

In Fig. 15-2a, lines of magnetic inductance of various direction must pass along the magnetic paths of mutual inductance through the stator and the rotor due to the mutually opposed magnetizing forces of the stator and the rotor, as a result of which the resultant field shown in Fig. 15-2b is obtained. It is easy to see that the flux linkages of all the windings are the same as at the initial moment (Fig. 15-1). Since,

owing to the increase in the current in the field winding, its leakage flux correspondingly increases in comparison with the value at the initial moment $t=0$ (Fig. 15-1)

$$\Phi'_{\sigma exc} > \Phi_{\sigma exc}$$

then the mutual-inductance flux decreases correspondingly

$$\Phi'_{m. exc} < \Phi_{m. exc}$$

It is possible to construct an equivalent flux map (Fig. 15-2c), however, in which the fluxes directly linked with the field winding at the moment $\gamma = \omega t = \frac{\pi}{2}$ will be exactly the same as at the initial moment $t=0$, but then there will appear an additional flux linked with the stator winding $B-B'$ passing successively through the air-gap and along the leakage paths of the excitation system. The fluxes linked with the $A-A'$ phase windings can be depicted in a similar manner; these fluxes are of the same nature as the fluxes of phase $B-B'$.

Let us denote the permeance of the mutual inductance path by Λ_{ad} , that of the stator winding leakage paths by $\Lambda_{\sigma a}$ and that of the rotor windings (the field and damper windings taken equal) by $\Lambda_{\sigma exc}$. These permeances correspond to the permeances of the relevant air-gaps (Fig. 15-2c).

According to Fig. 15-2c the flux linked with phase $A-A'$ is equal to the sum of two components, one of which passes through a path with the permeance $\Lambda_{\sigma a}$, the other, successively, through paths with the permeances Λ_{ad} and $\Lambda_{\sigma exc}$. Taking into account that in calculating the equivalent permeance, parallel permeances are added together, and with series-connected permeances their reciprocals—the reluctances—are added together, we find that the total permeance for all the mutual inductance and leakage fluxes linked with the stator windings will be

$$\Lambda'_d = \Lambda_{\sigma a} + \frac{1}{\frac{1}{\Lambda_{ad}} + \frac{1}{\Lambda_{\sigma exc}}} = \Lambda_{\sigma a} + \frac{\Lambda_{\sigma exc} \Lambda_{ad}}{\Lambda_{\sigma exc} + \Lambda_{ad}}$$

Since the sum of the fluxes shown in Fig. 15-2c linked only with the stator winding should be equal to the useful flux $\Phi_{m. exc}$ penetrating into winding $A-A'$ at the moment $\omega t = 0$, the current in stator windings $A-A'$ and $B-B'$, with the assumed number of turns per phase of $\omega_a = 1$, will be equal to

$$i_a = \frac{\Phi_{m. exc}}{\Lambda'_d \omega_a} = \frac{\Phi_{m. exc}}{\Lambda'_d}$$

The flux linkage picture in Fig. 15-2b makes it possible to construct an equivalent picture of the fluxes linked with the rotor windings (Fig. 15-2d).

The equivalent permeance for the field winding flux at the initial moment (Fig. 15-1) is equal to

$$\Lambda_{m.exc} = \Lambda_{\sigma exc} + \Lambda_{ad}$$

and for the moment $\omega t = \frac{\pi}{2}$ (Fig. 15-2d)

$$\Lambda'_{m.exc} = \Lambda_{\sigma exc} + \frac{\Lambda_{ad}\Lambda_{\sigma a}}{\Lambda_{ad} + \Lambda_{\sigma a}}$$

since the leakage flux $\Phi'_{\sigma exc}$ which the permeance $\Lambda_{\sigma exc}$ corresponds to, adds to the flux $\Phi'_{m.exc}$ forced out on the path of the stator winding leakage flux and is determined by the sum of the reluctances corresponding to the permeances Λ_{ad} and $\Lambda_{\sigma a}$

Since the resultant flux linkages for Figs. 15-1 and 15-2d are equal to $\Phi_{m.exc} + \Phi_{\sigma exc} = \Phi'_{m.exc} + \Phi'_{\sigma exc}$, the corresponding excitation currents will be, with $\omega_{exc} = 1$

$$i_{exc} = \frac{\Phi_{m.exc} + \Phi_{\sigma exc}}{\Lambda_{m.exc}\omega_{exc}} = \frac{\Phi_{m.exc} + \Phi_{\sigma exc}}{\Lambda'_{m.exc}}$$

and

$$i'_{exc} = \frac{\Phi'_{m.exc} + \Phi'_{\sigma exc}}{\Lambda'_{m.exc}\omega_{exc}} = \frac{\Phi_{m.exc} + \Phi_{\sigma exc}}{\Lambda_{m.exc}}$$

whence

$$i'_{exc} = \frac{\Lambda_{m.exc}}{\Lambda'_{m.exc}} i_{exc}$$

and the additional current surge in the field winding at the moment $\omega t = \frac{\pi}{2}$, as compared with the moment $t = 0$, will be

$$\begin{aligned} \Delta i'_{exc} &= i'_{exc} - i_{exc} = \frac{\Lambda_{m.exc} - \Lambda'_{m.exc}}{\Lambda'_{m.exc}} i_{exc} = \\ &= \frac{\Lambda_{ad}^2}{\Lambda_{\sigma exc}\Lambda_{ad} + \Lambda_{ad}\Lambda_{\sigma a} + \Lambda_{\sigma a}\Lambda_{\sigma exc}} i_{exc} \end{aligned}$$

Taking into account the relations between $\Phi_{m.exc}$ and $\Phi_{\sigma exc}$ in Fig. 15-1, let us assume that $\Lambda_{ad} = 3$ and $\Lambda_{\sigma exc} = 1$. Then, in accordance with the relations between $\Phi_{\sigma A}$ and Φ_{mA} , according to Fig. 15-2a, we have

$$\Lambda_{\sigma a} = \frac{\Phi_{\sigma A}}{\Phi_{mA}} \Lambda_{ad} = \frac{1}{2} \times 3 = \frac{3}{2}$$

By substituting these values for the permeance in the expression for $\Delta i'_{exc}$ we obtain

$$\Delta i'_{exc} = i_{exc}$$

i.e., in the given case, with a quarter turn of the rotor, the excitation current doubles.

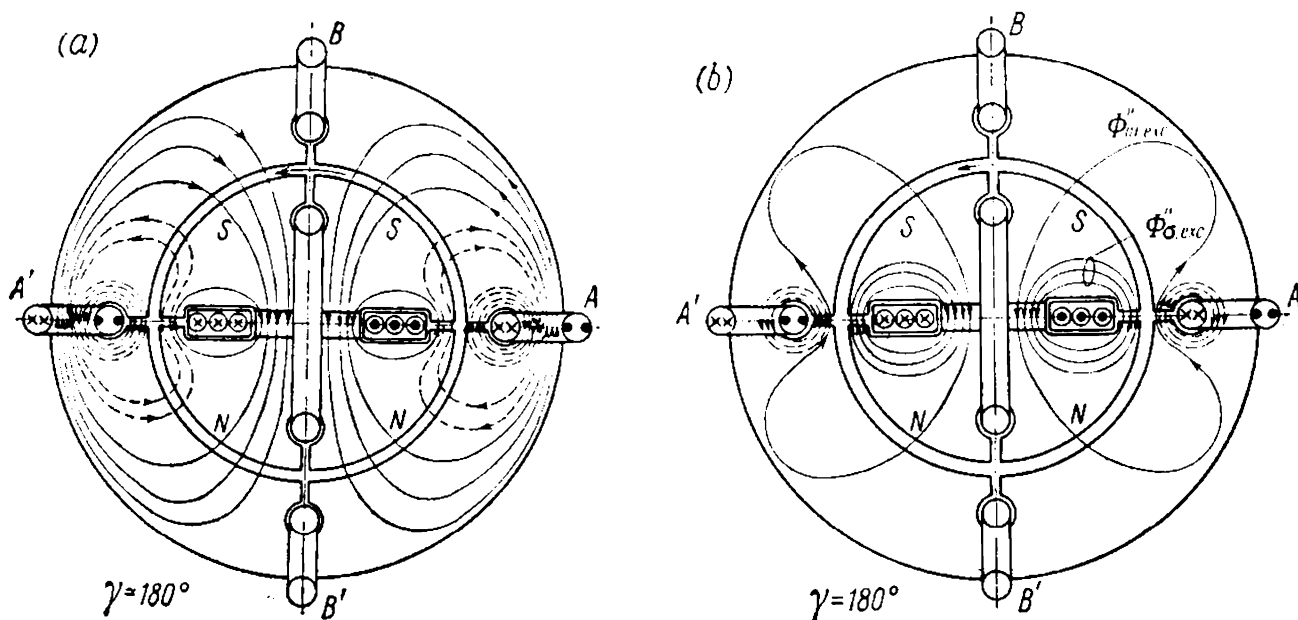


Fig. 15-3. Magnetic-flux paths of a synchronous machine one-half a period after the beginning of sudden short circuit

Let us consider in a similar manner the distribution of the flux linkages and currents for the moment $\omega t = \pi$, when the rotor and the excitation flux linked with it turn from the initial position ($t = 0$) through the angle $\gamma = 180^\circ$.

Now the rotor flux penetrates the circuits of the stator windings A-A' in the opposite direction, but since the flux linkages with these windings must be maintained equal to those for the initial moment $t = 0$ (Fig. 15-1), there must obviously appear around the stator windings a number of flux linkages double that existing at the moment $\omega t = \frac{\pi}{2}$ (Fig. 15-2c), and the general picture of the flux linkages will assume the form shown in Fig. 15-3a. To make doubling of the flux linkage possible, the current in these windings at the moment $\omega t = \pi$ must obviously be double that at the previous moment $\omega t = \frac{\pi}{2}$. Conversely, in the phase windings B-B' the current becomes equal to zero at this moment, since these windings now occupy a coaxial position with respect to the field winding and the useful flux $\Phi_{m. exc}$ produced by it.

The flux linkage map of Fig. 15-3a may be reduced to an equivalent map of the flux linkages coupled with the field winding (Fig. 15-3b). The flux $\Phi_{m. exc}''$ according to Fig. 15-3b occupies only a quarter of the cross section of the stator leakage flux path, and the resultant permeance for the excitation flux is therefore

$$\Lambda_{m. exc}'' = \Lambda_{\sigma exc} + \frac{\Lambda_{ad} \times \frac{1}{4} \Lambda_{\sigma a}}{\Lambda_{ad} + \frac{1}{4} \Lambda_{\sigma a}}$$

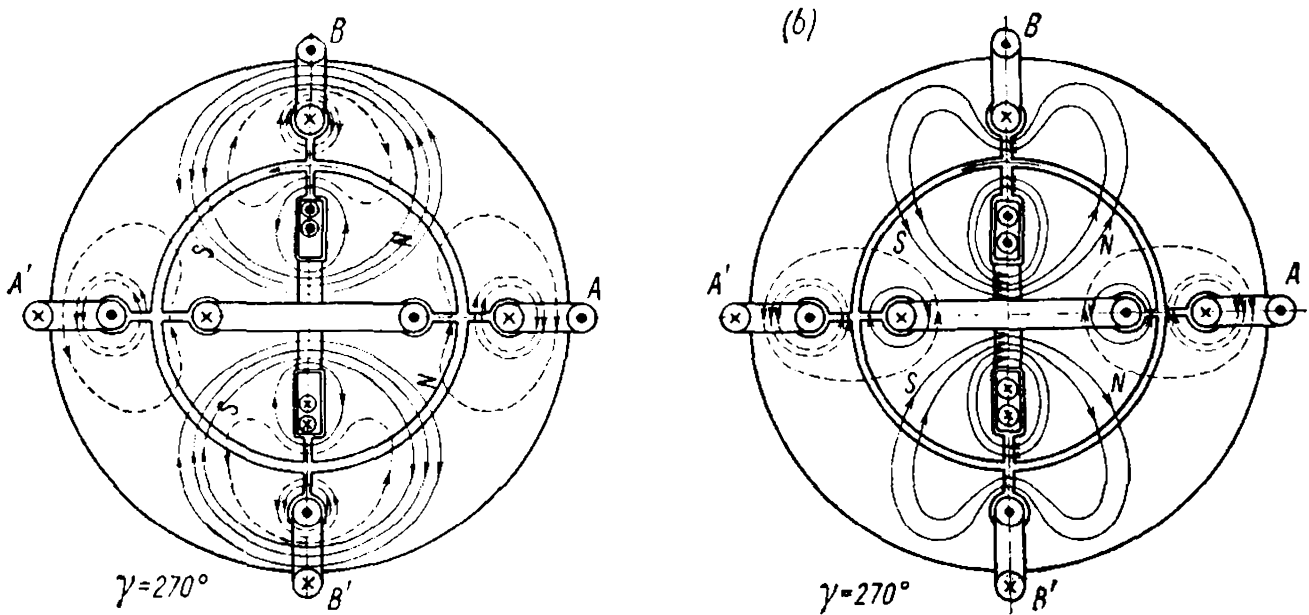


Fig. 15-4. Magnetic-flux paths of a synchronous machine three-quarters of a period after the beginning of sudden short circuit

while the surge of the excitation current relative to its value at the moment $t=0$ will equal

$$\Delta i_{exc}'' = \frac{\Lambda_{m. exc} - \Lambda_{m. exc}''}{\Lambda_{m. exc}''} i_{exc} = \frac{\Lambda_{ad}^2}{\Lambda_{\sigma exc} \Lambda_{ad} + \frac{1}{4} \Lambda_{ad} \Lambda_{\sigma a} + \frac{1}{4} \Lambda_{\sigma a} \Lambda_{\sigma exc}} i_{exc}$$

Substituting their values for the permeance, we get

$$\Delta i_{exc}'' = 2i_{exc}$$

i.e., at the moment $\omega t = \pi$ the excitation current will increase three-fold.

In a similar manner we can construct the equivalent flux linkages for the stator phase windings $B-B'$ and $A-A'$ (Fig. 15-4a) and for the rotor windings (Fig. 15-4b) at the following moment $\omega t = \frac{3\pi}{2}$.

The flux linkage map of the field windings and the stator phase winding $B-B'$ for the moment $\omega t = \frac{3\pi}{2}$ is identical to the flux linkages in these windings at the moment $\omega t = \frac{\pi}{2}$ (Fig. 15-2c), but the flux linkages and currents in the phase windings $B-B'$ change their sign, since the direction of the excitation flux reverses.

The flux linkages and the currents in the windings at the moment $\omega t = 2\pi$ corresponding to a turn of the rotor through 360° from the initial position completely correspond to the initial position of the rotor at $t=0$. With the winding resistances equal to zero, identical pictures of the distribution of currents and flux linkages are obtained

in a similar way for the moments

$$\omega t = \frac{\pi}{2}, \frac{5\pi}{2}, \frac{9\pi}{2}, \dots$$

$$\omega t = \pi, 3\pi, 5\pi, \dots$$

$$\omega t = \frac{3\pi}{2}, \frac{7\pi}{2}, \frac{11\pi}{2}, \dots$$

The currents in the stator phase windings and in the rotor field and damper windings for moments of time corresponding to various angular positions of the rotor after the initial moment $t=0$ of a sudden short circuit can be shown by curves (Fig. 15-5). Figure 15-5a gives the curves of the e.m.f. e_A and current i_A in phase winding $A-A'$ corresponding to the pictures of the flux linkages and currents in Figs. 15-1, 15-2b, 15-3a and 15-4a, from which it is seen that the current i_A can be resolved into two components—aperiodic i_{Aap} and symmetrical periodic i_{Asym} which is displaced by 90° from the e.m.f. e_A induced in this winding by the mutual inductance flux $\Phi_{m.exc.}$

The curves in Fig. 15-5a correspond to the connection of a circuit with a self-inductance L and resistance $r=0$ across a sine e.m.f. e_A passing at the initial moment $t=0$ through zero:

$$e_A = E_{max} \sin(\omega t + \psi) = L \frac{di_A}{dt}$$

which gives the following expression for the current:

$$i_A = \frac{1}{L} \int_0^t E_{max} \sin(\omega t + \psi) dt = -\frac{E_{max}}{\omega L} \cos(\omega t + \psi) + \frac{E_{max}}{\omega L} \cos \psi$$

where $\psi=0$ in the case under consideration.

The curves in Fig. 15-5b give the e.m.f. e_B and the current i_B in phase winding $B-B'$ when the e.m.f. passes through its negative maximum at the initial moment, this taking place when the initial phase shift is $\psi = -\frac{\pi}{2}$. Here the current is $i_B = \frac{E_{max}}{\omega L} \sin \omega t$.

Figure 15-5c gives a curve showing the variation in the excitation current i_{exc} corresponding to Figs. 15-1, 15-2b, 15-3b and 15-4b.

The resultant excitation current i_{exc} can be resolved into the following three components:

1. The initial excitation current $i_{exc,0}$ existing at the moment $t=0$ and created at the expense of the exciter e.m.f.

2. The aperiodic component $i_{exc.ap}$ which is equal to the additional surge of the excitation current $\Delta i'_{exc}$ at the moments $\omega t = \frac{\pi}{2}$ and $\omega t = \frac{3\pi}{2}$.

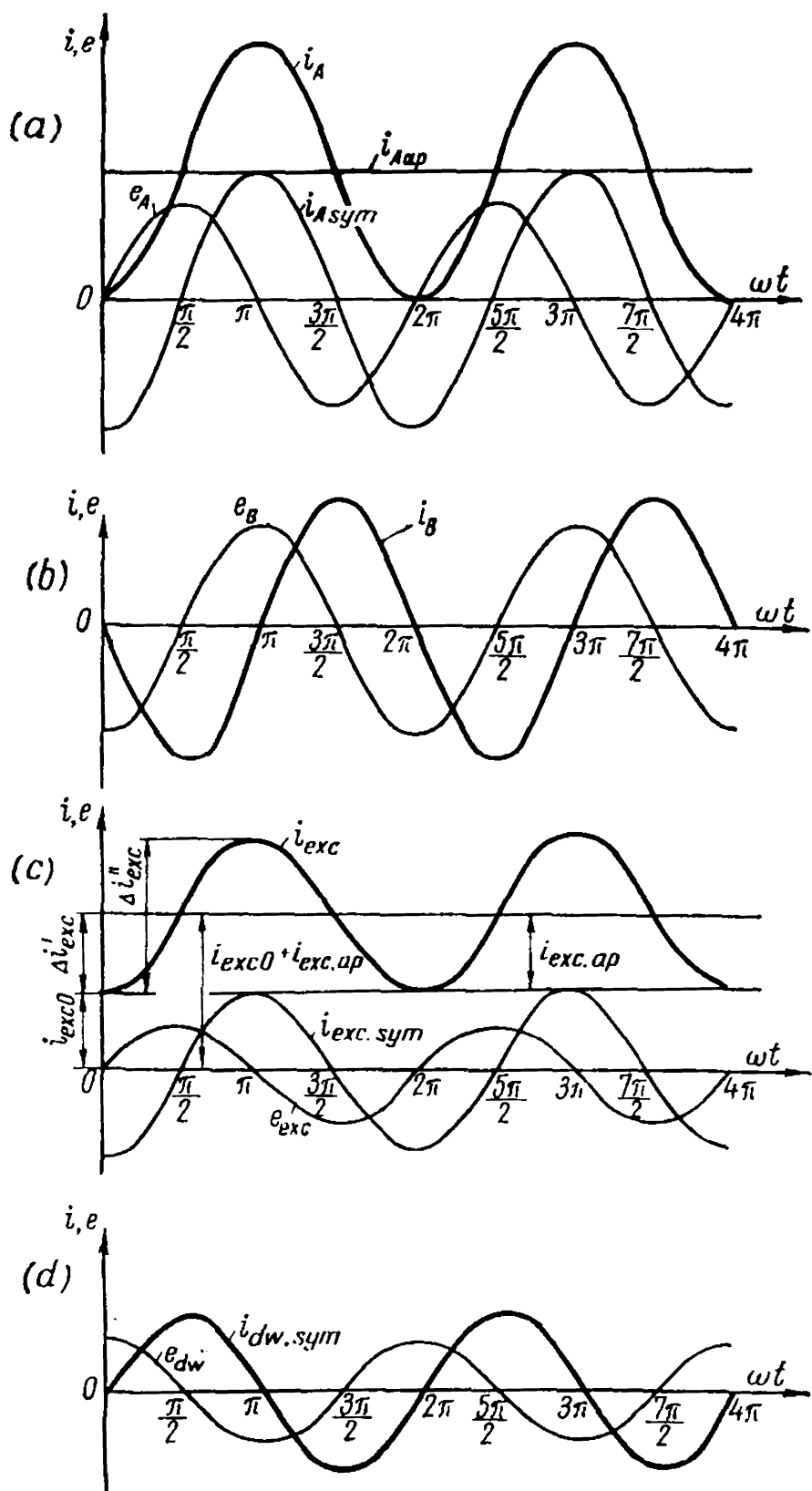


Fig. 15-5. Curves showing change in synchronous machine stator and rotor winding currents with a sudden short circuit in the absence of damping

3. The periodic symmetrical component of the excitation current $i_{exc. sym}$ with an amplitude

$$I_{exc. sym. max} = \Delta i'_{exc}$$

The maximum deviation of the excitation current from its initial value $i_{exc.0}$ is equal to:

$$2I_{exc. sym. max} = \Delta i_{exc}''$$

Thus, the resultant current is

$$i_{exc} = i_{exc.0} + i_{exc.ap} + i_{exc.sym}$$

Since the stator and rotor windings are transformer-linked circuits of a rotating transformer, it may be assumed that the constant component of the excitation current $i_{exc.0} + i_{exc.ap} = i_{exc.0} + \Delta i_{exc}'$ induces in the stator phase windings $A-A'$ and $B-B'$ periodic short-circuit currents $i_{A sym}$ and $i_{B sym}$, while the aperiodic component of the stator windings $i_{A ap}$ induces in the field winding a periodic current $i_{exc.sym}$.

Figure 15-5d shows the curve of the change in the current $i_{dw.sym}$ in the damper winding arranged along the quadrature axis and of the e.m.f. e_{dw} induced in the damper winding by the aperiodic stator current.

In the case being considered, the aperiodic component of the stator current, having a magnitude equal to the amplitude of the periodic component of the stator current, appeared in phase $A-A'$, because at the initial moment of the short circuit the field winding produced with this phase a maximum flux linkage, and the e.m.f. induced in it was zero. In phase $B-B'$ only the periodic current component of the current $i_{B sym}$ appeared, since at the initial moment of the short circuit the flux linkage of this phase was zero, and the e.m.f. e_B equalled its maximum value.

With another mutual position of the stator and rotor windings at the initial moment of the short circuit, the aperiodic current component may appear only in phase $B-B'$, or in both phases $A-A'$ and $B-B'$. When the resistances of the windings are taken into account, the aperiodic components of the stator and rotor fluxes, as will be shown below, do not remain invariable, but gradually decay in accordance with definite time constants.

15-2. Flux Linkages of Stator and Rotor Windings of a Synchronous Machine [85, 99a]

For quantitative analysis of the process of a sudden short circuit, the relations between the flux linkages and currents of the separate windings of a machine and their mutual positions must be determined.

The dependence of the stator and rotor winding flux linkages on their angular positions can be expressed analytically on the basis of the following.

Figure 15-6 shows the relative positions of the rotor and stator windings of a two-phase non-salient-pole synchronous machine at the moment t , when the direct axis of the rotor has turned through an

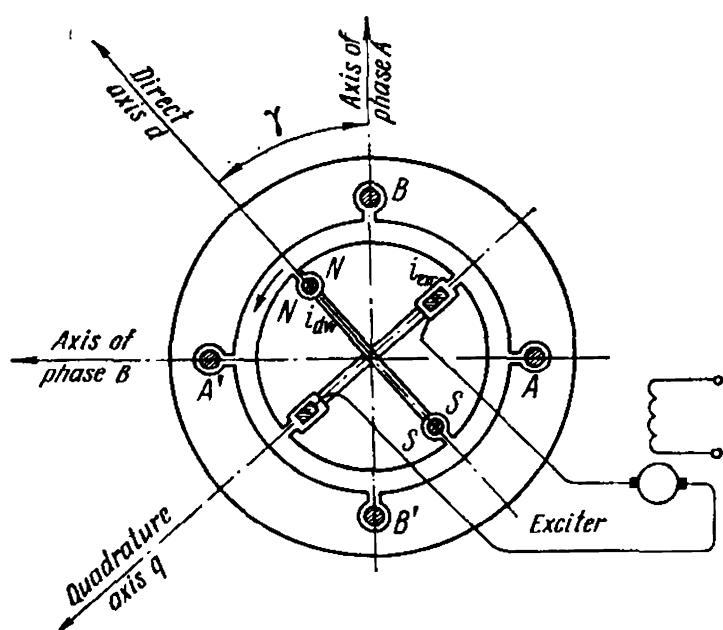


Fig. 15-6. Relative positions of synchronous generator stator and rotor windings and their axes at a random moment

angle γ from the axis of phase $A-A'$. It is assumed that the direction of the main excitation flux of the rotor is the positive direction of the direct axis. The positive direction of the quadrature rotor axis leads its direct axis by 90° . The positive directions of the stator winding axes are assumed to coincide with the directions of the fluxes produced by the stator windings when the current passes from the start of the winding to its finish. For simplicity, the number of rotor circuit turns is assumed to be reduced to the number of sta-

tor phase winding turns $w_{exc} = w_{dw} = w_a$.

The flux linkage of the stator phase $A-A'$ produced by the rotor magnetizing force is obtained by projecting, in accordance with Fig. 15-6, the fluxes of the field and damper windings acting along the d and q axes onto the axis of phase $A-A'$:

$$\Psi_{Ar} = k\Lambda_{ad}w_a^2 i_{exc} \cos \gamma - k\Lambda_{aq}w_a^2 i_{dw} \sin \gamma$$

Correspondingly, the flux linkage of phase $B-B'$ with the rotor fluxes is equal to:

$$\Psi_{Br} = k\Lambda_{ad}w_a^2 i_{exc} \sin \gamma + k\Lambda_{aq}w_a^2 i_{dw} \cos \gamma$$

Here $\gamma = \omega t + \gamma_0$ is the angle, varying in time, between the positive directions of the direct rotor axis and the axis of phase $A-A'$ of the stator winding $A-A'$; Λ_{ad} and Λ_{aq} are the permeances of the mutual-inductance paths of the direct and quadrature rotor axes, assumed to be equal in a non-salient-pole synchronous machine; k is a proportionality factor, and γ_0 defines the angular position of the rotor taken as the original one.

The currents i_A and i_B of the stator phases produce magnetizing forces in the positive directions of the direct and quadrature rotor axes equal to

$$F_d = k w_a \left[i_A \cos \gamma + i_B \cos \left(\frac{\pi}{2} - \gamma \right) \right] = k w_a [i_A \cos \gamma + i_B \sin \gamma]$$

$$F_q = k w_a \left[-i_A \sin \gamma + i_B \sin \left(\frac{\pi}{2} - \gamma \right) \right] = k w_a [-i_A \sin \gamma + i_B \cos \gamma]$$

The flux linkage of phase $A-A'$ created by the stator winding magnetizing forces is equal to

$$\Psi_{As} = k\Lambda_d \omega_a^2 \cos \gamma [i_A \cos \gamma + i_B \sin \gamma] + k\Lambda_q \omega_a^2 \sin \gamma [i_A \sin \gamma - i_B \cos \gamma]$$

where $\Lambda_d = \Lambda_{\sigma a} + \Lambda_{ad}$ and $\Lambda_q = \Lambda_{\sigma a} + \Lambda_{aq}$ are the total permeances of the stator along the direct and quadrature axes.

Similarly, the flux linkages of phase $B-B'$ due to the stator magnetizing force are equal to

$$\Psi_{Bs} = k\Lambda_d \omega_a^2 \sin \gamma [i_A \cos \gamma + i_B \sin \gamma] - k\Lambda_q \omega_a^2 \cos \gamma [i_A \sin \gamma - i_B \cos \gamma]$$

For simplicity, we shall consider a non-salient-pole synchronous machine.

For such a machine $\Lambda_d = \Lambda_q = \Lambda_a$ and, therefore,

$$\Psi_{As} = k\Lambda_d \omega_a^2 2i_A$$

and, in a similar manner, for phase $B-B'$

$$\Psi_{Bs} = k\Lambda_d \omega_a^2 i_B$$

The full flux linkages of phases $A-A'$ and $B-B'$ with all the fluxes produced by the stator and rotor magnetizing forces will, for a non-salient-pole machine, be equal to

$$\Psi_A = \Psi_{Ar} + \Psi_{As} = k\Lambda_{ad} \omega_a^2 [i_{exc} \cos \gamma - i_{dw} \sin \gamma] + k\Lambda_d \omega_a^2 i_A \quad (15-1)$$

$$\Psi_B = \Psi_{Br} + \Psi_{Bs} = k\Lambda_{ad} \omega_a^2 [i_{exc} \sin \gamma + i_{dw} \cos \gamma] + k\Lambda_d \omega_a^2 i_B \quad (15-2)$$

Correspondingly, the expressions for the flux linkages of the rotor circuits along its direct and quadrature axes due to the stator winding magnetizing forces are, according to Fig. 15-6, as follows:

$$\Psi_{ds} = k\omega_a^2 \Lambda_{ad} [i_A \cos \gamma + i_B \sin \gamma]$$

$$\Psi_{qs} = k\omega_a^2 \Lambda_{ad} [-i_A \sin \gamma + i_B \cos \gamma]$$

The rotor circuit flux linkages of the rotor fluxes closing through the stator and also of the leakage fluxes of the rotor windings are equal to

$$\Psi'_{d.exc} = k\omega_a^2 (\Lambda_{ad} + \Lambda_{\sigma exc}) i_{exc}$$

$$\Psi'_{q.dw} = k\omega_a^2 (\Lambda_{aq} + \Lambda_{\sigma dw}) i_{dw}$$

Assuming $\Lambda_{\sigma exc} \cong \Lambda_{\sigma dw}$ and denoting

$$\Lambda_{ad} + \Lambda_{\sigma exc} \cong \Lambda_{aq} + \Lambda_{\sigma dw} \cong \Lambda_{exc}$$

we obtain the following expressions for the full rotor flux linkages

$$\Psi_{d.exc} = \Psi'_{d.exc} + \Psi_{ds} = k\omega_a^2 \Lambda_{exc} i_{exc} + k\omega_a^2 \Lambda_{ad} [i_A \cos \gamma + i_B \sin \gamma] \quad (15-3)$$

$$\Psi_{q.dw} = \Psi'_{q.dw} + \Psi_{qs} = k\omega_a^2 \Lambda_{exc} i_{dw} + k\omega_a^2 \Lambda_{ad} [-i_A \sin \gamma + i_B \cos \gamma] \quad (15-4)$$

If, with $t=0$, we take angle γ_0 as the original angular position of the rotor axis d relative to the axis of phase $A-A'$ in the expression for the full flux linkages of the stator and rotor windings, assuming $\gamma = \omega t + \gamma_0$, we obtain their following relations to time

(a) for the stator windings

$$\Psi_A = k\Lambda_{ad}\omega_a^2 [i_{exc} \cos(\omega t + \gamma_0) - i_{dw} \sin(\omega t + \gamma_0)] + k\Lambda_d\omega_a^2 i_A \quad (15-5)$$

$$\Psi_B = k\Lambda_{ad}\omega_a^2 [i_{exc} \sin(\omega t + \gamma_0) + i_{dw} \cos(\omega t + \gamma_0)] + k\Lambda_d\omega_a^2 i_B \quad (15-6)$$

(b) for the rotor windings

$$\Psi_{d. exc} = k\Lambda_{exc}\omega_a^2 i_{exc} + k\Lambda_{ad}\omega_a^2 [i_A \cos(\omega t + \gamma_0) + i_B \sin(\omega t + \gamma_0)] \quad (15-7)$$

$$\Psi_{q. dw} = k\Lambda_{exc}\omega_a^2 i_{dw} + k\Lambda_{ad}\omega_a^2 [-i_A \sin(\omega t + \gamma_0) + i_B \cos(\omega t + \gamma_0)] \quad (15-8)$$

The coefficients of equations (15-5), (15-6), (15-7) and (15-8) are the inductances and mutual inductances, namely,

(a) the stator phase inductance

$$L_d = k\Lambda_{ad}\omega_a^2 \quad (15-9)$$

(b) the inductance of the field and damper windings

$$L_{exc} = L_{dw} = k\Lambda_{exc}\omega_a^2 \quad (15-10)$$

(c) the mutual inductance between the stator and the rotor with $\omega_a = \omega_{exc}$

$$M_{ad} = k\Lambda_{ad}\omega_a^2 \quad (15-11)$$

Besides, let us denote in equations (15-5) and (15-6)

$$i_{rA} = i_{exc} \cos(\omega t + \gamma_0) - i_{dw} \sin(\omega t + \gamma_0) \quad (15-12)$$

$$i_{rB} = i_{exc} \sin(\omega t + \gamma_0) + i_{dw} \cos(\omega t + \gamma_0) \quad (15-13)$$

where the value i_{rA} may be called the equivalent rotor current with respect to the phase $A-A'$ and i_{rB} the same with respect to phase $B-B'$.

Taking into account these notations, the stator flux linkages according to equations (15-5) and (15-6) can be rewritten as follows

$$\Psi_A = M_{ad}i_{rA} + L_d i_A \quad (15-14)$$

$$\Psi_B = M_{ad}i_{rB} + L_d i_B \quad (15-15)$$

Similar to equations (15-7) and (15-8), the rotor flux linkages can be rewritten as

$$\Psi_{d. exc} = L_{exc}i_{exc} + M_{ad}i_{ad} \quad (15-16)$$

$$\Psi_{q. dw} = L_{exc}i_{dw} + M_{ad}i_{aq} \quad (15-17)$$

where

$$i_{ad} = i_A \cos(\omega t + \gamma_0) + i_B \sin(\omega t + \gamma_0) \quad (15-18)$$

and

$$i_{aq} = -i_A \sin(\omega t + \gamma_0) + i_B \cos(\omega t + \gamma_0) \quad (15-19)$$

are the corresponding equivalent stator currents along the rotor axes d and q .

The expressions obtained for the flux linkages are valid for any duties of a machine with any time relations of the stator and rotor currents.

From equations (15-14), (15-15), (15-16) and (15-17) it follows that when considering the full flux linkages of the stator system, the equivalent rotor currents i_{rA} and i_{rB} are, similar to the effective stator currents i_A and i_B , sine-wave functions having amplitudes equal to i_{exc} and i_{dw} . Therefore, the differential equations of the stator system can be reduced to the equations of a static transformer with stator currents i_A and i_B and equivalent rotor currents i_{rA} and i_{rB} .

Similarly, the differential equations of the rotor system can also be reduced to the equations of a static transformer with the actual rotor currents i_{exc} and i_{dw} and the equivalent stator current i_{ad} and i_{aq} .

15-3. Analytical Investigation of the Sudden Short-Circuit Process

In considering the short-circuit process analytically, we shall assume that the parameters of the field and damper windings have been reduced to the stator winding, without indicating this by means of special symbols.

When a short circuit occurs, the e.m.f. in the stator winding circuit is created only at the expense of changes in the flux linkages Ψ_A and Ψ_B . If we take the resistances of the stator and rotor windings equal to zero, the resultant e.m.f. of phase $A-A'$ should also be zero:

$$-\frac{d\Psi_A}{dt} = 0$$

which, according to equation (15-14), gives

$$L_d \frac{di_A}{dt} + M_{ad} \frac{di_{rA}}{dt} = 0 \quad (15-20)$$

The excitation current i_{exc} can be represented as the sum

$$i_{exc} = i_{exc.0} + \Delta i_{exc}$$

where $i_{exc.0}$ is the invariable (main) component of the excitation current, i.e., the no-load excitation current created at the expense of the exciter e.m.f., and Δi_{exc} is the current induced by the currents in the stator windings.

Then, according to equation (15-12), the second term of equation (15-20) contains:

$$-\omega M_{ad} i_{exc.0} \sin(\omega t + \gamma_0) = -E_{m.max} \sin(\omega t + \gamma_0) \quad (15-21)$$

which is the stator winding no-load e.m.f. at the initial phase $\psi = \gamma_0$.

By assuming further that the current i_{rA} no longer contains the component corresponding to $i_{exc. 0}$, we can finally rewrite equation (15-20) of the stator circuit as

$$L_d \frac{di_A}{dt} + M_{ad} \frac{di_{rA}}{dt} = E_{m. max} \sin(\omega t + \psi) \quad (15-22)$$

According to equation (15-22), as also follows from the above physical analysis of the phenomenon, a sudden short circuit of an excited synchronous machine at no-load with a terminal voltage $e_0 = E_{m. max} \sin(\omega t + \psi)$ is equivalent to sudden connection of the same machine, but unexcited, to the line of an external power circuit with a voltage $E_{m. max} \sin(\omega t + \psi)$ at the moment of connection of the same magnitude and phase, the only difference being that in the latter case the field winding current will not contain a no-load component due to the exciter.

Equation (15-22) determines the change in the stator current during the short-circuit process, but it contains two unknowns, and for its solution we use an additional equation for the equivalent rotor circuit:

$$L_{exc} \frac{di_{rA}}{dt} + M_{ad} \frac{di_A}{dt} = 0 \quad (15-23)$$

By determining $\frac{di_{rA}}{dt}$ from equation (15-23) and substituting it in equation (15-22), we obtain the following differential equation of the first degree:

$$\left(L_d - \frac{M_{ad}^2}{L_{exc}} \right) \frac{di_A}{dt} = L_d' \frac{di_A}{dt} + E_{m. max} \sin(\omega t + \psi) \quad (15-24)$$

whence, taking into account that when $t = 0$ the current $i_A = 0$, we get

$$\begin{aligned} i_A &= \frac{1}{L_d'} \int E_{m. max} \sin(\omega t + \psi) dt + C = \\ &= -\frac{E_{m. max}}{\omega L_d'} \cos(\omega t + \psi) + \frac{E_{m. max}}{\omega L_d'} \cos \varphi = \\ &= i_{A sym} + i_{A ap} \end{aligned} \quad (15-25)$$

Here

$$\begin{aligned} L_d' &= L_d - \frac{M_{ad}^2}{L_{exc}} = (M_{ad} + L_{\sigma a}) - \frac{M_{ad}^2}{M_{ad} + L_{\sigma exc}} = \\ &= L_{\sigma a} + \frac{1}{\frac{1}{M_{ad}} + \frac{1}{L_{\sigma exc}}} \end{aligned} \quad (15-26)$$

is a quantity equivalent to the stator winding leakage inductance, which takes into account the transformer linkages of the stator winding with the rotor circuits, $L_{\sigma a}$ and $L_{\sigma exc}$ being, respectively, the leakage inductances of the stator winding and the rotor field winding.

The inductive reactance

$$x'_d = \omega L'_d$$

contained in equation (15-25) is referred to as the direct-axis transient reactance of the stator winding. It is obvious that this reactance is less than the direct-axis synchronous reactance

$$x_d = \omega L_d$$

At the initial phase angle $\psi = 0$, the current in phase A will be

$$i = -\frac{E_{m. max}}{\omega L'_d} \cos \omega t + \frac{E_{m. max}}{\omega L'_d} = i_{sym} + i_{ap} \quad (15-27)$$

and contains the maximum value of the aperiodic component i_{ap} , while at $\psi = \frac{\pi}{2}$ there remains only the periodic component

$$i = -\frac{E_{m. max}}{\omega L'_d} \sin \omega t = i_{sym} \quad (15-28)$$

which corresponds to the current of phase $B-B'$ in the case shown in Fig. 15-5.

Likewise, the current i_{rA} can be determined from the equation

$$\left(\frac{L_d L_{exc}}{M_{ad}} - M_{ad} \right) \frac{di_{rA}}{dt} = L'_{exc} \frac{di_{rA}}{dt} = -E_{m. max} \sin (\omega t + \psi) \quad (15-29)$$

obtained from equations (15-22) and (15-23) by excluding i_A from them. By solving equation (15-29) we obtain

$$i_{rA} = \frac{E_{max}}{\omega L'_{exc}} \cos (\omega t + \psi) - \frac{E_{max}}{\omega L'_{exc}} \cos \psi \quad (15-30)$$

where

$$L'_{exc} = \frac{L_d L_{exc} - M_{ad}^2}{M_{ad}} \quad (15-31)$$

For the initial phase angle $\psi = 0$ we find the equivalent current i_{rA} producing the rotor circuit magnetizing force along the axis of phase $A-A'$:

$$i_{rA} = \frac{E_{m. max}}{\omega L'_{exc}} \cos \omega t - \frac{E_{m. max}}{\omega L'_{exc}} = i_{rA sym} + i_{rA ap}$$

By substituting $\psi = -\frac{\pi}{2}$ in equation (15-30), we find for this case of short circuit the equivalent current i_{rB} producing the rotor magnetizing force along the axis of phase B :

$$i_{rB} = \frac{E_{m. max}}{\omega L'_{exc}} \sin \omega t = i_{rB sym}$$

The actual rotor winding currents can be found from equations (15-12) and (15-13) if we solve them for i_{exc} and i_{dw} and substitute in them the above values for i_{rA} and i_{rB} , assuming that $\gamma_0 = 0$:

$$i_{exc} = i_{rA} \cos \omega t + i_{rB} \sin \omega t = -\frac{E_{m. max}}{\omega L'_{exc}} \cos \omega t + \frac{E_{m. max}}{\omega L'_{exc}} = i_{exc. sym} + i_{exc. ap} \quad (15-32)$$

$$i_{dw} = -i_{rA} \sin \omega t + i_{rB} \cos \omega t = \frac{E_{m. max}}{\omega L'_{exc}} \sin \omega t = I_{dw. sym. max} \sin \omega t = i_{dw. sym} \quad (15-33)$$

These values of i_{exc} and $i_{dw. sym}$ correspond to the curves in Fig. 15-5, with the exception that the value of i_{exc} does not contain the component $i_{exc.0}$ produced by the exciter.

Up to now the rotor and stator resistances were assumed to be zero. If we first take into account the resistance r_a of the stator windings, then to the left side of differential equation (15-24) there must be added the term $r_a i_A$, after which the equation becomes

$$L'_d \frac{di_A}{dt} + r_a i_A = E_{m. max} \sin (\omega t + \psi) \quad (15-34)$$

and, since when $t = 0$ we have $i_A = 0$, its solution will be

$$i_A = \frac{E_{m. max}}{\sqrt{r_a^2 + \omega^2 L_d'^2}} \sin (\omega t + \psi - \varphi') - \frac{E_{m. max} e^{-\frac{t}{T_a}}}{\sqrt{r_a^2 + \omega^2 L_d'^2}} \sin (\psi - \varphi') \quad (15-35)$$

where

$$\varphi' = \arctan \frac{\omega L'_d}{r_a} \quad (15-36)$$

and the time constant

$$T_a = \frac{L'_d}{r_a} \quad (15-37)$$

Hence it follows that when a stator winding resistance is present, the aperiodic component of the short-circuit current will no longer remain constant, but will decay with the time constant T_a .

In a similar manner, if in the system of differential equations (15-29) for the rotor circuits we take into account the resistance of the field winding and take the resistance of the stator winding equal to zero, equation (15-29) will become

$$L'_{exc} \frac{di_{rA}}{dt} + r_{exc} i_{rA} = -E_{m. max} \sin (\omega t + \psi) \quad (15-38)$$

and its solution gives the following expression for the excitation current

$$i_{rA} = - \frac{E_{m. max}}{\sqrt{r_{exc}^2 + \omega^2 L_{exc}'^2}} \sin(\omega t + \psi - \varphi'') + \frac{E_{m. max} e^{-\frac{t}{T_d'}}}{\sqrt{r_{exc}^2 + \omega^2 L_{exc}'^2}} \sin(\psi - \varphi'') \quad (15-39)$$

where

$$\varphi'' = \arctan \frac{\omega L_{exc}'}{r_{exc}} \quad (15-40)$$

and the time constant

$$T_d' = \frac{L_{exc}'}{r_{exc}} \quad (15-41)$$

Thus, the aperiodic current component in the field winding also does not remain constant and will decay with the time constant T_d' . The equivalent inductances L_d' and L_{exc}' practically differ very little from each other and the difference between T_a and T_d' therefore depends mainly on the difference between the relative values of the resistances r_a and r_{exc} . In synchronous machines r_a is usually 5 to 10 times larger than r_{exc} and the time constant T_d' is therefore appreciably greater than T_a .

The periodic components of the stator winding current are proportional to the sum of the constant component of the excitation current $i_{exc.0}$ produced by the exciter and the aperiodic component of the excitation current $i_{exc.ap}$, that is, $i_{exc.0} + i_{exc.ap}$, since the periodic stator currents are induced by rotor currents constant in direction. Since the excitation current component $i_{exc.ap}$ decays with the time constant T_d' , it is obvious from the physical point of view that the corresponding part of the periodic stator current, called the *transient component*, decays with the same time constant. Correspondingly, the periodic rotor currents due to the aperiodic stator current decay with the time constant T_a .

To take into account the influence of the resistances of the rotor windings on the decay of the periodic stator current, and the influence of the stator resistances on the decay of the periodic rotor currents, it is necessary to solve the system of differential equations (15-22) and (15-23) with the addition of the terms $r_a i_A$ and $r_{exc} i_{rA}$ to their left-hand parts. The precise solution is rather complicated, however. With the actual relations existing between the parameters, a solution sufficiently correct for practice can be obtained in the following way.

In accordance with what was stated when determining the stator current with the decay of its transient component taken into account, the amplitude of the no-load e.m.f. $E_{m. max}$ can be represented in the

form of two components, one of which, $E'_{m. max}$, is proportional to the constant component of the excitation current $i_{exc.0}$ and constant in time, while the other, with the amplitude $E''_{m. max}$ at the initial moment, is proportional to the aperiodic current of the field winding $i_{exc.ap}$ and decays with the time constant T'_d .

Thus

$$\begin{aligned} E'_{m. max} + E''_{m. max} &= E_{m. max} \\ E'_{m. max} &= \frac{i_{exc.0}}{i_{exc.0} + i_{exc.ap}} E_{m. max} = \frac{I_d}{I'_d} E_{m. max} \\ E''_{m. max} &= \frac{i_{exc} - i_{exc.0}}{i_{exc.0} + i_{exc.ap}} E_{m. max} = \frac{I'_d - I_d}{I'_d} E_{m. max} = \frac{x_d - x'_d}{x_d} E_{m. max} \end{aligned}$$

since to the no-load excitation current $i_{exc.0}$ there corresponds the steady-state short-circuit stator current I_d (effective value) proportional to it

$$I_d = \frac{E_{m. max}}{\sqrt{2} \omega L_d} = \frac{E_{m. max}}{\sqrt{2} x_d} \quad (15-42)$$

while to the total excitation current at the initial moment of the short circuit $i_{exc} = i_{exc.0} + i_{exc.ap}$ there corresponds the initial periodic short-circuit stator current I'_d (effective value) which is proportional to it and equal to

$$I'_d = \frac{E_{m. max}}{\sqrt{2} \omega L'_d} = \frac{E_{m. max}}{\sqrt{2} x'_d} \quad (15-43)$$

Thus, the equations necessary for the determination of stator current can be written as follows:

$$\left. \begin{aligned} L_d \frac{di_A}{dt} + M_{ad} \frac{di_{rA}}{dt} + r_a i_A &= \\ &= \left(E'_{m. max} + E''_{m. max} e^{-\frac{t}{T'_d}} \right) \sin(\omega t + \varphi) \\ L_{exc} \frac{di_{rA}}{dt} + M_{ad} \frac{di_A}{dt} + r_{exc} i_{rA} &\cong L_{exc} \frac{di_{rA}}{dt} + M_{ad} \frac{di_A}{dt} = 0 \end{aligned} \right\} \quad (15-44)$$

It should be noted that if we neglect the term $r_{exc} i_{rA}$ in the second equation, then when solving the system of two equations we can obtain a resultant differential equation not of the second, but of the first degree, and the equations can be solved much simpler without affecting the accuracy of the results obtained. Solution of the system of these equations for the stator current with the above simplifications

gives

$$i_A = \frac{E'_{m. max} + E''_{m. max} e^{-\frac{t}{T'_d}}}{\sqrt{r_a^2 + \omega^2 L_d'^2}} \sin(\omega t + \psi - \varphi') - \frac{E_{m. max} e^{-\frac{t}{T_a}}}{\sqrt{r_a^2 + \omega^2 L_d'^2}} \sin(\psi - \varphi') \quad (15-45)$$

If we take the initial moment of short circuit $t = 0$ so that for phase $A-A'$ the angle $\psi = 0$, then with $\varphi' \cong \frac{\pi}{2}$ we shall have $\psi - \varphi' \cong -\frac{\pi}{2}$, and for phase $B-B'$ we can use equation (15-45) with $\psi - \varphi' = -\pi$. The current equations for these phases then become

$$i_A = -\frac{E'_{m. max} + E''_{m. max} e^{-\frac{t}{T'_d}}}{z'_d} \cos \omega t + \frac{E_{m. max} e^{-\frac{t}{T_a}}}{z'_d} = i_{A sym} + i_{A ap} \quad (15-46)$$

$$i_B = \frac{E'_{m. max} + E''_{m. max} e^{-\frac{t}{T'_d}}}{z'_d} \sin \omega t = i_{B sym} \quad (15-47)$$

Similarly, for the excitation current, since its periodic component will decay with the time constant T_a , and its aperiodic component with the time constant T'_d , the equation without the constant component will have the form

$$i_{exc} = -\frac{E''_{m. max} e^{-\frac{t}{T_a}}}{z'_{exc}} \cos \omega t + \frac{E'_{m. max} e^{-\frac{t}{T'_d}}}{z'_{exc}} \quad (15-48)$$

In equations (15-46), (15-47) and (15-48) we have denoted

$$z'_d = \sqrt{r_a^2 + \omega^2 L_d'^2} \quad \text{and} \quad z'_{exc} = \sqrt{r_{exc}^2 + \omega^2 L_{exc}'^2} \quad (15-49)$$

The resistances r_a and r_{exc} are very small compared with the inductive reactances

$$x'_d = \omega L'_d \quad \text{and} \quad x'_{exc} = \omega L'_{exc} \quad (15-50)$$

and, therefore, it may be assumed that

$$z'_d \cong x'_d, \quad z'_{exc} \cong x'_{exc}$$

The reactance x'_d is called the *transient direct-axis stator reactance*, and x'_{exc} , the *transient reactance of the field winding*.

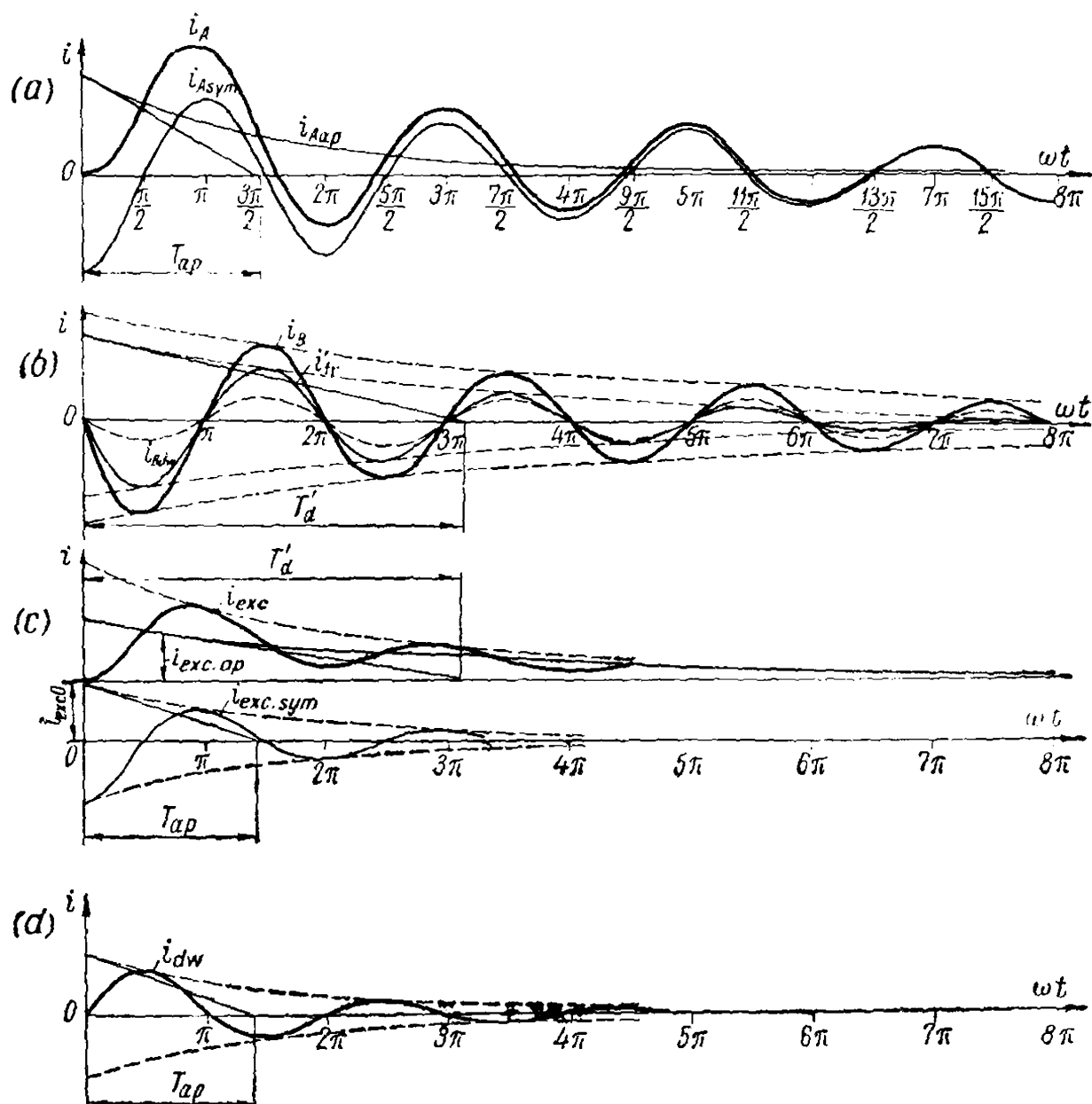


Fig. 15-7. Curves showing change in stator and rotor winding currents of a synchronous machine upon sudden short circuit with damping.

Figure 15-7 gives curves showing the change in the stator currents i_A and i_B and the excitation current i_{exc} for the case considered above.

The periodic component of the phase B current in Fig. 15-7 is resolved into two components: the sustained short-circuit current $i_{B,s}$ and the transient component i'_{tr} , attenuating with the time constant T'_d .

15-4. Sudden Short Circuit of a Synchronous Non-Salient-Pole Machine with Damper Windings on the Direct and Quadrature Axes

In the previous discussion of sudden short-circuit phenomena, a case was analysed where the damper winding was arranged only on the quadrature axis and its parameters (the reduced inductances and resistance) were equal to the parameters of the excitation system. In

actual cases the damper winding is arranged not only on the quadrature axis, but also on the direct axis, and its reduced inductance becomes somewhat smaller, and the reduced resistance, on the contrary, much larger than that of the field winding.

If the resistance of the damper winding is taken into account by means of an e.m.f. component in the stator circuit decaying with the time constant $T_d'' = \frac{L_{dw}''}{r_{dw}}$, and the resistance of the field winding is neglected, the differential equations of the transformer linkages between the stator and rotor circuits for the direct axis acquire the following form:

$$\left. \begin{aligned} L_d \frac{di_A}{dt} + M_{ad} \frac{di_{exc.A}}{dt} + M_{ad} \frac{di_{dw.A}}{dt} + r_a i_A &= \\ &= \left[E_{m.max}^{III} + E_{m.max}^{IV} e^{-\frac{t}{T_d''}} \right] \sin(\omega t + \psi) \\ L_{exc} \frac{di_{exc.A}}{dt} + M_{ad} \frac{di_A}{dt} + M_{ad} \frac{di_{dw.A}}{dt} &\cong 0 \\ L_{dw} \frac{di_{dw.A}}{dt} + M_{ad} \frac{di_A}{dt} + M_{ad} \frac{di_{exc.A}}{dt} &\cong 0 \end{aligned} \right\} \quad (15-51)$$

where $i_{exc.A}$ and $i_{dw.A}$ are the equivalent currents of the field and damper windings of the rotating rotor reduced to the stationary system of the stator circuits.

By excluding $i_{exc.A}$ and $i_{dw.A}$ from equations (15-51), we get

$$L_d'' \frac{di_A}{dt} + r_a i_A = \left[E_{m.max}^{III} + E_{m.max}^{IV} e^{-\frac{t}{T_d''}} \right] \sin(\omega t + \psi) \quad (15-52)$$

where L_d'' is the equivalent direct-axis leakage inductance of the stator winding with the screening effect of the field and damper windings taken into account, equal to

$$\begin{aligned} L_d'' &= (L_d - M_{ad}) + \frac{M_{ad}(L_{exc} - M_{ad})(L_{dw} - M_{ad})}{L_{exc}L_{dw} - M_{ad}^2} = (L_d - M_{ad}) + \\ &+ \frac{1}{\frac{1}{M_{ad}} + \frac{1}{L_{exc} - M_{ad}} + \frac{1}{L_{dw} - M_{ad}}} = L_{oa} + \frac{1}{\frac{1}{M_{ad}} + \frac{1}{L_{oexc}} + \frac{1}{L_{odw}}} \end{aligned} \quad (15-53)$$

By solving equation (15-52) for the current i_A , we find

$$i_A = \frac{E_{m. max}^{III} + E_{m. max}^{IV} e^{-\frac{t}{T_d''}}}{\sqrt{r_a^2 + \omega^2 L_d''^2}} \sin(\omega t + \psi - \varphi''') - \frac{E_{m. max} e^{-\frac{t}{T_a}}}{\sqrt{r_a^2 + \omega^2 L_d''^2}} \sin(\psi - \varphi''') = i_{A sym}'' + i_{A ap}'' \quad (15-54)$$

Here T_a is the time constant of decay of the aperiodic stator current with a damper winding on the rotor direct axis, equal to

$$T_a = \frac{L_d''}{r_a} \quad (15-55)$$

and T_d'' is the time constant of decay of the aperiodic current of the damper winding and of the corresponding periodic current component of the stator winding, equal to

$$T_d'' = \frac{L_{dw}''}{r_{dw}} \quad (15-56)$$

In the above expressions L_{dw}'' is the equivalent direct-axis leakage inductance of the damper winding, equal to

$$\begin{aligned} L_{dw}'' &= (L_{dw} - M_{ad}) + \frac{1}{\frac{1}{M_{ad}} + \frac{1}{L_{exc} - M_{ad}} + \frac{1}{L_d - M_{ad}}} = \\ &= L_{\sigma dw} + \frac{1}{\frac{1}{M_{ad}} + \frac{1}{L_{\sigma exc}} + \frac{1}{L_{\sigma a}}} \end{aligned} \quad (15-57)$$

With damper windings on the direct and quadrature axes, a greater current surge occurs during the initial short-circuit period in the stator windings and in the rotor damper winding than when there is no damper winding on the direct axis, since

$$L_d'' < L_d'$$

Seeing that the relative resistance r_{dw} of a damper winding is considerably greater than the resistance r_{exc} of a field winding, however, the time constant

$$T_d'' < T_d'$$

and, therefore, the current surge in the damper winding rapidly decays. After this a slower decay takes place in the field winding with the time constant T_d' corresponding to the sudden short-circuit process occurring without a damper winding considered earlier.

In accordance with the above, the periodic stator current contains the so-called subtransient component i_{tr}'' corresponding to the aperi-

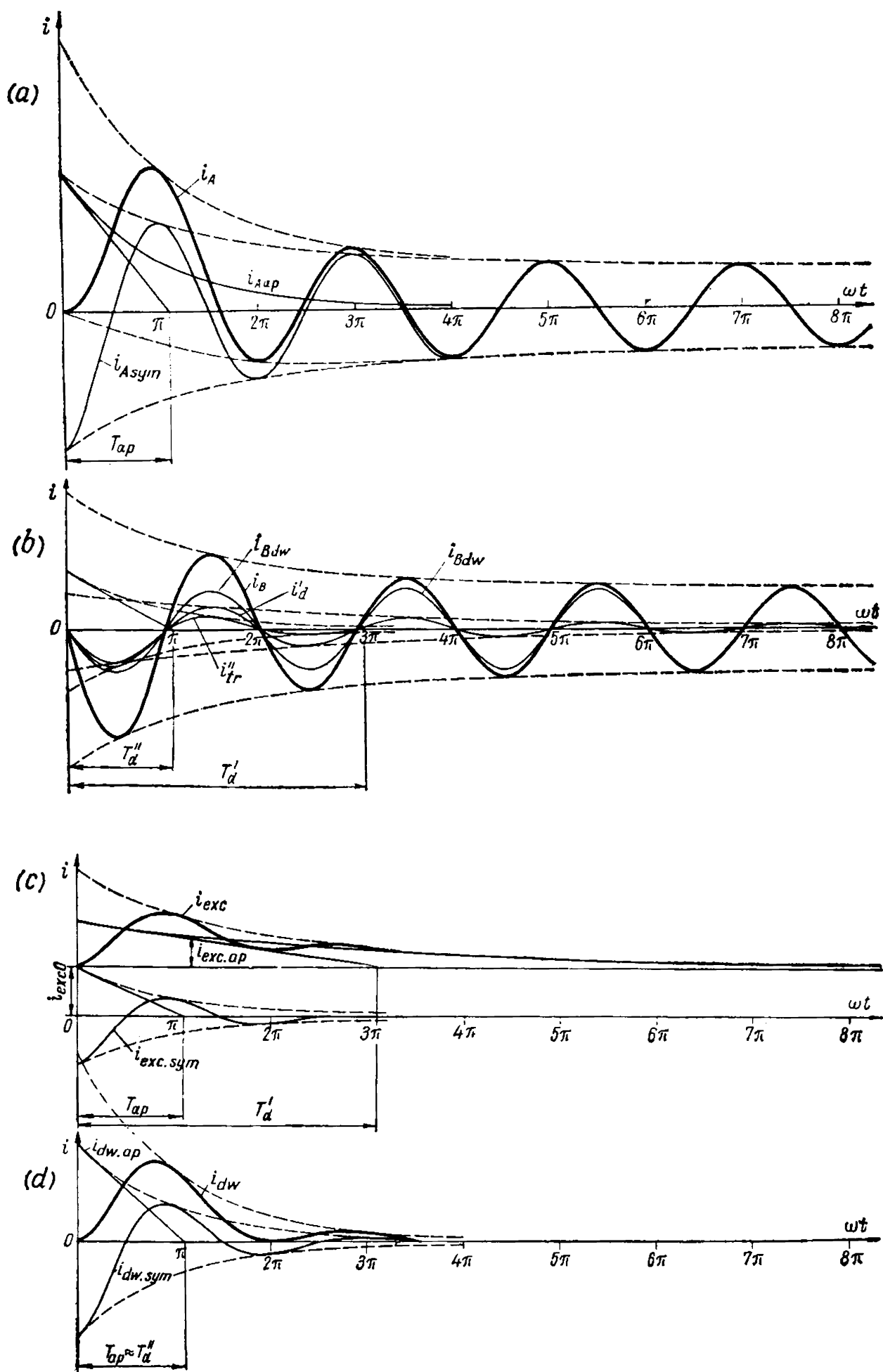


Fig. 15-8. Curves of short-circuit currents and their components

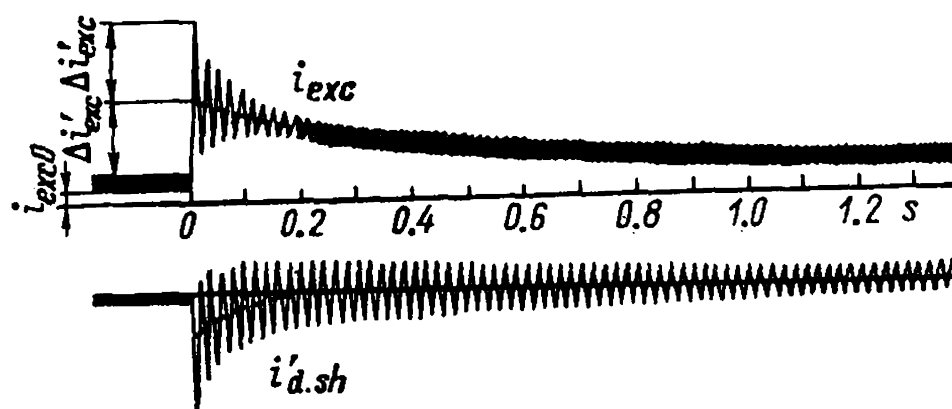


Fig. 15-9. Oscillograms of stator and rotor currents for sudden short circuit of a synchronous generator without damper winding on rotor

odic current $i_{dw.ap}$ of the damper winding and decaying with the time constant T'_d , and a transient component i'_{tr} corresponding to the aperiodic current $i_{exc.ap}$ of the field winding and decaying with the time constant T'_d .

Figure 15-8 shows curves of the short-circuit currents with a damper winding on the direct axis. The time constants T_a and T'_d are generally close in value, and in Fig. 15-8 they are assumed to be equal.

Figures 15-9 and 15-10 depict oscillograms of sudden short-circuit currents for a generator without and with a damper winding.

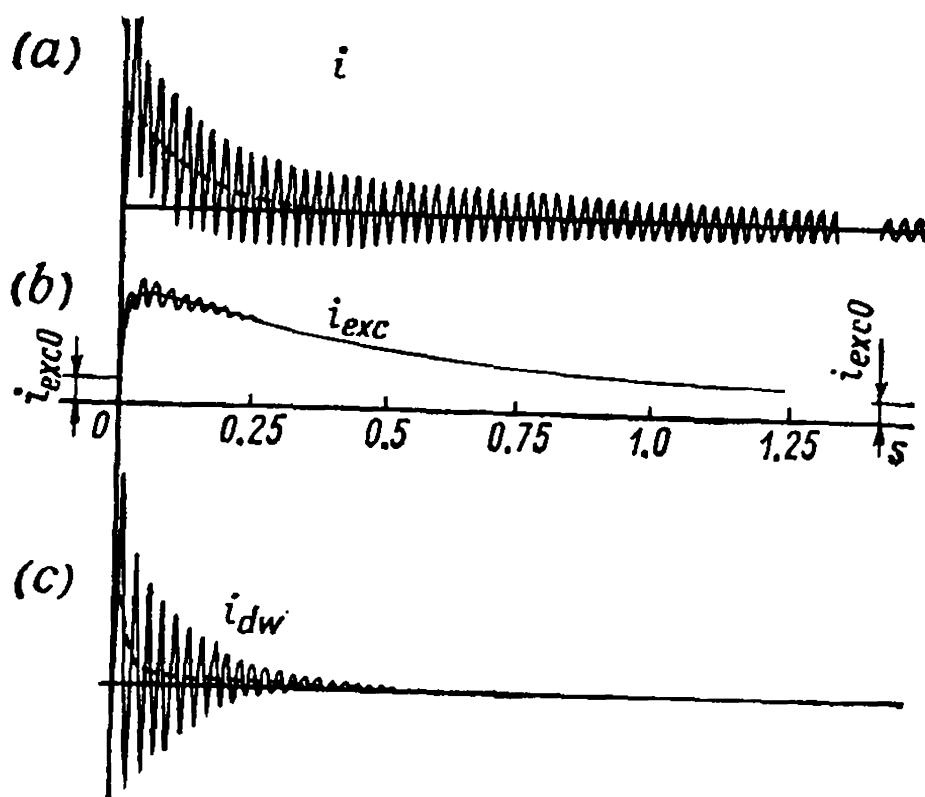


Fig. 15-10. Oscillograms of stator, field and damper winding currents for sudden short circuit

15-5. Equivalent Circuits for Synchronous Machine Inductive Reactances with a Sudden Short Circuit

The expression for the inductive reactance

$$x = \omega L = \omega k \Lambda \omega^2$$

shows that at a constant frequency $f = \frac{\omega}{2\pi}$ the inductive reactance x is proportional to the inductance L and, correspondingly, to the permeance Λ . If we express the inductive reactance in relative units, then

$$\underline{x} = \frac{x I_r}{E_r} = \frac{x}{x_r} = \frac{L}{L_r} = \underline{L} = \frac{\Lambda}{\Lambda_r} = \underline{\Lambda} \quad (15-58)$$

i.e., in relative units the inductive reactance x becomes equal to the relative inductance \underline{L} and relative permeance $\underline{\Lambda}$.

Hence, it follows that the equivalent circuits for the relative inductive reactances can simultaneously serve as equivalent circuits for the inductances and permeances, with the only difference that with physical units between x , L and Λ there is a direct proportionality. In relative units the sign of equality can be placed between the quantities \underline{x} , \underline{L} and $\underline{\Lambda}$.

If the inductance \underline{L} and the resistance r are expressed in physical units of the SI system, their ratio $\frac{L}{r}$ gives the time constant T in seconds. If they are expressed in relative units, their ratio $\frac{\underline{L}}{\underline{r}}$ gives the time constant in radians $\underline{T} = \omega T$, where the time T is expressed in seconds.

Thus, the expressions obtained for the permeance and the inductive reactance for a sudden short circuit, with only a field winding on the direct axis, have the following form:

$$\Lambda'_d = \Lambda_{\sigma a} + \frac{1}{\frac{1}{\Lambda_{ad}} + \frac{1}{\Lambda_{\sigma exc}}}; \quad L'_d = L_{\sigma a} + \frac{1}{\frac{1}{M_{ad}} + \frac{1}{L_{\sigma exc}}}$$

which makes it possible to write the corresponding expression for the direct-axis transient inductive reactance:

$$x'_d = \omega L'_d = x_{\sigma a} + \frac{1}{\frac{1}{x_{ad}} + \frac{1}{x_{\sigma exc}}} = x_{\sigma a} + \frac{x_{ad} x_{\sigma exc}}{x_{ad} + x_{\sigma exc}} \quad (15-59a)$$

and construct the equivalent circuit in Fig. 15-11 for x'_d . Similarly, for a sudden short circuit with two windings (field and damper) on

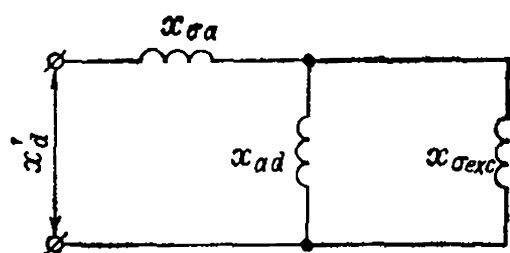


Fig. 15-11. Equivalent circuit for direct-axis transient inductive reactance

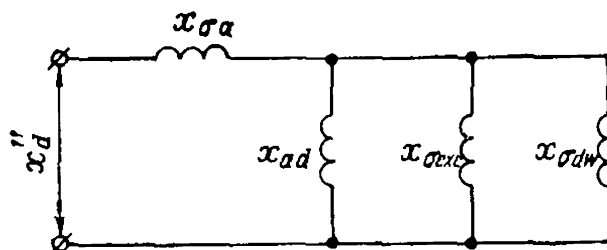


Fig. 15-12. Equivalent circuit for direct-axis subtransient inductive reactance

the rotor direct axis, we obtain the following expressions:

$$\Lambda_d'' = \Lambda_{\sigma a} + \frac{1}{\frac{1}{\Lambda_{ad}} + \frac{1}{\Lambda_{\sigma exc}} + \frac{1}{\Lambda_{\sigma dw}}}$$

$$L_d'' = L_{\sigma a} + \frac{1}{\frac{1}{M_{ad}} + \frac{1}{L_{\sigma exc}} + \frac{1}{L_{\sigma dw}}}$$

which makes it possible to write the expression for the direct-axis subtransient reactance:

$$x_d'' = \omega L_d'' = x_{\sigma a} + \frac{1}{\frac{1}{x_{ad}} + \frac{1}{x_{\sigma exc}} + \frac{1}{x_{\sigma dw}}} \quad (15-59b)$$

and construct the equivalent circuit in Fig. 15-12 for x_d'' .

With the stator winding open $L_{\sigma a} = \infty$ and the equivalent leakage inductance of the damper winding along the direct axis

$$L_{dw.0} = L_{a.dw} + \frac{1}{\frac{1}{M_{ad}} + \frac{1}{L_{\sigma exc}}}$$

The equivalent diagrams for the direct-axis transient and subtransient inductive reactances of the damper winding with an open and closed stator windings are shown in Figs. 15-13 and 15-14. The rotor resistances in these diagrams are reduced to the stator system and expressed in stator relative units (Sec. 11-1).

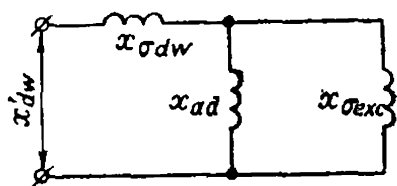


Fig. 15-13. Equivalent circuit for direct-axis transient inductive reactance of damper winding

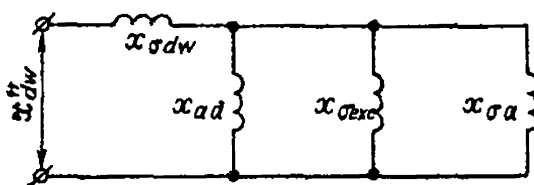


Fig. 15-14. Equivalent circuit for direct-axis subtransient inductive reactance of damper winding

These diagrams make it possible to write expressions for the transient and subtransient inductive reactances of the damper winding:

$$x'_{dw} = x_{\sigma dw} + \frac{1}{\frac{1}{x_{ad}} + \frac{1}{x_{\sigma exc}}} = x_{\sigma dw} + \frac{x_{ad} x_{\sigma exc}}{x_{\sigma exc} + x_{ad}} \quad (15-59c)$$

$$x''_{dw} = x_{\sigma dw} + \frac{1}{\frac{1}{x_{ad}} + \frac{1}{x_{\sigma exc}} + \frac{1}{x_{\sigma a}}} = x_{\sigma dw} + \frac{x_{ad} x_{\sigma exc} x_{\sigma a}}{x_{\sigma exc} x_{\sigma a} + x_{ad} x_{\sigma a} + x_{ad} x_{\sigma exc}} \quad (15-59d)$$

From expressions (15-59a), (15-59b), (15-59c) and (15-59d) we get

$$\frac{x'_{dw}}{x'_d} = \frac{x_{\sigma dw} x_{\sigma exc} + x_{\sigma dw} x_{ad} + x_{ad} x_{\sigma exc}}{x_{\sigma a} x_{ad} + x_{\sigma a} x_{\sigma exc} + x_{ad} x_{\sigma exc}} = \frac{x''_{dw}}{x''_d}$$

whence

$$x''_{dw} = x'_{dw} \frac{x''_d}{x'_d}$$

Example 15-1. The leakage inductive reactances of the field winding and damper winding according to the machine data are, in relative units, $x_{\sigma exc} = 0.239$ and $x_{\sigma dw} = 0.172$, respectively.

The total inductive reactance of the excitation system

$$X_{exc} = x_{ad} + x_{\sigma exc} = 0.57 + 0.239 = 0.809$$

The parameters of the direct-axis transient and subtransient conditions (Figs. 15-11 and 15-12) according to the stator winding equivalent diagrams, are

$$x'_d = x_{\sigma a} + \frac{1}{\frac{1}{x_{ad}} + \frac{1}{x_{\sigma exc}}} = 0.125 + \frac{1}{\frac{1}{0.57} + \frac{1}{0.239}} = 0.293$$

$$x''_d = x_{\sigma a} + \frac{1}{\frac{1}{x_{ad}} + \frac{1}{x_{\sigma exc}} + \frac{1}{x_{\sigma dw}}} = 0.125 + \frac{1}{\frac{1}{0.57} + \frac{1}{0.239} + \frac{1}{0.172}} = 0.211$$

The parameters for the direct-axis transient conditions according to field winding [formula (15-61)] equivalent diagram are as follows:

$$x'_{exc} = x_{\sigma exc} + \frac{1}{\frac{1}{x_{ad}} + \frac{1}{x_{\sigma a}}} = 0.239 + \frac{1}{\frac{1}{0.57} + \frac{1}{0.125}} = 0.341$$

The parameters of the direct-axis subtransient conditions, considered according to the damper winding equivalent circuit are correspondingly

$$x''_{dw} = x_{\sigma dw} + \frac{1}{\frac{1}{x_{ad}} + \frac{1}{x_{\sigma a}} + \frac{1}{x_{\sigma exc}}} = 0.172 + \frac{1}{\frac{1}{0.57} + \frac{1}{0.125} + \frac{1}{0.239}} = 0.244$$

15-6. Time Constants of a Symmetrical Polyphase Short Circuit

The time constant T'_d introduced above is a time constant of a field winding with closed stator windings.

If we short-circuit a field winding with the current $i_{exc} = i_{exc.0}$ and with the stator windings open and there is no damper winding along the direct axis, the current i_{exc} will drop to zero according to the law determined by the equation

$$L_{exc} \frac{di_{exc}}{dt} + r_{exc} i_{exc} = 0$$

The solution of this equation for the initial condition $i_{exc} = i_{exc.0}$ at $t = 0$ gives

$$i_{exc} = i_{exc.0} e^{-\frac{t}{T_{d0}}}$$

where

$$T_{d0} = \frac{L_{exc}}{r_{exc}} = \frac{X_{exc}}{\omega r_{exc}} \quad (15-60)$$

is the time constant of the field winding with an open stator winding. The time constant T'_d of the field winding with a closed stator winding can be approximately expressed through the time constant T_{d0} :

$$T'_d = \frac{x'_{exc}}{\omega r_{exc}} = \frac{x'_{exc}}{X_{exc}} T_{d0}$$

The inductive reactance X_{exc} for the field winding reduced to the stator is

$$X_{exc} = x_{\sigma exc} + x_{ad}$$

When the stator winding is short-circuited, the main excitation magnetic flux is displaced along the leakage flux path of the stator winding, as is shown in Fig. 15-2d, and the equivalent permeance of the field winding is

$$\Lambda'_{exc} = \Lambda_{\sigma exc} + \frac{\Lambda_{ad}\Lambda_{\sigma a}}{\Lambda_{ad} + \Lambda_{\sigma a}}$$

since, according to Fig. 15-2d, the reluctances corresponding to the permeances $\Lambda_{\sigma a}$ and Λ_{ad} are in series.

The equivalent inductive reactance x'_{exc} of the field winding corresponding to the permeance Λ'_{exc} is

$$x'_{exc} = x_{\sigma exc} + \frac{x_{ad}x_{\sigma a}}{x_{ad} + x_{\sigma a}} \quad (15-61)$$

The ratio between x'_{exc} and X_{exc} will be

$$\begin{aligned} \frac{x'_{exc}}{X_{exc}} &= \frac{x_{\sigma exc} + \frac{x_{ad} x_{\sigma a}}{x_{ad} + x_{\sigma a}}}{x_{\sigma exc} + x_{ad}} = \frac{x_{ad} x_{\sigma exc} + x_{\sigma a} x_{\sigma exc} + x_{ad} x_{\sigma a}}{(x_{\sigma exc} + x_{ad})(x_{\sigma a} + x_{ad})} = \\ &= \frac{x_{\sigma a} + \frac{x_{\sigma exc} x_{ad}}{x_{\sigma exc} + x_{ad}}}{x_{\sigma a} + x_{ad}} = \frac{x'_d}{x_d} \end{aligned}$$

According to the above result, the time constant T'_d of the field winding with a closed stator is expressed through the time constant T_{d0} with an open stator as follows

$$T'_d = \frac{x'_d}{x_d} T_{d0} \quad (15-62)$$

The time constant of the subtransient current with a closed stator is

$$\boxed{T''_d = \frac{x''_{dw}}{\omega r_{dw}}} \quad (15-63a)$$

The quantity T''_d , because of the considerable resistance of the damper winding, is very small, and it may usually be assumed for turbo-generators that

$$T''_d \cong \frac{1}{8} T'_d \quad (15-63b)$$

Example 15-2. The parameters of the 57 200-kW hydrogenerator considered in Example 8-1 (p. 201) in relative units are $x_1 = x_d = 0.695$; $x'_d = 0.293$, $x''_d = 0.211$; $x_2 = 0.215$; $x'_{exc} = 0.341$; $X_{exc} = 0.809$; $x''_{dw} = 0.244$; $r_a = 0.00468$; $r_{exc} = 0.00058$; $r_{dw} = 0.0154$.

The time constants for the transient conditions corresponding to these parameters are:

1. The time constant for the field winding with an open stator winding, from formula (15-60)

$$T_{d0} = \frac{X_{exc}}{\omega r_{exc}} = \frac{0.809}{314 \times 0.00058} = 4.43 \text{ s}$$

2. The time constant for the transient conditions of the field winding

$$T'_d = \frac{x'_{exc}}{\omega r_{exc}} = \frac{0.341}{314 \times 0.00058} = 1.88 \text{ s}$$

or, by formula (15-62)

$$T'_d = \frac{x'_d}{x_d} T_{d0} = \frac{0.293}{0.695} \times 4.43 = 1.87 \text{ s}$$

3. The time constant for the subtransient conditions of the damper winding, according to formula (15-63a)

$$T_d'' = \frac{x_{dw}''}{\omega r_{dw}} = \frac{0.244}{314 \times 0.0154} = 0.0503 \text{ s}$$

4. The time constant for the aperiodic component of the stator winding current, by formula (15-65a) in Sec. 15-7

$$T_a = \frac{x_2}{\omega r_a} = \frac{0.215}{314 \times 0.00468} = 0.146 \text{ s}$$

The maximum asymmetric short-circuit current, according to formula (15-67)

$$i_{\max, asym} = \frac{1.8 \times 1.05 \sqrt{2} U_r}{x_d''} = \frac{1.8 \times 1.05 \sqrt{2} \times 1.0}{0.211} = 12.7$$

15-7. Sudden Short Circuit of a Polyphase Salient-Pole Synchronous Machine

In a salient-pole synchronous machine the quadrature-axis synchronous inductive reactance x_q is not equal to the direct-axis reactance x_d .

Let us consider the simplest case of a two-phase synchronous machine having one field winding on the direct axis and no damper windings.

When a sudden short circuit takes place in such a machine, the value of the aperiodic current component in the stator winding changes when the rotor turns through 90° , because, in the first case, the direct axis will be opposite the phase being considered and, in the second phase, the quadrature axis.

In the first case the initial value of the aperiodic current is

$$I_{ap. d. max} = \frac{E_{m. max}}{x_d'}$$

and in the second case

$$I_{ap. q. max} = \frac{E_{m. max}}{x_q'} = \frac{E_{m. max}}{x_q}$$

the average value of the aperiodic current at $t=0$ being

$$I_{ap. av. max} = \frac{1}{2} \left(\frac{1}{x_d'} + \frac{1}{x_q} \right) E_{m. max}$$

If we suppose that the change in the permeance from its average value, when passing from the direct to the quadrature axis, takes place as a sine-wave function of double frequency, then

$$i_{ap} = \frac{1}{2} E_{m. max} \left[\left(\frac{1}{x_d'} + \frac{1}{x_q} \right) \cos 2\psi + \left(\frac{1}{x_d'} - \frac{1}{x_q} \right) \cos 2(\omega t + \psi) \right] e^{-\frac{T}{T_{ap}}} \quad (15-64)$$

The quantity

$$\frac{2}{\frac{1}{x'_d} + \frac{1}{x_q}} = \frac{2x'_d x_q}{x'_d + x_q} = x_2 \quad (15-65)$$

is the negative-sequence inductive reactance corresponding to asynchronous operation of a synchronous machine.

When x_2 is known, the time constant of the stator winding current aperiodic component can be found by means of the formula

$$\boxed{T_{ap} = \frac{x_2}{\omega r_a}} \quad (15-65a)$$

Salient-pole design does not introduce any novel features with respect to the periodic short-circuit current.

15-8. Total, Maximum Asymmetric and Effective Currents of a Polyphase Symmetrical Short Circuit

The relations obtained above make it possible to find expressions for the total short-circuit current of the stator winding. Here, as usual, we may neglect the active components as compared with the reactive ones in the impedances. The expression for the current is determined on the assumption that the sudden short circuit occurs at no-load with the minimum rated voltage across the terminals. For simplification, the relations are written for non-salient-pole synchronous machines.

The short-circuit current at rated voltage is

$$I_{sh} = \frac{E_r}{x} = I_r \frac{1}{x}$$

Consequently, the amplitude of a sustained short-circuit current will be

$$I_{sh, max. 0} = I_{r, max} \frac{1}{x_d}$$

The amplitude of the initial transient symmetrical short-circuit current equals

$$I'_{sh, max. 0} = I_{r, max} \frac{1}{x'_d}$$

and the amplitude of the initial subtransient symmetrical short-circuit current is

$$I''_{sh, max. 0} = I_{r, max} \frac{1}{x''_d}$$

The maximum value of the initial aperiodic short-circuit current equals

$$I_{ap, \max. 0}'' = I_{\max. 0}'' = I_{r, \max} \frac{1}{x_d''}$$

When the short-circuit current decays, its resultant periodic component divides into three parts

$$I_{sh, sym} = i_{sym} + (i'_{sym} - i_{sym}) + (i''_{sym} - i'_{sym})$$

The transient component $i'_{tr} = i'_{sym} - i_{sym}$ decays with the time constant T_d' ; the subtransient component $i''_{tr} = i''_{sym} - i'_{sym}$ decays with the time constant T_d'' , while i_{sym} is the sustained short-circuit current. The aperiodic component i_{ap} decays with the time constant T_{ap} . Consequently, the equation for the resultant short-circuit current may be written in the following form

$$\begin{aligned} i_{sh} &= i_{sym} + (i'_{sym, 0} - i_{sym, 0}) e^{-\frac{t}{T_d'}} + (i''_{sym, 0} - i'_{sym, 0}) e^{-\frac{t}{T_d''}} + i_{ap, 0} e^{-\frac{t}{T_{ap}}} = \\ &= I_{r, \max} \left[\frac{1}{x_d} \cos(\omega t + \psi) + \left(\frac{1}{x_d'} - \frac{1}{x_d} \right) e^{-\frac{t}{T_d'}} \cos(\omega t + \psi) + \right. \\ &\quad \left. + \left(\frac{1}{x_d''} - \frac{1}{x_d'} \right) e^{-\frac{t}{T_d''}} \cos(\omega t + \psi) - \frac{1}{x_d''} e^{-\frac{t}{T_{ap}}} \cos \psi \right] \quad (15-66) \end{aligned}$$

According to GOST 183-66, the maximum asymmetric short-circuit current is the crest value of the stator current for a given excitation of a rotating machine which occurs at sudden short circuit across the terminals of the machine. The magnitude of the maximum asymmetric short-circuit current defines the mechanical forces acting on the windings and on the shaft of the machine when a short circuit occurs.

In the most unfavourable case the initial value of the aperiodic current equals the initial value of the periodic current $\frac{E_{max}}{x_d''}$ and the maximum current inrush in half a period. In the absence of attenuation the current would be equal to $\frac{2E_{max}}{x_d''}$.

In practice the maximum asymmetric short-circuit current is calculated by the formula

$$i_{\max. asym} \cong \frac{1.8 \times 1.05 \sqrt{2} U_r}{x_d''} \quad (15-67)$$

where U_r is the rated phase voltage; 1.8 is the average value of the so-called current factor allowing for the decay of the current during a half-period. It is assumed that the short circuit occurs at no-load and the factor 1.05 allows for possible operation of the machine at a voltage of $1.05 U_r$.

The USSR State Standards at present do not limit the value of the maximum asymmetric current, but each generator must withstand such a current at no-load voltage equal to 105% of the rated value. Practically, the maximum asymmetric current may attain a value 15 times the rated current amplitude.

Since the periodic current is a decaying alternating current, its effective value at any moment t can be determined in the usual way from the equation

$$\begin{aligned} I''_{sym.t} &= I_{sym} + (I'_{sym.0} - I_{sym}) e^{-\frac{t}{T'_d}} + (I''_{sym.0} - I'_{sym.0}) e^{-\frac{t}{T''_d}} = \\ &= I_{sym} + I'_{tr.0} e^{-\frac{t}{T'_d}} + I''_{tr.0} e^{-\frac{t}{T''_d}} \end{aligned} \quad (15-68)$$

Here $I''_{sym.0} = \frac{E_m}{x''_d}$ = initial effective value of the subtransient current

$I'_{sym.0} = \frac{E_m}{x'_d}$ = initial effective value of the transient current without taking account of the subtransient component

$I''_{tr.0} = I''_{sym.0} - I'_{sym.0}$ and
 $I'_{tr.0} = I'_{sym.0} - I_{sym}$ = initial effective values of the subtransient components of the periodic current

I_{sym} = effective value of the sustained short-circuit current.

The decaying of the effective value of the resultant periodic current is shown by curve 1 in Fig. 15-15. Obviously the ordinates of the curve in Fig. 15-15 are $\sqrt{2}$ times less than the enveloping curve in Fig. 15-8b.

The initial effective value of the resultant short-circuit current I''_0 is equal to the square root of the sum of the squares of the initial effective value of the periodic current component $I''_{sym.0}$ and the initial

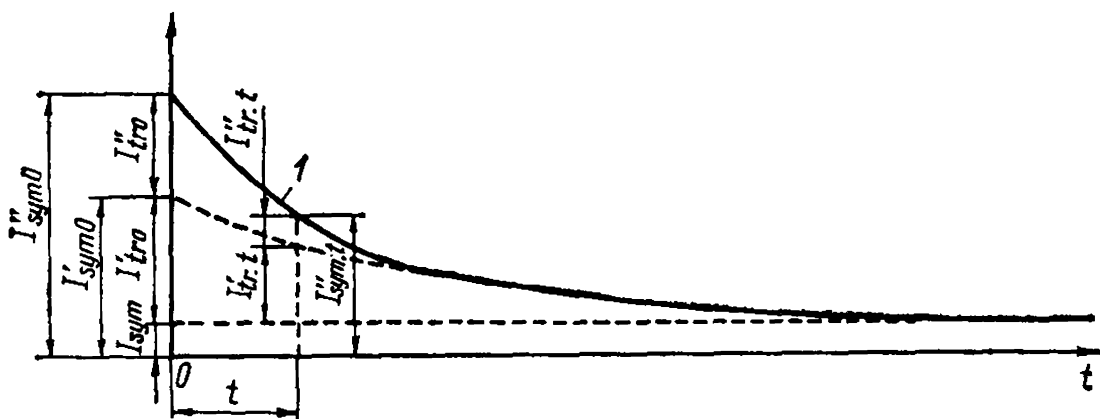


Fig. 15-15. Decay curves showing effective values of periodic current of sudden short circuit in a synchronous machine

value of the aperiodic component $I''_{ap.max.0}$, i.e.

$$I''_0 = \sqrt{I''^2_{sym.0} + I''^2_{ap.max.0}} = \sqrt{I''^2_{sym.0} + I''^2_{sym.max.0}} = \sqrt{I''^2_{sym.0} + (V\sqrt{2}I''_{sym.0})^2} = 1.73I''_{sym.0} \tag{15-69}$$

The current I''_0 is greater than the initial effective value of the periodic current component $I''_{sym.0}$ by $I''_{ap.0} = 0.73I''_{sym.0}$.

The difference between the effective value of the total current I''_0 and the effective value of the periodic current $I''_{sym.0}$ decays with a time constant T_{ap} and is represented by the expression

$$I''_{ap.t} = I''_{ap.0} e^{-\frac{t}{T_{ap}}} = 0.73I''_{sym.0} e^{-\frac{t}{T_{ap}}} \tag{15-70}$$

The effective value of the total current will be, therefore

$$I''_t = I''_{sym.t} + I''_{ap.t} = I_{sym} + I'_{tr.0} e^{-\frac{t}{T'_d}} + I''_{tr.0} e^{-\frac{t}{T''_d}} + 0.73I''_{sym.0} e^{-\frac{t}{T_{ap}}} \tag{15-71}$$

The effective value of the total current is shown by curve 1 in Fig. 15-16. Curve 2 is the aperiodic current component decay and curve 3, the decay of the effective value of the periodic current component.

TABLE

Type of synchronous machines	$\underline{x_d}$ (non-saturated values)	$\underline{x_q}$ (with rated current)	$\underline{x'_d}$ (with rated voltage)	$\underline{x''_d}$ (with rated voltage)	$\underline{x_2}$ (with rated current)	$\underline{x^*_0}$ (with rated current)
Two-pole turbogenerators	$\frac{1.10}{0.95-1.45}$	$\frac{1.07}{0.92-1.42}$	$\frac{0.155}{0.12-0.21}$	$\frac{0.090}{0.07-0.14}$	—	0.015-0.08
Four-pole turbogenerators	$\frac{1.10}{1.00-1.45}$	$\frac{1.08}{0.97-1.42}$	$\frac{0.23}{0.20-0.28}$	$\frac{0.15}{0.12-0.17}$	—	0.015-0.14
Synchronous generators with damper winding	$\frac{1.15}{0.60-1.45}$	$\frac{0.75}{0.40-1.00}$	$\frac{0.37}{0.20-0.50}$	$\frac{0.24}{0.13-0.35}$	$\frac{0.24}{0.13-0.35}$	0.02-0.20
Synchronous generators without damper winding	$\frac{1.15}{0.60-1.45}$	$\frac{0.75}{0.40-1.00}$	$\frac{0.35}{0.20-0.45}$	$\frac{0.32}{0.30-0.41}$	$\frac{0.55}{0.30-0.70}$	0.04-0.25
Synchronous motors	$\frac{1.8}{1.50-2.20}$	$\frac{1.15}{0.95-1.40}$	$\frac{0.40}{0.30-0.60}$	$\frac{0.25}{0.18-0.38}$	$\frac{0.24}{0.17-0.37}$	0.02-0.15

* x_0 varies considerably with a change in the winding pitch, therefore average values can be

** $\underline{r_a}$ varies considerably with the resistance of the damper winding.

*** $\underline{r_{a0}}$ and $\underline{r_a}$ depend on machine output. The limiting values are given for machines from winding.

The equation for the effective value of the current with a sudden short-circuit at a no-load equal to $U=U_r$ will be, in relative units

$$I_t'' = \frac{1}{x_d} + \left(\frac{1}{x_d'} - \frac{1}{x_d}\right)e^{-\frac{t}{T_d'}} + \left(\frac{1}{x_d''} - \frac{1}{x_d'}\right)e^{-\frac{t}{T_d''}} + 0.73\frac{1}{x_d''}e^{-\frac{t}{T_{ap}}} \quad (15-72)$$

This equation is obtained from equation (15-71) by substituting in it

$$\begin{aligned} I_{sym} &= \frac{U_r}{x_d}, & I'_{tr.0} &= U_r \left(\frac{1}{x_d'} - \frac{1}{x_d} \right) \\ I''_{tr.0} &= U_r \left(\frac{1}{x_d''} - \frac{1}{x_d'} \right) \\ I''_{sym.0} &= \frac{U_r}{x_d''} \end{aligned}$$

where

$$x_d = \frac{x_d U_r}{I_r}; \quad x_d' = \frac{x_d' U_r}{I_r}; \quad x_d'' = \frac{x_d'' U_r}{I_r}$$

and by dividing all the terms of this equation by I_r .

Typical synchronous machine parameters necessary for the calculation of short-circuit currents are given in Table 15-1. Inductive reactances are given in relative units, time constants, in seconds. The numerators are the average values, the denominators—the lower and the upper limiting values.

15-1

$\frac{x_p}{\text{(Potler reactance)}}$	r_{-2}^{**}	r_{-a}^{***}	r_{-a0}^{***}	T_{d0}	T_d'	T_d''	T_{ap}
$\frac{0.09}{0.07-0.14}$	0.025-0.04	0.003-0.008	0.0015-0.005	$\frac{4.4}{2.8-6.2}$	$\frac{0.6}{0.35-0.90}$	$\frac{0.035}{0.02-0.05}$	$\frac{0.09}{0.04-0.15}$
$\frac{0.17}{0.12-0.24}$	0.03-0.045	0.003-0.008	0.0015-0.005	$\frac{6.2}{4.0-9.2}$	$\frac{1.3}{0.9-1.8}$	$\frac{0.035}{0.02-0.05}$	$\frac{0.2}{0.15-0.35}$
$\frac{0.32}{0.17-0.40}$	0.012-0.20	0.003-0.015	0.003-0.020	$\frac{5.6}{1.5-9.5}$	$\frac{1.8}{0.5-3.3}$	$\frac{0.055}{0.01-0.05}$	$\frac{0.15}{0.03-0.25}$
$\frac{0.31}{0.17-0.38}$	0.03-0.045	0.003-0.010	0.003-0.020	$\frac{6.6}{3.0-10.5}$	$\frac{2.0}{1.0-3.3}$	—	$\frac{0.30}{0.1-0.5}$
$\frac{0.34}{0.23-0.45}$	0.025-0.07	0.004-0.010	0.002-0.015	$\frac{9.0}{6.0-11.5}$	$\frac{2.0}{1.2-2.8}$	$\frac{0.035}{0.02-0.05}$	$\frac{0.17}{0.1-0.3}$

given only approximately; x_0 varies from $0.1 x_d''$ to $0.7 x_d''$.

500 to 50 000 kVA. Here r_{a0} is the direct-current resistance and r_a , the resistance of the stator

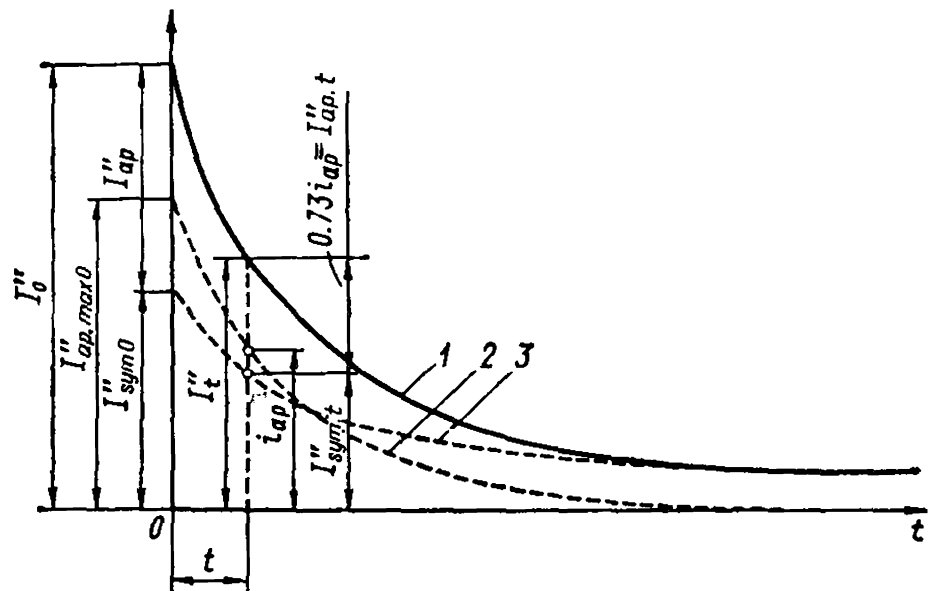


Fig. 15-16. Decay curves showing effective values of total short-circuit current and its components

15-9. Sudden Asymmetrical Short Circuit of a Synchronous Machine

Physical Aspects of the Phenomena. Let us consider the initial process of a two-phase and single-phase short circuits, neglecting decay of the currents in the stator and rotor windings.

Assume that the sudden short circuit occurs at the moment when the axis of the equivalent stator winding is perpendicular to the direct axis of the rotor (Fig. 15-17a), which will correspond to the case when only a periodic current is produced in the stator winding. The equivalent mutual inductance M of the stator and rotor windings will not be constant, as with a polyphase short circuit, but will vary pro-

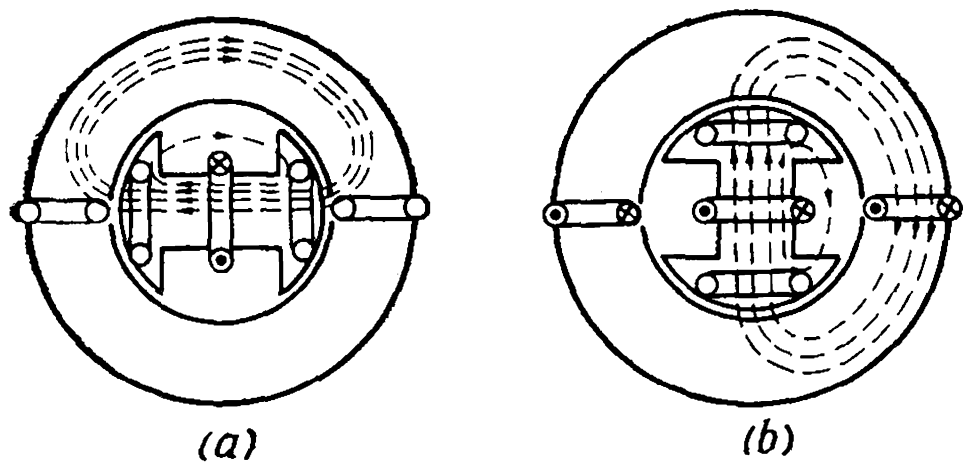


Fig. 15-17. Relative positions of stator and rotor windings at sudden single-phase short circuit:
a — with aperiodic stator current absent; b — with aperiodic stator current present

portional to $\sin \omega t$:

$$M = k\Lambda_{ad}\omega_a\omega_{exc} \sin \omega t$$

When the rotor turns from its initial position through an angle $\frac{\pi}{2}$, the mutual inductance will attain its maximum; therefore, for a constant initial value of the flux Φ_m in this position of the rotor, a maximum current surge equal to $\frac{E_m}{x'_d}$ will be created in the stator winding, and in the field winding we shall have

$$\Delta i_{exc} \cong \frac{x_d - x'_d}{x'_q} i_{exc 0}$$

which drops to the value

$$\Delta i_{exc} = \frac{x_q - x'_q}{x'_q} i_{exc 0} \cong 0$$

when the rotor turns through the angle π from its initial position, etc.

As a result, when there is only a periodic current component in the stator winding, an additional alternating component of the excitation current, whose peak values will attain the values of the constant additional component of a polyphase short circuit, will be created in the field winding, in contrast to a polyphase short circuit. As can be seen from the curves of the stator and field winding currents in Fig. 15-18a, the periodic current components in both windings will contain many harmonics. The appearance of these harmonics is easily explained by the fact that the pulsating magnetizing force

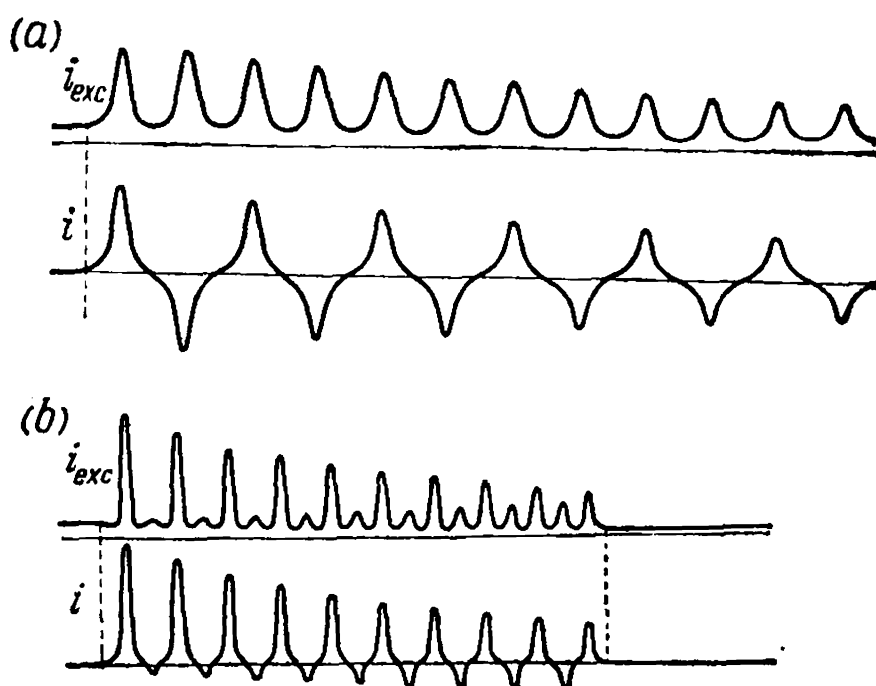


Fig. 15-18. Oscillograms of two-phase sudden short-circuit currents:

a — with aperiodic stator current absent; *b* — with aperiodic stator current present

of the stator winding produces not only a direct, but also a counter-rotating synchronous field, which, in the absence of a full damper system on the rotor, induces a double-frequency current in the field winding and a third-harmonic current in the stator winding, which, in turn, cause a number of even harmonics to appear in the field winding and a number of odd harmonics in the stator winding. Because of the resistance of the field winding, the fluxes in the machine will start to decay and, correspondingly, the currents in the stator winding will also start to decay, as can be seen from the oscillogram of the two-phase short circuit shown in Fig. 15-18*a*.

If a sudden two-phase or single-phase short circuit begins at the moment when the axes of the equivalent stator winding and of the field winding coincide (Fig. 15-17*b*), the mutual inductance of these windings will be maximum at the initial moment and at the moments corresponding to rotor displacements of $2k\pi$ from this position, where k is an integer.

An aperiodic current component will also appear in the stator winding and, therefore, if the resistances are neglected, the maximum initial current inrushes will be twice the value (Fig. 15-18*b*) than when there is only a periodic short-circuit current (Fig. 15-18*a*). The aperiodic component of the stator current will give rise to odd current harmonics in the field winding and to even ones in the stator winding, and as a result the entire process of current change will have the form shown in Fig. 15-18*b*. It can be seen from these curves that, after decay of the aperiodic current component, both current decay processes have the same nature as with a symmetrical short circuit. When the process of decay is over and the machine operates in conditions of a sustained short circuit, pronounced even current harmonics remain in the field winding, as can be seen from the oscillograms of Fig. 15-18*a* and *b*.

With a full damper winding on the rotor, or with a solid rotor of non-salient-pole turbo-type machines, the counter-synchronous field is practically damped; therefore, the current harmonics of the stator winding disappear, and the process begins to become similar to a polyphase short circuit, the values of the variable component in the excitation current also dropping somewhat.

With a sudden single-phase and two-phase short circuits in a three-phase machine, as well as with a short circuit in a single-phase machine, the value of the initial current will depend on the magnitude of the aperiodic current component. If the sudden short circuit occurs at the moment when the e.m.f. of the machine winding passes through zero, the maximum possible aperiodic component of the current is produced, and, therefore, the maximum possible inrush of initial current during the sudden short circuit takes place. If, on the contrary, the short circuit of the winding occurs at the moment when the e.m.f. of the winding passes through its maximum, the aperiodic current

component equals zero, and a periodic condition immediately sets in, during which the least possible inrush of the initial current of a sudden short circuit is obtained.

With a single-phase short circuit, the stator winding produces a pulsating magnetizing force, and, therefore, not only a synchronous field, but also a counter-synchronous armature field, which, in turn, produces a double-frequency current in the rotor windings.

Fundamental Relations. The initial effective values of currents for single-phase and two-phase short circuits are calculated by formulas similar to those for sustained currents of asymmetrical short circuits, in which only $x_1 = x_d$ is replaced by x'_d (or, correspondingly, by x''_d), while x_2 and x_0 remain practically the same both for the steady-state and transient conditions.

This is explained by the fact that the negative- and zero-sequence stator fluxes, as distinct from the positive-sequence flux, enter into transformer linkage with the rotor windings already in the steady-state condition, and, therefore, as concerns the manifestation and action of these fluxes, there is no significant difference between steady-state and transient conditions.

Thus, for the sustained and initial effective current values of a two-phase short circuit with $E_m = U_r$, we have

$$\left. \begin{aligned} I_{sym. 2} &= \frac{\sqrt{3} E_m}{x_d + x_2} = \frac{\sqrt{3} I_r}{x_d + x_2} \\ I'_{sym. 02} &= \frac{\sqrt{3} E_m}{x'_d + x_2} = \frac{\sqrt{3} I_r}{x'_d + x_2} \\ I''_{sym. 02} &= \frac{\sqrt{3} E_m}{x''_d + x_2} = \frac{\sqrt{3} I_r}{x''_d + x_2} \end{aligned} \right\} \quad (15-73)$$

and, correspondingly, for a single-phase short circuit

$$\left. \begin{aligned} I_{sym. 1} &= \frac{3E_m}{x_d + x_2 + x_0} = \frac{3I_r}{x_d + x_2 + x_0} \\ I'_{sym. 01} &= \frac{3E_m}{x'_d + x_2 + x_0} = \frac{3I_r}{x'_d + x_2 + x_0} \\ I''_{sym. 01} &= \frac{3E_m}{x''_d + x_2 + x_0} = \frac{3I_r}{x''_d + x_2 + x_0} \end{aligned} \right\} \quad (15-74)$$

For the root-mean-square value of a sudden short-circuit current we may write, in the general form, the following equation:

$$\begin{aligned} I_{vt} = I_{sym. v} + (I'_{sym. 0v} - I_{sym. v}) e^{-\frac{t}{T'_{dv}}} + (I''_{sym. 0v} - I'_{sym. 0v}) e^{-\frac{t}{T''_{dv}}} + \\ + I''_{d0v} e^{-\frac{t}{T_{apv}}} \end{aligned} \quad (15-75)$$

where v is a subscript characterizing the short circuit; $v=3$ for a three-phase, $v=2$ for a two-phase, and $v=1$ for a single-phase short circuit. The time constants T'_{dv} , T''_{dv} and T_{apv} are used in this equation in accordance with the type of short circuit.

The time constants of the subtransient current component may be assumed to be the same for all types of short circuits and equal to

$$T''_{d3} = T''_{d2} = T''_{d1} \cong \frac{1}{8} T'_d$$

The decay time constants of the transient current component are equal to:

$$\left. \begin{aligned} T'_{d3} &= T'_d = \frac{x'_d}{x_d} T_{d0} \\ T'_{d2} &= \frac{x'_d + x_2}{x_d + x_2} T_{d0} \\ T'_{d1} &= \frac{x'_d + x_2 + x_0}{x_d + x_2 + x_0} T_{d0} \end{aligned} \right\} \quad (15-76)$$

The decay time constants of the aperiodic current component are equal to:

$$\left. \begin{aligned} T_{ap3} &= T_{ap2} = \frac{x_2}{\omega r_{ap}} \\ T_{ap1} &= \frac{2x_2 + x_0}{3\omega r_{ap}} \end{aligned} \right\} \quad (15-77)$$

Example 15-3. Determine by formulas (15-76) and (15-77) the time constants for different kinds of sudden short circuit across the terminals at no-load for the 57 200-kW hydrogenerator considered in the previous examples, taking into account the values of the relative inductive reactances $\underline{x}_1 = \underline{x}_d = 0.695$, $\underline{x}'_d = 0.291$, $\underline{x}_2 = 0.215$, $\underline{x}_0 = 0.054$ and resistance $\underline{r}_{ap} = 0.00468$ found in those examples.

$$\begin{aligned} T'_{d3} &= T'_d = \frac{\underline{x}'_d}{\underline{x}_d} T_{d0} = \frac{0.291}{0.695} \times 4.43 = 1.87 \text{ s} \\ T'_{d2} &= \frac{\underline{x}'_d + \underline{x}_2}{\underline{x}_d + \underline{x}_2} T_{d0} = \frac{0.291 + 0.215}{0.695 + 0.215} \times 4.43 = 2.46 \text{ s} \\ T'_{d1} &= \frac{\underline{x}'_d + \underline{x}_2 + \underline{x}_0}{\underline{x}_d + \underline{x}_2 + \underline{x}_0} T_{d0} = \frac{0.291 + 0.215 + 0.054}{0.695 + 0.215 + 0.054} \times 4.43 = 2.57 \text{ s} \\ T_{ap3} &= T_{ap2} = \frac{\underline{x}_2}{\omega \underline{r}_{ap}} = \frac{0.215}{314 \times 0.00468} = 0.146 \text{ s} \\ T_{ap1} &= \frac{2\underline{x}_2 + \underline{x}_0}{3\omega \underline{r}_{ap}} = \frac{2 \times 0.215 + 0.054}{3 \times 314 \times 0.00468} = 0.11 \text{ s} \end{aligned}$$

Chapter 16

OSCILLATIONS OF SYNCHRONOUS MACHINES

16-1. General Physical Picture of Oscillations

A synchronous machine connected to a high-power mains with a constant voltage and a strictly constant frequency possesses the ability to oscillate near its average speed following disturbances in the equality between the torque M applied to its shaft and the electromagnetic torque M_{em} which it develops.

At a constant angular speed $\Omega = \text{const}$ the mechanical torque M applied to the shaft of a synchronous machine is balanced by the electromagnetic torque M_{em} , therefore the torque equilibrium equation has the following simple form:

$$M = M_{em}$$

If, for some reason, equilibrium is disturbed and $M \neq M_{em}$, then equilibrium is restored at the expense of the dynamic torque

$$M_j = J \frac{d\Omega}{dt}$$

which appears due to the change in angular speed of the machine:

$$M = M_{em} + M_j = M_{em} + J \frac{d\Omega}{dt} \quad (16-1)$$

where J is the moment of inertia of the rotating parts of a synchronous machine.

Assume, for example, that a very fast change occurs in the torque of the prime mover driving a non-salient-pole generator in which the preceding load corresponded to a certain angle of displacement θ' by which the e.m.f. \dot{E}_m leads the voltage vector \dot{U} (point a in Fig. 16-1a).

If we ignore the stator copper losses, the electromagnetic torque will be

$$M_{em} = \frac{P_{em}}{\Omega} = \frac{mE_m U}{\Omega x_d} \sin \theta$$

where $\Omega = \frac{\omega}{p}$ is the mechanical angular speed of the generator rotor.

With an increase in the torque from M' to M'' , upon a transition to a new state of equilibrium, the electromagnetic torque should also increase from M'_{em} to M''_{em} ; this requiring, with constant excitation ($E_m = \text{const}$), a change in the angle from θ' to θ'' . If the rotor system

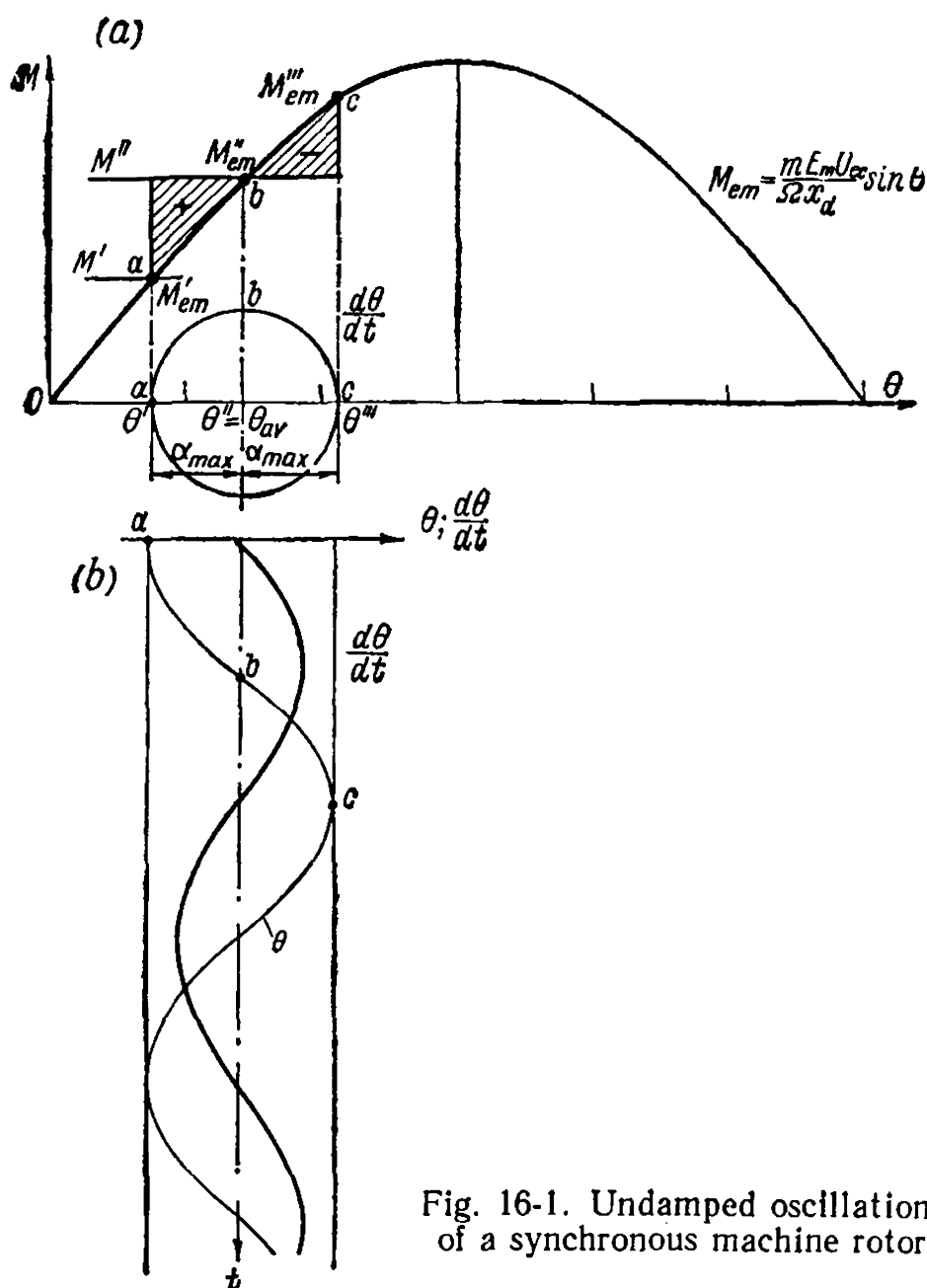


Fig. 16-1. Undamped oscillations of a synchronous machine rotor

of the synchronous machine had no inertia and kinetic energy, the rotor would instantaneously pass over to a new angular position, and a new condition of equilibrium would immediately set in between the applied and the electromagnetic torques $M'' = M_{em}$. Since the rotating rotor system has a definite moment of inertia J , however, the angle will change with a certain variable acceleration according to the equation

$$M'' = M_{em} + M_J = \frac{m E_m U}{\Omega x_d} \sin \theta + \frac{J}{p} \frac{d\omega}{dt}$$

if we do not consider the influence of the additional currents induced in the windings during the oscillation process with a change in the angle θ .

The rotor, receiving an angular acceleration $\frac{d\Omega}{dt} = \frac{1}{p} \frac{d\omega}{dt}$, begins to gradually increase its angular speed Ω , owing to which the angle of displacement θ of vector \vec{E} relative to vector \vec{U} also begins to change. When θ becomes equal to $\theta'' = \theta_{av}$ (point b in Fig. 16-1a), equilibrium

will be established between the torques $M'' = M''_{em} = M_{em.av}$. But, since during the period of transition from the angle θ' to θ'' the rotor accumulated an additional amount of kinetic energy $J \frac{\Omega''^2 - \Omega'^2}{2}$ and the angular speed Ω of the rotor becomes greater than the synchronous speed Ω_{syn} , the angle θ will continue to change, and equilibrium between the torques M and M_{em} will again be disturbed.

Now $M_{em} > M''$, and the acceleration $\frac{d\Omega}{dt}$ becomes negative. Therefore, the angular speed Ω begins to gradually decrease until the rotor again reaches its synchronous speed Ω_{syn} with a new value of the angle $\theta = \theta'''$ (point *c* in Fig. 16-1*a*) and with a new value of the electromagnetic torque M'''_{em} corresponding to this angle. At point *c* (Fig. 16-1*a*) the torques are not balanced, however, $M'''_{em} > M''$, the acceleration remains negative and the rotor continues to slow down. The rotor speed therefore becomes less than the synchronous speed, the angle θ begins to decrease until equilibrium between the torques $M'' = M_{em}$ is again restored at point *b* (Fig. 16-1*a*). The rotor speed at this point will be lower than the synchronous speed, therefore the angle θ continues to decrease, and the electromagnetic torque of the generator changes from point *b* to point *a* on the curve of Fig. 16-1*a*.

Here $M'_{em} < M''$, but since the rotor receives a positive acceleration, its speed will begin to increase, and at point *a* will reach the synchronous speed, i.e., the system returns to the previously considered initial position. The process will obviously begin again in the same sequence, if damping forces will not cause the oscillations to decay. When the oscillations decay, the system, after a certain time, reaches its final condition of equilibrium with $M'' = M_{em}$ and $\theta = \theta''$.

The change in the angle θ and in relative speed $\frac{d\theta}{dt}$ with time is shown in Fig. 16-1*b*.

It should be noted here that a synchronous machine may be brought out of equilibrium not only by a sudden change in the torque applied to its shaft, but also by a number of other causes. Among them are, for example, sudden changes in the external circuit parameters, disconnection from or connection of a portion of a parallel line to the line joining a synchronous machine with a high-capacity system; a short circuit followed by disconnection from the line; connection of the generator to the line when not sufficiently synchronized, etc.

The expression for the electromagnetic torque under oscillatory conditions can be written as follows:

$$M_{em} = \frac{mE_m U}{\Omega x_d} \sin(\theta_{av} + \alpha) = \frac{mE_m U}{\Omega x_d} \sin \theta_{av} \cos \alpha + \frac{mE_m U}{\Omega_{av} x_d} \cos \theta_{av} \sin \alpha \quad (16-2)$$

where α is the deviation of the angle θ from its average value θ_{av} .

If the changes of the angle θ are relatively small ($\alpha < 20^\circ$), it is then possible, without appreciable error to assume that $\cos \alpha \cong 1$, $\sin \alpha \cong \alpha$, and $\Omega \cong \Omega_{av}$. Then

$$\begin{aligned} M_{em} &\cong \frac{mE_m U}{\Omega_{av} x_d} \sin \theta_{av} + \frac{mE_m U}{\Omega_{av} x_d} \cos \theta_{av} \alpha \cong M_{em. av} + M'_{syn} \alpha = \\ &= M_{em. av} + M_{syn} \end{aligned} \quad (16-3)$$

where

$$M_{em. av} = \frac{mE_m U}{\Omega_{av} x_d} \sin \theta_{av}$$

is the mean electromagnetic torque balanced by the torque M on the shaft and $M'_{syn} \alpha$ is the unbalanced additional torque on the shaft, or the so-called synchronizing torque M_{syn} . Under the action of this torque, the rotor receives acceleration which tends to bring it into a position at which the torque on the shaft M'' and the electromagnetic torque M''_{em} balance each other (point b in Fig. 16-1a), this corresponding to normal synchronous operation.

The factor

$$M'_{syn} = \frac{mE_m U}{\Omega_{av} x_d} \cos \theta_{av} \quad (16-4)$$

is called the *synchronizing torque factor*.

If we assume that a synchronous machine is operating at synchronous speed, the machine, in oscillation conditions, is similar to a clock pendulum whose spring stiffness F is equivalent to the synchronizing torque factor M'_{syn} with the angle of twist of the spring from the zero position α corresponding to the angle of displacement θ of the e.m.f. E_m relative to the line voltage U .

In Fig. 16-2a such a pendulum is shown in a position where the spring is in positive tension and the angle $\alpha > 0$, which corresponds to point c in Fig. 16-1a. The pendulum is shown in Fig. 16-2b passing through its equilibrium position (point b in Fig. 16-1). Having the stored kinetic energy $J \frac{\Omega^2}{2}$, it passes through the equilibrium position with

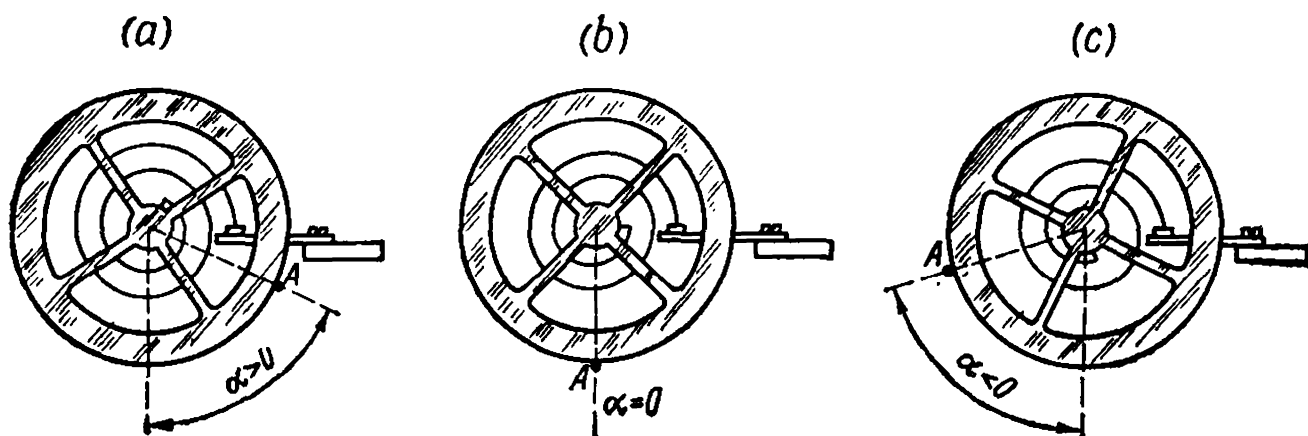


Fig. 16-2. Oscillations of mechanical watch pendulum

zero acceleration and the maximum speed, this permitting it to reach the position shown in Fig. 16-2c (point *a* in Fig. 16-1), at which its speed becomes zero and after which it begins to move in the opposite direction.

If no damping forces acted during pendulum motion, then, being once swung to the position of Fig. 16-2a, it would continue to oscillate for an infinitely long time with a steady amplitude and a definite natural frequency directly proportional to $\sqrt{\frac{F}{J}}$. However, the presence of damping forces such as air friction, bearing friction, etc., proportional to the speed and therefore having a maximum value when the pendulum is passing the position of equilibrium, leads to a gradual decrease in the swing until the pendulum stops in the position of equilibrium. Conversely, in the presence of compelling forces acting in resonance with the natural frequency of the pendulum, the amplitude of the oscillations may increase.

When a rotor in a synchronous machine oscillates near its synchronous speed, the principal damping forces which suppress its oscillations are the torques developed by the currents induced by the oscillations in the bars of a short-circuited damper winding, or in the solid rotor body of a turbogenerator, and also in the field winding.

In normal symmetrical operating conditions, when the rotor of a polyphase synchronous machine runs at synchronous speed together with the rotating field, no e.m.f. e_{dw} and currents i_{dw} appear in the damper winding bars. When the rotor oscillates with respect to the synchronous speed, however, e.m.f.s and currents of low frequency corresponding to the natural frequency of the synchronous machine (about 0.5-1.5 Hz) appear in these bars. Since the rotor oscillations are of a sine-wave character, the maximum value of the e.m.f. e_{dw} is reached at the maximum relative speed of oscillations $\frac{d\alpha}{dt}$, i.e., when the rotor passes through its equilibrium position. Since the frequency of the e.m.f. e_{dw} and of the current i_{dw} is very low and the resistance of the damper winding is high, the current slightly lags in phase behind the voltage and the current i_{dw} may be assumed to be in phase with the e.m.f. e_{dw} . The currents i_{dw} which interact with the resultant flux Φ_δ rotating at synchronous speed, produce retardation forces which act against the relative swing of the rotor and therefore develop a damping torque

$$M_{dw} = K_{dw} \frac{d\alpha}{dt} \quad (16-5)$$

which suppresses the oscillations similar to friction in a pendulum.

The currents induced in the massive metal parts of a rotor and in the field winding act in the same manner and contribute to the total damping torque M_{dw} . Natural-frequency currents are also induced

by the excitation flux in the stator winding, and, as a result of their interaction with the rotor field, the rotor is subjected to another component of the damping torque. When there is a damper winding in salient-pole machines and a massive rotor in turbogenerators, the action of the natural-frequency currents in the field and stator windings is relatively small and may be neglected in the first approximation. It should be noted that the factor K_{dw} in equation (16-5) is called the *damping torque factor*.

When a rotor runs with strictly synchronous speed, its axes are stationary both with respect to the resultant flux Φ_δ and to the armature-reaction flux Φ_a .

Therefore, the rotor oscillations with respect to the air-gap flux Φ_δ , which is rotating at synchronous speed, are equivalent to rotor oscillations relative to the conditionally stationary magnetizing forces and fluxes of the stator, this being equivalent to the flow of direct current in the stator.

Maps of such fluxes and currents for an overexcited synchronous generator operating in parallel with a network under no-load conditions ($\theta=0$) are shown in Fig. 16-3.

The cycle of the rotor oscillations is shown in Fig. 16-3 in four positions, Fig. 16-3*b* and *d* corresponding to the equilibrium position, Fig. 16-3*a* showing the maximum deviation of the rotor from equilibrium to the left and Fig. 16-3*c* to the right. For purposes of analogy, the corresponding positions of an imaginary pendulum are depicted in the lower part of each figure. The field winding with a current i_{exc} in the equilibrium position produces the flux Φ_m directed vertically downwards. The stator winding is shown as a two-phase winding with a 90° phase displacement. The conditional (in the sense pointed out previously) direct current flows only in phase *A* and produces a demagnetizing armature-reaction flux Φ_a directed upwards, which corresponds to the no-load conditions of an overexcited machine (see Fig. 12-11*a*). In phase *B* the current lags 90° behind the current in phase *A* and, therefore, its conditional direct current equals zero. Two damping circuits are shown on the rotor: one along the direct axis and the other along the quadrature axis. Upon oscillations of the rotor, the damper winding moves relative to the armature field directed downwards, and the excitation flux is displaced with respect to the stator windings. The directions of the natural-frequency currents induced in the above-mentioned windings can be determined by the right-hand rule, the directions of the forces developed by the left-hand rule.

A glance at Fig. 16-3 shows that when the rotor moves counterclockwise from the position in Fig. 16-3*a*, the stator field induces in the bars of the quadrature damper winding the e.m.f.s $e_{dw,q}$, whose direction is shown by a cross and a point in Fig. 16-3*b* corresponding to the amplitude of these e.m.f.s. The currents $i_{dw,q}$ of the quadrature damper winding are practically in phase with the e.m.f.s $e_{dw,q}$. Upon

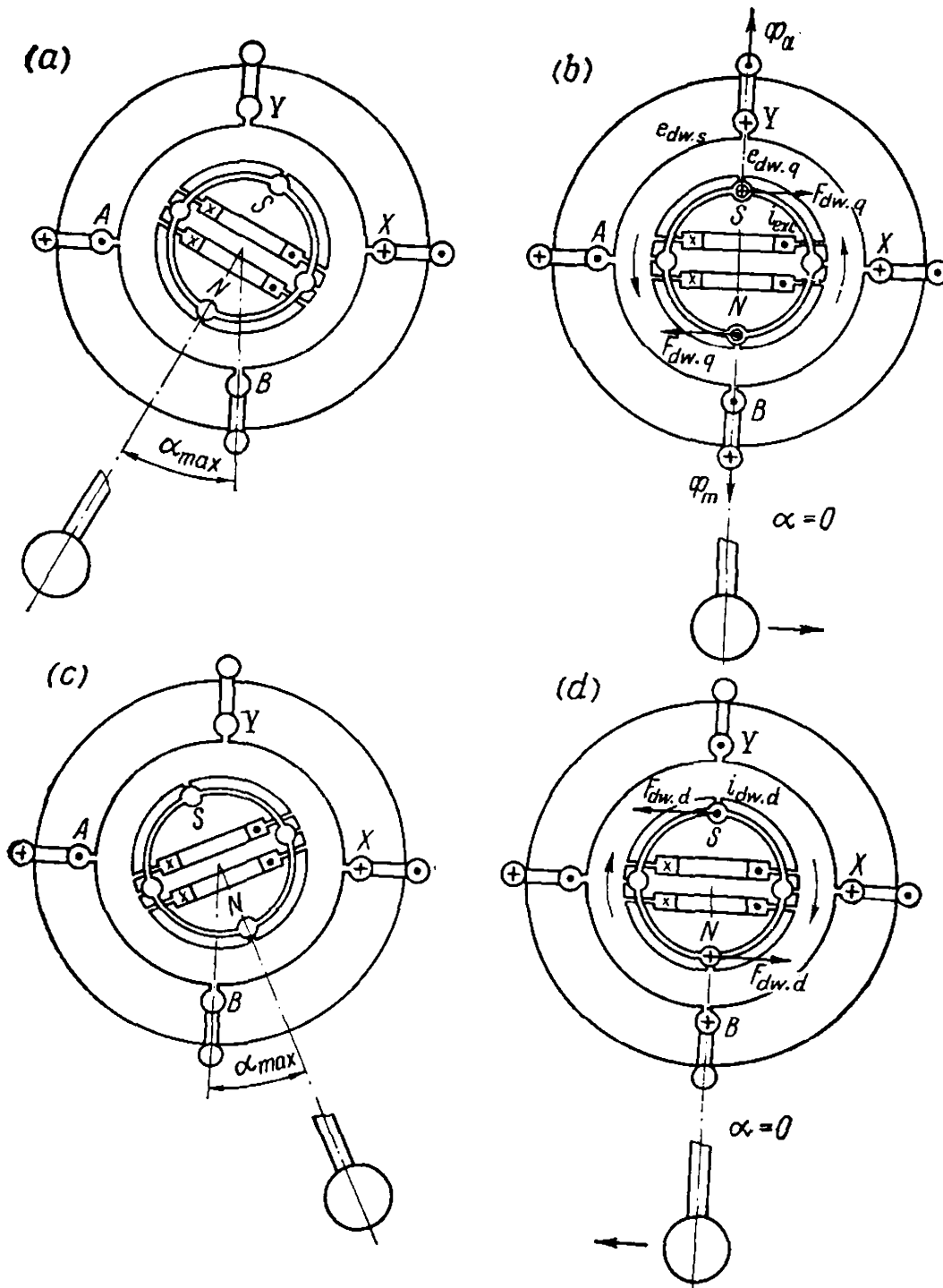


Fig. 16-3. Physical map of rotor oscillations

the interaction of these currents with the stator field, forces $F_{dw.q}$ appear and produce a torque opposite to the direction of rotor movement (Fig. 16-3b). When the rotor moves in the opposite direction from the other extreme position (Fig. 16-3c) and through the same equilibrium position (Fig. 16-3d), the currents $i_{dw.q}$ in the quadrature damper winding reverse their sign and produce a torque also acting opposite to the direction of movement. In both cases, as can be seen from Fig. 16-3b and d, the torque M_{dw} developed acts as a force damping rotor oscillations which develop near the synchronous speed. The damping torque $M_{dw} = K_{dw} \frac{d\alpha}{dt}$ is assumed in this case to be positive.

The effect of the direct-axis damper winding and field winding on the oscillations with an ideal no-load ($\theta=0$) and small amplitudes is practically reduced to zero, since in this case, as seen from Fig. 16-3, the e.m.f.s induced in them by the stator field are negligible.

The directions of the e.m.f.s $e_{dw.s}$ with the oscillation frequency and induced in stator phase B by the excitation flux during relative rotor movement are also shown in Fig. 16-3b and d by crosses and points. In these rotor positions the e.m.f.s $e_{dw.s}$ in phase B are equal to their amplitude values.

If the slip-frequency currents $i_{dw.s}$ in the stator winding are in phase with the e.m.f.s $e_{dw.s}$ and, consequently, have the same dire-

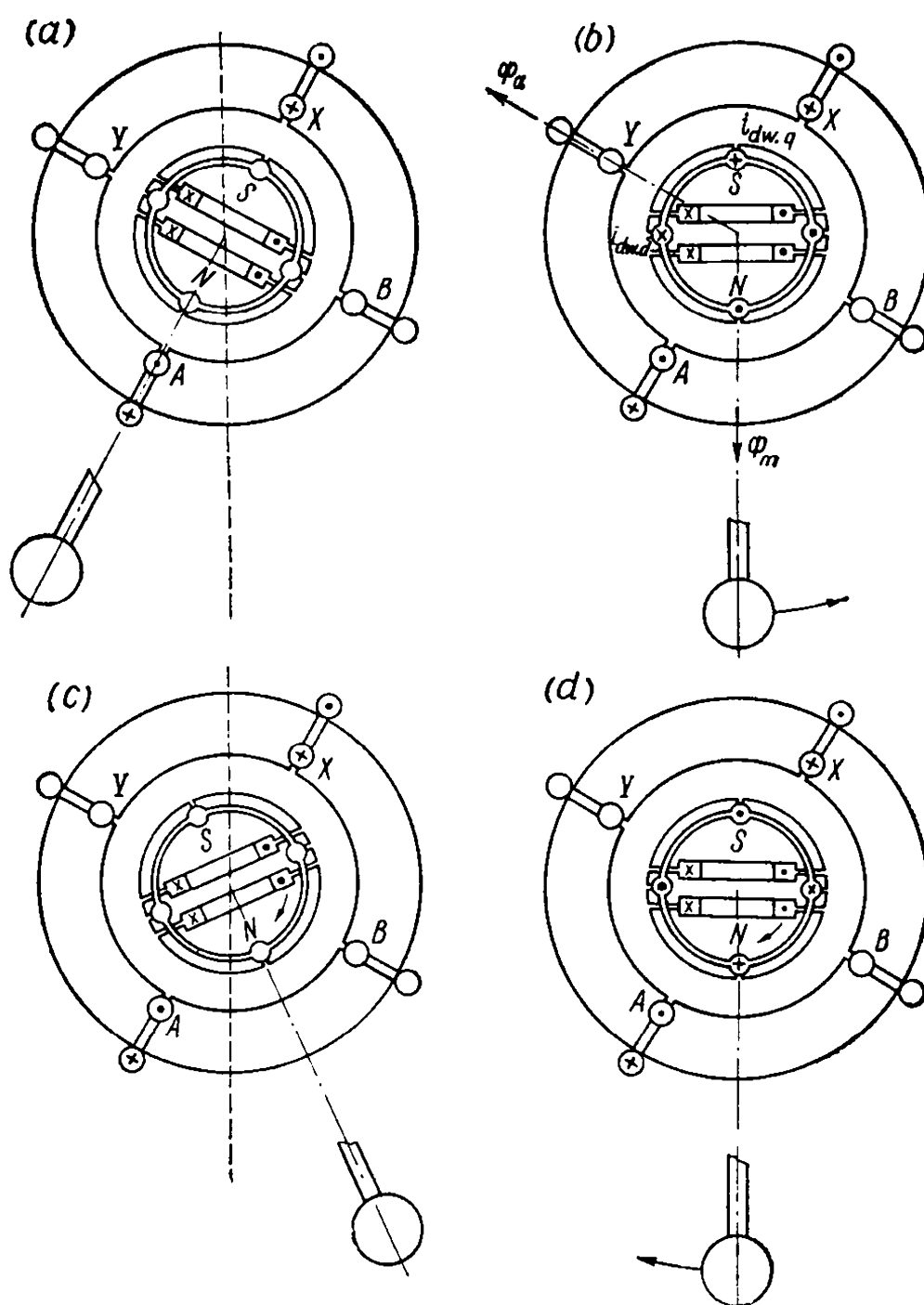


Fig. 16-4. Physical map of synchronous generator rotor oscillations under active load

ction as the latter at any moment, as can be seen from Fig. 16-3*b* and *d*, the interaction of these currents with the excitation flux or current produces a positive damping torque which suppresses the oscillations. The effect of the currents induced by the excitation flux in phase *A* as shown in Fig. 16-3 is negligible. Indeed, the resistance of the stator windings, as compared with their inductive reactance, is relatively small, the currents $i_{dw.s}$ therefore lag considerably behind the e.m.f.s $e_{dw.s}$, and the damping torque component produced by the stator winding is small.

Figure 16-4 shows oscillations of a synchronous machine when it is operating as a generator under active balanced loading (Fig. 16-4*b* and *d*) with an angle $\psi \cong 30^\circ$ (Fig. 12-9*a*). Figure 16-4*b* shows the directions of the axes of the excitation flux Φ_m and armature-reaction flux Φ_a . It can be seen from the figure that the direct-axis damper winding is now the more effective winding in which larger currents ($i_{dw.d}$) are induced. Also more effective, in comparison with the case of Fig. 16-3, is the damping action of the field winding.

Thus, the total magnitude of the damping torque of a synchronous machine depends both on the design characteristics of the machine and its conditions of operation. Formulas for the calculation of the total damping torque factor K_{dw} are generally given in special sources. It should also be noted that the damping torque factor K_{dw} for an overexcited synchronous machine under no-load, as has been shown by special investigations, may become negative if the resistance of the stator circuit is sufficiently high. In this case spontaneous oscillations of the synchronous machine rotor may occur and lead to the machine pulling out of step.

16-2. Forced Oscillations of a Synchronous Machine

Oscillations of a synchronous machine may appear, for example, under the action of external torques applied to the shaft from the prime-mover side of a generator, or from the driven-machine side of a motor.

If a synchronous generator is driven by a prime mover with irregular motion, for example, a reciprocating steam engine, oil engine, etc., *forced* oscillations are created which also give rise to variations in the electromagnetic power of the generator. Forced oscillations may appear both when the generator is operated alone and in parallel with a power network. In the latter case the forced oscillations, upon superposition onto the free oscillations, may cause dangerous oscillation resonance and the machine may fall out of step.

In a synchronous motor, as in a generator, free and forced oscillations may also occur. The latter occur, for instance, when synchronous motors are used as drives for piston compressors.

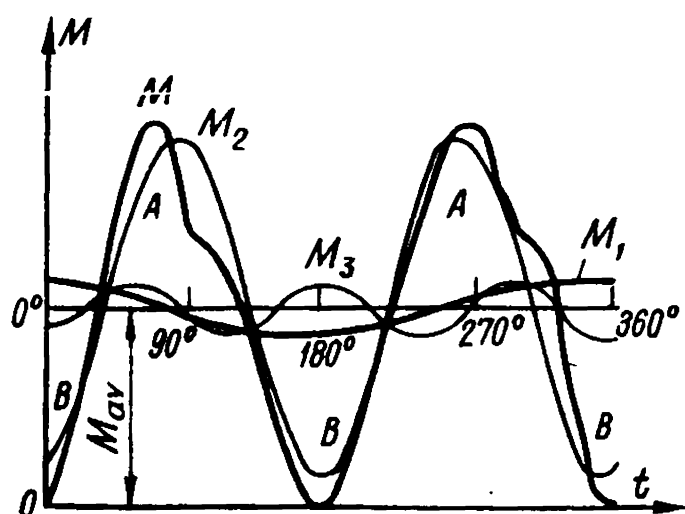


Fig. 16-5. Torque curve of a double-action steam engine

Prime movers of generators are divided into engines and machines with uniform and non-uniform motion. The former include water and steam turbines, the latter all the piston engines: steam engines, internal-combustion engines, gas engines. Among the machines with non-uniform motion driven by synchronous motors are piston compressors.

Engines and working machines with uniform rotation have a load or braking torque

which remains constant during a full revolution of the shaft, but when rotation is not uniform the torque undergoes periodic variations in value according to a definite law.

An approximate example of the torque curve for a tandem-type steam engine is given in Fig. 16-5. The torque changes twice from its maximum to its minimum value during one revolution. At the expense of the kinetic energy of the rotating masses there takes place a certain equalization of the power delivered by the generator to the mains. If for a given part of the revolution of the rotor an excess of power exists (area *A*), it is partly converted into kinetic energy of the rotating masses and is later returned when the rotor slows down and the energy input becomes less than consumption (area *B*).

The ratio

$$\Delta = \frac{\Omega_{max} - \Omega_{min}}{\Omega_{av}}$$

is called the degree of non-uniformity of motion. The torque curve can be resolved into a constant component, equal to the average value of torque, and harmonics. For the curve in Fig. 16-5 the resolution has the following form:

$$\frac{M}{M_{av}} = 1 + 0.142 \cos(\Omega_{av}t + 123^\circ) + 0.865 \cos(2\Omega_{av}t + 194^\circ) + \\ + 0.132 \cos(3\Omega_{av}t + 195^\circ) + \dots$$

where Ω_{av} is the average angular speed of the rotor. Here the second harmonic has the maximum amplitude, since in a tandem engine two main pulses occur during each revolution. Figure 16-5 also shows the curves of the first three harmonic torque components for which the axis of abscissas is the line of the average torque M_{av} .

In the general form the equation for the torque can be written as follows

$$M = M_{av} + \sum_{v=1}^{v=\infty} M_{vm} \cos(v\Omega_{av}t + \psi_v) \quad (16-6)$$

where v is the order of a harmonic, and M_{vm} is the amplitude of the harmonic.

A torque harmonic with a frequency determined by the number of working strokes or pulses N_p per revolution of the shaft, which depends on the kind of engine or machine, has the greatest amplitude and, correspondingly, the greatest influence on operation. In single-action four-stroke gas engines $N_p = \frac{1}{2}$, in two-cylinder engines $N_p = 1$, and in four-cylinder engines $N_p = 2$; in double-action two-stroke gas engines we have, correspondingly: $N_p = 2$ or 4 in two-cylinder engines, $N_p = 6$ in three-cylinder engines, etc.

Each harmonic of the torque causes forced oscillations of the speed of the rotating parts near its mean value with a frequency equal to the frequency of the given harmonic. The frequency of the forced oscillations due to the fundamental torque harmonic and the period of these oscillations are determined by the equations

$$f_1 = nN_p; \quad T = \frac{1}{f_1}$$

where n is the speed in rps.

16-3. Natural and Forced Oscillations of a Synchronous Generator on Infinite-Power Bus-Bar

According to the above discussion, in the general case of an oscillating synchronous machine operating in parallel with a powerful network the external torque M applied to the shaft of a machine is balanced by the following internal torques:

1. The electromagnetic torque, which for a non-salient-pole generator is equal to

$$M_{em} = \frac{mE_m U}{\Omega x_d} \sin \theta_{av}$$

2. The moment of inertia

$$M_J = \frac{J}{p} \frac{d\omega}{dt} = \frac{J}{p} \frac{d^2(\theta_{av} + \alpha)}{dt^2} = \frac{J}{p} \frac{d^2\alpha}{dt^2}$$

3. The synchronizing torque M_{syn} which with small oscillations is proportional to the deviation α of the angle θ from its average value θ_{av}

$$M_{syn} = M'_{syn}\alpha$$

4. The damping torque M_{dw} which with small oscillations is proportional to the variations of the angle α

$$M_{dw} = K_{dw} \frac{d\alpha}{dt}$$

The equation of rotor movement thus has the form

$$M = M_{em} + M_f + M_{syn} + M_{du}$$

With a non-uniform torque of the prime mover, the torque equations for a synchronous generator operating in parallel with a network acquires the form

$$M_{em} + \frac{J}{p} \frac{d^2\alpha}{dt^2} + K_{dw} \frac{d\alpha}{dt} + M'_{syn}\alpha = M_{av} + \sum_{v=1}^{v=\infty} M_{vm} \cos(v\Omega_{av}t + \psi_v) \quad (16-7)$$

If we consider only such speed variations with which the speed regulator of the prime mover has insufficient time to act, the average torque M_{av} of the motor during one revolution remains constant and balances the electromagnetic torque M_{em} . Owing to this the equation for the excess torque becomes

$$\frac{J}{p} \frac{d^2\alpha}{dt^2} + K_{dw} \frac{d\alpha}{dt} + M'_{syn}\alpha = \sum_{v=1}^{v=\infty} M_{vm} \cos(v\Omega_{av}t + \psi_v) \quad (16-8)$$

This equation is similar in form to equation (16-10) for currents in a circuit with series-connected L , C and r fed from a circuit with a voltage consisting of a number of harmonics:

$$L \frac{di}{dt} + ri + \frac{1}{C} \int i dt = \sum_{v=1}^{v=\infty} E_{vm} \sin(v\omega t + \psi_v) \quad (16-9)$$

where ω is the angular frequency of the first harmonic.

Differentiating the latter equation with respect to t , we get

$$L \frac{d^2i}{dt^2} + r \frac{di}{dt} + \frac{1}{C} i = \sum_{v=1}^{v=\infty} v\omega E_{vm} \cos(v\omega t + \psi_v) \quad (16-10)$$

Since equations (16-8) and (16-10) are similar, α , $\frac{J}{p}$, M'_{syn} , K_{dw} , M_{vm} in (16-8) conform to i , L , $\frac{1}{C}$, r , $v\omega E_{vm}$ in (16-10).

The solution of equations (16-8) and (16-10) consists of a partial steady-state solution of the form

$$\left. \begin{matrix} i \\ \alpha \end{matrix} \right\} = \sum_{v=1}^{v=m} \beta_m \sin(v\omega t + \psi_v - \varphi_v)$$

determining the forced oscillations, where in the first case

$$i = \sum_{v=1}^{v=m} \frac{E_{vm}}{\sqrt{r^2 + \left(v\omega L - \frac{1}{v\omega C}\right)^2}} \sin(v\omega t + \psi_v - \varphi_v) \quad (16-11)$$

and in the second case

$$\alpha = \sum_{v=1}^{v=m} \frac{M_{vm}}{v\Omega_{av} \sqrt{K_{dw}^2 + \left(v\Omega_{av} \frac{J}{p} - \frac{M'_{syn}}{v\Omega_{av}}\right)^2}} \sin(v\Omega_{av} t + \psi_v - \varphi_v) \quad (16-12)$$

and from the common integral of these equations without the free term

$$\left. \begin{matrix} i \\ \alpha \end{matrix} \right\} = Ae^{x_1 t} + Be^{x_2 t}$$

which defines the damper free oscillations of the machine under the action of a disturbing pulse.

Consider first the case when the equations do not contain damping terms ($r = 0$ and $K_{dw} = 0$). If in an electric circuit no dissipation of energy takes place ($r \cong 0$), the oscillations should be continuous, and equation (16-10) may be then rewritten as

$$\frac{d^2 i}{dt^2} + \frac{1}{LC} i = \frac{d^2 i}{dt^2} + \omega_0^2 i = 0$$

where

$$\omega_0 = \frac{1}{\sqrt{LC}}$$

is the angular frequency of the free electrical oscillations of a circuit containing L and C .

In a similar manner, if the damping torque factor of a synchronous machine is zero ($K_{dw} = 0$), the torque equation (16-8) can be rewritten as

$$\frac{d^2 \alpha}{dt^2} + \frac{M'_{syn} p}{J} \alpha = \frac{d^2 \alpha}{dt^2} + \omega_0^2 \alpha = 0 \quad (16-13)$$

where ω_0 is the angular frequency of the free mechanical oscillations, equal to

$$\omega_0 = \sqrt{\frac{p M'_{syn}}{J}} = \sqrt{\frac{P_{syn} p^2}{\omega_{ec} J} \frac{10^3}{g}} \quad (16-14)$$

Here P_{syn} is the synchronizing power factor [see equation (12-33)] and ω_{ec} is the angular frequency of the power-circuit voltage.

The solution of equation (16-13) for α has the form of

$$\alpha = A \sin \omega_0 t + B \cos \omega_0 t$$

where A and B are arbitrary constants determined from the initial conditions.

The speed of variation of the angle α equals

$$\frac{d\alpha}{dt} = \omega_0 A \cos \omega_0 t - \omega_0 B \sin \omega_0 t$$

Assuming that at the initial moment ($t=0$) we have $\alpha = \alpha_{max}$ and $\frac{d\alpha}{dt} = 0$, we find $A = 0$ and $B = \alpha_{max}$ and, consequently

$$\alpha = \alpha_{max} \cos \omega_0 t$$

whence it follows that the rotor oscillations are of a harmonic nature and the rotor oscillation amplitude α_{max} is equal to the maximum angle by which the rotor was displaced from its equilibrium position by an external force.

The frequency of free rotor oscillations equals

$$f_0 = \frac{1}{2\pi} \omega_0 = \frac{1}{2\pi \sqrt{\frac{J}{pM'_{syn}}}} = \frac{1}{2\pi} \sqrt{\frac{P_{syn} p^2}{\omega_{ec} J}} \quad (16-15)$$

and the free oscillation period is

$$T_0 = \frac{1}{f_0} = 2\pi \frac{\omega_{ec}}{P_{syn}} \frac{J}{p^2} \quad (16-16)$$

The free oscillation period is often expressed in terms of the so-called flywheel moment GD^2 of the rotor associated with the moment of inertia of the rotating parts J by the relation

$$J = mR^2 = \frac{GD^2}{4g}$$

where $m = G/g$ is the rotor mass, G is the rotor weight, g is the acceleration of gravity, $R = D/2$ is the centre of gravity.

Besides, taking account of the fact that the rated speed

$$n_r = \frac{60f_{ec}}{p} = \frac{60\omega_{ec}}{2\pi p}$$

equation (16-16) can be written in the following form

$$T_0 = 2\pi \sqrt{\frac{2\pi}{4 \times 60} \frac{GD^2 n_r}{gpP_{syn}}} \cong 1.02 \sqrt{\frac{GD^2 n_r}{gpP_{syn}}} \quad (16-17)$$

The same quantity can also be expressed by the so-called inertia constant of the rotor H_r , i.e., the time required to speed up the rotor from standstill to the rated speed n_r when the shaft is acted upon by a constant power equal to the rated power.

In modern electrical engineering practice total capacity in kilo-volt-amperes (expressed for a.c. machines) is taken as the rated ca-

capacity in calculating the inertia constant. Hence

$$H_{jP} = \frac{W}{P_r} = \frac{J\Omega_{sp}^2}{2P_r} = \frac{J\omega_{ec}^2}{2p^2P_r} = \frac{1}{102} \frac{GD^2}{2.4g} \left(\frac{2\pi n_r}{60} \right)^2 \frac{1}{P_r} = 1.37 \frac{GD^2}{P_r} n_r^2 \cdot 10^{-6} \text{ s} \quad (16-17a)$$

where $W = \frac{J\Omega_{sp}^2}{2}$ is the kinetic energy stored in the rotor when operating at the rated speed; GD^2 is the flywheel polar inertia of the rotor in kgf-m^2 ; n_r is the rated speed in revolutions per minute; and P_r is the total rated capacity in kVA.

It should be noted that in the USA, Great Britain, and in certain other countries, flywheel polar inertia (flywheel moment or effect) is defined as WR^2 , i.e., its value is only a quarter of that of GD^2 , and is expressed in pounds-feet squared. (1 lb. = 0.4536 kg, 1 ft = 0.3048 m). In this case formula (16-17a) yields

$$H_{jP} = 0.231 \frac{WR^2}{P_r} n^2 10^{-6} \text{ s}$$

If the flywheel polar inertia WR^2 is expressed in pounds-feet squared then, in order to find GD^2 in kgf-m^2 , we must multiply WR^2 (in pounds-feet squared) by the factor

$$0.4536 \times 0.3048^2 \times 4 = 0.168$$

For example, if $WR^2 = 23850$ pounds-feet squared, then

$$GD^2 = 23850 \times 0.168 = 4010 \text{ kgf-m}^2$$

In a number of other countries (the USSR, France, Switzerland, Japan) the inertia constant is taken as the time needed to accelerate the rotor from standstill to the rated speed under constant torque, which is found from the total rated capacity and the synchronous speed. Given that rotor speed rises uniformly, the average power applied to the shaft in acceleration will be

$$P_{av} = M_r \frac{\Omega_{sp}}{2} = \frac{P_r}{\Omega_{sp}} \frac{\Omega_{sp}}{2} = \frac{P_r}{2}$$

Thus, in this case

$$H_{jM} = \frac{W}{P_{av}} = \frac{2W}{P_r} = 2H_{jP} = 2.74 \frac{GD^2}{P_r} n_r^2 10^{-6} \text{ s} \quad (16-17b)$$

By introducing the value

$$\frac{\omega_{ec}J}{p^2} = \frac{H_{jM}P_r}{\omega_{ec}}$$

we obtain

$$T_0 = 2\pi \sqrt{\frac{H_{jM}P_r}{\omega_{ec}P_{syn}}} \quad (16-18)$$

or, with $f = 50$ Hz

$$T_0 = 0.355 \sqrt{H_{jM} \frac{P_r}{P_{syn}}}$$

It should be noted that the period of natural oscillations T_0 depends on the operating conditions of the machine. An increase in excitation, for example, will lead to an increase in the e.m.f. E_m and, at a constant load, to a decrease in the angle θ_{av} . Both these variations lead to an increase in the synchronization power factor P_{syn} and, consequently, to a reduction in the oscillation period T_0 .

When damping terms ($r \neq 0$ and $K_{dw} \neq 0$) are present, the common integral of the equations without the free term has the form

$$i \left\{ \begin{array}{l} A e^{x_1 t} + B e^{x_2 t} \end{array} \right.$$

Here A and B are arbitrary constants determined from the initial conditions, and x_1 and x_2 are the square roots of a characteristic equation of the form

$$x^2 + 2\delta x + \omega_0^2 = 0$$

equal to

$$x_{1,2} = -\delta \pm \sqrt{\delta^2 - \omega_0^2} = -\delta \pm j\omega'$$

where

$$\omega'^2 = \omega_0^2 - \delta^2$$

In the first case—for an electric circuit

$$\delta = \frac{r}{2L}; \quad \omega_0^2 = \frac{1}{LC}$$

and in the second case—for a synchronous machine

$$\delta = \frac{pK_{dw}}{2J}; \quad \omega_0^2 = \frac{pM'_{syn}}{J}$$

The oscillatory damping process takes place when $\delta < \omega_0$, which corresponds to the actual relations of these values for a synchronous machine. The solution for the first case—equation (16-9) with the right-hand side equal to zero—for the initial conditions $i = I_0$ and $\frac{di}{dt} = 0$ will be

$$i = I_0 e^{-\delta t} \sin \omega' t$$

Similarly, the solution of equation (16-8) with the right-hand side equal to zero, for the oscillations of a synchronous machine under the initial conditions $\alpha = \alpha_{max}$ and $\frac{d\alpha}{dt} = 0$ will be

$$\alpha = \alpha_{max} e^{-\delta t} \sin \omega' t$$

where ω' is the angular frequency of the oscillations, equal to

$$\omega' = \sqrt{\omega_0^2 - \delta^2} = \sqrt{\frac{pM'_{syn}}{J} - \left(\frac{pK_{dw}}{2J}\right)^2} \quad (16-19)$$

Correspondingly, the period of damping oscillations is

$$T = \frac{2\pi}{\omega'} = \frac{2\pi}{\sqrt{\frac{\rho M'_{syn}}{J} - \left(\frac{\rho K_{dw}}{2J}\right)^2}} = \frac{2\pi J}{\rho \sqrt{\frac{J M'_{syn}}{\rho} - \frac{K_{dw}^2}{4}}} \quad (16-20)$$

The period of damping oscillations, as seen from equation (16-20), depends on the value of the damping torque factor K_{dw} .

The logarithmic decrement of the oscillations, equal to the logarithm of the ratio of the amplitudes of the oscillation period being considered and the following one, will be

$$\vartheta = \delta T = \frac{\pi \rho K_{dw}}{J \sqrt{\frac{\rho M'_{syn}}{J} - \left(\frac{\rho K_{dw}}{2J}\right)^2}} = \frac{2\pi}{\sqrt{\frac{4 M'_{syn} J}{\rho K_{dw}^2} - 1}} \quad (16-21)$$

When $K_{dw} = 0$, the logarithmic oscillation decrement $\vartheta = 0$.

Figure 16-6a shows an oscillogram of the free oscillations of a synchronous machine connected through a model of a transmission line to infinite bus-bars. The initial surge was originated by a three-phase midline short circuit interrupted in 0.35 s. Figure 16-6b corresponds to a similar disturbance in the operating conditions of the same machine, when the latter pulled out of step during the first period of oscillation [79].

The equation for the operation of the generator alone, when synchronizing and damping torques are absent, is

$$\frac{J}{\rho} \frac{d^2 \alpha}{dt^2} = \sum_{v=1}^{v=m} M_{vm} \cos(v \Omega_{av} t + \psi_v)$$

this corresponding to the equation of an electric circuit with L , in which C and r are absent:

$$L \frac{d^2 i}{dt^2} = \sum_{v=1}^{v=m} v \omega E_{vm} \cos(v \omega t + \psi_v)$$

The amplitude of the steady-state current is

$$I_{0vm} = \frac{E_{vm}}{v \omega L}$$

The amplitude of the steady-state current for a circuit with L , C and r according to equation (16-11) is

$$I_{vm} = \frac{E_{vm}}{\sqrt{r^2 + \left(v \omega L - \frac{1}{v \omega C}\right)^2}}$$

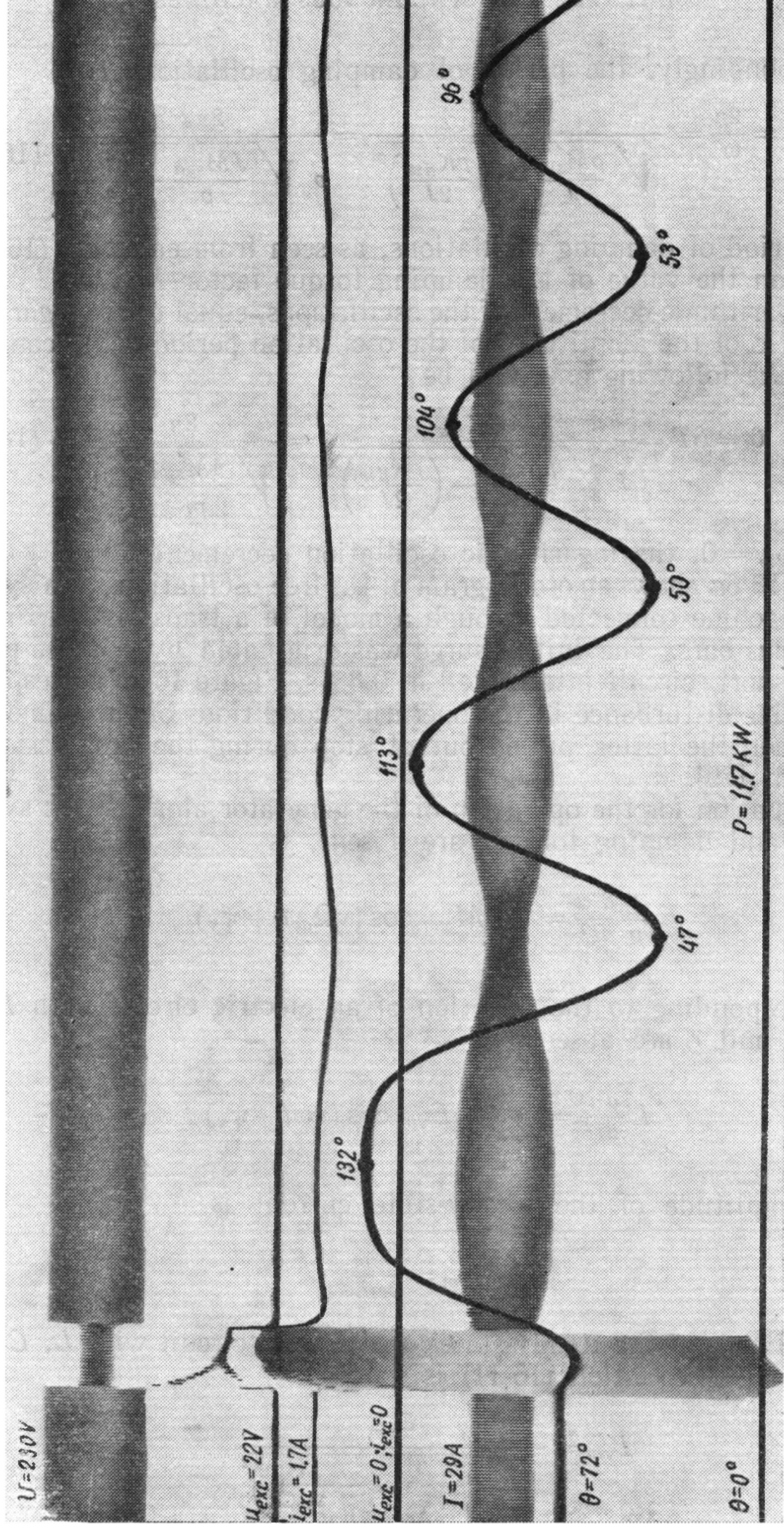


Fig 16-6a. Oscillogram of free oscillations of a synchronous generator when synchronism is retained

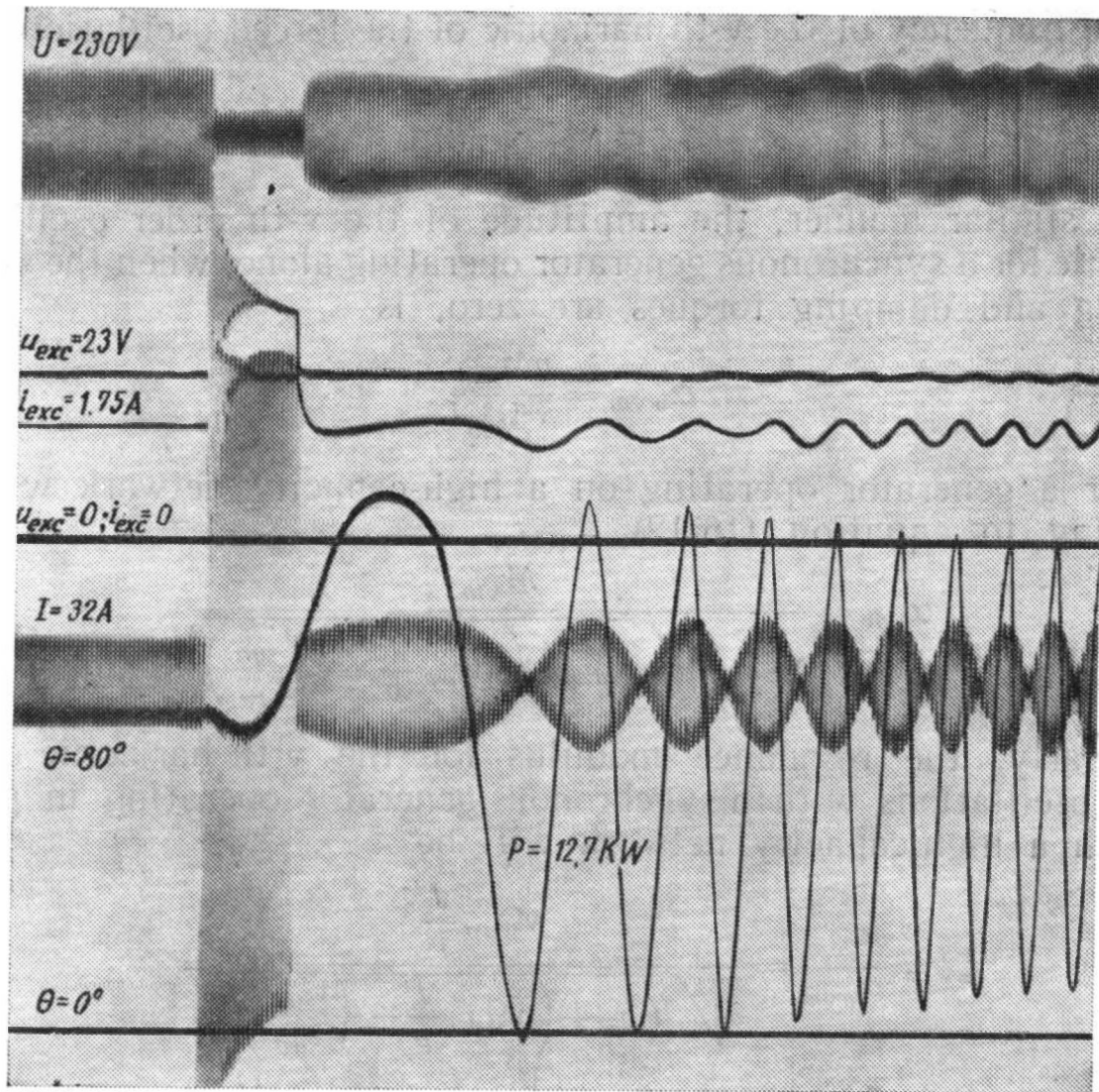


Fig. 16-6b. Oscillogram of free oscillations of a synchronous generator when it drops out of synchronism

With $\nu^2 \omega^2 LC = 1$ voltage resonance occurs for the given harmonic, and the current $I_{\nu m}$ reaches its highest possible value

$$I_{\nu m \max} = \frac{E_{\nu m}}{r}$$

The resonance modulus ζ_ν is equal to the current ratio $\frac{I_{\nu m}}{I_{0\nu m}}$, i.e.,

$$\begin{aligned} \zeta_\nu &= \frac{\nu \omega L}{\sqrt{r^2 + \left(\nu \omega L - \frac{1}{\nu \omega C} \right)^2}} = \frac{1}{\sqrt{\left(\frac{r}{\nu \omega C} \right)^2 + \left(1 - \frac{1}{\nu^2 \omega^2 LC} \right)^2}} = \\ &= \frac{1}{\sqrt{\left(\frac{r}{2\pi f_\nu L} \right)^2 + \left[1 - \left(\frac{f_0}{f_\nu} \right)^2 \right]^2}} \end{aligned} \quad (16-22)$$

where the natural oscillation frequency of the L and C circuit with $r = 0$ is

$$f_0 = \frac{1}{2\pi \sqrt{LC}}$$

and the frequency of the ν -th harmonic of the forced oscillations will be

$$f_\nu = \nu f_1 = \frac{\nu \omega}{2\pi}$$

In a similar manner, the amplitude of the ν -th order oscillation harmonic for a synchronous generator operating alone, when the synchronizing and damping torques are zero, is

$$\alpha_{0\nu m} = \frac{\rho M_{\nu m}}{\nu^2 \Omega_{av}^2 J}$$

and for a generator operating on a high-capacity network will be according to equation (16-12),

$$\alpha_{\nu m} = \frac{M_{\nu m}}{\nu \Omega_{av} \sqrt{K_{dw}^2 + \left(\nu \Omega_{av} \frac{J}{\rho} - \frac{M'_{syn}}{\nu \Omega_{av}} \right)^2}} \quad (16-23)$$

Similarly, the resonance modulus for the ν -th harmonic of the forced oscillations with a synchronous generator operating in parallel with a high-capacity network will be

$$\begin{aligned} \zeta_\nu &= \frac{\alpha_{\nu m}}{\alpha_{0\nu m}} = \frac{\nu \Omega_{av} \frac{J}{\rho}}{\sqrt{K_{dw}^2 + \left(\nu \Omega_{av} \frac{J}{\rho} - \frac{M'_{syn}}{\nu \Omega_{av}} \right)^2}} = \\ &= \frac{1}{\sqrt{\left(\frac{\rho K_{dw}}{2\pi f_\nu J} \right)^2 + \left[1 - \left(\frac{f_0}{f_\nu} \right)^2 \right]^2}} \end{aligned} \quad (16-24)$$

where the natural-oscillation frequency of the rotor, in accordance with equation (16-14), is

$$f_0 = \frac{1}{2\pi \sqrt{\frac{1}{\rho M'_{syn}}}}$$

and the frequency of the ν -th harmonic of the forced oscillations of the rotor is

$$f_\nu = \nu f_1$$

In the absence of a damping torque $K_{dw} = 0$, and the resonance modulus is

$$\zeta_\nu = \frac{1}{1 - \left(\frac{f_0}{f_\nu} \right)^2} \quad (16-25)$$

while if, in addition, the frequencies of the free and forced oscillations are equal ($f_0 = f_\nu$), i.e., for resonance, then $\zeta_\nu = \infty$.

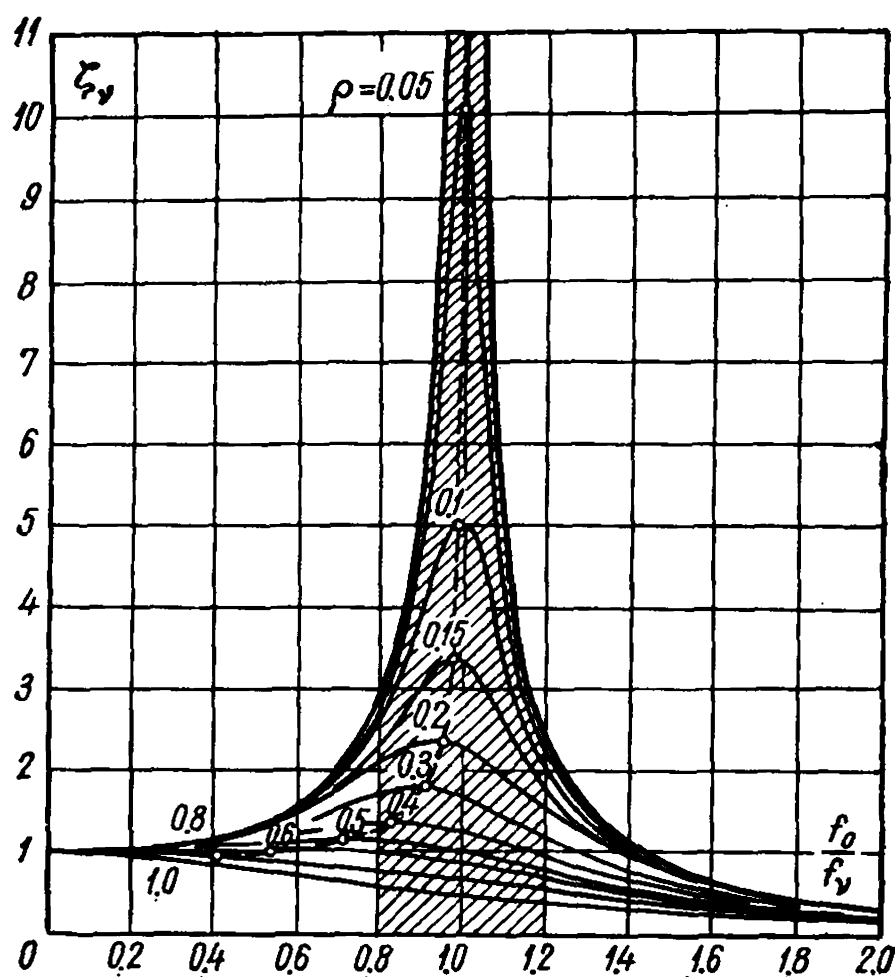


Fig. 16-7. Curves of resonance modulus versus ratio of frequencies of free and forced oscillations for different degrees of damping

As in an electric circuit, the existence of damping reduces the value of the resonance modulus, particularly in the most dangerous zone, when $\frac{f_0}{f_v} = 0.8$ to 1.2 .

Figure 16-7 gives curves of the dependence of the resonance modulus on the ratio $\frac{f_0}{f_v}$ for changes in f_v with various damping values

$$\rho = \frac{2\delta}{\omega_0} \begin{cases} \frac{r_0}{2\pi f_0 L} \\ \frac{\rho K_{dw}}{2\pi f_0 J} \end{cases} \quad (16-26)$$

As can be seen from these curves, the value of the resonance modulus ζ_v sharply increases with a decrease in damping, the maximum of ζ_v gradually shifting with an increase in ρ towards the decreasing values of $\frac{f_0}{f_v}$.

Example 16-1. A synchronous hydrogenerator with a power of $P_r = 71\,500$ kVA, $f = 50$ Hz, $2p = 96$, $n = 62.5$ rpm has a flywheel moment $GD^2 = 47\,000$ tonf·m². Its inertia constant, according to formula (16-17b), is equal to

$$H_{JM} = 2.74 \times \frac{GD^2 n^2}{P_r} 10^{-6} = 2.74 \times \frac{47\,000 \times 10^3 \times 62.5^2}{71\,500} \times 10^{-6} = 7.04 \text{ s}$$

Let us determine the period of the natural oscillations for the rated conditions according to formula (16-18), substituting in it the relative value of the rated power $P_r=2.4$ and the relative synchronizing power factor $P_{syn}=7.86$:

$$T_0 = 0.355 \times \sqrt{7.04 \times \frac{2.4}{7.86}} = 0.52 \text{ s}$$

The natural frequency

$$f_0 = \frac{1}{T_0} = \frac{1}{0.52} = 1.93 \text{ Hz}$$

16-4. Forced Oscillations of a Synchronous Generator Operating Alone

When a synchronous generator operates alone, there is no factor providing a constant magnitude and constant angular frequency of the voltage U across the generator terminals. Therefore, when forced oscillations due to speed variations of the prime mover occur, the angle θ between the vectors E_m and U remains constant.

The rotor speed may be considered as the sum of the constant component or average speed and the speed oscillation harmonics. The rotor oscillations, as with free oscillations, cause e.m.f.s of oscillation frequency to be induced in the stator windings. The forced-oscillation frequency of most of the harmonics is higher than the fundamental frequency of the stator e.m.f.s, owing to which the inductive reactance is predominant in the stator circuit; the e.m.f.s and currents of the forced oscillations are displaced by a considerable angle. For this reason, and owing to rotor inertia, the torques corresponding to the oscillation frequency currents in the stator are considerably less than the disturbing torques, and, for simplicity, we can assume that the electromagnetic torque developed by a generator remains constant, and that the damping torque of the stator winding is zero.

Since $\theta = \text{const}$, the synchronization torque factor

$$M'_{syn} = \frac{1}{\Omega_{sp}} \frac{\partial P_{em}}{\partial \theta}$$

is zero. Since the armature-reaction flux remains stationary with respect to the rotor, the damping torque components due to the field and damper windings are also equal to zero.

Thus, $M_{em} = M_{av}$ and, in accordance with equations (16-7) and (16-8), the equation for the machine oscillations becomes

$$\frac{J}{p} \frac{d^2 \alpha}{dt^2} = \sum_{v=1}^{v=\infty} M_{vm} \cos(v\Omega_{av}t + \psi_v) \quad (16-27)$$

By integrating equation (16-27) twice consecutively, we obtain expressions for the speed of oscillation and for rotor deviation

$$\frac{d\alpha}{dt} = \sum_{v=1}^{v=\infty} \frac{p}{J} \frac{M_{vm}}{v\Omega_{av}} \sin(v\Omega_{av}t + \psi_v) \quad (16-28)$$

$$\alpha = - \sum_{v=1}^{v=\infty} \frac{p}{J} \frac{M_{vm}}{(v\Omega_{av})^2} \cos(v\Omega_{av}t + \psi_v) \quad (16-29)$$

The maximum value of the angle oscillation speed for the v -th harmonic is

$$\left| \frac{d\alpha_v}{dt} \right|_{max} = \frac{p}{J} \frac{M_{vm}}{v\Omega_{av}} \quad (16-30)$$

and the corresponding oscillation amplitude is

$$\alpha_{vm} = \frac{p}{J} \frac{M_{vm}}{(v\Omega_{av})^2} \quad (16-31)$$

From formulas (16-29) and (16-31) it can be seen that the oscillation amplitude is inversely proportional to the square of the harmonic order and that the maximum deviation of the angle α_{max} , if taken with some margin of overstatement, is the algebraic sum of all the harmonic amplitudes.

Since motors have a low sensitivity to the oscillations in the voltage across the generator terminals due to oscillations in the speed of its rotor, the maximum allowable deviation is determined only by the sensitivity of the eye to variations in the luminous intensity of incandescent lamps. Usually α_{max} is limited to within ± 3 electrical degrees.

From formula (16-31) it is seen that, with a generator operating alone, the amplitude α_{vm} can be limited only by increasing the moment of inertia J , this being attainable either by increasing the moment of inertia of the rotor itself, or by mounting a special flywheel on the shaft of the synchronous generator.

Chapter 17

ROTARY CONVERTER

17-1. Operating Principle of a Rotary Converter and Its Basic Relations

The rotary converter is a machine used for changing alternating current into direct current, or vice versa. The converter is built in the form of a d.c. machine furnished not only with a commutator connected to a d.c. circuit, but also with leads brought out from the armature to slip-rings connected to an a.c. circuit (Fig. 17-1). The principle of operation of a rotary converter is based on the fact that an alternating voltage is induced in the armature of a d.c. machine and is rectified only by means of a commutator; therefore, when the armature winding is connected directly to slip rings, an a.c. voltage is obtained across the rings, and the machine may be connected through the latter to an a.c. circuit.

When converting alternating current into direct current, the machine operates with respect to the a.c. circuit as a synchronous motor, and with respect to the d.c. circuit as a d.c. generator. Conversely, when converting direct current into alternating current, the converter operates as a d.c. motor with respect to the d.c. circuit, and as a synchronous generator with respect to the a.c. circuit. If we disregard the losses in the converter proper, then, in both cases, the power taken from the a.c. side or delivered to this circuit is equal to the power delivered to the d.c. circuit or taken from it. Therefore, a rotary converter does not develop mechanical torque on its shaft, but only converts one kind of electric energy into another.

Below it is assumed that the flux density distribution along the armature surface may be considered sinusoidal.

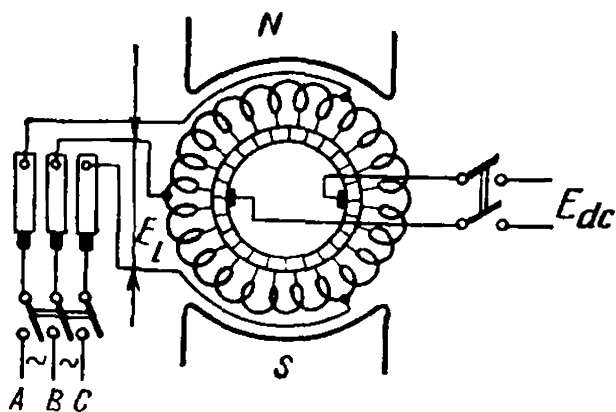


Fig. 17-1. Schematic view of a rotary converter

17-2. Relations Between Converter E.M.F.s

A rotary converter can be designed with a different number of phases m on the a.c. side, depending on the number of slip rings which the

armature leads are connected to. Since in a converter the alternating current and direct current e.m.f.s are induced in the same winding, the a.c. quantities are always definitely related to the d.c. ones.

The relation between the line e.m.f. E_l on the a.c. side and the e.m.f. E_{dc} on the d.c. side can be found as follows.

The e.m.f. on the d.c. side, according to formula (3-29) (Vol. I, Sec. 3-13), is equal to:

$$E_{dc} = pn \frac{N}{a} \Phi = 4\omega_s f \Phi$$

where $\omega_s = \frac{N}{4a}$ is the number of turns in a parallel path of the d.c. armature.

From the a.c. side the armature winding of a converter is mesh-connected and its phase e.m.f. equals the line e.m.f. Therefore, the line e.m.f. of the fundamental frequency at the slip rings, according to equation (2-37) for the e.m.f. of a synchronous machine, is equal to

$$E_l = \sqrt{2} \pi f \omega_{ph} k_w \Phi$$

Thus, the ratio of the e.m.f. on the a.c. side to the e.m.f. on the d.c. side is equal to:

$$k_E = \frac{E_l}{E_{dc}} = \frac{\sqrt{2} \pi}{4} \times \frac{\omega_{ph} k_w}{\omega_s} = \frac{\pi}{m \sqrt{2}} k_w \quad (17-1)$$

taking into account that $2\omega_s = m\omega_{ph}$.

If the number of slots per pole per phase is sufficiently large, then, according to equation (1-11), we have

$$k_w = \frac{\sin \frac{\pi}{m}}{\frac{\pi}{m}}$$

Substituting this value for k_w in equation (17-1), we obtain

$$k_E = \frac{\sin \frac{\pi}{m}}{\sqrt{2}} \quad (17-2)$$

The same value can be obtained from the potential circle of the armature winding of a converter (Fig. 17-2), if we take into account that the potential circle gives the amplitudes of the e.m.f. E_{ph2} , E_{ph3} , etc.

For a single-phase current, it is necessary to use $m=2$ in the formulas of the present section.

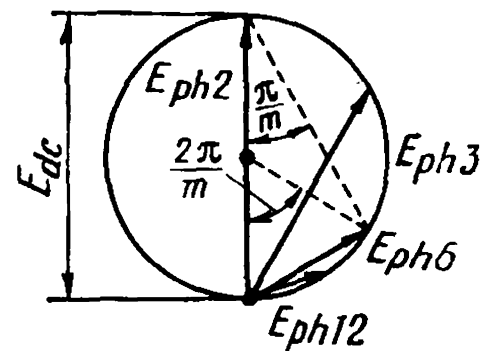


Fig. 17-2. Determination of line voltages of a rotary converter for different number of phases

17-3. Relations Between Converter Currents

Let us find the relations between the active a.c. component $I_{ph. a}$ in the armature phase and the direct current $I_{d c}$, disregarding the losses in the converter armature, i.e., assuming that the outputs and inputs on both the d.c. and a.c. sides are equal. Thence

$$E_{d c} I_{d c} = m E_{ph} I_{ph. a}$$

and

$$\frac{I_{ph. a}}{I_{d c}} = \frac{1}{m} \frac{E_{d c}}{E_{ph}} = \frac{1}{m k_E} = \frac{\sqrt{2}}{m \sin \frac{\pi}{m}} \quad (17-3)$$

Since the direct current in the parallel armature circuit equals $I'_{d c} = \frac{I_{d c}}{2a}$ and the active a.c. current component $I'_{ph. a} = \frac{I_{ph. a}}{a}$, the ratio between the alternating and the direct currents in the winding will be

$$k_{ia} = \frac{2I_{ph. a}}{I_{d c}} = \frac{2}{m k_E} = \frac{2 \sqrt{2}}{m \sin \frac{\pi}{m}} \quad (17-4)$$

Let k_{ir} be the ratio of the a.c. reactive component $I'_{ph. r} = \frac{I_{ph. r}}{a}$ in the winding circuit to the direct current $I'_{d c} = \frac{I_{d c}}{2a}$ in the winding. This ratio will be

$$k_{ir} = \frac{2I_{ph. r}}{I_{d c}} = \frac{2I_{ph. a}}{I_{d c}} \frac{I_{ph. r}}{I_{ph. a}} = k_{ia} \frac{\sin \psi}{\cos \psi} = k_{ia} \tan \psi \quad (17-5)$$

With an m -phase system the displacement between the currents of adjacent phases is $\frac{2\pi}{m}$. Since with a mesh connection the line current I_l is equal to the vector difference of the phase currents I_{ph} in adjacent phases, we obtain for the relation between I_l and I_{ph} the expression

$$I_l = 2I_{ph} \sin \frac{\pi}{m}$$

Taking this relation into account, from equation (17-3) we can obtain the following ratio between the active component of the line current and the direct current:

$$k_{ila} = \frac{I_{la}}{I_{d c}} = \frac{2 \sqrt{2}}{m} \quad (17-6)$$

The numerical values of the ratios between the quantities under consideration for different numbers of phases and in accordance with the expressions obtained above are given in Table 17-1. The values of these ratios for actual machines differ somewhat from the values given in the table because of the voltage drops and losses, as well as because of higher current harmonics.

TABLE 17-1

m	k_E	k_{ila}	k_{ia}	m	k_E	k_{ila}	k_{ia}
2	0.707	1.414	1.414	6	0.354	0.472	0.940
3	0.612	0.943	1.085	12	0.185	0.236	0.907

17-4. Losses in Armature Winding of a Converter

To determine the losses in the armature winding, it is necessary to know the instantaneous value of the current i in each armature coil section and to add together the losses in all the coil sections.

The instantaneous value of the current in an armature coil section is equal to the difference between the instantaneous values of the direct and alternating currents:

$$i = i'_{dc} - i'_{ph} \quad (17-7)$$

The instantaneous value of the direct current in a coil section is a rectangular curve which can be resolved according to the general rules into the fundamental and higher current harmonics:

$$\begin{aligned} i'_{dc} &= I_1 \sin \omega t + I_3 \sin 3\omega t + \dots + I_v \sin v\omega t + \dots = \\ &= I'_{dc} \frac{4}{\pi} \left(\sin \omega t + \frac{1}{3} \sin 3\omega t + \dots + \frac{1}{v} \sin v\omega t + \dots \right) \end{aligned} \quad (17-8)$$

where $\omega = 2\pi f = 2\pi pn$, the time $t = 0$ corresponding to the moment when the coil section passes a brush from one path of the winding into another.

The alternating-current e.m.f. in a phase passes through zero at the moment when its middle coil section is on the geometrical neutral (Fig. 17-3). If the current in the phase lags behind the e.m.f. by an angle ψ , the alternating current in the middle coil section varies according to the law

$$i'_{ph} = \sqrt{2} I'_{ph} \sin (\omega t - \psi)$$

The phase coil section displaced from the middle in the direction of rotation by an angle α (Fig. 17-3) crosses the neutral zone by the same angle earlier. Therefore, for this section, assuming also that $t = 0$ at the moment it crosses the neutral zone, the law of variation of the alternating current is determined by the expres-

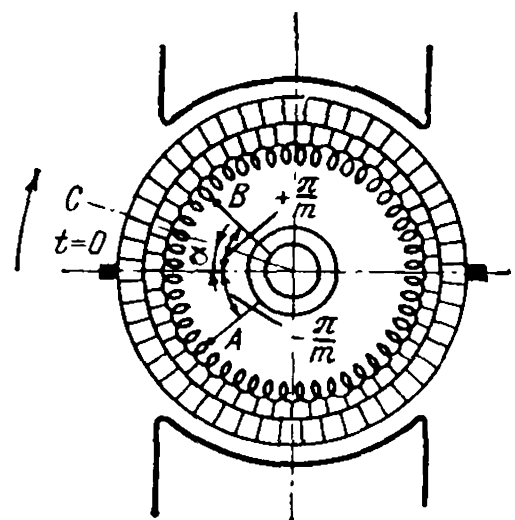


Fig. 17-3. Determination of losses in armature winding coil section of a rotary converter

sion

$$i'_{ph} = \sqrt{2} I'_{ph} \sin(\omega t - \psi - \alpha)$$

where α for different sections within the range of the given phase varies from $\alpha = +\frac{\pi}{m}$ to $\alpha = -\frac{\pi}{m}$ (Fig. 17-3).

By resolving $\sin(\omega t - \psi - \alpha)$ into components, and taking into account that the active and reactive a.c. components, according to the designations assumed previously, are

$$\begin{aligned} I'_{ph, a} &= I'_{ph} \cos \psi = k_{ia} I'_{dc} \\ I'_{ph, r} &= I'_{ph} \sin \psi = k_{ir} I'_{dc} \end{aligned}$$

we obtain for the current i'_{ph} the following expressions:

$$\begin{aligned} i'_{ph} &= \sqrt{2} I'_{ph} \sin(\omega t - \psi - \alpha) = \sqrt{2} (I'_{ph} \cos \psi \cos \alpha - \\ &- I'_{ph} \sin \psi \sin \alpha) \sin \omega t - \sqrt{2} (I'_{ph} \cos \psi \sin \alpha + I'_{ph} \sin \psi \cos \alpha) \cos \omega t = \\ &= \sqrt{2} I'_{dc} [(k_{ia} \cos \alpha - k_{ir} \sin \alpha) \sin \omega t - (k_{ia} \sin \alpha + k_{ir} \cos \alpha) \cos \omega t] \end{aligned} \quad (17-9)$$

The resultant current in the section, according to equations (17-7), (17-8) and (17-9), will be

$$\begin{aligned} i = i'_{dc} - i'_{ph} &= I'_{dc} \left\{ \left[\frac{4}{\pi} - \sqrt{2} (k_{ia} \cos \alpha - k_{ir} \sin \alpha) \right] \sin \omega t + \right. \\ &+ \sqrt{2} (k_{ia} \sin \alpha + k_{ir} \cos \alpha) \cos \omega t + \\ &\left. + \frac{4}{\pi} \left[\frac{1}{3} \sin 3\omega t + \dots + \frac{1}{v} \sin v\omega t + \dots \right] \right\} \end{aligned} \quad (17-10)$$

Figure 17-4 shows the resultant current curve with $m = 6$ for $\alpha = 0^\circ$, 15° , 30° and 60° .

The effective value of the resultant current of a coil section is equal to the square root of the half-sum of the squared amplitudes of all the current components:

$$\begin{aligned} I_{cs} &= I'_{dc} \sqrt{\frac{1}{2} \left\{ \left[\frac{4}{\pi} - \sqrt{2} (k_{ia} \cos \alpha - k_{ir} \sin \alpha) \right]^2 \times \right.} \\ &\times \left[\sqrt{2} (k_{ia} \sin \alpha + k_{ir} \cos \alpha) \right]^2 + \frac{16}{\pi^2} \left[\frac{1}{3^2} + \frac{1}{5^2} + \dots + \frac{1}{v^2} + \dots \right] \left. \right\}} = \\ &= I'_{dc} \sqrt{\frac{8}{\pi^2} + k_{ia}^2 + k_{ir}^2 - \frac{4}{\pi} \sqrt{2} (k_{ia} \cos \alpha - k_{ir} \sin \alpha) + \left(1 - \frac{8}{\pi^2} \right)} = \\ &= I'_{dc} \sqrt{1 + k_{ia}^2 + k_{ir}^2 - \frac{4}{\pi} \sqrt{2} (k_{ia} \cos \alpha - k_{ir} \sin \alpha)} \end{aligned} \quad (17-11)$$

since

$$\frac{1}{3^2} + \frac{1}{5^2} + \dots + \frac{1}{v^2} + \dots = \frac{\pi^2}{8} - 1$$

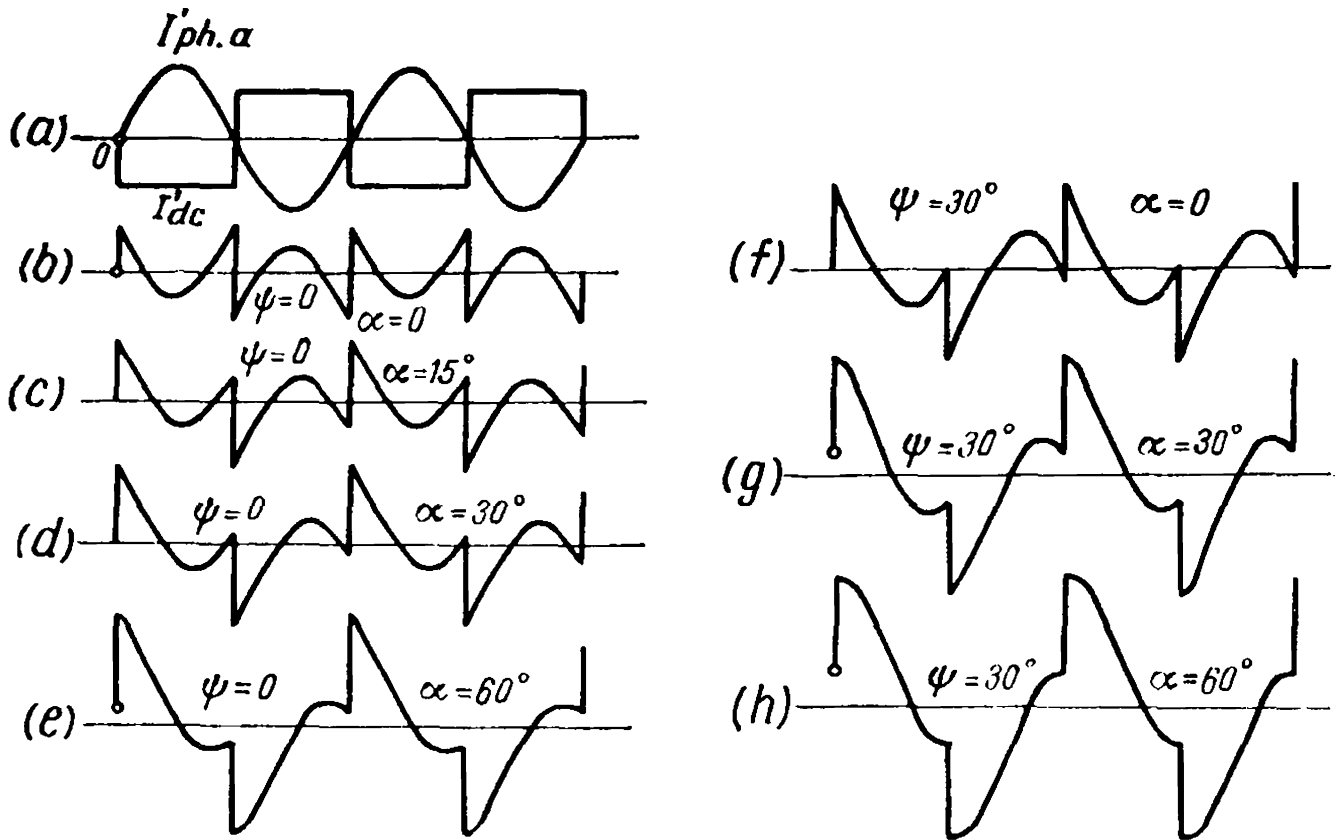


Fig. 17-4. Curves of current variation in armature winding coil sections of a rotary converter

The relation between the losses in the above coil section to the losses in it with a direct current I'_{dc} when the section is in a d.c. machine of the same capacity is

$$\left(\frac{I_{cs}}{I'_{dc}}\right)^2 = 1 + k_{ia}^2 + k_{ir}^2 - \frac{4}{\pi} \sqrt{2} (k_{ia} \cos \alpha - k_{ir} \sin \alpha) \quad (17-12)$$

The mean value of this ratio for the armature as a whole equals

$$k_v = \frac{m}{2\pi} \int_{-\frac{\pi}{m}}^{+\frac{\pi}{m}} \left(\frac{I_{cs}}{I'_{dc}}\right)^2 d\alpha = 1 + k_{ia}^2 + k_{ir}^2 - \frac{m}{2\pi} \times \frac{4}{\pi} \sqrt{2} \int_{-\frac{\pi}{m}}^{+\frac{\pi}{m}} (k_{ia} \cos \alpha - k_{ir} \sin \alpha) d\alpha = 1 + k_{ia}^2 + k_{ir}^2 - \frac{4 \sqrt{2} m k_{ia}}{\pi^2} \sin \frac{\pi}{m} \quad (17-13)$$

For the sine-wave field considered here, the values of the factors k_{ia} and k_{ir} are given by equations (17-4) and (17-5), and

$$\begin{aligned} k_v &= 1 + k_{ia}^2 + k_{ir}^2 - \frac{16}{\pi^2} = 1 - \frac{16}{\pi^2} + k_{ia}^2 (1 + \tan^2 \psi) = 1 - \frac{16}{\pi^2} + \frac{k_{ia}^2}{\cos^2 \psi} = \\ &= 1 - \frac{16}{\pi^2} + \frac{8}{m^2 \sin^2 \frac{\pi}{m} \cos^2 \psi} \end{aligned} \quad (17-14)$$

TABLE 17-2

<i>m</i>	cos $\psi=6$		cos $\psi=0.9$		<i>m</i>	cos $\psi=6$		cos $\psi=0.9$	
	k_v	$\frac{1}{\sqrt{k_v}}$	k_v	$\frac{1}{\sqrt{k_v}}$		k_v	$\frac{1}{\sqrt{k_v}}$	k_v	$\frac{1}{\sqrt{k_v}}$
2	1.380	0.85	1.88	0.73	12	0.207	2.20	0.42	1.54
3	0.567	1.33	0.87	1.07	∞	0.190	2.29	0.38	1.62
6	0.267	1.93	0.485	1.43					

If we denote by r_a the armature-winding resistance on the d.c. side, the losses in the converter armature will be equal to:

$$p_{cop. a} = k_v I_{dc}^2 r_a \tag{17-15}$$

If we assume that the armature losses of a rotary converter may be allowed to be the same as when it operates as a d.c. machine, the power of the converter, i.e., the a.c. or d.c. power converted by it, may be increased in the proportion $\frac{1}{\sqrt{k_v}}$.

Table 17-2 gives the values of k_v and $\frac{1}{\sqrt{k_v}}$ calculated from equation (17-14) for two cases: $\cos \psi = 1$ and $\cos \psi = 0.9$.

It can be seen from Table 17-2 that the armature losses at first markedly decrease with an increase in the number of phases, but with $m > 6$ this decrease begins to slow down and, in transition from $m = 12$ to $m = \infty$, the losses decrease very slightly.

With a single-phase current ($m = 2$), the losses in a converter are even higher than in a d.c. machine, and, therefore, rotary converters are generally built with a number of phases m not less than three. The most widely used converters are those with $m = 6$, since the six-phase system of feeding converters is accomplished in transformers without any specific design difficulties by changing the three-phase transformer secondary into a six-phase system (Fig. 17-5).

The armature losses of a converter increase with a re-

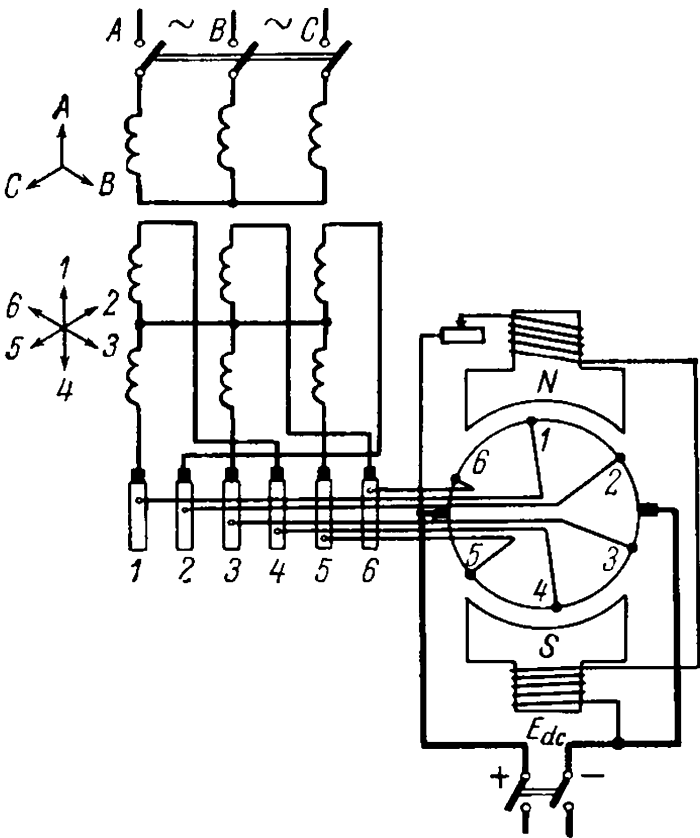


Fig. 17-5. Schematic diagram of a six-phase rotary converter

duction in $\cos \phi = \cos \psi$ on the a.c. side, since the a.c. wave begins to shift away from the d.c. wave and the mutual compensation of magnetizing forces produced by these currents is disturbed.

Figure 17-6 depicts curves of $\frac{1}{\sqrt{k_v}} = f(\cos \psi)$ for $m = 2, m = 3, m = 6$ and $m = 12$.

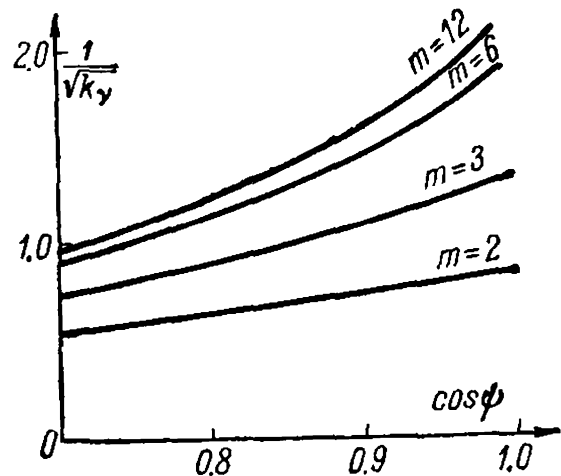


Fig. 17-6. Curves of armature loss factor vs power factor for a rotary converter

17-5. Starting of a Converter

A rotary converter can be started both from a d.c. and an a.c. sources. Direct current starting is possible in only a few cases, when a proper d.c. source, such as a storage battery, is available. Here the converter is started as a d.c. motor and is brought up to its synchronous speed, after which the converter is synchronized and connected to the a.c. power circuit. By this method the converter always obtains the correct polarity with respect to the d.c. circuit. Alternating current starting of the converter can be accomplished by several methods, of which the most important are the method of asynchronous starting of a synchronous motor, and the auxiliary-motor starting method.

Asynchronous starting of converters is the most widely used method. It is applicable when the pole shoes are fitted with a squirrel cage, because the converter can then develop sufficient starting and pull-in torques. Starting is accomplished at a reduced voltage (25 to 30% of the rated voltage) with the field winding closed through a resistor. When approaching synchronism, the converter begins to operate as an induction motor with a small slip, the polarity at its brushes periodically changing.

If the reactive torque of the converter is sufficient to pull it into synchronism, the latter may take place both with correct and with wrong polarity; in the latter case it is only necessary to change the direction of the current in the excitation circuit. If, on the contrary, the reactive torque is not sufficient for pulling the machine into step, it becomes necessary to switch-in the excitation circuit at the moment when the converter has the correct polarity.

When starting with an auxiliary induction motor, the number of pole pairs of the latter is usually taken one less than that of the converter.

The auxiliary motor allows the converter to be run through synchronism, when synchronization can be carried out by connecting the converter to the a.c. circuit.

17-6. Voltage Regulation of a Converter

Owing to mutual compensation of the magnetizing forces of the d.c. and a.c. sides, and to the correspondingly small armature reaction, the rotary converter has a very small inductive voltage drop. Since, at the same time, the electric losses in the converter armature are greatly reduced, the active voltage drop in the armature winding is also small. Therefore, the resultant voltage drop in a converter is only 2 to 5% of the rated voltage.

The rotary converter, as shown by equation (17-2), has a very strict relation between the voltages on the d.c. and a.c. sides. With an unvarying voltage $E_l \cong U_l = \text{const}$ on the a.c. side, the voltage on the d.c. side $U_{dc} \cong E_{dc}$ is quite definite, and its regulation requires additional devices, since a change in excitation will affect only the value of the reactive component of the alternating current, while the resultant flux Φ of the converter with $U_{dc} = \text{const}$ will also remain practically constant. Hence, it follows that to change the voltage on the a.c. side, we must change the voltage across the slip rings; therefore, for a given circuit voltage $U_l = \text{const}$, it is necessary to insert an additional device between the circuit and the slip rings to step up or step down the power circuit voltage. Such devices may be a voltage regulator (see Sec. 18-6), a reactor, or a booster machine. The first two are connected on the a.c. side, while the latter can be connected on either side, depending on whether it is a d.c. or an a.c. machine. The armature winding (or windings) of the booster is connected in series with the circuit, and the armature itself can be mounted on the shaft of the converter.

The voltage regulator allows considerable regulation to be obtained—up to 30% and more—of the rated voltage.

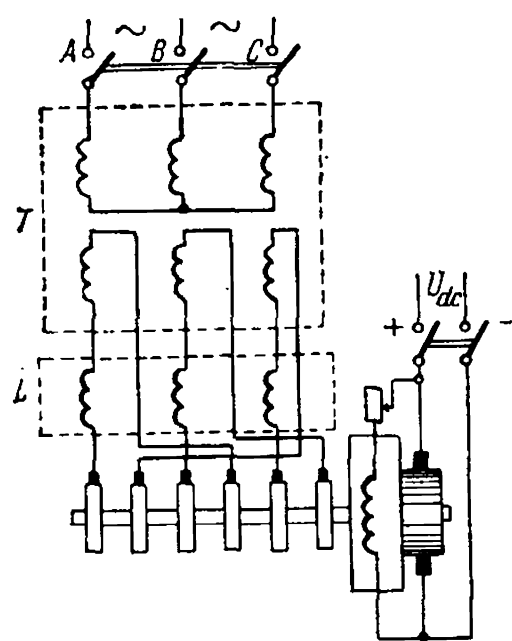


Fig. 17-7. Regulation of voltage of a rotary converter by means of a reactor

One of the simplest methods of rotary converter voltage regulation is the insertion of a reactor L (Fig. 17-7) between the secondary of transformer T and the slip rings, but it gives only relatively small limits of regulation which do not exceed $\pm 7.5\%$.

The method is based on the principle that a rotary converter operating with respect to the a.c. circuit as a synchronous motor will, with constant voltage and variable excitation, have different values of the resultant flux, whose change depends on the value of the inductive reactance x . This reactance may be both the intrinsic leakage reactance of the converter windings and the external inductive reactance. When overexcited, the

converter will operate with a leading current, and the voltage U_l across its slip rings, as can be seen from the voltage diagram in Fig. 17-8, will grow with a corresponding rise in the voltage on the d.c. side.

When underexcited, the converter will operate with a lagging current, and the voltage U_l , as seen from the diagram in Fig. 17-8b, will diminish with a corresponding decrease in the voltage U_{dc} .

Attention should be drawn to the fact that instead of employing a special reactor, use can be made of a transformer for feeding the converter which has a higher inductive reactance and then, with a constant voltage across the primary of the transformer, it will be possible to regulate the voltage of the converter by varying its excitation.

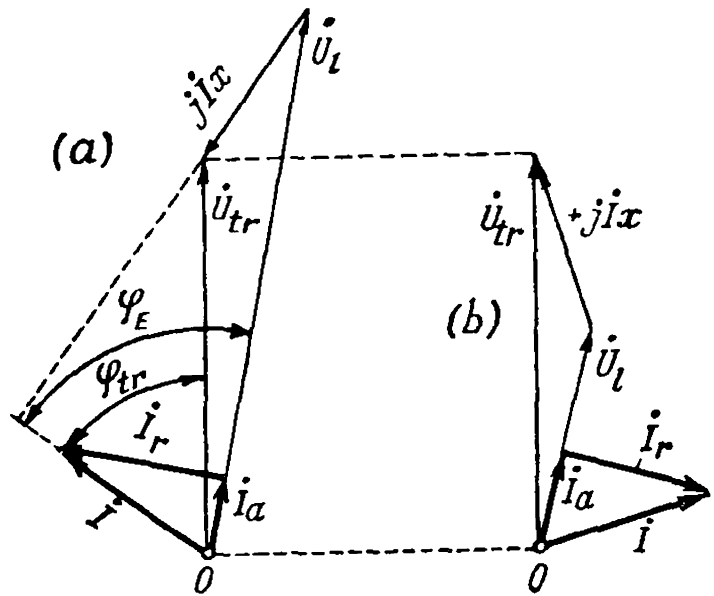


Fig. 17-8. Voltage diagram of a rotary converter operating with (a) leading and (b) lagging current

17-7. Oscillations of a Converter

A rotary converter operating with respect to the a.c. circuit as a synchronous motor may have, the same as the motor, forced and natural oscillations.

Forced oscillations appear when the synchronous generator which feeds the converter has variations in speed caused by non-uniform torque of the prime mover driving the generator.

Free oscillations may occur when the operating conditions of a converter change under the influence of load surges and short circuits.

Converters are often provided with damper windings arranged in the pole shoes of the main poles and acting as oscillation dampers; as a result forced oscillations are usually not observed. Free oscillations occurring during short circuits may lead to the converter being pulled out of step, but, when high-speed breakers are employed, the short circuit is disrupted before the angle of lag of the e.m.f. induced by the excitation flux behind the line voltage vector reaches 180° .

After breaking of the short circuit, the armature quickly returns to its normal speed under the action of the damper winding.

17-8. Application of Converters

Rotary converters built for a frequency of 50 Hz and outputs up to 5000 kW were very widely used for converting alternating current into direct current, especially for electrical traction, but at present they have been superseded in this field by the cheaper and more efficient mercury arc rectifiers. For voltage of 220 V and lower, however, the rotary converter is more economical than the mercury arc rectifier and therefore finds use at present in special installations.

At low outputs the rotary converter is often built without a feeding transformer, and with separate d.c. and a.c. windings on the armature, in order to make it possible to obtain any desired relation between the d.c. and a.c. voltages.

Machines with distributed windings are also used as generators producing both direct and alternating currents. In this case they are driven by some kind of prime mover, most often by internal-combustion engines.

Low-power synchronous generators of similar design are also built, their d.c. armature winding being used for feeding the field winding, thus making a separate exciter unnecessary.

PART THREE

INDUCTION MACHINES

Chapter

18

THREE-PHASE INDUCTION MACHINE WITH LOCKED ROTOR*

18-1. General

The object of this chapter is to show that, with the rotor locked, an induction machine is a transformer, differing from a conventional transformer only in design (distributed windings on the rotor and stator, the presence of an air-gap, etc.). As to the physical nature of the phenomena, it is similar in many respects. It is expedient, therefore, to begin the study of induction machines, like transformers, with consideration of the limiting operating conditions of the machine, i.e., the no-load and short-circuit conditions and then, in the following chapter, extend the concept of the induction machine as a transformer to a machine with its rotor running.

In further discussions we shall consider a three-phase induction machine with slip rings and a rotor which may be unlocked, short-circuited, or closed through a resistor. We shall consider all variables to be sine-wave functions of time or space, the role of the higher harmonics to be studied separately later. The voltages, e.m.f.s and currents are determined by their effective values, the magnetizing forces and fluxes by their maximum values. The winding phases are assumed to be symmetrical.

18-2. Induction Machine on No-Load, $n=0$

Assume that the rotor circuit of an induction machine is open (Fig. 18-1), the rotor at standstill, and the stator connected to a circuit with a voltage U_1 and frequency f_1 . Here the induction machine is a transformer at no-load. The stator of the machine is the primary winding, and the stationary rotor, the secondary. Correspondingly, all values pertaining to the stator will be called primary and denoted by "1", and to the rotor, secondary, denoted by "2".

The reasoning is, in principle, the same as for transformers (Vol. I, Chapter 13). Under the voltage U_1 a no-load current I_0 flows through the stator winding. The magnetizing force F_1 produced by this current gives rise to a flux, one part of which, Φ_m , is linked with the windings

* The operating principles and the design of non-commutator induction machines were dealt with previously, in Chapters 1, 3 and 5.

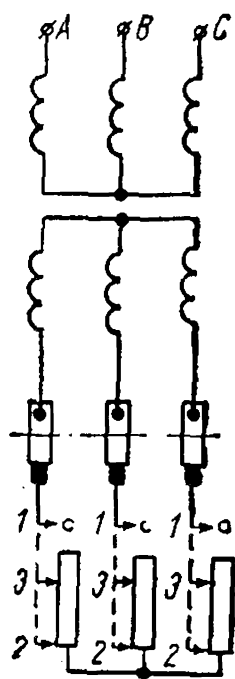


Fig. 18-1. Diagram of a motor with slip rings and rheostat

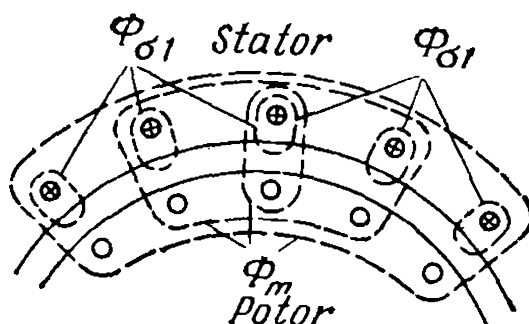


Fig. 18-2. Stator fluxes with rotor unlocked

of both parts of the machine, while the other part, $\Phi_{\sigma 1}$, is linked only with the stator winding (Fig. 18-2). The first flux is the main, the second, the leakage flux. If p is the number of pole pairs of the machine, then the speed n_1 of the magnetizing force F_1 and, correspondingly, of the flux Φ_m will be

$$n_1 = \frac{f_1}{p} \text{ rps} \quad (18-1)$$

The main flux causes in the stator and rotor windings the e.m.f.s E_1 and E_2 , determined by the formulas

$$\left. \begin{aligned} E_1 &= \sqrt{2} \pi f_1 \omega_1 k_{w1} \Phi_m \\ E_2 &= \sqrt{2} \pi f_1 \omega_2 k_{w2} \Phi_m \end{aligned} \right\} \quad (18-2)$$

The leakage flux $\Phi_{\sigma 1}$ causes in the stator winding a leakage e.m.f. $E_{\sigma 1}$ with

$$\dot{E}_{\sigma 1} = -j \dot{I}_0 x_1$$

where x_1 is the leakage inductive reactance of the stator winding.

In addition, the stator winding has a resistance r_1 ; taking into account its action in the form of a voltage drop $I_0 r_1$, we can write the primary e.m.f. equation of an induction machine in the same way as for transformers [see Vol. I, equations (13-16) and (13-22)], viz.:

$$\dot{U}_1 = -\dot{E}_1 + I_0 Z_1 \quad (18-3)$$

It should be recalled that in this equation $-\dot{E}_1$ and $I_0 Z_1$ are components of the voltage \dot{U}_1 , each of which is in equilibrium with the corresponding e.m.f.

Essentially identical no-load diagrams correspond to the identical equations of the primary e.m.f.s for a transformer and an induction machine. Therefore, we shall not repeat the diagram shown in Vol. I, Fig. 14-7. But, quantitatively, there is a noticeable difference between the two diagrams. Indeed, an induction machine has a relatively large air-

gap. For this reason the current I_0 in induction machines usually amounts to from 20 to 50% of the rated current I_r , i.e., it is considerably higher than the no-load current of the transformer (3 to 10% of I_r). Besides, the winding resistance in induction machines is also relatively higher than in transformers. The voltage drop in the stator winding of an induction machine at no-load therefore constitutes 2 to 5% of the rated voltage of the machine, while in transformers it does not generally exceed 0.1 to 0.4% of the latter.

The no-load currents of a three-phase induction machine form a symmetrical system, since the reluctances of all paths of the three-phase fluxes are the same. On the other hand, the shape of the no-load current is close to a sine wave, since in the presence of a relatively large air-gap the third harmonic of the current or, correspondingly, of the flux cannot be of any appreciable importance.

The *e.m.f.* or *voltage ratio* k of an induction machine is

$$k = \frac{E_1}{E_2} = \frac{\sqrt{2} \pi f_1 \omega_1 k_{w1} \Phi_m}{\sqrt{2} \pi f_1 \omega_2 k_{w2} \Phi_m} = \frac{\omega_1 k_{w1}}{\omega_2 k_{w2}} \quad (18-4)$$

In induction machines, as in transformers, the secondary winding is reduced to the primary one, i.e., the real secondary winding is replaced by another winding with the same number of phases and turns, winding pitch and number of slots per pole per phase as the primary one. The secondary parameters are then duly recalculated to retain the real power relations in the machine.

The *e.m.f.* of the equivalent secondary winding E'_2 is

$$E'_2 = kE_2 = E_1 \quad (18-5)$$

With the rotor unlocked and stationary, the only losses in the machine are the stator copper losses $m_1 I_0^2 r_1$, where m_1 is the number of stator phases, and the stator and rotor steel losses $p_{st1} + p_{st2}$. These losses are covered by the power P_{10} consumed by the machine from the external circuit. Thus,

$$P_{10} = m_1 I_0^2 r_1 + p_{st1} + p_{st2} \quad (18-6)$$

Since the current I_0 and resistance r_1 are relatively great in induction machines, the copper losses p_{cop1} make up a considerable part of the power P_{10} , whereas in transformers we may always disregard them.

Knowing P_{10} , we can determine the active current component I_{0a} from the formula

$$I_{0a} = \frac{P_{10}}{m_1 U_1}$$

The active current component I_{0a} is generally small in comparison with the reactive component I_{0r} of this current, and the angle φ_0 is equal to $\varphi_0 = 70$ to 80° .

The equivalent circuit of an induction machine at no-load does not differ in any way from the corresponding transformer circuit in Fig. 14-10 of Vol. I.

18-3. Short Circuit of an Induction Machine

If with the rotor braked ($n=0$) we move the sliding contact of the rheostat in the rotor circuit (Fig. 18-1) from position 1 to position 2, we shall obtain the short-circuit conditions of an induction machine. The physical essence of this short circuit is similar to that of a transformer short circuit (Vol. I, Chapter 17), but has some distinctions resulting from the design features of induction machines.

If we desire that the currents I_1 and I_2 in the stator and rotor windings should not exceed the rated values in a short circuit, then, as in transformers, we must reduce the voltage applied across the stator terminals to the value U_{sh} , which amounts to about 15 to 25% of U_r (compared with 5 to 17% in transformers). The currents I_1 and I_2 produce the stator and rotor magnetizing forces from which, according to the assumed conditions (see Sec. 18-1), we shall take the fundamental harmonic magnetizing forces F_1 and F_2 . With $n=0$ the rotor current frequency is equal to the stator current frequency f_1 . If p is the number of pole pairs in a machine, then the magnetizing forces F_1 and F_2 rotate in the same direction relative to the stationary stator and rotor and at the same speed $n_1 = \frac{f_1}{p}$, i.e., they are stationary with respect to each other and form the resultant magnetizing force F_{sh} which rotates at the speed n_1 and produces the main rotating flux Φ_{sh} linked with the stator and rotor windings. In addition, the magnetizing force F_1 induces the primary leakage flux $\Phi_{\sigma 1}$ linked only with the primary winding, while the magnetizing force F_2 produces the secondary leakage flux $\Phi_{\sigma 2}$ linked only with the secondary winding (Fig. 18-3).

As in a transformer, the magnetizing forces F_1 and F_2 in a short circuit are opposed to each other. Therefore, despite the considerable values of the currents I_1 and I_2 and magnetizing forces F_1 and F_2 produced by them, the resultant magnetizing force F_{sh} in a short circuit is relatively small, owing to which the flux Φ_{sh} is also small and, consequently, the main magnetic circuit is not saturated (Fig. 18-4).

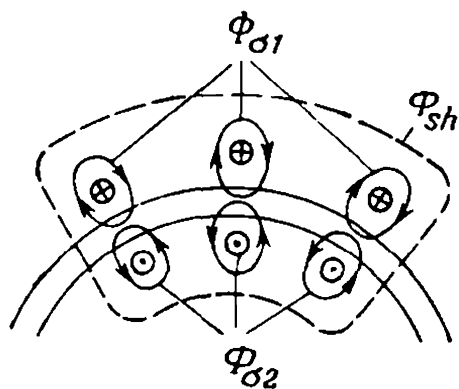


Fig. 18-3. Induction machine fluxes in short circuit

The primary current I_1 can be represented as the sum of two components, one of which (I_m) creates the magnetizing force F_{sh} and the other ($-I_2'$) creates the mag-

netizing force $-\dot{F}_2$ which compensates the magnetizing force \dot{F}_2 of the secondary current \dot{I}'_2 . Thus, we have

$$\dot{I}_1 = \dot{I}_m + (-\dot{I}'_2)$$

or

$$\dot{I}_1 + \dot{I}'_2 = \dot{I}_m \quad (18-7a)$$

Correspondingly,

$$\dot{F}_1 = \dot{F}_m + (-\dot{F}_2)$$

or

$$\dot{F}_1 + \dot{F}_2 = \dot{F}_m \quad (18-7b)$$

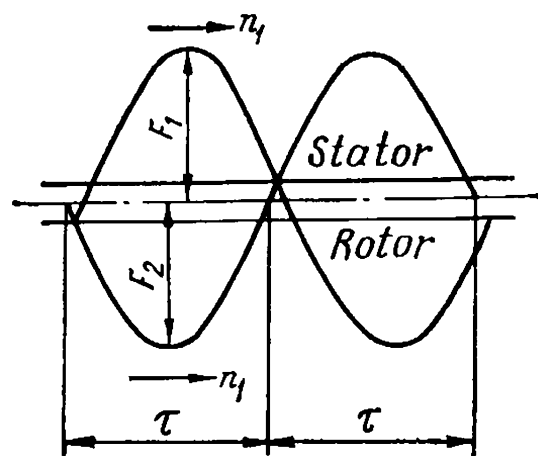


Fig. 18-4. Stator and rotor magnetizing forces in short circuit

the magnetizing forces \dot{F}_1 and \dot{F}_2 being determined from equation (4-36). Consequently,

$$\frac{m_1}{\pi} \sqrt{2} \frac{\omega_1 k_{w1}}{\rho} \dot{I}_1 + \frac{m_2}{\pi} \sqrt{2} \frac{\omega_2 k_{w2}}{\rho} \dot{I}_2 = \frac{m_1}{\pi} \sqrt{2} \frac{\omega_1 k_{w1}}{\rho} \dot{I}_m$$

Since $\dot{I}_1 = \dot{I}_m - \dot{I}'_2$, we get

$$-m_1 \omega_1 k_{w1} \dot{I}'_2 + m_2 \omega_2 k_{w2} \dot{I}_2 = 0$$

whence we find the *current ratio*:

$$k_i = \frac{\dot{I}_2}{\dot{I}'_2} = \frac{m_1 \omega_1 k_{w1}}{m_2 \omega_2 k_{w2}} \quad (18-8)$$

Therefore, the equivalent rotor current is

$$\dot{I}'_2 = \frac{1}{k_i} \dot{I}_2 \quad (18-9)$$

By using the voltage and current ratios [equations (18-4) and (18-8)], we can determine the equivalent rotor resistance r'_2 and reactance x'_2 .

When reducing r_2 to the stator, we shall proceed from the consideration that the copper losses in the rotor winding do not depend on this reduction. Consequently,

$$m_2 I_2^2 r_2 = m_1 I_2'^2 r'_2$$

whence

$$r'_2 = \frac{m_2}{m_1} \frac{I_2^2}{I_2'^2} r_2 = \frac{m_2}{m_1} \left(\frac{m_1 \omega_1 k_{w1}}{m_2 \omega_2 k_{w2}} \right)^2 r_2 = \frac{\omega_1 k_{w1}}{\omega_2 k_{w2}} \frac{m_1 \omega_1 k_{w1}}{m_2 \omega_2 k_{w2}} r_2 = k k_i r_2 = k_r r_2 \quad (18-10)$$

where

$$k_r = k k_i \quad (18-11)$$

is called the *resistance factor* or *ratio*.

When reducing the inductive leakage reactance x_2 to the stator, we proceed from the fact that angle ψ_2 between the e.m.f. E_2 and current I_2 is also independent of this reduction. Consequently,

$$\tan \psi_2 = \frac{x_2}{r_2} = \frac{x'_2}{r'_2}$$

whence

$$x'_2 = \frac{r'_2}{r_2} x_2 = k_r x_2 \quad (18-12)$$

The equations for the primary and secondary e.m.f.s of an induction machine in short circuit are written in exactly the same way as for transformers [Vol. I, equations (17-1) and (17-2)], namely,

$$\dot{U}_{1sh} = -\dot{E}_{1sh} + \dot{I}_1 Z_1 \quad (18-13)$$

and

$$\dot{E}_{2sh}' - \dot{I}_2' Z_2' = 0 \quad (18-14)$$

Here $Z_1 = r_1 + jx_1$ and $Z_2' = r'_2 + jx'_2$ are the impedances of the stator and rotor windings.

Taking into account that $\dot{E}_2' = \dot{E}_1$ and $\dot{I}_2' \cong -\dot{I}_1$, and solving equations (18-13) and (18-14) for \dot{I}_1 , we obtain

$$\dot{I}_1 \cong \frac{\dot{U}_{1sh}}{Z_1 + Z_2'} \quad (18-15)$$

according to which we have the same equivalent circuit for a short-circuited induction machine as for a transformer (Vol. I, Sec. 13-7) and the same short-circuit parameters, namely,

$$\left. \begin{aligned} r_{sh} &\cong r_1 + r'_2 \\ x_{sh} &\cong x_1 + x'_2 \end{aligned} \right\} \quad (18-16)$$

It should be noted, however, that for low-power induction machines with a relatively large magnetizing current ($I_0 > 50\%$ of I_r) special corrections have to be introduced into equation (18-16).

18-4. Squirrel-Cage Parameters

A squirrel cage can be imagined as a polyphase winding whose number of pole pairs is equal to the number of pole pairs of the rotating field. If N_s is the number of squirrel-cage bars, the e.m.f. displacement angle (as well as the current displacement angle) in adjacent bars should be equal to

$$\alpha = \frac{2\pi p}{N_s} \quad (18-17)$$

The current I_2 in a bar is the vector difference of the currents I_{ring} in two adjacent ring elements of a junction. Consequently,

$$I_2 = 2I_{ring} \sin \frac{\pi p}{N_2} \quad (18-18)$$

whence

$$I_{ring} = \frac{I_2}{2 \sin \frac{\pi p}{N_2}} \quad (18-19)$$

For practical calculations it is convenient to consider a squirrel cage as a polyphase winding with the number of phases m_2 equal to the number of slots N_2 :

$$m_2 = N_2 \quad (18-20)$$

The number of turns in a phase should then be taken equal to

$$w_2 = \frac{1}{2} \quad (18-21)$$

and the winding factor of a squirrel cage is

$$k_{w2} = 1$$

Under these conditions the current I_2 and the e.m.f. E_2 of a bar are the current and e.m.f. of the secondary winding, and the expressions obtained above for the winding e.m.f. and magnetizing force and for the ratios used to obtain the equivalent quantities are valid.

When considering the squirrel cage as a polyphase winding, it should be assumed to be star-connected and short-circuited. Then the ring element resistances should be allowed for by a corresponding increase in the bar resistances.

Two adjoining ring elements correspond to each bar, for instance, elements bd and ac correspond to bar ab , in Fig. 18-5a. Consequently, the resistance r_2 and, correspondingly, the inductive leakage reactance x_2 of each squirrel-cage phase consist of the sum of the cage bar resistance and reactance r_{bar} and x_{bar} and of the resistance and reactance

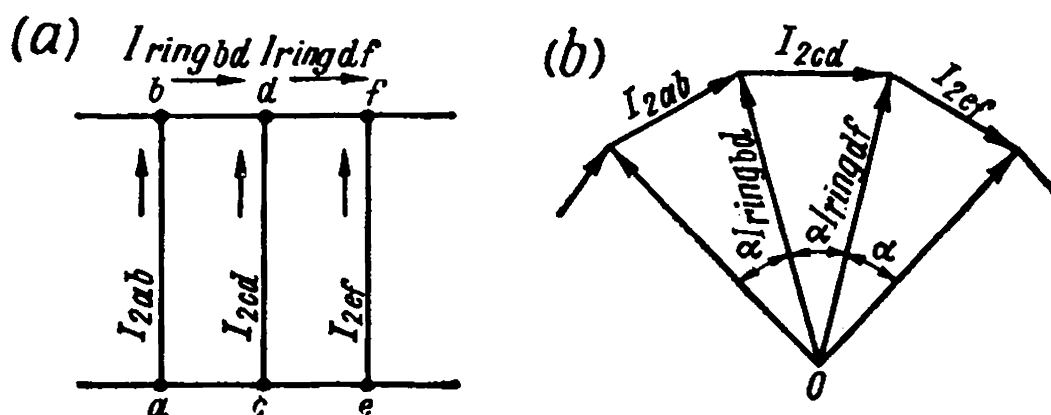


Fig. 18-5. Currents in rotor squirrel cage

of two ring elements, $2r'_{ring}$ and $2x'_{ring}$, i.e.,

$$\left. \begin{aligned} r_2 &= r_{bar} + 2r'_{ring} \\ x_2 &= x_{bar} + 2x'_{ring} \end{aligned} \right\} \quad (18-22)$$

The factor for reducing the resistance of the squirrel cage to the stator system, with the number of phase of the secondary system $m_2 = N_2$, the number of turns per phase $w_2 = \frac{1}{2}$ and $k_{w2} = 1.0$, is equal to

$$k_r = \frac{4m_1 (\omega_1 k_{w1})^2}{N_2} \quad (18-23)$$

Since the currents in the bar and ring are different, r'_{ring} should be considered as the ring element resistance referred to the current I_2 .

Proceeding from the equality of the main copper losses, we find

$$r'_{ring} = r_{ring} \left(\frac{I_{ring}}{I_2} \right)^2 = \frac{r_{ring}}{4 \sin^2 \frac{\pi p}{N_2}} \quad (18-24)$$

where r_{ring} is the actual resistance of a ring element.

Similarly

$$x'_{ring} = \frac{x_{ring}}{4 \sin^2 \frac{\pi p}{N_2}} \quad (18-25)$$

where x_{ring} is the inductive leakage reactance of a ring element.

The permeance of the end connections of a short-circuiting ring of an a.c. motor squirrel cage depends on the distance l_c between the ring centre C_{ring} and the centre C_s of the tangential equivalent ring of the end connection of the stator winding (Fig. 18-6) and can be expressed by the formula

$$\lambda_{ring} = \frac{N_2}{2pm_1} \cdot \frac{\tau}{l} g_{end} \quad (18-25a)$$

The value of g_{end} is determined from the curves of Fig. 18-6 for various ratios $\frac{\tau}{l_c}$ depending on $\frac{l_c}{\epsilon}$ [162], where

$$\epsilon = 0.223 (b_{ring} + h_{ring})$$

Here b_{ring} is the thickness of the short-circuiting ring, and h_{ring} is its height.

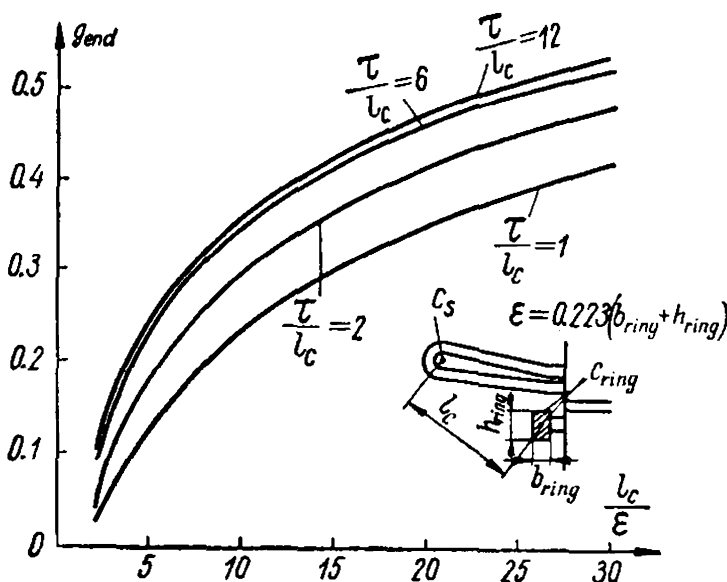


Fig. 18-6. Curves of g_{end} versus l_c/ϵ

The differential leakage of the toothzone of a short-circuited squirrel cage depends on the number of teeth of the secondary side per pole and can be determined by formula (5-27), where the factor k_{dif2} can be determined from the curves of Fig. 18-7 giving the relation

$$k_{dif2} = f\left(\frac{N_2}{2p}\right)$$

both for ordinary and for skewed slots per tooth pitch of the stator.

Example 18-1. Calculate the inductive reactances and resistances of the rotor windings of a three-phase 250-kW, 3000-V induction motor with a simple short-circuited winding in the form of a squirrel cage. The motor data are in the main those of Example 5-1: $2p=6$, pole pitch $\tau=275$ mm, length of active steel with ducts $l_0=364$ mm, effective length $l=334$ mm. The number of rotor slots $N_2=80$, number of turns per rotor phase $w_2=\frac{1}{2}$, air-gap $\delta=1.0$ mm, air-gap factor $k_\delta=1.6$ mm, saturation factor for differential leakage $k_{\mu dif}=1.1$, winding factor $k_{w2}=1.0$.

The rotor slot is of the form given in Fig. 5-3d; $d_s=12$ mm, $d_i=11.5$ mm, $h_2=1.0$ mm, $b_2=0.9$ mm. The overhang of the squirrel-cage winding bars on both sides of the rotor is $2 \times 55 = 110$ mm, the total length of the rotor bars $l_{bar}=364+110=474$ mm.

The cross section of the short-circuiting ring is

$$b_{ring}h_{ring}=12.5 \times 32.5 = 406 \text{ mm}^2$$

The leakage permeance of a rotor slot is

$$\lambda_s = 0.623 + \frac{1.0}{0.9} = 1.74 \text{ [formula (5-15d)]}$$

The leakage of the end connection of the short-circuiting ring winding is

$$\lambda_{end} = \frac{80}{2 \times 3 \times 3} \times \frac{275}{334} \times 0.31 = 1.14 \text{ [formula (18-25a)]}$$

where the end-connection leakage factor $g_{end}=0.31$ is determined from the curves of Fig. 18-6 for $l_C=115$ mm with

$$\epsilon = 0.223 \times (12.5 + 32.5) = 10.1 \text{ mm}$$

$$\frac{l_C}{\epsilon} = \frac{115}{10.1} = 11.4$$

$$\frac{\tau}{l_C} = \frac{275}{115} = 2.38$$

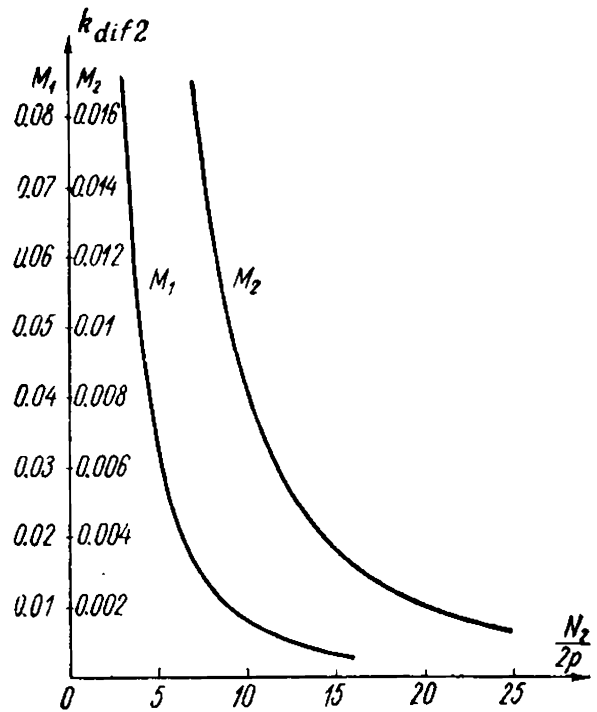


Fig. 18-7. Curves of k_{dif2} versus $N_2/2p$

The differential leakage permeance of the squirrel-cage rotor is

$$\lambda_{dif} = \frac{80}{2 \times 3 \times \pi^2} \times \frac{275 \times 1.0^2}{1.6 \times 1.1 \times 1.0} \times 0.0046 = 1.0 \text{ [formula (5-27)]}$$

where the differential leakage factor for

$$\frac{N_2}{2p} = \frac{80}{6} = 13.3$$

according to the curve of Fig. 18-7

$$k_{dif2} = 0.0046$$

The sum of the leakage permeances is

$$\sum \lambda = 3.88$$

The inductive reactance of the short-circuited rotor winding is

$$x_2 = 2\pi \times 1.26 \times 10^{-8} \times 50 \times 33.4 \times 3.88 = 0.00051 \Omega$$

The factor for referring the rotor secondary winding to the stator primary winding, according to formula (18-23), is

$$k_r = \frac{4 \times 3 \times (210 \times 0.91)^2}{80} = 5500$$

The equivalent rotor winding inductive reactance is

$$x_2' = x_2 k_r = 0.00051 \times 5500 = 2.8 \Omega$$

The resistance of one bar of the rotor squirrel cage is

$$r_{bar} = \rho_{75} \cdot \frac{l_{bar}}{q_{bar}} = 0.0217 \times \frac{0.474}{\frac{\pi}{4} \times 11.5^2} = 9.9 \times 10^{-5} \Omega$$

The resistance of two sections of the squirrel-cage short-circuiting rings with an average diameter $D_{ring} = 487$ mm at both sides of the rotor is

$$r_{ring} = 0.0217 \times \frac{0.0382}{406} = 20.4 \times 10^{-7} \Omega$$

where $l_{ring} = 2 \frac{\pi D_{ring}}{N_2} = 2 \times \frac{\pi \times 487}{80} = 38.2$ mm is the length of two adjacent sections of the ring;

$q_{ring} = 12.5 \times 32.5 = 406$ mm² is the cross section of the rings.

The resistance of two sections of the short-circuiting ring of the cage referred to the current in the bar [formula (18-24)] is

$$r'_{ring} = \frac{r_{ring}}{4 \sin^2 \frac{\pi p}{N_2}} = \frac{20.4 \times 10^{-7}}{4 \times \sin^2 \times \frac{\pi \times 3}{80}} = \frac{20.4 \times 10^{-7}}{0.055} = 3.7 \times 10^{-5} \Omega$$

The total resistance of the bar with two adjacent sections of the short-circuiting rings is

$$r_2 = r_{bar} + r'_{ring} = (9.9 + 3.7) 10^{-5} = 13.6 \times 10^{-5} \Omega$$

The resistance of the bar referred to the stator winding is

$$r_2' = r_2 k_r = 13.6 \times 10^{-5} \times 5500 = 0.75 \Omega$$

18-5. Locked-Rotor Induction Machine Under Load

Let us move the sliding contact of the rheostat inserted in the circuit of the locked rotor shown in Fig. 18-1 into position 3. Here the induction machine can be considered as a transformer under load. In the general case the load may be of a combined nature.

The physical processes here are absolutely the same as in transformers (Vol. I, Chapter 13), with the unimportant difference that here we have rotating magnetizing forces. Accordingly, the equations of e.m.f. and magnetizing force equilibrium, the vector diagram and the equivalent circuits have the same form as the transformers. We shall consider them here again to be able to compare in the next chapter the phenomena taking place in stationary and rotating induction machines.

The stator e.m.f. equation repeats the equation of the transformer e.m.f., namely,

$$\dot{U}_1 = -\dot{E}_1 + \dot{I}_1 \dot{Z}_1 \quad (18-26)$$

Assuming that the rotor has been reduced to the stator and that an additional impedance Z'_{add} referred to the stator has been inserted into the rotor circuit, we write the rotor e.m.f. equation in the form of equation (18-14), namely,

$$\dot{I}'_2(Z'_2 + Z'_{add}) = \dot{E}'_2 \quad (18-27)$$

The magnetizing force equation of a locked-rotor induction machine repeats the magnetizing force equation (18-7b) for the transformer linkages of the primary and secondary systems

$$\dot{F}_1 + \dot{F}_2 = \dot{F}_m \quad (18-28)$$

or

$$\dot{I}_1 + \dot{I}'_2 = \dot{I}_m \quad (18-29)$$

Both the stator and the rotor can be the primary system of an induction machine.

Figure 18-8 shows the sine waves of the magnetizing forces F_1 , F_2 and F_m rotating in the same direction and with the same speed $n_1 = f_1/p$, the sine wave F_2 being shifted from the sine wave F_1 by such an angle that the sum of the magnetizing forces F_1 and F_2 gives the magnetizing force F_m necessary to produce the main magnetic flux Φ_m .

By solving both the e.m.f. and magnetizing force equations for the current I_1 , we can obtain for it the same expression as for a transformer and, correspondingly, the equivalent circuit in Fig. 18-9 which repeats

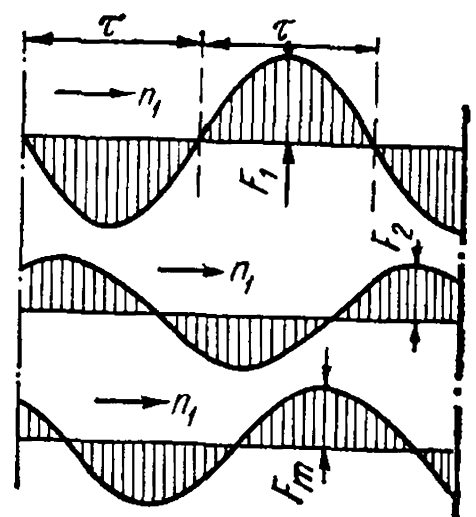


Fig. 18-8. Magnetizing force of a loaded induction machine at standstill

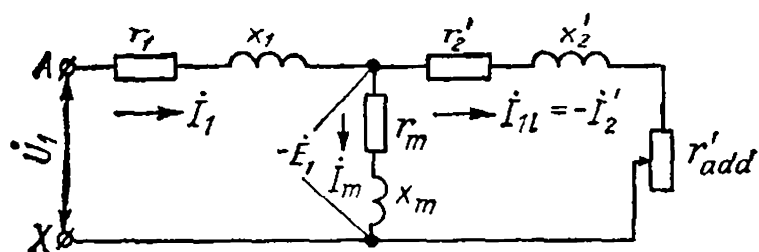


Fig. 18-9. Equivalent circuit diagram of an induction machine at standstill

the equivalent circuit of a transformer, with the assumption that only resistance ($Z_{add} = r_{add}$) has been inserted into the induction machine rotor circuit as is generally the rule for motors. The vector diagram corresponding to the equivalent circuit in Fig. 18-9 is plotted in Fig. 18-10. When constructing it, we lay off in the positive direction of the axis of ordinates the load component of the primary current $I_{1l} = -I_2'$. The vector $\overline{OD} = I_{1l}(r_2' + r_{add})$ is laid off in the same direction. The vector $\overline{DG} = jI_{1l}x_2'$ leads the vector \overline{OD} by 90° and, when added to the latter, gives the vector $\overline{OG} = -\dot{E}_1 = -\dot{E}_2$; the flux vector Φ_m lags behind the vector \overline{OG} by 90° ; the current vector I_m leads the flux vector Φ_m by an angle corresponding to the steel losses; the current $I_1 = I_{1l} + I_m$; by adding to vector \overline{OG} the vectors \overline{GK} and \overline{KA} of the active and inductive voltage drops in the stator I_1r_1 and jI_1x_1 , we obtain the voltage $\overline{OA} = \dot{U}_1$ across the machine terminals.

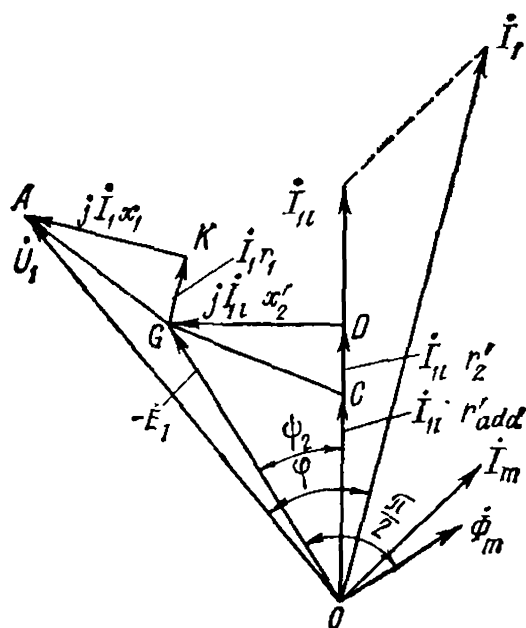


Fig. 18-10. Vector diagram of an induction machine at standstill

18-6. The Induction Regulator [156]

Operating Principle of the Induction Regulator. The induction regulator is an induction machine with a locked rotor that controls the circuit voltages. The most important are the three-phase induction regulators, while single-phase ones are used less frequently. For this reason we shall only consider the operation of three-phase regulators.

The connections of an induction regulator are given in Fig. 18-11. For reasons of practical convenience the rotor, whose angular position may be varied by means of some device, for instance, a worm gear, will be the primary, and the stator, which is stationary, will be the secondary.

The principle of operation of an induction regulator is as follows. The three-phase magnetizing current fed into the rotor produces a magnetic flux Φ_m rotating at the speed $n_1 = f_1 : p$ in a definite direction,

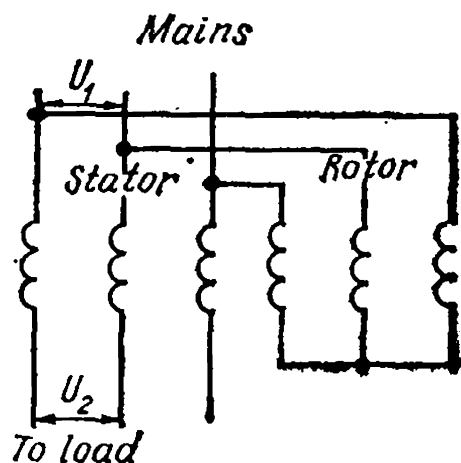


Fig. 18-11. Connections of induction regulator

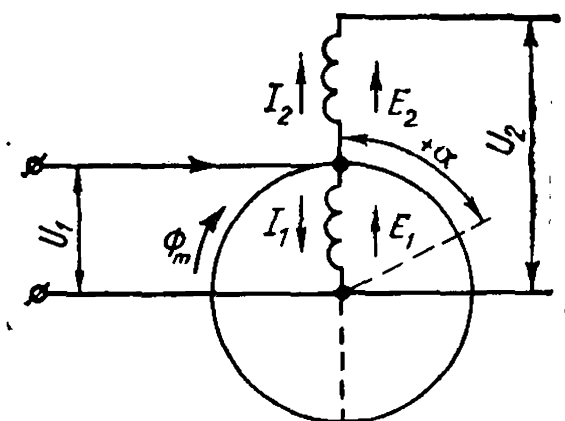


Fig. 18-12. E. m. f. s and currents of an induction regulator

for instance, clockwise. Assume that the rotor winding axes coincide in space with the corresponding stator winding axes (Fig. 18-12). The flux Φ_m now simultaneously runs into the windings of both parts of the machine and induces in them e.m.f.s E_1 and E_2 which coincide in phase and are identically directed with respect to the windings. Since all three phases are under the same conditions, it is sufficient to consider only one of them. We see that in these conditions the e.m.f. E_2 acts in concordance with the voltage. Owing to this, the voltage \dot{U}_2 across the terminals of the consumer circuit is the arithmetical sum of \dot{U}_2 and \dot{E}_2 , i.e. (Fig. 18-13),

$$\dot{U}_2 = \dot{U}_{max} = \overline{OA_1} = \dot{U}_1 + \dot{E}_2$$

We shall consider this position of the rotor as the initial one, and the angles will be reckoned from it.

Upon turning the rotor through the angle $\alpha = \pm 180^\circ$, we get

$$\dot{U}_2 = \dot{U}_{min} = \overline{OA_2} = \dot{U}_1 - \dot{E}_2$$

This position of the induction regulator may be called its second main position.

In the general case the rotor may be turned through any angle. Assume the angles to be positive when the rotor is turned in the direction of flux rotation, and negative when the rotor is turned against flux rotation.

Turn the rotor through an angle $\alpha > 0$ (Fig. 18-13). Since the voltage U_1 supplied to the rotor and the frequency f_1 are assumed constant, the flux Φ_m , as follows from the e.m.f. equilibrium equation, does not change in magnitude. But now it runs first onto the stator winding and then onto the rotor

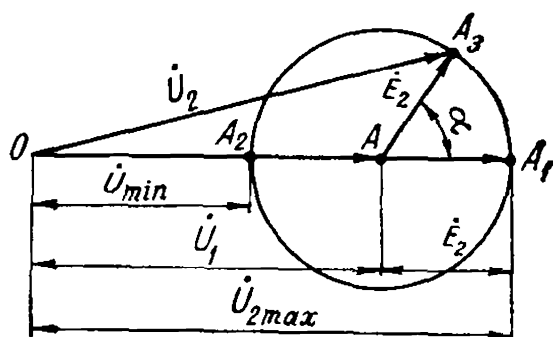


Fig. 18-13. E. m. f. diagram of an induction regulator

winding. Therefore, the e.m.f. vector $E_2 = \overline{AA_1}$, while not changing in magnitude, turns through an angle α in the direction of vector rotation. Obviously, with a change in the angle α , the locus of the ends of the e.m.f. vector E_2 and, therefore, of the voltage \dot{U}_2 is a circle described from point A as the centre by a radius

$$\dot{E}_2 = AA_1$$

The resultant voltage of the induction regulator is

$$\dot{U}_2 = \dot{U}_1 + \dot{E}_2$$

Currents and Power of the Induction Regulator. For simplicity, let us disregard the voltage drops in the primary and secondary windings of the induction regulator.

Figure 18-12 shows the direction of the currents I_1 and I_2 in the rotor and stator when $\alpha = 0$, i.e., in the initial position of the regulator. We see that the currents I_1 and I_2 produce the magnetizing forces $F_1 \equiv I_1 w_1$ and $F_2 \equiv I_2 w_2$ directed, as in an ordinary transformer, opposite to each other. From the magnetizing force equilibrium condition we have

$$I_1 w_1 k_{w1} + I_2 w_2 k_{w2} = I_m w_1 k_{w1} \quad (18-30)$$

Disregarding the higher magnetizing force harmonics, we can represent the magnetizing forces F_1 and F_2 by two sine waves rotating in the same direction at the same speed. These two magnetizing forces are shifted relative to each other so that the resultant magnetizing force is sufficient to produce the flux Φ_m (Fig. 18-8).

Let us show that when the rotor is turned through an angle α the mutual disposition of the waves of the magnetizing forces F_1 and F_2 remains the same as for $\alpha = 0$, it does not depend on the angle of rotor displacement.

Indeed, in Fig. 18-12 we turned the rotor from its original position through an angle $\alpha > 0$. If the phase of current I_1 did not change, the wave of the rotor magnetizing force F_1 , following the winding axis, would also turn by an angle α with respect to the wave of the stator magnetizing force F_2 . But, since the flux Φ_m runs onto the rotor winding by an angle α later than onto the stator winding, the current vector I_1 shifts in phase through the angle $-\alpha$ relative to the position which it occupied when $\alpha = 0$. Thus, the position of the magnetizing force F_1 depends simultaneously on two factors—on turning of the rotor winding axis through an angle α , and on the change in phase of the current I_1 by an angle $-\alpha$. As a result of mutual compensation of both factors, the position of the rotor magnetizing force wave F_1 with respect to the magnetizing force wave F_2 remains the same as for $\alpha = 0$.

The induction regulator allows smooth regulation of voltage under load over a sufficiently wide range. The conditions of the stator and rotor winding insulation in the slots limit the application of induction regulators to circuits with voltages of 6 to 12 kV, but there are separate units in service for voltages up to 18 kV and higher.

Speaking of the power of an induction regulator, we should differentiate between the external and internal apparent power.

By the external power of an induction regulator is meant the power which is delivered to or taken from it. That part of the external power which is transformed by the regulator is called its internal power. This power determines the dimensions of the regulator. Generally, both power ratings of a regulator and, in addition, the regulated voltage U and the voltage regulation range are given on its nameplate.

Three-phase induction regulators for distribution circuits are built with voltage regulation ranges of $\pm (10 \text{ to } 15)\%$. In comparison with the so-called regulating transformers, the induction regulator is heavier, has a larger magnetizing current and heavier losses. Lately, however, it has become possible to reduce the weight of the induction regulator by approximately 25 to 30% by designing it with two poles instead of four, using better grades of steel, and increasing somewhat the electromagnetic loading of the regulator.

Of very great importance are the cooling conditions of an induction regulator. For low power and small voltages, the regulators are made with natural or forced air cooling. Medium- and high-power regulators for distribution circuits and rectifiers are most often provided with oil cooling. The housing of such regulators is of the same form as that of ordinary transformers, but the regulator is mounted vertically in order to utilize the natural oil movement in the vertical channels for cooling, as in conventional transformers.

Double Induction Regulator. The regulator considered above is called a single regulator. The voltages U_1 and U_2 of such a regulator differ from each other both in magnitude and in phase. It is therefore impossible to carry out the regulation process when the regulator operates in parallel with an ordinary transformer. In addition, appreciable torques appear on the shaft of a single regulator in certain rotor positions for which it is necessary to design the parts for driving and braking the regulator.

To eliminate these disadvantages, two single regulators can be connected into a double induction regulator as shown in Fig. 18-14a. The rotors are fixed on the same shaft and their windings are connected to the circuit in parallel. The phase sequence of the rotor and stator windings in one of the regulators is reversed by interchanging the ends of two phases (Fig. 18-14a) so that when the rotor of one regulator turns in the direction of its field rotation, the rotor of the other regulator turns opposite to the direction of its field rotation. If the rotors turn in one direction, the stator e.m.f.s shift in opposite directions

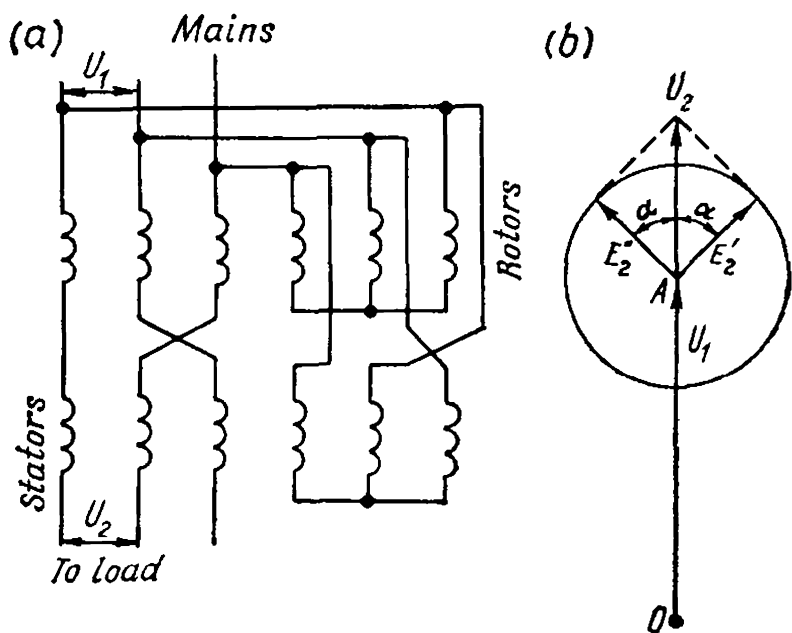


Fig. 18-14. Double induction regulator:
a—connections; b—vector diagram

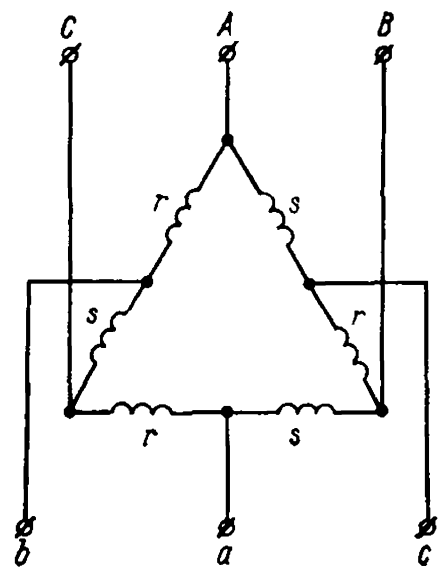


Fig. 18-15. Induction regulator with delta-connected windings

(Fig. 18-14b); if we disregard the voltage drops in the regulator, the voltage U_2 will always be in phase with the voltage U_1 . The torques produced by each of the single regulators are in opposition to each other and, consequently, the resultant torque on the shaft of the double regulator is zero.

Induction Regulator with Common Delta-Connected Windings. The stator and rotor windings of a locked-rotor induction machine, connected in series by phases, can be electrically joined into a common triangle (Fig. 18-15) and the vertices A, B, C of the triangle connected to a supply circuit with $U_1 = \text{const}$. When the rotor of the machine turns, the voltage U_2 between the terminals a, b and c will change in magnitude and, in the general case, also in phase.

If the number of effective rotor and stator turns are equal, i.e., $\omega_s k_{w.s} = \omega_r k_{w.r}$, and we neglect the voltage drops in the leakage resistances of the windings, the shift of the voltage U_2 with respect to

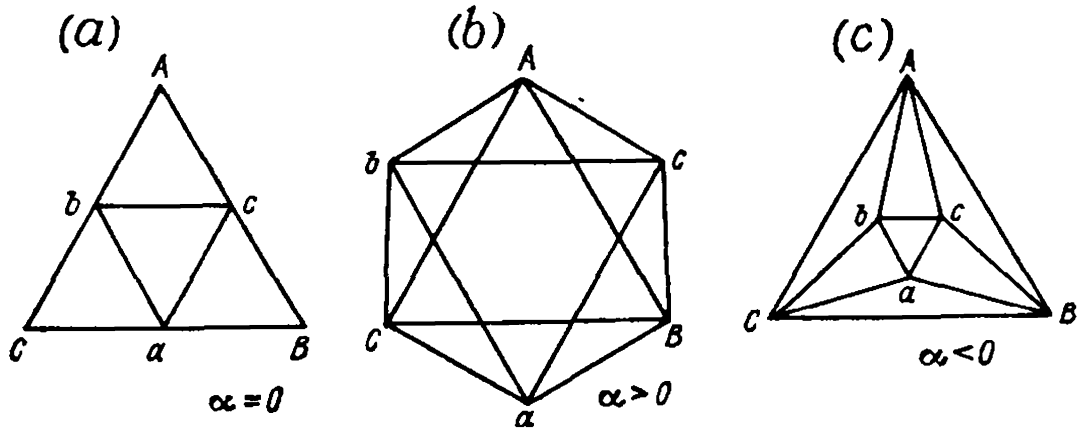


Fig. 18-16. Diagram of voltages of an induction regulator with delta-connected windings having equal number of turns in stator and rotor

U_1 will be 180° or 0 . Figure 18-16 shows diagrams of the regulator voltages in this case for several values of angle of rotation α of the regulator rotor.

The triangle ABC in Fig. 18-16 is a system of invariable line voltages on the primary side. For any values of the angle α , the vector sum of the stator and rotor phase e.m.f.s \dot{E}_s and \dot{E}_r of one side of the triangle must be equal (with opposite sign) to the primary line voltage of this side. With a change in the angle α , a change equal to this angle will also occur in the phase displacement of the

e.m.f.s \dot{E}_s and \dot{E}_r , and in their magnitudes. As a result, the size of triangle abc of the secondary voltages will change.

A change proportional to the e.m.f.s E_s and E_r will also occur in the main magnetic flux of the regulator, while in the single three-phase regulator it remains practically constant.

Phase Shifter. The phase shifter is an induction machine with a locked rotor made in accordance with the diagram in Fig. 18-17. By turning the rotor relative to the stator we smoothly change the phase of the rotor e.m.f. without changing its magnitude. This type of phase shifter is widely used in laboratory practice.

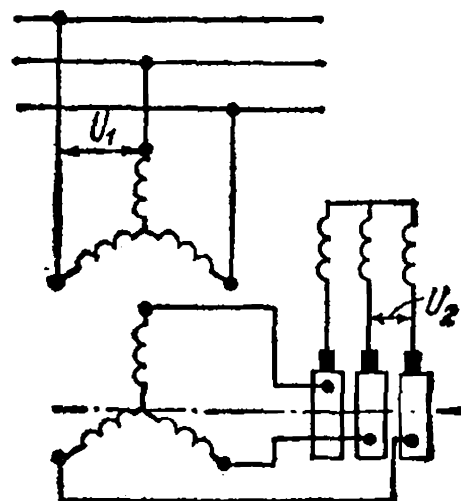


Fig. 18-17. Phase shifter

Chapter

19

THREE-PHASE INDUCTION MACHINE WITH ROTOR RUNNING

19-1. Principal Phenomena

The induction machine may be considered as a transformer not only with the rotor locked, but also when it is running. Here the machine is a universal transformer, i.e., a transformer in which not only the voltages, currents and number of phases undergo transformation, but also the frequency and the kind of energy. As a result, having written the e.m.f. equations of an induction machine and solved them for the current, we obtain essentially the same equivalent circuits as for a transformer. Being descriptive and simple, the equivalent circuits are very useful for solving a number of problems, including that of circle diagram construction. Here we must make the following assumptions:

(a) only the first harmonics of the variables (voltages, currents, etc.) are taken into account, as previously, since they embrace and determine the main group of processes in an induction machine;

(b) the processes occurring in the rotor with the latter running at any speed will be considered irrespective of the cause which makes the rotor run, to make the analysis as generalized as possible.

Suppose the stator of an induction machine is connected to a circuit with a given voltage U_1 and a constant frequency f_1 . The main flux Φ_m , rotating at a speed $n_1 = f_1 : p$, produces the fundamental e.m.f. E_1 in the stator winding. In the same winding the primary leakage flux $\Phi_{\sigma 1}$ induces the leakage e.m.f. $\dot{E}_{\sigma 1} = -jI_1x_2$. If, in addition, we take account of the stator winding resistance r_1 , it can be seen that the stator of an induction machine with the rotor running has the same e.m.f.s as in a locked-rotor machine, in accordance with this, the e.m.f. equation is written identically in both cases (see above, Sec. 18-5), namely,

$$\dot{U}_1 = -\dot{E}_1 + \dot{I}_1 Z_1 \quad (19-1)$$

According to the assumptions, the rotor can run either in the same direction as the field, or in the opposite direction. In the first case we shall assume the rotor speed n to be positive, in the second, negative.

Let us consider what occurs in the rotor, supposing its circuit to be open meanwhile; for this purpose the sliding contact of the rheostat in Fig. 18-1 is shifted to position 1.

Frequency of the E.M.F. Induced in the Rotor Winding. When a rotor runs at a speed n in a magnetic field rotating at a speed n_1 , everything takes place as if the rotor were stationary and the flux Φ_m rotated with respect to the rotor at a speed

$$n_2 = n_1 - n$$

The frequency of the e.m.f. induced in the rotor winding is therefore equal to

$$f_2 = pn_2 = p(n_1 - n) = n_1 p \frac{n_1 - n}{n_1} = f_1 s \quad (19-2)$$

where f_1 is the supply circuit frequency and s is the slip [see formula (1-3)]. We see that with a given frequency the e.m.f. in the rotor changes in direct proportion to the slip. For brevity, the frequency f_2 is referred to as the slip frequency.

In accordance with the slip variation range from $s = -\infty$ in generator duty to $s = +\infty$ in electromagnetic brake duty ($n < 0$), the frequency f_2 also varies from $f_2 = -\infty$ to $f_2 = +\infty$. The plus and minus signs at a frequency f_2 have an arbitrary meaning, determining the change in the sign of the induced e.m.f. when passing from one duty to another.

Rotor E.M.F. According to the general expression [equation (2-37)], for the rotor e.m.f. we have

$$E_{2s} = 4.44 f_2 \omega_2 k_{w2} \Phi_m = 4.44 f_1 s \omega_2 k_{w2} \Phi_m = E_2 s \quad (19-3)$$

or, if the rotor winding is reduced to the stator winding,

$$E'_{2s} = E'_2 s \quad (19-4)$$

i.e., for a given main flux Φ_m the e.m.f. induced in the rotor during rotation is equal to the e.m.f. E_2 with the rotor locked multiplied by the slip. If, for example, at $n = 0$ with the rotor circuit open we obtain across the rings a voltage $U_2 = E_2 = 600$ V, by gradually increasing the speed of the rotor in the direction of the field from $n = 0$ to $n = n_1$ we obtain a linear variation of E_{2s} from $E_{2s} = 600$ V to $E_{2s} = 0$; when $n > n_1$ the e.m.f. E_{2s} begins to rise, having a negative value, i.e., its phase changes with respect to the initial phase by 180° .

Rotor Winding Resistance. Suppose the rotor circuit is closed through an additional resistance; for this we shift the sliding contact of the rheostat inserted in the rotor circuit from position 1 to position 3 (Fig. 18-1). Assume this to be a resistance, and not a reactance, since it corresponds more closely to the actual service conditions of an induction machine with slip rings. The resistance of the rotor circuit will then be $R_2 = r_2 + r_{add}$, where r_2 is the resistance of the rotor winding proper and r_{add} is the additional resistance, connected to the rotor circuit via slip rings.

If the phenomenon of skin-effect in the rotor winding conductors and the change in the winding resistance due to the change in temperature are disregarded, it may be assumed that

$$R_2 = r_2 + r_{add} = \text{const}$$

or, reducing these resistances to the stator winding

$$R'_2 = r'_2 + r'_{add} = \text{const}$$

The leakage inductive reactance of the locked rotor $x_2 = 2\pi f_1 L_{\sigma 2}$, where $L_{\sigma 2}$ is the inductance due to the secondary leakage flux. Since the leakage fluxes pass mainly through air, $L_{\sigma 2} \cong \text{const}$. Consequently, the inductive reactance of the rotor during rotation is

$$x_{2s} = 2\pi f_2 L_{\sigma 2} = 2\pi f_1 s L_{\sigma 2} = x_2 s \quad (19-5)$$

or, when reduced to the stator winding

$$x'_{2s} = x'_2 s \quad (19-6)$$

that is, the inductive reactance of a rotor winding during rotation is equal to that of the locked rotor multiplied by the slip.

19-2. Rotor E.M.F. Equation and Current

If the rotor circuit is closed, the current I_2 flows through it, produces a leakage flux $\Phi_{\sigma 2}$ (Fig. 19-1a) and meets a resistance r_2 . Accordingly, in the rotor winding there exists an e.m.f. $\dot{E}_{2s} = \dot{E}_2 s$ produced by the main flux Φ_m and a leakage e.m.f. $\dot{E}_{\sigma 2} = -j\dot{I}_2 x_{2s} = -j\dot{I}_2 x_2 s$. Then, according to Kirchhoff's second law

$$\dot{E}_{2s} + \dot{E}_{\sigma 2} = \dot{E}_2 s - j\dot{I}_2 x_2 s = \dot{I}_2 r_2$$

or

$$\dot{E}_2 s = \dot{I}_2 Z_{2s} \quad (19-7)$$

where $Z_{2s} = r_2 + jx_{2s}$ is the impedance of the real rotor.

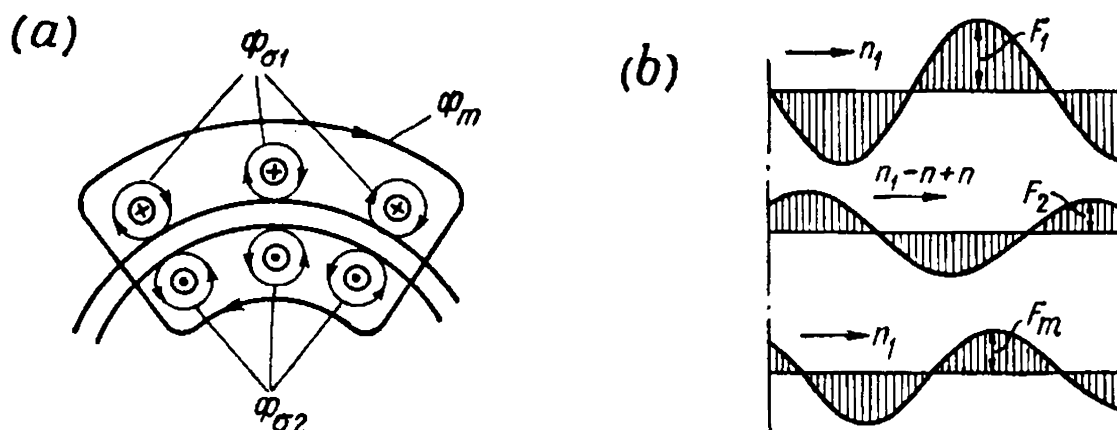


Fig. 19-1. Fluxes and magnetizing forces of an induction machine with rotor running

Consequently

$$\dot{I}_2 = \frac{\dot{E}_{2s}}{Z_{2s}} = \frac{\dot{E}_{2s}}{r_2 + jx_2s} \quad (19-8)$$

and

$$I_2 = \frac{E_{2s}}{\sqrt{r_2^2 + x_2^2 s^2}} \quad (19-9)$$

If the rotor winding is reduced to the stator winding, then

$$\dot{E}'_{2s} = \dot{I}'_2 Z'_{2s} \quad (19-10)$$

where $Z'_{2s} = r'_2 + jx'_2s$ is the impedance of the equivalent rotor.

Hence

$$\dot{I}'_2 = \frac{\dot{E}'_{2s}}{r'_2 + jx'_2s} \quad (19-11)$$

and

$$I'_2 = \frac{E'_{2s}}{\sqrt{r'^2_2 + x'^2_2 s^2}} \quad (19-12)$$

19-3. Speed of Rotation of Rotor Magnetizing Force

In flowing through the rotor winding, the current I_2 produces a magnetizing force F_2 rotating with respect to the rotor at a speed n_2 which corresponds to the rotor current frequency f_2 . Furthermore, the rotor itself runs at a speed n . Consequently, the rotor magnetizing force F_2 runs with respect to some fixed point in space and, also, therefore, with respect to the stator at a speed $n_2 + n$. But

$$n_2 = \frac{f_2}{p} = \frac{f_1 s}{p} = n_1 s = n_1 \frac{n_1 - n}{n_1} = n_1 - n$$

Thus

$$n_2 + n = n_1 - n + n = n_1$$

that is, the rotor magnetizing force always rotates in space (i.e., irrespective of operating conditions) at the same speed and in the same direction as the stator magnetizing force. We again recall that, in speaking of the magnetizing forces of an induction machine, we agreed to consider only their first harmonics.

19-4. Magnetizing Force Equation and Flux Vector Diagrams of an Induction Machine

Magnetizing Force Equation. Since in an induction machine the stator and rotor magnetizing forces F_1 and F_2 both rotate in space at the same speed and in the same direction, it may be assumed that they are stationary with respect to each other and, consequently, produce a

common rotating sine wave of the magnetizing force F_m . The sine wave of F_2 must be shifted in space with respect to that of F_1 by an angle that makes the resultant magnetizing force F_m sufficient to produce the main magnetic flux Φ_m required for the conditions of e.m.f. equilibrium.

Thus

$$\dot{F}_1 + \dot{F}_2 = \dot{F}_m \quad (19-12a)$$

Substituting here for the magnetizing forces their values from equation (4-36), we get

$$m_1 \omega_1 k_{w1} \dot{I}_1 + m_2 \omega_2 k_{w2} \dot{I}'_2 = m_1 \omega_1 k_{w1} \dot{I}_m \quad (19-12b)$$

or

$$\dot{I}_1 + \frac{m_2 \omega_2 k_{w2}}{m_1 \omega_1 k_{w1}} \dot{I}_2 = \dot{I}_1 + \frac{1}{k_i} \dot{I}_2 = \dot{I}_1 + \dot{I}'_2 = \dot{I}_m \quad (19-12c)$$

We see that the magnetizing force equations for an induction machine with the rotor running repeat the magnetizing force equations (Fig. 18-7a and b) for an induction machine with $n = 0$. Accordingly, the magnetizing force picture in Fig. 19-1b repeats the picture of the magnetizing force in Fig. 18-8, with the only difference that the speed in space n_1 of the magnetizing force F_2 in Fig. 19-1b is made up of the speed $n_2 = n_1 - n$ of the magnetizing force F_2 with respect to the rotor and the speed n of the rotor proper.

The conclusion reached above is true for any duty of an induction machine. When it operates as a motor, the speed n_2 is positive, i.e., the rotor magnetizing force rotates in the same direction as the rotor. When the machine operates as a generator, the speed n_2 is negative, i.e., the rotor magnetizing force runs in a direction opposite to rotor rotation. The same occurs when the machine operates as an electromagnetic brake.

Vector Diagrams of an Induction Machine as a Particular Case of a Transformer. The mutual inductance flux Φ is determined by the value of the magnetizing current \dot{I}_m which is equal to the vector sum of the current \dot{I}_1 and the equivalent current \dot{I}'_2 . Neglecting the losses in the steel, it may be assumed that the flux $\Phi = \Phi_m$ is in phase with the current \dot{I}_m . Let us introduce into the discussion the fictitious fluxes $\dot{\Phi}_1$ and $\dot{\Phi}_2$ coinciding in phase with the currents \dot{I}_1 and \dot{I}_2 and proportional to these currents, so that

$$\frac{\dot{\Phi}_m}{\dot{I}_m} = \frac{\dot{\Phi}_1}{\dot{I}_1} = \frac{\dot{\Phi}_2}{\dot{I}_2}$$

Here it may be assumed that the flux $\dot{\Phi}_m$ is equal to the vector sum of the fluxes $\dot{\Phi}_1$ and $\dot{\Phi}_2$

$$\dot{\Phi}_m = \dot{\Phi}_1 + \dot{\Phi}_2$$

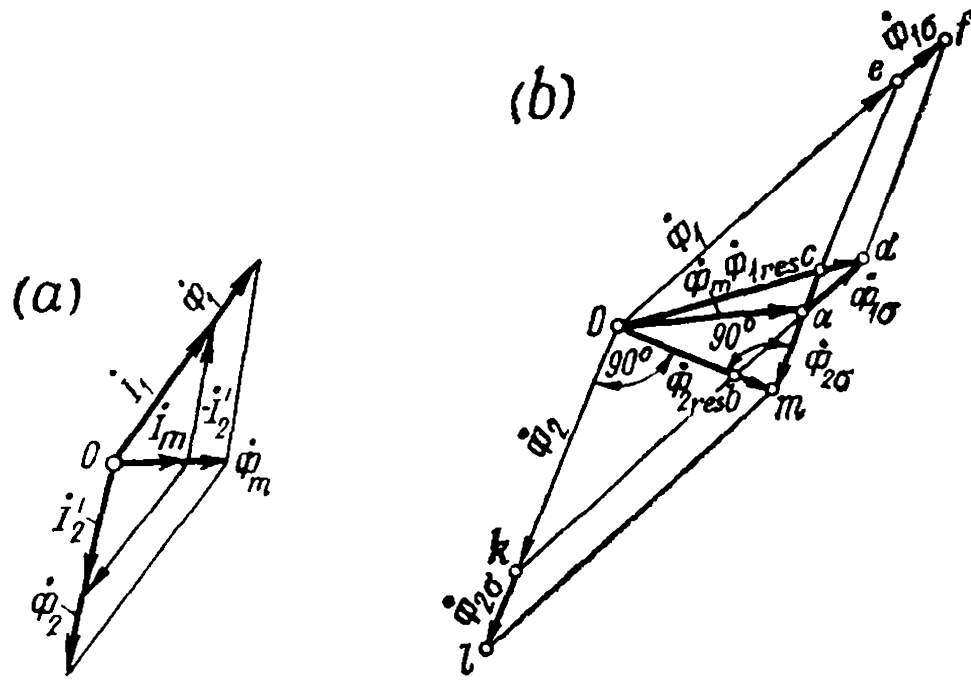


Fig. 19-2. Current and flux vector diagrams of an induction machine as a particular case of a transformer

The vector diagram of currents and fluxes will have the form shown in Fig. 19-2a.

It follows from the current vector diagram that I_2' is the primary current component which compensates the magnetic action of the secondary circuit on the primary circuit.

Since the flux is equal to the magnetizing force divided by the reluctance, then the following relations can be written for all the fluxes indicated above:

$$\begin{aligned}\dot{\Phi}_m &= \frac{\dot{F}_m}{R_m} = \frac{\omega_1 \dot{I}_m}{R_m} \\ \dot{\Phi}_1 &= \frac{\dot{F}_1}{R_m} = \frac{\omega_1 \dot{I}_1}{R_m} \\ \dot{\Phi}_2 &= \frac{\dot{F}_2}{R_m} = \frac{\omega_2 \dot{I}_2}{R_m}\end{aligned}$$

where R_m is the reluctance of the main circuit along the mutual inductance path.

Let us now plot the vector diagram for the fluxes of an induction machine, introducing into it the leakage fluxes $\dot{\Phi}_{1\sigma}$ and $\dot{\Phi}_{2\sigma}$.

The primary leakage flux is

$$\dot{\Phi}_{1\sigma} = \frac{\omega_1 \dot{I}_1}{R_{1\sigma}} \tag{19-13a}$$

and the secondary

$$\dot{\Phi}_{2\sigma} = \frac{\omega_2 \dot{I}_2}{R_{2\sigma}} \tag{19-13b}$$

where $R_{1\sigma}$ and $R_{2\sigma}$ are the reluctances of the primary and secondary circuits along their leakage paths. Since $\dot{\Phi}_1$ and $\dot{\Phi}_2$ are in phase with \dot{I}_1 , they are consequently in phase with each other and can therefore be summated algebraically. Correspondingly, $\dot{\Phi}_2$ and $\dot{\Phi}_{2\sigma}$ are in phase with \dot{I}_2 and can also be summated algebraically.

By vector summation of the total flux ($\dot{\Phi}_1 + \dot{\Phi}_{1\sigma}$) and the flux $\dot{\Phi}_2$, we obtain the resultant flux $\dot{\Phi}_{1res}$ and of the total flux ($\dot{\Phi}_1 + \dot{\Phi}_{2\sigma}$) and the flux $\dot{\Phi}_2$ —the resultant flux $\dot{\Phi}_{2res}$. The vector diagram of all the fluxes indicated above is presented in Fig. 19-2b. From this diagram it follows, on the other hand, that

$$\begin{aligned}\dot{\Phi}_{1res} &= \dot{\Phi}_m + \dot{\Phi}_{1\sigma} \\ \dot{\Phi}_{2res} &= \dot{\Phi}_m + \dot{\Phi}_{2\sigma}\end{aligned}$$

The vector diagram of Fig. 19-2b makes it possible to separate the actually existing fluxes in an induction machine from the fictitious fluxes necessary for similarity in diagram construction. By comparing the flux picture in Fig. 19-2a with the vector diagram in Fig. 19-2b, it is easy to carry out the following division of the fluxes.

The mutual inductance flux $\dot{\Phi}_m$ exists in the air-gap between the stator and rotor. The leakage flux $\dot{\Phi}_{1\sigma}$ exists along the leakage paths of the primary circuit, the leakage flux $\dot{\Phi}_{2\sigma}$, along the secondary circuit leakage paths. The flux $\dot{\Phi}_{1res}$ is the total flux piercing the primary winding of the machine, and the flux $\dot{\Phi}_{2res}$ is the total flux piercing the secondary winding of the machine. The other fluxes $\dot{\Phi}_1$ and $\dot{\Phi}_2$ are fictitious. $\dot{\Phi}_1$ is the mutual inductance flux which would exist if the primary current were equal to the current \dot{I}_1 and the secondary circuit were open. Here the mutual inductance reluctance R_m must remain the same as with the resultant magnetizing current \dot{I}_m ; similarly, $\dot{\Phi}_2$ corresponds to the current \dot{I}_2 when $\dot{I}_1 = 0$ and the reluctance R_m remains invariable. The actually existing fluxes are shown in the diagram of Fig. 19-2b by heavy lines, the fictitious fluxes, by thin lines.

The introduction of the concept of fictitious fluxes $\dot{\Phi}_1$ and $\dot{\Phi}_2$ makes it possible not only to construct a complete vector diagram of the fluxes (Fig. 19-2b) but also to introduce the concept of leakage factors, which play an important part in the study of the processes of induction machine operation. The primary leakage factor τ_1 is equal to the ratio of $\dot{\Phi}_{1\sigma}$ to the flux $\dot{\Phi}_1$ which would be set up at the same current \dot{I}_1 but with the reluctance of the mutual inductance circuit R_m corresponding to the normal magnetizing current \dot{I}_m . Similarly, the secondary leakage factor τ_2 is equal to the ratio of $\dot{\Phi}_{2\sigma}$ to $\dot{\Phi}_2$.

Thus

$$\tau_1 = \frac{\dot{\Phi}_{1\sigma}}{\dot{\Phi}_1} = \frac{R_m}{R_{1\sigma}} = \frac{\lambda_{1\sigma}}{\lambda_m} = \frac{x_1}{x_m}$$

and

$$\tau_2 = \frac{\dot{\Phi}_{2\sigma}}{\dot{\Phi}_2} = \frac{R_m}{R_{2\sigma}} = \frac{\lambda_{2\sigma}}{\lambda_m} = \frac{x'_2}{x_m}$$

since

$$x_1 \equiv \lambda_{1\sigma}; \quad x_2 \equiv \lambda_{2\sigma} \quad \text{and} \quad x_m \equiv \lambda_m$$

where $\lambda_{1\sigma}$, $\lambda_{2\sigma}$ and λ_m are the permeances of the leakage paths and of the main circuit.

The full leakage factor τ , the concept of which was introduced by Heyland, is [153]

$$\tau = \tau_1 + \tau_2 + \tau_1\tau_2$$

19-5. Equivalent Circuits of an Induction Machine

It is often more convenient to consider not a real induction machine representing a system of two (or in the general case several) electromagnetically linked circuits, but an equivalent electrical system, constructing for this purpose a corresponding equivalent circuit similar to the equivalent circuit of a transformer.

Actual Physically Existing Equivalent Circuit of the Primary and Secondary Circuits. The physical picture of the fluxes in an induction machine with the rotor running (Fig. 19-1) similar to the flux picture for a short circuit (Fig. 18-3) makes it possible to represent it in the form of an equivalent circuit (Fig. 19-3). The primary and secondary circuits of the machine are transformer-coupled by means of the mutual inductance flux Φ_m , inducing in the secondary circuit, when the rotor is running, the e.m.f. $E_{2s} = E_2s$. This e.m.f. produces in the secondary circuit the current determined by equation (19-8).

Physical Equivalent Circuit Referred to a Stationary Rotor. The expression for the current I_2 according to equation (19-8) can be transformed as follows:

$$I_2 = \frac{\dot{E}_2 s}{r_2 + jx_2 s} = \frac{\dot{E}_2}{\frac{r_2}{s} + jx_2} \quad (19-14)$$

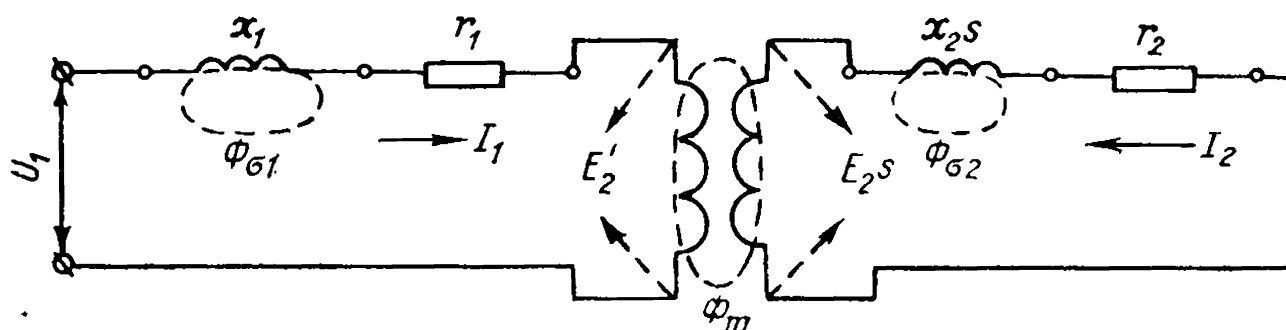


Fig. 19-3. Physical picture of the primary and secondary circuit coupling

The new expression for I_2 has a new physical meaning which may be formulated as follows. In the secondary circuit, there now exists, instead of the e.m.f. $\dot{E}_2 s$ having the frequency $f_1 s$ when the rotor is running, the e.m.f. \dot{E}_2 with the frequency f_1 when the rotor is locked. Correspondingly, instead of the reactance $x_2 s$ with a running rotor, there acts in the secondary circuit the reactance x_2 with a locked rotor. To have a current I_2 of the same value and phase with respect to E_2 flow in the secondary circuit with the rotor locked, it is necessary, instead of r_2 acting when the rotor is running, to insert a new resistance equal to

$$\frac{r_2}{s} = r_2 + r_2 \frac{1-s}{s}$$

Thus, if with the rotor locked it is desirable to have the same current in it, an additional resistance must be inserted into the secondary circuit equal to

$$r_2 \frac{1-s}{s}$$

In both cases the phase shift of the current from the e.m.f. which produces it will be the same. Indeed, in the first case

$$\tan \psi_2 = \frac{x_2 s}{r_2}$$

and in the second

$$\tan \psi_2 = \frac{x_2}{\frac{r_2}{s}} = \frac{x_2 s}{r_2}$$

Evidently, the stator current I_1 here also remains the same in magnitude and in phase and, consequently, the power consumed from the circuit or delivered to it will not change. Since the electric losses in the primary and secondary windings remain as before, the power developed by the motor on its shaft during rotation will be equal to the power consumed in the additional resistance $r_2 \frac{1-s}{s}$. This concept makes it legitimate to analyse, instead of a running motor, a motor at standstill and having the indicated additional resistance, the power consumed in the latter being equal to the mechanical power developed by the rotor during its rotation.

When an induction machine operates as a generator ($-\infty < s < 0$), or acts as an electromagnetic brake ($1 < s < \infty$), the additional resistance $r_2 \frac{1-s}{s}$ becomes negative. Physically, this corresponds to the fact that under these conditions the machine takes mechanical power from the shaft equal to

$$P = m_2 I_2^2 r_2 \frac{1-s}{s}$$

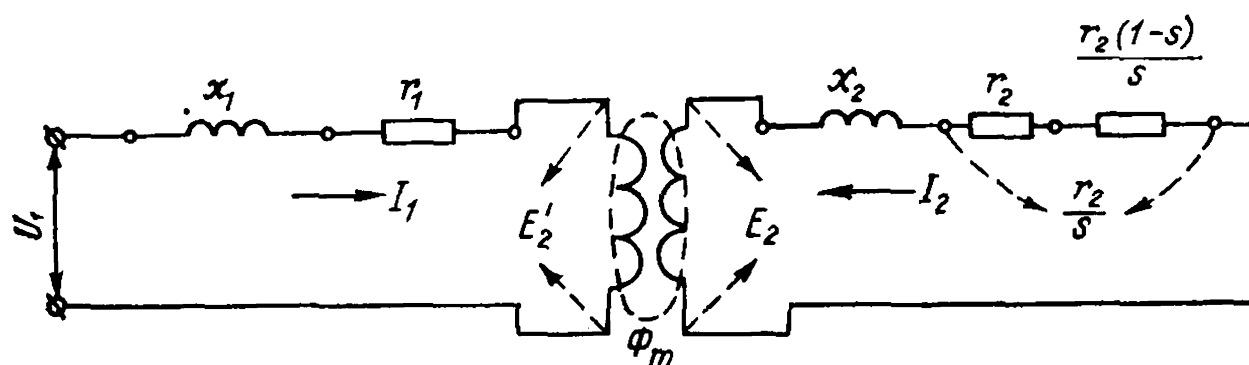


Fig. 19-4. Physical equivalent circuit reduced to locked rotor

and, in comparison with motoring, the direction of power flow is now reversed, owing to which the power P must also be considered negative. It is hence possible to imagine that in these operating conditions an a.c. generator with a frequency f_1 is connected to the equivalent rotor circuit which develops a power per phase equal to

$$I_2'^2 r_2' \frac{1-s}{s} = I_2^2 r_2 \frac{1-s}{s}$$

The equivalent circuit in Fig. 19-3 can be replaced by the equivalent circuit in Fig. 19-4 for a static transformer with an additional resistance $r_2 \frac{1-s}{s}$. This makes it possible to study the circuit in Fig. 19-4 instead of the circuit for a machine with a running rotor in Fig. 19-3 and apply all the conclusions made from a study of the second circuit to the first circuit.

Equivalent Circuit of Induction Machine as a Transformer. To convert the equivalent circuit in Fig. 19-4 into a transformer equivalent circuit, the secondary circuit should be reduced to the primary one as was done in Sec. 18-3. Here the equivalent quantities, denoted by a prime, are expressed according to Sec. 18-3 in terms of the non-reduced quantities as follows

$$\begin{aligned} E_2' &= k E_2; & I_2' &= \frac{I_2}{k_i}; \\ x_2' &= k k_i x_2 = k_r x_2; & r_2' &= k k_i r_2 = k_r r_2 \end{aligned}$$

The secondary current value I_2' reduced to the primary circuit is determined through the equivalent e.m.f. value E_2' and the equivalent values of the resistances of the secondary circuit as follows:

$$I_2' = \frac{\dot{E}_2'}{\frac{r_2'}{s} + jx_2'} = \frac{\dot{E}_2'}{Z_2'} \quad (19-15)$$

where

$$Z_2' = \frac{r_2'}{s} + jx_2' \quad (19-16)$$

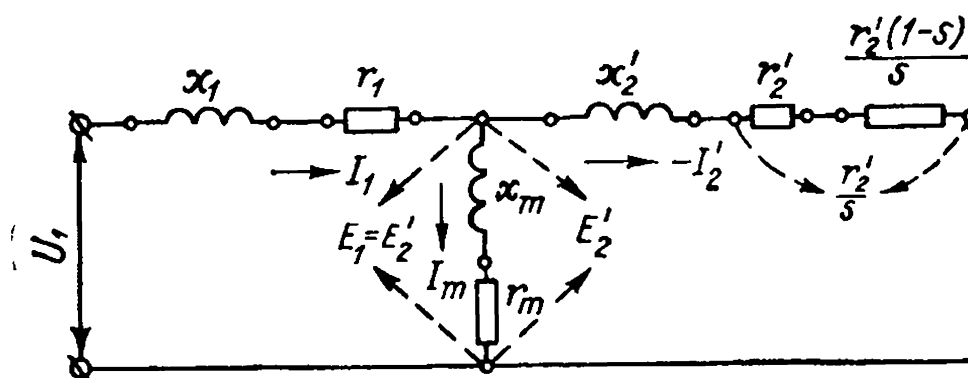


Fig. 19-5. Equivalent circuit of an induction machine as a transformer

The phase shift of the equivalent secondary current I_2' from the equivalent secondary e.m.f. \dot{E}_2' is equal to the displacement of the current \dot{I}_2 from the e.m.f. \dot{E}_2 , as follows from what is described in Sec. 19-5.

Let us now show the complete equivalent circuit for an induction machine. Since we obtain the same voltage $E_1 = E_2'$ across the magnetizing circuit terminals in the primary and secondary circuits, the common equivalent points of both circuits in Fig. 19-4 can be superposed and the equivalent circuit shown in Fig. 19-5 obtained.

In the circuit in Fig. 19-5 the magnetizing branch circuit contains a reactance x_m of mutual induction of the equivalent secondary circuit and primary circuit, equal to the self-induction reactance of the stator phase due to the air-gap flux fundamental harmonic [see Sec. 5-1, equation (5-5)], and a resistance r_m taking into account the losses in the steel. The current in the magnetizing branch of the circuit in Fig. 19-5 is equal to the vector sum of the currents \dot{I}_1 and \dot{I}_2'

$$\dot{I}_m = \dot{I}_1 + \dot{I}_2' \quad (19-17)$$

consequently,

$$\dot{E}_1 = \dot{E}_2' = \dot{I}_m (r_m + jx_m) = \dot{I}_m Z_m \quad (19-18)$$

Since the reactances and resistances in the circuit given in Fig. 19-5 are arranged in the form of the letter T, this circuit is referred to as a T-circuit.

Equivalent Circuit of Induction Machine with the Magnetizing Branch Circuit Brought out to the Power-Circuit Terminals. Unlike a transformer, which only converts electric energy of one voltage into that of another voltage, the induction motor is a device which converts electric energy into mechanical energy. When the load drops, the terminal voltage usually remains constant, while the mutual inductance flux and the e.m.f. $E_1 = E_2'$ corresponding to it and existing across the magnetizing branch circuit terminals in Fig. 19-5, with the change in load under the influence of the voltage drop $\dot{I}_1 Z_1$ in the primary, both undergo a change.

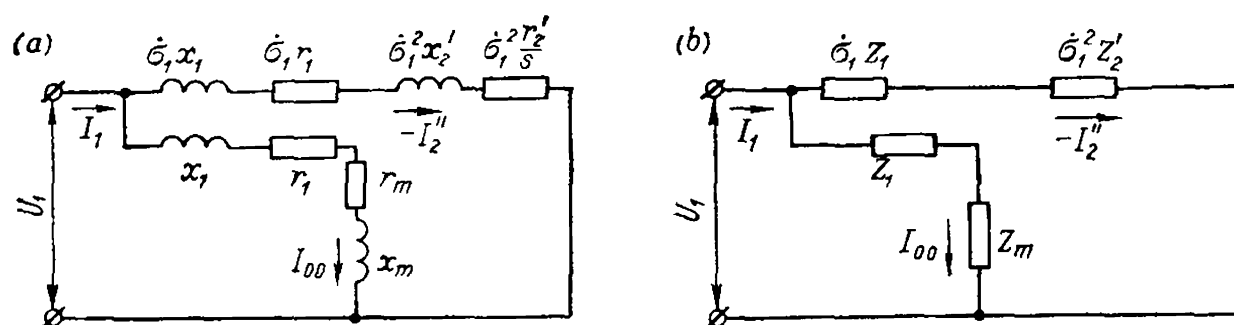


Fig. 19-6. Exact equivalent circuits with magnetizing branch circuit brought out to primary terminals

An equivalent L-circuit has appreciable advantages in investigating the processes in an induction machine over the T-circuit used in studying transformer processes [197, 212].

In transformers the magnetizing circuit is between the primary and secondary sides, and makes it possible to study the phenomena involved when the direction of the energy flux changes.

In contrast to a transformer, an induction motor, being a consumer of power, must be considered with a constant voltage across its terminals, i.e., with $U_1 = \text{const}$. Here, with an equivalent T-circuit, the currents change not only in the main circuit, but also in the branch magnetizing circuit, and for this reason all the currents I_1 , I_2 and I_m depend on the duty, i.e., they change with a change in the slip and in accordance with the speed. With an equivalent L-circuit, with $U_1 = \text{const}$, the current I_{00} in the branch circuit remains constant when the slip s changes, and only the current in the main circuit changes.

Generator and braking duties in an induction machine are also studied with a constant voltage across the terminals ($U_1 = \text{const}$), and therefore the equivalent L-circuit has the same advantages for these duties as for motoring.

Let us determine the main circuit current— I_2'' of the modified circuit (Fig. 19-6) as the vector difference of the main circuit current I_1 and the ideal no-load current I_{00} for $s = 0$ in the T-circuit of a transformer.

According to Fig. 19-5, we have

$$I_1 = \frac{\dot{U}_1}{Z_1 + \frac{Z_2' Z_m}{Z_2' + Z_m}} = \frac{Z_2' + Z_m}{Z_1 Z_2' + Z_1 Z_m + Z_2' Z_m} \dot{U}_1 \quad (19-19)$$

and the magnetizing circuit current with $s = 0$ will be

$$I_{00} = \frac{\dot{U}_1}{Z_1 + Z_m} = \frac{\dot{U}_1}{Z_m \left(1 + \frac{Z_1}{Z_m} \right)} = \frac{\dot{U}_1}{Z_m \dot{\sigma}_1} = \frac{\dot{U}_1}{Z_m'} \quad (19-20)$$

where

$$\dot{\sigma}_1 = 1 + \frac{Z_1}{Z_m} \quad (19-21)$$

and

$$Z'_m = \dot{\sigma}_1 Z_m = Z_1 + Z_m \quad (19-22)$$

The main circuit current for the modified circuit is

$$\begin{aligned} -j_2'' = i_1 - i_{00} &= \dot{U}_1 \left(\frac{Z'_2 + Z_m}{Z_1 Z'_2 + Z_1 Z_m + Z'_2 Z_m} - \frac{1}{Z_1 + Z_m} \right) = \\ &= \frac{\dot{U}_1 Z_m^2}{(Z_1 + Z_m)(Z_1 Z'_2 + Z_1 Z_m + Z'_2 Z_m)} = \frac{\dot{U}_1}{Z_1 \left(1 + \frac{Z_1}{Z_m} \right) + Z'_2 \left(1 + \frac{Z_1}{Z_m} \right)^2} = \\ &= \frac{\dot{U}_1}{Z_1 \dot{\sigma}_1 + Z'_2 \dot{\sigma}_1^2} = \frac{\dot{U}_1}{Z_1'' + Z_2''} \quad (19-23) \end{aligned}$$

where

$$Z_1'' = Z_1 \dot{\sigma}_1, \quad Z_2'' = Z'_2 \dot{\sigma}_1^2 \quad (19-24)$$

The relations obtained correspond to the equivalent L-type circuit in Fig. 19-6.

The current in the main part of the equivalent circuit (Fig. 19-5) is equal to

$$\begin{aligned} -j_2' &= \frac{\dot{U}_1 - i_1 Z_1}{Z'_2} = \frac{\dot{U}_1}{Z'_2} \left[1 - \frac{(Z'_2 + Z_m) Z_1}{Z_1 Z'_2 + Z_1 Z_m + Z'_2 Z_m} \right] = \\ &= \frac{\dot{U}_1}{Z_1 + Z'_2 \left(1 + \frac{Z_1}{Z_m} \right)} = \frac{\dot{U}_1}{Z_1 + Z'_2 \dot{\sigma}_1} = \frac{\dot{U}_1 \dot{\sigma}_1}{Z_1'' + Z_2''} \quad (19-25) \end{aligned}$$

Therefore, the ratio of the currents in the main parts of the T- and L-circuits will be

$$\frac{j_2'}{j_2''} = 1 + \frac{Z_1}{Z_m} = \dot{\sigma}_1 \quad (19-26)$$

The equivalent secondary impedance of the main part of the L-type equivalent circuit for synchronous no-load operation, corresponding to a slip $s=0$, will be $Z'_2 \dot{\sigma}_1^2 = \infty$, and as a result the current in the main part $j_2''=0$ and the primary current $i_1 = i_{00}$. Consequently, the no-load current of the modified circuit is equal to that of the fundamental T-circuit with $s=0$.

The correction factor $\dot{\sigma}_1$ modifies the fundamental parameters of the main and magnetizing parts of the circuit and the currents both in magnitude and in phase angle, but does not depend on the slip. Since $r_m \ll x_m$, the correction factor $\dot{\sigma}_1$ may be represented as

$$\dot{\sigma}_1 = 1 + \frac{Z_1}{Z_m} \cong \left(1 + \frac{x_1}{x_m} \right) - j \frac{r_1}{x_m} = \sigma_1 - j \frac{r_1}{x_m} \quad (19-27)$$

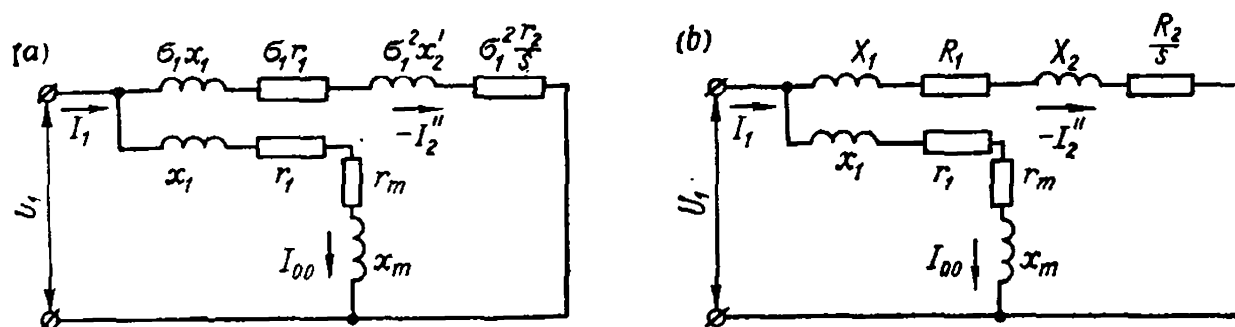


Fig. 19-7. Improved equivalent circuits with magnetizing part of circuit brought out to primary terminals

where

$$\sigma_1 = 1 + \frac{x_1}{x_m} = 1 + \frac{\Phi_{\sigma 1}}{\Phi_m} = 1 + \tau_1 \quad (19-28)$$

is the total leakage factor of the primary circuit, and $\tau_1 = \frac{\Phi_{\sigma 1}}{\Phi_m}$ is the leakage factor of the primary circuit.

Modifying of the basic T-circuit into an L-circuit discussed above is possible for any values of s within the range of $-\infty \leq s \leq +\infty$.

Since the current I_{00} is constant when $U_1 = \text{const}$, the determination of the current I_1 for different values of s and, correspondingly, different values of $-I_2''$ from the L-type circuit does not present any difficulties.

Seeing that the ratio $\frac{r_1}{x_m}$ is generally very small, we may disregard the imaginary part of σ_1 and take into account in most cases only its real part equal to

$$\sigma_1 = 1 + \frac{x_1}{x_m}$$

In real machines

$$\sigma_1 = 1.04 \text{ to } 1.08$$

Improved Equivalent L-Type Circuit of Induction Machine. In calculating the currents, power and other ratings of induction machines, sufficiently accurate results are obtained from the improved equivalent circuit (Fig. 19-7) derived from the precise L-type circuit (Fig. 19-6) if we assume the main circuit correction factor to be the real number σ_1 given by equation (19-28). Here

$$\left. \begin{aligned} \sigma_1 Z_1 &= \sigma_1 r_1 + j\sigma_1 x_1 = R_1 + jX_1 \\ \sigma_1^2 Z_2' &= \sigma_1^2 \frac{r_2'}{s} + j\sigma_1^2 x_2' = \frac{R_2}{s} + jX_2 \end{aligned} \right\} \quad (19-29)$$

where

$$\left. \begin{aligned} R_1 &= \sigma_1 r_1, & R_2 &= \sigma_1^2 r_2' \\ X_1 &= \sigma_1 x_1, & X_2 &= \sigma_1^2 x_2' \end{aligned} \right\} \quad (19-30)$$

Thus, the improved equivalent circuit (Fig. 19-7) will contain the primary and secondary reactances and resistances increased σ_1 and σ_1^2 times, respectively.

The impedance of the parallel circuit is, as before,

$$Z'_m = Z_1 + Z_m$$

and the relation between the currents in the main circuit is

$$I'_2 = \sigma_1 I''_2$$

i.e., I''_2 is in phase with I'_2 and equals $\frac{I'_2}{\sigma_1}$.

In the improved L-type equivalent circuit the total inductive reactance can be introduced into the main part of the circuit

$$X_{sh} = X_1 + X_2 = \sigma_1 x_1 + \sigma_1^2 x'_2 \quad (19-31)$$

and with $s=1$ also the total resistance

$$R_{sh} = R_1 + R_2 = \sigma_1 r_1 + \sigma_1^2 r'_2 \quad (19-32)$$

The resistance R_{sh} and reactance X_{sh} are approximately equal to the respective short-circuit values of the machine ($s=1$), since with $s=1$ the magnetizing circuit impedance $Z_1 + Z_m$ is high compared to the main circuit impedance $R_{sh} + jX_{sh}$.

The quantity X_{sh} is determined by the magnitude of the leakage flux of the machine.

Example 19-1. Determine the parameters of an improved L-type equivalent circuit (Fig. 19-7) of a three-phase induction motor with a phase-wound and a simple squirrel-cage rotor.

The electrical ratings for the motor with a phase-wound rotor are: power at the shaft $P_2 = 250$ kW, number of phases $m = 3$, frequency $f = 50$ Hz, number of poles $2p = 6$, line voltage $U_1 = 3000$ V, phase voltage with a star connection $U_{1ph} = 1730$ V, rated phase current $I_{ph.r} = 60$ A, no-load current $I_0 = 17.5$ A, efficiency $\eta_r = 90\%$, $\cos \varphi_r = 0.89$.

The design data of the motor with a phase-wound rotor are: $D_a = 730$ mm, $D = 523.3$ mm, $\tau = 275$ mm, $l_0 = 364$ mm, $l = 334$ mm, $Z_1 = 90$, $Z_2 = 72$, $w_1 = 210$, $w_2 = 24$, $\beta_1 = 0.8$, $\beta_2 = 1.0$, $q_1 = 5$, $q_2 = 4$; the inductive reactance of the stator winding $x_1 = 2.78 \Omega$, its resistance $r_1 = 0.68 \Omega$; the inductive reactance of the rotor winding $x_2 = 0.07 \Omega$, its resistance $r_2 = 0.00818 \Omega$.

The inductive reactance of the magnetizing circuit, from formula (5-5), is

$$\begin{aligned} x_m &= 2mf \frac{\mu_0 D_i l}{k_\delta k_\mu \delta} \cdot \frac{w_1^2 k_{w1}^2}{p^2} = \\ &= 2 \times 3 \times 50 \times \frac{1.26 \times 10^{-8} \times 52.3 \times 33.4}{1.6 \times 1.75 \times 0.1} \times \frac{210^2 \times 0.91^2}{3^2} = 95.6 \Omega \end{aligned}$$

Here the air-gap factor is taken equal to $k_\delta = 1.6$ and the saturation factor of the entire magnetic circuit $k_\mu = 1.75$.

The inductive reactance of the no-load circuit is

$$x_0 = x_m + x_1 = 95.6 + 2.78 = 98.4 \Omega$$

The no-load impedance is

$$Z_0 = \frac{x_0}{\sin \psi_0} \cong \frac{98.4}{0.99} = 99 \, \Omega$$

The resistance of the no-load circuit is

$$r_0 = r_1 + r_m = \sqrt{Z_0^2 - x_0^2} = \sqrt{99^2 - 98.4^2} = 11.68 \, \Omega$$

The resistance of the magnetizing circuit is

$$r_m = r_0 - r_1 = 11.68 - 0.68 = 11 \, \Omega$$

The no-load current is

$$I_0 = \frac{U_{1ph}}{Z_0} = \frac{1730}{99} = 17.5 \, \text{A}$$

The relative no-load current is

$$\frac{I_0}{I_{ph. r}} = \frac{17.5}{60} = 0.292$$

The losses in the steel at no-load are

$$p_{st} = 3 \cdot I_0^2 r_m = 3 \times 17.5^2 \times 11 = 10\,125 \, \text{W}$$

The total ideal no-load losses with $s=0$ are

$$p_0 = 3 \cdot I_0^2 (r_1 + r_m) = 3 \times 17.5^2 \times 11.68 = 10\,750 \, \text{W}$$

$$\cos \varphi_0 = \frac{p_0}{3U_{1ph}I_0} = \frac{10\,750}{3 \times 1730 \times 17.5} = 0.118$$

The reduced correction factor, by formula (19-28), is

$$\sigma_1 = 1 + \frac{x_1}{x_m} = 1 + \frac{2.78}{95.6} = 1.03$$

$$\sigma_1^2 = 1.03^2 = 1.06$$

The referred rotor winding inductive reactance and resistance are

$$x'_2 = 0.07 \times \left(\frac{210 \times 0.91}{24 \times 0.958} \right)^2 = 4.85 \, \Omega$$

$$r'_2 = 0.00818 \times \left(\frac{210 \times 0.91}{24 \times 0.958} \right)^2 = 0.57 \, \Omega$$

where $k_{w1}=0.91$ and $k_{w2}=0.958$ are the winding factors of the stator and rotor.

The parameters of the main circuit of a three-phase induction motor with a phase-wound rotor, with the no-load circuit brought out to the terminals

according to the diagram in Fig. 19-7, are

$$\begin{aligned}
 R_1 &= r_1 \sigma_1 = 0.68 \times 1.03 = 0.7 \, \Omega \\
 R_2 &= r'_2 \sigma_1^2 = 0.57 \times 1.06 = 0.604 \, \Omega \\
 X_1 &= x_1 \sigma_1 = 2.78 \times 1.03 = 2.86 \, \Omega \\
 X_2 &= x'_2 \sigma_1^2 = 4.85 \times 1.06 = 5.15 \, \Omega \\
 R_{sh} &= R_1 + R_2 = 0.7 + 0.604 = 1.304 \, \Omega \\
 X_{sh} &= X_1 + X_2 = 2.86 + 5.15 = 8.01 \, \Omega \\
 Z_{sh} &= \sqrt{1.304^2 + 8.01^2} = 8.1 \, \Omega \\
 I''_{sh} &= \frac{1730}{8.1} = 214 \, \text{A} \\
 \frac{I'_{sh}}{I_{ph. r}} &= \frac{I''_{sh} \sigma_1}{I_{ph. r}} = \frac{214 \times 1.03}{60} = 3.66 \\
 \cos \varphi''_{sh} &= \frac{1.304}{8.1} = 0.161
 \end{aligned}$$

For a squirrel-cage induction motor with the same stator and with $N_2 = 80$ bars in the rotor, the parameters of the main circuits of the equivalent diagrams with the no-load circuit brought out to the terminals (Fig. 19-7) are

$$\begin{aligned}
 r_1 &= 0.68 \, \Omega, \quad R_1 = r_1 \sigma_1 = 0.68 \times 1.03 = 0.7 \, \Omega \\
 x_1 &= 2.78 \, \Omega, \quad X_1 = x_1 \sigma_1 = 2.78 \times 1.03 = 2.86 \, \Omega \\
 r'_2 &= 0.75 \, \Omega, \quad R_2 = r'_2 \sigma_1^2 = 0.75 \times 1.06 = 0.795 \, \Omega \\
 x'_2 &= 2.8 \, \Omega, \quad X_2 = x'_2 \sigma_1^2 = 2.8 \times 1.06 = 2.97 \, \Omega \\
 R_{sh} &= R_1 + R_2 = 0.7 + 0.795 = 1.495 \, \Omega \\
 X_{sh} &= X_1 + X_2 = 2.86 + 2.97 = 5.83 \, \Omega \\
 Z_{sh} &= \sqrt{1.495^2 + 5.83^2} = 6.01 \, \Omega \\
 I''_{sh} &= \frac{1730}{6.01} = 287 \, \text{A}, \quad \frac{I'_{sh}}{I_r} = \frac{I''_{sh} \sigma_1}{I_r} = \frac{287 \times 1.03}{60} = 4.91 \\
 \cos \varphi''_{sh} &= \frac{1.495}{6.01} = 0.248
 \end{aligned}$$

The parameters of the magnetizing circuit are taken the same as for a phase-wound motor.

19-6. Operating Conditions and Vector Diagrams of an Induction Machine

The vector diagrams of an induction machine, like those of a transformer, are constructed in accordance with the equivalent T-circuit of the machine, which corresponds to its physical operating conditions. The diagrams are plotted for one phase with the rotor winding referred to the stator winding.

Motor Operating Duty. This duty, as was indicated previously, is the main operating condition of an induction machine. Here energy is transmitted through the magnetic field from the primary side to the secondary, as in a transformer. Therefore, the vector diagram of

an induction machine in motoring operation is quite similar to that of a transformer.

The vector diagram of a motor is shown in Fig. 19-8.

The main flux Φ_m induces the e.m.f. $\dot{E}_1 = \dot{E}_2$ equal to the voltage across the magnetizing circuit terminals of the T-circuit (Fig. 19-5). The magnetizing circuit current \dot{I}_m leads Φ_m by an angle corresponding to the losses in the stator steel, since the losses in the rotor steel are small at the low values of the slip in normal operating conditions ($s=0$ to 0.05).

The current \dot{I}'_2 lags on the e.m.f. \dot{E}'_2 by an angle ψ_2 , and its magnitude and phase are determined by the secondary circuit impedance Z'_2 .

The primary current \dot{I}_1 is equal to the vector sum of the current \dot{I}_m and the load component of the primary current $\dot{I}'_1 = -\dot{I}'_2$

$$\dot{I}_1 = \dot{I}_m + (-\dot{I}'_2)$$

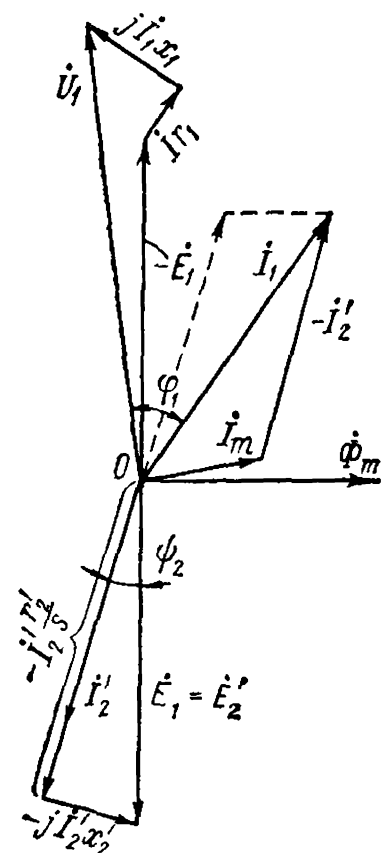


Fig. 19-8. Vector diagram of an induction motor

The primary voltage \dot{U}_1 is equal to the sum of the component which balances the e.m.f. \dot{E}_1 and the voltage drops $jx_1\dot{I}_1$ and $r_1\dot{I}_1$.

The current \dot{I}_1 lags on the voltage \dot{U}_1 by an angle $\varphi_1 < \frac{\pi}{2}$. The primary power

$$P_1 = m_1 U_1 I_1 \cos \varphi_1 \quad (19-33)$$

is positive here, this corresponding to power consumption from the circuit.

With an increase in the load on the shaft the slip s grows, since to obtain a greater torque an increase in the secondary current I_2 is required, and as a result the e.m.f. $E_{2s} = E_2 s$ induced in a running rotor must also increase. With an increase in load, the current I_2 and, with it, the primary current I_1 grow, the voltage drop also increases and, consequently, with $U_1 = \text{const}$, the e.m.f.s $E_1 = E'_2$, the flux Φ_m and the current I_m decrease.

The reduction in the main flux Φ_m with a change in load from zero to the nominal value is small, however, and amounts to only several per cent. For this reason, with approximate calculations and $U_1 = \text{const}$, it is sometimes assumed that $\Phi_m = \text{const}$.

In the following chapters motoring operation of an induction machine will be discussed in more detail.

Generator Operating Duty. Assume that an induction machine is connected to a circuit with a voltage $U_1 = \text{const}$ and a frequency $f_1 = \text{const}$. If it operates as a motor, then $n < n_1$.

Let us gradually decrease the load on the motor. If, for simplicity, we disregard the voltage drop in the stator winding, then the flux $\Phi_m = \text{const}$, the current $I_m = \text{const}$, while the secondary current I_2 decreases, and the end of the primary current vector \dot{I}_1 begins to move on the diagram of Fig. 19-8 up to the no-load point, when $\dot{I}_1 = \dot{I}_m$.

Now let us raise the speed of the induction machine rotor with the help of a motor so that $n = n_1$, i.e., up to the synchronous speed. Since the induction machine remains connected to the same circuit, then Φ_m and I_m remain constant. The power necessary to compensate the winding (p_{cop1}) and the steel (p_{st}) losses of the stator is delivered from the mains, and the power necessary to compensate the mechanical (p_{mech}) and additional (p_{add}) losses is supplied by the motor driving the induction machine (the prime mover).

If we further accelerate the induction machine, the speed n becomes higher than n_1 , and the slip s becomes negative. The flux Φ_m , remaining constant in magnitude, continues to rotate in space at the former speed n_1 . But its rotation relative to the rotor is reversed, with a corresponding change in the sign of the e.m.f. $E_{2s} = E_2 s$ induced in the rotor.

The active and reactive components of the rotor current will be

$$I_{2a} = \frac{E_{2s}}{Z_2} \cos \psi_2 = \frac{E_2 s r_2}{r_2^2 + x_2^2 s^2} \quad (19-34)$$

$$I_{2r} = \frac{E_{2s}}{Z_2} \sin \psi_2 = \frac{E_2 s^2 x_2}{r_2^2 + x_2^2 s^2} \quad (19-35)$$

We see that the sign of the active component I_{2a} of the secondary current changes with a negative slip, while the inductive component I_{2r} of this current retains its former sign.

The current I_2 produces the magnetizing force F_2 which, as indicated in Sec. 19-2, rotates in space at a synchronous speed n_1 determined by the frequency f_1 of the excitation current, and relative to the rotor at a speed $n_1 - n$. Since $n > n_1$, the magnetizing force F_2 rotates in the direction opposite to rotor rotation and, when interacting with the magnetizing force F_1 , develops the electromagnetic torque M_{em} directed against rotor rotation. Consequently, the torque M_{em} is a braking torque, and the induction machine operates as a generator.

To construct the vector diagram of an induction generator, let us superpose the main flux vector Φ_m on the positive direction of the axis of abscissas (Fig. 19-9). The current vector \dot{I}_m and the e.m.f. vector $\dot{E}_1 = \dot{E}'_2$ will occupy their usual positions on the diagram, but the current vector \dot{I}'_2 , in accordance with formulas (19-34) and (19-35), will

now be in the second and not in the third quadrant, as in motoring. The primary current $\dot{I}_1 = \dot{I}_m - \dot{I}'_2$. The voltage across the stator terminals $\dot{U}_1 = -\dot{E}_1 + \dot{I}_1 Z_1$. The angle $\varphi_1 > 90^\circ$, i.e., the electric power of the machine is negative. This means that in the conditions considered above the mechanical power delivered to the induction machine from the prime mover is converted into electric power and is supplied to the circuit.

The magnetic flux Φ_m is produced in an induction generator by the magnetizing current I_m . For this purpose synchronous generators are used to feed the external circuit together with the induction generator. Since the current I_m amounts to 25-45% of I_r and is fed to the generator at line voltage, the excitation power (in kVA) amounts to the same 25-45% of the generator rating. In other words, if 2 to 4 induction generators of equal output are installed in a power station, their excitation will take the full output of one synchronous generator of the same capacity as each of the induction generators. Recall that the power of excitation of a large synchronous generator is less than 1%. This difference in excitation power, which is unfavourable for the induction generator, is its essential drawback compared with the synchronous generator. In addition, the current I_m lags on the voltage by practically 90° . Consequently, parallel operation of induction and synchronous generators results in a considerable reduction in the power factor ($\cos \varphi$) of both even when the external load is purely active.

The connection of an induction generator to a circuit is not difficult. The rotor is brought into motion in the same direction in which the flux is rotating at a speed as close as possible to synchronous. When a generator is connected to the circuit the same phenomena occur as when transformers or induction motors are connected. The active power supplied by the generator to the circuit, as with synchronous generators, is changed by varying the mechanical power applied to the generator shaft. The efficiency of an induction generator is not lower than that of a synchronous generator.

In practice induction generators are used only in low-power stations, most frequently in automatic hydropower stations and wind-driven installations.

If an induction generator is to operate separately in an external circuit, the magnetizing current can be obtained in the process of

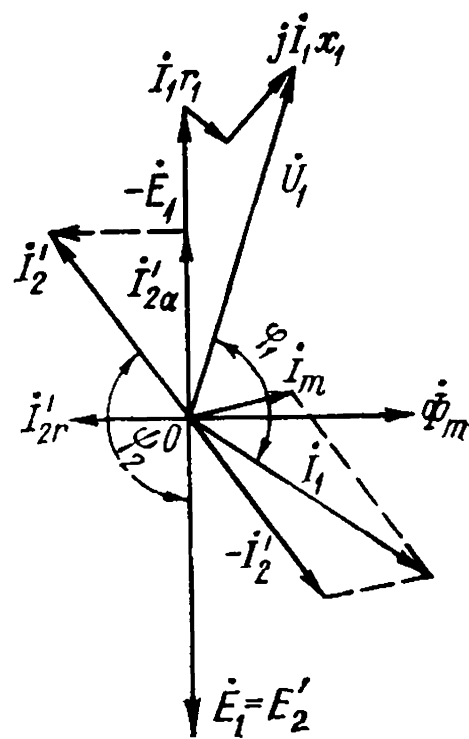


Fig. 19-9. Vector diagram of an induction generator

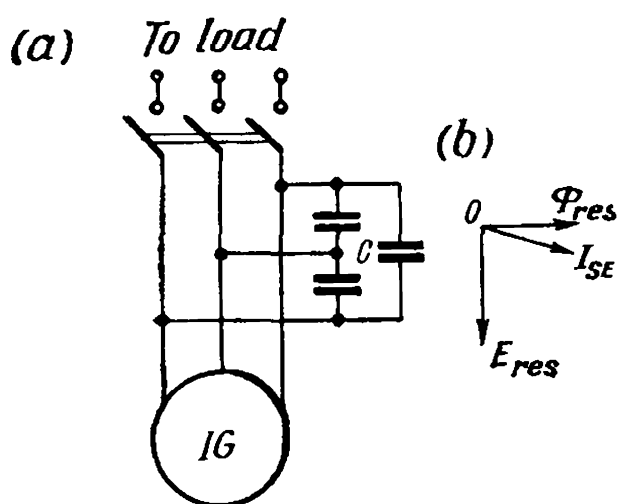


Fig. 19-10. Self-excited induction generator

its self-excitation. For this purpose it is necessary to connect to the stator terminals a group of properly selected capacitors (Fig. 19-10a) and run the rotor at the required speed. An indispensable condition for self-excitation of an induction generator is the presence of a residual magnetic flux in the rotor steel. With the external stator circuit open the residual magnetic flux Φ_{res} produces a certain e.m.f. E_{res} in the stator winding, which induces a current I_{se} in the capacitor group,

thus increasing the flux Φ_{res} (Fig 19-10b). The process then proceeds as in self-excitation of shunt generators (see Vol. I).

A costly part of induction self-excited generators is the group of capacitors. This is why such generators have not obtained wide use.

Electromagnetic Braking Duty. If we continue to load a motor more and more, its speed will drop and then, when the load torque exceeds the maximum motor torque, the motor will stall. After this, we can run the rotor against the flux with the help of an auxiliary motor. We have previously agreed to call these operating conditions electromagnetic braking.

The speed n in these conditions is negative, and thus $1 < s < \infty$.

Since the slip s is large, the rotor current

$$\dot{I}'_2 = \frac{\dot{E}'_2}{\frac{r'_2}{s} + jx'_2}$$

is also large and lags on E'_2 by the angle ψ_2 , which at the limit with $s = \infty$ equals 90° . Correspondingly large is the primary current I_1 and its angle of displacement φ_1 with respect to the voltage U_1 . The vector diagram for braking conditions is similar to that for motoring conditions (Fig. 19-8), with all the above-mentioned features.

Since $\varphi_1 < 90^\circ$, the machine draws power from the circuit. Besides, it obtains mechanical power from the prime mover. All the power consumed by the machine is spent in covering the machine losses, which are quite high. Therefore, from the viewpoint of heating these conditions are also very severe, and with $U_1 = U_r$ are permissible only for a relatively short period.

When an additional resistance is connected to the secondary circuit of an induction motor, the latter will consume a considerable part of the power supplied to the primary circuit of the machine. An increase in $\cos \varphi$ will take place, and the operation of the induction machine in electromagnetic braking conditions will be more effective.

Chapter

20

TORQUES AND POWER OF AN INDUCTION MACHINE

20-1. Energy Diagrams of an Induction Machine

Of great importance in induction motor operation is the conversion of electric energy consumed from the mains into mechanical energy and, in induction generator operation, the conversion of mechanical energy obtained from the prime mover into electric energy delivered to the circuit. In both cases the energy is transferred through the air-gap magnetic field from the stator to the rotor or vice versa. The energy transfer through the air-gap is connected with the forces of electromagnetic origin developed on the rotor and producing the electromagnetic torque of the machine. The conversion of energy from one kind into another is inevitably accompanied by losses in the various parts of a machine. Therefore, the rates of energy flow, the losses, and the torques are problems of considerable importance in the study of induction machine performance.

Consider the power diagrams of an induction machine.

Let us examine the conversion of electric energy delivered to the motor into mechanical energy at the shaft.

Let P_1 be the electric power delivered to the motor (Fig. 20-1a). A part of this power p_{cop1} is spent for covering the stator copper losses, the remainder being converted into rotating flux power. Here other losses appear, however—losses in the steel of the machine p_{st} ; practically only the stator steel losses should be taken into account, since the frequency f_2 of steel magnetization reversal in the rotor is usually very low (1 to 3 Hz), and the losses in the rotor steel are therefore very small. Thus, the electromagnetic power is

$$P_{em} = P_1 - p_{cop1} - p_{st} \quad (20-1)$$

This electromagnetic power is transferred through the air-gap to the rotor. If the rotor had no losses, this power would be totally converted into mechanical power. But, when a current flows through the rotor winding, losses occur in its copper or aluminium conductors. Let us consider a copper winding and deal with the copper losses p_{cop2} . Consequently, the total mechanical power developed by a motor at its shaft is

$$P_{mech} = P_{em} - p_{cop2} \quad (20-2)$$

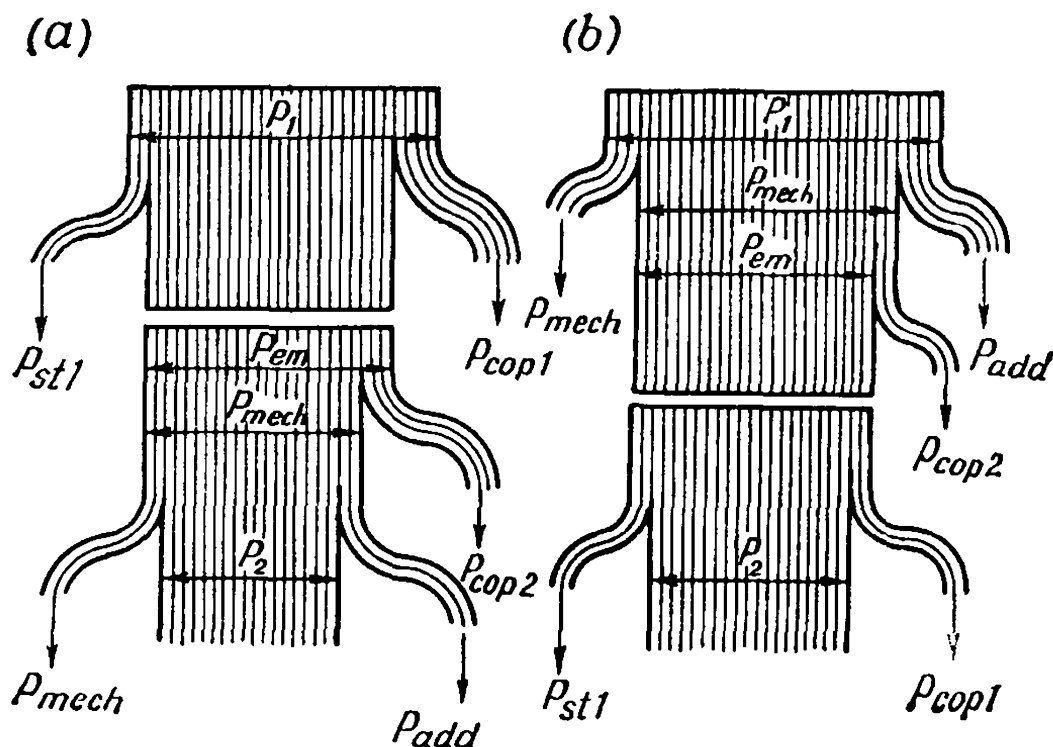


Fig. 20-1. Power diagrams:
a — induction motor; b — generator

The useful mechanical power P_2 delivered by a motor is less than the power P_{mech} by the mechanical losses p_{mech} and additional losses p_{add} . The losses p_{add} are incurred during rotation of the machine in its windings and steel and are due to stator and rotor toothings and to the quazi-sinusoidal distribution of the magnetizing forces in space (for more detail see Sec. 20-18).

Additional losses give rise to an additional braking torque and of the same nature as the mechanical losses, and, therefore, are compensated in the same way. When the energy flow in motor operation is analysed they are added to the mechanical losses. Thus

$$P_2 = P_{mech} - p_{mech} - p_{add} \quad (20-3)$$

Hence, for an induction motor we obtain the following relations:

$$P_1 = P_{em} + p_{cop1} + p_{st} \quad (20-4)$$

$$P_{em} = P_{mech} + p_{cop2} \quad (20-5)$$

$$P_{mech} = P_2 + p_{mech} + p_{add} \quad (20-6)$$

The efficiency of a motor is

$$\eta = \frac{P_2}{P_1} \quad (20-7)$$

An energy-flow diagram for an induction motor is pictured in Fig. 20-1a.

When an induction machine operates as a generator the mechanical power P_1 is delivered to its shaft. Upon subtraction of the mechanical and windage losses p_{mech} and the additional losses p_{add} from P_1 , we obtain the useful mechanical power P_{mech} . By subtracting the copper losses p_{cop2} in the secondary circuit from the power P_{mech} , we obtain the electromagnetic power P_{em} , and, subtracting from the latter the losses in the steel p_{st} and primary circuit copper p_{cop1} , we obtain the delivered power P_2 .

Hence, for generator conditions the following relations are obtained:

$$P_{mech} = P_1 - p_{mech} - p_{add} \quad (20-8)$$

$$P_{em} = P_{mech} - p_{cop2} \quad (20-9)$$

$$P_2 = P_{em} - p_{cop1} - p_{st} \quad (20-10)$$

The efficiency of a generator is

$$\eta = \frac{P_2}{P_1} \quad (20-11)$$

The total energy diagram for an induction generator is shown in Fig. 20-1b.

20-2. Torques of an Induction Machine

As in d.c. motors, an induction motor in steady-state conditions ($n = \text{const}$) overcomes the load torque M_l consisting of the no-load braking torque M_0 and the useful braking torque M_2 . Therefore, the electromagnetic torque M_{em} developed on the rotor of the motor at constant speed contains two components, each of which is in equilibrium with the corresponding braking torque component. Thus

$$M_{em} = M_0 + M_2 \quad (20-12)$$

Here

$$M_0 = \frac{p_{mech} + p_{add}}{\Omega} = \frac{p_{mech} + p_{add}}{2\pi n} \quad (20-13)$$

$$M_2 = \frac{P_2}{\Omega} = \frac{P_2}{2\pi n} \quad (20-14)$$

where P_2 = useful mechanical power delivered by the motor
 n = rotor speed.

The total mechanical power corresponding to the electromagnetic torque M_{em} developed in the rotor and determined by relation (20-6) is

$$P_{mech} = M_{em}\Omega = M_{em}2\pi n \quad (20-15)$$

whence

$$M_{em} = \frac{P_{mech}}{\Omega} = \frac{P_{mech}}{2\pi n} \quad (20-16)$$

The torque M_{em} results from the interaction of the rotating magnetic flux Φ_m and the current I_2 in the rotor. But the flux Φ_m rotates

in space at an angular speed $\Omega_1 = 2\pi n_1$, where $n_1 = \frac{f_1}{p}$. The power developed here is the electromagnetic power P_{em} of the motor. Consequently

$$P_{em} = M_{em} \Omega_1 \quad (20-17)$$

whence

$$M_{em} = \frac{P_{em}}{\Omega_1} = \frac{P_{em}}{2\pi n_1} \quad (20-18)$$

From equations (20-16) and (20-18) we get

$$P_{mech} = \frac{n}{n_1} P_{em} = (1-s) P_{em} \quad (20-19)$$

Substitution of this value for P_{mech} in (20-2) yields

$$p_{cop2} = s P_{em} \quad (20-20)$$

i.e., the secondary-circuit copper losses or, in the general case, the electric power P_e developed in the secondary circuit is equal to the electromagnetic power P_{em} multiplied by the slip.

Thus, the electromagnetic power P_{em} is divided into the components P_{mech} and p_{cop2} determined from equations (20-19) and (20-20) depending on the slip.

By determining from equation (20-20) the value of P_{em} and substituting it in equation (20-18), we get another expression for the magnitude of the electromagnetic torque

$$M_{em} = \frac{p_{cop2}}{s \Omega_1} = \frac{p_{cop2}}{2\pi n_1 s} \quad (20-21)$$

Although in establishing the relations obtained in this section we proceeded from motor conditions, they are valid for any values of the slip s , i.e., for all operating conditions of a machine.

20-3. Electromagnetic Torque of an Induction Machine

The electromagnetic torque results from the interaction between the rotor winding conductors carrying the current I_2 and the fundamental-harmonic rotating field or flux Φ_m .

Assume at first that the rotor winding is squirrel-cage. Then, the fundamental sine wave of the resultant rotating field will induce in each conductor an e.m.f. $e_{\alpha 1}$, whose value varies along a space coordinate α in accordance with the sine law. In the general case the current in a single conductor $i_{\alpha 1}$ will lag behind the e.m.f. $e_{\alpha 1}$ which produces it by an angle ψ_2 in the direction of rotation of the resultant magnetic field. The wave of the ordinates $e_{\alpha 1}$, which are the instantaneous values of the e.m.f.s induced in the given conductors, is in phase with

the wave of the flux densities $B_{\alpha 1}$ at the given points, while the wave of the currents $i_{\alpha 1}$ will be shifted in the direction opposite to flux density wave movement by the same angle ψ_2 (Fig. 20-2).

The field with the flux density $B_{\alpha 1}$ travelling around the rotor periphery and the current $i_{\alpha 1}$ in the conductor produce the elementary force

$$f_{\alpha 1} = B_{\alpha 1} i_{\alpha 1} l$$

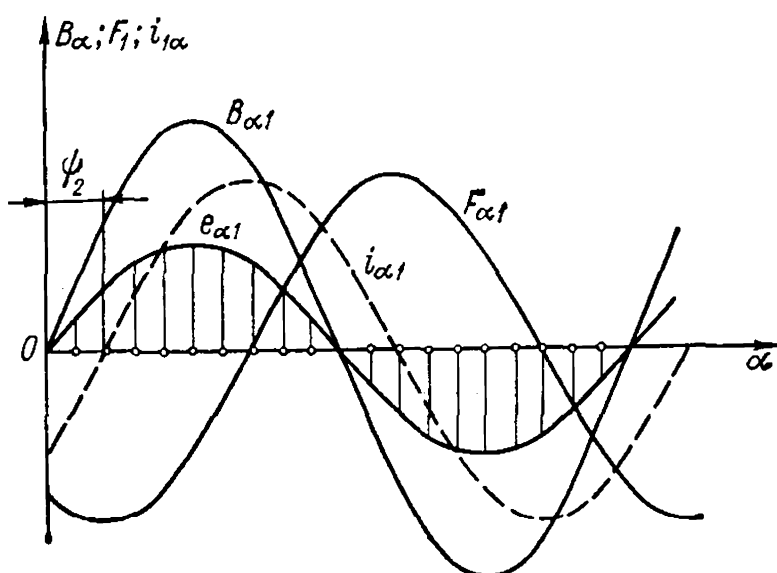


Fig. 20-2. Distribution of magnetic flux density, e. m. f.s and currents of rotor along the air-gap

where l is the active length of the rotor steel.

The torque produced by one current-carrying conductor is

$$m_{\alpha 1} = f_{\alpha 1} \frac{D}{2} = B_{\alpha 1} i_{\alpha 1} l \frac{D}{2}$$

where D is the rotor diameter. The number of conductors within the space angle $d\beta$ of the rotor periphery is $\frac{N}{2\pi} d\beta$. Since $B_{\alpha 1}$ and $i_{\alpha 1}$ vary along the space coordinate in accordance with the sine law, then

$$B_{\alpha 1} = B_m \sin \beta p \quad \text{and} \quad i_{\alpha 1} = I_{2m} \sin (\beta p - \psi_2)$$

$$B_{\alpha 1} i_{\alpha 1} = B_m I_{2m} \sin \beta p \sin (\beta p - \psi_2)$$

The total torque produced by all rotor conductors per pole division of a machine is

$$M_r = \int_0^{\frac{2\pi}{2p}} \frac{B_m \sin \beta p I_{2m} \sin (\beta p - \psi_2) l D N}{2 \times 2\pi} d\beta$$

The average value of the resultant torque produced by the rotor conductors of all poles is

$$M_{av} = 2p M_r = \frac{2p B_m I_{2m} l D N}{2 \times 2\pi} \int_0^{\frac{\pi}{p}} \sin \beta p \sin (\beta p - \psi_2) d\beta =$$

$$= \frac{2p B_m I_{2m} l D N}{2 \times 2\pi} \frac{1}{p} \left[\frac{\cos \psi_2}{2} \beta p - \frac{\sin (2\beta p - \psi_2)}{4} \right]_0^{\frac{\pi}{p}} =$$

$$= \frac{2p B_m I_{2m} l D N}{2 \times 2\pi} \frac{\pi}{2p} \cos \psi_2 = p \frac{B_m l D}{p} \frac{I_{2m} N}{4} \cos \psi_2$$

Taking into account that

$$I_{2m} = I_2 \sqrt{2}; \quad B_m = B_{av} \frac{\pi}{2}; \quad D = \frac{2p\tau}{\pi}$$

we get

$$\frac{B_m l D}{\rho} = B_{av} l \tau = \Phi_m$$

and the average torque, with $N = 2\omega_2 m_2$, will be

$$M_{av} = \frac{1}{2\sqrt{2}} p \Phi_m I_2 N \cos \psi_2 = \frac{1}{\sqrt{2}} m_2 p \omega_2 \Phi_m I_2 \cos \psi_2$$

This expression is true for a rotor with a squirrel-cage type winding for which the winding factor $k_{w2} = 1.0$. If the rotor has a phase winding, the latter is equivalent to a squirrel cage in which the number of turns is $\omega_2 k_{w2}$, where $k_{w2} = k_{d2} k_{p2}$.

In this case for the average value of the induction machine torque we have

$$M_{av} = \frac{1}{\sqrt{2}} m_2 p \omega_2 k_{w2} \Phi_m I_2 \cos \psi_2$$

Figure 20-3a contains a curve showing the change in the elementary torques m_α along the air-gap with $\psi_2 \cong 0$, which corresponds to small slips ($s \cong 0.01$ to 0.02). The curve in Fig. 20-3b is for $\psi_2 = 60^\circ$, which approximately corresponds to a slip $s = 1$, i.e., to a rotor at rest. Figure 20-3c corresponds to $\psi_2 = 90^\circ$, when the resultant torque $M_{av} = 0$. Figure 20-3d shows generator conditions at small slips.

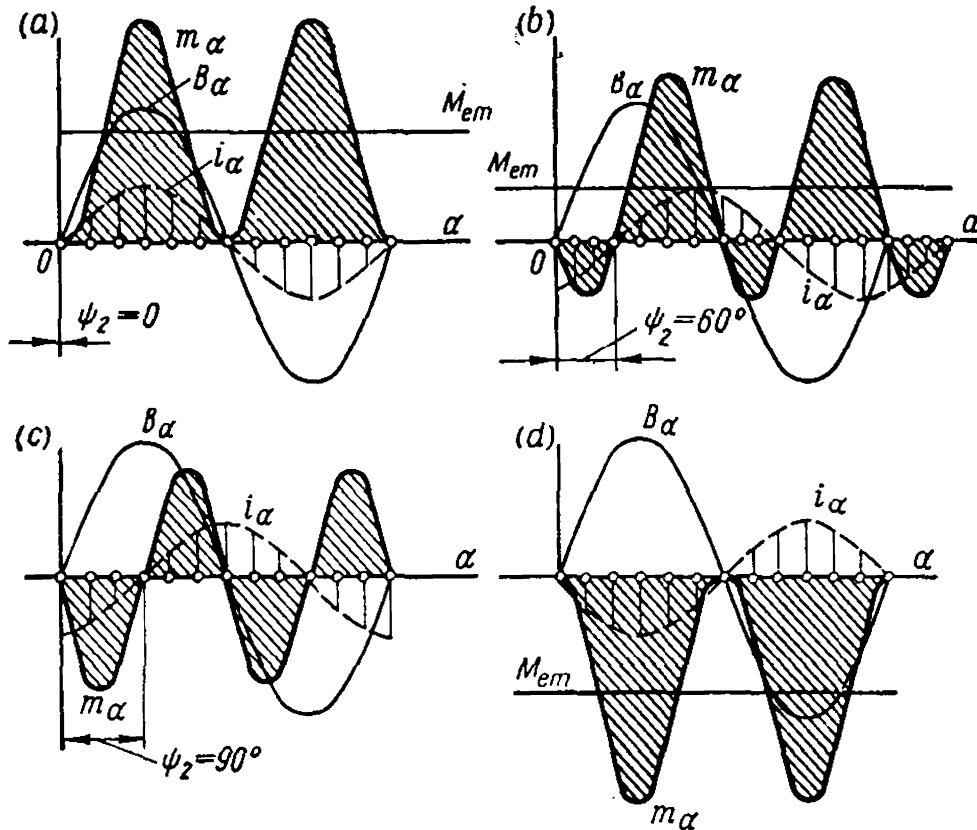


Fig. 20-3. Distribution of fundamental harmonics of magnetizing force, current and flux density along the air-gap

The expression for the electromagnetic torque M_{av} can also be obtained through the electromagnetic power P_{em} transferred from the stator to the rotor

$$P_{em} = m_2 E_2 I_2 \cos \psi_2 = M_{av} \Omega_1 = M_{av} \frac{2\pi f_1}{p}$$

Hence

$$\begin{aligned} M_{av} &= \frac{m_2 E_2 I_2 \cos \psi_2}{\frac{2\pi f_1}{p}} = \frac{\rho m_2 \pi \sqrt{2} \Phi_m \omega_2 k_{w2} f_1 I_2 \cos \psi_2}{2\pi f_1} = \\ &= \frac{1}{\sqrt{2}} m_2 p \omega_2 k_{w2} \Phi_m I_2 \cos \psi_2 \end{aligned}$$

considering that in the equivalent T-circuit of Fig. 19-5 this corresponds to the power released in the resistance $\frac{r_2'}{s}$.

The current I_2'' of the equivalent L-circuit (Fig. 19-7b) is

$$I_2'' = \frac{U_1}{\sqrt{\left(R_1 + \frac{R_2}{s}\right)^2 + (X_1 + X_2)^2}} \quad (20-22)$$

and the current of the equivalent T-circuit (Fig. 19-5) will be, according to equation (19-26),

$$I_2' = \sigma_1 I_2'' = \frac{\sigma_1 U_1}{\sqrt{\left(R_1 + \frac{R_2}{s}\right)^2 + (X_1 + X_2)^2}} \quad (20-23)$$

The change in rotor current according to equation (20-23) is shown in Fig. 20-4, the currents for generator operating conditions ($s < 0$) being shown as negative values. The current I_2' is obviously maximum at $s = \pm\infty$.

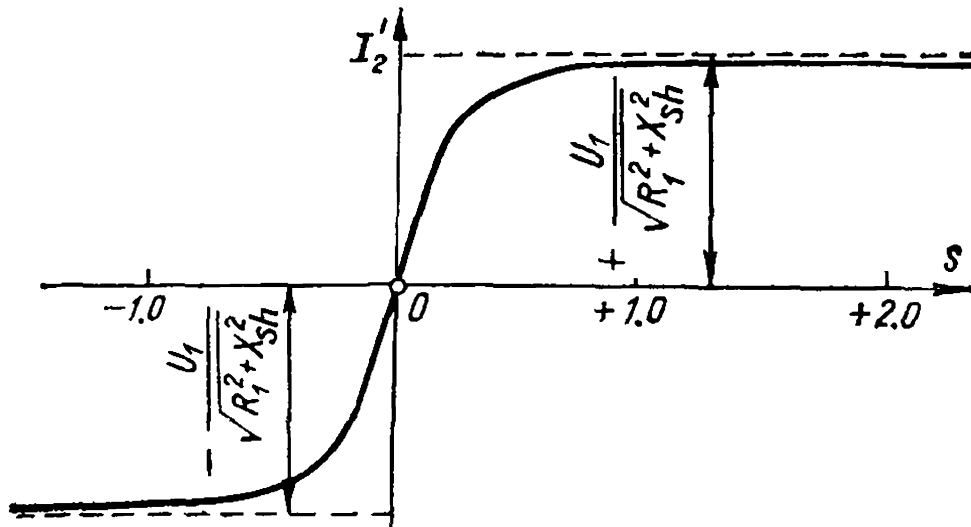


Fig. 20-4. Rotor current I_2' against slip s

According to the equivalent circuits of Figs. 19-4 and 19-5, the expression for the electromagnetic power P_{em} can be written as

$$P_{em} = m_2 I_2^2 \frac{r_2}{s} = m_1 I_2'^2 \frac{r_2'}{s} = m_1 I_2''^2 \frac{R_2}{s} \quad (20-24)$$

Substituting for I_2'' its value from equation (20-22) in equation (20-24), we obtain the dependence of the electromagnetic power on the voltage U_1 , slip s and the machine parameters

$$P_{em} = \frac{m_1 U_1^2 \frac{R_2}{s}}{\left(R_1 + \frac{R_2}{s}\right)^2 + (X_1 + X_2)^2} \quad (20-25)$$

while from equations (20-18) and (20-25) we find the expression for the electromagnetic torque

$$M_{em} = \frac{pm_1 U_1^2 \frac{R_2}{s}}{2\pi f_1 \left[\left(R_1 + \frac{R_2}{s}\right)^2 + (X_1 + X_2)^2 \right]} \quad (20-26)$$

Expression (20-26) could also have been obtained from formula (20-21) if we took into account that the electrical losses in the secondary circuit are

$$p_{cop2} = m_2 I_2^2 r_2 = m_1 I_2'^2 r_2' = m_1 I_2''^2 R_2 \quad (20-27)$$

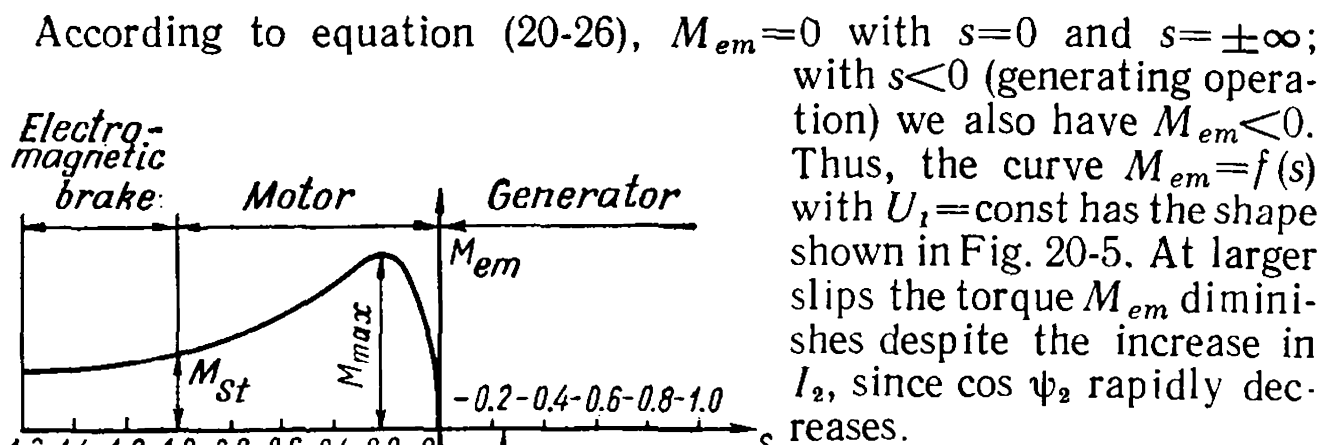


Fig. 20-5. Torque curve $M = f(s)$ for $U_1 = \text{const}$, $f = \text{const}$ and $r_{add} = 0$

In the above expressions the torques, when SI units are used, are in newton-metres. By dividing these values by 9.81 the torques are obtained in kilogram-metres.

20-4. Relation Between Torque M_{em} and Slip

Formula (20-26) is of very great importance. When we analysed it initially, all quantities except the slip s were considered constant, since some of them (m_1 , p , R_1 , R_2 , X_1 and X_2) are specified by design and others (U_1 and f_1), by the circuit which feeds the motor.

We shall investigate the torque of a motor beginning with the moment when it is connected to a circuit, i.e., when $s=1$. Let the torque M_{em} developed by the motor when $s=1$ be sufficient to overcome the load torque. The motor will then start running with a certain acceleration and continue to increase its speed until the torque becomes equal to the braking torque. After this the starting process is over, and the motor continues to run under steady-state conditions.

Corresponding to continuous increase in speed, the slip of the motor continuously diminishes from $s=1$ at starting to a certain value which is a positive proper fraction. Simultaneously, the numerator and the denominator in equation (20-26) also increase. Assume that the additional resistance in the rotor circuit $r_{add}=0$, and, consequently, $R_2=\sigma_1^2 r_2'$. Here the relation $M_{em}=f(s)$ takes the form of the curve in Fig. 20-5. The shape of the curve is explained by the fact that the inductive reactances X_1 and X_2 are generally much greater than the resistances R_1 and R_2 . Therefore, when the motor is accelerated, the numerator in formula (20-26) first increases more rapidly than the denominator, then the denominator becomes predominant and the torque M_{em} decreases. At synchronous speed, i.e., at $s=0$, the torque $M_{em}=0$.

Since the deduction of formula (20-26) was based on general premises, it is true for any operating conditions of an induction machine. When the machine starts to work as a generator, the slip reverses its sign ($s<0$) and the torque M_{em} becomes negative, i.e., a braking torque. The nature of the generator torque curve is the same as for a motor (the part of the curve to the right of the axis of ordinates in Fig. 20-5), but the maximum torque is somewhat higher (see Sec. 20-6). The torque curve, when the machine operates as an electromagnetic brake ($s>+1$), is the prolongation of the motor torque curve.

20-5. Maximum Electromagnetic Torque and Maximum Power

Expressions (20-25) and (20-26) based on the equivalent circuit make it possible to find expressions for the maximum electromagnetic torque M_{max} and the maximum electromagnetic power $P_{em, max}$ proportional to it, assuming all the quantities in these expressions except the slip s to be constant.

To find the slip $s=s_m$ corresponding to $P_{em. max}$, we take the derivative of equation (20-25) in respect to s and equate it to zero

$$\begin{aligned} \frac{dP_{em}}{ds} &= \frac{m_1 U_1^2 \left\{ - \left[\left(R_1 + \frac{R_2}{s} \right)^2 + X_{sh}^2 \right] \frac{R_2}{s^2} + \frac{R_2}{s} 2 \left(R_1 + \frac{R_2}{s} \right) \frac{R_2}{s^2} \right\}}{\left[\left(R_1 + \frac{R_2}{s} \right)^2 + X_{sh}^2 \right]^2} = \\ &= \frac{m_1 U_1^2 \frac{R_2}{s^2} \left[-R_1^2 - X_{sh}^2 + \frac{R_2^2}{s^2} \right]}{\left[\left(R_1 + \frac{R_2}{s} \right)^2 + X_{sh}^2 \right]^2} = 0 \end{aligned}$$

For the derivative $\frac{dP_{em}}{ds}$ to equal zero, the member in brackets in the numerator of the above expression must equal zero

$$-R_1^2 - X_{sh}^2 + \frac{R_2^2}{s_m^2} = 0$$

whence

$$\frac{R_2}{s_m} = \pm \sqrt{R_1^2 + X_{sh}^2}$$

and

$$s_m = \pm \frac{R_2}{\sqrt{R_1^2 + X_{sh}^2}} \quad (20-28)$$

Here the plus sign corresponds to motoring operation of the induction machine, and the minus sign to generating operation.

In conventional induction machines R_1 is considerably less than X_{sh} (R_1 is only 10 to 12% of X_{sh}). For this reason R_1^2 is so much less than X_{sh}^2 that it may be disregarded. Thus

$$s_m \cong \frac{R_2}{X_{sh}} = \frac{R_2}{X_1 + X_2}^* \quad (29-29)$$

Substituting the expression from equation (20-28) for s_m in expression (20-25) for P_{em} , we find the maximum electromagnetic power

$$\begin{aligned} P_{em. max} &= \pm \frac{m_1 U_1^2 \sqrt{R_1^2 + X_{sh}^2}}{R_1 \pm (\sqrt{R_1^2 + X_{sh}^2})^2 + X_{sh}^2} = \\ &= \pm \frac{m_1 U_1^2 \sqrt{R_1^2 + X_{sh}^2}}{2 [\pm R_1 \sqrt{R_1^2 + X_{sh}^2} + (R_1^2 + X_{sh}^2)]} = \pm \frac{m_1 U_1^2}{2 (\pm R_1 + \sqrt{R_1^2 + X_{sh}^2})} \quad (20-30) \end{aligned}$$

* In approximate analysis of the main principles of the induction machine in Chapter I with $\Phi_m = \text{const}$, we obtained expression (1-9): $s_m = \pm \frac{r_2}{x_2}$, which differs from expression (20-29). This is because expression (1-9) was obtained essentially for a T-type equivalent circuit with a constant voltage across the branch circuit $E_1 = \text{const}$. With $U_1 = \text{const}$ across the primary terminals and, correspondingly, with $\Phi_m \neq \text{const}$, which corresponds to an L-type equivalent circuit, the denominator takes account not only of the inductive reactance x_2 , but also of the reactance x_1 , i. e., the total short-circuit inductive reactance $X_{sh} = X_1 + X_2$.

where plus also corresponds to motoring and minus to generating operation.

Disregarding R_1^2 in equation (20-30) as being negligible compared with X_{sh}^2 we find an approximate expression for the maximum electromagnetic power

$$P_{em. max} \cong \pm \frac{m_1 U_1^2}{2(\pm R_1 + X_{sh})} \quad (20-31)$$

For the maximum electromagnetic torque, according to equations (20-30) and (20-31), we find

$$M_{max} = \pm \frac{pm_1 U_1^2}{2 \times 2\pi f_1 [\pm R_1 + \sqrt{R_1^2 + X_{sh}^2}]} \quad (20-32)$$

or, approximately

$$\begin{aligned} M_{max} &\cong \pm \frac{pm_1 U_1^2}{4\pi f_1 (\pm R_1 + X_{sh})} = \pm \frac{m_1 U_1^2}{2\Omega_{syn} (\pm R_1 + X_{sh})} = \\ &= \pm \frac{pm_1 U_1^2}{4\pi f_1 \sigma_1 (r_1 + x_1 + \sigma_1 x_2')} \end{aligned} \quad (20-33)$$

From the above formulas it follows that the maximum torque M_{max} :

(a) with a given frequency and given machine parameters is proportional to the square of the voltage U_1^2 ;

(b) does not depend on the resistance of the secondary circuit (rotor);

(c) is obtained with a slip which is the greater, the larger is the ratio $\frac{R_2}{X_{sh}}$ and, in particular, with a slip which is the greater, the larger the resistance of the secondary circuit;

(d) with a given frequency is almost inversely proportional to the sum of the reactances $(X_1 + X_2)$, i.e., is the smaller, the greater the inductive leakage reactances of the primary and secondary circuits.

For the relation between M_{max} and the frequency see Sec. 20-8.

The magnitude of the torque M_{max} is of special importance when an induction machine operates as a motor. The maximum torque of a motor is frequently referred to as the *stalling torque*.

The ratio

$$k_{ov} = \frac{M_{max}}{M_r}$$

is called the *overload capacity factor* of an induction motor.

20-6. Starting Torque of an Induction Motor

Along with the torque M_{max} , the starting torque M_{st} of a motor is one of the most important performance characteristics. The value of M_{st} is obtained from the general torque formula (20-26) when $s=1$:

$$M_{st} = \frac{pm_1 U_1^2 R_2}{2\pi f_1 [(R_1 + R_2)^2 + (X_1 + X_2)^2]} = \frac{pm_1 U_1^2 R_2}{2\pi f_1 (R_{sh}^2 + X_{sh}^2)} \quad (20-34)$$

If we desire the torque M_{st} to be maximum at starting, then, as follows from equation (20-28), it is necessary that

$$R_2^2 = \sigma_1^2 (r_2' + r_{add}')^2 = R_1^2 + X_{sh}^2 \quad (20-35)$$

or, approximately

$$r_2' + r_{add}' = x_1 + x_2' \quad (20-36)$$

From the above formulas it can be seen that the torque M_{st} :

(a) with a given frequency f_1 and given machine parameters is directly proportional to the square of the voltage U_1^2 ;

(b) reaches its maximum value when the resistance of the rotor circuit is equal to the inductive leakage reactance of the machine;

(c) with other conditions equal, is the smaller, the greater the inductive leakage reactance of the machine X_{sh} .

For the relation between M_{st} and the frequency see Sec. 20-8.

The torque M_{st} is usually expressed by the ratio

$$k_{st} = \frac{M_{st}}{M_r}$$

called the *starting torque ratio*.

Example 20-1. Calculate the power and torques of a squirrel-cage three-phase induction motor according to the parameters given in Sec. 19-5: $P_2 = 250$ kW; $\eta_r = 90\%$; $\cos \varphi_r = 0.89$; $U_1 = 3000$ V; $U_{1ph} = 1730$ V; $I_{1r} = 60$ A; $2p = 6$;
 $P_1 = \frac{P_2}{\eta} = \frac{250}{0.9} = 278$ kW.

The total losses are

$$\sum_p = \frac{P_2 (1 - \eta)}{\eta} = \frac{250 \times 0.1}{0.9} = 27.8 \text{ kW}$$

$$R_1 = 0.7 \Omega, R_2 = 0.795 \Omega; X_{sh} = 5.83 \Omega$$

The mechanical losses are taken equal to 0.7% of P_1

$$p_{mech} = 0.007 \times 278 \cong 2 \text{ kW}$$

The additional losses, according to the standards, are equal to 0.5% of P_1

$$p_{add} = 0.005 \times 278 = 1.4 \text{ kW}$$

The total mechanical power

$$P_{mech} = P_2 + p_{mech} + p_{add} = 250 + 2.0 + 1.4 = 253.4 \text{ kW}$$

The reduced (referred) current of the main part of the equivalent circuit is

$$I_{2r}'' = \frac{I_1 \cos \varphi_r - I_0 \cos \varphi_0}{\cos \psi_2} = \frac{53.3 - 2.05}{0.985} = 52.0 \text{ A}$$

where

$$I_1 \cos \varphi_r = 60 \times 0.89 = 53.3 \text{ A}$$

$$I_0 \cos \varphi_0 = 17.5 \times 0.118 = 2.05 \text{ A}$$

$$\cos \psi_2 \text{ (preliminarily)} = 0.985$$

The losses in the copper of the main part of the equivalent circuit with the no-load circuit brought out to the terminals are

$$p_{cop1} = 3 I_2''^2 R_1 = 3 \times 52^2 \times 0.7 \times 10^{-3} = 5.67 \text{ kW}$$

The losses in the secondary main circuit part are

$$p_{cop2} = 3 I_2''^2 R_2 = 3 \times 52^2 \times 0.795 \times 10^{-3} = 6.46 \text{ kW}$$

The electromagnetic power at rated load is

$$P_{em} = P_{mech} + p_{cop2} = 253.4 + 6.46 \cong 260 \text{ kW}$$

The slip of the motor at rated load is

$$s_r = \frac{p_{cop2}}{P_{em}} = \frac{6.46}{260} = 0.0249$$

The value of

$$\frac{R^2}{s_r} = \frac{0.795}{0.0249} = 31.9 \Omega$$

The quantity

$$\cos \psi_2 = \frac{R_1 + \frac{R_2}{s_r}}{\sqrt{\left(R_1 + \frac{R_2}{s_r}\right)^2 + X_{sh}^2}} = \frac{0.7 + 31.9}{\sqrt{(0.7 + 31.9)^2 + 5.83^2}} = \frac{32.6}{33.1} = 0.985$$

The rotor speed is

$$n = n_1 (1 - s_r) = 1000 \times (1 - 0.0249) = 975.1 \text{ rpm}$$

The useful torque of the motor is

$$M_{2r} = \frac{250 \times 10^3}{2\pi \times \frac{975.1}{60}} = 2450 \text{ N}\cdot\text{m}$$

or

$$M_{2r} = \frac{2450}{9.81} = 250 \text{ kgf}\cdot\text{m}$$

The no-load torque is

$$M_0 = \frac{p_{mech} + p_{add}}{2\pi \cdot \frac{n}{60}} = \frac{3.4 \times 10^3}{2\pi \times \frac{975.1}{60}} = 33.3 \text{ N}\cdot\text{m}$$

The electromagnetic torque is

$$M_{em.r} = M_{2r} + M_0 = 2450 + 33.3 = 2483.3 \text{ N}\cdot\text{m}$$

The final electromagnetic power is

$$P_{em} = \frac{3 \cdot U_{1ph}^2 \cdot \frac{R_2}{s_r}}{\left(R_1 + \frac{R_2}{s_r}\right)^2 + X_{sh}^2} = \frac{3 \times 1730^2 \times 31.9 \times 10^{-3}}{32.6^2 + 5.83^2} = 261.5 \text{ kW}$$

The final electromagnetic torque is

$$M_{em.r} = \frac{P_{em}}{2\pi n_1} = \frac{261.5 \times 10^3}{2\pi \times \frac{1000}{60}} = 2495 \text{ N}\cdot\text{m}$$

According to formula (20-32), the maximum torque is

$$M_{max} = \frac{3 \times 3 \times 1730^2}{2 \times 2 \times \pi \times 50 (0.7 + \sqrt{0.7^2 + 5.83^2})} = 6530 \text{ N}\cdot\text{m}$$

Thus

$$\frac{M_{max}}{M_{em. r}} = \frac{6530}{2495} = 2.62$$

The starting torque according to formula (20-34) is

$$M_{st} = \frac{m_1 U_{1ph}^2 R_2}{\frac{2\pi f}{p} (R_{sh}^2 + X_{sh}^2)} = \frac{3 \times 3 \times 1730^2 \times 0.795}{2\pi \times 50 \times (1495^2 + 5.83^2)} = 1900 \text{ N}\cdot\text{m}$$

$$\frac{M_{st}}{M_{em. r}} = \frac{1900}{2495} = 0.763$$

The total losses are

$$\sum p = (p_{mech} + p_{add}) + 3 \cdot I_2''^2 R_{sh} + p_0 = 3.4 + 3 \times 52^2 \times 1.495 \times 10^{-3} + 11.68 = 27.2 \text{ kW}$$

where $p_0 = 11.68 \text{ kW}$ are the losses in the no-load part of the equivalent circuit.

The efficiency

$$\eta = \left(1 - \frac{27.2}{250 + 27.2} \right) \times 100 = (1 - 0.0983) \times 100 = 90.17\%$$

Example 20-2. In a similar manner calculate the powers and torques of a three-phase induction motor with a phase-wound rotor according to the parameters given in Example 19-1.

The initial data of the motor: $P_2 = 250 \text{ kW}$, $\eta_r = 90\%$, $\cos \varphi_r = 0.875$, $U_1 = 3000 \text{ V}$, $U_{1ph} = 1730 \text{ V}$, $I_r = 60 \text{ A}$, $2p = 6$, $P_1 = 278 \text{ kW}$, $\sum p = 27.8 \text{ kW}$, $R_1 = 0.7 \Omega$, $R_2 = 0.604 \Omega$, $X_{sh} = 8.01 \Omega$, $s_r = 0.019$.

According to the formulas used for calculating the squirrel-cage motor, we find

$$\frac{R_2}{s_r} = \frac{0.604}{0.019} = 31.8 \Omega$$

$$\cos \psi_2 = \frac{0.7 + 31.8}{\sqrt{(0.7 + 31.8)^2 + (8.01)^2}} = \frac{32.5}{33.4} = 0.97$$

$$I_1 \cos \varphi_r = 60 \times 0.875 = 53.5 \text{ A}, \quad I_0 \cos \varphi_0 = 17.5 \times 0.118 = 2.05 \text{ A}$$

$$I_{2r}'' = \frac{I_1 \cos \varphi_r - I_0 \cos \varphi_0}{\cos \psi_2} = \frac{53.5 - 2.05}{0.97} = 52 \text{ A}$$

$$P_{em} = \frac{3 \times 1730^2 \times 31.8 \times 10^{-3}}{(0.7 + 31.8)^2 + (8.01)^2} = 259 \text{ kW}$$

$$M_{em. r} = \frac{259 \times 10^3}{2\pi \times \frac{1000}{60}} = 2470 \text{ N}\cdot\text{m}$$

$$M_{max} = \frac{3 \times 3 \times 1730^2}{2 \times 2 \times \pi \times 50 (0.7 + \sqrt{0.7^2 + 8.01^2})} = 4920 \text{ N}\cdot\text{m}$$

$$\frac{M_{max}}{M_{em. r}} = \frac{4920}{2470} = 1.99$$

(according to the Manufacturer's data for the type AM-6 280-kW, 3000-V motor, the ratio $\frac{M_{max}}{M_{em,r}} = 2.0$).

$$\sum p = 3.4 + 3 \times 52^2 \times 1.304 \times 10^{-3} + 11.68 = 25.7 \text{ kW}$$

$$\eta = \left(1 - \frac{25.7}{250 + 25.7} \right) \times 100 = 90.65\%$$

20-7. Relation Between Torque and Resistance of Rotor Circuit

If $r_{add}=0$ and, consequently, $R_2=\sigma_1^2 r_2'$, the ratio $\frac{R_2}{X_{sh}}$ is generally small. Therefore, the torque M_{em} passes through its maximum at relatively small slips of about $s=0.12$ to 0.20 (Fig. 20-5). But the starting torque M_{st} in motors with phase-wound rotors, which have a larger rotor leakage reactance than squirrel-cage motors, may fall below the limit required for starting, and the motor will not start. To avoid this, an additional resistance r_{add} should be introduced into the circuit of the phase-wound rotor. As follows from equations (20-28) and (20-32), the torque maximum does not change, but the slip s_m increases.

Figure 20-6 shows four curves of the torque M_{em} corresponding to four different values of the additional resistance r_{add} . Curve 1 is obtained with $r_{add}=0$ and repeats the torque curve in Fig. 20-5. Curve 3 corresponds to such a value of r_{add3} for which $\sigma_1^2(r_2' + r_{add}) = X_{sh}$; here $s_m=1$, i.e., the torque attains its maximum at the initial moment of motor starting. Curve 2 corresponds to the resistance $r_{add2} < r_{add3}$ and curve 4 to the resistance $r_{add4} > r_{add3}$; in the latter case the torque attains its maximum when the slip $s_m > 1$, i.e., when the machine operates as an electromagnetic brake.

It should be noted that when the additional resistance is introduced into the secondary circuit, a simultaneous decrease in starting current is attained, according to equation (20-22).

Below, in Chapters 23 and 24, the curves of Fig. 20-6 will be used for explaining the starting of induction motors by means of a rheostat and the regulation of their speed.

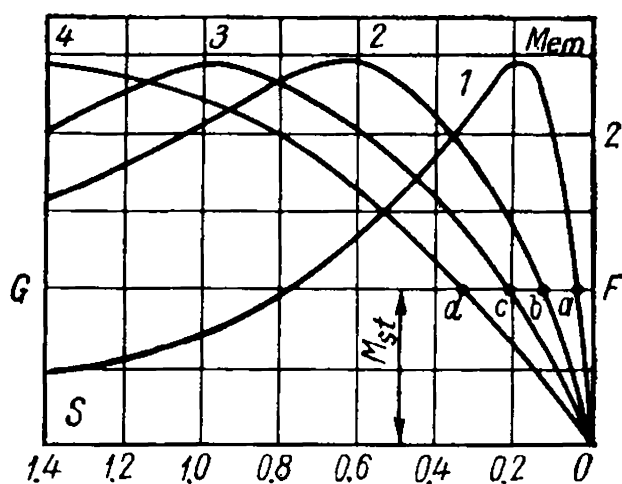


Fig. 20-6. Curves of $M = f(s)$ for different rotor circuit resistances

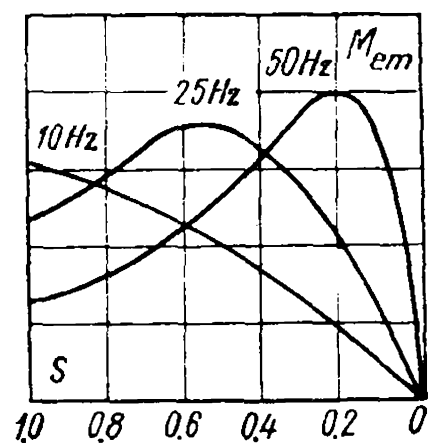


Fig. 20-7. Curves of $M_{em} = f_1(s)$ with $\frac{U_1}{f_1} = \text{const}$

20-8. Relation Between Torque M_{em} and Frequency f_1 with $\frac{U_1}{f_1} = \text{const}$

The frequency f_1 of the power circuit usually remains constant, but in some installations it may vary within certain limits if the voltage U_1 across the motor terminals varies with the frequency, the change in U_1 and f_1 more frequently being such that $\frac{U_1}{f_1} = \text{const}$.

To answer the question as to the nature of the curves $M_{em} = f(s)$ in these conditions at different frequencies we shall make use of the simplified formulas (20-29) and (20-33). According to the first of these, the slip s_m with $R_2 = \text{const}$ varies inversely to the frequency. In other words, in these conditions the torque M_{em} passes through a maximum at a slip which is the greater, the lower the frequency f_1 . On the other hand, the value of M_{max} is influenced by three variables: U_1 , f_1 and $X_{sh} = \sigma_1 x_1 + \sigma_2^2 x_2'$. If we had disregarded R_1 , then, as can be seen from equation (20-33), the change in U_1 would have been compensated by a proportional change in f_1 and X_{sh} . In this case the torque M_{max} would have remained constant. Actually it decreases somewhat with a decrease in frequency.

This discussion is illustrated by three torque curves for $f_1 = 50, 25$ and 10 Hz shown in Fig. 20-7.

20-9. Kloss's Formula for Relative Torque

When problems of electrical drive motion are being solved, it is important to determine the relation $M = f(s)$ from the data given in electrical motor catalogues. These data usually make it possible to determine the value of the torque M_r for the rated load, the slip s_r for this load, and the overload capacity factor k_{ov} , which can be used to determine the maximum torque $M_{max} = k_{ov} M_r$ for the rated voltage. We shall demonstrate how the relation $M = f(s)$ can be determined from the above data considering the motor parameters as independent of the slip.

Relations (20-26) and (20-32) give the value of the torque for any slip and also the value of the maximum torque.

By taking the ratio of equations (20-26) and (20-32), using only the plus sign (motor conditions) and omitting the subscript em , we get

$$\frac{M}{M_{max}} = \frac{2 \frac{R_2}{s} [R_1 + \sqrt{R_1^2 + X_{sh}^2}]}{\left(R_1 + \frac{R_2}{s}\right)^2 + X_{sh}^2} \quad (20-37)$$

According to equation (20-28), we have

$$\sqrt{R_1^2 + X_{sh}^2} = \frac{R_2}{s_m}$$

Introducing this value of the square root into expression (20-37), we obtain

$$\begin{aligned} \frac{M}{M_{max}} &= \frac{2R_2 \left[R_1 + \frac{R_2}{s_m} \right]}{\left[\left(\frac{R_2}{s_m} \right)^2 + \left(\frac{R_2}{s} \right)^2 + \frac{2R_1R_2}{s} \right] s} = \frac{2 \frac{R_2^2}{s_m} \left[\frac{R_1}{R_2} s_m + 1 \right]}{\frac{R_2^2}{s_m} \left[\frac{s}{s_m} + \frac{s_m}{s} + 2 \frac{R_1}{R_2} s_m \right]} = \\ &= \frac{2 \left(1 + \frac{R_1}{R_2} s_m \right)}{\frac{s}{s_m} + \frac{s_m}{s} + 2 \frac{R_1}{R_2} s_m} \end{aligned} \quad (20-38)$$

In induction machines with no additional resistance in the rotor circuit we usually have $r_1 \cong r_2$, and, consequently, also $R_1 \cong R_2$. Therefore, when the ratio $\frac{R_1}{R_2}$ cannot be determined more precisely, it may be assumed that

$$\frac{M}{M_{max}} = \frac{2(1 + s_m)}{\frac{s}{s_m} + \frac{s_m}{s} + 2s_m} \quad (20-39)$$

Knowing M_r , k_{ov} and s_r from the catalogue data, we can determine s_m from equation (20-39) and then with the aid of this equation obtain the relative torque for any slip s .

For small values of slip in the range of normal loads, only the term $\frac{s_m}{s}$ in the denominator of equation (20-39) can be taken into account, and thus

$$\frac{M}{M_{max}} \cong \frac{2(1 + s_m)}{s_m} s$$

The expression obtained above shows that in the normal load range the torque M varies with the slip, as shown in Figs. 20-5 and 20-6.

If in equation (20-39) we were to neglect s_m in the numerator and the term $2s_m$ in the denominator, we obtain an approximate relation sometimes used in calculations:

$$\frac{M}{M_{max}} \cong \frac{2}{\frac{s}{s_m} + \frac{s_m}{s}} \quad (20-40)$$

20-10. Maximum Mechanical Power

The expression for the maximum value of the mechanical power P_{mech} developed on the rotor of an induction machine can be obtained in the same way as the expression for the maximum electromagnetic power $P_{em. max}$.

On the basis of equations (20-19) and (20-20), the mechanical power is

$$P_{mech} = \frac{1-s}{s} p_{cop2} = \frac{1-s}{s} m_1 I_2'^2 R_2 \quad (20-41)$$

or, substituting here for I_2' its value from the equivalent L-circuit of Fig. 19-7

$$P_{mech} = \frac{1-s}{s} \frac{m_1 U_1^2 R_2}{\left(R_1 + \frac{R_2}{s}\right)^2 + X_{sh}^2} \quad (20-42)$$

To find the slip $s=s_p$ corresponding to the maximum value of P_{mech} we take the derivative of P_{mech} with respect to s and equate it to zero

$$\frac{dP_{mech}}{ds} = \frac{m_1 U_1^2 \left[-(R_1 + R_2)^2 - X_{sh}^2 + \left(-R_2 + \frac{R_2}{s_p} \right)^2 \right] \frac{R_2}{s^2}}{\left[\left(R_1 + \frac{R_2}{s} \right)^2 + X_{sh}^2 \right]^2} = 0$$

For the derivative $\frac{dP_{mech}}{ds}$ to equal zero, it is necessary to equate to zero the multiple of the numerator in brackets

$$-(R_1 + R_2)^2 - X_{sh}^2 + \left(-R_2 + \frac{R_2}{s_p} \right)^2 = 0$$

whence

$$\frac{R_2}{s_p} = R_2 \pm \sqrt{(R_1 + R_2)^2 + X_{sh}^2} = R_2 \pm Z_{sh}$$

where

$$Z_{sh} = \sqrt{(R_1 + R_2)^2 + X_{sh}^2} = \sqrt{R_{sh}^2 + X_{sh}^2} \quad (20-43)$$

Consequently

$$s_p = \frac{R_2}{R_2 \pm Z_{sh}} \quad (20-44)$$

The plus sign corresponds to motor operation of an induction machine, and the minus sign to generator operation.

By substituting the expression obtained for s_p with the plus sign into the general expression (20-42) for the power P_{mech} , we obtain for motor operation the maximum mechanical power equal to

$$P_{mech. max} = \frac{m_1 U_1^2 R_2 \left[\frac{R_1 + Z_{sh}}{R_2} - 1 \right]}{(R_{sh} + Z_{sh})^2 + X_{sh}^2} = \frac{m_1 U_1^2 Z_{sh}}{2Z_{sh} (R_{sh} + Z_{sh})}$$

or, finally,

$$P_{mech.max} = \frac{m_1 U_1^2}{2(R_{sh} + Z_{sh})} \quad (20-45)$$

The maximum power P_{2max} on the motor shaft differs from $P_{mech.max}$ according to (20-45) by the value of the mechanical and additional losses.

For generator operation, when the minus sign is used in equation (20-44), we obtain for the maximum mechanical power on the rotor the expression:

$$P_{mech.max} = - \frac{m_1 U_1^2}{2(-R_{sh} + Z_{sh})} \quad (20-46)$$

The minus sign indicates here that this power is not delivered to the shaft, but taken from it.

20-11. Hysteresis Torque

The rotor steel losses consist of the hysteresis losses p_h and the eddy-current losses p_{ed} , the former, as is known, varying in proportion to the magnetic reversals of the rotor frequency $f_2 = f_1 s$, and the latter in proportion to the square of this frequency. If we denote the values of these losses at the frequency f_1 , i.e., when the rotor is at standstill, by p_{h0} and p_{ed0} , respectively, then, with $\Phi_m = \text{const}$

$$p_h = p_{h0} s \quad (20-47)$$

$$p_{ed} = p_{ed0} s^2 \quad (20-48)$$

To these losses, as also to the rotor copper losses p_{cop2} , correspond their individual electromagnetic torques. Indeed, the eddy currents appear as a result of the e.m.f.s being induced in the rotor steel laminations by the rotating field. They do not differ in principle from the currents in the rotor winding. Owing to the hysteresis in the rotor steel, the magnetic field change in the rotor steel lags and in motoring operating conditions the direction of the magnetic flux lines in the air-gap is not radial, but deviates on the rotor surface in a direction opposite to rotation (Fig. 20-8), and a hysteresis torque is produced acting in the direction of rotation, i.e., a positive torque. In generating operating conditions the sign of the hysteresis torque is reversed.

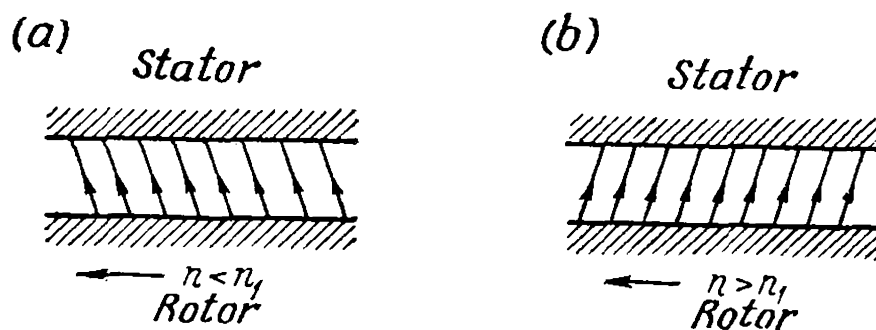


Fig. 20-8. Hysteresis torque:
a — in motoring conditions; b — in generating conditions

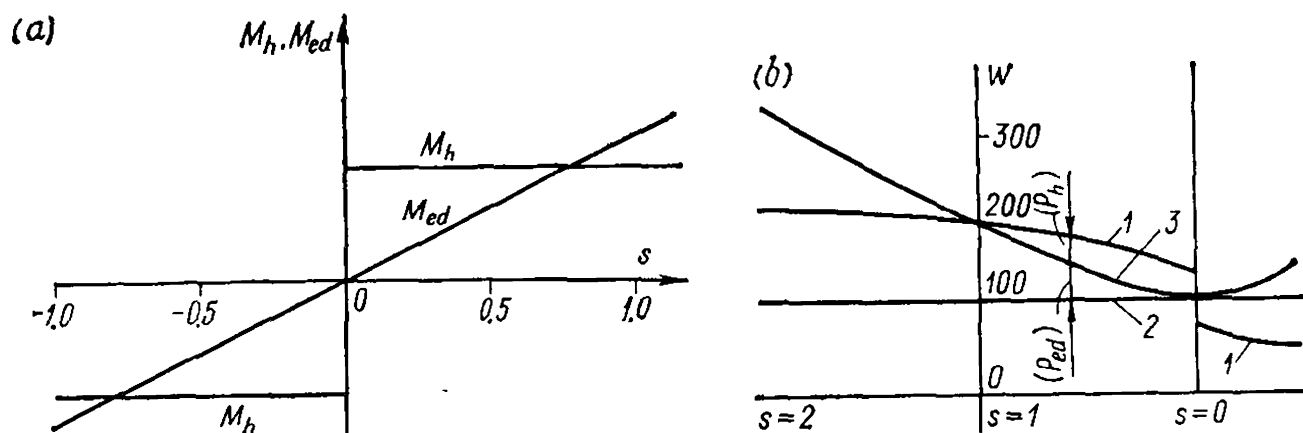


Fig. 20-9. Torques (a) and losses (b) due to hysteresis and eddy currents

In accordance with equation (20-21), the hysteresis torque M_h and the eddy-current torque M_{ed} are respectively equal to

$$M_h = \frac{p_h}{s\Omega_1} = \frac{p_{h0}}{\Omega_1} \quad (20-49)$$

and

$$M_{ed} = \frac{p_{ed}}{s\Omega_1} = \frac{sp_{ed0}}{\Omega_1} \quad (20-50)$$

Thus, the value of the hysteresis torque M_h does not depend on the slip. The torque, with $\Phi_m = \text{const}$, is constant in magnitude and only changes its sign when $s=0$. The eddy-current torque M_{ed} varies in proportion to the slip.

Both torques, M_h and M_{ed} , act on the rotor in the same manner as the main electromagnetic torque, and are therefore useful torques.

Figure 20-9a shows the relations $M_h = f(s)$ and $M_{ed} = f(s)$. The torque M_{ed} under ordinary operating conditions is very small. In some machines, in which the rotors are not made of electrical steel, the torque M_h has a higher value.

The no-load test makes it possible to determine the losses in the stator copper p_{cop1} , the stator steel losses p_{st1} , additional no-load losses p_{add0} and the mechanical losses p_{mech} :

$$P_0 = p_{cop1} + p_{st1} + p_{add0} + p_{mech}$$

Since the stator copper losses at no-load are

$$p_{cop1} = 3I_0^2 r_1$$

then with I_0 and r_1 known, we can determine the total losses

$$p_{st1} + p_{add0} + p_{mech} = P_0 - p_{cop1}$$

If we determine P_0 for various voltages, then, since p_{cop1} and p_{add0} are proportional to B^2 and, therefore, to U_1^2 , the mechanical losses

can be determined according to the values of P_0 for two values of U_1 :

$$a = P'_0 - p'_{cop1} = (p'_{st1} + p'_{add0}) + p_{mech}$$

$$b = P''_0 - p''_{cop1} = (p''_{st1} + p''_{add0}) + p_{mech} = (p'_{st1} + p'_{add0}) \left(\frac{U''_1}{U'_1} \right)^2 + p_{mech}$$

whence

$$c = p'_{st1} + p'_{add0} = \frac{b - a}{\left(\frac{U''_1}{U'_1} \right)^2 - 1}$$

and, consequently, $p_{mech} = a - c$.

Figure 20-9b shows curve 1 for the power obtained from a 5-kW induction machine with a phase-wound rotor run by a separate motor. The straight line 2 is the sum of the stator copper and steel losses. The difference between curves 1 and 2 gives the sum of the hysteresis and eddy-current losses in the rotor. The difference between curves 3 showing the change in the eddy-current losses and curve 2 gives the power p_{ed} corresponding to the eddy currents in the rotor, while the difference between curves 1 and 3 gives the power p_h corresponding to the hysteresis torque.

In ordinary induction machines the torques M_h and M_{ed} are usually not taken into account in calculations, but lately wide use is being made of low-power motors (up to 200 W) so-called hysteresis ones. The rotor of such a motor is round, without a winding, and made of steel sheets with a wide hysteresis loop. The motor is started by the hysteresis and eddy-current torques. Under the action of the hysteresis torque, the motor is pulled into step and then runs as a synchronous motor. With a 200-W output the efficiency may be as high as 80%.

Hysteresis motors find use in clock and tape transport mechanisms, in sound-recording and reproducing apparatus, etc. Such motors are most often single-phase, and use the relevant method of starting (see Sec. 25-4).

20-12. Parasitic Torques of an Induction Motor [186, 196, 202]

Besides the main or fundamental torque due to the first harmonics of the flux and current, a number of additional or parasitic torques appear in induction motors, which may, in certain conditions, disturb motor operation and even make it impossible.

We distinguish the following parasitic torques:

- (a) asynchronous torques due to higher magnetizing force harmonics, including the tooth harmonics;
- (b) synchronous torques that appear at a certain speed and with certain relations between the number of stator and rotor slots Z_1 and Z_2 ; and

(c) vibration torques also due to unfavourable relations between the number of slots Z_1 and Z_2 .

Furthermore, the higher-order (temporary) voltage harmonics have a certain influence on motor operation, but they may be disregarded because it is usually small.

We shall assume that the properties of the space and tooth-ripple harmonics are already known (Chapter 4) and we shall consider only squirrel-cage motors, since the presence of parasitic torques is particularly harmful for their operation.

20-13. Asynchronous Parasitic Torques

Speaking of induction motor operation, we showed in Sec. 19-3 that the first magnetizing force harmonics of the stator and rotor rotate in space always in one direction and at the same speed n_1 , the speed of the fundamental magnetizing force rotor harmonic being the sum of the speed $n_1 - n$ of its rotation with respect to the rotor and of the rotor speed n .

Let us extend this concept of the relation between the stator and rotor magnetizing forces to the magnetizing force harmonics of any order. If the stator first magnetizing force harmonic rotates at a speed n_1 , then the stator magnetizing force harmonic of the v -th order will rotate at a speed $n_{1v} = \pm \frac{n_1}{v}$. Here the plus sign relates to the magnetizing force rotating in the same direction as the fundamental magnetizing force harmonic, and the minus sign to the magnetizing force rotating in the opposite direction. For short, the former magnetizing forces will be called direct, and the latter backward spacial harmonic magnetizing forces.

The slip corresponding to a given harmonic is

$$s_v = \frac{\pm n_{1v} - n}{\pm n_{1v}} = 1 \pm \frac{n_1 - (n_1 - n)}{\frac{n_1}{v}} = 1 \pm (1 - s)v \quad (20-51)$$

Here s is the rotor slip with respect to the fundamental magnetizing force or, in short, the fundamental slip.

The frequency of the current induced in the rotor by the flux of the stator v -th magnetizing force harmonic is determined by formula (19-2):

$$f_{2v} = f_1 s_v = f_1 [1 \pm (1 - s)v] \quad (20-52)$$

Since $n_{1v} = \pm \frac{n_1}{v}$, the rotor v -th magnetizing force harmonic rotates with respect to the rotor at a speed

$$n_{2v} = \pm \frac{n_1}{v} - n \quad (20-53)$$

Consequently, the speed of the rotor v -th harmonic in space equals

$$n_{2v} + n = \pm \frac{n_1}{v} - n + n = \pm \frac{n_1}{v} \quad (20-54)$$

i.e., it is equal to the speed of rotation of the stator v -th magnetizing force harmonic.

On this basis we can calculate the induction torques produced by the higher magnetizing force harmonics from formula (20-26), substituting in it the values corresponding to the given harmonic.

The effect of the parasitic induction torques depends on the direction of rotation of the magnetizing force harmonics.

Let us consider first the effect of a direct magnetizing force harmonic of the v -th order. We know that the synchronous speed of rotation of such a harmonic is $n_{1v} = \frac{n_1}{v}$. This corresponds to the slip

$$s = \frac{n_1 - \frac{n_1}{v}}{n_1} = 1 - \frac{1}{v}$$

Within the slip range from $s=1$ to $s=1-\frac{1}{v}$ the rotor runs at a lower speed than the harmonic, and in the range from $s=1-\frac{1}{v}$ to $s=0$, at a greater speed. In the first case the v -th magnetizing force harmonic produces a motor torque, in the second case—a generator torque, i.e., a braking torque. The motor torque of the harmonic adds to the fundamental torque, while the generator torque subtracts from the latter. Curve 1 in Fig. 20-10 shows the fundamental torque, while curve 2 shows the torque of the seventh harmonic.

Let us now consider the effect of the backward spacial magnetizing force harmonics. Since in motoring operating conditions the rotor runs in the direction opposite to the direction of rotation of these harmonics, an induction motor acts with respect to them as an electromagnetic brake. Therefore, for all slips within the range from $s=1$ to $s=0$ the reverse magnetizing force harmonics produce braking torques, as shown by curve 3 of the torque produced by the fifth-order reverse harmonic. But, if we rotate the rotor opposite to the fundamental magnetizing force rotation, i.e., in the direction of the backward spacial harmonic, then, at a slip $s=1+\frac{1}{v}$ corresponding to synchronous rotation of the rotor within the flux of this har-

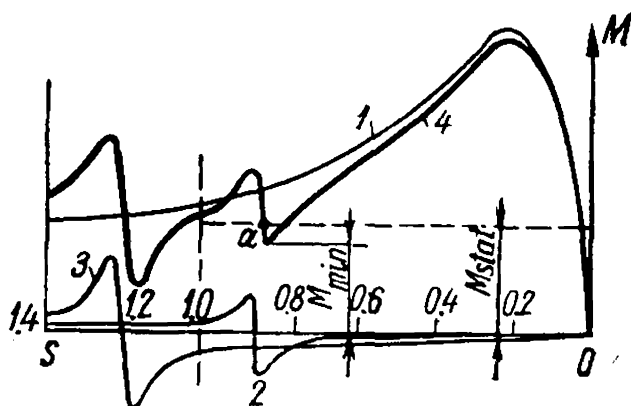


Fig. 20-10. Influence of higher harmonic asynchronous torques of stator magnetizing force on torque curve

monic, its torque will pass through zero and then, when $s > 1 + \frac{1}{v}$, will acquire a positive value.

By summing the ordinates of curves 1, 2 and 3 in Fig. 20-10, we obtain curve 4, the resultant torque of the motor. We see that it has two dips: one when $s = 1 - \frac{1}{7} = \frac{6}{7}$, the other when $s = 1 + \frac{1}{5} = 1.2$. Of special importance is the first dip. Indeed, if the static torque M_{stat} proves to be greater than the minimum driving torque M_{min} , the motor, when accelerated, will reach point a , but will not pass through the dip in the torque curve and, consequently, will operate steadily at a speed much lower than the rated value, consuming a current considerably higher than the rated current.

20-14. Tooth-Ripple Harmonics

Of all the stator harmonics that develop asynchronous torques, special attention should be paid to the tooth-ripple harmonics, i.e., the harmonics which in the general case have an order $v_{t1} = k \frac{Z_1}{p} \pm 1$ (Sec. 2-4). Here k is any positive integer. The tooth harmonic for $k=1$ is considered to be the fundamental harmonic, the others, the higher harmonics. The higher tooth-ripple harmonics may be neglected.

The primary importance attached to stator tooth-ripple harmonics as regards the development of parasitic induction torques is due chiefly to the fact that for the tooth harmonics the winding distribution factor is equal to the distribution factor of the first harmonic [formula (2-15)], while for magnetizing force harmonics of other orders it is considerably less. As a more detailed analysis shows, the value of the parasitic induction torque depends mainly on the ratio $\left(\frac{k_{wv}}{k_{w1}}\right)^2$, where k_{w1} and k_{wv} are the winding factors for the first and v -th harmonics. Thus, for tooth-ripple harmonics, the above ratio is greater than for other harmonics. This explains the importance attached to the tooth-ripple harmonics.

The effect of the stator tooth harmonics and the torques produced by them can be greatly limited by a proper choice of the number of rotor slots Z_2 . Special analysis shows that for this purpose we must have

$$Z_2 \leq 1.25 \left(\frac{Z_1}{p} \pm 1 \right) p \leq 1.25 (Z_1 \pm p) \quad (20-55)$$

20-15. Synchronous Torques

In the general case the synchronous torque is defined as the torque appearing at a certain rotor speed as the result of interaction between stator and rotor harmonics of the same order, i.e., at $v_1 = v_2$ and at

such a rotor speed at which these harmonics rotate in synchronism. In particular, of primary importance are the synchronous torques which are produced when the stator and rotor tooth-ripple harmonics are of the same order, i.e., at

$$v_{t1} = v_{t2} \quad (20-56)$$

Assuming $k=1$ (see above, Sec. 20-14), we have

$$\frac{Z_1}{p} \pm 1 = \frac{Z_2}{p} \pm 1$$

Consequently, the synchronous torques occur when

$$Z_1 = Z_2; \quad Z_1 - Z_2 = \pm 2p \quad (20-57)$$

Therefore, these relations between the number of stator and rotor slots should be avoided. The case when $Z_1 = Z_2$ is rarely met with, however, since rotor sticking which occurs when the rotor is at standstill has long been known.

For illustration, Fig. 20-11a and b shows torque curves for a four-pole motor with $Z_1 = 24$ and $Z_2 = 24 \pm 4 = 28$ or 20 slots.

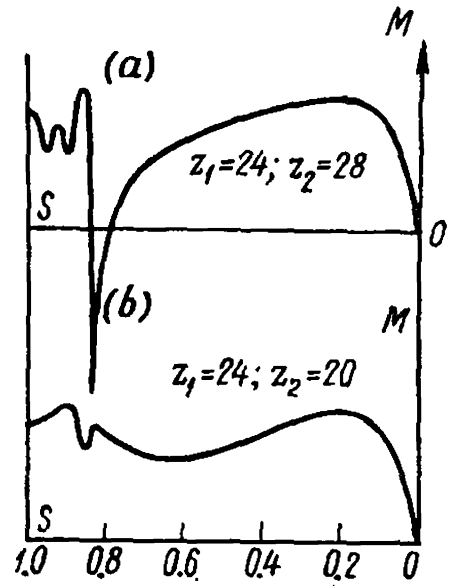


Fig. 20-11. Torque curves with $2p = 4$

20-16. Vibration Torques

When a rotor runs, its teeth continuously move with respect to the stator teeth; periodical variations of the flux density occur in the stator and rotor teeth, causing various acoustical effects: hum, whistling, etc. Besides, when the axes of the stator and rotor teeth coincide, a unidirectional pulling force appears between the stator and rotor at a given point on the stator periphery. When the rotor runs, this force moves along the gap at a definite speed and causes the rotor to vibrate. At a certain speed of the rotor these vibrations may begin to resonate with the natural (mechanical) oscillations of the rotor. If this phenomenon develops to a considerable extent, it may make operation impossible. Analysis shows that vibration torques appear if

$$Z_1 - Z_2 = \pm 1 \pm 2p \quad (20-58)$$

Some investigations show that such relations between the number of slots are undesirable when

$$0.5 \times (Z_1 - Z_2) = \pm 1 \pm 2p$$

or

$$Z_1 - Z_2 = \pm 2 \pm 4p \quad (20-59)$$

Since $Z_1 = 2pm_1q_1$, then, with q_1 an integer, Z_1 becomes an even number. Here condition (20-58) leads to the conclusion that a rotor with an

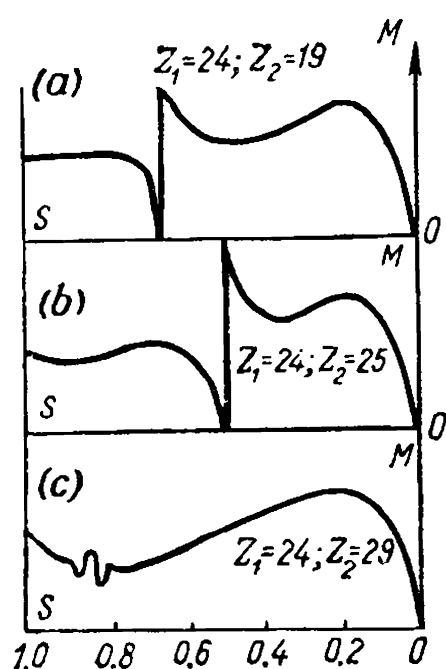


Fig. 20-12. Vibration torques, $2p = 4$;
 $Z_1 = 24$, $Z_2 = 24 + 1$
 and $Z_2 = 24 \pm (1 + 4)$

odd number of slots is undesirable, this having been experimentally confirmed.

Shown in Fig. 20-12a, b and c are torque curves for $Z_1 = 24$; $Z_2 = 24 + 1$; $Z_2 = 24 \pm (1 + 4)$ with $2p = 4$, given for purposes of illustration.

20-17. Preventive Measures Against Parasitic Torques

From the above it follows that the induction motor may be represented as a number of additional induction and synchronous motors mounted on the same shaft as the main motor. We have seen that these additional motors may disturb the operating conditions of the main motor or even make operation impossible. Therefore, the parasitic torques of the induction motor should be eliminated as fully as possible.

The simplest way to eliminate them is to weaken the stator winding magnetizing force harmonics. For this purpose fractional-pitch windings with an integral number of slots per pole per phase are used. Windings with a fractional number of slots per pole per phase produce magnetizing force systems asymmetrically distributed along the stator periphery and facilitate the appearance of noise in the motor. Therefore fractional-slot windings, in contrast to synchronous motor practice, are seldom used in induction motors. The number of slots of a rotor must meet the condition of formula (20-55).

Very effective means against parasitic induction torques is the skewing of the rotor or stator slots.

The rotor slot skew is made equal to the stator tooth pitch t_1 , or is decreased to $t_1 \frac{Z_1}{Z_1 + p}$. In the first case we partially paralyze the action of the direct and reverse tooth-ripple harmonics of the order $\frac{Z_1}{p} \pm 1$, while in the second case we eliminate the action of the most dangerous direct harmonic $\frac{Z_1}{p} + 1$. Indeed, the slot skew factor can be determined from formula (3-1), if we insert in it the following values: $v = \frac{Z_1}{p}$ or $v = \frac{Z_1}{p} + 1$; $c = t_1$ or $c = t_1 \frac{Z_1}{Z_1 + p}$. In both cases the slot skew factor k_{sk} and, consequently, the e.m.f.s induced by the tooth-ripple harmonics are equal to zero. The same can be seen in Fig. 20-13. The conductor ab of the rotor is skewed by t_1 and e.m.f.s are induced in the conductor which mutually balance each other.

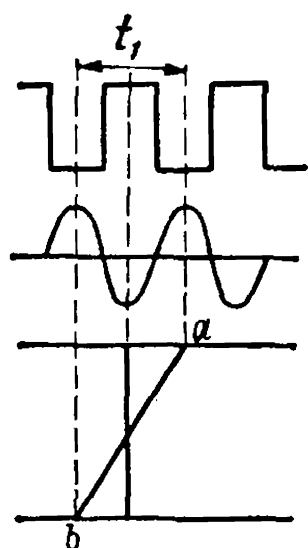


Fig. 20-13. Influence of slot skewing on e. m. f. tooth-ripple harmonics

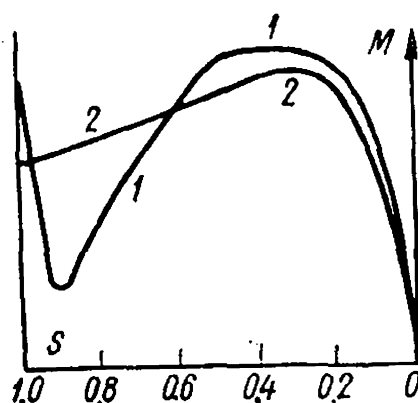


Fig. 20-14. Torque curves for straight-tooth (1) and skewed-tooth (2) slots

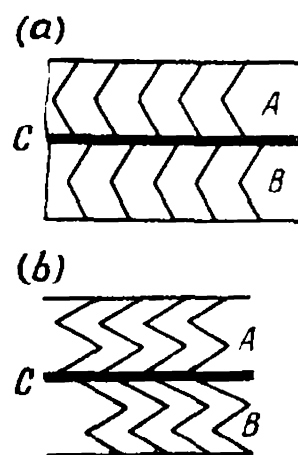


Fig. 20-15. Zigzag-tooth rotor slots

When the stator slot skew is made equal to the rotor tooth pitch t_2 , the results are the same.

Curve 1 in Fig. 20-14 depicts the torque of a motor without slot skewing, and curve 2 with skewed slots. It is easy to notice how favourably skewing influences the elimination of parasitic torques.

To reduce noise in motors, zigzag-tooth slots (see Fig. 20-15 *a* and *b*) are sometimes used instead of straight-tooth slots. The rotor is divided lengthwise into two parts *A* and *B* so that the slots of one part are displaced with respect to those of the other; adjacent ends of both halves of the winding are attached to the common connecting ring *C*.

It should not be forgotten, however, that slot skewing is equivalent to an additional reduction in the winding factor. It increases the leakage flux in the motor and thus decreases somewhat the performance of the motor, in particular its power factor and the overload capacity. This can also be seen from Fig. 20-14.

An increase in the air-gap reduces parasitic torques, and also the additional losses. But an increased air-gap leads to an increase in no-load current and, as a result, to a poorer motor power factor ($\cos \varphi$). Therefore, only in motors of high reliability, for mechanical reasons, is the air-gap made larger than usual.

To avoid synchronous and vibration torques, a proper choice of the respective number of slots for the stator and rotor is necessary. Summarizing everything mentioned in this connection, we obtain the following undesirable relations between the number of slots Z_1 and Z_2 :

$$Z_1 - Z_2 = \pm 2p; Z_1 - Z_2 = \pm 1 \pm 2p; Z_1 - Z_2 = \pm 2 \pm 4p$$

Moreover, odd numbers of rotor slots are also undesirable. Consequently, on the whole the choice of the number of rotor slots is a re-

latively complex problem which in practice can be solved only experimentally.

For illustration below are given the favourable numbers of rotor slots Z_2 for four-pole motors without slot skewing:

with $Z_1=24$

$$Z_2=18, 30, 34 \text{ and } 38$$

with $Z_1=36$

$$Z_2=10, 14, 22, 26, 30, 42, 46, 50, 54 \text{ and } 58$$

with $Z_1=48$

$$Z_2=10, 14, 18, 30, 34, 42, 54, 58, 62 \text{ and } 66$$

The favourable effect of these recommended rotor slot numbers on the motor torque is mainly confirmed experimentally.

20-18. Performance Characteristics of an Induction Motor

The performance characteristics of an induction motor, as of a synchronous motor, are those that give the relations:

$$n, M, \eta \text{ and } \cos \varphi = f(P_2) \text{ with } U_1 = \text{const and } f_1 = \text{const}$$

In addition, the following data are also important: the overload capacity factor k_{ov} and for squirrel-cage motors, also the multiplicity factor of the starting current and the starting torque.

Speed of Motor $n = f(P_2)$. From formula (1-3) for the slip it follows that

$$n = n_1(1-s) \quad (20-60)$$

On the other hand, according to equation (20-20),

$$s = \frac{p_{cop2}}{P_{em}} \quad (20-61)$$

Thus, the slip of an induction motor is numerically equal to the ratio of the losses p_{cop2} in the rotor winding to the electromagnetic power P_{em} developed by the motor.

The no-load losses p_{cop2} are diminishingly small in comparison with the power P_{em} , and we have $s \cong 0$ and $n \cong n_1$. As the load increases, the ratio (20-61) grows, but for obtaining a high motor efficiency it is limited to a very narrow range. Usually at the rated load, the ratio $\frac{p_{cop2}}{P_{em}} \cong \frac{p_{cop2}}{P_2} = 1.5-5.0\%$. The smaller figure relates to larger motors, the greater to small 3-10-kW motors. The relation $n = f(P_2)$ is a curve with a very slight incline to the axis of abscissas (Fig. 20-16). It can be seen that the induction motor has a speed characteristic similar to that of a d.c. shunt motor.

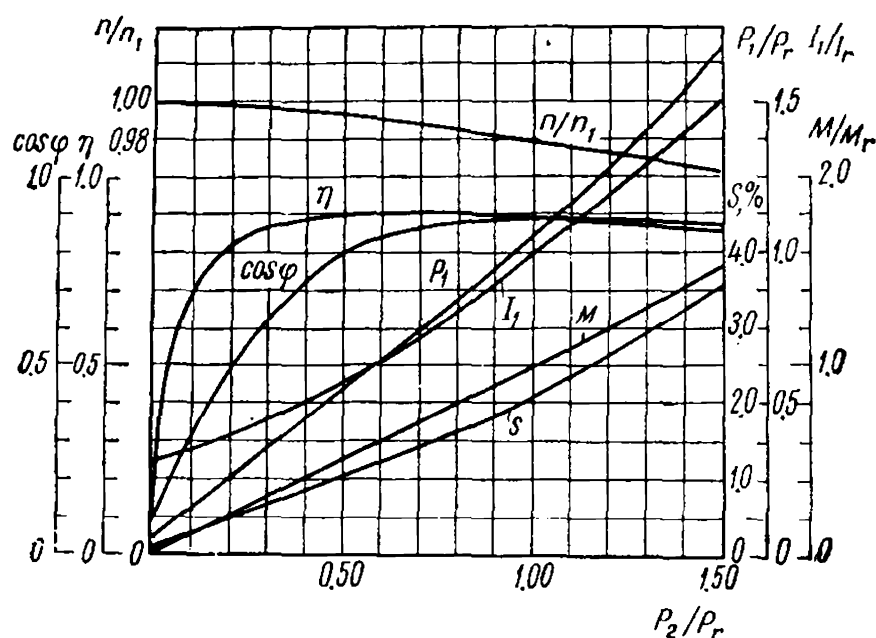


Fig. 20-16. Performance curves of 50-kW, 220/380-V, 1470-rpm squirrel-cage induction motor in relative units

Relation $M=f(P_2)$. In steady-state operating conditions $M=M_2+M_0$, where M_2 is the useful braking torque of a motor and M_0 is the no-load torque. Since with a change in load in the range from no-load to rated load the speed of induction motors remains almost constant, the relation $M=f(P_2)$ of an induction motor is nearly linear (Fig. 20-16).

Motor Losses and Efficiency. In induction motors the same kinds of losses occur as in all other electrical machines, i.e., mechanical, steel, copper, and additional losses.

The main kinds of losses in induction machines are determined by formulas similar to those given in previous sections (see Vol. I, Chapter 7, Vol. II, Secs. 11-8 and 20-11). The additional losses form a special group. They include additional copper and additional steel losses. With sinusoidal voltage across the motor terminals the additional copper losses are partly due to the influence of higher magnetizing force harmonics, and partly to the skin effect.

The additional copper losses due to higher magnetizing force harmonics occur mainly in the windings of a squirrel-cage rotor. When the rotor runs in magnetic field produced by the higher harmonics of the stator magnetizing force, currents appear in the rotor winding with a frequency differing from the slip frequency and depending on the rotor speed. To reduce these losses, the following steps may be taken: (a) shortening of the stator winding pitch, which leads to a decrease in the higher order magnetizing force harmonics, (b) skewing of the rotor slots with respect to the stator slots, this being equivalent to pitch shortening, and (c) proper choice of the number of stator and rotor slots Z_1 and Z_2 . Analysis shows that if the additional rotor los-

ses should not exceed 10% of the fundamental losses due to the current first harmonic, then, for non-skewed slots, $Z_2 \leq \frac{4}{3} Z_1$.

The skin effect phenomenon is observed both in stator and in rotor windings, especially in those with a squirrel cage. Here the effect can be used for improving the starting characteristics of motors with a squirrel-cage rotor. However, during normal operating conditions the frequency of the current in the rotor does not exceed 3 Hz. Under such conditions the skin effect is practically imperceptible. The phenomena occurring in starting and connected with the skin effect in the rotor are examined in Chapters 22 and 23.

Since the additional losses due to the higher magnetizing force harmonics are produced by currents with a frequency different from the current first harmonic, they are compensated by the mechanical power developed by the motor.

It may be assumed with sufficient accuracy that the additional copper losses are proportional to the square of the current.

The additional losses in the steel of induction machines consist, as in synchronous machines, of pulsation losses and surface losses.

The pulsation losses are caused by direct-axis pulsations of the magnetic flux due to variations in the magnetic permeance as a result of the continuous change in mutual position of the stator and rotor teeth during rotation of the rotor. The pulsation frequency in the stator is $f_{t1} = Z_2 n$, and in the rotor is $f_{t2} = Z_1 n$, where Z_1 and Z_2 are the number of stator and rotor slots and n the speed of the rotor. The calculation of these losses is the subject of a special course.

The surface losses are due mainly to the fact that the slots cause dips to appear in the curve of flux density distribution in the air-gap (Fig. 20-17). The frequency of the surface pulsations is the same as that of the pulsations in the teeth. Analysis shows that the surface losses depend on the frequency to the power 1.5 and on the square of the mean value of the flux density in the gap.

Since the additional losses in the steel have a frequency differing from the fundamental frequency, they are compensated by the mechanical power developed by the motor.

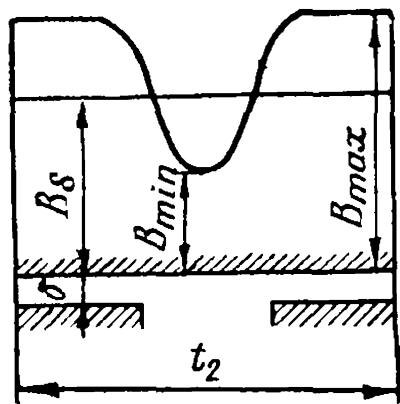


Fig. 20-17. Curve of flux density in the air-gap

It can be assumed with sufficient accuracy that the additional losses in the steel change in proportion to the square of the voltage across the motor terminals.

The degree of accuracy which the additional losses are calculated with is rather small. They are, therefore, usually taken into account by approximation as a certain per cent of the output when the machine operates as a generator, or of the supplied power when the machine operates as a motor. According to GOST 183-66, the

additional losses p_{add} in induction machines at rated load amount to 0.5% of the supplied power. It should be remembered, however, that this is an average figure, found experimenally and from which considerable deviations are often observed.

The total losses in a motor are equal to

$$\sum p = p_{cop1} + p_{cop2} + p_{st} + p_{mech} + p_{add} \tag{20-62}$$

At loads from idling to rated load the losses p_{st} define only losses in the stator core, since with the usual frequencies in the rotor (1 to 3 Hz), the losses in the steel tend to vanish.

With an increase in load the sum of the losses $p_{st} + p_{mech}$ decreases somewhat owing to a reduction in the main flux and to a decrease in speed. Usually this reduction does not exceed 4-8%, therefore these losses are referred to as the constant losses of the motor.

In contrast to the losses in steel, the losses in copper are proportional to the square of the current.

The additional losses, as we have already seen, depend partly on the current, and partly on the voltage. For simplicity it is assumed that they are proportional to the supplied power.

Reasoning in the same way as with d.c. machines (Vol I, Sec. 7-8), we come to the conclusion that the maximum efficiency is reached when the constant and the variable losses are equal; thus, by a corresponding redistribution of the losses, we can obtain motors having efficiency curves of different shapes. Figure 20-16 shows a typical efficiency curve for an induction motor, the curve reaching its maximum at approximately 75% of the rated load.

Table 20-1 gives, for purposes of illustration, efficiency values for slip-ring and squirrel-cage motors with power ratings of $n = 1000$ rpm and $2p = 6$.

TABLE 20-1

Slip-ring motors				Squirrel-cage motors			
U, V	P_r, kW	$\eta, \%$	$\cos \varphi$	U, V	P_r, kW	$\eta, \%$	$\cos \varphi$
220/380	8.0	83.0	0.80	220/380	9.1	86.0	0.825
220/380	13.5	85.0	0.81	220/380	15.2	87.1	0.835
220/380	29.0	87.0	0.845	220/380	32	89.0	0.855
220/380	44.0	88.2	0.870	220/380	48	90.3	0.87
220/380	67	89.5	0.88	220/380	72	90.7	0.88
220/380	100	91.5	0.88	220/380	100	91.5	0.88
6000	260	91.0	0.86	6000	260	91.0	0.85
6000	430	92.5	0.88	6000	430	92.5	0.87
6000	875	93.5	0.89	6000	875	93.5	0.88

It should be noted that in this table the efficiency of low-power spuirrel-cage motors is higher than that of slip-ring motors. A cer-

tain, though non-essential reduction in efficiency results in an increased voltage.

Power Factor $\cos \varphi = f(P_2)$. An induction motor, as a transformer, consumes lagging current from the power circuit almost independent of the load. Therefore, its power factor is always less than unity. At no-load the power factor ($\cos \varphi$) does not usually exceed 0.2, but under load it grows rather rapidly (Fig. 20-16) and reaches its maximum at a power close to the rated value. With a further increase in load the speed of the motor falls; this increases the angle $\psi_2 = \arctan \frac{sX_2}{r_2}$ and reduces $\cos \psi_2$ and $\cos \varphi$ (Fig. 20-16). The change of $\cos \varphi$ with load can be more distinctly observed on the circle diagram described in the following chapter.

Table 20-1 illustrates values of $\cos \varphi$ for different types of motors. Squirrel-cage motors are designed as deep-slot or double-cage motors, and their $\cos \varphi$ is somewhat lower than that of slip-ring motors of the same power rating (for greater detail see Chapter 23).

Motor Overload Capacity. The overload capacity of an induction motor or its stalling torque is the ratio of the maximum torque of the motor to its rated torque, i.e.,

$$k_{ov} = \frac{M_{max}}{M_r}$$

Usually for low- and medium-power motors $k_{ov} = 1.6-1.8$. For medium- and high-power motors $k_{ov} = 1.8-2.5$. For motors of special design k_{ov} reaches 2.8-3.0 and even more.

Chapter

21

CIRCLE DIAGRAMS FOR AN INDUCTION MACHINE

21-1. Main Concepts of Theory of Loci of A. C. Machines in Symbolic Form

The properties of a.c. machines can be properly investigated with the aid of the loci of the ends of the primary current vectors when the machine consecutively passes through different operating conditions. Very convenient for investigating many loci is the method of analysis of curve equations in the symbolic form.

Line and Circle. If \dot{B} is a complex number, representing a certain vector, and p a real parameter which assumes any value within the limits of $\pm\infty$, then the product $\dot{B}p$ represents all vectors, coinciding in direction with vectors \dot{B} and $-\dot{B}$, and, therefore, an equation of a straight line passing through the origin of coordinates has the form $\dot{U} = \dot{B}p$. Accordingly the equation of a line which passes parallel to vector \dot{B} through the end of vector \dot{A} (Fig. 21-1) has the form

$$\dot{U} = \dot{A} + \dot{B}p$$

When inverting a line expressed by the equation

$$\dot{U} = \dot{C} + \dot{D}p$$

we obtain the equation of a circle (Fig. 21-2a) passing through the origin of coordinates and having the symbolic form of

$$\dot{U} = \frac{1}{\dot{C} + \dot{D}p}$$

where $\dot{C} = c_1 + jc_2$; $\dot{D} = d_1 + jd_2$.

An equation of the form

$$\dot{U} = \frac{\dot{E}}{\dot{C} + \dot{D}p}$$

also represents a circle, passing through the origin of coordinates, but turned through an angle equal to the argument of the complex \dot{E} and multiplied by its modulus.

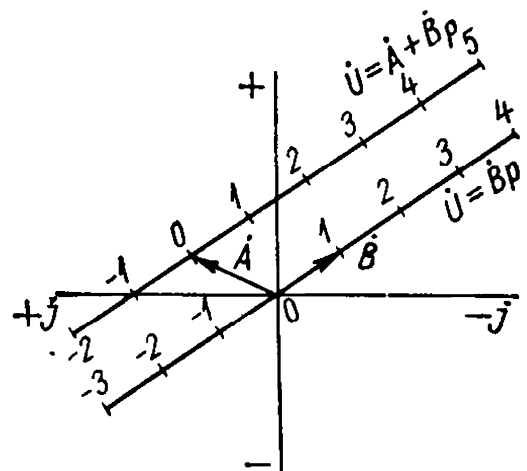


Fig. 21.1 Straight lines on a complex plane

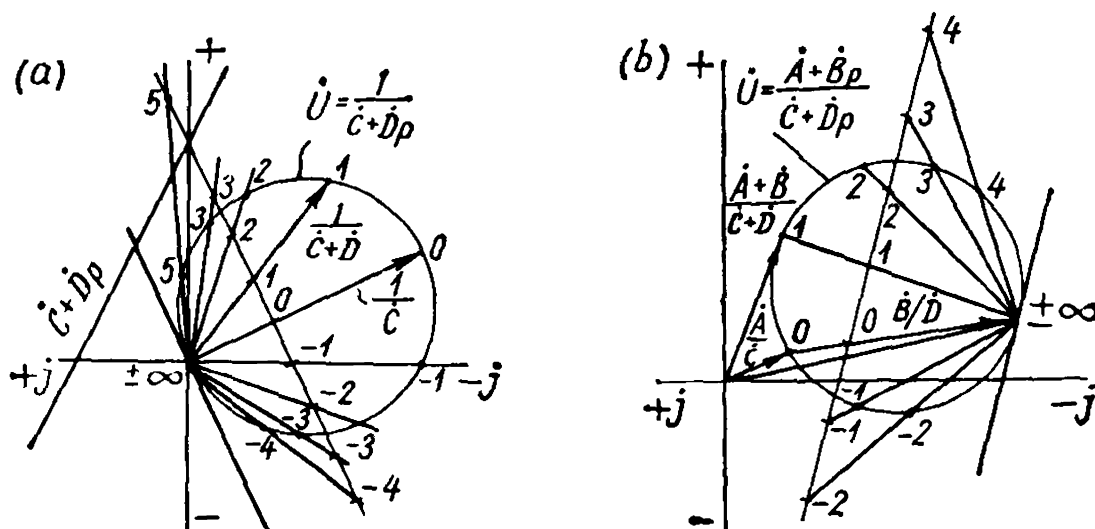


Fig. 21-2. Circles on a complex plane

When shifting the origin of coordinates by a constant segment expressed by the complex \dot{F} , we obtain the equation of a circle in the general form, not passing through the origin of coordinates (Fig. 21-2b):

$$\dot{U} = \dot{F} + \frac{\dot{E}}{\dot{C} + \dot{D}p} = \frac{\dot{A} + \dot{B}p}{\dot{C} + \dot{D}p}$$

where $\dot{A} = \dot{C}\dot{F} + \dot{E}$; $\dot{B} = \dot{F}\dot{D}$.

With $p = 0$

$$\dot{U}_0 = \frac{\dot{A}}{\dot{C}}$$

with $p = \pm \infty$

$$\dot{U}_\infty = \frac{\dot{B}}{\dot{D}} = \dot{F}$$

with $p = 1$

$$\dot{U} = \frac{\dot{A} + \dot{B}}{\dot{C} + \dot{D}}$$

The equation of a circle can also be represented as

$$\dot{U} = \dot{M} + Re^{j\theta} = (x_m + jy_m) + (x_r + jy_r)e^{j\theta}$$

where \dot{M} is the vector of the centre of the circle, $Re^{j\theta}$ is the radius-vector of the circle and θ an angle varying from 0° to 360° (Fig. 21-3).

The relations between the complex coefficients in the circle equations are

$$\dot{A} = \dot{M}\dot{C} + \dot{R}\dot{C}$$

$$\dot{B} = \dot{M}\dot{D} + \dot{R}\dot{D}$$

and

$$\dot{M} = \frac{\dot{A}\dot{D} - \dot{B}\dot{C}}{\dot{C}\dot{D} - \dot{D}\dot{C}}$$

$$\dot{R} = \frac{\dot{B}\dot{C} - \dot{A}\dot{D}}{\dot{C}\dot{D} - \dot{D}\dot{C}}$$

where \dot{C} and \dot{D} are conjugate numbers.

Accordingly, the coordinates of the centre M are:

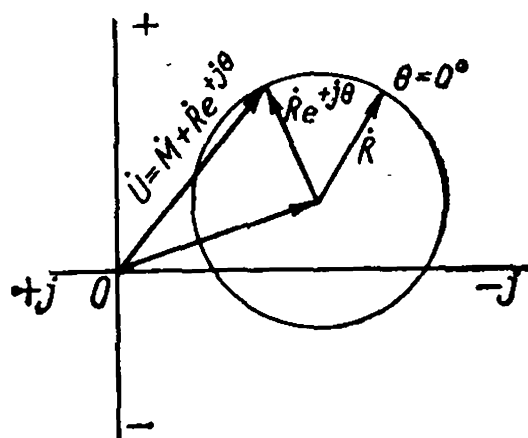


Fig. 21-3. Circle in arbitrary position on the complex plane

$$x_M = \frac{a_1d_2 - a_2d_1 - b_1c_2 + b_2c_1}{2(c_1d_2 - c_2d_1)}$$

$$y_M = \frac{a_1d_1 + a_2d_2 - b_1c_1 - b_2c_2}{2(c_1d_2 - c_2d_1)}$$

The coordinates of the radius-vector \dot{R} with $\theta = 0$ are

$$x_R = \frac{a_1d_2 + a_2d_1 - b_1c_2 - b_2c_1}{2(c_1d_2 - c_2d_1)}$$

$$y_R = -\frac{a_1d_1 - a_2d_2 - b_1c_1 + b_2c_2}{2(c_1d_2 - c_2d_1)}$$

Parameter Scale for Circle. To construct a circle it is necessary to plot \dot{U} in a complex plane (Fig. 21-4), next plot its mirror reflection in the axis of real quantities, and then inverse this straight line. If we lay off the value of parameter p on the reflected line \dot{U} , and connect the origin of coordinates O ($p = \pm\infty$) by means of straight lines with points corresponding to the values of the parameter p , we get points with the same parameter values at their intersections with the circle. Obviously, at the intersection of these lines with any other straight line parallel to the reflected line, the same distribution of the parameter p is obtained. Thus the parameter scale can in the general case be constructed on any straight line parallel to a tangent at point $p = \pm\infty$. If two points are known on the scale with two values of the parameter, for example, points with $p = 0$ and $p = 1$, then the scale of the parameter can be readily marked for other values of p .

Higher-Order Curves. In the theory of alternating current, of importance is the bicircular curve of the fourth order, expressed by the equation

$$\dot{U} = \frac{\dot{A} + \dot{B}p + \dot{C}p^2}{\dot{D} + \dot{E}p + \dot{F}p^2}$$

The most important is a bicircular curve which represents a limited section of a circle with two-digit value of the parameter p (Fig. 21-5).

the form of a Pascal's limaçon (Fig. 21-7), whose equation has the form:

$$\dot{U} = \dot{A} + \dot{B}e^{-j\theta} + \dot{C}e^{-j2\theta}$$

21-2. Improved Circle Diagram

Preliminary Remarks. The performance curves and other characteristics of the induction machine which determine its properties can be obtained by testing the machine under load. However, tests under load are often difficult to carry out and even impossible, as, for instance, with high-power machines built at electrical machine-building works. In such cases the characteristics of a machine can be obtained with the help of its circle diagram based on data obtained from comparatively easily performed no-load and short-circuit tests.

The circle diagram can also be constructed on the basis of the design data of the machine to obtain the design performance and other characteristics.

The circle diagram is the locus of the end of the primary-current vector I_1 of the machine, with $U_1 = \text{const}$ and the slip varying within the range $-\infty \leq s \leq +\infty$. This locus, as will be indicated below, is a circle only when the resistances and reactances of the machine may be considered as constant and independent of the current and slip. The latter, with certain approximations, is true for machines of normal design, i.e., for machines with slip rings and single squirrel cages made of round rods.

The present chapter considers the loci of machines with constant parameters. At the end of the chapter are considered the problems when normal-type machine loci depart from a circular form. The loci of machines with essentially non-linear parameters (deep-slot motors, double-cage motors) are considered in Chapter 23.

Construction of Circle Diagram. An improved circle diagram is based on the improved L-type equivalent circuit (see Fig. 19-7b) in which the correction factor σ_1 is assumed to be a real number σ_1 [see equation (19-28)]. In this circuit

$$\begin{aligned} R_1 &= r_1 \sigma_1; & R_2 &= r'_2 \sigma_1^2 \\ X_1 &= x_1 \sigma_1; & X_2 &= x'_2 \sigma_1^2 \\ \dot{I}_2'' &= \dot{I}_2' \sigma_1 \end{aligned}$$

Since the expression for the resistance of the branch part of the equivalent circuit does not include the slip s , the current in this part with $U_1 = \text{const}$ remains unchanged for all variations of the slip s and, consequently, for all loads of the induction machine. In the main part all the resistances and inductive reactances are series-connected, the slip s being only in the denominator of the total resistance $\frac{R_2}{s}$;

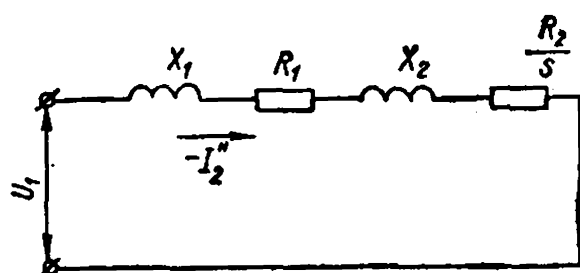


Fig. 21-8. Main part of L-type equivalent circuit

magnetizing branch part of the circuit and the variable current vector $-I_2''$ of the main part, which varies together with the change in the slip s :

$$I_1 = I_{00} + (-I_2'')$$

Obviously, it is sufficient here to find the law of displacement of the end of the current vector $-I_2''$ with a change in s , since this will simultaneously give the law of displacement of the end of the current vector I_1 coinciding with the end of the vector $-I_2''$.

Let us separate from the equivalent circuit in Fig. 19-7b the main part, whose resultant impedance Z_{res} depends on the slip s (Fig. 21-8). For the current of the main part the following equation can be written:

$$-I_2'' = \frac{\dot{U}_1}{Z_{res}} = \frac{\dot{U}_1}{\left(R_1 + \frac{R_2}{s}\right) + j(X_1 + X_2)} \quad (21-1)$$

Correspondingly,

$$\tan \psi_2'' = \frac{X_1 + X_2}{R_1 + \frac{R_2}{s}}; \quad \sin \psi_2'' = \frac{X_1 + X_2}{Z_{res}}; \quad \cos \psi_2'' = \frac{R_1 + \frac{R_2}{s}}{Z_{res}} \quad (21-2)$$

Let us direct the axis of ordinates in Fig. 21-9a along line OA and lay off the current vector $\overline{OB} = -I_2''$ at an angle ψ_2'' to it. Let us draw from end B of this vector a perpendicular to intersect the axis of abscissas at point C and the axis of ordinates at point A . The length OC on the axis of abscissas cut off by this perpendicular is

$$OC = \frac{OB}{\sin \psi_2''} = \frac{U_1}{Z_{res}} \frac{Z_{res}}{X_1 + X_2} = \frac{U_1}{X_1 + X_2} = \frac{U_1}{X_{sh}}$$

Since we assume the values of the inductive reactances X_1 and X_2 to be independent of the current $-I_2''$ and, therefore, of the slip s , the length $OC = \text{const}$ at any values of $-I_2''$ and s .

Seeing that a curve which includes one and the same angle $\angle OBC = 90^\circ$ is a semi-circle, the end of the current vector $-I_2''$ with a change

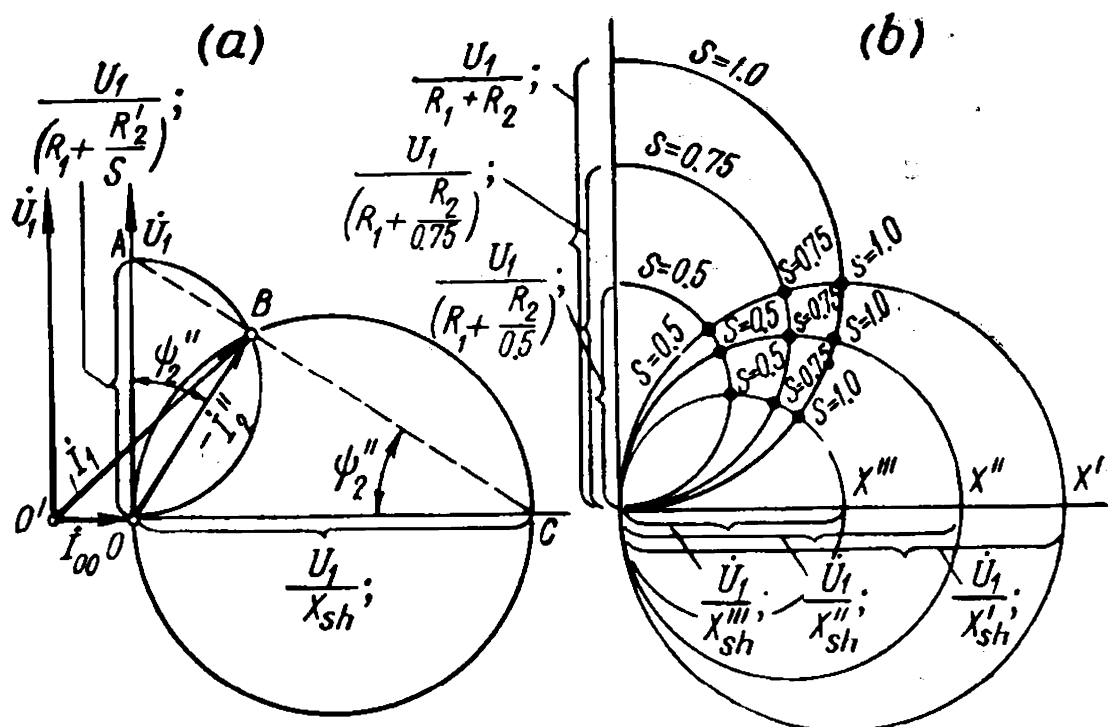


Fig. 21-9. Approximate circle diagrams of an induction machine

in the slip s from $-\infty \leq s \leq +\infty$ will describe a circle. Having laid off length $\overline{OO'} = I_{00}$ to the left of point O , i.e., the value of the no-load current when $s=0$, we obtain vector $\overline{O'B}$ of the primary current I_1 whose end will also describe the same circle.

The diameter of the circle $D = OC$ is, evidently, equal to

$$D = \frac{U_1}{X_1 + X_2} = \frac{U_1}{X_{sh}} \quad (21-3)$$

The length OA cut on the axis of ordinates in Fig. 21-9a by the perpendicular to the end of the current vector $\overline{OB} = I_2''$ equals:

$$OA = \frac{OB}{\cos \psi_2''} = \frac{U_1}{Z_{res}} \frac{Z_{res}}{R_1 + \frac{R_2}{s}} = \frac{U_1}{R_1 + \frac{R_2}{s}} \quad (21-4)$$

Hence it follows that once the current circle is found, we can easily find on it, for any given value of the slip, a point corresponding to the ends of the vectors $-I_2''$ and I_1 at the given slip s . For this purpose the segment $OA = \frac{U_1}{R_1 + \frac{R_2}{s}}$ should be laid off on the axis of ordinates

and point A connected with fixed point C , constant by condition. Obviously, point B at the intersection of line AC with the current circle will be the sought point of the current vector end. Instead of drawing the straight line AC we can also describe a circle around OA as the diameter and find its intersection with the current circle at the same point B .

When $s = 0$, point A , according to equation (21-4), coincides with the origin of coordinates. Therefore, for synchronous no-load operation $-I_2'' = 0$ and $I_1 = I_{00}$, as was to be expected. With a short circuit $s = 1.0$, and according to equation (21-4)

$$[OA]_{s=1} = \frac{U_1}{R_1 + R_2}$$

and when $s = \pm \infty$

$$[OA]_{s=\pm\infty} = \frac{U_1}{R_1}$$

Thus, by laying off along the axis of ordinates lengths corresponding to various slips, we can determine the points on the current circle corresponding to any value of the slip.

The diameter of the circle diagram according to equation (21-3) is inversely proportional to the short-circuit inductive reactance X_{sh} . With an increase in X_{sh} the diameter of the current circle decreases and, conversely, with a decrease in X_{sh} the diameter increases. In Fig. 21-9b current circles are shown for three different values of the reactance X_{sh} .

From the expression for the diameter of the auxiliary circle (21-4) it follows that with a change in the total short-circuit reactance X_{sh} with $s = \text{const}$ the end of the current vector also describes a circle, this circle now having the diameter OA and its centre on the axis of ordinates. In Fig. 21-9b current circles are given for three different values of the slip: $s = 0.5$; $s = 0.75$ and $s = 1.0$.

The active component of the no-load current when $s = 0$, i.e., of the current of the branch part in Fig. 19-7, is, according to equation (19-20), equal to:

$$I_{00a} = I_{00} \cos \varphi_0 = \frac{U_1}{z_m'} \frac{r_1 + r_m}{z_m'} = \frac{U_1 (r_1 + r_m)}{z_m'^2}$$

and the reactive component will be

$$\begin{aligned} I_{00r} &= I_{00} \sin \varphi_0 = \frac{U_1}{z_m'} \frac{x_1 + x_m}{z_m'} = \\ &= \frac{U_1 (x_1 + x_m)}{z_m'^2} \end{aligned}$$

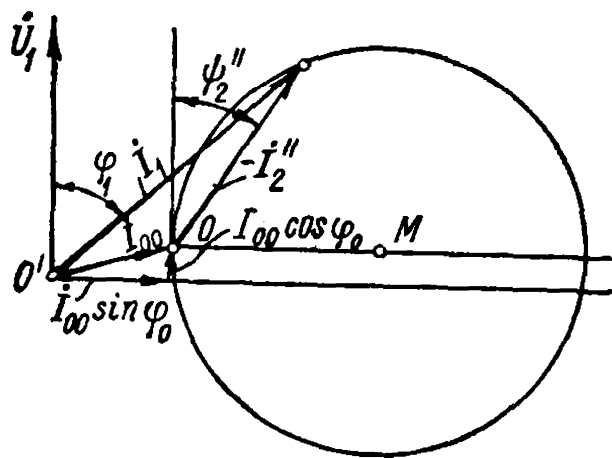


Fig. 21-10. Approximate circle diagram of an induction machine with account of the active component of the no-load current

By laying off from the beginning O of the current vector $-I_2''$ the active component of the current I_{00a} along the axis of ordinates and the reactive component I_{00r} along the axis of abscissas (Fig. 21-10), we obtain the origin of coordinates for

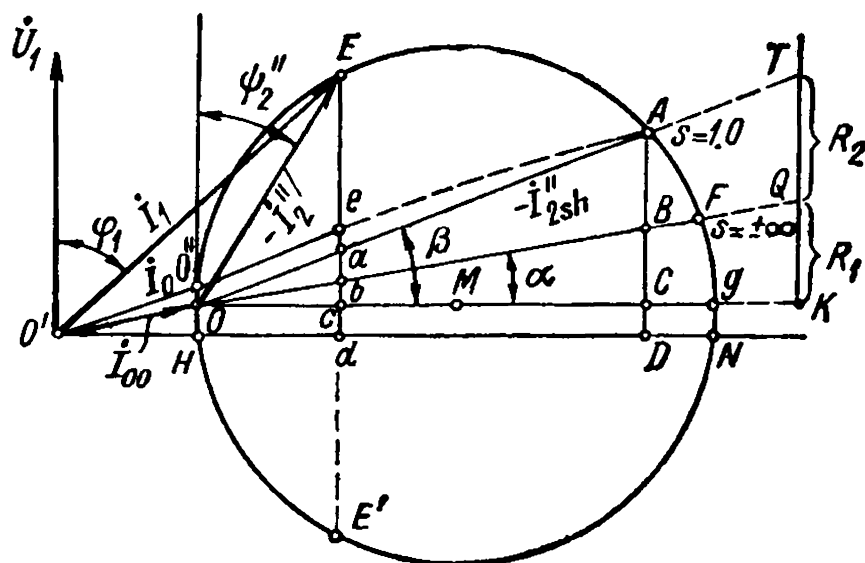


Fig. 21-11. Determination of losses and power from improved circle diagram corresponding to the equivalent circuit of Fig. 19-7

the beginning of the current vector \dot{I}_1 , whose end describes the same circle as the end of the current vector $-\dot{I}_2''$.

It should be noted here that we sometimes use a less exact circle diagram than the one considered in this discussion, assuming that the diameter of the circle diagram is

$$D = \frac{U_1}{x_1 + x_2}$$

Let us call this circle diagram a simplified one. It is obtained by removing the magnetizing circuit branch to the primary terminals without introducing the correction factors σ_1 and σ_1^2 for the parameters of the main part of the equivalent circuit.

As distinct from the simplified diagram, we shall call the circle diagram considered in this section, and based on the L-type equivalent circuit with the introduction of the real correction factors σ_1 and σ_1^2 , an improved diagram.

Expression of Losses and Power by Segments on the Circle Diagram. Figure 21-11 pictures an improved circle diagram corresponding to the improved L-type equivalent circuit of an induction machine (see Fig. 19-7). This circle diagram shows: (1) point F corresponding to $s = \pm \infty$; (2) point A corresponding to $s = 1.0$; (3) point O corresponding to $s = 0$, and (4) point E corresponding to a load in motor operation ($0 < s < 1.0$).

The arc OEA of the circle diagram corresponds to motoring ($0 < s < 1$); the arc AFN —to electromagnetic braking ($1 < s < \infty$) and the arc $OE'N$ —to generating ($-\infty < s < 1$).

Since the introduction of the correction factors σ_1 and σ_1^2 changes the inductive reactances only quantitatively, the circle diagram here

will also be a circle with the diameter

$$D = \frac{U_1}{x_1\sigma_1 + x_2'\sigma_1^2} = \frac{U_1}{X_1 + X_2}$$

Connect points A and F of the circle diagram in Fig. 21-11 with point O and draw perpendiculars to the axis of abscissas from points A and E . We thus obtain the intersection points a, b, c, d and A, B, C, D shown in Fig. 21-11.

Let us first show that if we draw on the diagram of Fig. 21-11 any vertical line, the lines OA, OF and the diameter line Og will cut off on this vertical line lengths proportional to the resistances R_1 and R_2 and the length of the circle-diagram diameter from point O to the indicated vertical line will be, with the same proportionality factor, the reactance $X_{sh} = X_1 + X_2$. Let us corroborate the discussion by using as an example the vertical line AC .

When $s = 1$, the current I_2'' is equal to

$$[I_2'']_{s=1} = \frac{U_1}{z_{sh}} = \frac{U_1}{\sqrt{R_{sh}^2 + X_{sh}^2}} = \frac{U_1}{\sqrt{(R_1 + R_2)^2 + (X_1 + X_2)^2}}$$

The tangent of the angle of displacement of this current relative to the voltage U_1 is, on the one hand, $X_{sh} : R_{sh}$. On the other hand, this angle, in Fig. 21-11, is equal to $\angle OAC$, whose tangent is $OC : AC$. Consequently,

$$\frac{OC}{AC} = \frac{X_{sh}}{R_{sh}} = \frac{X_1 + X_2}{R_1 + R_2} \quad (21-5)$$

When $s = \infty$, the impedance of the main part of the equivalent circuit in Fig. 19-7 is $R_1 + jX_{sh}$, since $\frac{R_2}{s} = 0$, and the current

$$[I_2'']_{s=\infty} = \frac{U_1}{\sqrt{R_1^2 + X_{sh}^2}}$$

Considering in a similar manner the tangent of the angle $[\psi_2'']_{s=\infty} = \angle OBC$, we get

$$\frac{OC}{BC} = \frac{X_{sh}}{R_1} = \frac{X_1 + X_2}{R_1} \quad (21-6)$$

Thus, if $OC = X_1 + X_2 = X_{sh}$ to a certain scale, then to the same scale $AC = R_1 + R_2 = R_{sh}$ and $BC = R_1$ and, consequently, $AB = AC - BC = R_{sh} - R_1 = R_2$.

The reactances and resistances X_{sh}, R_1 and R_2 are shown in Fig. 21-11 by OK, KQ and QT .

Let us now prove that ab, bc and cd show to a definite scale the separate losses of the machine for a given slip s corresponding to the load point E , and that AB, BC and CD show, to the same scale, the losses with $s = 1.0$.

From the geometrical construction (Fig. 21-11) we have

$$\begin{aligned} I_{2sh}''^2 &= m_i^2 OA^2 = m_i^2 OgOC \\ \tan \beta &= \frac{AC}{OC} = \frac{R_1 + R_2}{X_1 + X_2} \\ m_i Og &= \frac{U_1}{X_{sh}} \end{aligned}$$

where m_i is the current scale, i.e., the number of current units (amperes) per unit length of the segment on the diagram.

From the above relations we obtain

$$AC = OC \tan \beta = \frac{OA^2}{Og} \frac{R_1 + R_2}{X_1 + X_2} = \frac{I_{2sh}''^2 X_{sh} m_i}{m_i^2 U_1} \frac{R_1 + R_2}{X_{sh}} = \frac{1}{U_1 m_i} I_{2sh}''^2 (R_1 + R_2)$$

Since when $s = 1$ the losses in the machine corresponding to the current I_2'' of the main part of the equivalent circuit in Fig. 19-7 are equal to

$$p_{cop.sh} = m_1 I_{2sh}''^2 (R_1 + R_2) \quad (21-7)$$

then, according to the expression obtained for AC ,

$$p_{cop.sh} = m_p AC \quad (21-8)$$

where

$$m_p = m_1 U_1 m_i \quad (21-9)$$

is the power scale of the circle diagram.

The losses $p_{cop.sh}$ are, with a sufficient accuracy, the short-circuit losses of a machine for the voltage which the circle diagram was constructed for.

From Fig. 21-11 we have further that

$$\tan \alpha = \frac{R_1}{X_{sh}} = \frac{BC}{OC}$$

and, consequently,

$$\begin{aligned} BC &= OC \tan \alpha = \frac{OA^2}{Og} \frac{R_1}{X_{sh}} = \frac{1}{U_1 m_i} I_{2sh}''^2 R_1 \\ AB &= AC - BC = \frac{1}{U_1 m_i} I_{2sh}''^2 (R_1 + R_2) - \frac{1}{U_1 m_i} I_{2sh}''^2 R_1 = \frac{1}{U_1 m_i} I_{2sh}''^2 R_2 \end{aligned}$$

whence, for the short-circuit losses in the primary and secondary windings of the machine, we obtain with the same degree of accuracy:

$$\left. \begin{aligned} p_{cop1.sh} &= m_1 I_{2sh}''^2 R_1 = m_p BC \\ p_{cop2.sh} &= m_1 I_{2sh}''^2 R_2 = m_p AB \end{aligned} \right\} \quad (21-10)$$

Consider now motoring operation under load with $0 < s < 1.0$, expressed by point E on the circle diagram in Fig. 21-11.

From the geometrical construction we have in this case

$$\begin{aligned} OE^2 &= Og \cdot Oc \\ \tan \beta &= \frac{R_1 + R_2}{X_{sh}} = \frac{ac}{Oc} \\ \tan \alpha &= \frac{R_1}{X_{sh}} = \frac{bc}{Oc} \end{aligned}$$

whence

$$\begin{aligned} ac &= Oc \tan \beta = \frac{OE^2}{Og} \frac{R_1 + R_2}{X_{sh}} = \frac{1}{U_1 m_i} I_2'^2 (R_1 + R_2) \\ bc &= Oc \tan \alpha = \frac{OE^2}{Og} \frac{R_1}{X_{sh}} = \frac{1}{U_1 m_i} I_2'^2 R_1 \\ ab &= ac - bc = \frac{1}{U_1 m_i} I_2'^2 R_2 \end{aligned}$$

and, consequently, the losses in the copper of the primary and secondary windings and the sums of these losses for given operating conditions will be

$$\left. \begin{aligned} p_{cop1} &= m_1 I_2'^2 R_1 = m_p bc \\ p_{cop2} &= m_1 I_2'^2 R_2 = m_p ab \\ p_{cop} &= p_{cop1} + p_{cop2} = m_p ac \end{aligned} \right\} \quad (21-11)$$

where m_p is the same power scale factor.

The synchronous no-load losses of a machine, equal to the losses in the branch part of the equivalent circuit in Fig. 19-7 increased m_1 times, are found in a similar manner:

$$p_0 = m_1 I_{00}^2 (r_1 + r_m) = m_1 U_1 m_i OH = m_p OH = m_p cd \quad (21-12)$$

Thus, length bc expresses, to a scale previously established for the short circuit, the losses in the machine primary winding for a given current I_2' , length ab expresses, to the same scale, the losses in the secondary winding, and cd the no-load losses consisting of the no-load losses in the stator winding and the losses in the steel.

With the help of these lengths, expressing the losses, the lengths which express power can also be found.

The input power of an induction motor is

$$P_1 = m_1 U_1 I_1 \cos \varphi_1 = m_1 U_1 m_i Ed = m_p Ed \quad (21-13)$$

Thus, Ed expresses the motor input power to the same scale which the losses were previously determined to.

The mechanical power on the rotor of a motor is

$$P_{mech} = P_1 - p_0 - p_{cop} = P_1 - m_1 I_{00}^2 (r_1 + r_m) - m_1 I_2'^2 (R_1 + R_2)$$

Since Ed expresses the power P_1 , length cd synchronous no-load losses, and $ac = bc + ab$ the load losses in the windings, then, evident-

ly,

$$Ea = Ed - cd - ac$$

will express the power

$$P_{mech} = m_p Ea \quad (21-14)$$

If we add p_{cop2} to P_{mech} , we obtain the electromagnetic power P_{em} ; therefore

$$Eb = Ea + ab$$

expresses to the previously established scale the power P_{em} :

$$P_{em} = m_p Eb \quad (21-15)$$

as well as the electromagnetic torque M_{em} to the scale

$$m_t = \frac{m_p}{2\pi n_1} = \frac{pm_p}{2\pi f_1} \quad (21-16)$$

when measuring the torque in newton-metres and to the scale

$$m_t = \frac{pm_p}{9.81 \times 2\pi f_1} \quad (21-17)$$

when measuring the torque in kilogram-metres.

Thus, the electromagnetic torque for a given load is equal to

$$M_{em} = m_t Eb \quad (21-18)$$

Since the slip s equals the ratio of the secondary copper losses to the electromagnetic power, we have

$$s = \frac{p_{cop2}}{P_{em}} = \frac{ab}{Eb} \quad (21-19)$$

In the previous considerations all the losses were taken into account except the mechanical losses (due to friction and windage) p_{mech} and the additional losses p_{add} . Since both these losses may be considered as some additional braking torque applied to the shaft, the sum of these losses may be expressed by a common term $p_{mech.add}$. Evidently, at real no-load of a motor the additional braking torque due to these losses should increase the active component of the no-load current and force the rotor to rotate with a very small slip s_0 . Thus, for real no-load the end of the no-load current vector will be somewhat above point O for the slip $s=0$ and will occupy the position, for example, of point O'' in Fig. 21-11.

Within the range of normal loads and overloads of an induction motor, the slip, which does not usually exceed 3 to 5%, influences the speed so little that the mechanical and additional losses, which depend on the speed to the 1.5th power, may be considered invariable.

Therefore, over this section, the sum of the losses $p_{mech.add}$ may be accounted for by the segment parallel to the axis of ordinates between line OA and line $O''e$ parallel to it and passing through point O'' . With large overloads, when the slip begins to increase sharply and the speed to reduce, the parallelism is disturbed and these lines begin to converge to meet at point A when the slip $s = 1.0$, as shown by the dotted line in Fig. 21-11.

For the chosen point E the losses $p_{mech.add}$ may be expressed, to the previously established scale, by the segment $ea = OO''$

$$p_{mech.add} = p_{mech} + p_{add} = m_p ea \quad (21-20)$$

Thus, the useful power applied to the shaft $P_2 = P_{mech} - p_{mech.add}$ is expressed by the corresponding segment $Ee = Ea - ea$

$$P_2 = m_p Ee \quad (21-21)$$

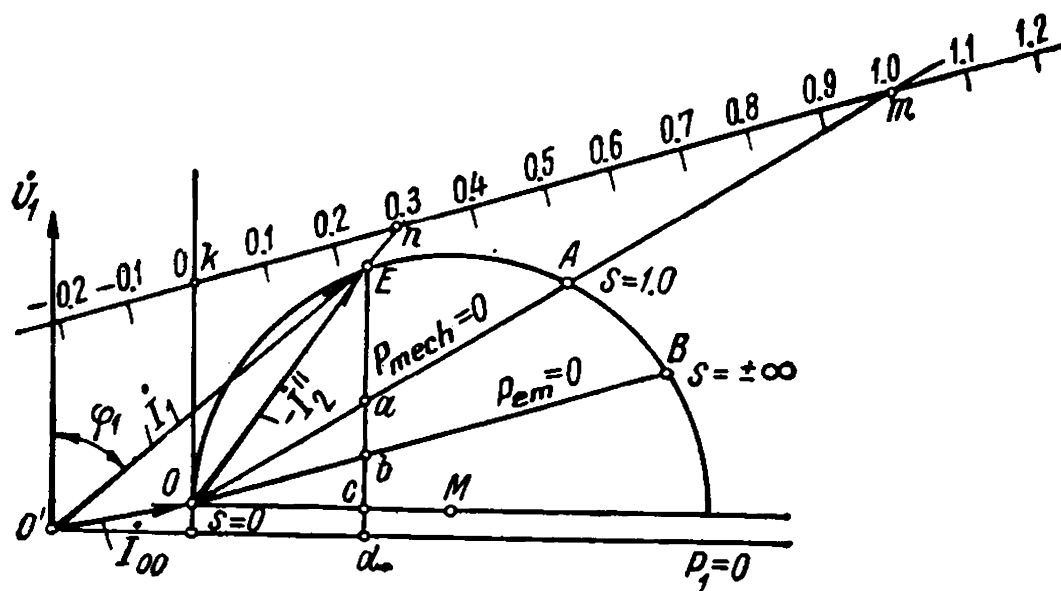
The efficiency of a motor $\eta = \frac{P_2}{P_1}$ can therefore be expressed as the ratio of the segments Ee and Ed

$$\eta = \frac{Ee}{Ed} \quad (21-22)$$

The above analysis of the elements of a circle diagram reveals the significance of the various lines taking part in the constructions. Since a perpendicular dropped to the axis of abscissas gives, to a definite scale, the motor input power, this axis may be called the line of primary power, complying with the equation $P_1 = 0$. In the same way the line OF connecting points on the circle with slips $s = 0$ and $s = \pm \infty$ is the line of electromagnetic power complying with the equation $P_{em} = 0$. The line OA connecting the points $s = 0$ and $s = 1.0$ is the line of mechanical power complying with the equation $P_{mech} = 0$. Finally, the line $O''e$ is the line of useful power $P_2 = 0$.

In our case we determine the powers P_{em} , P_{mech} and P_2 by the lengths between a point on the circle and one of the corresponding power lines $P_{em} = 0$, $P_{mech} = 0$ and $P_2 = 0$, but, instead of using this method, we might, according to the general theory of circle diagrams discussed in books devoted to the theoretical fundamentals of electrical engineering, draw from the given point on the circle a perpendicular to each of the lines of power. These perpendiculars would also express the powers to some definite, though different, scales for each line of power, and, therefore, the previous method, for which all the powers and losses have the same scale, is more convenient.

Construction of the Slip Scale. Draw the tangent Ok to the circle (Fig. 21-12) at point O with a slip $s = 0$ and line knm parallel to line OB of the electromagnetic power $P_{em} = 0$ at such a distance that length km can be readily divided into 100 parts. Let us prove that the exten-



sion of the line of secondary current $-I_2''$ will mark the slip corresponding to point E at point n on the scale km .

Triangles Okm and Oab are similar, since two of their sides are parallel, and the third side is common. Hence, we have the following proportion:

$$\frac{ab}{Ob} = \frac{Ok}{km}$$

For the same reason triangle Okn is similar to triangle OEb , and

$$\frac{Ob}{Eb} = \frac{kn}{Ok}$$

By multiplying these two proportions, we get

$$\frac{ab}{Eb} = \frac{kn}{km}$$

But it was previously shown that the slip

$$S = \frac{p_{cop2}}{p_{em}} = \frac{ab}{Eb}$$

whence

$$\frac{kn}{km} = s$$

Part km of the scale gives slips for motoring operation of an induction machine. If we continue the slip scale km to both sides and mark it out to the same scale as km , then to the right of point m we shall have values of $s > 1.0$, and to the left of point k negative values, $s < 0$. The slips within the range $1 < s < +\infty$ correspond to braking operation of the induction machine, and the negative slips ($s < 0$) to generating operation.

wer $P_1 = 0$; then the line parallel to the line $p_{cop} = 0$ will be the line of total losses of both parts $p_{cop} + p_0 = 0$. To take the mechanical and additional losses of the motor into account, it is necessary to bear in mind that for no-load the end of the current vector is not at point O , but at point O'' (Figs. 21-14 and 21-15).

By drawing through point O'' (Fig. 21-15) a straight line parallel to the line $P_{mech} = 0$, we obtain the line of useful power $P_2 = 0$, which at the intersection with the line $P_1 = 0$ gives point t . By drawing through t a straight line parallel to the axis of ordinates, we get the line of total losses $\Sigma p = 0$.

Since, as a result of the construction, the lines $\Sigma p = 0$ and $P_2 = 0$ were found to be identical with those of the previous geometrical construction, the efficiency scale will also be obtained in the form of a length parallel to the line $P_1 = 0$ and confined between the lines $P_2 = 0$ and $\Sigma p = 0$.

Determination of Power Factor ($\cos \varphi$). To determine $\cos \varphi$ for a given value of the current $I_1 = m_i OD$, the simplest way is to lay off on the axis of ordinates a length easily divisible into 10 parts (Fig. 21-17a) and construct a semi-circle on it, using it as a diameter. The length Oh at the intersection of the current vector I_1 or its extension with semi-circle Of is a measure of the power factor of the motor, since

$$\cos \varphi = \frac{Oh}{Of}$$

Motor Overload Capacity (Stalling Torque). The overload capacity of a motor is the ratio (see Sec. 20-5)

$$k_{ov} = \frac{M_{max}}{M_r}$$

To determine the torque M_{max} from the circle diagram, we draw from the centre O_1 of the current circle a perpendicular to the line of electromagnetic power $P_{em} = 0$ (Fig. 21-17a) and extend it to the intersection with the current circle at point S . The length

$$Sl = \frac{M_{max}}{m_t}$$

and, consequently,

$$k_{ov} = \frac{M_{max}}{M_r} = \frac{Sl}{dD}$$

provided that point D of the diagram corresponds to rated operating conditions.

Point S can also be found by drawing a tangent to the current circle parallel to the line of electromagnetic power $P_{em} = 0$.

Next we construct the short-circuit current vector of the main part of the circuit for the slip $s=1.0$ (\overline{OA})

$$I'_{sh} = I''_{2sh} = 214 \text{ A}, \quad \cos \varphi_{sh} \cong 0.161$$

We draw a perpendicular to the axis of abscissas from point A (Fig. 21-11) for the slip $s=1.0$ to its intersection with line Og at point C , line Og being drawn parallel to the axis of abscissas from the end of the no-load current vector I_0 and divide length AC at point B in the ratio

$$R_1 : R_2 = 0.7 : 0.604$$

Line OB , drawn from the end of the no-load current vector I_{00} through point B , is the line of electromagnetic power $P_{em}=0$ and, correspondingly, the line of the torque $M=0$.

Line OA is the line of mechanical power $P_{mech}=0$, and the axis of abscissas—the line of primary power $P_1=0$.

We draw from the middle of line OA a perpendicular to its intersection with line Og at point M , which is the centre of the current circle with a radius OM . On the current circle (point E) is located the end of the current vector at rated load $I_1 = I_{ph.r} = 60 \text{ A}$, $\cos \varphi = \cos \varphi_r = 0.89$. The magnitude of the active current is expressed by length $Ed \perp HN$. The sum of the mechanical and additional losses for the rated load

$$p_{mech} + p_{add} = 2 + 1.4 = 3.4 \text{ kW}$$

which makes it possible to determine the corresponding component of the active current

$$ea = \frac{p_{mech} + p_{add}}{\sqrt{3} U_1} = \frac{3.4 \times 10^3}{\sqrt{3} \times 3000} = 0.65 \text{ A}$$

We draw a straight line parallel to OA at a distance $ea=0.65 \text{ A}$, which is the line of useful power $P_2=0$. The efficiency at rated load is equal to the ratio of useful power P_2 to the primary power P_1 , or

$$\eta = \frac{Ee}{Ed} = \frac{96 \times 100}{105} = 91.5\%$$

The secondary current of the main part of the equivalent circuit is

$$I''_{2r} = OE = 52 \text{ A}$$

By constructing a circle diagram for a squirrel-cage induction motor we find the values of the current and electromagnetic torque for different slips (Fig. 21-17b). The obtained values of the currents in amperes and the torques in newton-metres, for the corresponding slips, are shown in the figure. The torques found graphically, correspond to the effective values, determined in Example 20-1.

21-3. Precise Circle Diagram [189, 191, 197, 213]

The complete equivalent circuit (Fig. 19-5) transformed into a precise equivalent circuit with the magnetizing part removed to the terminals (Fig. 19-6) makes it possible to construct a precise circle diagram. In this equivalent circuit only the resistance $\frac{r'_2}{s} \dot{\sigma}_1^2$ of the main part depends on the slip, while all other parameters, both of the main

and of the branch parts, do not depend on it. Hence the same methods can be used for constructing the circle diagram and its analysis as for an improved circle diagram. A precise transformed equivalent circuit is shown in Fig. 19-6.

The correction factor σ_1 , when the losses in the steel are neglected ($r_m = 0$), can be represented as follows:

$$\dot{\sigma}_1 = 1 + \frac{Z_1}{Z_m} \cong 1 + \frac{r_1 + jx_1}{jx_m} = \left(1 + \frac{x_1}{x_m}\right) - j \frac{r_1}{x_m} = \sigma_1 e^{-j\psi} \quad (21-23)$$

where the modulus of $\dot{\sigma}_1$ is

$$\sigma_1 = |\dot{\sigma}_1| = \sqrt{\left(1 + \frac{x_1}{x_m}\right)^2 + \left(\frac{r_1}{x_m}\right)^2} \cong 1 + \frac{x_1}{x_m} \quad (21-24)$$

and its argument ψ is determined from the relation

$$\tan \psi = \frac{r_1}{x_1 + x_m}$$

The expression for the impedance of the main part, taking into account equation (21-23), can be transformed as follows:

$$\begin{aligned} Z_{res} &= Z_1 \dot{\sigma}_1 + Z'_2 \dot{\sigma}_1^2 = Z_1 \sigma_1 e^{-j\psi} + Z'_2 \sigma_1^2 e^{-j2\psi} = e^{-j2\psi} [Z_1 \sigma_1 e^{j\psi} + Z'_2 \sigma_1^2] = \\ &= e^{-j2\psi} \left[(r_1 + jx_1) \sigma_1 (\cos \psi + j \sin \psi) + \left(\frac{r'_2}{s} + jx'_2\right) \sigma_1^2 \right] \end{aligned} \quad (21-25)$$

Since r_1 is usually very small compared with $(x_1 + x_m)$, then $\sin \psi$ and $\cos \psi$ can be assumed equal to

$$\begin{aligned} \sin \psi &= \frac{r_1}{\sqrt{r_1^2 + (x_1 + x_m)^2}} \cong \frac{r_1}{x_1 + x_m} \\ \cos \psi &= \frac{x_1 + x_m}{\sqrt{r_1^2 + (x_1 + x_m)^2}} \cong 1 \end{aligned}$$

Hence

$$\begin{aligned} Z_{res} &= e^{-j2\psi} \left\{ \left[\left(r_1 - x_1 \frac{r_1}{x_1 + x_m} \right) \frac{x_1 + x_m}{x_m} + \frac{r'_2}{s} \sigma_1^2 \right] + \right. \\ &\quad \left. + j \left(x_1 \sigma_1 + x'_2 \sigma_1^2 + \frac{r_1^2}{x_1 + x_m} \sigma_1 \right) \right\} = \\ &= e^{-j2\psi} \left[\left(r_1 + \frac{r'_2}{s} \sigma_1^2 \right) + j \left(X_{sh} + \frac{r_1^2}{x_m} \right) \right] = e^{-j2\psi} Z_{res\psi} \end{aligned} \quad (21-26)$$

where

$$Z_{res\psi} = \left(r_1 + \frac{R_2}{s} \right) + j \left(X_{sh} + \frac{r_1^2}{x_m} \right) \quad (21-27)$$

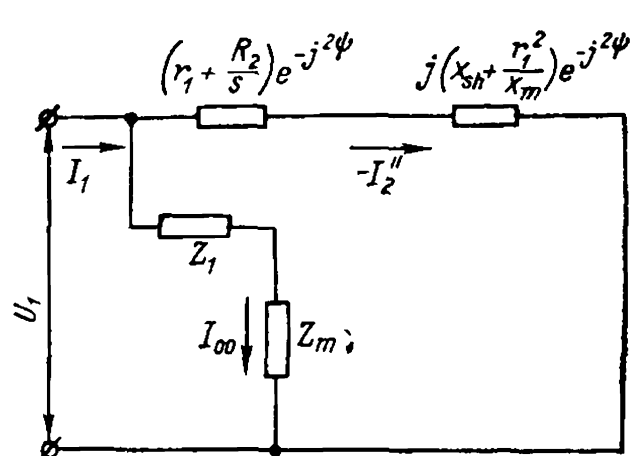


Fig 21-18. Precise equivalent circuit

and

$$\left. \begin{aligned} R_2 &= r_2' \sigma_1^2 \\ X_{sh} &= X_1 + X_2 = x_1 \sigma_1 + x_2' \sigma_1^2 \end{aligned} \right\} \quad (21-28)$$

and 2ψ is determined from the relation

$$\tan 2\psi \cong 2 \tan \psi = \frac{2r_1}{x_1 + x_m} \quad (21-29)$$

According to the above transformations, the precise equivalent circuit can be represented in the developed form as depicted in Fig. 21-18.

The current of the main part of the circuit in Fig. 21-18, according to expressions (21-26) and (21-27), is equal to

$$-I_2'' = \frac{\dot{U}_1}{Z_{res}} = \frac{\dot{U}_1 e^{j2\psi}}{Z_{res\psi}} = \frac{\dot{U}_1 e^{j2\psi}}{\left(r_1 + \frac{R_2}{s}\right) + j\left(X_{sh} + \frac{r_1^2}{x_m}\right)} \quad (21-30)$$

The denominator $Z_{res\psi}$ in equation (21-30) for the current $-I_2''$ in the precise equivalent circuit, as also the denominator Z_{res} with improved equivalent circuit [equation (21-1)], has only one term $\frac{R_2}{s}$ depending on the slip. It has been shown above that the end of the current vector $-I_2''$ of the improved equivalent circuit describes a circle when s changes. Obviously, here the end of the current vector $-I_2''$ will also describe a circle, but since the numerator includes the additional multiplier $e^{j2\psi}$, the current circle will be turned through an angle 2ψ counterclockwise with respect to the current circle of Fig. 21-10.

The diameter of the precise circle diagram according to equation (21-30) is

$$D = \frac{U_1}{X_{sh} + \frac{r_1^2}{x_m}} \quad (21-31)$$

The denominator in the expression for the diameter of a precise circle diagram compared with the diameter of an improved circle diagram [equation (21-3)] differs by the presence of the additional term $\frac{r_1^2}{x_m}$. Since the term $\frac{r_1^2}{x_m}$ is usually very small compared with X_{sh} , its influence on the value of the current circle diameter is manifested in small machines and in normal-type machines only when an additio-

nal resistance is inserted in the primary circuit of the motor, or with a large decrease in frequency which noticeably reduces X_{sh} . In all other cases the diameter of the circle diagram, both for construction of the precise and improved circle diagrams, can be assumed equal to:

$$D = \frac{U_1}{X_{sh}} = \frac{U_1}{X_1 + X_2} \tag{21-32}$$

When the current circle of the main part is turned counterclockwise through an angle 2ψ , the circle diameter, the line $p_{cop} = 0$ of the copper losses in the main circuit, and the line $\Sigma p = 0$ of the total losses also turn through the same angle with respect to the voltage vector.

Figure 21-19a shows a precise circle diagram with the above features of its construction and the corresponding slip and efficiency scales.

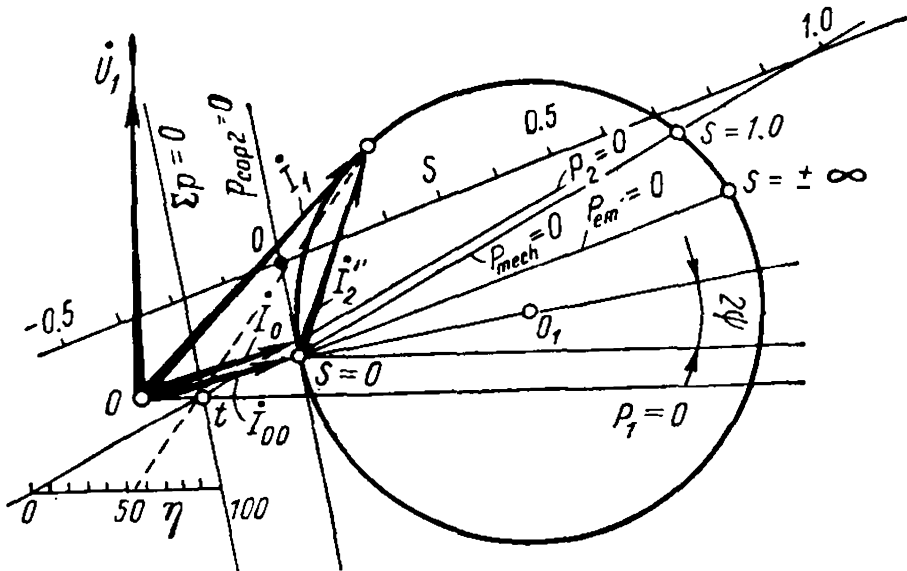


Fig. 21-19a. Precise circle diagram of an induction machine

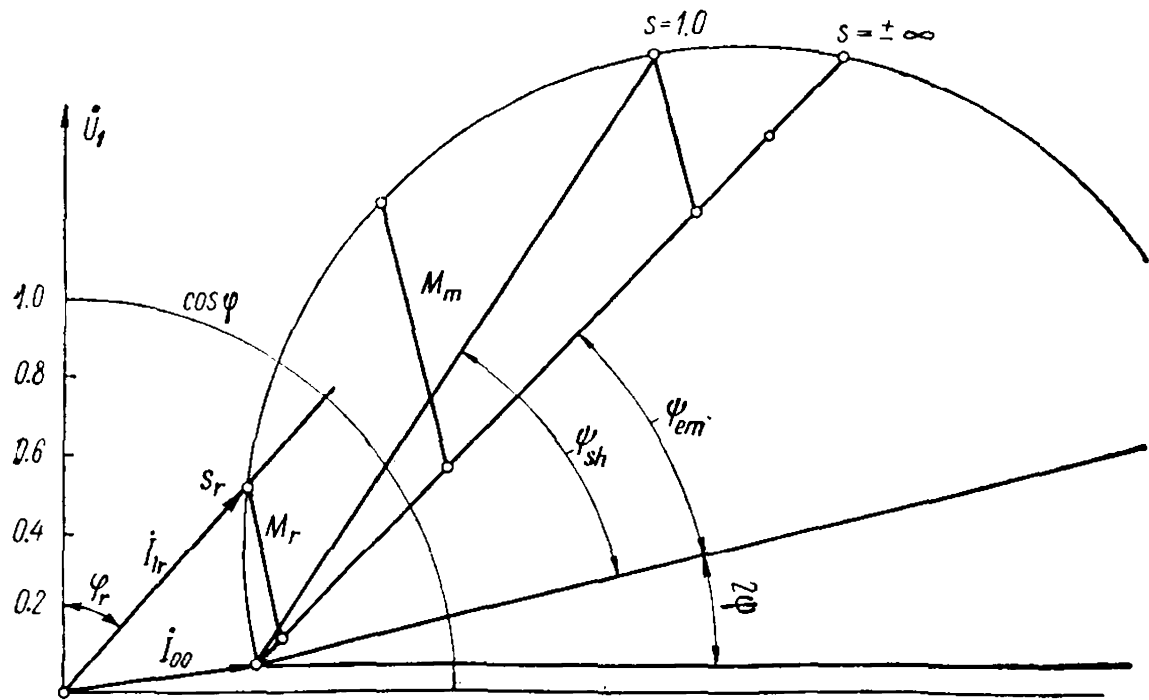


Fig. 21-19b. Precise circle diagram of an induction machine plotted from data given in the example

For convenience of construction, the efficiency scale is placed below the axis of abscissas.

Example 21-2. Determine the inductive reactances and resistances of the windings and their corresponding parameters for constructing the precise circle diagram (Fig. 21-19a) for a low-power three-phase induction motor with a squirrel-cage rotor.

The data of the motor are: $P_2 = 120$ W; $U_1 = \frac{380}{220}$ V, $I_{1ph} = 0.44$ A, $\eta = 0.58$, $\cos \varphi = 0.72$, $2p = 4$, $D_a = 102$ mm, $D = 60$ mm, $\tau = 47$ mm, $l = 46$ mm, the number of stator slots $Z_1 = 24$ and rotor slots $N_2 = 18$, the number of series-connected turns of the stator $w_1 = 1016$, the winding is a single-layer one with a diametrical pitch of the type shown in Fig. 3-7 with the number of slots per pole per phase $q_1 = 2$. The stator slots (of the form shown in Fig. 5-3c): $h_1 = 9$ mm, $h_2 = 0.5$ mm, $h_3 = 0.5$ mm, $h_4 = 0.5$ mm, $b_1 = 7.5$ mm, $b_2 = 1.8$ mm, $b_3 = 5.3$ mm, the winding factor $k_{w1} = k_{d1} = 0.966$ (according to Table 2-2).

The leakage permeance of the slot portion of the stator winding $\lambda_{s1} = 2.4$.

The leakage permeance of the stator winding end connections, according to formula (5-20), is equal to:

$$\begin{aligned}\Lambda_{end1} &= q\lambda_{end} \frac{l_{end}}{l} = 2 \times \left(0.67 - 0.43 \frac{\tau}{l_{end}} \right) \frac{l_{end}}{l} = \\ &= 2 \times \left(0.67 - 0.43 \times \frac{4.7}{9.2} \right) \frac{9.2}{4.6} = 1.80\end{aligned}$$

The air-gap $\delta = 0.25$, air-gap factor $k_\delta = 1.2$, magnetic circuit saturation factor $k_\mu = 1.1$, the differential leakage permeance, by formula (5-27) for a differential leakage factor $k_{dif} = 0.028$ (see curves in Fig. 5-5 for $q = 2$ with a diametrical winding pitch) is

$$\lambda_{dif1} = \frac{3 \times 2 \times 0.966^2 \times 4.7}{\pi^2 \times 1.2 \times 1.1 \times 0.025} \times 0.028 = 2.27$$

The sum of the stator winding leakage permeance is

$$\sum \lambda_1 = 2.4 + 1.80 + 2.27 = 6.47$$

The stator winding inductive reactance, by formula (5-14), is

$$x_1 = 4\pi \times 50 \times 1.26 \times 10^{-8} \times \frac{4.6 \times 1016^2}{2 \times 2} \times 6.47 = 60.6 \Omega$$

The resistance of the stator winding at 75 °C is

$$r_1 = 108.5 \Omega$$

The inductive reactance of the magnetizing circuit, by formula (5-5), is

$$x_m = 2 \times 3 \times 50 \times \frac{1.26 \times 10^{-8} \times 6 \times 4.6 \times 1016^2 \times 0.966^2}{1.2 \times 1.1 \times 0.025 \times 2^2} = 815 \Omega$$

The ratios are:

$$\frac{x_1}{x_m} = \frac{60.6}{815} = 0.075; \quad \frac{r_1}{x_m} = \frac{108.5}{815} = 0.133;$$

$$\frac{r_1^2}{x_m} = 143 \Omega$$

The leakage permeance of the rotor winding slot part is

$$\lambda_{s2} = 1.40$$

The leakage permeance of the rotor winding end connection, by formula (18-25a), is

$$\lambda_{ring} = \frac{18 \times 4.7}{2 \times 2 \times 3 \times 4.6} \times 0.14 = 0.22$$

where $g_{end} = 0.14$ with $\frac{l_c}{e} = 3.77$ and $\frac{\tau}{l_c} = 2.35$ (Fig. 18-6).

The differential leakage permeance, by formula (5-27), is

$$\lambda_{dif2} = \frac{18 \times 4.7 \times 0.966^2}{2 \times 2 \times \pi^2 \times 1.2 \times 1.1 \times 0.025} \times 0.07 = 4.53$$

where $k_{dif2} = 0.07$ with $\frac{N_2}{2p} = 4.5$ (Fig. 18-7).

The sum of the rotor winding leakage permeances is

$$\sum \lambda_2 = 1.40 + 0.22 + 4.53 = 6.15$$

The inductive reactance of the squirrel-cage rotor winding is

$$x_2 = 2\pi \times 1.26 \times 10^{-8} \times 50 \times 4.6 \times 6.15 = 0.000112 \Omega$$

The coefficient for referring the rotor winding to the stator winding is

$$k = \frac{4 \times 3 \times 1016^2 \times 0.966^2}{18} = 644\,000$$

The rotor winding inductive reactance referred to the stator winding is

$$x'_2 = 0.000112 \times 644\,000 = 72.0 \Omega$$

The ratio

$$\frac{x'_2}{x_m} = 0.087$$

The resistance of one bar of the rotor squirrel cage is

$$r_{bar} = 5.74 \times 10^{-5} \Omega$$

The resistance of two sections of the squirrel-cage short-circuiting rings with an average diameter $D_{ring} = 44.5$ mm and a cross-sectional area 130 mm^2 on both sides is

$$r_{ring} = 0.52 \times 10^{-5} \Omega$$

The resistance of two sections of the short-circuiting rings referred to the resistance of one bar of the squirrel cage, by formula (18-24), is

$$r'_{ring} = 1.11 \times 10^{-5} \Omega$$

The total resistance of a rod with two adjoining sections of the short-circuiting rings is

$$r_2 = r_{bar} + r'_{ring} = 6.84 \times 10^{-5} \Omega$$

The secondary winding resistance referred to the primary winding is

$$r'_2 = r_2 k = 6.84 \times 10^{-5} \times 64.4 \times 10^4 = 44.0 \Omega$$

The ratio

$$\frac{r_2'}{x_m} = \frac{44}{815} = 0.053$$

The modulus of the correction factor, by formula (21-24), is

$$\sigma_1 = \sqrt{(1 + 0.075)^2 + 0.133^2} = 1.08$$

and its argument

$$\psi = \arctan \frac{108.5}{60.6 + 815} = \arctan 0.124$$

The parameters of the main part of an exact L-type equivalent circuit, according to formula (21-28), are

$$R_p = 51.5 \, \Omega; \quad X_{sh} = 151.4 \, \Omega$$

The diameter of the circle of a precise circle diagram, by formula (21-31), is

$$D = \frac{U_1}{X_{tot. sh}} = \frac{220}{165.7} = 1.33 \, \text{A}$$

where

$$X_{tot. sh} = X_{sh} + \frac{r_1^2}{x_m} = 151.4 + 14.3 = 165.7 \, \Omega$$

The angles between the diameter of the circle diagram and the lines of the electromagnetic and total mechanical powers are

$$\begin{aligned} \psi_{em} &= \arctan \frac{r_1}{X_{tot. sh}} = \arctan \frac{108.5}{165.7} = \arctan 0.656 \\ \psi_{sh} &= \arctan \frac{r_1 + R_2}{X_{tot. sh}} = \arctan \frac{108.5 + 51.5}{165.7} = \arctan 0.97 \end{aligned}$$

The current of the magnetizing circuit with $s=0$, by formula (19-20), taking into account formula (19-27), is

$$i_{00} = \frac{\dot{U}_1}{Z_m \sigma_1} \cong \frac{\dot{U}_1}{j x_m \left(\sigma_1 - j \frac{r_1}{x_m} \right)} = 0.030 - j0.245 \, \text{A}$$

(the resistance r_m is disregarded because of its low value).

The data obtained has been used to plot the circle diagram in Fig. 21-19b.

21-4. Current Loci for Induction Machines with Variable Parameters

In precise analysis all the machine parameters are considered to be variable, since the resistances depend on the winding temperature, while the inductive reactances x_m , x_1 and x_2' are determined by the degree of saturation of the steel by the main magnetic flux or the leakage fluxes.

The active steel of an induction machine, especially in the tooth belt, is usually very greatly saturated, and the result is that the curve of flux density along the air-gap with a sinusoidal magnetizing force

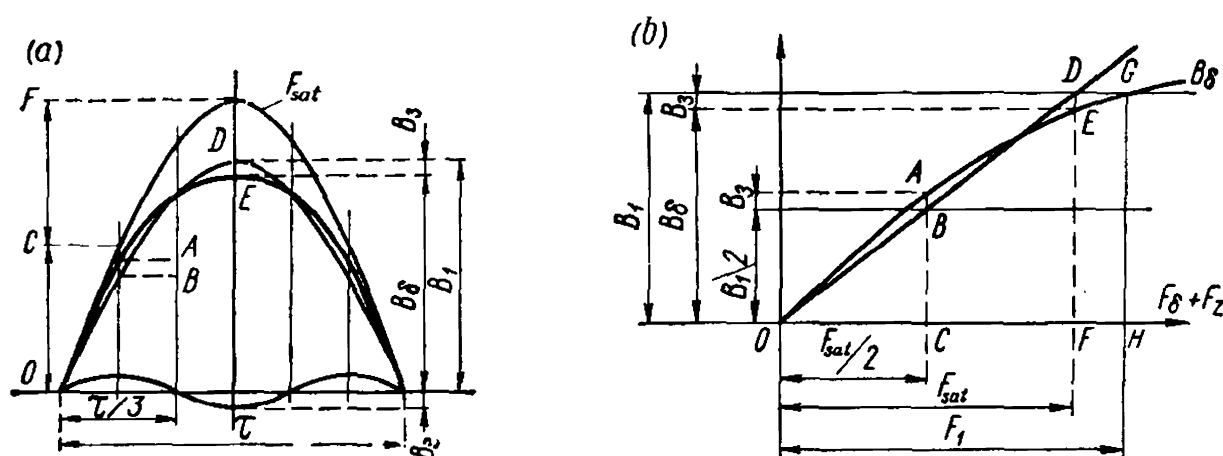


Fig. 21-20. Determination of actual flux densities and magnetic flux in a saturated machine

noticeably deviates from the sinusoidal form (Fig. 21-20a). Such a flat response of the field curve affects the reduction of the magnetizing current and the increase in the steel losses; therefore in detailed designing of an induction machine this influence should be taken into account. Let us assume that the magnetizing force is distributed according to the sinusoidal law along the pole pitch (Fig. 21-20a, curve F_{sat}). Owing to saturation of the steel, mainly in the stator and rotor tooth belt, the curve of the magnetic field is flat (curve B_δ). Disregarding the higher harmonics of the field, except the third one, it may be assumed that the field curve consists of the fundamental harmonic B_1 and the third harmonic B_3 . The fundamental harmonic induces in the primary winding the fundamental e.m.f. harmonic, but the third field harmonic does not affect a three-phase winding.

The magnitude of the fundamental flux density harmonic B_1 is determined by the value of the fundamental e.m.f. harmonic. The third harmonic of the magnetic field can be determined from the magnetization curve (Fig. 21-20b). Let us divide length GH , corresponding to the flux density B_1 , into two equal parts and draw through point G and through the middle of GH lines parallel to the axis of abscissas. From the origin of coordinates we draw another line at an angle such that $AB = DE$. Then $EF = B_\delta$ is the real flux density in the air-gap, and OF is the amplitude of the magnetizing force producing the magnetic flux. Similarly, the lengths $AB = ED$ are the amplitudes of the third harmonic of the field B_3 . Thus, instead of the amplitude value of the first harmonic of the flux density we obtain the real density $B_\delta < B_1$; the density in the teeth decreases correspondingly. On the other hand, the magnetizing force F_1 decreases to the value F_{sat} . But in the backs of the stator and rotor cores, on the contrary, the flux density increases, since owing to the third harmonic, the total flux Φ increases (Fig. 21-20a):

$$\Phi = \frac{2}{\pi} \tau l B_1 + \frac{2}{\pi} \frac{\tau}{3} l B_3 = \frac{2}{\pi} \tau l \left(B_1 + \frac{B_3}{3} \right)$$

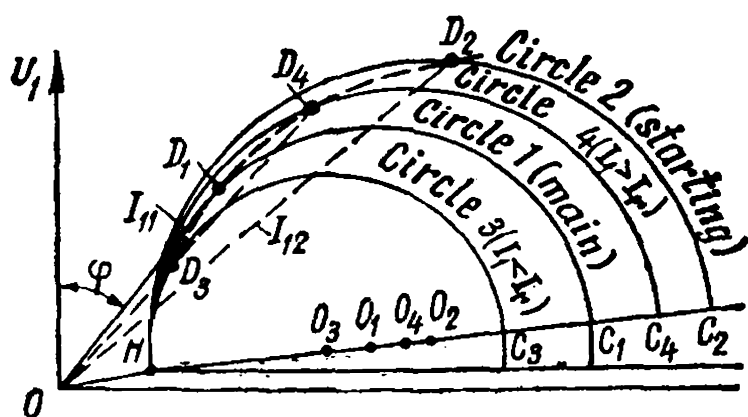


Fig. 21-21. Construction of current loci for $X_{sh} = f(I_1)$

The value of Φ is used to determine the magnetizing current and the flux densities which the losses in the steel depend on.

In addition, the parameters are affected by the skin effect. Sometimes the parameters change with a change in the operating conditions of an induction machine, so that the current locus loses its circular form.

The current loci for motors with deep-bar and double-squirrel cage rotors are considered below in Chapter 23; here we shall discuss the current locus for a standard motor with a variable inductive reactance $X_{sh} = X_1 + X_2$. Tests show that in squirrel-cage motors with closed rotor slots the reactance X_{sh} is half as much when the current changes from $I_1 = I_r$ to $I_1 \cong 5I_r$ owing to saturation of the "bridge" between the teeth by the slot leakage flux. Here the diameter of the current circle $D = U_1 : X_{sh}$ continuously changes, growing with an increase in the current. Since to each current value there corresponds one value of the inductive reactance and, therefore, one current diameter, it is theoretically possible to plot an infinite number of such circles. The most frequent practice is to limit them to two circles constructed for two values of X_{sh} —one corresponding to the short-circuit current with the voltage $U_{sh} = U_r$, and the other corresponding to the current $I_{sh} = I_r$. The first circle serves for determining the starting characteristics, the second corresponds to the rated operating conditions and serves to determine the characteristics corresponding to these conditions (Fig. 21-21). The first circle may be called the *starting* circle, the second the *main* circle. The centres of both circles O_1 and O_2 are practically on straight line HC_1C_2 . The diagram is constructed for both circles, but only for that part which concerns each given circle. In more complicated cases it is possible to construct, similarly, several circles, for example four conditions for four values of the current I_{11} , I_{12} , I_{13} and I_{14} , the main and starting circles 1 and 2 corresponding to the currents I_{11} and I_{12} , and the additional circles 3 and 4 to the currents I_{13} and I_{14} . By laying off the corresponding currents on these circles, we get points D_1 , D_2 , D_3 and D_4 and, after joining them with a continuous curve, we plot the locus of the current of a motor with the inductive reactance $X_{sh} = f(I_1)$. If the function $X_{sh} = f(I_1)$ is hyperbolic, then, as was shown by Prof. L. Piotrovsky, the current locus for an induction machine is the internal loop of Pascal's limaçon.

21-5. No-Load Test

The point of no-load operation H on the circle diagram can be found from design or experimental data.

When testing a motor under no-load conditions the rated voltage U_r at the rated frequency f_1 is applied. The voltage should be practically sinusoidal. To avoid accidental errors, the supplied voltage is changed within certain limits, usually between $0.5U_r$ and $1.2U_r$. The curves of I_0 , I_{0r} , $P_{00} = P_0 - m_1 I_0^2 r_1$ in relative units and of the power factor ($\cos \varphi$) are given in Fig. 21-22.

At voltages close to the rated value the curves of the no-load current I_0 and of its inductive component I_{0r} practically coincide, but then they begin to diverge more and more, since with a reduction in U_1 the active component I_{0a} attains greater and greater importance. With $U_1 = U_r$ we usually have $\cos \varphi \leq 0.12$, but it grows appreciably with a reduction in voltage.

The curve P_{00} is an almost regular parabola, since the losses $p_{mech} = \text{const}$ and the losses $p_{st} + p_{add}$ are proportional to the square of the e.m.f. E_1 and, consequently, to the voltage U_1 .

21-6. Short-Circuit Test

To determine the short-circuit parameters we perform a short-circuit test similar to that of a three-phase transformer (Vol. I, Chap. 17).

To prevent the short-circuit current from reaching an excessive value, the voltage U_{sh} applied across an induction machine on short circuit is lowered compared with the rated voltage value U_r . But the resistances and reactances of induction machines are relatively larger than those of transformers, therefore, the short-circuit voltage $U_{sh} = \frac{U_{sh}}{U_r} \times 100\%$ corresponding to the current $I_{sh} = I_r$ is also higher.

Practically $U_{sh} = 15$ to 25% . Consequently,

$$I_{sh.r} = (7 \text{ to } 4) I_r$$

where $I_{sh.r}$ is the short-circuit current with $U_{sh} = U_r$.

The short-circuit parameters are determined in the same way as for transformers, with the same assumption that the short-circuit power P_{sh} is spent only to cover the losses in the copper of the primary and secondary windings of the machine.

The main difference between the short-circuit parameters of trans-

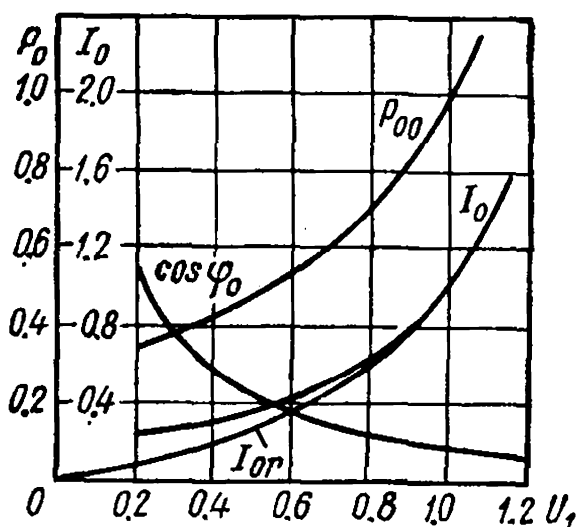


Fig. 21-22. No-load characteristics of an induction motor

formers and induction machines is that, with a given winding temperature and frequency, the short-circuit parameters of transformers do not practically depend on the current I_{sh} , while this dependence always exists in induction machines and is sometimes of a very pronounced nature.

Such a difference is mainly determined by the tothing of the rotor and stator of the induction machine and, in particular, by the shape of their slots, i.e., by the geometry of the slotted belt.

Two main cases should be distinguished: when the stator and rotor slots have an open or semi-closed shape, and when the stator slots have a semi-closed and the rotor slots a closed shape (see Fig. 1-19).

In the first case the short-circuit leakage fluxes weakly saturate the stator and rotor teeth. Therefore, the short-circuit parameters, in particular X_{sh} , vary within relatively narrow limits. This can be illustrated by the curves for R_{sh} , X_{sh} and Z_{sh} as functions of U_{sh} shown in Fig. 21-23 for a 4.5-kW, 380/220-V, 8.8/15.2-A, 50-Hz, 1440-rpm motor with star-connected stator windings. Such curves are obtained for deep-slot motors and motors with phase-wound rotors.

In the second case the bridge which covers the slot is rapidly saturated already with small currents; with an increase in current the saturation belt becomes larger and embraces the tooth addendum and the tooth proper. Therefore, the inductive reactance of such machines changes appreciably with a change in the voltage U_{sh} , acquiring a hyperbolic nature. This can be illustrated by the curves R_{sh} and $X_{sh} = f(U_{sh})$ shown in Fig. 21-24 for a 1-kW, 380/220-V, 2.15/3.72-A, 50-Hz, 1420-rpm motor with delta-connected stator windings. It can be seen that the inductive reactance X_{sh} varies from $X_{sh} = 21.6$ ohms with $I_{sh} = I_r = 3.72$ A to $X_{sh} = 11.6$ ohms with $U_{sh} = U_r = 220$ V, i.e., in the ratio of 1 : 0.54. The curve $X_{sh} = f(U_{sh})$ is a

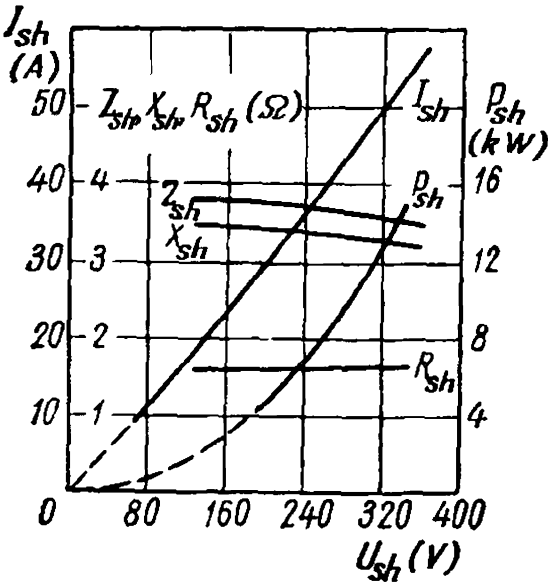


Fig. 21-23. Short-circuit characteristic of an induction motor

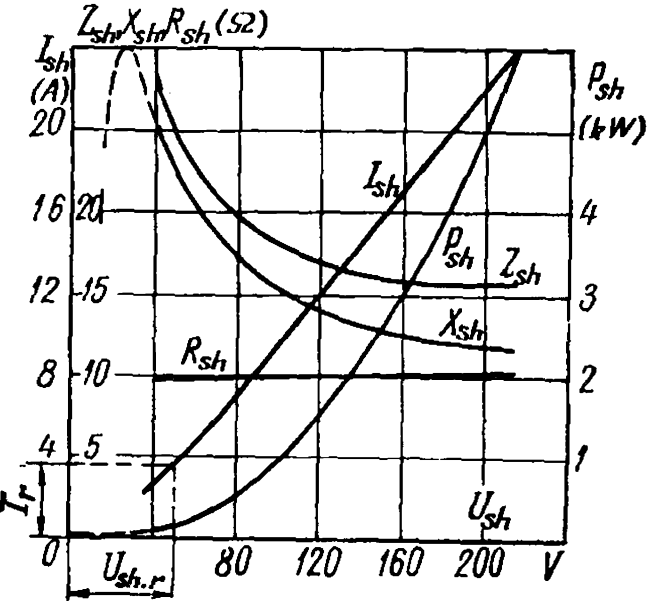


Fig. 21-24. Short-circuit characteristic of a squirrel-cage motor

nearly regular hyperbola which can be expressed by the equation $X_{sh} = 8.55 + \frac{655}{U_{sh}}$ ohms.

The function $X_{sh} = f(I_{sh})$ is also a curve close to a hyperbola, since the current I_{sh} is nearly proportional to the voltage U_{sh} .

It should be noted that the curve $X_{sh} = f(I_{sh})$ retains its hyperbolic nature only up to a certain minimum value of the current, after which X_{sh} begins to decrease, as shown by the dotted line in Fig. 21-24. This is explained by the fact that with very small currents and, consequently, with very weak saturation of the steel, the permeability begins to decrease.

If the short-circuit parameters of an induction machine may be, with sufficient accuracy, considered constant, the function $I_{sh} = f(U_{sh})$ is a straight line (Fig. 21-24). Here the recalculation of the short-circuit test data obtained for a reduced voltage U_{sh} to the rated voltage U_r is not difficult and is performed with the aid of the formulas

$$I_{sh.r} = I_{sh} \frac{U_r}{U_{sh}} \quad \text{and} \quad P_{sh.r} = P_{sh} \left(\frac{U_r}{U_{sh}} \right)^2$$

Here

I_{sh} , U_{sh} and P_{sh} = test current, voltage and power values; $I_{sh.r}$ and $P_{sh.r}$ = current and power corresponding to the rated voltage U_r .

As with transformers, the values of all the resistances are also reduced to 75° C.

In machines with semi-closed or closed rotor slots the curve $I_{sh} = f(U_{sh})$ departs from a straight line (Fig. 21-25). But this departure is noticeable only with currents $I_{sh} < I_r$, while with currents $I_{sh} > I_r$ the curve $I_{sh} = f(U_{sh})$ is practically a straight line. Here the following procedure is used. The short-circuit test is performed so as to obtain the curve $I_{sh} = f(U_{sh})$ for currents within the limits from $I_{sh} \cong I_r$ to $I_{sh} \cong 2.5I_r$ (Fig. 21-25). This part of the curve can already be considered a straight line. By extrapolating it for the voltage $U_{sh} = U_r$, we get the current $I_{sh.r}$.

The same result can also be obtained by calculation. For this purpose it is sufficient to extend the linear part of the curve $I_{sh} = f(U_{sh})$ to its intersection with the axis of abscissas at point a . This gives us the voltage U_0 . Then

$$I_{sh.r} = \frac{U_r - U_0}{U_{sh} - U_0} I_{sh}$$

and

$$P_{sh.r} = \left(\frac{U_r - U_0}{U_{sh} - U_0} \right)^2 P_{sh}$$

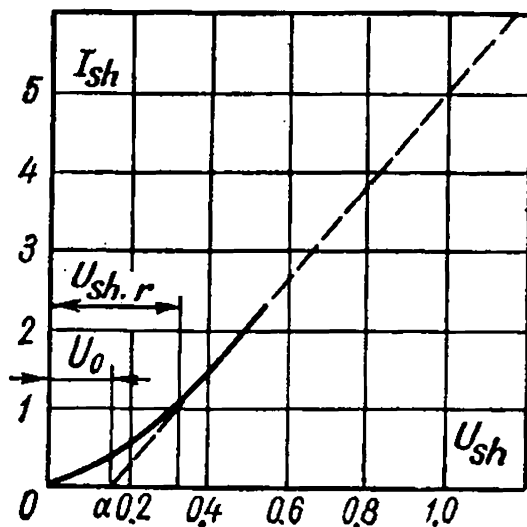


Fig. 21-25. Determination of short-circuit current corresponding to rated voltage

the ratio $\frac{BC}{AC} = \frac{R_1}{R_{sh}}$. Then, by drawing a straight line through points O'' and B up to its intersection with the circle, we find point F corresponding to the slip $s = \pm \infty$. Straight line $O''F$ is the line of electromagnetic power $P_{em} = 0$.

The slip scale is constructed as in Figs. 21-12 and 21-13, and the efficiency scale as in Figs. 21-13, 21-14, 21-15 and 21-16.

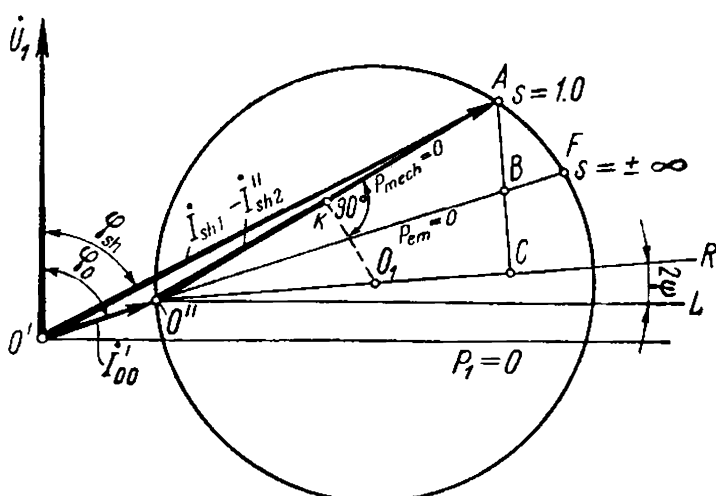


Fig. 21-27. Construction of precise circle diagram according to experimental data

To find the centre line when constructing a precise circle diagram, we draw (Fig. 21-27) line $O''R$ at an angle $2\psi = \arctan \frac{2r_1}{x_1 + x_m} = \arctan \frac{2I_0 r_1}{U_1}$ to line $O''L$ running parallel to the axis of abscissas through point O'' of the ideal no-load. Then, from the middle K of chord $O'A$, we draw a perpendicular to intersect line $O''R$ at point O_1 which is the centre of the current circle. A perpendicular to line $O''R$ is drawn from point A and length AC is divided at point B in the ratio $\frac{BC}{AC} = \frac{r_1}{R_{sh}}$. Then we draw through points O'' and B a straight line to its intersection with the circle at point F , which is a point with a slip $s = \pm \infty$. Straight line OF is the line of electromagnetic power $P_{em} = 0$. The slip and efficiency scales are further constructed in the same way as in the improved circle diagram.

21-8. Application of Approximate Circle Diagram

Determination of $(\cos \varphi)_{max}$ (Fig. 21-28). An approximate circle diagram can be used to derive approximate formulas for determining such important quantities as $(\cos \varphi)_{max}$, $\cos \varphi$ and P_{2max} .

From the no-load and short-circuit tests we find I_0 , I_{sh} and $\cos \varphi_{sh}$. The ideal short-circuit current $I_{sh.i} = O'g$ can be determined approximately from these data if we assume that $\angle O'Ag = 90^\circ$. Then

$$I_{sh.i} \cong \frac{I_{sh}}{\sin \varphi_{sh}}$$

Let us draw a tangent to the current circle from the origin of coordinates O' ; the circle radius is then

$$R = EM = O'M \cos (\varphi_{min}) = (R + I_0) \cos (\varphi_{min})$$

but

$$R \cong \frac{I_{sh.i} - I_0}{2}$$

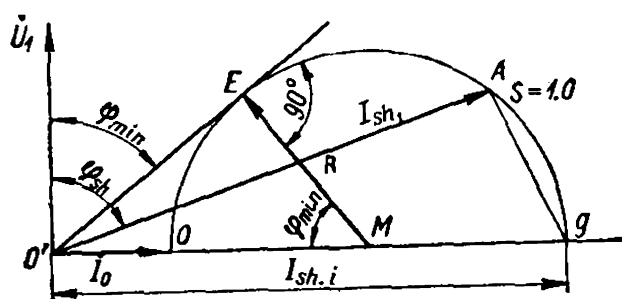


Fig. 21-28. To determination of $(\cos \varphi)_{max}$

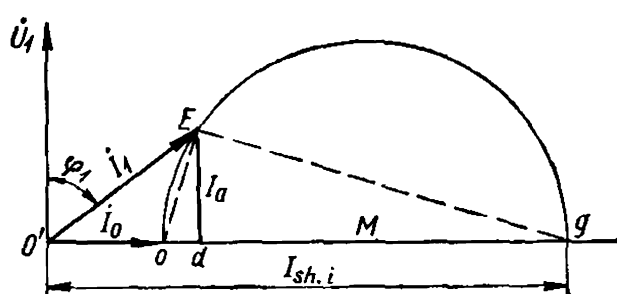


Fig. 21-29. To determination of $\cos \varphi$

whence

$$\cos (\varphi_{min}) = (\cos \varphi)_{max} = \frac{R}{R + I_0} = \frac{I_{sh.i} - I_0}{2 \left(\frac{I_{sh.i} - I_0}{2} + I_0 \right)} = \frac{I_{sh.i} - I_0}{I_{sh.i} + I_0} \quad (21-33)$$

Determination of $\cos \varphi$ (Fig. 21-29):

$$\cos \varphi = \frac{1}{\sqrt{\tan^2 \varphi + 1}}$$

but

$$\tan \varphi = \frac{O'd}{Ed} = \frac{I_0 + Od}{I_a}$$

where I_a is the active component of the current equal to

$$I_a = \frac{P_1}{\sqrt{3}U_1\eta} \cong \frac{P_1}{\sqrt{3}U_1}$$

We further have

$$I_a^2 = (Ed)^2 = Od \cdot dg \cong Od (I_{sh.i} - O'd) \cong Od (I_{sh.i} - I_0)$$

whence

$$Od = \frac{I_a^2}{I_{sh.i} - I_0}$$

Thus

$$\tan \varphi = \frac{I_0}{I_a} + \frac{I_a}{I_{sh.i} - I_0}$$

and

$$\cos \varphi = \frac{1}{\sqrt{\left(\frac{I_0}{I_a} + \frac{I_a}{I_{sh.i} - I_0} \right)^2 + 1}} \quad (21-34)$$

(Spektor's formula, Kharkov Electrical Engineering Plant).

Determination of P_{2max} (Fig. 21-30). We plot an approximate circle diagram, placing the no-load current vector $I_0 \cong O'O$ on the axis of abscissas and assuming that line OA is the line of the useful secondary power $P_2 = 0$. We draw tangent LN to the current circle

parallel to the line $P_2 = 0$ and join the point of tangency D to centre M of the circle. We then drop a perpendicular from point D onto the axis of abscissas; the length Oa is P_{2max} . We draw tangent OQ to the current circle at point O and assume approximately that the angle $\varphi'_{sh} \cong \varphi_{sh}$. Since $\angle QOA = \varphi'_{sh}$, then

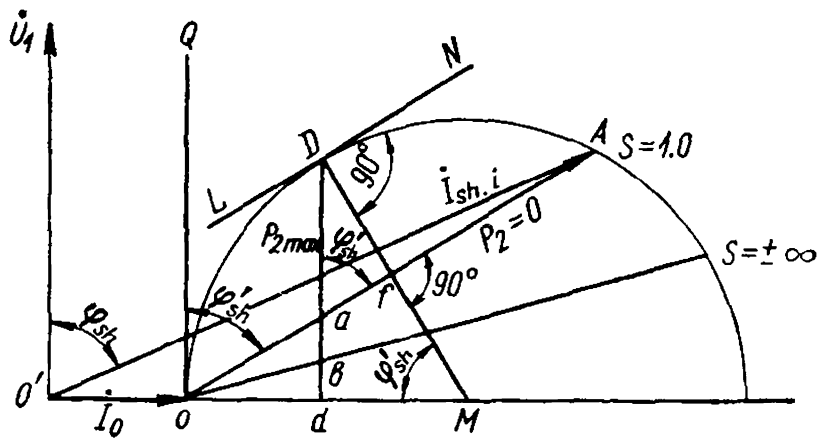


Fig. 21-30. To determination of P_{2max}

$$P_{2max} = Da = \frac{Df}{\sin \varphi'_{sh}} \cong \frac{Df}{\sin \varphi_{sh}}$$

but

$$Df = OM - Mf = R - Mf$$

and

$$Mf = OM \cos \varphi'_{sh} = OM \cos \varphi_{sh} = R \cos \varphi_{sh}$$

therefore,

$$Df = R - R \cos \varphi_{sh} = R (1 - \cos \varphi_{sh})$$

Thus

$$P_{2max} \cong \frac{Df}{\sin \varphi_{sh}} = \frac{R (1 - \cos \varphi_{sh})}{\sin \varphi_{sh}} = \frac{R (1 - \cos \varphi_{sh}) (1 + \cos \varphi_{sh})}{\sin \varphi_{sh} (1 + \cos \varphi_{sh})} = \frac{R \sin \varphi_{sh}}{1 + \cos \varphi_{sh}}$$

Since $R = \frac{I_{sh.i} - I_0}{2}$ then, finally, in relative units

$$P_{2max} = \frac{(I_{sh.i} - I_0) \sin \varphi_{sh}}{2 (1 + \cos \varphi_{sh})} \quad (21-35)$$

Since the angle φ_{sh} is very close to 90° , it can be assumed with a still greater approximation that

$$\sin \varphi_{sh} \cong 1.0$$

and then

$$P_{2max} = \frac{I_{sh.i} - I_0}{2 (1 + \cos \varphi_{sh})} \quad (21-35a)$$

Example 21-3. For a three-phase squirrel-cage motor

$$I_0 = 17.5 \text{ A}; \quad I_{sh.i} = 312.5 \text{ A} \text{ and } I_a = 50 \text{ A}$$

according to formula (21-33)

$$(\cos \varphi)_{max} = \frac{312.5 - 17.5}{312.5 + 17.5} = \frac{295}{330} = 0.893$$

(the circle diagram gives 0.89).

For a phase-wound rotor $I_0 = 17.5$ A, $I_{sh.i} = 232.5$ A, $I_a = 50$ A, according to formula (21-33),

$$(\cos \varphi)_{max} = \frac{232.5 - 17.5}{232.5 + 17.5} = \frac{215}{250} = 0.86$$

(the circle diagram gives 0.87).

For a squirrel-cage motor according to formula (21-34)

$$\cos \varphi_{sq} = \frac{1}{\sqrt{\left(\frac{17.5}{50} + \frac{50}{295}\right)^2 + 1}} = \frac{1}{1.122} = 0.89$$

(the circle diagram gives 0.89).

For a motor with a phase-wound rotor

$$\cos \varphi_{ph} = \frac{1}{\sqrt{\left(\frac{17.5}{50} + \frac{50}{215}\right)^2 + 1}} = \frac{1}{1.155} = 0.865$$

(the circle diagram gives 0.865).

The maximum relative useful power according to formula (21-35) for motor with a phase-wound rotor ($\cos \varphi_{sh} = 0.165$) is

$$P_{2max} = \frac{215 \times 0.987}{50 \times 2 \times 1.165} = 1.83$$

(the circle diagram gives 1.9).

For a squirrel-cage motor ($\cos \varphi_{sq} = 0.25$)

$$P_{2max} = \frac{295 \times 0.97}{50 \times 2 \times 1.25} = 2.29$$

(the circle diagram gives 2.38).

Chapter

22

STARTING OF THREE-PHASE INDUCTION MOTORS

22-1. General

The main problems in starting induction motors are the magnitudes of the starting torque and starting current.

For a rotor to start, the starting torque developed by the motor must be greater than the braking torque at the shaft due to the coupled driven mechanism. A considerable starting torque, equal to the rated torque or even larger, is often required (for instance, when starting ball mills, crushers, compressors and the like).

On the other hand, the strength of the starting current for a given mains should not exceed certain limits, which depend on the power capacity of the mains. With large motors and low-power mains the strength of the starting current should be reduced.

The starting current of a squirrel-cage induction motor can be lowered by reducing the voltage across the motor terminals at starting, but the starting torque is reduced in proportion to the square of the voltage. This method can therefore be used only in easy starting conditions. In severe starting conditions a normal squirrel-cage induction motor may be unable to develop sufficient starting torque, even with across-the-line starting at rated voltage. Here use can be made of motors with phase-wound rotors or squirrel-cage motors with a special type of rotor, i.e., with double squirrel-cages or deep-bar rotors (Chap. 23).

In double motors with phase-wound rotors favourable conditions for starting (a large starting torque at a small starting current) are easily attained by inserting a starting rheostat in the rotor circuit. These motors, however, are more costly than squirrel-cage motors, and the starting rheostat makes installation and maintenance more complicated.

Of essential importance are also the problems of starting duration, energy losses in the windings and their heating, and the transient processes in starting.

These problems will be discussed in detail below.

22-2. Starting Currents of Induction Motors

Two limiting cases are distinguished: when a motor is switched on to a line with its rotor circuit open, and when the motor is switched on with its rotor short-circuited.

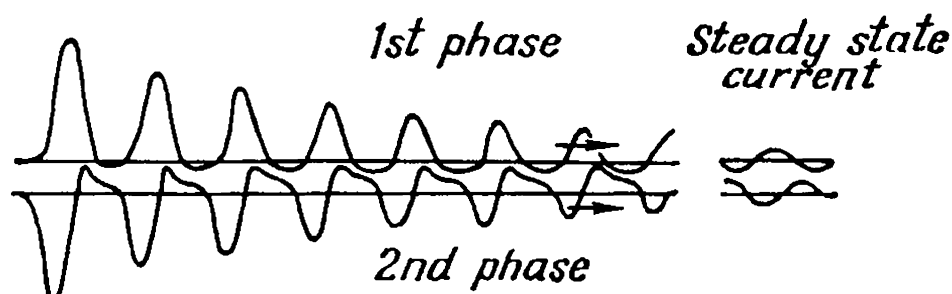


Fig. 22-1. Connection of an induction motor with the rotor circuit open

In the first case the process is qualitatively the same as with a transformer switched on to the power supply with its secondary open (see Vol. I, Sec. 21-2). The most dangerous moment of switching is the one when the voltage passes through zero. Here the magnetic flux of each phase has two components; a symmetrical component $\Phi_m \cos \omega t$ and an aperiodic component Φ_{ap} mutually superposed on each other and owing to which the resultant flux at the moment of connection may theoretically attain twice the value of the flux of the machine for steady-state operating conditions. In a polyphase machine the periodic flux components of the individual phases form a resultant flux rotating in space with a speed $n_1 = f_1 : p$, while the aperiodic flux components form a flux which is stationary in space.

The doubled resultant flux highly saturates the steel of the machine. The amplitude of the no-load inrush current of an induction motor I'_{0m} , therefore, greatly exceeds the amplitude of the steady-state no-load current I_{0m} . In comparison with transformers, the $\frac{I'_{0m}}{I_{0m}}$ ratio for induction motors is smaller, since, owing to the presence of the air-gap, the magnetization curve of the motors has a gradual slope and the residual magnetization flux is lower. Nevertheless, the no-load inrush current may be several times greater than the rated current I_r . Thus, for instance, during a test of a three-phase 500-kW, 1500-rpm motor, the no-load inrush current exceeded the steady-state no-load current 14 times and the rated current of the motor three times (Fig. 22-1).

The no-load inrush current of an induction motor decays relatively slowly, but faster than in transformers, since the time constant of decay for the latter is comparatively larger.

Let us now consider the case when a motor with a shorted rotor is switched on to the line. Since at the first moment the speed is $n = 0$, the phenomena occurring here are qualitatively the same as in a suddenly short-circuited transformer (Vol. I, Sec. 21-2). If for simplicity we neglect the magnetizing current, the sudden short-circuit current in an induction motor can be determined from the formula

$$i_{sh} = i_{st. st} + i_{sh. ap} = - \frac{U_{1m}}{\sqrt{R_{sh}^2 + X_{sh}^2}} \cos(\omega t + \varphi_{sh}) + \frac{U_{1m}}{\sqrt{R_{sh}^2 + X_{sh}^2}} \cos \varphi_{sh} e^{-\frac{\omega R_{sh}}{X_{sh}} t}$$

As with the no-load inrush current, it has two components, of which one—the periodic component $I_{st.st}$ —corresponds to the short-circuit current, and the other—the aperiodic component $I_{sh.ap}$ —decays according to the exponential rule. The current decays very quickly, since the decay time constant $\frac{X_{sh}}{\omega R_{sh}}$ is small. Therefore, this second current component is usually neglected and the magnitude of the starting current I_{st} of a motor is understood to be the periodic short-circuit current. In general

$$\frac{I_{st}}{I_r} = 4 \text{ to } 7$$

Of still less importance is the magnetizing short-circuit current $I_{m.sh}$. Usually $\frac{I_{m.sh}}{I_r} \times 100 < 5\%$.

22-3. Disconnection of an Induction Motor from the Line

A running induction motor contains a certain amount of stored electromagnetic energy determined, in the main, by the size of the air-gap. The greater the gap, the greater the amount of stored electromagnetic energy. Therefore, the stored energy is relatively greater in induction machines than in transformers, and in synchronous machines greater than in induction machines.

When a machine is disconnected from the line, the energy of its magnetic field must be dissipated in one form or another. If the rotor circuit of an induction motor is open, the rapid disappearance of the flux Φ produces considerable overvoltages in the stator and leads to the appearance of a breaking arc. According to experimental data, the overvoltages appearing in disconnection of an induction motor with an open rotor circuit from the line exceed the rated voltage three to four times, i.e., are positively dangerous.

The same phenomena, though in a weaker form, occur when the rotor of an induction motor is closed through a large resistance, since the latter promotes fast decay of the flux.

From the above it follows that an induction machine is best disconnected from the line when its rotor is short-circuited, since when the flux disappears the energy in its secondary winding is gradually dissipated.

22-4. Acceleration of an Induction Motor at Starting

Duration of Acceleration. When an induction motor with a short-circuited rotor is started, the duration of its acceleration depends on the braking torque M_{stat} on the shaft, the inertia torque M_{in} of the rotating masses and the shape of the motor torque curve $M = f(s)$.

Let us consider the most simple case: acceleration of a motor starting at no load ($M_{stat} = 0$, $M_{in} = M$).

Since

$$M_{in} = J \frac{d\Omega}{dt} = J \frac{d(2\pi n)}{dt}$$

then when acceleration is uniform $M_{in} = \text{const}$. The duration of acceleration up to the synchronous speed $\Omega = \Omega_{syn}$ with $M = M_{max} = \text{const}$ will then be

$$t = \int_0^{\Omega_{syn}} \frac{J}{M_{in}} d\Omega = \frac{J}{M_{max}} \Omega_{syn} = T_{st} \quad (22-1)$$

since $\Omega = 0$ with $t = 0$.

The quantity T_{st} is called the starting time constant.

Let the torque curve of a motor be given in the form of equation (20-40). The mechanical and additional losses, as well as the torque M_0 corresponding to them, will be neglected. Then, when starting a motor at no-load, according to equations (22-1) and (20-40),

$$\begin{aligned} \frac{M}{M_{max}} &= \frac{J}{M_{max}} \frac{d\Omega}{dt} = \frac{J\Omega_{syn}}{M_{max}} \frac{d}{dt} \left(\frac{\Omega}{\Omega_{syn}} \right) = \\ &= T_{st} \frac{d(1-s)}{dt} = -T_{st} \frac{ds}{dt} = \frac{2}{\frac{s_m}{s} + \frac{s}{s_m}} \end{aligned} \quad (22-2)$$

whence, in starting from $s = 1.0$ to s the time is determined by the integral

$$t = -\frac{T_{st}}{2} \int_1^s \left(\frac{s_m}{s} + \frac{s}{s_m} \right) ds = -\frac{T_{st}}{2} \left[\frac{s^2}{2s_m} + s_m \log_e s \right]_1^s$$

and, consequently,

$$t = \left(\frac{1-s^2}{4s_m} + \frac{s_m}{2} \log_e \frac{1}{s} \right) T_{st} \quad (22-3)$$

At starting the speed first grows very quickly, but near to $s = 0$

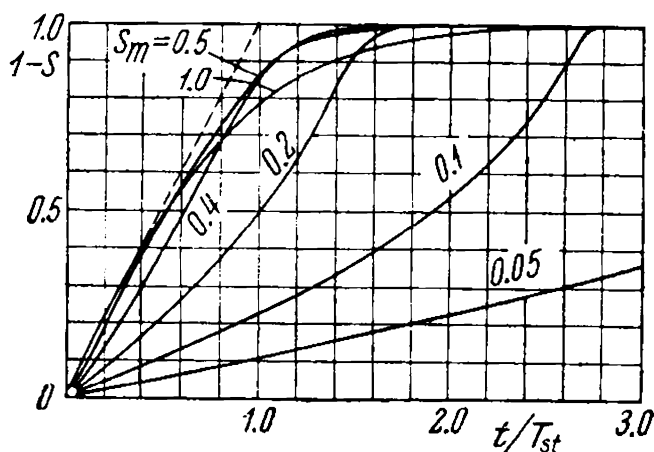


Fig. 22-2. Relative speed $1-s$ of an induction motor versus relative starting time

$$\frac{t}{T_{st}}$$

it approaches the steady-state speed asymptotically. Figure 22-2 shows the relation between the relative speed $(1-s)$ and the relative starting time for different values of s_m . Acceleration of the motor, as can be seen from Fig. 22-2, is the highest with $s_m \geq 0.4$.

Heat Liberated in Motor windings at Starting. In acceleration of an induction motor the current appreciably exceeds its rated value, and, therefore, a large quantity of heat is liberated in the

windings. If we neglect the no-load current I_0 and assume that $I_1 = I'_2$, the losses of energy in the windings at starting are equal to

$$A = \int_0^t m_1 I_2'^2 (r_1 + r_2') dt = \int_0^t m_1 I_2''^2 (R_1 + R_2) dt = \int_0^t m_1 I_2''^2 R_{sh} dt \quad (22-4)$$

For the current I_2'' , on the basis of the equivalent circuit of Fig. 19-7b, assuming $R_1 \cong R_2$ and taking into account the relation $R_2 = s_m X_{sh}$, we obtain

$$I_2'' = \frac{U_1}{\sqrt{\left(R_1 + \frac{R_2}{s}\right)^2 + X_{sh}^2}} \cong \frac{U_1}{\sqrt{\left(\frac{R_2}{s}\right)^2 + \left(\frac{R_2}{s_m}\right)^2}} = \frac{U_1}{\frac{R_2}{s_m} \sqrt{1 + \frac{s_m^2}{s^2}}}$$

When $s = 1.0$

$$I_{2sh}'' \cong \frac{U_1}{\frac{R_2}{s_m} \sqrt{1 + s_m^2}} \cong \frac{s_m U_1}{R_2} \quad (22-5)$$

and, consequently,

$$I_2'' \cong \frac{I_{2sh}''}{\sqrt{1 + \frac{s_m^2}{s^2}}} \quad (22-6)$$

From equation (22-2) we have

$$dt = -\frac{T_{st}}{2} \left(\frac{s_m}{s} + \frac{s}{s_m} \right) ds = -\frac{T_{st}}{2} \left(1 + \frac{s_m^2}{s^2} \right) \frac{s}{s_m} ds \quad (22-7)$$

Substituting in equation (22-4) for dt and I_2'' their values from equations (22-6) and (22-7), we have

$$A = -\frac{m_1 I_{2sh}''^2 R_{sh} T_{st}}{2s_m} \int_1^s s ds = m_1 I_{2sh}''^2 R_{sh} T_{st} \frac{1-s^2}{4s_m} \quad (22-8)$$

The amount of heat increases with speed, according to equation (22-8), along a parabola and reaches a finite limit when synchronism is attained, with $s = 0$.

From equation (22-8) it follows that during the starting period from $s = 1.0$ to $s = 0$ the energy losses in the windings are equal to

$$A_1 = m_1 I_{2sh}''^2 R_{sh} \frac{T_{st}}{4s_m} \quad (22-9)$$

When a motor is reversed, the lower limit of the integral (22-8) is equal to $s = 2$, and, therefore

$$A_2 = m_1 I_{2sh}''^2 R_{sh} \frac{T_{st}}{s_m} \quad (22-10)$$

Thus, in reversing, four times more heat is liberated than in starting from standstill.

With a view to equation (22-1), we obtain for the losses developed in the secondary winding at starting

$$A'_1 = m_1 I_{2sh}''^2 R_2 \frac{T_{st}}{4s_m} = \frac{m_1 I_{2sh}''^2 R_2}{s_m} \frac{J\Omega_{syn}^2}{4P_{em. max}} \quad (22-11)$$

But

$$P_{em. max} = m_1 I_{2m}''^2 \frac{R_2}{s_m}$$

Therefore, taking into account that equation (22-6) with $s = s_m$ gives $I_2'' = I_{2m}'' \cong \frac{I_{2sh}''}{\sqrt{2}}$, from equation (22-11) we get

$$A'_1 = \frac{1}{2} J\Omega_{syn}^2 \quad (22-12)$$

From equation (22-12) it follows that the quantity of heat liberated in the rotor winding during acceleration of an induction motor is equal to the kinetic energy of the rotor proper and of the rotating masses connected with it. Thus, one half of the electromagnetic energy transferred from the stator to the rotor is converted into kinetic energy of the rotating masses, while the other half is converted into thermal energy in the secondary circuit. If we insert an additional resistor r_{add} into the secondary circuit, the energy will be distributed between the internal and external resistances in the ratio $r_2 : r_{add}$.

The greater the moment of inertia of the rotating masses on the motor shaft, the slower is the acceleration and the greater the quantity of heat liberated in the secondary system of the motor.

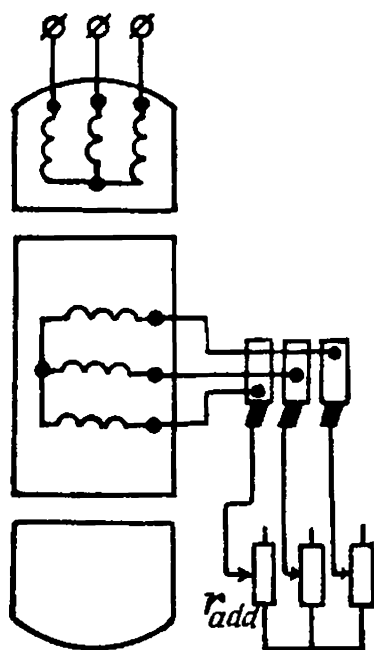


Fig. 22-3. Connection of additional resistors to rotor circuit

22-5. Starting of Phase-Wound Motors

The starting current of a motor with a phase-wound rotor can be reduced by connecting an additional resistor to the rotor circuit. The connection of an inductive reactance would simultaneously result in a reduction of the secondary current I_2 , and in an increase in the phase angle ψ_2 between the current and the e.m.f. E_2 , and would lead to a large decrease in torque. But, when a resistance is connected to the rotor circuit, the angle ψ_2 reduces and, therefore, the torque, despite the reduction in the current I_2 , in certain conditions even grows. This is why only connection of a resistance in the rotor circuit is of practical importance (Fig. 22-3).

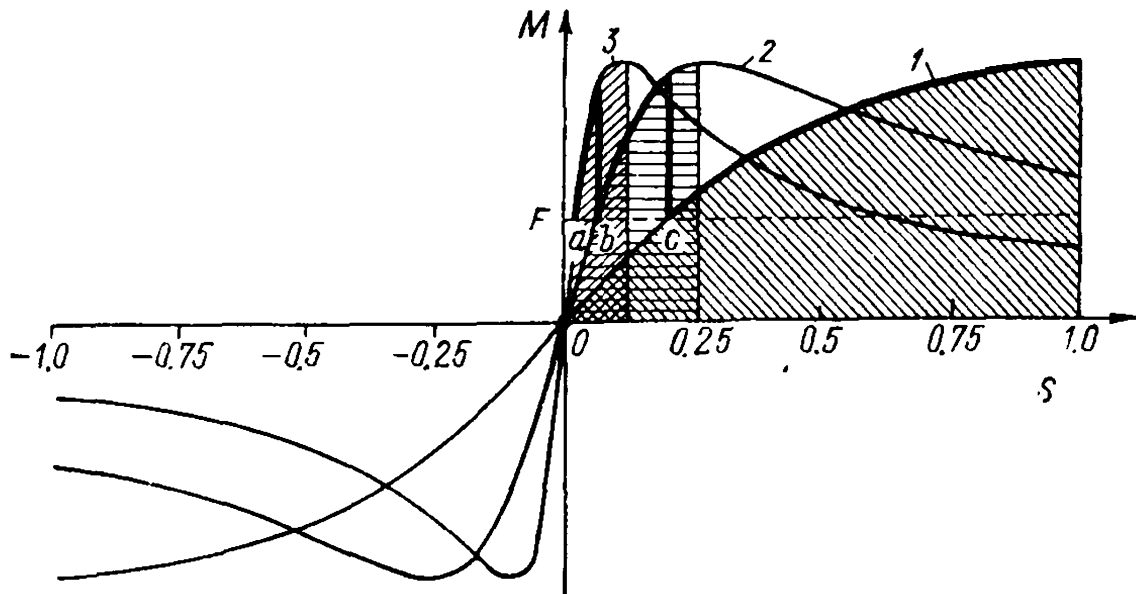


Fig. 22-4. Dependence of electromagnetic torque on slip for different values of the additional resistance in the rotor circuit:

1 — for $(R_2 + R_{add})/X_{sh} = 1.0$; 2 — for $(R_2 + R_{add})/X_{sh} = 0.25$;
3 — for $R_2/X_{sh} = 0.125$

Analysis of equivalent circuits and circle diagrams of an induction motor has shown that the maximum torque does not depend on R_2 , but only on the sum $R_1 + X_{sh}$ [formula (20-33)]:

$$M_{max} = \frac{m_1 U_1^2}{2\Omega_{syn} (R_1 + X_{sh})}$$

When the secondary resistance changes, only the slip s_m at which the torque is maximum changes and

$$s_m = \frac{R_2}{\sqrt{R_1^2 + X_{sh}^2}} \cong \frac{R_2}{X_{sh}}$$

Hence, it follows that if we introduce into the secondary circuit an additional resistor r_{add} for which

$$s_m = \frac{R_2 + R_{add}}{\sqrt{R_1^2 + X_{sh}^2}} = 1.0 \quad (\text{where } R_{add} = \sigma_1^2 r'_{add} = \sigma_1^2 k_r r_{add})$$

the starting torque will reach its maximum possible value (Fig. 22-4). The starting torque ratio will then be equal to the overload capacity:

$$k_{ov} = \frac{M_{max}}{M_r}$$

The torque-slip curves for different values of the additional resistance r_{add} are shown in Figs. 20-6 and 22-4. These curves make it possible to establish fundamental rules for selecting additional resistances when starting an induction motor. If the torque M_{stat} applied to the motor shaft is greater than the electromagnetic torque which it can develop when $s = 1.0$, the motor will obviously remain statio-

nary. For the motor to develop the maximum possible torque in starting, the additional resistance of the rheostat should be

$$r_{add} = \frac{\sqrt{R^2 + X_{sh}^2} - R_2}{\sigma_1^2 k_r} \cong \frac{X_{sh} - R_2}{\sigma_1^2 k_r}$$

Let us consider the starting process at this value of the additional resistance.

If the applied braking torque (OF in the figure) is less than the starting torque M_{st} , the motor will begin to rotate, and the electromagnetic torque developed by it will begin to decrease along curve 1 in Fig. 22-4. The slip of the motor will begin to decrease, and the speed to rise until equilibrium sets in between the braking and the electromagnetic torques. If we again decrease the additional resistance, the motor will pass over to the electromagnetic torque curve 2; the electromagnetic torque again becomes greater than the braking torque, and the motor begins to accelerate until equilibrium is reached between the developed and applied torques at the new and smaller slip. After this, we can again decrease the additional resistance of the starting rheostat and raise the speed. Cutting out of the additional resistances can be continued till $r_{add} = 0$, after which the motor passes over to its natural torque curve 3 corresponding to the value of its rotor resistance.

In practice, however, when a motor is started by means of a rheostat made of metal resistors, the stages of the rheostat are cut out not at the moment when equilibrium is attained between the running and static braking torques, but somewhat earlier, when the motor current drops to a certain value. This leads to a reduction in starting time.

For each torque curve corresponding to a certain resultant value of the secondary resistance $r_2 + r_{add}$ the portion of the curve from $s = 0$ to $s_m \cong \frac{R_2 + R_{add}}{X_{sh}}$ at which the torque reaches its maximum is the stable region of motor operation; the part from s_m to $s = 1.0$ is, correspondingly, the unstable region of operation. Within the stable-operation region an increase in braking torque causes an increase in slip, a decrease in speed and an increase in the electromagnetic torque until a new state of equilibrium sets in. Conversely, within the unstable-operation region an increase in braking torque and slip causes the electromagnetic torque to decrease in magnitude, as a result of which the motor does not attain a new state of equilibrium at another speed and slip, and comes to a standstill.

From a comparison of the torque curves for different values of r_{add} it can be seen that for motor operating conditions from $s = 0$ to $s = +1.0$ the only fully stable-operation curve is that for which $s_m = 1.0$, i.e., such an electromagnetic torque curve at which the maximum torque is obtained at $s_m = 1.0$.

An induction motor with slip rings (Fig. 22-3) is started by connecting the stator to the power line, the additional resistance r_{add} being fully cut in in the rotor circuit, in the form of a starting rheostat, after switching on the stator, the rheostat is gradually cut-out until the winding is short-circuited. Starting rheostats are usually metal with oil or liquid cooling.

To reduce the secondary resistance and decrease the friction losses of the brushes on the slip rings, the motors are frequently provided with a device for short-circuiting the rings while running and for further lifting the brushes.

22-6. Starting of Squirrel-Cage Motors

Across-the-Line-Starting. This method of starting is prevalent today because electrical systems now possess sufficient power capacity. Such starting is exceedingly simple, but at the same time it entails more or less considerable current surges which may harmfully affect the power supply line. For illustration Table 22-1 gives the starting currents and torques of 5- to 100-kW motors rated for speeds of $n = 1500$; 1000 and 750 rpm.

The above data relate to general-purpose motors.

In motors of special design we have, for the same or larger starting torques, smaller starting currents (Chap. 23).

Starting by Means of a Reactor in the Stator Circuit. The starting circuit is shown in Fig. 22-5. Here S is the stator, R —the rotor, R_c —the reactor. Suppose that the starting current in the external circuit is limited to $I_{st.ec}$.

$$I_{st.ec} = k_{st.ec} I_r$$

where $k_{st.ec}$ is the permissible starting current ratio.

Assuming for simplicity that $I_1 \cong I'_2$ we have, according to formulas (20-18) and (20-24):

$$M_{st} = \frac{m_1 I_{st.ec}^2 r'_2}{\Omega_1} = k_{st.ec}^2 \frac{m_1 I_r^2 r'_2}{\Omega_1} \equiv k_{st.ec}^2$$

Thus, when starting a motor with a reactor, the starting torque depends on the square of the coefficient $k_{st.ec}$.

TABLE 22-1

n_1 , rpm	I_{st}/I_r	M_{st}/M_r	M_{max}/M_r
1500	6.5-6	1.4-1.1	1.8
1000	6	1.3-1.1	1.8
750	5.5	1.1	1.6

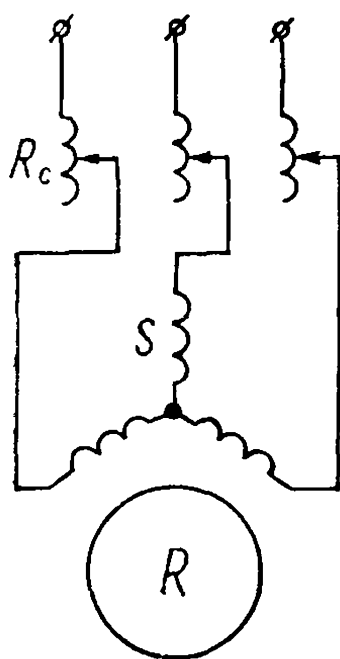


Fig. 22-5. Reactor starting

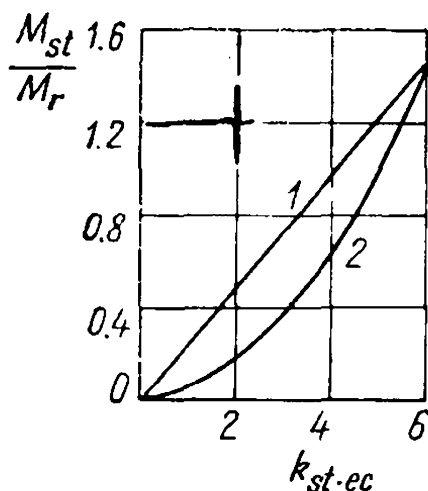
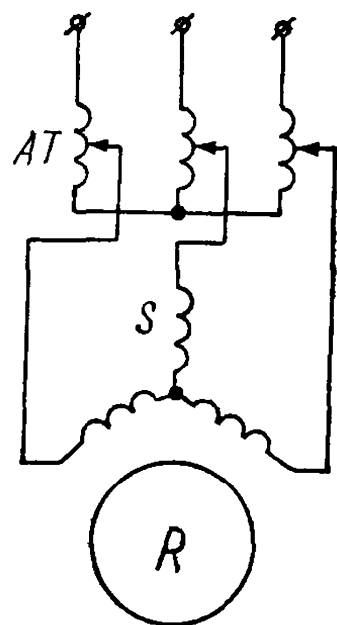
Fig. 22-6. Relation $\frac{M_{st}}{M_r} = f(k_{st.ec})$ for starting by means of autotransformer (1) and reactor (2)

Fig. 22-7. Autotransformer starting

But

$$M_r = \frac{m_1 I_r^2 \frac{r_2'}{s_r}}{\Omega_1}$$

where s_r is the slip at rated operating conditions.

Consequently,

$$\frac{M_{st}}{M_r} = k_{st.ec}^2 s_r \quad (22-13)$$

The relation $\frac{M_{st}}{M_r} = f(k_{st.ec})$ is shown in Fig. 22-6 by curve 2 plotted for a slip of $s_r = 4\%$. It can be seen that with $\frac{I_{st.ec}}{I_r} = 3$ the starting torque does not reach 40% of its rated value. In other words, this method of starting is admissible only where the magnitude of the starting torque is not essential.

Autotransformer Starting. The starting circuit is shown in Fig. 22-7. Here S is the stator, R is the rotor and AT is the autotransformer. Let U_{ec} and $I_{st.ec}$ be the voltage and starting current of the external circuit; $U_{st.mot}$ the voltage across the motor terminals and $I_{st.mot}$ the current in the stator; k_A is the voltage ratio of the autotransformer. The voltages and the currents are calculated per phase.

If z_{sh} is the impedance of one motor phase, then, neglecting for simplicity the autotransformer resistance, we have

$$U_{st.mot} = \frac{U_{ec}}{k_A}; \quad I_{st.mot} = \frac{U_{st.mot}}{z_{sh}} = \frac{U_{ec}}{k_A z_{sh}}$$

and

$$I_{st. ec} = \frac{I_{st. mot}}{k_A} = \frac{1}{k_A^2} \frac{U_{ec}}{z_{sh}} = \frac{1}{k_A^2} I_{sh} \quad (22-14)$$

where I_{sh} is the short-circuit current of the motor at rated voltage.

Thus, when an autotransformer is used for starting, the starting current in the circuit decreases k_A^2 times in comparison with the starting current obtained during across-the-line starting of the motor.

However, $M_{st} \equiv U_{st. mot}^2$ and since $U_{st. mot} = \frac{U_{ec}}{k_A}$, the starting torque also decreases k_A^2 times in comparison with the torque with across-the-line starting.

Hence, it follows that this method of starting, as also the previous one, can only be used when the braking torque is small at starting. Otherwise the motor will not start.

As compared with the previous one, this method of starting has a considerable advantage with respect to the starting torque. Indeed

$$M_{st} = \frac{m_1 I_{st. mot}^2 r_2'}{\Omega_1} = \frac{m_1 (I_{st. ec} k_A)^2 r_2'}{\Omega_1}$$

and

$$M_r = \frac{m_1 I_r^2 \frac{r_2'}{s_r}}{\Omega_1}$$

Consequently,

$$\frac{M_{st}}{M_r} = \frac{I_{st. ec}^2 k_A^2}{I_r^2} s_r = \frac{I_{st. ec}}{I_r} \times \frac{k_A^2 I_{st. ec}}{I_r} s_r$$

The ratio

$$\frac{I_{st. ec}}{I_r} = k_{st. ec}$$

is the starting current ratio in the external circuit. Besides, according to equation (22-14),

$$k_A^2 = \frac{I_{sh}}{I_{st. ec}}$$

Therefore,

$$\frac{M_{st}}{M_r} = k_{st. ec} s_r \frac{I_{sh}}{I_r} \quad (22-15)$$

The relation $\frac{M_{st}}{M_r} = f(k_{st. ec})$ is a straight line, since for given values of $\frac{I_{sh}}{I_r}$ and s_r , the torque $M_{st} \equiv k_{st. ec}$. Curve 1 in Fig. 22-6 giving the relation $\frac{M_{st}}{M_r} = f(k_{st. ec})$ was plotted for $\frac{I_{sh}}{I_r} = 6$ and $s_r = 0.04$.

By comparing formulas (22-15) and (22-13), we see that when starting through a reactor the torque $M_{st. r} \equiv k_{st. ec}^2$, while when starting

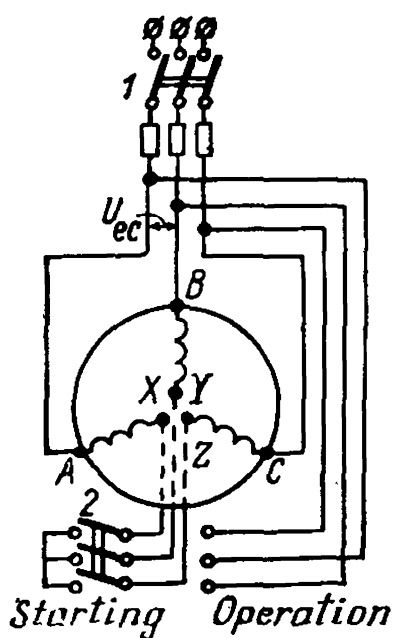


Fig. 22-8. Starting of a squirrel-cage motor by star-delta switching

through an autotransformer we have $M_{st.A} \equiv \equiv k_{st.ec} \frac{I_{sh}}{I_r}$. Since $\frac{I_{sh}}{I_r} > k_{st.ec}$, then $M_{st.A} > M_{st.r}$. Only in the limiting case, when $k_{st.ec} = \frac{I_{sh}}{I_r}$ (across-the-line starting), do we have $M_{st.r} = M_{st.A}$.

Star-Delta Starting (Y/Δ). This starting diagram is shown in Fig. 22-8. If switch 2 is in its "start" position, the stator winding is star-connected, if it is in its "operation" position, the winding is delta-connected.

The starting procedure is as follows. We set switch 2 in its "start" position and close switch 1. When the motor reaches a steady-state speed, switch 2 is quickly changed over to "operation". This completes starting.

Let U_{ec} be the line voltage, U_Y and U_{Δ} the voltages per phase for star and delta connections of the winding; $I_{st.ecY}$, $I_{st.ec\Delta}$, $I_{st.phY}$ and $I_{st.ph\Delta}$ —the starting currents in the line and in the phases of the stator winding when it is star- and delta-connected; z_{sh} —the short-circuit impedance of one phase.

Then

$$I_{st.phY} = I_{st.ecY} = \frac{U_Y}{z_{sh}} = \frac{U_{ec}}{\sqrt{3} z_{sh}} \quad (22-16)$$

If we connect the motor to the circuit with its winding delta-connected, we would obtain

$$I_{st.ph\Delta} = \frac{U_{\Delta}}{z_{sh}} = \frac{U_{ec}}{z_{sh}}$$

and

$$I_{st.ec\Delta} = \sqrt{3} I_{st.ph\Delta} = \frac{\sqrt{3} U_{ec}}{z_{sh}} \quad (22-17)$$

By comparing these two formulas, we see that

$$\frac{I_{st.ecY}}{I_{st.ec\Delta}} = \frac{1}{3} \quad (22-18)$$

Thus, the starting current in the circuit when the stator winding is star-connected is one-third of that when it is delta-connected. However, the starting torque M_{st} also decreases three times. Indeed,

$$M_{st.Y} \equiv U_Y^2 = \frac{U_{ec}^2}{3}$$

whereas

$$M_{st.\Delta} \equiv U_{\Delta}^2 = U_{ec}^2$$

This method of starting may be considered as a particular case of starting by means of an autotransformer with $k_A = \sqrt{3}$.

The method of reconnecting the stator windings, but in the reverse sequence, i.e., Δ/Y , is sometimes used to improve the power factor $\cos \varphi$ at loads not exceeding 30 to 40% of the rated load.

To see how the operating conditions of a motor change when switched over from a delta to a star connection, the simplest way is to construct two combined circle diagrams (Fig. 22-9): one for a delta-connected stator winding (circle *a*) and the other for a star-connected one (circle *b*). The diagrams are constructed by plotting the no-load points H_a and H_b and the short-circuit points K_a and K_b . In reconnection the voltage per phase increases $\sqrt{3}$ times, the flux Φ growing correspondingly; the no-load current (per phase), however, increases more than $\sqrt{3}$ times because of saturation of the steel. The short-circuit current $I_{sh.a} = \frac{U_{ec}}{z_{sh}}$, while $I_{sh.b} = \frac{U_{ec}}{\sqrt{3} z_{sh}}$. Consequently,

$$I_{sh.a} = I_{sh.b} \sqrt{3}.$$

The curves of the relations η , $\cos \varphi$ and $I = f(P_2)$ with delta- and star-connected stator windings are shown in Fig. 22-10. It can be seen that Δ/Y reconnection at small loads has a favourable effect on the power factor $\cos \varphi$ and is one of the possible ways of improving the external circuit power factor.

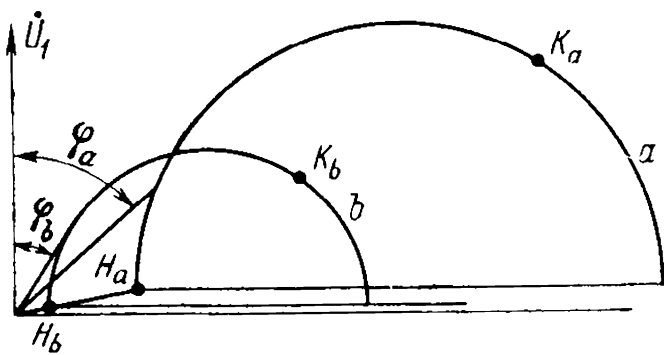


Fig. 22-9. Combined circle diagrams for operation with delta- (a) and star-connected (b) stator winding

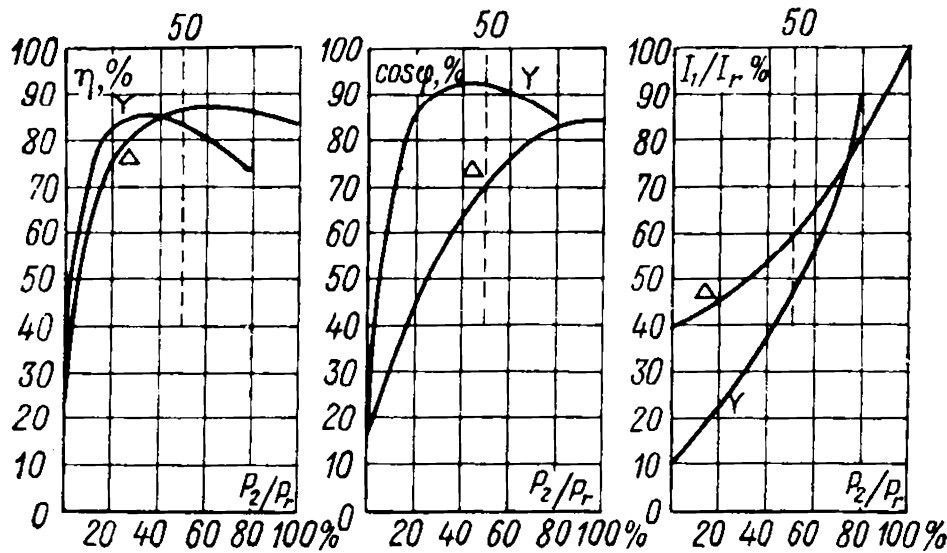


Fig. 22-10. Performance curves for a motor with delta- and star-connected stator winding

In the usual Y/ Δ reconnection procedures the stator is disconnected from the line for a very short time. The motor speed practically does not change, and, since it is near synchronous speed, when the motor is again connected, the process proceeds as if the rotor of the motor were open-circuited ($\frac{r_2}{s} \cong \infty$). Here a sharp surge of the no-load current is observed. This fault can be eliminated by means of special switches not disrupting the current at the expense of a more complex design.

Chapter 23

INDUCTION MOTORS USING SKIN EFFECT IN THE ROTOR WINDING

23-1. Double Squirrel-Cage Motor [163, 178, 179, 192, 193, 194, 209, 210, 211]

Designs. The double squirrel-cage motor was suggested by M. Dolivo-Dobrovolsky and is one of the varieties of the squirrel-cage induction motor using the skin-effect phenomenon in the rotor winding to improve the starting properties of the motor.

The stator of such a motor does not differ from that of a conventional motor, but its rotor consists of two cages (Fig. 23-1a). The upper cage nearer to the air-gap, is made of a high-resistant material—brass, aluminium bronze, etc., while the lower cage is made of copper, the two cages being separated by narrow slits of the slots. As a result, the lower cage has a high permeance for the leakage fluxes and the upper cage a relatively low permeance, owing to which the leakage inductive reactance of the lower cage is considerably greater than that of the upper cage. The part of the upper cage placed in the steel has practically no leakage flux of its own (Fig. 23-2), since the leakage flux $\Phi_{\sigma op. st}$ which links the two windings, is their mutual inductance flux and is determined by the vector sum of the currents flowing in the upper and lower bars.

The upper and lower cages may have either a common short-circuiting end ring (Fig. 23-1b), or each winding has its own short-circuiting end ring (Fig. 23-1c). In the first case the current flowing through the ring equals the vector sum of the currents in both windings, owing to which the leakage flux of the ring simultaneously becomes their mutual inductance flux; in the second case each of the windings has its own ring leakage flux and a certain flux linking both rings. In practice, however, the design generally used incorporates separate rings (Fig. 23-1c), because in this case the bars of the separate cages,

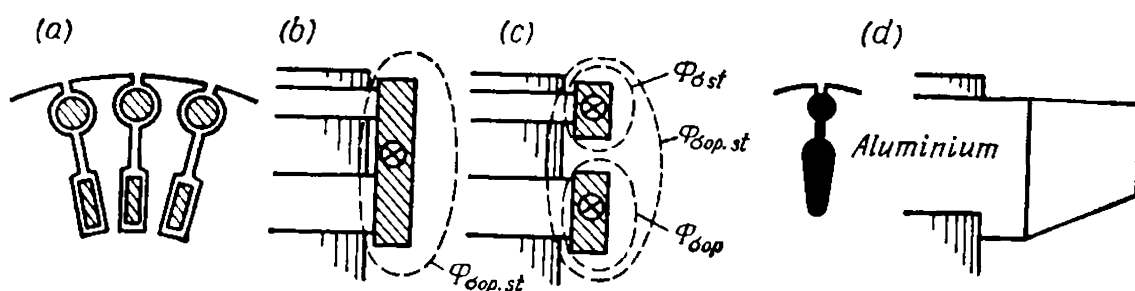


Fig. 23-1. Design of rotor windings of a double squirrel-cage motor

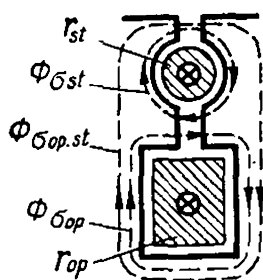


Fig. 23-2. Leakage flux path in rotor slot of a double squirrel-cage motor

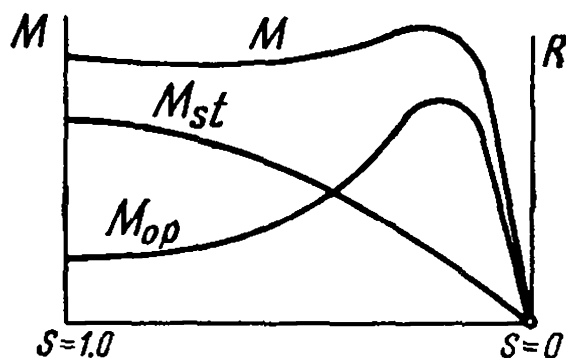


Fig. 23-3. Torque curves for a double squirrel-cage motor

each heating to a different degree during starting, can elongate freely and independently.

Double squirrel-cage motors with cast-in aluminium cages are made with appropriately shaped slots (Fig. 23-1d). Here the high resistance of the upper cage is obtained only by reducing its cross section. This is not dangerous from the point of view of heating, since the two windings are connected together through the aluminium bridge which also fills the slit between them.

Principle of Operation. At starting, the frequency of the rotor current is high and equal to the frequency in the line. The current is distributed between the upper and lower windings in inverse proportion to their impedances, and, since the lower winding has a very high inductive reactance, its impedance is several times that of the upper cage, whose reactance is practically zero. The current of the lower cage is thus appreciably smaller than that of the upper cage. Furthermore, owing to the high leakage inductive reactance of the lower cage, the current in it lags behind the e.m.f. induced by the mutual inductance flux by a large angle and the winding consequently produces a small torque. Conversely, the current in the upper cage at starting is not only of considerable magnitude, but is also nearly in phase with the mutual inductance e.m.f. because of the negligible inductive reactance and high resistance of the cage, owing to which this winding produces a very great torque.

The torque during the starting period is hence developed mainly by the upper cage, which, in consequence, is referred to as the *starting* cage.

As the motor speed increases, the frequency in the rotor winding begins to decrease, this resulting in a reduction of the inductive reactance and an increase in the current in the lower cage accompanied by a corresponding decrease in the phase angle between the current and the voltage. Consequently, this cage gradually begins to develop a greater and greater increasing torque. When the motor develops full speed and has a very small slip s , the inductive reactance of the lower cage becomes negligible in comparison with its resistance. The total

TABLE 23-1

M_{st}/M_r	2.0	1.5	1.0
I_{st}/I_r	5-4.5	3.8-3.5	3.5-3.2

working current of the motor secondary winding will be divided between the windings inversely proportional to their resistances, and, since the upper winding has a resistance which is 5 to 6 times that of the lower winding, the current in the upper cage becomes considerably smaller than that in the lower cage. Hence the torque is mainly developed by the lower cage, called the *operating* cage.

Figure 23-3 shows approximate torque curves for the upper and lower cages, as well as the total torque curve of both cages.

Possible values for the starting torque and starting current ratios for double squirrel-cage motors according to data of the “Elektrosila” Works are given in Table 23-1.

Equivalent Circuit for Double Squirrel-Cage Motor. The leakage flux paths inside a slot of a motor are shown in Fig. 23-2. The leakage flux $\Phi_{\sigma op. st}$ links the circuits of both currents—of the upper and lower cages—and is determined by the vector sum of these currents; this sum is the equivalent current I_2 of the secondary circuit. The inductive reactance $x_{op. st}$ corresponds to this flux. The leakage flux $\Phi_{\sigma op}$ links only with the lower cage and is determined by the current I_{op} in this cage. The leakage inductive reactance x_{op} corresponds to this flux. The leakage flux $\Phi_{\sigma st}$ should link only with the upper cage and is determined by the current I_{st} in this cage, but, since the lines of this flux passing through the slit between the cages are directed opposite to the lines of the flux $\Phi_{\sigma op}$, this results in the equivalent flux $\Phi_{\sigma op. st}$ which envelopes both cages jointly. It should be noted here that the flux $\Phi_{\sigma st}$ must cross two air-gaps, while the fluxes $\Phi_{\sigma op. st}$ and $\Phi_{\sigma op}$ cross only one gap. Owing to the above reasons, it may be assumed for an unsaturated magnetic circuit that the flux $\Phi_{\sigma st} \cong 0$ and, correspondingly, the inductive leakage reactance $x_{st} \cong 0$. Only when there are separate end rings for each cage conditions are created for producing a small flux around the end ring of the upper cage. Here it should be assumed that the upper cage has a small independent inductive leakage reactance x_{st} .

Therefore, taking into consideration the above, the equi-

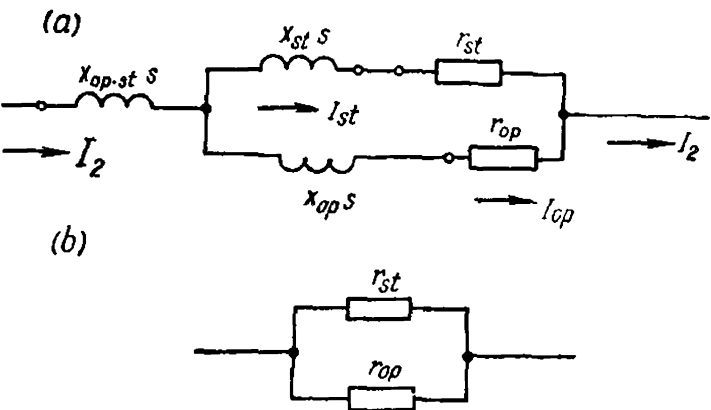


Fig. 23-4. Equivalent circuits for a double squirrel-cage motor rotor

valent circuit for the rotor with a slip s will have the form shown in Fig. 23-4a.

Let us write the expression for the impedance of the entire secondary circuit:

$$Z_{2s} = Z_{op. st. s} + \frac{Z_{st. s} Z_{op. s}}{Z_{st. s} + Z_{op. s}} = jx_{op. st} s + \frac{(r_{st} + jx_{st}s)(r_{op} + jx_{op}s)}{(r_{st} + r_{op}) + j(x_{st} + x_{op})s} \quad (23-1)$$

By multiplying the numerator and denominator of the fraction in the expression (23-1) by the conjugated complex of the denominator, we obtain

$$Z_{2s} = \left[jx_{op. st} + \frac{r_{st}r_{op}(r_{st} + r_{op}) + (r_{st}x_{op}^2 + r_{op}x_{st}^2)s}{s[(r_{st} + r_{op})^2 + (x_{st} + x_{op})^2 s^2]} + \right. \\ \left. + j \frac{r_{st}^2 x_{op} + r_{op}^2 x_{st} + (x_{st} \cdot x_{op})(x_{st} + x_{op})s^2}{(r_{st} + r_{op})^2 + (x_{st} + x_{op})^2 s^2} \right] \quad (23-1a)$$

Equations (23-1) and (23-1a) for Z_{2s} are rather complicated for analysis. But in most cases, as was shown previously, for example for a motor with a double squirrel cage, it may be assumed that $x_{st} \cong 0$, and then formula (23-1a) becomes more simple and convenient for analysis. Here no separate slot leakage of the upper cage, but only a very small separate end-connection leakage remains for the upper and lower cages when there are separate end rings.

With a common end ring for both cages, there are also no separate leakages, and only common leakage of both cages in the slot portion and in the end connections remains, which is already part of the mutual leakage inductive reactance $x_{op. st}$. With $x_{st} = 0$ the formula (23-1a) will have the form:

$$Z_{2s} = s \left\{ jx_{op. st} + \frac{r_{st}r_{op} + jr_{st}x_{op}s}{s[(r_{st} + r_{op}) + jx_{op}s]} \right\} = \\ = s \left\{ jx_{op. st} + \frac{r_{st}r_{op}(r_{st} + r_{op}) + r_{st}x_{op}^2 s^2}{s[(r_{st} + r_{op})^2 + x_{op}^2 s^2]} + \right. \\ \left. + j \frac{r_{st}^2 x_{op}}{[(r_{st} + r_{op})^2 + x_{op}^2 s^2]} \right\} \quad (23-2)$$

The complete equivalent circuit for a double squirrel-cage motor will be of the form shown in Fig. 23-5a. Since there are several parts, the analysis of this circuit is rather difficult. If the circuit of Fig. 23-5a is transformed into a circuit with the magnetizing branch part brought out, as in Sec. 19-5 for a conventional induction machine, and the correction factor σ_1 is taken to be a real number, we obtain the improved equivalent circuit in Fig. 23-5b. In this circuit the slip does not influence the current in the magnetizing branch part. As a result, only one parallel branch remains in the transformed circuit, considerably simplifying its analysis. In the circuit in Fig. 23-5b

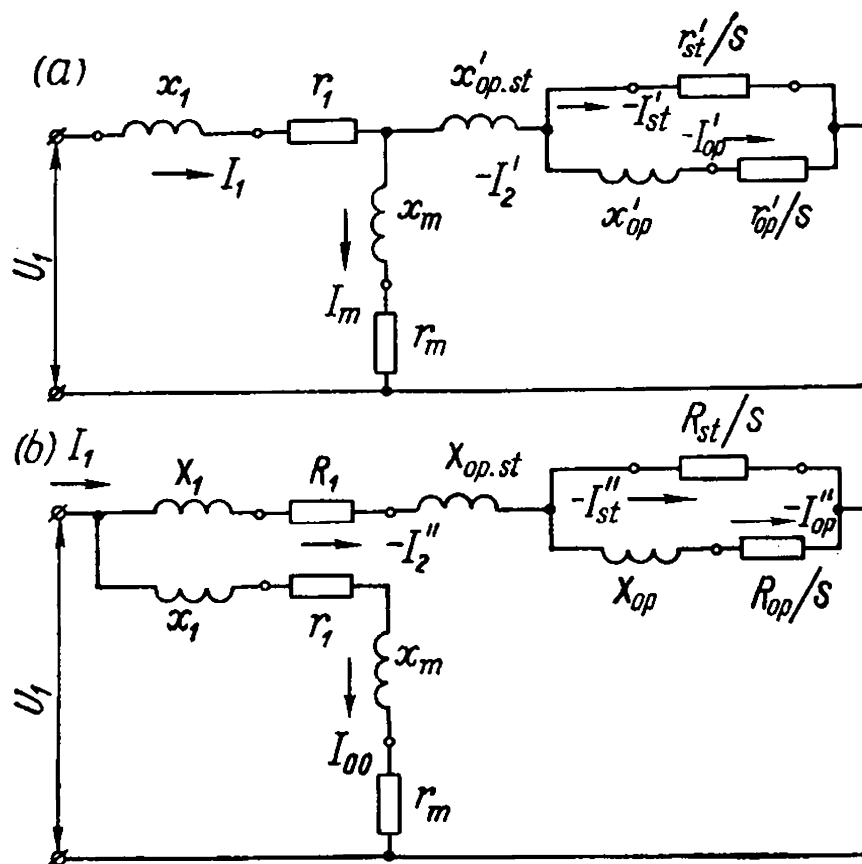


Fig. 23-5. Precise (a) and improved (b) equivalent circuits for a double squirrel-cage motor

we have

$$\begin{aligned} X_1 &= x_1 \sigma_1; & R_1 &= r_1 \sigma_1; & X_{op.st} &= x'_{op.st} \sigma_1^2 \\ R_{st} &= r'_{st} \sigma_1^2; & X_{op} &= x'_{op} \sigma_1^2; & R_{op} &= r'_{op} \sigma_1^2 \end{aligned}$$

where the correction factor σ_1 , if we neglect the resistances r_1 and r_m , is equal to the primary leakage factor.

Now let us consider separately the operating conditions of a motor with small slips, when $s \approx 0$ (rated load) and the operating conditions for $s \approx 1$ (starting and braking conditions).

Small-Slip Conditions ($s \approx 0$). Here we may neglect the terms containing s^2 in equation (23-2). The expression for the secondary circuit impedance then acquires the following form:

$$\begin{aligned} Z_{2s} &\approx s \left[jx_{op.st} + \frac{r_{st}r_{op}}{s(r_{st} + r_{op})} + j \frac{r_{st}^2}{(r_{st} + r_{op})^2} x_{op} \right] = \\ &= s \left[jx_{op.st} + \frac{r_{eq}}{s} + jx_{eq} \right] \end{aligned} \quad (23-3)$$

where

$$r_{eq} = \frac{r_{st}r_{op}}{r_{st} + r_{op}}; \quad x_{eq} = \frac{r_{st}^2}{(r_{st} + r_{op})^2} x_{op}$$

Hence it follows that the equivalent resistance with small slips is equal to the equivalent resistance of the two parallel-connected

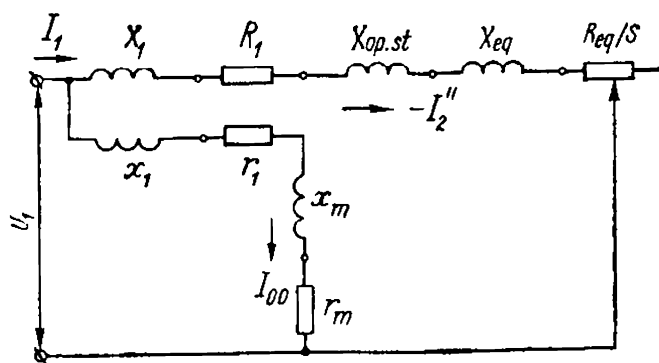


Fig. 23-6. Approximate equivalent circuit for a double squirrel-cage motor with small slips

resistances r_{op} and r_{st} (Fig. 23-4b), and that the equivalent inductive reactance x_{eq} is equal to the reactance x_{op} of the lower cage multiplied by the square of the resistance ratio:

$$\left(\frac{r_{st}}{r_{op} + r_{st}} \right)^2$$

By substituting for the resistances of the branch part in the equivalent circuit of Fig. 23-5b the resistance and reactance $R_{eq} = r'_{eq} \sigma_1^2$ and $X_{eq} = x'_{eq} \sigma_1^2$, we obtain the circuit in Fig. 23-6, which is the equivalent circuit of a motor with the inductive reactance $X_2 = X_{op.st} + X_{eq}$ and resistance $\frac{R_2}{s} = \frac{R_{eq}}{s}$ in its secondary circuit.

If this two-cage motor were made as a conventional squirrel-cage motor with only the upper cage, but with a resistance R_{eq} , and the stator circuit remaining as before, such a motor would then have the same primary circuit resistance and reactance, and its secondary circuit would have a resistance $\frac{R_2}{s} = \frac{R_{eq}}{s}$ and a reactance $X_2 = X_{op.st}$. Both motors would have the same no-load current, but the diameters of their circle diagrams would be different. For a conventional-type motor

$$D_a = \frac{U_1}{X_1 + X_2} = \frac{U_1}{X_1 + X_{op.st}} \quad (23-4)$$

and for a double squirrel-cage motor

$$D_{eq} = \frac{U_1}{X_1 + X_{op.st} + X_{eq}} \quad (23-5)$$

It is obvious that $D_a > D_{eq}$ and the circle diagrams of these motors will be of the form shown in Fig. 23-7. Since we assumed that the pri-

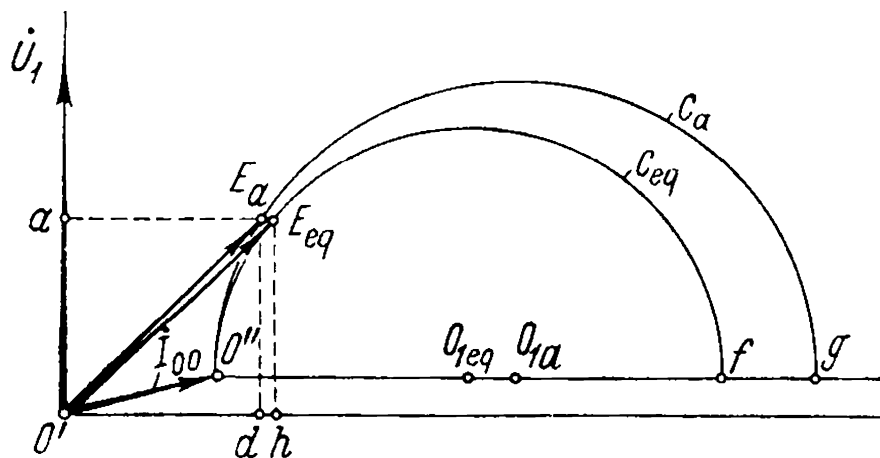


Fig. 23-7. Circle diagrams of normal induction motor (C_a) and double squirrel-cage motor (C_{eq})

mary and secondary resistances of these motors are equal, the motors will have approximately equal efficiencies. At the same load the motors will have the same active current component $E_a d = E_{eq} h$, but the inductive current component for the conventional induction motor $O'd$ is less than the inductive component $O'h$ for the double squirrel-cage motor. Hence, the power factor $\cos \varphi$ of the double squirrel-cage motor is usually lower than that of the normal induction motor; this is more pronounced in low-speed motors than in high-speed ones. Consequently, an increased starting torque in the double squirrel-cage motor is attained at the expense of a somewhat decreased power factor at practically the same efficiency when compared with a conventional squirrel-cage induction motor.

Large-Slip Conditions ($s \cong 1.0$). With large slips we may neglect the small resistance $\frac{R_{op}}{s}$ of the lower cage in the branched secondary circuit as compared with the relatively high inductive reactance X_{op} of this cage. Assuming that $R_{op} \cong 0$, we obtain for the main branch of the motor the approximate equivalent circuit of Fig. 23-8a.

Let us compare the circuit of Fig. 23-8a with the complete equivalent circuit for a conventional induction motor (Fig. 19-5) in which the losses in the steel are neglected ($r_m \cong 0$). The latter circuit can be transformed into the improved equivalent circuit shown in Fig. 19-7. If in the same manner we transform the circuit in Fig. 23-8a into a circuit with its parallel part brought out to the terminals, we obtain the equivalent circuit shown in Fig. 23-8b. From this circuit it follows that at large slips the end of the current vector will describe a circle whose diameter is

$$D_{st} = \frac{U_1}{(X_1 + X_{op.st}) \sigma'_1} \quad (23-6)$$

where

$$\sigma'_1 = 1 + \frac{X_1 + X_{op.st}}{X_{op}} \quad (23-7)$$

By substituting its value for σ'_1 in the expression for the diameter, we get

$$D_{st} = \frac{U_1 X_{op}}{(X_1 + X_{op.st})(X_1 + X_{op.st} + X_{op})} \quad (23-8)$$

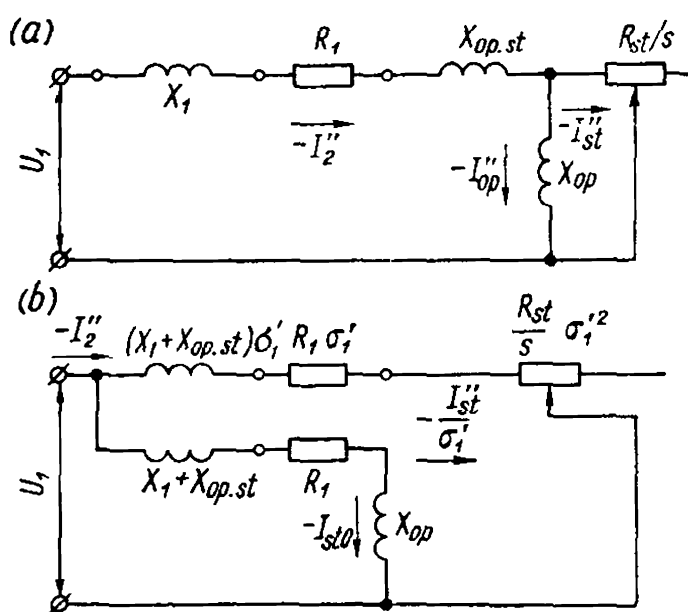


Fig. 23-8. Approximate equivalent circuits for an induction motor with large slips

The conditional no-load current for this circle, which is valid only for large slips s , will be

$$I_{st0} = \frac{U_1}{\sqrt{R_1^2 + (X_1 + X_{op.st} + X_{op})^2}} \quad (23-9)$$

Let us now consider the current circle when the upper cage is open-circuited, i.e., assuming in the diagram in Fig. 23-5b that $R_{st} = \infty$. We obtain a single-cage induction motor where the current circle diameter will be equal to

$$D_0 = \frac{U_1}{X_1 + X_{op.st} + X_{op}} \quad (23-10)$$

and the current for a slip $s = \pm\infty$ will be equal to

$$I_{0\infty} = \frac{U_1}{\sqrt{R_1^2 + (X_1 + X_{op.st} + X_{op})^2}} \quad (23-11)$$

Hence, we come to the conclusion that the no-load current of circle C_{st} corresponding to the circuit in Fig. 23-8b is equal to the current for the slips $s = \pm\infty$ of the circle C_0 corresponding to operation of the motor with its upper cage open.

It is interesting to note the following relation between the diameters of the circles considered above:

$$D_{st} = \frac{U_1 X_{op}}{(X_1 + X_{op.st})(X_1 + X_{op.st} + X_{op})} = \frac{U_1}{X_1 + X_{op.st}} - \frac{U_1}{X_1 + X_{op.st} + X_{op}} = D_a - D_0 \quad (23-12)$$

The points with the slip $s = \pm\infty$ for the circles C_a and C_{st} coincide. Indeed, for the first circle (the circuit in Fig. 23-6 with $X_{eq} = 0$) we have

$$I_{a\infty} = \frac{U_1}{\sqrt{R_1^2 + (X_1 + X_{op.st})^2}} \quad (23-13)$$

and for the second circle C_{st} (the circuit in Fig. 23-8b)

$$I_{st\infty} = \frac{U_1}{\sqrt{R_1^2 + (X_1 + X_{op.st})^2}} \quad (23-14)$$

whence

$$I_{a\infty} = I_{st\infty}$$

All the circles considered above and their mutual arrangement are shown in Fig. 23-9.

A more detailed analysis proves that the centre M_a of circle C_a , the centre M_{st} of circle C_{st} and the point with the slip $s = \pm\infty$ on circles C_a and C_{st} lie on one straight line $M_a - M_{st} - F$.

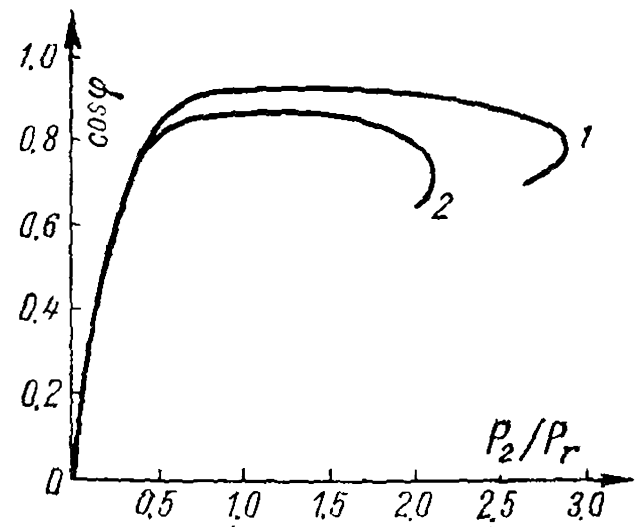


Fig. 23-10. Dependence of power factor upon load for four-pole 29-kW motors of the conventional (1) and double squirrel-cage (2) types

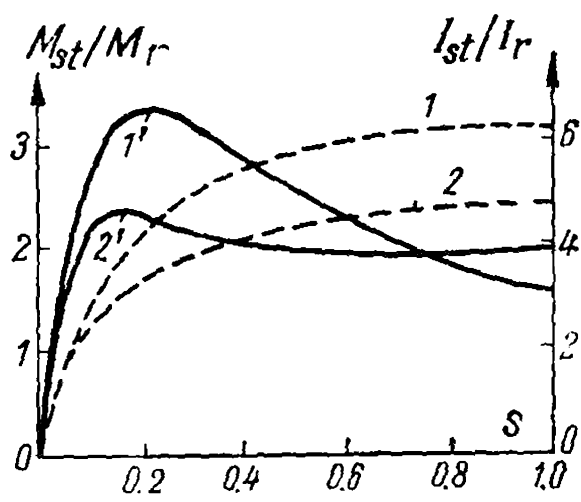


Fig. 23-11. Dependence of torque ($1'$ and $2'$) and current (1 and 2) upon slip for four-pole 29-kW motors of the conventional (1 and $1'$) and double squirrel-cage (2 and $2'$) types

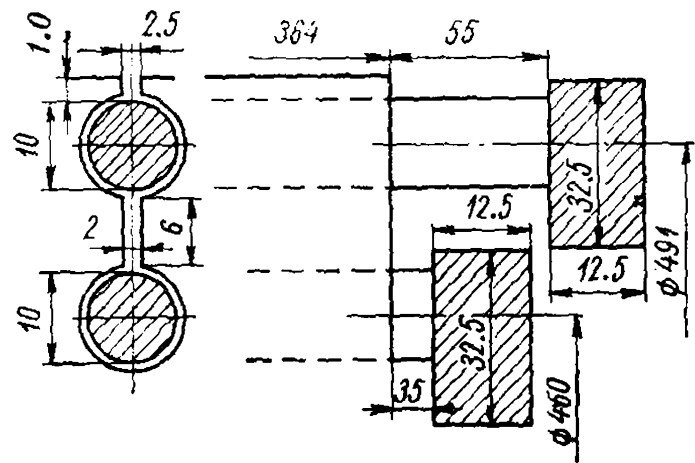


Fig. 23-12a. Shape of slot of rotor with a double squirrel cage

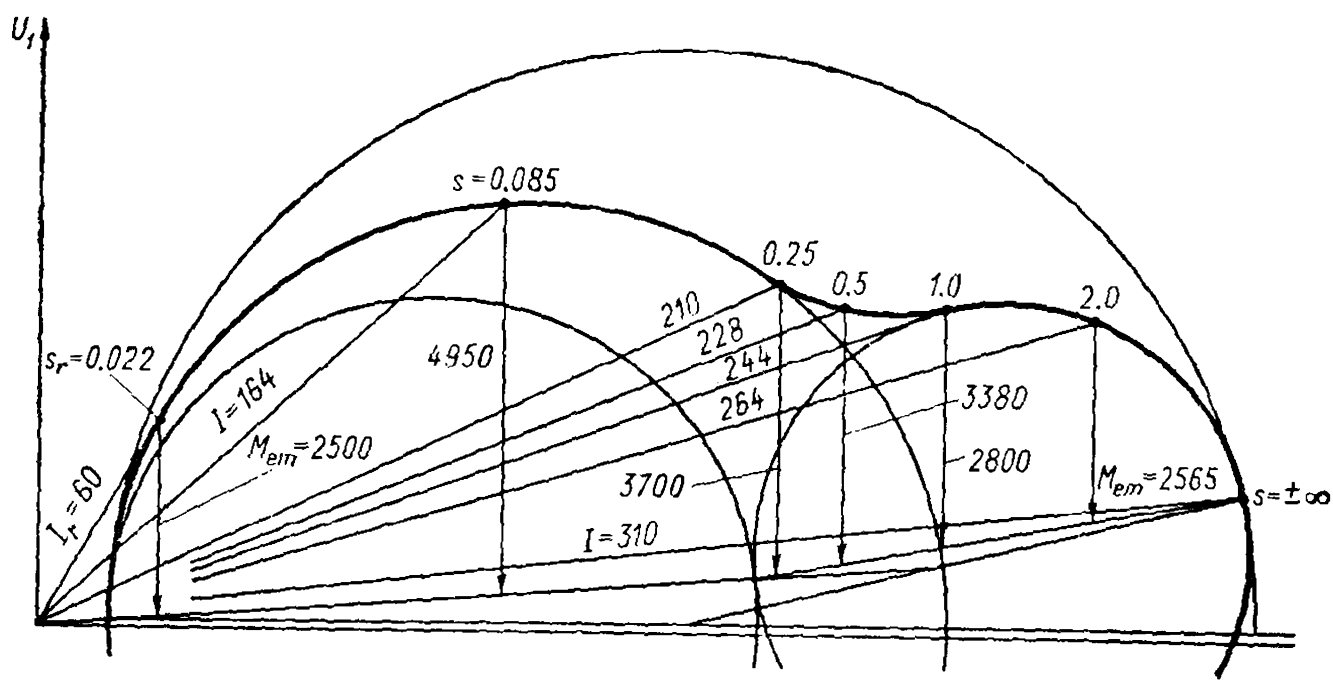


Fig. 23-12b. Circle diagram of a double squirrel-cage motor (according to data given in Example 23-2) and of the current and torque values at different slips

The stator and the parameters of the magnetizing loop of the equivalent circuit are assumed the same as for a conventional squirrel-cage motor (see Example 19-1).

The data of the rotor are: number of rotor slots $N_2=80$, number of slots per pole per phase $q_2=4.44$.

The shape and the main dimensions of the rotor slot are shown in Fig. 23-12a.

Rotor slot permeance:
upper cage (brass)

$$\lambda_{st. bar1} = 0.623 + \frac{1}{2.5} = 1.023 \text{ [formula (5-15d)]}$$

$$\lambda_{end. bar1} = 1.14 \text{ [formula (18-25a)]}$$

$\lambda_{dif. bar1} = 1.7$ [formula (5-27), the factor k_{dif2} has been taken from Fig. 18-7 for $\beta=1.0$ and $q_2=4.44$]

$$\sum \lambda_{bar1} = 1.023 + 1.14 + 1.7 = 3.86$$

$$x'_{op. st} = 2\pi \times 1.26 \times 10^{-8} \times 50 \times 33.4 \times 3.86 \times k = 0.00051 \times 5500 = 2.8 \Omega$$

where $k=5500$ is the reduction factor;
lower cage (copper)

$$\lambda_{s. bar2} = 0.623 + \frac{6}{2} = 3.62$$

$$\lambda_{end. bar2} = 1.14$$

$$\sum \lambda_{bar2} = 4.76$$

$$x'_{op} = 2\pi \times 1.26 \times 10^{-8} \times 50 \times 33.4 \times 4.76 \times k = 6.29 \times 10^{-5} \times 5500 = 3.45 \Omega$$

The resistance of the upper cage bars is

$$r_{bar1} = \rho_{75^\circ} \frac{l_{bar1}}{q_{bar1}} = 0.0744 \times \frac{0.474}{78.5} = 45 \times 10^{-5} \Omega$$

where

$$l_{bar1} = 364 + 2 \times 55 = 474 \text{ mm}$$

$$d_{bar1} = 10 \text{ mm}$$

$$q_{bar1} = \frac{\pi}{4} \times 10^2 = 78.5 \text{ mm}^2$$

$$\rho_{15^\circ} = 0.06 \Omega \cdot \text{mm}^2/\text{m}$$

$$\rho_{75^\circ} = 1.24 \times 0.06 = 0.0744 \Omega \cdot \text{mm}^2/\text{m}$$

The resistance of two adjacent sections of the copper end ring of the upper cage is

$$r_{cage1} = \rho_{cop75^\circ} \frac{l_{cage1}}{q_{ring1}} = 0.0217 \times \frac{0.0386}{406} = 20.6 \times 10^{-7} \Omega$$

where

$$q_{ring1} = 12.5 \times 32.5 = 406 \text{ mm}^2$$

$$l_{cage1} = 2 \times \frac{\pi \times 491}{80} = 38.6 \text{ mm}$$

The resistance of two sections of the ring reduced to the resistance of a bar, according to formula (18-24), is

$$r'_{ring1} = \frac{20.6 \times 10^{-7}}{0.055} = 3.75 \times 10^{-5} \Omega$$

The total resistance of the upper cage, referred to the stator primary system, is

$$r'_{st} = (r_{bar1} + r'_{cage1}) k = (45 + 3.75) \times 10^{-5} \times 5500 = 2.68 \Omega$$

Lower copper cage

$$l_{bar2} = 364 + 2 \times 35 = 434 \text{ mm}$$

$$d_{bar2} = 10 \text{ mm}$$

$$q_{bar2} = \frac{\pi \times 10^2}{4} = 78.5 \text{ mm}^2$$

$$r_{bar2} = 0.0217 \times \frac{0.434}{78.5} = 12 \times 10^{-5} \Omega$$

$$q_{ring2} = 12.5 \times 32.5 = 406 \text{ mm}^2$$

$$l_{cage2} = 2 \times \frac{\pi \times 450}{80} = 35.4 \text{ mm}$$

$$r_{cage2} = 0.0217 \times \frac{0.0354}{406} = 18.9 \times 10^{-7} \Omega$$

The resistance of two sections of the end rings of the lower cage reduced to the resistance of a squirrel cage bar [formula (18-24)] is

$$r'_{ring2} = \frac{18.9 \times 10^{-7}}{0.055} = 3.45 \times 10^{-5} \Omega$$

The total resistance of the lower cage, referred to the primary system, is

$$r'_{op} = (r_{bar2} + r'_{ring2}) k = (12 + 3.45) \times 10^{-5} \times 5500 = 0.85 \Omega$$

The complete equivalent diagram of a motor with a squirrel cage is according to Fig. 23-5a, where

$$x_1 = 2.78 \Omega; \quad r_1 = 0.68 \Omega; \quad x'_{op, st} = 2.8 \Omega$$

$$\frac{r_{st}}{s} = \frac{2.68}{s}; \quad x'_{op} = 3.45 \Omega$$

$$\frac{r'_{op}}{s} = \frac{0.85}{s}; \quad x_m = 95.6 \Omega; \quad r_m = 11 \Omega$$

The equivalent diagram with the no-load part brought out to the terminals is according to Fig. 23-5b where

$$\sigma_1 = 1 + \frac{2.78}{95.6} = 1.03; \quad \sigma_1^2 = 1.06$$

$$R_1 = 0.68 \times 1.03 = 0.7 \Omega; \quad X_1 = 2.78 \times 1.03 = 2.86 \Omega$$

$$X_{op, st} = 2.8 \times 1.06 = 2.96 \Omega; \quad X_{op} = 3.45 \times 1.06 = 3.65 \Omega$$

$$R_{st} = 2.68 \times 1.06 = 2.84 \Omega; \quad R_{op} = 0.85 \times 1.06 = 0.9 \Omega$$

Example 23-2. Calculation of powers and torques of an induction motor with a double squirrel cage, and construction of primary current locus.

The total mechanical power is

$$P_{mech} = p_{mech} + p_{add} + P_2 = 2.0 + 1.4 + 250 = 253.4 \text{ kW}$$

The reduced current of the main circuit, owing to a somewhat reduced $\cos \varphi$, is taken equal to $I_2'' = 53 \text{ A}$ (for a simple squirrel-cage motor $I_2'' = 52 \text{ A}$). Here

$$p_{cop2} = 3I_2''^2 \cdot R_2 = 3 \times 53^2 \times 0.683 \times 10^{-3} = 5.74 \text{ kW}$$

$$P_{em} = P_{mech} + p_{cop2} = 253.4 + 5.74 = 259.14 \text{ kW}$$

$$s_r = \frac{p_{cop2}}{P_{em}} = \frac{5.74}{259.14} = 0.0221$$

$$\frac{R_2}{s_r} = \frac{0.683}{0.0221} = 30.9 \text{ } \Omega$$

$$\cos \psi_2 = \frac{R_1 + \frac{R_2}{s_r}}{\sqrt{\left(R_1 + \frac{R_2}{s_r}\right)^2 + X_{sh}^2}} = \frac{0.7 + 30.9}{\sqrt{(0.7 + 30.9)^2 + 7.93^2}} = \frac{31.6}{32.6} = 0.97$$

$$P_{em.r} = \frac{3U_{1ph}^2 \frac{R_2}{s_r}}{\left(R_1 + \frac{R_2}{s_r}\right)^2 + X_{sh}^2} = \frac{3 \times 1730^2 \times 30.9 \times 10^{-3}}{(0.7 + 30.9)^2 + 7.93^2} = 261.5 \text{ kW}$$

$$M_{em.r} = \frac{P_{em.r}}{2\pi n} = \frac{261.5 \times 10^3}{2\pi \times \frac{1000}{60}} = 2500 \text{ N}\cdot\text{m}$$

according to formula (20-32)

$$M_m = \frac{3 \times 3 \times 1730^2}{2 \times 2\pi \times 50 (0.7 + \sqrt{0.7^2 + 7.93^2})} = 4950 \text{ N}\cdot\text{m}$$

$$\frac{M_m}{M_{em.r}} = \frac{4950}{2500} = 1.98$$

$$\sum p = (p_{mech} + p_{add}) + 3I_2''^2 R_{sh} + p_0 = 3.4 + 11.6 + 11.68 = 26.7 \text{ kW}$$

$$\eta = \left(1 - \frac{26.7}{250 + 26.7}\right) \times 100 = (1 - 0.0966) \times 100 = 90.34\%$$

For low slip conditions within the normal load range the equivalent diagram can be represented in a simplified form with the resistances and inductive reactances of the main branched circuit part replaced by equivalent resistances and reactances connected in series

$$R_{eq} = R_{op} \alpha = 0.9 \times 0.76 = 0.683 \text{ } \Omega$$

and

$$X_{eq} = X_{op} \alpha^2 = 3.65 \times 0.578 = 2.11 \text{ } \Omega$$

where

$$\alpha = \frac{R_{st}}{R_{st} + R_{op}} = \frac{2.84}{2.84 + 0.9} = 0.76 \text{ and } \alpha^2 = 0.578$$

For low slip conditions ($s < 0.1$) the equivalent diagram has the simplified form shown in Fig. 23.6, where

$$\begin{aligned} R_{sh} &= R_1 + R_{eq} = 0.7 + 0.683 = 1.383 \, \Omega \\ X_{sh} &= (X_1 + X_{op, st}) + X_{eq} = 5.82 + 2.11 = 7.93 \, \Omega \\ Z_{sh} &= \sqrt{R_{sh}^2 + X_{sh}^2} = \sqrt{1.383^2 + 7.93^2} = 8.02 \, \Omega \\ I_{sh} &= \frac{1730}{8.02} = 216 \, \text{A}, \quad \cos \varphi_{sh} = \frac{1.383}{8.02} = 0.173 \end{aligned}$$

For great slips ($s > 1$) the simplified equivalent diagram of the main circuit acquires the form shown in Fig. 23-8a and can be transformed into a simplified equivalent circuit with the conditional magnetizing part removed to the terminals as shown in Fig. 23-8b. Here

$$\begin{aligned} \sigma'_1 &= 1 + \frac{X_1 + X_{op, st}}{X_{op}} = 1 + \frac{5.82}{3.65} = 2.6; \quad \sigma'^2 = 6.75 \\ X_{sh} &= (X_1 + X_{op, st}) \sigma'_1 = 5.82 \times 2.6 = 15.2 \, \Omega \\ R_{sh} &= R_1 \sigma'_1 + R_{st} \sigma'^2_1 = 0.7 \times 2.6 + 2.84 \times 6.75 = 20.92 \, \Omega \\ R_{st} \sigma'^2_1 &= 2.84 \times 6.75 = 19.1 \, \Omega \\ Z_{sh} &= \sqrt{20.92^2 + 15.2^2} = 25.8 \, \Omega \\ I''_{s1} &= \frac{1730}{25.8} = 67 \, \text{A} \end{aligned}$$

according to formula (20-34)

$$\begin{aligned} M_{st} &= \frac{3 \times 3 \times 1730^2 \times 19.1}{2 \times \pi \times 50 \times 665} = 2470 \, \text{N-m} \\ \frac{M_{st}}{M_{2r}} &= \frac{2470}{2440} = 1.025 \end{aligned}$$

The parameters of an induction motor with a double squirrel cage for different slips are calculated more accurately by formulas (23-1) and (23-2), corresponding to the equivalent circuit of Fig. 23-5

$$\begin{aligned} Z_{st} &= R_1 + j(X_1 + X_{op, st}) + \frac{R_{st} R_{op} (R_{st} + R_{op}) + R_{st} X_{op}^2 s^2}{s [(R_{st} + R_{op})^2 + X_{op}^2 s^2]} + \\ &\quad + j \frac{R_{st}^2 X_{op}}{[(R_{st} + R_{op})^2 + X_{op}^2 s^2]} = 0.7 + j5.82 + \\ &\quad + \frac{2.84 \times 0.9 \times (2.84 + 0.9) + 2.84 \times 3.65^2 s^2}{s [(2.84 + 0.9)^2 + 3.65^2 s^2]} + \\ &\quad + j \frac{2.84 \times 3.65}{(2.84 + 0.9)^2 + 3.65^2 s^2} = 0.7 + j5.82 + \frac{9.56 + 37.8 s^2}{s (13.9 + 13.2 s^2)} + \\ &\quad + j \frac{29.3}{(13.9 + 13.2 s^2)} \end{aligned}$$

with $s=1.0$

$$Z_{st} = 0.7 + j5.82 + \frac{47.36}{27.1} + j \frac{29.3}{27.1} = 0.7 + 1.75 + j6.9$$

$$Z_{st} = 7.33 \, \Omega$$

$$I_{st} = \frac{U_1}{Z_{st}} = \frac{1730}{7.33} = 236 \, \text{A}$$

$$\cos \varphi'' = \frac{R_{st}}{Z_{st}} = \frac{2.45}{7.35} = 0.334$$

$$\frac{I_{st}}{I_r} = \frac{236 \times 1.03}{60} = 4.06$$

according to formula (20-34)

$$M_{st} = \frac{3 \times 3 \times 1730^2 \times 1.75}{2 \times \pi \times 50 \times 7.33^2} = 2800 \, \text{N-m}$$

$$\frac{M_{st}}{M_{em.r}} = \frac{2800}{2500} = 1.12$$

We perform the calculations for other values of the slip s in a similar way. These values can also be found graphically from a circle diagram. Figure 23-12*b* presents a circle diagram for a motor plotted according to the data given above. The values of the currents are in amperes and torques, in newton-metres for different slips of the motor.

23-2. Deep Bar Motor [184, 188, 195]

Principle of Operation. The deep bar motor, similar to the double squirrel-cage motor has better starting characteristics compared with the conventional squirrel-cage motor. The shape of the slots of a deep bar motor with one of the most widely used methods of connecting the bars to the short-circuiting end rings is shown in Fig. 23-13. Bars of other than rectangular cross section are also used, for instance trapezoidal and bottle-shaped (see Fig. 1-22). In further discussion only bars with a rectangular cross section will be considered, since they are the main ones and of the simplest shape with respect to design and manufacture.

In deep bar motors use is made of the skin effect in the rotor winding bars caused by the slot leakage fluxes.

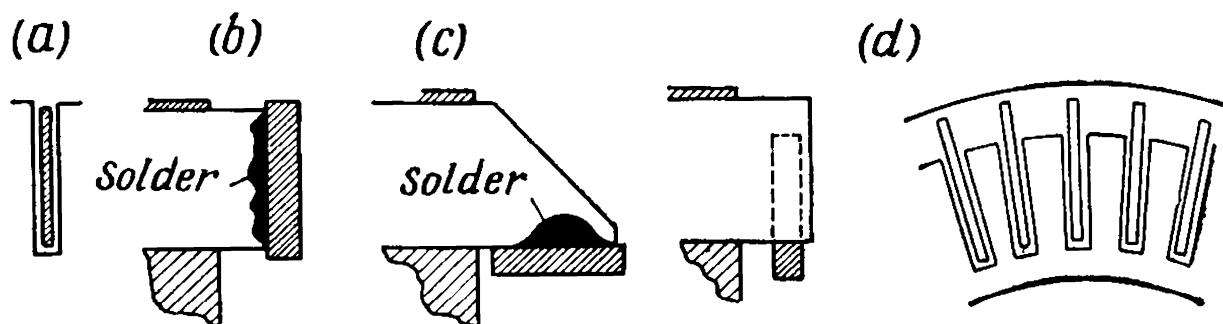


Fig. 23-13. Details of design of an induction motor deep bar rotor

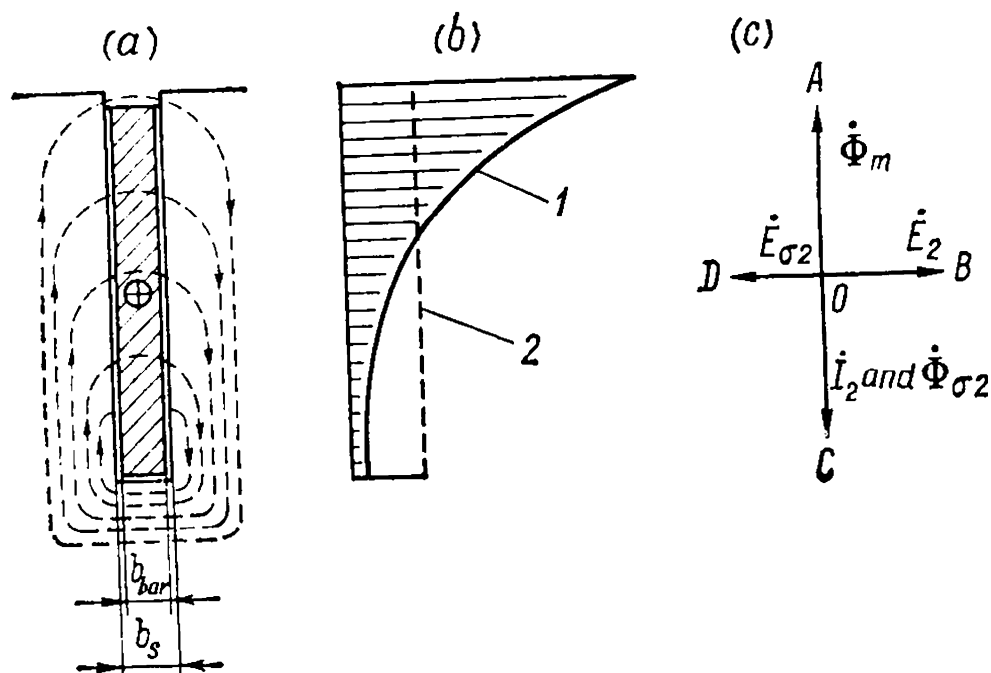


Fig. 23-14. Leakage flux in rotor slot of a deep bar motor and distribution of current density in rotor conductor

Let us first consider the phenomena at starting. At the initial moment $s=1$, and the frequency in the rotor is equal to the line frequency. The slot leakage flux paths of the rotor for these conditions are depicted in Fig. 23-14a. A glance at this figure shows that bar portions of different height are linked by different numbers of leakage flux lines; the lower parts, with the greatest number of lines, the upper parts, with the least number. For this reason the maximum leakage e.m.f.s are induced in the lower parts of the bar, the minimum e.m.f.s in the upper parts.

The action of the leakage e.m.f. will be found in the simplest way by means of the diagram in Fig. 23-14c when the resistance of the conductor is assumed to be equal to zero. Here the vector $\overline{OA} = \dot{\Phi}_m$ is the main flux of the motor, \overline{OB} is the main e.m.f. \dot{E}_2 produced by the flux $\dot{\Phi}_m$ in the rotor conductor and lagging on it by 90° . When $r_2=0$, the current in the conductor $\dot{I}_2 = \overline{OC}$ and, correspondingly, the leakage flux is in quadrature with the e.m.f. \dot{E}_2 ; $\dot{E}_{\sigma 2}$ being the leakage e.m.f. lagging behind the flux $\dot{\Phi}_{\sigma 2}$ by 90° .

It can be seen that the e.m.f. $\dot{E}_{\sigma 2}$ is directed opposite to the main e.m.f. \dot{E}_2 , but, according to the previous discussion, it is greater in the lower parts of the conductor than in its upper parts. Consequently, less current should flow through the lower parts than through the upper ones; in other words, the current is forced to the outside of the conductor (skin effect). Hence the current density is distributed along the conductor height as shown by curve 1 in Fig. 23-14b.

The skin effect takes place in all types of motors. With the usual conductor height of 10-12 mm, however, it is almost unnoticeable.

In deep bar motors, where the bars are 20-50 mm high, the effect is very strong and appreciably changes the rotor parameters.

To answer the question as to what direction the resistance and inductive reactance of the rotor change in, imagine the lower part of the conductor to be absent due to distribution of the current density (Fig. 23-15). Since the conductor cross section is reduced, on distribution of the current the resistance of the rotor rises. On the other hand, the centre of the lines of the slot leakage flux rises to the outside of the conductor and the leakage flux for a given current in the conductor decreases. Therefore, when the current is forced, the rotor inductive reactance decreases with respect to the reactance of a rotor with the same slot without current distribution, but it is of the same order as the rotor reactance of a conventional motor. A deep bar motor therefore has a relatively smaller current at a relatively higher starting torque, i.e., it has better starting characteristics than a conventional motor.

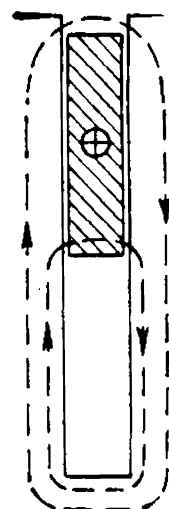


Fig. 23-15.
Explanation of
skin effect

As the motor accelerates, the frequency of the current in the rotor falls to values corresponding to steady-state operating conditions, i.e., to $f_2 = 1$ to 3 Hz. The skin effect gradually diminishes, and the current becomes more uniformly distributed over the conductor cross section (see dotted line 2 in Fig. 23-14b). The resistance of the rotor gradually decreases, and the inductive reactance related to the circuit frequency increases. At normal speed the deep bar motor is a conventional squirrel-cage motor with the usual resistance, but with a somewhat higher inductive reactance of the rotor, owing to which the power factor and the overload capacity of the motor are somewhat reduced.

Rotor Resistance and Inductive Reactance. The skin effect takes place practically only in that part of the conductor which lies in the slot, and is absent in the end connections of the winding. Therefore, the resistance r'_2 and inductive reactance x'_2 of the rotor winding can be expressed as follows:

$$r'_2 = k_{res} r'_{2s} + r'_{2end} \quad (23-15)$$

$$x'_2 = k_x x'_{2s} + x'_{2end} \quad (23-16)$$

Here r'_{2s} = resistance of the slot part of the rotor winding with uniform current distribution along the conductor cross section

k_{res} = factor allowing for the increase of the resistance r'_{2s} due to the skin effect

r'_{2end} = constant-value resistance of the rotor winding end connections

x'_{2s} and x'_{2end} = leakage inductive reactances of the slot and end connec-

tions of the rotor winding with uniform current distribution over the conductor cross section and with a frequency $f_2 = f_1$

k_x = factor allowing for the decrease of the inductive reactance x'_{2s} due to the skin effect.

Analysis of this complicated problem shows that

$$k_{res} = \xi \frac{\sinh 2\xi + \sin 2\xi}{\cosh 2\xi - \cos 2\xi} \quad (23-17)$$

$$k_x = \frac{3 \sinh 2\xi - \sin 2\xi}{2\xi \cosh 2\xi - \cos 2\xi} \quad (23-18)$$

where

$$\xi = h \sqrt{\pi \mu_0 \frac{b_{bar}}{b_s} \frac{f^2}{\rho}} \quad (23-19)$$

Here h = height of the bar
 b_{bar} and b_s = bar and slot widths, respectively
 f_2 = frequency of the current in the bar
 ρ = resistivity of the bar material.

This formula is written in the rationalized system of units.

By inserting in formula (23-19) the dimensions of all the quantities included in it, it will be seen that ξ is dimensionless. It is called the equivalent conductor height, since, for a given frequency f_2 and a given conductor material, the value of ξ is directly proportional to h .

In the SI system the linear dimensions are expressed in metres, $\mu_0 = 4\pi \times 10^{-7}$ H/m and ρ is measured in $\Omega \cdot m$. In practical calculations the lengths are expressed in centimetres, and ρ in $\Omega \cdot mm^2/m$ and then, if we insert, additionally, $f_2 = f_1 s = 50s$ Hz

$$\begin{aligned} \xi &= \frac{h}{100} \sqrt{\pi \times 4\pi \times 10^{-7} \frac{b_{bar}}{b_s} \frac{50s}{\rho \times 10^{-6}}} = \\ &= \frac{2\pi \sqrt{5}}{100} h \sqrt{\frac{b_{bar}}{b_s} \frac{s}{\rho}} = 0.14h \sqrt{\frac{b_{bar}}{b_s} \frac{s}{\rho}} \end{aligned}$$

If the conductor is of copper, then, at a temperature of about $50^\circ C$, we have $\rho = 0.02 \Omega \cdot mm^2/m$. Furthermore, the rotor winding of a deep bar motor has no insulation and its conductors may be tightly arranged in the slots; here $b_{bar} = b_s$. Thus, if h is measured in centimetres

$$\xi = h \sqrt{s}$$

that is, with $f = 50$ Hz and $s = 1$, the value of ξ is numerically equal to the copper conductor height in centimetres.

Knowing ξ , we can determine the factors k_{res} and k_x from equations (23-17) and (23-18).

For values of $\xi > 2$ we have $\sinh 2\xi \cong \cosh 2\xi$, where $\sinh 2\xi$ and $\cosh 2\xi$ are considerably greater than $\cos 2\xi$ and $\sin 2\xi$. Therefore, for $\xi > 2$

$$k_{res} = \xi \quad (23-20)$$

$$k_x \cong \frac{3}{2\xi} \quad (23-21)$$

These formulas greatly facilitate the determination of the rotor parameters of a deep bar motor and, consequently, facilitate the analysis of its operation at large slips and, particularly, at starting, since for these conditions we always have $\xi > 2$. As to operation at small slips—from no-load to $M = M_{max}$ —we may assume here that $k_{res} = k_x = 1$.

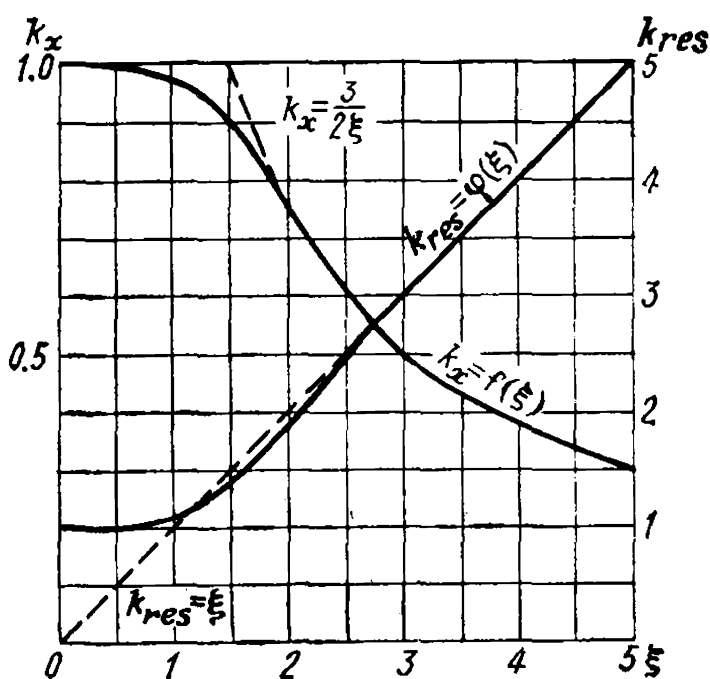


Fig. 23-16. Factors k_{res} and k_x versus ξ

Figure 23-16 shows curves of the functions $k_{res} = f(\xi)$ and $k_x = f(\xi)$ calculated by the exact formulas (23-17) and (23-18).

Equivalent Circuit. The equivalent circuit of a deep bar motor differs from that of a conventional motor only in that each of the secondary part parameters is the sum of a constant and a variable addends [see equations (23-15) and (23-16)]. Accordingly, the improved equivalent circuit with its magnetizing part brought out to the terminals has, for a deep bar motor, the form shown in Fig. 23-17, where

$$X_1 = x_1 \sigma_1; \quad X_s = x'_{2s} \sigma_1^2; \quad X_{end} = x'_{2end} \sigma_1^2$$

$$R_1 = r_1 \sigma_1; \quad R_s = r'_{2s} \sigma_1^2; \quad R_{end} = r'_{2end} \sigma_1^2$$

The motor shown by the equivalent circuit in Fig. 23-17 is a motor with variable parameters, since k_{res} and k_x are functions of the slip s .

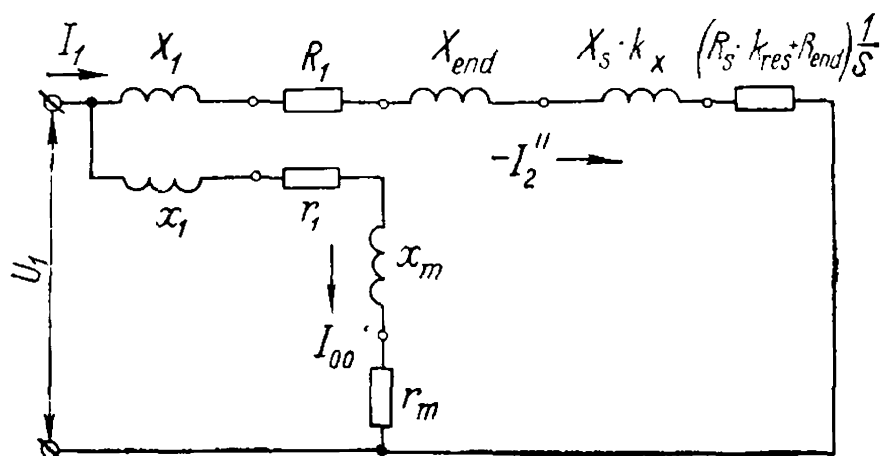


Fig. 23-17. Improved equivalent circuit for a deep bar motor

Example 23-3. Calculation of parameters of equivalent circuit of three-phase induction motor with deep-bar rotor.

The stator and the parameters of the magnetizing part are the same as for a conventional squirrel-cage motor (see Sec. 21-3).

The rotor data: number of rotor slots $N_2=80$, $q_2=4.44$. The shape of the slot is according to Fig. 5-3a: $h_1=40$ mm, $h_3=0.5$ mm, $h_4=0.8$ mm, $b_1=30$ mm, $b_2=1.5$ mm.

The leakage permeances for small slips are

$$\lambda_{s.bar} = \frac{1}{3} \times \frac{40}{3} + \frac{0.5 \times 2}{3 + 1.5} + \frac{0.8}{1.5} = 5.2 \text{ [formula (5-15a)]}$$

$$\lambda_{end.bar} = 1.14 \text{ [formula (18-25a)]}$$

the factor k_{dif2} is taken according to Fig. 18-7 with $\beta=1.0$ and $q_2=4.44$

$$\lambda_{dif.bar} = 1.7$$

The sum of the permeances for low slip conditions $s < 0.1$ is

$$\sum \lambda_{bar} = 5.2 + 1.14 + 1.7 = 8.04$$

The rotor inductive reactance referred to the stator primary winding is

$$x'_2 = 2\pi\mu_0 f l \sum \lambda_{bar} k = 2\pi \times 1.26 \times 10^{-8} \times 50 \times 33.4 \times 8.04 \times 5500 = 5.8 \Omega$$

With great slips ($s=1.0$), when the bar height $h_1=4$ cm

$$k_x = 0.38$$

$$\lambda'_{s.bar} = \frac{1}{3} \times \frac{40}{3} \times 0.38 + 0.22 + 0.53 = 2.44$$

$$\sum \lambda_{bar} = 2.44 + 1.14 + 1.7 = 5.28$$

$$x'_{2(s=1)} = 5.8 \times \frac{5.28}{8.04} = 3.8 \Omega$$

$$X_2 = x'_2 \sigma_1^2 = 3.8 \times 1.06 = 4.03 \Omega$$

The cross section of the rotor bar is selected equal to that of the bar of a conventional copper squirrel cage, with a diameter $d_{bar}=11.5$ mm

$$q_{bar} = \frac{\pi}{4} \times 11.5^2 = 103.5 \text{ mm}^2 = 2.6 \times 40 \text{ mm}^2$$

The length of a bar with a 30-mm overhang on each side is

$$l_{bar} = 364 + 2 \times 30 = 424 \text{ mm}$$

The radial ventilating channels are $6 \times 10 = 60$ mm.

With small slips

$$r_{bar} = \rho_{75^\circ} \frac{l_{bar}}{q_{bar}} = 0.0217 \times \frac{0.424}{103.5} = 8.9 \times 10^{-5} \Omega$$

The resistance of the sections of the end rings, adjoining to a bar at both sides of it with a ring diameter of 475 mm and a cross section of $12.5 \times 50 = 625 \text{ mm}^2$ is

$$l_{cage} = 2 \times \frac{\pi \times 475}{80} = 37.4 \text{ mm}$$

$$r_{cage} = 0.0217 \times \frac{0.0374}{625} = 13 \times 10^{-7} \Omega$$

The resistance of two sections of the ring reduced to the resistance of a bar, according to formula (18-24), is

$$r'_{cage} = \frac{13 \times 10^{-7}}{0.055} = 2.36 \times 10^{-5} \Omega$$

The total resistance of the secondary circuit referred to the stator primary circuit is

$$r'_2 = (r_{bar} + r'_{cage}) k = (8.9 + 2.36) 10^{-5} \times 5500 = 0.62 \Omega$$

With great slips ($s > 0.5$) the displacement of the current (skin effect) takes place in the slot portions of the bars. For example, the resistance growth factor with $h_{bar} = 4$ cm and $f_2 = 50$ Hz is equal to $k_{res} = 0.4$.

With a total length of 424 mm, there is 304 mm of it embedded in the steel, and 120 mm are outside the steel, as well as the short-circuiting rings. Therefore

$$r'_2 \left[8.9 \left(\frac{304 \times 4}{424} + \frac{120}{424} \right) + 2.36 \right] \times 10^{-5} \times 5500 = 1.68 \Omega$$

The parameters of the main part of the equivalent circuit with the no-load part brought out to the terminals in low slip conditions $s < 0.1$ (the operating conditions) are

$$R_1 = 0.7 \Omega; \quad R_2 = 0.62 \times 1.06 = 0.656 \Omega$$

$$X_1 = 2.86 \Omega; \quad X_2 = 5.8 \times 1.06 = 6.15 \Omega$$

$$R_{sh} = 0.7 + 0.656 = 1.356 \Omega$$

$$X_{sh} = 2.86 + 6.15 = 9.01 \Omega$$

$$Z_{sh} = \sqrt{1.356^2 + 9.01^2} = 9.15 \Omega$$

$$\cos \varphi_{sh}'' = \frac{1.356}{9.15} = 0.148$$

$$I_{sh}'' = \frac{1730}{9.15} = 189 \text{ A}$$

$$\frac{I_{sh1}}{I_r} = \frac{I_{sh}'' \sigma_1}{I_r} = \frac{189 \times 1.03}{60} = 3.15$$

Current Diagrams. At low slips corresponding to a change in s from no-load to the maximum torque, we have $k_{res} \cong k_x \cong 1.0$, and, therefore, for the normal load region the equivalent circuit of Fig. 23-17, when simplified, becomes an equivalent circuit of a conventional induction motor with constant parameters. The operation circle diagram C_{eq} corresponding to this operating range is shown in Fig. 23-18a, where the point B conditionally corresponds to the slip $s = \pm \infty$.

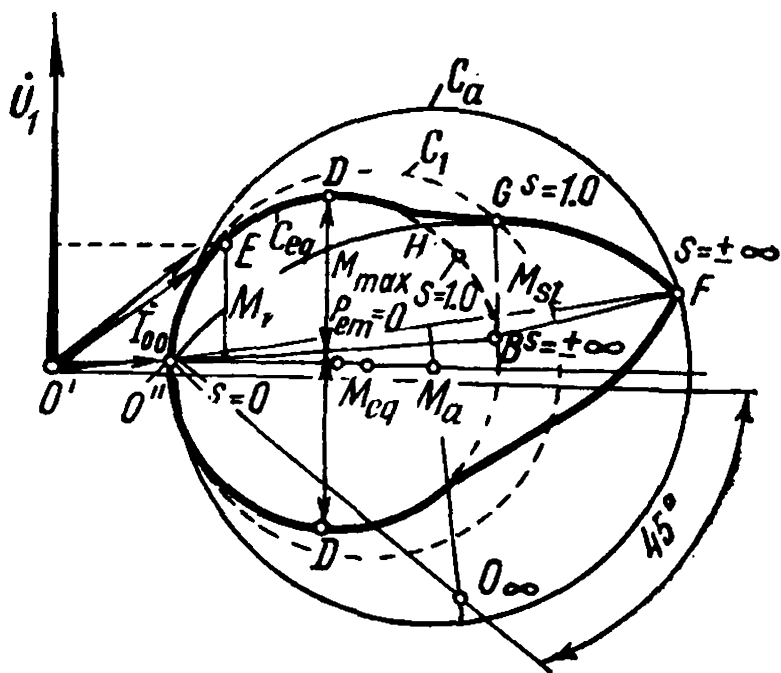


Fig. 23-18a. Current diagram for a deep bar motor

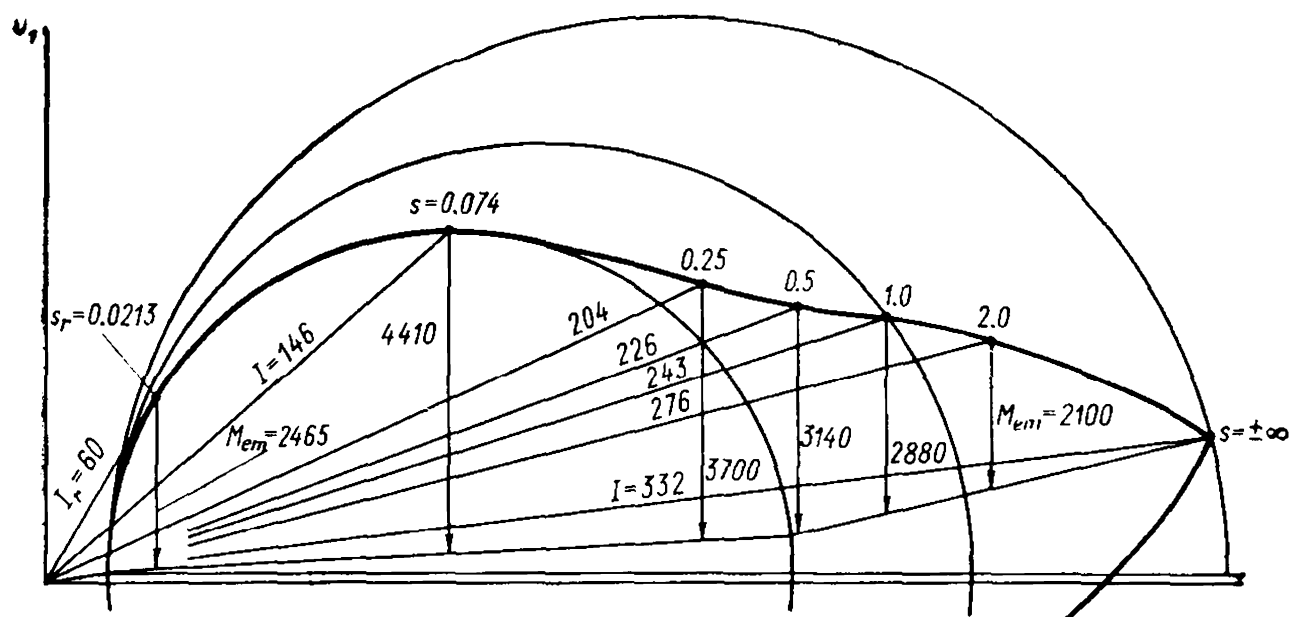


Fig. 23-18b. Circle diagram of deep bar motor (according to data given in example 23-4) and of the torque and current values at various slips

At a slip $s = \pm\infty$ the actual position of the end of the current vector is on circle C_a corresponding to the operating conditions of the machine as an induction motor with constant secondary circuit parameters $x_2 \approx x_{2end}$ and $r_2 \approx r_{2end} + k_{res}r_{2s}$.

At high slips ($s > s_m$) a deep bar motor represents an induction machine with variable parameters. It is as if each slip has its own circle diagram, therefore, for the point of greatest interest for us with a slip $s = 1.0$ we obtain the conditional circle diagram C_1 depicted in Fig. 23-18a by a dotted line.

If we connect point D corresponding to the maximum torque M_{max} with point G for $s = 1.0$ and point F for $s = \pm\infty$ by a smooth curve, we obtain the curve which is described by the current vector end with a change in s . In the same way the other half of the curve, which corresponds to generator performance of the machine, can be drawn. If we connect point O'' with point B by a straight line we obtain the line of electromagnetic power $P_{em} = 0$ for the current circle C_{eq} .

The electromagnetic power line for the current curve on the section DGF will pass somewhat higher than point B and, on the right-hand end part of it, will coincide with the straight line connecting points B and F .

After drawing the line $P_{em} = 0$, we find the values of the maximum torque M_{max} and the starting torque M_{st} in the usual manner.

Having constructed the operation circle C_{eq} and found on it the conditional point H with a slip $s = 1.0$, and point B with the conditional slip $s = \pm\infty$, the scales of slip s and efficiency η for determining the operating conditions of the machine are plotted in the same way as for the conventional induction motor.

Example 23-4. Calculation of currents, powers and torques of a three-phase deep bar induction motor.

The total mechanical power is

$$P_{mech} = P_2 + p_{mech} + p_{add} = 250 + 2.0 + 1.4 = 253.4 \text{ kW}$$

The reduced current of the main part of the circuit, owing to the lower $\cos \varphi$, as in a motor with a double squirrel cage, is taken equal to $I_2'' = 53 \text{ A}$.

Here we find:

$$p_{cop2} = 3I_2''^2 R_2 = 3 \times 53^2 \times 0.656 \times 10^{-3} = 5.52 \text{ kW}$$

$$P_{em} = P_{mech} + p_{cop2} = 253.4 + 5.52 = 258.92 \text{ kW}$$

$$s_r = \frac{p_{cop2}}{P_{em}} = \frac{5.52}{258.92} = 0.0213$$

$$\frac{R_2}{s_r} = \frac{0.656}{0.0213} = 30.8 \Omega$$

$$\cos \psi_2 = \frac{R_1 + \frac{R_2}{s_r}}{\sqrt{\left(R_1 + \frac{R_2}{s_r}\right)^2 + X_{s1}^2}} = \frac{0.7 + 30.8}{\sqrt{(0.7 + 30.8)^2 + 9.01^2}} = 0.965$$

$$P_{em.r} = \frac{3U_{1ph}^2 \frac{R_2}{s_r}}{\left(R_1 + \frac{R_2}{s_r}\right)^2 + X_{sh}^2} = \frac{3 \times 1730^2 \times 30.8 \times 10^{-3}}{(0.7 + 30.8)^2 + 9.01^2} = 259 \text{ kW}$$

$$M_{em.r} = \frac{P_{em.r}}{2\pi \cdot n} = \frac{259 \times 10^3}{2\pi \times \frac{1000}{60}} = 2470 \text{ N}\cdot\text{m}$$

according to formula (20-32)

$$M_m = \frac{3 \times 3 \times 1730^2}{2 \times 2\pi \times 50(0.7 + \sqrt{0.7^2 + 9.01^2})} = 4410 \text{ N}\cdot\text{m}$$

$$\frac{M_m}{M_{em.r}} = \frac{4410}{2470} = 1.78$$

$$\begin{aligned} \Sigma_p &= (p_{mech} + p_{add}) + 3I_2''^2 R_{sh} + p_0 = 3.4 + 3 \times 53^2 \times 1.356 \times 10^{-3} + \\ &+ 11.68 = 26.6 \text{ kW} \end{aligned}$$

$$\eta = \left(1 - \frac{26.6}{250 + 26.6}\right) 100 = 90.35\%$$

TABLE 23-2

$M_{em}/M_{em,r}$														
I_1/I_r														
Squirrel-cage motor			Double squirrel-cage motor		Deep-bar motor									
s	I_1, A	I_1/I_r	s	I_1, A	I_1/I_r	Squirrel-cage motor		Double squirrel-cage motor		Deep-bar motor				
						$M, N\cdot m$	M/M_r	s	$M, N\cdot m$	M/M_r	s	$M, N\cdot m$	M/M_r	
0.0249	60	1	0.022	60	1.0	0.0249	2490	1.0	0.022	2500	1.0	0.0213	2465	1
0.075	210	3.5	0.085	164	2.73	0.075	6530	2.62	0.085	4950	1.98	0.075	4410	1.78
0.25	262	4.37	0.25	207	3.45	0.25	5580	2.24	0.25	3700	1.48	0.25	3700	1.5
0.5	291	4.85	0.5	228	3.8	0.5	3540	1.42	0.5	3380	1.35	0.5	3140	1.27
1.0	304	5.06	1.0	244	4.06	1.0	1900	0.763	1.0	2800	1.12	1.0	2880	1.16
2.0	308	5.13	2.0	280	4.67	2.0	995	0.4	2.0	2565	1.02	2.0	2100	0.85
∞	312	5.2	∞	310	5.16	∞	0	0	∞	0	0	∞	0	0

Starting conditions with $s = 1.0$; $k_{res} = 4$; $k_x = 0.38$:

$R_1 = 0.7 \Omega$; $R_2 = 1.78 \Omega$

$X_1 = 2.86 \Omega$; $X_2 = 4.03 \Omega$

$R_{sh} = 0.7 + 1.78 = 2.48 \Omega$,

$X_{sh} = 2.86 + 4.03 = 6.89 \Omega$

$Z_{sh} = \sqrt{2.48^2 + 6.89^2} = 7.31 \Omega$

$\cos \varphi_{sh} = \frac{2.48}{7.31} = 0.339$

$I''_{sh} = \frac{1730}{7.31} = 236 \text{ A};$

$\frac{I'_{sh}}{I_r} = \frac{I''_{sh}\sigma_1}{I_r} = \frac{236 \times 1.03}{60} = 4.05$

$M_{st} = \frac{3 \times 1730^2 \times 1.78}{100 \times \frac{\pi}{3} \times 53.2} = 2880 \text{ N}\cdot\text{m}$

$M_{em,r} = \frac{253.4 \times 10^3}{2\pi \times \frac{979.4}{60}} = 2465 \text{ N}\cdot\text{m}$

$\frac{M_{st}}{M_{em,r}} = \frac{2880}{2465} = 1.16$

The other values of the slip can be calculated in a similar way. The values can also be found graphically by means of a circle diagram. Figure 23-18*b* shows a circle diagram for deep bar induction motor, plotted according to the data given above. The currents in the circle diagram are in amperes and the torques in newton-metres for different values of the slip.

23-3. Comparison of Double Squirrel-Cage and Deep Bar Motors

Table 23-2 compares the torques $\frac{M}{M_r}$ and the primary currents $\frac{I_1}{I_r}$ for various slips of a conventional squirrel-cage motor (SC), a deep bar motor (DB) and a double squirrel-cage motor (DC) calculated in the previous examples and having the same overall dimensions and speed.

When a double squirrel-cage motor is started, only the upper winding functions, as a rule. To avoid excessive overheating of this winding, its cross section should be increased and the winding made of a high-resistivity material. With a deep bar motor only the top part of the rotor conductor carries the current at starting, but, since the heat conductivity of copper is high, the whole conductor warms up; therefore, when the cage is made of copper, the average starting current density is not excessive. As a result, a double squirrel-cage motor utilizes the rotor copper to a smaller degree and such a motor is more costly than a deep bar motor.

The possibility of a wide choice of double squirrel-cage motor starting characteristics by properly selecting the resistances r_{st} , r_{op} and the reactance x_{op} , x_{st} is its appreciable advantage. In a double squirrel-cage motor any position of the short-circuit point within the area of the circle diagram C_a of a normal motor (Fig. 23-9) can be obtained, i.e., the motor can be designed for any desired starting torque and different starting current ratios, retaining the operation circle C_{eq} and its characteristics invariable. In a deep bar motor these possibilities are more limited, since the short-circuit point can be displaced only along the conditional circle C_1 (Fig. 23-18).

In contrast to a deep bar motor, its double squirrel cage counterpart makes possible a very great rise in starting torque (to 2.5-3 times the rated value) with a certain decrease in the diameter of the operation circle C_{eq} , owing to which the characteristic of the motor begins to approach that of a series d.c. motor. Figure 23-19 combines the characteristics of the torque and the starting current for an ordinary squirrel-cage motor, a double squirrel-cage motor with a very high value of the starting torque and a deep bar motor as a function of the slip s . These properties of double squirrel-cage motors permit us to use them in a number of special cases, where such mechanical characteristics are required, for example, in cranes, elevators, winches, and centrifuges.

To construct the operation circles C_{ed} of double squirrel-cage and deep bar motors from no-load and short-circuit tests and to avoid the influence of the skin effect, B. Kuznetsov [204] proposed to perform the latter test at a frequency of $f_r=5$ to 10 Hz. To plot point H (Fig. 23-18) of the conditional short circuit corresponding to the operation circle, it is necessary to recalculate the short-circuit inductive reactance X_{sh} for the rated frequency f_1 :

$$X_{sh} = \frac{f_1}{f_r} X_{sh \cdot r}$$

After finding point H , the operation circle is constructed in the usual way.

The short-circuit test carried out at the rated frequency f_1 permits the true short-circuit point (Fig. 23-18) of the current diagram to be found.

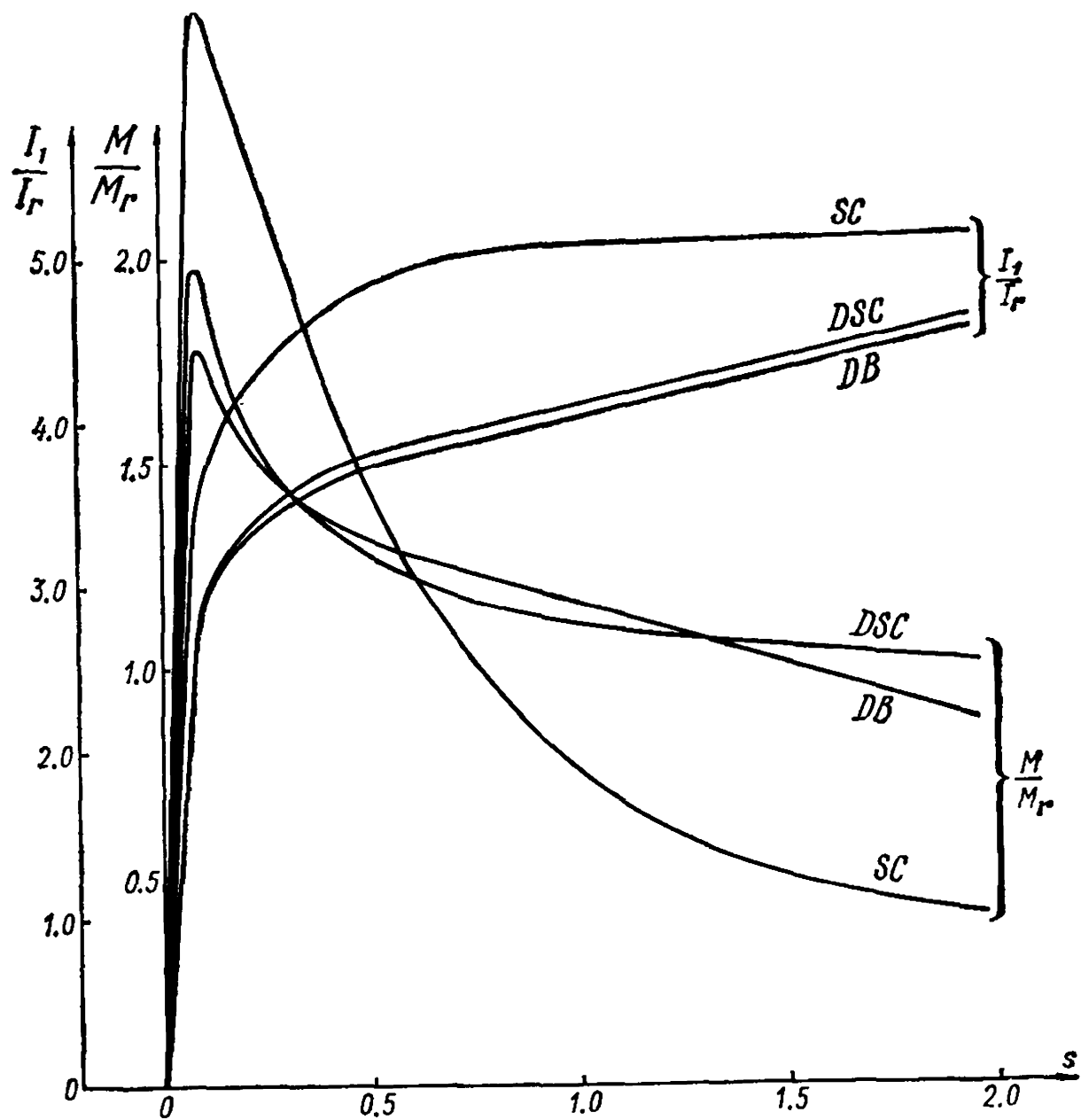


Fig. 23-19. Torque and current versus slip for double squirrel-cage motor (DSC), deep bar (DB) and ordinary squirrel-cage motor (SC)

23-4. Calculation of Starting Characteristics of a Salient-Pole Synchronous Motor with a Damper System

In asynchronous starting of a synchronous motor with a damper system, the motor is similar to an induction machine, but has its specific features. Let us consider these features by calculating for various slips the starting characteristics of a 225-kW, six-pole ($2p=6$) three-phase salient-pole synchronous motor having a powerful damper system of brass bars with copper short-circuiting rings. The main parameters of the motor were determined in Example 13-1.

The ohmic-resistance of one brass bar of the damper winding with six bars per pole, each $l_{bar}=480$ mm long, with a diameter of $d_{bar}=14$ mm, together with two adjacent sections of a short-circuiting

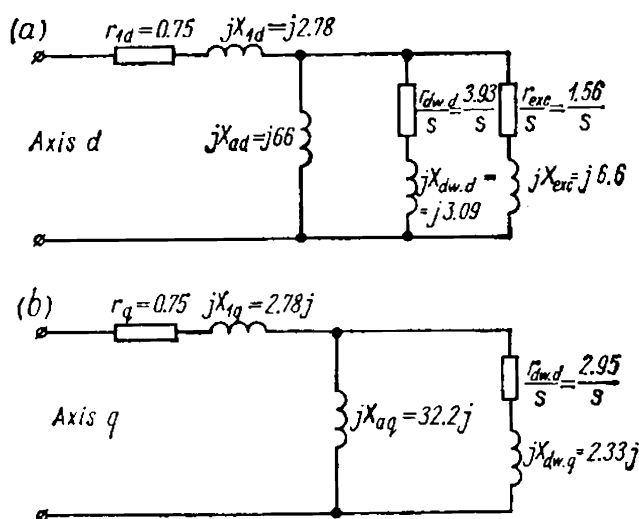


Fig. 23-20. Equivalent circuits of synchronous motor:
a—along direct axis;
b—along quadrature axis

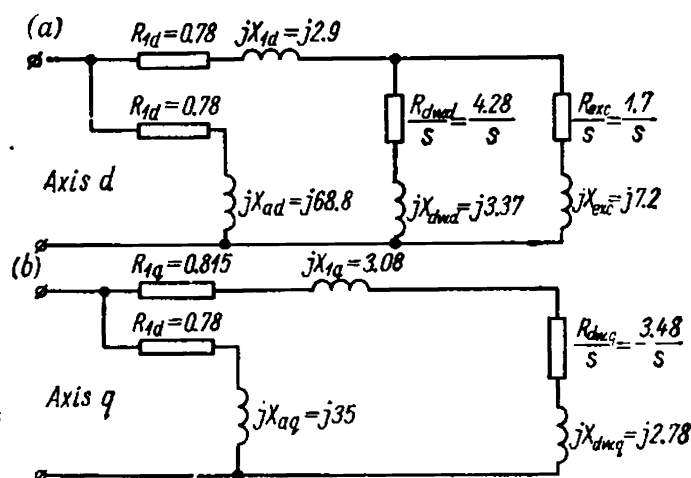


Fig. 23-21. Equivalent circuits of a synchronous motor with the magnetizing parts brought out to the terminals:
a—along direct axis; b—along quadrature axis

copper ring with a diameter $D_{ring} = 505$ mm and a cross section $q_{ring} = 14 \times 20 = 280$ mm², is

$$r_{dw.d} = r_{bar} + 2r_{ring} = \rho_{a.br75^\circ} \frac{l_{bar}}{q_{bar}} + 2\rho_{cop75^\circ} \frac{l_{ring}}{q_{ring} 2 \sin^2 \frac{\pi p}{Z_2}} =$$

$$= 0.087 \times \frac{0.48}{153} + 2 \times 0.0217 \times \frac{0.041}{280} \times 7.42 = 0.000273 +$$

$$+ 0.0000505 = 0.000324 \Omega$$

The ohmic resistance of the damper winding, referred to the stator system, according to formula (18-23), is equal to:

$$r'_{dw.d} = r_{dw.d} \frac{4m(\omega_1 k_{w1}^2)^2}{Z_2} = 0.000324 \times \frac{4 \times 3 \times 36500}{36} = 3.93 \Omega$$

$$r'_{dw.q} \cong 0.75 r'_{dw.d} = 0.75 \times 3.93 = 2.95 \Omega$$

$$\underline{r}_{dw.d} = \frac{3.93}{29.1} = 0.132, \quad \underline{r}_{dw.q} = \frac{2.95}{29.1} = 0.102$$

The complete equivalent circuits of a salient-pole synchronous motor for the direct (d) and quadrature (q) axes are given in Fig. 23-20.

The complete equivalent circuits can be transformed into equivalent circuits with the magnetizing parts brought out to the terminals along both axes d and q .

The parameters for the equivalent circuits with the magnetizing parts brought out to the terminals (Fig. 23-21) will have the following

values:

$$\begin{aligned}
 \sigma_{1d} &= 1 + \frac{2.78}{66} = 1.042; & \sigma_{1q} &= 1 + \frac{2.78}{32.2} = 1.086 \\
 \sigma_{1d}^2 &= 1.042^2 = 1.09; & \sigma_{1q}^2 &= 1.086^2 = 1.18 \\
 jX_{ad} &= j(2.78 + 66) = j68.8; & jX_{aq} &= j(2.78 + 32.2) = j35 \\
 R_{1d} &= 0.75 \times 1.042 = 0.78; & R_{1q} &= 0.75 \times 1.086 = 0.815 \\
 jX_{1d} &= j2.78 \times 1.042 = j2.9; & jX_{1q} &= j2.78 \times 1.086 = j3.08 \\
 jX_{dw.d} &= j3.09 \times 1.09 = j3.37 \\
 R_{dw.q} &= 2.95 \times 1.18 = 3.48; & R_{exc} &= 1.56 \times 1.09 = 1.7 \\
 jX_{dw.q} &= j2.33 \times 1.18 = j2.78; & jX_{exc} &= 7.2 \\
 R_1 &= \frac{R_{1d} + R_{1q}}{2} = \frac{0.78 + 0.815}{2} = 0.8; & R_{dw.d} &= 3.93 \times 1.09 = 4.28
 \end{aligned}$$

The parameters of the main parts of the equivalent circuits along the d and q axes with the magnetizing part brought out to the terminals have the following values:

$$\begin{aligned}
 \dot{Z}_d &= \dot{Z}_{1d} + \dot{Z}_{2d} = (R_{1d} + jX_{1d}) + \frac{\left(\frac{R_{dw.d}}{s} + jX_{dw.d}\right) \left(\frac{R_{exc}}{s} + jX_{exc}\right)}{\left(\frac{R_{dw.d}}{s} + jX_{dw.d}\right) \left(\frac{R_{exc}}{s} + jX_{exc}\right)} \\
 \dot{Z}_q &= \dot{Z}_{1q} + \dot{Z}_{2q} = (R_{1q} + jX_{1q}) + \left(\frac{R_{dw.q}}{s} + jX_{dw.q}\right)
 \end{aligned}$$

The equivalent total resistance of the branch part of the circuit with the magnetizing part brought out to the terminals will be

$$\begin{aligned}
 \dot{Z}_{2d} &= \frac{\frac{1}{s} R_{dw.d} R_{exc} (R_{dw.d} + R_{exc}) + (R_{dw.d} X_{exc}^2 + R_{exc} X_{dw.d}^2) s}{(R_{dw.d} + R_{exc})^2 + (X_{dw.d} + X_{exc})^2 s^2} + \\
 &+ j \frac{R_{dw.d}^2 X_{exc} + R_{exc}^2 X_{dw.d} + (X_{dw.d} X_{exc}) (X_{dw.d} + X_{exc}) s^2}{(R_{dw.d} + R_{exc})^2 + (X_{dw.d} + X_{exc})^2 s^2}
 \end{aligned}$$

The currents in the main part along the axes d and q determined by the expressions:

$$\dot{I}_d = \frac{\dot{U}}{2} \frac{1}{\dot{Z}_d}; \quad \dot{I}_q = \frac{\dot{U}}{2} \frac{1}{\dot{Z}_q}$$

With slips other than $s=0.5$, the positive-sequence current is proportional to the half-sum of the currents along the axes d and q :

$$\dot{I}_1 = \frac{1}{2} (\dot{I}_d + \dot{I}_q) = \frac{U}{2} \left(\frac{1}{\dot{Z}_d} + \frac{1}{\dot{Z}_q} \right) = I_a + jI_r$$

The negative-sequence current is proportional to half the difference of the currents along the axes d and q :

$$i_2 = \frac{1}{2} (i_d - i_q) = \frac{\dot{U}}{2} \left(\frac{1}{\dot{Z}_d} - \frac{1}{\dot{Z}_q} \right) = I_a - jI_r$$

At a slip exactly equal to $s=0.5$ the positive-sequence current is inversely proportional to the half-sum of the impedances \dot{Z}_d and \dot{Z}_q [73]:

$$i_{1(s=0.5)} = \dot{U} \left(\frac{2}{\dot{Z}_d + \dot{Z}_q} \right) = I_a + jI_r$$

The resultant main torque is proportional to the active component of the positive-sequence current I_a less the losses due to the resultant positive-sequence current I_a in the primary resistance R_1 . To take into account the losses due to the negative-sequence currents in the primary resistance the latter is multiplied by $(1-2s)$; therefore for slips $1 < s < 0.5$ these losses are added to the positive-sequence losses, and for $0.5 < s < 0$ these losses are subtracted from the positive-sequence losses.

Thus, the resultant starting torque of a synchronous motor is proportional to

$$M_{st} \equiv P_{st} = 3U_{ph}I_a - 3I_1^2r_1 - 3I_2^2r_1(1-2s)$$

The resultant positive-sequence current along the d -axis of the main and branch parts of the equivalent circuit is equal to:

$$I = \sqrt{I_a^2 + \left(I_r + \frac{U}{x_{ad}} \right)^2}$$

These formulas make it possible to calculate the torques and currents for different slips.

For a slip $s=1.0$, and $1-2s=-1$:

$$\begin{aligned} \dot{Z}_{2d} &= \frac{4.28 \times 1.7 (4.28 + 1.7) + 4.28 \times 7.2^2 + 1.7 \times 3.37^2}{(4.28 + 1.7)^2 + (3.37 + 7.2)^2} + \\ &\quad + j \frac{4.28^2 \times 7.2 + 1.7^2 \times 3.37 + 3.37 \times 7.2 \times (3.37 + 7.2)}{(4.28 + 1.7)^2 + (3.37 + 7.2)^2} = \\ &= \frac{43.5 + 222 + 19.2}{35.7 + 111.5} + j \frac{132 + 9.75 + 2.56}{35.7 + 111.5} = 1.8 + j2.52 \\ \dot{Z}_d &= (0.78 + j2.9) + (1.8 + j2.52) = 2.58 + j5.42 \\ \dot{Z}_q &= (0.815 + j3.02) + (3.48 + j2.78) = 4.3 + j5.8 \\ i_1 &= \frac{\dot{U}}{2} \left(\frac{1}{\dot{Z}_d} + \frac{1}{\dot{Z}_q} \right) = \frac{1730}{2} \left(\frac{1}{2.58 + j5.42} + \frac{1}{4.3 + j5.8} \right) = 134 - j225 \\ I_1 &= \sqrt{134^2 + 225^2} = 262 \text{ A} \\ i_2 &= \frac{\dot{U}}{2} \left(\frac{1}{\dot{Z}_d} - \frac{1}{\dot{Z}_q} \right) = \frac{1730}{2} \left(\frac{-17 - j74}{1890} \right) = -7.7 - j34 \\ I_2 &= \sqrt{7.7^2 + 34^2} = 34.8 \text{ A} \\ P_{st} &= (3 \times 1730 \times 134 - 3 \times 262^2 \times 0.78 + 3 \times 34^2 \times 0.78) \times 10^{-3} = \\ &= 695 - 163 + 2.84 = 534.9 \text{ kW} \end{aligned}$$

The starting torque ratio

$$k_{st. M} = \frac{M_{st}}{M_r} = \frac{P_{st}}{P_r} = \frac{534.9}{225} = 2.37$$

The starting phase current is

$$I_{st} = \sqrt{134^2 + \left(225 + \frac{1730}{68.8}\right)^2} = \sqrt{134^2 + (225 + 25.2)^2} = 300 \text{ A}$$

The starting current ratio is

$$k_{st. i} = \frac{300}{59.5} = 5.05$$

$$\cos \varphi = \frac{I_a}{I_{st}} = \frac{134}{300} = 0.446$$

The parameters are calculated in a similar manner for other values of the slip.

The data obtained for the starting conditions of a synchronous motor for various slips are given in Table 23-3.

TABLE 23-3

s	I_{st}, A	I_2, A	P_{st}, kW	$k_{st. M}$	$k_{st. i}$	$\cos \varphi$
1.0	300	34.8	534.9	2.37	5.05	0.446
0.5	203	0	654.0	2.90	4.00	0.615
0.25	137	42.2	528.1	2.34	2.57	0.720
0.1	82	35.6	384.7	1.71	1.60	0.805
0.06	53.2	36.8	258.4	1.15	1.08	0.890

Chapter

24

SPEED CONTROL OF THREE-PHASE INDUCTION MOTORS

24-1. Methods of Speed Control

The problem of speed control of electrical motors in general and of induction motors in particular is of great practical importance.

In a number of industries motors must satisfy very strict speed characteristic requirements, both with respect to the range and smoothness of control and also with respect to economical operation. From the viewpoint of speed-control characteristics, induction motors are inferior to d.c. motors, the greater, the wider the range of control.

Many investigations have been carried out to find means of improving the speed-control characteristics of induction motors, but as yet they have not superseded d.c. motors in fields where the requirements of motor speed control are exacting.

Methods of speed control are distinguished according to the main action on the motor: (1) from the stator side, and (2) from the rotor side.

The following methods of speed control from the stator side are used:

- (a) changing of the applied voltage;
- (b) changing of the number of pole pairs;
- (c) changing of the power circuit frequency.

From the rotor side the speed may be controlled:

- (a) by changing the resistance in the rotor circuit;
- (b) by introducing into the rotor circuit an additional e.m.f. of the same frequency as the fundamental e.m.f. of the rotor.

For the latter method of speed control an additional electrical machine or several such machines are required. A set consisting of a regulated induction motor and one or more additional electrical machines connected to it electrically or mechanically is called a cascade. Commutator machines are commonly used as the additional machines. Therefore, cascades, with the exception of cascades of two induction motors without commutators, will be considered in Chapter 31.

The speed control of induction motors by changing the primary voltage is of secondary importance, since it does not allow control to be accomplished within wide limits and is not economical. Therefore, this method of speed control is employed only for induction motors of very low power in special installations where economical performance is not important.

The influence of voltage variation on motor speed is discussed in Chapter 26.

Various special motor designs have been suggested to improve speed control, as, for instance, a design with a double rotor.

24-2. Changing the Number of Poles

The synchronous speed is determined from the relation

$$n_1 = \frac{f_1}{p} \quad (24-1)$$

If the frequency f_1 is given, then, with a change in p , the synchronous speed n_1 and, consequently, the speed of the motor n also change. But here the speed is controlled not continuously, but in steps, very frequently in two steps with a speed ratio 2 : 1. Such motors are called double-speed motors.

At present two-, three- and four-speed motors are produced in the USSR.

The number of pole pairs in the stator can be changed as follows:

(a) by placing one winding on the stator and changing the number of poles by correspondingly reconnecting its parts;

(b) by placing two independent windings on the stator;

(c) by providing two independent stator windings, each with reconnection of the poles.

Double-speed motors are usually made with one winding on the stator, the number of poles being changed in the ratio 1 : 2. Three- and four-speed motors are provided with two windings on the stator, one or both of which are made with changing of the number of poles. For example, if it is desired to obtain a motor for four synchronous speeds: 1500, 1000, 750 and 500 rpm, two windings should be placed on the stator, one of which gives $p=2$ and $p=4$ pole pairs, the other $p=3$ and $p=6$.

If the motor has a phase-wound rotor, the number of pole pairs must be changed simultaneously on the stator and rotor. This complicates the design of the rotor. Therefore, motors with changing of the number of poles usually have a short-circuited rotor with a squirrel-cage winding. Such a rotor can operate without any reconnections with any number of stator poles. We shall consider only motors of this type below.

There exist several methods of switching over the pole pairs of a winding. The one most frequently used is the method of changing the direction of the current in the separate halves of each phase winding or, shorter, in the half-windings. Schematic diagrams of the half-winding commutation for changing the number of poles in the ratio of 2 : 1 are given in Fig. 24-1a, b and c. The diagrams in Fig. 24-1a and b are called series commutations and in Fig. 24-1c—parallel

commutation. The phase windings may also be commutated from star to delta and vice versa. Thus, when the number of poles is changed, in the general case, all the characteristics of the winding change and, correspondingly, also the gap flux density.

As is known,

$$E = \pi \sqrt{2} f \omega k_w \Phi_m$$

If the flux density is sinusoidally distributed in the gap, then

$$\Phi_m = \frac{2}{\pi} B_m \tau l = B_m \frac{D}{p} l$$

where B_m = maximum flux density in the air gap

D = diameter of the stator bore

p = number of pole pairs.

Let us designate quantities corresponding to the smaller number of poles by the subscript 1, and to a double number of poles by the subscript II. Then, omitting the subscript m of the

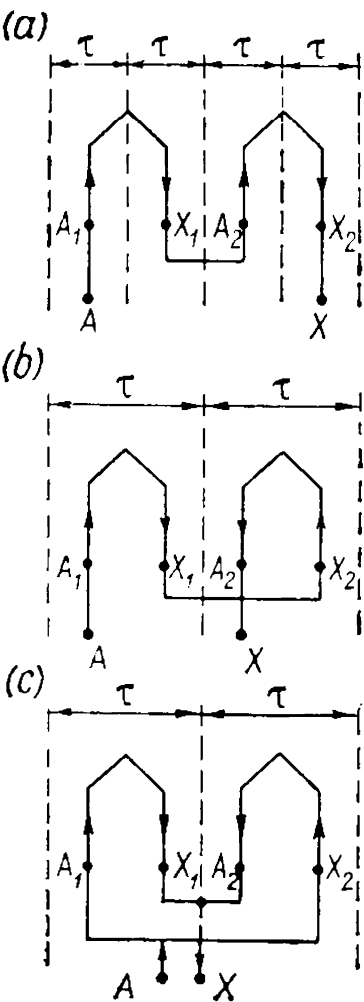


Fig. 24-1. Schematic diagrams of pole number changing

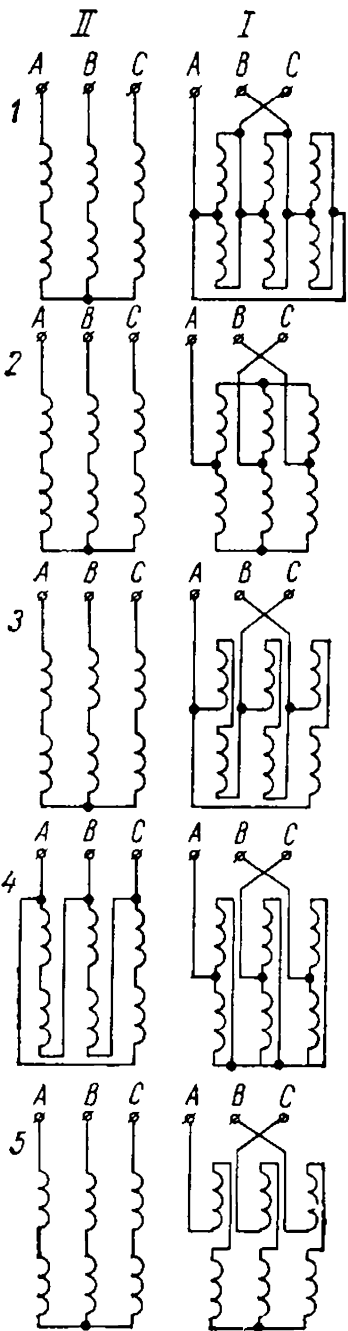


Fig. 24-2. Changing number of poles

flux density, we get

$$\frac{E_1}{E_{11}} = \frac{\omega_1 k_{w1} B_1 \rho_{11}}{\omega_{11} k_{w11} B_{11} \rho_1} \quad (24-2)$$

In equations (24-2) and (24-3), ω is the number of turns of one parallel branch of the phase. With an invariable voltage U_1 across the terminals, if we neglect the voltage drop in the winding, $E = \frac{U_1}{\sqrt{3}}$ for a star connection and $E = U_1$ for a delta connection.

By varying the methods of half-winding and phase-winding connection, the ratios $\frac{B_{11}}{B_1}$ can be changed over a rather wide range. Figure 24-2 shows five commonly used commutation diagrams for stator windings. When changing-over from a large number of poles to a smaller one it is necessary to switch-over the leads of the phase windings, so as to retain the previous direction of rotation of the motor. The ratios of $\frac{B_{11}}{B_1}$ obtained with the winding connections shown in Fig. 24-2 are given in Table 24-1. For simplicity we assume $k_{w1} = k_{w11}$.

The ratio $\frac{B_{11}}{B_1}$ is closely related to the ratio of the torques $\frac{M_{11}}{M_1}$ developed by a motor with a double and single number of pole pairs. Indeed, the torque can be expressed by the formula

$$M = \frac{1}{\sqrt{2}} m_1 \omega k_w p \Phi_m I'_2 \cos \psi_2 \quad (24-3)$$

which can be obtained from relations (20-18) and (20-24), if we insert

$$I'_2 \frac{r_2}{s} = E'_2 = E_1 = \sqrt{2} \pi f \omega k_w \Phi_m$$

and take into account equation (24-1). Assuming as before that $k_{w1} = k_{w11}$ and neglecting the difference between $\cos \psi_{211}$ and $\cos \psi_{21}$, we get

$$\frac{M_{11}}{M_1} = \frac{\omega_{11} I'_{211} \rho_{11} \Phi_{11}}{\omega_1 I'_{21} \rho_1 \Phi_1}$$

But

$$\rho_{11} \Phi_{11} = \rho_{11} B_{11} \frac{D}{\rho_{11}} l = B_{11} D l$$

and

$$\rho_1 \Phi_1 = B_1 D l$$

Besides, it can be assumed that

$$\omega_{11} I'_{211} \cong \omega_1 I'_{21}$$

Indeed, since the number of stator phases and the diameter of its bore do not depend on the number of poles, each of the products $\omega_{11} I'_{211}$

TABLE 24-1

Diagram No.	Double number of poles ($2 \times 2p$). Subscript II, Fig. 24-2		Single number of poles ($2p$). Subscript I, Fig. 24-2		Ratio $\frac{B_{II}}{B_I}$
	Half-winding connection	Phase connection	Half-winding connection	Phase connection	
1	Series	Y	Parallel	Δ	0.58
2	Series	Y or Δ	Parallel	YY or Δ	1.00
3	Series or parallel	Y	As with double number of poles	Δ	1.16
4	Series	Δ	Parallel	YY	1.73
5	Series or parallel	Y or Δ	As with double number of poles	Y or Δ	2

and $\omega_1 I'_{21}$ is approximately proportional to the line load, which may be assumed to have a given value in connection with the permissible heating of the motor. Thus, for maximum loads from the viewpoint of heating

$$\frac{M_{II}}{M_I} \approx \frac{B_{II}}{B_I} \quad (24-4)$$

The braking torque of a driven machine often does not depend on speed. The driving motor must develop identical torques at both speeds, i.e., $M_{II} = M_I$. Such a motor is referred to as a constant-torque motor. According to equation (24-4), here we must have $B_{II} = B_I$. From Table 24-1 it can be seen that diagrams 2 and 3 suit this purpose.

If a pole-changing motor is built as a constant-power motor, then $\frac{M_{II}}{M_I} = \frac{B_{II}}{B_I} = 2$. Diagrams 4 and 5 of Table 24-1 suit this purpose.

Diagram 1, on the contrary, corresponds to the minimum value of the torque ratio and can be used for fan-type drives.

In designing pole-changing motors, special care should be taken to see that the magnetizing force curves for both numbers of poles are as close as possible to a sine wave. The type and design of winding, and, in particular, the pitch factor, should be appropriately selected.

A three-phase winding having a 60° phase belt gives the best shape of the magnetizing force curve when the pitch differs from the full one by one-sixth of a pole pitch, i.e., has a relative pitch $\beta = \frac{5}{6} = 0.833$

or $\beta = 1\frac{1}{6} = 1.167$, while a winding with a 120° phase belt gives the best results with a full pitch ($\beta = 1$). Pole-changing windings for the smaller number of pole pairs (p_I) have a 60° phase belt. With a double number of pole pairs (p_{II}), the phase belt becomes 120° , since the number of coil sections in a belt does not change, while the pole pitch

TABLE 24-2

Power, kW	Speed, rpm	s, %	η , %	$\cos \varphi$	I_{st}/I_r	M_{st}/M_r	M_{max}/M_r
4	750	2.4	80.5	0.778	4.2	1.3	2.0
4.5	1500	3.1	79.0	0.92	4.6	1.4	1.9
10.8	750	2.6	83.5	0.79	5.0	1.5	2.3
10.8	1500	3.1	82.5	0.935	5.5	1.5	2.2
46	750	1.4	90.0	0.825	6.4	1.5	2.8
46	1500	2.1	88.5	0.935	5.3	1.0	2.3

becomes halved. In this connection the best results with respect to the shape of the magnetizing force curve are obtained if, for the greater number of pole pairs (p_{II}), we choose $\beta_{II} > 1.0$, for example, $\beta_{II} = 1.4$; then, for the smaller number of poles (p_I) we obtain $\beta_I < 1$, for example, $\beta_I = 0.7$.

Table 24-2 gives the main characteristics of three-phase double-speed squirrel-cage induction motors, Type MA-200, rated for 1500/750 rpm, 380 V. A glance at the table shows that these motors develop constant power with both numbers of pole pairs and that the efficiency of the motors is somewhat higher at a lower speed than at a higher one, but the power factor $\cos \varphi$ is considerably lower. The other characteristics differ very little.

Pole-changing motors are built mainly as double-speed ones and, less frequently, as three- and four-speed motors of low power rating. But these motors are sometimes designed for high ratings in installations of special importance. For instance, there are installations having motors with pole changing from $2p = 22$ to $2 \times 2p = 44$, each being rated for 1655/4050 kW, $U_1 = 5$ kV and $n = 317/162$ rpm. The rotors of these motors each has two windings; one a squirrel-cage, the other a phase-wound one with its leads brought out to slip rings.

Attempts to build motors with more than four speed steps have not been successful because of the involved design of both the motor and the pole-changing device.

24-3. Changing the Primary Frequency [174, 187, 265]

This method of speed control is possible only when a motor is fed from special installations. The frequency can be changed over a wide range by making synchronous generators run at a varying speed or according to the Yapolsky-Kostenko scheme using commutator a.c. generators, and also by using installations with gas-filled valve converters, for example, according to the scheme proposed by D. Zavali-shin.

The following main cases of speed control are possible:

- (a) with constant torque, i.e., with $M = \text{const}$;
- (b) with constant power, i.e., with $P_2 = \text{const}$;
- (c) when the torque is proportional to the square of the frequency, i.e., with $M \propto f_1^2$.

The investigation of this problem by M. Kostenko [187] has shown that if we want a motor to operate at different frequencies with practically constant values of its efficiency, power factor, overload capacity and a constant absolute slip, then, with the steel unsaturated simultaneously with the change in frequency we must also change the voltage U_1 in relation to the frequency and torque according to the following law:

$$\frac{U'_1}{U_1} = \frac{f'_1}{f_1} \sqrt{\frac{M'}{M}} \quad (24-5)$$

Here U'_1 and M' are the voltage and torque corresponding to the frequency f'_1 , and U_1 and M to the frequency f_1 .

When $M = \text{const}$, we have

$$\frac{U'_1}{U_1} = \frac{f'_1}{f_1} \quad (24-6)$$

i.e., the voltage supplied to the motor must vary in proportion to the frequency.

With a constant power, the motor torque varies inversely proportional to the speed and, accordingly, to the frequency, i.e.,

$$\frac{M'}{M} = \frac{f_1}{f'_1}$$

whence

$$\frac{U'_1}{U_1} = \sqrt{\frac{f_1}{f'_1}} \quad (24-7)$$

If $M \propto f_1^2$, then

$$\frac{U'_1}{U_1} = \left(\frac{f'_1}{f_1} \right)^2 \quad (24-8)$$

i.e., voltage fed to the motor must vary as the square of the frequency.

In practice, however, we have to depart somewhat from these deductions, because the core steel of the machine is always more or less saturated, and because the cooling conditions of a machine vary with a change in speed.

24-4. Changing the Resistance in the Rotor

In motors with slip rings the speed can be controlled with the aid of a rheostat in the rotor circuit.

The control diagram does not differ from the ordinary diagram of an induction motor with a phase-wound rotor (Fig. 22-3). The control

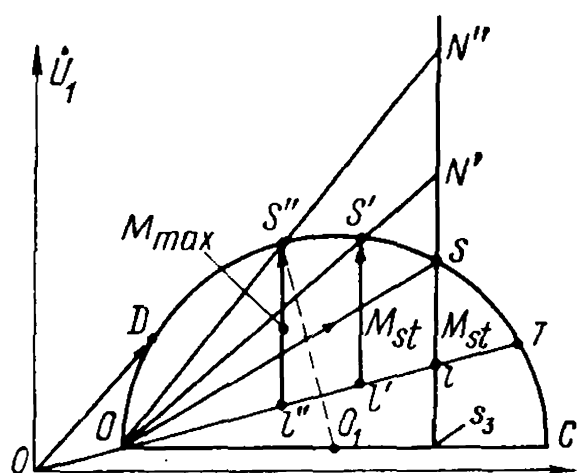


Fig. 24-3. Circle diagram for different values of additional resistance in rotor circuit

rheostats, of the metal or water type, are similar to starting rheostats, but are designed for continuous operation.

The physical aspects of the process taking place in speed control are the same as in d.c. motors. Indeed, at the first moment after switching in the control rheostat, when the speed of the motor has not yet had time to change, the rotor current decreases. This causes the torque at the motor shaft to decrease, and a negative dynamic torque appears at the shaft.

The speed of the motor begins to fall, and the e.m.f. and the current in the rotor rise. The process proceeds until the rotor current reaches a value at which the motor rotational and static loading torques are mutually balanced.

Let us consider the curves $M=f(s)$ in Fig. 20-6. If $M_{stat}=\text{const}$, stable operation of a motor corresponds to points a, b, c, d on the intersection of the torque curves with the straight line FG . It can be seen that by introducing a resistance into the rotor we can regulate the speed downward from the synchronous value over rather wide limits. This results in a considerable reduction in motor efficiency, however, since a large part of the power is spent in the control rheostat.

To answer the question of how the motor characteristics change when an additional resistance is introduced into the rotor circuit, we can construct a circle diagram (Fig. 24-3).

Since the voltage applied to the motor and the circuit frequency remain constant, the current I_0 does not change, and the no-load point O continues to occupy its previous position on the circle diagram. The diameter of the circle diagram also remains the same, but the position of the short-circuit point S on the current circle depends on the value of the additional resistance inserted into the rotor circuit (Fig. 24-3). This determines the new position of the line of useful power and, correspondingly, the new values of the slip and the efficiency. Let, for example, the static torque be $M_{stat}=\text{const}$. Then, when $U_1=\text{const}$ and $f_1=\text{const}$, we have

$$\Phi_m = \text{const}; \quad I'_{2a} = I'_2 \cos \psi_2 = \text{const}$$

Consequently, the end of the secondary current vector and, hence, the end of the primary current vector (Fig. 24-3) continue to occupy their previous positions in the circle diagram.

The primary power $P_1 = m_1 U_1 I_1 \cos \varphi_1$ remains unchanged. The electromagnetic power $P_{em} = M_{em} \Omega_1$ also remains unchanged, while the useful power $P_2 = M_{em} \Omega$ decreases practically proportional to the

speed. The motor efficiency $\eta = \frac{P_2}{P_1} \equiv \Omega$ decreases in the same proportion, i.e., this method of speed control is not economical. The slip

$$s = \frac{m_1 I_2'^2 (r_2' + r_{add}')}{M_{em} \Omega_1} \equiv r_2' + r_{add}'$$

increases in proportion to the increase in the resistance in the rotor circuit.

The case of $M_{stat} = \text{const}$ considered above is the simplest, but in other cases analysis of the operating conditions can be carried out in a similar manner.

Although it is uneconomical, speed control by means of a rheostat in the rotor circuit is widely used in practice, mainly for low-power motors and in overhead cranes. It is sometimes used, however, for speed regulation of rolling mills especially where they are provided with flywheels for reducing the load peaks in the circuit. Here the rheostat, called the slip regulator, is automatically switched in when the load increases, and as a result the slip increases and part of the load is compensated at the expense of the kinetic energy of the flywheel. Conversely, when the load decreases, the resistance in the rotor circuit is decreased; the speed grows and the flywheel begins to store kinetic energy.

24-5. Cascaded Induction Motors [190a]

Instead of dissipating energy in the control rheostat in controlling the speed, this energy can be fed to another induction motor connected to the first one in cascade, and converted into mechanical energy. Hence the energy consumed from the power line can be utilized more effectively.

For normal operation of the cascade, motors *I* and *II* (Fig. 24-4) must be coupled both electrically and mechanically. An electrical connection alone does not suffice, since motor *I* begins to operate from a circuit with normal voltage and frequency, and runs at normal speed, whereas motor *II* receives a very low voltage with a very low frequency from the rings of motor *I*. Hence motor *II* does not develop any torque and is only an additional resistance introduced into the rotor circuit of motor *I*.

Motors *I* and *II* should be selected so that their characteristics correspond to each other. Thus, for instance, if both motors are identical in design (conditions prevailing in railway traction), the stators

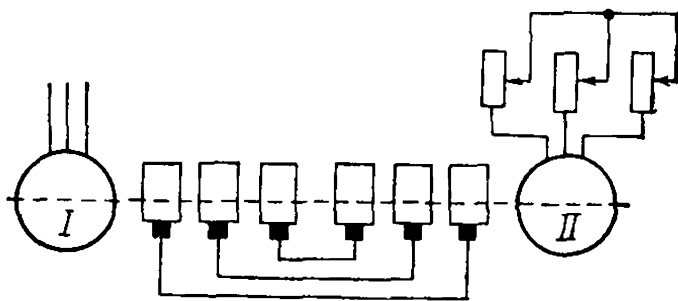


Fig. 24-4. Cascaded induction motors

of the motors being high-voltage circuits and the rotors low-voltage circuits, it is necessary to interconnect the rotors of both motors; to connect the rotor of motor *I* to the stator of motor *II* would not be rational. In special installations motor *II* may have a squirrel-cage rotor; here the rotor of motor *I* is connected to the stator of motor *II*, but the characteristics of both circuits should be matched. Steps should also be taken to add together the torques developed by both motors.

The cascade connection will be stable in operation if the frequency in the secondary circuit of motor *II*, i.e., in the stator in Fig. 24-4 will, at its limit, be close to zero.

Let f_1 be the power circuit frequency; f_2 the frequency in the secondary circuit of motor *I* corresponding to the synchronous speed of the cascade connection $n_{c. syn}$; p_1 and p_{II} the numbers of pole pairs of motors *I* and *II*, and n_{1I} and n_{1II} the synchronous speeds of these motors. Then

$$n_{1I} = \frac{f_1}{p_1}; \quad f_2 = (n_{1I} - n_{c. syn}) p_1$$

In motor *II* a flux is produced which rotates relative to the rotor at a speed

$$n_{1II} = \frac{f_2}{p_{II}} = (n_{1I} - n_{c. syn}) \frac{p_1}{p_{II}}$$

The condition for stable operation of the cascade will be satisfied if the speed n_{1II} is equal in value to the synchronous speed $n_{c. syn}$ of the cascade. In this case

$$n_{c. syn} = n_{1II} = (n_{1I} - n_{c. syn}) \frac{p_1}{p_{II}}$$

whence

$$n_{c. syn} = n_{1I} \frac{p_1}{p_1 + p_{II}} = \frac{f_1}{p_1 + p_{II}} \quad (24-9)$$

Thus, a cascade of two electrically coupled motors is like a single induction motor in which the number of pole pairs is equal to the sum of the pole pairs of both motors. The actual speed of the cascade is $n_c < n_{c. syn}$ since the cascade, as any ordinary motor, operates with some slip depending on the load.

The installation in Fig. 24-4 can be modified so that each motor will be able to operate independently or in cascade. Here we obtain three stages of speed corresponding to the numbers of pole pairs p_1 , p_{II} and $p_1 + p_{II}$.

The power distribution in a cascade is the same as in a normal motor. According to formula (20-5), $P_{em} = P_{mech} + p_{cop2}$. The power P_{mech} is proportional to the speed n , and the power dissipated in the rotor winding is proportional to the slip s . Let the speed of the cascade

be n_c ; the slip will then be

$$s = \frac{n_{11} - n_c}{n_{11}}$$

If P_{em} is the electromagnetic power of the cascade transmitted from the stator to the rotor of motor I , the power transmitted to the cascade shaft in the form of mechanical energy will be

$$P_{mech} = P_{em} \frac{n_c}{n_{11}}$$

The remaining power

$$P_{sec} = P_{em} \frac{n_{11} - n_c}{n_{11}}$$

is transmitted in the form of electric power to the second circuit and is there partially converted into mechanical power. If we assume that $n_c \cong n_{c, syn}$, then

$$\frac{P_{mech}}{P_{sec}} = \frac{n_c}{n_{11} - n_c} \cong \frac{p_1}{p_{11}} \quad (24-10)$$

A cascade of two induction motors has substantial disadvantages. Indeed, the magnetizing current I_{0c} necessary to produce the fluxes in both motors is drawn from the external circuit through motor I . Therefore, the no-load current I_{0c} of the cascade is appreciably greater than the no-load current I_0 of one motor. On the other hand, motor II is connected in series with motor I . This is why the short-circuit current of the cascade $I_{c, sh} < I_{shI}$, where I_{shI} is the short-circuit current of motor I . Therefore, the locus of the primary current I_{1c} of the cascade is inside the current circle of a motor operating alone (Fig. 24-5). More detailed investigations show that the locus is actually a fourth-degree curve approaching a circle.

The cascade characteristics are much inferior to the corresponding characteristics of a motor operating alone. A cascade of two induction motors is therefore used only in special cases, mainly on railways with three-phase current.

To obtain a greater number of speed steps, each of the motors constituting a cascade connection may be made with pole changing.

Example 24-1. Let us consider a cascade connection of two three-phase induction motors A and B , of 250 kW each, with phase-wound rotors having $2p=6$ and $2p=4$ poles.

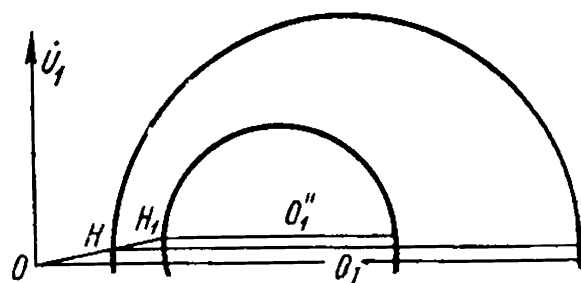


Fig. 24-5. Circle diagram of a separate induction motor and of a cascade of two motors

Motor *A* has the following inductive reactances and resistances (see Examples 5-1 and 19-1):

$$\begin{aligned} r_{1A} &= 0.68 \, \Omega; & r_{mA} &= 11 \, \Omega \\ jx_{1A} &= j2.78 \, \Omega; & x_{mA} &= j95.6 \, \Omega \\ r'_{2A} &= 0.57 \, \Omega; & \sigma_{1A} &= 1 + \frac{x_{1A}}{x_{mA}} = 1 + \frac{2.78}{95.6} = 1.03 \\ jx'_{2A} &= j4.7 \, \Omega; & \sigma_{1A}^2 &= 1.03^2 = 1.06 \end{aligned}$$

Three-phase 250-kW induction motor *B* with a phase-wound rotor and $2p = 4$ poles, computed in the same way as motor *A*, has the following resistances and inductive reactances:

$$\begin{aligned} r_{1B} &= 0.335 \, \Omega; & r'_{mB} &= 11.7 \, \Omega; & jx_{1B} &= j2.74 \, \Omega \\ jx'_{mB} &= j99 \, \Omega; & r'_{2B} &= 0.274 \, \Omega \\ \sigma_{1B} &= 1 + \frac{x'_{1B}}{x'_{mB}} = 1 + \frac{0.392}{99} \cong 1.04 \\ jx'_{2B} &= j3.92 \, \Omega \end{aligned}$$

The complete T-type equivalent circuit for the cascade of two three-phase motors *A* and *B*, neglecting the resistance of the magnetizing circuit r'_{mB} of the second motor, has the form shown in Fig. 24-6a.

The complete T-type equivalent circuit for motors *A* and *B* is considerably simplified when the magnetizing part of the motor *A* connected to the power line is brought out to the primary terminals.

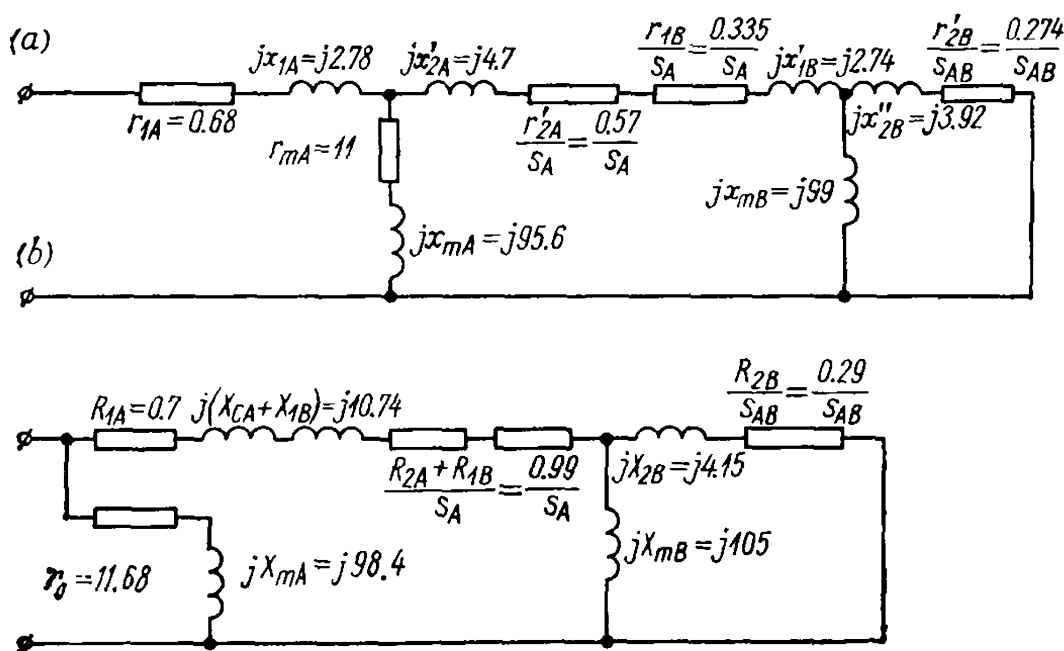


Fig. 24-6. Equivalent diagrams of two cascaded induction motors

The parameters of the equivalent circuit with the magnetizing part brought out to the terminals are:

$$\begin{aligned}
 R_{1A} &= r_{1A} \sigma_{1A} = 0.68 \times 1.03 = 0.7 \, \Omega \\
 jX_{1A} &= jx_{1A} \sigma_{1A} = j2.78 \times 1.03 = j2.86 \, \Omega \\
 R_{2A} &= r'_{2A} \sigma_{1A}^2 = 0.57 \times 1.06 = 0.604 \, \Omega \\
 jX_{2A} &= x'_{2A} \sigma_{1A}^2 = j4.7 \times 1.06 = j4.98 \, \Omega \\
 R_{1B} &= r'_{1B} \sigma_{1A}^2 = 0.335 \times 1.06 = 0.355 \, \Omega \\
 jX_{1B} &= jx'_{1B} \sigma_{1A}^2 = j2.74 \times 1.06 = j2.9 \, \Omega \\
 R_{2B} &= r'_{2B} \sigma_{1A}^2 = 0.274 \times 1.06 = 0.29 \, \Omega \\
 jX_{2B} &= jx''_{2B} \sigma_{1A}^2 = j3.92 \times 1.06 = j4.15 \, \Omega \\
 jX_{mA} &= jx_{1A} + jx_{mA} = j2.78 + j95.6 = j98.4 \, \Omega \\
 r_0 &= r_{1A} + r_{mA} = 0.68 + 11 = 11.68 \, \Omega \\
 jX_{mB} &= jx_{mB} \sigma_{1A}^2 = j99 \times 1.06 = j105 \, \Omega \\
 jX_{cA} + jX_{1B} &= jX_{1A} + jX_{2A} + jX_{1B} = j2.86 + j4.98 + j2.9 = j10.74 \, \Omega \\
 R_{1A} + R_{2B} &= 0.7 + 0.29 = 0.99 \, \Omega
 \end{aligned}$$

The equivalent circuit with the magnetizing part brought out to the primary terminals is shown in Fig. 24-6b.

The parameters of the branched part of two circuits connected in parallel can be reduced to equivalent series-connected impedances, where for simplicity the resistance of the magnetizing part is neglected.

Hence the equivalent impedance is

$$\begin{aligned}
 Z_{eq} = R_{eq} + jX_{eq} &= \frac{\frac{R_{2B}}{s_{AB}} X_{mB}^2}{\left(\frac{R_{2B}}{s_{AB}}\right)^2 + (X_{2B} + X_{mB})^2} + \\
 &\quad + j \frac{\left(\frac{R_{2B}}{s_{AB}}\right)^2 X_{mB} + X_{2B} X_{mB} (X_{2B} + X_{mB})}{\left(\frac{R_{2B}}{s_{AB}}\right)^2 + (X_{2B} + X_{mB})^2} = \\
 &= \frac{\frac{0.29}{s_{AB}} \times 105^2}{\left(\frac{0.29}{s_{AB}}\right)^2 + (4.15 + 105)^2} + j \frac{\left(\frac{0.29}{s_{AB}}\right)^2 \times 105 + 4.15 \times 105 \times (4.15 + 105)}{\left(\frac{0.29}{s_{AB}}\right)^2 + (4.15 + 105)^2} = \\
 &= \frac{3190s_{AB}}{0.084 + 11900s_{AB}^2} = j \frac{8.82 + 47500s_{AB}^2}{0.084 + 11900s_{AB}^2}
 \end{aligned}$$

Let us determine the values of the impedances Z_{st} , the current I_{st} and $\cos \varphi_{st}$ of the main cascaded part for various and more essential slips of the cascade, which makes it possible to plot the current vectors and the corresponding circle diagrams of the cascade connection:

1. $s_A = 0$, $s_{AB} = -1$.

Such conditions correspond to no-load operation of the first motor A, connected to the line when only the magnetizing part brought out to the terminals remains.

TABLE 24-3

s_A	$-\infty$	-0.2	-0.05	0	$+0.05$	0.2
s_{AB}	$+\infty$	-1.135	-1.066	-1.083	-9.34	1.0
I_{st}	117	112.2	71	17.6	69.3	111
$\cos \varphi_{st}$	0.0322	-0.291	-0.795	0.185	0.81	0.329

Continued

s_A	0.585	0.6	0.61	0.65	1.0	1.5
s_{AB}	-0.0292	0	0.0122	0.081	0.161	1.5
I_{st}	102	14.95	55	110	116	117
$\cos \varphi_{st}$	-0.392	0.0203	0.77	0.332	0.14	0.1035

Here

$r_0 = 11.68 \, \Omega; \quad jX_{mA} = j98.4 \, \Omega$
 $Z_0 = 98.8 \, \Omega; \quad I_0 = \frac{1730}{98.8} = 17.5 \, A$
 $\cos \varphi_0 = \frac{11.68}{98.8} = 0.118$

2. $s_A = +0.05; \quad s_{AB} = -0.581$. In this case

$\frac{R_{2A} + R_{1B}}{s_A} = \frac{0.99}{0.05} = 19.8 \, \Omega; \quad \frac{R_{2B}}{s_{AB}} = \frac{0.29}{-0.581} = -0.5 \, \Omega$
 $R_{1A} = 0.7 \, \Omega; \quad j(X_{cA} + X_{1B}) = j10.74 \, \Omega$
 $jX_{1B} = j4.15 \, \Omega; \quad jX_{mB} = j105 \, \Omega$
 $Z_{eq} = -0.472 + j3.99$
 $Z_{st} = (0.7 + 19.8 - 0.472) + j(10.74 + 3.99) = 20.03 + j14.73$

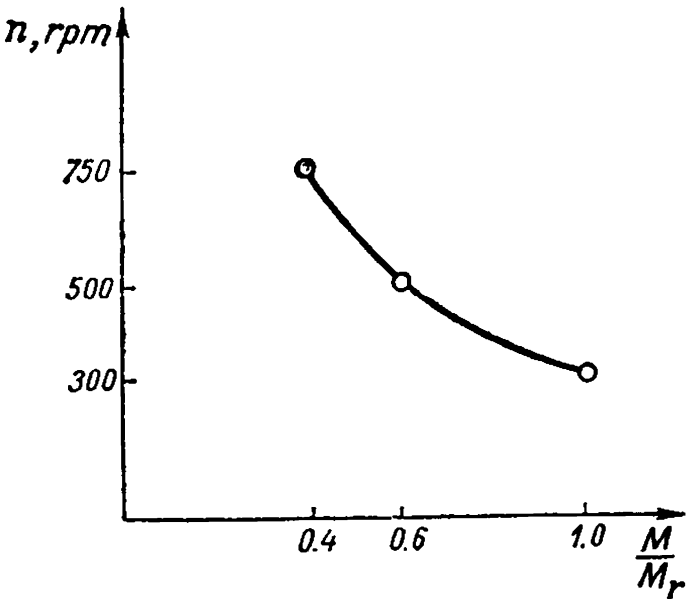


Fig. 24-7. Relation $n = f\left(\frac{M}{M_r}\right)$

$Z_{st} = \sqrt{20.03^2 + 14.73^2} = 25 \, \Omega$
 $I_{st} = \frac{1730}{25} = 69.3 \, A$
 $\cos \varphi_{st} = 0.805$

The calculations for other values of the slip are performed in a similar way. The data are given in Table 24-3.

The data obtained can be used to plot the current circle diagram, which comprises two circles, intersecting near the point $s_A = 1.0$.

A curve of the torque at the shaft of the cascade connection for various speeds is shown in Fig. 24-7.

Chapter

25

SINGLE-PHASE INDUCTION MOTORS

25-1. Principle of Operation

Single-phase motors are fed from a single-phase a.c. mains. In accordance with this, their stators have one operating winding connected to the mains. The rotor winding of a single-phase motor is usually short-circuited and has the form of a squirrel cage. The stator also carries an additional starting winding which most often is connected to the mains only during starting of the motor. The function of this winding will be explained later.

Let us first consider the operation of a single-phase motor when the starting winding is switched-off.

The operating winding arranged on the stator of a single-phase motor (Fig. 25-1a) is fed from a single-phase a.c. external circuit. The current in this winding produces a pulsating magnetic field which can be resolved into two fields rotating in opposite directions at the same speed and with the same amplitudes, equal to one-half the amplitude of the pulsating field.

According to the above, a single-phase motor is equivalent to two identical three-phase motors whose rotors are fitted on a common shaft, and whose stator windings are connected in series, so that the magnetic fields produced by them rotate in space in opposite directions (Fig. 25-1b). These two motors, in turn, are equivalent to one three-

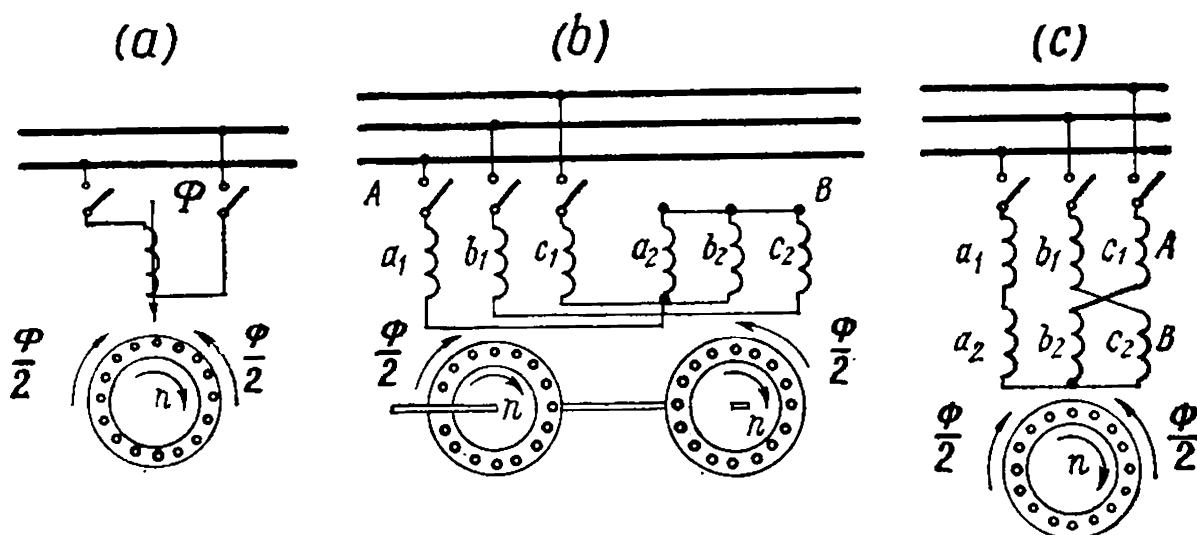


Fig. 25-1. Principle of operation of a single-phase motor

phase motor with two identical series-connected three-phase windings which produce fields rotating in opposite directions (Fig. 25-1c).

Both in a real single-phase motor and in its two indicated modifications the currents induced in the rotor winding by the two rotating stator fields and interacting with them, produce equal and mutually opposed electromagnetic torques when the motor is at standstill, owing to which the resultant torque is zero, and the motor cannot start, even in the absence of a braking torque on the shaft.

If we bring the rotor of the motor up to a speed n in any direction, for instance, in the direction which the field of coil A rotates in (Fig. 25-1c), this field will induce in the rotor winding a current having the frequency

$$f_{2A} = p(n_1 - n) = \frac{n_1 - n}{n_1} p n_1 = s f_1 \quad (25-1)$$

where s is the rotor slip relative to field A .

With respect to the backward rotating field of winding B , the rotor will have a relative speed equalling the sum of the field and rotor speeds, and, therefore, the frequency of the current induced in the rotor winding will be

$$f_{2B} = p(n_1 + n) = p[2n_1 - (n_1 - n)] = (2 - s)f_1 \quad (25-2)$$

where $(2-s)$ is the slip of the rotor relative to the backward rotating field.

Let us assume that the torque M_A produced by winding A in the direction of rotor rotation is positive. Then the torque M_B created by the backward rotating field of winding B will be negative and, evidently, be a braking torque.

The curve of the torque M_A against the slip will be of the same nature as that of a three-phase induction motor, and, with an increase in rotor speed, the positive torque will rise to a certain maximum and, when $s=0$, will vanish.

When $0 < s < 1$, the slip relative to the backward rotating field will be $(2-s) > 1$, and the motor operates in braking conditions with respect to this field. When $1 < s < 2$, i.e., when the rotor runs in the

direction of the B -winding field, the slip $(2-s)$ relative to this field will be $0 < (2-s) < 1$. With respect to this field the machine is motoring, and with respect to the A -winding field it is braking. Assuming the torques to be positive when they act in the direction of rotating field A , we obtain

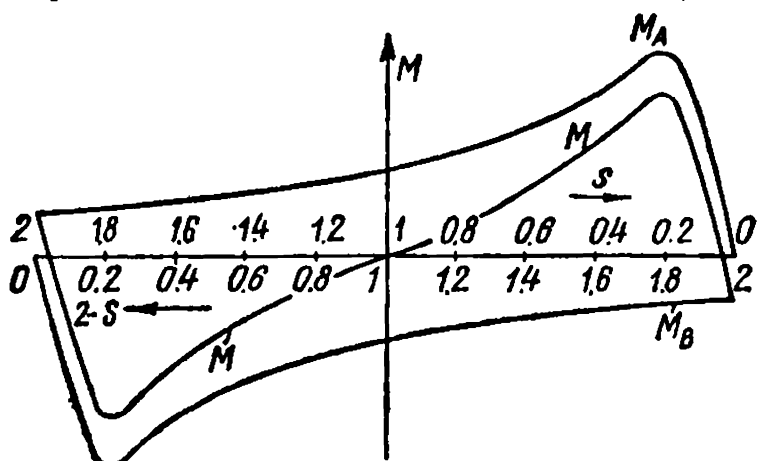


Fig. 25-2. Single-phase motor torques

the torque curves M_A and M_B for windings A and B shown in Fig. 25-2.

The resultant torque

$$M = M_A + M_B \quad (25-3)$$

is also shown in Fig. 25-2.

As follows from the general considerations and from Fig. 25-2, we have $M=0$ when $s=1$, and the motor cannot start rotating independently when there is only one single-phase winding on the stator. The operating conditions with the rotor running in either direction at a certain speed n will be identical.

25-2. Equivalent Circuit for a Single-Phase Motor

On the basis of the above, the equivalent circuit of a single-phase motor is of the type shown in Fig. 25-3, where the secondary circuit with the inductive reactance x'_2 and resistance $\frac{r'_2}{s}$ corresponds to the forward rotating field, and the circuit with x'_2 and $\frac{r'_2}{2-s}$ corresponds to the backward rotating field.

Let us consider the operation of a motor when it rotates in the direction of the forward field ($-\infty < s < 1$) and combine the left pair of parallel parts in Fig. 25-3 into one common part. The impedance of this part will be

$$\begin{aligned} Z_{2-s} &= \frac{\left(\frac{r'_2}{2-s} + jx'_2\right) jx_m}{\frac{r'_2}{2-s} + jx'_2 + jx_m} = \frac{\frac{r'_2}{2-s} + jx'_2}{1 + \frac{x'_2}{x_m} - j \frac{r'_2}{(2-s)x_m}} \cong \\ &\cong \frac{r'_2}{2-s} \frac{1}{\sigma_2} + jx'_2 \frac{1}{\sigma_2} \end{aligned} \quad (25-4a)$$

where

$$\sigma_2 = 1 + \frac{x'_2}{x_m} \quad (25-4b)$$

is a correction factor equal to the leakage factor of the rotor.

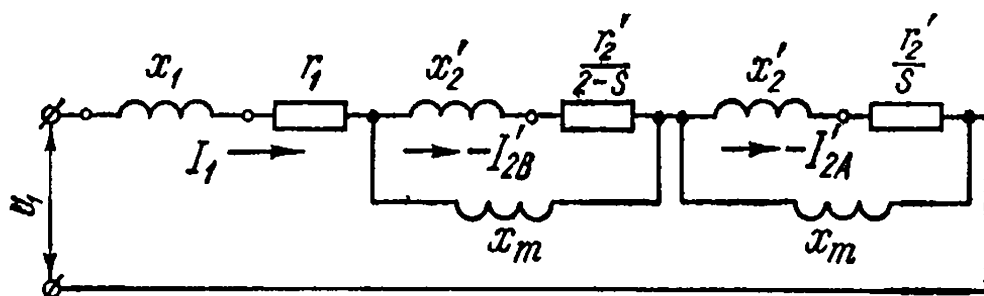


Fig. 25-3. Equivalent circuit of a single-phase induction motor

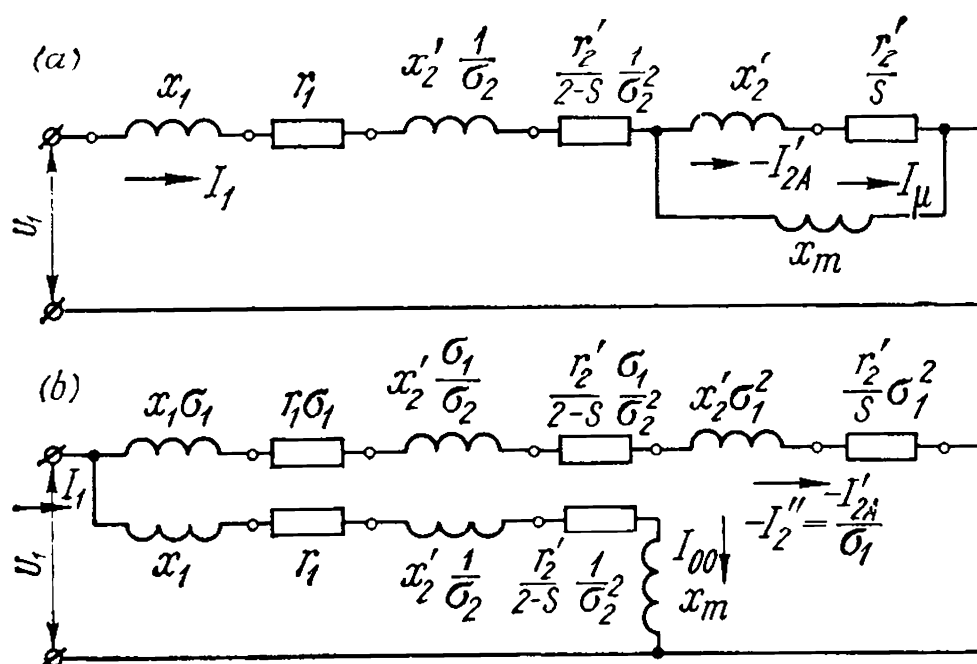


Fig. 25-4. Improved equivalent circuits of a single-phase induction motor

Here we have neglected the imaginary part $j \frac{r_2'}{(2-s)x_m}$, which in the considered range of the slip s is relatively small.

After this, the combined equivalent circuit assumes the form shown in Fig. 25-4a. Let us bring out the parallel branch containing the inductive reactance x_m to the primary terminals. We then obtain the equivalent circuit of Fig. 25-4b, where the correction factor σ_1 , neglecting its imaginary part, is equal to

$$\sigma_1 = 1 + \frac{x_1 + x_2' \frac{1}{\sigma_2}}{x_m} \quad (25-5)$$

It may be assumed for the magnetizing part of the equivalent circuit in Fig. 25-4b, that $s=0$, since here x_m is great compared with the other resistances and reactances.

The ideal no-load current ($s=0$), equal to the current of the magnetizing part in Fig. 25-4b, with account of the resistance r_m of the magnetizing circuit, will be

$$I_{00} = \frac{U_1}{\left(r + \frac{r_2'}{2} \frac{1}{\sigma_2^2} + r_m \right) + j \left(x_1 + x_2' \frac{1}{\sigma_2} + x_m \right)} \quad (25-6)$$

while the current in the main part of the circuit in Fig. 25-4b is

$$-I_2'' = \frac{\dot{U}_1}{\left(r_1 \sigma_1 + \frac{r_2'}{s} \sigma_1^2 + \frac{r_2'}{2-s} \frac{\sigma_1}{\sigma_2^2} \right) + j \left(x_1 \sigma_1 + x_2' \sigma_1^2 + x_2' \frac{\sigma_1}{\sigma_2} \right)} \quad (25-7)$$

On the basis of the equivalent circuit in Fig. 25-4b we can write expressions for the power, torques and losses in the windings.

The losses at ideal no-load ($s = 0$) are

$$p_{cop0} = I_{00}^2 \left(r_1 + \frac{r_2'}{2} \frac{1}{\sigma_2^2} + r_m \right) \quad (25-8)$$

At slips $s = 0$ and $s = 2$ the resistances $\frac{r_2'}{s}$ and $\frac{r_2'}{2-s}$ become equal to infinity, and, therefore, the current in the main circuit is $I_2'' = 0$.

When $s \neq 0$, the losses in the primary and secondary circuits increase by the value

$$\left. \begin{aligned} p_{cop1} &= I_2''^2 r_1 \sigma_1 \\ p_{cop2} &= I_2''^2 \left(r_2' \sigma_1^2 + r_2' \frac{\sigma_1}{\sigma_2^2} \right) \end{aligned} \right\} \quad (25-9)$$

The electromagnetic power transmitted from the primary to the secondary circuit is

$$P_{em} = P_{emA} + P_{emB} = I_2''^2 \frac{r_2'}{s} \sigma_1^2 + I_2''^2 \frac{r_2'}{2-s} \frac{\sigma_1}{\sigma_2^2} \cong 2 I_2''^2 r_2' \frac{1}{s(2-s)} \quad (25-10)$$

The power corresponding to the electromagnetic torque of the motor is

$$P_M = P_{emA} - P_{emB} \cong 2 I_2''^2 r_2' \frac{1-s}{s(2-s)} = p_{cop2} \frac{1-s}{s(2-s)} \quad (25-11)$$

With ideal no-load $s = 0$, and with a short circuit $s = 1.0$, hence $P_M = 0$, since in the first case $I_2'' = 0$ and in the second $(1 - s) = 0$.

At small slips corresponding to motor operation under load it may be assumed that $s^2 = 0$, and, therefore,

$$P_M \cong \frac{p_{cop2}}{2} \frac{1-s}{s} = I_2''^2 r_2' \frac{1-s}{s} \quad (25-12)$$

The motor slip can be determined from equation (25-10):

$$s(2-s) = \frac{p_{cop2}}{P_{em}} \quad (25-13)$$

The mechanical power of a motor according to equation (25-11), within the range of normal operating slips, is

$$P_{mech} = P_M (1-s) = \frac{(1-s)^2}{s(2-s)} p_{cop2} = \frac{(1-s)^2}{s(2-s)} 2 I_2''^2 r_2' \quad (25-14)$$

25-3. Circle Diagram of a Single-Phase Motor

In the considered range ($-\infty < s < 1$) the influence of the slip s on the value of the current of the magnetizing part of the equivalent circuit in Fig. 24-4b is slight, and the current in this part can be assu-

med equal to its value when $s=0$ [equation (25-6)]. In the range of normal loads ($0 < s \ll 1$), the term $\frac{r'_2}{s} \sigma_1^2$ in the denominator of equation (25-7) is predominant over the term $\frac{r'_2}{2-s} \frac{\sigma_1}{\sigma_2^2}$, and the latter may therefore be replaced by the term $\frac{r'_2}{2-s} \sigma_1^2$ and the sum of both these terms will be

$$\frac{r'_2}{s} \sigma_1^2 + \frac{r'_2}{2-s} \frac{\sigma_1}{\sigma_2^2} \cong \frac{r'_2}{s} \sigma_1^2 + \frac{r'_2}{2-s} \sigma_1^2 = \frac{2r'_2 \sigma_1^2}{q}$$

where

$$q = s(2-s) \quad (25-15)$$

Then, instead of equation (25-7), we obtain

$$-I_2'' = \frac{\dot{U}_1}{\left(r_1 \sigma_1 + \frac{2r'_2 \sigma_1^2}{q}\right) + j \left(x_1 \sigma_1 + x'_2 \sigma_1^2 + x'_2 \frac{\sigma_1}{\sigma_2}\right)} \quad (25-16)$$

When q varies within the limits $-\infty \leq q \leq +\infty$, the end of the current vector $-I_2''$, similar to the case considered in Sec. 21-2, describes a circle with a diameter

$$D = \frac{U_1}{x_1 \sigma_1 + x'_2 \sigma_1^2 + x'_2 \frac{\sigma_1}{\sigma_2}} \quad (25-17)$$

As a result, for a single-phase motor we obtain the circle diagram given in Fig. 25-5. The diagram and its scales are constructed in the

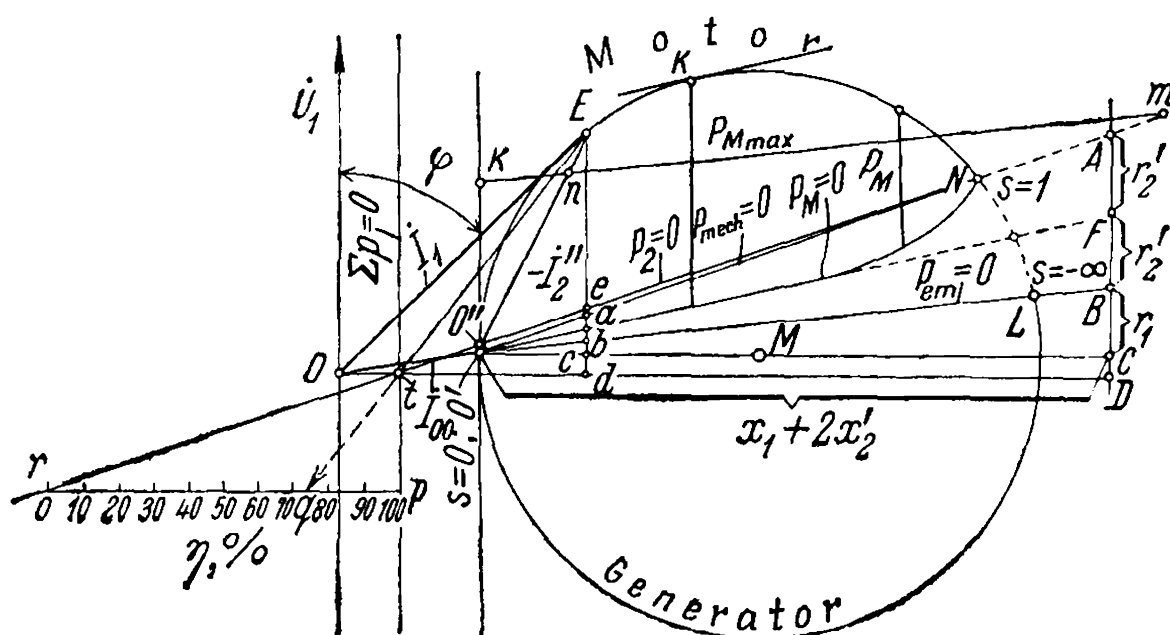


Fig. 25-5. Circle diagram of a single-phase induction motor

same way as for the approximate circle diagram of a three-phase motor, the only difference being that, instead of the scale of the slip s , we obtain the scale of the parameter q , and the value of s is determined through q from the relation

$$s = 1 - \sqrt{1 - q} \quad (25-18)$$

which follows from equation (25-15). It should be borne in mind that the diagram is valid when $-\infty \leq s \leq 1$ and, correspondingly, when the values of q are within the limits $-\infty \leq q \leq 1$.

Thus a circle diagram for a single-phase induction motor has a double scale from the parameter s (see Sec. 21-1).

Chapter 26

SPECIAL OPERATING CONDITIONS AND TYPES OF INDUCTION MACHINES

26-1. Electrical Braking of Induction Motors

The proper operation of many industrial installations requires rapid and smooth motor braking in exact accordance with a given speed schedule. Braking may be mechanical or electrical, but the latter has many advantages, particularly where precise control of the stopping moment and smoothness of operation are needed.

There are three main methods of electrical braking of induction motors: plugging, regenerative braking, and dynamic braking.

Plugging. The rotation of the stator field is reversed by interchanging any two stator connections. Here the rotor rotates against the field with a slip greater than unity ($s > 1$).

If the motor has a slip-ring rotor, we insert a resistance r_{add} into the rotor circuit to limit the plugging current. We have already seen (Fig. 22-4) that the torque maximum, remaining constant in magnitude, shifts with increase in r_{add} in the direction of greater positive slips. Therefore, we may select such a resistance r_{add} at which the induction motor, in passing over to electromagnetic braking, will develop the required braking torque. The torque curves $M = f(s)$, however, acquire a very gentle slope.

The circuit most widely used is shown in Fig. 26-1. Its features are that the stator is switched across the line as a single-phase stator during braking, and that two of the phase windings are short-circuited. The latter is of special importance, since without the shorted circuit we would have a usual single-phase motor without a braking torque.

An analysis of this circuit shows that everything takes place as if we had two three-phase motors on one shaft, developing opposed torques. The braking characteristics of this circuit are favourable.

Its disadvantages are: poorer utilization of a single-phase machine in comparison with a three-phase one, unfavourable influence of a single-phase load on the symmetry of the three-phase line voltage, and a low power factor of the machine. In most cases, however, these disadvantages are not essential.

Regenerative Braking. This is used mainly in motors with pole changing. If the motor operates

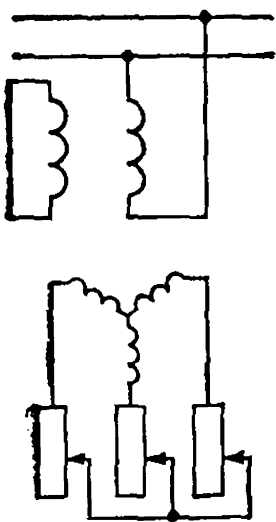


Fig. 26-1. Braking circuit of an induction motor

with a smaller number of poles $2p$, i.e., at a higher speed $n_1 = \frac{f}{p}$, then, by switching it over to a greater number of poles $2 \times 2p$, we accomplish regenerative braking within the range from $n_1 = \frac{f}{p}$ to $n'_1 = \frac{f}{2p}$. To continue braking below the speed n'_1 , plugging must be used.

Regenerative braking is also used in hoisting equipment when lowering heavy loads. Here the machine returns the energy produced by the lowering load to the mains.

Dynamic Braking. In this method the stator is disconnected from the mains and excited by direct current from some d.c. source—an exciter or rectifier. One of the possible schemes is shown in Fig. 26-2. Here St is the stator, two phase windings of which are series-connected and fed in braking from a dry rectifier DR ; Rot is a squirrel-cage rotor, Sw_1 and Sw_2 are switches which cut in the rectifier for braking. Other connections of the stator windings are also possible, for instance, all three phase windings can be connected in series, according to the circuit $(A-X)-(Y-B)-(Z-C)$, two parallel windings are series-connected to the third, etc.

A glance at the circuit in Fig. 26-2 shows that an induction machine in dynamic braking conditions is an inverted synchronous generator in which the stator produces a stationary magnetic field in space, while the rotor is the armature of the generator. The braking energy is absorbed in the rotor. In slip-ring motors we can insert, in braking, a resistance r_{add} and thus influence the braking torque curve of the machine, which, as analysis shows, is almost identical with the torque curve of an induction machine. In squirrel-cage motors the braking torque is varied by controlling the d.c. voltage. Here we must take into account the unilateral pull between the stator and rotor.

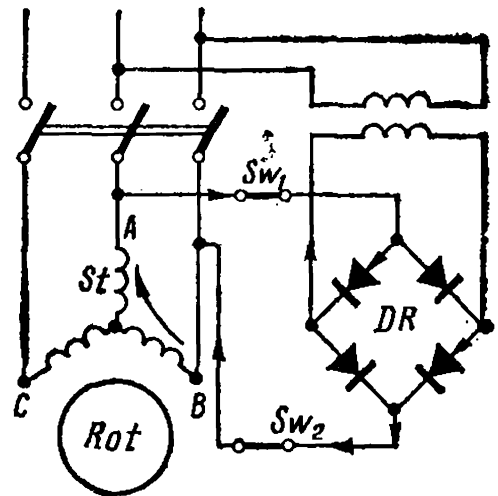


Fig. 26-2. Dynamic braking circuit of a squirrel-cage motor

26-2. Doubly Fed Induction Motor [190b]

Power is usually supplied to an induction motor only from the stator side. But in slip-ring motors we can supply power to both parts of the machine, i.e., to the stator and the rotor, connecting their windings in series or in parallel.

Such a motor is called a doubly fed motor.

Assume that the stator and rotor are connected in parallel (Fig. 26-3) and determine the conditions necessary for the operation of a doubly fed motor.

The current I_1 supplied from the mains to the stator produces a magnetizing force whose first harmonic rotates relative to the stator at a speed $n_1 = \frac{f}{p}$.

The current I_2 delivered from the mains to the rotor produces a magnetizing force rotating with respect to the rotor at a speed $n_2 = \frac{f}{p}$. The direction of rotation of this magnetizing force may coincide with the direction of rotor rotation and may be against it. If n is the speed of the rotor, the speed of the rotor magnetizing force in space will be, correspondingly, $n + n_2$ or $n - n_2$.

To develop a torque, the stator and rotor magnetizing forces (the first harmonics) should be stationary with respect to each other, i.e.,

$$n_1 = n \pm n_2 \text{ or } n = n_1 \mp n_2 \quad (26-1)$$

Here the top sign refers to rotation of the rotor magnetizing force in the same direction as the rotor, and the bottom sign in the opposite direction.

Since $n_1 = n_2$, the motor operates under doubly fed conditions when $n = 0$, and $n = 2n_1$. In the second case we have a machine which rotates at double synchronous speed and has many properties of a synchronous machine. In particular, to realize conditions of double speed, the motor must be brought up to this speed by some external means. One of the weak points of such a machine is its pronounced tendency towards oscillations.

When $U = \text{const}$, the flux Φ of the doubly fed machine also remains practically constant, and, therefore, the resultant magnetizing force F_m of the rotor and stator windings. At no-load the axes of the magnetizing forces F_1 of the stator winding and F_2 of the rotor winding coincide and, hence, considering F_1 and F_2 as spatial vectors, we may write

$$\dot{F}_1 + \dot{F}_2 = \dot{F}_m$$

When the motor is loaded, the rotor will shift with respect to the stator through a

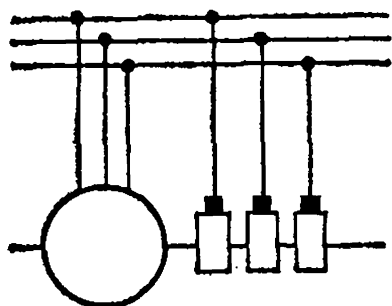


Fig. 26-3. Doubly fed machine

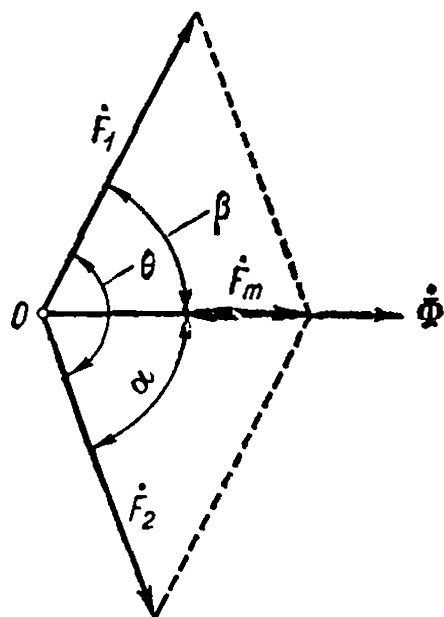


Fig. 26-4. Magnetizing force vector diagram for a doubly fed motor

certain angle θ , and then

$$\dot{F}_1 + \dot{F}_2 e^{-j\theta} = \dot{F}_m$$

which the vector diagram in Fig. 26-4 corresponds to. The magnetizing forces \dot{F}_1 and \dot{F}_2 will grow correspondingly and together with them the stator and rotor currents will increase.

The doubly fed motor can also operate in asynchronous speed conditions, but the machine delivers slip-frequency currents to the circuit which are harmful both for the latter and the synchronous generators feeding it. For this reason the practical value of a doubly fed induction machine operating at synchronous and asynchronous speeds is rather small.

In the general case the doubly fed machine can operate from a circuit with different voltages and frequencies and have a rotor and stator with different parameters. This was investigated by V. Kasyanov, who evolved general expressions for the currents and e.m.f.s of such a machine and proved that it may be considered as a general case of an a.c. machine.

Doubly fed machines, both three-phase, and especially, single-phase, are widely used in synchronous-drive systems.

26-3. Electromagnetic Slipping Clutches

An electromagnetic slipping clutch is used as an elastic coupling between a prime mover and an operating mechanism. It comprises a driven, usually internal part, practically representing the rotor of an induction machine with a phase wound or, more frequently, with a squirrel-cage winding, and an external or driving part having salient poles excited by direct current. The driven part of the clutch is mechanically coupled to the operating mechanism, the driving part to the prime mover. When the excited driving part rotates, it interacts electromagnetically with the driven part and endows it with rotary motion with a slip s , in the same way as the rotating field in an induction motor acts on the rotor. In steady-state operation $s = 1$ to 2%.

By regulating the excitation current, it is possible to easily and very smoothly engage and disengage the driving and driven parts. At the same time, in accordance with each given value of the excitation current, the clutch develops a definite stalling torque and thus serves as a safety device for protecting the prime mover from excessive overloads and shock loads. By making the driven part with two squirrel cages, it is possible to obtain a clutch developing very high starting torques. The main field of application of electromagnetic clutches is ship propulsion installations. Recently such clutches have been used in aerodynamic installations. One of such installations has a rating of 8800 kW.

26-4. Induction Machines for Automatic Devices

In automatic, telecontrol and computer systems various types of subfractional horsepower electrical machines (miniature machines) are used. These machines have to meet high demands as regards precision of operation, and in this connection their manufacture resembles the production of precision apparatus. A few types of such machines are discussed below.

Two-Phase Hollow-Rotor Machines. These machines are widely used as actuating motors (servomotors). In automatic control circuits they have to respond to changes in certain electrical quantities (signals), and in accordance with the intensity and duration of the action of this quantity they have to perform a definite function by acting upon other elements of the automatic control equipment.

The design of a hollow-rotor motor is shown in Fig. 26-5. Stator 2 of this motor is designed similar to that of an ordinary induction machine and comprises winding 5 with two phases displaced relative to each other in space by 90 electrical degrees. The motor also has internal stator 4, i.e., a stationary stack of electrical steel laminations, designed to reduce the reluctance of its magnetic circuit. Rotor 3 is a hollow thin-wall (less than one millimetre thick) cylinder of a non-magnetic metal or alloy (usually aluminium). The rotor is fixed on bushing 1 through which it transmits rotation to the shaft. With such a design the rotor has a negligible inertia which is very important from the viewpoint of quick response of the motor to the appearance and disappearance of a signal.

One of the stator winding phases is the field winding which, during operation of the automatic equipment, is energized by a constant-value a.c. voltage U_{exc} . The other phase is the control winding into which the so-called signal is fed in the form of an a.c. voltage U_{sig} of the same frequency (Fig. 26-6).

The signal voltage is shifted 90° in phase from the excitation voltage and can be varied from zero to a definite value.

The asymmetrical two-phase system of voltages \dot{U}_{exc} and \dot{U}_{sig} (Fig. 26-6a) can be resolved into a positive-sequence voltage system (Fig. 26-6b) with the magnitude

$$\dot{U}_1 = \frac{\dot{U}_{exc} + j\dot{U}_{sig}}{2}$$

and a negative-sequence voltage system (Fig. 26-6c) with the mag-

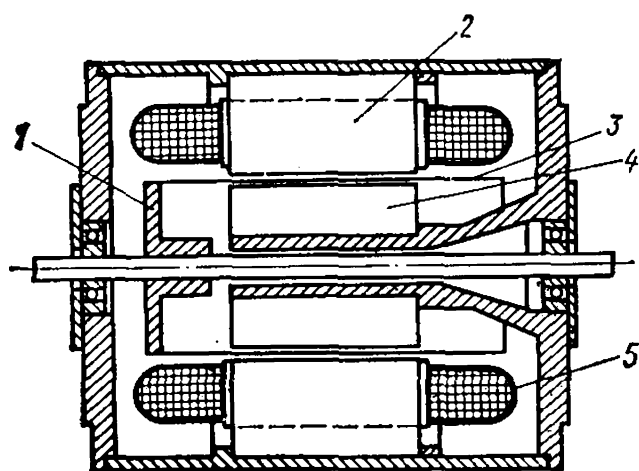


Fig. 26-5. Two-phase hollow-rotor induction machine:

1 — rotor bushing; 2, 4 — stator; 3 — hollow rotor; 5 — stator winding

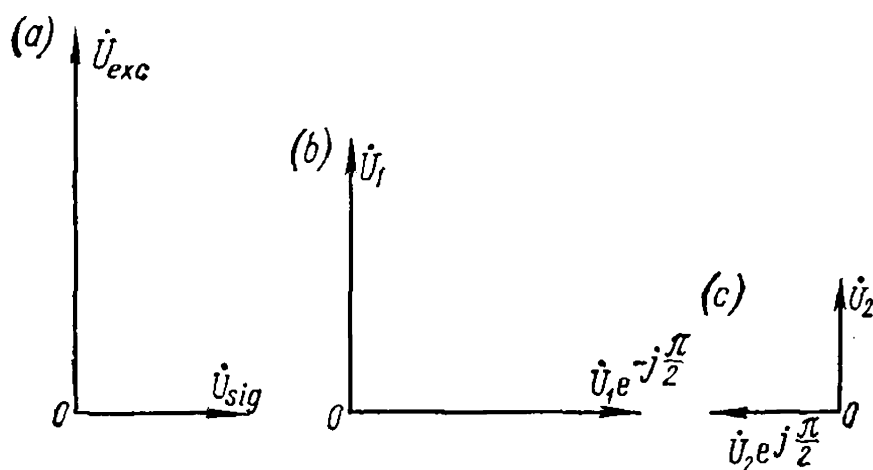


Fig. 26-6. Two-phase system voltages:
 a — winding voltages; b — positive-sequence voltages;
 c — negative-sequence voltages

nitude

$$\dot{U}_2 = \frac{\dot{U}_{exc} - j\dot{U}_{sig}}{2}$$

When the signal voltage U_{sig} is zero, $U_1 = U_2$, the motor develops no torque, and the rotor remains standstill. When $U_{sig} > 0$, we have $U_1 > U_2$ and the motor develops a torque which is practically proportional to the signal voltage U_{sig} . If this torque exceeds the braking torque on the shaft, the motor will immediately begin to rotate.

Hollow-rotor machines are also widely used as tachogenerators. The field winding is connected to a source of a constant a.c. voltage, and as a result a pulsating magnetic flux Φ_{exc} appears (Fig. 26-7). When the rotor is at standstill, this flux will induce in the rotor only the so-called transformation e.m.f., as a result of which there appear the currents i_1 (Fig. 26-7), whose flux acts along the axis of the field winding and does not induce any e.m.f. in the control winding. But, with the rotor running, rotational e.m.f.s are induced in the winding and currents i_2 (Fig. 26-7) appear, whose flux, being directed along the axis of the control winding pulsates with the frequency of the field winding current and induces in the control winding an e.m.f. whose magnitude is practically proportional to the speed of rotation.

In automatic control systems a tachogenerator serves as a speed measuring element acting on some circuit element through the e.m.f. induced in the control winding.

Rotary Transformers. In automatic control systems it is sometimes necessary to obtain voltages which are functions of the displacement angle α of a certain mechanism. These voltages, in turn, act on other elements of the

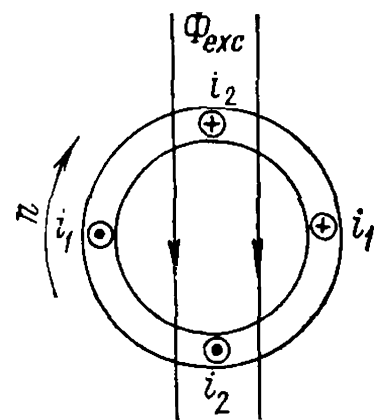


Fig. 26-7. Rotor currents of a tachogenerator

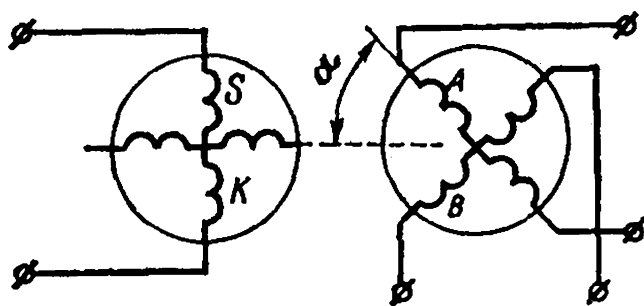


Fig. 26-8. Winding connections of a sine-cosine rotary transformer

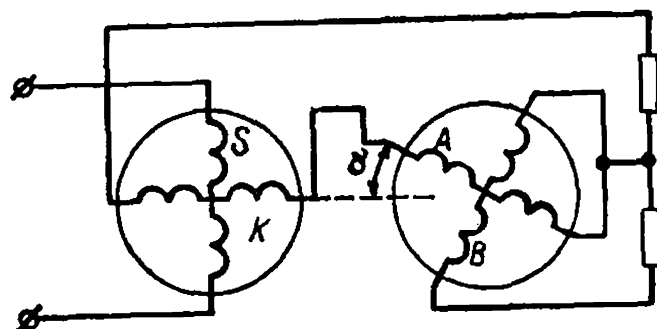


Fig. 26-9. Winding connections of a linear rotary transformer

system, which perform regulation as a function of the angle of displacement.

For such purposes use is made of rotary transformers (Fig. 26-8), similar in design to normal induction machines, with two windings (S , K) on the stator and two similar windings (A , B) on the rotor. In such transformers steps are taken to have the magnetic density distributed along the air-gap as near as possible to sinusoidal. If in these conditions one of the stator windings, for instance, winding S in Fig. 26-8, is fed with alternating current, e.m.f.s will be induced in rotor windings A and B that are proportional to $\sin \alpha$ and $\cos \alpha$, respectively. Such a transformer is called a sine-cosine transformer, and the voltages in windings A and B will also be proportional to $\sin \alpha$ and $\cos \alpha$ if these windings and their external loads are the same. Otherwise distortions arise due to the quadrature flux, which is directed perpendicular to the axis of winding S . They can be reduced to a minimum if we close winding K on a small external resistance. Such a procedure is called balancing.

If the windings are connected as shown in Fig. 26-9 and winding S is fed with an alternating current, the voltage across the terminals of the series-connected windings A and K , for values of α from zero to 65° , will vary practically in direct proportion to the angle α . To achieve balance, winding B is closed on an external resistance. Such a rotary transformer is called a linear transformer.

PART FOUR

ALTERNATING-CURRENT COMMUTATOR MACHINES

Chapter

27

GENERAL THEORETICAL PROBLEMS

27-1. Brief History of A. C. Commutator Machines

The first attempts to use the series d.c. motor for operation from a single-phase a.c. circuit were made as far back as the middle eighties of the past century. Indeed, since in a series motor the change in current occurs simultaneously in the armature and in the field winding, the torque developed by the motor does not depend on the direction of the current. To improve the performance of the motor, its magnetic system was completely made of steel laminations, and to avoid the harmful effects of the pulsating armature-reaction magnetizing force, a compensating winding was used in the form of a short-circuited turn, its axis coinciding with the armature-winding axis.

By this time a single-phase repulsion motor was developed, in which, as in an induction motor, the stator and rotor are coupled only electromagnetically, but in which, nevertheless, all the properties of a single-phase series motor are retained.

The invention of the three-phase induction motor by M. Dolivo-Dobrovolsky opened a new era in electrical machine design and for some time interrupted the development of the a.c. commutator machine. Only at the beginning of the current century, when it became obvious that the induction motors have unsatisfactory regulation characteristics and a power factor less than unity, especially low-speed motors, or at small loads, interest in a.c. commutator machines, chiefly motors, revived. Indeed, by providing an asynchronous a.c. motor with a commutator, we obtain an entirely new type of motor close to the d.c. motor in its characteristics.

The a.c. commutator machine has found the widest application in electrical traction, in the form of a single-phase series motor. Experience gained in the operation of main-line electrified railways has shown that they can be operated successfully both on high-voltage direct current (3300 V) and on single-phase alternating current of reduced frequency (25 and $16\frac{2}{3}$ Hz). Today single-phase commercial-frequency current at 50 and 60 Hz is being widely used for railway traction in many countries.

During the period from 1900 to 1914 three-phase commutator machines developed in the following main directions:(a) as series and shunt

motors permitting continuous speed control to be accomplished within a wide range; (b) as motors with an improved power factor; (c) as phase advancers connected to the rotor circuit of induction non-commutator machines to improve the power factor, and (d) as a.c. generators for cascade and special installations.

Three-phase shunt motors were suggested as early as 1891, but began to be developed only in the current century. The most widely used motor was the inverted motor (i.e., fed from the rotor—see Sec. 29-7), with two sets of brushes on the commutator, a rigid speed characteristic and a variable speed range of 1 : 3 and more (the Schrage-Richter motor).

The asynchronous compensated and synchronized motors were substantially developed in the twenties of the present century to improve the power factor of electric power systems. The main idea of these machines is that we, so to say, build an additional commutator machine into a normal induction motor. The aim pursued is attained by this, but it is reached at the relatively high cost of disregarding the major advantages of the normal induction motor, i.e., its low cost, cheap maintenance and reliability in operation. Therefore, at present it is preferred to improve the power factor of low-power motors by the use of static capacitors, and of high-power motors by the use of phase advancers.

The first phase advancers with rotor excitation were suggested in the mid-nineties of the past century. Phase advancers of this system improve the power factor only when under load. A number of other systems have been suggested, both with self-excitation and with separate excitation. Phase advancers, notwithstanding their additional cost, are a valuable means of improving the power factor of induction motors and are often used for this purpose. By appropriate selection of the phase advancer, an induction motor can be made to operate with a leading power factor.

A.c. commutator machines are widely used in cascades and serve both for speed regulation at higher efficiency and for power factor compensation. The fundamental types of cascades were developed during the period from 1908 to 1916 (the Kramer cascade and Scherbius cascade) and make it possible to vary the speed either only below synchronism, or above and below it within the range of $\pm 25\%$. The cascades have found a certain use in those branches of industry where the required range of speed control does not exceed the ratio 1 : 2.

The a.c. commutator machine can be used as a variable-frequency generator operating at constant speed. One of the best systems of this kind, the so-called compensated commutator generator with independent a.c. excitation, was developed in the USSR by N. Yapolsky and M. Kostenko in 1921. In 1946-47 M. Kostenko suggested a circuit with a commutator generator which makes it possible to main-

tain a constant frequency and constant voltage under variations in speed of the prime mover.

Thus, the induction commutator machine should be considered as a special type of electrical machine, which, although it cannot compete with normal types of electrical machines, still finds rather wide and multiform application in a number of special cases.

27-2. E.M.F.s Induced in Armature of an A. C. Commutator Machine

In the general case two kinds of e.m.f.s are induced in the armature of an a.c. commutator machine: the transformer e.m.f. E_{tr} , since the field and armature windings linked by an alternating field may be considered as the primary and secondary windings of a transformer, and the rotational e.m.f. E_{rot} developed in the armature winding when it revolves in the magnetic field as in a d.c. machine. Let us consider the properties of these e.m.f.s first for the simplest case of a single-phase commutator machine.

Transformer E.M.F. Produced by a Pulsating Field in the Armature of a Single-Phase Commutator Machine. Assume that the field winding FW (Fig. 27-1) produces a flux Φ_m pulsating with a frequency f and that the armature Arm is stationary in space, i.e., $n = 0$. Since the plane of coil section 1-1 is parallel to the lines of the flux Φ_m , its transformer e.m.f. E_{tr} equals zero. In coil section 2-2 located on one side of section 1-1 the e.m.f. E_{tr} has one sign, for instance "cross-to-point", while in coil section 3-3 arranged symmetrically about section 2-2 on the other side of coil section 1-1 the e.m.f. E_{tr} has the opposite sign, "point-to-cross". Thus, in the conductors of the armature winding arranged on different sides of the axial line of the field winding e.m.f.s of different signs are induced. The maximum value of the transformer e.m.f. E_{tr} across the brushes A and B is obtained when they are placed along the field winding axis (Fig. 27-1a). The frequency

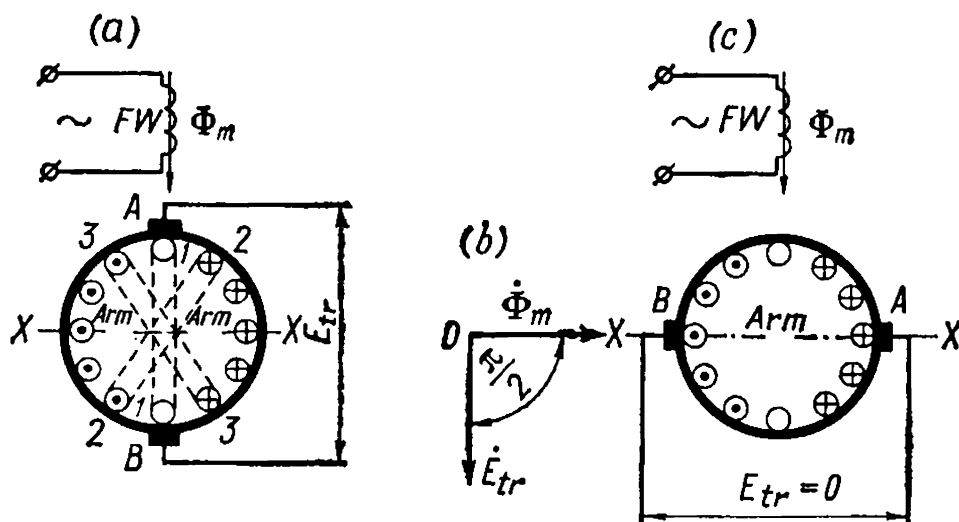


Fig. 27-1. E. m. f. E_{tr} produced in the armature winding by pulsating field at $n = 0$

of the transformer e.m.f. both in the coil sections and across the brushes is equal to the frequency f on the pulsating flux Φ or the corresponding exciting current i_{exc} .

In the following we shall assume that the flux Φ varies as a sine wave with time and consider for simplicity that the flux is sinusoidally distributed over the armature periphery.

The e.m.f. E_{tr} also varies with time sinusoidally, its effective value being equal to

$$E_{tr} = \pi \sqrt{2} f \omega_a k_w \Phi_m \quad (27-1)$$

where Φ_m is the magnetic flux amplitude.

If N is the number of armature-winding conductors, and $2a$ the number of parallel branches, then $\omega_a = \frac{N}{2 \times 2a}$. In addition, with sinusoidal field distribution over the armature periphery, the winding factor of a single-phase armature is $k_w = \frac{2}{\pi}$ (the ratio of the diameter to the half-circumference). For these conditions we have

$$E_{tr} = f \frac{N}{a} \frac{\Phi_m}{\sqrt{2}} \quad (27-1a)$$

The e.m.f. E_{tr} lags behind the flux Φ_m by 90° in phase (Fig. 27-1b).

If we place brushes A - B on the geometrical neutral X - X (Fig. 27-1c), then $E_{tr} = 0$, since each path of the armature winding includes the same number of coil sections with opposed e.m.f.s.

When the brushes are shifted from the neutral by an angle α we have

$$E_{tr\alpha} = E_{tr} \sin \alpha \quad (27-2)$$

Transformer E.M.F. Produced by a Circular Rotating Field. Assume that the flux Φ_m rotates in space clockwise at a speed $n_1 = \frac{f}{p}$ and that $n = 0$ as before. The rotating flux can be replaced by two equal magnetic fluxes Φ_x and Φ_y pulsating with the frequency f and shifted 90° in time and in space (Fig. 27-2). If brushes A and B are shifted from the line X - X by an angle α , the flux Φ_x produces an e.m.f. $E_{tr.x} = E_{tr} \cos \alpha$ across the brushes, and the flux Φ_y produces an e.m.f. $E_{tr.y} = E_{tr} \sin \alpha$, these e.m.f.s, as well as the fluxes which produce them, being shifted in time by 90° . Consequently,

$$E_{tr(A-B)} = \sqrt{E_{tr.x}^2 + E_{tr.y}^2} = E_{tr} \quad (27-3)$$

i.e., a circular rotating field produces a transformer e.m.f. across the brushes which varies with a frequency f and retains a constant value E_{tr} irrespective of the position of the brushes on the commutator.

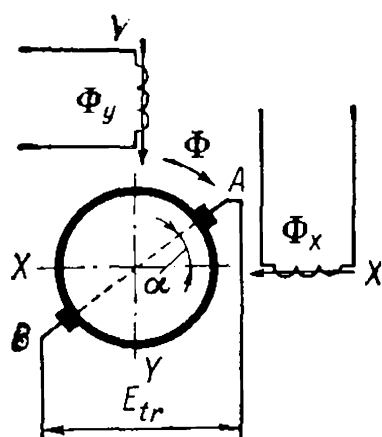


Fig. 27-2. E. m. f. E_{tr} induced by a rotating field at $n = 0$

The phase of the e.m.f. E_{tr} with respect to the flux Φ_m is the same as in Fig. 27-1b.

Rotational E.M.F. Produced by a Pulsating Field. Assume first that $\Phi_m = \text{const}$, i.e., that we have a d.c. machine. If an armature runs in this field at a speed n , then, as we already know: (a) in each coil of the armature winding an alternating e.m.f. with a frequency $f_{rot} = pn$ is induced; (b) the e.m.f. E_{rot} is produced across the brushes with a frequency $f = 0$, corresponding to the flux Φ stationary in space and constant in time; (c) at a given speed of armature rotation n , the e.m.f. E_{rot} attains its maximum value if the brushes are placed on the geometrical neutral and, if the brushes are shifted from the neutral by 90° , the e.m.f. $E_{rot} = 0$; the voltage in the general case being $E_{rot\alpha} = E_{rot} \cos \alpha$, where α is the angle by which the brushes are shifted from the neutral; (d) a change in speed n leads to a change in the magnitude and frequency of the coil section e.m.f., but the e.m.f. across the brushes changes only in magnitude ($E_{rot} \propto n$) and retains the frequency $f = 0$.

Assume now that the excitation flux Φ_m pulsates with a frequency f . In each coil section of the armature winding there now appears an e.m.f. which is the result of superposition of two e.m.f.s—the rotational e.m.f. with a frequency $f_{rot} = pn$ and the transformer e.m.f. with the frequency f .

The properties of the rotational e.m.f. across the brushes are different. Let us suppose that the brushes are placed on the line $X-X$ (Fig. 27-3a), i.e., in such a position that $E_{tr} = 0$ and that the flux varies sinusoidally with time (curve 1 in Fig. 27-3b). For a given speed n the e.m.f. $E_{rot} \propto \Phi_m$. Consequently, the e.m.f. E_{rot} also varies sinusoidally with time, and passes through zero and attains its maximum value in step with the flux Φ_m (curve 2 in Fig. 27-3b). With a change in speed, the e.m.f. E_{rot} varies only in magnitude, while the frequency as before remains equal to the frequency f of the pulsating flux.

If we reverse the direction of armature rotation ($-n$) without any change in the excitation circuit, we shall obtain a rotational e.m.f. E_{rot} which is in antiphase with the flux Φ (dotted line 3 in Fig. 27-3b and, correspondingly, the vector \dot{E}_{rot} in Fig. 27-3c). Thus, we may say that the frequency of the e.m.f. across the brushes does not depend on the speed of armature rotation and is determined only by the frequency f of the excitation flux; that the rotational e.m.f. is in phase or in antiphase with the

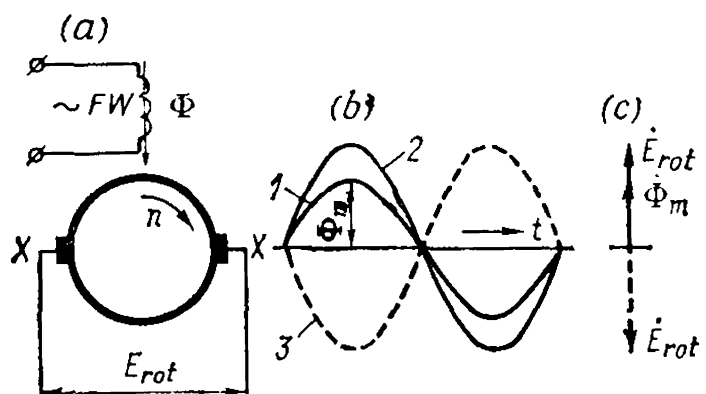


Fig. 27-3. Rotational e. m. f. E_{rot} produced in the armature winding by a pulsating field

flux Φ_m ; and that the e.m.f. E_{rot} reaches its maximum value when the brushes are on the geometrical neutral line, it being equal to

$$E_{rot} = \sqrt{2} \pi f_{rot} \omega_a k_w \Phi_m \quad (27-4)$$

or, since $\omega_a = \frac{N}{2 \times 2a}$ and $k_w = \frac{2}{\pi}$

$$E_{rot} = f_{rot} \frac{N \Phi_m}{a \sqrt{2}} = \frac{p n N \Phi_m}{a \sqrt{2}} \quad (27-5)$$

When brushes $A-B$ are shifted from the neutral by an angle α , we obtain the e.m.f.

$$E_{A-B} = \sqrt{E_{tr}^2 \sin^2 \alpha + E_{rot}^2 \cos^2 \alpha}$$

with the frequency f , since each e.m.f. has this frequency across the brushes.

E.M.F. Across the Brushes with a Circular Rotating Field. If the magnitude of the excitation flux is specified ($\Phi_m = \text{const}$) and stationary in space as in d.c. machines, the e.m.f. across the brushes has a definite value and the frequency $f = 0$. Assume now that the flux Φ_m , remaining constant in magnitude, begins to rotate (Fig. 27-4a). If the brushes remain stationary as before, the e.m.f. across the brushes varies with the same speed as the flux Φ_m ; in other words, *the frequency of the rotational e.m.f. across the brushes is determined, as with a pulsating flux, only by the excitation flux frequency and does not depend on the speed of armature rotation.*

To determine the magnitude of the rotational e.m.f., let us resort to the same procedure as before, namely, let us replace the rotating magnetic flux by two equivalent fluxes Φ_x and Φ_y pulsating with a frequency f and shifted relative to each other by 90° in time and space. Let us suppose that the brush line coincides with the axis of one of the fluxes, for instance, flux Φ_x (Fig. 27-4a). This flux produces only a transformer e.m.f. across brushes $A-B$, which is determined from formula (27-1) and lags behind Φ_x by 90° (Fig. 27-4b).

The flux Φ_y produces only the rotational e.m.f. across brushes $A-B$, with the same frequency f as the transformer e.m.f.; here when the

field and the armature rotate concurrently, as shown in the figure, their relative speed will be $n_1 - n$; if they rotate in opposite directions, we have the speed $n_1 + n$. In the first case the e.m.f. \dot{E}_{rot} , whose phase is determined by the flux $\dot{\Phi}_y$, must be directed against \dot{E}_{tr} , so that the resultant e.m.f. across the brushes $\dot{E}_{A-B} = \dot{E}_{tr} - \dot{E}_{rot}$.

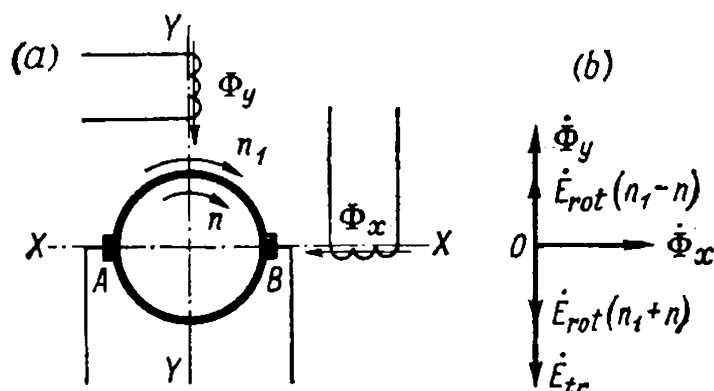


Fig. 27-4. E. m. f. produced in the armature by a rotating field when $n = 0$

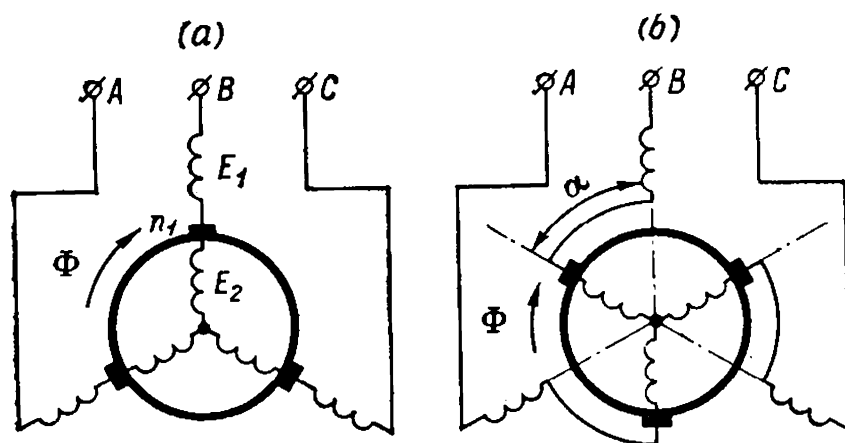


Fig. 27-5. E. m. f. across brushes of a three-phase (polyphase) commutator machine:
 a — the angle $\alpha = 0^\circ$; b — brushes are shifted opposite to field rotation

When $n = n_1$, we have $\dot{E}_{rot} = \dot{E}_{tr}$ and $\dot{E}_{A-B} = 0$, since in this case the field is stationary with respect to the rotating armature. In the second case $\dot{E}_{A-B} = \dot{E}_{tr} + \dot{E}_{rot}$.

By using formulas (27-1) and (27-4), we get

$$E_{A-B} = E_{tr} \mp E_{rot} = \sqrt{2}\pi (f \mp f_{rot}) \omega_a k_w \Phi_m \quad (27-6)$$

The minus sign corresponds to armature rotation in the direction of the rotating field, the plus sign to rotation in the reverse direction.

If the fluxes Φ_x and Φ_y , while remaining displaced by 90° in time and space, are not equal in magnitude, then

$$E_{A-B} = E_{tr} \mp E_{rot} = \pi \sqrt{2} f \omega_a k_w \Phi_x \mp \pi \sqrt{2} f_{rot} \omega_a k_w \Phi_y \quad (27-7)$$

In a still more general case, the fluxes Φ_x and Φ_y may be displaced in time by an angle other than 90° . Here the e.m.f.s E_{tr} and E_{rot} are summated vectorially, i.e.,

$$\dot{E}_{A-B} = \dot{E}_{tr} \mp \dot{E}_{rot}$$

E.M.F. Across the Brushes of a Polyphase Commutator Machine.

Assume the most frequent case of a three-phase commutator machine, i.e., $m = 3$. The armature phase windings are delta-connected which can always be reduced to an equivalent star. If the axes of the stator and rotor windings coincide (Fig. 27-5a), the e.m.f.s induced in them by the rotating flux Φ_m also coincide in phase.

When $n = 0$, the e.m.f. of the rotor, reduced to a star connection, will be

$$E_2 = \pi \sqrt{2} f \omega_2 k_{w2} \Phi_m \quad (27-8)$$

Correspondingly, the stator-phase e.m.f. is

$$E_1 = \pi \sqrt{2} f \omega_1 k_{w1} \Phi_m \quad (27-9)$$

Hence

$$E_1 = k_e E_2 = E'_2 \tag{27-10}$$

where

$$k_e = \frac{\omega_1 k_{w1}}{\omega_2 k_{w2}}$$

and E'_2 is the e.m.f. of the rotor phase across the brushes referred to the e.m.f. of the stator phase.

When the rotor is in motion, $E'_{2s} = sE'_2$. If we shift the brushes through an angle α , for instance, *against the rotation* of the flux Φ_m , the e.m.f. across the brushes will not change in magnitude, but will begin to lead the e.m.f. E_1 in phase by the angle α , since in these conditions the flux Φ first meets the rotor winding axis and then, with a phase shift equal to α , the stator winding axis. With the brushes shifted in the direction of flux rotation, the e.m.f. across the brushes will lag on the e.m.f. E_1 by the angle α . Hence

$$\dot{E}'_{2s} = sE'_2 e^{\mp i\alpha} \tag{27-11}$$

27-3. Armature Currents of an A. C. Commutator Machine

The main feature of armature supply of an a.c. commutator machine, in contrast to a normal d.c. machine, is that the number of armature feed points per pole pair may be more than two, the angles between adjacent brushes being in the general case not equal to each other.

Single-Phase Machines. The simplest way of feeding current to the armature of a single-phase commutator machine is, as in a d.c. machine, through two diametrically arranged points on the potential circle of the commutator (Fig. 27-6a). The second way is through four points on two mutually perpendicular axes—the method used in so-called compensated single-phase motors and corresponding to the feeding of a rotary amplifier armature. Here two independent systems of currents exist, as it were, in the armature, adding together in some parts and subtracting in others (Fig. 27-6b). The third way of feeding, through

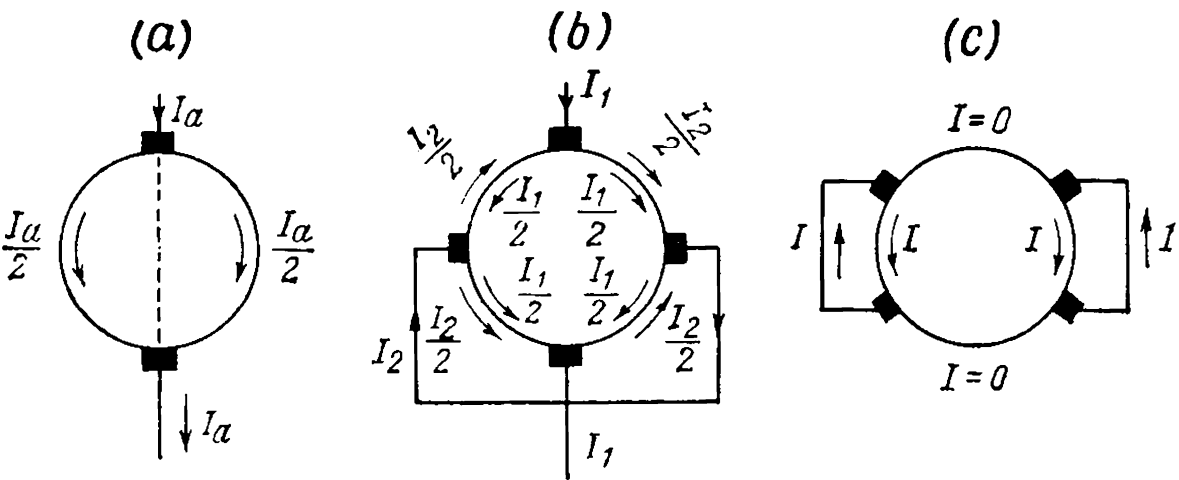


Fig. 27-6. Systems of feeding single-phase machine armatures

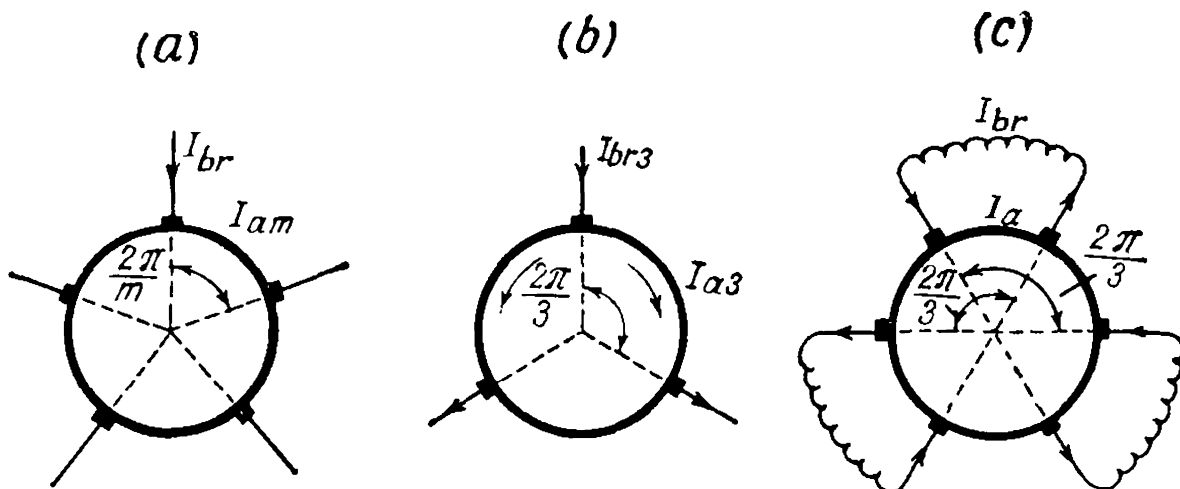


Fig. 27-7. Feeding of polyphase machine armatures

two systems of symmetrical movable brushes, which can converge and diverge, is used in single-phase repulsion motors (see Chap. 28). Here only those parts of the armature winding that are connected through the brushes are live, while the other armature sections are dead (Fig. 27-6c).

Polyphase Machines. When the armature is fed with a polyphase symmetrical current, the armature winding is mesh-connected. The current I_{br} flowing through a brush into the armature winding is the vector difference I_a of two phase currents of this winding. If the number of phases is m , the angle between two phase currents is $\frac{2\pi}{m}$ (Fig. 27-7a). Thus,

$$I_{br} = 2I_{a \cdot m} \sin \frac{\pi}{m} \quad (27-12)$$

With a three-phase current (Fig. 27-7b) we have

$$I_{br3} = 2I_{a3} \sin \frac{\pi}{3} = I_{a3} \sqrt{3} \quad (27-13)$$

With polyphase current the armature may be fed from an open polyphase system. The distance between the armature feed points may be varied by moving the brushes. Figure 27-7c illustrates such a system for a three-phase Schrage-Richter motor (see Chap. 29). It can be seen that only the armature sections between interconnected brushes are live, the other sections being dead because the currents in the outer sections of all phases balance each other. It may be assumed that now the current flowing through a brush I_{br} is equal to the current I_a flowing in the inner section.

27-4. Armature Winding Magnetizing Force of a Polyphase Commutator Machine

A drum armature winding of an a.c. commutator machine is designed in the same way as in d.c. machines, viz., of form-wound coils or bars forming a turn. One side of such a turn is placed in the upper

layer of the winding, the other in the lower one. The winding generally has a full or nearly full pitch, but in some special cases a considerably shorter pitch is used (for example, in the Scherbius machine, see Chap. 31).

Full-Pitch Winding. If a machine has an even number of phases, for instance six, the current will flow through the armature in the same manner as in each of the separate layers dividing the winding into a number of phase belts equal to the number of armature phases (Fig. 27-8a). Here the time phases of the currents in the upper and lower layers of each slot are shifted by 180° , but since the lower layer contains the return conductor of each phase, the result will be that the direction of the currents in opposite bars of the upper and lower layers is the same. These currents induce magnetizing forces that coincide in phase; for example, the currents i_{a1} , $-i_{a4}$, i_{a2} , $-i_{a5}$, etc., have in Fig. 27-8a identically directed arrows in both layers. In the belts *a*, *b*, *c*, *d*, *e* and *f* the upper and lower layers of the winding carry currents in the same direction. Thus, the six-phase current star of the upper layer coincides with the current star of the lower layer and forms the resultant six-phase system of magnetizing forces from \vec{F}_a to \vec{F}_f shown in Fig. 27-8b. If the machine has an odd number of phases, for example $m = 3$, as shown in Fig. 27-9a, then the resultant armature current system is formed with a double number of belts for current distribution in only the upper or the lower layer of the winding. The currents in the upper and lower layers are here phase-shifted by 180° with respect to the magnetizing forces produced by them. The combined effect of the upper- and lower-layer magnetizing forces on the magnetic system of the machine can be shown as a resultant current flowing through the conductors of the upper and lower layers in the same direction.

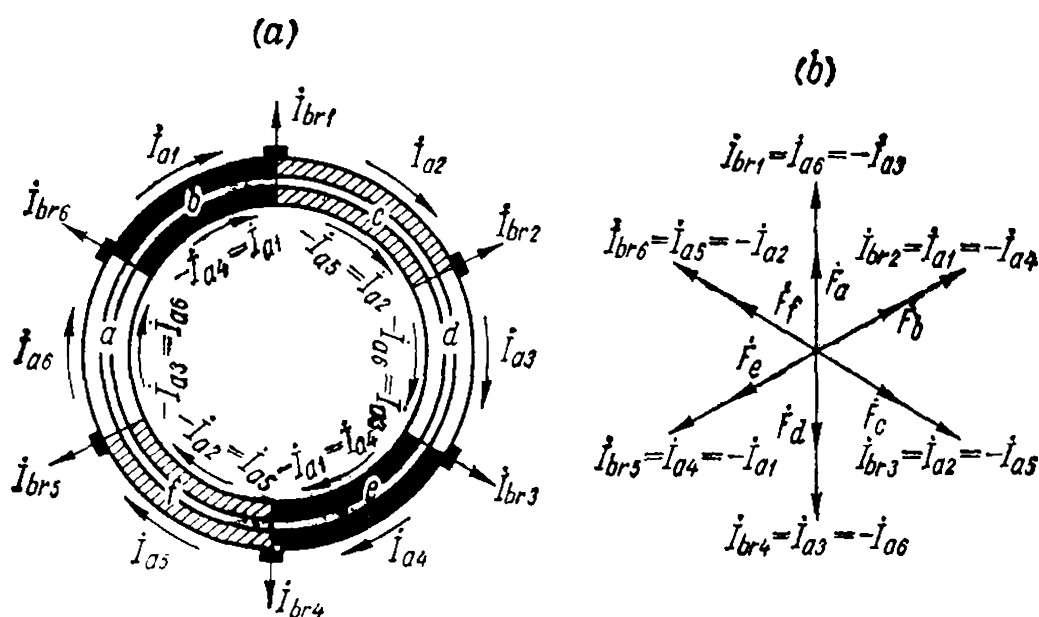


Fig. 27-8. Phase belts with an even number of phases

The direction of the upper-layer currents for the most widely used three-phase system is shown in the timing chart (Fig. 27-9b) by the vectors \dot{I}_{a1} , \dot{I}_{a2} and \dot{I}_{a3} , and that of the lower-layer current by vectors $-\dot{I}_{a1}$, $-\dot{I}_{a2}$ and $-\dot{I}_{a3}$. Here six belts are formed with the equivalent currents shown in Fig. 27-9b by vectors \dot{F}_a , \dot{F}_b , ..., \dot{F}_f and representing the magnetizing forces to the scale of currents and which the currents \dot{I}_{br1} , \dot{I}_{br2} and \dot{I}_{br3} flowing through the brushes will coincide with in phase. Thus, the magnetizing forces of an armature with a diametral-pitch winding give the same results with an odd number of phases as of an armature fed from a system with a double number of phases.

A comparison of the diagrams in Figs. 27-8 and 27-9 shows that the equivalent armature magnetizing force with a six-phase system is $\frac{2}{\sqrt{3}}$ times greater than that of a three-phase system, since the magnetizing forces of the upper and lower layers add together algebraically in the first case and vectorially in the second. Owing to this, with a three-phase system of brush distribution along the commutator, the current flowing through a brush is 1.15 times that in a six-phase system.

Fractional-Pitch Windings. If the winding pitch is $y = \frac{2}{3}\tau$, i.e., the pitch shortening is $\frac{1}{3}\tau$, the current will flow through the armature windings as shown in Fig. 27-10. It can be seen that the winding now forms as many equivalent belts as there are brush system phases, and no belt doubling takes place as previously. The magnetizing force curve of such a system noticeably differs from a sine wave, and, as a result, strongly pronounced space harmonics appear in it. Such a winding is used, for instance, in the Scherbius machine, described in Chap. 31.

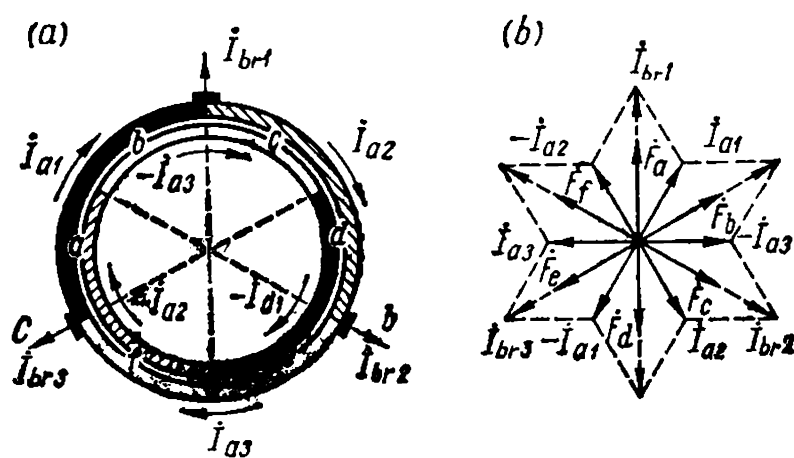


Fig. 27-9. Phase belts with an odd number of phases

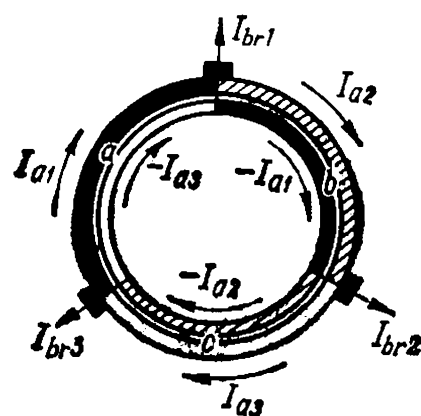


Fig. 27-10. Phase belts of winding with pitch $y = \frac{2}{3}\tau$

27-5. Commutation in A. C. Commutator Machines [238]

Commutation in Single-Phase Machines. Suppose the current i_a varies with time sinusoidally (Fig. 27-11). Current commutation may start at any moment, i.e., at any instantaneous value of the current i_a . The commutated current at the initial moment will differ somewhat in strength from the current at the final moment of commutation, but at normal motor speeds this circumstance is of no importance, since the commutating period T_{com} usually lasts a maximum of 0.001 s.

During the commutating period two e.m.f.s are produced in the coil section undergoing commutation: the reactive e.m.f. e_r and the transformer e.m.f. $e_{tr.com}$.

The reactive e.m.f. depends on the magnitude of the change in the current when the coil section passes from one parallel path to the other. Consequently, it reaches its maximum value when $i_a = I_m$ and is zero when $i_a = 0$ (Fig. 27-11). Thus, the reactive e.m.f. is in phase with the current i_a . The effective value of the reactive e.m.f. is determined from the same formula as for the d.c. machine (see Vol. I, Chapter 5), namely,

$$F_r = 2\omega_{cs}v_a l \Lambda' A \quad (27-14)$$

where A is the effective value of the rotor current loading.

The transformer e.m.f. appears in the coil section undergoing commutation owing to the pulsations of the pole flux Φ_{exc} (Fig. 27-12). If the winding has a full pitch $y = \tau$ and if the flux changes sinusoidally with time, then

$$E_{tr.com} = \pi \sqrt{2} f \omega_{cs} \Phi_m \quad (27-15)$$

Here Φ_m is the amplitude of the flux passing into the armature. In further discussion the subscript *com* in $E_{tr.com}$ will be omitted.

The transformer e.m.f. lags behind the flux Φ_{exc} and, therefore, behind the current I_{exc} by 90° . In series motors (see Fig. 28-1), in which the current I flows through the field and armature windings connected in series, the e.m.f.s E_r and E_{tr} are at 90° with respect to each other; they consequently summate vectorially and form in the coil undergoing commutation an e.m.f.

$$E_{res} = \sqrt{E_r^2 + E_{tr}^2} \quad (27-16)$$

Under the influence of this e.m.f. a current $I_{com} = \frac{E_{res}}{z_{com}}$ is produced in the coil section, z_{com} being the coil section impedance, including the contact resistance of the brushes. Usually z_{com} is small and, therefore, the current I_{com} may reach a high value, exceeding 10-12 times the normal current of the coil section. This leads to very non-uniform distribution of the current density under the brush and may cause heavy sparking of the motor.

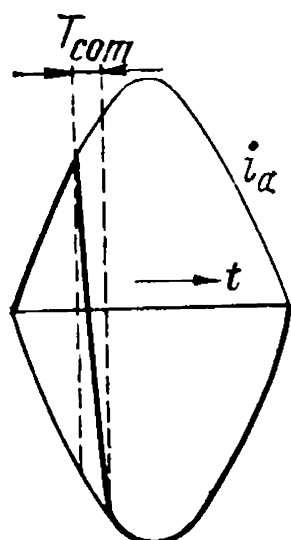


Fig. 27-11. Commutation of current in a single-phase commutator machine

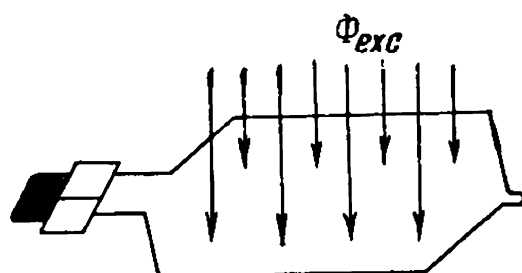


Fig. 27-12. Flux Φ_{exc} in a coil section undergoing commutation

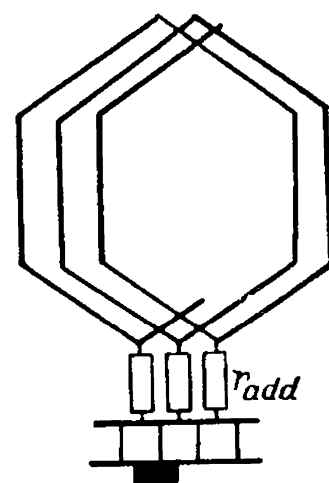


Fig. 27-13. Additional resistors r_{add}

To reduce the current I_{com} we may:

- (a) increase the impedance z_{com} ;
 - (b) reduce the e.m.f. E_{res} by reducing one or both of its components;
- and
- (c) compensate the e.m.f.s E_r and E_{tr} by introducing additional e.m.f.s into the commutating circuit.

Methods of the first kind include the selection of hard grades of brushes having a large contact resistance, and the introduction of special additional resistors r_{add} between each armature-winding coil section and the corresponding commutator bar (Fig. 27-13).

If the motor current I is given, then, other conditions being equal, the selection of hard brushes which allow a lower current density to be used leads to an increase in the required working surface of the brushes and to a corresponding increase in the mechanical losses due to friction between the brushes and the commutator, and losses in the brush contact.

The additional resistors are usually made of a material with a relatively high resistivity and are inserted in the same slots as the armature winding. A high current density may be allowed in them, since each additional resistor conducts the current for a comparatively short interval of time, during which commutation takes place in the section corresponding to the given resistor.

Additional resistors are mainly used in single-phase traction motors. They are most favourable for improving the commutating conditions of a motor, but considerably complicate motor design, lower the efficiency of the motor under load by 1 to 2% and increase its heating.

Furthermore, in starting a motor, when it is still at standstill, only one of the groups of additional resistors carries current; there-

fore, if the motor does not gain speed immediately, this group may overheat and burn out. For this reason the use of additional resistors was at one time discontinued, but at present they are being used again in single-phase 25- and 50-Hz traction motors, since they make it possible to increase the voltage across the commutator and, with the appropriate design, ensure reliable operation of the motor under heavy loads and prolonged train startings.

When we speak of decreasing the e.m.f. E_{res} , we must bear in mind, first of all, the e.m.f. E_{tr} . Indeed, the reactive e.m.f. E_r appearing in a.c. commutator machines is, in its origin, the same as in d.c. machines. It is equal to zero at starting and depends on the speed and load of the motor when the latter is running [see equation (27-14)]. Consequently, to compensate the e.m.f. E_r in a.c. commutator machines, we may use the same method as for d.c. machines, viz., employ additional series-excitation poles.

Contrary to the reactive e.m.f., the transformer e.m.f. E_{tr} becomes manifest during any operating conditions, i.e., both with the armature stationary ($n=0$) and running. But, when $n=0$, for instance, when starting the motor, the e.m.f. produced by compoles is zero, and, therefore, the e.m.f. E_{tr} is not compensated. Practice shows that satisfactory commutation is possible only when the non-compensated e.m.f. in the commutating section does not exceed 1.2 to 1.5 V.

Commutation in Three-Phase Machines. In the coil section of a three-phase, or, generally, of a polyphase machine undergoing commutation, the same e.m.f.s e_r and e_{tr} develop as in a single-phase machine. But the phenomenon occurring here is more complicated, as are the expressions for these e.m.f.s.

Let us first consider the e.m.f. e_r , supposing that we have a three-phase machine, i.e., that $m=3$. Let, for instance, the time T_{rev} , during which the armature makes one revolution be equal to $\frac{3}{2}T$, where T is the time of one period of the alternating current (Fig. 27-14). Since the brushes are distributed along the commutator equidistantly, the time during which the armature-winding coil section moves from one brush to the adjacent brush is

$$\frac{T_{rev}}{3} = \frac{1}{2} T$$

Assume that the internal currents in phases A , B and C vary sinusoidally and that the armature runs from left to right. Then, within the time $\frac{1}{2}T$ during which the coil section F passes from brush a to brush b , the current in this section varies according to the heavy portion of the sine line A from i_{aA1} to i_{aA2} . During the commutation period T_{com} section F passes from phase A to phase B , and the commutated current must change accordingly from i_{aA2} to i_{aB1} .

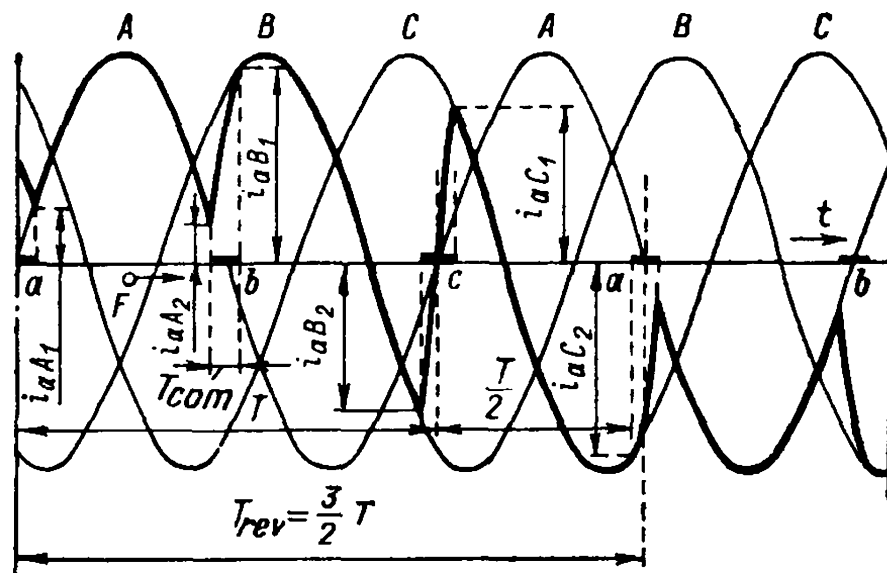


Fig. 27-14. Commutation of current in a three-phase commutator machine

Here and further it will be assumed that the commutation is rectilinear. Further current changes in the section, as it passes from one brush to the other, and during the commutating period, are similar (heavy lines in Fig. 27-14). It should be emphasized that the pattern of current change in different coil sections is not the same, since some coil sections are contacted by the brush and undergo commutation earlier than section F , and others later.

A glance at the figure shows that a change in the commutating current in a given coil section is equal to the instantaneous current difference between the two phases which the coil section belongs to before and after commutation. If we assume that the commutating period is infinitely small ($T_{com} = 0$), then this difference is actually the instantaneous value of the line current entering the brush which contacts the coil section undergoing commutation.

By using effective values, we can say that the mean effective value of the e.m.f. E_r during the commutating period T_{com} is determined by the vectorial difference of the effective values of the two phase currents or, consequently, by the effective value of the current passing through the brush (see Fig. 27-9a). If the brush width is equal to the width of one commutator interval, then $E_r = L_{cs} \frac{I_{br}}{T_{com}}$ or, since $I_{br} = 2I_a \sin \frac{\pi}{m}$ [see equation (27-12)], then

$$E_r = L_{cs} \frac{2I_a}{T_{com}} \sin \frac{\pi}{m} \quad (27-17)$$

where L_{cs} is the inductance of an armature-winding coil section.

Formula (27-17) differs from the corresponding formula (5-35), Vol. I, for d.c. machines only by the factor $\sin \frac{\pi}{m}$. Therefore, in poly-

phase commutator machines we have

$$E_r = 2\omega_{cs}v_a l \Lambda' A \sin \frac{\pi}{m} \quad (27-18)$$

When calculating the permeance Λ' , we should distinguish between windings with an odd and even number of phases. In Fig. 27-9a, a two-layer full-pitch armature winding of a three-phase machine ($m = 3$, an odd number) was shown schematically. It can be seen that while the conductors in the upper layer of the slot which is under brush a undergo commutation, conductors b in the lower layer of the same slot do not undergo commutation. Conversely, in a six-phase machine ($m = 6$, an even number) whose armature has a two-layer full-pitch winding, all the conductors in the slot under the brush undergo commutation simultaneously (see Fig. 27-8a). Thus, in the second case the magnitude of the commutating current in the slot is twice the value in the first case. Just as in d.c. machines (Vol. I, Sec. 5-8), we have, in machines with an *odd number of phases*

$$\Lambda' = \Lambda_s + \Lambda_t + \frac{l_{end}}{l} \Lambda_{end} \quad (27-19)$$

in machines with an *even number of phases*

$$\Lambda' = 2(\Lambda_s + \Lambda_t) + \frac{l_{end}}{l} \Lambda_{end} \quad (27-20)$$

If the width of the brush is greater than that of the commutator bar, then everything holds that was said in Vol. I, Sec. 5-7 about this question.

From equation (27-18) it follows that the e.m.f. e_r reaches its highest value when the electric loading A or, in other words, the current I attains its maximum. Consequently, the vector E_r of the reactive e.m.f. is in phase with the current vector I .

Let us now consider the e.m.f. E_{tr} appearing in the short-circuited coil section cut by the rotating magnetic flux Φ_m .

The value of E_{tr} depends on the number of series-connected turns w_{cs} in the short-circuited coil section, on the magnitude of the flux Φ_m and on its speed $n_1 \mp n$ with respect to the coil section. The minus sign relates to the case when the flux rotates in the same direction as the armature and, consequently, when the relative speed decreases, the plus sign when the flux and the armature rotate in opposite directions and the relative speed increases.

Hence

$$E_{tr} = \pi \sqrt{2} \frac{p(n_1 \mp n)}{60} w_{cs} \Phi_m = \pi \sqrt{2} (f \mp f_{rot}) w_{cs} \Phi_m \quad (27-21)$$

According to the general rule, the transformer e.m.f. vector E_{tr} lags behind the flux vector by 90° .

Since in the general case the e.m.f.s E_r and E_{tr} do not coincide in phase, the resultant e.m.f. in the short-circuited coil section is the vector sum of the e.m.f.s E_r and E_{tr} . As in single-phase machines, satisfactory commutation of three-phase commutator machines is possible only when the non-compensated e.m.f. in the coil section undergoing commutation is $E_{res} \leq 1.2$ to 1.5 V. Similarly, the means of improving commutation are the same as those indicated in Sec. 27-5. Special features of the commutation process of some types of machines are considered separately.

Chapter 28

SINGLE-PHASE COMMUTATOR MOTORS

28-1. Principle of Operation and Torque of a Single-Phase Series Motor

A schematic diagram of a single-phase series motor is given in Fig. 28-1. Here *Arm* is a normal d.c. machine armature; *FW* is a field winding connected in series with the armature; *CP* denotes commutating poles which, as in d.c. machines, are used for improving commutation; *CW* is a compensation winding which improves the power factor of the motor by compensating the armature reaction. The entire magnetic system of the motor is built up of steel laminations to minimize eddy-current losses. The brushes are on the geometrical neutral.

Since the field winding is connected in series with the armature, the current i_a in the armature and the magnetizing force F_{exc} produced by the poles coincide in phase. But the flux Φ_{exc} , which is produced by the magnetizing force F_{exc} and passes through the armature, lags behind the current by an angle γ (Fig. 28-2b) owing to the influence of the steel losses and, particularly, of the currents in the short-circuited armature-winding coil sections electromagnetically linked with the field winding of the motor (see Sec. 28-2 and Fig. 28-3). Assume that the current i_a and the flux Φ_{exc} vary sinusoidally with time, i.e., $i_a = I_{am} \sin \omega t$ and $\Phi_{exc} = \Phi_m \sin (\omega t - \gamma)$. Since a single-phase motor is essentially a d.c. motor fed with alternating current, the instantaneous value of the torque on the shaft of its armature can be expressed by equation (10-6), Vol. I for the electromagnetic torque of a d.c. motor, viz.,

$$M_t = \frac{Ni_a}{\pi} p\Phi_{exc} = \frac{NI_{am}}{\pi} p\Phi_m \sin \omega t \sin (\omega t - \gamma) \quad (28-1)$$

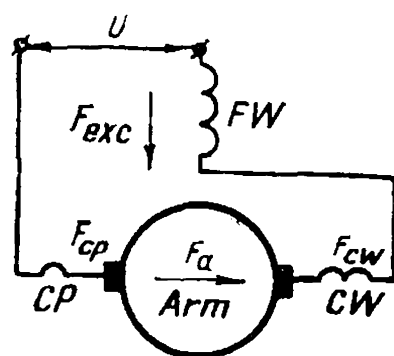


Fig. 28-1. Schematic diagram of a single-phase series motor

If we assume that the angle γ equals zero, then

$$M_t = \frac{NI_{am}}{\pi} p\Phi_m \sin^2 \omega t \quad (28-2)$$

Here the torque of a single-phase series motor remains positive during the whole period T , varying sinusoidally during the half-cycle from zero to the maximum value $M_m = \frac{NI_{am}}{\pi} p\Phi_m$ (Fig. 28-2a).

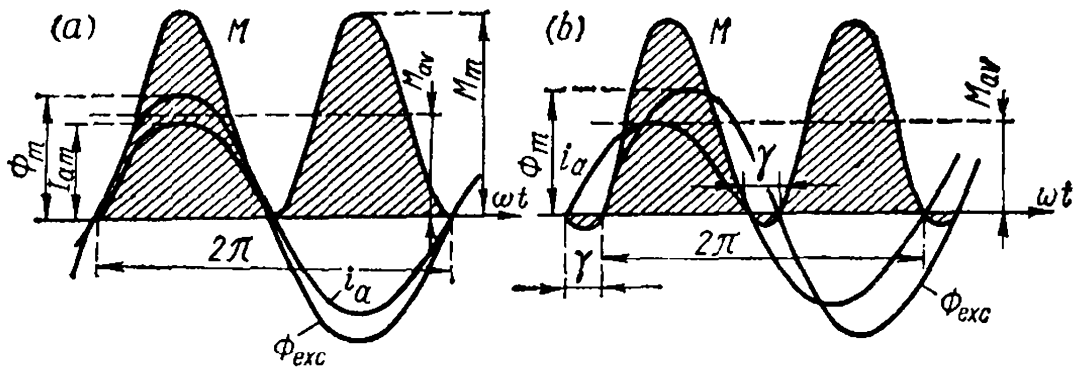


Fig. 28-2. Torque of single-phase commutator motors:
 a — armature current in phase with flux; b — armature current out of phase with flux

When the angle γ is not equal to zero, the motor torque has the form shown in Fig. 28-2b, i.e., it remains positive during the time interval corresponding to the angle $\pi - \gamma$ and has negative values during the interval corresponding to the angle γ . The average value of the torque on the motor shaft is

$$\begin{aligned}
 M_{av} &= \frac{1}{\pi} \int_0^\pi M_t dt = \\
 &= \frac{1}{\pi} \int_0^\pi \frac{NI_{am}}{\pi} \cdot p\Phi_m \sin \omega t \sin (\omega t - \gamma) dt = \\
 &= \frac{NI_{am}}{2\pi} p\Phi_m \cos \gamma = \frac{NI_a}{\pi} p \frac{\Phi_m}{\sqrt{2}} \cos \gamma \quad (28-3)
 \end{aligned}$$

Here I_a = effective value of the current in one parallel path of the motor armature winding
 Φ_m = main magnetic flux amplitude.

28-2. Vector Diagram of a Single-Phase Series Motor

When the current I flows in a motor, there exist the excitation magnetizing force F_{exc} , the armature magnetizing force F_a , the compensation winding magnetizing force F_{cw} , the magnetizing force F_{cp} of the compoles and the magnetizing force F_{com} produced by the currents in the coil sections undergoing commutation.

The field winding magnetizing force F_{exc} sets up the full flux of the poles Φ_m ; one part of this flux Φ_m penetrates the armature winding and forms the main flux of the motor, the other part links only with the field winding and forms the leakage flux $\Phi_{exc\sigma}$ of this winding.

The magnetizing forces F_a and F_{cw} are oppositely directed. Usually $F_a = F_{cw}$ and these magnetizing forces produce only leakage fluxes $\Phi_{a\sigma}$ and $\Phi_{cw\sigma}$ each of which is linked only with the corresponding winding.

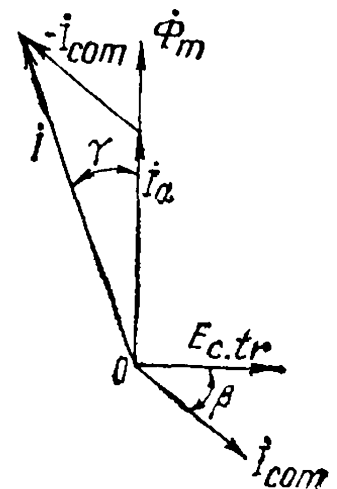


Fig. 28-3. Action of commutating current

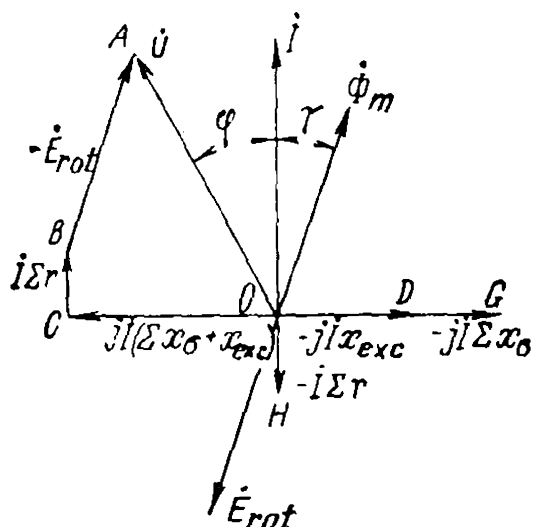


Fig. 28-4. Vector diagram of a single-phase series motor

The magnetizing force F_{cp} produces the flux Φ_{cp} , the action of this flux being the same as in d.c. machines (Vol. I, Sec. 6-4).

The action of the magnetizing force F_{com} is shown in Fig. 28-3 on the assumption that the main importance is attributed to the transformer e.m.f. $\dot{E}_{com.tr}$ which is in quadrature lagging with the main excitation flux $\dot{\Phi}_m$. The current \dot{I}_{com} produced by e.m.f. \dot{E}_{tr} in the coil sections undergoing commutation lags on it by angle β determined by the parameters of these coil sections. Thus, along the pole axis

we have a transformer whose primary is the field winding and whose secondary, the section undergoing commutation. Having constructed the current diagram in the conventional manner for transformers, we find that the current \dot{I} leads the flux $\dot{\Phi}_m$ by the angle γ .

In accordance with the above, a vector diagram of a series motor has been constructed in Fig. 28-4. Suppose the motor runs at a speed n and the brushes are placed on the geometrical neutral. The transformer e.m.f. produced across the brushes by the main excitation flux $\dot{\Phi}_m$ is zero (Fig. 28-1); the e.m.f. \dot{E}_{rot} produced by the same flux is in antiphase with the flux $\dot{\Phi}_m$, since when the machine operates in motoring duty the e.m.f. \dot{E}_{rot} opposes the flow of the current \dot{I} . The following e.m.f.s also exist in the motor: (a) the e.m.f. $\overline{OD} = -j\dot{I}x_{exc}$, where x_{exc} is the inductive reactance of the field winding corresponding to the full excitation flux Φ_{exc} ; (b) the e.m.f. $\overline{DG} = -j\dot{I}\Sigma x_{\sigma}$, where Σx_{σ} is the inductive reactance corresponding to the leakage fluxes of the armature, compensating winding and the compole flux; (c) the e.m.f. $\overline{OH} = -\dot{I}\Sigma r$, where Σr is the sum of all the resistances of the motor, including the contact resistance of the brushes. The equation for the motor e.m.f.s will then be written as

$$U = j\dot{I}(\Sigma x_{\sigma} + x_{exc}) + \dot{I}\Sigma r + (-\dot{E}_{rot}) = \overline{OC} + \overline{CB} + \overline{BA} = \overline{OA}$$

Here \overline{OC} , \overline{CB} and \overline{BA} are the components of the voltage \overline{OA} supplied to the motor, each of them being in equilibrium with the corresponding e.m.f. The phase displacement between the voltage \dot{U} and current \dot{I} is determined by the angle φ . The means for improving $\cos \varphi$ and its numerical values are dealt with in Sec. 28-4.

28-3. Methods of Improving Commutation of Single-Phase Series Motors

From a previous discussion (Sec. 27-5) it follows that commutation in single-phase series motors is more complicated than commutation in d.c. series motors, since in the a.c. motor, in addition to the reactive e.m.f. E_r , the transformer e.m.f. E_{tr} also appears in the coil section undergoing commutation. To provide normal operation of single-phase series motors, the compensation of both e.m.f.s should be as complete as possible.

Compensation of Reactive E.M.F. E_r . We have seen above (Sec. 27-5), that the e.m.f. \dot{E}_r is in phase with the current \dot{I} and is directly proportional to the armature speed. To compensate this e.m.f., the flux Φ_{cr} coincident in phase with the current \dot{I} should be produced (Fig. 28-5). This can be done by means of series-excited compoles, whose polarity is selected as in d.c. machines (see Vol. I, Sec. 6-4). When the armature rotates in the field of these poles, there appears in the coil section undergoing commutation an e.m.f. \dot{E}_{cr} directed against the e.m.f. \dot{E}_r . If the flux Φ_{cr} varies sinusoidally with time, we have

$$E_{cr} = 2\omega_{cs} v_a l \frac{B_{cr}}{\sqrt{2}} \quad (28-4)$$

where B_{cr} is the maximum value of the flux density in the gap under the compole.

Complete compensation is attained when the condition $E_{cr} = E_r$ is observed. Substituting the corresponding values for the e.m.f.s E_{cr} and E_r [equations (28-4) and (27-14)], and cancelling where possible, we obtain

$$B_c = \sqrt{2} \Lambda' A \quad (28-5)$$

Hence it can be seen that when equation (28-5) is observed, the compoles, when connected in series, produce a correct commutating field which allows the e.m.f. \dot{E}_r to be compensated at all speeds and values of the load current.

Compensation of Transformer E.M.F. E_{tr} . It was stated above (Sec. 27-5) that the e.m.f. \dot{E}_{tr} does not depend on the armature speed and lags 90° behind the current \dot{I} , i.e., it is in quadrature with the e.m.f. \dot{E}_r (Fig. 28-5). With the motor running, the transformer e.m.f. as well as the reactive e.m.f. can be compensated, with the help of compoles. For this purpose the flux $\Phi_{c.tr}$ should be produced in quadrature with the flux

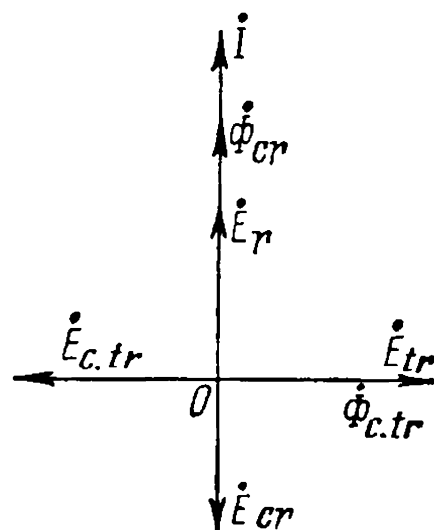


Fig. 28-5. Compensation of e. m. f. s E_r and E_{tr}

Φ_{cr} and, correspondingly, with the current I . With proper polarity of the compoles, the e.m.f. $E_{c.tr}$ produced in the coil section undergoing commutation by the flux $\Phi_{c.tr}$ with the armature running will be directed against the e.m.f. E_{tr} .

Similar to formula (28-4), we have

$$E_{c.tr} = 2\omega_{cs}v_a l \frac{B_{c.tr}}{\sqrt{2}} \quad (28-6)$$

By comparing this formula with formula (27-15) for the e.m.f. E_{tr} , we get

$$B_{c.tr} = \frac{\pi f \Phi_{exc}}{lv_a} \quad (28-7)$$

The relations between the e.m.f.s E_{tr} and $E_{c.tr}$ for various operating conditions of the motor are shown in Fig. 28-6a, b, and c. The compoles are assumed to be non-saturated, i.e., it may be supposed that the flux of the compole varies as the current I_{cp} . Figure 28-6a depicts curves of E_{tr} and $E_{c.tr}$ against the current I with a constant speed n . In conformance with formula (27-15), we have $E_{tr} = C\Phi_m$, i.e., the curve E_{tr} resembles the magnetization curve, whereas $E_{c.tr} = CB_{c.tr} \equiv I$.

Figure 28-6b shows the same curves as functions of the speed n with $I = \text{const}$. For the general case of motor operation at various speeds and corresponding load currents, the curves of E_{tr} and $E_{c.tr}$ are as shown in Fig. 28-6c; with $n = 0$ the e.m.f. $E_{c.tr} = 0$, while E_{tr} may attain a considerable magnitude corresponding to the increase in current I and flux Φ_m in starting of the motor. With small loads, it may be assumed that the flux $\Phi_{c.tr}$ is proportional, and the armature speed is inversely proportional to the current I ; correspondingly, $E_{c.tr} = Cn\Phi_{c.tr} \cong \text{const}$, and E_{tr} decreases in proportion to the decreasing current I .

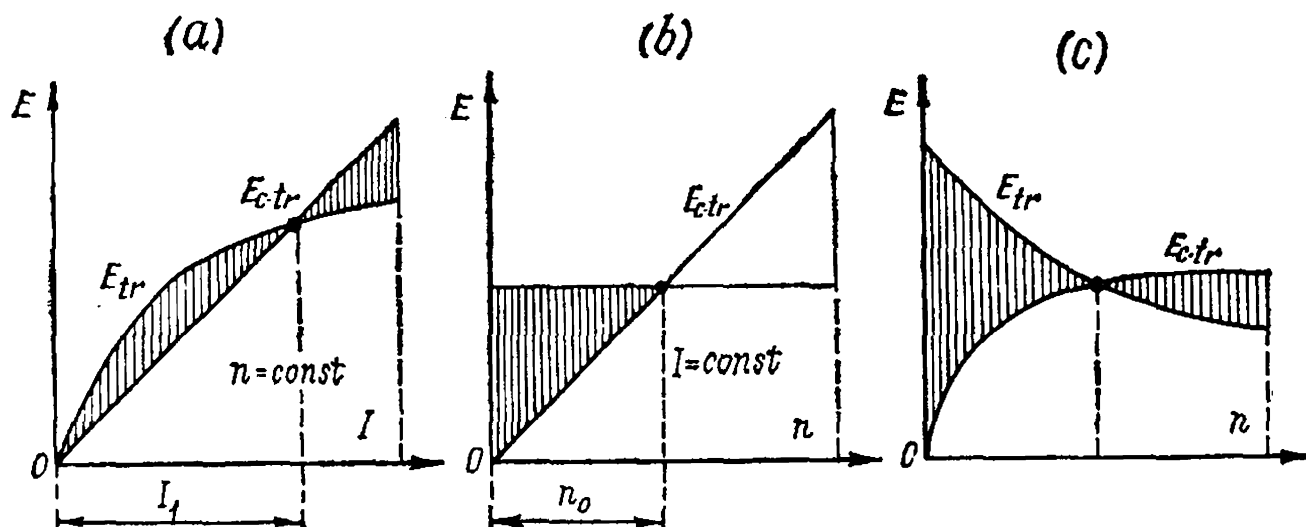


Fig. 28-6. Curves of E_{tr} and $E_{c.tr}$ for different operating conditions of a motor

The diagrams given above show that full compensation of the e.m.f.s E_{tr} and $E_{c.tr}$ is possible only at one point; as we move away from this point the unbalance of e.m.f.s and, consequently, the danger of disturbance in commutation become more acute.

To produce the flux $\Phi_{c.tr}$, we can place a special winding on the stator and connect it across the motor terminals (to the mains). But a more convenient method is to shunt the winding of the series-connected compole CP (Fig. 28-7) by means of a resistance. The corresponding vector diagram is shown in Fig. 28-8a. Assume that the compole winding has only an inductive reactance; here the current $I_R = \overline{AB}$ in the resistor R and the current $I_{cp} = \overline{OA}$ in the compole winding are in quadrature, and $I_R + I_{cp} = I = \overline{OB}$, where I is the current in the motor armature. The current I_{cp} produces the commutating flux Φ_{com} which has two components: $\Phi_{cr} = \overline{OC}$, in the direction of current I , and $\Phi_{c.tr} = \overline{CA}$, lagging on the current by 90° . With correct polarity of the compoles, the fluxes Φ_{cr} and $\Phi_{c.tr}$ produce e.m.f.s E_{cr} and $E_{c.tr}$ which balance the e.m.f.s E_r and E_{tr} (see Fig. 28-5).

We have seen from Fig. 28-6 that for given operating conditions full compensation of the e.m.f. E_{tr} is possible only at one point. To widen the range of compensation, we connect the capacitors C_1 and C_2 across the compole winding of traction motors in addition to the resistance R (Fig. 28-7). The winding of the compoles and the capacitors constitute a sort of resonant circuit. With a given current in the non-branched part of the circuit the current in the compole winding grows from I_{cp} to I'_{cp} (Fig. 28-8b); the voltage across the terminals will increase correspondingly and the current I_R in the resistor will rise to I'_R . Point A will move to point A' , and the flux $\Phi_{c.tr}$ will grow to $\Phi'_{c.tr}$. By a proper choice of the capacitors it is possible to widen the zone

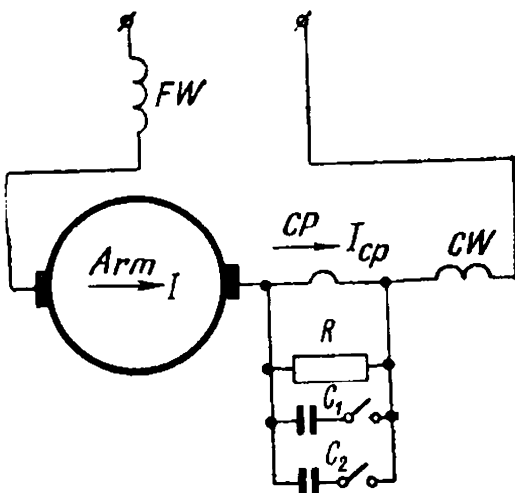


Fig. 28-7. Compensation of e. m. f. E_{tr}

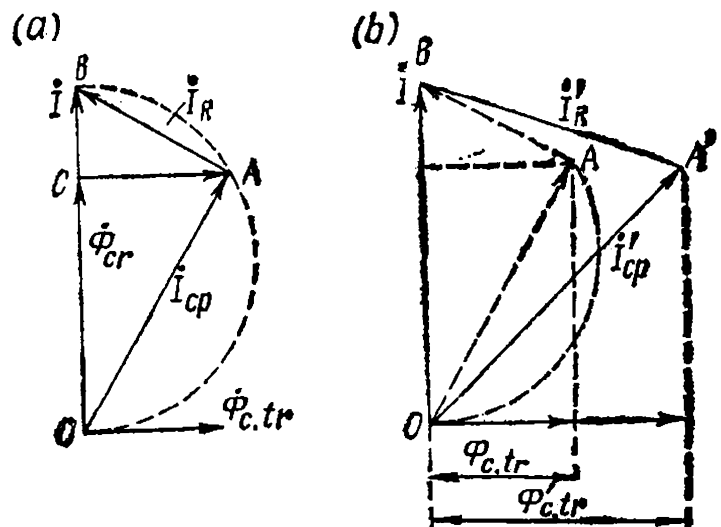


Fig. 28-8. Vector diagrams for compoles:
a — shunted by resistance; b — shunted by resistance and capacitance

of compensation of the e.m.f. E_{tr} and thus improve the conditions of commutation in the motor.

In addition to capacitors, regulated inductive reactances can be used, and the shunting resistors can be connected to the compole winding through a transformer.

It follows from the above that, as regards compensation of the e.m.f. E_{tr} , the single-phase commutator motor starts in exceptionally difficult conditions. Here the e.m.f. E_{tr} grows due to an increase in starting current and a corresponding increase in the excitation flux Φ_{exc} , while the compensating e.m.f. $E_{c.tr}$ at the initial moment of starting ($n = 0$) is equal to zero. Practice shows that the e.m.f. E_{tr} must not exceed 3.5 to 3.75 V when starting if special measures have not been taken to limit the additional short-circuit current arising in the coil section undergoing commutation under the action of the e.m.f. E_{tr} . On the other hand, with smaller values of E_{tr} the dimensions of the motor grow; this is especially objectionable for motors of high rating, such as motors of trunk-line electric locomotives (ratings of the order of 400 to 800 kW).

An urgent need in single-phase industrial frequency railway electrification is to increase the admissible limits of the e.m.f. E_{tr} . With this end in view, industrial frequency traction motors are provided with additional resistors inserted between the armature winding and the commutator (see Fig. 27-13). These resistors prove very effective for such frequencies. For the same purpose in French industrial frequency traction motor designs a complex lap winding with equalizer connections of the second type is used (see Vol. I, Figs. 3-47 and 3-62). Here only one-half of the e.m.f. E_{tr} induced in an armature winding turn by the main flux acts between two commutator bars, in accordance with which a greater e.m.f. E_{tr} per turn may be permitted. The design suggested is of essential importance for motors of a high rating.

28-4. Characteristics of a Single-Phase Series Motor

The speed characteristic $n = f(M)$ of a single-phase series motor with $U = \text{const}$ and $f = \text{const}$ has the same nature as that of a d.c. series motor. With a varying voltage this relation does not change its nature, but the curve $n = f(M)$ on the diagram will lie lower if the voltage U decreases, and higher, if it increases.

Figure 28-9 shows curves of $n = f(M)$ and $I = f(M)$ for different voltages across the terminals of a 36.5-kW, 1000-rpm crane motor. These curves show that to obtain the rated torque when starting, the motor requires 47 per cent of the rated voltage, while at $M_{st} = 1.8 M_r$ it requires 60 per cent of U_r .

To regulate the voltage, the motor is connected to the power line through a transformer T with a tapped secondary (Fig. 28-10). With

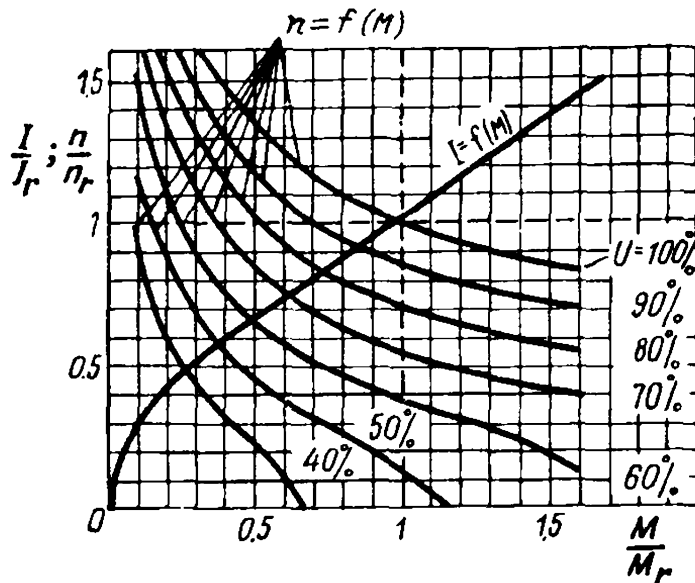


Fig. 28-9. Curves $I = f(M)$ and $n = f(M)$ for different voltages

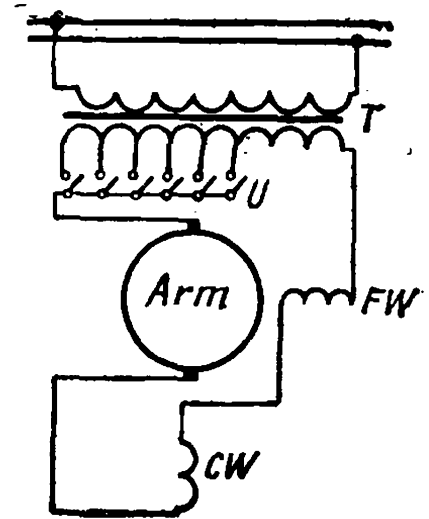


Fig. 28-10. Diagram of a single-phase commutator crane motor

such a method of regulation it is not necessary to have any regulating resistance in the main circuit, and this is a feature of single-phase commutator motors which distinguishes them from d.c. motors. Regulation by means of a transformer is effected almost without any losses, and the efficiency of the motor in service is raised.

The curve $I = f(M)$ shown in Fig. 28-9 is of the same nature as the corresponding curve of a d.c. series motor. With small loads and, consequently, low saturations, the torque developed by a single-phase series motor is proportional to the square of the current, and the initial part of the curve $I = f(M)$ is of a quadratic nature. With an increase in saturation this curve becomes more and more rectilinear.

Figure 28-11 gives curves of the power factor $\cos \varphi = f(M)$ and efficiency $\eta = f(M)$ for the same crane motor for different voltages across the motor terminals. When the voltage decreases and a given torque is maintained on the shaft, the power factor of the motor and its efficiency decrease.

To raise the power factor, it is necessary to have as small a reactive voltage drop as possible in the main circuit of the motor (component \overline{OC} in Fig. 28-4). For this purpose motors are provided with

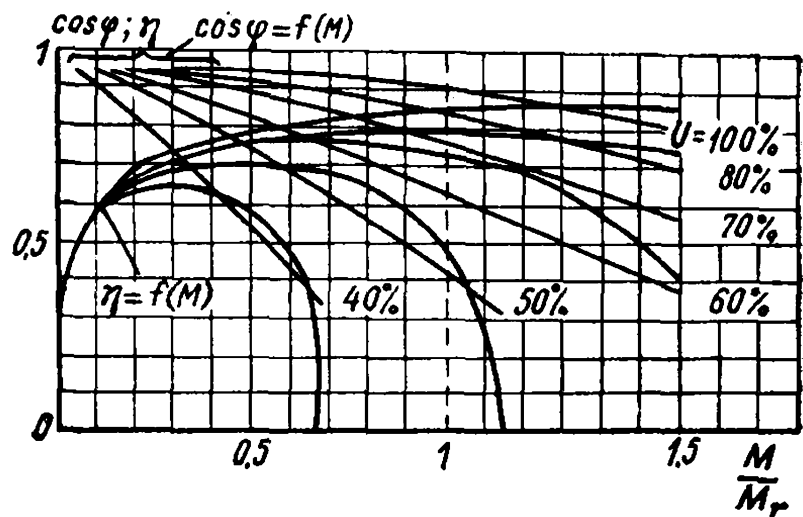


Fig. 28-11. Curves of $\cos \varphi = f(M)$ and $\eta = f(M)$ for different values of U

the smallest possible air-gap, so that the number of turns in the field winding is minimum. Usually in motors up to 100 kW the air-gap $\delta = 1.5$ to 2.5 mm, in motors of a higher rating $\delta = 2$ to 4 mm (the air-gap under the main poles). The second means of improving the power factor is compensation of the armature reaction by means of a compensating winding. Recently, however, some single-phase commutator motors have been built without a compensating winding. A somewhat lower power factor of such motors is compensated by several inherent advantages: less copper, simpler design, better conditions for conducting the magnetic flux through the air-gap under the main pole and a lower leakage reactance.

The efficiency of a single-phase series motor is less than that of a d.c. series motor of the same rating. This is explained by somewhat greater losses in the steel of a single-phase motor and by relatively higher additional losses, mainly of a commutating nature, owing to the more severe conditions for commutation.

The power factor and the efficiency of single-phase commutator traction motors depend on the frequency which the motor normally operates at. We have already mentioned above that to improve commutating conditions the compoles are shunted with a resistor (see Fig. 28-7). Calculations show that for $16\frac{2}{3}$ Hz (this frequency is widely used in Germany, Switzerland and Sweden) the losses in the shunting resistor do not exceed 1%; with 25 Hz (used in the USA) the losses reach 2-2.5%, and with 50 Hz (used in France, etc.) they rise to 5-7%. Therefore, the $16\frac{2}{3}$ -Hz motors have a power factor of 0.96 to 0.97 at rated operating conditions, and their efficiencies are about 90%, while motors of the same type operating at 50 Hz have a power factor of 0.86 to 0.89 and efficiencies of about 85 to 89%.

28-5. Application of Single-Phase Commutator Motors

Single-phase commutator motors are used mainly for single-phase current electric traction.

The problem of a.c. railway electrification appeared at the beginning of the current century.

The first single-phase current electrified railways using single-phase commutator motors were put into commission almost simultaneously in Germany and the USA. To facilitate the operation of the motor, it was suggested that railway lines be supplied with current of a lower frequency (with respect to industrial frequency). In Europe, mainly in Germany, the $16\frac{2}{3}$ -Hz single-phase current system was developed, in the USA the 25-Hz system.

The lower frequency necessitated the use of convertor installations or the construction of special power plants. Therefore, as early as the twenties of the current century there arose the problem of supplying railways from industrial frequency power systems.

The solution of the problem has several alternatives; first, conversion of the single-phase alternating current of the supply circuit into d.c. power in the electric locomotive by using rotary convertors or static ignitron rectifiers, dry-contact rectifiers; locomotives with the latter type of rectifiers due to their high efficiency and good starting properties, are now being used on an exceptionally large scale both abroad and in the USSR. Other alternatives are: the conversion of single-phase current into a system of three- or two-phase current and, finally, the direct utilization of single-phase current by using single-phase industrial frequency commutator motors.

The development of the commutator motor required for the last alternative presented considerable difficulties and required much research on the part of many French, Swiss and German designers. This work resulted in the creation of a motor with many features: the motor was designed both with and without a compensating winding, with the compoles shunted by a resistor and a capacitor, with additional resistors inserted between the armature winding and the commutator, and designed with increased ventilation.

Such motors were installed in electrical locomotives operating on the railway lines of northern and north-eastern districts of France which were electrified at the beginning of the current century.

One of the obstacles met with in the development of a system of single-phase series commutator motors of industrial frequency were the severe conditions of prolonged starts, unavoidable in trunk-line freight locomotive service. However, for passenger electrical locomotives and multiple-unit trains, the single-phase industrial frequency commutator motors often give quite satisfactory results.

28-6. Repulsion Motor with Two Windings on the Stator

A schematic diagram of a repulsion motor with two windings on the stator is shown in Fig. 28-12. This circuit is obtained by modifying the circuit of a series motor with an electrically disconnected compensating winding acting as a transformer secondary with respect to the armature winding. But nothing will change if armature winding *Arm* serves as the secondary circuit and the compensating winding *CW* is joined to the power circuit in series with the field winding *FW* as shown in Fig. 28-12. This is why the armature of a repulsion motor can be built for a lower voltage without using a step-down transformer.

To find the properties of a repulsion motor, let us construct an e.m.f. vector diagram for conditions of armature rotation. Let us lay off on the axis of ordinates the vector of the current I_1 flowing through

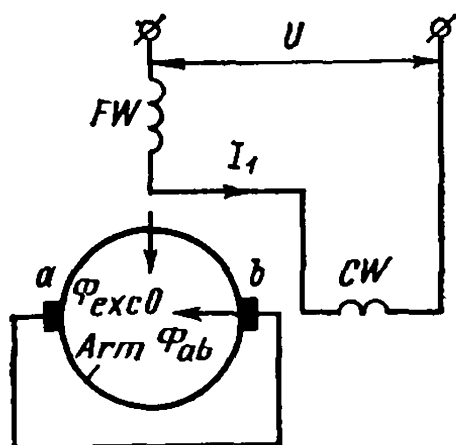


Fig. 28-12. Repulsion motor with two windings on the stator

its primary windings (Fig. 28-13). In phase with current I_1 is the flux Φ_{exc0} produced by the field winding FW . Due to transformation linkage between windings Arm and CW , the current I'_2 is induced in the armature.

The magnetizing forces \dot{F}_1 and \dot{F}_2 produced by the currents I_1 and I'_2 add together vectorially and form the resultant magnetizing force $\dot{F}_m = \dot{F}_1 + \dot{F}_2$ which produces the flux Φ_{ab} directed in space along the brush line $a-b$ and lagging with time behind the current I_1 by an angle β .

Let us consider first the e.m.f. in the secondary circuit of the motor, i.e., in the armature winding.

The flux Φ_{ab} produces at brushes $a-b$ the pulsation e.m.f. $E'_{ap} = \overline{OA}$ lagging on it by 90° . When the armature cuts the flux Φ_{exc0} , the rotational e.m.f. $\dot{E}'_{a,rot} = \overline{OB}$ appears across the brushes $a-b$, coinciding in phase with the flux Φ_{exc0} , since it tends to oppose the flow of the current I'_2 . Besides, there also exists the armature-winding leakage flux e.m.f. $-jI'_2x'_{a\sigma}$ and the resistance e.m.f. $-I'_2r'_a$. Since the armature winding is short-circuited on itself, then

$$\dot{E}'_{a,rot} + \dot{E}'_{ap} - jI'_2x'_{a\sigma} - I'_2r'_a = \overline{OB} + \overline{BC} + \overline{CD} + \overline{DO} = 0$$

Now consider the e.m.f.s in the primary circuit. Owing to the pulsation of the fluxes Φ_{exc} and Φ_{ab} , the pulsation e.m.f.s E_{exc} and E_{cw} are produced in the windings FW and CW . They lag behind their respective fluxes by 90° . The components of the voltages $-\dot{E}_{exc}$ and $-\dot{E}_{cw}$ lead the fluxes Φ_{exc} and Φ_{ab} by 90° . By vector addition of the above components to the voltage drops $I_1(r_{exc} + r_{cw})$ and $jI_1(x_{exc\sigma} + x_{cw\sigma})$ in

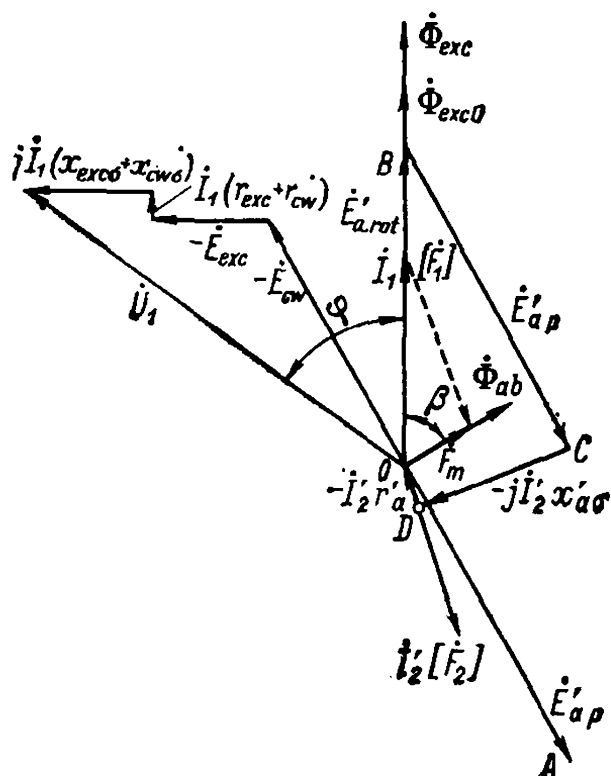


Fig. 28-13. Vector diagram of a repulsion motor with two windings on the stator

windings FW and CW , we obtain the voltage \dot{U}_1 across the motor terminals leading the current \dot{I}_1 in phase by an angle φ .

It follows from the diagram that a repulsion motor having two windings on the stator always operates with a lagging power factor.

Another very interesting feature of the repulsion motor follows from the same diagram.

The fluxes Φ_{exc0} and Φ_{ab} are shifted in space precisely by 90° (Fig. 28-12) and in time practically by 90° (Fig. 28-13), but in the general case they are not equal to each other in magnitude. Thus, the *repulsion motor is a system with an elliptical rotating field*. At the synchronous speed of the armature, however, this field becomes circular. Indeed, if we disregard the impedance of the armature circuit Z_a , the absolute magnitudes of the voltages are then $E_{a.rot} = E_{ap}$ [equation (27-1)], i.e.,

$$\pi \sqrt{2} f_{rot} \omega_a k_{w.exc} \Phi_{exc0} = \pi \sqrt{2} f \omega_a k_{wa} \Phi_{ab}$$

whence

$$\Phi_{ab} = \Phi_{exc0} \frac{f_{rot}}{f} \quad (28-8)$$

Here $f_{rot} = pn$ is the rotational frequency, and f —the frequency of the supply circuit. When $f_{rot} = f$, i.e., when the *motor runs at synchronous speed*, $\Phi_{av} = \Phi_{exc0}$ and the *elliptical field becomes circular*.

The torque of a repulsion motor is usually expressed by the formula

$$M = c_M I_2 \Phi_{exc0} \cos(\hat{I}_2 \Phi_{exc0}) \quad (28-9)$$

or, since

$$\cos(\hat{I}_2 \Phi_{exc0}) \cong 1$$

then

$$M = c_M I_2 \Phi_{exc0} \quad (28-10)$$

The commutation process in the short-circuited turns of the repulsion motor armature winding of starting goes on in the same way as in a series motor. The commutating conditions *for a running repulsion motor not provided with compoles are better, however, than in a series motor because of the creation of an elliptical field*. In the particular case when $f = f_{rot}$ the transformer e.m.f. in the short-circuited turn vanishes and the commutating process depends only on the reactive e.m.f. E_r . The most advantageous rotational speed of a repulsion motor is about 20% below synchronous speed. This dependence of the most advantageous operating conditions of a repulsion motor on the synchronous speed is a feature by which it differs from a series motor.

28-7. Repulsion Motor with One Winding on the Stator and with One Set of Brushes (Thomson Motor) [245]

This motor has a stator with one winding St and an armature Arm with a set of brushes $a-b$, whose axis may occupy a position at any angle α with respect to the stator winding axis.

Assume that $\alpha=90^\circ$, i.e., the axis of the brushes $a-b$ and, consequently, the axis of the armature winding are perpendicular to the axis of the stator winding (Fig. 28-14a). Here the sum of the e.m.f.s in each branch of the armature winding is zero (see Fig. 27-1b) and, accordingly, the armature current and the torque developed by the motor are also zero. The motor may be considered as a transformer with an open secondary circuit.

The position of the brushes corresponding to the angle $\alpha=90^\circ$ is termed the *no-load position*.

If $\alpha=0$, the axes of windings St and Arm coincide (Fig. 28-14b). The current I_2 appears in the armature and produces the magnetizing force F_2 directed against the magnetizing force F_{stat} produced by winding St . The motor again cannot develop a torque (as in a d.c. motor, when the brush axis coincides with the field winding axis) and can be considered as a transformer under short-circuit conditions. Therefore such a position of the brushes is referred to as the *short-circuit position*.

With intermediate values of the angle α (Fig. 28-14c), the Thomson repulsion motor may be reduced to a repulsion motor with two windings on the stator if we divide the stator winding St into two windings, the axis of one coinciding with the line of the brushes $a-b$ and of the other being perpendicular to the brush line. The first acts as the winding CW in the diagram in Fig. 28-12, the second as the field winding FW . Correspondingly, the operating conditions of the motor are the same as for a motor with two windings on the stator, and the vector diagrams of the motors are identical.

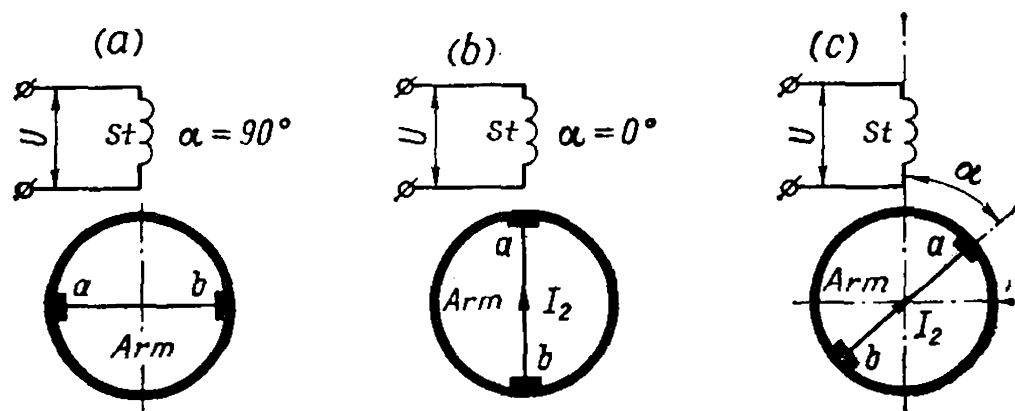


Fig. 28-14. Thomson repulsion motor:

a — brush position at no-load; b — brush position at short circuit;
 c — intermediate brush position

28-8. Characteristics of a Thomson Repulsion Motor

Below is a simplified deduction of a formula for the torque of this motor. Let w_{stat} be the number of turns of the stator winding; then, according to the above, we can suppose that along the brush axis a - b there is a winding with $w_{cw} = w_{stat} \cos \alpha$ turns, and in the perpendicular direction a winding with $w_{exc} = w_{stat} \sin \alpha$ turns. According to the general rule

$$M \cong c_M I_2 \Phi_{exc0} \quad (28-11)$$

If the steel of the motor is not saturated, then

$$\Phi_{exc0} = c_{exc} I_1 w_{exc} = c_{exc} I_1 w_{stat} \sin \alpha$$

Further, we may neglect the magnetizing current induced as a result of the transformation linkage between the stator and rotor windings. Then

$$\frac{I_2}{I_1} = \frac{w_{cw}}{w_a} = \frac{w_{stat} \cos \alpha}{w_a}$$

whence

$$I_2 = I_1 \frac{w_{exc} \cos \alpha}{w_a}$$

and formula (28-11) becomes

$$M = c_M I_1^2 \sin 2\alpha \quad (28-12)$$

It follows from this formula that the *torque of the motor attains a maximum at $\alpha = 45^\circ$* . Upon a change in current I_1 with a change in angle α , however, the torque maximum is displaced. Curves $M = f(\alpha)$ and $I_1 = f(\alpha)$ for $U_1 = \text{const}$, $f = \text{const}$ and $n = 0$ are shown in Fig. 28-15.

Since the torque of a repulsion motor depends on the square of the current I_1 , a repulsion motor and, particularly, a motor with one winding on its stator and one set of brushes has the same speed and current characteristics $n = f(M)$ and $I = f(M)$ as single-phase series motors (Fig. 28-9). The angle of brush rotation α here plays the part of the regulated voltage U .

The commutation of a Thomson repulsion motor is characterized by the motor having to operate with a changing position of the brushes on the commutator; the position of the brush short-circuited commutation circuit of the motor, therefore, changes with the operating conditions. Consequently, an improvement of commutation by means of compoles cannot be achieved, since such poles require that the position of the circuit undergoing commutation be fixed with respect to the stator. In the no-load position of brushes (Fig. 28-14a) there is

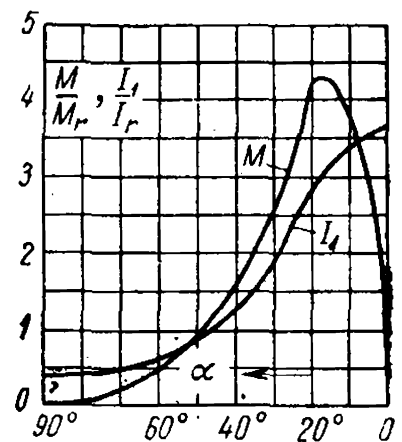


Fig. 28-15. Curves of $M = f(\alpha)$ and $I_1 = f(\alpha)$ for Thomson repulsion motor

a transformation linkage between the coil sections undergoing commutation and transformer winding and they are, therefore, under short-circuit conditions with respect to this winding.

In the short-circuit position of the brushes (Fig. 28-14*b*) the coil sections undergoing commutation are in the no-load position, since the circuits of these turns are not penetrated by the stator winding flux.

It follows, consequently, that starting of a Thomson repulsion motor from the no-load position is more difficult from the viewpoint of its commutation, since the transformer e.m.f. E_{tr} is maximum here; such starting takes place when the operating conditions of the drive require only a small starting torque on the motor shaft.

Conversely, if a considerable starting torque has to be developed, as, for instance, in hoisting installations, starting is then carried out from a position close to that of the short-circuit, here the commutation of the repulsion motor takes place in relatively favourable conditions.

Since the Thomson motor has no compoles, the commutation of this motor takes place in sufficiently favourable conditions only at speeds close to synchronism. Here a rotating magnetic field of almost circular shape is produced in the motor (see Sec. 28-6) with which the transformer e.m.f. E_{tr} in the coil section undergoing commutation disappears and only the reactive e.m.f. E_r remains. A departure from synchronism impairs the commutation or, in other words, the commutation of a repulsion motor with one winding on the stator, as with two windings on the stator, depends on the speed of the motor.

Motors with one winding on the stator are built for low ratings, generally not more than a few kilowatts. Figure 28-16 gives curves of $\eta = f(M)$ and $\cos \varphi = f(M)$ with $U = \text{const}$ and $\alpha = \text{var}$ for a motor with a one-hour rating of 13 kW, 250 V, 50 Hz, and 750 rpm. The angle α is expressed not in degrees but in per cent of 90° .

It can be seen from the curves that the values of η and $\cos \varphi$ of this motor are smaller than, for instance, those of induction motors.

The overload capacity of this motor, as can be seen from Fig. 28-15, is relatively high.

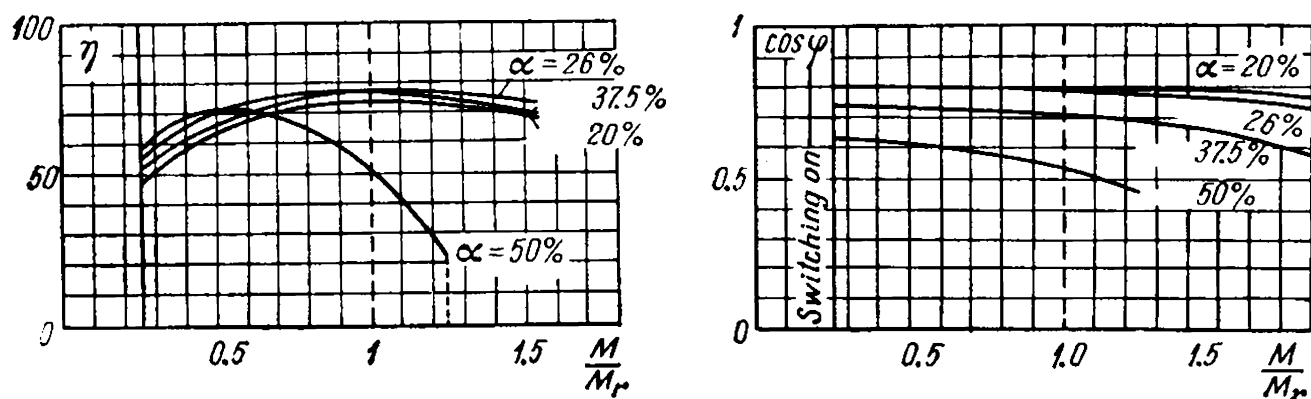


Fig. 28-16. Curves of η and $\cos \varphi = f(M)$ for Thomson repulsion motor

28-9. Repulsion Motor with One Winding on the Stator and Two Sets of Brushes (Deri Motor)

The circuit of this motor (Fig. 28-17) incorporates a double set of brushes $a-b$ and $a'-b'$ which are arranged on the armature commutator. Brushes a and a' are stationary and spaced 180° apart. Brushes b and b' are connected to brushes a and a' , respectively, and can be moved over the commutator. The axis of the stationary brushes $a-a'$ generally coincides with the axis of the stator winding St .

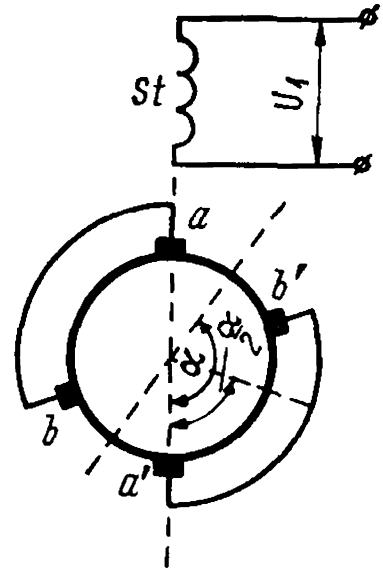


Fig. 28-17. Deri repulsion motor

When brushes $b-b'$ coincide with brushes $a-a'$, the angle $\alpha=0$. Such a position of the brushes is called the *no-load position*.

When the brushes $b-b'$ are turned through an angle $\alpha=180^\circ$, brush b' coincides with brush a , and brush b with brush a' . This position of the brushes is termed the *short-circuit position*. In both cases the torque M developed by the motor equals zero.

When brushes $b-b'$ are turned through an angle α , the axis of the armature magnetizing force is displaced in space only by $\frac{\alpha}{2}$. Correspondingly, α must be introduced into formula (28-12) for the torque M instead of 2α . This makes it possible to give the curve $M=f(\alpha)$ of the motor a gentler slope and thus provide finer speed control than in a similar motor with one set of brushes. This is an essential advantage of the Deri motor.

A second very important advantage of this motor over a motor with one set of brushes is that it has better commutation characteristics. Indeed, it can be seen from Fig. 28-17 that both in the no-load and in the short-circuit positions the plane of the coil section undergoing commutation is parallel to the flux lines produced by the stator winding. Therefore, in both cases the transformer e.m.f. $E_{tr}=0$.

During operation the current in the coil section undergoing commutation varies not from $+i_a$ to $-i_a$ (see Fig. 27-11), but only from $+i_a$ to 0, since in the parts $a-b'$ and $a'-b$ of the armature the currents vanish. For this reason the reactive e.m.f. E_r decreases.

A disadvantage of the Deri motor, when compared with a similar motor with one set of brushes, is the more complicated double set of brushes.

These motors are built for ratings of up to 100 kW. Their performance characteristics n , η and $\cos \varphi=f(M)$ are practically the same as those of motors having one winding on the stator and one set of brushes.

Chapter

29

THREE-PHASE SHUNT AND SERIES COMMUTATOR MOTORS

29-1. General

With the development of the electrical drive, the problem of more economical and reliable wide-range speed control of the induction motor became more urgent.

The following paths were chosen to solve this problem: (a) by improvements in the already known types of three-phase commutator machines, and by designing new types of such machines, and (b) by developing cascades. The problem of the power factor of a regulated system as a whole was also raised, but its solution became urgent only in the twenties of the current century in connection with the rationalization of electrical power system operation. This led to the development of compensated and synchronized commutator motors and phase advancers both with self- and with separate excitation.

The principal means for ensuring both speed regulation within the given limits and improvement of the power factor is the introduction of an *additional e.m.f. E_{com} into the secondary circuit of an asynchronous machine*, which is specifically orientated with respect to the main e.m.f. E_{2s} of this circuit. Naturally, the e.m.f. E_{com} must, under all operating conditions, have the same frequency as the e.m.f. E_{2s} , since only then do the two e.m.f.s interact. This principle is of very great importance and underlies the operation of a number of a.c. commutator machines and cascaded systems.

29-2. General Principles of Shunt Polyphase Commutator Machines

The shunt commutator motor is to serve as a polyphase machine with speed regulated within certain limits, retaining the shunt speed characteristic at each stage of regulation, i.e., with a relatively small change in speed in transition from no-load to full-load. The speed is regulated by introducing into the secondary main circuit, which in essence serves as the main secondary circuit of an asynchronous machine, an additional e.m.f. E_{2com} . If this e.m.f. is directed against the main e.m.f. of the secondary circuit E_{2s} , the motor reduces its speed to below the synchronous one. If the e.m.f. E_{2com} coincides in phase with the e.m.f. E_{2s} , then the motor transfers to a speed above the synchronous one. The magnitude of the e.m.f. E_{2com} at each speed stage should

not change under the influence of the change in the magnitude of the secondary current I_2 . If the additional e.m.f. $E_{2com}=0$, the machine acquires the properties of an ordinary asynchronous machine and at no-load gives a speed close to the synchronous one. Under load the speed drops below the synchronous one by the value of the slip s . When transferring from one speed to another only the magnitude of the e.m.f. E_{2com} changes, its phase in relation to the e.m.f. E_{2s} remaining unchanged. If the e.m.f. E_{2com} changes in certain known stages, then we get a corresponding stepped change in speed. If the system makes it possible to obtain a continuous change in the e.m.f., then a smooth change of speed within the given limits can be achieved.

If, besides a change in speed, it is also desired to improve the power factor, then the additional e.m.f. E_{2com} should have, besides the main component which causes a change in speed, a small component which produces a leading phase component of the secondary current, as a result of which the power factor is improved up to the required value.

The additional e.m.f. E_{2com} is produced on the primary side of the machine in a special system comprising an additional winding, an additional regulating transformer or a potential regulator. Since the primary side of the machine has the frequency of the primary circuit f_1 , and the secondary additional e.m.f. E_{2com} must have the secondary circuit frequency $f_2=f_1s$, then for transforming the frequency E_{2com} without changing its magnitude a commutator is used.

It should be noted that irrespective of whether the primary side is on the rotor or on the stator, the commutator in both cases is on the rotor.

29-3. General Equations of Polyphase Shunt Commutator Machine Operation and Their Circle Diagrams

A schematic diagram of a shunt machine is shown in Fig. 29-1.

Here the commutator C is shown schematically, since depending on the method of energizing the machine it may be related either to the primary or the secondary side. The axis of the primary winding w_a is taken as the main axis, and the angular positions of the regulating (commutating) winding w_{com} and main winding w_d can be determined relative to it. Let us assume that the axes of the windings w_d and w_a coincide, and the axis of winding w_{com} is shifted in the direction of rotation of the field by an angle β from the axis of winding w_a .

Let us compile expressions for the e.m.f. and magnetizing force of the windings and

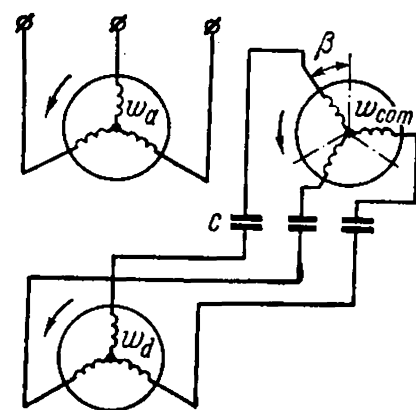


Fig. 29-1. Schematic diagram of a shunt commutator machine

find the current and voltage ratios in the complex form:

$$\begin{aligned}\dot{E}_a &= \pi \sqrt{2} \Phi \omega_a k_a f_1 = \dot{E}'_2 \\ \dot{E}_{com} &= \pi \sqrt{2} \Phi \omega_{com} k_{com} f_1 e^{-i\beta}\end{aligned}$$

Let us assume that the secondary system rotates with respect to the primary with a slip s . Then the e.m.f. induced in winding ω_d by the flux Φ will be

$$\dot{E}_d = \pi \sqrt{2} \Phi \omega_d k_d f_1 s$$

The resultant e.m.f. of the secondary circuit is

$$\dot{E}_2 = \dot{E}_{com} + \dot{E}_d = \frac{\dot{E}'_2}{k_e}$$

where the voltage ratio

$$k_e = \frac{\dot{E}'_2}{\dot{E}_2} = \frac{\omega_a k_a}{\omega_{com} k_{com} e^{-i\beta} + \omega_d k_d s} \quad (29-1)$$

The resultant magnetizing force of the secondary system is

$$\dot{F}_{com} + \dot{F}_d = \dot{F}'_2 = m_1 \dot{I}'_2 \omega_a k_a = m_2 \dot{I}_2 (\omega_{com} k_{com} e^{+i\beta} + \omega_d k_d)$$

Hence we obtain the following expression for the referred secondary current:

$$\dot{I}'_2 = \frac{\dot{I}_2}{k_i}$$

where the current ratio is equal to:

$$k_i = \frac{m_1}{m_2} \frac{\omega_a k_a}{\omega_{com} k_{com} e^{+i\beta} + \omega_d k_d} \quad (29-2)$$

For the secondary current \dot{I}_2 and secondary referred current \dot{I}'_2 we obtain the following expressions:

$$\dot{I}_2 = \frac{\dot{E}'_2}{z_2} = \frac{\dot{E}'_2}{z_2 k_e}; \quad \dot{I}'_2 = \frac{\dot{I}_2}{k_i} = \frac{\dot{E}_2}{z_2 k_e k_i} = \frac{\dot{E}'_2}{z_2 k} = \frac{\dot{E}'_2}{z'_2}$$

Let us introduce the following notation:

$$\frac{m_1}{m_2} = m_{12}; \quad \frac{\omega_a k_a}{\omega_d k_d} = k_{ad} \text{ and } \frac{\omega_{com} k_{com}}{\omega_d k_d} = k_{cd}$$

The total transformation ratio k_{tr} is equal to

$$\begin{aligned}k_{tr} &= k_e k_i = m_{12} \frac{k_{ad}^2}{(k_{cd} + s e^{+i\beta})(k_{cd} + e^{-i\beta})} = \\ &= m_{12} \frac{k_{ad}^2}{(k_{cd} + s \cos \beta + j s \sin \beta)(k_{cd} + \cos \beta - j \sin \beta)}\end{aligned} \quad (29-3)$$

The denominator of the complex transformation ratio \dot{k}_{tr} has the form of the product of two complexes:

$$(A + jB)(D + jE) = C(\cos \alpha + j \sin \alpha) = Ce^{j\alpha} \quad (29-4)$$

where

$$\cos \alpha = \frac{AD + BE}{C} = \frac{k_{cd}^2 + k_{cd}(1+s) \cos \beta + s}{C} \quad (29-5)$$

$$\sin \alpha = \frac{BD + AE}{C} = -\frac{k_{cd}(1-s) \sin \beta}{C} \quad (29-6)$$

$$\begin{aligned} C^2 &= (A^2 + B^2)(D^2 + E^2) = \\ &= (k_{cd}^2 + 2k_{cd}s \cos \beta + s^2)(k_{cd}^2 + 2k_{cd} \cos \beta + 1) \end{aligned} \quad (29-7)$$

Hence

$$\dot{k}_{tr} = m_{12} \frac{k_{ad}^2}{Ce^{j\alpha}} = m_{12} \frac{k_{ad}^2}{C} e^{-j\alpha} \quad (29-8)$$

The referred values of the secondary impedance are

$$z'_2 = z_2 \dot{k}_{tr} = z_2 k_{tr} e^{-j\alpha} = (r_2 + jx_2) k_{tr} (\cos \alpha - j \sin \alpha) = r'_2 + jx'_2 \quad (29-9)$$

Hence for the total impedance $z_{tot} = z_1 + z'_2$ we have for the resistance and inductive reactance:

$$r_{tot} = r_a + r'_2 = r_1 + k_{tr} (r_2 \cos \alpha + x_2 \sin \alpha) \quad (29-10)$$

$$x_{tot} = x'_a + x'_2 = x_1 + k_{tr} (x_2 \cos \alpha - r_2 \sin \alpha) \quad (29-11)$$

If the magnetizing circuit is brought out to the primary terminals without corrections, then for the primary current:

$$\begin{aligned} \dot{I}'_2 &= \frac{\dot{U}_1}{z_{tot}} = \frac{\dot{U}_1}{z_1 + z_2 \dot{k}_{tr}} = \\ &= \frac{U_1 (k_{cd} + s \cos \beta + js \sin \beta) (k_{cd} + \cos \beta - j \sin \beta)}{z_1 (k_{cd} + s \cos \beta + js \sin \beta) (k_{cd} + \cos \beta - j \sin \beta) + m_{12} k_{ad}^2 z_2} \end{aligned} \quad (29-12)$$

Since in the expression for \dot{I}'_2 the real part of the slip parameter s is contained in the numerator and denominator in the first degree, then with a change in the parameter s within the range $\pm \infty$ the end of the primary current vector describes a circle (see Sec. 21-1).

Having determined the values of the equivalent resistances and inductive reactances for any three values of the slip s and by plotting for them the current vectors \dot{I}'_2 , it is possible to draw through the three points a current circle for the given value of the angular position of the brushes on the commutator β . If we add to the current vector \dot{I}'_2 the vector of the magnetizing current \dot{I}_0 , then we obtain the vector $\dot{I}_1 = \dot{I}'_2 + \dot{I}_0$ of the primary current.

The expressions for the equivalent inductive reactances x_{tot} can be found for the most convenient and characteristic values of slip

$s=0$, $s=\pm\infty$ and $s=+1$, as in the case of the induction machine, and they can be used to find the corresponding current vectors $\dot{I}_{s=0}$, $\dot{I}_{s=+1}$ and $\dot{I}_{s=\pm\infty}$.

Since three points are sufficient for construction of the current circle, the fourth point, for example, for $s=-1$, can be used to check whether the current circle has been constructed properly. Since the values of the currents for the slips $s=0$, $s=\pm\infty$ and $s=+1.0$ are required, as in induction machines, for construction of the torque, slip, curves, etc., then this method is the simplest one for constructing the current circle for a given value of the angle β and a variable slip s and for studying the operation of a commutator shunt machine by means of it.

The angle β of displacement of the regulating winding ω_{com} with respect to the main primary winding ω_a is ordinarily very small, therefore, it is possible to assume $\cos \beta \cong 1.0$. Hence for slips $s=1.0$, $s=\pm\infty$ and $s=0$ we obtain the following values of the referred resistances and inductive reactances:

$$x_2 = x_d s + x_{com}$$

for $\beta \neq 0$, $s = 1.0$:

$$r_{tot1} = r_a + r'_2 = r_a + \frac{m_{12} k_{ad}^2 r_2}{(k_{cd} + 1)^2}$$

$$x_{tot1} = x_a + \frac{m_{12} k_{ad}^2}{(k_{cd} + 1)^2} (x_d + x_{com})$$

for $s=0$

$$r_{tot0} = r_a + \frac{m_{12} k_{ad}^2 [r_2 (k_{cd} + 1) - x_{com} \sin \beta]}{k_{cd} (k_{cd} + 1)^2}$$

$$x_{tot0} = x_a + \frac{m_{12} k_{ad}^2 [x_{com} (k_{cd} + 1) + r_2 \sin \beta]}{k_{cd} (k_{cd} + 1)^2}$$

for $s = \pm\infty$

$$r_{tot \pm\infty} = r_a + \frac{m_{12} k_{ad}^2 k_{cd} \sin \beta}{(k_{cd} + 1)^2} x_d$$

$$x_{tot \pm\infty} = x_a + \frac{m_{12} k_{ad}^2}{(k_{cd} + 1)} x_d$$

With complete absence of angular shift of the winding ω_{com} with respect to the winding ω_a it is necessary to assume not only that $\cos \beta \cong 1.0$, but also that $\sin \beta = 0$ and thus the above formulas for the parameters r_{tot} and x_{tot} for $s=1.0$, $s=\pm\infty$ and $s=0$ are still greater simplified:

for $\beta = 0$, $s = 1.0$

$$r_{tot1} = r_a + \frac{m_{12} k_{ad}^2}{(k_{cd} + 1)^2} r_2$$

$$x_{tot1} = x_a + \frac{m_{12} k_{ad}^2}{(k_{cd} + 1)^2} (x_d + x_{com})$$

for $s = 0$

$$r_{tot0} = r_a + \frac{m_{12}k_{ad}^2}{k_{cd}(k_{cd} + 1)} r_2$$

$$x_{tot0} = x_a + \frac{m_{12}k_{ad}^2}{(k_{cd} + 1)k_{cd}} x_{com}$$

for $s = \pm \infty$

$$r_{tot \pm \infty} = r_a; \quad r'_2 = 0$$

$$x_{tot \pm \infty} = x_a + \frac{m_{12}k_{ad}^2}{(k_{cd} + 1)k_{cd}} x_d$$

29-4. Introduction of an Additional E.M.F. into the Secondary Circuit of an Induction Machine

Regulation of Speed. Assume that an induction motor with slip rings operates at $U_1 = \text{const}$, $f = \text{const}$ and $M_{stat} = \text{const}$. If we disregard the voltage drop in the stator, then, regardless of the motor operating conditions, $U_1 \cong E_1 \cong C_E \Phi_m = \text{const}$. Let $\overline{OA} = \dot{E}_{2s} = s\dot{E}_2$ be the vector of the main e.m.f. in the rotor lagging 90° behind the flux vector Φ_m (Fig. 29-2a). Hence

$$I_2 = \frac{E_2 s}{\sqrt{r_2^2 + x_{2s}^2}} = \frac{sE_2}{\sqrt{r_2^2 + (sx_2)^2}}$$

Under usual conditions of motor operation $r_2^2 \gg (sx_2)^2$; therefore it may be assumed that the current vector $\dot{I}_2 = \frac{s\dot{E}_2}{r_2}$ is in phase with the e.m.f. \dot{E}_{2s} .

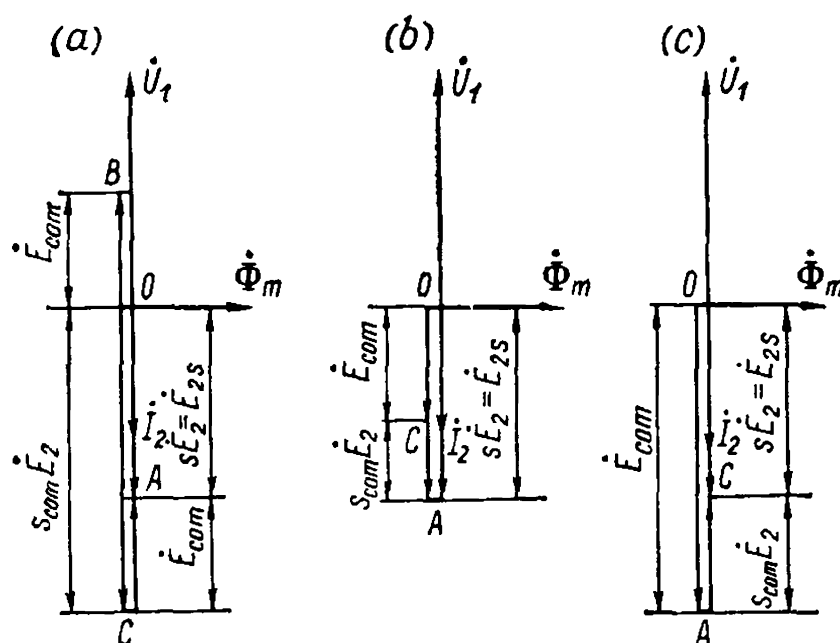


Fig. 29-2. Speed regulation of an induction motor by introducing an additional e. m. f. E_{com} into the rotor circuit

Let us introduce into the secondary circuit (i.e., into the rotor circuit) of the motor an additional e.m.f. $E_{com} = \overline{OB}$ directed against the main e.m.f. $E_{2s} = \overline{OA}$. At the initial moment, when the speed has not yet changed because of the inertia of the rotating parts of the motor, the secondary circuit e.m.f. drops to the value $sE_2 - E_{com}$, in accordance with which the current I_2 and, consequently, the torque $M = c_M I_2 \Phi_m$ decrease in the ratio $\frac{sE_2 - E_{com}}{sE_2}$. But since it has been assumed that the load torque remains constant, a negative dynamic torque develops on the shaft, and the motor speed begins to drop. This process of motor speed reduction and, consequently, of slip and main e.m.f. increase will continue until the current in the rotor and, consequently, the drive torque attain their previous values.

Let s_{com} be the new value of the slip and $s_{com} E_2$ the new value of the main rotor e.m.f. for steady-state operation of the motor after introduction of the additional e.m.f. E_{com} . Since with small values of s we neglect the inductive reactance $x_{2s} = sx_2$ in our discussion, we have

$$I_2 \cong \frac{s_{com} E_2 - E_{com}}{r_2} = \frac{s E_2}{r_2}$$

whence

$$s_{com} = s + \frac{E_{com}}{E_2} \quad (29-13)$$

Thus, when the e.m.f. E_{com} is introduced in opposition to the main e.m.f. E_{2s} , the speed of the motor drops and the slip becomes greater.

In principle, an additional e.m.f. E_{com} for which $s_{com} = 1$ can be introduced. But for this it is necessary that

$$1 = s + \frac{E_{com}}{E_2} \text{ or } E_{com} = E_2 (1 - s)$$

In no-load duty the slip $s \cong 0$; consequently, when the speed is regulated under these conditions equation (29-13) becomes

$$s_{0com} = \frac{E_{com}}{E_2} \quad (29-14)$$

where s_{0com} is the no-load slip corresponding to the additional e.m.f. E_{com} .

If $E_{com} = E_2$, the slip $s_{0com} = 1$ and the motor is similar to a static transformer without load.

Let us now introduce an additional e.m.f. $E_{com} = \overline{OB}$ (Fig. 29-2a) which is in phase with the e.m.f. E_{2s} under the same conditions as previously. Equation (29-13) now becomes

$$s_{com} = s - \frac{E_{com}}{E_2} \quad (29-15)$$

Reasoning as before, we may observe that *when the e.m.f. E_{com} is introduced concurrent with the main e.m.f. E_{2s} , the speed of the motor increases and the slip decreases.*

If $\frac{E_{com}}{E_2} > s$, the slip s_{com} becomes negative, and the induction machine, maintaining its motor duty, runs at a speed above synchronous so that the e.m.f. $s_{com}\dot{E}_2$ is directed against the e.m.f. \dot{E}_{com} (Fig. 29-2c). Here the current I_2 , which determines the torque of the motor, is produced not by the main slip e.m.f., but by another e.m.f. introduced from without, i.e., from another generator circuit which produces the additional e.m.f. E_{com} .

If the motor operates without load, equation (29-15) becomes

$$s_{com} = -\frac{E_{com}}{E_2} \quad (29-16)$$

By combining formulas (29-13) and (29-15) for $M_{stat} = \text{const}$ and formulas (29-14) and (29-16) for $M_{stat} = 0$, we get

$$s_{com} = s \pm \frac{E_{com}}{E_2} \quad (29-17)$$

and

$$s_{0com} = \pm \frac{E_{com}}{E_2} \quad (29-18)$$

The plus sign corresponds here to the action of the additional e.m.f. E_{com} when it opposes the main e.m.f. E_{2s} , and the minus sign to concurrent action.

Regulation of $\cos \varphi$. Let us assume as before that $U_1 = \text{const}$, $f = \text{const}$ and $M_{stat} = \text{const}$. Neglecting the voltage drop in the stator, we have $E_1 = \text{const}$ and $\Phi_m = \text{const}$.

Let us introduce into the secondary circuit of the motor the additional e.m.f. $\dot{E}_{com} = \overline{CD}$ at an angle $+90^\circ$ with respect to the main e.m.f. $\dot{E}_{2s} = \overline{OC}$, assuming that the e.m.f. E_{com} has the same slip frequency $f_2 = sf$ as the e.m.f. \dot{E}_{2s} (Fig. 29-3a). If $\dot{I}'_{2s} = \overline{OA}$ and $\dot{I}'_{2com} = \overline{AB}$ are the currents referred to the stator winding and due to the e.m.f.s E_{2s} and E_{com} then the current $\dot{I}'_2 = \dot{I}'_{2s} + \dot{I}'_{2com} = \overline{OB}$. The current in the primary circuit $\dot{I}_{1com} = \dot{I}_m + (-\dot{I}'_{2s}) + (-\dot{I}'_{2com}) =$

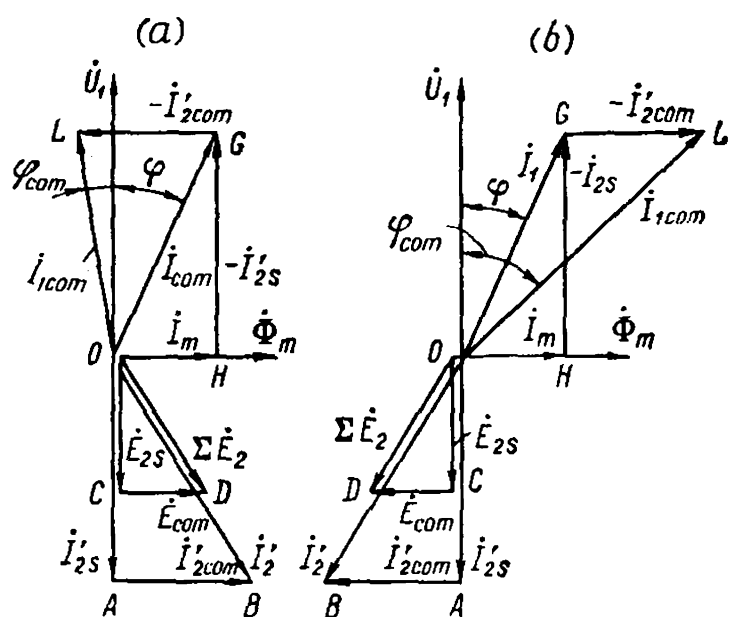


Fig. 29-3. Compensation of power factor ($\cos \varphi$) by introducing an additional e. m. f. into the rotor circuit

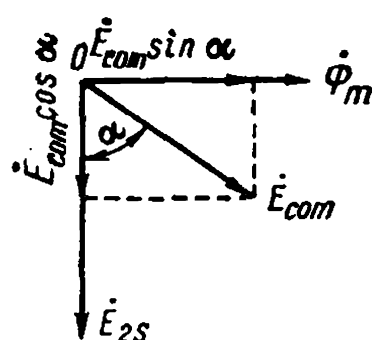


Fig. 29-4. General case of asynchronous motor regulation

$=\overline{OH}+\overline{HG}+\overline{GL}=\overline{OL}$. Thus, in the primary circuit of the motor there appears a current component $-I'_{2com}=\overline{GL}$ which positive compensation of the power factor $\cos \varphi$ is due to.

If the e.m.f. \dot{E}_{com} is introduced at an angle -90° to the e.m.f. \dot{E}_{2s} (Fig. 29-3b), this will cause an increase in the magnetizing current consumed from the power circuit by $-I'_{2com}$ and, consequently, a negative compensation of the power factor, i.e., a reduction of $\cos \varphi$.

By comparing Fig. 29-3a and b, we can see that the operation of an asynchronous motor, when $U_1=\text{const}$, $f=\text{const}$, $M_{stat}=\text{const}$ and the e.m.f. E_{com} varies, but when its phase remains either at $+90^\circ$ or -90° , can be assumed, from the viewpoint of the change in $\cos \varphi$, to be similar to synchronous motor operation with a U-curve characteristic (Sec. 12-5).

General Case. In the general case the additional e.m.f. \dot{E}_{com} may be at some angle α with the main e.m.f. \dot{E}_{2s} (Fig. 29-4). Here the e.m.f. \dot{E}_{com} is resolved into two components, $\dot{E}_{com} \cos \alpha$ and $\dot{E}_{com} \sin \alpha$, of which the first affects the speed of the motor, and the second its power factor.

29-5. Power Supplied from the Source of an Additional E.M.F.

According to the general rule, the active power of the additional e.m.f. source can be expressed by the formula

$$P_{com\ a} = m_2 E_{com} I_2 \cos (\widehat{E_{com} I_2})$$

where I_2 is the secondary circuit current of the motor.

If the e.m.f. E_{com} is in phase with the current I_2 , $P_{com\ a}$ will be directly proportional to E_{com} . If E_{com} is perpendicular to the direction of I_2 , the active power is zero, and the additional e.m.f. source delivers purely reactive power to the secondary circuit of the motor.

The above relations determine the energy balance in commutator machines and cascade systems and will later be applied to various types of these machines and systems.

29-6. Frequency Conversion by Means of a Commutator

It is known that the frequency of the additional e.m.f. must be equal to the slip frequency, regardless of the operating conditions of the machine. To produce such an e.m.f., we can use the property of an a.c. commutator machine to convert the frequency while retaining

the magnitude of the voltage across the brushes. The machine designed for this purpose has a rotor which is a d.c. machine armature whose winding is connected on one side, at points $a_1-b_1-c_1$ to the three-phase current system $A_1-B_1-C_1$ through three rings and the brushes set on them, and on the other side it is brought out to the commutator on which three brushes $a_2-b_2-c_2$ are set 120° apart (Fig. 29-5). The ring side will be referred to as the primary side of the frequency converter, and the commutator side as the secondary side. The stator is not shown in the circuit since it may have no winding and act only as a magnetic-circuit element.

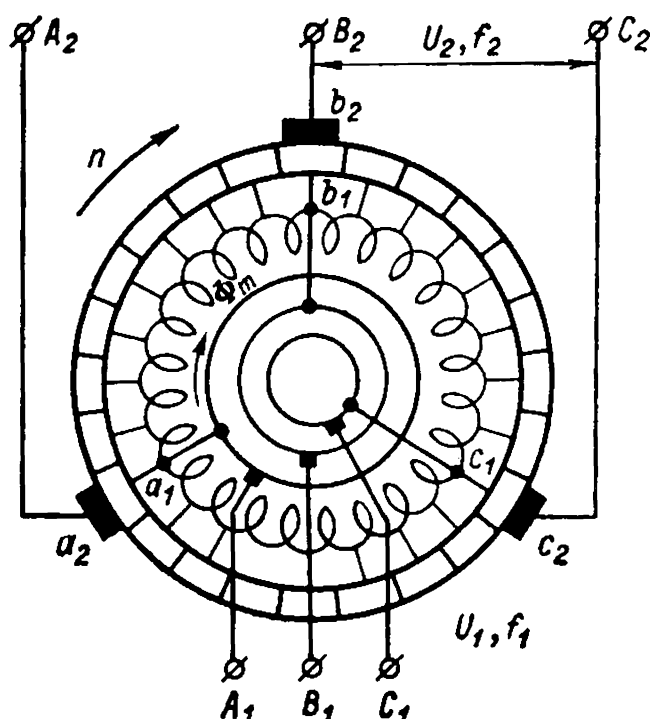


Fig. 29-5. Frequency converter

Consider first operation of the frequency converter when $n=0$. Let the brushes $a_2-b_2-c_2$ be placed on the commutator as shown in Fig. 29-5, i.e., opposite points $a_1-b_1-c_1$. This position of the brushes will be considered as the initial position and the angles of brush turn α will be counted from it.

The three-phase current flowing through the winding produces the flux Φ_m which rotates with respect to the rotor and, consequently, also in space with a speed $n_1 = \frac{f}{p}$ in one direction, for example, clockwise. If w_{ph} is the number of series-connected turns of one phase of the rotor winding and k_w is its winding factor, then, assuming that the e.m.f. E_2 produced by the flux Φ_m varies sinusoidally with time, we have $E_2 = \pi \sqrt{2} f w_{ph} k_w \Phi_m$.

Suppose the rotor winding is connected to the commutator in the simplest possible manner, i.e., each section of the winding is brought out to the adjacent commutator bar (Fig. 29-5). Hence the voltage distribution which at the given moment exists in the winding also exists on the commutator. The curve of voltage distribution on the commutator is referred to as the *potential wave of the commutator*. In the following discussion it will be considered sinusoidal (Fig. 29-6).

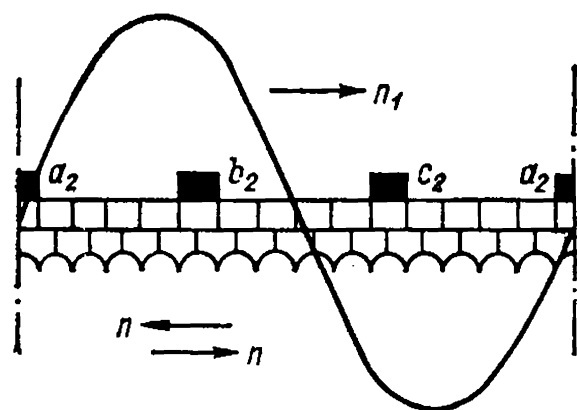


Fig. 29-6. Potential wave of commutator

The potential wave of the commutator rotates with respect to the rotor in the same direction as the flux Φ_m and at the same speed $n_1 = \frac{f}{p}$. Consequently, we obtain across the brushes on the commutator a three-phase voltage system with a frequency $f_2 = f = pn$. Neglecting the voltage drop in the armature winding, we have

$$\dot{U}_2 = \dot{E}_2 = \dot{U}_1 \quad (29-19)$$

If we displace brushes $a_2-b_2-c_2$ from the position shown in Fig. 29-5, the voltage \dot{U}_2 , while remaining constant in magnitude, will change in phase. Indeed, with a shift of the brushes (the potential wave) against the direction of flux rotation the axes of the windings between brushes a_2-b_2 , b_2-c_2 and c_2-a_2 are displaced in space in the same direction and by the same angle; consequently, the flux Φ_m now runs earlier past the axis of each winding indicated above by an angle α , and we have, accordingly,

$$\dot{U}_2 = \dot{U}_1 e^{+j\alpha}$$

With a shift of brushes in the direction of flux rotation we have

$$\dot{U}_2 = \dot{U}_1 e^{-j\alpha} \quad (29-20)$$

In the general case

$$\dot{U}_2 = \dot{U}_1 e^{\pm j\alpha}$$

Now let us make the rotor revolve at a speed n in any direction, for instance, against the potential wave. Since the voltage U_1 and frequency f of the supply circuit have not changed, the voltage wave, constant in magnitude, continues to run with respect to the rotor at the previous speed $n_1 = \frac{f}{p}$. But in space and, consequently, with respect to brushes $a_2-b_2-c_2$ which remain stationary in space, the wave now rotates at a speed $n_2 = n_1 - n$. When the rotor runs in the direction of the potential wave we have $n_2 = n_1 + n$. Accordingly, the frequency of the e.m.f. across brushes $a_2-b_2-c_2$ can, in the general case, be written as

$$f_2 = pn_2 = p(n_1 \pm n) = pn_1 \frac{n_1 \pm n}{n_1} = fs \quad (29-21)$$

According to formula (29-19), the voltage U_2 does not depend on the rotor speed n . On the other hand, the phase U_2 , as with a stationary rotor, is determined solely by the angle α , which fixes the spatial position of the windings a_2-b_2 , b_2-c_2 and c_2-a_2 with respect to the rotating flux Φ_m .

Thus, the system shown in Fig. 29-5 allows the frequency f_2 and the phase of voltage U_2 to be regulated with a practically constant voltage across the brushes, i.e., with $U_2 = \text{const}$. This valuable property of

the commutator is widely used both for speed regulation of asynchronous machines and for improving the power factor.

If it is necessary to change the voltage U_2 across the terminals of a frequency converter, this may be done by varying the voltage U_1 across the rings, for instance, by means of a transformer tapped on the secondary side and supplying the frequency converter from the slip-ring side.

29-7. Three-Phase Shunt Motor with Double Set of Brushes (Schrage-Richter Motor) [242, 250, 251, 264, 268a, 269]

This motor is an illustrative example of a machine in which the principle of introduction of an additional e.m.f. into the secondary circuit of the motor is used for regulation of the speed and partly of the power factor. A schematic diagram of this motor is shown in Fig. 29-7. Here R and Com are the windings arranged on the rotor, and St is the stator winding. The winding R is a usual three-phase winding which is connected through slip rings and terminals $A_1-B_1-C_1$ to a power circuit with the voltage U_1 and the frequency f . Thus, winding R serves as the primary winding of the motor. The secondary of the motor is stator winding St , consisting of three separate phase windings whose beginnings $A-B-C$ are connected to one set of brushes $a_1-b_1-c_1$, and whose ends $X-Y-Z$ are connected to the other set of brushes $a_2-b_2-c_2$. Winding Com serves for the production of an additional e.m.f. E_{com} and is a d.c. commutator-type winding wound in the same slots as winding R and electrically connected to stator winding St by means of the two brush sets mentioned above. For simplicity, winding Com is combined in Fig. 29-7 with the commutator and shown by a thick solid line. The brush sets $a_1-b_1-c_1$ and $a_2-b_2-c_2$ are fixed to two brush rockers which can be shifted in opposite directions, so that the angle 2γ between brushes a_1-a_2 , b_1-b_2 and c_1-c_2 may be reduced to zero or increased to a certain value.

The brush control device of the motor and its mechanical features are shown in Fig. 29-8a and b. Two fundamental designs of the mechanical drive for brush rockers 4-4' carrying brushes 5-5' are used. In both designs the rockers can be moved in opposite directions, but in the first one (Fig. 29-8a) rotation of handwheel 1 is transmitted to the rockers by means of gear train 2 and drive sheaves with cables 3-3'; while in the second design by means of gear trains 3-3'

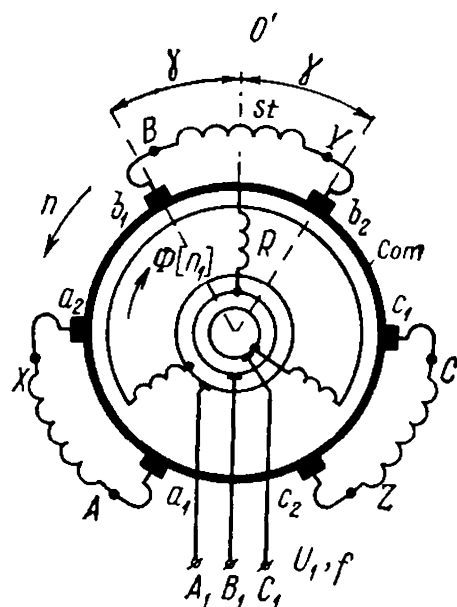


Fig. 29-7. Schematic diagram of Schrage-Richter motor

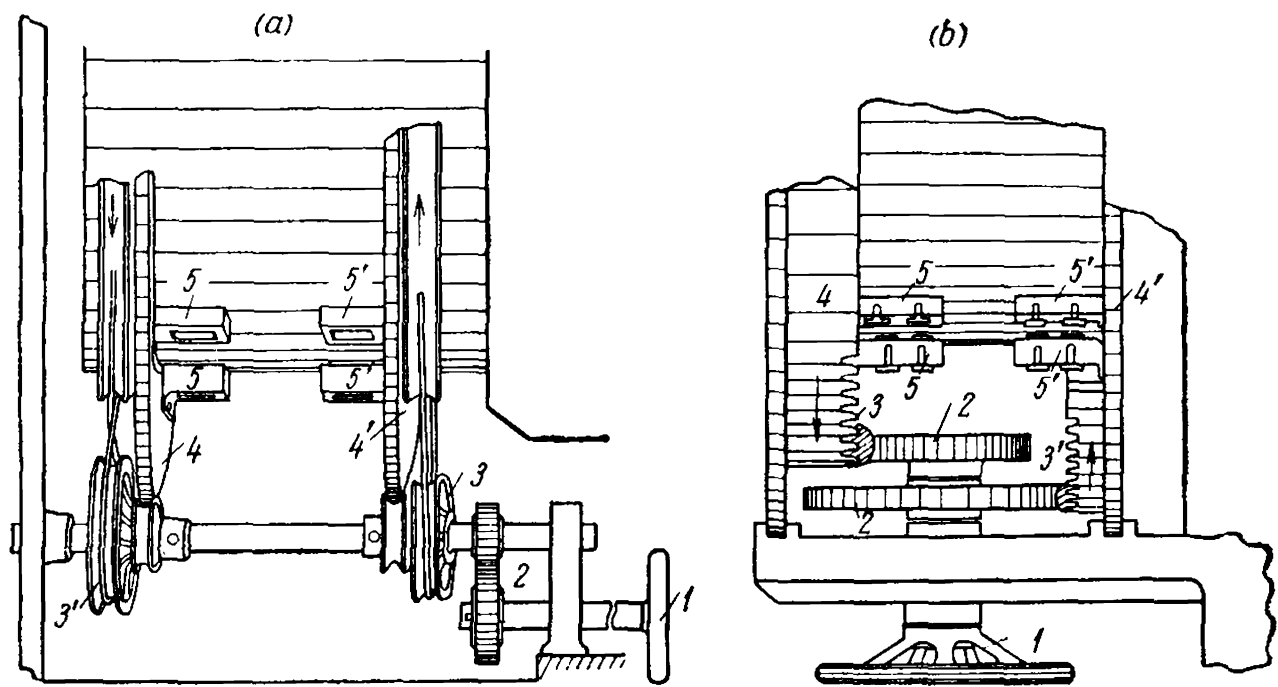


Fig. 29-8. Brush gear of Schrage-Richter motor

(Fig. 29-8b). Depending on whether the gear ratios in the first and second designs are the same or different, the brush rockers are displaced from their initial positions by the same or different angles (see Fig. 29-9a, b and c). Practice has shown that in small motors gearing systems are relatively costly. For this reason, small-diameter cables have found use, for example, in textile motors.

29-8. Regulation of Speed and Power Factor of Schrage-Richter Motor

Regulations of Speed. Let us assume the initial brush position on the commutator to be that in which each brush pair, for instance, the pair b_1 - b_2 , lies on the line coinciding with axis OO' of the stator winding St (dotted line in Fig. 29-9a). Here the angle 2γ between the

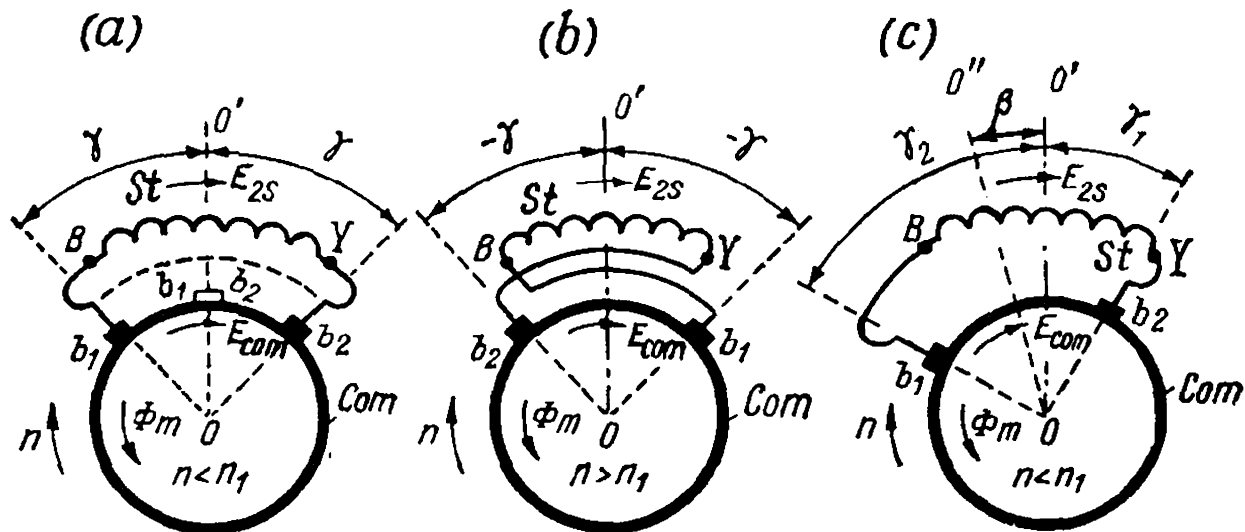


Fig. 29-9. Speed and power factor regulation of Schrage-Richter motor

brushes is zero, the additional e.m.f. E_{com} is also zero, and the motor operates as an inverted induction motor, rotating in the direction opposite to that of the flux Φ_m .

When brushes b_1 - b_2 are shifted through equal angles γ with respect to axis OO' , the circuit b_1 - B - Y - b_2 - b_1 is formed with the e.m.f.s E_{2s} and E_{com} . The axis of the part of winding Com between brushes b_1 and b_2 is fixed in space by the position of these brushes. Therefore, the flux Φ_m moves with respect to brushes b_1 - b_2 and, consequently, with respect to the part of the winding included between them with the

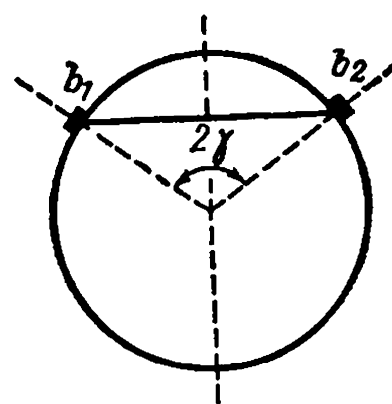


Fig. 29-10. Potential circle of winding Com

same speed as with respect to the stator winding St . The e.m.f. E_{com} produced by winding Com and applied across brushes b_1 - b_2 has the same slip frequency $f_2 = sf$ as the stator e.m.f. E_{2s} . Besides, the axes of windings Com and St coincide in space and, accordingly, the e.m.f.s E_{2s} and E_{com} coincide in phase. Assume that windings St and Com are wound in the same direction. The e.m.f.s E_{2s} and E_{com} now act in the circuit b_1 - B - Y - b_2 - b_1 against each other, this corresponding to the motor operating at subsynchronous speed (see Fig. 29-2a).

If the brush rockers are shifted so that brushes b_1 - b_2 change places (Fig. 29-9b), the e.m.f.s E_{2s} and E_{com} act in phase in the circuit b_2 - Y - B - b_1 - b_2 and the motor begins to operate at hypersynchronous speed (see Fig. 29-2c).

Let us consider the limits of speed regulation of a motor in the simplest case of no-load operation. According to equation (29-18), the slip at no-load is $s_{0com} = \pm \frac{E_{com}}{E_2}$. In the motor under consideration, the e.m.f. E_{com} is produced by the part of winding Com contained in the angle 2γ . Let ω_{com} be the number of turns of winding Com between two adjacent brushes of a rocker (for instance, between brushes b_1 - c_1 in Fig. 29-7); $\omega_{com\gamma}$ —the number of turns of this winding within the angle 2γ ; ω_2 —the number of turns in the stator winding phase; $K_{w,com}$, $k_{w\gamma}$, k_{w2} —the winding factors corresponding to these numbers of turns. Then

$$E_{com} = \pi \sqrt{2} f_2 \omega_{com\gamma} k_{w\gamma} \Phi_m$$

$$E_2 = \pi \sqrt{2} f_2 \omega_2 k_{w2} \Phi_m$$

But, from the potential circle for winding Com (Fig. 29-10) we have

$$b_1 b_2 = \omega_{com\gamma} k_{w\gamma} = \omega_{com} k_{w,com} \sin \gamma$$

Consequently,

$$s_{0com} = \pm \frac{E_{com}}{E_2} = \frac{\omega_{com} k_{w,com}}{\omega_2 k_{w2}} \sin \gamma \quad (29-22)$$

The plus and minus signs in this expression refer to the sign of the angle γ . The latter should be assumed positive when E_{com} opposes E_{2s} , and negative when these e.m.f.s are concurrent.

Since $s_{ocom} = \frac{n_1 - n_0}{n_1}$, where n_0 is the speed of the rotor at no-load,

$$n_0 = n_1 \left(1 - \frac{\omega_{com} k_{w.com}}{\omega_2 k_{w2}} \sin \gamma \right) \quad (29-23)$$

We see that the speed n_0 depends on the ratio between the number of turns in windings *Com* and *St* and on the angle γ between the brushes.

With the given ratio of $\frac{\omega_{com} k_{w.com}}{\omega_2 k_{w2}}$ the speed of a motor will be minimum when $\gamma = +90^\circ$ and maximum when $\gamma = -90^\circ$. Thus, for instance, with $\frac{\omega_{com} k_{w.com}}{\omega_2 k_{w2}} = \frac{1}{2}$ the speed of the motor can be regulated within the limits of 1 : 3.

Regulation of $\cos \varphi$. When the motor operates at subsynchronous speed, the power factor is relatively very small (see below, Fig. 29-13). To improve it, brushes b_1 - b_2 are shifted through different angles γ_1 and γ_2 with respect to axis OO' , so that axis OO'' of winding *Com* is displaced from axis OO' of winding *St* by an angle β in the direction of rotation of the flux Φ_m (Fig. 29-9c). The e.m.f. E_{com} now leads the e.m.f. E_{2s} , which corresponds to positive compensation of $\cos \varphi$ (Fig. 29-3a); but such compensation also affects the speed, since for the conditions under consideration formula (29-23) becomes

$$n_0 = n_1 \left(1 - \frac{\omega_{com} k_{w.com} \cos \alpha}{\omega_2 k_{w2}} \sin \gamma \right) \quad (29-24)$$

29-9. Vector Diagrams of Schrage-Richter Motor

Consider the vector diagrams of this motor for three operating conditions, namely, for sub- and hypersynchronous speed in the absence of the compensating effect, and for subsynchronous speed with simultaneous compensation of $\cos \varphi$. A vector diagram for subsynchronous speed is plotted in Fig. 29-11a. Here $\overline{OA} = sE_2$ is the main e.m.f. induced by the flux Φ_m in the motor secondary circuit (in stator *St*) in the absence of the additional e.m.f.; $\overline{CA} = \dot{E}_{com}$ is the additional e.m.f. directed opposite to the main e.m.f.; $\overline{OC} = s_{com} \dot{E}_2$ is the e.m.f. at the slip s_{com} ; $\overline{OB} = \dot{I}_2$ is the secondary current of the motor corresponding to the main e.m.f.; $\overline{DB} = \dot{I}_{2com}$ and $\overline{OD} = \dot{I}_{2s}$ are two imaginary currents of which the first corresponds to the e.m.f. E_{com} and the second to the e.m.f. $s_{com} E_2$. The magnetizing force of the secondary circuit is the arithmetical difference between the magnetizing forces of the stator windings and the additional winding on the rotor. If \dot{I}_s

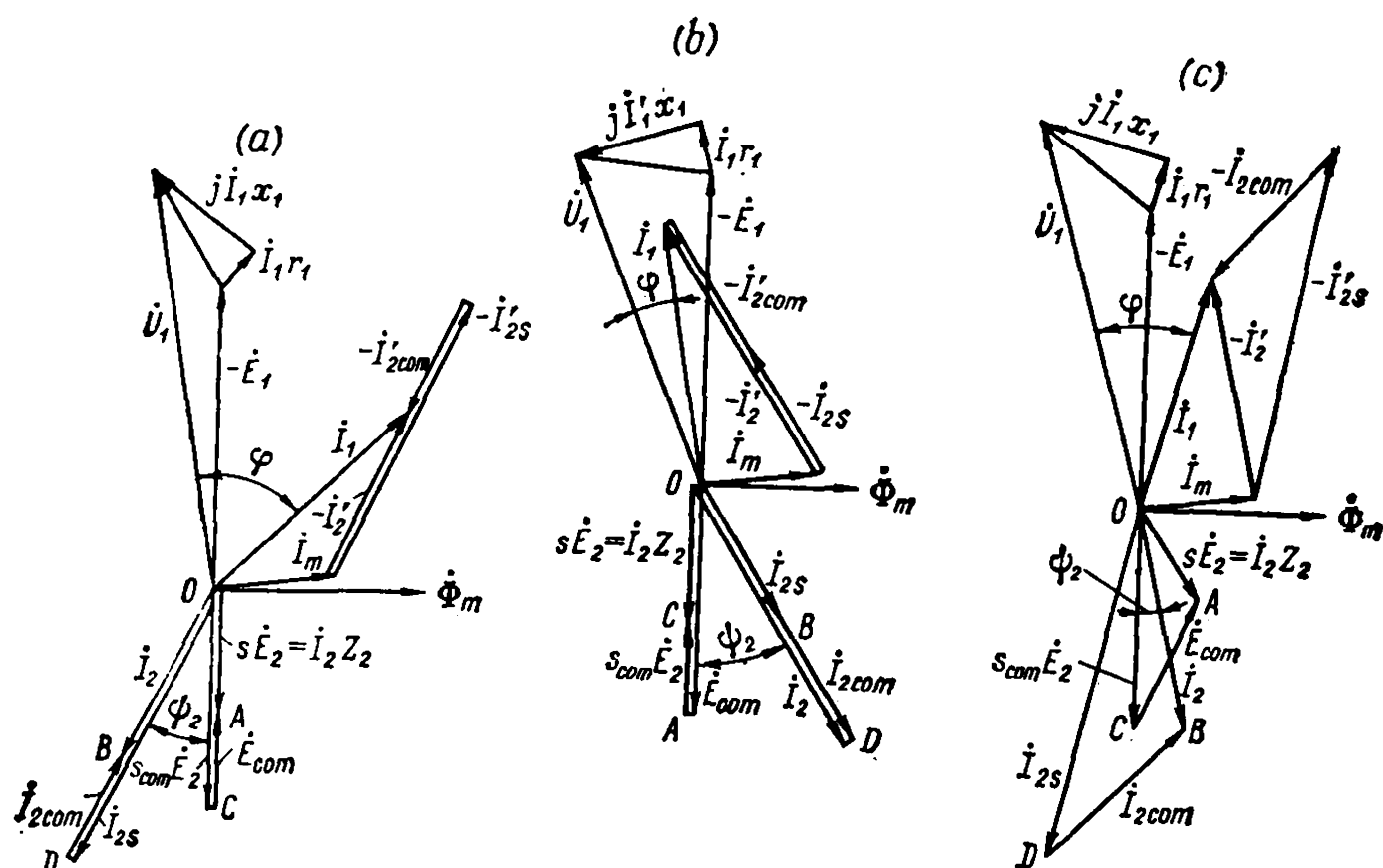


Fig. 29-11. Vector diagrams of Schrage-Richter motor:
 a — when $n < n_1$; b — when $n > n_1$; c — when $n > n_1$ with compensation of $\cos \varphi$

is the secondary current referred to the primary winding, then

$$m_1 \omega_1 k_{w1} \dot{I}'_2 = m_2 \omega_2 k_{w2} \dot{I}_2 - m_2 \omega_{com} \gamma k_{w\gamma} \dot{I}_2$$

or

$$\dot{I}'_2 = \dot{I}'_{2s} - \dot{I}'_{2com} \quad (29-25)$$

where

$$\dot{I}'_{2s} = \frac{m_2 \omega_2 k_{w2}}{m_1 \omega_1 k_{w1}} \dot{I}_2$$

and

$$\dot{I}'_{2com} = \frac{m_2 \omega_{com} \gamma k_{w\gamma}}{m_1 \omega_1 k_{w1}} \dot{I}_2$$

Consequently,

$$\dot{I}_1 = \dot{I}_m + (-\dot{I}'_2) = \dot{I}_m + (-\dot{I}'_{2s}) + (+\dot{I}'_{2com})$$

and, correspondingly,

$$\dot{U}_1 = -\dot{E}_1 + \dot{I}_1 r_1 + j \dot{I}_1 x_1$$

Figure 29-11b shows a vector diagram plotted for hypersynchronous speed. Since here the e.m.f.s $\dot{E}_{2s} = s\dot{E}_2$ and \dot{E}_{com} act concurrently, the magnetizing force of the secondary circuit is expressed as the sum of the magnetizing forces of the stator and additional windings. Si-

milar to formula (29-25) we have

$$\dot{I}'_2 = \dot{I}'_{2s} + \dot{I}'_{2com} \quad (29-26)$$

At hypersynchronous speed the slip s is negative. Therefore, the current \dot{I}'_2 leads the e.m.f. $s\dot{E}_2$ by an angle

$$\psi_2 = \arctan \left(-\frac{x_2 s_{com}}{r_2} \right)$$

and the motor operates with a $\cos \varphi$ considerably improved over that at subsynchronous speed.

Figure 29-11c also shows a vector diagram of a motor plotted for subsynchronous speed with simultaneous compensation of the power factor. The secondary circuit magnetizing forces is here the vector sum of the magnetizing forces produced by the currents \dot{I}'_{2s} and \dot{I}'_{2com} , i.e.,

$$\dot{I}'_2 = \dot{I}'_{2s} + \dot{I}'_{2com}$$

It can be seen from the diagram that the power factor of a motor operating at subsynchronous speed can be substantially improved in comparison with operation without compensation of $\cos \varphi$.

29-10. Characteristics of Schrage-Richter Motor

Since at $U_1 = \text{const}$ and $f = \text{const}$ the main flux $\Phi_m \cong \text{const}$, the mechanical characteristic of the motor $n = f(M)$ at a given angle 2γ between the brushes is of a rigid nature. Figure 29-12 gives curves showing this relation for three values of the angle 2γ . It follows from the curves that the motor at the limiting magnitudes of 2γ (the lower and upper curves) has relatively increased speed changes. This can be explained by the fact that the resistance of the secondary circuit in the machine is greater under these conditions than the resistance under asynchronous conditions, i.e., when $2\gamma = 0$. Figure 29-13 shows curves of $\cos \varphi = f(M)$ for the same values of 2γ .

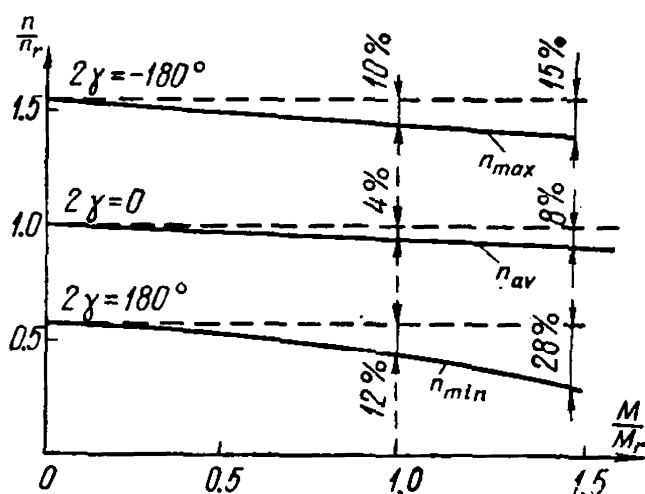


Fig. 29-12. Curves of $n = f(M)$ for Schrage-Richter motor with $\gamma = \text{var}$

For the lowest speed stage the curve $\cos \varphi = f(M)$ is given for conditions of compensation of the power factor.

The stalling torque of the motor over the speed regulation range of 3 : 1 is relatively high, viz., $\frac{M_{max}}{M_r} \cong 5.5$ at the maximum speed; $\frac{M_{max}}{M_r} \cong 2.8$ at the average speed and $\frac{M_{max}}{M_r} \cong 2$ at the minimum speed.

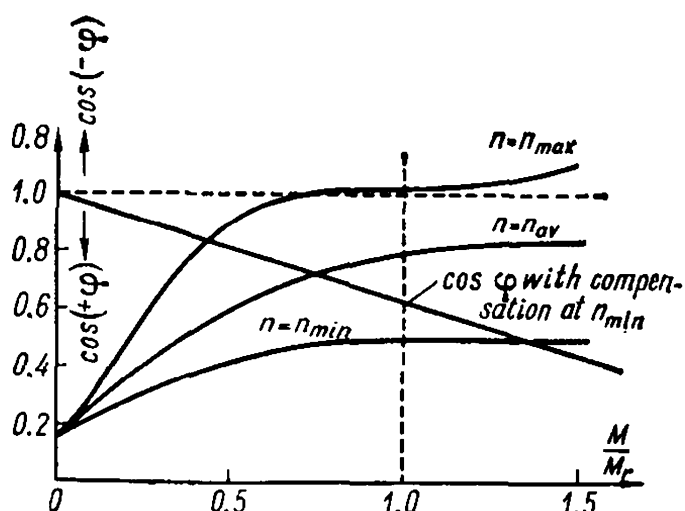


Fig. 29-13. Curves of $\cos \varphi = f(M)$ for Schrage-Richter motor with $\gamma = \text{var}$ and $\beta = \text{var}$

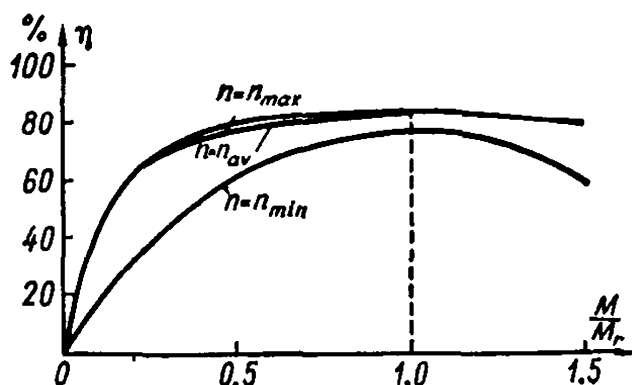


Fig. 29-14. Curves of $\eta = f(M)$ for Schrage-Richter motor with $\gamma = \text{var}$

Figure 29-14 shows curves of $\eta = f(M)$. The curve of maximum efficiency corresponds to the upper speed characteristic, and that of minimum efficiency to the lower one, although under the conditions of the former the mechanical and copper losses of the primary winding are greater. The increase in efficiency is explained by the increase in power developed by the motor at high speeds, since its power output at the shaft when $M = \text{const}$ (normal operating conditions of the motor) rises in direct proportion to its speed.

The starting characteristics of the motor are relatively favourable. There is no need in a special starting rheostat, since its role is performed by the additional e.m.f. E_{com} which, when the motor is started, must be directed against the main e.m.f. Here the starting current in the secondary circuit is $I_{st} = \frac{E_2 - E_{com}}{z_2}$

and can be limited in accordance with the relation between E_2 and E_{com} .

Figure 29-15 shows curves of the starting torque and starting current for a motor with speed regulation as a function of the angle 2γ between the brushes. It can be seen that when $2\gamma = 180^\circ$ the starting torque is relatively high ($M_{st} \cong 2.2M_r$), and the starting current ($I_{st} \cong 1.6I_r$) greatly reduced.

A disadvantage of the Schrage-Richter motor is that it is fed from the rotor side through a system of rings and brushes. Practice has shown that such a system functions reliably only when the voltage supplied to the motor is $U_1 \leq 500 \text{ V}$. On the other hand, the commutating con-

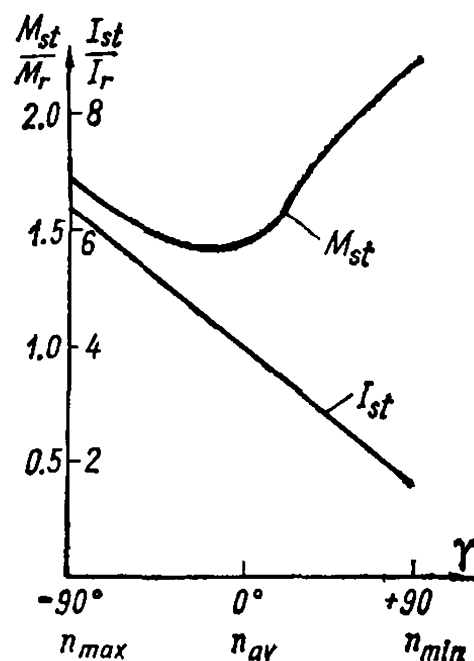


Fig. 29-15. Curves of $M_{st} = f(\gamma)$ and $I_{st} = f(\gamma)$

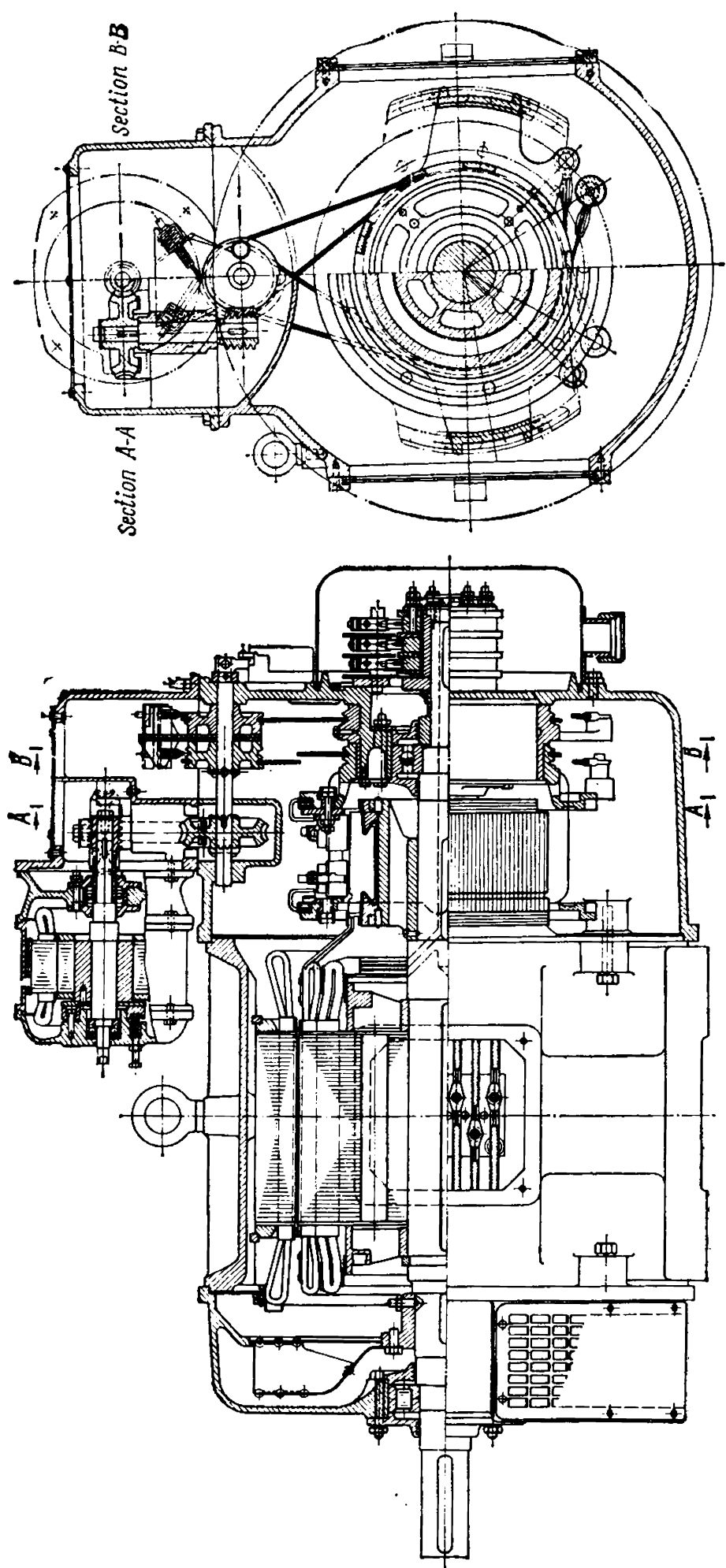


Fig. 29-16. Cross section of Schrage-Richter commutator motor

ditions of the motor are such that the power per pole pair is limited to 20-30 kVA at 50 Hz. These limits can be considerably extended, however, by employing a double squirrel-cage winding (see Vol. I, Sec. 3-13). Accordingly, motors of this type are mainly built with low ratings, though their power may sometimes reach 250 to 500 kW.

These motors have attained wide use in many branches of industry: textile, paper, printing, etc.

Example 29-1. Calculate the parameters and construct the circle diagrams of a shunt commutator motor supplied through the rotor (the Schrage-Richter type).

Initial data: the motor is of open design (Fig. 29-16) with speed regulation from 500 to 1400 rpm. The line voltage $U_1=220/380$ V, $f=50$ Hz. In the range of speed variation from 50 to 140%, the synchronous torque at the shaft remains constant. The power and other data are given in Table 29-1. The number of poles of the motor $2p=6$, the external diameter of the stator iron $D_a=370$ mm, the diameter of the stator bore $D_i=290$ mm, the pole pitch $\tau=151$ mm, the length of the active iron $l=190$ mm, the number of rotor slots $z_1=36$, the number of series-connected turns of the primary rotor winding $w_a=116$, the number of slots per pole and phase $q_a=2$, the winding pitch is from slot 1 to slot 6, the relative rotor winding pitch $\beta_a=\frac{5}{6}=0.833$.

The rotor slots (with a shape according to Fig. 29-17a) have the following data: $h_1=26.15$ mm, $h_2=10.0$ mm, $h_3=7.65$ mm, $h_4=1.0$ mm, $b_1=9$ mm, $b_2=14$ mm, $b_2''=15.3$ mm, $b_3=3.3$ mm, the rotor winding factors $k_{da}=0.966$, $k_{pa}=0.966$, $k_a=0.936$.

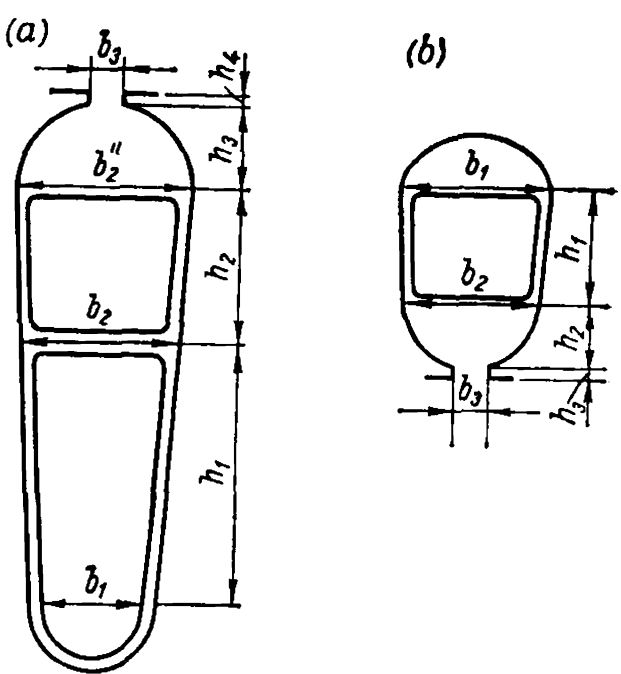


Fig. 29-17. Rotor and stator slots of Schrage-Richter commutator motor

TABLE 29-1

Parameter	Operating condition		
	hypersyn- chronous	asynchro- nous	subsynchron- ous
Speed, rpm	1,400	920	500
Power, kW	12.0	7.7	4.3
Primary current I_1 , A	22.7	17.0	15.3
Secondary current I_2 , A	56.2	56.4	63.2
Efficiency, %	80.3	85.0	74.0
$\cos \varphi$	~ 1.0	0.815	0.575
Slip, %	7	8	18
Angle between brushes, degrees	76°	0°	$-48^\circ 30'$

In the same slot as the primary winding of the rotor is the regulating (compensating) winding with $w_{com}=16$ series-connected turns and with $q_{com}=2$, pitch 1-6, $\beta_{com}=0.833$ and winding factors $k_{d.com}=0.960$, $k_{p.com}=0.966$, $k_{com}=0.927$.

The number of stator slots $z_2=54$, the number of slots per pole per phase $q_d=3$, number of series-connected turns $w_d=30$, the stator winding pitch is from slot 1 to slot 9, $\beta_d=0.889$, the winding factors $k_{d.d}=0.960$, $k_{p.d}=0.985$, $k_d=0.945$. The dimensions of the stator slot (Fig. 29-17b): $h_1=8.5$ mm, $h_2=5.9$ mm, $h_3=1.0$ mm, $b_1=12.8$ mm, $b_2=11.8$ mm, $b_3=3.2$ mm.

Parameters of motor winding in various operating conditions.

The permeance of the slots of the rotor part of the primary winding is

$$\lambda_{sa} = \lambda_{sa1} + \lambda_{sa2}$$

$$\lambda_{sa1} = \left[\frac{2h_1}{3(b_1+b_2)} + \frac{1}{2} \times 0.66 + \frac{2h_2}{b_2+b_2''} + \frac{2h_3 \times 0.75}{b_2''+b_3} + \frac{h_4}{b_3} \right] \times \frac{3\beta_a+1}{4} = 2.35$$

$$\lambda_{sa2} = \left[\frac{1}{2} \times \frac{2h_1}{b_2+b_2''} + \frac{2h_3 \times 0.75}{b_2''+b_3} + \frac{h_4}{b_3} \right] \frac{3\beta_a+1}{4} \times$$

$$\times \frac{w_{com} \frac{2}{\pi} \sin \gamma}{w_d k_d + w_{com} \frac{2}{\pi} \sin \gamma} = 1.1 \times \frac{15.3 \sin \gamma}{28.4 + 15.3 \sin \gamma}$$

The end-connection permeance is

$$\lambda_{end.a} = 0.75 \frac{\tau q_a}{l} \frac{3\beta_a-1}{2} = 0.68$$

The differential leakage permeance is

$$\lambda_{dif.a} = \frac{m_1 q_a k_{com}^2 \tau}{\pi^2 \delta k_\mu k_\delta} k_{dif} \left(1 - \frac{w_{com} \frac{2}{\pi} \sin \gamma}{w_d k_d + w_{com} \frac{2}{\pi} \sin \gamma} \right) = 1.65 \times \frac{28.4}{28.4 + 15.3 \sin \gamma}$$

The regulating winding slot portion permeances are

$$\lambda_{s.com} = \lambda_{s.com1} + \lambda_{s.com2}$$

$$\lambda_{s.com1} = \left[\frac{2h_2}{3(b_2+b_2'')} + \frac{2h_3 \times 0.75}{b_2''+b_3} + \frac{h_4}{b_3} \right] \frac{3\beta_{com}+1}{4} = 1.01$$

$$\lambda_{s.com2} = \left[\frac{2h_2}{2(b_2+b_2'')} + \frac{2h_3 \times 0.75}{b_2''+b_3} + \frac{h_4}{b_3} \right] \frac{3\beta_{com}+1}{4} \times$$

$$\times \frac{w_d k_d + w_{com} \frac{2}{\pi} \sin \gamma}{w_d k_d} = 1.152 \times 0.875 \frac{28.4 + 14.8 \sin \gamma}{28.4}$$

The end-connection permeance is

$$\lambda_{end.com} = \lambda_{end.a} = 0.68$$

The differential leakage permeance is

$$\lambda_{dif.com} = \frac{m_1 q_a k_d^2 \tau}{\pi^2 \delta k_\mu k_\delta} k_{dif} \left(1 - \frac{w_d k_d + w_{com} \frac{2}{\pi} \sin \gamma}{w_{com} \frac{2}{\pi} \sin \gamma} \right) = 1.65 \times \frac{28.4}{15.3 \sin \gamma}$$

The permeance of the slot portion of the main secondary winding is

λ_{sd} = [2h₁ / (3(b₁ + b₂)) + 1/2 × 0.66 + 2h₂ × 0.75 / (b₂ + b₃) + h₃ / b₃] (3β_d + 1) / 4 = 1.34

The permeance of the end connections is

λ_{end.d} = 0.57 (τ q_d / l) (3β_d - 1) / 2 = 1.13

The differential 'eakage permeance is

λ_{dif.d} = (m₂ q_d k_d² τ / (π² δ k_δ k_μ)) k_{dif} = 1.24

The inductive reactance is

x_m = (U_Φ - I₁ r₁) / I_m = (220 - 17.2 × 0.287) / 8.86 = 24.3 Ω

where I_m = 2 × (1.11 p F_Σ / (m ω_a k_a)) = (2 × 1.11 × 3 × 423.7) / (3 × 116 × 0.935) = 8.86 A

TABLE 29-2

Calculated quantities	Operating condition		
	hypersynchro- nous γ = -76°, β = 0°	asynchronous γ = 0°, β = 0°	subsynchronous γ = 48.5°, β = 0°
Primary winding			
λ _{sa1}	2.35	2.35	2.35
λ _{sa2}	-0.38	0	0.75
λ _{sa}	1.97	2.35	3.10
λ _{end a}	0.68	0.68	0.68
λ _{dif.a}	1.085	1.65	2.76
Σ λ	3.74	4.68	6.54
x _a	1.27	1.58	2.21
r _a	0.287	0.287	0.287
Regulation winding			
λ _{s.com1}	1.01	—	1.01
λ _{s.com2}	-3.22	—	1.63
λ _{s.com}	-2.21	—	2.64
λ _{end.com}	0.68	—	0.68
λ _{dif.com}	3.17	—	4.09
Σ λ	-4.71	—	7.41
x _{com}	-0.0485	0	0.0312
r _{com}	0.0232	0	0.0148
Resistance of brush contact	0.0285	0.0284	0.0253
λ _{sd}	—	1.34	—
λ _{end.d}	—	1.13	—
λ _{dif.d}	—	1.24	—
Σ λ	—	3.71	—
x _d	—	0.055	—
r _d	—	0.0254	—

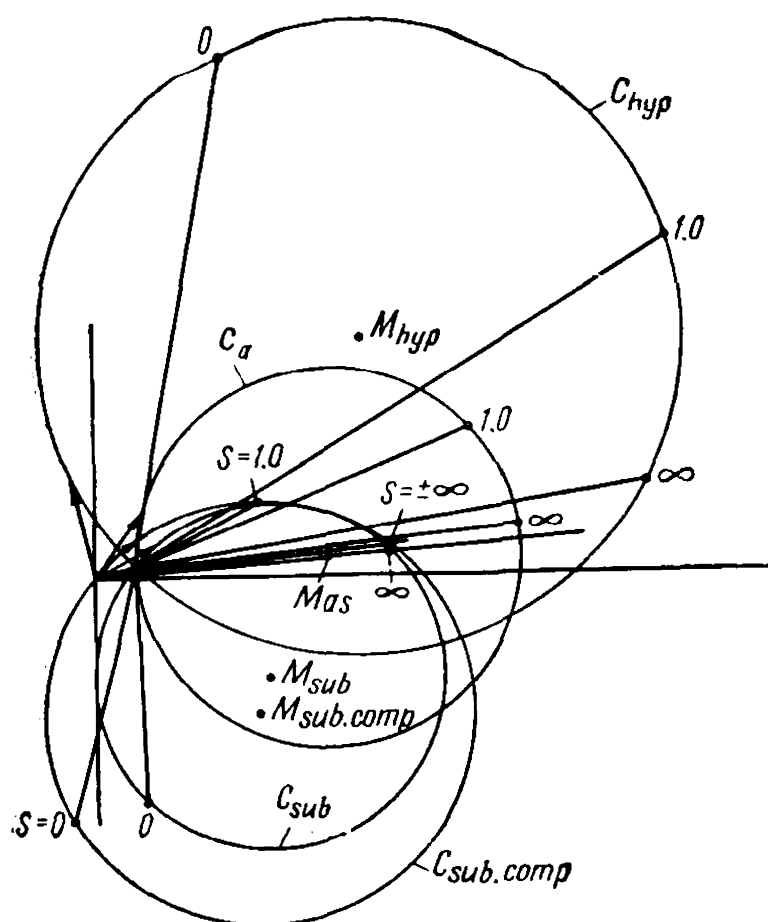


Fig. 29-18. Circle diagrams to example of Schrage-Richter commutator motor at hypersynchronous (C_{hyp}), asynchronous (C_{as}) and subsynchronous (C_{sub}) speeds, and at subsynchronous speed with compensation ($C_{sub.comp}$)

Main motor operation data: for hypersynchronous conditions $P = 12$ kW, $I = 22.7$ A, $\cos \varphi = 0.966$; for asynchronous conditions $P = 7.7$ kW, $I = 17$ A, $\cos \varphi = 0.815$; for subsynchronous conditions $P = 4.3$ kW, $I = 15.3$ A, $\cos \varphi = 0.46$; for subsynchronous compensated conditions $P = 4.3$ kW, $\cos \varphi = 0.655$

result of which at no-load the motor has a power factor $\cos \varphi \approx 1$, and under load an increased value of $\cos \varphi$.

Commutator motors with stator feeding have the main winding on the stator, and additional voltage E'_{2com} can be obtained both from an additional winding on the stator, and from a potential regulator. An interesting type of motor is the AEG commutator motor in which additional voltage is obtained simultaneously both from an additional winding on the stator, and from a small potential regulator [255].

29-11. Three-Phase Series Commutator Motor. Diagrams and Operating Principle [236, 237, 240]

Figure 29-19 shows a schematic diagram of a three-phase series commutator motor. It has two windings: winding St with ω_1 turns, arranged on the stator and wound as a.c. three-phase windings, and winding

The leakage factor is

$$\sigma_1 = 1 + \frac{x_1}{x_m} = 1 + \frac{x_1}{24.3}$$

The calculated values of the permeances, resistances and inductive reactances of the motor windings are given in Table 29-2.

The calculated parameters of the motor circle diagram for points $s = 1.0$, $s = 0$ and $s = \pm \infty$ in the hypersynchronous, asynchronous and subsynchronous operating conditions (with $\beta = 0$ and $\beta = 8^\circ$) are given in Table 29-3. These data have been used to plot the circle diagrams in Fig. 29-18 for hypersynchronous (circle C_{hyp}), subsynchronous with and without compensation (circles C_{sub} and $C_{sub.comp}$) and for asynchronous speeds of the motor (circle C_{as}).

Analysis of the circle diagrams in Fig. 29-18 shows that at hypersynchronous speed the reactive component of the current begins to decrease in comparison with the no-load current and therefore the motor has a very high $\cos \varphi$, close to unity, under load.

At subsynchronous speeds, on the contrary, the reactive component of the current begins to grow and therefore $\cos \varphi$ has a relatively low value. Here $\cos \varphi$ can be improved by introducing a compensating voltage, as a re-

TABLE 29-3

Calculated quantities	Operating conditions			
	hypersynchro- nous $\gamma = -76^\circ$, $\beta = 0^\circ$	asynchro- nous $\gamma = 0^\circ$, $\beta = 0^\circ$	subsynchro- nous $\gamma = +48.5^\circ$, $\beta = 0^\circ$	subsynchro- nous with com- pensation $\gamma = 48.5^\circ$, $\beta = 8^\circ$
$s = 1.0$				
r_1	0.287	0.287	0.287	0.287
x_1	1.25	1.58	2.21	2.21
r_2	0.0538	0.0538	0.0538	0.0538
x_d	0.055	0.055	0.055	0.055
x_{com}	-0.0485	0	0.0312	0.0312
$x_2 = x_d s + x_{com}$	0.0065	0.055	0.0862	0.0862
σ_1	1.05	1.065	1.09	1.09
σ_2	1.10	1.14	1.19	1.19
$r'_1 = r_1 \sigma_1$	0.301	0.306	0.313	0.313
$x'_1 = x_1 \sigma_1$	1.32	1.68	2.41	2.41
$r'_2 = r_2 \sigma_1^2$	0.0847	0.0614	0.078	0.078
$x'_2 = x_2 \sigma_1^2$	0.00715	0.0626	0.1025	0.1025
$r'_{2com} = \frac{m_{12} k_{ad}^2 r'_2}{(k_{cd} + 1)^2}$	0.534	0.900	3.20	3.20
$x'_{2com} = \frac{m_{12} k_{ad}^2 x'_2}{(k_{cd} + 1)^2}$	0.045	0.919	4.20	4.20
$r_{tot1} = r'_1 + r'_{2com}$	0.835	1.206	3.513	3.513
$x_{tot1} = x'_1 + x'_{2com}$	1.365	2.605	6.610	6.610
$z_{tot1} = \sqrt{r_{tot1}^2 + x_{tot1}^2}$	1.60	2.88	7.48	7.48
$\cos \varphi_{tot1} = \frac{r_{tot1}}{z_{tot1}}$	0.522	0.419	0.470	0.470
$I_{tot1} = \frac{U_1}{z_{tot1}}$	137.5	76.4	29.5	29.5
$s = 0$				
r_1	0.287	0.287	0.287	0.287
x_1	1.25	1.58	2.21	2.21
r_2	0.0538	0.0538	0.0538	0.0538
x_d	0.055	0.055	0.055	0.055
x_{com}	-0.0485	0	0.0312	0.0312
$x_2 = x_d s + x_{com}$	-0.0485	0	0.0312	0.0312
σ_1	1.05	1.065	1.09	1.09
σ_1^2	1.10	1.14	1.19	1.19
$r'_1 = r_1 \sigma_1$	0.301	0.306	0.313	0.313

Calculated quantities	Operating conditions			
	hypersynchro- nous $\gamma = -76^\circ$, $\beta = 0^\circ$	asynchro- nous $\gamma = 0^\circ$, $\beta = 0^\circ$	subsynchro- nous $\gamma = +48.5^\circ$, $\beta = 0^\circ$	subsynchronous with compensa- tion $\gamma = 48.5^\circ$, $\beta = 8^\circ$
$x'_1 = x_1 \sigma_1$	1.32	1.68	2.41	2.41
$r'_2 = r_2 \sigma_1^2$	0.0847	0.0614	0.078	0.078
$x'_2 = x_2 \sigma_1^2$	-0.0534	0	0.037	0.037
$r'_{2com} = \frac{m_{12} k_{ad}^2 [r'_2 (k_{cd} + 1) - x'_2 \sin \beta]}{k_{cd} (k_{cd} + 1)^2}$	1.56	∞	-4.74	-4.20
$x'_{2com} = \frac{m_{12} k_{ad}^2 [x'_2 (k_{cd} + 1) + r'_2 \sin \beta]}{k_{cd} (k_{cd} + 1)^2}$	-0.98	0	-2.24	-3.33
$r_{toto} = r'_1 + r'_{2com}$	1.86	∞	-4.43	-3.89
$x_{toto} = x'_1 + x'_{2com}$	-0.34	1.68	0.17	-0.92
$z_{toto} = \sqrt{r_{toto}^2 + x_{toto}^2}$	1.89		4.44	4.00
$\cos \varphi_{toto} = \frac{r_{toto}}{z_{toto}}$	0.985	1.0	0.999	0.972
I_{toto}	116	0	49.6	55.0
	$s = \pm \infty$			
r_1	0.287	0.287	0.287	0.287
x_1	1.25	1.58	2.21	2.21
r_2	0.0538	0.0538	0.0538	0.0538
x_d	0.055	0.055	0.055	0.055
x_{com}	-0.0485	0	0.0312	0.0312
x_2	0.055	0.055	0.055	0.055
σ_1	1.05	1.065	1.09	1.09
σ_1^2	1.10	1.14	1.19	1.19
$r'_1 = r_1 \sigma_1$	0.301	0.306	0.313	0.313
$x'_1 = x_1 \sigma_1$	1.32	1.68	2.41	2.41
$r'_2 = r_2 \sigma_1^2$	0.0847	0.0614	0.078	0.078
$x'_2 = x_2 \sigma_1^2$	0.0605	0.0627	0.0655	0.0655
$r'_{2com} = \frac{m_{12} k_{ad}^2 k_{cd} \sin \beta \cdot x'_2}{(k_{cd} + 1)^2}$	0	0	0	0.150
$x'_{2com} = \frac{m_{12} k_{ad}^2 x'_2}{k_{cd} + 1}$	0.585	0.919	1.60	1.60
$r_{tot\infty} = r'_1 + r'_{2com}$	0.301	0.306	0.313	0.463
$x_{tot\infty} = x'_1 + x'_{2com}$	1.905	2.60	4.01	4.01
$z_{tot\infty} = \sqrt{r_{tot\infty}^2 + x_{tot\infty}^2}$	1.93	2.62	4.02	4.04
$\cos \varphi_{tot\infty} = \frac{r_{tot\infty}}{z_{tot\infty}}$	0.156	0.117	0.073	0.114
$I_{tot\infty}$	114.0	84.0	54.7	54.5

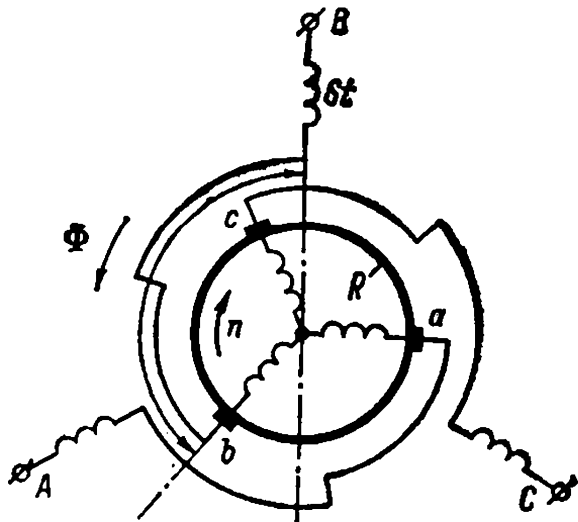


Fig. 29-19. Schematic diagram of a three-phase series commutator motor

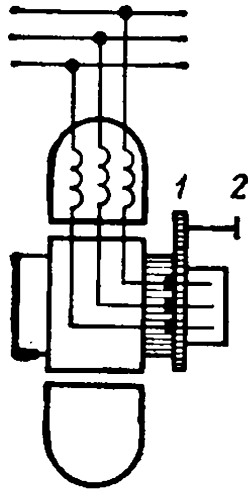


Fig. 29-20. Device for shifting brush system in a three-phase series commutator motor

R with w_2 turns, arranged on the rotor and wound as a d.c. winding with a commutator. To simplify the discussion, the delta-connected rotor winding has been replaced by an equivalent star-connected winding. In the simplest case the motor may have no intermediate transformer: the phase ends of the stator winding are connected on one side to brushes $a-b-c$ and on the other to external terminals $A-B-C$. The rocker carrying the brush system can be shifted in either direction through an arbitrary angle ρ by means of gear train 1 and handwheel 2 (Fig. 29-20). Since all the phase windings are symmetrical, only one phase, for instance, $B-b$ will be shown in the following discussion.

When the axes of the stator and rotor windings coincide, i.e., when the angle of displacement between them $\rho=0$, the no-load position is obtained (Fig. 29-21a). Here the motor in each phase has the maximum possible equivalent number of turns, therefore, the resultant

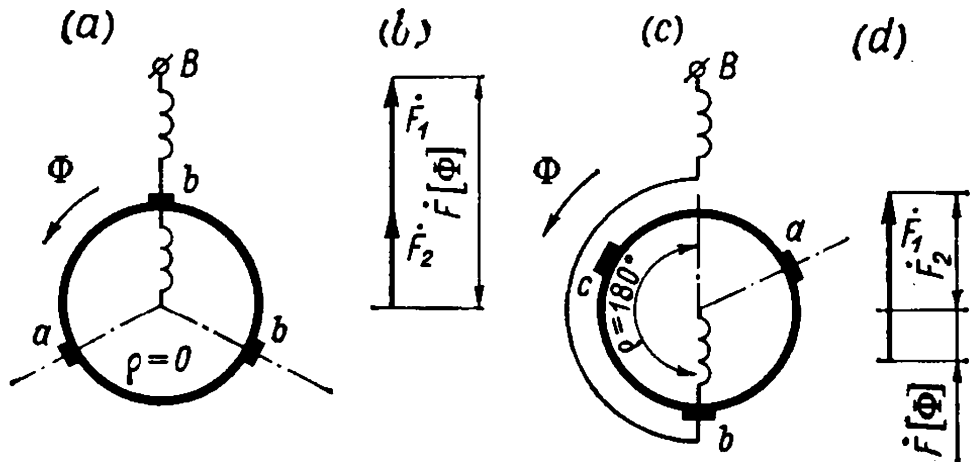


Fig. 29-21. Position of brushes of a three-phase motor:
 a — no-load; b — short-circuit

magnetic flux

$$\Phi_m \cong \frac{U_1}{\pi \sqrt{2} (\omega_1 k_{w1} + \omega_2 k_{w2}) f} \quad (29-27)$$

is minimum. Here ω_1 and ω_2 are the number of turns in the stator and rotor windings, and k_{w1} and k_{w2} are the winding factors.

If the brushes are turned through $\rho = 180^\circ$ from the no-load position, the short-circuit position will be obtained (Fig. 29-21c). Now the stator and rotor windings are as if bifilarly coiled; the equivalent number of turns in each phase is, therefore, the difference of the effective stator and rotor turns, corresponding to which the magnetic flux has the maximum value:

$$\Phi_m \cong \frac{U_1}{\pi \sqrt{2} (\omega_1 k_{w1} - \omega_2 k_{w2}) f} \quad (29-28)$$

In the no-load position the magnetizing forces F_1 and F_2 , produced by the current I flowing in the stator and rotor windings act concurrently and, therefore, the resultant magnetizing force $\dot{F} = \dot{F}_1 + \dot{F}_2$ (Fig. 29-21b). Conversely, in the short-circuit position the magnetizing forces \dot{F}_1 and \dot{F}_2 are in opposition and, therefore, $\dot{F} = \dot{F}_1 - \dot{F}_2$ (Fig. 29-21d). In the first case the axis of the flux Φ_m produced by the resultant magnetizing force F coincides with the axis of the rotor magnetizing force F_2 , whereas in the second case they are in opposition. Therefore, in both cases the torque of the motor is zero, since to develop torque on the shaft it is necessary that some angle α of displacement in space should exist between the axes of the flux Φ_m and rotor magnetizing force F_2 .

To obtain this angle, let us shift the brushes from the no-load position by an angle ρ in some direction, for instance, in the direction of rotation of the flux Φ_m (Fig. 29-19). Here the

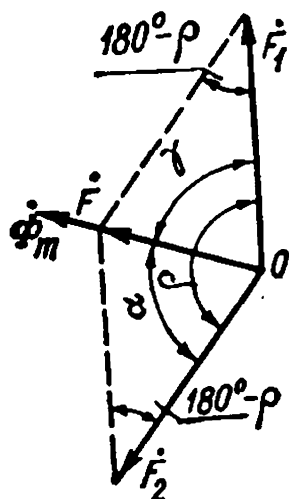


Fig. 29-22. Magnetizing force diagram of a three-phase series motor

space vector diagram of the stator and rotor magnetizing forces will acquire the form shown in Fig. 29-22. The resultant magnetizing force of the motor is expressed by the vector sum of the magnetizing forces \dot{F}_1 and \dot{F}_2 , i.e., $\dot{F} = \dot{F}_1 + \dot{F}_2$. The magnetizing force \dot{F} produces a flux $\dot{\Phi}_m$ shifted with respect to the magnetizing force \dot{F}_2 by an angle α .

The direction of rotor rotation depends on the direction of shifting the brushes from their no-load position. According to the general rule, the axis of the rotor winding tends to coincide with the axis of the stator winding, since here the flux penetrating the rotor winding reaches its maximum. Consequently, when the brushes are shifted against the direction of rotation of the flux Φ_m ,

the rotor will rotate concurrently with the flux, and, when the brushes are shifted in the direction of flux rotation, it will run against the flux. In this way the motor can be reversed. It should not be forgotten, however, that when the rotor runs against the field the steel losses increase in accordance with the frequency $f_2 = p(n_1 + n)$ and the transformer e.m.f. in the coil sections short-circuited by the brush also increases in accordance with the same frequency. Therefore, the normal direction of rotor rotation will be assumed to be the direction which coincides with flux rotation, this simultaneously decreasing the losses in the steel and improving the conditions of commutation.

29-12. Fundamental Equations of Three-Phase Series Commutator Motors

The voltage applied across the terminals of the stator primary winding will be

$$\dot{U}_1 = \dot{I}(z_1 + z_2) - \dot{E}_1 - \dot{E}_2$$

where z_1 and z_2 are the impedances of the stator and rotor windings w_1 and w_2 , and \dot{E}_1 and \dot{E}_2 are the e.m.f.s induced in these windings by the rotating mutual inductance fluxes Φ_m of both windings.

The mutual inductance flux is

$$\Phi_m = \dot{F}\lambda_m = \frac{4}{\pi^2} \sqrt{2} \cdot \frac{m_1}{2} \cdot \dot{I}_m \cdot \frac{w_1 k_{w_1}}{p} \cdot \lambda_m \quad (29-29)$$

where the permeance of the air-gap is

$$\lambda_m = \mu_0 \frac{\tau l}{\delta} \quad (29-30)$$

and the resultant motor magnetizing current is

$$\dot{I}_m = \frac{m_1 \dot{I} w_1 k_{w_1} + m_1 \dot{I} w_2 k_{w_2} e^{j\rho}}{m_1 w_1 k_{w_1}} = \dot{I} (1 + k_{21} e^{j\rho}) = \dot{I} + \dot{I}'_2 \quad (29-31)$$

The current \dot{I}_m is produced by the geometrical sum $\dot{I} + \dot{I}'_2$ of the reduced currents of windings w_1 and w_2 and can be expressed in the scale of the stator winding current I . The ratio of the effective number of turns is denoted by

$$k_{21} = \frac{w_2 k_{w_2}}{w_1 k_{w_1}}$$

If the brushes on the commutator are shifted in the direction of rotor rotation through the angle $+\rho$, then the magnetizing force

$$\dot{F}_2 \equiv \dot{I}'_2 = I k_{21} e^{+j\rho}$$

of winding w_2 will lead the magnetizing force $\dot{F}_1 \equiv \dot{I}_1 = \dot{I}$ of winding w_1 by the angle ρ . The resultant magnetizing force is equal to the geometrical sum of the magnetizing force of the stator and rotor systems

$$\dot{F} = \dot{F}_1 + \dot{F}_2$$

and can be expressed through the product of the current \dot{I} and the equivalent number of turns w :

$$\dot{F} = \dot{F}_1 + \dot{F}_2 = \dot{I}w_1k_{w_1} + \dot{I}w_2k_{w_2}e^{+j\rho} = \dot{I}w \quad (29-32)$$

$$w = w_1k_{w_1} [(1 + k_{21} \cos \rho) + jk_{21} \sin \rho] \cong$$

$$\cong w_1k_{w_1} \sqrt{1 + 2k_{21} \cos \rho + k_{21}^2} = w_1k_{w_1}k_m$$

here

$$k_m = \sqrt{1 + 2k_{21} \cos \rho + k_{21}^2}$$

The torque is

$$M = k\Phi_m F_2 \sin \alpha \cong k' F F_2 \sin \alpha$$

but since

$$\sin \alpha = \frac{F_1}{F} \sin \rho = \frac{\sin \rho}{k_m}$$

therefore

$$M = k' F_2 F_1 \sin \rho = k' F_2^2 k_{21} \sin \rho = k'' I_2^2 \sin \rho = k''' \Phi_m^2 \sin \rho \quad (29-33)$$

Denoting the inductive reactance of the magnetizing circuit with w_1 stator turns by x_m , we obtain the resultant impedance of the motor circuit:

$$z = z_1 + z_2 + jx_mk_m^2$$

The starting current, with the machine at standstill, is

$$\dot{I} = \frac{\dot{U}_1}{z} = \frac{\dot{U}_1}{z_1 + z_2 + jx_mk_m^2}$$

and, accordingly, the starting torque is

$$M = k'' I^2 \sin \rho = \frac{U_1^2 k'' \sin \rho}{[z_1 + z_2 + jx_m(1 + 2k_{21} \cos \rho + k_{21}^2)]^2}$$

If with a change in the angle ρ the voltage across the terminals \dot{U}_1 is regulated so that the starting current I remains constant, then the maximum torque is obtained with $\rho = 90^\circ$. If the angle ρ is changed with $\dot{U}_1 = \text{const}$, then the starting current will change, and the maximum torque will now be obtained when $90^\circ < \rho < 180^\circ$. The e.m.f.

of the stator winding produced by the mutual induction flux is

$$\begin{aligned}\dot{E}_1 &= -j\pi \sqrt{2} \Phi_m \omega_1 k_{w1} f_1 = \\ &= -j\pi \sqrt{2} \frac{4}{\pi^2} \frac{\sqrt{2}}{2} \frac{m_1}{2} I_m \frac{\omega_1 k_{w1}}{p} \lambda_m \omega_1 k_{w1} f_1 = -j I_m x_m\end{aligned}$$

where

$$x_m = \frac{4m_1\omega_1^2 k_{w1}^2 f_1 \lambda_m}{\pi p} \quad (29-34)$$

In a corresponding manner the e.m.f. produced in the rotor winding when the brushes are turned through an angle ρ in the direction of rotor motion is

$$\dot{E}_2 s = \dot{E}_2 \frac{\omega_2 k_{w2}}{\omega_1 k_{w1}} s e^{-i\rho} = -j \dot{I}_m x_m k_{12} s e^{-i\rho}$$

where the slip s takes into account the relative speed of the winding ω_2 in relation to the mutual induction flux Φ_m . The equation for the e.m.f. now becomes

$$\begin{aligned}\dot{U}_1 &= \dot{I} (z_1 + z_2) - \dot{E}_1 - \dot{E}_2 s = \dot{I} (z_1 + z_2) + j \dot{I}_m x_m (1 + k_{21} s e^{-i\rho}) = \\ &= \dot{I} (z_1 + z_2) + j \dot{I} x_m (1 + k_{21} e^{+i\rho}) (1 + k_{21} s e^{-i\rho})\end{aligned} \quad (29-35)$$

hence

$$\begin{aligned}\dot{I} &= \frac{\dot{U}_1}{z_1 + z_2 + j x_m (1 + k_{21} e^{+i\rho}) (1 + k_{21} s e^{-i\rho})} \cong \\ &\cong \frac{\dot{U}_1}{(r_1 + r_2) + j [(x_1 + x_2 s) + x_m \sqrt{(1 + 2k_{21} \cos \rho + k_{21}^2) (1 + 2k_{21} \cos \rho s + k_{21}^2 s^2)}]} \\ &\cong \frac{\dot{U}_1}{(r_1 + r_2) + j [(x_1 + x_2 s) + x_m k_m k_{ms}]} \quad (29-36)\end{aligned}$$

where x_2 is the inductive reactance of the rotor winding when $s=1$ and

$$k_{ms} = \sqrt{1 + 2k_{21} \cos \rho s + k_{21}^2 s^2}$$

The torque when the machine operates with a slip s is

$$M = k'' I^2 \sin \rho = \frac{U_1^2 k'' \sin \rho}{(z_1 + z_2 + j x_m k_m k_{ms})^2} \quad (29-37)$$

If we neglect the leakage inductive reactances of the stator and rotor windings and their resistances which are small compared with the mutual inductive reactance of the magnetizing circuit, then

$$M = k'' I^2 \sin \rho \cong \frac{U_1^2 k'' \sin \rho}{x_m^2 k_m^2 k_{ms}^2} \quad (29-38)$$

Here for the e.m.f. equation the following simplified expression is obtained:

$$\begin{aligned}\dot{U}_1 &\cong -\dot{E}_1 - \dot{E}_2 s = -\dot{E}_1 (1 + k_{21} e^{-j\rho s}) = \\ &= (\pi \sqrt{2} \omega_1 k_{w1}) \dot{\Phi}_m [(1 + k_{21} e^{-j\rho s}) - j k_{21} \sin \rho s] \cong \\ &\cong (\pi \sqrt{2} \omega_1 k_{w1}) \dot{\Phi}_m \sqrt{1 + 2k_{21} \cos \rho s + k_{21}^2 s^2}\end{aligned}$$

Taking into account that

$$\Phi_m^2 \equiv I^2 \equiv \frac{M}{k'' \sin \rho}$$

and also that

$$1 + 2k_{21} \cos \rho s + k_{21}^2 s^2 = \frac{U_1^2 k'' \sin \rho}{(\pi \sqrt{2} \omega_1 k_{w1} f_1) M} = \frac{U_1^2 \sin \rho}{k M}$$

we find from the quadratic equation with respect to the variable s that

$$\frac{n_2}{n_1} = (1 - s) = \left(1 - \frac{\cos \rho}{k_{21}}\right) \pm \sqrt{\frac{U_1^2 \sin \rho}{k M} - \frac{\sin^2 \rho}{k_{21}}} \quad (29-39)$$

where

$$k = \frac{k''}{\pi \sqrt{2} \omega_2 k_{w2} f_1}$$

To obtain stable operation of the motor the sign “+” before the root is selected, which corresponds to the angle of brush shift $90^\circ < \rho < 180^\circ$. To determine the slip s_m at which the torque is maximum, it is necessary to take the derivative $\frac{dM}{ds}$ from the expression (29-39) and equate it to zero:

$$\frac{dM}{ds} \frac{k}{\sin \rho} = \frac{U_1^2 2 \left(\cos \rho + \frac{s}{k_{21}} \right)}{(1 + 2k_{21} \cos \rho s + k_{21}^2 s^2)^2} = 0$$

whence $\cos \rho + \frac{s_m}{k_{21}} = 0$ and, therefore,

$$s_m = -\frac{\cos \rho}{k_{21}}$$

The torque M with $s=s_m$ reaches its maximum value, and with $s > s_m$ begins to decrease. From equation (29-39) it follows that with $M=0$ we have $n_2=\infty$ and when M increases the speed of the motor begins to noticeably drop along a curve having a hyperbolic nature. Consequently, the three-phase series motor with an increase of the torque has a series speed characteristic similar to that of a d.c. series motor.

29-13. Circle Diagrams of Current and Voltage

According to expression (29-36) the general equation for the current of a three-phase series commutator motor can be written as follows

$$I = \dot{U}_1 \frac{1}{\dot{C} + \dot{D}s} \tag{29-40}$$

where

$$\dot{C} = (r_1 + r_2) + j [x_1 + x_m (1 + k_{21} \cos \rho)]$$

and

$$\dot{D} = x_2 + jx_mk_{21} (\cos \rho + k_{21})$$

According to the general rule for loci (Sec.21-1), the current vector \dot{I} with a change in the parameter s within the limits $\pm \infty$ and a constant angle ρ will describe a circle passing through the origin of coordinates when the slip $s = \pm \infty$. For plotting the current circle three points of the circle can be used, namely, the currents for the slips $s = 0$

$$I = \dot{U}_1 \frac{1}{\dot{C}}$$

$s = 1.0$

$$I = \dot{U}_1 \frac{1}{\dot{C} + \dot{D}}$$

$s = \pm \infty$

$$I = 0$$

When the angle of brush shift ρ changes, the diameter of the current circle also changes and for various constant values of the angle we obtain a family of circles passing through the origin of coordinates. Figure 29-23 shows a family of four circles for angles of $\rho = 155^\circ$,

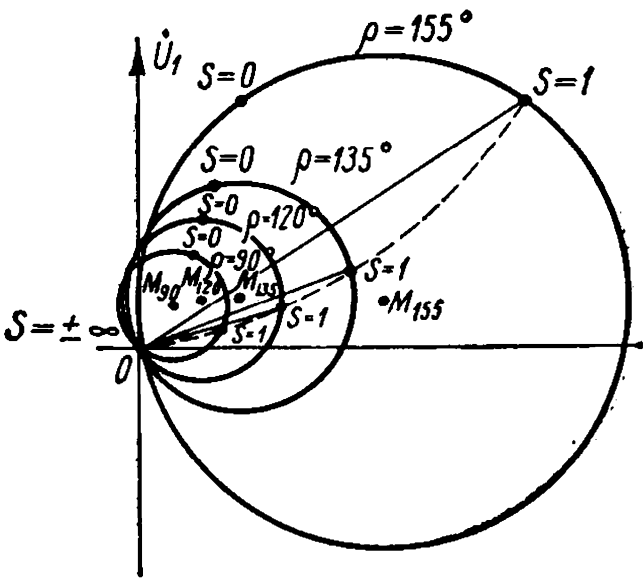


Fig. 29-23. Circle diagrams of a series commutator motor for various values of the angle ρ

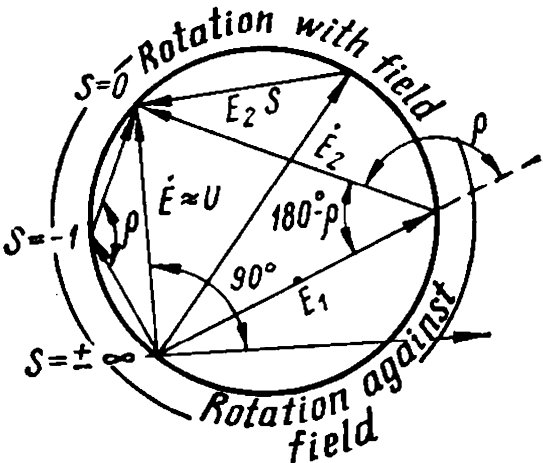


Fig. 29-24. Vector diagram of voltages for various slips with $\rho = \text{const}$

135°, 120° and 90°. From expression (29-35) for the approximate equality of the voltages

$$\dot{U}_1 = -\dot{E}_1 - \dot{E}_2 s e^{-j\rho}$$

it follows that when the slip s changes with $\dot{U}_1 = \text{const}$ the e.m.f.s \dot{E}_1 and $\dot{E}_2 s$ change both in magnitude and in phase. Since with $\rho = \text{const}$ the angle of displacement of the e.m.f.s \dot{E}_1 and $\dot{E}_2 s$ and also their vector sum remains constant, then with a change in the slip s the ends of e.m.f. vectors \dot{E}_1 and $\dot{E}_2 s$ travel along a circle, maintaining the given angle $180^\circ - \rho$ (Fig. 29-24). Shown in Fig. 29-24 are vector diagrams of the e.m.f.s \dot{E}_1 and $\dot{E}_2 s$ for $\omega_1 k_{w1} = \omega_2 k_{w2}$ at slips:

$$s = 1.0; 0 < s < 1 \text{ and } s = -1.0$$

29-14. Connection Diagrams of a Three-Phase Series Commutator Motor, Its Characteristics and Applications

Connection Diagrams of Motor. A series motor in operation cannot have more than 30 to 40 V per phase between commutator brushes because of commutating conditions, and this is why it is generally used with a transformer T which reduces the voltage across the rotor. A series motor can be designed with a conversion or intermediate-frequency transformer. The first diagram (Fig. 29-25a and b) is used when a voltage over 500 V is fed to a motor, the second (Fig. 29-25c and d) is for voltages from 500 to 110 V. A conversion transformer should be designed for full power of the motor, while an intermediate-frequency transformer only for that portion of the power which is supplied to the rotor of the motor or is electrically taken from it. Since the power of the rotor depends on the speed regulation range with respect to its synchronous speed, the dimensions of an intermediate transformer are the smaller, the less the range of regulation.

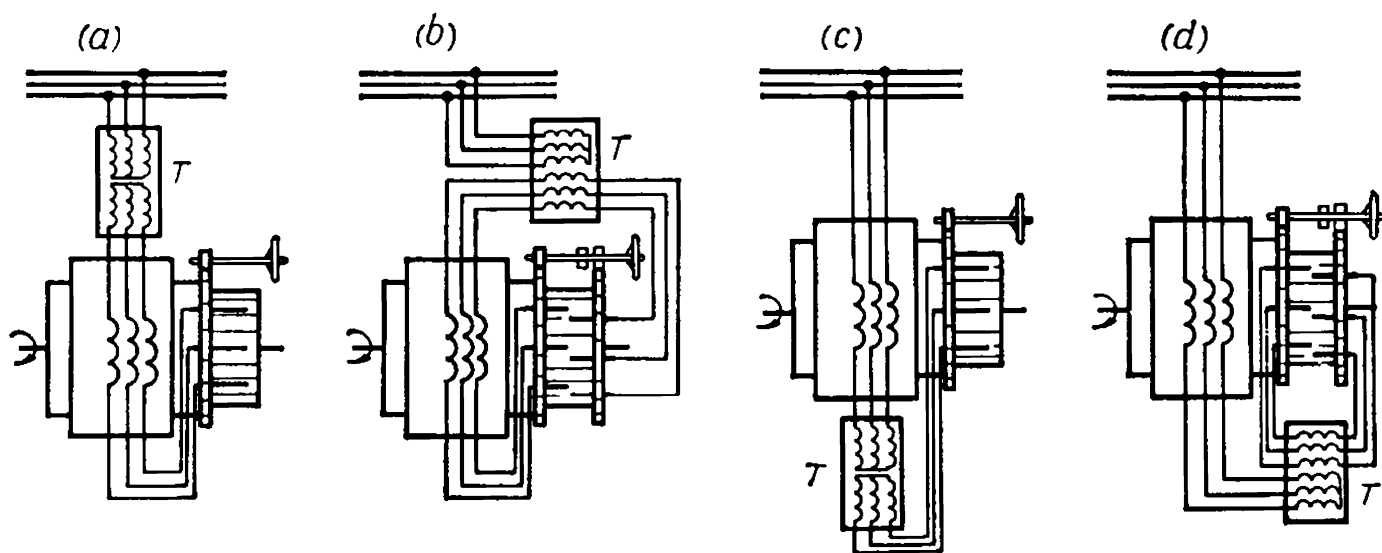


Fig. 29-25. Connection diagram of a three-phase series commutator motor

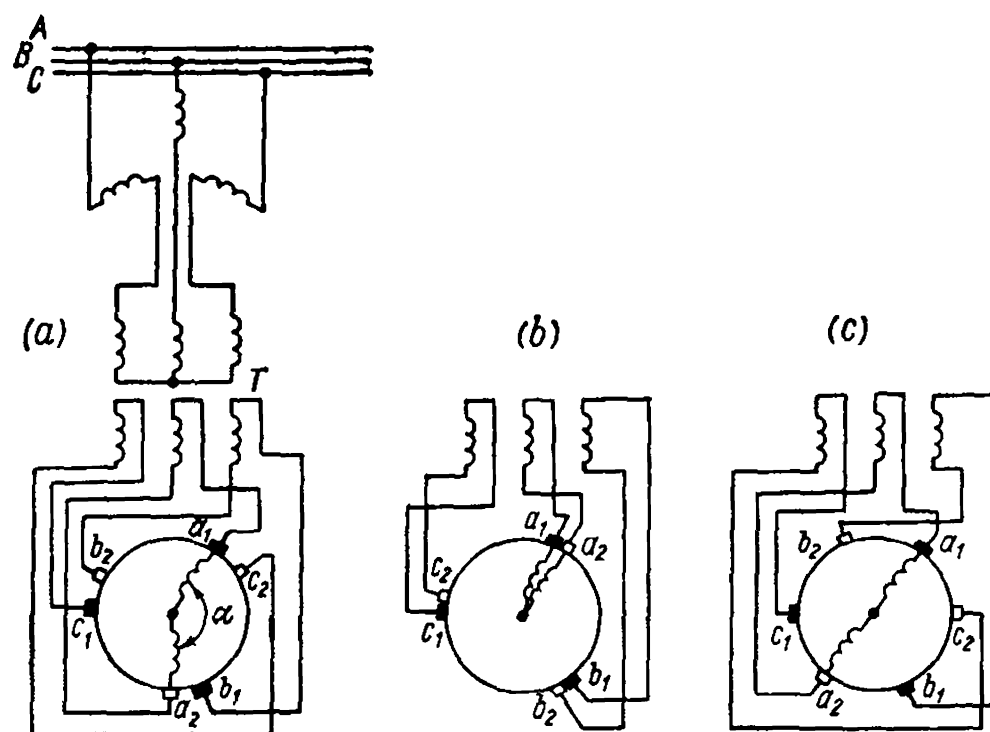


Fig. 29-26. Three-phase series commutator motor with a double system of brushes

Series Three-Phase Commutator Motor with Double Number of Brushes. To obtain the maximum torque for the given values of the current I and flux Φ_m , and, correspondingly, to obtain the maximum stability of the motor, the resultant magnetizing force F must form a right angle $\alpha = 90^\circ$ with the rotor magnetizing force, which is attained when $\sin \alpha = 1.0$.

This condition will be complied with automatically in a motor with a double number of brushes. This motor has a stationary system of brushes $a_1-b_1-c_1$ and a movable system $a_2-b_2-c_2$ (Fig. 29-26a).

Each pair of brushes belonging to one phase consists of one stationary and one movable brush, joined to the ends of one phase of the secondary circuit of intermediate transformer T .

The transformer primary winding is connected on one side to the terminals of the stator winding, and on the other is star-connected. With this diagram only part of the rotor winding contained between the stationary and movable brushes is connected to the transformer. In the no-load position the rotor winding is completely disconnected (Fig. 29-26b), and with a short circuit the entire rotor winding is connected (Fig. 29-26c). When the angle of brush rotation is varied, the magnitude of the connected portion of the rotor winding is changed, and also the angle between the rotor and stator winding axes.

Figure 29-27 shows a magnetizing force diagram for a motor with a double system of brushes, with an equal number of turns $\overline{AO} = \overline{OC}$. At no-load both systems coincide, and no voltage is delivered to the transformer secondary winding. If the movable brushes are turned

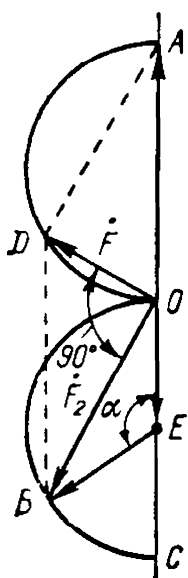


Fig. 29-27. Diagrams of magnetizing forces of a three-phase series commutator motor with a double system of brushes

through an angle α , the magnetizing force of the stationary brushes \overline{OE} retains its position, and the magnetizing force of the movable brushes shifts to position \overline{BE} , so that the resultant rotor magnetizing force will be depicted in magnitude and direction by vector \overline{OB} , while the resultant motor magnetizing force \overline{OD} will be equal to the vector sum of the magnetizing forces of the stator \overline{OA} and rotor \overline{OB} . When constructing the magnetizing force parallelogram \overline{OB} is equal and parallel to \overline{AD} , the latter being on the circumference ODA , therefore the angles ODA and BOD are right angles. Since for any value of the angular position of the brushes the angle between the resultant magnetizing force \vec{F} and the rotor magnetizing force \vec{F}_2 ($\angle DOB$) remains a right angle, the motor is always stable in operation at the most advantageous conditions of torque formation.

Characteristics and Applications of Series Three-Phase Commutator Motor. When the motor starts ($s=1.0$) its starting current I is determined by expression (29-36), and the starting torque M by expression (29-37).

Figure 29-28 shows the starting characteristics of a motor with an intermediate-frequency transformer.

Figure 29-29 depicts the motor mechanical characteristics $n=f(M)$ for various angular positions of the brushes on the commutator from $\rho=100^\circ$ to $\rho=160^\circ$ for a motor with one system of brushes, and in Fig. 29-30 for a motor with a double system of brushes when the angle changes from $\alpha=140^\circ$ to $\alpha=50^\circ$. A glance at the curves in Fig. 29-29 shows that the mechanical characteristics when the angle ρ changes from 100° to 135° have a limited range of stability, increasing with the angle ρ , while when it changes from 140° to 160° stable conditions of motor operation are obtained.

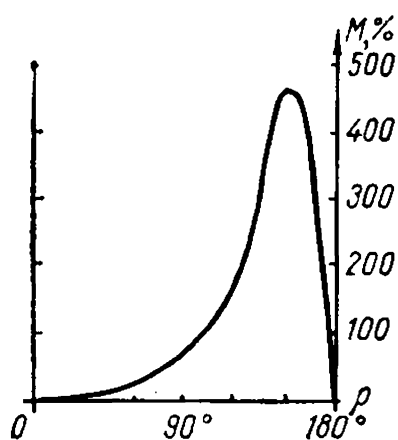


Fig. 29-28. Curve of starting torque versus angle ρ

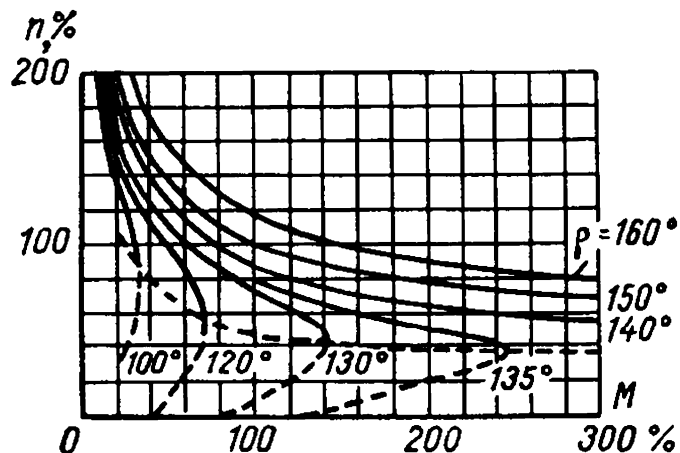


Fig. 29-29. Characteristic $n=f(M)$ with various values of ρ for a three-phase series commutator motor with one system of brushes

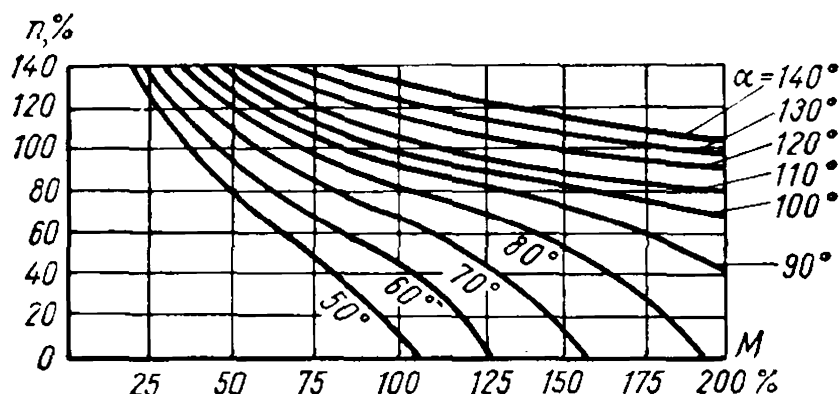


Fig. 29-30. Characteristic $n = f(M)$ with various values of α for a three-phase series commutator motor with a double system of brushes

From the mechanical characteristics (Fig. 29-30) it can be seen that for a motor with a double system of brushes we obtain stable conditions of operation for all angular positions of the brushes on the commutator, since here it is possible to obtain $\sin \alpha = 1.0$ for all angles.

Figure 29-31 gives the brake characteristics of a motor depending on the change in the torque at the shaft (n , $\cos \varphi$, η , I) for $\rho = 160^\circ$.

The series motor is used for drives where a definite torque at the shaft corresponds to each speed. These types of drives include centrifugal pumps and fans, compressors, crane and hoisting installations, printing presses, ring-spinning frames. With varying speed and a constant torque on the shaft speed regulation is possible in the ratio of 1 : 2.5, the speeds being limited to 20-30% above the synchronous and 50% below the synchronous speed. The lower limit is established by motor ventilating conditions, the upper by commutating conditions. When working with drives in which the torque at the shaft varies in proportion to the square of the speed (fans, centrifugal pumps, etc.) it is possible to have speed regulation up to 1 : 4. Here the increase in speed above the synchronous value should also not exceed 20-30%. A speed much lower than the synchronous value, up to 5 per cent of it, is possible, since with the small power developed in this case by the motor, its losses at low speeds are small and, therefore, poor ventilation will not cause trouble. When a motor must work with a varying torque at the shaft and constant speeds for the given conditions, it becomes more difficult to use a series motor, since for each value of the torque it is necessary to have another angular position of the brushes on the commutator; therefore, it is preferable to use motors with a parallel speed characteristic.

Series three-phase motors can be designed for relatively high powers, up to several hundred kilowatts.

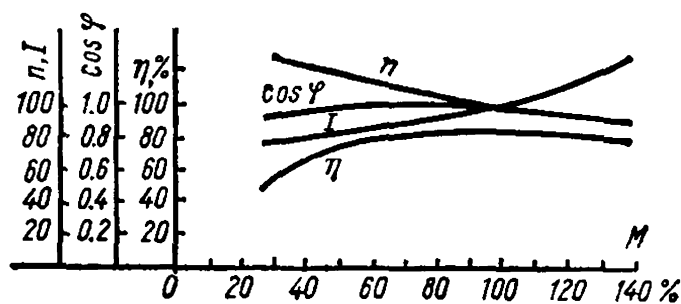


Fig. 29-31. Brake characteristics versus torque at shaft

Chapter

30

CASCADE CONNECTIONS OF INDUCTION AND COMMUTATOR MACHINES

30-1. General

Cascade-connected induction machines are systems designed for smooth and economic speed regulation of induction motors by introducing an additional e.m.f. into their secondary circuit. Simultaneously, this e.m.f. can also be used for regulation of the power factor of the cascade. Thus, cascade systems pursue, in fact, the same aim as the Schrage-Richter motor (Chap. 29), but in the latter the commutator machine, which is the source of the additional e.m.f., is built into the main induction machine. This makes the motor compact, but restricts the upper limit of its power from the viewpoint of both supply and commutation. Therefore, it is more expedient to build high-power induction motors as normal-type machines and use one or more d.c. or a.c. commutator machines for producing the additional e.m.f.

A large number of cascade systems are in existence, and sometimes they are very complicated.

The following basic types are distinguished: (a) mechanical cascades, where power is transmitted from one machine to the other through a shaft, and (b) electrical cascades, where power is electrically transmitted to the other machine. Besides, there are distinguished cascades where the magnitude of the e.m.f. E_{com} or E_{adv} is: (a) practically independent of the load current, (b) dependent on it to a great extent, and (c) dependent on the load only to a certain degree. In the first case the speed of the motor changes only slightly with the load, in the second case it changes considerably, and in the third the change is intermediate between the previous two cases. The first type of cascade is called the parallel, the second—the series, and the third—the mixed type.

Cascade connections with induction machines are used in drives with a relatively narrow speed regulation range (see Sec. 30-3) since experience shows that the more these limits are extended, the more it becomes expedient to employ d.c. motors fed from special converter installations.

30-2. Mechanical Cascade of an Induction Motor with a Rotary Converter and a D.C. Motor as the Regulating Machine (Kramer Cascade)

Figure 30-1 shows a schematic diagram of a Kramer cascade, with a mechanical connection [227]. The cascade consists of an induction motor IM with a phase-wound rotor, a d.c. machine DCM and a rotary converter RC . Machine DCM is mechanically coupled to the shaft of motor IM . During normal operation of the cascade the rings of motor IM are connected to the rings of excited converter RC , and the brushes on the commutator of the converter are connected to the brushes of excited machine DCM . Let us consider the process of speed and power factor regulation of the cascade, assuming that the load torque at the shaft remains constant, i.e., $M_{stat} = \text{const.}$

Let the cascade be connected to the power circuit and run at a speed $n_c < n_1$, where n_1 is the synchronous speed of motor IM . The converter RC operates on the a.c. side as a synchronous motor and converts the slip power into d.c. power. The direct-current machine DCM operates as a motor and, in converting electric power into mechanical power, returns to the shaft of the cascade the slip power less the losses in the auxiliary machines.

If we increase the excitation current of motor DCM , then at first moment when the cascade continues to rotate at its previous speed by inertia, the back e.m.f. of motor DCM increases. This causes the current I_a drawn by motor DCM from converter RC , and the current I_2 drawn from the rotor of motor IM into converter RC to decrease. The result is a reduction in the torque M of motor IM and, consequently, a rise in the negative dynamic torque at the shaft of the cascade, since, according to the given conditions, $M_{stat} = \text{const.}$ The speed of the cascade decreases, and accordingly the slip of motor IM , the frequency and the voltage across the rings of converter RC , its speed and, finally, the currents I_a and I_2 begin to increase. This process will continue until the current I_2 and, correspondingly, the torque M of the induction motor reach their previous magnitudes.

If we reduce the excitation current of motor DCM , its e.m.f. decreases and the process reverses in

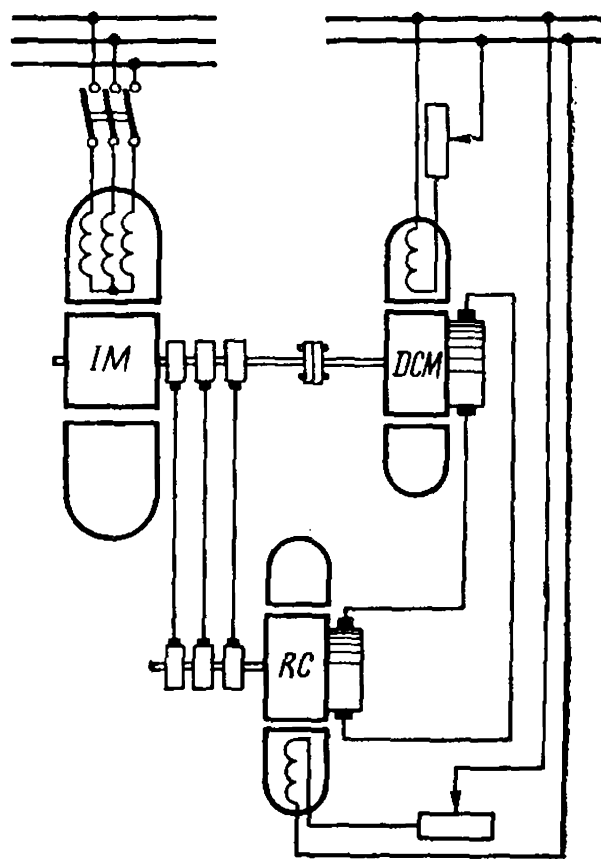


Fig. 30-1. Mechanical cascade of the Kramer type for subsynchronous speed

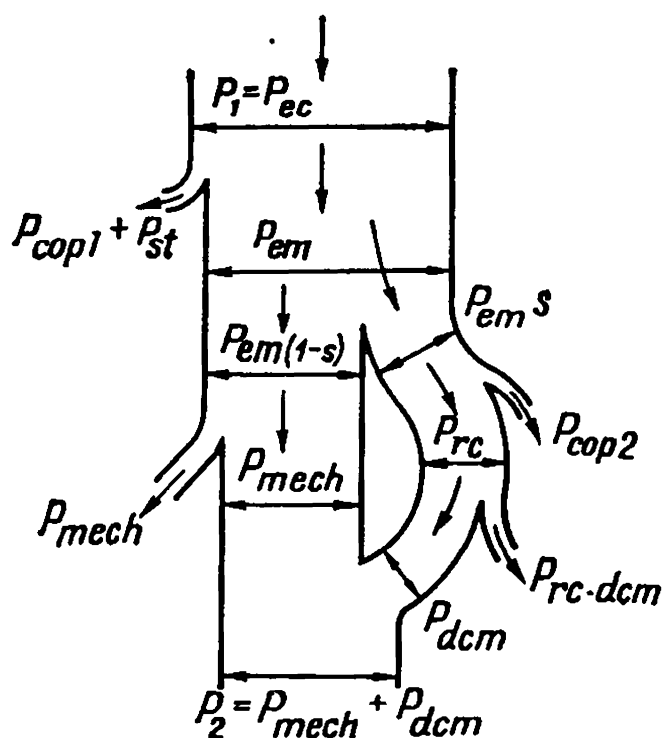


Fig. 30-2. Power-flow diagram of the Kramer cascade for subsynchronous speed

comparison with the previous one. The speed of the cascade increases and the slip frequency decreases, in accordance with which the speed of converter RC also drops. When the speed n_c of the cascade is close to the synchronous speed n_1 of motor IM , converter RC runs at a very low speed determined by the expression $n_{rc} = f_2 : p_{rc}$ and practically plays the role of a resistor connected to the secondary circuit of the induction motor. Under these conditions the additional e.m.f. introduced into the secondary circuit of motor IM equals zero. Consequently, the above cascade with mechanical connection permits the speed of induction motor IM to be regulated only downward from synchronous speed, i.e., it is a system with so-called *single-zone regulation*.

It follows that *speed regulation of a Kramer cascade is accomplished by changing the excitation current of the d.c. machine*.

Let us set the speed n_c of the cascade below its synchronous speed n_1 and, keeping the excitation of motor DCM and the load torque M_{stat} constant, alter the excitation current of converter RC . Since now the frequency and the voltage U_2 across the rings of motor IM remain approximately constant, converter RC operates as a synchronous motor under conditions of U-curve regulation. The increase in the excitation current of converter RC leads to the appearance of the current I_2 in the secondary circuit of motor IM , which leads the voltage U_2 across the rings of this motor; conversely, a decrease in the excitation current will result in lagging of I_2 behind U_2 . It should be noted that the degree of possible power factor regulation of a cascade depends on the slip frequency f_2 , since at low frequencies stable operation of converter RC in overexcited synchronous motor operating conditions is impossible.

It follows that *power factor regulation of a cascade is accomplished by altering the excitation current of the rotary converter*.

Figure 30-2 shows the power flow diagram of a Kramer cascade with mechanical connection. Here $P_1 = P_{ec}$ is the power consumed by motor IM from the external circuit; $P_{em} = P_1 - p_{cop1} - p_{st}$ is the electromagnetic power of motor IM ; $P_{em}(1-s)$ is the power transmitted by motor IM to the cascade shaft; P_{ems} is the slip power; p_{cop2} is the power which covers the copper losses in the rotor of motor IM ; P_{rc} is the

power delivered to converter RC ; $p_{rc, dcm}$ is the power which covers the losses in auxiliary machines RC and DCM ; P_{dcm} is the power transmitted to the shaft of the cascade by means of auxiliary machine DCM ; p_{mech} is the power which covers windage and mechanical losses of motor IM ; P_{mech} is the mechanical power developed by motor IM on the shaft of the cascade IM - RC - DCM ; and $P_2 = P_{mech} + P_{dcm}$ is the useful mechanical power on the shaft of the cascade.

According to the circuit in Fig. 30-1 and the power flow diagram in Fig. 30-2, the efficiency of the cascade is

$$\eta = \frac{P_2}{P_1 + U_{exc}i_{exc}} \times 100\%$$

where $U_{exc}i_{exc}$ is the power which covers the losses in the excitation circuits of auxiliary machines RC and DCM . From the power flow diagram in Fig. 30-2 it follows that if we disregard the losses in the cascade, the power rating of converter RC must be equal to the power rating of machine DCM , which, in turn, is proportional to the maximum value of the slip s which the cascade is rated at.

Thus, for instance, for speed regulation of the cascade in the range of up to 50%, the power rating of converter RC on the basis of the above assumption will be $P_{em}s = P_{em} \times 0.5 \cong 0.5P_1$. The power rating of the d.c. machine must also equal this value.

30-3. Cascade with Electrical Connection (Scherbius Cascade) [227]

A schematic diagram of a cascade with an electrical connection is shown in Fig. 30-3. Here, in contrast to the circuit in Fig. 30-1, the direct current machine DCM is mechanically coupled to an induction machine im , and only electrically connected to the main motor IM . This cascade circuit, similar to the one mentioned above, permits the speed to be regulated only downward from synchronous speed.

The power flow diagram of this cascade for speeds below synchronous is shown in Fig. 30-4. The power of the motor primary system P_1 is equal to the sum of the external circuit power P_{ec} and the secondary

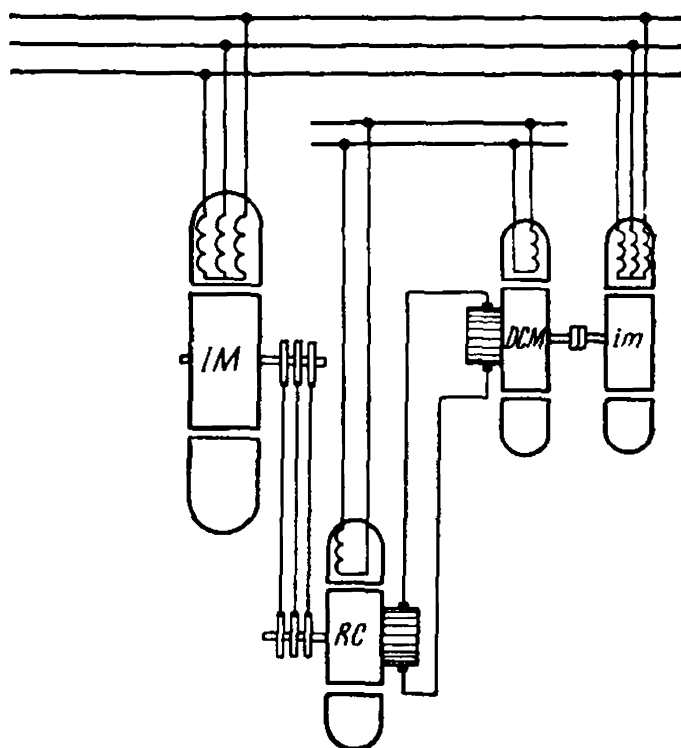


Fig. 30-3. Cascade with electrical connection for subsynchronous speed

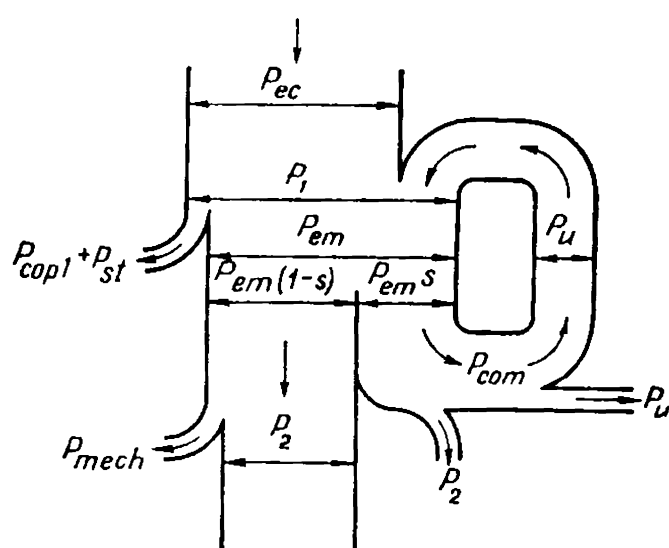


Fig. 30-4. Power flow diagram of cascade with electrical connection for subsynchronous speed

power P_u of the regulating unit, i.e., $P_1 = P_{ec} + P_u$.

The power P_1 less the losses $p_{cop1} + p_{st}$ in the stator winding and steel is converted into electromagnetic power P_{em} which is divided into the power $P_{em}(1-s)$ transmitted to the rotor of motor *IM* and the slip power $P_s = P_{em}s$ which is transmitted to the regulating unit; thus, $P_{em} = P_{mech}(1-s) + P_{em}s$.

The power $P_{em}(1-s)$ is converted into the total mechanical power of the motor P_{mech} ; by subtracting from this power the mechanical losses and the additional losses in the steel p_{mech} , we obtain the useful mechanical power of motor *IM* which, in view of the electrical connection between this motor and the regulating unit, is the power P_2 on the shaft of the entire unit; thus, $P_2 = P_{mech} - p_{mech}$.

The power P_{com} obtained by the regulating unit from the rings of motor *IM* is equal to the slip power $P_{em}s$ less the losses p_2 in the secondary circuit of the motor, i.e., $P_{com} = P_{em}s - p_2$. Finally, by subtracting from the power P_{com} the losses p_u in the regulating unit, we obtain the power P_u which is returned by the regulating unit to the primary circuit terminals of the motor; consequently, $P_u = P_{com} - p_u$.

From a comparison of the power flow diagrams in Figs. 30-2 and 30-4 it follows that a cascade with mechanical connection will operate most economically with constant power of the shaft, while a cascade with electrical connection will operate most efficiently with constant torque.

30-4. Characteristics of Mechanical and Electrical Cascade Connections

Characteristics of Kramer Mechanical Cascade Connections. The Kramer cascade is mainly used in rolling mills. To smooth out the peak loads on the power circuit feeding the cascade, the induction motor is mounted on the same shaft with a flywheel. Effective utilization of the kinetic energy of the flywheel is obtained provided that the speed-torque mechanical characteristic of the cascade $n = f(M)$ has a gradually drooping shape (curves 3 and 4 in Fig. 30-5). For this purpose, the series field winding is arranged on the main poles of motor *DCM* (Fig. 30-1), so that the magnetizing force produced by the winding is in the same direction as the e.m.f. of the shunt

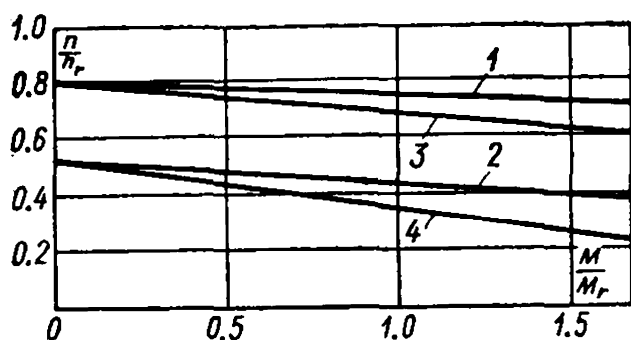


Fig. 30-5. Curves $n = f(M)$ for Kramer cascade

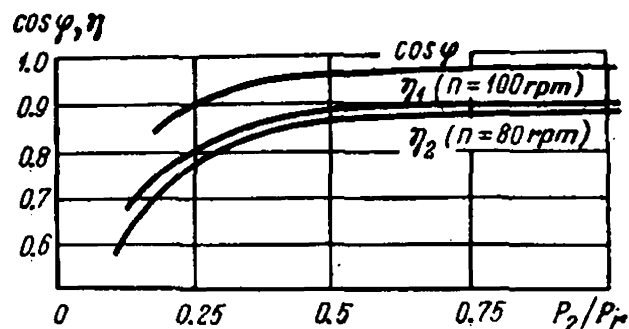


Fig. 30-6. Curves of efficiency η and power factor $\cos \varphi$ against P_2 for Kramer cascade

winding; the same results can be obtained by means of a special excitation unit.

The Kramer cascade allows the speed of the induction motor to be regulated down to 50% below synchronous speed. Figure 30-5 shows curves $n = f(M)$ for the Kramer cascade for two speed stages, curves 1 and 2 corresponding to cascade operation without the series field winding, and curves 3 and 4 with the winding.

As already mentioned (Sec. 30-2), the cascade is regulated by over-exciting the rotary converter; however, a strong overexcitation of the latter involves decrease in cascade efficiency η due to the increase in the losses of the converter. For this reason it is good to raise the power factor of the cascade to about 0.96. To keep the power factor of the cascade at its maximum value with variable speed, the poles of converter RC , in addition to the separate field winding provided on them, also carry another parallel or shunt winding which is connected across the d.c. terminals of the converter.

Figure 30-6 shows the power factor and efficiency ($\cos \varphi$ and η) characteristics of a 2200-kW, 125-rpm, 5500-V, 50-Hz Kramer cascade as functions of the shaft output power P_2 for two speeds: $n = 100$ and $n = 80$ rpm.

Characteristics of Scherbius Electrical Cascade. [228, 243, 257]. Originally, the Scherbius system was built only for single-zone regulation below the synchronous speed, but in 1916 a system with two-zone speed regulation was developed which is now relatively widely used.

Figure 30-7 depicts a schematic diagram of a Scherbius cascade for two-zone speed regulation. A compensated commutator generator CG with stator excitation (the generator is described in the next chapter) serves as the regulating commutator machine connected to the secondary circuit of regulated induction motor IM . The field winding FW of the commutator generator has its leads connected on one side to the generator main terminals through autotransformer AT and on the other side to the brushes of frequency converter FC which is mounted on the same shaft as the induction motor and connected to the same

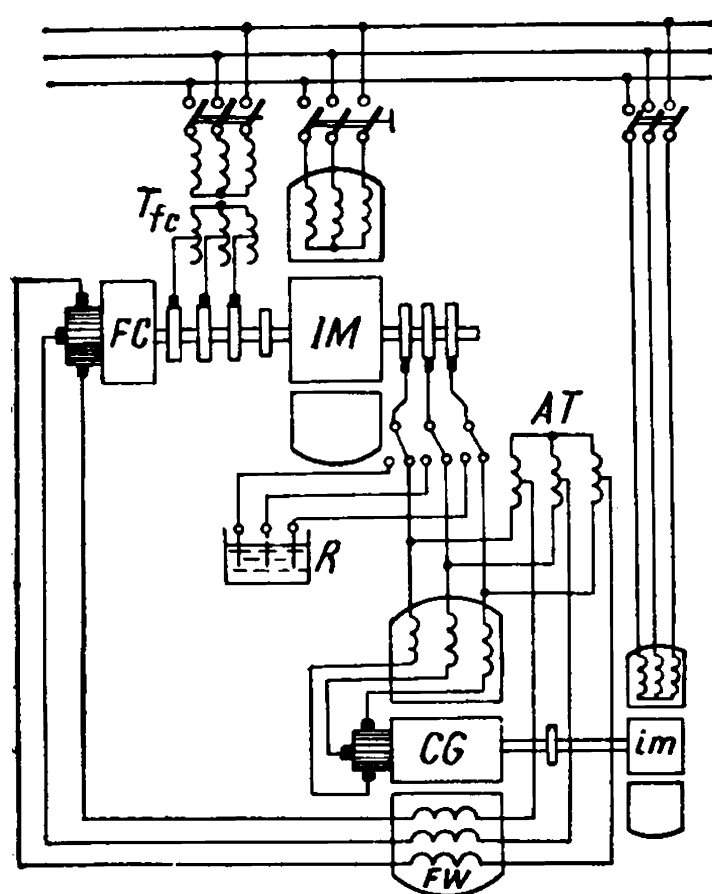


Fig. 30-7. Scherbius cascade for two-zone speed regulation

power circuit as the motor through transformer T_{fc} tapped on the secondary side. Commutator generator CG and autotransformer AT serve for speed and power factor regulation of the cascade under operating conditions more or less remote from the synchronous speed. As the machine approaches synchronism, the voltage across the rings of the induction motor continually decreases, and the action of generator CG and autotransformer AT becomes insufficient. It is therefore impossible to bring the cascade up to a speed over 95 to 96% of the synchronous speed.

To pass through synchronism, i.e., to obtain a cascade system with two-zone speed regulation, it is necessary to introduce an e.m.f. into

field winding FW of the commutator generator, such that an exciting current is provided at synchronous speed and speeds close to it. For this purpose a small frequency converter FC (Sec. 29-6) is used, the e.m.f. introduced by it into field winding FW having its magnitude regulated by transformer T_{fc} and its phase changed by shifting the brushes on the converter commutator. Thus, at speeds near synchronous, the frequency converter can affect both the speed and the power factor of the cascade connection.

When the cascade passes through synchronous speed, the starts and finishes of field winding FW must change places in accordance with the change in sign of the slip in the induction motor.

The commutator machine in the cascade in Fig. 30-7 may be built for power ratings from 1000 to 1100 kVA and a maximum frequency of 12 to 16 Hz. Therefore when the cascade has a speed regulation range of $\pm 25\%$, it may reach a power of 4000 kW which varies with regulation of the speed from 3000 to 5000 kW.

Chapter

31

POLYPHASE COMMUTATOR GENERATORS

31-1. Operating Principle and Fundamental Relations

In a synchronous generator the e.m.f. and frequency are directly related. It is often necessary, however, to obtain a voltage characteristic independent of the frequency or dependent upon it according to a specific law, for instance, according to a quadratic law. It is especially important to be able to obtain a three-phase voltage of the required magnitude at zero frequency. Since a synchronous generator cannot meet these requirements, a polyphase commutator generator is used for this purpose.

Commutator generators are built in the form of salient-pole machines with three or six salient poles per double-pole pitch, and non-salient-pole machines resembling normal induction machines. Here only two types of generators will be described: (1) the compensated commutator salient-pole generator with its field winding on the stator (the Scherbius generator), and (2) the compensated commutator non-salient-pole generator with its field winding on the stator or the rotor (commutator generator of the N. Yapolsky and M. Kostenko system).

31-2. Compensated Commutator Salient-Pole Generator with Field Winding on Stator (Scherbius Generator) [228]

A schematic diagram of this generator with three salient poles per double-pole pitch is shown in Fig. 31-1. The phases A_1 , B_1 , C_1 of the excitation system are arranged on the respective salient poles and produce three pulsating fluxes displaced 120° both in space and in time.

The rotor winding is designed as a double-layer d.c. one with the pitch shortened by $\frac{1}{3}\tau$, by virtue of which the commutating coil sections are placed in the spaces between the salient poles. This allows the commutation of the machine to be improved by using composites with a series and a parallel winding. The objective pursued thereby is the same as in single-phase series motors (Sec. 28-3), viz., the series winding of the composites produces an e.m.f. which balances the reactive e.m.f. of the commutating section, while the parallel winding, which is connected in parallel with the field winding (not shown in

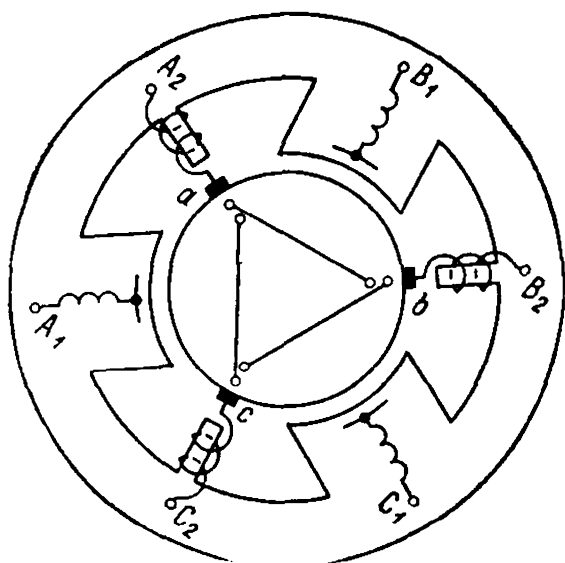


Fig. 31-1. Compensated salient-pole generator with a field winding on stator

Fig. 31-1), produces the transformer e.m.f. of the same coil section. Owing to this, the commutation of the generator is satisfactory. It should be understood, however, that the magnetizing force curve of a three-phase armature with a fractional pitch of $y = \frac{2}{3} \tau$ greatly deviates from a sinusoidal curve, is unsymmetrical, and sharply variable in shape with time. To compensate such a magnetizing force, a special compensating winding is arranged on the salient poles of the stator, which allows complete compensation of the armature magnetizing force to be attained with very simple connections of the ex-

ternal circuit to the generator terminals.

As has already been mentioned, the Scherbius generator may be built for power ratings up to 1000 kVA and frequencies of 12 to 15 Hz and is used in cascade connections, and as a phase advancer for improving the power factor of induction motors.

31-3. Compensated Commutator Non-Salient-Pole Generator [265]

The generator may be designed with excitation on the stator, and with excitation on the rotor. A schematic diagram of a generator with excitation on the stator is shown in Fig. 31-2. Field winding FW , with w_{exc} turns, is arranged on the stator and is wound as a normal a.c. winding. It may be star- or delta-connected and brought out to terminals $A_1-B_1-C_1$ which are the external terminals of the generator excitation system. Another winding CW , with w_{cw} turns, is also arranged on the stator, and is called the compensating winding. The latter is also wound as an a.c. winding and placed in the same slots as winding FW . The ends of the compensating winding phases are brought out, on one side, to the main terminals $A_2-B_2-C_2$ of the machine and, on the other side, to brushes $a-b-c$ placed on the commutator of the generator rotor. Finally, winding A , with w_a turns, is arranged on the rotor, this being a closed d.c. winding brought out to a commutator connected in series with winding CW through brushes $a-b-c$.

The numbers of turns w_a and w_{cw} of the windings are in a definite relation, namely, the effective number of turns of the rotor phase winding referred to an equivalent star must be equal to the effective number of turns of the compensating phase winding, i.e. $w_a k_{wa} = w_{cw} k_{wcw}$. When the brushes are set with $\alpha = 180^\circ$, the machine acquires the properties of a compensated commutator generator. This

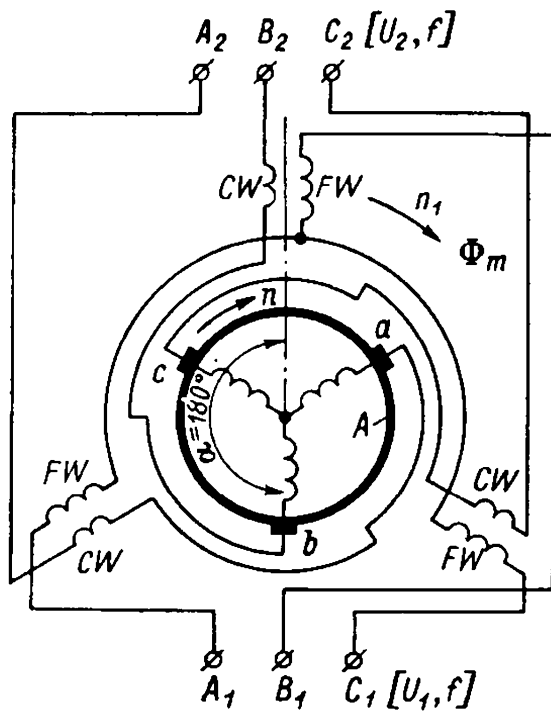


Fig. 31-2. Compensated non-salient-pole generator with excitation on stator

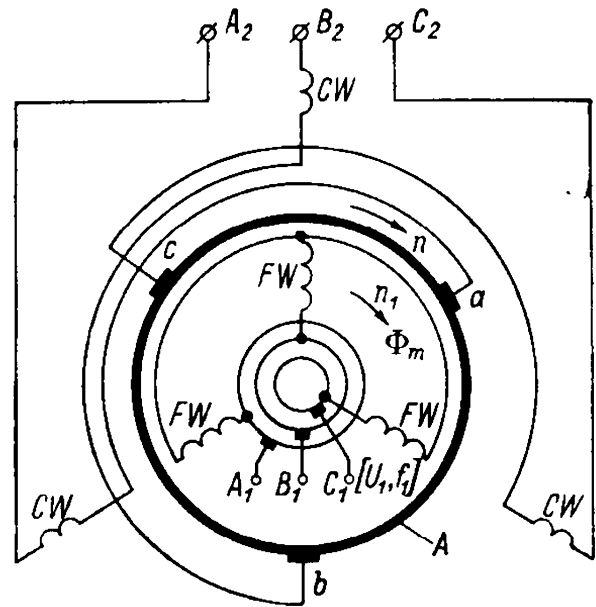


Fig. 31-3. Compensated non-salient-pole generator with excitation on rotor

is considered to be the fundamental position of the brushes. Figure 31-3 shows a schematic diagram of a commutator generator with excitation on the rotor. This circuit differs from the previous one only in that the field winding FW , with w_{exc} turns, is arranged in the rotor slots together with the rotor winding. At three points of symmetry the field winding is connected to slip rings whence it is brought out to terminals A_1, B_1, C_1 of the exciting system.

Let us consider first the operating principle of the commutator generator with excitation on the stator (Fig. 31-2). Let us apply a voltage U_1 to terminals A_1, B_1, C_1 from a power circuit with a frequency f . A flux Φ_m rotating at a speed n_1 in the direction of the phase sequence of the field winding will appear in the machine. Let the rotor of the generator run at a constant speed n in the direction of rotation of the flux Φ_m . An e.m.f. E_a will be produced in turns w_a of winding A equal to

$$E_a = \pi \sqrt{2} (f - f_{rot}) w_a k_{wa} \Phi_m \quad (31-1)$$

where $f_{rot} = pn$. Since the flux Φ_m rotates at the full speed n_1 with respect to stationary brushes a, b, c , however, the frequency of the e.m.f. E_a at the brushes will be equal to the frequency f of the exciting system.

In turns w_{cw} of the compensating winding an e.m.f. E_{cw} will be produced which has the frequency f and is determined by the expression

$$E_{cw} = \pi \sqrt{2} f w_{cw} k_{w.cw} \Phi_m \quad (31-2)$$

Windings A and CW are connected in series and have their axes turned through 180° . Therefore, on the main terminals A_2, B_2, C_2 there appears a voltage U_2 determined by the expression

$$U_2 = E_{cw} - E_a = \pi \sqrt{2} f_{rot} \omega_a k_{wa} \Phi_m + \pi \sqrt{2} f (\omega_{cw} k_{wc} - \omega_a k_{wa}) \Phi_m \quad (31-3)$$

Since the machine is compensated, the second term of equation (31-3) is zero and we have

$$U_2 = \pi \sqrt{2} f_{rot} \omega_a k_{wa} \Phi_m \quad (31-4)$$

Thus, the voltage U_2 acts across the main terminals $A_2-B_2-C_2$, its magnitude depending, as in d.c. machines, on the speed of rotation n of the generator rotor, the effective number of turns of the rotor winding, and the magnitude of the flux Φ_m . The frequency of this voltage is equal to the frequency f of the excitation voltage U_1 . An e.m.f.

$$E_{exc} = \pi \sqrt{2} f \omega_{exc} k_{w_{exc}} \Phi_m \quad (31-5)$$

is induced in the field winding.

Figure 31-4 shows the characteristics of U_2 , its components E_{cw} , E_a and E_{exc} as functions of the frequency f provided that the flux Φ_m and the speed of the generator rotor n are constant. The same relations are shown in Fig. 31-5, but on condition that $\Phi_m \equiv f$ and $f_{rot} = \text{const}$.

In view of the fact that the voltage U_2 across the terminals of a compensated commutator generator is determined, according to equation (31-4), by the speed of rotation of its rotor, the voltage U_2 is called the rotational e.m.f. Consequently, it can be said that the voltage across the terminals of a compensated commutator generator is equal to its rotational e.m.f.

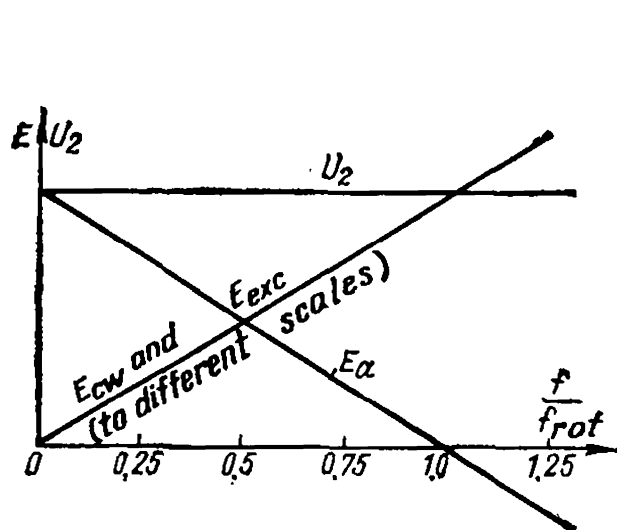


Fig. 31-4. Relation between E_{cw} , E_a and E_{exc} and $U_2 = f(f/f_{rot})$ with $\Phi_m = \text{const}$ and $f_{rot} = \text{const}$

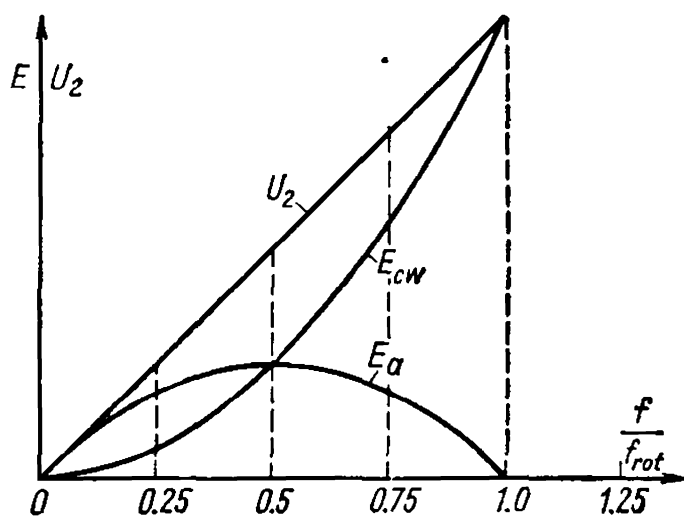


Fig. 31-5. Relation between E_{cw} , E_a and $U_2 = f(f/f_{rot})$ with $\Phi_m \equiv f$ and $f_{rot} = \text{const}$

The above relations remain unchanged even if the rotor runs against the flux Φ_m . This is not advisable for a generator with excitation on the stator, however, since it causes the rotor steel losses to increase and considerably aggravates commutation of the generator.

Let us now consider the operating principle of a commutator generator with excitation on the rotor (Fig. 31-3).

Apply the voltage U_1 with a frequency f to terminals A_1 - B_1 - C_1 of field winding FW and run the rotor at a speed n in any direction, say, in the direction of the flux Φ_m . Reasoning as before, we obtain the same formula (31-4), i.e., other conditions being equal, the voltages U_2 across the terminals of both types of generators are equal. But in the generator with excitation on the rotor the frequency of the voltage U_2 is determined by the frequency of the excitation current and the speed of the rotor according to formula (27-21). Consequently, in the given case we have $f_2 = f + f_{rot}$. If the rotor runs opposite to the flux Φ_m , then $f_2 = f - f_{rot}$.

31-4. Applications of a Commutator Generator

The commutator generator makes it possible to regulate the speed of an induction motor by varying the frequency, with the generator driven at constant speed by the prime mover. Figure 31-6 shows a schematic diagram of a fan drive, where IM is the induction motor which drives the fan (or propeller); CG is the compensated commutator generator with excitation on the stator according to the circuit in Fig. 31-2; SE is the synchronous exciter which feeds field winding FW of the generator and is driven by d.c. motor DCM over the required range of speed regulation. The power rating of generator CG must be equal to the power rating of the induction motor; the power rating of the exciter expressed in volt-amperes amounts to from 25 to 35% of the power of generator CG ; the power of the d.c. motor with generator CG fully compensated covers only the losses in the exciter unit.

Generator CG is driven at constant speed by some kind of prime mover and operates with a frequency which is determined by the frequency of the exciter unit; the voltage U_2 across terminals A_2 - B_2 - C_2 of generator CG depends, according to equation (31-4), on the speed n of the generator rotor and on the magnitude of the flux Φ_m produced by the synchronous exciter. The speed of the induction motor is regulated by changing the speed of the d.c. motor, i.e., on the excitation circuit side of generator CG . Hence it follows

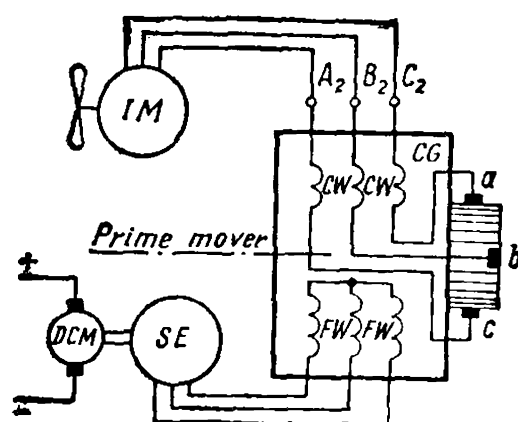


Fig. 31-6. Speed regulation by means of a compensated commutator generator with excitation on stator

that with simultaneous regulation of the excitation circuit frequency and voltage, this system is an a.c. system similar to the d.c. Ward-Leonard system.

In addition to installations of the type described above, the commutator generator can be used in a number of special installations, for example, for driving roller conveyers [270].

31-5. Thyristors or Silicon Controlled Rectifiers

Thyristors or silicon controlled rectifiers first appeared in 1957-8 and have since then found wide application in various branches of electronics and electrical engineering. Their characteristics are similar to those of thermionic rectifiers (thyratrons, ignitrons, etc.). One of their main applications is in combination with a.c. electrical machines: i.e., in frequency circuits, cascade circuits, and thyatron-motor circuits. Thyristors have several advantages over thermionic rectifiers: namely, a much lower voltage drop in conducting (1-2 V instead of the 10-20 V of thermionic rectifiers), a much smaller size and mass, high mechanical strength and simplicity of construction, a broad range of permissible operating temperatures, immediate readiness, and the absence of the need for constant supervision and servicing.

BIBLIOGRAPHY

GENERAL INFORMATION ON A. C. MACHINES

1. Arnold, E. *Die Wechselstromtechnik*: (a) Bd. 1. Theorie der Wechselströme, J. La. Cour, O. Bragstad, 1910; (b) Bd. 3. Die Wicklungen der Wechselstrommaschinen, Arnold, E., 1912; (c) Bd. 4. Die synchronen Wechselstrommaschinen, Arnold, E., J. La Cour, 1913; (d) Bd. 5. Die asynchronen Wechselstrommaschinen: Teil 1. Induktionsmaschinen, Arnold, E., J. La Cour, Fraenkel, A. 1909; Teil 2, Die Wechselstromkommutatormaschinen, Arnold, E. J. La Cour, Fraenkel, A., 1912. Berlin, J. Springer.
2. Bloch, O. *Die Ortskurven der graphischen Wechselstromtechnik*. Zürich, Rascher, 1917.
3. Hawkins, C. *The Dynamo. Its theory, design and manufacture*. Vol. 3. (Alternators). London, I. Pitman, 1925.
4. Mauduit, A. *Machines électriques*: (a) T. 1. Dynamos, alternateurs, transformateurs statiques, 1931, (b) T. 2. Moteurs d'induction, machines synchrones, commutatrices, moteurs alternatifs à collecteurs, redresseurs. Paris, Dunod, 1931.
5. Postnikov, I. M. *Obobshchennaya teoriya i perekhodnye protsessy elektricheskikh mashin*. (General theory and transient processes of electrical machines). Kiev, Tekhnika, 1966.
6. Kostenko, M. P., Sukhanov, L. A., Aksenov, V. N. *Sovremennye moshchnye gidrogeneratory*. (Modern high-power hydrogenerators). Moskva, Informstandtelektro, 1967.
7. Voldek, A. I. *Elektricheskie mashiny*. (Electrical machines). Leningrad, Energiya, 1966.
8. S. E. T. *Spravochnaya kniga dlya elektrotehnikov*. (a) T. 5. Obshchaya chast, sinkhronnye mashiny. (b) T. 6. Induktsionnye mashiny, kollektornye mashiny, vrashchayushchiesya preobrazovateli, spetsialnye tipy mashin i transformatorov, ionnye preobrazovateli s upravlyaemym razryadom. (Handbook for electrical engineers: (a) General, synchronous machines; Vol. 5. (b) Induction machines, commutator machines, rotary converters, special types of machines and transformers, gas filled tube rectifiers with grid-control). Kouboutch, 1934.
9. Richter, R. *Elektricheskie mashiny*: (a) T. 2. Sinkhronnye mashiny i odnoyakovnye preobrazovateli. (Electrical machines. Synchronous machines and converters); ONTI, 1936; (b) T. 4. Induktsionnye mashiny. (Induction machines); ONTI, 1939; (c) T. 5. Kollektornye mashiny odnofaznogo i mnogofaznogo toka, regulirovochnye agregaty. (Single-phase and polyphase commutator motors controlling units), Moskva-Leningrad, 1950; Gosenergoizdat, 1961; (d) Kurzer Lehrbuch der elektrischer Maschinen. Berlin, J. Springer, 1949; (e) Lehrbuch der Wicklungen elektrischer Maschinen, Karlsruhe, G. Braun, 1952.
10. Kron, G. *The application of tensors of the analysis of rotating electrical machinery*. Schenectady, General Electric Review, 1942.
11. Kron, G. *Equivalent circuit of electric machinery*, J. Wiley, New York, 1951.
12. Langsdorf, A. *Theory of alternating current machinery*. New-York. London, Mc. Graw-Hill, 1955.

13. Petrov, G. N. *Elektricheskie mashiny*. (a) Ch. 1. Vvedenie, transformatory, 1956, (b) Ch. 2. Asinkhronnye i sinkhronnye mashiny, 1963, (c) Ch. 3. Kollektornye mashiny postoyannogo i peremennogo toka, 1968. (Electrical machines. 2nd ed. (a) P. 1. Introduction, transformers, (b) P. 2. Induction and synchronous machines, (c) P. 3. D. C. and A. C. commutator machines). Moskva-Leningrad, Gosenergoizdat.
14. Titov, V. V., Khutoretsky, G. M., Zagorodnaya, G. A., Vartanyan, G. P., Zaslavsky, D. I., Smotrov, I. A., *Turbogeneratory. Raschet i konstruktsiya* (Turbogenerators. Design and construction). Leningrad, Energiya, 1967.
15. Bödeteld, T., Sequenz, H. *Elektrische Maschinen, Einführung in die Grundlagen*. Wien, J. Springer, 1942.
16. Komar, E. G., Britsyn, M. L. *Turbogeneratory serii T-2. Tekhnicheskii spravochnik*. (Technical manual. Turbogenerators of the T-2 series). Lenizdat, 1945.
17. Bewley, L. (a) *Alternating current machinery*. New-York, Mc. Millan, 1949; (b) *Tensor analysis of electric circuit and machines*. U. S. A., P. Press, 1961.
18. Zherve, G. K. *Promyshlennye ispytaniya elektricheskikh mashin*. (Industrial tests of electrical machines). Leningrad, Energiya, 1968.
19. Adkins, B. *General theory of electrical machines*. London, Chapman and Hall, 1959.
20. Gibbs, W. *Tensors in electric machine theory*. London, Chapman and Hall, 1952.
21. Lyon, W. *Transient analysis of alternating current machinery. An application of the method of symmetrical components*. New York. J. Wiley, 1954.
22. Gruzov, L. N. *Metody matematicheskogo issledovaniya elektricheskikh mashin*. (Methods of mathematical investigation of electrical machines). Moskva-Leningrad, Gosenergoizdat, 1953.
23. Alekseev, A. E. *Konstruktsiya elektricheskikh mashin*. (Construction of electrical machines). Moskva-Leningrad, Gosenergoizdat, 1958.
24. Postnikov, I. M. *Proektirovanie elektricheskikh mashin*. (Design of electrical machines, 2nd ed.). Kiev, Gostekhizdat Ukr. SSR, 1960.
25. Kostenko, M. and Piotrovski, L. *Electrical machines*, Part one, 1962. Part two, 1963. Moscow, Mir Publishers.
26. Kazovsky, E. Ya. (a) *Nekotorye voprosy perekhodnykh protsessov v mashinakh peremennogo toka*. (Particular problems of transient processes in a. c. machines). Moskva-Leningrad, Gosenergoizdat, 1953. (b) *Perekhodnye protsessy v elektricheskikh mashinakh peremennogo toka*. (Transient processes in a. c. machines). Moskva-Leningrad, Acad. Sc. USSR, 1962.
27. Kovács, K. und Rácz, I. *Transiente Vorgänge in Wechselstrommaschinen*. Bd. 1. Budapest. Ungarischen Akademie der Wissenschaften, 1959.
28. Strakhov, S. V. *Perekhodnye protsessy v elektricheskikh tsepyakh, sodержashchikh mashiny peremennogo toka*. (Transient processes in electric circuits with a. c. machines). Moskva-Leningrad, Gosenergoizdat, 1960.
29. Sequenz, H. *Die Wicklungen elektrischen Maschinen*: (a) Bd. 1. Wechselstrom-Ankerwicklungen, 1950. (b) Bd. 2. Wenderwicklungen, 1952. (c) Bd. 3. Wechselstrom-Sonderwicklungen, 1954. (d) Bd. 4. Herstellung der Wicklungen. Wien, J. Springer, 1955.
30. Livshitz-Garik, M. *Obmotki mashin peremennogo toka*. (A. C. machine windings). Moskva-Leningrad, Gosenergoizdat, 1959.
31. Kucera, J. und Hapl, J. *Wicklungen der Wechselstrommaschinen*. Berlin, VEB Technik, 1956.
32. Alper, T. I. Sergievskaya, T. G., *Okhlazhdenie gidrogeneratorov*. (Cooling of hydrogenerators). Moskva, Energiya, 1969.
33. Gotter, G. *Erwarmung und Kühlung elektrischer Maschinen*. Berlin-Göttingen-Heidelberg, Springer-Verlag, 1959.
34. Hawkins, C., Smith, S. and Neville, S. *Papers of the design of alternating-current machinery*. London, I. Pitman, 1919.
35. Filippov, I. F. *Voprosy okhlazhdeniya elektricheskikh mashin*. (Cooling of electrical machines). Leningrad, Energiya, 1964.

36. Chechet, Yu. S. *Elektricheskie mikromashiny avtomaticheskikh ustroystv*. (Electrical fractional horse-power machines of automatic devices). Moskva-Leningrad, Gosenergoizdat, 1957.
37. Goldenberg, S. I., Moz, L. S., Neyman, Z. B., Pekne, V. Z. *Sinkhronnye kompensatory. Voprosy proektirovaniya, montazha i ekspluatatsii*. (Synchronous phase modifiers. Design, erection and maintenance). Moskva, Energiya, 1969.
38. Neyman, L. R., Glinernik, S. R., Emelyanov, A. V., Novitsky, V. G. *Elektroperedacha postoyannogo toka kak element energeticheskikh sistem*. (Direct current transmission as an element of energy systems). Moskva-Leningrad, Acad. Sc. USSR, 1962.
39. Burdun, G. D., Kalashnikov, N. V., Strotsky, L. R. *Mezhdunarodnaya sistema edinits*. (International system of units). Moskva, Vysshaya shkola, 1964.
40. *Elektricheskie mashiny. Gosudarstvennye standarty SSSR*. (Electrical machines. State standards of the USSR). Moskva, Standartgiz, 1968.

SYNCHRONOUS MACHINES

41. Heuillard, J. (a). Progrès techniques dans la construction des turbo-alternateurs de grande puissance. *Alsthom*, 1967, June. (b) Essais en plate-forme de l'alternateur de 600 MW de la centrale de Havre. *Alsthom*, 1968, July-August.
42. Shiki, M. Four-pole turbogenerator for nuclear power station. *Mitsubishi Denki Eng-r*, 1969, June.
43. Kai, T. Turbogenerators for nuclear power station. *Mitsubishi Denki Eng-r*, 1971, March.
44. Hill, E. *Rotary Converters*. London, Chapman and Hall, 1927.
45. Barrère, M. *Commutatrices et convertisseurs rotatifs*. Paris, J. Baillière, 1931.
46. Bennett, R. Water cooling of turbine generator rotor windings. *E. El. Journal*, 1968, March-April.
47. Wiedemann, E. Fully water cooled turbogenerators. *B. B. Rev.*, 1966, 9.
48. Berger, A. Ya. *Turbogeneratory peremennogo toka*. (A. C. turbogenerators) Vol. 1, 1935; Vol. 2, 1937, Vol. 3, 1941. Moskva-Leningrad, Gosenergoizdat.
49. Alekseev, A. E., Kostenko, M. P. *Turbogeneratory*. (Turbogenerators). Moskva-Leningrad, Gosenergoizdat, 1939.
50. Anempodistov, V. P., Kasharsky, E. G., Urusov, I. D. *Problemy krupnogo turbogeneratorostroeniya*. (Problems of large turbogenerator construction). Moskva-Leningrad, Acad. Sc. USSR, 1960.
51. Britsyn, M. L., Khutoretsky, G. M. *Turbogeneratory moshchnostyu 100 Mt i vyshe s neposredstvennym okhlazhdeniem obmotok*. (Turbogenerators rated at 100 MW and higher with direct cooling of windings). Moskva-Leningrad, Acad. Sc. USSR, 1960.
52. Komar, E. G. (a) *Voprosy ekspluatatsii turbogeneratorov*. (Turbogenerator maintenance). Moskva-Leningrad, Gosenergoizdat, 1950. (b) *Voprosy proektirovaniya turbogeneratorov*. (Turbogenerator design). Moskva-Leningrad, Gosenergoizdat, 1955.
53. Khutoretsky, G. M. *Proektirovanie i raschet sovremennykh dvukhpolutnykh turbogeneratorov*. (Design and calculation of modern double-pole turbogenerators). L. P. I. im. M. I. Kalinina, 1962.
54. Holley, C., Willyoung, D. Stator winding systems with reduced vibratory forces for large turbine generators, *IEEE Trans.*, 1970, PAS-89, 8.
55. Dombrovsky, V. V., Ipatov, P. M., Pinsky, G. B. *Proektirovanie gidrogeneratorov*. Ch. 1. *Elektromagnitnye raschety*. (Design of hydrogenerators. P. 1. Electromagnetic calculations). Leningrad, Energiya, 1965. Ch. 2. *Konstruktsii. Mekhanicheskie raschety*. (P. 2. Construction. Mechanical calculations). Leningrad, Energiya, 1968.
56. Large hydroelectric generators of the Soviet Union. CIGRE. Session 1954, Report 150. Auth.: Ivanov, N., Yeremeyev, A., Luter, R., Kaplan, M.

57. Grgic, A. Leistungsgrenzen für zwei und vierpolige Turbogeneratoren auf Grund mechanischen Beanspruchungen. *BB-Mitt.*, 1969, 8.
58. Mulra, H. Design features of recent waterwheel generators. *Mitsubishi Denki Eng-r*, 1970, 24, April.
59. Ringland, W., Kilbourne, C., Kilgore, L. American development in generator cooling. CIGRE. Session 1956, rep. 127.
60. Noser, R., Krawz, R. Turbo-alternator with liquid-cooled rotor. CIGRE. Session 1966, rep. 111.
- 61a. Ipsen, P., Massingill, Y. 800 MW expansion of big sandy plant of the AEP system. *Amer. Power Conference*, 1968, April 23-25, pt. 3.
- 61b. Barby, C. und Kunoth, K. (a) Die 160 MVA Generatoren Wasserkraftanlage Furnas (Brasilien.) *Siemens Zeit.*, 1962, 5. (b) Die Generatoren des Pumpspeicherwerks Vlianden. *Siemens Zeit.*, 1963, 1.
- 61c. Strömberg, T. The 150 MVA generators at stornorrfor. *ASEA Fourn.*, 1960, 1-2.
- 61d. Matthias, F., Travers, F., Ducan, J. Planning and construction of the chute des passes hydroelectric power project. Canada. *The Engineering Journal*, 1960, January.
- 61e. Thorgerson, T. and Basileco, J. Electric features of the Niagara power project *El. Engineering*. 1961, October.
62. Wiedemann, E. Wasserkraftgeneratoren mit Flüssigkeitskühlung in Stator und Rotor. *BB-Mitt.*, 1964, 5.
63. Kasharsky, E. G., Safiullina, R. Kh., Urusov, I. D. *Nauchno-metodicheskie voprosy sozdaniya serii krupnykh sinkhronnykh mashin.* (Scientific and methodological problems of production of large synchronous machine series). Moskva-Leningrad, Acad. Sc. USSR, 1962.
64. Landhalt, H., Nordberg, B. 345 MVA water-cooled synchronous condenser for dumont station, Part 2. Design, construction and testing. *IEEE. Winter power meeting*, 1971, 9.
65. Haydock, J. and Warnock, J. Giant-sized hydraulic turbines—review and forecasts. *Amer. Power Conference*, 1968.
66. Baltsberger, K., Gamlesaeter, K. Betriebserfahrungen mit vollständig wassergekühlte Schenkelpolmaschinen. *BB-Mitt.*, 1971, 1.
67. Fukawa, K. Modern large hydropower equipment. *Toshiba Rev.*, 1971, March.
68. Berglund, B., Tengstrand, C. Technical features and economic implications of the seitevare water-cooled hydrogenerator. *Proc. Amer. Power Conference*, 1969, Vol. 31.
69. Mc. Connel, P. Application of large hydrogenerators in Canada. *Proc. Amer. Power Conference*, 1969, Vol. 31.
70. Crary, S. *Power system stability*. Vol. 1. Steady state stability, 1945. Vol. 2. Transient Stability, 1947, New York, J. Wiley.
71. Gorev, A. A. (a) *Perekhodnye protsessy sinkhronnoi mashiny.* (Transient processes in synchronous machines). Moskva-Leningrad, Gosenergoizdat, 1950. (b) *Izbrannye trudy po voprosam ustoychivosti elektricheskikh sistem.* (Selected works on problems of stability of electric systems). Moskva-Leningrad, Gosenergoizdat, 1960.
72. Vazhnov, A. I. (a) *Osnovy teorii perekhodnykh protsessov sinkhronnoi mashiny.* (Fundamentals of theory of transient processes in synchronous machines). Moskva-Leningrad, Gosenergoizdat, 1960. (b) *Elektricheskie mashiny.* (Electrical machines). Leningrad, Energiya, 1969.
73. Concordia, Ch. *Synchronous machines. Theory and performance.* New York, J. Wiley, 1951.
74. Babbist, J. Large hydroelectric generators for Grand Coulee third power plant. *Proc. Amer. Power Conference*, 1969, Vol. 31.
75. Kimbark, E. *Power system stability*. Vol. 3. Synchronous machines. New York, J. Wiley, 1956.
76. Laible, T. Moderne Methoden Zur Behandlung Nichtstationärer Vorgänge

- in elektrischen Maschinen, Bulletin des Schweizerischen elektrotechnischen Vereins, 1950, July, Bd. 41, No. 14, Berlin, J. Springer, 1952.
77. Venikov, V. A. *Perekhodnye elektromekhanicheskie protsessy v elektricheskikh sistemakh*. (Transient electromechanical processes in electric systems). Moskva, Energiya, 1964.
 78. Apsit, V. V. *Sinkhronnye mashiny s kogteobraznymi polusami*. (Synchronous machines with claw-type poles). Riga, Publ. House Latvia SSR, 1959.
 79. *Elektrodinamicheskoe modelirovanie energeticheskikh sistem*. [Sbornik statei]. Pod red. Kostenko M. P. (Electrodynamic simulation of energy systems. Collected articles). Moskva-Leningrad, Acad. Sc. USSR, 1959.
 80. Urusov, I. D. *Lineinaya teoriya kolebanii sinkhronnoi mashiny*. (Linear theory of synchronous machine oscillations). Moskva-Leningrad, Acad. Sc. USSR, 1960.
 81. Potier, A. Sur la réaction d'induit des alternateurs. Paris, L'Eclairage Electrique, 1900, t. 24.
 82. Ashley, E. Operation and maintenance of large hydroturbines on the Columbia and Snake rivers. *Proc. Amer. Power Conference*, 1970, Vol. 32.
 83. Fujuta, J. Kisen'yama pumped-storage power station. pt. 2, 250 MVA/MW generator-motor. *Toshiba Rev.*, 1971, February.
 84. Holley, C., Willyoung, D. Conductor-cooled rotor for large turbogenerators; experience and prospects. CIGRE, 1970, 23rd Session, Vol. 1, 1 section, group 11, papers 11-06.
 85. Doherty, R. and Shirley, O. Reactance of synchronous machines and its applications. *AIEE Trans.*, 1918.
 86. Glebov, I. A. *Sistemy vozbuzhdeniya sinkhronnykh generatorov s upravlyаемymi preobrazovatelyami*. (Excitation systems of synchronous generators with controlled converters). Moskva-Leningrad, Acad. Sc. USSR, 1960.
 87. Hossli, W. Die 1160 MW Turbine für Kernkraftwerk "Donald C. Cook" der AEP. *BB-Mitt.*, 1972, 1.
 88. Hoover, D. B. The brushless excitation system for large a. c. generators. *Westinghouse Engineer*, 1964, 9.
 89. Venikov, V. A., Gertsenberg, G. R., Sovalov, S. A., Sokolov, N. I. *Sil'noe regulirovanie vozbuzhdeniya*. (Strong excitation control). Moskva-Leningrad, Gosenergoizdat, 1963.
 90. Venikov, V. A., Ivanov-Smolensky, A. V. *Fizicheskoe modelirovanie elektricheskikh sistem*. (Physical simulation of electrical systems). Moskva-Leningrad, Gosenergoizdat, 1956.
 91. Hiebler, H. Der 1333 MVA-Generator für das Kernkraftwerk "Donald C. Cook" der AEP. *BB-Mitt.*, 1972, 1.
 92. Turbine generators for nuclear power stations. *Mitsubishi Denki Eng-r*, 1971. 31. Auth.: Kai, T., Oishi, N., Hayami, K., Ito, H., Amagasa, N.
 93. Noser, R., Pohl, H. Cooling large turbogenerators without hydrogen. *IEEE, PAS-90*, 1971, 5.
 94. Concordia, C., Brown, P. Transient behavior of synchronous machine and shunt-connected thyristor exciter under system faults. *IEEE, PAS-90*, 1971, 5.
 95. Blondel, A. (a) Complément à la theorie des alternateurs à deux reactions. *R. G. E.*, 1922, t. 12, (b) Application de la methode de deux reactions à l'étude des phénomènes oscillatoires des alternateurs couplés. *R. G. E.*, 1923, t. 13.
 96. *Tekhniko-ekonomicheskie problemy elektrogeneriruyushchego oborudovaniya energosistem*. [Sbornik statei]. (Technical and economical problems of electrical generating equipment for energy systems. Collected articles). Leningrad, Nauka, 1968.
 97. Weber, A. et Orliac, M. Les alternateurs de la Centrale de Malgovert. *Révue Electr. Mecan.*, 1955, 99-100.
 98. Doherty, R. and Nickle, C. Synchronous machines: (a) Parts 1 and 2. An extension of Blondel's two reaction theory. Steady state power angle characteristics. *AIEE Trans.*, 1926. (b) Part 3. Torque-angle characteristics under transient

- conditions. *AIEE Trans.*, 1927. (c) Part 4. Synchronous machines, single phase short circuit. *AIEE Trans.*, 1928. (d) Part 5. Three-phase short circuit synchronous machines. *AIEE Trans.*, 1930.
99. **Park, R.** (a) Definition of an ideal synchronous machine and formula for the armature flux linkage. *G. E. R.*, 1928. (b) Two-reaction theory of synchronous machines—generalised method of analysis. Part 1. *AIEE Trans.*, 1929, Part 2. *AIEE Trans.*, 1933.
 100. **Wieseman, R.** Graphical determination of magnetic fields (practical applications to salient pole synchronous machine design). *AIEE Trans.*, 1927.
 101. **Alger, P.** The calculation of armature reactance of synchronous machines. *AIEE Trans.*, 1928.
 102. **Linville, T.** Starting performance of salient pole synchronous machines. *AIEE Trans.*, 1930.
 103. **Tolwinski, W.** Das Problem der unsymmetrischen Belastung des synchron Drehstromgenerators und des Drehstromtransformators. *A. f. E.*, 1930, Bd. 23, 5.
 104. **Nauchno-tehnicheskie problemy krupnogo turbo- i gidrogeneratorostroeniya.** [Sbornik statei] (Scientific and technological problems of large turbo- and hydrogenerator construction. Collected articles). Leningrad, Nauka, 1967.
 105. **Teoreticheskie i eksperimental'nye issledovaniya turbo- i gidrogeneratorov bol'shoi moshchnosti.** [Sbornik statei]. (Theoretical and experimental studies of high-power turbo- and hydrogenerators. Collected articles). Leningrad, Nauka, 1968.
 106. **Kasharsky, E. G.** *Spetsial'nye voprosy rascheta i issledovaniya sinkhronnykh mashin s massivnym rotorom.* (Special problems on calculation and study of synchronous machines with solid rotors). Leningrad, Nauka, 1965.
 107. **Gorev, A. A.** Osnovnye uravneniya perekhodnykh protsessov sinkhronnoi mashiny. (Fundamental equations of transient processes of synchronous machines). *Elektrichestvo*, 1938, 2.
 108. **Luter, R. A.** O momentakh vrashcheniya sinkhronnoi mashiny pri periodicheskikh eyo kachaniyakh. (Synchronous machine torques during periodic swingings). *Elektrichestvo*, 1940, 2.
 109. **Liwchitz, M.** (a) Positive and negative damping in synchronous machines. *AIEE Trans.*, 1941. (b) Damping and synchronising torque of double-fed asynchronous machines. *AIEE Trans.*, 1941.
 110. **Concordia, Ch.** (a) Rotating electrical machine time constants at low speeds. *AIEE Trans.*, 1946. (b) Synchronous machine damping and synchronising torques. *AIEE Trans.*, 1951, pt. 1.
 111. **Teoriya, raschet i issledovanie vysokoispol'zovannykh elektricheskikh mashin.** [Sbornik statei]. (Theory, calculation and study of highly-utilized electrical machines. Collected articles). Leningrad, Nauka, 1965.
 112. **Sistemy vozbuzhdeniya i regulirovaniya sinkhronnykh mashin i moshchnye staticheskie preobrazovateli.** [Sbornik statei]. (Excitation and control systems of synchronous machines and high-capacity static converters. Collected articles). Leningrad, Nauka, 1967.
 113. **Elektricheskie mashiny** (Issledovaniya, voprosy teorii i rascheta). [Sbornik statei]. [Electrical machines. (Studies, theory and calculation). Collected articles]]. Leningrad, Nauka, 1965.
 114. **Hoard, B. and Weiner, L.** Matching electrical characteristics of McNary generators and transformers with bonnevillie power administration transmission system. *AIEE Trans.*, 1949.
 115. **Issledovanie elektromagnitnykh polei, parametrov i poter' v moshchnykh elektricheskikh mashinakh.** [Sbornik statei]. (Investigation of electromagnetic fields, parameters and losses in high-power electrical machines. Collected articles). Leningrad, Nauka, 1966.
 116. **Kostenko, M. P., Konik, B. E.** Opredeleniye osnovnoi i tretyei garmonik polya yakorya i polya polosov yavnopolusnoi sinkhronnoi mashiny. (Determination

- of fundamental and third harmonic of armature and pole fields of salient-pole synchronous machine). *Elektrichestvo*, 1951, 3.
117. Honsinger, V. Theory of end winding leakage reactance. *AIEE Trans.*, 1959, August, pt. 3.
 118. Tegopoulos, J. (a) End component of armature leakage reactance of turbine generators. *AIEE Trans.*, 1963, Vol. 82, pt. 3; 1964, June, Vol. 83. (b) Forces on the end winding of turbo-generators. *IEEE Trans.*, PAS-85, 1966, 2.
 119. Voldek, A. I. Metodika rascheta vektornogo magnitnogo potentsiala lobovykh chastei obmotok elektricheskikh mashin. (Method of calculation of magnetic potential vector of electrical machine winding end connections.) *Trudy LPI im. M. I. Kalinina*, 1964, 241; *Elektrichestvo*, 1963, 1.
 120. Harrington, D. and Elligott, U. Mc. New developments in armature windings arrangements for large turbine generators. *AIEE Trans.*, 1954, pt. 3-A.
 121. Paulus, C., Fitzgerald, J. and Bellack, J. Application of conductor-cooled generators. National Power Conference, Cincinnati, Ohio, 1963, September.
 122. Venikov, V. Strow, V. Power system stability as affected by automatic control of generators. *IEEE*, Pap. 71TR-RWR. Winter Power Meeting, 1971, 9.
 123. Canay, M. Ersatz Schemata der Synchronmaschine zur Berechnung von Pohlradgrößen bei nichtstationären Vorgängen sowie asynchronen Anlauf. T. 1. Turbogeneratoren, *BB-Mitt.*, 1969, 2.
 124. Canay, M. Entwicklungsstand der Turbogeneratoren. *BB-Mitt.*, 1969, 8.
 125. Nippes, P. Short-circuit torques in turbine generators, *AIEE Trans.*, 1959, pt.3.
 126. Althammer, P. Berechnung des magnetischen Feldes in den Wickelköpfen von Turbogeneratoren. *BB-Mitt.*, 1964, 5.
 127. Baudry, R. and King, R. I. Improved cooling increases generator capabilities. *Westinghouse Engineer*, 1964, 11.
 128. Lawrenson, P. Calculation of machine end-winding inductances with special reference to turbogenerators. *Proc. IEE*, 1970, Vol. 117, 6.
 129. Kozyrev, N. A. *Izolyatsiya elektricheskikh mashin i metody eyo ispytaniya*. (Insulation of electrical machines and methods of its testing.) Moskva-Leningrad, Gosenergoizdat, 1962.
 130. Akers, H. Present trends in design of large turbine generators. *Proc. Amer. Power Conference*, 1970, Vol. 32.
 131. Harrington, J. Trends and advancements in the design of large generators. *Proc. Amer. Power Conference*, 1970, Vol. 32.
 132. Davies, E. Airgap windings for large turbogenerators. *Proc. IEE*, 1971, Vol. 118, 3/4.
 133. Evolution of large generators. *El. Rev.*, 1971, 15.
 134. Olmsted, L. 8th steam station design survey reveals sharp upturn in unit size., *El. World*, 1964, 19 October.
 135. Houser, W., Hindle, W. and Tyerman, J. Production and installation of vertical water-generators. *AIEE Trans.*, 1955, pt. 3.
 136. Leupin, G. Generatoren für das Wasserkraftwerk Assuan am Nill. *BB-Mitt.*, 1956, 12.
 137. Kilbourn, C. and Holley, C. Liquid cooling of turbine-generator winding. *AIEE Trans.*, 1956, pt. 3.
 138. Floyd, G. and Sills, H. The evolution of the modern waterwheel generators in Canada. *AIEE Trans.*, 1958, pt. 3.
 139. Wiedemann, E. Grenzleistungs-Turbo-Generatoren. *BB-Mitt.*, 1958, 1.
 140. Knox, R. British developments in the design of very large synchronous generators. *EL. News and Eng-g*, 1971, April.
 141. Stanislavsky, L. Ya. (a) Turbogeneratory moshchnostyu ot 30 do 300 Mvt zavoda HETZ. (30 to 300 MW turbogenerators of the Kharkov electrical works.) *Elektrichestvo*, 1958, 3; (b) Opytnyi turbogenerator s vnutrennim vodorodnym okhlazhdeniem obmotok statora i rotora pri davlenii 3 atm. (Experimental turbogenerator with internal hydrogen cooling of stator and rotor windings at 3-atm pressure.) *Elektrichestvo*, 1958, 8.

142. **Kazovsky, E. Ya., Kostenko, M. P.** Sovremennye metody rassmotreniya perekhodnykh protsessov v elektricheskikh mashinakh peremennogo toka. (Modern investigation of transient processes in a. c. electrical machines.). *Energetika i avtomatika*, 1959, 4.
143. **Harrington, D. and Whittlesey, J.** The analysis of sudden short circuit oscillograms of steam turbine generators. *AIEE Trans.*, 1959, pt. 3.
144. **Design, construction and operation of brownlee hydroelectric development.** *AIEE Trans.*, 1959, pt. 3-B, Auth.: G. Soule, T. Heikes, W. Mitchell, O. Schaufelberger.
145. **Alyabiev, M. I.** Uravneniya elektricheskikh mashin peremennogo toka v fizicheskikh i otnositelnykh edinitsakh. (Equations of a. c. machines in physical and relative units). *Elektrichestvo*, 1960, 1.
146. **Carpantier, L.** Moyens de reculer des limites de réalisation de grands alternateurs hydrauliques. *R. G. E.*, 1960, 6.
147. **Modern powerful turbo- and hydro-generators, their cooling systems and performance.** CIGRE, Session 1964, Paris, rep. 129. Auth.: M. P. Kostenko, E. J. Kazovsky, N. P. Ivanov, L. J. Stanislavsky, K. F. Potekhin.
148. **Water-cooled rotors.** *Energy International*, 1971, February.
149. **Kidd, K.** Peace river hydroelectric development begins. *El. World*, 1960, July, 2.
150. **Dureault, M., Kohn, S. et Loyez R.** Part 1. Wolfhugel A., Therby M.; Part 2. Evolution et construction des turboalternateurs modernes de grande puissance. *R. G. E.*, 1962, 2.
151. **Kostenko, M. P., Karpov G. et Kazovsky E.** D'eterminacion des paramètres des puissants alternateurs de centrales hydroélectriques de la Basse-Volga. CIGRE, Session 1962, rap. 124.

INDUCTION MACHINES

152. **Hobart, H.** *Electric motors, their theory and construction*. Vol. 2. *Polyphase current*. London, Pitman, 1923.
153. **Heubach, J.** *Der Drehstrommotor*. Berlin, J. Springer, 1923..
154. **Vickers, M.** *The induction motor in theory, design and practice*. London, Pitman, 1925.
155. **Rummel, E.** *Die Asynchronmotoren und ihre Berechnung*. Berlin, J. Springer, 1926.
156. **Shait, G.** *Induktsionnye regulatory tryokhfaznogo toka*. (Three-phase induction regulators,) ONTI, 1933.
157. **Krug, K. A.** *Beskollektornye asinkhronnye dvigateli*. (Non-commutator induction motors. 2nd ed.). Kouboutch, 1928.
158. **Sallinger, F.** *Die asynchronen Drehstrommaschinen mit und ohne Stromwender*, Berlin, J. Springer, 1928.
159. **Benischke, G.** *Die asynchronen Wechselfeldmotoren, Kommutator und Induktionsmotoren*. Zweite Auflage. Berlin, J. Springer, 1929.
160. **Chapman, F.** *A study of the induction motor*. New-York, J. Wiley, 1930.
161. **Blomquist, T.** Die Eisensättigung des Drehstrommotoren. *E.T.Z.*, 1923, 23.
162. **Baffrey, M.** Zur Vorausberechnung von Kurzschlussankermotoren. *A. f. E.*, 1926, Bd. 17.
163. **Punga, P. and Raydt, O.** *Drehstrommotoren mit Doppelkäfiganker*. Berlin, J. Springer, 1931.
164. **Vasiliev, D. V.** (a) *Elektricheskie mashiny v skhemakh sinkhronnoy soyazi*. (Electrical machines in synchro systems). ONTI, 1935; (b) *Induktsionnye sistemy sinkhronnoi soyazi*. (Induction synchro systems). Moskva-Leningrad, Gosenergoizdat, 1949.
165. **Aparov, B. P.** *Mashiny peremennogo toka*. T. 1. Asinkhronnye mashiny. (A. C. machines. Vol. 1. Induction machines). ONTI, 1936.

166. Trapeznikov, V. A. *Osnovy proektirovaniya serii asinkhronnykh mashin*. (Fundamentals of designing induction machine series). ONTI, 1937.
167. Veinott, C. *Fractional horsepower electric motors*. New York, McGraw-Hill, 1948.
168. Lopukhina, E. M., Solomina, G. S. *Raschet asinkhronnykh mikrodvigatelei odnofaznogo i trekhfaznogo toka*. (Calculation of single- and three-phase induction fractional horsepower motors). Moskva-Leningrad, Gosenergoizdat, 1961.
169. Adamenko, L. I. *Odnofaznye kondensatornye dvigateli*. (Single-phase capacitor motors). Kiev, Izd-vo AN Ukr. SSR, 1960.
170. Syromyatnikov, I. A. *Rezhimy raboty asinkhronnykh dvigatelei* (Operating duties of induction motors). Moskva-Leningrad, Gosenergoizdat, 1950.
171. Alger, P. *The nature of polyphase induction machines*. New-York, J. Wiley, 1951.
172. Schuisky, W. *Elektromotore*. Wien. J. Springer, 1951.
173. Spreadbury, F., *Fractional, H. P. electric motors*. London, I. Pitman, 1951.
174. Bulgakov, A. A. *Chastotnoe upravlenie asinkhronnykh elektrodvigatelei*. (Frequency-control of induction motors). Moskva-Leningrad, Acad. Sc. USSR, 1955.
175. Mkrtchan, D. P., Khrushchev, V. V. *Odnofaznye selsiny*. (Single-phase selsyns). Leningrad, Sudpromgiz, 1957.
176. Piotrovsky, L. M., Vasyutinsky, S. B., Nesgovorova, E. D. *Ispytaniya elektricheskikh mashin (transformatory i asinkhronnye mashiny)*. (Testing of electrical machines. Transformers and induction machines). Moskva-Leningrad, Gosenergoizdat, 1960.
177. Ermolin, N. P. *Elektricheskie mashiny maloi moshchnosti*. (Low-power electrical machines). Moskva, Vysshaya shkola, 1962.
178. Dolivo-Dobrowolsky, M. Die neuesten Drehstrommotoren ohne Schleifkontakte der A. E. G. E. T. Z., 1893.
179. Boucherot, P. Moteurs à courant polyphase à induits fermés sur eux memes et démarrants en charge. *L'Industrie Electrique*, 1898; *L'Eclairage Electrique*, Vol. 14.
180. Heyland, A. (a) Ein graphisches Verfahren zur Vorausberechnung von Transformatoren und Mehrphasenmotoren. *E. T. Z.*, 1894; (b) A propos du moteur asynchrone polyphase et de son diagramme, *R. G. E.*, t. 24, 1928; (c) Das Kreisdiagramm des kompensierten Motoren. *E. T. Z.*, 1903.
181. Goldschmidt, R. Diagramme für Induktionsmotoren. *E. T. Z.*, 1900.
182. Osnos, M. Ein neues Verfahren zum Kompensieren der Phasenverschiebung in asynchronen Wechselstrommaschinen. *E. T. Z.*, 1902.
183. Bragstad, O. und Fraenkel, A. Untersuchung und Berechnung der zusätzlichen in Asynchronmotoren. *E. T. Z.*, 1908.
184. Rüdenberg, R. Asynchronmotoren mit Selbstanlauf durch tertiäre Wirbelströme. *E. T. Z.*, 1918.
185. Anderson, E. General characteristics of electric ship propulsion equipments. *G. E. R.*, 1919, 5.
186. Dreyfus, L. *Die Theorie des Drehstrommotoren mit Kurzschlussanker*. Stockholm, Gunnar Tiesells, 1924.
187. Kostenko, M. P. Rabota mnogofaznogo asinkhronnogo dvigatelya pri peremennom chisle periodov. (Operation of a polyphase induction motor with variable cycles). *Elektrichestvo*, 1925, 2.
188. Liwschitz, M. Asynchronmotoren mit Kurzschlussläufer für hohen Anlaufmoment und niedrigen Anlaufstrom. *Siem. Zeitschrift*, 1925, 1927, 1928; *A. f. E.*, 1925, Bd. 14.
189. Kafka, H. Zur Konstruktion des genauen Kreisdiagramms. *A. f. E.*, 1927, Bd. 18.
190. Kasyanov, V. T. (a) Mnogokratnye kaskady iz trekhfaznykh induktionnykh mashin. (Cascade-connections of three-phase induction machines). *Elektrichestvo*, 1926, 2, 1927, 5; (b) Elektricheskaya mashina dvoynogo pitaniya kak obshchii

- sluchai mashiny peremennogo toka. (Double-feed electrical machine as a general case of an a. c. machine). *Elektrichestvo*, 1931, 22.
191. **Hemmeter, H.** Eine neue einfache Konstruktion des genauen Kreisdiagramms. *A. f. E.*, 1927, Bd. 18, 1.
 192. **Lund, H.** (a) Ein graphisches Verfahren zur Berechnung des Boucherot-Motors *A. f. E.*, 1928, 4; (b) Der A. E. G.-Doppelnutmotor. *A. E. G.-Mitt.*, 1928, 1.
 193. **Böttcher, A.** Berechnung des Doppelnutmotors. *A. E. G.-Mitt.*, 1928.
 194. **Kostenko, M. P.** Theory and calculation of Boucherean motors in electrical engineering. In: *Electromashinostroenie* (Electrical machine building). NTOE, 1930.
 195. **Schenfer, C. und Moskwitin, A.** Experimentelle Untersuchungen des Skineffektes. *A. f. E.*, 1930, H. 24, 6.
 196. **Möller, H.** Über die Drehmomente beim Anlauf von Drehstrommotor mit Käfigläufer. *A. f. E.*, 1930, H. 24.
 197. **Kostenko, M.** Das Kreisdiagramm und das demselben entsprechende Ersatzschema der Asynchronmaschine. *E. u. M.*, 1931, 38.
 198. **Hoseason, D.** (a) The predetermination of the performance of induction motors. London, *I.E.E. Journal*, 1925; (b) The cooling of electrical machines. *Ibidem*, 1931.
 199. **Koch, C.** Measurement of stray load loss in polyphase induction motors. *AIEE Trans.*, 1932.
 200. **Morgan, T. and Narboutovskih, P.** Stray-load test on induction machines. *AIEE Trans.*, 1934.
 201. **Linville, T. and Woodward, J.** Selsyn instruments for position systems. *Electr. Eng.*, 1934, November.
 202. **Heller, F.** Zusätzliche Momente beim Anlauf von Käfigankermotoren. *A. f. E.*, 1935, Bd. 29.
 203. **Stanley, H.** An analysis of the induction machine. *AIEE Trans.*, 1938.
 204. **Kuznetsov, B. I.** Diagramma toka dvigatelya s glubokim pazom i dvigatelya Bushero po dannym opyta kholostogo khoda i korotkogo замыкания. (Current diagrams of deep-bar motor and Boucherean motor by no-load and short-circuit data). *Elektrichestvo*, 1940, 1.
 205. **Himerbrook, F.** Single-phase induction-motor performance calculation. *AIEE Trans.*, 1941.
 206. **Concordia, Ch., Crary, S. and Kron, G.** The double fed machine. *AIEE Trans.*, 1942.
 207. **Trickey, P.** Performance calculation on polyphase reluctance motors (Synchronous motors without field excitation). *AIEE Trans.*, 1946.
 208. **Piotrovsky, L. M.** (a) Diagramma tokov induktsionnogo dvigatelya s peremennym induktivnym soprotivleniem. (Current diagram of induction motor with variable inductive resistance). *Elektrichestvo*, 1937, 14; (b) Geometricheskoe mesto tokov asinkhronnoi mashiny s peremennym nasyshcheniem stali. (Current loci of induction machine with variable steel saturation). *Elektrichestvo*, 1946, 2; (c) Razvitie krugovoi diagrammy za 50 let. (A 50-year development of the circle diagram). *Elektrichestvo*, 1946, 6.
 209. **Alger, P. and Wray, J.** Double and triple squirrel cage for polyphase induction motors. *AIEE Trans.*, 1953, pt. 3.
 210. **Godman, J.** A design method for double squirrel cage induction motors. *AIEE Trans.*, 1953, pt. 3.
 211. **Courtin, J.** Report on double-cage rotor symposium. *AIEE Trans.*, 1953, pt. 3.
 212. **Midendorf, W.** Circulation of induction motor torque and power. *AIEE Trans.*, 1958, pt. 3.
 213. **Kaasik, P. Yu.** Tochnaya krugovaya diagramma asinkhronnoi mashiny maloi moshchnosti. (Precise circle diagram for low-power induction machine). *Izv. vuzov. Elektromekhanika*, 1961, 1.
 214. **Larionov, A. N., Mastyaev, N. Z., Orlov, I. N., Panov, D. N.** Obshchie voprosy teorii gisterezisnykh elektrodvigatelyei. (General problems of hysteresis motor theory). *Elektrichestvo*, 1958, 7.

215. Jordan, H. Synthesis of double-cage induction motor design. *AIEE Trans.*, 1959, pt. 3.
216. Veinott, C. (a) Induction machinery design being revolutionised by the digital computer. *AIEE Trans.*, 1956, Vol. 75, pt. 3; (b) Synthesis of induction motor design on a digital computer. Ibidem. 1960, pt. 3.
217. Heller, B., Hamata, V. *Přidavna pole, síly a ztráty v asynchronním stroji*. Praha, 1961.
218. Garreau, M. *La Traction Electric*. Edition Scientific Riber. Paris, 1965 (2^e) bl. de Sevastopol.
219. Dembo, A. R., Kozhevnikov, V. A., Kochnev, A. V., Pruss-Zhukovsky, V. V. *Parametry sovremennykh tyagovykh dvigatelei elektrovozov i autonomnykh lokomotivov*. (Parameters of modern traction motors of electric locomotives and autonomous locomotives). Leningrad, Nauka, 1964.
220. Graybeal, T. Derivation of the basic constants of the general induction machine in terms of winding parameters. *AIEE Trans.*, 1961, Vol. 80, pt. 3.
221. Agarwal, P. and Alger, P. Saturation factors for leakage reactance of induction motor. *AIEE Trans.*, 1960, Vol. 79, pt. 3.
222. Angst, G. Polyphase induction motor with solid rotor effects of saturation and finite length. *AIEE Trans.*, 1961, Vol. 80, pt. 3.

A. C. COMMUTATOR MACHINES AND CASCADE CONNECTIONS

223. Jacquin, Ch. *Les alternateurs à collecteur monophasés et polyphasés*. Paris, Gauter-Villard, 1907.
224. Schenkel, M. *Die Kommutatormaschinen für einphasigen und mehrphasigen Wechselstrom*. Berlin, W. de Gruyter, 1924.
225. Walker, M. *The control of the speed and power factor of induction motors*. London, Ernest Benn, 1924.
226. Olliver, C. *The A. C. commutator motor*. London, Chapman and Hall, 1927.
227. Zabransky, H. *Die wirtschaftliche Regelung von Drehstrommotoren durch Drehstrom-Gleichstrom-Kaskaden*. Berlin, J. Springer, 1927.
228. Dreyfus, L. *Kommutatorkaskaden und Phasenschieber*. Berlin, J. Springer, 1931.
229. Schait, H. *Kompensierte und synchronisierte Asynchronmotoren*. Berlin, J. Springer, 1929.
230. Shenfer, K. I. *Kollektornye dvigateli peremennogo toka* (A. c. commutator motors). GONTI 1933.
231. Kostenko, M. P. *Kollektornye mashiny peremennogo toka*. (A. c. commutator motors). Kouboutch, 1933.
232. Addkins, B. and Gibbs, W. *Polyphase commutator machines*. Cambridge, University Press, 1951.
233. Benedikt, Otto. *Die neue elektrische Maschine "Autodyne"*. Berlin, Akad. Verlag, 1957.
234. Taylor, E. *The performance and design of a. c. commutator motors*. London, I. Pitman, 1958.
235. Klíma, V., Rosek, J. *Trojfázové Kommutátorové derivací motory*. Praha, Československé akad. ved., 1962.
236. Schenkel, M., *Der Drehstrom-Reihenschlussmotor der Siemens-Schuckert-Werke*. *E. T. Z.*, 1912.
237. Ivanov, N. A. *Trekhfaznaya posledovatel'naya kollektornaya mashina kak dvigatel i generator*. (Three-phase series commutator machine as motor and generator). *Elektrichestvo*, 1912.
238. Schenfer, C. (a) Kommutierungsstromkurven bei Einphasen-Kollektormotoren. *E. u. M.*, 1911, 53; (b) Kommutationsstromkurven bei Mehrphasenkollektormotoren, *E. u. M.*, 1912, 17; (c) Experimentelle Untersuchung der Kommutierung bei dem Einphasenkollektormotorender SSW. *E. u. M.*, 1914, 12.

239. **Helsen, H.** Die Kompensation des Phasenverschiebung von Induktionsmaschinen durch selbsterregte Hauptstromdrehfeld-Erregermaschinen, *E. T. Z.*, 1917.
240. **Altes, W.** (a) The brush-shifting polyphase series motor. *G. E. R.*, 1916; (b) The polyphase shunt motor. *Ibidem*, 1918.
241. **Latour, M.** Commutation in alternating current machinery. *AIEE Proc.*, 1918.
242. **Schrage, H.** (a) Ein neuer Drehstrom-Kommutatormotor mit Nebenschlussregelung durch Bürstenverschiebung. *E. T. Z.*, 1914; Die Oberfelder beim rotorspeisten Kollektormotors. *E. u. M.*, 1935; (c) Mehrfachparallelwicklungen für Drehfeld Kommutatormaschinen. *Bull. Schweiz. Elektrotechn. Verein*, 1943.
243. **Hull, J.** Theory of speed and power-factor control of large induction motors by neutralised polyphase alternating-current commutator machines. *G. E. R.*, 1920.
244. **Ridsdale, J.** *The theory of the three-phase shunt commutator motor*. London, *Electrician*, 1912.
245. **Siegel, E.** Das Kreisdiagramm des Repulsionmotors. *E. u. M.*, 1921.
246. **Kade, F.** Die Theorie und Wicklungsweise der kompensierten Asynchronmotoren. *E. T. Z.*, 1924.
247. **Kaden, H.** Die Theorie der kompensierten Asynchronmaschine. *A. f. E.*, 1925, H. 14, 5.
248. **Kostenko, M. P., Lyuter, R. A.** Trekhfaznye kompensirovannyye asinkhronnyye dvigateli. (Three-phase compensated induction motors). *Elektrichestvo*, 1925, 1.
249. **Weiler, W.** Drehzahlregelung von Asynchronmotoren durch netzerregte Drehstrom-Erregermaschine. *E. T. Z.*, 1925.
250. **Kostenko, M. P.** Kollektornyi shuntovoi mnogofaznyi dvigatel sistemy Shrage. (Commutator shunt polyphase motor of the Schrage system). *Elektrichestvo*, 1925, 8.
251. **Richter, R.** Der Läuferspeiste Drehstrom-Nebenschluss-Motor und neue Ausführung des fremderregten Erequenzwandler. *E. T. Z.*, 1925.
252. **Walz, H.** Über die Ortskurven des Primärstromes einer Induktionsmaschine eigenerregten Drehstromer Megermaschine. *E. u. M.*, 1927.
253. **Liwschitz, M.** Die Drehfeldmaschine in Verbindung mit fremderregter Erregermaschine. *A. f. E.*, 1927, Bd. 19.
254. **Hess, H.** Zur Theorie des kompensierten Asynchronmotors. *A. f. E.*, 1928, Bd. 20, 1.
255. **Rosenthal, H.** Stufenlosregelbare Drehstrom-Nebenschlussmotoren mit Ständer-speisung. *A. E. G.-Mitt.*, 1929.
256. **Kostenko, M. P., Zavalishin, D. A.** (a) Sovremennyye fazovyye kompensatory s sobstvennym vzbuzhdeniem. (Modern phase advancers with self-excitation). *Elektrichestvo*, 1929, 11-12; (b) Eksperimentalnoye issledovaniye fazovykh kompensatorov sobstvennogo vzbuzhdeniya. (Experimental study of phase-compensators with self-excitation). *Elektrichestvo*, 1929, 19-20.
257. **Seiz, W.** Die Regelung der Drehzahl von Induktionsmotoren im unter- und übersynchronen Gebiet nach System Brown-Boveri-Scherbius. *E. u. M.*, 1924; *E. T. Z.*, 1926; *BB-Mitt.*, 1925, 1930.
258. **Kostenko, M. P.** Die mehrphasigen Kollektor und Induktionsmaschinen als Sonderfall des "Allgemeinen transformators". *A. f. E.*, 1930, Bd. 23, 4.
259. **Kostenko, M. P.** Kaskadnyye soedineniya asinkhronnoi i kollektornoi mashin kak chastnyye sluchai "vseobshchego transformatora". (Cascade-connected induction and commutator machines as special cases of "universal transformers"). *Vestnik elektrotehniki*, 1930, 11.
260. **Kostenko, M. P. und Zavalishin, D. A.** Experimentelle und theoretische Kreisdiagramm der mehrphasigen Kollektormaschinen nach der Methode des "Allgemeinen Transformators". *E. u. M.*, 1931, 6.
261. **Hellmund, R. and Ludwig, L.** Sparking under brushes of commutator machines. *AIEE Trans.*, 1933.

262. Coulthard, W. A Generalized equivalent circuit in the theory of polyphase commutator motors. *AIEE Trans.*, 1941.
263. Conrad, A., Zweig, F. and Clarke, J. Theory of the brush-shifting a. c. motor. *AIEE Trans.*, pt. 1, 2, 1941, pt. 3,4, 1942.
264. Franklin, P. (a) The circle diagram of the polyphase brush-shifting commutator motor (Schrage type). *AIEE Trans.* 1947; (b) A study of the 3-phase commutator armature with six adjustable brushes. *Ibidem*, 1948.
265. Kostenko, M. P. Kompensirovannyi mnogofaznyi alternator s krugovym vrashchayushchimsya polem i nezavisimym vozbuzhdeniem peremennogo toka. (Compensated polyphase alternator with circular rotating field and with separate a. c. excitation). *Elektrichestvo*, 1925, 7; 1948, 2.
266. Cučera, T. La theorie du motor à collecteur Schrage. *R G E*, 1962, 6.
267. Kostenko, M. P., Gnedin, L. P. *Teoriya i raschet trekhfaznykh kollektornykh mashin i kaskadnykh soedinenii*. (Theory and calculation of three-phase commutator machines and cascade-connections). Leningrad, Nauka, 1964.
268. Rauhut, P. (a) Der rotorgespeiste Dreiphasen-Nebenschluss-Kommutatormotor und seine Entwicklung, *BB-Mitt.*, 1949, 3-4; (b) Scherbiusmaschinen für Drehzahlregelung, Phasenkompensation und Leistungsregelung von Asynchronmaschinen. *BB-Mitt.*, 1951, 5-6; (c) Der Kommutator-Frequenzumformer, ein Hilfsmittel für den Langsamgang von Arbeitsmaschinen. *BB-Mitt.*, 1951, 5-6; (d) Wann, wo und wie wählt man die Scherbiusregelung. *BB-Mitt.*, 1954, 12; (e) Der Umformer für elastische Netzkupplung. *BB-Mitt.*, 1955, 9; (f) Der Netzkupplungs-Umformer Auhof der Österreichischen Bundesbahnen. *BB-Mitt.*, 1958, 5; (g) Der Scherbius-Regelsatz zum Hauptumformer des CENR. Genf. *BB-Mitt.*, 1959. 6.
269. Lerner, A. Sinkhronizatsiya vrashcheniya kollektornykh dvigatelei tipa Shrage-Rikhtera. (Synchronization of rotation of Schrage-Richter commutator motors). *Elektrichestvo*, 1940 7.
270. Koch, H. Scherbiusmaschinen als Niederfrequenzgeneratoren für Rollgangantriebe. *BB-Mitt.*, 1961, 11/12; 1963, 11/12.

SUPPLEMENT

271. Danilevich, Ya., B., Dombrovsky, V. V., Kazovsky, E. Ya. *Parametry elektricheskikh mashin peremennogo toka*. (Parameters of A. C. electrical machines). Leningrad, Nauka, 1965.
272. Alyabev, M. I. *Obshchaya teoriya sudovykh elektricheskikh mashin*. (General theory of marine electrical machines). Leningrad, Sudostroenie, 1965.
273. Treshchev, I. I. *Nesimmetrichnye rezhimy sudovykh mashin peremennogo toka*. (Unbalanced duties of a. c. marine machines). Leningrad, Sudostroenie, 1965.
274. Baudry, R. and King, E. Improved cooling for generators of large rating. *AIEE Trans.*, Power App. and Syst., 1955., 2.
275. King, E. and Batchelor, J. Effects of unbalanced current on turbine-generators. *AIEE Trans.*, Power App. and Syst., 1965, 2.
276. Rosenberg, L. Developments in gas conductor-cooled generators. *IEER Trans.*, Power App. and. Syst., 1965, 2.
277. Jones, N., Temoshok, M. and Winchester, R. Design of conductor-cooled steam turbine-generators and application to modern power systems. *IEEE Trans.*, PAS-84, 1965, 2.
278. Gheorghiu, I. *Masini electrice*. Vol. 4. Masini alternative cu colector. Bucuresti, Didactică si pedagogica, 1965.
279. Rziha, E. V. *Starkstromtechnik Taschenbuch für Elektrotechniker*. Bd. 1, 2, Achte Auflage. Berlin, W. Ernst, 1955.
280. Wiedemann, E. und Kellenberger, W. *Konstruktion elektrischer maschinen*. Berlin, 1967.

281. **Kazovsky, E. Ya., Danilevich, Ya. B., Kasharsky, E. G., Rubisov, G. V.** *Anormalnye rezhimy krupnykh sinkhronnykh mashin.* (Abnormal operation of large synchronous machines). Leningrad, Nauka, 1969.
282. **Zavalishin, D. A., Parfenov, E. E., Bobrova, R. F.** Kaskad elektricheskikh mashin (Cascade-connected electrical machines), Moscow. Part No. 135956, Bull. of inventions, 1961, 4.
283. **Parfenov, E. E.** Utochnennyyi raschet asinkhronnykh poluprovodnikovyykh kaskadov s vypriamitelem v rotornoi tsepi, ekvivalentnym dvenadtsatifaznomy. *Avtomatizirovannyyi elektroprivod.* (Improved calculation of induction semiconductor cascade connections with rectifier in rotor circuit equivalent to 12-phase rectifier. In book *Automated electric drive*). Leningrad, Nauka, 1965.
284. **Parfenov, E. E., Rovinsky, P. A.** *Asinkhronno-ventilnye kaskady dlya dvukhfaznogo regulirovaniya skorosti asinkhronnykh elektrodvigateli.* (Induction rectifier cascade connections for two-zone regulation of speeds of induction motors). Leningrad, Nauka, 1969.
285. **Kurita, S., Kataoka, M., Nimura, H.** Super-synchronous static Scherbius (Type SS) thyristor motors. *Mits., Denki Eng.*, 1972, 34.
286. **Kazovsky, E. Ya., Sidelnikov, A. V., Troyanskaya, D. O.** Ustanovivshiesya i perekhodnye protsessy v asinkhronnom dvigatele, pitaemom ot preobrazovatelya chastoty (Steady-state and transient processes of induction motor fed from a frequency converter). *Elektrotehnika*, 1973, 4.

INDEX

- A.c. commutator machine
 - development, 595-7
 - polyphase
 - armature currents, 602-3
 - armature winding m.m.f., 603-5
 - shunt, 628-33
 - single-phase
 - armature currents, 602
 - commutation, 606-8
 - three-phase, commutation, 608-11
 - uses, 595-6
 - A.c. commutator motor
 - single-phase
 - repulsion, 621-27
 - characteristics, 625-6
 - commutation, 623, 625, 627
 - Deri, 627
 - with one winding on stator, 624-7
 - Thomson, 624-6
 - torque, 624-6
 - with two windings on stator, 621-3
 - series, 612-21
 - characteristics, 618-20
 - improving commutation, 615-8
 - operating principle, 612-3
 - torque, 612-3
 - uses, 620-1
 - vector diagram, 613-4
 - three-phase
 - Schrage-Richter, 639-52
 - characteristics, 644-7
 - design, 639-40
 - power factor regulation, 642
 - speed regulation, 640-2
 - vector diagram, 642-4
 - series, 650, 654-63
 - characteristics, 662-3
 - circle diagrams, 659-60
 - connection diagrams, 660
 - design, 650
 - with double number of brushes, 660-2
 - fundamental equations, 655-8
 - uses, 663
 - shunt, 639-50
- Air, properties, 160
- Air-gap
 - flux density, 118, 125-6, 195, 480, 510-2
 - distribution, 108-9, 455-7
 - influence on generator performance, 246
 - magnetic field, 110
 - inductive reactances, 128-9
 - non-uniform, 51-2
 - permeance, 110, 125-6, 655
 - variation, 86-7
 - shape, 197, 477
 - size, 6-19
 - tooth ripples, 85-6
- Alternator, *see also* Synchronous generator
 - armature reaction, 183-6
 - current distribution 183-4
 - flux distribution, 183-4
- Angle
 - between current and e.m.f., 183
 - power, 203
- Antinode, wave, 104
- Band rings, rotor, 24
- Bearing, thrust, 36
- Belts, phase, 603-5
- Blondel, A., 190, 205, 208
- Brush(es)
 - gear, 640, 650, 654
 - position, 624-5, 627, 654
 - shifting device, 654
- Cage, rotor, 41-2
- Capacitors, for e.m.f. compensation, 617-8
- Capacity, overload, 263-5, 288, 482, 626
- Cascade, 565, 573-8, 596
 - motor connection, 572-3
 - selection of motors, 573
- Circle, *see also* Diagram, circle equation, 483-4

- main, 513
- parameter scale, 484
- starting, 513
- Circuit
 - equivalent, 362
 - deep bar motor, 553-4
 - direct-axis, 216-7
 - induction machine, *see* Induction machine, equivalent circuit
 - single-phase induction motor, 581-4
 - synchronous motor, 560-1
 - double squirrel-cage motor, 537-9
 - magnetic, saturation, 331
- Clutch, electromagnetic, 590
- Coefficient
 - convection, 150
 - pole-arc, 190
 - radiation emissivity, 150
 - synchronizing power, 265-7, 284
 - synchronizing torque, 265-7
 - of thermal conductivity, 148-9, 151
- Coil
 - crank-shaped, 81
 - group, 56, 80-1, 83
 - m.m.f., 111-4
 - insulation, 98-100
 - straight, 81-2
- Commutation
 - in single-phase machines, 606-8, 615-8, 623, 625, 627
 - in three-phase machines, 608-11
- Commutator, 630
- Condenser, synchronous, *see* Synchronous condenser
- Conductor height, equivalent, 552
- Convection
 - artificial, 150-1
 - natural, 150
- Converter, rotary, *see* Rotary, converter
- Cooling
 - closed circuit, 164
 - open-circuit, 164
 - transformer, 165-78
- Copper, utilisation in windings, 49, 74, 81
- Core
 - stator, 24-5
- Current
 - active component, 416, 447
 - aperiodic component 343-5, 351-5, 355, 366-8, 373-4
 - armature, 602-3
 - commutating, 609-10
 - direct-axis component, 211, 214
 - double-frequency, 235
 - eddy, 469
 - effective value, 370-1, 408-9
 - equalizing, 591-2
 - equivalent
 - rotor, 348, 351
 - stator, 348
 - excitation, 228, 237, 339-40, 349, 352
 - surge, 341
 - unit, 238
 - instantaneous, 402
 - magnetizing, 655
 - negative-sequence, 312, 563
 - no-load, 277, 415, 541-2, 573
 - ideal, 582
 - inrush, 522-3
 - positive-sequence, 331, 562
 - quadrature-axis component, 211, 214
 - for railway traction, 595
 - reactive, 270-1
 - reactive component, 448
 - resultant, 404-5
 - rotary converter, 403-4
 - rotor, 458
 - short-circuit, 324-5, 354, 366, 513, 516, 522, 575
 - ideal, 517
 - shock, 367-8
 - starting, 292, 301-3, 309-10, 321-2, 529-32, 559, 564, 647, 656
 - stator, 354, 437
 - subtransient component, 368-9, 367, 375
 - symmetrical periodic, 343-4, 351, 353, 355, 367-8, 373
 - transient component, 353, 367, 369, 376
 - zero-sequence, 317-8
- Curve
 - bicircular, 485-6
 - cooling, 156-7
 - current decay, 368-9
 - flux density distribution, 109-11, 194
 - heating, 156-7
 - higher-order, 485-7
 - magnetizing, 510-1, 521
 - m.m.f., 111, 118-27, 569
 - integral method of construction, 119-20
 - performance, 479
 - short-circuit current, 343, 356, 359, 370-1
 - torque, 386, 477, 537
 - torque-slip, 46, 290-1, 295, 459, 465-6, 562-3, 580
- Diagram
 - Blondel, 202

circle, 487, 583-4, 650
 approximate, 517-9
 construction, 487-92, 516-8, 659
 corrected, 492-3
 diameter, 490, 506-7, 540-2
 efficiency scale construction, 498-502
 exact, 504-10
 expression of losses, 492-6
 expression of power, 494-7
 power factor determination, 502-3
 simplified, 492
 slip scale construction, 497-8
 stalling torque determination, 503

current
 circle, 274, 275-8
 deep bar motor, 555-6
 equation, 274-6
 Pascal limaçon, 278-280
 e.m.f., 205-7, 208-9, 211, 221, 239, 621-2
 with AIEE correction, 231
 comprasion, 231-2
 modified, 211-13
 short-circuit, 213-5
 simplified, 230-1
 e.m.m.f., 205, 207-9, 221-4, 227-9
 applicability, 226-7
 practical construction, 225-7
 simplified, 226-8, 230
 energy-flow, 452-53
 equivalent, 362 *see also* Circuit, equivalent
 m.m.f., 208, 210, 654, 661-2
 Potier, 205, 223-4, 227-30
 Swedish, 226-8, 230
 vector, 424, 434-7, 446, 449
 e.m.f. 613-5, 642-3, 659-10
 voltage, 203-32, 236, 257, 262, 267-70, 274, 276, 285-6
 rotary converter, 408
 for short circuit, 327-8
 simplified, 286
 for unbalanced load, 328-31
 uses, 203, 218-9
 winding, 69-70, 72, 76, 77-9, 80-4, 90, 95

Dolivo-Dobrovolsky, M. 535, 595

Duty
 continuous, 157-9
 short-time, 158-60
 intermittent, 158, 160-1

Efficiency
 generator, 249-50, 453, 499-500
 motor, 287, 452, 481-2, 496, 498-9, 570, 571-3, 619-20, 626, 644

Electrical machine(s)
 external self-cooling, 163
 heat transfer, 148-52
 by conduction, 148-9
 by convection, 151-2
 by radiation, 149-50
 heating, 152-7
 independent cooling, 163
 internal self-cooling, 160-3
 investigation of operating conditions, 269-73
 natural cooling, 160
 rated duties, 157-8, *see also* Duty
 thermal calculations, 158-9
 ventilation, *see also* Cooling, Ventilation, 145, 166-9

Ellipse, 486-7

E.m.f., *see also* Harmonics, e.m.f.
 additional, 628-9, 633-6, 639
 armature reaction, 210
 direct-axis, 209, 215
 quadrature-axis, 209
 conductor, 51-5
 effective value, 52-5, 56, 58, 608-9
 equivalent, 284
 frequency, 54, 117, 431
 induction machine, slip frequency, 43
 instantaneous value, 51, 56
 internal, 332
 leakage, 130-32, 207, 226, 414, 432, 550
 main parameters, 51
 maximum value, 56
 mutual inductance, 130
 no-load, 354
 phase, 320
 pulsation, 622
 reactive, 606, 608-10
 compensation, 615-6
 resultant, 70, 75, 92, 207, 214, 601, 630
 rotary converter, 398-9
 rotational, 593-601
 across brushes, 600-3, 622
 rotor, 423, 431-3
 self-inductance, 128, 193
 stator, 423, 430
 transformer, 597-9, 601, 606-8, 609-11, 614, 654
 compensation, 615-8
 turn, 55, 60, 62
 vector duagram, 86, *see also* Diagram, vector,
 wave shape, 51, 60
 winding, 55-67
 winding phase, 68

Factor

- air-gap, 85, 126
- armature-reaction, 190, 195
- damping torque, 385
- differential, leakage, 139-40
- direct-axis armature-reaction field form, 192, 196-8
- direct-axis reaction, 193, 196-9
- excitation field form, 186, 192, 196, 199
- field form, 52, 199, 201
- leakage, 315, 437, 442
- overload capacity, 461, 466, 482
- pitch, 62-3
- pole-arc flux, 198
- pole-shoe skew, 87
- power, 270, 288, 482, 588, 619-20, 626, 645
 - determination, 502-3, 517-8
 - improvement, 306-7, 532-3, 595, 620, 629, 639, 644
 - maximum, 586
 - regulation, 633-5, 640, 664-6, 669
- quadrature-axis reaction, 196-8
- quadrature-reaction field form, 195-7
- relative winding, 65
- shock, 368
- slot skew, 476
- static overload capacity, 265
- steel saturation, 126
- synchronization torque, 398
- winding, 60, 63, 86-87, 112
- winding distribution, 47-48, 57, 60, 77

Field

- armature-reaction, 184-6, 314
- circular rotating, 598
- clunter-synchronous, 233-5, 314
- differential leakage, 134
- excitation, 193-4
- leakage, 130-1
- magnetic
 - of a.c. winding, 125-6
- air-gap, 109
 - inductive reactance, 128-30
 - in no-load conditions, 215
 - pulsating, 104-7
 - rotating, 105-8
 - slot-linkage, 132
 - speed of rotation, 43
 - in steady-state short-circuit conditions, 215
 - strength, 109
- pulsating, 597-99

Flux

- commutating, 617
- demagnetizing, 382
- density

- distribution, 51-2, 103, 109-10, 183-4
- effective, 52
- harmonics, 52-5, 511
- instantaneous, 109
- maximum, 192
- excitation, 338
- fictitious, 434, 436-7
- harmonics, 53-4
- induction machine, 433-4
- leakage, 130-1, 133-4, 200, 206, 339, 414, 435, 535-6, 549
 - differential, 140
 - end connection, 138
 - stator, 249
- linkage, 135, 337, 341-3, 345-8
- main, 414, 447
- mutual inductance, 436, 655
- pulsating, 591, 600
- pulsations, 87
- resultant, 206, 214, 216, 281, 436, 522, 653

Frequency

- conversion, 636-8
- converter, 637
- current, 580
- e.m.f., 598-99, 638
- influence of efficiency, 621
- oscillation, 387, 395

Generator

- a.c. commutator, *see* A.c. commutator generator
- induction, *see* Induction generator
- synchronous, *see* Synchronous generator

Gorodskoy, D., 313

Harmonics

- e.m.f.
 - first (fundamental), 56-9, 62, 64
 - higher, 58-60, 65
- flux, 54
- flux density, 53-4, 510
- instantaneous amplitude value, 110-12
- m.m.f.
 - direct, 472-3
 - direction of rotation, 117
 - first (fundamental) 111, 114-5, 126, 192, 195, 318, 456, 624
 - higher, 112, 114, 116, 126, 249, 479
 - lower-order, 125
 - reverse, 472
 - speed of rotation, 118
- tooth-ripple, 56-60, 62-3, 85-7, 249, 474

- Heat
 - rejection
 - from ventilated surfaces, 152
 - from winding surface, 177
 - specific, 149
- Heyland, 437
- Hydrogenerator, 21, 30-7, 75, 139, 312
 - losses, 250
 - rotor, 32-6
 - stator, 34-35
 - ventilation, 33
 - vertical-shaft, 30
 - suspended-type, 30-1
 - umbrella-type, 30
- Impedance
 - excitation circuit, unit, 239
 - rated, 238
 - secondary circuit, 538-40, 630
 - subtransient, 317
- Inductance
 - equivalent, 353, 357, 358, 361
 - mutual, 129, 139, 348, 372-4
 - stator phase, 348
 - winding, 130, 348
 - leakage, 130-2, 357, 358, 362
- Induction generator, *see also* Induction machine
 - drawbacks, 449
 - self-excitation, 450
 - vector diagram, 448
- Induction machine(s)
 - with additional e.m.f. in secondary circuit, 633-36
 - circle diagrams, 483-520
 - corrected, 487-491
 - definition, 19
 - design, 42
 - electromagnetic brake operation, 43, 438, 450
 - electromagnetic torque, 45-6, 297
 - energy-flow diagrams, 451-53
 - equivalent circuit, 416, 418, 423-4, 430, 437, 450
 - as transformer, 439-40
 - equivalent L-circuit, 441-6, 487-8
 - equivalent T-circuit, 446
 - fluxes, 434-6
 - generator operation, 441, 439, 448-50, *see also* Induction generator
 - under load, 423-4
 - magnetizing force equation, 433
 - motoring operation, 42-3, 446-7, *see also* Induction motor
 - on no-load, 413-16
 - operating principle, 42-3
 - operation in synchronous drive system, 589
 - phase-wound rotor, 40-1
 - power, *see* Power
 - rotor, 40-2
 - short circuit, 416-18
 - parameters, 513-15
 - slip, *see* Slip
 - squirrel-cage, 41-2
 - parameters, 418-21
 - stator, 40
 - torque, *see* Torque
 - two-phase hollow-rotor, 590-2
 - vector diagrams, 433-7, 446
- Induction motor, *see also* Induction machine
 - braking
 - circuits, 587-9
 - dynamic, 587
 - electrical, 586
 - regenerative, 586-7
 - characteristics
 - efficiency, 479
 - no-load, 513
 - overload capacity, 482, 502
 - power factor, 482
 - short-circuit, 513
 - speed, 478
 - deep bar, 549
 - comparison with other motors, 580-2
 - current diagrams, 555-6
 - design, 549
 - equivalent circuit, 553-4
 - operating principle, 549-51
 - doubly fed, 587
 - operation
 - phase-wound, starting, 526-8
 - plugging, 586
 - single-phase
 - applications, 613-4
 - circle, diagram, 583-4
 - equivalent circuit, 581-3
 - operating principle, 579-81
 - slip-ring, 481, 587
 - speed regulation, 633-36
 - starting, 526
 - speed, 45
 - squirrel-cage, 479, 570
 - starting, 529-30
 - with autotransformer, 530-31
 - three-phase
 - speed control, 565-70
 - by changing number of poles, 566-70
 - by changing primary frequency, 570-1

- methods, 565-6
 - with rheostat in rotor circuit, 571-2
 - using cascade of motors, 573-78
- starting, 521-34
 - acceleration, 523-4
 - energy losses, 525
 - disconnection from the line, 523
- double squirrel-cage motor, 535-549
 - comparison with other motors, 543, 558-9, 580-2
 - design, 535
 - equivalent circuit, 537-8
 - large-slip conditions, 541-43
 - operating principle, 536-7
 - small-slip conditions, 539-40
- Induction regulator
 - currents, 426
 - with delta-connected windings, 428-9
 - design, 427
 - double, 427
 - operating principle, 424-6
 - power, 426-7
- Inertia constant, 390
- Insulation, *see also* Materials, insulating
 - combined, 99
 - compound-impregnated, 101
 - continuous, 99-100
 - end connection, 100
 - properties, 102
 - winding, 98-102
- Jumper, bypassing, 94-5
- Kasyanov, V., 589
- Konik, B., 198
- Kostenko, M., 198, 313, 571, 596
- Kraemer, W., 596
- Kuznetsov, B., 559
- Lamp, phasing, 252-57
- Law, total current, 109
- Lines, transmission
 - reactances, 334
 - voltage regulation, 306-7
- Load
 - asymmetrical, 311
 - capacitive, 207, 217
 - inductive, 205, 207, 217, 224, 232
 - unbalanced, 328-31
- Locomotives, electric, 620-1
- Lomonosova, L., 313
- Losses
 - additional, 87, 248, 452, 479-80, 495
 - basic, 248
 - copper, 283, 415, 451, 470, 479, 513
 - eddy-current, 471
 - electrical, 237, 458
 - expression on circle diagram, 493-6
 - field winding, 198
 - hysteresis, 469-71
 - mechanical, 470-1, 495, 516
 - motor, 479-82
 - no-load, 494, 582
 - pulsation, 480
 - rotary converter, 403, 405
 - short-circuit, 493-4
 - in shunting resistor, 620
 - steel, 451, 480, 655
 - surface, 249, 480
 - windage, 162
- Machine(s)
 - a.c., *see also* Induction machines, Synchronous machines
 - commutator, *see* A.c. commutator machines
 - winding design, 46-9
 - asynchronous, *see* Induction machines
 - induction, *see* Induction machines
 - Scherbius, 605
 - synchronous, *see* Synchronous machines
- Materials, insulating
 - classes, 143-4
 - limiting temperature, 143
 - properties, 144-5
 - service life, 144
- M.m.f., *see also* Harmonics, m.m.f.
 - armature-reaction, 184-6, 206, 236
 - direct-axis, 191-4, 209, 220
 - quadrature-axis, 194-7, 209, 227
- armature winding, 603-5
- coil, 108-11, 119
- counter-synchronous, 234-5
- equivalent field, 188, 194, 196
- field winding, 613
- fractional-pitch winding, 112-4, 124-6
- full-pitch coil group, 111-2
- resultant, 115-7, 189-90, 208, 416, 434, 588, 622, 630, 655, 662
- rotor, speed, 433
- sinusoidal, 116, 511
- speed, 119
- three-phase winding, 114-9, 122
- wave shape, 114
- winding, 119
- winding phase, 112-4
- Modulus, resonance, 396-7
- Moment, flywheel, 391

Motor(s)

- a.c. commutator, *see* A.c. commutator motor
- asynchronous, *see also* Induction motor
- crane, 618-9
- hysteresis, 469
- induction, *see* Induction motor
- pole-changing, 566-70
- Schrage-Richter, 596, 603, 640-47
- synchronous, *see* Synchronous motor
- traction, 608, 618, 620
- double speed, 566, 570

Node, wave, 104**Oil, dielectric properties, 172****Oscillations,**

- forced, 385-7, 396, 409
- free, 389, 393-6, 409
- pendulum 381
- rotor, 382-85, 390

Oscillograms, current, short-circuit, 360, 373**Pal, E., 313****Pascal limaçon, 487****Period**

- damping oscillation, 393
- free oscillation, 390

Permeance

- air-gap, 110, 126, 655
- counter-synchronous, field, 233-4
- damper system, 141
- end connection, 138-9, 420-1
- equivalent, 132, 135, 339
- leakage, 241
- slot, 134-8
- for stator current flux, 216
- for sudden short circuit, 361
- total, 339

Phase

- advancer(s), 596, 628, 672
- belts, 49
- shift, 286

Piotrovsky, L., 512**Pitch**

- coil, 32, 80
- relative shortening, 62
- resultant, 75
- winding, relative, 60, 63

Pole

- commutator, 615-18, 655
- skewed, 86-7

shoe, design, 51**stator, imaginary, 281****Potential**

- circle, 47
- polygon, 46

Power

- electromagnetic, 260, 263, 267, 280, 282-3, 287, 451, 454, 458, 495, 583
- maximum, 459-61
- expression on circle diagram, 495-7
- mechanical, 453, 495, 583
- maximum, 468-71
- synchronizing, 265-7
- synchronous machine, 257-63
- useful, 496, 572
- maximum, 538-9

Prime movers, 400-1**Railways, electrified, 620-1****Ratio**

- current, 417, 630
- flux density, 567-8
- resistance, 417, 419
- starting torque, 371, 526, 537, 564
- transformation, 631
- voltage, 415, 417, 630

Reactance, inductive, 361, 371

- air-gap magnetic field, 128-30
- armature, 188
- direct-axis armature reaction, 194, 240
- end connection, 133
- equivalent, 539, 631
- excitation winding, 241, 364
- leakage, 130-4, 140, 314, 537
- differential, 139
- negative-sequence, 313-317, 367
- for plotting e.m.m.f. diagram, 226
- positive-sequence, 313, 331
- quadrature-axis armature reaction, 194, 240-1
- relative, 240
- rotor, 432, 551
- short-circuit, 313-4, 559
- in steady-state balanced operation, 215-18
- subtransient, 362-3
- synchronous, 208, 212, 215, 230
- transient, 362, 351
- zero-sequence, 318-19

Reactor, 408**Regulator, induction, *see* Induction regulator****Resistance**

- additional for induction motor starting, 527

- equivalent, 539
- negative-sequence, 316-17
- positive-sequence, 316
- rotor, 551
- subtransient, 317
- Resistors, additional, 607, 618
- Rheostat
 - speed control, 572
 - starting, 521, 526
- Rotary converter, 400-10
 - armature winding, 48
 - losses in armature winding, 403-06
 - operating principles, 400
 - oscillations, 409
 - relations between currents, 402
 - relations between e.m.f.s., 400-1
 - starting, 407
 - uses, 400, 409
 - voltage regulation, 408-9
- Rotor
 - band rings, 24
 - cooling, 170
 - deep-bar, 41
 - hydrogenerator, 31-6
 - induction machine, 40-2
 - radial-slot, 24-5
 - single-cage, 41
 - squirrel-cage, 41-2
 - turbogenerator, 23-7
 - double squirrel-cage, 41-2
- Scherbius, A., 596
- Short circuit
 - asymmetrical, 319-27, 372
 - balanced, 213
 - steady-state, 213, 215
 - sudden, 336-376
 - sustained, 368, 389
- Skin effect, 480, 549-51
- Slip, 43, 472, 478, 495, 573
 - for electromagnetic braking, 44, 497
 - generator, 44, 497
 - for maximum power, 459-61, 468
 - for maximum torque, 45, 461
 - motor, 45, 497, 583, 586
- Slot(s)
 - closed, 98-100
 - number, 87, 94-5, 477, 480
 - open, 98-100
 - rotor, 23, 41-2
 - skewed, 476
 - semi-closed, 98-100
 - semi-open, 98-100
 - shapes, 98-100, 549
 - stator, skewed, 87, 476
- Star, e.m.f., 68-74, 77-8, 82, 92
 - see also* Diagram, vector
- Stator
 - cooling, 161
 - hydrogenerator, 31, 33-4
 - induction machine, 40
 - split, 84-5
 - turbogenerator, 23-5
- Steel
 - band-ring, 27
 - rotor, 24, 25
 - saturation factor, 126
 - stator core, 24
- Synchronization devices, 256, 288
- Synchronous condenser, 29-37, 270, 306-10
 - rated capacity, 319
 - starting, 310
 - utilization factor, 309
 - voltage diagrams, 205
- Synchronous-drive system, 589
- Synchronous generator, *see also* Alternator characteristics
 - external, 247-8
 - load, 246-7
 - no-load, 214, 242-3
 - regulation, 248
 - short-circuit, 243-4
 - efficiency, 249-50
 - losses, 248-50
 - magnetic field, 215-16
 - output, 236-7, 265
 - parallel connection, 252-57
 - parallel operation, 251, 263-5, 273
 - self-synchronization in parallel operation, 257
 - short-circuit ratio, 245-6
 - single-phase
 - armature reaction, 233-37
 - non-salient-pole, 233
 - parallel connection, 252
 - salient-pole, 233
 - three-phase
 - asymmetrical loading, 311
 - asymmetrical short circuits, 319
 - on balanced load, 203-32
 - non-salient-pole, 205-8
 - parallel connection, 252-7
 - salient-pole, 208-13
- Synchronous machine(s), *see also* Synchronous condenser, Synchronous generator, Synchronous motor characteristics
 - power-angle, 258
 - static, 263
 - definition, 19
 - design, 21-5
 - duties, 281-2
 - excitation, 19, 24

- field winding reduction to stator, 198-9
- high-frequency, 37
- leakage inductive reactance, 139-40
- non-salient-pole, 21-3, 128, 218, 225, 236, 247, 260, 263-5, 269, 275-6
see also Tubogenerator armature reaction, 186-9
- design, 51
 - short circuit, 336, 349-56
- operating principle, 19-20
- reaction, 276-7
- salient-pole, 21, 140, 217, 226, 231
260, 276-80, 314 *see also* Hydrogenerator armature reaction, 189-198
 - direct-axis, 191-4
 - quadrature-axis, 194-97
- design, 51, 141
 - short circuit, 366-370
- static overload capacity, 263-5
- uses, 19
- Synchoronous motor,
 - characteristics, 287-8
 - efficiency, 287
 - equivalent circuits, 583-4
 - non-salient-pole, 301
 - power
 - maximum, 282
 - useful, 282, 287
 - reaction, 276
 - salient-pole, 283
 - starting characteristics, 582-6
 - starting
 - asynchronous, 289-306
 - autotransformer, 301-2
 - by combined scheme, 303-4
 - direct, 300
 - pull into synchronism, 295-7
 - uniaxial, 293
 - reactance, 302
 - with auxiliary motor, 289
 - frequency change, 289
 - voltage diagrams, 205
- Tachogenerator, 591
- Tape, mica, 100
 - allowable limit, 148
 - measurement, 145
 - rise, 145, 150, 153-7
- Theory, two-reaction, 189, 205, 209
- Time constant, 352-6, 358, 364-5, 367, 376
 - heating, 153-7, 160
 - starting, 523
- Tolvinsky, V., 232, 330
- Tooth ripples, 85-7
- Torque
 - asynchronous, 298
 - average, 456, 613
 - damping, 382, 385, 388, 398
 - dynamic (excess), 298, 377, 403
 - eddy-current, 470-1
 - electromagnetic, 45, 282
 - maximum, 45-6, 459-61
 - equilibrium equation, 377
 - harmonics, 387
 - hysteresis, 469-71
 - of inertia, 387
 - maximum, 625, 290, 527, 656, 658
 - parasitic, 471
 - asynchronous, 472-3
 - prevention, 476-7
 - synchronous, 474
 - vibration, 475
 - pull-in, 290
 - pull-out, 290
 - relative, 466
 - resultant, 563, 581
 - stalling, 461, 502, 631, 644, 691
 - starting, 290-2, 302, 465, 521, 526, 529-34, 559, 563, 584, 629, 662
 - synchronizing, 251, 266, 380, 387
- Triangle, reactive (short-circuit), 214, 331-35
- Turbogenerator, 25-9, 187, 226, 231, 312, 333
 - losses, 250
 - rotor, 21-3
 - stator, 24-5
 - ventilation, 28, 160-4
- Units, relative, 238-43
- Values, per unit, *see* Units, relative
- Vasilyev, D., 631
- Ventilation
 - axial-flow, 162-3
 - exhaust, 161-2
 - forced-draught, 160-1
 - hydrogenerator, 33, 176
 - radial, 162-3
 - turbogenerator, 25, 164-6
- Voltage
 - across terminals, 204, 207
 - drop, 218-22, 223-4, 230-31, 236-7, 408
 - excitation circuit, unit, 238-9
 - regulation, 441, 427, 618
 - rise, 218-23, 227, 230, 232
- Voltmeter, null, 254, 256

Wave

- antinodes, 104
- commutator potential, 638
- nodes, 104
- pulsating, 103-5, 110
- travelling, 104-5, 115-6

Wedges, rotor-slot, 24-5

Weight, specific, 147-8

Winding(s)

a.c., machine

design, 68-102

inductive reactances, 128-42

magnetomotive force, 103-27, *see*
also M.m.f.

armature, drum, 603

bar, 77

chain, 79-80

compensation, 612, 620

concentrated, 56, 60, 63

dampers, 32, 231, 234-5, 336, 356-60,
409, 560

differential leakage field, 134

distributed, 55-60, 64

distribution factor, 49-50

double-layer, 133, 136, 138

end connections, 74, 77-85

insulation, 98-102

leakage permeance, 141-2

fractional, 87-96

double-layer, 90-3

full-pitch, 68-71, 74, 84

heating, 524

insulation, 98, 102

lap

double-layer, 68-75

fractional, 87-96

single-layer, 77-8

laying methods, 98-9

leakage field, 130-1

leakage inductance, 131

magnetic field, 103

phase belt, 48-9

pitch factor, 62-3

pole-changing, 569

potential polygon, 46

rotor, 57

design, 533, 611,

end connections, 24

short-pitch, 69, 74, 77-8

single-layer, 77-85, 132-3

chain, 79-80

concentric, 80-5

three-tier, 83, 84, 133, 138

two-tier, 80-3, 133, 137

involute, 77-9

mush, 80-1

single-phase, 59-60, 138

starting, 37, 41, 579

symmetrical, 49

test voltages, 101

three-phase, 60-1, 68-85, 88-98

wave

double-layer, 75-7

fractional, 94-8

Yapolsky, N., 570, 596

Zavalishin, D., 570